COMBINED PROCEEDINGS OF THE NIGERIAN MATERIALS CONGRESSES (NIMACON-2010 & 2011) / NIGERIAN-MRS MEETING

COMBINED PROCEEDINGS OF THE NIGERIAN MATERIALS CONGRESSES

(NIMACON-2010 AND NIMACON-2011)

And Meeting of the

NIGERIAN MATERIALS RESEARCH SOCIETY

(Nigerian-MRS)

NIMACON 2010

Held at:

Universal Hotel, Aguleri Street,
Independence Layout, Enugu, Nigeria

November 23 – 26, 2010

NIMACON 2011

Held at:

Conference Hall, Engineering Materials
Development Institute, Km 4 Ondo Road,
Akure, Nigeria

November 21 – 24, 2011



COMBINED PROCEEDINGS

of the

NIGERIAN MATERIALS CONGRESSES

(NIMACON-2010 AND NIMACON-2011)

And Meeting of the

NIGERIAN MATERIALS RESEARCH SOCIETY (Nigerian-MRS)

Copyright © 2012. Materials Science and Technology Society of Nigeria (MSN)
ISBN 978-060-609-21
All Rights Reserved 2012

Published by

Materials Science and Technology Society of Nigeria (MSN)
National Headquarters
Engineering Materials Development Institute, Km 4 Ondo Road,
PMB 611, Akure, Nigeria
info@msn-ng.org
www.msn-ng.org

Printed by:
TIFODANT PRESS AND PUBLISHING CO.
Tel: 08038054359

COMBINED PROCEEDINGS OF THE

NINETH AND TENTH NIGERIAN MATERIALS CONGRESSES (NIMACON-2010 AND NIMACON-2011)

NIMACON 2010 Held at

Universal Hotel, Aguleri Street, Independence Layout, Enugu, Nigeria
November 23 – 26, 2010

Theme: **Materials in Clean Technologies Development**

NIMACON 2011 Held at

Conference Hall, Engineering Materials Development Institute, Km 4 Ondo Road, Akure, Nigeria
November 21 – 24, 2011

Theme: **Materials Processing for Sustainable Environment and National Development**

DR. A.T. OYELAMI, PROF. B.O. ADEWUYI AND PROF. D.A. PELEMO

PUBLISHED BY THE MATERIALS SCIENCE AND TECHNOLOGY SOCIETY OF NIGERIA (MSN)

LIST OF SPONSORS

NIMACON 2011

1. Materials Science and Technology Society of Nigeria (MSN)
2. Federal Ministry of Science and Technology, Abuja
3. National Agency for Science and Engineering Infrastructure (NASENI) Abuja
4. Engineering Materials Development Institute (EMDI) Akure
5. Prototype Engineering Development Institute (PEDI) Ilesa
6. Sheda Science and Technology Complex (SHESTCO), Abuja
7. Centre for Energy Research and Development (CERD) Ile Ife
8. Postgraduate School, University of Ibadan

NIMACON 2010

1. Projects Development Institute (PRODA), Enugu
2. National Agency for Science and Engineering Infrastructure (NASENI) Abuja
3. Scientific Equipment Development Institute (SEDI), Enugu
4. Prototype Engineering Development Institute, Ilesha
5. Engineering Materials Development Institute (EMDI), Akure
6. National Engineering Design and Development Institute, Nnewi
7. INNOSON Technical and Industrial Company
8. Lad Fluid Controls Services/TCR Engineering, Port Harcourt
9. Nnabuife Enterprises Nigeria, Ltd., Ogui Rd., Enugu
10. Mirabeth Suites, Abakpa, Enugu
11. Professor C.A. Nebo
12. Engr. Nathan Abia-Bassey

MATERIALS SCIENCE AND TECHNOLOGY SOCIETY OF NIGERIA (MSN)

NIGERIAN MATERIALS CONGRESS 2010 (NIMACON 2010)

HELD AT
UNIVERSAL HOTEL, AGULERI STREET, INDEPENDENCE LAYOUT, ENUGU, NIGERIA
NOVEMBER 23 – 26, 2010

COMMUNIQUE –NIMACON2010

The Materials Society of Nigeria held its 9th Annual Congress, tagged "NIMACON 2010" in the city of Enugu, co-hosted by Projects Development Institute (PRODA), Enugu and Scientific Equipment Development Institute (SEDI) Enugu from 23rd to 26th November, 2010.

The conference theme was "MATERIALS IN CLEAN TECHNOLOGIES DEVELOPMENT" and drew participants from all geopolitical zones of Nigeria as well as the African continent. Contemporary issues and scholarly papers were presented and discussed.

At the end of deliberations, Congress rose with the following communiqué:

1. That government should be more committed and provide the leadership in the global drive for clean technologies through deliberate policies aimed at improving the science and technology infrastructure of Nigeria. Congress places particular emphasis is placed on the need for cleaner technology in the development of fossil fuels like coal.

2. That the paucity of research laboratories in most higher institutions and the poorly equipped or in existent ones of government established research institutions does not bode well for sustainable technological development. Congress calls for the establishment of at least one centre of excellence in each geopolitical zone aimed at materials research and able to address clean technology needs.

3. That government should engage the relevant professional bodies like the Materials Society of Nigeria (MSN), Nigerian Society of Engineers (NSE), Nigerian Metallurgical Society (NMS), Chemical Society of Nigeria (CSN) and others to highlight the key issues in science and technology development and materials research to ensure implementation of agreed policies.

4. That research institutes, academia and industries should collaborate and synergize for more meaningful impact in the country's technological development.

5. That eligible professionals should make affiliation with professional bodies an important call to duty and take advantage of the opportunities offered to enhance their professional development and add value to the technological development drive.

6. That students should be encouraged and sponsored to attend conferences and workshops to ensure the growth and sustenance of the materials profession.

MATERIALS SCIENCE AND TECHNOLOGY SOCIETY OF NIGERIA (MSN)

NIGERIAN MATERIALS CONGRESS 2011 (NIMACON 2011)
HELD AT
CONFERENCE HALL, ENGINEERING MATERIALS DEVELOPMENT INSTITUTE, KM 4 ONDO ROAD, AKURE, NIGERIA
NOVEMBER 21 – 24, 2011

COMMUNIQUE – NIMACON2011

The Materials Science and Engineering Society of Nigeria (MSN) held its 10th Annual Nigerian Materials Congress (NIMACON 2011) from 21st – 24th November, 2011 at the EMDI, Akure, Ondo State with a theme "Materials Processing for Sustainable Environment and National Development".

In all, a total of 1 keynote address, 4 plenary papers, 79 technical papers and 52 poster presentations covering different aspects of materials science and engineering were discussed. At the end of deliberations, the following communiqué was presented.

1. The need for an effective tripartite linkage between Government, Industry and Academia for sustainable environment and economic development of any nation cannot be overemphasized. Congress therefore urges Government to take the lead in strengthening and sustaining this all-important mutual relationship in Nigeria as the only panacea for our national development.

2. Congress notes the current ugly and unacceptable trend in which most if not all the multinationals operating in the country have their research facilities outside Nigeria, only to import the results back for implementation. Congress urges Government to institute relevant policies that would mandate these multinationals to install these facilities within the country as way of accelerating our economic and technological advancement as a nation.

3. Congress notes the recent incidents of lead poisoning during mining activities in some states in Nigeria. Congress recommends that Government should encourage mining companies to adopt the emerging global concept of integrating mine closure activities in mining project proposals. For a start, intending companies wishing to operate in the mining sector of the economy should be mandated to set aside at least 30% of total cost of the project for mine closure activities before being licensed to operate.

4. Congress notes the near total absence of research laboratories in most Nigerian Universities which has hampered our technological growth over the years. Congress therefore reiterates the need for centre of excellence and recommends that at least one such centre be established in each of the six geo-political zones in the country as a way of boistering research activities for our industrial and technological advancement.

5. Congress notes the growing number of professors emerging from our universities, especially in science and engineering as good development. Congress encourages Government to ensure that the potentials of these eminent Nigerians be maximally harnessed through the provision of enabling environment for practice vis-a-vis the establishment of research laboratories, libraries and better working conditions in our universities.

FROM THE EDITORS' DESK

This is the first time two proceedings of the Nigerian Materials Congress (NIMACON) will be combined in a single volume. The reason for the combination is to ensure that the Society maintains its 10-year unbroken record of producing quality conference proceedings. The inability to print the proceeding for NIMACON 2010 was purely due to logistics. We are therefore happy to present to the materials community and the academic society as a whole another edition of well-researched works with academic and practical contents cutting across virtually all engineering and science-related disciplines.

Another interesting thing about the proceeding is the quality of plenary/keynote papers contained therein, which for obvious reason, we could not include them all.

NIMACON 2010 revolved round the theme "Materials in Clean Coal Technology" with the following sub-themes

* Materials in Clean Technologies for Transportation
*Materials in Clean Technologies for the Oil and Gas Industry
*Advanced Renewable Energy Materials
*Modelling and Simulation in Clean Technologies
*Clean Technologies in Materials Processing
*Clean Technologies, Energies and Environment

NIMACON 2011 on the other hand focused on Materials Processing for Sustainable Environment and National Development and quite a large number of papers were presented on all the sub-themes covering:

* Biomaterials and Biometrics,
* Nanomaterials and Nanotechnology,
* Materials in Constructions and Communications,
* Reverse Engineering and Adaptive Technology,
* Electronic Materials,
* Polymeric Materials,
* Minerals Processing,
* Modeling and Simulations,
* Innovation and Development in Materials Research

The editors have made painstaking efforts to format and edit the papers to ensure uniformity. Any error and omission noticed is unintended and is regretted.

Adekunle Oyelami (EMDI, Akure)
Benjamin Adewuyi (FUTA, Akure)
David Pelemo (OAU, Ile Ife)

NIMACON 2010 LOCAL ORGANIZING COMMITTEE

Engr. N. Abia-Bassey (PRODA)	-	Chairman
Engr. J.U. Odo (UNIZIK)	-	Member
Prof. R.U. Osuji (UNN)	-	Member
Dr. F.I. Ezema (UNN)	-	Tech. Sec.
Engr. C.N. Mbah (ESUT)	-	Member
Mr. I. Ita (SEDI-E)	-	Member
Engr. R.N. Okeke (ESUT)	-	Member
Engr. E.C. Ufomba (SEDI-E)	-	Member
Engr. J.N. Ogbodo (SEDI-E)	-	Member
Engr. T.C. Udeinya (PRODA)	-	Member
Engr. C.S. Obayi (UNN)	-	Member
Engr. Mrs. L. A. Nnodi (SEDI-E)	-	Member
Engr. S. Adikwuanduaba (POLY NEKEDE)	-	Member
Dr. N.E. Idenyi (EBSU)	-	Member
Engr. P. Okoye (POLY NEKEDE)	-	Member
Engr. P. Nwosu (POLY NEKEDE)	-	Member
Engr. C.C. Njoku (PRODA)	-	Secretary

NIMACON 2011 LOCAL ORGANIZING COMMITTEE

1.	Prof. B.O. Adewuyi (FUTA)	-	Chairman
2.	Engr. B.A. Olunlade (EMDI)	-	Member
3.	Prof. J.O. Borode (FUTA)	-	Member
4.	Dr. O.T. Adewara (FUTA)	-	Member
5.	Dr. A.R. Adetunji (PEDI)	-	Member
6.	Dr. M.B.O. Shitta (UNAD)	-	Member
7.	Mr. B.E. AttahDaniel (EMDI)	-	Member
8.	Engr. A.K. Ogunkoya (EMDI)	-	Member
9.	Engr. J.O. Alasoluyi (EMDI)	-	Member
10.	Engr. A.T. Oyelami (EMDI)	-	Secretary

BOARD OF TRUSTEES

Engr. Kunle Ogunade (Petro Organico, Lagos)	-	Chairman
Prof. O.O. Adewoye (NASENI, Abuja)	-	Secretary
Prof. A.B. Okorie (ESUT, Enugu)	-	Member
Prof. P. Onwualu (RMRDC, Abuja)	-	Member
Prof. Wole Soboyejo (Princeton, USA)	-	Member

NATIONAL EXECUTIVE BOARD MEMBERS (2008 – 2010)

NATIONAL PRESIDENT
Prof. F.E. Okieimien,
Department of Chemistry,
University of Benin, Benin City.
okieimen@uniben.edu.ng

VICE PRESIDENT (MATERIALS SCIENCE)
Dr. B. Babatope,
Department of Engineering Physics,
Obafemi Awolowo University, Ile-Ife.
bbabatop@oauife.edu.ng

VICE PRESIDENT (MATERIALS ENGINEERING)
Prof. K.J. Osinubi,
Department of Civil Engineering,
Ahmadu Bello University, Zaria.
kosinubi@yahoo.com

NATIONAL SECRETARY
Prof. A.O. Olorunnisola,
Department of Agricultural Engineering,
University of Ibadan, Ibadan.
abelolorunnisola@yahoo.com

ASST. NATIONAL SECRETARY
Dr. A. Giwa,
Department of Textiles Technology,
Ahmadu Bello University, Zaria.
giwafat2002@yahoo.com

MEMBERSHIP SECRETARY
Engr. A.T. Oyelami,
Engineering Materials Development Institute,
Km 4 Ondo Road, P.M.B. 611, Akure.
atoyelami@yahoo.com

PUBLICATION SECRETARY
Dr. Z. Kana,
Sheda Science and Technology Complex,
Sheda, Abuja.
zebaze@shestco.org

FINANCIAL SECRETARY
Engr. J.U. Odo,
Dept. of Met. and Materials Engineering,
Nnamdi Azikwe University, Awka.
odojis@yahoo.com

TREASURER
Dr. (Mrs.) E.U. Ikhuoria,
Department of Chemistry,
University of Benin, Benin City.
ikhuoria@uniben.edu.ng

PUBLIC RELATIONS OFFICER
Dr. S. Odusanya,
Sheda Science and Technology Complex,
Sheda, Abuja.
shola2@hotmail.com

AUDITOR
Dr. A.R. Adetunji,
Prototype Engineering Development Institute
Old Ile-Ife Road, Ilesa
aadetunj@oauife.edu.ng

CONTINUOUS PROFESSIONAL DEVELOPMENT OFFICER
Dr. S.B. Hassan CPD Officer
Dept. of Metallurgical Engineering
Ahmadu Bello University, Zaria.
hassbolaji@yahoo.com

FIRST ORDINARY MEMBER
Dr. (Mrs.) A. Boyo,
Department of Physics,
Lagos State University, Lagos
nikeboyo@yahoo.com

SECOND ORDINARY MEMBER
Miss O.O. Olatunbi,
Federal College of Chemical and Leather Technology, Zaria.
opicferra@yahoo.com

THIRD ORDINARY MEMBER (AND PIONEER NATIONAL PRESIDENT)
Prof. O.O. Adewoye *FAS*
National Agency for Science and Engineering Infrastructure,
Idu Industrial Layout, Garki, Abuja.
oadewoye@yahoo.co.uk

NATIONAL EXECUTIVE BOARD MEMBERS (2010 – 2012)

NATIONAL PRESIDENT
Prof. A.O. Olorunnisola,
Department of Agricultural Engineering,
University of Ibadan, Ibadan.
abelolorunnisola@yahoo.com

VICE PRESIDENT (MATERIALS SCIENCE)
Prof. (Mrs.) E. U. Ikhuria,
Department of Chemistry,
University of Benin, Benin City.
ikhuoria@uniben.edu.ng

VICE PRESIDENT (MATERIALS ENGINEERING)
Prof. S.B. Hassan
Dept. of Metallurgical Engineering
Ahmadu Bello University, Zaria.
hassbolaji@yahoo.com

NATIONAL SECRETARY
Dr. A. Giwa,
Department of Textiles Technology,
Ahmadu Bello University, Zaria.
giwafat2002@yahoo.com

ASST. NATIONAL SECRETARY
Dr. N. E. Idenyi
Department of Industrial Physics
Ebonyi State University, Abakaliki
edennaidenyi@yahoo.com

MEMBERSHIP SECRETARY
Engr. Dr. A.T. Oyelami,
Engineering Materials Development Institute,
Km 4 Ondo Road, P.M.B. 611, Akure.
atoyelami@yahoo.com

PUBLICATION SECRETARY
Prof. D. A. Pelemo,
Centre for Energy Research and Development,
Obafemi Awolowo University, Ile-Ife
dpelemo@cerd.gov.ng

FINANCIAL SECRETARY
Dr. (Mrs) A. Boyo,
Dept. of Physics, Lagos State University, Ojo,
Lagos
nikeboyo@yahoo.com

TREASURER
Engr. Dr. J.U. Odo,
Dept. of Met. and Materials Engineering,
Nnamdi Azikwe University, Awka.
odojis@yahoo.com

PUBLIC RELATIONS OFFICER
Prof. B. I. Imasogie,
Department of Materials Science and
Engineering,
Obafemi Awolowo University, Ile-Ife
imasogie@oauife.edu.ng

AUDITOR
Engr. A. K. Ogunkoya
Engineering Materials Development Institute,
Km 4 Ondo Road, P.M.B. 611, Akure
tjoguns607@yahoo.com

CONTINUOUS PROFESSIONAL DEVELOPMENT OFFICER
Engr. N Abia-Bassey
Projects Development Institute,
PMB 01609 Nchatancha Emene WD/Lout,
Enugu
nyab2001@yahoo.co.uk

FIRST ORDINARY MEMBER (AND IMMEDIATE PAST NATIONAL PRESIDENT)
Prof. F.E. Okieimien,
Department of Chemistry,
University of Benin, Benin City.
okieimen@uniben.edu.ng

SECOND ORDINARY MEMBER (AND PIONEER NATIONAL PRESIDENT)
Prof. O.O. Adewoye *FAS*
National Agency for Science and Engineering Infrastructure,
Idu Industrial Layout, Garki, Abuja.
oadewoye@yahoo.co.uk

THIRD ORDINARY MEMBER
Engr. Dr. B. A. Olunlade
National Agency for Science and Engineering Infrastructure,
Idu Industrial Layout, Garki, Abuja
koleolunlade@yahoo.com

FOURTH ORDINARY MEMBER
Engr. Dr. S.O.O. Olusunle
Engineering Materials Development Institute,
Km 4 Ondo Road, P.M.B. 611, Akure
tolusunle@yahoo.co.uk

Table of Contents

LIST OF SPONSORS iii

COMMUNIQUE –NIMACON2010 iv

COMMUNIQUE – NIMACON2011 v

FROM THE EDITORS' DESK vi

NIMACON 2010 LOCAL ORGANIZING COMMITTEE vii

NIMACON 2011 LOCAL ORGANIZING COMMITTEE vii

BOARD OF TRUSTEES viii

NATIONAL EXECUTIVE BOARD MEMBERS (2008 – 2010) ix

NATIONAL EXECUTIVE BOARD MEMBERS (2010 – 2012) ix

TABLE OF CONTENTS x

TECHNICAL PAPERS FOR NIMACON 2010 xi

TECHNICAL PAPERS FOR NIMACON 2011 xiii

NIMACON 2010 LIST OF PARTICIPANTS xvii

NIMACON 2011 LIST OF PARTICIPANTS xix

TECHNICAL PAPERS FOR NIMACON 2010

S/N	TITLE OF PAPERS	NAME(S) OF AUTHOR(S)	E-MAIL	PAGE
1.	Solar Energy: A Veritable And Sustainable Power Generation Source For Domestic Use, Material Processing And Technological Advancement	C. I. Nwoye and J. U. Odo	chikeyn@yahoo.com	13
2.	Microstructural Development On Fired Nigerian Clay Of South-west, Nigeria	[*1]Olokode O.S., [1]Aiyedun P.O., [2]Oluwadare G.O., [3]Lee, W.E	atoyelami@yahoo.com	20
3.	Performance Evaluation Of Blowers Of Different Impeller/vane Profiles	Oyelami A.t.[1], Adejuyigbe S.b.[2], Waheed M.a.[2], Ogunkoya A.k.[1] And Iliya D.		25
4.	Development Of Spin – Casting Machine For Production Of Nano-structured Parts	O. Olaniran, B.O. Adewuyi and J.O. Borode	dayo525@yahoo.com	32
5.	Strength Classes Of Some Common Nigerian Timber Species	I. Abubakar[1], J. M. Kaura[1] And S. Dahiru[2]	jdanbala@yahoo.co.uk, salisudahiru@ymail.com	35
6.	Renewable, Recycled And Re-used Materials As Major Pillar Of Sustainable Construction In Developing Countries	Dauda Dahiru and Abdulazeez Darda'u		45
7.	Fuel Production From Biomass For Renewable Energy	1.1Ocheri C.[1], Agboola, J.b[.2] Oyelaran O.a[3] & Barnabas A.[4]	ocheri4c@yahoo.com,joe_agboola@yahoo.com ajanioyelaran@yahoo.com, barnabelad20012000@yahoo.com	52
8.	Materials In Advanced Clean Coal Technologies	1.2Ocheri C.[1], Agboola, J.b[-2] Oyelaran O.a[3] & Barnabas A.[4]	ocheri4c@yahoo.com, joe_agboola@yahoo.com ajanioyelaran@yahoo.com , barnabelad20012000@yahoo.com	59
9.	Municipal Solid Waste Management (mswm): Issues, Challenges And Agenda For Ac*tion.*	Oyelaran O.A.[1], Ocheri C[2]. and Barnabas A.[3]	ocheri4c@yahoo.com, ajanioyelaran@yahoo.com , barnabelad20012000@yahoo.com	64
10.	Synthesis And Characterization Of Some Hematite (α- Fe_2o_3) Samples	Adegoke H.I[+]. and Adekola F.A.	ihalimat@yahoo.com	68
11.	The Effect Of Heat Treatment Processes On The Mechanical Failure Of Engineering Parts Used In Cocoa Industry (ile - Oluji Cocoa Industry As A Case Study)	[1]Alo F. I, [2]Shitta M. B. O, [1]Adetunji A. R	Iretispecial2005@yahoo.com	73
12.	The Optimal Driving Speed As A Means Of Enhancing A Cleaner Environment	Igweh C.O., *Unachukwu G.O.		79
13.	Comparative Modeling And Simulation Of Structural Behaviour Of Steel Component Welded With Different Brands Of Electrodes Using Pro-e Mechanica And Comsol Multiphysics	[*]Oyelami A.T., Ogunkoya A.K., Ogundare O. and Olunlade B.A	atoyelami@yahoo.com	81
14.	Finite Element Analysis Of Thermoelastic Contact Problem Of Disc Brake With Frictional Heat Generation.	*Moses Omolayo Petinrin; John Ogheneortega Oji	*layopet01@yahoo.com	90

TECHNICAL PAPERS FOR NIMACON 2011

S/N	TITLE OF PAPERS	NAME(S) OF AUTHOR(S)	E-MAIL	PAGE
1.	Effects Of Water Temperature On The Hardness And Toughness Of Water Quenched Medium Carbon Steel	*A.A. Alabi, A.I. Obi And Magani S.S	abdulmm2001@hotmail.com	97
2.	The Influence Of Carburizing Variables On The Mechanical Properties Of AISI 1034 (2-D Approach)	[1]Adegbola A. A., [1]adegbenjo. O.A, [1]Olaiya. K.A, [2]omotoyibo J.A And [2]Olaniran .O	kunleade2002@yahoo.com	101
3.	Effect Of Starch On The Mould Characteristics Of Ngwo Foundry Sand	[1]Nwonye E.I. And [2]odo J.U.	emmanuel_nwonye@yahoo.com, odoju@yahoo.com	107
4.	Evaluation Of The Inhibitive Properties Of Black Cream On Ductile Iron	Ibegbulam, C.M; Olowonubi, J.A; Aigbogun, O.J; Olunlade, B.A And Ukoba, O.K	c_m_ibe@yahoo.com	115
5.	Coal Processing In The Coke Oven And By Product Plant Of The Ajaokuta Steel Company Limited	Ocheri C.1, Agboola, J.B.2	ocheri4c@yahoo.com	119
6.	Influence Of Hammer Mill Operating Parameters On Grinding Energy Requirement Of Two Hard Nutshells	[A]Kayode, O. And [B]Koya, O. A.	adeolakunle@yahoo.com	125
7.	Mechatronics For Sustainable Environment And National Development	[1,2]Onipede B.O., [1,3]Omole F.O, [1,4]oji J.O., [1,5]Adetunji A. R.	*deleonipede@gmail.com, omolfemi65@yahoo.com*	131
8.	Design Of A Compression Based Hand Operated Brick Moulding Machine	[1,2]Yakubu A.M., [1,2]Oji J.O., [1]Ogar M.O., [1,2]Oduola M.O., [1,3]Adetunji A. R.	yakmoji79@yahoo.com	135
9.	A Study Of The Solvent Extraction Of Tantalum(V) From Aqueous Sulphate/Fluoride Columbite Leach Using Trioctyl Amine In Mibk	O. Sanda[1]*, E. A. Taiwo[2] And G. A. Osinkolu[1]	osanda@cerd.gov.ng	139
10.	Potentials Of Ukwa Tree (Sterculia Setigera) As A Source Of Raw Material For Pulp And Paper Making	[1]Anyanwu, B.U, [2]olokode, O.S, [3]Aiyedun, P.O, [4]oyeleke Y.T.	engr_olokode@yahoo.com	145
11.	Synthesis And Comparative Analysis Of Samples Of Dye Sensitized Solar Cells Using TiO_2 Films	Nwanya A. C.[1], Ezema F.[1.2] And Oparaku O.U[1].	chinweasum@yahoo.com	150
12.	Characterization Of Vacuum Thermally Deposited Aluminium Zinc Nano Thin Film	O.R. Adetunji [1]; P.O.Aiyedun[2]; T.A.Arowolo [3] ; O.J.Alamu [4]	adetunjiolayide@yahoo.co.uk	159
13.	Investigation On Properties Of Recycled Acrylonitrile-Butadiene-Styrene (Abs) From Different Fridge Brands	A.O. Aroke*, A. S. Ahmed And B.O. Aderemi	kenlamin@yahoo.com	164
14.	Effect Of Delignified Native Bamboo (Bambusa Vulgaris) Cellulosic –G-Poly (Acrylonitrile) On The Growth Of Okro (Abelmoschus Esculentus) Seedlings	L. O. Ekebafe*[1], M.O.Ekebafe[2], S.O. Ugbesia[1], J.A. Idiaghe[1]	lawekebafe@gmail.com	169

15.	Development and Applicability of Synthetic Polymeric Materials for Corrosion Inhibition; A Sustainable Technology for Pipelines and Allied Structures Integrity	C. I. Nwoye[1*], J. U. Odo[1], E. O. Obidiegwu[2], and C. C. Ugwuegbu[3]	chikeyn@yahoo.com	174
16.	Determination Of Flammability Properties Of Acetaldehyde Homo-Polymer	Nsikak S. A. ,Edward O., Bashir I., Nkechinyere N. E. Uduak-Obong I. I. And Martins K. U.	ikem404umi@yahoo.com	181
17.	Production Of Silicon Slurry As A High Temperature Protective Coating For Mild Steel In A Salt Admixture	[1,2]Liadi, A. A., 1taiwo, A. T., [1]Akinluwade, K. J; And [1,3]Adetunji, A. R.	abiodunliadi@yahoo.com	185
18.	Production Of Particleboard From Sugarcane Bark, Bagasse And Their Composite	[1] M. T. Isa*, [1], Abdulaziz Atta, [1]Baba Abdul, [1] T. K. Bello And [2] S. A. Yusuf	mtisaz@yahoo.com mtisa@abu.edu.ng	190
19.	Effect Of Dioctyl Phthalate On The Properties Of Unsaturated Polyester Resin	M. T. Isa *[A], A. S. Ahmed [A], B. O. Aderemi [A], R. M. Taib [B], I. A. Mohammed-Dabo[a]	mtisaz@yahoo.com, mtisa@abu.edu.ng	193
20.	Production Of Carbon Nanotubes CNTs Using Alcohol Catalytic Chemical Vapour Deposition (ACCVD) Technique: A Review	Adewuyi B. O. And Aladejebi O. A.	tayo_adewuyi@yahoo.com	197
21.	The Use Of Operational Amplifier In Providing Safety For Electronic Devices	Oluyamo S.S. And Olusola O.I.	olajideibk@yahoo.com oluyamos@yahoo.com	341
22.	Base And Precious Metal Values In End-Of-Life Electronics	Ogunniyi I. O.	mrolatunji@yahoo.com	328
23.	Potential Applications Of Carbon Nanotubes Cnts: A Review	Adewuyi B. O. And Aladejebi O. A.	tayo_adewuyi@yahoo.com	209
24.	Correlation Between Structural And Optical Properties Of PVA/TiO_2 Nanocomposites	Ahmed, T. O., Akusu, P. O., Alu, N.,Ismaila, A. & Shiga, Y. A.	tajahmol@yahoo.co.uk abdu.ismaila@gmail.com abdulgaladima2@yahoo.com	212
25.	Microstructural Evolution And Properties Of Titanium Thin Films Prepared By D. C. Magnetron Sputtering Technique	E. Ajenifuja*, A. Y. Fasasi, G. A. Osinkolu	emmanuelaje@yahoo.com , eajenifuja@cerd.gov.ng	
26.	Comparative Analysis Of Corrosion In Different Aluminium Plates Concentration Of Lime Solutions	Owoeye, F.T., Olokode, O.S., Aiyedun, P.O.	engr_olokode@yahoo.com	223
27.	Effects Of Chemical Additives On The Hydration Behaviour Of Cement Composites From Calamus Deerratus And Laccosperma Secundiflorum Canes	Adefisan, O.O And Olorunnisola, A.O.	femiadefisan@yahoo.co.uk, bolajide96@hotmail.com	228
28.	Process Of Sinter Production For Use In The Blast Furnace Of The Ajakuta Steel Company Limited	Ocheri C.[1], Oyelaran O.A[2] & Barnabas A.[3] Agboola, J.B.[4] Aji Daniel [5]	ocheri4c@yahoo.com	233
29.	Characterization Of Ugwu-Ogba Clay Deposit For Furnace Refractory Production	*Odo, J.U; [+]Agbo, A. O;*Nwoye C.I. And *Adinna B.O.	odojus@yahoo.com, alfredagbo@yahoo.com	237
30.	Microbial Corrosion of Mild and Medium Carbon Steels	J. E. O. Ovri, Okeahialam, S. I., And Onyemaobi O. O.	jimvri@yahoo.com	243

31.	Synthesis of Nanoporous Silica Membrane from Corn Hob Ash (Zea mays) by Sol-gel Method	OGUNFOWOKAN. A.O., Ezenwafor. T. C and Imosili. P	marrisconso@yahoo.com	337
32.	Magnetic And Optical Properties Of Nano-Crystalline Chemical Bath Deposition Metal-Sulphide And Metal-Oxide Thin Films	Oluyamo S.S., Ogunjo S.T., Oluwasusi, F.F.	ogunjosam@yahoo.com	
33.	Production Of Bamboo-Lam From Flat Bamboo Strip Prepared From *Bambusa Vulgaris* Schrad	Adewole A. N.[1] And Olayiwola H. O.[2]	dabukyo@yahoo.com, an.adewole@mail.ui.edu.ng	346
34.	Comparative Study Of Thevetia Peruviana And Jatropha Curcas Seed Oils As Feedstock For Grease Production	[1]Olisakwe, H.C.,* [2]Tuleun, L.T., [3] Eloka-Eboka, A.C.	fatherfounder@yahoo.com	351
35.	Effects of Eggshell on the Microstructures and Properties of Al-Cu-Mg/Eggshell Particulate Composites	Hassan .S. B and Aigbodion.V.S	hassbolaji@yahoo.com, aigbodionv@yahoo.com	355
36.	Effect Of Fibre Extraction And Chemical Treatment On The Tensile Properties Of Sisal Fibre Reinforced Polypropylene Composites	Oladele I.O [1,3], Omotoyinbo J.A [1,3]., Adewuyi B.O [1,3]., Adewara J.O.T [1,3.], And Kavishe F. P.L. [2,3]	wolesuccess2000@yahoo.com	362
37.	Model For Analysis And Prediction Of Ethanol Production Based On Treatment Temperature And Microbial Growth During Biodegradation Of Sugar Cane Molasses	C. I. Nwoye*[1], J. U. Odo[1], B. C. Chukwudi[2] And C. N. Mbah[3]	chikeyn@yahoo.com	372
38.	Virtual Reality As A Tool For Reducing Road Design/Construction Cost	Laseinde, O. T, Adejuyigbe, S.B. And Ismaila S.O.	famefresh@gmail.com	379
39.	Application Of Virtual Reality (VR) For The Production Of Spur Gears	Laseinde, O. T And Adejuyigbe, S.B.	famefresh@gmail.com	384
40.	Application of Optimization and Mathematical Modeling to Research & Industrial Formulation	Idowu G. O. And Okorie N. N.	gabrielolufemiidowu@yahoo.com	389
41.	Model For Evaluation And Assessment Of Energy Transmissivity By Solar Collector Based On The Reflectivities Of Beam And Diffused Components Of Radiation	*C. I. Nwoye[1], U. C. Nwoye[2], And J. U. Odo[1].	chikeyn@yahoo.com	396
42.	Biodegradable Metals For Biomedical Applications: A Paradigm Shift In Metallic Biomaterials.	[A]C.S. Obayi, [B]B.A. Okorie, [C]d.O.N. Obikwelu, [D]r.E. Njoku, [E]diego Mantovani.	camillus.obayi@unn.edu.ng	403
43.	Powder Metallurgy; An Alternative Process Route For Duplex Stainless Steel Nanocomposite – Review	Olaniran O.S.[A & B], Olubambi P.A[a & B]. Adewuyi B.O.[B] And Oladele I.O.[B]	dayo525@yahoo.com tayo_adewuyi@yahoo.com	410
44.	Hardening And Corrosion Behaviour Of Copper Added Sus 304h AUSTenitic Steels Subjected To Thermal Cycling	Kenneth Kanayo Alaneme[1, 2]*, Upadrasta Ramamurty[2], Olanrewaju Bello[1]	kalanemek@yahoo.co.uk	
45.	Mechanical Behaviour Of Cold Deformed And Solution Heat-Treated Alumina Reinforced AA 6063 Metal Matrix Composites	Kenneth Kanayo Alaneme*	kalanemek@yahoo.co.uk	414
46.	Adsorption Of Cadmium Ions On Kankara Kaolin	Edomwonyi-Otu L.C*, Alonge J. K, Ajiboye O.O, Bawa, G. S	osas1law@yahoo.com, lcotu@abu.edu.ng	321

47.	Evaluation Of The Compressive Strength Of Hybrid Clay Bricks	* O. Azeez, *1 O. Ogundare, * T.E. Oshodin, O.A. Olasupo, And *B.A. Olunlade	*suppiedee@yahoo.com*	426
48.	Studies On The Five (5) Selected Clays In Abeokuta, Nigeria	[1]Aiyedun, P.O, [2]olokode, O.S, [3]Oyeleke Y.T. [4]lee, W.E, Anyanwu, B.E	engr_olokode@yahoo.com	429
49.	Alternative Production Of Xylaneses Using Sawdust And Different Local Digestive Bran As Substrates	M.I. Alibe, A.S. Magaji, A.M. Sule, B.Inuwa, G. Mohammed, I. A. Suleiman, I. Khalid, M.H. Aliyu	ibrahim_mstpha@yahoo.com.com	435
50.	Production And Utilization Of Ceramic Glaze From Locally Sourced Materials Of Nigerian Origin	[1]Eloka-Eboka, A.C.,* [2]Ajiwe, V.I.E, [3]Oshuoha, I.C.	fatherfounder@yahoo.com	439
51.	Effect Of Volume Ratio On The Tensile Properties Of Rice Husk Flour (RHF) Polyester Composite	Imoisili P. E, Olunlade B. A.,*Tomori W. B.	patrickehis2002@yahoo.com	443
52.	Production Of Alumina In The Aluminum Silicate And Refractory Shop Of The Ajaokuta Steel Company Limited	Ocheri C.[1], Oyelaran O.A[2] & Barnabas A.[3] Agboola, J.B.[4] Aji Daniel [5]	ocheri4c@yahoo.com	446
53.	Characterization Of Solid Waste In Nigeria: Akure Metropolis As A Case Study	O. P. Fapetu, T. I. Ogedengbe* And O. T. Ajayi	tioged@yahoo.com	449
54.	Fate Of Nanoparticles In The Environment	Akpotu, S.O. And Oketola, A.A.	soulmanlegendry@yahoo.com	454
55.	Gold Nanoparticles: A Review	[1,2]ogundare, O., [2]adeoye, M.O., [2, 3]adetunji, A.R., And *Adewoye, O.O.	*suppiedee@yahoo.com*	459
56.	Synthesis And Characterization Of Chemical Bath Deposited $BaTiO_3$ Mixed Oxide Thin Films On Seeded TiO_2	F. I. Ezema[1a], B. A. Ezekoye[1], P. O. Ike[1],A. B. C. Ekwealor[1]	fiezema@yahoo.com	465
57.	Characterization Of Sol-Gel Deposited Barium Stannate Films And Powder	Odo V. C.1, Amaechi C. I.1, Asogwa P. U.1, Ezema F. I.1, And Osuji R. U.1,2	ifeanyichukwuonline@yahoo.com	472
58.	Decolourization And Degradation Of Textile Wastewater Using Tio_2 Nanoparticles	A. Giwa*, P.O. Nkeonye, K.A. Bello, E.G. Kolawole	agiwa@abu.edu.ng	478
59.	Effects Of Some Hexose Sugars On The Retrogradation And Stability To Sunlight And Heat Of Maize (*Zea Mays*) And Wheat(*Triticun Aestivum*) Starches	[1]*Abba, H., [2]Adamu, I. K., [3]Kogo, A.A. And [2]Bello, H.	hamzaabbah@yahoo.com	483
60.	Modifying Meionite Silicate For Effective Removal Of Organic Contaminants From Solutions	Ikhuoria E.U And Enivwenae B.Ovie	ikhuoria@uniben.edu.ng	487

61.	Mechanical Behaviour Of Cold Deformed And Solution Heat-Treated Alumina Reinforced AA 6063 Metal Matrix Composites	Kenneth Kanayo Alaneme*	kalanemek@yahoo.co.uk	414
62.	Adsorption Of Cadmium Ions On Kankara Kaolin	Edomwonyi-Otu L.C*, Alonge J. K, Ajiboye O.O, Bawa, G. S	osas1law@yahoo.com, lcotu@abu.edu.ng	421
63.	Evaluation Of The Compressive Strength Of Hybrid Clay Bricks	* O. Azeez, *1 O. Ogundare, * T.E. Oshodin, O.A. Olasupo, And *B.A. Olunlade	*suppiedee@yahoo.com*	426
64.	Studies On The Five (5) Selected Clays In Abeokuta, Nigeria	[1]Aiyedun, P.O, [2]olokode, O.S, [3]Oyeleke Y.T. [4]Iee, W.E, Anyanwu, B.E	engr_olokode@yahoo.com	429
65.	Alternative Production Of Xylaneses Using Sawdust And Different Local Digestive Bran As Substrates	M.I. Alibe, A.S. Magaji, A.M. Sule, B.Inuwa, G. Mohammed, I. A. Suleiman, I. Khalid, M.H. Aliyu	ibrahim_mstpha@yahoo.com.com	435
66.	Production And Utilization Of Ceramic Glaze From Locally Sourced Materials Of Nigerian Origin	[1]Eloka-Eboka, A.C.,* [2]Ajiwe, V.I.E, [3]Oshuoha, I.C.	fatherfounder@yahoo.com	439
67.	Effect Of Volume Ratio On The Tensile Properties Of Rice Husk Flour (RHF) Polyester Composite	Imoisili P. E, Olunlade B. A.,*Tomori W. B.	patrickehis2002@yahoo.com	443
68.	Production Of Alumina In The Aluminum Silicate And Refractory Shop Of The Ajaokuta Steel Company Limited	Ocheri C.[1], Oyelaran O.A[2] & Barnabas A.[3] Agboola, J.B.[4] Aji Daniel [5]	ocheri4c@yahoo.com	446
69.	Characterization Of Solid Waste In Nigeria: Akure Metropolis As A Case Study	O. P. Fapetu, T. I. Ogedengbe* And O. T. Ajayi	tioged@yahoo.com	449
70.	Fate Of Nanoparticles In The Environment	Akpotu, S.O. And Oketola, A.A.	soulmanlegendry@yahoo.com	454
71.	Gold Nanoparticles: A Review	[1,2]ogundare, O., [2]adeoye, M.O., [2, 3]adetunji, A.R., And *Adewoye, O.O.	*suppiedee@yahoo.com*	459
72.	Synthesis And Characterization Of Chemical Bath Deposited $BaTiO_3$ Mixed Oxide Thin Films On Seeded TiO_2	F. I. Ezema[1a], B. A. Ezekoye[1], P. O. Ike[1],A. B. C. Ekwealor[1]	fiezema@yahoo.com	465
73.	Characterization Of Sol-Gel Deposited Barium Stannate Films And Powder	Odo V. C.1, Amaechi C. I.1, Asogwa P. U.1, Ezema F. I.1, And Osuji R. U.1,2	ifeanyichukwuonline@yahoo.com	472
74.	Decolourization And Degradation Of Textile Wastewater Using Tio_2 Nanoparticles	A. Giwa*, P.O. Nkeonye, K.A. Bello, E.G. Kolawole	agiwa@abu.edu.ng	478
75.	Effects Of Some Hexose Sugars On The Retrogradation And Stability To Sunlight And Heat Of Maize (*Zea Mays*) And Wheat(*Triticun*	[1]*Abba, H., [2]Adamu, I. K., [3]Kogo, A.A. And [2]Bello, H.	hamzaabbah@yahoo.com	483
76.	Modifying Meionite Silicate For Effective Removal Of Organic Contaminants From Solutions	Ikhuoria E.U And Enivwenae B.Ovie	ikhuoria@uniben.edu.ng	487

NIMACON 2010 CONFERENCE ATTENDANCE

	NAME		AFFILIATION
1	Abba	H.	ABU, Zaria
2	Abia-Bassey	Nathan	PRODA Enugu
3	Adegoke	Haleemat I.	UNILORIN
4	Adeluju	Kelvin A.	UNIADO, Ado-Ekiti
5	Adeoye	Abiodun E.	EMDI Akure
6	Adesakin	A.O.	EMDI Akure
7	Aduloju	K.A.	UNAD, Ado-Ekiti
8	Agbadua	Segun A.	NEDDI, Nnewi
9	Agboola	J.B.	FUT, Minna
10	Aiyedun	Peter O.	UNAAB, Abeokuta
11	Ajao	John A.	CERD, OAU, Ile-Ife
12	Ajenifuja	Emmanuel	CERD, OAU, Ile-Ife
13	Akinluwade	Kunle J.	PEDI Ilesha
14	Alayande	Oluwagbemiga S.	CERD, OAU, Ile-Ife
15	Alo	Ayotunde O.	OAU, Ile-Ife
16	Amaechi	Chinedu I.	UNN
17	Asogwa	Paul U.	UNN
18	Attah	Daniel B.	EMDI Akure
19	Ayinde	Wasiu B.	UNAAB, Abeokuta/PEDI
20	Baba	Alafara A.	UNILORIN
21	Bello	Afeez A.	OSU, Oshogbo
22	Borokini	Adebowale S.	OAU, Ile-Ife
23	Boyo	Adenike	LASU, Ojo
24	Daniyan	A.A.	EMDI Akure
25	Dauda	Benjamin	ABU, Zaria
26	Ebisike	Kelechi	EMDI Akure
27	Eze	Ifeanyi S.	UNN
28	Ezeaba	Chioma O.	NAU, Awka
29	Ezekoye	B.A.	UNN
30	Ezema	Fabian I.	UNN
31	Fagbulu	Adebayo A.	EMDI Akure
32	Fasasi	Niyi Y.	CERD, OAU, Ile-Ife
33	Giwa	Abdulraheem	ABU, Zaria
34	Hassan	S.B.	ABU, Zaria
35	Ibeagha	Doris C.	PRODA Enugu
36	Ibrahim	Balarabe M.	CHELTEC, Zaria
37	Idenyi	Ndubuisi E.	EBSU Abakaliki
38	Idowu	A.S.	EMDI Akure
39	Ijimdiya	T.S.	ABU, Zaria
40	Ikhuoria	Esther U.	UNIBEN
41	Imasogie	Benjamin I.	OAU, Ile-Ife
42	Imosili	Patrick E.	EMDI Akure
43	Isikaku-Ironkwe	Paul O.	MOUA, Umidike
44	Ita	Israel A.	SEDI Enugu
45	Kollere	A.S.	RMRDC, Abuja
46	Latif	Bakary M.	CERD, OAU, Ile-Ife
47	Marut	Ayuba J.	CHELTEC, Zaria
48	Nebo	Chinedu O.	UNN

49	Njoku	Christian C.	PRODA Enugu
50	Nkeonye	Peter O.	ABU, Zaria
51	Nnadi	Augustine C.	SEDI Enugu
52	Nnamani	P.O.	UNN
53	Nnodi	Linda	SEDI Enugu
54	Nnoruka	Josephine N.	PRODA Enugu
55	Nnuka	E.E.	NAU, Awka
56	Nwobodo	Gloria U.	NAU, Awka
57	Obele	C.M.	NAU, Awka
60	Oboh	Johnson	CHELTEC, Zaria
61	Ocheri	Cyril	Ajaokuta Steel Coy.
62	Ochu	Sumaila A.	PRODA Enugu
63	Odo	Jerome U.	NAU, Awka
64	Odoemelam	Chidiebere	ESUT, Enugu
65	Ogbodo	Joy N.	SEDI Enugu
66	Ogundare	O.	EMDI Akure
67	Ogunkoya	Adetunji K.	EMDI Akure
68	Ogunmola	Enoch D.	EMDI Akure
69	Oji	John O.	PEDI Ilesha
70	Okafor	Wilson C.	ANSU, Uli
71	Okieimen	Felix E.	UNIBEN
72	Okorie	Ngozi N.	EMDI Akure
73	Okorie	Boniface A.	UNN
74	Olabode	Victor O.	CHELTEC, Zaria
75	Olaniran	Oladayo	FUTA
76	Olorunnisola	Abel O.	UNIBADAN
77	Olunlade	B.O.	SEDI Enugu
78	Onwughalu	Chiagozi C.	NAU, Awka
79	Osuji	Rose U.	UNN
80	Ottih	Ifeyinwa E.	ANSU, Uli
81	Oyegunwa	Olufemi	EMDI Akure
82	Oyelami	Adekunle T.	EMDI Akure
83	Ozoeemena	Kenneth	CSIR, South Africa
84	Pelemo	David A.	CERD, OAU, Ile-Ife
85	Petirin	Moses O.	PEDI Ilesha
86	Putshak'a	Julius D.	CHELTEC, Zaria
87	Sanda	Olayinka	CERD, OAU, Ile-Ife
88	Shitta	Mohamed B.O.	UNAD, Ado-Ekiti
89	Taiwo	Adeyinka T.	PEDI Ilesha
90	Udeinya	Thaddeus C.	PRODA Enugu
91	Udoh	Matthew E.	SEDI Enugu
92	Ufomba	Emmanuel C.	SEDI Enugu
93	Ugwunali	B.I.	SEDI Enugu
94	Ugwuoke	Cletus N.	SEDI Enugu
95	Ukoba	Kingsley O.	EMDI Akure

NIMACON 2011 LIST OF PARTICIPANTS

S/N	TITLE	NAME	INSTITUTE
1.	MRS.	A. AKINSELOYIN	ENGINEERING MATERIALS DEVELOPMENT INSTITUTE, AKURE
2.	MR.	A. AKOREDELE	AHMADU BELLO UNIVERSITY, ZARIA
3.	MR.	A. B. AYENI	UNIVERSITY ILORIN
4.	MR.	A. C. ELOKA- EBOKA	UNIVERSITY OF AGRICULTURE, MAKURDI
5.	DR.	A. GIWA	AHMADU BELLO UNIVERSITY, ZARIA
6.	ENGR.	A. I. USMAN	ENGINEERING MATERIALS DEVELOPMENT INSTITUTE, AKURE
7.	MR.	A. O. ADESAKIN	ENGINEERING MATERIALS DEVELOPMENT INSTITUTE, AKURE
8.	DR.	A. O. AJAGUNNA	F FEDERAL UNIVERSITY OF TECHNOLOGY, AKURE
9.	MR.	A. O. ALADEJEBI	FEDERAL UNIVERSITY OF TECHNOLOGY, AKURE
10.	PROF.	A. O. OLORUNSOLA	UNIVERSITY OF IBADAN
11.	MR.	A. OLUWAGBEMIGA	CERD, OBAFEMI AWOLOWO UNIVERSITY ILE-IFE
12.	ENGR.	A. S. IDOWU	ENGINEERING MATERIALS DEVELOPMENT INSTITUTE, AKURE
13.	ENGR.	A.K. OGUNKOYA	ENGINEERING MATERIALS DEVELOPMENT INSTITUTE, AKURE
14.	DR.	A.R. ADETUNJI	PROTOTYPE ENGINEERING DEVELOPMENT INSTITUTE, ILESHA
15.	MR.	ABIODUN LIADI	PROTOTYPE ENGINEERING DEVELOPMENT INSTITUTE, ILESHA
16.	MR.	ADEBAYO A. FASHINA	AFRICAN UNIVERSITY OF SCIENCE AND TECHNOLOGY, ABUJA
17.	DR.	ADEDAPO N. ADEWOLE	UNIVERSITY OF IBADAN
18.	MR.	ADEGBOLA ADEKUNLE AMOS	THE POLYTECHNIC, IBADAN
19.	PROF.	ADEJUYIGBE S.B.	UNIVERSITY OF AGRICULTURE, ABEOKUTA
20.	ENGR.	ADEKUNLE T. OYELAMI	ENGINEERING MATERIALS DEVELOPMENT INSTITUTE, AKURE
21.	DR.	ADENIYI FASASI	CERD, OBAFEMI AWOLOWO UNIVERSITY ILE-IFE
22.	MR.	ADESINA A.J.	YABA COLLEGE OF TECHNOLOGY, YABA LAGOS
23.	MR.	ADEYINKA T. TAIWO	PROTOTYPE ENGINEERING DEVELOPMENT INSTITUTE, ILESHA
24.	MR.	AJAYI MOMOH J.YAKUBU	PROTOTYPE ENGINEERING DEVELOPMENT INSTITUTE, ILESHA
25.	MR.	AKINRIBIDE O.J.	ENGINEERING MATERIALS DEVELOPMENT INSTITUTE, AKURE
26.	MR.	AYODELE DANIYAN	ENGINEERING MATERIALS DEVELOPMENT INSTITUTE, AKURE
27.	PROF.	B. A. OKORIE	UNIVERSITY OF NIGERIA NSUKKA
28.	MR.	B. E. ATTAHDANIEL	ENGINEERING MATERIALS DEVELOPMENT INSTITUTE, AKURE

29.	PROF.	B. I. IMASOGIE	OBAFEMI AWOLOWO UNIVERISTY, ILE -IFE
30.	MR.	B. K. AHMED NASIR	UNIVERSITY OF ABUJA
31.	PROF.	B. O. ADEWUYI	FEDERAL UNIVERSITY OF TECHNOLOGY, AKURE
32.	MR.	B. O. ONIPEDE	PROTOTYPE ENGINEERING DEVELOPMENT INSTITUTE, ILESHA
33.	DR.	BOLA ELERUJA	OBAFEMI AWOLOWO UNIVERISTY, ILE -IFE
34.	DR. (MRS)	BOYO	LAGOS STATE UNINVERSITY
35.	PROF.	C. E. ADEEYINWO	THE FEDERAL UNIVERSITY OF TECHNOLOGY, AKURE
36.	MR.	C. OGBUNAOFOR	ENUGU STATE UNIVERSITY OF SCIENCE AND TECHNLOGY, ENUGU
37.	MR.	C. S.OBAYI	UNIVERSITY OF NIGERIA NSUKKA
38.	MR	CHARLES A. IKUTEGBE	PROTOTYPE ENGINEERING DEVELOPMENT INSTITUTE, ILESHA
39.	DR.	CHUKWUKA I. NWOYE	NNAMDI AZIKWE UNIVERSITY, AWKA
40.	PROF.	D.A. PELEMO	OBAFEMI AWOLOWO UNIVERISTY, ILE -IFE
41.	MR.	DALYOP DABORO ILIYA	ENGINEERING MATERIALS DEVELOPMENT INSTITUTE, AKURE
42.	MR.	DAMILOLA MOMODU	AFRICAN UNIVERSITY OF SCIENCE AND TECHNOLOGY, ABUJA
43.	MS	DEBORAH O. OLALEKAN	SHESTCO, ABUJA
44.	MR.	EKEBAFE LAURENCE	AUCHI POLYTECHNIC, EDO STATE
45.	MR.	EMMANUEL AJENIFUJA	CERD, OBAFEMI AWOLOWO UNIVERSITY ILE-IFE
46.	MR.	EMMANUEL FEMI OLU	INDIAN INSTITUTE OF SCIENCE, BANGALORE, INDIA
47.	MR.	EMMANUEL O. VODAH	AFRICAN UNIVERSITY OF SCIENCE AND TECHNOLOGY, ABUJA
48.	MR.	ENIVWENAE OVIE BENEDICT	DELTA STATE SCHOOL OF MARINE TECHNOLOGY, BURUTU DELTA STATE
49.	MISS	EZENWANFOR T.C.	ENGINEERING MATERIALS DEVELOPMENT INSTITUTE, AKURE
50.	MR.	FEMI O. OMOLE	PROTOTYPE ENGINEERING DEVELOPMENT INSTITUTE, ILESHA
51.	MISS	FUNLOLA AKIODE	NIGERIAN COMMUNICATIONS COMMISSION
52.	MR.	HAMMED T. O.	ENGINEERING MATERIALS DEVELOPMENT INSTITUTE, AKURE
53.	DR.	HAMZA ABBA	AHMADU BELLO UNIVERSITY, ZARIA
54.	MR.	HASAN O. BAKARE	NATIONAL AGENCY FOR SCIENCE & ENGR. INFRASTRUCTURE, ABUJA
55.	MR.	HASSAN O. BAKARE	NATIONAL AGENCY FOR SCIENCE & ENGR. INFRASTRUCTURE, ABUJA
56.	MR.	I. C. AMAECHI	UNIVERSITY OF NIGERIA NSUKKA

NIMACON 2011 LIST OF PARTICIPANTS

57.	DR.	I. O. OGUNIYI	FEDERAL UNIVERSITY OF TECHNOLOGY, AKURE
58.	ENGR.	I. O. OLAKUNLE	FEDERAL UNIVERSITY OF TECHNOLOGY, AKURE
59.	DR.	I. OGEDENGBE	FEDERAL UNIVERSITY OF TECHNOLOGY, AKURE
60.	DR.	IDENYI N. E.	EBONYI STATE UNIVERSITY, ABAKALIKI
61.	MR.	IFEANYI O. AMAECHINA	YABA COLLEGE OF TECHNOLOGY, YABA LAGOS
62.	MR.	IKE PATRICK OKEZIE	UNIVERSITY OF NIGERIA NSUKKA
63.	MR.	IORKYAA AHEMEN	UNIVERSITY OF AGRICULTURE, MAKURDI
64.	MR.	ISAAC JOHN ORAH	FEDERAL COLLEGE OF EDUCATION, GOMBE
65.	MR.	ITOPA MONDAY MOMOH	ENGINEERING MATERIALS DEVELOPMENT INSTITUTE, AKURE
66.	MR.	IYIPORO DANYUO	AFRICAN UNIVERSITY OF SCIENCE AND TECHNOLOGY, ABUJA
67.	MR	J. A.OLOWONUBI	ENGINEERING MATERIALS DEVELOPMENT INSTITUTE, AKURE
68.	ENGR.	J. O. ALASOLUYI	ENGINEERING MATERIALS DEVELOPMENT INSTITUTE, AKURE
69.	DR.	J. O. T. ADEWARA	FEDERAL UNIVERSITY OF TECHNOLOGY, AKURE
70.	PROF.	J. O.BORODE	FEDERAL UNIVERSITY OF TECHNOLOGY, AKURE
71.	ENGR.	J.U. ODO	NNAMDI AZIKWE UNIVERSITY, AWKA
72.	DR.	JAMES E.O. OVRI	FEDERAL UNIVERSITY OF TECHNOLOGY OWERRI
73.	DR.	JOHN ADEGBINDIN AJAO	CERD, OBAFEMI AWOLOWO UNIVERSITY ILE-IFE
74.	MR.	JOHN DAVID OBADEYI	AFRICAN UNIVERSITY OF SCIENCE AND TECHNOLOGY, ABUJA
75.	DR.	JOHNSON AGUNSOYE	UNIVERSITY OF LAGOS
76.	MR.	JOSEPH ASARE	AFRICAN UNIVERSITY OF SCIENCE AND TECHNOLOGY, ABUJA
77.	MISS	K. T. OGUNDELE	CERD, OBAFEMI AWOLOWO UNIVERSITY, ILE -IFE
78.	MR.	KELECHI EBISIKE	ENGINEERING MATERIALS DEVELOPMENT INSTITUTE, AKURE
79.	MR.	KENNETH K. ADAMA	SHESTCO, ABUJA
80.	MR.	KINGSLEY K. AJEKWENE	YABA COLLEGE OF TECHNOLOGY, YABA LAGOS
81.	MR	KINGSLEY O.UKOBA	ENGINEERING MATERIALS DEVELOPMENT INSTITUTE, AKURE
82.	MR.	KUNLE J. AKINLUWADE	PROTOTYPE ENGINEERING DEVELOPMENT INSTITUTE, ILESHA
83.	MR.	M. I. ALIBE	NATIONAL RESEARCH INSTITUTE FOR CHEMICAL TECHNOLOGY, ZARIA
84.	ENGR.	M. O.PETINRIN	PROTOTYPE ENGINEERING DEVELOPMENT INSTITUTE, ILESHA
85.	MRS.	M. U.OKHUAROBO	YABA COLLEGE OF TECHNOLOGY, YABA LAGOS
86.	DR.	M.B.O. SHITTA	EKITI STATE UNIVERSITY, ADO EKITI
87.	DR.	M.T. ISA	AHMADU BELLO UNIVERSITY, ZARIA

88.	MR.	OCHERI C.	AJAOKUTA STEEL COMPANY LIMITED, AJAOKUTA, KOGI STATE
89.	MR.	OGAR MARK OGAR	PROTOTYPE ENGINEERING DEVELOPMENT INSTITUTE, ILESHA
90.	MR.	OJI JOHN	PROTOTYPE ENGINEERING DEVELOPMENT INSTITUTE, ILESHA
91.	ENGR.	OLADAYO AZEEZ	ENGINEERING MATERIALS DEVELOPMENT INSTITUTE, AKURE
92.	ENGR.	OLAGOKE O. AJAYI	NATIONAL AGENCY FOR SCIENCE & ENGR. INFRASTRUCTURE, ABUJA
93.	MR.	OLAKUNLE KAYODE	OSUN STATE UNIVERSITY, OSOGBO
94.	MR.	OLANIYI GLADIUS BABATUNDE	ENGINEERING MATERIALS DEVELOPMENT INSTITUTE, AKURE
95.	MR.	OLAYINKA SANDA	CERD, OBAFEMI AWOLOWO UNIVERSITY ILE-IFE
96.	ENGR.	OLAYODE A. OLASUPO	NATIONAL AGENCY FOR SCIENCE & ENGR. INFRASTRUCTURE, ABUJA
97.	MR.	OLUFEMI KOMOLAFE	ENGINEERING MATERIALS DEVELOPMENT INSTITUTE, AKURE
98.	MR.	OLUSEGUN A. ODEJOBI	PROTOTYPE ENGINEERING DEVELOPMENT INSTITUTE, ILESHA
99.	DR.	OLUSOLA S. ODUSANYA	SHESTCO, ABUJA
100.	MR.	OLUWASEUN OYEWOLE	AFRICAN UNIVERSITY OF SCIENCE AND TECHNOLOGY, ABUJA
101.	MR.	OMAR AROKE AMINU	AHMADU BELLO UNIVERSITY, ZARIA
102	MISS	OMOYEME OBERAIFO	AFRICAN UNIVERSITY OF SCIENCE AND TECHNOLOGY, ABUJA
103.	ENGR.	OPEYEOLU TIMOTHY LASEINDE	FEDRAL UNIVERSITY OF AGRIC, ABEOKUTA
104.	MR.	OSAGIE JOLLY AIGBOGUN	ENGINEERING MATERIALS DEVELOPMENT INSTITUTE, AKURE
105.	PROF.	OSINKOLU	CERD, OBAFEMI AWOLOWO UNIVERSITY ILE-IFE
106.	DR.	P. I. CHUKWU	ANAMBRA STATE UNIVERSITY ULI, ANAMBRA STATE
107.	PROF.	P. NKEONYE	AHMADU BELLO UNIVERSITY, ZARIA
108.	PROF.	P. O. AIYEDUN	U. I. / UNAAB
109.	MR.	P.E. IMOSILI	ENGINEERING MATERIALS DEVELOPMENT INSTITUTE, AKURE
110.	MR.	R. SAADU	UNIVERSITY OF ABUJA
111.	ENGR.	RAFIU OGUNYEMI	NATIONAL AGENCY FOR SCIENCE & ENGR. INFRASTRUCTURE, ABUJA
112.	MR.	RAFIU OGUNYEMI	NATIONAL AGENCY FOR SCIENCE & ENGR. INFRASTRUCTURE, ABUJA
113.	PROF.	S. A. THOMAS	SHESTCO, ABUJA

114.	PROF.	S. B. HASSAN	AHMADU BELLO UNIVERSITY, ZARIA
115.	ENGR.	S. O. O. OLUSUNLE	NATIONAL AGENCY FOR SCIENCE & ENGR. INFRASTRUCTURE, ABUJA
116.	MR.	SALIFU TAHIRU AZEKO	AFRICAN UNIVERSITY OF SCIENCE AND TECHNOLOGY, ABUJA
117.	MR.	SHAWN HENRY ENEJE	UNIVERSITY OF NIGERIA NSUKKA
118.	MR.	SHIGA ABIGAIL YUSUF	AHMADU BELLO UNIVERSITY, ZARIA
119.	ENGR.	SMART A. OLUBAYODE	ENGINEERING MATERIALS DEVELOPMENT INSTITUTE, AKURE
120.	MR.	SOLOMON GAJERE BAWA	AHMADU BELLO UNIVERSITY, ZARIA
121.	DR.	T. O. AHMED	AHMADU BELLO UNIVERSITY, ZARIA
122.	DR. (MRS)	T. U. ONUEGBU	NNAMDI AZIKWE UNIVERSITY, AWKA
123.	ENGR. (MRS)	T.E. OSHODIN	ENGINEERING MATERIALS DEVELOPMENT INSTITUTE, AKURE
124.	ENGR.	TAIBAT . O. ADEKUNLE	ENGINEERING MATERIALS DEVELOPMENT INSTITUTE, AKURE
125.	MRS.	TAIWO ADENIKE ONI	ENGINEERING MATERIALS DEVELOPMENT INSTITUTE, AKURE
126.	MR.	TANIMOWO OLUWASEYI ALIU	PROTOTYPE ENGINEERING DEVELOPMENT INSTITUTE, ILESHA
127.	MR.	THOMAS IMALERIO	SHESTCO, ABUJA
128.	MR.	TIMOTHY SUNDAY AIYEEIAN	KOGI STATE POLYTECHNIC, LOKOJA
129	MR.	TOLULOPE IDOWU ADEJUGBE	ENGINEERING MATERIALS DEVELOPMENT INSTITUTE, AKURE
130.	PROF	TUNDE OJUMU	CAPE PENINSULA UNIVERSITY OF TECH., CAPE TOWN, SOUTH AFRICA
131	MR.	VICTOR K. ODEYEMI	# 3 KAYOSOLA CLOSE IJAPO ESTATE, AKURE
132.	MR.	VITALIS CHIOH ANYE	AFRICAN UNIVERSITY OF SCIENCE AND TECHNOLOGY, ABUJA
133.	MR.	WASIU AJIBOLA OLADOSUN	NATIONAL AGENCY FOR SCIENCE & ENGR. INFRASTRUCTURE, ABUJA
134.	MR.	YAQUB A. OMOFOYEWA	EKITI STATE UNIVERSITY, ADO EKITI
135.	MR.	ZAKARI ABDULLAHI	SHESTCO, ABUJA
136.	DR.	ZEBAZE KANA M. G.	SHESTCO, ABUJA

TRENDS IN THE CLEAN ENERGY TECHNOLOGIES PHENOMENON: DEVELOPMENTS IN THE POWER SECTOR AND THE CHALLENGES FOR MATERIALS ENGINEERS IN NIGERIA

A keynote address presented at the 9th Nigerian Materials Congress, Enugu, Enugu State, Nigeria on the 23rd of November 2010.

By, Professor Bart Nnaji, NNOM, CON.
Special Adviser to the President on Power and
Chairman Presidential Task force on Power (PTFP)
Presented on his behalf,
By Chike Madueke
Technical Adviser,
Presidential Task Force on Power, Abuja

Protocols

Distinguished Ladies and gentlemen,

You will recall that in the early days of his administration, the President and Commander in Chief of the Federal Republic of Nigeria, Dr. Goodluck Ebele Jonathan GCFR, established the Presidential Action Committee on Power (PACP) of which I am a member by virtue of my appointment as the Presidential Adviser. In the same vein, the Presidential Task Force on power (PTFP) was set up as the engine room to design and drive a reform roadmap of the power sector in the country. I also serve as the Chairman of this taskforce

In the course of our work, we have been able to study the existing systems, observed and the operations and practices of this very complex sector and have scientifically modeled a roadmap with which we commenced the drive towards the total reengineering and repositioning of the sector. This drive started in earnest since the past three months with the launching of the Roadmap on the 26th of August 2010 by the president.

The lessons from the uncensored realities that characterise the Nigerian power sector, albeit global developments has enabled me to put together some critical facts and challenging issues that are meant to stimulate vigorous discussions amongst participants as we examine the challenges facing materials scientists and engineers in Nigeria.

I therefore thank you for the opportunity this conference has provided me as I am very pleased and honoured to be here to share and compare notes with you, my fellow colleagues. I do hope that at the end of this week-long conference, we would all leave here better informed, fulfilled, better prepared and much more motivated to put in our best for our society and indeed our country Nigeria and for the betterment of mankind.

I shall therefore open up this address with an elementary introduction of this all-new, all-embracing but topical rave of the moment referred to as "Clean Technologies"

INTRODUCTION

Whilst there is no hard and fast definition for the term 'Clean Technology', we can describe it as the application of processes that differ from conventional methods and which aim towards the reduction of emissions and the reduction in the depletion of natural resources by processes of recycling or reuse or elimination and or improvement on the efficiencies of conventional technologies.

Clean Energy Technologies therefore refer to those processes applied in the energy sector for the reduction and elimination of generation and operation emissions and its impact on the environment. Clean Technologies are tending towards pushing these to zero position.

It is in this wise that I wish to include those technologies applied in the improvement of the inefficient energy generating systems that are geared towards the elimination of emission, and those aiming towards zero emission and improved fuel efficiency for the benefit of this discuss.

Against the backdrops of these descriptions therefore, I wish to firstly discuss the various conventional energy sources (which abound in Nigeria) for the production of electricity, the technological processes utilised to harness the said energy sources, the technological efforts, changes and developments in these fields as driven by the renewed searches for cleaner technology applications.

The challenges that face scientists and engineers in research and the actual retrofitting exercises in these fields are peculiar and as they concern materials scientists and engineers.

.

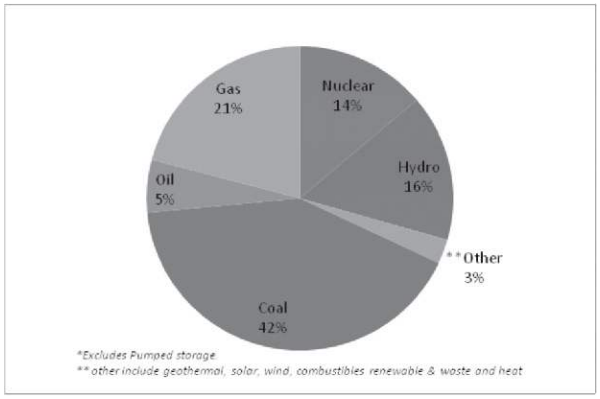
WORLD ENERGY MIX

In the generation of electricity, six principal fuel sources are prominent. These are Hydro, Coal, Gas, Oil, Nuclear and Others. Others refer mostly to geothermal and renewables or much of what can be termed to be "Clean Technologies Compliant". See Fig 1.

Amongst these six fuel sources, Coal, Oil and Gas are considered as “Not so Clean”. Whilst Hydro, Solar, Wind, Geothermal, are considered clean, Nuclear is facing a classification problem if the waste disposal issues are considered, so also is biomass

World Electricity by Energy Source. 2007

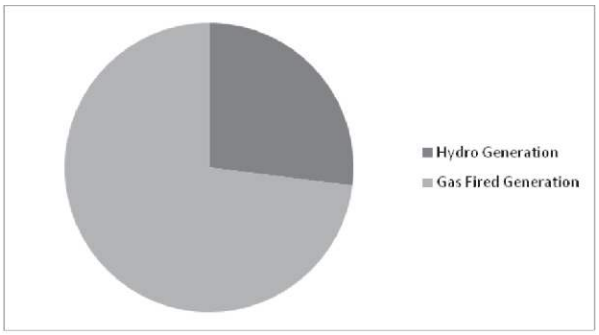
Fig 1.



In order to understand the processes of electricity extraction from the aforementioned energy sources, we shall broadly discuss the sources, the conventional processes for the production of electricity and the developments and progress made in recent times and or technologies being developed in the effort to advance towards zero Emission.

Fig 2.

Nigeria's Total Energy Mix by Source. -2010



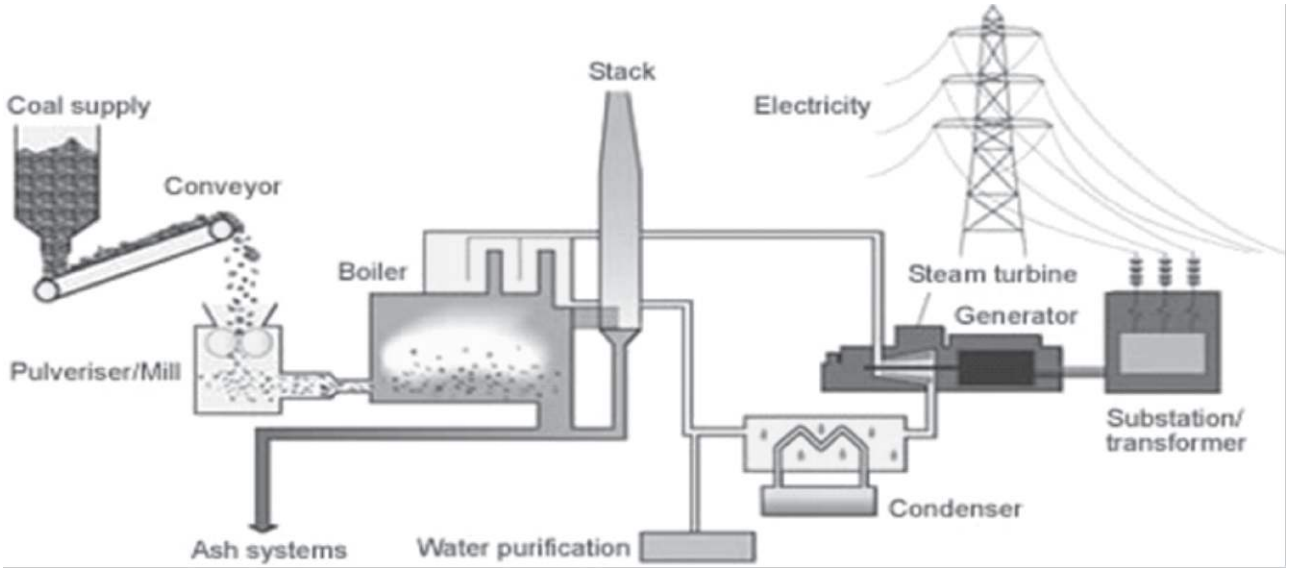


Fig 3. Pulverised Coal Conversion -PCC

This System of electricity has poor emission control and very inefficient in terms of energy conversion. It is generally referred as a 'dirty process'.

In response to the call for cleaner energies, newer technologies introduced the use of coal using the Coal Gasification System. This technology converts pulverized coal in the presence of Oxygen to form Synthetic gas, (Carbon monoxide and Hydrogen) fondly called "Syngas".

Whilst this syngas is used to fire the turbines the effluent heat is recovered and used to fire steam turbines also for the generation of electricity.

There is an improved fuel efficiency and reduced emission (about 20%) in combined configuration plants.

Newer technologies are even looking at the capture, solidification and storage of the emitted carbon in what is called Carbon Capture and Storage CCS. This is Clean Technology on the move and it is aiming towards zero emission.

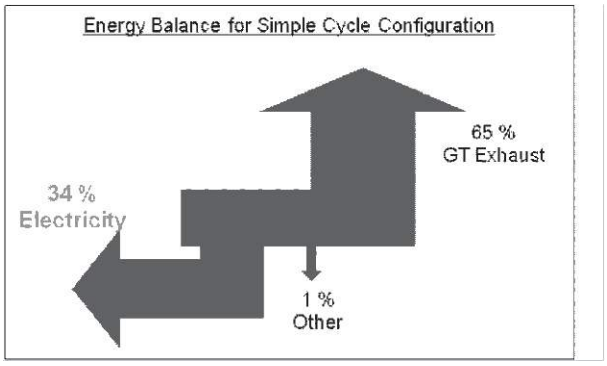
The combination of these processes is tending to what is now referred to as "Clean Coal" technology but currently this process is yet to be ratified by the countries subscribing to the Kyoto protocol.

Much as it is capital intensive, scientists and engineers cannot afford to rest on their oars now and in the near future until coal generation comes very clean and new plants are built using the new technologies and old plants promptly retrofitted to comply.

NATURAL GAS

In the generation of electricity, natural gas tends to be the cleanest fossil fuel in terms of carbon emission. In Nigeria, it accounts for the bulk of the generation capacity and indeed for future power investments.

Also referred to as thermal plant, it has a relatively low capital cost, short design to commission periods and as long as gas is available and equipment in good stead, it is able to produce power all year round. Fuel efficiency here is put at about 34% for single cycle



Plants

In the light of this and in the quest to achieve cleaner power generation systems, the combined cycle was introduced. Here gas is fired to turn the gas turbines and the resulting exhaust heat is harnessed to generate steam which in turn is utilised to power electricity in what is now referred to as Combine Cycle. Fuel efficiency here is generally about 50%. Lately though, Mitsubishi has announced that it recorded 59.1using their single shaft turbines.

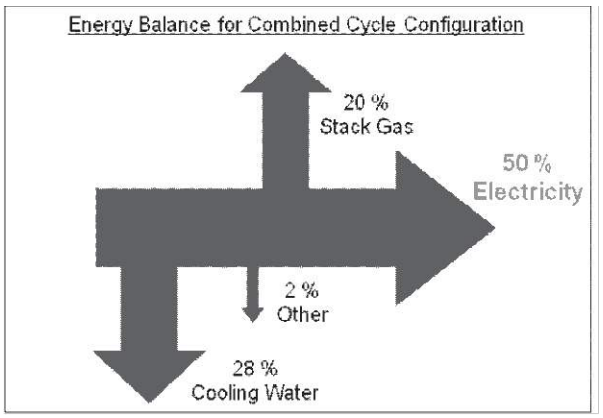


Fig 6. Reduced Emission

These achievements stem from the development of high temperature, high wear resistant materials as we continue to push towards zero emission. Note is also taken of the attendant high maintenance demand in terms of man and manpower and may in part explain the high breakdown rate of most Nigerian plants as in fig 8.

HYDRO

Readily the cheapest power plants to run, Hydro power production systems are capital intensive with long gestation periods. They are affected by the seasons and the structural requirement is intensive and the land requirement is immense. The ecological impact is as significant as the resources a well harnessed infrastructure can deliver.



Fig 7. Typical Hydro electric power dam

The use of gravity and heads to spin turbines makes it a most simple mechanism to operate. Emission is minimal but the demand on water is to say the least challenging.

The presence of dissolved ions, humidity and chemicals tend to increase corrosion rate of both immersed and partially immersed components and materials. In the quest for clean technologies and improved efficiencies, corrosion resistant materials must come to play.

The costs and environmental impacts of constructing a dam make traditional hydroelectric projects difficult to construct.

In the further search to improve on the efficiency of this hydro source, there has been the introduction of hydrokinetics, which harnesses tidal flows and requiring barely no physical infrastructures and tending towards a plug and play situation. Requiring no relocation of inhabitants hydro kinetics demands minimal footprint. It is often referred as "damless hydro".

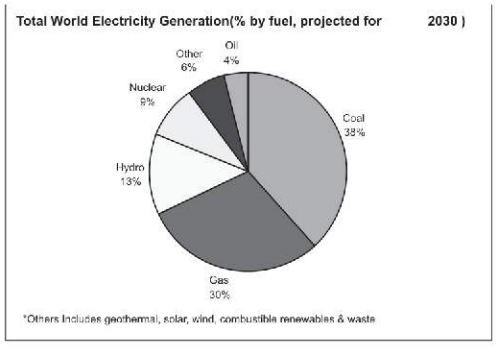
Hydrokinetics tends to have brought to bear solutions to negative ecological and environmental impact of hydro dams and damming on living organisms especially fishes and vegetation, There has also been cases of decayed vegetation resulting from rising waters. The decayed vegetation tend to form methane which is a far worse greenhouse gas than carbon dioxide

The choice, design and selection of materials for submerged hydrokinetic turbines, moving parts and controls is a subsisting challenge to Materials engineers if this new Clean Technological process will survive.

NUCLEAR ENERGY.

Nuclear Energy for electric power stems from a carefully controlled fission or fusion of nuclear particles using nuclear reactors.

It is a high-end technology and it is very capital intensive. It has long gestation and construction period and has limited room for plant shut down in a case of load reduction. It is often classified as clean technology but the nagging problem of the waste management tends to question this classification.



17 Source: World Coal Institute: Coal Fact, 2007

-Solar

The Sun's radiation can produce heat, generate electricity, or cause chemical reactions. That is Solar Energy. In modern times the harnessing of this energy and the translation from one form to the other, forms the core of studies and intellectual works in renewable energies or Clean Technologies.

Solar collectors collect solar radiation and transfer it as heat to a carrier fluid. It can then be used for heating. Solar cells convert solar radiation directly into electricity by means of the photovoltaic effect.

This form of energy is inexhaustible and has zero emission, but due to its inefficiency in the conversion of solar radiation to electricity and the high cost of producing a massive number of solar cells and panels, this energy source is yet to be a commercial success. The challenge in the production and design of readily affordable and optimized solar cells is still a tough one for materials engineers.

In Nigeria, this source of energy is abundant in Nigeria. It is currently being used for street lights for cities and remote areas. However the poor success rate in Nigeria still remains a challenge to the materials engineer.

-Wind

Wind Energy is a strong member of the renewable energy family. It has grown from the 0.5kW stand alone windmills of yester years to multi megawatt machines that can be laid out in multiples as is the case in wind farms. This has gained tremendous acceptance in the past five to ten years.

Despite recorded successes and roll outs, the challenges here for the materials engineer is still enormous.

For instance one of the biggest worries remains the reliability of gearboxes in wind turbines. A former chief wind turbine engineer at the National Renewable Energy Laboratory in Colorado was quoted as saying that the wind industry expects today's gearboxes to to last 7-10 years. This markedly contracts with the 20year design life time of wind turbines.

The implication for the industry is huge, since changing a gearbox is typical a lengthy and extremely costly exercise.

According to Jordi Puigcorbe and Alexis de-Beaumont in their article in Renewable Energy World magazine, May-June 2010 Volume 13 Number 3, the gear box's reputation for a high failure rate is linked to extreme engineering challenge that the gearbox technology faces in wind applications and the difficulty in properly assessing the loads –and in particular the non torsional loads that pass through the gearbox and how these affect

bearings and gears.
In combating this challenge, some manufacturers have chosen to move to direct drives in order to reduce the number of moving parts exposed to wear. This has come with extra challenges that are making the equipment manufacturer specific and lacking the amount of O &M concept of flexibility expected by customers.
The challenge therefore still remains for the materials engineer.

- Tidal.
Tidal energy sources and Waves are coming on strongly and as described earlier in the Hydro section, hydro kinematics is providing answers to the challenges of costly dams and environmental impacts of damming.
-Biomass Power Generation
This energy source though may exist in Nigeria for private captive generation is not part of the energy mix in the national grid.
In most countries where large scale agriculture is practiced, it is a majour sustainable source of power using wastes from Sugar, Palm Oil, Rice, Wood and other agro and allied processes.
Typical plants range from 5-15MW capacities. Even these too face pollution control issues and depletion of fuel supply.
As a measure towards clean technology, pollution control equipment such as Electrostatic Precipitators (ESPs), filters and multi cyclones are applied. Even these face loss in efficiency resulting in higher emissions to the environment

-Bio-Fuels
Input from agricultural products e.g cassava, sugarcane, maize, jathropha etc'
Can have a great multiplier effect on the Agricultural development of the country and result in increased food with application of adapted technology
Nevertheless, the abundance of crude in Nigeria has not made it very an interesting area of venture. In Brazil, the development is huge and the application versatile.
There are however several recorded private interests and investments in Nigeria in this respect

CHALLENGES, CHALLENGES
There are other exploits in geothermal energy sources, Combined Heat and Power, CHP, etc, but despite these exploits and the developments in renewables, Angela Neville of Power magazine of June 2010, decries the big limitation of renewable energy sources. She posits that they are available on an intermittent basis due to fluctuations in natural conditions. For example, the variable nature of wind generation poses special challenges to grid operators who must constantly balance the supply of and demand for electricity grid.
In facing these challenges, the new and emerging energy storage (ES) technologies are positioning towards the the development of renewable energy resources by increasing their efficiency and dependability in providing electrical energy to any nation's electric grid.
The attraction of bulk ES technologies is the ability to harness the power of renewable in such a way as to allow for the selective use of same when needed and not just when generated as is the situation now. These emerging technologies now functioning as :time machines" that allows this condition to be solved.
Examples of ES technologies include
Large –scale advanced electrochemical batteries which allows for the conversion of chemical reactions to store energy. The challenges of highly conductive materials and of slow eroding materials remain squarely on the shoulders of materials scientists and engineers. We are beginning to see some of them on our high streets.
Another example is the Pumped storage hydroelectric facilities which pumps water from lower to higher elevations during off-peak periods for release through turbines during peak periods. The design and choice of impeller materials, seals O-sings and those of other high speed moving parts with ability to withstand escalated heat and chemical resistance rest fully on the shoulders of the materials specialists.

WORLD ENERGY CHALLENGES AND CLEAN TECHNOLOGY APPLICATIONS
There are no doubts that the quest for economic development and indeed in the emerging economies and nay the developing world requires an increase in the demand, supply and consumption of energy in all forms.
The challaenge of this assertion is the fact that whilst supply is expected to increase say five folds in these regions in the next twenty years, is it possible to increase emissions resulting from these activities say by a factor of two.
In Nigeria for instance, is it possible to increase power generation from say 4,000MW of today to say 20,000 MW in the next 10 years without causing a corresponding increase in emissions resulting from the activities of these development?
In a nut-shell, that is the challenge of clean technologies facing scientists and engineers

MATERIAL CHALLENGES
The design and introduction of new processes and process changes in obedience to clean technology

demands requires changes in the application of materials of use as a rule.. This is often taken for granted but the fact is clear that any change in technological process comes with changes in the conditions of matters in contact with the applied and processing materials and indeed the environment.

The challenges of high temperatures and pressures, high speeds and frequency changes, quick start-offs and shut downs, load and no-load conditions, submerged and non-submerged situations bring to bear tremendous strain and stress to materials so much so that the consequences like creep, fatigue, corrosion, yield and failures become realities.

Fig 8. TYPICAL DAILY POWER GENERATION REPORT IN NIGERIA.

POWER PLANTS	AVAILABLE UNITS	INSTALLED AVAILABLE CAPACITY (MW)	ACTUAL GENERA-TION CAPABILITY (MW)	GENERA-TION AT 06:00 HRS	REMARKS
HYDRO POWER PLANT #1	1G8, 10 & 11 **-3**	260	170	123	1G5- Awaiting rehabilitation. 1G6 – Out on gov. fault. 1G7 – Out on rotor E/F and stator winding insulation resistance failure. 1G9 – Out due to H2O leakage from the throat ring. 1G10 – Limited to 20MW on observation. 1G12 – Out on governor fault.
HYDRO POWER PLANT #2	2G1 - 5 **-5**	482	450	348	2G4 – On standby due to faulty 330kV synchronising breaker. 2G6 - Out due to burnt AVR.
HYDRO POWER PLANT #3	411G1, 3 & 4 **-3**	450	450	448	411G2 – Under going repairs.
STEAM POWER PLANT #4	ST2 – 5 **-4**	880	880	655	ST1 – Out on bearing problem. ST6 – Generator rotor being awaited.
STEAM POWER PLANT #5	ST1	120	90	61	ST2 – Out due to boiler feed pump problem. ST3 - Rehabilitation work in progress. ST6 - Out on high turbine rotor vibration.
GAS PLANT #6	----	----	---	--	GT5 – Out due to speed control problem. GT17 – Shutdown due to sparking carbon brushes. GT18 – Out due to turbine bade failure. GT19 – Bearing Nos 3 & 4 leaking lube oil. GT20 – Out on inspection.
GAS PLANT #7	GT6, 9, 11, 12, 14, 16 & 18 **-7**	320	300	253	GT3 & 5 – Generator winding fault. GT4 – Out due to starting device problem. GT7 – Out due to fire outbreak in the load gear compartment. GT10 – Out due to high vibration. GT13 – High vibration. Awaiting investigation and repairs. GT15 – Turbine blade failure. GT17 – Out due to accessory gear problem. GT19 – Tripped on generator hydogen purge shutdown. GT20 – Out due to hydrogen elakage.

A typical example is as is the case with failures resulting in power outages caused by material failures. The question is, how many materials engineers are working in the power plants? How much of materials limitations and allowances are observed in the course of operation and maintenance of these power plants? How much of preventive maintenance is practiced in power generation, transmission and distribution in Nigeria. How much of the outages, breakdown and shutdowns can be attributed to material failures? How much awareness can be credited to the operators in this wise

Every material is like a piece of cloth which if old woul naturally tear apart. At the same time if a clothing it is sewn not to fit and enough allowances not given to make for movements required, the result will be a tear.

To a non-trained eye, every metal is an iron or at best steel. To an untrained professional, every electrode can be used for any weldment and so also any material can work in any environment. Oh! And indeed any

bearing can be used for any moving part and so would any gauge of material be configured for fabrication of storages, containers and structures. That is fallacy.

CHALLENGES TO MATERIALS ENGINEERS IN NIGERIA

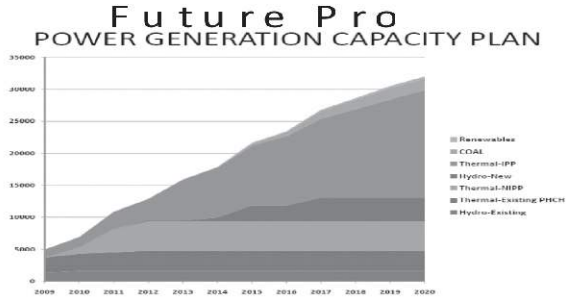
It is important to look at the profile of the Energy mix in Nigeria (Fig 2) as compared to the total World energy mix in fig 1 in order to envisage the complexity of the challenges of clean energy technology development in Nigeria.

Short of a 10MW wind power plant project in the Kaduna, Katsina axis, there is hardly any significant real Clean Technology plants coming up in Nigeria. This is not correct.

From the Key world Energy Statistics of the International Agency, 2009, the growth in world renewable has been tremendous in the last 24-25years has been tremendous. In 1973, Other fuel sources (renewables) contributed a total of 0.6%. In 2007 it had grown to 2.6% or about 433%

Nigeria has contributed zero in this respect.

However, all hope are not lost as can be seen in the project profile published by the Federal Ministry of power in February 2010.



CONCLUSION

The world and indeed Nigeria requires nothing short of an energy revolution. This energy revolution requires that we think about energy in new and innovative ways.

The Roadmap of the Presidential Task Force on Power launched in August is a start.

Captive applications of these renewables are one of such innovations, the introduction of nuclear generation in our energy mix in the near future is another.

Experts are even advocating for hybrid energy systems much like our modern hybrid electric car, these hybrid energy systems will combine nuclear and fossil or renewable and nuclear technologies to yield improved efficiency and reduced impact on the environmental.

The Ultimate goal is Zero Emission, the veritable vehicle is Clean Technology, the time to start is now, the place to start is here and vanguard and indeed the drivers are Materials Engineers and Scientists.

I thank you.

References.

Power Sector Outlook; Looking Ahead. A paper presented by Engr. Clement A. Oke at the 2010 Annual Conference of the National Association of Engineering Economist.

Renewable Energy World Magazine; May-June 2010 Volume 13 Number 3

Power Business and Technology for Global Generation Industry Vol. 154. No. 5. May 2010

Power Business and Technology for the Global Generation Industry. Vol. 154. No. 6. June 2010

Renewable Energy World Magazine; July-August 2010. Vol. 13 Number 4.

Arul Joe Mathias and Dr. P.K. Balasankari. Trends in Biomas: Opportunities for global Equipment Suppliers in Asia. Renewable Energy world Magazine. 2010-2011 Review Issue, July-August 2010

PLENARY PAPER ON
CURRENT ADVANCES IN COMMUNICATIONS MATERIALS

A plenary paper presented at the 10th Nigerian Materials Congress, Akure, Ondo State, Nigeria on 21st November 2011.
By Dr. Eugene I. Juwah
Executive Vice Chairman
Nigerian Communications Commission

Presented on his behalf,
By Funlola Akiode (Ms.)
Director, Corporate Planning & Strategy,
Nigerian Communications Commission

INTRODUCTION

Distinguished Ladies and Gentlemen. All protocols duly observed. I am delighted to welcome all of you to this Nigerian Material Congress 2011 (NIMACON 2011). I am highly honoured to address this special gathering of distinguished Government officials, policy makers, Academia, professionals and Stakeholders in the industry on the topic: "Current Advances in Communications Materials".

Gathering this group is the best way forward for Nigeria's technological advancement and in particular advances in the ICT materials in view of the convergence of Information and Communications Technologies.

May I also commend the organizers of this congress for their foresight in assembling technocrats and stakeholders to rub minds together to proffer solutions via these brainstorming sessions on current advances in ICT materials, the current and future applications in ICT and the way in which all these affect our socio-economic lives as individuals and as a nation, with an eye on environment sustainability.

BACKGROUND - CONVERGENCE OF TECHNOLOGY

In the world today, the telecommunications and Information Technology sectors are moving very fast on the track of technological development which has resulted in the convergence of Information and Communication Technologies. These two phenomena to a large extent, have become inseparable. Integrated systems have powered the convergence of both data communication and voice communication (i.e. Telecommunication). System Integration has made it possible to have integrated digital system to cater for both technologies at the same time.

Electronic systems had started with vacuum tubes (electronic valves) and then transistors which later got integrated as ICs. These tremendous improvements owe their successes to great advancement in electronic materials.

Switching systems used to be discrete, just like other components of electronic devices such as modulation, amplifiers, oscillators, transmission schemes, etc. These are now part of integrated systems. This cannot be unconnected with the advances in ICT materials which has brought the possibility of reduction in latency and jitters, increased speed, capacity, miniaturization, low power consumption, light weight, etc., in Packet Switching transmission and other systems.

Advances in ICT materials have brought about advancement in manufactured ICT equipment. These directly impact on information processing schemes. Information has therefore become a strategic resource, a commodity and foundation of every human activity. It can be managed and processed to give data which are vital in any sector of the economy. In fact, ICT could be classified as a utility such as water and electricity and hence, it has become a major factor in socio-economic development of every nation. ICT now plays a major role in education, learning and research, agriculture, health, commerce and even in poverty alleviation by generating or creating jobs through numerous investment opportunities. It has also helped in capacity building.

This paper attempts to x-ray Nigeria's advancement in the ICT superhighway, in order to steer investors towards the great opportunities ahead. Places like the USA, Japan etc created conducive environment for technological advances in material science. For instance, advances in research works from places like Silicon Valley, Massachuset Institute of Technology (both of USA), and Tsukuba Science City of Japan etc. have greatly impacted on ICT growth. It is a well known fact that the ICT market in Nigeria has a very large potential which has come to limelight within the past few years.

Let us also remember that in addition to the need to gear up stakeholders and investors for the opportunities in this sector, there is also the need to brace up for the challenges of e-waste which may become a monster if proper measures are not put in place to preserve our environment and sustain it.

ADVANCES IN ENGINEERING FIELD OF APPLICATIONS OF ICT MATERIALS

The field of Information and Communications Technology employs a broad range of materials in the fabrication of the components of a typical Communications Systems (CS). To a very large extent, the materials used for the fabrication of a specific component are strongly tied to the intended application of

the component. In addition, the materials used range from metals (and their various alloys in varying compositions), through plastics and polymers, to ceramics and silicates.

CONSIDERATIONS FOR ELECTRONIC MATERIALS

Materials used for manufacturing communications equipment need to comply with the following considerations:

1. The materials (and by extension, the finished product) comply with the acceptable safety Standards of the industry. That is, that it does not pose/constitute a threat to Safety of the users of the equipment;
2. The materials do not cause any undue interference to other telecommunications equipment and can also accept interference from other equipment within its neighborhood. All these are summarized as Electromagnetic Compatibility (EMC) and can be broken down to Immunity and interference from intentional and non-intentional radiators as the case may be.
3. The materials do not impair, or degrade the performance of the networks in the Nigerian telecommunications system. In order words, the materials used must be standard materials.
4. These materials should have good heat resistance, to be able to absorb or dissipate heat internally generated by systems/devices.

Ladies and Gentlemen, the predominant form of radiation in telecommunication systems is electromagnetic and most of the materials used in these systems serve to aid the beneficial manipulation of this radiation. Common characteristics of these materials that are of interest include, but, are not limited to:

a) Electrical Conductivity/Resistivity
b) Magnetic property
c) Dielectric property
d) Elastic
e) Thermal Conductance
f) Optical properties like, Refractive index, reflectivity etc.

The above enumerated characteristics of ICT materials in one way or the other affect the way the materials can be used and these properties are being studied deeply for further advancement in ICT materials. In examining the Current Advances in ICT Materials, permit me to divide the materials into:

1. Civil materials;
2. Mechanical and Metallurgical materials;
3. Electronics materials and
4. Optical materials;
5. Chemical Materials

For all intents and purposes, this categorization which is solely for this paper is however, by no means, exhaustive.

Civil Materials

The materials used in civil structure related to ICT applications consist of

1. Designed reinforced concrete mixes for the foundations of masts, building substructures etc;
2. Designed reinforced Aluminum alloys used for the mast superstructure on which the antennas are mounted;
3. Pre-fabricated Base Transceiver Station (BTS) shelter

In its basic components, these are said to be mixture of silicon (sand), rocks, limestone refined into cement, alloys and steels used in mast, tower, shelters and so on. Advances are being made in the mixture techniques and concentration percentage for better results.

Metallurgical and Mechanical Materials

These are the metallic materials in their purest form and in varying alloy amalgam used in ICT related applications. They consist of:

1. Copper (Cu) Conductors for site wiring, earthing, waveguide and antenna termination; and
2. Gold plated metals [and sometimes pure gold (Au)] for super-conducting applications.
3. Casing and weight bearing framework.

Electronics Materials

Electronic materials form a considerable portion of the materials used in electronic devices and components found in most ICT equipment. The evolutionary path was from tubes to transistor to Integrated Circuit (IC) and now, to Very Large Scale Integrated Circuit (VLSI).

Optical Materials

The term photonics was developed as an outgrowth of the first practical semiconductor light emitters invented in early 1960s and optical fibers developed in the 1970s. The science of photonics includes the generation, emission, transmission, modulation, signal processing, switching, amplification, detection and sensing of light. Photonics emphasizes that photons have dual nature of particle and wave with applications over the whole spectrum. Most applications are, however, in the visible region and near infrared light.

Chemical Materials

Advances in chemical engineering of electronic materials have enabled the production of sensors, semiconductors, biometric devices, different kinds of electrolytes, measurement devices, and the ability of equipment to work under stressful conditions without losing the main characteristics.

All these advances in material Science have enabled integration of not only electronic components but also functions, applications and services. These led to reduced sizes of electronic packaging, giving rise to microelectronics where high scale of integration is implemented. Every year new materials are being discovered. It is the aggregation of the advances in optical materials, electronic materials, and metallurgical/mechanical materials, chemical materials etc., that have helped in miniaturizing the electronics of the Communications technology. It is not possible to treat them in isolation as all the components are interlinked chemically. Micro-electronics is a product of advanced material Science and the enabling technology for miniaturization. It is the prospects of these advances in material science and growth that give rise to Moore's Law.

MINIATURIZATION

Moore's law describes a long-term trend in the history of computing hardware. The number of transistors that can be placed inexpensively on an integrated circuit doubles approximately every two years, and this trend has continued for more than half a century.

This law is not only applicable to the computer hardware but rather the whole field of ICT. The implication of this is that advances in Communications materials tend to make the size of ICT materials smaller, making us to talk more of chips, which are embodiments of VLSI. This is actually the current trend which has brought about the advent of the highly sophisticated field of nanotechnology and the molecular nanotechnology which are the future of ICT. Nanotechnology and molecular nanotechnology are the latest success story with research works still on in MIT and the likes. The main objective in nanotechnology is to understand nanoscale rules and mechanism in order to implement new ICT systems that are more economic, more reliable with little materials. Ladies and gentlemen, this is the future of advances in ICT materials as it stands today, and research works are still on to unleash the potentials of this hi-tech field of advancements.

POSITIONING IN THE GLOBAL ECONOMY AND CHALLENGES

The intent behind this benchmarking is to create a high-tech environment and infrastructure that can attract national and international investors and create spillover effects in the rest of the economy. The objective of this can be a replication of the conditions that can bring Nigeria to the limelight of global market like the economic successes of Silicon Valley. This concept of having Nigeria's Silicon Valley is to use this as a starting point for the development of ICT basic components like chips, and to develop spin-off applications intended to transform major sectors of the society through the use of ICT as a platform on which education, healthcare, e-government, commerce and manufacturing will ride. We have already started seeing a bit of these in our society. However, until broadband is fully optimized, and Nigeria Technology Village is established, we may not find ourselves at that level.

The Malaysian government was one of the first to attempt to replicate the Silicon Valley model amongst the developing countries. In her attempt to move the technology sector to attract domestic and foreign private investment, the Malaysian government invested in creating a world class physical and information infrastructure. This US$40 billion initiative, called the Multimedia Super Corridor (MSC), serves as the backbone for the country's information superhighway [3]. This is brought about by advancement in ICT infrastructure through the use of optical fibre and other advanced ICT materials with a capability of unending broadband which supports economic, cost effective solutions and less materials usage. We believe that this is also possible in Nigeria with concerted effort of all the professionals present here today channeled towards advances in ICT materials.

Nigeria's ICT sector has been able to build on a relatively good infrastructure and a small, but highly skilled, IT professional base. Local software development production grew in Lagos, because of the high level of commercial activities in SMEs and even large scale enterprises. However, most of the development has been limited to small scale local projects. Currently packaged software is over 90 percent imported. Research and Development (R&D) spending has thus far been very low and there is room for expansion, both in terms of the range of products available and the huge domestic market.

ACHIEVEMENTS

Presently, Nigeria is experiencing a quantum leap in socio-economic development due to the advent of the Internet, laying of fibre optics cable, satellite communications and the arrival of Global System for Mobile Communication and now planning for the 4th Generation systems.

Essentially, the areas in which the advances in ICT materials have transformed into more effective equipment and efficient ICT infrastructures which have improved the socio-economic status of Nigeria with resultant effect on national development include but not limited to:

1) **BANKING**

Banking in Nigeria is so dynamic and competitive. Before the advent of ICT, the business of banking in Nigeria was so difficult because it involved the normal banking routine of using papers and registers for the implementation of banking transaction and when a transaction involves two banks the bureaucratic bottleneck involved in the transaction was quite enormous and time consuming.

Presently, banking is more interesting as banking transactions can be done within the split of a second in these banks due to the deployment of ICT infrastructures which make transactions fast, dynamic, and effective. Using the gains of mobile technology, the Nigerian economy is moving towards a digital economy. To that end, the NCC is

collaborating with the Central bank of Nigeria to ensure that mobile payment mechanism is effectively entrenched in the Nigerian financial system, while also demanding networks optimization to handle these financial services seamlessly.

2) BETTER SECURITY NETWORK

The work of law enforcement agent, which seems a herculean task, has been eased with improved ICT infrastructure providing better option in communications for building an improved security network because of its tetherless nature. Robbery menace has been alleviated, though not totally eradicated, as victims of armed robbery can easily contact police officers for rescue operations at the touch of a button on a phone.

3) ELECTRONIC COMMERCE

This a fast growing sector in the commerce industry because of its effective nature. The Internet makes it possible for buyers and sellers to interact on-line without physical contact. These are made possible because of advances in web-based applications and the ICT hardware components.

A buyer can just visit a web site click on a particular item he wants to buy and pays via a credit card, e.g., Master Card, Visa Card e.t.c. This has really improved the modus operandi of commercial activities and there is a paradigm shift from the normal physical contact commercial activity to virtualization.

4) DIRECT AND INDIRECT JOBS

Many Nigerians are employed in various works directly or indirectly related to building the ICT capacity of the nation. For example, mobile operators and Private Telecommunication Operators (PTOs) employ Nigerians in the provision of the communication services to Nigerians thereby increasing the socio-economic activities of the country.

There are other indirect jobs these include:

i. Establishment of tele-centers
ii. Establishment of business centers
iii. Hawking of recharge cards and telecommunications accessories etc.

All these improve the socio-economic life of Nigerians. Other indirect employment opportunities involve award of contracts to indigenous IT firms, media consultants, etc.

The nearest future still hold the following for Nigeria. Although, we have started seeing a tip of the iceberg of the positive effects of these advances, the truth is that, these phenomena are not yet optimized for full benefits. These include amongst others:

5) TELEMEDICINE

In Nigeria, telemedicine is new and it is increasingly becoming popular in the medical sector. However, this has not been fully optimized. Telemedicine offers the following advantages:

i. It reduces the number of patient going to the hospital to seek the attention of medical doctors.
ii. It brings about maximization of medical personnels' expertise.
iii. It improves the health status of the populace by the distant treatment being offered to them by the specialist doctors which may have a busy schedule.

The road ahead of telemedicine in Nigeria is promising. Nigerians living in rural areas will definitely have access to the type of health services in the urban centers. Telemedicine applications allow a group of specialist surgeons (in different locations) to carry out operation together, while sharing sight of a video signal broadcast from the operating theatre, as well as full reference into a patient's medical records. A surgeon roaming in another country could indicate directly on the video exactly where an incision should be made. This can only be optimized through broadband infrastructure.

The Internet can also be harnessed in telemedicine so that a patient can visit a website where diseases have already been diagnosed all he needs do is to read the symptoms and make a diagnostic conclusion through the help of a medical personnel on the phone.

6) VIDEO CONFERENCING

Executive management decisions are being made via video conferencing. This has made the meeting of industry captains, professionals, investors, and other stakeholder in every sector to be possible in the virtual world. This can be done by setting up a virtual private network (VPN) which can only be assessed by the intended executives. The VPN is a highly secured network on which activities like video conferencing can take place. This has been made possible by the application of advances in material development

The advantages of video conferencing cannot be over emphasized. These include but not limited to:

i. It is a highly secured medium in which important security decisions can be made.
ii. It lessens the movement of the executives, thereby preventing exposure to attacks by mafias, hoodlums and other touts.
iii. It saves time and energy in the conveyance of such meeting because less physical arrangement is involved in conveying such a meeting.

7) E-GOVERNANCE

The application of ICT in governance (i.e. e-government) has a great prospect in the future of

governance. If the whole 774 local governments in the federation are hooked up to the Internet and also, Wide Area Network there will be information flow from one arm of government to the other without any delay. Governors and local government chairman will need not travel to Abuja all the time to get information. They can even go ahead to have an online chat with the officials they intend to meet thereby reducing expenses on trips and at the same time save time. All these are still coming to stay in Nigeria when we fully embrace the advances in the future

CONCLUSION

In all, current advances in ICT materials have brought a lot of development globally and into our country Nigeria. Applications of the current advances have also stepped up the speed of activities and development in other economic sectors, while the socio-economic development presently manifesting in the country is as a result of the supersonic growth of ICT development in Nigeria. With good collaboration for research into advances in materials and their applications by the professionals, academia and relevant government agencies, who are present here today, Nigeria can become a model ICT based economy in the next few years.

Furthermore, the field of nanotechnology and molecular nanotechnology that are not yet fully developed will definitely explode to become a reference indicator in standardizing the advances in ICT. However, efforts in sustaining our environment should be proportional to the current advances in ICT materials development.

Distinguished audience, we therefore challenge the professionals here present and beyond to seize the immense opportunities being presented in the ICT field to explore the possibility of utilizing our local materials in producing ICT technologies for the deployment of ICT infrastructure, not just for the Nigerian market, but for the African and global market of the future.

I thank you for your attention.

Dr. Eugene I. Juwah
Executive Vice Chairman/Chief Executive Officer,
Nigerian Communications Commission.

REFERENCES

1. **Wikipedia Moore's Law, http://en.www.wikipadia.org/wiki/Moore%27s_law**

2. **Wikipedia Photonics, http://en.www.wikipadia.org/wiki/Photonics**

3. **Professor Clement Dzidonu,** (2002) **"**A blueprint for developing national ICT policy in Africa". **ISBN No. 9966-916-87-3**

4. Factors Affecting E-Payment Adoption in Nigeria, http://www.irma-international.org/viewtitle/46947/

SOLAR ENERGY: A VERITABLE AND SUSTAINABLE POWER GENERATION SOURCE FOR DOMESTIC USE, MATERIAL PROCESSING AND TECHNOLOGICAL ADVANCEMENT

C. I. Nwoye and J. U. Odo
Department of Materials and Metallurgical Engineering, Nnamdi Azikiwe University Awka, Nigeria.
chikeyn@yahoo.com

Abstract
This paper presents a review of intensive research works on collection, harnessing and conversion of Sun's radiation into electrical and heat energy which meet the daily energy requirement for domestic use such as heating-up rooms and cooking, materials processing and technological advancement such as space innovations. Solar electricity is produced following incidence and absorption of Sun's radiation on the solar cells (diodes). Equipment needful of only solar radiation (as a source of energy) for its operation such as drying, refrigerating and cooking have all been found to be 100% environmentally friendly since such operations are devoid of emitting harmful gases into the atmosphere. Global commercialization of these equipment is expected to not only reduce largely the effects of global warming, particularly the green house effects but also put in check desertification, deforestation and obstruction of the ecosystem. Critical analysis of the challenges facing power generation from Sun's radiation indicates high dependence of Sun's radiation on the environmental weather condition, dependence of Sun's radiation on the collection location and the duration of the radiant inflow, dependence on the time of the day at which the Sun's radiant heat is being collected, dependence on angle of incidence (i.e the angle between the normal to the solar array and a light ray from the Sun), dependence on solar distance (i.e the distance of the array from the Sun) as well as dependence on light transmission losses in cover glasses, cover adhesive and other optical elements. Based on inevitable natural constraints, these challenges persist recurrently due to variations in the optimal conditions of all these factors

Keywords: Solar Energy, Power Generation, Domestic Use, Material Processing and Technological advancement.

1.0 Introduction

There are great potentials for the development and utilization of solar energy in developing countries due epileptic power supply as well as high cost of conventional fuel such as petrol and diesel. In so many cases, solar energy has shown to be superior to fossil fuels because the latter has continued to raise a lot of environmental concerns. Environmentally, solar energy is one of the least destructive of all the sources of energy [1].

A good knowledge of the global solar radiation dynamics especially the intensity of solar radiation at a given location is of fundamental importance for all solar energy conversion systems [2]. This is because the length of time and proportion of the amount of solar energy radiation reaching the earth varies from place to place due to the earth's orientation and attenuation factors [3].
The Sun generates radiant energy by combination of hydrogen atoms to form helium. The energy released in this process directly supplies most of the natural energy systems on earth which can be utilized by conversion of the heat to electricity [4].

Report [5] on solar energy indicates that it is silent, inexhaustible and non-polluting source of energy which provides daylight, heats the earth and meets up the energy requirement for plant growth. The Sun is viewed as a natural nuclear power plant which generates radiant energy to the tune of 3.8×10^{23} kW. The earth intercepts only a fraction of this energy (1.8×10^{14} kW) and on a very bright day, a square meter of surface facing the Sun receives about 1Kw. It was also discovered [5] that the amount of solar energy falling on the earth in three days is equal to the known fossil fuel reserve of the world. This implies that there is sufficient energy from the Sun to meet the present and future energy needs if properly harnessed and utilized. In a similar vein it has been suggested [6] that the energy available on the earth surface is approximately 50% of the incident radiation. This was attributed to the fact that the solar radiation scatters on reaching the earth, and then get absorbed by dusts, gas molecules and water vapour as it passes the earth's atmosphere. This way the actual magnitude of radiant energy reaching the earth is reduced.

TYPES OF SOLAR CELL AND MATERIALS FOR ITS DESIGN

Solar cells called photovoltaics made from thin slices of crystalline silicon, gallium arsenide, cadmium sulphide, specific components of copper indium silinide (CIS) or other semiconductor materials convert solar radiation directly into electricity [6]. These cells being the building block of a PV system are diodes that allows incident light to be absorbed and subsequently converted to wavelengths. Some solar electric cells have laelectricity [6]. Light can be separated into many different wavelengths. Consequently, the light that hits the power cell has a wide range of energies, and different semiconductor materials react differently to different light yers of semiconductor mediums, even layers of

different mediums, in an attempt to maximize efficiencies. The most common type of solar cell is **Crystalline Silicon**, of which there are two primary types; **Single-Crystalline Silicon** and **Poly-Crystalline Silicon [7]**. Single-Crystalline is more efficient but also more expensive to produce (usually limited to commercial and residential applications). Both are still very fragile, and usually sandwiched between rigid sheets of glass, for protection.

SOLAR ENERGY GENERATION FOR DOMESTIC USE

Solar radiation incident and absorbed on the collectors (solar cells) is converted to electricity for use in water and space heating. Homes employ collectors fixed in place on roofs. In the Northern Hemisphere, they are oriented to face true south (± 20°); in the Southern Hemisphere, they are oriented to face north [8]. For year-round applications such as providing hot water in homes (Fig. 1), they are tilted relative to the horizontal at an angle equal to the latitude ± 15° [8]. The electricity generated in this way in homes could be used to run the fans, light the electric bulbs and heat-up the rooms (during cold) and boilers. Furthermore, the electricity produced could also be used to keep televisions, radios and computers usefully on. In addition to the flat plate collectors, typical hot-water and space heating systems include circulating pumps, temperature sensors, automatic controllers to activate the circulating pump, and a storage device [8].

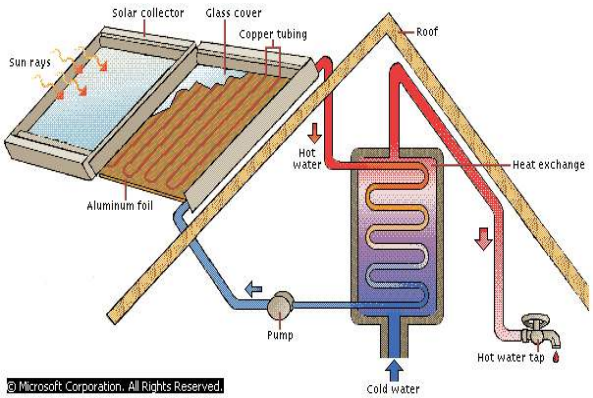


Fig.1: Flat plate collector [8]

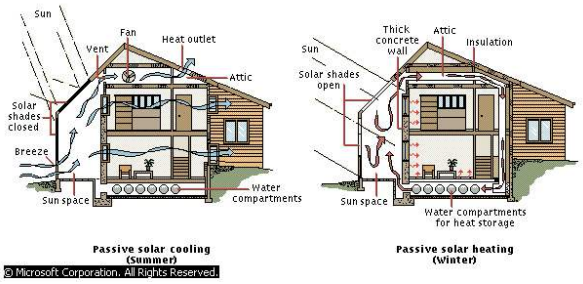


Fig. 2: Showing solar cooling and heating system for summer and winter [8]

Either air or a liquid (water or a water-antifreeze mixture) can be used as the fluid in the solar heating system [8] (Fig. 2). A rock bed or a well-insulated water storage tank typically serves as an energy storage medium. Concentrating collectors are used for air conditioning, central power generation, and many industrial heat requirements where flat plate collectors cannot provide carrier fluids at high enough temperatures to be effective. The concentrators move to track the Sun using devices called heliostats.

SOLAR COOKER

Solar cooker was designed and developed [9] as an alternative to the conventional electric stove of power rating 1000W. The performance test of this solar cooker on clear sky days shows satisfactory performance in terms of the variety, quantity of food and the time of completion of the cooking. The cooker [9] was able cook satisfactorily 5kg yam in 40 minutes. It also boiled 3 eggs in 12 minutes and prepared an egg stew in 15 minutes. In comparison with an electric stove of power rating 1000W, the cooker performance was found competitive as the time duration for the cooking were approximately the same as shown in Tables 2 and 3 [9]. Commercialized usage of this solar cooker implies saving the high cost of fuel procurement and then investing the fund into other sectors of the economy.

Table 1 : Performance Test on Solar Cooker [9]

Food Stuff	Mass of food (kg)	Cooking Time (mins.)	Ambient Temperature
3eggs + water	1	12	27^0C
Yams	5	40	27^0C
4 eggs, oil, tomatoes, pepper	1	12	27^0C

Table 2 : Performance Test on E lectric Stove (Rating: 1000W) [9]

Food Stuff	Mass of food (kg)	Cooking Time (mins.)	Electric Voltage (V)
3eggs + water	1	11	220
Yams	5	35	220
4 eggs, oil, tomatoes, pepper	1	12	220

There is indication [9] that the operation of the cooker is also free from smoke and fire hazards associated with conventional cooking methods and electric shock of the electric stove. Also the incessant incident of kerosene stove explosion will be highly reduced. Usage of the solar energy in this form shows that the solar cooker is 100% environmental friendly as its operation does not emit harmful gases. Therefore, usage of this solar cooker will largely reduce the effects of global warming, particularly the green house effects.

SOLAR ENERGY GENERATION FOR MATERIAL PROCESSING

Application of solar energy has really covered vast areas in solar processing of agricultural materials to food, heating, desalination process, refrigeration, air conditioning, heat and electricity generation for domestic use and materials processing in the industries. The solar cookers use sunlight for cooking, dryimg and pasteurization. Solar cooking cuts-off fuel cost, reduces demand for fuel or fire wood and improves air quality since it is not associated with emission of harmful gases and smoke. This equipment has become instrument for checking desertification and deforestation. They are particularly suitable for use in rural areas where the risk of fire is considered important [10].

SOLAR DRIER

Studies [10-18] have shown that Sun could be used for drying of agricultural products, heating, boiling of water, refrigeration etc. Cassava is a staple food in Nigeria, especially in the eastern Nigeria. Drying the cassava chip as a mode of processing it for storage using sophisticated chemical methods is expensive while drying in by ordinary smoking method using wood is prone the problems already expounded [19,20]. A solar drier was designed and developed [18] for processing wet cassava chips to a dry condition for storage. This allows preparation of this cassava chips for meals at convenient times. Past report [21] indicates that cassava chips prepared from a freshly harvested cassava have 70% moisture content. Using the designed solar drier [Iwuoha],the moisture content of the cassava chips was reduced to only 30%.

In the drier, very hot air at a temperature of about 80^0C flowing into the solar absorber enters the drying chamber by natural convection through the inlet to the drying chamber control gate, adjustable between 0 to 90^0C, to regulate the inflow of heat entering the drying chamber [18]. As the heated air-flow passes over the systematically sliced cassava chips, moisture is removed and exhausted through the chimney.

In a similar vein, a design of an energy saving drier for preservation of agricultural produce has been carried out [22]. The energy saving was achieved by the incorporation of a heat exchanger between the fresh air inlet and the exit air from the drying chamber in such a manner that the exit air from the drying chamber preheats the incoming air. Results of the experimental tests [22] reveal that an energy saving of up to 22% is

possible. The results also show that the moisture content of agricultural products (both grated and non grated) so preserved dropped from between 29-31%wb to about 15%wb.

SOLID ADSORPTION SOLAR REFRIGERATOR

The design and development [23] of solid adsorption solar refrigerator was embarked on to explore the possibility of cold production from the solar radiation. Several scientists [24-27] have all reported successful production of cold using this technology. It has been discovered that the use of solar energy powered system to produce cold depends on the availability and intensity of solar energy in the region of interest. Results generated from similar research [25, 28] shows that solar energy intensity in the range 11-12 MJ/m^2 and above is required if a solid adsorption solar refrigeration system using activated carbon/methanol pair is to be effectively used cold production. This cold production technology for preserving bacteria cultures, agricultural products and foods could be a viable alternative to the conventional method in remote regions without grid connected electricity or farm settlement with abundant solar radiation.

SOLAR POND

Research [29] has shown that a potentially cheaper and more effective energy solution especially in the rural areas is the solar pond. Solar pond captures and stores sunlight (in form of heat) via body of water, in the form of energy supply [29]. This factor makes it an attractive form of energy supply for out-of-town usage and in industrial heat application for materials processing. The convecting solar pond consists of merely water in a containment area with some basic measure to reduce convective version and uses a medium such as salt or a membrane to achieve heat loss reduction [29]. Some solar ponds use brine to set up a salinity gradient required to prevent the occurrence of convection current in the water. This helps to improve the solar gathering performance of the pond. With proper insulation, the trapped heat will be available 24 hours a day.

The salt gradient solar pond has three operational layers of water that determines its behaviour [30]. These are Upper Convective Zone (UCZ), the Non-Convective Zone (NCZ) and the Lower Convective Zone (LCZ). The LCZ is made of concentrated brine, a supersaturated solution of salt that absorbs the incident solar heat rays and stores the energy in the form of heat [30]. Generally, the LCZ will reach temperatures in the range 45 to 90^0 Celsius in operational solar ponds as found El Paso in Texas [31] and the Bhuj solar pond in India [32] Concentrated salt solution is denser than water, counter-acting the tendency of the hot solution to rise to the surface [30]. The UCZ is a layer of fresh water that allows sunlight penetration in this concept [30]. This layer has a varying salt concentration, changing from salty to fresh water as the depth decreases [30]. This layer acts as a barrier to any convective currents trying to reach the upper surface of the pond, reducing the heat transfer rate.

SOLAR ENERGY GENERATION FOR TECHNOLOGICALADVANCEMENT

Solar or photovoltaic cells are basically grouped together to form 'PV modules' that may in turn be arranged in solar arrays referred to as solar panels. Such solar arrays have been used to power orbiting satellites and other space crafts [33]. Normally, the photovoltaic power generated is determined by calculating the number of solar panels to ascertain the solar energy flux (W/m^2) [33]. However, for satellite application, there are several factors which determine the solar power generation capacity required on board the satellite. These includes: end of life (EOL), begin of life (BOL), temperature coefficients, radiation degradation remaining factors, loss factors (cell mismatch, calibration error and solar aspect angle) [33]. Very importantly, these factors need be known, adjusted and controlled for the required PV power to be generated.

Table 3: Photovoltaic Installation C apacity in some countries of the world as at the year 2004 [6]

Countries		
Cumulative connection Grid-tied (kW) (kW)	Off-grid PV Total (kW)	Grid Total (kW)
Japan	84,24	5
1,047,746 267,016	1,131,991	272,368
Germany	26,000	
768,000 360,000	794,000	363,000
United State	189,000	
175,000 62,000	365,200	90,000
Australia	48,640	
6,760 780	52,300	6,670
Holland	4,769	
44,310 3,071	49,079	3,162
Spain	14,000	
23,000 8,460	37,000	10,000
Italy	12,000	
18,700 4,400	30,700	4,700
France	18,300	
8,000 4,183	26,300	5,228
Switzerland	3,100	
20,000 2,000	23,100	2,100
Austria	2,687	
16,493 1,833	17,180	2,347
Mexico	18,172	
10 0	18,182	1,041
Canada	13,372	
512 107	13,884	2,054
Korea	5,359	
4,538 3,106	9,892	3,454
United Kingdom	776	
7,386 2,197	8,164	2,261
Norway	6,813	
75 0	6,888	273

The PV power installation has been on the increase in various countries of the world. As at 2004, (as in Table 3) PV power installation has found its place in 15 countries; both developed and developing countries with total

installed capacity in the range of 273 and 363,000 kW [6].

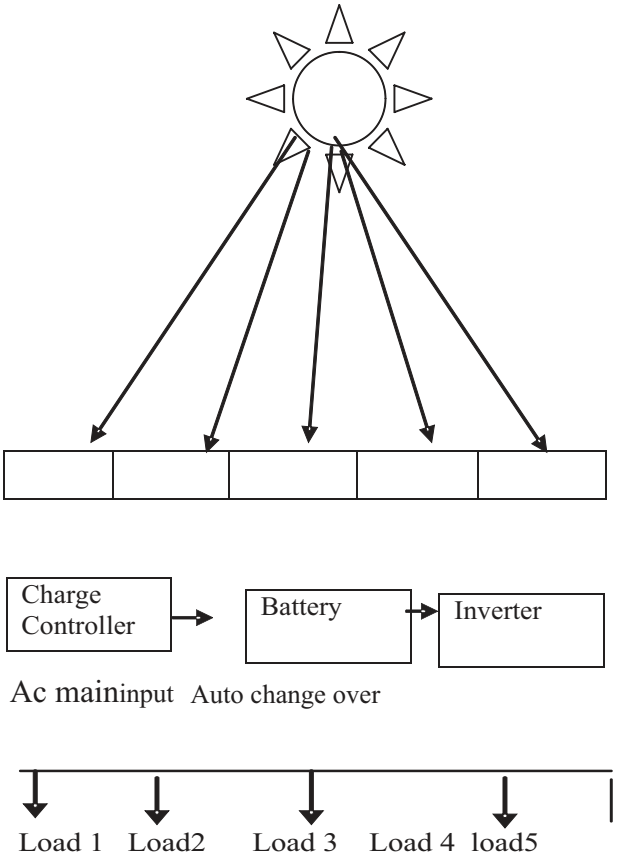


Fig. 3: Block diagram of Solar Electric Power Inverter [6]

Most PV generator systems currently in use in recent time employ rechargeable electric storage batteries for this purpose (Fig.3). The standard solar cell modules are designed to provide the correct out put voltage to effectively charge these batteries. The solar energy provides all the power required by the load over the year. The storage battery is made to act as a 'buffer' between the solar ray and the load, and go ahead to supply power to the load during the period of low sunlight [6]. The conversion of solar radiation into electricity (in homes for domestic use) by means of the PV cell is at present the most sophisticated technology development in solar energy devices [5].

It has been discovered [34] that thermal power plant (condensing power plant) can convert the energy of a chemical fuel into mechanical energy which is then converted into electrical energy by a generator. Thermal energy conversion can be classified into three categories, namely: low temperature range (< 10^0C), medium temperature range (10-150^0C) and higher temperature range (>150^0C) [35].

ELECTRIC POWER GENERATION FOR SPACE OPERATIONS

There are numerous artificial satellite missions' objectives, which includes environmental surveillance, scientific probes, communication links for data acquisition, change monitoring and impact assessment in the lower orbit and deep space [36, 37]. Basically, all these satellites practically need electrical power to sustain their operations while in space.

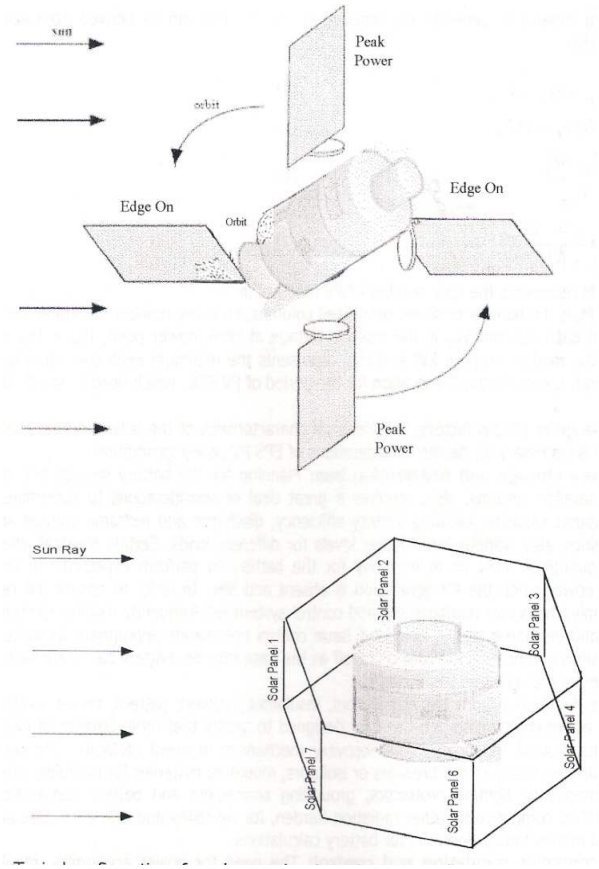
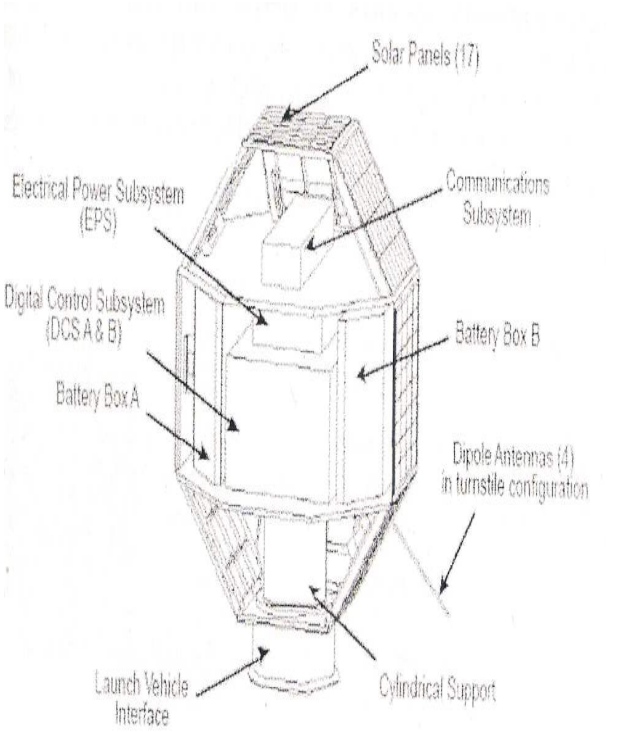


Fig. 4: Typical configurations for solar panels orientations on satellites [33]

Renewable energy source from Sun distinguishes itself as the energy source of preference in the solar system , particularly for satellites' missions closer to the Sun [38]. Photovolta ic array design take into cognizance variations in solar flux, electron and proton fluxes, meteor showers and ultraviolet radiation which degrade performance by about 2% per year [33]. Basically, depending on the satellite power demand and mass considerati on, special mechanism like SADM (solar array drive mechanism) in SPOT 4 and ERS 1 and 2 can be incorporated to redirect t he solar panels to the Sun [39, 40] (Fig. 4).



sub-system (EPS) on board artificial satellites [33]. Considering satellites varied mission objectives, orbit position, the capacity and scale of EPS implantation are based on the power demand for the various satellites' sub systems for navigation, sensing and communication [33]. This implies that the EPS has the responsibility of providing adequate and reliable electrical power, over the entire life of the satellite in the orbit. Achievement of this requires an efficient and effective means of generation, storage, managing and distribution of power using intelligent electronic power control systems technologies [33].

It was suggested [33] that the appropriate number of batteries, operation temperature, nominal and operating voltages, storing ampere-hours and mass of each, be determined to support the satellite electrical energy consumption for the period when solar energy is not available. This arrangement incorporates both battery chargers and electronic switch-over gadgets into the EPS.

The electrical power on board is distributed to other satellite sub-systems and payload through determined rated bus voltage arrangement. Most importantly, the batteries have a specified cycle and level of charge and discharge that must be conformed to in order to maintain efficient performance. There is need for the EPS to be very intelligent, enough (in collaboration with the on-board computer) to manage the electric energy generated for usage in the satellite over its life cycle in the orbit. Indicators for battery status such as voltage, temperatures, current charge and discharge limits need be monitored and controlled in the satellite to ensure steady power supply and system protection.

MAJOR CHALLENGES OF HARNESSING SUN'S RADIANT HEAT INTO USEFUL ENERGY

Realization of the potentials inherent in Sun's radiation as a sustainable energy source has been celebrated globally for industrial growth. However, in both developing and developed countries, there are un-avoidable challenges facing the conversion of sunlight to electric and heat energy for domestic and industrial use. These includes; high dependence of Sun's radiation on the environmental weather condition, dependence of Sun's radiation on the collection location and the duration of the radiant inflow, dependence on the time of the day at which the Sun's radiant heat is being collected, dependence on angle of incidence (i.e the angle between the normal to the solar array and a light ray from the Sun), dependence on solar distance (i.e the distance of the array from the Sun) [43] and dependence on light transmission losses in cover glasses, cMango, Pineapple and Fish," Annual Research Report, Department of Farm Power and Machinery, Bangladesh, Agricultural University, Mymensign, Bangladesh.

[13]Othieno, G., and Iwidell, I. (1992). "Application of Small Crop Drier to Maize Drying in Kenya, Energy for Rural Island Communities, Pergamon Press, London.

[14]Schirmer, P. S., Janjai, A., Esper, R. Smitabhindu, W. M. (1996). "Experimental Investigation of the Performance of the Solar Dryer for Drying Bananas" Renewable Energy, 7(2):119-129.

[15]Sachthananthan, K., Trim, D. S., Speirs, C. I. (1985). A Solar Dome Drier for Drying Fish, FAO Fisheries Report No. 329 (Supply), Fish Processing in Africa, Proceedings the FAO Expert Consultation of Fish Technology in Africa, Lusaka, Zambia.

[16]Mukherjee, S., Bandgapadhay, S. and Rose, A. N. (1990). An Improved Solar Drier for Fish Drying in the Coastal Belt, Journal of Ed. Sc. Tech. 27: 175-177.

[17]Akanbi, C. T., Olumess, A. O., Taiwo, K. A., Ojo, A., and Akinwands, B. A. (2003). "Effect of Balanching Medium on Drying and Storage Characteristics of Paper" Nigerian Drying Symposium Series, 1:95-107.

[18]Iwuoha, S. I. (2003). "Solar Fish Dryer for Imo State of Nigerian Environment" Nigerian Drying Symposium Series, 1:123-130.

[19]Shittu, T. A. (2003). "Smoke Drying Technology: Implication for the Efficiency and Saftey of Drying Fermented Cassava Roots'' Nigerian Drying Symposium Series, 1:85-94

[20]Dzisi, A. K. and Mirth, J. (1991). "Cassava Drying in A Wood Fired Bed Crop Dryer" in Proceeding of 8th Symposium of the 1 STRC, October 20-26, Accra, Ghana.

[21]Okpala, K. O., Orga, A. C., and Onyelucheya, O. E. (2003). Drying Kinetics of Cassava Slices. Nigerian Drying Symposium Series, 1:1-14.

[22]Ogueke, N. V. (2009).Energy Saving Agricultural Produce Dryer. Advances in Science and Technology,3(2):113-119.

[23]Ibrahim, J. S., Kucha, E. I., and Igwue, G. A. (2009). Modelling of Solar Absorption Refrigeration Using Local Gin (Ogogoro) As Refrigerant.

[24]Anyanwu, E. E., and Ezekwe, C. I. (2003). "Design, Construction and Test Run of a Solid Adsorption Solar

Refrigerator Using Activated Carbon/Methanol as Adsorbent/Adsorbate Pair", Energy Convention and Management, 44:2879-2892.
[25]Pons, M., and Grenier, P. H. (1987). "Experimental Data on a Solar Powered Ice Maker Using Activated Carbon and Methanol Adsorption Pair", Journal of Solar Engineering, 109;303-310.
[26]Grenier, P. H., Guilleminot, J. J., Mester, M., Meunier, F., and Pons, M. (1983). " Experimental Results on a12m^2 Solar Powered Cold Store", ISES Congress, Perth, Australia.
[27]Critoph, R. E. (1993). Laboratory Testing of Ammonia/Carbon Solar Refrigerator. ISES, Solar World Congress,Budapest, Hungary, August 23-26.
[28] Anyanwu, E. E., and Ogueke, N. V. (2001). "Computer Prediction of the Performance of a Solar Powered Asorption Refrigerator in Some Nigerian Cities." Indian Journal of Engineering and Materials Sciences, 8:261-270.
[29]Imaekhai, L. (2009). "Development of a Small-Scale Solar Pond Technology Test Bed for Education Purposes." International Journal of Mechanical Engineering, 1(1):48-52
[30]Sukhatme, S. P. (1997). Solar Energy-Principle of Thermal Collection and Storage, Second Edition, McGraw Hill International.
[31]http://www.solarpond.utep.edu/
[32]http://www.teriin.org/case/bhuj.htm
[33]Okafor, E. C. N., Okoro, C. E., and Ejimanya, J. I. (2008). Design Algorithm of Electrical Power Generation, and Control for Satellite Systems. International Journal of Natural and Applied Sciences, 4(2):131-138.
[34]Zia, Y. A., Juan, L., and Balar, Jr. (1994). Electromechanical Energy Devices and Power Systems. John Wiley and Sons, New York.
[35]Tiwari, G. N. (2006). Solar Energy Fundamentals, Design, Modelling and Applications, 3rd Edition, New Delhi: Narosa Publishing House.
[36]Ononiwu, N. (1994). Appraisal of Role of Satellite Systems in Acquisition of Data for Monitoring and Evaluating Global Climatic Changes with Respect to Reservoir Energy Generation. Global Climate Change Impact on Energy Development Journal, 165-171.
[37]Ejimanya, J. I. (1999). Communication Electronics. Prints Konzults, Lagos, Nigeria.
[38]Van den berg, E., and Kroon, M. (2002). Algorithm and Performance of a Space Dedicated Solar Array Modelling Tool. Space Power, Proceedings of Sixth European Conference, Portugal, Pp 527.
[39]France National Satellite Programme SPOT 4 Bulletin.
[40]European Remote Sensing Satellite, (1995). ERS-2. European Aerospace Bulletin, No. 83.
[41]PANSAT (1993). Prelimnary Design Review. Collection of View Graphs Presented at Petit Amateur Satellite (PDR, Naval Post Graduate School, Monterey, California, April 27.
[42]NASA (1983) Galileo Mission to Jupiter FACT Sheet, NASA FACTS, National Aeronautic Space Administration, Washington.
[43]Far Ultraviolet Spectroscopic Explorer, FUSE: Space Based Astronomy, FACT Sheet, NASA, (1999)

MICROSTRUCTURAL DEVELOPMENT ON FIRED NIGERIAN CLAY OF SOUTH-WEST, NIGERIA

[*1]Olokode O.S., [1]Aiyedun P.O., [2]Oluwadare G.O., [3]Lee, W.E
[*1,1]Mechanical Engineering Department, University of Agriculture, P.M.B. 2240, Abeokuta, Nigeria.
[2]Depatment of Chemical Sciences, Bells University of Technology, Otta, Nigeria.
[3] Department of Materials, Imperial College London, SW7 2AZ, UK.
[*]Author for correspondence

ABSTRACT
Thermal transformation of Asero clay minerals were studied using inductively coupled plasma (ICP), X-ray diffraction and Scanning Electron Microscopy (SEM), and the results indicated two clay minerals namely kaolin and illite. The major properties investigated were drying and firing behaviour, apparent density, bulk density, apparent porosity and moisture content.
Similarly, thermal breakdown and phase development scheme were ascribed to the presence of interlayer cations and accessory minerals. These results provide a basis for predicting phase development on firing Asero clay for lining furnaces, stoneware, tiles and fire clay bricks.

Keywords: microstructure, spinel, bulk density, firing, lining, kaolin, illite,

INTRODUCTION

Clay is the chief raw material for many commercial structural ceramic products such as roofing tiles, building bricks and whitewares including sanitaryware, floor and wall tiles and furnace lining. Clays are used in enormous quantities in these applications and different clays are often blended to give the most desirable properties. Lately, clays are also used in what might be termed more advanced applications such as in combination with zeolite for catalyst supports in hydrocarbon cracking[1] as additive to cement to act as binder or plasticizer[2] and in refractories to act as a binder[3].

Kaolinites have 1:1 layered structures consisting of alternate sheets of silicate tetrahedral arranged in rings and metal hydroxide (gibbsite structure) octahedral.

Pure kaolinite has the formula $Al_4[SiO_{10}](OH)_8$. The other two main classes of clay minerals, illite and smectite, however, have 2:1 structures made up of an octahedral layer between two layers of inward-pointing silica tetrahedral with additional interlayer cation that charge-balance substitution in the octahedral and tetrahedral layers, making the compositions in the 2:1 clays difficult to define exactly. Illites substitution of Al^{3+} for Si^{4+} occurs in the tetrahedral layer with charged balance provided by interlayer K^+ so that an illite might have the appropriate formula
$K_{1.5\text{-}1.0}Al_4[(Si_{6.5\text{-}7.0}Al_{1.5\text{-}1.0})O_{20}](OH)_4$.

On firing, the kaolinite mineral dehydroxylates at 500^0-600^{0}C, forming metakaolin, which consists of the kaolinitic lattice after the removal of most of the hydroxyl groups. Scanning electron microscopy (SEM) studies of this transformation reveal the characteristics pseudo-hexagonal morphology of the kaolinite crystals is retained by the metakaolin. As heating proceeds, a spinel-type phase crystallizes within the metakaolin, beginning at around 900^{0}C. This has been reported by some researchers[4,5] to be a γ-Al_2O_3 spinel phase with some residual amorphous SiO_2 and by others[6] as a single phase containing more Si and having a composition nearer to mullite. Mullite itself also begins to form at this stage, and the development of these continues to 1000^{0}C. SEM analysis of kaolinite fired to this temperature shows 10-30nm crystals of spinel-type phase identifiable by electron diffraction and primary mullite crystals on the 10-30nm scale[7, 8]. Amorphous, Si-rich, material is also visible at this temperature, having developed from the metakaolin. At about 1100^0-1200^{0}C, spinel is lost and elongated mullite crystals up to 0.5μm long begin to develop. By 1300^{0}C, cristobalite begins to form from amorphous Si-rich phases, until eventually mullite and cristoballite are the only crystalline phases remaining in the body. The phases formed on firing illite group clays have been studied for many years, but there have been comparatively few studies of microstructural evolution in this material. Asero clay transformation sequences have been studied using techniques such as X-rays diffraction[9] (XRD), thermal analysis[10] and Scanning Electron Microscopy (SEM). The microstructural development on firing Nigerian clay has been assessed during thermal analysis, for Asero clay in Abeokuta for furnace lining.

2. Material and Methods

The geomorphology of the township, Abeokuta and its environs is made up of flat topped hills, escapements and lowlands. The hills geologically are the Olden granite masses and other rocks such as gneisses and migmatites, commonly referred to as crystalline basement or basement complex. These escapements are of cretaceous age. Alluvial terraces are well dissected by the Ogun River and where underlying rock is deeply weathered. The clay settlement is situated 9.6km east of Abeokuta. The site consists of a strip approximately 7.6km north to south by 2.0km east to west as shown in Figure 1. Approximately 10kg of clay was taken from the Asero clay deposit in Abeokuta, South West Nigeria. Chemical analysis of the raw material was performed using inductively coupled plasma atomic emission

spectroscopy (ICP-Varian Vista Pro ICP-AEP), where sample in the form of aqueous solutions were introduced as aerosols into plasma flame to produce characteristics emission of the sought elements. The loss on ignition was measured by calculating the wt% difference between unfired sample and after firing for 2hours 1000^{0}C. Table 1 shows the chemical composition of the raw materials in the form of oxides, together with the loss on ignition.

The crystalline and glassy phases in the fired sample were identified using an XRD instrument (Model PW 1700 series) automated powder diffractometer using CuK and radiation operating at 40KV and 40Ma from 5^0<2? <85^0 with step size 0.04 at the counting time of 2seconds. The XRD spectra were fed into a computer running a software (Siehilt) and interpreted by search and match method with the international centre for diffractometre data (ICDD) to identify the crystalline phases.

Asero clay was dried overnight in an oven at 100^{0}C, grounded to a fine powder in an agate mortar, moistened (10wt % water) and uniaxially pressed ~ 40Mpa for 60 seconds into 25mm diameter disks using laboratory hydraulics press model assemblages and morphologies, samples were ground and polished (only samples fired at ≥ 1000^{0}C were etched in 5% HF for 3minutes) and subsequently carbon or gold coated. Both SE (Secondary electron) and BSE (Base-scattered electron) images were obtained using an SEM (JSM 5000) equipped with energy dispersive spectroscope.

PHYSICAL PROPERTIES

Sample Preparation

Asero sample was dried in a drying oven at 110°C for 24 hours, then crushed with a jaw crusher and milled in a ball mill for 8 hours. The raw materials slips were removed from the ball mill and again dried at 110°C, ground in a mill to a particular size of ~1mm. Moisture was added by means of a spray gun to achieve a moisture content of ~5%. The sample was then screened through a 1mm sieve in order to break up the lumps and to obtain even distribution of the added moisture.

Pressing

Dry pressing is commonly used to produce ceramic particles thicker than 0.5mm. Stages of dry pressing include: filling of the die, compaction, shaping and ejection.

Approximately 8mm diameter die were pressed using a laboratory hydraulic press Model 15010. The desired pressure applied, 40 MPa was maintained for about 60 seconds to allow for particle rearrangement. Freshly compacted test specimen were measured, weighed, marked for further identification and dried in an oven type MOV 112 at 110°C overnight prior to firing. Dry shrinkage, fired shrinkage and total shrinkage of these samples was determined at various temperatures of 600, 700, 800, 900, 1000, 1100, 1200°C. A micrometer with accuracy of 0.01mm was used to measure the length of the samples directly after pressing, and the length of the dried samples. After firing at specific temperatures, the fired length for each temperature was measured. The formula for the calculation of dry shrinkage is:

$$\% DS = \frac{L_2 - L_3}{L_2} \times 100 \quad (1)$$

Where, DS = Dry Shrinkage

L_2 = length of sample directly after pressing (mm)

L_3 = length of dry pressed sample (mm)

The formula used for the calculation of the fired shrinkage at each temperature is:

$$\%TS = \frac{L_2 - L_4}{L_2} \times 100 \quad (2)$$

where, TS = Total Shrinkage

L_2 = length of sample directly after pressing (mm)

L_4 = length of fired sample at a specific individual temperature (mm)

Water Absorption

Water absorption measurements were carried out according to British Standard EN 99 (19 91). Fired pellets were soaked in boiling water in a beaker, and left to cool down to room temperature still soaked in water. Excess water was removed from the pellets surface using a moistened cloth prior to weighing. The wet weight (W_w) was then measured. Pellets were left drying in an oven at 110 ℃ overnight, and the dry weight was measured (W_d). Water absorption (WA) was computed as:

$$WA = \frac{W_w - W_d}{W_d} \times 100$$

As boiling water will penetrate open or interconnected pores of the specimen, the higher the water absorption the more porous is the material in terms of that specific type of porosity. Open pores are common in under fired stoneware, where not enough liquid has bee n produced to close the porosity of the ware on firing. In over fired specimens, gas escaping from inside the ware will create blistering on its surfaces.

Bulk Density

The bulk density of the fired samples was determined by water displacement using

Archimedes principle. The experimental set-up allows the weights of the beaker partially filled with water, with and without the pellet immersed in water, to be measured. The difference gives weight of water displacement, according to the Archimedes principle. The weight of water displaced can be easily related to the volume of water displaced, as the density of water is known. The volume of water immersing in the water using a precision balance. Thus, the bulk density (BD, g/cm³) is given in terms of sample mass (S_m) and the sample volume (S_v) as:

:

$$LS = \frac{D_d - D_f}{D_d} \times 100 \qquad (5)$$

The measurements were made using digital calliper. As the ceramic body densifies, it shrinks in all direction. The shrinkage along the disk diameter gave more results than that of the height.

Pressing Moisture

A representative batch of pressed test pieces were weighed (M2), dried at 110°C for 24 hours and then weighted (M1) again. The difference in mass was divided by the initial mass, multiplied by the initial mass, multiplied by the average pressing moisture of the sample is:

$$\%MC = \frac{M_1 - M_2}{M_2} \times 100$$

6)

Where, MC = moisture content

M1 = weight of the sample after drying

M2 = weight of the sample before pressing.

Moisture Expansion

Most fired clay materials exhibit irreversible expansion over a period of time as a consequence of moisture absorption from the atmosphere. This expansion is usually rapid during the early life of the material but slows down to a negligible value over a period of 5years.

3. Results and Discussions

The microstructural evolution on firing clays has been the subject of several recent studies[11-13]. Figure 5 reveals the porous microstructure of Asero clay, the iron seems to have re-distributed in the clay as a result of liquid formation on firing. Loss on ignition (LOI) of Asero clay was 8.43wt% (Table 1) compared to theoretical kaolinite clay that could lose 13.9wt% of its mass on ignition due to dehydroxylation with water release. This material dehydroxylated at around 100 ^{0}C, and the metakaolin formed began to break down at 520 ^{0}C, forming nanometer scale spinal crystals and a silica-rich liquid phase.

XRD of unfired Asero clay reveals that the major mineral is illite, with small quantities of kaolin, quartz present as accessory mineral as shown in figure 2.

Differential scanning calorimetric (DSC) analysis of the raw clay (Fig. 4) confirms the clay dehydroxylates to form metakaolin below 600^{0}C. An endothermic event occurs at ~520^{0}C and a spinel $A1_20_3$ phase is formed at ~963^{0}C. Bulk density, apparent density, percentage moisture content and apparent porosity were fired in oxidising atmosphere, shows the bulk density reached a maximum after firing at ~1100°C while apparent density remained unchanged at ~900-1000°C. Likewise, the percentage apparent porosity at ~900-1000°C followed by a decrease at 1200°C as in the works of Souza (2004) [13].

These results indicate the potential for using local raw materials for fire bricks, in furnace lining in Nigerian foundry works.

Conclusions

In the present study, the use of local clay from Asero from Abeokuta South West, Nigeria was investigated for the production of fire bricks for furnace lining. The clay was found to have moderate shrinkage 8-16%, the colour characteristics ranged from whitish brown to yellowish brown on firing. The SEM/BS image for the etched specimen of Asero clay reveals the presence of interlayer cations, encourages liquid formation which in turn influences the morphology in the final fired product.

Acknowledgements

This research at Imperial College London for Dr. Olokode O.S was supported by the Commonwealth Scholarships Commission programme. He gratefully acknowledges the Materials Department of Imperial College for providing the equipment used and extends his thanks to Mr. Richard Sweeney and Dr. Mahmood Adrakani for their experimental assistance.

References

1. P. B. Malla and L. A. Arrington-Webb, (1994). 'Properties and Characterisation of Porous Material Prepared by Hydrothermal Treatment of Kaolin: Better Ceramics through Chemistry VI', MRS Symp. Proc., 346, 475 – 480
2. M. S. Morsy, A. F. Galal, and S. A. Abo-El-Enein, (1998). 'Effect of Temperature on Phase Composition and Microstructure of Artificial Pozzolana-Cement Pastes Containing Burnt Kaolinite Clay', Cement Concr. Res., 28[8] 1157 –11 63.
3. P. Shelest, (1992) 'Refractories from Troshkov Clays for Lining Steel casting Ladles', Refractories, 33[3/4] 215 – 218.
4. F. Onike, G. D. Martin, and A. C. Durham, (1986).'Time-Temperature Transformation Curves for Kaolinite', Mater. Sci. Forum, 7, 73 – 82
5. Sonuparlak, M. Sarikaya, and I. A. Aksay, (1987). 'Spinal Phase Transformation during the 980°C Exothermic Reaction in the Kaolinite-to-Mullite Reaction Series', J.Am. Ceramics Soc., 70[11] 837 – 42
6. K. Srikrishna, G. Thomas, R. Martinez, M. P. Corral, S. De Aza, and J. S. Moya, (1998). 'Kaolinite-Mullite Reaction Series: A SEM/TEM Study', J. Mater. Sci., 25, 607 – 12 McConville, W. E. Lee, and J. H. Sharp, 'Microstructural Evolution in Kaolinite Powders and Dense Clay Bodies', Br. Ceramic Proc., 58, 75 – 92
7. J. McConville, W. E. Lee, and J. H. Sharp, (1998). 'Microstructural Evolution in Fired Kaolinite', Br. Ceramic Trans., 97[4] 162 –168
8. R. E. Grim, and W. F. Brandley, (1940). 'Investigation of the Effect on the Clay Minerals Illite and Montmorillonite', J.Am. Ceram. Soc., 23[8] 242 –248
9. S. J. Chipera, and D. L. Bish, (2002). 'Thermal Evolution of Fluorine from Smectite and Kaolinite', Clays Clay Miner., 50[1] 38 – 46
10. Y. Iqbal, and W. E. Lee, (2000). 'Microstructural Evolution in Triaxial Porcelain', J.Am Ceram. Soc., 83[12] 3121 – 3127

12 C. Y. Chen, G. S. Lan, and W. H. Tuan, (2000). 'Microstructural Evolution of Mullite during the Sintering of Kaolinite Powder Compacts', Ceram. Int., 26[7] 715 – 720

13 Souza, G.P. (2004). Microstructural variations in Porcelain Stoneware as a function of flux system. J. Am. Ceram. Soc. Vol. 87. Issue, 10pgs, 1959-1966.

Table 1.

Chemical Composition of Asero clay deposit (wt %) used

Raw Material	SiO_2	AI_2O_3	TiO_2	Fe_2O_3					
	MgO	CaO	Na_2O	K_2O	P_2O_5	LOI			
Asero clay	66.8	21.3	0.45	2.94	0.07				
	0.08	0.02	0.45	0.06	8.43				

Table 2

Shrinkage test for Asero clay deposit in Abeokuta South-West, Nigeria.

Temperature °C	Ajebo clay					
	Original diameter (mm)	Dry Shrinkage (mm)	Fixed length (mm)	% Dry fired Shrinkage	% Wet Dry Shrinkage	Total Shrinkage
600	8	7.6	7.30	7.54	10.29	9.0
700	8	7.94	7.23	7.62	10.40	10.0
800	8	7.80	7.09	7.76	10.60	11.5
900	8	7.76	7.06	7.67	10.48	12.0
1000	8	7.62	6.97	7.58	10.35	13.0
1100	8	7.66	6.78	7.49	10.22	15.0
1200	8	7.20	6.65	7.38	10.01	17.0

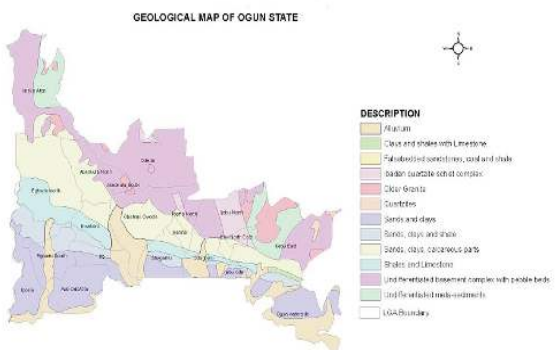


Figure 1.
Geocal locations of minerals (Asero clay deposit) in South-West Nigeria (Abeokuta).

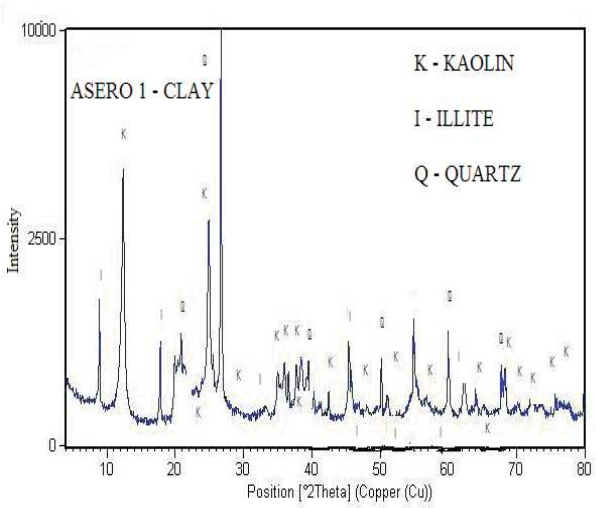


Fig 2.

XRD traces of the untreated Asero clay from Nigeria.

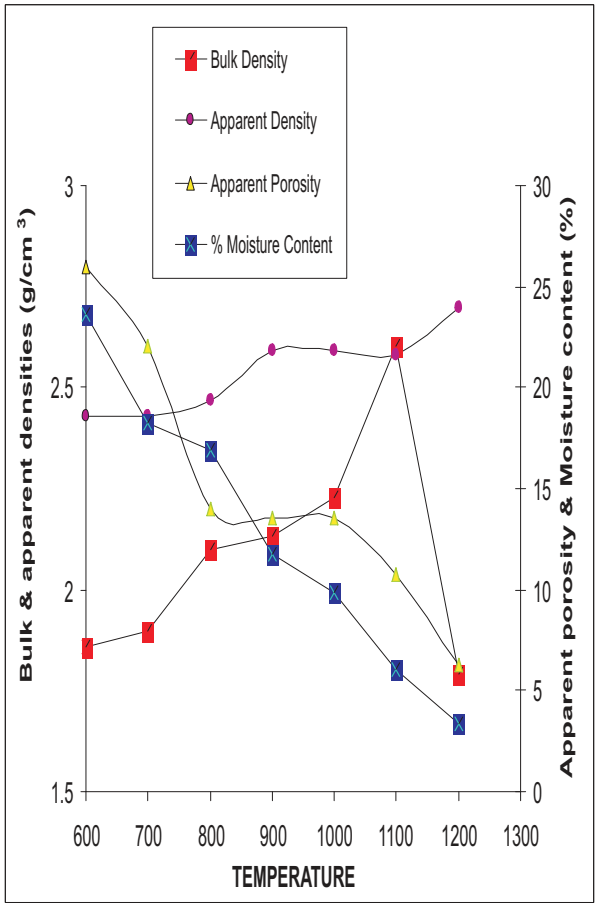


Figure 3.
Bulk density, apparent density, Percentage moisture Content, and apparent p orosity as a function of firin g temperature.

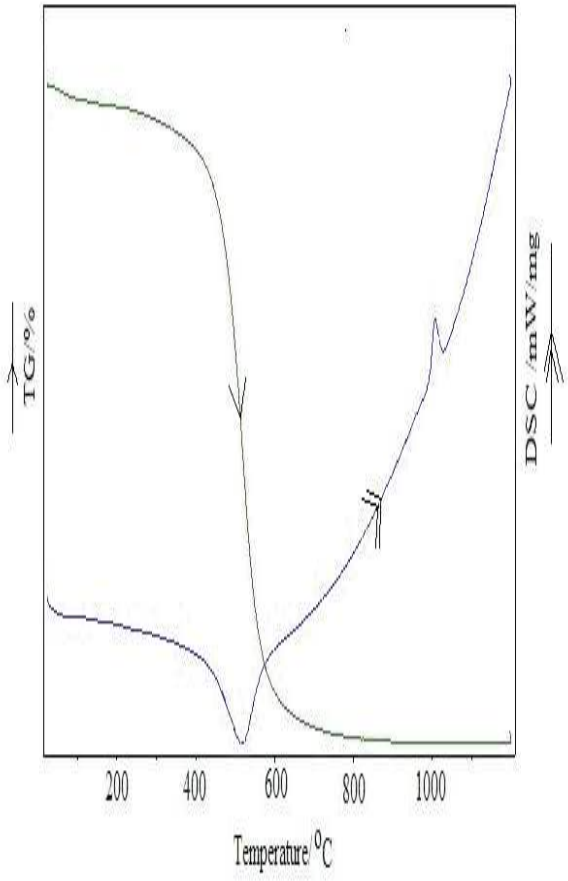
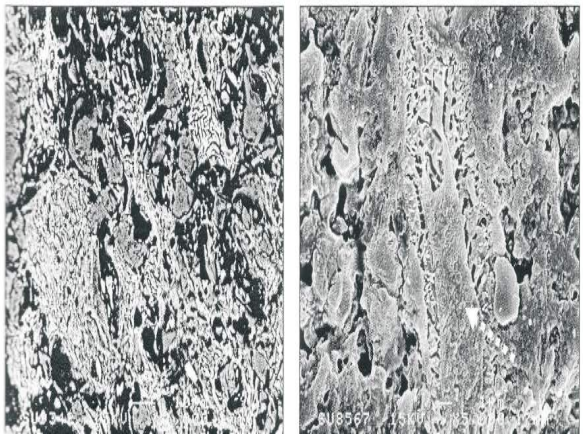


Figure 4.
Thermogravimetric analysis/Differential scanning calorimetric TG/DSC of Asero raw clay from Abeokuta, Ogun-State.

900^0C
1100^0C

Figure 5.



SEM/SE images of Asero clay cross sectioned fired at 900 - 1100^0C.

PERFORMANCE EVALUATION OF BLOWERS OF DIFFERENT IMPELLER/VANE PROFILES

Oyelami A.T.[1], Adejuyigbe S.B.[2], Waheed M.A.[2], Ogunkoya A.K.[1] and Iliya D.[1]
[1]Engineering Materials Development Institute, P.M.B 611 Akure, Ondo State, Nigeria
[2]Department of Mechanical Engineering, University of Agriculture, Abeokuta, Nigeria
All Correspondences to: **atoyelami@yahoo.com**

ABSTRACT
Centrifugal blowers which utilize **radial-flow impellers were designed and developed. Different designs of two of the most important parts of the blower – the impeller and the volute casing – were done and their operational performances evaluated.** In all the designs, fluid enters the inlet port at the center of the rotating impeller which is the suction eye. As the impeller spins, it thrusts the fluid outward radially, causing centrifugal acceleration. As it does this, it creates a vacuum in its wake, drawing even more fluid into the inlet. The volute casing performs the function of slowing the fluid and increasing the pressure. The impeller, driven by the blower shaft adds the velocity component to the fluid by centrifugally casting the fluid away from the impeller vane tips. The amount of energy given to the fluid is proportional to the velocity at the edge or vane tip of the impeller. Whereas two designs of the volute casings done were essentially the same, differing only on the direction of impelling; seven different impellers were designed and developed. The differences in the impeller designs are not only attributable to the vane profile but also on whether the impeller is open or close. The designed and developed closed-impellers include backward and forward curved vanes while the open-impellers comprise of backward and forward curved; backward and forward inclined; and radial vanes. The performance evaluation carried out with the aid of an anemometer revealed that the closed impeller with backward curved vanes has the best performance cum efficiency with respect to the output speed and flow rate.

Keywords: *Centrifugal Blower, Impeller, Volute Casing, Suction Eye, Vane, Anemometer*

1.0 Introduction

The principle involved in the design of a blower is similar in virtually every important aspect as that of a centrifugal pump except for the fact that the term "centrifugal pump" is often associated with liquid as its working fluid while the blower is meant to work on air (Edward, H.S. 1995). The blower can therefore be described as a device, which converts 'driver' energy to kinetic energy in a fluid by accelerating it to the outer rim of a revolving device known as an impeller. The impeller is always placed directly onto the shaft of the Suction Motor so that it spins at a very high speed. The effects of centrifugal force acting upon the spinning air within the impeller create the suction. As the impeller rotates, the spinning air moves outward away from the hub, creating a partial vacuum which causes more air to flow into the impeller. The impeller is often considered an integral part of the suction motor since it, the impeller housings and the motor are assembled as a unit.

The impeller, driven by the blower shaft adds the velocity component to the fluid by centrifugally casting the fluid away from the impeller vane tips. The key idea here is that the energy created is *kinetic energy*. The amount of energy given to the fluid corresponds to the velocity at the edge or vane tip of the impeller. Addison (1995) established that the faster the impeller revolves or the bigger the impeller is, the higher will be the velocity of the fluid at the vane tip and the greater the energy imparted to the fluid.

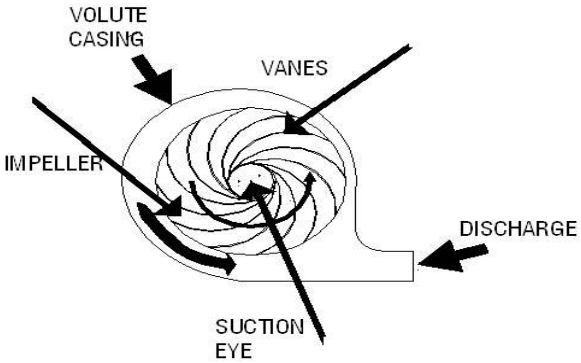


Figure 1: Sectional drawing of a blower

Figure 1 illustrates a cross-section of the blower designed. Fluid enters the inlet port at the center of the rotating impeller, or the suction eye. As the impeller spins in a counter-clockwise direction, it thrusts the fluid outward radially, causing centrifugal acceleration. As it does this, it creates a vacuum in its wake, drawing even more fluid into the inlet. Centrifugal acceleration creates energy proportional to the speed of the impeller (Csanady 1981). The faster the impeller rotates, the faster the fluid movement and the stronger its force. Impellers are the rotating blades that actually move the fluid. They are connected to the drive shaft that rotates within the blower casing. The impeller is designed to impart a whirling or motion to the air in the blower

2.0 The Impeller

As the impeller rotates, it creates vacuum at its inlet suction side through centrifugal force. In turn, the impeller creates a positive pressure, inducing a force of air on the discharge side. Impeller is the most important part of the blower components because of the fact that its performance inadvertently determines the blower's performance. An impeller is essentially a disk shaped structure with vanes that create the actual suction in a blower. The impeller is always placed directly onto the shaft of the electric motor so that it spins at a very high speed. The effects of centrifugal force acting upon the spinning air within the impeller create the suction. As the impeller rotates, Von Cube and Steimle (1981) confirms that the spinning air moves outward away from the hub, creating a partial vacuum which causes more air to flow into the impeller. The most important impeller parameters can be grouped into three categories:

- Geometrical Parameters: Tip diameter, hub diameter and tip width;
- Operating conditions: Inlet total pressure, inlet total temperature and fluid density;
- Performance characteristics: mass flow parameter, pressure ratio and specific speed.

3.0 Technical Performance Data

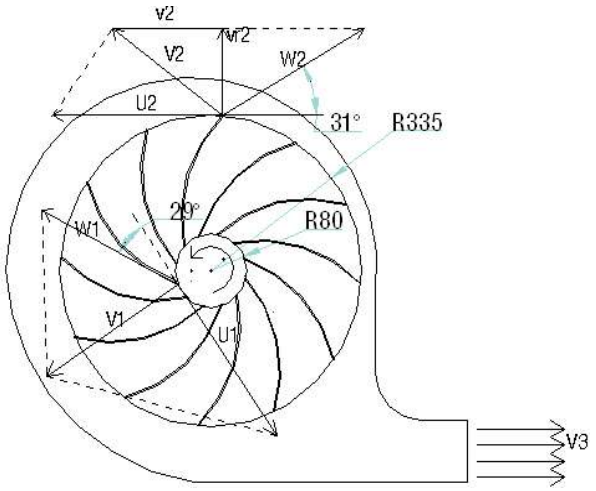


Figure 1: Impeller cross-section in the blower volute's casing showing the velocity diagrams

Figure 2 shows the velocity triangle of the air flow leaving the impeller. Since there are no inlet guide vanes, the entering flow has no tangential component of motion. The entering flow is therefore in radial direction, and v_{r1} which is the radial component of the absolute velocity is the same as the inlet velocity, V_1.

That is $v_{r1} = V_1$.

It is assumed that the flow is completely guided by the blades and that the flow angles coincide with the blade angles.

Inlet Vane Angle

$\beta_1 = 29^0$

Outlet Vane Angle $\beta_2 = 31^0$

Volute Inside radius r_1=0.08m

Volute Outside radius r_2=0.335m

Vane Width at the Suction Eye b_1=0.0355m

Vane Width at the tapered end b_2=0.024m

Rotational Speed N=3430rpm

Linear Speed at the inlet is

$$U_1 = r_1\omega = \frac{2\pi \times 3430 \times 0.08}{60} = 28.74 m/s$$

$$V_1 = v_{r1} = U_1 \tan\beta_1 = 28.74 \tan 29 = 15.93 m/s$$

The expected flow rate is

$$\dot{Q} = 2\pi r_1 b_1 v_{r1} = 2\pi \times 0.08 \times 0.0355 \times 15.93 = 0.2842 m^3/s$$

Applying continuity concept at the blower discharge

$$V_3 = \frac{\dot{Q}}{A_3} = \frac{0.2842}{0.134 \times 0.134} = 15.83 m/s$$

Applying Bernoulli equation between the room and blower discharge at 3,

$$\frac{P_{atm}}{\rho g} + (\Delta h_t)_{1\to 2} = \frac{P_{atm}}{\rho g} + \frac{V_3^2}{2g}$$

where

V_3 = the discharge velocity

$\dot{Q}$ = Fluid flow rate

A_3 = Cross-sectional area at the discharge end

P_{atm} = Atmospheric pressure

$(\Delta h)_{1\to 2}$ = The total head change

ρ = Air density

g = acceleration due to gravity

The total head change imparted to t he flow by the blower is then

$$(\Delta h_t)_{1\to 2} = \frac{V_3^2}{2g} = \frac{15.83^2}{2 \times 9.81} = 12.77 m$$

But $(\Delta h_t)_{1\to 2} = \dfrac{U_2 v_{\theta 2} - U_1 v_{\theta 1}}{g}$ (Alan M. 1979)

Where v_θ is the tangential component of the fluid absolute velocity

Since the flow enters radially, $v_{\theta 1} = 0$,

$$v_{\vartheta 2} = \frac{(\Delta h_t)_{1\to 2}}{U_2}$$

Where v_θ is the tangential component of the fluid absolute velocity

Since the flow enters radially, $v_{\theta 1} = 0$,

$$v_{\vartheta 2} = \frac{(\Delta h_t)_{1\to 2}}{U_2}$$

Where

$$U_2 = r_2\omega = \frac{2\pi N}{60} r_2 = \frac{2\pi \times 3430}{60} \times 0.335 = 120.33 m/s$$

$$v_{r2} = \frac{\dot{Q}}{2\pi r_2 b_2} = \frac{0.2842}{2\pi \times 0.335 \times 0.024} = 5.625 m/s$$

$$\tan\beta_2 = \frac{v_{r2}}{U_2 - v_{\theta 2}}$$

$$v_{\theta 2} = U_2 - \frac{v_{r2}}{\tan\beta_2} = 120.33 - \frac{5.625}{\tan 31} = 110.97 m/s$$

$$V_2 = \sqrt{v_{\theta 2}^2 + v_{r2}^2} = \sqrt{110.97^2 + 120.33^2} = 163.69 m/s$$

The power input to the blower is

$$P = \rho \dot{Q} gh = 1.239 \times 0.2842 \times 9.81 \times 12.77 = 44.11 W$$

4.0 Methodology

Apart from dimensions and materials used for construction, what essentially differentiate two impellers from each other are:

1. Shape / Profile of the Vane
2. Presence / Absence of Guiding Vanes
3. Whether the impeller is closed or open

Since the aim of this work is to evaluate performance of blowers of different impeller/vane profiles, seven different possibilities of impeller designs were explored. They all had same base-plate dimensions without guiding vanes. These include

1. Backward-Curved-Vane Open Impeller
2. Forward-Curved-Vane Open Impeller
3. Backward-Curved-Vane Closed Impeller
4. Forward-Curved-Vane Closed Impeller
5. Backward-Inclined-Vane Open Impeller
6. Forward-Inclined-Vane Open Impeller
7. Radial-Vane Open Impeller

(See Plates 1 – 4)

Two volute casings were constructed to allow for clockwise and anticlockwise rotation of the impellers (Figures 3 – 5 and Plates 5 – 6). Each of the impellers was subjected to dynamic balancing (Plate 7) where out-of-balance mass was added to ensure stability and minimize vibration (Plate 8)

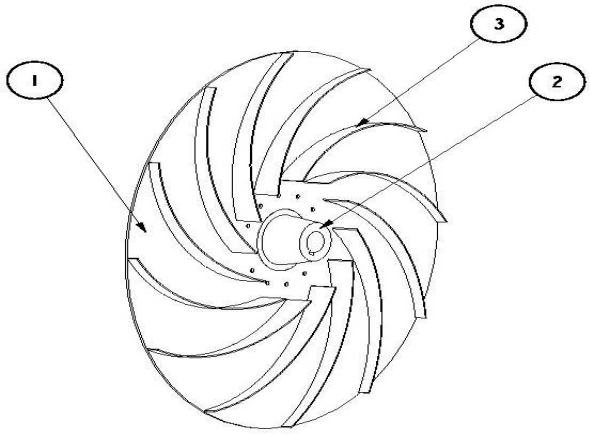


Figure 1: 3D Drawing of Backward -Curved-Vane Open Impeller

[1) base-plate; 2) Backward -Curved-Vane; 3) Coupler

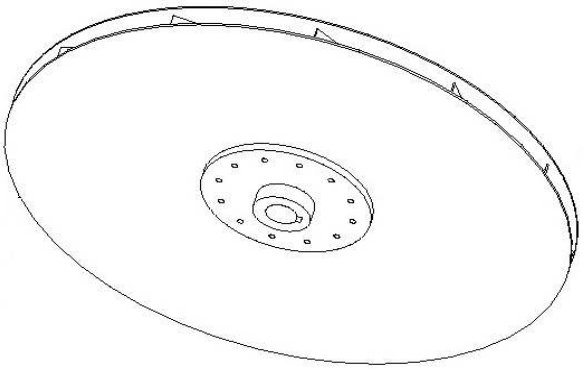


Figure 1: 3D Drawing of Backward-Curved-Vane Closed Impeller

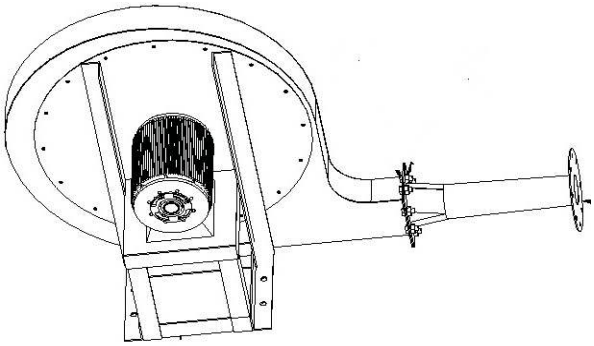


Figure 1: 3D Assembly Drawing of the developed Blower



Plate 1: Forward-Inclined Impeller under Construction



Plate 1: Backward Curved Impeller under Construction



Plate 1 : Radial Impeller under Construction



Plate 1 : Newly constructed Backward Curved Closed Impeller



Plate 1: Anti-Clockwise Volute Casing under Construction



Plate 1: Clockwise and Anti-Clockwise Volute Casings under Construction

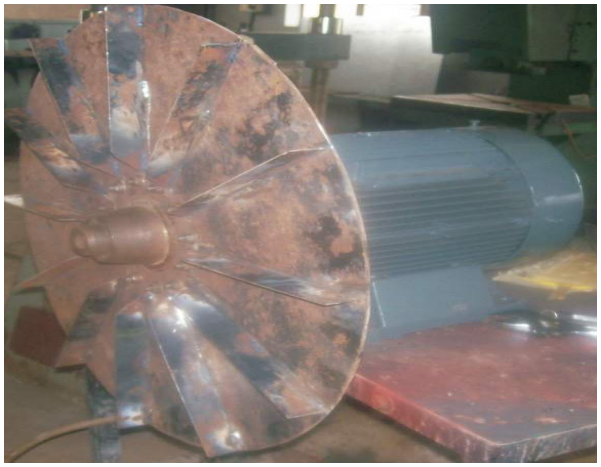


Plate 1: Radial Impeller undergoing Dynamic Balancing



Plate : Out-of-Balance Mass added for Impeller Dynamic Balance



Plate 1: Blower being assembled for Test Running



Plate 1: Anenometer - used for Blower Performance Characterization (for measuring Airflow, Temperature, Relative Humidity and Air Velocity)



Plate 1: Blower Performance being measured at a distance x



Plate 1: Blower Performance being measured at a distance y



Plate 1: Blower Performance being measured at a distance z

1.1 5.0 ***Results and Discussions***

As previously explained, impeller is the most important part of the blower components because of the fact that its performance inadvertently determines the blower's performance. It is the impeller's vanes that create the actual suction in a blower. The effects of centrifugal force acting upon the spinning air within the impeller create the suction. As the impeller rotates, the spinning air moves outward aay from the hub, creating a partial vacuum which causes more air to flow into the impeller. The impeller speed, which determines the suction rate, was measured at different points, for different vane types/ profiles, from the outlet/discharge of the blower and the results are as shown in Table 1. The measurements were done with the aid of an Airflow Anenometer (see plates 10 – 13). The graph showing Blower Speed

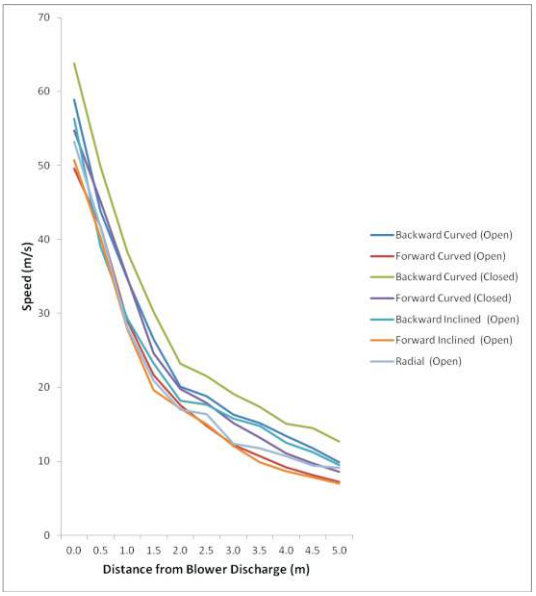


Figure 6: Blower Speed Variations with different types of Impeller

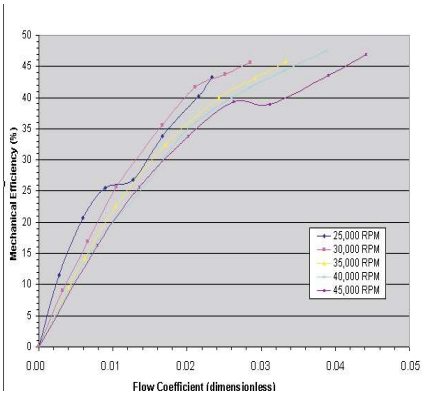


Figure 1: Variation of Blower Mechanical Efficiency with Flow Coefficient for different RPMs

Figure 7: Variation of Blower Mechanical Efficiency with Flow Coefficient for different RPMs

Table 1: Blower Performance Characteristics

S/N	Vane Type	Vane Profile	Impeller Type	0m	0.5m	1m	1.5m	2.0m	2.5m	3.0m	3.5m	4.0m	4.5m	5.0m
1.	Backward Curved		Open	58.9	43.8	34.7	26.5	20.1	18.8	16.3	15.2	13.4	11.8	9.9
2.	Forward Curved		Open	49.6	41.8	29.0	21.7	17.6	14.8	12.2	10.7	9.2	8.1	7.2
3.	Backward Curved		Closed	63.8	49.9	38.3	30.2	23.2	21.5	19.1	17.4	15.1	14.5	12.7
4.	Forward Curved		Closed	54.7	45.2	34.8	24.6	19.8	17.9	15.2	13.2	11.1	9.7	8.6
5.	Backward Inclined		Open	56.3	39.1	29.3	23.3	18.2	17.7	15.8	14.8	12.5	11.2	9.5
6.	Forward Inclined		Open	50.7	40.3	27.9	19.6	17.1	15.0	12.1	9.9	8.7	7.8	7.0
7.	Radial		Open	53.2	41.7	28.1	20.9	17.0	16.4	12.4	11.8	10.7	9.4	9.1

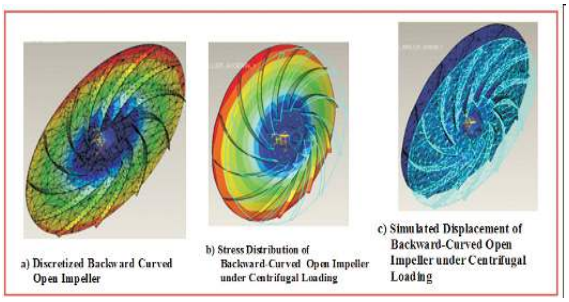


Figure 8: Failure Analyses of the Developed Impellers

6.0 Sources of Blower Failures/Poor Performance

There are generally four reasons why a blower will not perform optimally. These reasons can be categorized into four. They are Vibration, Lack of Performance, Excessive Noise and Premature Component Failure (Edward, H.S. 1995).

6.1 Vibration

There are generally eight sources of vibration in a blower. These are summarized thus:

1. Material build-up on the wheel.
2. Loose mounting setscrews, bearings, bolts, or couplings.
3. Misalignment or excessive wear of belts coupling or bearings.
4. Bent shaft.
5. Material build-up on the wheel.
6. Excessive system pressure or restriction of airflow due to closed dampers.
7. Inadequate structural support or mounting.
8. Externally transmitted vibration.

6.2 Lack of Performance

The general reasons for lack of performance of a blower are:

1. Incorrect system design calculation or testing procedures.
2. Incorrect blower RPM.
3. Blower wheel rotating in wrong direction - check motor leads.
4. Improper wheel to inlet cone clearance.
5. Inlet or discharge air leaks, clogged filters, coils or damper settings.

6. System effect due to improper inlet or discharge connection.

6.3 Excessive Noise

The various causes of noise during a blower's operation are

1. Fan operating near "stall" due to incorrect system design or installation.
2. Vibration originating elsewhere in the system.
3. System resonance or pulsation.
4. Improper location or orientation of fan intake and discharge.
5. Inadequate or faulty design of supporting structures.
6. Nearby sound reflecting surfaces.
7. Loose accessories or components.
8. Worn bearings.

6.4 Premature Component Failure

Component failure will occur due to any of the following causes:

1. Abrasion or corrosion of internal fan components.
2. Vibration due to Impeller out of balance.
3. Lack of lubrication of bearings.
4. Misalignment or power transmission components or bearings.
5. Bearing failure from incorrect or contaminated lubricant or grounding through the bearings while arc welding.
6. Extreme ambient or air-stream temperatures.

7.0 Conclusion

The performance evaluation of the developed blower with different impeller/vane profiles revealed that:

- the performance differences in the seven (7) impeller designs are not only attributed to the vane profile but also on whether the impeller is open or close.
- the closed impeller with backward curved vanes has the best performance cum efficiency with respect to the output speed and flow rate.

Therefore, the data obtained can serve as a tool in selecting blower design type for different applications.

8.0 References

Addison, H. 1995. *Centrifugal and other Rotordynamic Pumps, 2nd ed., Chapman & Hall, London, England*

Alan, M. 1979. Engineering Fluid Mechanics McGraw-Hill Int. Book Co., Auckland, New Zealand.

Budynas- Nisbett 2006. Shigley's Mechanical Engineering Design. 8th Edition, McGraw- Hill Primis, U.S.A.

Csanady G.T, (1964) *Theory of Turbomahines,* McGraw-Hill, New York.

Dryden, I.G.C. 1982. The Efficient Use of Energy. Butterworth, Surrey, England

Horlock, J.H. 1984. Axial Flow Compressors. Butterworths, London, England.

Edward, H.S. (1995) *Mechanical Engineers Reference Book,* 12th Edition, The Bath Press, Bath, Great Britain.

Oyelami, A.T., and Adejuyigbe, S.B. 2006. The design of a radiation-recuperative heat exchanger for a 200kg capacity rotary furnace. AU J.T. 10: 100-4

Tuton, R.K. 1984. Principles of Turbo-machinery. S & FN Spon, London, England.

Von Cube, H.L.; and Steimle, F. 1981. Heat Pump Technology. Butterworth, London, England.

http://www.engineeringpage.com (2005)

http://www.fanair.com (2006)
http://www.flowmetric.com/products/ (2006)

DEVELOPMENT OF SPIN – CASTING MACHINE FOR PRODUCTION OF NANO-STRUCTURED PARTS

O. Olaniran, B.O. Adewuyi and J.O. Borode
Department of Metallurgical and Materials Engineering Federal University of Technology, Akure.
dayo525@yahoo.com

ABSTRACT
Nanostructure is the characteristic appearance of materials of less than 100nm in size. There are basically three methods of achieving this nano-structured materials; transforming the whole bulk into nano-crystalline structure, transforming the surface into nano-crystalline structure and deposition of nano-crystalline structures on a base material. This research will therefore center on the first method; transforming the whole bulk into nano-crystalline structure by spin-casting process. The procedures include designing and fabrication of a casting machine for producing machine parts of high integrity. Close tolerance nano-structured parts can be achieved by spin casting process that uses centrifugal force to produce highly detailed castings in a variety of technical grade materials. Almost any part that is designed for other casting processes can be produced by spin casting process in an inexpensive timely fashion. Casting finds wide applications as it enables production of parts from a few grams to hundreds of tons and with dimensions up to tens of meters to be manufactured from alloys of practically any composition, including those which are difficult to shape by plastic working. The theory and practice of metal casting at the modern stage permit the manufacture of articles with high working properties. This is evidenced by reliable casting operation in jet engines, nuclear power plants, space crafts and other critical machines and installations. Spin casting in other words is a precision casting process producing high integrity, close tolerance parts comparable to die casting or plastic injection techniques.
Key words: Nano-structure, fabrication, spin-casting, nano-crystalline and centrifugal force.

INTRODUCTION

Macrostructure is the appearance and physical arrangement as observed with the naked eye or with a low power magnification. Microstructure on the other hand is the characteristic appearance and physical arrangement of material as observed with a microscope [6]. Naturally these two groups of characteristics are closely related with each other and knowledge of both is essential for a full understanding of any materials. Micrography concerns itself with the smallest characteristics directly observable with optical assistance; macrography deals with conditions in the massive range within the scope of unaided or slightly aided observation.

Nanostructure is the characteristic appearance of materials of less than 100nm in size [1]. There are basically three methods of achieving this nano-structured materials; transforming the whole bulk into nano-crystalline structure, transforming the surface into nano-crystalline structure and deposition of nano-crystalline structures on a base material. This research will therefore center on the first method; transforming the whole bulk into nano-crystalline structure by spin-casting process.

Most casting methods require machining and cutting operations which could be very expensive. These operations result in material wastage and losses thereby increasing the production cost. These are considerably taken care of in spin casting operation. The procedures include designing and fabricating of a casting machine for producing machine parts. High integrity, close tolerance parts can be achieved by spin casting process that uses centrifugal force to produce highly detailed castings in a variety of technical grade materials. As a prototype and short run manufacturing procedure, it has few application limitations. Almost any part that is designed for other casting processes can be produced by spin casting process in an inexpensive timely fashion.

In machine building, instrument making, civil engineering and other branches of the national economy, various metal articles and semi finished products are manufactured by hot or cold plastic working, machining, pressing and sintering of powders (powder metallurgy), welding and casting. Castings are produced by pouring the superheated molten metal of the specified composition into a mould whose internal space (impression) reproduces the configuration and dimension of the future cast article with maximum accuracy [2]. On cooling, the metal solidifies and acquires the configuration of the mould. Most of the metal working processes involve an intermediate stage of producing cast articles (or ingots). This shows that casting is an efficient method of making articles of desired metal, with low expenditures of energy, materials and labour.

Casting finds wide applications as it enables production of parts from a few grams to hundreds of tons and with dimensions up to tens of meters to be manufactured from alloys of practically any composition, including those which are difficult to shape by plastic working. The theory and practice of metal casting at the modern stage permit the manufacture of articles with high working properties. This is evidenced by reliable casting operation in jet engines, nuclear power plants, space crafts and other critical machines and installations. Spin casting in other words is a precision casting process producing high integrity, close tolerance parts comparable to die casting or plastic injection techniques [2]. It is a simple, cost effective alternative for prototyping.

COMPUTER AIDED DESIGN OF A SPIN CASTING MACHINE

A spin casting machine is designed by the use of computer termed 'computer aided design'[5] defined Computer-Aided Design (CAD) as the use of computer system to assist in the creation, modification, analysis or optimization of a design. According to Wikipedia encyclopedia, CAD is the use of computer technology to aid in the design and especially, the drafting of a part of a product. It is both visual and symbol-based method of communication whose conventions are particular to a specific technical field. Drafting is the integral communication of technical drawings. CAD is used in the design of tools and machinery used in the manufacture of components and in the drafting and design of industrial structure. The designed spin casting machine is in fig. 1. below.

MATERIALS AND METHOD

The selection of materials for use in any engineering application depends on the appropriate mechanical properties that are peculiar to the service which such materials are subjected to. In this design, low alloy (carbon) steel was used for the fabrication of the components machine prototype. Other components include, electric motor with reducing gear (low speed, 220V, 3 core), Variable speed resistor, bearings (2Nos) odometer, industrial belt, nuts and screws.

FABRICATION OF A SPIN CASTING MACHINE

The fabrication of the spin casting machine was done by electric arc welding, after which assembling of the various components was done to make the spin-casting machine as shown in figure 3. The machine consists of a mould compartment supported by a plate, which is allowed to rotate freely about its axis. An electric motor is mounted on the other side of the table with an industrial belt to connect with the shaft carrying the mould compartment. The pulleys are fixed on the shaft carrying the mould compartment. The variable speed resistor provides speed variation and /regulation such that the speed of rotation could be varied. The pulleys are fixed on the shaft and the electric motor to control the speed of rotation when connected to electricity source. The shafts are fixed into bearings to prevent wobbling [6 & 7]. Various components of the spin casting machine are shown in the exploded diagram, figure 2.

DESIGN CALCULATION

The variance in the diameter of the groove apart from the speed regulator can also be employed in order to achieve varying motor speed, it implies that the speed varies as the diameter, hence the use of the following expression

$n_1 d_1 \gamma = n_2 d_2$

Where n_1 is the speed of electric motor = 1420rpm

n_2 is the speed of the main shaft

d_1 is the diameter of the driving pulley on the electric motor shaft = 550mm

d_2 is the diameter of the driven pulley on the main shaft

d_{2a} = 650mm, d_{2b} = 960mm, d_{2c} = 1350mm and

γ is the safety factor constant = 0.9 (chua et al,1998)

For case A

Speed of pulley A =

$$\frac{n_2 d_1 \gamma}{d_{2a}}, \frac{1200 \times 550 \times 0.9}{594} = 1000\text{rpm}$$

For case B

Speed of pulley B =

$$\frac{n_2 d_1 \gamma}{d_{2b}}, \frac{1200 \times 550 \times 0.9}{848} = 700rpm$$

DETERMINATION OF HOPPER VOLUMETRIC FLOW RATE

In the determining the volumetric flow rate of the ceramic hopper the principle of fluid flow as stated by the Torricelli theorem is expressed mathematically as follows:

$$V_x = c\ \sqrt{2gh}$$

Where

V_x = velocity of the fluid at point of exit

C = discharge coefficient due to change in cross sectional area into the orifice.

g = gravitational acceleration=9.8m/s

h = vertical liquid height

Volumetric flow rate Q = A x V……from law of continuity

Where

A = cross sectional area o section in consideration

V = velocity of the fluid in section in consideration

$A_c V_c = A_{cy} V_{cy}$

Ac = area of conical section of hopper, πrl where l = r + h

A_{cy} = area of cylinder section of hopper,

V_c = velocity of fluid in conical section of hopper

V_{cy} = velocity of fluid in cylindrical section of hopper

Velocity of fluid at the end of cylindrical section determines the nature of flow, i.e. whether turbulent, laminar or transient.

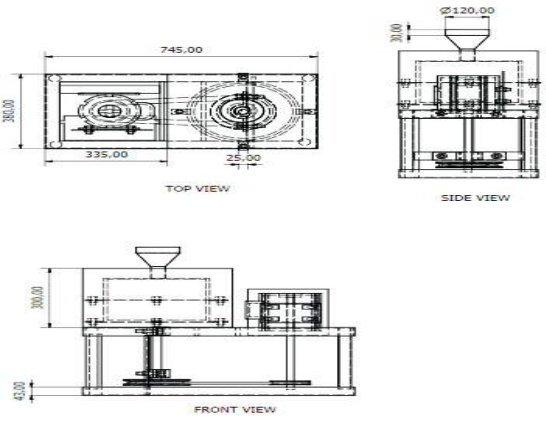


FIG.1: DESIGN OF A SPIN CASTING MACHINE

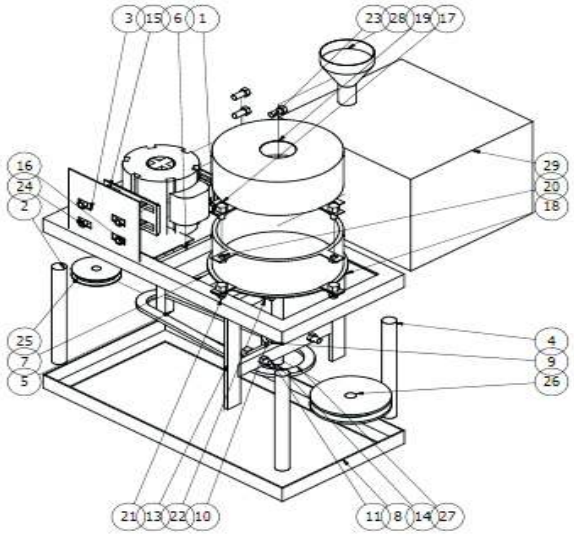


FIG. 2: EXPLODED VIEW OF THE SPIN CASTING MACHINE



FIG. 3: FABRICATED SPI N CASTING MACHINE

Table 1: Components of a Spin Casting Machine

S/N	COMPONENT	S/N	COMPONENT
1	Hook	8&9	Angle bar
2	Angle bar	10	Bearing
3	Motor screw	11&12	Nut
4	Motor screw	13	Bar
5	Industrial belt	14	
6	Angle bar	115	
7	Drag support	16	

REFERENCES

1 Adejuyigbe, S.B CAD/CAM for Manufacturing, TOPFUN Publication Akure, Nigeria, Pp 12- 15. (2008):

2 Adewuyi B.O., **Olaniran O.** and Olaseinde O.A., Research and Development in Nanotechnology – Application and Implication of the New Technology on the Society. A review Journal of Engineering Science and Technology. V2 N4, 48-52, (2007).

3 Anahim L.R, Typical Tekast System, www.tekast.com (2007).

4 Froes, F.H., Suryanarayana C., Guo-Hao Chen, Abdulbaset Frefer and Garrett R. Hyde, Nanostructure Processing for Titanium-Base Materials, The Journal of The Minerals, Metals & Materials Society, Vol. 44 No 5, 26-28, (1992).

5 Kalpakjan Serope and Steven R. Schimid. Manufacturing Engineering and Technology, 5th edition, Pearson, ISBN 0-13-148965-8; Pp108-124, (2006):

6 Mikhailov A.M. (1987): Metal casting, Mir publications Moscow; Pp58-70.

7 **Olaniran O.**, Adewuyi B.O. and Aribo Sunday, Development of Rapid Solidification Casting Machine for Ball Production, Proceedings of the Nigerian Metallurgical Society's 25th Annual Conference, Nigerian Metallurgical Society, (74-78), (2008).

STRENGTH CLASSES OF SOME COMMON NIGERIAN TIMBER SPECIES

I. ABUBAKAR[1], J. M. KAURA[1] AND S. DAHIRU[2]
[1]Department of Civil Engineering, Ahmadu Bello University Zaria
[2]Department of Civil Engineering Technology, Nuhu Bamalli Polytechnic Zaria
jdanbala@yahoo.co.uk, salisudahiru@ymail.com

ABSTRACT

The grade determining properties (density, modulus of elasticity and bending strength) of some common timber species in Nigeria, were presented in this paper. The properties were adjusted to 12% moisture content in order to comply with the Eurocode 5 (2004) and EN 338 (2008) requirements. 18% moisture content adjustment was also made in order to generate data that suit the Nigerian Environmental condition according to the Nigerian Code of Practice for Permissible Stress Design of Timber Members (NCP2, 1973). The tested species were Alstonia Boonei (Ahun), Triplochiton Scleroxylon (Arere), Terminalia Ivorensis (Idigbo) and Terminalia Superba (afara). The moisture content, density, modulus of elasticity and bending strength were determined according to the relevant on EN standard procedures. The density, moisture content, bending strength and modulus of elasticity varied significantly as indicated by their coefficients of variations. Least square regression models were established for the prediction of the bending strength and modulus of elasticity, once the density of the species at 12% is established. Each specie was assigned to an appropriate strength class based on its bending strength and modulus of elasticity at 12% moisture content. Alstonia Boonei was assigned to strength class C16, Triplochiton Scleroxylon to strength class C14, Terminalia Ivorensis to strength class C22, and Terminalia Superba to strength class C30.

INTRODUCTION

The knowledge of wood mechanical properties is of primordial importance for its selection and application in the various domains of engineering. The knowledge of the mechanical properties allows the characterisation of material behaviour when submitted to mechanical solicitations.

The Eurocode 5 is a new design code for timber structures in Europe, that replaced BS 5268. To use a particular timber specie in the design of timber structures based on the Eurocode 5, the strength class of the specie is required based on EN 338 (2008). In the determination of the strength class, the density, bending strength and modulus of elasticity have to be established. These are know as the grade determining properties (Antti et al, 2006; Ravenshorst et al, 2004; Ridley-Ellis et al, 2008; Baltrusaitis and Pranckevocene, 2003; JCSS PMC, 2006). Most timber usage in Nigeria, is on roof truss fabrication. There is the need to properly classify the timber species in Nigeria in order to use Eurocode 5, for Engineered design, since British standard have for long been the reference standard in Nigeria. Alstonia Boonei, Triplochiton Scleroxylon, Terminalia Ivorensis and Terminalia Superba are among the most commonly used timber species in Nigeria for roof truss pubrication (Lucas et al, 2006; Akindele, 2003; RMDC, 1998). In this paper the grade determining properties of these timber species are presented along with the appropriate strength classes based on EN 338 (2008).

PREPARATION OF TEST SPECIMEN

Procedures in accordance with International Standard Organisation (ISO) 3129 (1975) and ISO 3349 (1975) standard were followed to prepare test specimens. The sample boards for each specie were sawn into 50 mm x 75 mm x 1500 mm. Support and load position were marked and arrive at 1350 mm between supports living 75 mm overhang on each side of the beams. Third points between the supports were marked as the load points. These specimens are used for the bending tests.

DETERMINATION OF PROPERTIES

Density

Wood density is often considered to be the single most important wood property because of its strong influence on the quality of a wide range of solid wood and fiber products and has as such, received the most attention

(Cown et al, 2002). Bunn (1981) states that "density is probably the most important intrinsic wood property for most wood products", while Bamber and Burley (1983) point out, "of all the wood properties, density is the most significant in determining end use". Similarly, Zobel and van Buijtenen (1989) states that "density largely determines the value and utility of wood and overshadows the importance of other wood properties". However, the importance of density as an indicator of wood of wood quality alone is debatable because variability is due to many intrinsic factors, defects and variations inherent in basic wood structures. The density was obtained using the air dry volume and air dry and oven dry weight of each specimen. The density of samples are determine using equations1.0 and 2.0.

$$\text{Wet density } \rho_b = \frac{m_u}{V} \quad (1.0)$$

$$\text{Dry density } \rho_d = \frac{m_o}{V} \quad (2.0)$$

Moisture Content

Moisture content of each specie was determined in accordance with EN 13183-1 (2002) procedure. All test specimens were weighed to obtain the air dry weight and then oven dried at a temperature of 103±2^{0}C to constant weight to obtain the dry weight. The moisture content of were obtained using eqn.

Moisture content (%) = x100 (3.0)

Where, m_u is the bulk mass of sample in kg

M_0 is the oven dry mass in kg

V is the volume of sample in mm

ρ_u is the bulk density

ρ_d is the dry density in kg/m^3

ρ_d is the dry density in kg/m^3

Modulus of Elasticity (E_m) and Bending Strength (f_m)

An important element of wood quality is that of "stiffness" or its modulus of elasticity (MOE). The end-use of wood material, especially for structural timber is strongly related to MOE (Kumar, 2004; Piter and Zerbino, 2003). Modulus of elasticity defines the relationship between stress and strain within the elastic region. Timber is considered to be an isotropic material with three mutually perpendicular axes in the longitudinal, radial and tangential directions (Xu, 2000). The longitudinal modulus of elasticity is a quantitative measure of the stiffness of the wood along the grain. It is the most commonly measured elastic property and the most important elastic constant. Elasticity implies that deformations produced by the low stress are completely recoverable after loads are removed, and this is the accepted criterion of stiffness.

The Modulus of Elasticity were generated from four point bending test as specified in accordance with EN 408 (2003) using the Denison Universal Testing Machine. Twenty pieces of each specie (75mm x 50mm x 1500mm) were tested. The distance between supports is 1350mm. The span depth ration is 18, as specified in the code. Two point loads are applied at the central third of each test piece. The testing arrangement is shown in Figure 1.0.

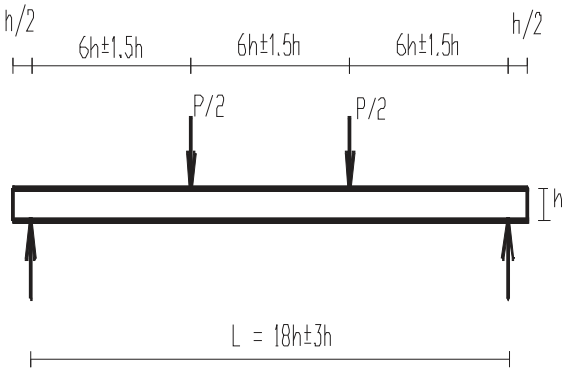


Figure 2.0 Four Point Bending Test Setup (EN 408, 2003)

Based on linear regression analysis, the Modulus of Elasticity for each test piece was obtained from equation 4.0. The Bending Strengths were obtained from equation 5.0.

$$E_m = \frac{L^3(F_2-F_1)}{4.7bh^3(w_2-w_1)} \quad (4.0)$$

$$f_m = \frac{aF_{max}}{2W} \quad (5.0)$$

where (F_2-F_1), L, b, h. (w_2-w_1) and F_{max} are as defined above

a is the distance between one load and the nearest support in mm

W is the section modulus of the beam in mm^3.

RESULTS

Moisture Content

The mean, standard deviation and the coefficient of variation of the moisture content of each specie are presented in Table 1.0. The mean values of the moisture contents for Alstonia boonei, Triplochiton Scleroxylon, Terminalia Ivorensis and Terminalia Superba are 20.59%, 16.83%, 19.26% and 20.96% respectively with the corresponding coefficients of variation of 0.34, 0.29, 0.24 and 0.23. The moisture content of Alstonia boonei is

slightly above its Fiber Saturation Point (FSP) of 0.32 (Cirad, 2009). However, the moisture contents of all the other three species were below their FSP of 0.29, 0.27, and 0.28 for Triplochiton Scleroxylon, Terminalia Ivorensis and Terminalia Superba respectively. The timber specimens were initially air dried for almost six month (from October, 2009 to March, 2010) to achieve equilibrium moisture content, and since the measured moisture contents were all close to their FSP values. Dimensional stability is therefore expected.

TABLE 1.0 MEAN AND STANDARD DEVIATION MOISTURE CONTENT

TIMBER SPECIE	Moisture Content (%)		
	MEAN	STANDARD DEVIATION	CEFFICIENT OF VARIATION
Alstonia Boonei	20.59	7.04	0.34
Triplochiton Acleroxylon	16.83	4.85	0.29
Terminalia Ivorensis	19.26	4.65	0.24
Terminalia Superba	20.96	4.81	0.23

Density

As shown in Table 2.0 the mean values of the density of Alstonia Boonei, Triplochiton Scleroxylon, Terminalia Ivorensis and Terminalia Superba are 384.23kg/m^3, 327.25kg/m^3, 449.10kg/m^3 and 421.51kg/m^3. From this table, it is observed that the coefficients of variation of density for the Alstonia Boonei, Triplochiton acleroxylon, Terminalia Ivorensis and Terminalia superba, are 11%, 18%, 15%, 16% respectively.

TABLE 2.0 MEAN, STANDARD DEVIATION AND COEFFICIENTS OF VARIATION OF DENSITY

SPECIE	Density (kg/m^3)		
	MEAN	STANDARD DEVIATION	CEFFICIENY OF VARIATION
Alstonia Boonei	384.23	41.06	0.11
Triplochiton Acleroxylon	327.25	57.60	0.18
Terminalia Ivorensis	449.10	73.88	0.16
Terminalia Superba	421.59	68.74	0.15

Modulus of Elasticity E_m, and Bending Strength f_m

In the four point bending tests, the central deflection of each test piece was measured relative to the end supports by means of a dial gauge graduated at 1/100 th of a millimeter. The measurement were made at interval of 1000 N up to the failure load. Load-deflection scatter plot were made for each test piece. The modulus of elasticity were obtained from the least square lines of the load deflection plots developed for each specimen in MS EXCEL, 2007. The test data have been analysed statistically, to generate the average values, standard deviation and coefficient of variation of the strength and stiffness properties of each of the four species.

The European strength class system EN, 338 is based on material properties with a reference moisture content equal to 12%. Likewise, the reference moisture content in Nigeria as specified in NCP2 is 18%. For easy comparison, the modulus of elasticity, bending strength and density values were adjusted to 12% and 18% reference moisture content using equations 6.0 to 8.0. Bostron, 1994; Heikkila and Hijarvi, 2008). The 12% moisture content adjustment equation for bending strength is given by equation 6.0 (Kucera, 1992).

$$f_{m,12\%} = \frac{f_{measured}}{1+0.0295(12-u)} \quad (6.0)$$

were $f_{m,12\%}$ is the bending strength at 12% moisture content

$f_{measured}$ is the bending strength at the measured moisture content

u = is the measured moisture content in %

The 12% moisture content adjustment equation for modulus of elasticity is given by equation 7.0 (Bostrom, 1994).

$$E_{12} = \frac{E_{measred}}{1+0.0143*(12-u)} \quad (7.0)$$

Likewise, Heikkila and Herajarvi (2008) gave moisture adjustment factor for density as:

$$\rho_{12} = \rho_w\left(1-\frac{(1-2)(w-12)}{100}\right) \quad (8.0)$$

Also, the volume effect for bending is dealt with in the European standard EN 384 and Eurocode 5. For solid timber, the reference depth in bending is 150 mm. For depths in bending less than 150 mm, the characteristic values for bending strength, $f_{m,k}$ are increased by the factor k_h given by equation 9.0 (Eurocode 5, 2004).

$$k_h = \left(\frac{150}{h}\right)^{0.2} \quad (9.0)$$

The generated bending strength were first corrected for the reference depth of 150mm accordingly. The point statistics (mean, standard deviation and coefficient of variations) are presented in Tables 3.0 to 6.0.

TABLE 3.0 VARIATION IN THE STRENGTH AND STIFFNESS PROPERTIES OF ALSTONIA BOONEI

ALSTONIA BOONEI

S/NO	PROPERTY	UNIT	MC	MEAN	STD DEV.	COV
1	DENSITY	kg/m^3	0.21	384.23	11.53	0.03
			0.12	367.73	11.03	0.03
			0.18	362.97	10.89	0.03
2	MODULUS OF ELASTICITY	N/mm^2	0.21	7691.60	461.50	0.06
			0.12	8768.72	526.12	0.06
			0.18	9105.98	546.36	0.06
3	BENDING STRENGTH	N/mm^2	0.21	28.89	4.04	0.14
			0.12	38.70	5.42	0.14

In Table 3.0, the mean values, standard deviation and coefficients of variation of the grade determining properties for Alstonia Boonei are presented. The Moduli of elasticity and the bending strengths were generated from the four point bending tests. These values were adjusted to 12% moisture content and 18% moisture content as required by EN 338 and NCP2. The coefficient of variation for density, modulus of elasticity and bending strength are 3%, 14% and 17% respectively.

Table 4.0, shows the mean values, standard deviation and coefficients of variation of the grade determining properties (density, modulus of elasticity and bending) for Triplochiton Scleroxylon, are presented. The Moduli of elasticity and the bending strengths were also generated from the four point bending tests.

TABLE 4.0 VARIATION IN THE STRENGTH AND STIFFNESS PROPERTIES OF TRIPLOCHITON SCLEROXYLON

S/NO	PROPERTY	UNIT	MC	MEAN	STD DEV.	COV
1	DENSITY	kg/m^3	0.17	327.25	42.54	0.13
			0.12	319.35	41.52	0.13
			0.18	321.22	41.76	0.13
2	MODULUS OF ELASTICITY	N/mm^2	0.17	6350.20	1397.04	0.22
			0.12	6821.34	1500.70	0.22
			0.18	6709.09	1476.00	0.22
3	BENDING STRENGTH	N/mm^2	0.17	41.73	7.09	0.17

In Table 5.0, the mean values, standard deviation and coefficients of variation of the grade determining properties for Terminalia Ivorensis are presented. The Moduli of elasticity and the bending strengths were generated from the four point bending tests. These values were adjusted to 12% moisture content and 18% moisture content as required by EN 338 and NCP2. The coefficient of variation for density, modulus of elasticity and bending strength are 14%, 19% and 20% respectively.

In Table 6.0, the mean values, standard deviation and coefficients of variation of the grade determining properties for Terminalia Superba are presented. The Moduli of elasticity and the bending strengths were generated from the four point bending tests. These values were adjusted to 12% moisture content and 18% moisture content as required by EN 338 and NCP2. The coefficient of variation for density, modulus of elasticity and bending strength are 16%, 08% and 07% respectively. The statistical parameter presented in Tables 4.0 to 7.0 are among the important requirement for the reliability analysis and design of timber structures.

TABLE 5.0 VARIATION IN THE STRENGTH AND STIFFNESS PROPERTIES OF TERMINALIA IVORENSIS

S/NO	PROPERTY	UNIT	MC	MEAN	STD DEV.	COV
1	DENSITY	kg/m^3	0.19	449.10	62.87	0.14
			0.12	432.80	60.59	0.14
			0.18	430.07	60.21	0.14
2	MODULUS OF ELASTICITY	N/mm^2	0.19	9964.50	1893.26	0.19
			0.12	11118.84	2112.58	0.19
			0.18	11322.85	2151.34	0.19
3	BENDING STRENGTH	N/mm^2	0.19	48.91	9.78	0.20
			0.12	62.24	12.45	0.20
			0.18	64.64	12.93	0.20

TABLE 6.0 VARIATION IN THE STRENGTH AND STIFFNESS PROPERTIES OF TERMINALIA SUPERBA

S/NO	PROPERTY	UNIT	MC	MEAN	STD DEV.	COV
1	DENSITY	kg/m^3	0.21	421.59	67.45	0.16
			0.12	402.70	64.43	0.16
			0.18	396.74	63.48	0.16
2	MODULUS OF ELASTICITY	N/mm^2	0.21	10970.00	877.60	0.08
			0.12	12582.12	1006.57	0.08
			0.18	13138.24	1051.06	0.08
3	BENDING STRENGTH	N/mm^2	0.21	61.48	4.30	0.07
			0.12	83.57	5.85	0.07
			0.18	91.56	6.41	0.07

The general observation is that, high variability exists not only between timber specie, but also within the species. This is not the case with other construction materials like concrete and steel, which properties could be controlled through manufacturing process. There is great implication of these variability on the issue of acceptability of the European strength classification system (EN 338, 2008), which is used in conjunction with the Eurocode 5. In this classification system, solid timber species that have minimum values of the grade determining properties (density, modulus of elasticity and bending strength) of a particular strength class are assigned to that strength class. There is the need to include criteria that can accommodate the issue of the high variability in the properties of structural timber. This can be achieved through the adoption of full probabilistic approach to design of timber structures.

PREDICTION MODELS FOR STRENGTH AND STIFFNESS

Prediction models for the bending strengths and moduli of elasticity for the tested specie were calibrated through linear regression analysis, with density as the independent variables. The advantage of these models is that, the bending strength and modulus of elasticity of any timber piece belonging to any of the four species tested, can be assessed without subjecting the piece to destructive bending test. First, the density has to be adjusted to 12% moisture content through equation 8.0.

Figure 2.0 to 5.0, shows the scatter plots and the least square regression lines for the bending strength obtained from the four point bending test against the density of Alstonia Boonei, Triplochiton Scleroxylon, Terminalia Ivorensis and Terminalia Superba. The prediction models for the bending strength f_m are given by equations 10.0 to13.0 for the respective species.

$$f_m = 0.011\rho + 20.71 \quad (10.0)$$

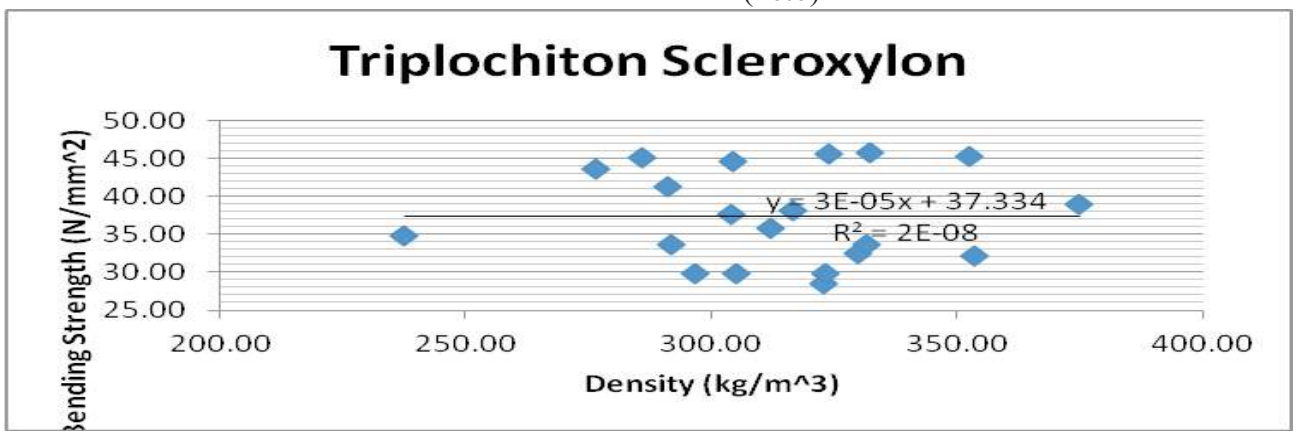


Table 3.0 Relation between density and f_m (Triplochiton Scleroxylon)

$$f_m = 3E\text{-}05\rho + 37.33 \quad (11.0)$$

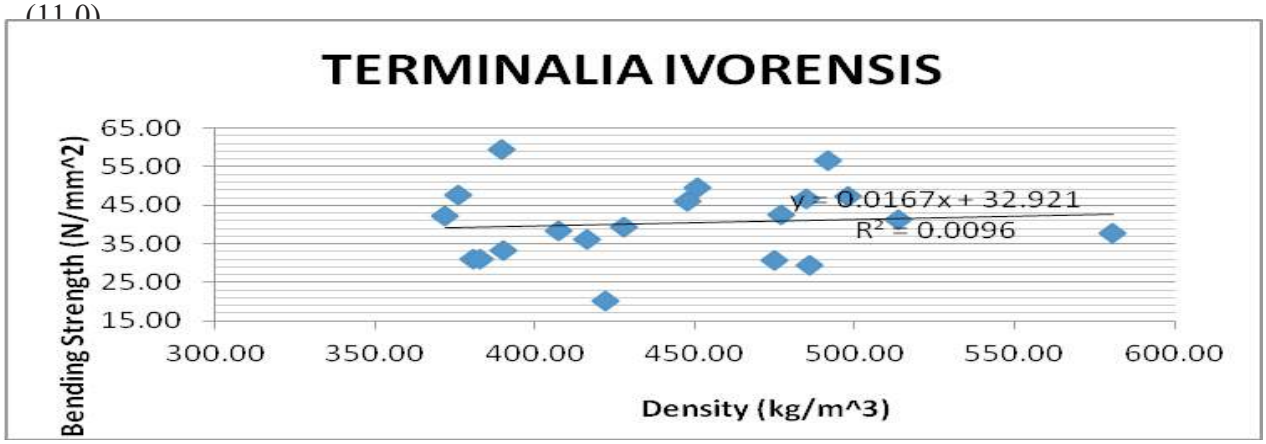


Table 4.0 Relation between density and f_m (Terminalia Ivorensis)

$$f_m = 0.016\rho + 32.92 \quad (12.0)$$

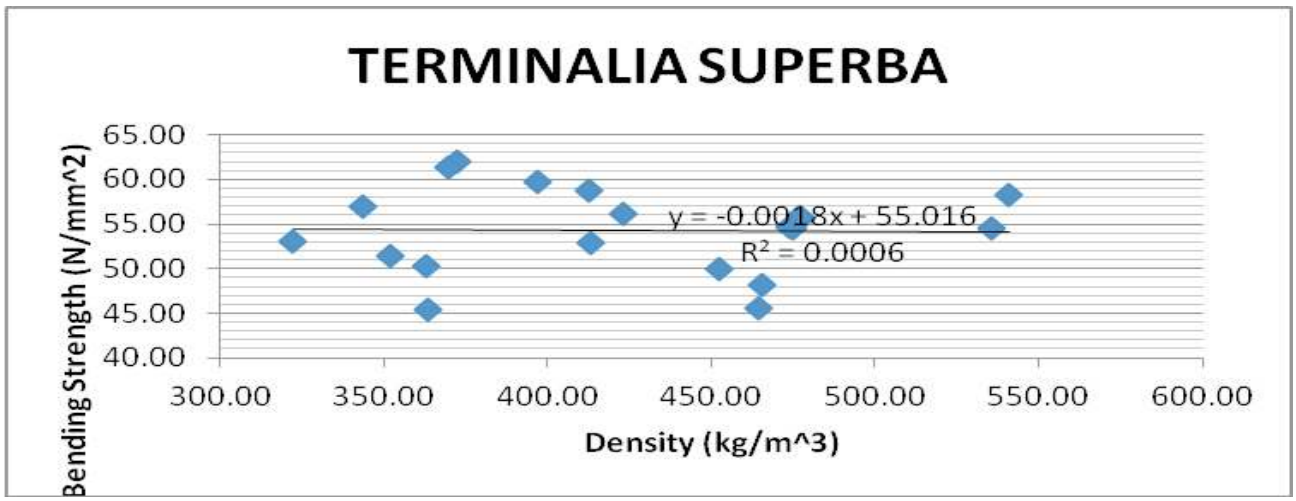


Table 5.0 Relation between density and f_m (Terminalia Superba)

$f_m = 0.001\rho + 55.01$
(13.0)

Figure 6.0 to 9.0, shows the scatter plots and the least square regression lines for the moduli of elasticity also obtained from the four point bending test against the density of Alstonia Boonei, Triplochiton Scleroxylon, Terminalia Ivorensis and Terminalia Superba. The prediction models for the modulus of elasticity MOE are given by equations 14.0 to17.0 for the respective species.

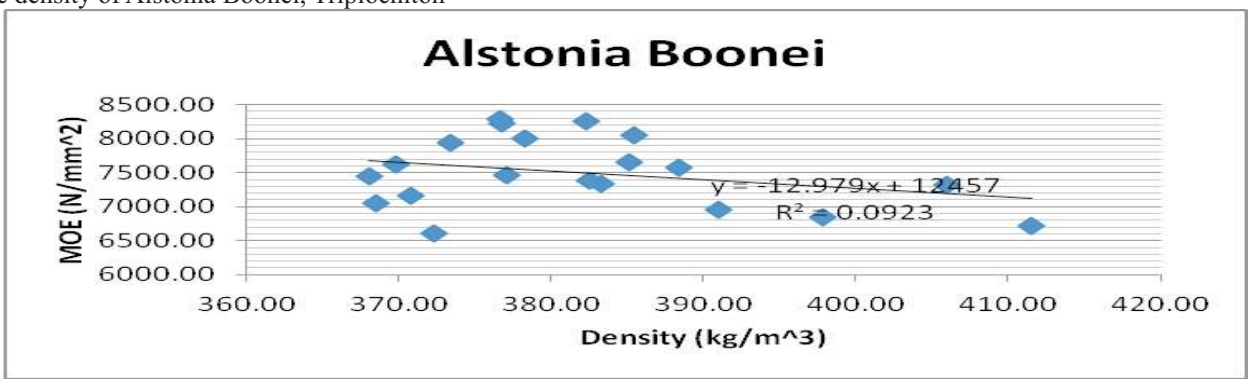


Figure 6.0 Relation between density and MOE (Alstonia Boonei)
$MOE = 12.97\rho + 12457$
(14.0)

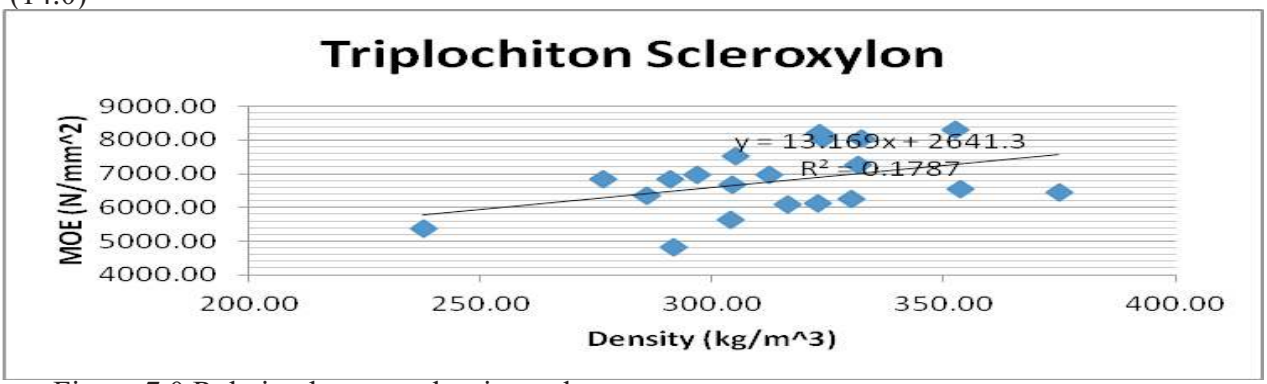


Figure 7.0 Relation between density and MOE (Triplochiton Scleroxylon)
$MOE = 1316\rho + 2641$
(15.0)

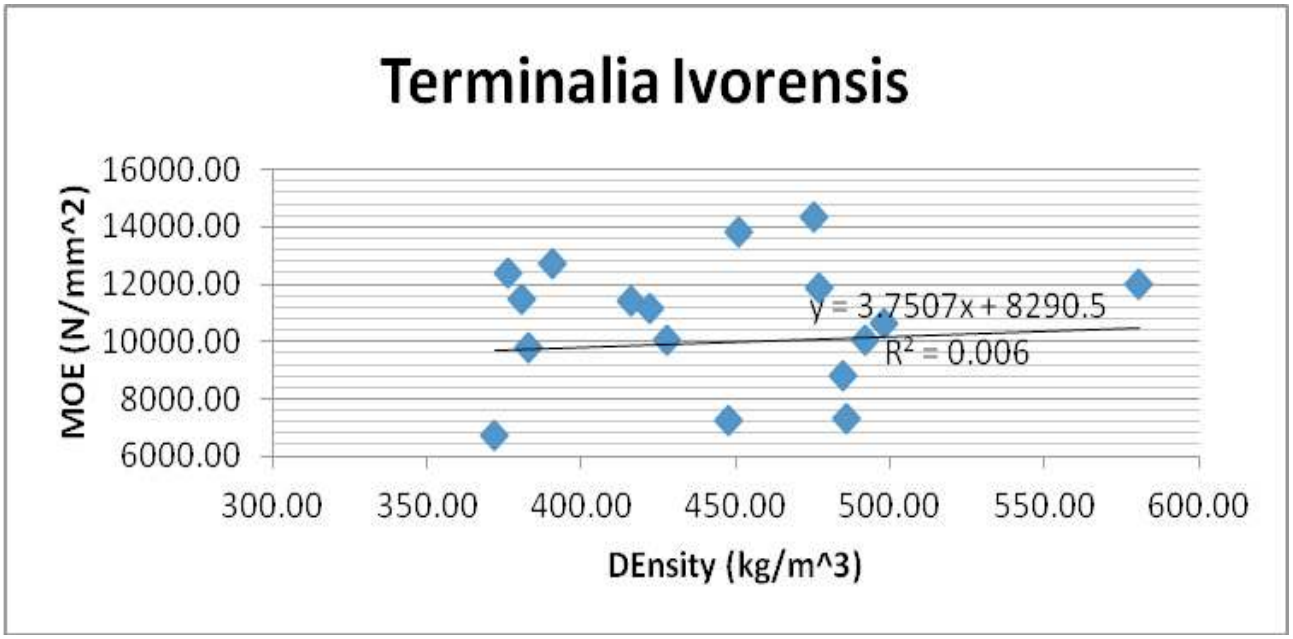


Figure 8.0 Relation between density and MOE (Terminalia Ivorensis)

$MOE = 3.750\rho + 8290$ (16.0)

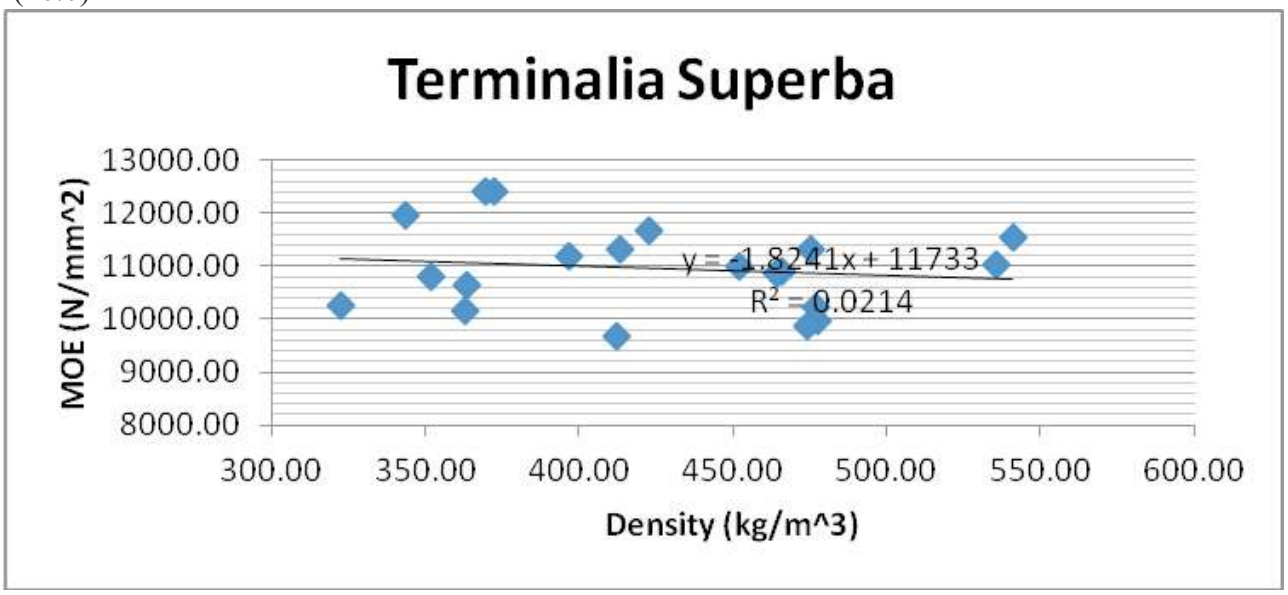


Figure 9.0 Relation between density and MOE (Terminalia Superba)

$MOE = 1.824\rho + 11733$ (17.0)

STRENGTH CLASSES

The European strength classification system defined the minimum characteristic bending strength for each strength class. For example, solid timber of strength class C16 is for timber species with minimum characteristic bending strength equal to $16N/mm^2$. The bending strength of solid timber obtained through equation 18.0 (Ranta-Maunus, 2004; EN 384, 2002).

$$f_{m,k} = 1.12f_{0.05} \quad (18.0)$$

were $f_{m,k}$ is the characteristic value of bending strength

$f_{0.05}$ is the 5% fractile value of bending strength

The 5% fractile values and the Characteristic values of bending strength are presented in Table

8.0. Alstonia Boonei was assigned to solid timber strength class C16 (EN 338, 2008) based on its minimum characteristic bending strength of 17.92N/mm^2 and minimum mean elastic modulus of 8070N/mm^2. The characteristic bending strength and modulus of elasticity for strength class C16 are 16N/mm^2 and 8000N/mm^2 respectively. Triplochiton Scleroxylon was assigned to strength class C14, because the minimum measured characteristic bending strength and minimum mean modulus of elasticity are 32.48N/mm^2 and 6821N/mm^2 respectively. The characteristic bending strength and mean modulus of elasticity for strength class C14 are 14N/mm^2 and 7000N/mm^2 respectively. Likewise, Terminalia Ivorensis was assigned to strength class C22, because its minimum characteristic bending strength and minimum mean elastic modulus are 23.52N/mm^2 and 11119N/mm^2 respectively. The characteristic bending strength and mean elastic modulus for strength class C22 are 22N/mm^2 and 10000N/mm^2 respectively. Terminalia Superba was assigned to strength class C30, because its minimum characteristic bending strength and minimum mean elastic modulus are 36.96N/mm^2 and 12582N/mm^2 respectively. The characteristic bending strength and mean elastic modulus of strength class C30 are 30N/mm^2 and 12000N/mm^2 respectively.

TABLE 8 5% FRACTILE VALUES AND CHARACTERISTIC STRENGTHS OF BENDING STRENGTH

Test Method	Alstonia Boonei		Triplochiton Scleroxylon		Terminalia Ivorensis		Terminalia Superba	
	$f_{0.05}$ (N/mm^2)	f_k (N/mm^2)	$f_{0.05}$ (N/mm^2)	f_k (N/mm^2)	$f_{0.05}$ (N/mm^2)	f_k (N/mm^2)	$f_{0.05}$ (N/mm^2)	f_k (N/mm^2)
3 point Bending	16.0	17.92	36.0	40.32	30.0	33.6	33.0	36.96
4 point Bending	20.00	22.40	29.0	32.48	21.0	23.52	45.0	50.40

CONCLUSION AND RECOMMENDATIONS

The mean values. Standard deviation and coefficient of variation of the grade determining properties (density, bending strength and modulus of elasticity) of four commonly used timber species in Nigeria were determined based on the European standards. Based on these properties, each specie was assigned to the appropriate strength class according to EN 338 (2008) procedure. Least square regression equations were also established for the prediction of bending strength and modulus of elasticity of each specie, once the specie density is known. The following recommendations are made:

1. To fully utilized the benefit of the EC 5, there most be a transition from prescriptive to engineered design. With the result in this study, engineered design of solid timber roof trusses can be undertaking based on the EC5.
2. A formalized national annex to EC5 need to be developed, to accommodate properties that suit Nigerian environmental conditions, especially moisture content which variation affect the properties of timber to a extent.
3. It is further recommended that the large uncertainties in the properties of solid timber should be accommodated into the design rules of the EC5 through reliability based design. The mean values and standard deviations generated in this study can provide adequate background in that direction

REFERENCES

Ang A. H., and Tang T. H., (1975). "Probability Concept in Engineering Planning and Design". Vol. 1. John Wiley and Sons. New York.

ASTM D-143-94 (2000) "Standard Method of Testing Small Clear Specimens of Timber," American Society for Testing and Materials, USA.

Antti, H. Ranta-Maunus, A. and Goran, T. (2006) "Potential of Strength Grading Of Timber with Combined Measurement Technique. Report of the Cambridge Poject – phase 1.

Akindele, S. O. (2003) Volume Prediction from Stump Diameters of Ginelina Arboria (Rocb) trees in Akure Forest Reserve. Nigeria. Niger J. Forestry 33 (2), 116-123.

Bostrom. L. (1994) Machine Strength Grading . Comparison of For Different Systems Swedish National Testing and Research Institute Building Technology sp. Report 1994, 49, 57p.

Bostrom, L. and Ormassn, S. (1999) Measurement of Modulus of Elasticity in Bending of Structural Timber-Determination of Some Physical and Mechanical Properties.

Baltrusaitis, A and Pranckevicene, V. (2003) "Strength Grading of the StructuralTimber" Material Science Journal, Vol 9, No 3. Pp 284-287

Bamber, R. K. and Burley, J. (1983) The Wood Properties of Radiata Pine. Commonwealth Agricultural Bureu. England.

Burkill, H. M. (1994) Useful Plants of West Tropical Africa. Vol. 2. Families E-I. Royal Botanical Gardens, Kew.

Burley J, and Styles B. T. (1976) Tropical Trees: Variation, Breeding and Conservation. Linnean Society Symposium Series No. 2. Academic Press.

Bunn, E. H. (1981) The nature of the Resource. New Zealand Journal of Forestry. 26 (2): 162-199.

Cirad (2009) Tropix-African Wood. The Production and Processing of Tropical Woods, Research Unit of Cirad (Centre de Cooperation Internationale en Recherche Agronomique pour le Development. Web document: http://tropix.cirad.fr/africa/africa.html. Retrieved on 26th February, 2010

Ditlevsen, O. (1981) Uncertainty Modeling. McGraw Hill

Eurocode 5 (2004) "Design of Timber Structures; Part 1-1: General Rules and Rules for Buildings. Brussels, 2004.

EN 338 (2008) Structural Timber – Strength Classes.

EN 408 (2002) Timber Structures-Structural Timber and Glued Laminated Timber- Determination of Mechanical Properties.

EN 384 (1995) "Structural Timber-Determination of Characteristic Values of Mechanical Properties and Density.

EN 350-2 (1994) Durability of Two Wood-Based Products. Guide to Natural Durability and Treatability of Selected Wood Species of Importance in Europe.

EN 13153-1 (2002) Moisture Content of a Piece of Sawn Timber-Part 1. Determination byOven Dry Method.

Engineering Statistics (2006) Handbook http://www.itl.nist.gov/div898/handbook/eda/eda.htm Online Statistics Handbook retrieved 26th July, 2010.

JCSS (2006) "Probabilistic Model Code: Material Properties for Timber" Joint Committee on Structural Safety

Jorascav, H., and Pavel, K. (2010) Analysis of selected Mechanical Properties Of Construction Wood KVH and Paraliam 2.0 E. DRVNA INDUSTRIJA 61 (1) pp 15-25.

Heikkila, K. and Herajarvi, H. (2008) Stiffness and Strength of 45X95mm beams Glued from Norway Spruce Using 8 Different Structural Models. Conference COST E53 29-30. Delft, the Netherlands.

Kucera, L. (19920 Skandinaviske Mormer for Testing av ama Feilfric Prover ac Heltre Skogs Forsk, Norwegian Forest Research Institute. Agricultural University of Norway. 104p.

Lucas, E. Olorunmisola, A. and Adewole, N. (2006) Preliminary Evaluation of Guava (Psidium Guajava L.) Tree Branches for Truss Fabrication in Nigeria. Agricultural Engineering International: CIGR Ejournal vol VIII.

NCP 2 (1973) "Timber Design Manual" Nigerian Industrial Standard, 1973.

Piter, J. C. Zerbino, R. L. Blab, H. J. (2003) Relationship Between Local and Global Modulus Of Elasticity in Beams of Argentinian Eucalyptus Grandis. Maderas Ciencia y Technologia 5(2); 107-116.

Ranta-Maurus, A., Forselius, M., Kurkela, J. and Toratti, T (2001) Reliability Analysis of Timber Structures. Nordic Industrial Fund. Technical Research Centre of Finland.

Ridley-Ellis D., Moore J., and Lyon A. (2008) Strength Grading and the End User - Lessons from the SIRT Project at Napier University. Conference COST E53, 29-30th October, 2008, Delft, the Netherlands.

Ravenshorst, G., van der Linden, M., Vrouwenveider, T., and Kuilien, W. (2004) An Economic Method to Determine the Strength Class of Wood Species. HERO, Vol, 49 No 4.

Raw Materials and Development Council, RMRDC (1998). Local Building and Construction Materials. Report of the Multi-Disciplinary Task Force on the Survey and Update of The Report on Local Sourcing of Raw Materials for Building and Construction Industry in Nigeria, 27-39

Schoome, D (2003) A Step Towards a More Precise Prediction of the Bending Strength of Spruce. Report of a Short Term Scientific Mission to CNR-IVALSA.

Solli, K. H. (2000) "Modulus of Elasticity-Local or Global

Solli, K. H. (1996) "Determination of Modulus of Elasticity in Bending According

to EN 408

Thelandersson, S (1995) "Serviceability Limit States-Deformation. In Timber Engineering STEP 1 pp. A17/8. Centrum Hout, The Netherlands.

Zobel, B. J. and Buijtenen, J. P. (1989) Wood Variation-Its Cause and Control. Springer Series in Wood Science. Springer-verlag. Berlin, Germany.



Plate 1 Four point Bending Test Set up in the Denison Universal Testing Machine

RENEWABLE, RECYCLED AND RE-USED MATERIALS AS MAJOR PILLAR OF SUSTAINABLE CONSTRUCTION IN DEVELOPING COUNTRIES

Dauda Dahiru and Abdulazeez Darda'u
Department Of Building, Faculty of Environmental Design, Ahmadu Bello University, Zaria – Nigeria

ABSTRACT
Exponential increase in population has led to corresponding increase in construction activities this in turn lead to excessive consumption of natural resources thus leading to negative impact which threatens the survival of mankind. This paper examines the use of renewable material as an important step towards the achievement of sustainable built environment. First major problems caused by construction activities, most especially construction materials, measures taken by government as part of effort made by various nations all over the world in order to ensure the achievement of Sustainability. These include among others legislations such as the Environmental Impact Assessment law, establishment of ministry of environment, Use of the Building Code/Regulation, etc were examined. It was noted that such measures, although, they are good but they proved ineffective due to some problems such as low level of awareness, poverty failure to enforce these legislation, lack of concern by the communities, etc. The paper examines the use of renewable construction materials as one of the viable options of sustainable built environment; in which various types of renewable materials, their use, advantages and how their application can assist in the achievement of sustainability. Part of the conclusions drawn, are that it is inevitable to use construction materials and that such use leads to serious depletion of natural resources and environmental problems. Therefore it was recommended that problems associated with construction activities should be viewed as common problem that affect all. As such developed countries have a responsibility tohelp.Government should create an enabling environment for the use of renewable materials, research institutes, professional bodies and educational institutions should encourage research on renewable construction materials. Regional Building Code should be developed and it should to include measures that will promote sustainable built environment.
KEYWORDS: High Consumption, Renewable Construction Materials, Depletion, Environmental degradation, Sustainability.

0 INTRODUCTION

Construction of buildings for human habitation and other purposes is one of the major attributes of civilization. It is an absolutely indispensable developmental activity that dates back to ancient times. However, in almost all human activities, there are ramifying consequences some of which are ecological in nature. For, the construction, maintenance and use of buildings all have significant impact on the environment both locally and globally. These impacts may produce effects in short or long term; they may even, lead to irreversible change in the world climate, atmosphere and ecosystems.

This is particularly true in recent times in which the cumulative effect of unplanned exploitation are manifesting in the present day consequences such as soil erosion, smog and environmental pollution. Added to the fact that there is exponential increase in population, this leads to corresponding increase in developmental activities so as to meet human needs. This in turn, leads to high consumption of resources depletion of natural resources, excessive emission of waste and environmental degradation. According to CIOB (2001) in Dahiru (2005) the construction industry consumes approximately 40 % of world natural resources and it is responsible for the emission of about 40 %waste. That is why it is referred to as the 'forty percent industry'. In view of the high consumption of resources, question is increasingly being asked as to whether current rates of exploitation of the planet's resources can be sustained without serious implication s for the future. (Taylor, 2005: 59)

Recently, awareness has arisen that unless this trend is checked, the future of man is doomed. Looking at the various efforts made by governments, at the local, national and international levels, it can be said that the reciprocal impacts between human actions and the biophysical world have been recognized by governments at different levels. That is why the concept of sustainability and sustainable development gain currency in recent times. According Brundtland report sustainability is the extent to which current needs can be fulfilled without compromising the needs of future generations. In other words sustainability is improving the quality of human life while living within the carrying capacity of supporting ecosystems. According to DOE (1990) in Glasson *et al* (2005) sustainability means living on earth's income rather than eroding its capital. Thus sustainability is a call for adoption of a new way of thinking and acting responsibly towards the context of our existence.

In order to ensure the achievement of sustainable development, various measures were introduced by governments at different levels. Besides that, researches were carried out on various aspects of environmental problems. In order to come up with mitigating measures that will reduce or completely eliminate the negative side effects of developmental activities on the environment. For example, in the building construction industry there are many researches

on re-cycling of construction materials, renewable energy and high performance buildings which are also called green building or environmentally friendly buildings, introduction of various legislations. All these are aimed at achieving sustainable built environment. However, according to CED (2008).due to man short sightedness and selfishness, these measures have not succeeded in stemming the increasing damage to the environment by physical developments. According to experts the carrying capacity of the environment is as limited as other natural resources and therefore, judicious use of it should be ensured to guide against catastrophes due man's unplanned modification of the environment by project developments (CED, 2008).

One important mea sure of mitigating the negative impact of construction work, hence the achievement of sustainable built environment, is by the use of renewable and recycled construction materials This paper discusses one of the a viable means of mitigating the negative effect of excessive consumption of resources as a means of achieving sustainable construction in the developing countries through the use of these important constructions materials - renewable and recycled construction materials.

2.0 PROBLEMS ASSOCIATED WITH THE USE OF CONSTRUCTION MATERIALS

2.1 Excessive Consumption of Natural Resources

Construction industry is regarded as the highest consumer of natural resources. According to Bokinni, (2008) buildings consume approximately 40% of the materials and resources entering the global economy each year. They account for one-fourth of the world's wood harvest, two-fifths of its material and energy usage, and one-sixth of its fresh water usage. Lessen and Roadman (1995) in Huby (2005) noted that the building of homes and offices, alone is estimated to consume between one-sixth and one-half of the world's physical resources: wood, minerals, energy, and water. In view of the good qualities of timber such as strength, light weight, easy transportability, free from corrosion or rusting, etc. it is widely used either directly as timber or to make plywood, chipboard or veneers. It was estimated that approximately one-fifth of the world's forest have been cut and cleared since 1950 and that around one-acre of tropical forest, was being destroyed every second. According to Agenda 21 for Sustainable Construction Countries (2001), the biggest culprit s are the materials that form the basis of modern construction – concrete and steel. Twice as much concrete is used in construction around the world than the total of all other building materials including wood, steel, plastic tons/year. According to Mehta and Monetrio, (2006) it is estimated that the present consumption of concrete in the world is of the order of 11 billion metric tonnes every year. Besides, the current cement production rate of the world is approximately 1.2 billion tons/year and this is expected to grow to about 3.5 billion tons/year by 2015. (Coutinho, 2003). In Nigeria the local cement production as of 2008 was 6.5 million metric tonnes and the annual demand of cement is 18 million metric tonnes and there is the possibility that the local need may double this amount in the near future (Salau, 2008). According to Kolawole and Anigbogu (2005) the production of 1 tonne of cement involves 2.6 to 2.8 tonnes of raw materials: clinker gypsum, oil or coal. Furthermore, water, which is also a key sustainability concern, is needed for the production of concrete and it is supposed to be portable tap water. However, water is also scarce in most of the cities in developing countries, not to talk of the rural areas.According to Agenda 21 for Sustainable Construction Countries (2001), only 62% of households in urban areas have access to a safe drinking water Despite this problem, the construction industry accounts for one-sixth of total global fresh water consumption.

Furthermore, 30 to 40% of total global energy is used in the manufacture of construction materials such as brick, steel, glass, etc. Steel is one of the most energy – intensive materials. The production of iron and steel is responsible for 4.1% of global energy use (World Resource Institute, 2000). Copper is used extensively in construction work for pipes and electrical wiring. The United States alone uses 530,000 tonnes per year for these purposes (Huby, 2005). Besides that, some materials used in housing construction are wholly manufactured often using materials such as coal and coal products, Polyvinyl Chloride (PVC), for example, is used in construction for window and door frames, pipes, paneling gutters and cables. It (PVC) is used inside housing in flooring, wallpaper, blinds and shower curtains

.

2.2 Serious Environmental Degradation

Exploitation of wood for construction purposes leads to forest destruction. Deforestation has both local and global impacts on the environment, affecting soil conditions, water relations, greenhouse, gas production and biodiversity. Even areas where selective logging of valuable trees, is carried out, extensive damage to surrounding areas occurs, in the process. It is estimated that the deforestation of tropical moist forests leads to the extinction of 12,000 – 57,000 species each year. This reduction in biodiversity represents the loss of a rich source of generic potential for example, for the development of new pharmaceutical products or of new improved strains of food crops from forest species. (Huby, 2005: 69) The extraction of raw materials such as mineral ores, stone and cement for building necessitates quarrying and mining for their distribution, can have negative effects on the wildlife and amenity value of the country side. According to Huby (2005) damage caused to landscape and wildlife, habitats, is often underestimated due to the fact that the negative impacts is caused at distance from the point at which the extraction of material take place. In Nigeria, Gandu (2005) noted that ecological impact is still being felt in Plateau state, Nigeria, today as a result of several years of tin mining activities. It was also noted that effect of suspended solids deposits from the processing of cement is glaring around the cement company of Northern Nigeria (CCNN) Sokoto. Abdulkarim & Muktar (2005) noted that the excavated or borrow pits due to construction activities in Zaria have subsequently turned

into artificial ponds. These ponds have become nuisance sites and that their impact has negatively affected humans and animals health, safety and beauty of the environment. Also the manufacture of heavily processed materials for use in housing results in more obvious environmental damage. For example, copper used for construction of buildings must be purified for low grades ores, thus producing massive amounts of waste ores or 'tailings'. In addition, to the environmental problem posed by mining and waste production, the copper purification process releases toxic metals such as arsenic and cadmium, and sulphur dioxide which contributes to acid deposition. Also PVC created environmental damage or problems through the generation of numerous toxic pollutants which contaminate air and water during production processes and when it is disposed of after use by incineration. The manufacture, use and disposal of paints and chemicals for treating timber can also cause toxic pollution of land, water and air.

Another major problem associated with the resource use and material processing for construction work, is that it produces massive amount of waste including potentially toxic manufactured materials as well as more inert forms of waste or rubble. According to Lenssen and Roadman (1995: 98) in Huby (2005) erecting a typical 150 tonnes home in the United States sends some 7 tonnes of refuse to the local dump. Also production of cement leads to some environmental problems. Cement is manufactured through the extraction and processing of mineral resources such as limestone. This affects the visual landscape. Also, during its production, it leads to the emission of CO_2. According to Bremner (2001) with every ton of cement produced, almost a ton of CO_2 is emitted. About 0.5 tonnes comes from decomposition of the limestone and the balance is generated by the power plant supplying the electricity to turn the kiln and ball mills to grind the cement plus the fuel burned to fire the kiln. Other generation such as operating ready mix trucks adds to the CO_2. Also, as regards to conventional concrete mixes, about 480kg of CO_2 is emitted per cubic metre of concrete or 20kg of CO_2 per 100kg of concrete produced. This, according to Bremner (2001) amounts to approximately 7% of the total CO_2 generated worldwide.

Cement production even in the developed countries like, US, UK, Canada etc leads to other problems such as particulate emissions. From the exhaust gas ranging from 0.3 to 1.0kg/tone, visual pollution arising from Quarries used to gain raw materials for cement production or for obtaining sand and gravel, noise pollution during production. There are also adverse health effects. Ozone (which is formed when nitrogen oxide and volatile organic compound mix in sunlight) cause health such as asthma attack, sore throat, coughing. Also, increased chromium content of cement has side effects. According to Walton (1990) in Dahiru (2005), cement powder causes disease called dermatitis when it is inhaled and frequent contact with it leads to skin disease.

2.3 Health Hazards and Indispensability of Construction Material

Considering the excessive amount of resources used in the processing and use of construction materials, in addition to the serious environmental damage, it can be concluded that the best remedy is not to construct any structure (Kolawole and Anigbogu, 2005).However; construction materials are absolutely indispensable, for many reasons. First, no any construction work can take place without materials. Secondly, they account for 50-80% of the total value of construction (Arora and Bindra, 2005). Also, the quality of any construction work or structure largely depends the quality of materials used in constructing such structure. That is why Taylor (2005) noted that there is relationship between material quality, material behavior and material failure – and hence, building failure. That is why, expert are of the view that building pathology, the study of building failure, is a valuable way of understanding material physiology (Taylor, 2005). According to Ayodeji (1995), 13% of the failure of buildings structures in Nigeria investigated was as a result of the use of poor quality materials

.

Another important issue worthy of note is the debate over the possible health hazards posed by construction materials and products or additives e.g. formaldehyde. According to Frey, (2002) in AbdulGaffar, (2009) there is greater public awareness of chemical compounds contained in building shells. This has led to change in general positive basic attitude towards modern products in recent years. With new construction or conversion, developers today expect exact costs and also information on energy, ecology and health. Since the use of construction materials cannot be avoided this means measures must be put in place to control their use and hence, mitigate the negative impact of their use.

3.0 MEASURES ADOPTED BY COUNTRIES TO MITIGATE THE NEGATIVE IMPACT OF CONSTRUCTION WORK

3.1 Legislations Aimed at Controlling Development ntrolling Development

For the fact that construction activities are absolutely indispensable, and that such activities exert pressures on the environment and change its state in terms of its quality and its stocks of natural resources. This leads to response by the society through general environmental, economic and sectorial policies, and through changes in behaviour. Measures put in place by nations all over the world are meant to ensure that developmental activities are in harmony with environment; and that the activities do not compromise the ability of future generation to achieve their needs

It is in realization of the negative impact that in Nigeria, the Federal and State governments have taken positive steps to mitigate such problems by enacting

laws. These include, among others Decree 58 of 1988 establishing Federal Environmental Protection Agency (FEPA), Decree No. 86 of 1992 for Environmental Impact Assessment (EIA). Besides that, in 1995 sectional guidelines for EIA were also developed to take care of the various sectors of Nigerian economy such as coastal development project, ports and harbor, transportation, railways, highways, roads, airports, urban development project, etc (Gandu, 2005). State governments have enacted environmental edicts and agencies for example Kaduna State Environmental Protection Edicts and Kaduna State Environmental Protection Agency (KEPA).Similar effort was made by many developing countries especially on EIA (Glasson *et al,* 2005)

3.2 Problems Faced by Developing Countries

There is no doubt that both the developed and developing countries's construction industries are responsible for excessive consumption of natural resources and emission of waste, leading to environmental degradation. However, developed countries are responsible for major part of such problem. According to Taylor (2005) estimates suggest that when normal living and energy requirements are added to these relating to supply and maintenance of a 'developed world' life style, they amount to as much as 2kW continuously per individual throughout life whereas corresponding consumption by individual in the 'developing world' would be a minute fraction of the figure. Besides that, Elkin and McLaren, (1991:34) in Huby (2005), noted that over 2 million doors were imported from tropical countries in 1989. However, the negative impact is more pronounced in developing countries (Agenda 21 for Sustainable Construction in Developing countries, 2000). This is due to many reasons. First, many of the raw materials used for the production of construction materials are obtained in the developing countries. Secondly, there is the problem of poverty, war and an exhausting debt burden (Adebayo, 2001 in Dahiru, 2005. This makes it very difficult for people to observe some of the measures put in place for the achievement of sustainability. Because societies and government faced with the extreme survival issues prevalent in the developing world tend to make a crisis-management approach to development, with little regard about the long term impact their actions will have on both the environment and the society. Since the main concern is the issue of survival as such, it will be difficult to make the environment as a nation priority. Another major factor that serves as an impediment is lack of awareness. Many people in developing countries are ignorant on, not only the problems caused by developmental activities but also on their role or responsibility on such problem. They view such an issue as something that does not concern them. But when these measures are examined closely it will be observed that the success of these measures require the support and participation of pressure groups, non-governmental organizations and the general public. For example, for legislation on Environmental Impact Assessment to serve its purpose it requires the active participation of the people especially those that are close to the place where such activity will take place. According to Warren (1996) before application for planning permission for projects like road construction is approved, in the United Kingdom, the general public must be informed. Once, it is decided to go ahead with the project, and the design is completed, an order is published in the local press for six weeks stating the intention of the Department of Transport. Besides that our level of development is very low as such, some of the facilities needed in order to assist in mitigating such negative impacts are either not available or grossly inadequate. **For instance according to Ibrahim (2006).there are no adequate equipment for effective evacuation of waste, no single engineered landfill and other disposal sites** in Nigeria .Added to the fact that there is no commitment on the part of many governments in the developing countries.

4.0 USE OF RENEWABLE AND RECYCLED MATERIALS AS AN A REMEDY TO THE NEGATIVE IMPACT OF CONSTRUCTION ACTIVITIES

Looking at the aforementioned issues, it would be noted that one of the prominent factors responsible for the serious problems due to construction activities, is the excessive consumption of resources. It is because of this, that the construction industry is always referred to as the 'forty percent industry'- due to the fact that it consumes approximately 40% of global natural resources and emits about 40% waste (CIOB, 2001 in Dahiru, 2005). Thus, any measure aimed at mitigating the negative impact of construction activities and hence the achievement of sustainable built environment, must take into consideration the problem of consumption of resources and the serious side effects. According to Bremner (2001) improved efficiency in production of such materials like cement is not likely to change the problem but development of alternative materials that are not associated with such problems is the only remedy. One viable means of achieving sustainability is through the use of renewable, recycled and re-used construction materials.

4.1Renewable Construction Materials

Renewable materials are substances derived from a living tree, plant, animal or ecosystem which has the ability to regenerate itself. A renewable material can be produced again and again. For example, when we use plantation wood to make roof trusses or frames we can plant more trees to replace it. Earth's mineral resources are finite, and often energy-intensive, but renewable materials like timber, can be produced indefinitely, with strong environmental benefits. Earth's mineral resources are finite, and processing them is often energy-intensive. Renewable materials can be produced indefinitely, with strong environmental benefits.

Renewable materials do not deplete resources, if managed properly, may have reduced net emissions of CO_2 across their life cycle compared to materials from fossil fuels which result in biodegradable waste. Maistry (2007) in AbdulGaffar (2009) asserted that renewable and biodegradable materials not only consume less energy in their preparation, but also are less problematic

to dispose of at the end of their useful life. Result of a study show that the substitution of 6% of materials by weight (steel for wood) resulted in a substantial percentage increase in all of the environmental performance indices except solid waste; which was unchanged. In another research, in order to determine the difference between wood and timber design, a 8,000kg of concrete was replaced with wood in the exterior wall structure, as both designs used similar concrete and wood floors. Results of the study shows that the substitution of wood resulted in a substantial percentage increase in all the environmental performance indices except water, which was unchanged. With two exceptions, all the construction index measures indicated significantly, lower environmental risk, for the wood framing design – as a renewable material - compared to non wood framing alternatives.

The use of wood materials was substantially more efficient than fossil intensive substitutes like steel and concrete. For the concrete frame used 250% more fossil energy than the wood frame. While the substitution of concrete block, mortar and steel requires 63GJ energy as against the wood energy use of only 36GJ. (Maistry, 2007 in AbdulGaffar, 2009),

According to Eric (2007) materials currently available, that have been developed from renewable materials, include:

i. Insulation materials
ii. Paints
iii. Natural fibre floor and wall covering
iv. Geo textile
v. Renewable Flooring
vi. Renewable Interior Doors
vii. Cellulose Roofing
viii. Renewable Wall Panels
ix. Renewable Tire Flooring
x. Cork floors and walls
xi. River-recovered Wood
xii. Certified Wood
xiii. Renewable plastic lumber
xiv. Thatch, etc.

Others include: Bamboo, Cork and Straw, natural and bio fiber composites, such as kenaf, hemp, flax, jute, and henequen and pineapple leaf fibre. Some of the uses of renewable materials are:

- Bamboo flooring and window screen
- Laminate Floors from Renewable Timber Reserves: Some 90% of the materials used to make Traffic Zone and Natural Reflections hardwood floors comes from renewable timber reserves. The manufacturing process utilizes trees, tree branches and windblown timber
- Renewable Natural Cork Flooring
- Renewable Wall Panels
- Cellulose Roofing
- Whole building was constructed with renewable material (Bamboo)

4.2 Re-Use Construction Materials

This refers to employing buildings or components for new applications with minimal alteration. There is the high need to consider the provision of flexibility for possible re-use when designing buildings – since society is dynamic, living habits always changes as such, taste regarding style of design and construction changes. Demolition in such case is inevitable. According to Dahiru and Garba (2010) emphasis is made, in recent times on how construction materials can be re-used or recycled. Some examples of situation where construction materials re-used are:

- Adaptation of older structures to other uses for example conversion of old factory building to other use – like office
- Use of part of the building such as re-use of bricks/blocks and simple structural timber sections like the joist.
- The use of stones recovered from demolished building to construct wall.
- Construction of roof with slates from old building.
- Construction of external paving by the use of cobbles which was formerly used for paving purposes.

4.3 Re-Cycled Construction Materials

Recycling is the conversion of the previous material into some other forms; mostly by the production of a lesser grade product. Recycling is mostly employed where deterioration has taken place as such; it is not possible to re-use such material. One major area where much attention is focused recent times is on recycling of waste materials for the production of construction materials. This has the twin advantage of cleaning the environment and making optimum use of materials. Some of the recycled materials are:

- Recycled Rubber Tiles: Flex-tuft Rubber Tile is an anti-slip flooring made from recycled tires. The product is available in 12x12 and 12x30 inches.
- Ceilings Made from Recycled Materials: Armstrong ceilings are made from recycled materials. Some of the highest performing noise-reducing and light-reflecting ceilings containing up to 70% recycled material. Armstrong also offers reclamation and recycling program for used ceilings made from renovation projects.
- Modular Furniture Made From Recycled Material and Recycled Interior Doors
- PVC Decking System and Recycled Insulation

5.0 SUMMARY, CONCLUSION AND RECOMMENDATIONS

5.1 Summary and Conclusion

The use of construction materials are not only desirable but necessary, however, there are many problems associated with the extraction, processing and use. These problems affect the environment and even the users of such structures. Governments all over the world have recognized this. As such, measures aimed at mitigating these problems were put in place. However, due to many problems in the developing countries, these measures could not bring the desired effect .This calls for a new approach. One viable option that is the use of Re-used, Re-cycled and Renewable construction materials.

Recommendations

- Problems due to developmental activities on the environment should be viewed as a common and should be treated as such. That means the developed countries should assist the developing countries in this respect.
- Research Institutes, Professional bodies and Higher institution of learning have a big role to play in ensuring the use of these materials gain currency in the construction industry in the developing countries. Attention should be paid to, and effort should be intensified in undertaking various researches on the development of recycled and renewable materials.
- A regional Building Code should be developed; such code should be used to control the excessive use of non-renewable materials. For instance, certain percentage of renewable or recycled materials should be used in the construction of buildings.
- Governments should encourage the use of renewable and recycled construction materials by :
  i,) Making it compulsory to use certain percentage of renewable or recycled construction materials for the construction of any public building
  ii) Establishing a trust fund in which construction firms and construction materials manufacturing companies would c contribute funds to such trust fund. The money realized, should be used to remedy the problem of environmental degradation caused by construction activities – especially the extraction and processing of raw materials for the production of construction materials. Besides that, such funds should be used to sponsor research on renewable and recycled construction materials, renewable energy and ways and means of enhancing the environment.
- Governments in the developing countries should emulate some of the developed countries in taking serious measures aimed at controlling or reducing the negative impacts of developmental activities on the environment, similar to Polluters Pay Principle, used by the developed countries like the United States of America. For instance, any firm that is responsible for any problem relating to environmental degradation, should either remedy the problem or be made to pay for mitigating/remedying the problem.
- An enlightenment campaign should be carried out on sustainability.

REFERENCES

Abdulkarim, B. & Muktar, A.A. (2005): Shelter and the Environmental Implication of Artificial Ponds in the Savanna: A Case Study of Zaria City – Kaduna State – Nigeria." *Conference Proceedings of the 2nd National Conference tagged: "Towards a Sustainable Built Environment."* Ahmadu Bello University, Zaria. 21st – 23rd September.

AbdulGaffar,S, (2009): "A Study on How the Application of Renewable Building Materials can be Enhanced in Building Construction Industry in Nigeria." An Unpublished B.Sc Project, Department of Building, Ahmadu Bello University, Zaria - Nigeria

Agenda 21 For Sustainable Construction in Developing Countries, First Discussion Document, UN New--York,USA

Arora, S.P. and Bindra,S.P. (2005): "The Text Book of Building Construction" 5th Edition,Dhanpat Rai Publications New – Delhi, India Pp 5.1 - 5.45

Ayodeji, A.O.(1995)"Handling of Concrete and its Constituents Material on Site – A Survey of Site Practice" Paper Presented at a Seminar, Department of Building, Ahmadu Bello University, Zaria Nigeria. October,1995.

Bokinni, K. S (2008) "An Overview of Building Code," A paper presented at the Nigerian Institute of Building Annual Conference at Oshogbo, Osun State, 15th – 19th 2008.

Bremner, T.W. (2001): "Environmental Aspects of Concrete – Problems and Solutions." *Invited Paper for the Plenary Session of the 1st All – Russian Conference on Concrete and Reinforced Concrete 9 – 14 September 2001.*

CED (2008): "Environmental Impact Assessment

Training." NWRI, Kaduna

Countinho J.S. (2003). "The Combined Benefits of CPF and RHA in Improving the Durability of Concrete Structures." Cement Concrete. Comp.; 25:51-9.

Dahiru, D. (2005): "Measures of Ensuring Sustainability in the Nigerian Construction Industry." *Conference Proceedings of the 2nd National Conference tagged: "Towards a Sustainable Built Environment."* Ahmadu Bello University, Zaria. 21st – 23rd September.

Dahiru, D. and Garba, M.M.(2010) "Study of the Compressive Strength of Mortar made With Recycled Sandcrete Blocks" *The Environ journal,* Faculty of Environmental design, Ahmadu Bello University, Zaria - Nigeria

Eric C. F, (2007)**."** Green Building, Remodeling For Dummies," 1st Edition Amazon.com, USA

Gandu, Y.J. (2005): "Impact of Construction Activities on the Environment." *Conference Proceedings of the 2nd National Conference tagged: "Towards a Sustainable Built Environment."* Ahmadu Bello University, Zaria. 21st – 23rd September.

Glasson *et al,* (1999): "Introduction to Environmental Impact Assessment: Principles and Procedures, Process, Practice and Prospects." UCL Press, London.

Ibrahim, A.T. (2006): "The Use of Solid waste for Producing Energy and Other Benefits." Senate Committee on Environment and Ecology, N.A. Abuja – Nigeria.

Mehta, K.P. and Monterio, P.J.M. (2006): "Concrete: Microstructure, Properties and Materials." McGraw Hill Ltd, California .U.S.A.

Huby, M. (2005): "Social Policy and the Environment." Open University Press, Buckingham, MK 18 IX W, United Kingdom.

Kolawole, J. & Anigbogu (2005): "Impact of Construction Activities on the Environment." *A Paper Presented at the 2nd National Conference Towards a Sustainable Built Environment.* Ahmadu Bello University, Zaria – Nigeria. Sept. 21st – 23rd.

Salau, M.A.(2008): "Abundant Local Structural Engineering Materials without Affordable Structures" An Inaugural Lecture delivered at the University of Lagos-Nigeria. 23rd April, 2008

Taylor, G.D.(2005) "Materials in Construction, Principles Practice and Performance 2nd Edition, Pearson Education Ltd; United Kingdom.

Warren, C (1996) 'Civil Engineering Construction – Design, management and Construction" Palgrave, London U.K.

World Resource Institute (2000) World Resources 2000 – 2001 Online

FUEL PRODUCTION FROM BIOMASS FOR RENEWABLE ENERGY

1.1 *OCHERI C.[1], AGBOOLA, J.B[2] OYELARAN O.A[3] & BARNABAS A.[4]*

1.2 Foundry Shop, Ajaokuta Steel Company Limited, Ajaokuta, Kogi State[1]
Department of Mechanical Engineering, Federal University of Technology, Minna, Niger State[2]
Hydraulic Equipment, Development Institute, Kano [3]
Department of Metallurgical & Materials Engineering, Federal University of Technology, Akure[4]
E-mail:ocheri4c@yahoo.com,joe_agboola@yahoo.com
ajanioyelaran@yahoo.com,barnabelad20012000@yahoo.com

ABSTRACT
The penetration of renewable energy into the energy system of human settlements on Earth is from one point of view nearly 100%. The energy system seen by the inhabitants of the Earth is dominated by the environmental heat associated with the greenhouse effect, which captures solar energy and stores it within a surface-near sheet of topsoil and atmosphere around the Earth. Only 0.02% of this energy system is currently managed by human society. Within this economically managed part of the energy sector, renewable energy sources currently provide about 25% of the energy supplied. A large part of this renewable energy is in the form of biomass energy, either in food crops or in managed forestry providing wood for industrial purposes or for incineration .This paper therefore discusses the conversion of fuels, fuel cell in technology, the conversion of biological materials, heat production from Biomass, production of Biogas through Thermo chemical gasification of Biomass and generation of liquid biofuels.
Key words: Renewable, Energy, Biomass, Biological materials and Biofuels

INTRODUCTION

Renewable energy sources are typically characterized by a theoretical maximum rate at which energy may be extracted in a "renewable" mode, i.e. the rate at which new energy is arriving or flowing into the reservoirs associated with many of the renewable energy flows. In some cases, the additional loop on a given renewable energy cycle, caused by man's utilization of the source, will by itself modify the rate at which new energy is arriving (for instance, utilization of temperature differences in the oceans may alter surface evaporation rates and the velocities of ocean currents; in both cases the mechanisms for establishing the temperature differences may become altered.
Renewable energy resources are first placed in the framework of current economic thinking, as a preliminary effort to quantify some of the considerations which should be made in constructing a viable energy supply system. Then follows a survey of indirect economic factors to consider, which leads to the description of the methodology of life-cycle analysis, which together with the scenario technique constitutes the package for an up-to-date economic analysis. It is then used in concrete examples, as a tool for systems assessment. The renewable energy research and development areas most important for the immediate and the near future for solving the challenges associated to energy consumption globally.

2.0 THE ENERGY FUTURE AND THE ROLE OF RENEWABLE ENERGY

There are very large differences between the energy use of the leading countries or leading persons within countries, as compared with the least energy-using inhabitants of poor countries. This feature is currently changing, as the level of global interaction increases and every world citizen becomes aware of the kind of life-style that is "possible". However, the current development does not seem to indicate a diminishing ratio of the energy use of those using most and those using least energy. This is also true of other commodities related to living standard. Energy use and resource depletion does not, of course, constitute the primary goals of any society or individual within a society. For example, average Europeans or Japanese use about half as much energy as the average North American, but have a living standard, which certainly is not lower than that of the North American citizens.

This development in energy use is linked to another problem that may serve to accelerate the energy transition, namely the increased awareness of the negative implications of environmental impacts of energy production and use. Early man was capable of causing environmental disturbance only on a very local scale. However, extensive burning of forests, for example, to provide land for agriculture, which would later be abandoned when overexploitation diminished the crop or grazing yields, may have been instrumental in creating the desert and semi-desert regions presently found at low latitudes (Bryson, 1971). This is already an important example of a possibly man-made climatic change. Recently, man has reached a technological level enabling him to convert energy at rates which can be maintained over extended areas and which are no longer small compared to the energy fluxes of solar origin that are responsible for the climate.

The average heat flux of anthropogenic origin (i.e. from fossil fuels) in an industrial and urban area such as the Los Angeles Basin (about 1010 m^2) was estimated

in 1970 to be 7 Wm^{-2} (Lees, 1970). The global average value around 1970 was 0.015 Wm^{-2}, and the average solar flux absorbed by the Earth–atmosphere system is 240 Wm^{-2}.

For comparison, a forest fire, which would burn down an area of fertile, tropical forests in one week, would release a heat flux of about 1000 Wm^{-2}. Yet the average heat flux from forest fires in all continental regions, the average being over several years, is less than the average anthropogenic heat flux. The nuclear weapons arsenal built up during the last 50 years is somewhere in the range of 104–105 megatons (Feld, 1976), the higher figure corresponding to about 4.4×1020 J. If these weapons were detonated within a 24-hour interval, the average energy flux would be 5×1015 W, and if the target area were 1012 m^2, the average heat flux would be 5000 Wm^{-2}.

Radioactive contamination of the environment would cause additional death and decay, and would establish further mechanisms for climatic disturbance (e.g. destruction of the stratospheric ozone shield), in addition to the difficulty presented to human survival as the dominant species on our planet. It has been suggested that fusion energy constitutes an alternative to renewable energy as the long-term solution. It is not clear at present whether fusion energy on Earth will ever become a feasible and practical source of controlled energy supply. It will create nuclear waste in amounts similar to those of fission technologies, and will counteract the development towards decentralized technologies characterizing the present trend. It is probably an exaggeration to imagine that the introduction of one kind of energy technology rather than another will determine or solve such institutional problems. What may be true, though, is that certain types of technology are more suitable for societies organized in a particular way, and that the kind of technology imagined in connection with the use of certain renewable energy resources fits well both with the needs of sophisticated, decentralized societies based upon information technology and with the needs of the presently under-privileged regions.

2.0 CONVERSION OF BIOLOGICAL MATERIAL

Traditional uses of organic fuels as energy carriers comprise the use of fresh biomass, i.e. storage and combustion of wood fuels, straw and other plant residues, and in recent centuries notably storage and combustion of fossilized biomass, i.e. fuels derived from coal, oil and natural gas. While the energy density of living biomass is in the range of 10- 30 MJ per kg dry weight, the several million years of fossilation processes typically increase the energy density by a factor of two . The highest energy density is found for oil, where the average density of crude oil is 42 MJ kg-1.

The known reserves of fossil fuels that may be economically extracted today, and estimates of further resources exploitable at higher costs, can be seen as indicated in Table 1. The finiteness of such resources is of course, together with the environmental impact issues, the reason for turning to renewable energy sources, including renewable usage of biomass resources. Coal to peat classification and selected properties. The dashed lines indicate the fractional content of oxygen and of fixed carbon. The remaining fraction consists of volatile matter (Based on US DoE, 1979).

Source	Reserves (EJ	Resources (>-50% prob.)	Occurrence (speculative)	1990 use (EJ)	Accum. Use 1860–1990
Coal				91	5 203
hard coal	15 000	100 000	900 000		
brown coal/ lignite	4 000	30 000	90 000		
peat	0	4 000	4 000		
Oil				128	3 343
conventional	5 000	3 000	13 000		
unconventional	7 000	9 000	20 000		
Natural gas				71	1 703
conventional	5 000	5 000	15 000		
unconventional in hydrates	7 0000	20 0000	25 000 100 000		

Table 1.0. Fossil reserves, resources and consumption in EJ (UN, 1981; Jensen and Sørensen, 1984; Nakicenovic *et al*., 1996).

However, fresh biomass is a large potential source of renewable energy that in addition to use for combustion may be converted into a number of liquid and gaseous biofuels. This may be achieved by thermo chemical or by biochemical methods.

Biomass is not just stored energy; it is also a store of nutrients and a potential raw material for a number of industries. Therefore, bio- energy is a topic that cannot be separated from food production, timber industries (serving construction purposes, paper and pulp industries, etc.), and organic feedstock-dependent industries (chemical and biochemical industries, notably).

Furthermore, biomass derives from plant growth and animal husbandry, linking the energy aspect to agriculture, livestock, silviculture, aquaculture, and quite generally to the management of the global ecological system. Thus procuring and utilizing organic fuels constitute a profound interference with the natural biosphere, and the understanding of the range of impacts as well as the elimination of unacceptable ones should be an integral part of any scheme for diversion of organic fuels to human society.

3.0 HEAT PRODUCTION FROM BIOMASS-Producing Heat By Burning

Heat may be obtained from biological materials by burning, eventually with the purpose of further conversion. Efficient burning usually requires the reduction of water content, for example, by drying in the Sun. The heat produced by burning cow dung is about 1.5 x 10^7 J per kg dry matter, but initially only about 10% is dry matter, so the vaporization of 9 kg water implies an energy requirement of 2.2x 10^7 J, i.e. the burning process is a net energy producer only if substantial sun-drying is possible. Firewood and other biomass sources constitute stores of energy, since the drying may be performed during summer, such that these biological fuels can be used during winter periods when the heating requirement

may be large and the possibility of sun drying may not exist.

The heat produced by burning 1 kg of dry wood or sawmill scrap is about 1.25 $x10^7$ J (1 kg in these cases corresponds to a volume of approximately $1.5x10^{-3}$ m^3), and the heat from burning 1 kg of straw (assumed water content 15%) is about $1.5x10^7$ J (Eckert, 1960). The boilers used for firing with wood or straw have efficiencies that are often considerably lower than those of oil or gas burners. Typical efficiencies are in the range 0.5- 0.6 for the best boilers. The rest of the enthalpy is lost, mostly in the form of vapour and heat leaving the chimney (or other smoke exit), and therefore not available at the load area.

Combustion is the oxidation of carbon-containing material in the presence of sufficient oxygen to complete the process

$C + O_2 \rightarrow CO_2$

Wood and other biomass is burned for cooking, for space heating, and for a number of specialized purposes, such as provision of process steam, electricity generation. In rural areas of many Third World countries a device consisting of three stones for outdoor combustion of twigs is still the most common. In the absence of wind, up to about 5% of the heat energy may reach the contents of the pot resting on top of the stones. In some countries, indoor cooking on simple Chulas is common. A chula is a combustion chamber with place for one or more pots or pans on top, resting in such a way that the combustion gases will pass along the outer sides of the cooking pot, and leave the room through any opening.

Most biological material is not uniform, and some pre-treatment can often improve both the transportation and storage processes and the combustion (or other final use). Irregular biomass (e.g. twigs) can be chopped or cut to provide unit sizes fitting the containers and burning spaces provided. Furthermore, compressing and pelletizing the fuel can make it considerably more versatile. For some time, straw compressors and pelletizers have been available, so that the bulky straw bundles can be transformed into a fuel with volume densities approaching that of coal. Other biomass material can conceivably be pelletized with advantage, including wood scrap, mixed biomass residues, and even aquatic plant material (Anonymous, 1980).

Particularly in the rich countries, a considerable source of biomass energy is urban refuse, which contains residues from food preparation and discarded consumer goods from households, as well as organic scrap material from commerce and industry. Large-scale incineration of urban refuse has become an important source of heat, particularly in Western Europe, where it is used mainly for district heating (de Renzo, 1978).

Particulates are not normally regulated in home boilers, but for power plants and industrial boilers, electrostatic filters are employed with particulate removal up to over 99%. Compared to coal burning without particle removal, wood emissions are 5- 10 times lower. When starting a wood boiler there is an initial period of very visible smoke emission, consisting of water vapour and high levels of both particulate and gaseous emissions. After reaching operating temperatures, wood burns virtually without visible smoke. When stack temperatures are below 60°C, again during start- up and incorrect burning practice, severe soot problems arise.

In general, the environmental impacts of biomass utilization through combustion may be substantial and comparable to, although not entirely of the same nature as, the impacts from coal and oil combustion (see Table 4.4). In addition, ashes will have to be disposed of. For boiler combustion, the sulphur dioxide emissions are typically much smaller than for oil and coal combustion, which would give 15- 60 kg t-1 in the absence of flue gas cleaning.

If ash is re-injected into the wood-burner, higher sulphur values appear, but still below the fossil fuel emissions in the absence of sulphur removal efforts.

Substance emitted	Emissions (kg/103kg)
Particulates	---
Organic compounds	1.0
Sulphur dioxide	0- 1.5b
Nitrogen oxides	5.0
Carbon monoxide	1.0

Table 2. Uncontrolled emissions from biomass combustion in boilers (kg per tonne
of fuel, based on woody biomass; US EPA, 1980). a Hydrocarbons including methane
and traces of benzo(a)pyrine. b Upper limit is found for bark combustion. Ten times
higher values are reported in cases where combustion ashes are re-injected.

4.0 FUEL PRODUCTION FROM BIOMASS: OVERVIEW AND GENERATION OF GASEOUS FUELS

Fuels are biological material (including fossilised forms), hydrocarbons or just hydrogen, which can be stored and used at convenient times. "Usage" traditionally means burning in air or pure oxygen, but other means of conversion exist, for example, fuel cells .

A number of conversion processes aim at converting one fuel into another which is considered more versatile. Examples are charcoal production from wood (efficiency of conversion about 50%), liquefaction and gasification (Squires, 1974). Figure 1.0 gives an overview of all the non-food uses
of biomass.

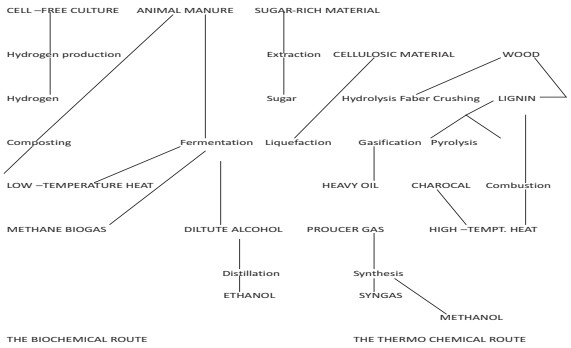


Fig:1 shows Non –Food energy uses of Biomass

Coal is gasified to carbon monoxide and hydrogen, which is then, by the Fischer- Tropsch process (passage through a reactor, e.g., a fluidized bed, with a nickel, cobalt, or iron catalyst), partially converted into hydrocarbons. Sulphur compounds have to be removed as they would impede the function of the catalyst. The reactions involved are of the form

Non-food energy uses of biomass and conversion efficiencies range from 21% to 55% (Robinson, 1980).

$$(2n + 1)H_2 + nCO \rightarrow CnH2n+2 + nH_2O,$$
$$(n + 1)H_2 + 2nCO \rightarrow CnH2n+2 + nCO_2$$

Alternative coal liquefaction processes involve direct hydrogenation of coal under suitable pressures and temperatures. Pilot plants have been operating in the United States, producing up to 600 t a day (slightly different processes are named "solvent refining", "H-coal process", and "donor solvent process", cf. Hammond, 1976). From an energy storage point of view, either coal or the converted product may be stockpiled. For use in the transportation sector, production of liquid hydrocarbons such as methanol from natural gas could be advantageous.

5.0 BIOGAS

Conversion of (fresh) biological material into simple hydrocarbons or hydrogen can be achieved by a number of anaerobic fermentation processes, i.e. processes performed by suitable microorganisms and taking place in the absence of oxygen. Such anaerobic "digestion" processes work on the basis of most fresh biological material, wood excepted, provided that the proper conditions are maintained (temperature, population of microorganisms, stirring, etc.). Thus biological material in forms inconvenient for storage and use may be converted into liquid or gaseous fuels that can be utilized in a multitude of ways, like oil and natural gas products.

The "raw materials" that may be used are slurry or manure (e.g. from dairy farms or "industrial farming" involving large feedlots), city sewage and refuse, farming crop residues (e.g. straw or parts of cereal or fodder plants not normally harvested), or direct "fuel crops", such as ocean- grown algae or seaweeds, water hyacinths (in tropical climates) or fast growing bushes or trees. The deep-harvesting necessary in order to collect crop residues may not be generally advisable, owing to the role of these residues in preventing soil erosion.

Among the fermentation processes, one set is particularly suited for producing gas from biomass in a wet process . It is called *anaerobic digestion*. It traditionally used animal manure as biomass feedstock, but other biomass sources can be used within limits. There are three discernible stages. In the first, complex biomass material is decomposed by a heterogeneous set of microorganisms, not necessarily confined to anaerobic environments. These decompositions comprise hydrolysis of cellulosic material to simple glucose, using enzymes provided by the microorganisms as catalysts.

The second stage involves dehydrogenation (removing hydrogen atoms from the biomass material), such as changing glucose into acetic acid, carboxylation (removing carboxyl groups) of the amino acids, and breaking down the long-chain fatty acids into short-chain acids, again obtaining acetic acid as the final product. These reactions are fermentation reactions accomplished by a range of acidophilic (acid-forming) bacteria.

Finally, the third phase is the production of biogas (a mixture of methane and carbon dioxide) from acetic acid by a second set of fermentation reactions performed by methanogenic bacteria. These bacteria require a strictly anaerobic (oxygen-free) environment. Often all processes are made to take place in a single container, but separation of the processes into stages will allow greater efficiencies to be reached.

6.0 THERMOCHEMICAL GASIFICATION OF BIOMASS

Conversion of fossil biomass such as coal into a gas is considered a way of reducing the negative environmental impacts of coal utilization. However, in some cases the impacts have only been moved but not eliminated. Consider, for example, a coal-fired power plant with 99% particle removal from flue gases. If it were to be replaced by a synthetic gas-fired power plant with gas produced from coal, then sulphur could be removed at the gasification plant, using dolomite-based scrubbers. This would practically eliminate the sulphur oxide emissions, but on the other hand, dust emissions from the dolomite processing would represent particle emissions twice as large as those avoided at the power plant by using gas in-stead of coal (Pigford, 1974). Of course, the dust is emitted at a different location.

This example, as well as the health impacts associated with coal mining, whether on the surface or in mines (although not identical), has sparked interest in methods of gasifying coal *in situ*. Two or more holes are drilled. Oxygen (or air) is injected through one, and a mixture of gases, including hydrogen and carbon oxides, emerges at the other holes. The establishment of proper communication between holes, and suitable underground contact surfaces, has proved difficult, and recovery rates are modest.

The processes involved would include

$$2C + O_2 \rightarrow 2CO,$$
$$CO + H_2O \leftrightarrow CO_2 + H_2$$

The stoichiometric relation between CO and H_2 can then be adjusted using the shift reaction which may proceed in both directions, depending on steam temperature and catalysts. This opens the way for methane synthesis through the reaction:

$$CO + 3H_2 \rightarrow CH_4 + H_2O.$$

At present, the emphasis is on improving gasifiers using coal already extracted.

Traditional methods include the Lurgi fixed-bed gasifier (providing gas under pressure from non-caking coal at conversion efficiency as low as 55%) and the Koppers- Totzek gasifier (oxygen input, the produced gas unpressurised, also of low efficiency).

Improved process schemes include the hy-gas process, requiring a hydrogen input, the bi-gas concept of brute force gasification at extreme, high temperatures, and the slagging Lurgi process, capable of handling

powdered coal (Hammond, 1976). Promising, but still at an early stage of development, is catalytic gasification (potassium catalyst), where all processes take place at a common, relatively low temperature, so that they can be combined in a single reactor (Fig. 4.123).

The primary reaction here is *Figure 4.123.* Schematic diagram of catalytic gasification process (SNG is synthetic natural gas) (From Hirsch *et al*., 1982. Reprinted from *Science*, 215, 121-127, 8, January 1982, with permission. Copyright 1982 American Association for the Advancement of Science.)

$C + H_2O \rightarrow H_2 + CO$,

(H2O being in the form of steam above 550°C), The catalyst allows all processes to take place at 700°C. Without catalyst, the gasification would have to take place at 925C and the shift reaction and methanation at 425°C, that is, in a separate reactor where excess hydrogen or carbon monoxide would be lost (Hirsch *et al*., 1982).

In a coal gasification scheme storage would be (of coal) before conversion. Peat can be gasified in much the same way as coal, as can wood

7.0 FUEL PRODUCTION FROM BIOMASS: Generation Of Liquid Biofuels

Anaerobic fermentation processes may also be used to produce liquid fuels from biological raw materials. An example is the ethanol production (4.152) from glucose, known as standard yeast fermentation in the beer, wine and liquor industries. It has to take place in steps, such that the ethanol is removed (by distillation or dehydrator application) whenever its concentration approaches a value (around 12%) which would impede reproduction of the yeast culture.

In order to reduce the primary biological material (e.g. molasses, cellulose pulp or citrus fruit wastes) to glucose, the hydrolysis process may be used. Some decomposition takes place in any acid solution, but in order to obtain complete hydrolysis, specific enzymes must usually be provided, either directly or by adding microorganisms capable of forming such enzymes.

The yeast fungi themselves contain enzymes capable of decomposing polysaccharides into glucose.

The theoretical maximum efficiency of glucose-to-ethanol conversion is 97%, and, according to Calvin (1977), the Brazilian alcohol industry in 1974 obtained 14% of the energy in the raw sugar input, in the form of ethanol produced by fermentation of just the molasses residues from sugar refining, i.e. in addition to the crystallized sugar produced. A current figure is 25% for an optimized plant design (EC, 1994).

Mechanical energy input, e.g. for stirring, could be covered by the fermentation wastes if they were burned in a steam power plant. In the European example (EC, 1994), these inputs amount to about a third of the energy inputs through the sugar itself.

Alternative fermentation processes based on molasses or other sugarcontaining materials produce acetone- butanol, acetone- ethanol or butanol-isopropanol mixtures, when the proper bacteria are added. In addition, carbon dioxide and small amounts of hydrogen are formed (Beesch, 1952; Keenan, 1977).

Conversion of fossilized biomass into liquid fuels was briefly mentioned at the beginning in conjunction with the overview showing the conversion routes open for biofuel generation. Among the nonfood energy uses of biomass, there are several options leading to liquid fuels which may serve as a substitute for oil products.

The survey of conversion processes given indicates liquid end products as the result of biochemical conversion either using fermentation bacteria or as the result of a thermochemical conversion process involving gasification and, for example, further methanol synthesis. The processes, which convert biomass into liquid fuels that are easy to store, are discussed below, but first the possibility of direct production of liquid fuels by photosynthesis is presented.

7.1 Direct photosynthetic production of hydrocarbons

Oil from the seeds of many plants, such as rape, olive, groundnut, corn, palm, soy bean, and sunflower, are used as food or in the preparation of food. Many of these oils will burn readily in diesel engines, and can be used directly or mixed with diesel oil of fossil origin, as they are indeed in several

pilot projects around the world.

However, in most of these cases the oil does not constitute a major fraction of the total harvest yield, and any expansion of these crops to provide an excess of oil for fuel use would interfere with food production. A possible exception is palm oil, because inter-cropping of palm trees with other food

crops may provide advantages such as retaining moisture and reducing wind erosion.

7.2 Methanol from biomass.

There are various ways of producing methanol from biomass sources, as indicated

in Fig. 1 Starting from wood or isolated lignin, the most direct routes are by liquefaction or by gasification. The pyrolysis alternative gives only a fraction of the energy in the form of a producer gas.

By high-pressure hydrogenation, biomass may be transformed into a mixture of liquid hydrocarbons suitable for further refining or synthesis of methanol (Chartier and Meriaux, 1980), but all methanol production schemes so far have used a synthesis gas, which may be derived from wood gasification or coal gasification. The low-quality "producer gas" resulting directly from the wood gasification (used in cars throughout Europe during World War II) is a mixture of carbon monoxide, hydrogen gas, carbon dioxide, and nitrogen gas. If air is used for gasification, the energy conversion efficiency is about 50%, and if pure oxygen is used instead, some 60% efficiency is possible, and the gas produced has less nitrogen content (Robinson, 1980). Gasification or pyrolysis could conceivably be performed with heat from (concentrating) solar collectors, for example, in a fluidised bed gasifier maintained at 500°C.

The producer gas is cleaned, CO2 and N2 as well as impurities are removed (the nitrogen by cryogenic separation), and methanol is generated at elevated pressure by the reaction

$2H2 + CO \rightarrow CH3OH$ (4.160)

The carbon monoxide and hydrogen gas (possibly with additional CO2) is called the "synthesis gas," and it is usually necessary to use a catalyst in order to maintain the proper stoichiometric ratio between the reactants of (Cheremisinoff *et al.*, 1980). A schematic process diagram is shown in

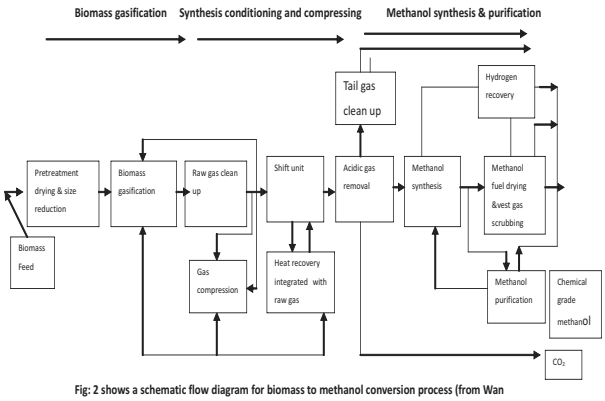


Fig: 2 shows a schematic flow diagram for biomass to methanol conversion process (from Wan simamins and Ngayen , 1981, Reported from Biomass Gasification (T Reed ,ed) , with permission , copyright 1981 , Noyes Data corporation)

An alternative is biogas production from the biomass followed by the methane to methanol reaction,

$2CH4 + O2 \rightarrow 2CH3OH$ (4.161)

also used in current methanol production from natural gas (Wise, 1981). Change of the H2/CO stoichiometric ratio for is obtained by the "shift reaction" Steam is added or removed in the presence of a catalyst (iron oxide, chromium oxide).

The conversion efficiency of the synthesis gas to methanol step is about 85%, implying an overall wood to methanol energy efficiency of 40- 45%.

Improved catalytic gasification techniques raise the overall conversion efficiency to some 55% (Faaij and Hamelinck, 2002). The currently achieved efficiency is about 50%, but all life-cycle estimates of energy inputs have not been included or performed (EC, 1994).

The octane number of methanol is similar to that of ethanol, but the heat of combustion is less, amounting to 18 MJ kg-1. However, the engine efficiency of methanol is higher than that of gasoline, by at least 20% for current motor car engines, so an "effective energy content" of 22.5 MJ kg-1 is sometimes quoted (EC, 1994). Methanol can be mixed with gasoline in standard engines, or used in specially designed Otto or diesel engines, such as a spark ignition engine run on vaporised methanol, the vaporisation energy being recovered from the coolant flow (Perrin, 1981). Uses are similar to those of ethanol, but several differences exist in the assessment of environmental impacts from production to use (e.g. toxicity of fumes at filling stations).

Conclusion

In conclusion we can observe that the use of renewable energy has become important in the all sectors of our social lives. The traditional use of biomass for combustion is still the dominating use of renewable energy, although it takes more efficient forms in many industrialized countries.

Only slightly less (146 W/cap.) is the use of food energy in biomass of animal or vegetable origin (the nutrient value of food being in any case more than that of the energy it provides). Next comes hydropower (50 W/cap.) and then geothermal power, which only in part can be classified as renewable

(as many steam reservoirs are exploited at a rate that will exhaust the reservoir over periods of decades). At the level of 1 W/cap., i.e. two orders of magnitude under the energy in food intake, one finds biomass waste (used for power or heat), biogas, liquid biofuels (used in the transportation

sector), wind power and geothermal heat (used for district heating). At the bottom comes solar heat, tidal power and solar power, the latter below 0.01 W/cap. However, the fastest growing markets are those of wind and solar power, both currently adding 35% of installed power each year.

The market characteristics of the various renewable energy forms exhibit differences linked to the nature of each source. For food energy, the price is influenced by variations in production due to climatic variations, the choices made in regard to area use, livestock holdings, fish quotas and the competitive behaviour of the food processing and marketing industry. Yet the bulk prices of different commodities seem remarkably consistent with their energy content, varying only between some 70 US or euro cents per kWh (heat value) and 200 c/kWh. Translating OECD data (OECD, 2002) to energy

units, the current whole-sale price of cereals such as rice or wheat are around70 c/kWh, while the whole-sale price of typical meat and diary products are about 100 c/kWh. Only specialized gourmet products obtain higher prices in the marketplace. Consumer retail prices are typically five times higher than the bulk prices just quoted. This is more than 30 times the current consumer price of a kWh of electricity produced from fossil fuels. Wholesale market prices for biomass waste and fuel wood range from Wholesale market prices for biomass waste and fuel wood range from about 1 c per kWh (of "burning value", i.e. energy of combustion) in India (FAO-Asia, 2003) to some 2 c/kWh in industrialized countries (e.g. straw, wood chips 1.6 c/kWh and wood pellets 1.9 c/kWh; Danish Energy Agency, 1996; Alakangas *et al.*, 2002). For comparison, the cost of coal before considering

externalities is 0.5 c/kWh (Danish Energy Agency, 2002). The production cost of biogas is 3.6-7 c/kWh (Danish Energy Agency, 1992), while that of wind power is 3-7 c/kWh (depending on wind conditions) and that of photovoltaic solar power 40-130 c/kWh (IEA-PVPS, 2002).

REFERENCES

[1] Ackermann, T. (2002). Transmission systems for offshore wind farms. *Renewable Energy*
World, vol. 5, no. 4, pp. 49-61.

[2] Alakangas, E., Hillring, B., Nikolaisen, L. (2002). Trade of solid biofuels and fuel
prices in Europe, pp. 62-65 in "12th European Biomass Conf.", ETA Firenze &

WIP Munich.
[3] Barbier, E. (1999). Geothermal energy: a world overview. *Renewable Energy World,* 2,
148-155
[5] Berglund, M., Börjesson, P. (2002). Energy efficiency in different types of biogas systems,
pp. 219-222 in "12th European Biomass Conf.", ETA Firenze & WIP Munich.
Berkner, L. and Marshall, L. (1970).
[6] In "The Encyclopedia of Geochemistry and Environmental
Sciences" (R. Fairbridge, ed.), Vol. 4A, pp. 845–861. Van Nostrand,
New York.
[7] Biomass Energy Institute (1978). "Biogas Production from Animal Manure", Winnipeg,
Manitoba.
[8] Bockris, J. and Shrinivasan, S. (1969). "Fuel Cells: Their Electrochemistry".
McGraw- Hill, New York.
[9] Brown, S. (1998). The automakers' big- time bet on fuel cells. *Fortune Mag.*, 30 March,
12 pages (http://www.pathfinder.com/fortune/1998/980330).

MATERIALS IN ADVANCED CLEAN COAL TECHNOLOGIES

1.2 OCHERI C.[1], AGBOOLA, J.B[2] OYELARAN O.A[3] & BARNABAS A.[4]
Foundry Shop, Ajaokuta Steel Company Limited, Ajaokuta, Kogi State[1]

Department of Mechanical Engineering, Federal University of Technology, Minna, Niger State[2]
Hydraulic Equipment, Development Institute, Kano [3]
Department of Metallurgical & Materials Engineering,
Federal University of Technology, Akure, Ondo State[4]
E-mail:ocheri4c@yahoo.com, joe_agboola@yahoo.com ajanioyelaran@yahoo.com ,
&barnabelad20012000@yahoo.com

ABSTRACT
Coal is a critical component in the international energy portfolio, used extensively for electricity generation. Coal is also readily converted to liquid fuels and/or hydrogen for the transportation industry. However, energy extracted from coal comes at a large environmental price: coal combustion can produce large quantities of ash and carbon dioxide, as well as other pollutants. Advanced technologies can increase the efficiencies and decrease the emissions associated with burning coal and provide an opportunity for carbon dioxide capture and sequestration. However, these advanced technologies increase the severity of plant operating conditions and thus require improved materials that can stand up to the harsh operating environments. The materials in advanced clean coal technologies must be use to solving problem associated to burning coal, make it acceptable economically and environmentally through sound choice for producing energy
Key Words: Coal, Clean, Technologies, Advanced Materials

1.0 INTRODUCTION

Coal, a combustible organic rock composed primarily of carbon, hydrogen, and oxygen. Coal is burned to produce energy and is used to manufacture steel. It is also an important source of chemicals used to make medicine, fertilizers, pesticides, and other products. Coal comes from ancient plants buried over millions of years in Earth's crust, its outermost layer. Coal, petroleum, natural gas, and oil shale are all known as fossil fuels because they come from the remains of ancient life buried deep in the crust.

Coal is rich in hydrocarbons (compounds made up of the elements hydrogen and carbon). All life forms contain hydrocarbons, and in general, material that contains hydrocarbons is called organic material. Coal originally formed from ancient plants that died, decomposed, and were buried under layers of sediment during the carboniferous period, about 290 million to 360 million years ago. As more and more layers of sediment formed over this decomposed plant material, the overburden exerted increasing heat and weight on the organic matter. Over millions of years, these physical conditions caused coal to form from the carbon, hydrogen, oxygen, nitrogen, sulfur, and inorganic mineral compounds in the plant matter. The coal formed in layers known as seams. Plant matter changes into coal in stages. In addition, coal contains a number of inorganic impurities, and its combustion results in the emission of the "criteria pollutants" sulfur dioxide (SO_2), nitrogen oxides and particulates, as well as mercury. Both the specific impurities present in a coal feedstock and their quantities depend on the type of coal and where it is mined, but at least 10 wt% of any coal is some combination of volatile and noncombustible inorganic components, present primarily in the form of minerals. Some coals consist of 50 wt%, or more, of these non-carbon–based constituents.

As a result, any viable coal combustion technology must be able to accommodate the presence of these impurities at elevated temperatures and to remove them from the plant waste stream to levels mandated by local environmental regulations. Good environmental stewardship would seek complete removal and benign sequestration of all pollutants wherever possible in the conversion of this necessary fuel to energy.

Technology advancement to address the world's growing demand for clean and affordable energy will require simultaneous advances in materials science and technology in order to meet the performance demands of new power systems.

This is particularly true for coal-based technologies, where the drive for increased efficiencies and reduced environmental impact— the drive to extract as much energy as possible from every ton of coal—calls for the use of increased system operating temperature sand pressures, as well as the ability to perform effectively in increasingly aggressive environments. The addition of alternative feed stocks, such as the combustion of coal and biomass to produce electricity and/or liquid fuels, can also place a huge stress on the materials of construction, to the point where the development of new materials with improved performance characteristics and/or new materials protection strategies are warranted. Each of the evolving clean coal technologies must address specific materials in order to achieve widespread commercialization.

2.0 Clean Coal Technologies

Since the mid-1980s, a worldwide push to reduce the environmental impact of coal's conversion to energy has resulted in the advancement of a group of technologies known collectively as clean coal technologies (CCTs). Designed with the combined goals of minimizing emissions and maximizing energy efficiency for each ton of coal processed, the suite of CCTs in development today comprises advanced pollution controls for new and existing power plants, including CO_2 capture and sequestration; advanced combustion technologies; and gasification- based systems.

Another goal for these systems is fuel flexibility, allowing for the use of a range of different types of coals, or combinations of coal and other opportunity fuels such as petroleum coke or biomass, without impacting plant performance. Beyond electricity generation, coal gasification systems are also being designed for product flexibility, offering the option of producing liquid fuels and/or hydrogen from coal while minimizing impact on the environment.

3.0 Advanced Combustion Technologies

Pulverized coal combustion (PCC), in which finely divided coal particles are combusted in air in a boiler to create steam that is passed through a steam turbine to generate electricity, accounts for over 90% of coal-fired capacity worldwide. Modern PCC technology is well developed, and today's sub critical coal-fired power plant, operating at a steam temperature of 540°C and a steam pressure of 16.5 MPa, has a thermal efficiency of approximately 35%.

However, more energy extracted per unit coal means an increase in power plant output and a relative decrease in emissions, and thus, advanced combustion technologies seek to maximize the thermal efficiency of the power plant through increases in steam temperatures and/or pressures above the critical point. Additional increases in thermal efficiencies are being sought through additional increases in steam temperatures and pressures, but these will require further advances in materials technology to be realized at a commercial scale.

The coefficients of thermal expansion (expansion of material with increasing temperature) must be compatible in those components that are joined with other components, such as the turbine rotors and blades. In addition, the alloys must be resistant to sulfide and chloride attack on the fire side (i.e., inside the boiler, where the coal is combusted) and to oxidation on the steam side (i.e., inside steam piping and within the steam turbine). For many alloys, a chemistry and microstructure optimized for creep resistance are not optimum for required environmental resistance, so effective coating and/or cladding strategies will also have to be considered.

Beyond performance, fabricability and weldability must also be designed into the materials being developed. In all cases, because of the very large volume of materials required to construct a power plant, reliability must be obtained at an affordable cost.

Combusting coal in oxygen, as opposed to air, can lead to a significant reduction in NO*x* emissions and also simplify CO_2 capture for sequestration, so combined with USC technology; it can significantly reduce the environmental impact of PCC plants. Currently, no commercial-scale oxy-fired PCC plants are in operation, although several such new plant constructions were announced recently in the United States. Existing PCC plants could also be retrofitted with oxy-fuel burners, thereby providing a carbon capture option for the existing power fleet.

However, with no oxy-fired retrofit boilers currently in operation, there is no experience in how the resulting change in operating environment will impact the boiler materials of construction or the operation of the plant as a whole. Perhaps the single greatest materials challenge associated with oxy-fuel combustion is in the production of oxygen.

Oxygen produced by cryogenic air separation methods can be prohibitively expensive for this application, and a reliable, affordable alternative method for producing oxygen is needed for this as well as other advanced coal combustion technologies.

Fluidized-bed combustion (FBC) is another of the advanced combustion technologies that has evolved from efforts to develop an environmentally friendly combustion process that does not require external emission controls. FBC systems burn coal, and other carbon-containing feedstock, in a bed of heated particles suspended in flowing air. The fluidizing action promotes more complete coal combustion at lower flame temperatures, between 760°C and 925°C, which greatly reduces NO*x* emissions (nitrogen oxides are typically formed at temperatures approaching 1370°C).

In addition, the particle bed includes a sulfur-absorbing sorbent such as limestone or dolomite, which can reduce SO_2 emissions by more than 95%. As a result, FBC systems can meet most environmental standards for SO_2 and NO*x*, without the need for post-combustion pollution controls. Atmospheric-pressure FBCs are available in either a bubbling FBC or circulating FBC configuration, with a power-generating efficiency similar to that of a standard PCC plant. Popular primarily because of its fuel flexibility—an FBC can burn any carbon-containing material, from low-rank coals to municipal waste—and environmental performance, there are now more than 400 FBC units operating worldwide. A second type of FBC system, the pressurized fluidized-bed combustion (PFBC) system, operates at elevated pressures to produce a gas stream that can drive a gas turbine. However, this technology has yet to find widespread market acceptance.

Materials challenges inherent to FBC systems depend primarily on the type of feedstock utilized, and FBCs sometimes experience excessive materials wastage through corrosion and wear. Combustion of biofuels can result in the formation of alkaline sulfates and chlorides at the tube surfaces, resulting in an accelerated corrosion-erosion of the tube walls. In PFBC systems, product gas streams require removal of fly ash particulate by a series of candle filters before entering the turbine, and filter reliability can be an issue.

Post-combustion CO_2 capture for subsequent sequestration is a challenge for existing coal combustion plants without oxyfuel firing, because it requires the

separation of dilute concentrations of CO_2 (13–15 vol% in a typical coal plant) from the low-pressure flue gas stream. Amine absorbents are currently commercially available that can remove as much of 90% of the CO_2 from the flue gas; however, regeneration of the solvents is an energy-intensive process, resulting in a decrease in plant electricity output of approximately 15%. In addition, amine solvents degrade in the presence of other trace impurities in the flue gas, such as particulates, SO*x*, and NO*x*. New absorbent materials and processes that can more effectively and efficiently remove CO_2 from the flue gas of conventional coal combustion plants will be needed if CO_2 sequestration is to become a reality for the existing coal combustion fleet.

4.0 Gasification Technologies

The gasification process reacts a carbon-containing material, such as coal, with steam and controlled amounts of air or oxygen at high pressures and temperatures to form a synthesis gas composed primarily of carbon monoxide and hydrogen.6 Synthesis gas, or syngas, can then be used as a fuel to generate electricity and/or steam, or it can be used as a basic chemical building block for the formation of a variety of liquid fuels or other chemical products.

The gasification of coal is not a new technology: "Town gas" (another name for syngas) was widely used in North America and Europe until it was replaced in the 1950s by natural gas, and Germany used this process to produce substantial amounts of liquid fuels during World War II. However, the technology's fuel and product flexibility, combined with its relatively lower emissions of criteria pollutants compared to advanced combustion technologies and the relatively straightforward extraction of CO_2 from the syngas for subsequent sequestration, have brought renewed interest in gasificationin recent years. In order to promote healthy atmosphere, the use of many fuels which releases carbon emissions into the atmosphere has to be reduced. Heating the coal under controlled conditions with insufficient air to provide complete combustion produces a gaseous fuel known as syngas, which is also known as town gas. Coal has been gasified ever since the industrial revolution to produce "town gas". This was once done in the local gas works, and every town had one.

4.1 The advantage of **Coal gasification** is that the use of synthesis gas as fuel and its origin is more than direct combustion, because the high temperature fuel cells can be burned. Carnot's rule can be efficient or effective as on the thermodynamics of the upper limit not apply. Internal combustion engine directly used to produce methanol and hydrogen. In addition, the high-temperature combustion refines out corrosive ash elements such as chloride and potassium, allowing clean gas production from otherwise problematic fuels.

Oxygen gasification or steam at high temperatures with the control of the reaction of the raw materials from coal, oil or biomass, such as carbon monoxide and hydrogen for the conversion of carbonaceous materials is one method. Gasification is a very efficient method for extracting energy from many different types of organic materials, and also has applications as a clean waste disposal technique.

Coal gasification technology is at the forefront in the efforts to develop alternatives for conventional furnaces. It is of particular interest because it offers an opportunity to use the product fuel gas in integrated gasification combined-cycle electric power generation (IGCC). Great hopes are pinned on IGCC as a highly efficient and low polluting emissions technology. Gasification can also be fueled by materials that are not otherwise useful fuels, such as biomass or organic waste.

5.0 Hydrogen from Coal

Hydrogen can be produced from coal by first gasifying the coal to produce a cleaned synthesis gas and subjecting the gas to the water–gas shift reaction (H_2O + CO « H_2 + CO_2) in a catalytic reactor to increase the hydrogen content and convert the CO to CO_2. The CO_2 can then be separated for subsequent sequestration, leaving a relatively pure hydrogen stream to be used as a fuel in a hydrogen turbine or in a fuel cell. However, although this process is technically feasible today, issues with efficiency and cost still need to be addressed.

From a materials standpoint, this means research to develop improved catalysts for the water–gas shift and membranes for hydrogen separation that are more tolerant of impurities such as sulfur, ammonia, and chlorides. Alternatively, CO2-selective membranes can be used to purify the hydrogen stream. Successful separation membranes will have a high flux at low pressure drops and operate at temperatures between 250°C and 500°C. When the hydrogen from coal is intended for use in a fuel cell, membrane selectivity must ensure that carbon monoxide is present at concentrations of less than 10 ppm and that sulfur-containing compounds are present at concentrations of less than 10 ppb.

Successful transfer of membrane technology will require the development of effective high-temperature seals for membrane module assembly, as well as manufacturing methods that can reliably and affordably produce defect-free membranes. At a more fundamental level, a more complete understanding of membrane separation mechanisms will lead ultimately to the design of more effective separation systems.

Historically, hydrogen membranes have been fabricated from various combinations of metals, ceramics, and polymers, with dense metal membranes yielding the highest selectivity and porous-based membranes providing the highest .Carbon dioxide separation membranes, on the other hand, are typically based on polymers and depend on physical solubility to separate gases.

The most advanced polymeric membranes today have selectivity values for CO_2 to H_2 of ~10. More recent research trends have focused on CO_2- selective membranes utilizing a facilitated transport mechanism such as ionic liquids and molten salts, which have shown the potential to increase performance under conditions associated with gasification. However, these chemically enhanced transport mechanisms suffer from instability

and volatility of the transport media.

6.0 Advanced Land-Based Combustion Turbines

As with other components in advanced coal power plants, research continues into the development of next-generation stationary land-based combustion turbines that include both increased efficiency and reduced impact on the environment.

These efforts are exemplified by DOE's FutureGen initiative, which aims to demonstrate a coal-fired IGCC power system that combines product flexibility and greater than 50% system efficiency with zero emissions by 2015.

To accomplish this goal, turbines that are fuel flexible and capable of operating at temperatures in excess of 1400°C will be required. In the nearer term, these will be hydrogen turbines, capable of reliably burning fuel that contains a majority of hydrogen at high temperatures to maximize efficiency. In the longer term, it is expected that these will be oxy-fuel turbines, capable of combusting fuels consisting of nearly 100% hydrogen.

From a materials standpoint, realization of the next generation of advanced turbines will require innovation in aerothermal concepts for cooling and heat-transfer management, combined with significant advances in materials technology. Traditionally, new materials and materials processes for land based combustion turbines have been adapted from those developed for the aircraft engine industry, although not without significant challenges resulting from the much larger sizes of the stationary land-based turbines.

This sharing of materials technology might continue in the future; however. Refractory materials exposed to the operating environment inside a slagging coal gasifier must be designed to resist slag penetration and attack. Interaction with the slag at the hot face of this chromium oxide refractory results in a significant change in the refractory microstructure and ultimately loss of material. Hydrogen/CO_2 separation membranes currently under development: (left) Poly-ionic liquid membrane for CO_2 removal; (center) multilayered, dense metal hydrogen separation membrane; and (right) copper-based, alumina-supported metal organic framework membrane for CO_2 separation. The temperature requirements for land-based turbines and jet engines are merging, and the materials systems that can reliably and affordably withstand the DOE requirements for turbine technology have not yet been identified. In addition to high temperature, the hydrogen and oxy-fuel land-based turbines will operate with substantially higher moisture contents than current commercial turbines, placing additional requirements for environmental resistance on the materials of construction.

For next-generation land-based hydrogen turbines, exhaust gases are expected to contain around 17% H_2O, whereas oxy-fuel turbines are predicted to have exhaust gases composed of up to 90% H_2O. This is in comparison to modern syngas turbines, where steam makes up less than 10% of the gas exhaust.

Within the hot section of the turbine, materials of construction will need to be resistant to oxidation, hot corrosion, creep, fatigue, and wear at temperatures in excess of 1400°C for long periods of operation.

Current generation nickel- and cobalt-based super alloys cannot withstand sustained metal temperatures greater than approximately 1100°C, requiring internal cooling as well as thermal-barrier and oxidation-resistant coatings to meet today's turbine performance requirements. As a result, it appears likely that the next generation of land-based turbines will require the development of new substrate materials, combined with new coating strategies, to meet the substantially higher temperature requirements.

With sufficient internal cooling, silicides, nitrides, and refractory metal-based alloys all have potential to meet the temperature requirements presented by the next-generation turbine; however, each has significant issues with regard to environmental stability, especially in the presence of moisture that will likely require mitigation through some form of protective coating strategy. In addition, the production and processing of these next-generation materials will be nontrivial, especially at the scale required for land-based turbine systems. In some cases, completely new processing strategies might need to be developed.

Regardless, because of the need for long-term reliability in these components, defects introduced during processing will have to be kept to an absolute minimum. Computational methods that link various length and time scales to define a complete materials chemistry, microstructure, and processing strategy could be key to accelerating development of these next-generation materials.

In addition to the development of structural materials and improved coatings, sensors that can provide real-time turbine process information (temperature, pressure, gas composition) to the operator are needed to fully optimize system performance. These requirements are very similar to those necessary for gasifier systems. In addition, *in situ* sensors that can monitor component reliability and nondestructive methods for assessing component health during maintenance shutdowns are needed to maximize materials performance in this application.

7.0 Coal to Liquid Fuels

Utilizing the Fischer–Tropsch (FT) process, the synthesis gas produced by a coal gasifier can be condensed over a suitable metal catalyst to produce liquid fuels and/or chemical feed stocks. Transportation fuels produced by this methodology are sulfur-free, low in particulates, and low in nitrogen oxides. Although this is not a new process—South Africa has been producing coal-derived fuels since 1955 and currently produces more than 30% of that country's gasoline and diesel from indigenous coal—there is still room for improvement, particularly in the area of reaction chemistries.

In FT synthesis, carbon monoxide is reacted with hydrogen in the presence of a solid metal catalyst, such as iron, cobalt to produce liquid hydrocarbons.

Iron catalysts are most often employed for coal-derived syngas because iron has a higher water–gas shift

activity and a significantly lower cost than cobalt. However, research is still needed to define the optimum catalyst size and shape for maximum activity and selectivity and to improve catalyst stability and lifetime. A better understanding is also needed of catalyst behavior in the reactor environment, so that processes can be optimized for efficiency and yield.

Computational studies, followed by experimental verification, will be key to identifying and optimizing promising reaction chemistries and chemical processing routes. Liquid fuels, such as high-octane gasoline, can also be produced from coal by a direct liquefaction process called Bergius hydrocracking. However, because of its relatively high cost and poor environmental performance, this process is not currently commercialized.

Summary

Clean coal technologies are being developed that can make the conversion of coal to energy an efficient and environmentally benign process; however, their successful realization will require simultaneous advancements in materials science and technology. New materials that can reliably meet the demands of increased temperatures and pressures, and increasingly severe service environments while maintaining required performance characteristics are needed, as are advanced processing technologies that can economically produce components at the required scale.

Computational methodologies that can accurately link the various scales of materials development, materials processing, and materials performance will help speed the time from concept development to component reality.

RESOURCES COAL

References

1. *The Coal Resource—A Comprehensive Overview of Coal* (World Coal Institute, Richmond-upon-Thames, UK, 2005); www.worldcoal.org/assets_cm/files/PDF/thecoalresource.pdf (accessed January 2008).
2. *The Future of Coal—Options for a Carbon-Constrained World* (Massachusetts Institute of Technology, Cambridge, MA, 2007); http://web.mit.edu/coal (accessed January 2008).
3. "Annual Energy Outlook 2007 With Projections to 2030" [Report DOE/EIA- 0383(2007), U.S. Department of Energy, Washington, DC, 2007]; http://tonto.eia.doe.gov/ftproot/forecasting/0383(2007).pdf (accessed January 2008).
4. R. Viswanathan, A.F. Armor, G. Booras, *Power* **148**, 42 (2004).
5. "Fluidized Bed Technology—Overview" (Office of Fossil Energy, U.S. Department of Energy, Washington, DC, 2007); www.fossil.energy.gov/programs/powersystems/combustion/fluidizedbed_overview.html (accessed January 2008).
6. "What is Gasification?" (Gasification Technologies Council, Arlington, VA, 2007); www.gasification.org/Technology.htm (accessed January 2008).
7. N. Holt, *Proceedings of the 2001 Gasification Technologies Conference* (Gasification Technologies Council, Arlington, VA, 2007); www.gasification.org/Docs/2001_Papers/GTC01052.pdf (accessed January 2008).
8. "Hydrogen from Coal—Future Technologies" (Office of Fossil Energy, U.S. Department of Energy, Washington, DC, 2007); www.fossil.energy.gov/programs/fuels (accessed January 2008).
9. T.M. Nenoff, R.J. Spontak, C.M. Aberg, *MRS Bull.* 31 (10), 735 (2006).
10. M.V. Mundschau, X. Xie, C.R. Evenson, in *Nonporous Inorganic Membranes*, A.F. Sammells, M.V. Mundschau, Eds. (Wiley-VCH, New York, 2006), chap. 4.
11. J. Giove III, J. Daniels, V.K. Der, *Power Ind. Dev.* **12**, 27 (2006).
12. *The Turbines of Tomorrow* (Office of Fossil Energy, U.S. Department of Energy, Washington, DC, 2007); www.fossil.energy.gov (accessed January 2008).
13. M. Jacoby, *Chem. Eng. News* **84**, 57 (2006).

MUNICIPAL SOLID WASTE MANAGEMENT (MSWM): ISSUES, CHALLENGES AND AGENDA FOR ACTION.

OYELARAN O.A. [1], OCHERI C[2]. AND BARNABAS A.[3]
Hydraulic Equipment Development Institute, Kano[1], Foundry Shop, Ajaokuta Steel Company, Ajaokuta[2] and
Dept of Metallurgical Engineering, Federal University of Technology, Akure. [3]

ABSTRACT
Municipal solid waste management constitutes one of the most crucial health and environmental problems facing both the Local and state governments of Nigeria. Poor management of urban waste represents a serious urban environmental and public health problem. The presence of waste in residential areas, at markets, roadsides, schools etc. poses grave health hazards to the populace. At the same time poor urban waste management is primarily due to the lack of sufficient resources to collect and properly dispose of municipal waste. Municipal wastes, which are always a function of population, increase proportionally. The paper attempts to examine the issues of Municipal waste Management, its challenges, how to face the various challenges and the agenda for action. After defining Municipal Solid Waste Management (MSWM), waste management is then examined, trailing its stages. In conclusion, the paper suggests some solutions to current waste management problems which included Public Private Partnership, Volume reduction, closing the loop (recycling of waste), Minimize waste at source of design, Improve waste collection systems and strict anti-littering laws.
Keywords: Municipal Solid Waste Management (MSWM), Public Private Partnership, recycling, Incineration

INTRODUCTION

Municipal Solid Waste (MSW) is Waste material from households and businesses in a community that is not regulated as hazardous.

Poor management of Municipal waste represents the most serious urban environmental and public health problem in Nigeria. It has dire environmental and public health consequences. Public health-wise, the presence of waste in residential areas, at markets, roadsides, etc. poses serious health hazards to people in general and children in particular. Much municipal waste in developing countries contains animal and human excreta, which play a major role in the transmission of communicable diseases like cholera, plague, tetanus, etc. Pathogens are known to survive for long periods of time in urban garbage [ ]. It has also been found that during the rainy seasons, uncollected municipal waste is washed by water, causing not only pollution of surface and ground water sources but also blocking the water drains, a situation which causes flooding [ ]. During the dry seasons, improperly managed urban waste decomposes causing serious air pollution, just as burning of solid waste does. In a nutshell, poor urban waste management has a lot of deleterious environmental and public health effects especially in high-density areas which are the typically characteristic of most major urban centres in Nigeria.

Even though many factors influence municipal solid waste management, population size is an important one. There is a positive correlation between city population size and both the percentage of waste moved and rate of households enjoying regular waste collection. This suggests that increasing city size poses a greater problem to the solid waste [ ]. With the steady increase in urban population and the decline in municipal services, urban waste has become a major problem in Nigeria with an estimated 30-50% of it remaining uncollected. The World Bank estimates the per capita daily refuse production to be between 0.7 and 1.8 kg for urban centres in industrialised countries and between 0.4 and 0.9 for those in developing countries. This translates to a rate of about 400 -900 metric tonnes of waste each day for a city on one million inhabitants [Fobil J. N et al: 2005]. Urban waste is a fast growing problem driven by rapid urban population growth, which is generally, at least twice the respective national population growth rates. This is evidenced by the increasing illegal dumpsites, irregular collection of garbage, and rising garbage piles and dumps in city alleys, streets and residential areas. Based on this most cities and towns could not cope with the increasing growth of waste production.

2. ISSUE: Municipal Solid waste management

Most of the waste management budget is dedicated to waste transportation alone, still only a very small percentage is moved to the waste disposal centre. Two main collection systems can be identified: the primary or pre-collection at household level and the secondary collection by the Refuse management board or Refuse removal contractors.

Various categories of collection dumper trucks fitted with corresponding specialized devices for removing and dumping waste have been imported for use. Sweeping of some main streets is done manually as well as with mechanical van where it exists. These equipment breakdowns quite often and they are also very expensive to run and maintain. waste today-a great improvement, however, many problems still exist of the big problem is the pre-collection of large amounts of waste trapped in inaccessible residential quarters, prior to its transport to the nearest official regular waste management facility. Such areas constitute more than 65 percent of the city area

and are inhabited mostly by low-income members of the communities. There is no
house-to-house collection, so pre-collection from homes to the public or communal skips placed at strategic spots in the city, has to be organized by households or some informal private groups
Conflict over zones of exploitation is only one of such problems. Dr. Kolawole Raheen in Megafu (2003), advising the Lagos State Government on its waste management, draws their attention to one other danger of multinationals thus: 'Multinational companies all over the world are known for managing wastes the cheapest way by dumping them into rivers where people would not understand what have been dumped". Giving a concrete example (Marchand 2002) cites the disposal of refuse in the middle of a South African township by SITA, an affiliate of the French Conglomerate Suez. According to this source, the township unknowingly accepted a quantity of toxic waste, mostly medical. This was in complete disregard of the welfare of the township' s inhabitants and especially children who were exposed to poisoned used syringes. The author characterizes it as double standards because different rules are applied in different places for the same situation–"keeping the north clean and the south dirty" (Marchand 2002:1). This company was active at the Johannesburg Earth Summit, the same source remarks.

3. CHALLENGES: WASTE EXPLOSION

The traditional approach where municipal authorities monopolise waste management, ignoring other stakeholders, This approach does not improve much the waste management situation in Nigerian cities. The noninvolvement of the major stakeholders worsens the scenario. Asomani-Boateng et al. (1999:1), quoting Adedibu and Okekunle (1989) use the case of Lagos, Nigeria to illustrate what looks like a common phenomenon in many African cities. They ranked Lagos as the dirtiest capital in the world and further expanded: ..in most parts of the city, streets are partially or wholly blocked by solid waste. Similarly open spaces, marketplaces are littered with solid waste. In most cases drains are clogged or totally blocked and many compounds are hemmed in by solid waste. Similar conditions exist in many other cities of Nigeria where only 21 percent of the people benefit from home collection of their solid waste, the uncollected waste is illegally dumped in open spaces, water bodies, storm-drainage channels, buried, burnt or deposited along the streets or roadsides. Blocked drainage channels cause flooding in the cities. Many authors attribute the prevalence of parasites, tetanus, malaria, hookworm, cholera, and diarrhea so common in many African to unsanitary conditions caused by waste being simply strewn around (McMicheal 2000); (Mwanthi et al. 1997).

Economic growth: The development of the solid waste sector in the last decade shows rapid changes. Mass consumption and a throwaway ethic are reasons for the growing amount of solid waste. Growing quantities of waste demand additional capacities for transportation, storage, treatment and disposal. While appropriate technology and environmental concerns have to be considered, social aspects and community involvement are equally important.

Population growth: Even though many factors influence municipal solid waste management, population size is an important one. There is a positive correlation between city population size and both the percentage of waste moved and rate of households enjoying regular waste collection. This suggests that increasing city size poses a greater problem to the solid waste management. With the steady increase in urban population and the decline in municipal services, urban waste has become a major problem in Nigeria.

Rising affluence (high consumption pattern, high expectations.): One other source of solid waste in African cities is imported second hand goods from the developed world. These old goods are near the end of their life cycle and spend little time with their final owners before being put aside as waste. Cases of accepting imported foreign waste in exchange for 'hot' currencies have been reported in Africa. Current studies on Bamenda city in Cameroon by Eric Achankeng indicate that one new and increasing element in waste composition is that of non-biodegradable waste. Electronic waste or E-waste, and waste from white goods are increasing [Achankeng E.: 2003]. In regular household waste generation, plastics, paper and cartons, tin cans, glass, bottles and fibre are on the increase Their rates of generation have a relationship with the different socio-economic parts of the city- a trend that suggests the increasing influence of globalization and changing consumption habits.

4. AGENDA FOR ACTION

INCINERATION (VOLUME REDUCTION): This remains a low option for Africa. The high organic and water content of the waste stream make incinerators energy consumers rather than energy producers. Incinerators are also very expensive to construct and run. The failed cases of incineration in Tanzania and Nigeria demonstrate that incinerators are not sustainable for Africa (UNEP-IETC1996).

Composting: Many authors identify the organic content of solid waste in African cities to be as high as70 percent (Achankeng E.: 2003). This suggests that composting could be a very viable recovery alternative (Mustafa et al. 2002). However this has been tried in various countries at different scales with very poor results. International NGOs have sponsored small scale composting in Benin, Cameroon, Egypt, Kenya, Nigeria, South Africa, and Zambia; but the practice has not had significant impact on the cities MSW reduction (UNEP-IETC 1996). Poor quality of the manure resulting from inadequate segregation of waste appears to have increased the low demand. In a recent study of composting in Bamako, Mali and Cameroon (Keita: 2003) demonstrates how increasing quantities of strange global products such as plastics and packaging have invaded compost manure, rendering it unacceptable by farmers. The project has ended due to many problems, but one key reason being poor quality as a consequence of plastic materials.

Sustainable solution closing the loop (recycling of waste). Waste minimization, through segregation of recyclable materials like plastics, glass, metals, etc. is another aspect, which needs special attention. NGOs may come forward to promote the activity. Waste pickers may be trained so that the segregation of recyclable items can be done in a more systematic and organized way.

Source Reduction: The United States Environmental Protection Agency defines the term, source reduction; as follows "Source reduction is the design, manufacture, purchase, or use of materials or products (including packages) to reduce their amount or toxicity before they enter the municipal solid waste stream. Because it is intended to reduce pollution and conserve resources, source reduction should not increase the net amount or toxicity of wastes generated throughout the life of a product." Good package design helps reduce the volume of our waste stream, while maximizing cost effectiveness and product protection. Less material means smaller packages, reducing the number of truckloads required to ship and the associated transportation impact. In addition to reduced packaging cube size, a majority of the products we now provide expand on-site at time of use, reducing warehouse space requirements and associated energy resources. The goal is to provide more efficient solutions for our customers with the lowest possible environmental impact

Strict anti-littering: laws on regulation of solid waste disposal and facilities and its enforcement. Providing inspection and oversight to ensure that the laws are effectively implemented and enforcing standards. Violators should be prosecuted accordingly.
Involve the community (Public Private Partnership) Residents, Businesses, Schools, Grassroots organizations, Government agencies, NGOs.[Programs/Initiatives: Recycling Corners in Schools, Environment Clubs, Dialogue/feedback, Community-led activities, Products stewardship, Recycling Day, Clean & Green Week etc]The development of the solid waste sector in the last decade shows rapid changes. Mass consumption and a throwaway ethic are reasons for the growing amount of solid waste. Growing quantities of waste demand additional capacities for transportation, storage, treatment and disposal. While appropriate technology and environmental concerns have to be considered, social aspects and community involvement are equally important. It is very essential that before any project is implemented, a public participation meeting be held to make the public aware of the technology used and the impacts.

Approach (Communication, Engagement and empowerment). Environmental education is a way of increasing understanding of problems, cooperation among stakeholders, environmental entrepreneurship and environmental performance. The training should be a regular feature of MSWM, with hands on training on sorting and collection. After training there should be follow up of the practices

5.0 Conclusion

This paper's findings believe ministry of Environment do not have any sustainable method of municipal solid waste management. It is all a history of trials and abandonment with many issues seemingly unresolved. Africa's national and urban governments are copying ill-adapted global strategies and technologies not suitable to the local realities. They are not adequately exploring and using local initiatives and strategies, which could go a long way to improve solid waste management. Imported waste management technologies have not adequately solved the problem. Local and adapted techniques involving collaboration with the stakeholders and coordinated by the government would be important. Decentralised participatory management with mutual respect and close collaboration is indispensable. Globalization and urbanization have come to stay. They have benefits as well as a good number of irking problems. Finding solutions to problems associated with urbanization and globalization, while at the same time realizing their positive prospects would be the better way out. The ability to deal with this new situation will require effective capacity building for cities and communities toward participatory and good governance. Such will produce city leaders who will not close their eyes to the environmental degradation by multinationals while opening their pockets, but forward looking leaders who will put their city, its environment and its people ahead of every other consideration. Such a strong city government will also be able to place checks on the power of transnational corporations, press for certain minimums including share profits of their less regulations and free trade barriers.

References

Achankeng E.(2003) Globalization, Urbanization and Municipal Solid Waste Management in Africa African Studies Association of Australasia and the Pacific 2003 Conference Proceedings - African on a Global Stage

Asomani-Boateng, R. and M. Haight (1999). Reusing organic solid waste in urban farming in African cities: A challenge for urban planners. Ontario, IDRC, International Development Research Centre: 9.

Fobil J.N.,Carboo D.and Armah N.A.(2005) Evaluation of municipal solid wastes (MSW) for utilisation in energy production in developing countries 76 Int. J. Environmental Technology and Management, Vol. 5, No. 1, 2005

4Keita, M. (2003). Improving the stakeholder involvement in solid waste collection in
Bamako. CWG Workshop, Dar es Salaam

Kishimba M.A. (2009).Energy recovery from Municipal Waste: Making Cities more Productive and Cleaner;

Converting an Environmental and Public Health liability into a Social-economic and Poverty alleviation Asset.

Kreith, F. (1994) *Hand Book of Municipal Solid Waste Management,* McGraw-Hill, Inc.,
New York, pp.11.1–11.82.

Marchand, A. (2002). Impunity for multinationals. ATTAC, Global policy forum.

McMicheal, A. J. (2000). The urban environment and health in a world of increasing globalization:issues for developing countries. Bulletin of the World Health Organisation, 200, 78. W. H. Organisation, World Health Organisation. 78 (9).

Megafu, S. (2003). Expert Raise Alarm on Filth in Lagos, THISDAYonline. 2003.

Mwanthi, M. A., L. O. Nyabola, et al. (1997). "Solid Waste Management in Nairobi City: Knowledge and Attitudes." Environmental Health Dec. 1997(Dec. 1997): 23-29.

UNEP-IETC, U. N. E. P.-I. E. T. C. (1996). International Source Book on Environmentally Sound Technologies for Municipal Solid Management. Osaka/Shiga, UNEP International Environmental Technology Centre

SYNTHESIS AND CHARACTERIZATION OF SOME HEMATITE (A-FE_2O_3) SAMPLES

Adegoke H.I[+]. and Adekola F.A.
Dept of Chemistry, University of Ilorin, Ilorin, Nigeria.
[+]Corresponding author: **ihalimat@yahoo.com**

Abstract
Hematites of different morphology were prepared using four (4) different methods of preparation. The synthesized hematite were characterized by X-ray diffraction, X-ray fluorescence and Scanning electron microscopy. The pH of the sample ranged from 6.30 to 9.06 and the point of zero charge of one of the sample was also determined using potentiometric mass titration method. The morphology of the sample ranges from plate-like to spherical shape from the Scanning Electron Micrograph, the XRD spectra and XRF results show that the sample is hematite. The particle sizes of the various hematite sample were in the range of 41.4- 41.7nm.

Introduction

The preparation and properties of iron oxides continue to attract considerable interest and attention because of their importance in magnetic materials technology [1]. The formation of iron oxides in aqueous system involves nucleation and crystal growth[2]. Iron oxide samples often display a wide range of particle sizes indicating that nucleation and crystal growth took place simultaneously over the bulk of the reaction. Nucleation and crystal growth must be separated in order to obtain a product with a fairly narrow size distribution[2]. Almost all the iron oxides and hydroxides can be prepared by a number of synthesis routes; the method of synthesis frequently influences the properties of the product, particularly crystal morphology, degree of crystallinity, surface area and water content. The methods of synthesis are hydrolysis of acidic solution of Fe(III) salts, transformation of ferrihydrite in alkaline media, oxidative hydrolysis, phase transformation and decomposition of metal chelates[2].

Hematite, akaganeite and ferrihydrite may be obtained by hydrolysis of Fe^{3+} solutions. The product formed is influenced by variety of factors including rate of hydrolysis, solution pH, temperature, [Fe^{3+}] and the nature of the anion present. Hydrolysis reactions are:

$$Fe^{3+} + H_2O \rightarrow FeOH^{2+} + H^+$$
$$Fe^{3+} + 2H_2O \rightarrow Fe(OH_2)^+ + 2H^+$$
$$Fe^{3+} + 2H_2O \rightarrow FeOOH + 3H^+$$
$$2Fe^{3+} + 3H_2O \rightarrow Fe_2O_3 + H^+$$

The reaction condition must be carefully controlled in order not to get mixtures, rather than a single produc[2]. Some researchers have investigated the synthesis method intensively and shown the various way in which the reaction product and also morphology may be influenced by reaction conditions[3,4].

Hematite (α-Fe_2O_3) crystallizes in the rhombohedral system space group R_3C. its crystal structure consist of Fe^{3+} cations octahedrally coordinated hexagonal close packed oxygen atoms. The arrangement belonging to the corundum (α-Al_2O_3) structure typed[5,6]

Hematite occurs as rouge red earthy masses of finely divided particles, it is the major red coloring agents in rocks and is common interstitial cement in sediments. The color is blood red in thin fragment and streak and powder are rouge red: hardness is 6 on mohs scale and specific gravity is 5.25. The mineral is weakly magnetic[6].

Hematite is one of the most frequently used catalyst in chemical industries and are potential candidate ad a photo anode for possible photo electrochemical cells[7-10.]

Several researchers have synthesized and characterize different types of hematite nanoparticles. They observed that small changes in the reaction condition led to remarkable changes in final size and shape of hematite crystallites[3, 11-13]

The methods of characterization used by various researchers include-ray diffraction, raman spectrum, transmission electron microscopy and scanning electron microscopy.

The main objective of this paper is to synthesize hematite samples of different morphology and characterize them by physicochemical and spectroscopic methods.

Materials and Methods

All chemical agents were purchased from Sigma Aldrich Chemical Company and used without further purification. Deionized water of conductivity 110.1μS was used for all solution preparation

Synthesis of Hematite

The hematite particles were prepared using four different methods.

Method 1

Synthesis of hematite particle (ADE1) was carried out by acid hydrolysis method by mixing 2L of preheated 0.002M HNO_3 and 16.6g of $Fe(NO_3)_3$. $9H_2O$ at 98°C.The mixture was stirred vigorously and aged in the oven at 98°C for seven days. The red sediment was centrifuged, dialyzed in deionized water to remove the nitrate ion, filtered using a 0.45μm Millipore filter paper in a vacuum filtration system and dried in the oven at 40°C[2].

Method 2

Synthesis of hematite particle (ADE 2) was also carried out by acid hydrolysis method,

1L of 0.002M hydrochloric acid solution was preheated in the oven at 100°C and 10.80g of $FeCl_3$. $6H_2O$ was

dissolved in the hot solution to make 0.02M Fe^{3+} solution with and vigorous stirring to form a reddish brown homogeneous solution. The mixture was aged in the oven at 100°C for seven days. The reddish- brown sediment was centrifuged, dialyzed in deionized water to remove the chloride ions, filtered using a 0.45µm Millipore filter paper in a vacuum filtration system and dried in the oven at 40°C [11].

Method 3

The method of Sugimoto et al was employed in the synthesis of hematite particle ADE3

100ml of 5.4M NaOH aqueous solution was prepared and added slowly into a well stirred100ml 2.0M $FeCl_3$ aqueous solution in 250ml Pyrex flask for. The mixture was stirred for 10 minutes and the flask containing a reddish brown mixture was placed in an oven preheated to 100°C for 8days. The sediment was centrifuged, dialyzed in deionized water to remove the chloride ions, filtered using a 0.45µm Millipore filter paper in a vacuum filtration system and dried in the oven at 40°C [12].

Method 4

Synthesis of hematite particle (ADE 4) was also carried out by acid hydrolysis method 40g of $Fe(NO_3)_3.9H_2O$ was dissolved in 500ml deionized water preheated to 90°C, 300ml of 1M KOH preheated to 90°C was added to the brown solution and a deep brown suspension was observed. 50ml of 1M $NaHCO_3$ preheated to 90°C was added to the brown suspension in a closed flask, the mixture was aged in the oven at 90°C for 48hours.

The product was centrifuged, dialyzed in deionized water to remove the nitrate ion, filtered using a 0.45µm Millipore filter paper in a vacuum filtration system and dried in the oven at 40°C [2].

Characterization of the prepared Sample

The prepared samples have been characterized using the following physical and spectroscopic methods: pH, Point of zero charge (PZC), X-ray fluorescence (XRF), X-ray diffraction (XRD), Infra red spectroscopy (IR).

The pH of the sample was determined by taking 1: 10(w/v) suspension of sample in deionized water, this was performed by using a pH meter (model pHS -25).

The point of zero charge of the sample ADE 4 was determined using potentiometric and mass titration method.

The structure of the samples were examined by X-ray diffraction. Powder XRD patterns were recorded with a PW3050/60 Goniometer using CuKα, with a scanning speed of 2° min^{-1}. The characteristic reflection peaks were matched with the JCPDS data files and the crystalline phases were identified.

The elemental abundances normalized to 100 weight was accomplished using a Leo 1430VP Scanning Electron Microscope. The composition s quantified by EDS analysis using an Oxford Instument 133KeV detector and Oxford INCA software. Beam conditions during analyses were 20KV and approximately 1.5nA, with a working distance of 13mm and a specimen beam current of -3.92nA.

Scanning electron microscopy (SEM) was used in inspecting the morphology of the hematite particles. The instrument used was a Leo 1430VP Scanning Electron Microscope

Results and Discussion

The physical properties of the samples are shown in the Table 1 below:

Table1: Physical Properties of the samples

Samples	1	2	3	4
Colour	Reddish brown	Brown	Reddish brown	Reddish brown
pH	6.30	6.65	7.47	9.06
PZC	–	–	–	9.06–9.35
Texture % yield	Fine 62.4	Fine 83.1	Fine 91.7	Fine 81.3

The colour of the samples ranges from reddish brown to brown, this in line with the colour revealed in literature for hematite samples [2].

The pH is in the range 6.30 and 9.06 for the various hematite particles and the point of zero charge determined by potentiometric mass titration method for the hematite sample ADE 4 is in the range 9.06-9.35. The value is in the range of values stated by Marek [13] for point of zero charge for hematite.

XRD spectra

Figures 1a- 1d show the XRD spectra for the samples Ade1- 4. They revealed that all the samples were hematite crystals when the JCPDS constant values obtained were compared with the standard values. The particle sizes of the samples were obtained from the XRD spectra using the Scherer formular. The results obtained for the particle sizes for the samples is in the range 41.4-41.7nm which is in line with the values reported by Gee et al [11] and Cornell and Schwertmann [2] for particle sizes of hematite of 35-45nm and 30-50nm respectively.

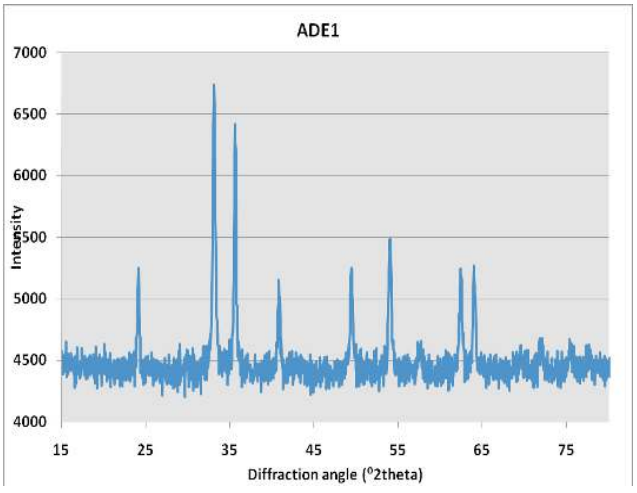


Fig 1a: XRD pattern of hematite ADE1

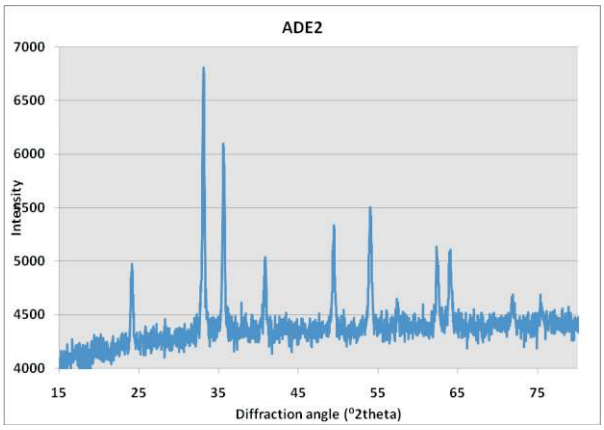


Fig 1b: XRD pattern of hematite ADE2

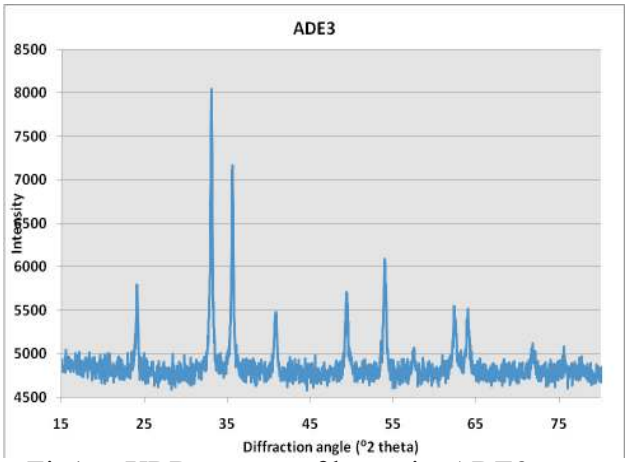


Fig1 c: XRD pattern of hematite ADE3

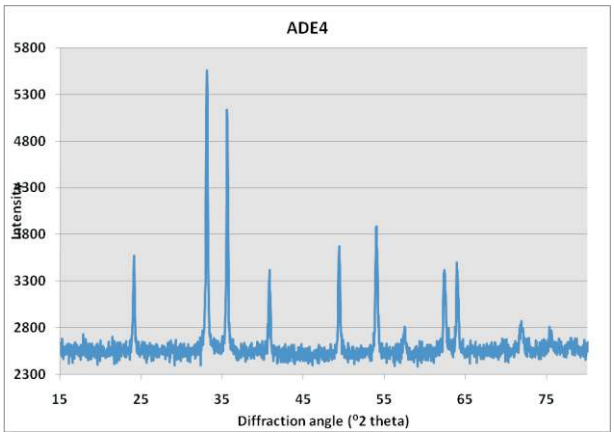


Fig 1d: XRD pattern of hematite ADE4

XRF result

The result of elemental composition of synthesized samples are shown in Table 2. As evidenced by XRD, the results of XRF clearly showed that the samples were hematite. The samples can be ranked thus in terms of %.

Table 2: Elemental Abundances of the samples

Samples	O	Al	Si	Cr	Fe	Co	Total
ADE I	46.05	0.15	0.14		53.50	0.16	100.00
ADE 2	44.98	0.12	0.16		54.60	0.15	100.00
ADE 3	27.19	-	-	0.56	72.25	-	100.00
ADE 4	45.55	-	-	-	54.45	-	100.00

The presence of other metals such as Al, Si, Co and Co all at concentration less than 0.6% could be traced to the level of purity of the Fe $(NO_3)_3$ and $FeCl_3.6H_2O$ used in t he preparation of the samples. .

Table 3: Infra-red data of hematite ADE4

PEAKS(cm^{-1})	FUNCTIONAL GROUP
3449.78	Hydroxyl group
468.40 – 544.14	Characteristic band of hematite

the Infra-red spectra, the characteristic band of hematite shows that the iron oxide is hematite, the colour of the sample which was brownish-red also reveals that the sample is hematite and the X-ray diffraction result further supported the identification of the sample is hematite .

SEM result

The Scanning Electron microg raphs for the samples are shown in Figures 2a-2d

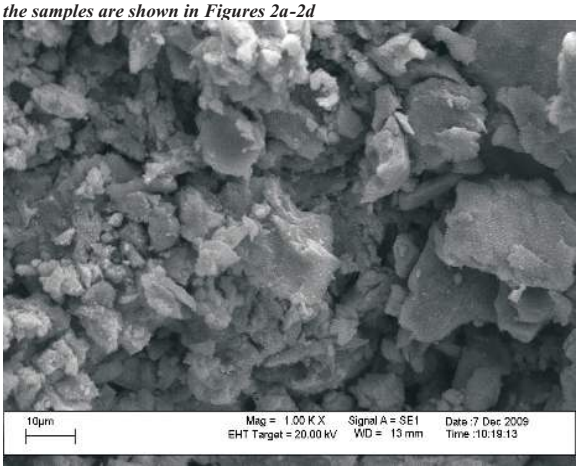


Fig 2a: SEM image of hematite ADE1

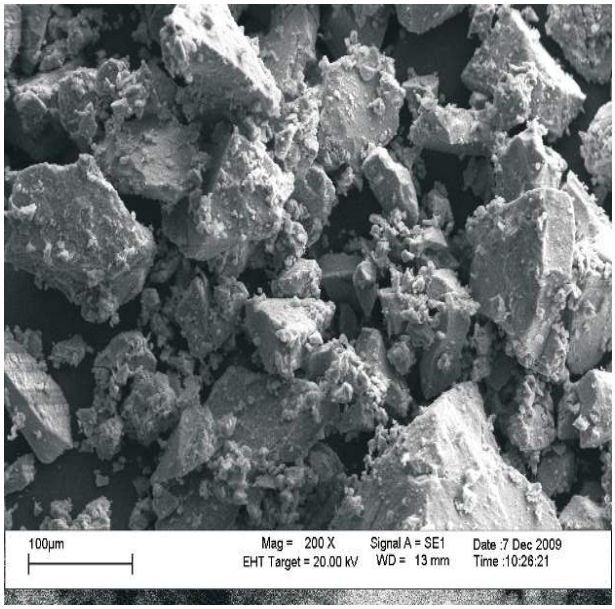


Fig 2b: SEM image of hematite ADE 2

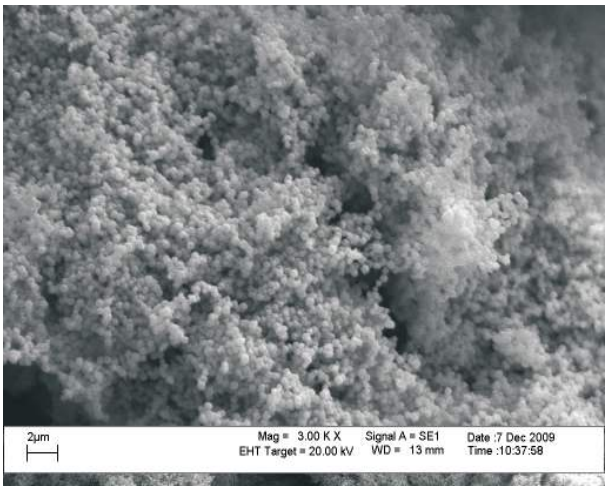


Fig 2c: SEM image of hematite ADE3

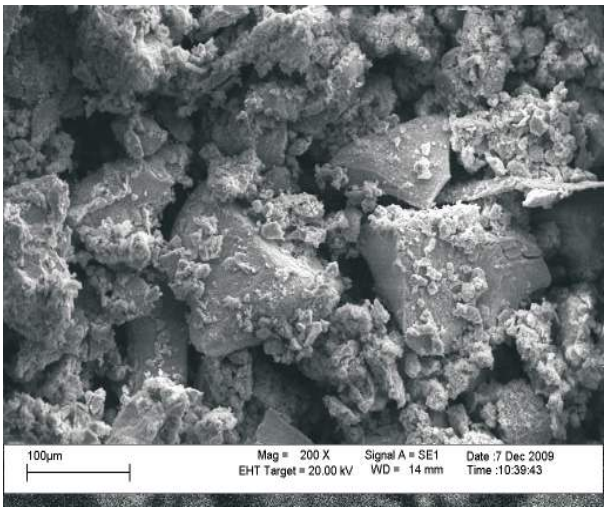


Fig 2d: SEM image of hematite ADE4

The Scanning Electron Micrograph for sample Ade 1 identified it to be platelike (i.e hexagonal in shape) at magnification 100micrometer

The shape of Ade2 is regular and it is pentagonal in shape at magnification 100 micrometer. The thickness of the shape is 27µm.

Ade 3 was identified to be spherical in shape, the thickness of material is 0,25µm (i,e nanomaterial)

Ade 4 was identified to be platelike and the thickness is 200µm. (i.e. largely hexagonal).

Conclusion

Iron oxides naturally, are composed mainly of iron and oxygen and are used industrially in different field. Due to their non-toxic nature and their resistance to moisture, they are graded safe for cosmetics use. Hematite, which is an iron oxide, can be synthesized in the laboratory and it can be used to absorb some heavy metal from aqueous solution.

References

1. M Sorescu O. Mihaila - Tarabasanu, L Diamodescu(1998). Appl Lett **72**, 2047
2. R M Cornell and U Schwertmam (1996) " The iron oxides structure, properties, reaction, occurrences and uses VCH weinhein 395-432"
3. E Matijevic and P Scheiners (1978) "Ferric hydrous oxide Sols III preparation of uniform particles by hydrolysis of Fe(111) chloride-nitrate and perchlorate solutions. J. Colloid interface sci: **63**,509-524.
4. M.Ozaki,S.Krathvil and E.Matijevic (1984) formation of monodispersed spindle type hematite particle. J. Colloid interface sci:102,146-151.
5. X .Wang, X. Chen, X. Ma, H. Zheng, M. Ji and Z. Zhang(2004) Low temperature synthesis of α-Fe_2O_3 nanoparticles with a closed cage structure. Chemical physics letter **384**,391-393
6. Mc Graw-Hill Encyclopiedia of science and technology New York, **8**,185-447
7. N. Mimura, I. Takahara and M.Ando(1998) c a t a l . Today 45,61 ln: X .Wang, X. Chen, X. Ma, H. Zheng, M. Ji and Z. Zheng (2004) Low temperature synthesis of -Fe_2O_3 nanoparticles w i t h a c l o s e d c a g e s t r u c t u r e . Chm.phys.Lett.**384**,391-393
8. J .Chang, S. Park and M.Park (1997) C h e m L e t t . 1 1 , 1 1 2 3 ln:X.Wang,X.Chen,X.Ma,H.Zheng,M.Ji and Z.Zheng(2004) Low temperature synthesis of Fe_2O_3 nanoparticles with a closed cage structure. Chem.phys.Lett. **384**, 391-393.
9. J. Turner, M .Hendewerk, J. Parmeter, D. N e i m a n a n d G . S o m o r j a l (1 9 8 4) J.Electrochem.Soc.131,177 ln: X. Wang, X. Chen, X. Ma, H .Zheng, M. Ji and Z. Zheng(2004) Low temperature synthesis of nanoparticles with a closed cage structure Chem.phys.Lett **384**,391-393.

10. L. Lindgren, H. Wang, N. Beermann, L. Vayssieres, A. Hagfeldt and S. Linguist(2002) Sol. Energ. Mat. Sol.C. 71,231 ln:X. Wang, X. Chen, X. Ma, H. Zheng and Z. Zheng (2004) Low temperature synthesis of nanoparticles with a closed cage structure Chen phys.Lett. **384**, 391-393
11. S. H. Gee, Y. K. Hong, J. C. Sur, D.W. Erikson, M. H. Park and F. Jeffers (2004) Spin orientation of Hematite(α- Fe2O3) Nanoparticles During the Morin Transition. IEEE Transactions on Magnetics 40(4),2691-2693.
12. T. Sugimoto, Y. Wang, H. Itoh and A.Muramatsu (1998) Systematic control of size shape and internal structure of monodisperse particles.Colloids an surfaces A. Physicochemical and Engineering Aspects **134**,265-279.
13. Marek Kosmulski (2002) The pH- dependent Surface Charging and the Points of Zero Charge"., J. Colloid Interface Sci., **253**, 77-87.

THE EFFECT OF HEAT TREATMENT PROCESSES ON THE MECHANICAL FAILURE OF ENGINEERING PARTS USED IN COCOA INDUSTRY (ILE - OLUJI COCOA INDUSTRY AS A CASE STUDY)

[1]ALO F. I, [2]SHITTA M. B. O, [1]ADETUNJI A. R
[1]Department of Material Science and Engineering, Obafemi Awolowo University Ile – Ife
[2]Department of Physics, University of Ado – Ekiti, Nigeria
Email: Iretispecial2005@yahoo.com

Corresponding Author: Alo F. I. Department of Material Science Engineering, Obafemi Awolowo University, Ile – Ife, Osun State.

ABSTRACT:

Cocoa processing industry has been in existence for quite some time and makes use of steel and cast iron as the major engineering components. Iron & steel are the most common of engineering metals used in far greater tonnage than all other metals put together. In service, they are subjected to conditions that promote failure and therefore lower the reliability of the machine performance. This work presents the result of an investigation on the effect of heat treatment processes on the mechanical failure of Engineering parts used in Cocoa industry. Fifty Six (56) pieces were machined from failed triangular bar used in powder processing plant from Ile - Oluji Cocoa industry and some were subjected to Austempering, martensitic hardening, Tempering, Carburizing, Annealing & Normalizing with the As-Received sample as the control. After heat treatment, Tensile, hardness and micro - structural analysis were carried out. The results showed that hardened sample exhibited the greatest Tensile Stress breaking at 632. 29 MPA while the Normalized sample showed the least strength of 168.27 MPA. Hardened sample exhibited the greatest value of 53.5HRC while the As-Received the least 32.5HRC. The impact strength value for Tempering sample is 10.1 x 10^{10}J while the Hardened sample showed the lease at 6.77 x 10^{10}J.
Key words: Cocoa, heat-Treatment, steel, failure, strength

INTRODUCTION

Cocoa is grown in Nigeria by small holders particularly in Ondo State where over 60% of national total output is produced (Akinwale, 2003). It is also a crop grown largely by small holder farmers in the lowland tropics, including parts of Latin America and Indonesia (Mangerete Fransen & Monique Borgerholf Mulder 2007).

Before the discovery of oil in Nigeria, cocoa was the most important economic foreign exchange earner for the country, even many African countries like Coted'ivore & Ghana depend on earnings from cocoa for running their countries.

The health value of cocoa could not be over emphasized, according to recent studies, cocoa flavanols, the unique compounds found naturally in cocoa can increase blood flow to the brain (www.marsbotanical.com). The long time improvement in brain blood flow could impart cognitive behavior, offering future potential for debilitating brain condition including dementia and stroke. In a scientific study of healthy, older adults ages 59 to 83, Harvard medical scientists found that study participants who regularly drank a cocoa flavanol rich beverage made using the Mars, incorporated cocoa preprocess had an eight percent increase in brain flow after one week, and 10 percent increase after two weeks. (www.healthy cocoa.com & www.marsbotanical.com) the role of these flavanols which helps to reduce heart related risk is much important. The use of cocoa product in daily diet has shown an increased rate of longevity. The chances of suffering from heart attacks are reduced substantially if you include cocoa containing foods in your diet. (Article source: http://ezinearticles.com /? Expert= Beverly clement/. Even cocoa shell-ash known to be rich in potash is used as an Alkalizing agent on cocoa products (Osundahinsi et al, 2007). Cocoa processing industry makes use of steel & cast iron as the major Engineering Components. In service, they are subjected to conditions that promote failure and therefore lower the reliability of the machine performance. The cheapest and most easily accessible metal for agro – processing equipment fabrication in Nigeria is plain carbon steel. However, there are some aggressive ions present in raw agricultural and food products, which may attack the steel components of these processing machinery resulting in their untimely failure in service (S.O Jekayinfa et al (2005).O. O. Oluwole et al (2008) opined that the unplated steel was found to be unsuitable for the fabrication of Cocoa processing machinery without some

form of surface treatment. Corrosion and wear rate are of paramount concerns to both Engineers and Machine Scientist during the design, material selection, fabrication of machine components and tools. A successful material must have satisfactory properties, be economically viable and easily available. Hence, the need for heat-treatment of the material. Umoru et al (2006) investigated the corrosion – wear of NST 60Mn steel in cocoa mucilage and concluded heat-treatments such as mar tempering, quenching and quenching plus low temperature tempering are capable of improving the structural integrity of the steel. Sorokin G.M et al (1991) said abrasive wear by sliding is characterized by a definite orientation of grooves coinciding with the direction of movement of the specimen or the abrasive. The stronger the resistance to cut, the greater is the wear resistance. In this research, therefore, the effect of heat-treatment processes on the failure analysis of an Engineering part used in cocoa industry is investigated and presented. The heat-treatments given are; Hardening (Martensitic hardening), Annealing, Normalizing, Austempering, Carburizing and Tempering.

MATERIALS AND METHODS

Work materials and Specimens preparation.

The materials used in this study were failed triangular bar steel used in powder processing plant from ile - Oluji cocoa industry in Ondo State of Nigeria. Twenty one (21) tensile specimens and twenty one (21) impact specimens followed by seven hardness specimens and seven micro structural specimens each were prepared from these materials using the lathe machine as shown in figure 1:

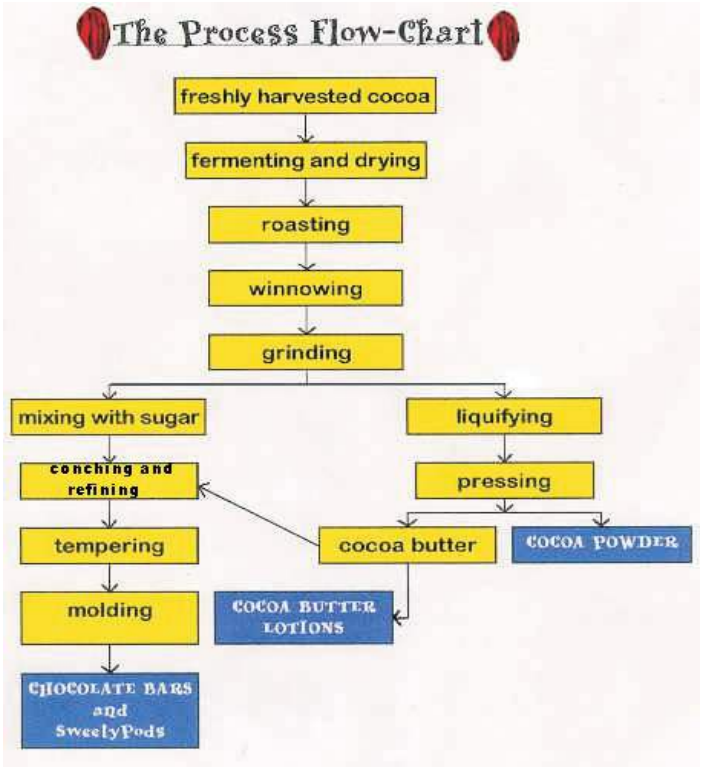


Table 1: **Chemical Composition of Steel Sample**

Steel Sample	% Composition					
	C	Si	Mn	S	P	Fe
Low carbon	0.225	0.6	0.55	0.042	0.38	98.103

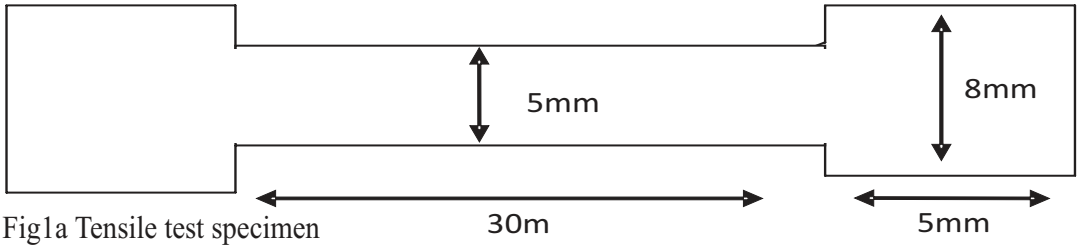


Fig1a Tensile test specimen

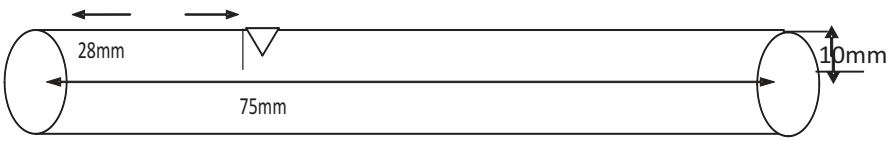


Fig 1b

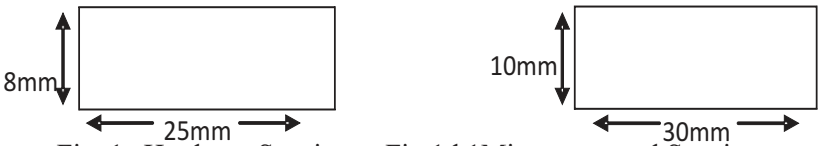


Fig. 1c Hardness Specimen Fig.1d 1Microstructural Specimen

The samples were subjected to heat-treatment according to the following procedures:

Carburizing Eight samples were packed in a metal box of 100-200mm diameter sandwiched by pulverized Anthracite coal (hard coal of fine particles which is the main source of carbon. The pulverized coal was mixed with an energizer which is $Baco_3$ (Barium Carbonate), in amount of 10-30%. The Box is top-closed with a well-fitting lid. The packed box was placed in a carbolite furnace in the materials science laboratory of Obafemi Awolowo University at Temperature of 840^0c for a period of 5 hours. The Box was removed after allowing it to cool. The Specimen washed and dried

.

Hardening: Thirty two (32) samples were placed in a metal box inside the furnace and heated to 840^0C and allowed to soak for one hour to attain (or to homogenize). After that eight samples were removed and place outside to cool in Air which is Normalizing, sixteen, samples were then cooled inside a bucket full of water. Eight of the samples cooled inside the water were later tempered at 300^0C. The remaining eight samples inside the furnace were left to cool which is Annealing process.

Austempered: The remaining eight samples were austenized at 840^0C, Soaked for one hour and quenched in salt bath which contained 30% KNO_3 and 70% $NaN0_3$. At a temperature of 300^0C and were later cooled to room temperature.

All the As-received samples did not undergo any heat-treatment processes. They only serve as control or reference sample. The Tensile samples were then tested to failure with the Universal Instron machine at EMDI (Engineering material development institute) at Akure.

Metallography The samples were ground on 240, 320, 400 & 600 grit emery papers in the materials laboratory at OAU Ile - Ife, then followed by initial polishing with selvt cloth swamped with solution of one micron of silicon carbide solution. Then, followed by the final polishing stage with the same selvt cloth swamped with solution of 0.5µm silicon carbide until a mirror-like surface is attainable. The mirror-like surface was etched in 2% NITAL (2% NITRIC ACID and 98% of Ethyl Alcohol) and later viewed under the metallurgical microscope.

Impact test: Impact specimens, shown from figure 1b which were notched to a depth of 2mm from 28mm end of the specimen to create an area of stress concentration for initiating fracture, were fixed on a 1zod impact testing machine to receive a blow from the pendulum from a fixed height. The reading on a dial gauge on the machine showed the impact energy absorbed by the respective specimen

Hardness Test: Hardness specimens from figure 1c had their surface grounded and smoothened on a 600 grit paper to have mirror like surface. The hardness was then read by using digital Rockwell hardness tester indentec.

RESULTS AND DISCUSSIONS

Sample Idea	Tensile stress MPA	Time to break in sec.	True strain(mm/mm)	Energy at break	Tensile stress at maxi(mpa)	Tensile stress at yield(mpa) yield stress	True strain at yield(mm/mm	hardness Test (Hrc)	impact test(J)
	A	B	C	D	E	F	G	H	I
As Received	201.58	132	0.564	145.58	143.2	355.43	0.45334	32.46	7.8637441
Austermpered	388.6	138.2	0.569	180.7	230.7	564.18	0.44	39.3	9.211653074
Annealing	433.07	125.2	0.533	148	243.5	617.58	0.4	38.86	8.541653074
Hardening	632.29	79.9	0.34	131.8	353.5	721.47	0.28	53.5	6.779089742
Carburizing	321.58	60.5	0.289	54.7	186.8	439.17	0.24	42.5	9.407256383
Normalizing	168.27	145.7	0.622	166.4	95.4	202	0.1	36.5	8.13490769
Tempering	267.81	147.7	0.602	152.9	160.2	388.01	0.1	33.06	10.16863461

Table 1

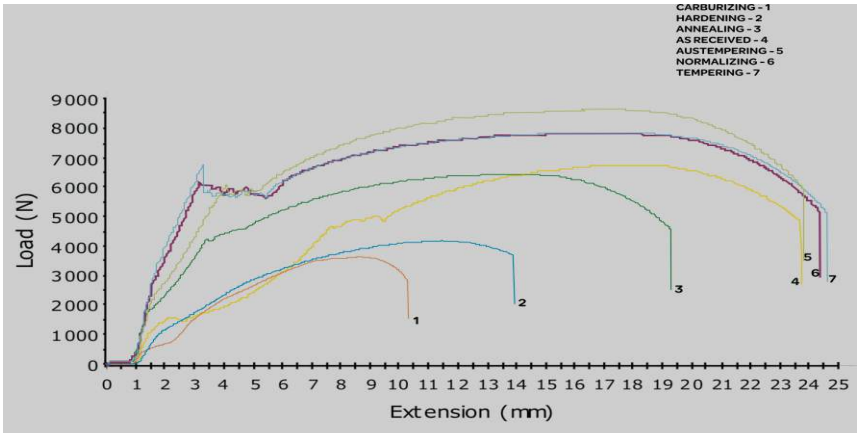


Fig 1: Tensile Graph of different heat-treated processes

Fig 2: Relationship between Impact and Tensile of different heat-treated process

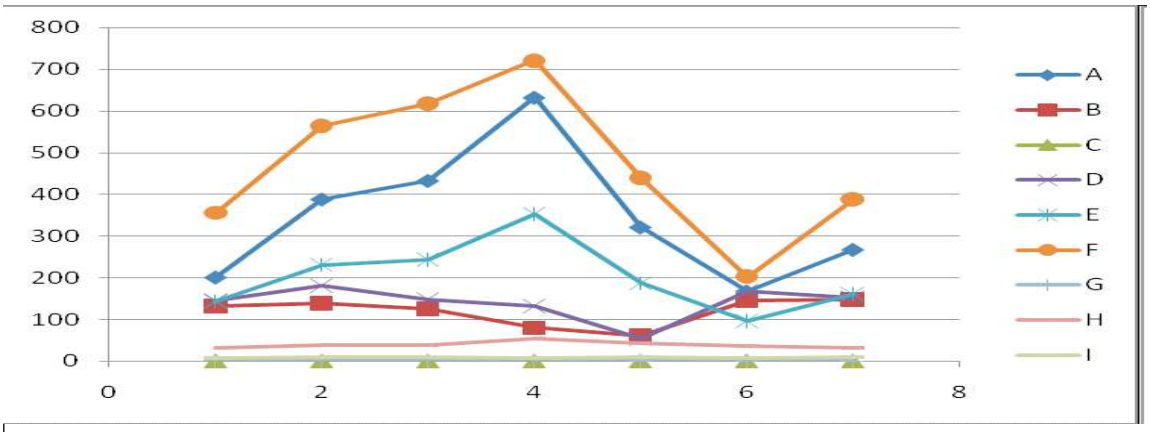


Fig 3: Relationship between the Tensile, Hardness and impact of different heat treated processes

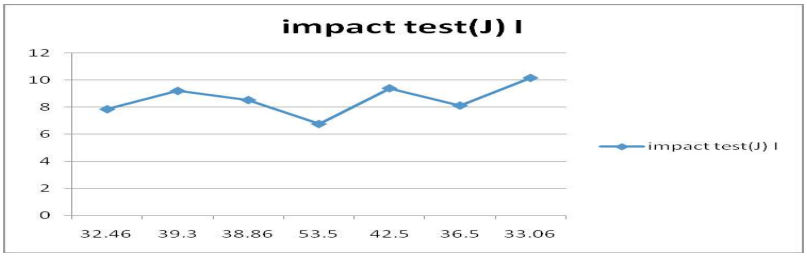


Fig 4: Relationship between hardness and impact of different heat-treated processes

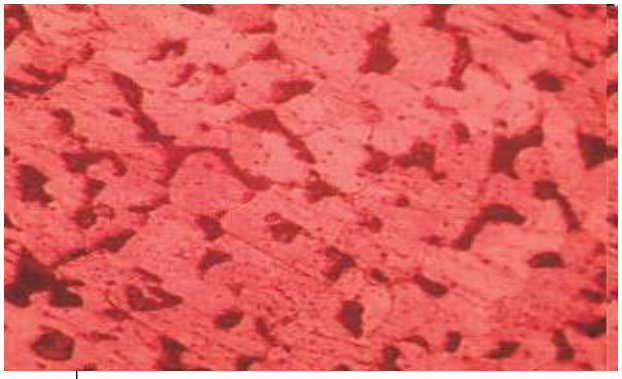




Figure 5 As Received sample

Figure 6 Austempered at 840°c

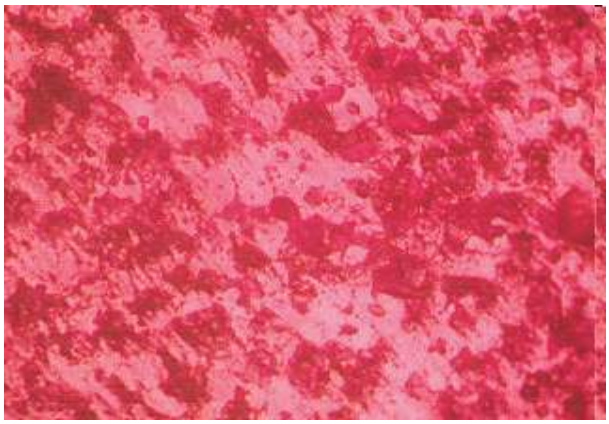


Fig 7 Nomalised at room temperature



Fig8 Tempered at 300°C

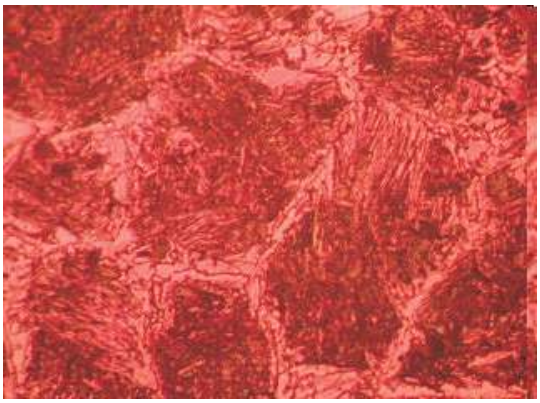


Fig 10 Carburized at 840°C

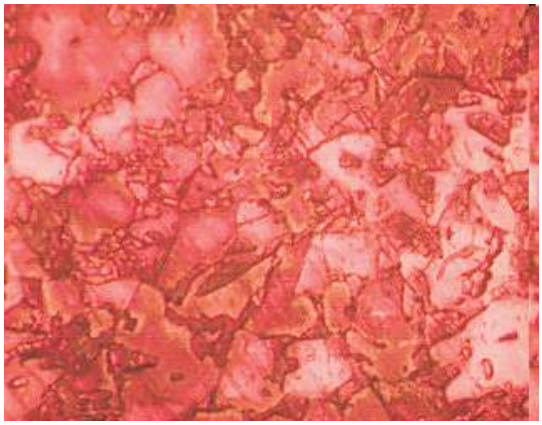


Fig 9 Hardened at 840°C

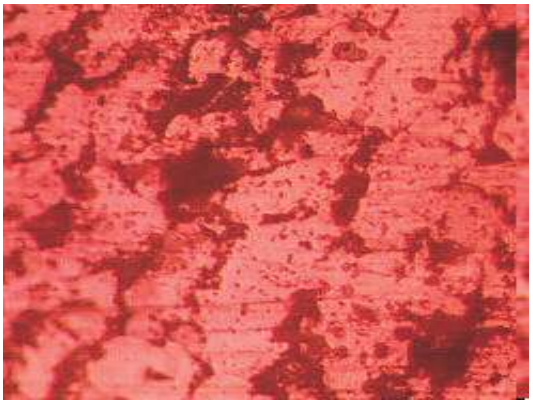


Fig11: Annealed at inside the furnace at room temperature

RESULTS AND DISCUSSION

Fig 1 shows the Tensile Graph of different heat-treated processes given to the specimens. Fig 2 shows the relationship between impact and tensile of different heat-treated processes. Fig 3: shows the graphical representation of tensile, hardness and impact. Fig 4 shows the relationship between hardness and impact of different heat-treated processes. Fig 5 – 11 shows the micro-structures of different heat-treated processes. The tensile stress at break (Mpa) is highest for the hardened sample, at 632.29 Mpa and hardness of 53.5Hrc. Reason is because of the martensitic structure that was formed as a result of the rapid cooling inside the water therefore exhibiting great resistance to wear, followed by the annealed sample which has coarse ferrite & pearlite grains (433.07MPA). The same pattern of result followed for tensile stress at maximum of hardened sample which is 353.5 MPA followed by annealed specimen of 243.5MPA. The Austempered specimen has hardness of 39.3 ARC and impact of 9.21 x 10 ^10J simply because of the Austenite which transforms isothermally to lower bainite. However Tempering which has Tensile stress of break of 267.81 MPA has the highest impact energy of 10.2 x 10^{10}J. This is because, impact is a measure of Toughness and is measured by the area under the entire stress – strain diagram up to the point of fracture. It then shows that a stronger material does not mean tougher. A stronger material may / may not be a tough material.

In conclusion: From the result of the work done in this research, the following deductions can be made:

(1) Heat – treatment of the samples can increase the lifespan of the material.
(2) Combination of hardening & annealing process will improve the hardness properties of the material.
(3) Tempering of the specimens tends also to improve the toughness of the material.
(4) The longer the carburized samples are allowed in the furnace, the higher the hardness value.

REFERENCES

1. Akinwale,O.(2003).The problems of Cocoa marketing and Trade in Nigeria: Pre-liberalization and liberalization Era. Cocoa Association of Nigeria publication 2003
2. Article source: http://ezineurticles.com|?Expert=Beverly clement.
3. G.M .Sorokin, S.P.Grigorev and A.G.Golova,(1991).Nature of Impact-abrasive wear of steels. Strength of materials volume 23,no 4,463-467,DOI:10,1007|BF00771977.
4. Mangaret Frozen & Morgue Borgerholf

Mulder, Biodivers Conservative (2007) Ecological, economic & social perspective on Cocoa production worldwide. 16:3835 – 3849,DOI: 10:1007/s 10531-007-9183-5

5. S.O. Jekayinfa, M.A. Waheed, K.A. Adebiyi, F.T. Adebiyi (2005). "Effect of Cassava fluid on corrosion performance of mild steel" Anti – corrosion methods & Materials, Vol.52 ISS: 5, PP286 – 292.
6. O.O. Oluwole, D.T. Oloruntoba and O. Awheme (2008). Effect of Zinc plating of low Carbon Steel on corrosion resistance in Cocoa fluid environment – journal of materials and Design. Volume 29, issue 6, 2008, pages 1266 – 1274.
7. Umoru L.E., A.O. Akinola and M.O. Adeoye (2006). Corrosion- wear of NST 60 Mn Steel in Cocoa Mucilage. Journal of Applied Science Research, 2 (9) : 529 – 532,2006 Insinet Publication.
8. O.F. Osundahunsi, M.k. Bolade AND A.A. Akinbinu (2007). Effect of Cocoa Shell Ash as an Alkalizing agent on Cocoa Products. Journal of Applied Sciences 7 (12): 1674 – 1678, 2007. ISSN 1812 – 5654, 2007 Asian Nerwork for Scientific Information.
9. www.healthy cocoa.com and www.marsbotanical.com
10. http://naturalhealthezine.com/health-benefits-of-cocoa/

THE OPTIMAL DRIVING SPEED AS A MEANS OF ENHANCING A CLEANER ENVIRONMENT

Igweh C.O., *Unachukwu G.O.
Eng. Mgt. And Eff. Unit, NCERD
National Centre for Energy Research and Development
University of Nigeria, Nsukka

ABSTRACT
In the world the need for minimization of the Environmental Pollution has forced man into several ways of controlling and maximizing the output of automobiles and fuel consuming machines.
This work looks into the best speed for the running of cars. Two models: high efficient and low efficient are looked into. For the high efficient cars we are taking the Audi 80 1.8s and the Mercedes Benz (190) for the low efficient.
The speed of these cars are taken and a model is then derived, which is simulated to find the best speed to run the car for any given distance, time or both combined, taking into consideration the cost of time as a function of the public cars' earn per trip.
Key words: Optimization, Fuel Consumption, Modeling, Simulation and Efficiency.

INTRODUCTION

Clean energy is not a single industry but instead involves a wide variety of very different industries. Some of the broad sub sectors under clean energy include Solar power, fuel cels, geothermal power, wave/tide power, biofuels, cleaner coal, and power efficiency (Asplund R.W. 2008).

In this work the power efficiency sub sector is being considered knowing that the extra inefficient power is a waste both detrimental to the Environment and the Economy.

Fossil fuel in the form of coal, petroleum, and natural gas has served the world very well in the provision of cheap supply of fuel to drive the age of industrialization. From the paper by Igweh C.O. etal (2009). The calculation of the percentage Co2 by mass emission of an 800 watts generator gives a value of 2.819% by mass. This is a cause for concern since the world's factories, houses and vehicles for many decades depend on the energy derived from burning fossil fuels.
According to (Asplund R.W. 2008); 'The U.S. Energy Information Adminstration fully expecting double fuel consumption by 2030.' The simple fact is that burning fossil fuels, whether in power plants or in internal combustion engines, releases CO2, other green house gases, and various contaminants into the atmosphere, causing pollution and global warning problems. Energy hence needs to be derived from cleaner sources that avoid these problems.

Transport coveys many benefits. It allows personal mobility for both work and leisure activities. In most industrialized countries people have a much wider choice of where they can live in relation to their employment than the enjoyed in the past. (Banister D and Buton K, 1993). Despite the unquestionable benefits that appropriate transport provision can bring, there is an inevitable opportunity cost involved. Some elements of this cost are taken into account in the charges borne by those supplying transport services and by the users of these services.

1.0 LITERATURE REVIEW:

Based on the monopoly of power, government subsidies, inefficient management, and a range of other factors the markets may well be offering a far from ideal level of transport provision and that the facilities which are available are not being used optimally even within the confines of these narrow markets.
(Banister D and Buton K, 1993). Transport has always been associated with impositions on environmental cost; this fact has always been appreciated by transport policy-makers.

The damaging effects of acid rain' on forests and water life mounted in the late 1970s and early 1980s and the importance of NOx and other gaseous emisions from automobiles was recognized as a major contributing factor. The issue of high level ozone depletion and the effects it might have for the long-term incidence of certain types of cancer also emerged at the same time. Transport contributes, albeit in a relatively minor way via the use of such things as CFCS in air-conditioning units, to the gases, which may cause this problem. (Banister D and Baton K, 1993).

The logistical problems of operating the transport modeling activity meant that the analytical framework for transport had to be established in detail well before the end of the study. However, the overall framework was committed progressively and was finalized only after some of the transport results were available and the method could not be altered.

According to (Creighton R.C., 1970), many of our views are constant (since we remain human animals with certain physical needs), but others are modified as time and technology change, as we live in different

places, as our productivity increases, and as al the various parts of our environment shift and change in time. Estimating the value of a person's time is much more difficult. There is clear evidence, however, that given a choice, people will pay for higher sped, and hence time. Studies of the choices people make between free and toll facilities permit the value of time to be deducted; values of $1.14 and $1.42 per automobile hour were calculated in this fashion.

A more recent study based on data from a sample of workers using free and toll roads to travel to five industrial plants allowed calculations to be made giving a value of $2.82 per person hour for commuter trips of over five miles. From the calculation (Tresider J.O., 1972), the accessibility index for transport analysis was defined as

$$I = [100 \sum [\sum(G_i A_j) *(T_t/T)]]/ \sum G_iA_j$$

Where I = accessibility index for the plan under test

G_i =generation from zone I

A_j = attraction from zone j

$\sum_{ij} (G_i A_j)_t$ = Sum of al 10 pairs of generations and attractions in zones time t

apart.

T_t = Mean number of trips of length t in the set of plans under test.

T = Mean number of total trips in the set of plans under test.

In any transport analysis time is a utility and must be considered. The delivery of gods and persons at desired time, is becoming increasingly important. Delays in transit cause spoilage and perhaps loss in market value in the critical market areas (fresh vegetable and fruit transportation) (Hay W.W., 1961). For an automobile assembly plant which receives car bodies from one city engine from another and electrical equipment from a third, it must have the components available when needed else would cause a slow down or stop entirely the assembly line.

The community at large will continue to resist the encroachment on the quality of life by any or al forms of transport and future developments will have to pay considerable regard to the amenity of the environment. It has yet to be fully recognized by society that in accommodating some of the technologies of the future a high price will have to be paid for the preservation of an acceptable environment. Those who provide future inter-city transport must decide which of the customers they are aiming to satisfy. and which of the features of inter-city travel they consider should be promoted. (Anon, 1972).
Specific fuel consumption of vehicles has been improved through technical changes in the last three decades. Studies of the impact of the behavioral aspects on the specific fuel consumption of vehicles has been little. The analytical tools developed recently have included options for quantifying the specific fuel consumption in certain predefined driving of cycles. Empirical studies have shown that real driving cycles are different from predefined ones. It has also been observed that optimal coordination of both sped of vehicle and gear ration are detrimental to the improved performance of a vehicle. (Saboohi Y and Farzaneh H., 2008).

METHODOLOGY:

The speed is varied for ten different data on a distance of ten (10)km. Then this is repeated for ten different increments on that distance at an addition of five kilometers. The model is derived and the line of best fit is derived.

The graphs and tables will be sent after acceptance of the work.

CONCLUSION:

With this we could calculate the best speed to go a distance given the time constraint. Also calculation of the best rate of rise of acceleration is got for the two models of car.

REFERENCES

Hay W.|W., (1961) An introduction to transportation Engineering, John Wiley & Sons, Inc.,m New York, USA.

Recent Developments in Inter-City transport and their relevance in Great Britain, Transport Engineering 1972 Proceedings of the conference organized by the Institution of Civil Engineers in London

Tresider J.O. (1972), Current Philosophy and Techniques of regional transport studies, Transport Engineering 1972) Proceedings of the Conference Organized by the Institution of Civil Engineers in London.

Wilson R.L. and Holland C.J. (1972), Transport aspects of the preparation of the
strategic plan for the South East, Transport Engineering 1972) Proceedings of the conference organized. 1982 World Survey of Current Research and Development on Roads and Road transport, Prepared for the Federal Highway Administration under contract no DTFH 61-81-c023, Washington D.C.

Creighton R.L. (1970), Urban Transportation Planning, 1970 Board of Trustees of the University of Illinois.

Banister D. and Buton K. (1993), Transport, the Environment and Sustainable Development, E $ FN Spon, London.

Saboli Y. and Farzaneh H.(208), Model for optimizing Energy Efficiency through controlling sped and gear ration, Energy Efficiency, Springer Netherlands, Vol I, No. I

Igweh C.O. etal, (208), Achieving a safe and clean Environment through the Deployment of Magneto hydrodynamics (MAD) technology.

COMPARATIVE MODELING AND SIMULATION OF STRUCTURAL BEHAVIOUR OF STEEL COMPONENT WELDED WITH DIFFERENT BRANDS OF ELECTRODES USING PRO-E MECHANICA AND COMSOL MULTIPHYSICS

[*]Oyelami A.T., Ogunkoya A.K., Ogundare O. and Olunlade B.A
Engineering Materials Development Institute, Km4 Ondo Road, P.M.B. 611, Akure, Nigeria
[*]Correspondence Author: atoyelami@yahoo.com

ABSTRACT
This work uses two of the world's leading FEA softwares - Pro/E Mechanica and COMSOL Multiphysics - to model the structural behavior of mild steel component welded with three distinctive brands of electrode using different approaches in the two softwares. The work utilized the approach of h-elements of low order interpolating polynomials for convergence in COMSOL Multiphysics while convergence was obtained in Pro/E Mechanica by increasing the order of the interpolating polynomials on each element, that is, using p-elements. The work demonstrates the versatility of the state-of-the-art FEA software – COMSOL Multiphysics – most especially in the area of structural analysis in comparison to a less versatile but highly resourceful in structural and thermal applications – Pro/E Mechanica. The maximum stress level (von Mises Stress) and static deflection found were compared with the material's yield strength and the time-dependent analysis respectively. The results obtained show the alarming deviation of some critical properties of mild steel and its electrodes in Nigerian markets when compared to the standards.

Keywords: Pro-E Mechanica, COMSOL Multiphysics, FEA, h-elements, p-elements, Convergence, von Mises Stress, Modeling and Simulation.

1.0 INTRODUCTION

Mathematical modeling has become an important part of the research and development work in engineering and science[5]. Competitive edge requires speed on the path between idea and prototype, and mathematical modeling and simulation provides a valuable shortcut for understanding both qualitative and quantitative aspects of scientific and engineering design[11]. COMSOL Multiphysics offers state-of-the art performance, being built from the foundation with Java3D interface and C/C++ solvers[4]. Pro-E Mechanica or simply MECHANICA is Finite Elements Analysis software which offers more than simply being an FEA engine. It is a design tool which allows parametric studies as well as design optimization to be set up quite easily. Moreover, unlike many other commercial FEM programs where determining accuracy can be difficult or time consuming, MECHANICA is able to compute results with some certainty as to the accuracy. This refers to the issue of convergence whereby the FEA results must be verified or tested so that they can be trusted[12]. An attempt has therefore been made in this work to model and simulate the structural behavior of steel component welded with different brands of electrodes using the leading FEA softwares – Pro/E Mechanica and COMSOL Multiphysics. The validity of the modeling and simulation was ascertained by comparison of the results obtained from the modeling and simulation to that obtained from experimental analysis. The essence of the work is to give an insight into an area of engineering application of the softwares and more importantly to ascertain the quality of mild steel and its electrodes in Nigerian market through the study of their structural behavior.

Progressive building collapse occurs when failure of a structural component leads to the failure and collapse of surrounding members, possibly promoting additional collapse[1]. There has been an unprecedented increase in the rate at which houses and structures are collapsing in Nigeria. The blame has always been put at the doorstep of the structural engineers who are often accused of incompetence. Findings however show that most of the times the fault is traceable to the use of sub-standard materials. The Structural Engineer for example might have based his design on the standard values of some critical properties of mild steel whereas results of this work show significant deviation of such critical properties from the established standard values.

Mild steel is the most common form of steel as its price is relatively low while it provides material properties that are acceptable for many applications. Mild steel has a low carbon content (up to 0.3%) and is therefore neither extremely brittle nor ductile[3]. It becomes malleable when heated, and so can be forged. It is also often used where large amounts of steel need to be formed, for example as structural steel. Density of this metal is 7,861.093 kg/m^3, the tensile strength is a maximum of 500 MPa and it has a Young's modulus of 210 GPa[17].

SMAW (shielded metal arc welding) electrodes are covered rods manufactured by concentrically extruding silicated chemical mixtures followed by an oven cure[18]. The SMAW process uses an arc between a covered electrode and the weld pool. The

arc and molten metal are shielded by the decomposition of the electrode covering. The SMAW electrode also supplies filler metal to the weld pool and to the weld metal. Ideally, the weldment produced by SMAW is expected to have approximately the same mechanical properties with the parent metals. This work is therefore an attempt to check the level of homogeneity of the weld properties when compared to the parent metals.

2.0 FINITE ELEMENTS ANALYSIS (FEA)

The Finite Element Analysis (or Finite Element Method) is a numerical analysis technique used by Engineers, Scientists, and Mathematicians to obtain solutions to the differential equations that describe, or approximately describe a wide variety of physical (and non-physical) problems[13]. Physical problems range in diversity from solid, fluid and soil mechanics, to electromagnetism or dynamics. Finite Element Analysis uses computer simulation technique for engineering analysis. It uses a numerical technique called the finite element method (FEM)[8].

The underlying premise of the method states that a complicated domain can be sub-divided into a series of smaller regions in which the differential equations are approximately solved. By assembling the set of equations for each region, the behavior over the entire problem domain is determined. Each region is referred to as an element and the process of subdividing a domain into a finite number of elements is referred to as discretization. Elements are connected at specific points, called nodes, and the assembly process requires that the solution be continuous along common boundaries of adjacent elements.

The majority of FEA programs will combine all of the individual elements into a mesh and then convert the problem from a set of continuous differential equations into a large set of simultaneous linear algebraic equations. This system will have several thousand equations in it, and the solution of the simultaneous linear algebraic equations represents an approximation of the continuous differential equations, which represented the mesh. This approximation can call into question the accuracy of the results. In theory, a mesh of infinite number will create the best approximation. However, this would produce a system of simultaneous linear algebraic equations of infinite size as well. The actual steps the programs take in solving a system of simultaneous linear algebraic equations can be complex, however they can be reduced to the following: The dependent variable in the governing partial differential equation is the displacement from a reference, which is usually the unloaded position. The material strain, displacement per unit length, is then computed from the displacement by taking the derivative with respect to its initial position. Finally, the stress components at any point in the material are computed from the strain at that point[5]. Thus, if the interpolating polynomial for the spatial variation of the displacement field is linear within that small element, then the strain and stress will be constant within that element since the derivative of the linear function representing that element is also constant.

2.1 Processing Steps

Often times in order to obtain results in a finite amount of time; several assumptions or simplifications must be made in order to have a final workable model. Workable means the FEA model must allow for the computation of the results of interest with sufficient accuracy and with acceptable time and resource usage. In order to simplify the model, some assumptions are made. One of such assumptions is that the materials assigned to the model are homogeneous, isotropic, and free of internal defects or flaws, another is to ignore aspects of the geometry that pose no anticipated effect on the results, such as chamfered edges along the outside of the part.

After making those assumptions, the model can be called a simplified physical model. The next step would be making further assumptions to create a mathematical model. This set of assumptions includes linear material properties and idealized loading conditions. To idealize the loading conditions, the loading must be steady, and placed on perfectly fixed points. At this time the model is converted into one or more differential equations that describe the variation in characteristics within the boundaries of the model. The next step is creating an FEA model from the mathematical model. This is where the conversion from one or more differential equations into an equal number of simultaneous linear algebraic equations occurs. A run processor actually performs the solution to the proposed problem. This run processor is an FEA engine that will use special numerical techniques and algorithms to exploit various properties within the system of equations. The output can be displayed graphically showing displaced shape, stress distribution, mode shapes and many other important features.

2.2 Convergence of H-elements

Most programs/PDE solution software (including COMSOL Multiphysics) use this classic approach of low order interpolating polynomials in each element[4]. The interpolating functions are typically linear (first order) within each element. In order to get a more accurate estimate of the stress, it is often necessary to use much smaller elements. This process is called mesh refinement. It may not always be possible to easily identify regions where mesh refinement is required, and quite often the entire mesh is modified. The process of mesh refinement continues until further mesh division and refinement does not lead to significant changes in the obtained solution. The process of continued mesh refinement leading to an acceptable solution is called convergence analysis

2.3 Convergence of P-elements

1.1.1.1 This convergence method is used by Pro/E Mechanica. Instead of constantly refining and recreating finer and finer meshes, convergence is obtained by increasing the order of the interpolating polynomials on each element. The mesh stays the same for every iteration, called a p-loop pass. The use of higher order interpolating polynomials for convergence analysis leads to p-element class of FEA methods, where the 'p' denotes polynomial[12]. P-elements have a different mathematical formulation when compared to h-elements:

· p-elements have shape functions with variable

polynomial order. Convergence is achieved by increasing the polynomial order for a given mesh.
- h-elements have a fixed shape function polynomial. Convergence is achieved by refining the mesh in regions where higher accuracy is needed.
- P-elements can capture more complex behavior with a coarser mesh than h-elements, but are more resource intensive, both computer memory and disk space.
- With P-elements, the user is not responsible for manually designing an accurate mesh.
- In ANSYS, p-elements cannot be mixed with h-elements and p-elements must be higher-order.
- Recent advances in (Mechanica) P-element capabilities: large deformation and contact problems, transient thermal and structural behavior, 2D modeling

3.0 METHOD

Four different specimens of mild steel of configuration shown in Figure 1 were prepared. One of the specimens was used as control while each of the remaining three was cut into two (mid-way) before being joined together by one of the three brands of the popular electrodes in Nigerian market (i.e. Oerlikon, FED and China electrodes). The actual mechanical properties of each of the specimen were obtained using the Universal Testing Machine and software driven micro-hardness testing machine. The results of the testing are as shown in Figures 2 to 5 and tables 1 and 3.

All the results obtained were later used as input in modeling and simulating the structural behaviour of steel. As illustrated in Figure 1, a longitudinal load is applied at the top end of the control test piece (this load varies depending on the experimental results obtained for a particular specimen). Boundary conditions are then set based on the fixed and free surfaces. Since the geometry was imported from Pro/E both to the COMSOL and MECHANICA environments, a single sub-domain was used while carrying out the static analysis. A static analysis has no explicit or implicit time dependencies[4]. This situation corresponds to the steady state of a transient analysis with constant boundary conditions and material properties which is normally aimed at finding:

The maximum stress level and compare it with the material's yield strength

The static deflection at the point where the load is applied and compare it with the time-dependent analysis.

4.0 RESULTS AND DISCUSSIONS

The various results of the experimental analyses and simulation and modeling are as shown in Figures 1 to 24 and Tables 1 to 4. The different approaches used for convergence in the two softwares (h- and p-elements) are evidenced in the density of the different meshes generated.

4.1 FEA Mesh in MECHANICA

The FEA mesh created by the automatic mesh generator is as shown in Figure 6. This FEA mesh will be taken to be a very poor mesh/ discretization by people who are used to some other FEA software which use h-elements. The seemingly justifiable reasons for such an allusion are:
- There are not very many elements involved in the model
- There are many long, slender elements (high aspect ratio)
- Element corners, even within the same element, can have very different angles
- Transitions in element size through the mesh are quite abrupt (long, slender elements are adjacent to short, wide ones)

In an h-code based method, all these would be signs of a poorly constructed and possibly lethal mesh, and would raise serious concerns about the accuracy of the solution.

In order to allay such palpable fear, some of the limits in the Mesh Generator default setting (AutoGem) was tampered with as shown in Figure 7. This adjustment resulted into increase in the number of the meshing elements from 170 to 2,251 (Figures 6 and 7). As can be seen from Table 2, there are no significant differences between the Von Mises Stresses (1.53MPa and 1.48MPa) and the maximum displacement values (0.12213mm and 0.12203mm) whereas the solution time significantly increases from 20.30s to 153.50s and the system memory usage increases from about 203MB to about 1.6GB. This shows that the mesh density in MECHANICA does not have a significant effect on the results in the final solution, although it significantly affects the solution time and the memory usage.

4.2 FEA Mesh in COMSOL

The default h-element type in COMSOL Multiphysics is quadratic Lagrange elements. The concept uses 2nd-order polynomials, which is often a good trade-off between memory usage and accuracy. Linear Lagrange elements are used to reduce memory consumption when accurate stress or strain results are not required. To improve the level of accuracy, the mesh is refined and the analysis is run again. It is then observed if the solution is converging to a stable value as the mesh is refined. If the solution changes when the mesh is refined, the solution is mesh dependent, so the model requires a finer mesh. This approach was used to generate the mesh until it was established that there was no significant difference between the current results and the preceding ones. All the meshes generated and the solutions obtained are as shown in Figures 12 to 24 and Table 4.

5.0 CONCLUSION

Structural behavior of mild steel component welded with three most popular mild steel electrodes in Nigerian market (Oerlikon, FED and China electrodes) has been investigated. Results of the experimental analysis carried out through mechanical testing of the components were used to model and simulate several other structural properties of mild steel components using-state-of-the-art FEA software – Pro/E Mechanica and COMSOL Multiphysics. The various results of the experimental analyses and that of the modeling and simulation are as shown in Figures 1 to 24 and Tables 1 to 4.

Some of the critical properties of mild steel obtained from the experimental analysis carried out vary significantly from the known standard values. The most

prominent of them are the Young Modulus and Yield Strength of Steel. The Young Modulus is supposed to be between 190 and 210MPa [6,7] while the Yield Strength is 353.4 [16]. The values obtained from the experimental analysis are however at a great variance from the standard values. The summarized results of the experimental analysis together with that of the Modeling and Simulation using Pro Mechanica and COMSOL Multiphysics are as shown in Table 4.

REFERENCES

1. Baldridge, S.M., and Humay, F.K. (2003), "Preventing progressive collapse in concrete buildings", Concrete International, November 2003, 73-79.

2. BOC Gases New Zealand Limited (2001), "General Purpose Mild Steel Electrodes: Statement of Hazardous Nature" 988 Great South Road, Penrose, Auckland, NZ

3. Carvill J. (2003), "Mechanical Engineer's Data Handbook", Butterworth-Heinemann Jordan Hill, Oxford OX2 8DP 200 Wheeler Road, Burlington MA 01803

4. COMSOL Multiphysics Modeling Guide (2008), Version 3.4, United States COMSOL, Inc. 1 New England Executive Park Suite 350Burlington, MA 01803

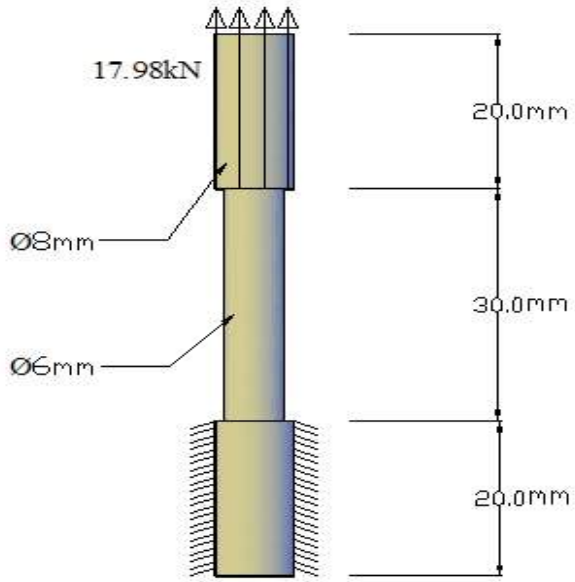
5. Crisfield M. A. (2000), "Non-linear Finite Element Analysis of Solids and Structures" (Volume 1), John Wiley & Sons Ltd. Bafins Lane, Chichester West Sussex PO19 IUD, England

6. Dan B.M. (2001), "Mechanical Engineer's Handbook" Academic Press, 525 B Street, Suite 1900, San Diego, California 92101-4495, USA

7. Edward H.S. (2000) "Mechanical Engineer's Reference Book" Buttenvorth-Heinemann Linacre House, Jordan Hill, Oxford OX2 SDP 225 Wildwood Avenue, Woburn, MA

8. Friedel H. and Casimir K. (2007), "Structural Analysis with Finite Elements", Springer-Verlag Berlin Heidelberg

9. Hartsuijker C. and Welleman J.W. (2006), Engineering Mechanics, Springer P.O. Box 17, 3300 AA Dordrecht, The Netherlands Manual on Tensile Test of Steel, University of New Mexico, Civil Engineering Department, Civil



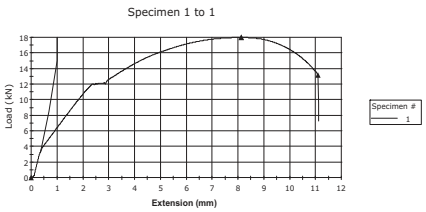


Figure 2: Graph of Load Vs Extension in the M

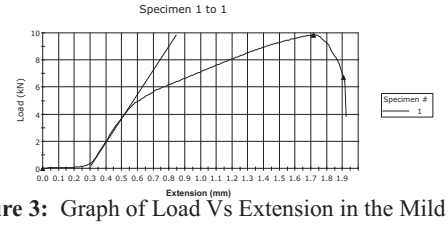


Figure 3: Graph of Load Vs Extension in the Mild Steel Test Piece welded with Oerlikon Electrode

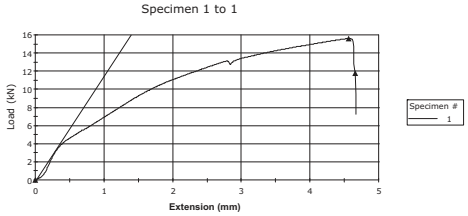


Figure 4: Graph of Load Vs Extension in the Mild Steel Test Piece welded with FED Electrode

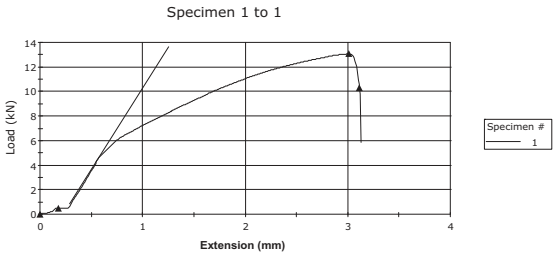


Figure 5: Graph of Load Vs Extension in the Mild Steel Test Piece welded with China Electrode

	SPECIMEN LABEL			
	S1	**S2**	**S3**	**S4**
Length (mm)	27.27000	28.0400	27.7000	27.520
Diameter (mm)	5.97000	5.94000	6.04000	5.8600
Area (mm^2)	27.99230	27.7117	28.6526	26.9703
Maximum Load (kN)	17.98000	9.84000	15.6100	13.070
Tensile stress at Maximum Load (MPa)	642.2800	355.190	544.640	484.440
Tensile strain at Maximum Load (%)	29.83000	6.12000	16.4900	10.9300
Load at Break (Standard) (kN)	13.17000	6.74000	11.7800	10.3000
Extension at Break (Standard) (mm)	11.09987	1.90850	4.65906	3.11687
Tensile stress at Break (Standard) (MPa)	470.4000	243.060	411.130	381.990
Tensile strain at Break (Standard) (%)	40.70000	6.81000	16.8200	11.3300
Tensile stress at Yield (Zero Slope) (MPa)	642.2800	355.190	-	19.1500
Modulus (E-modulus) (MPa)	13205.520	17277.6	14922.3	14124.8
Energy at Break (Standard) (J)	156.75044	11.2175	49.7934	26.3278
Energy at Maximum Load (J)	107.51298	9.52872	48.4319	24.9960
Energy at Yield (Zero Slope) (J)	107.51298	9.52872	-	0.03532
Extension at Yield (Zero Slope) (mm)	8.13337	1.71669	-	0.17487
Load at Yield (Zero Slope) (N)	17978.825	9842.91	-	516.466
Tensile strain at Yield (Zero Slope) (mm/mm)	0.29825	0.06122	-	0.00635
Energy to X-Intercept at Modulus (E-modulus) (J)	0.00747	0.02069	0.01525	0.06996

Table 1: Experimental Results of the Mechanical Testing of Mild Steel Test Pieces welded with three different brands of popular mild steel electrodes in Nigerian market

Legend

S1 - Mild Steel Control Test Piece
S2 - Mild Steel Test Piece welded with Oerlikon Electrode
S3 - Mild Steel Test Piece welded with FED Electrode
S4 - Mild Steel Test Piece welded with China

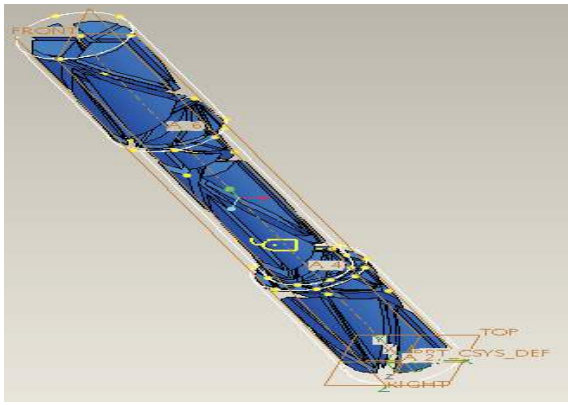
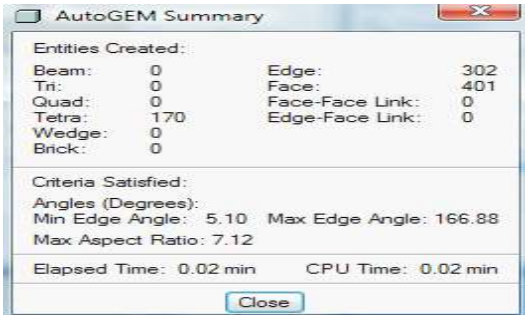


Figure 6: Mesh generated by MECHANICA using default setting (consisting of 170 elements)



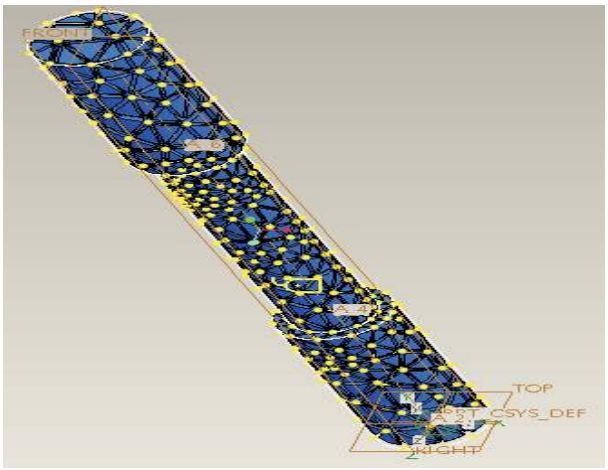
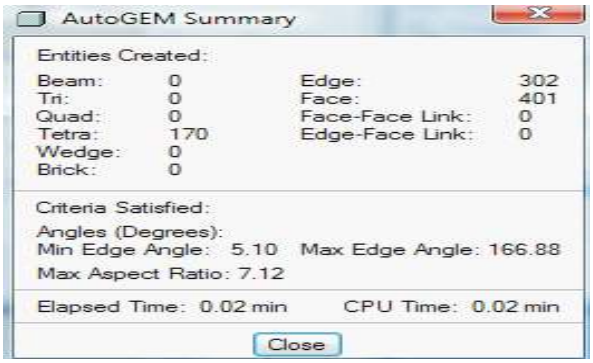


Figure7: Mesh generated by MECHANICA using user defined setting (consisting of 2251 elements)



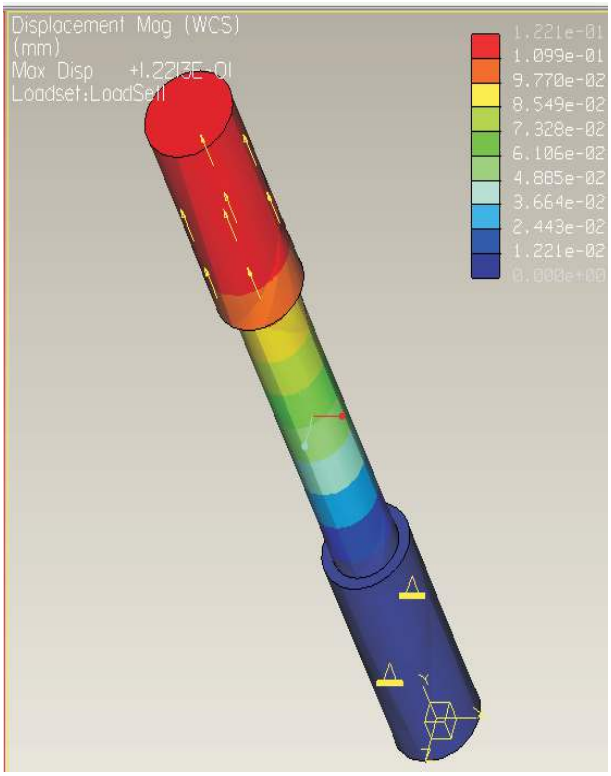


Figure 9: Displacement/extension before breaking using MECHANICA

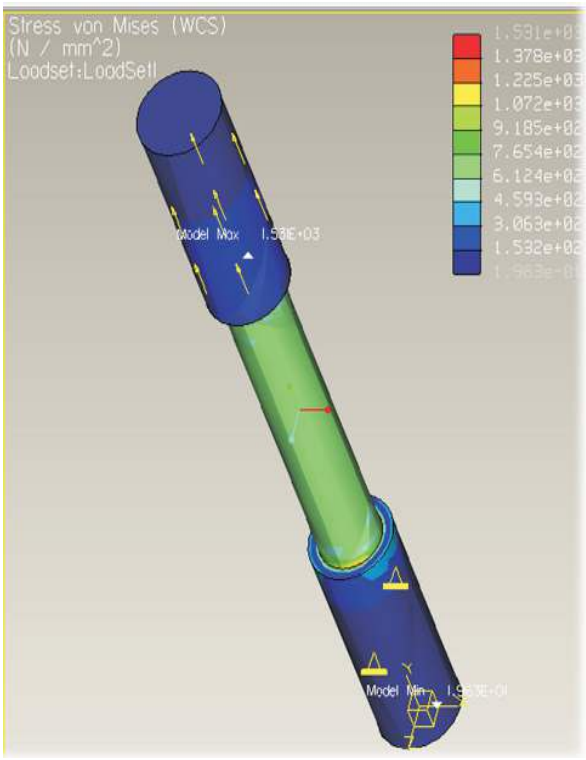


Figure 8: Von Mises Stress Distribution using MECHANICA

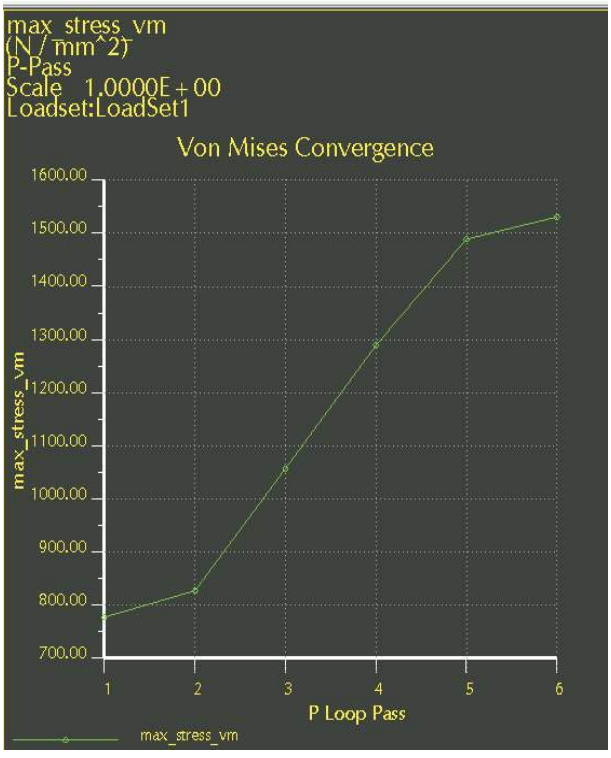


Figure 10: Convergence Test in MECHANICA using Von Mises Stress

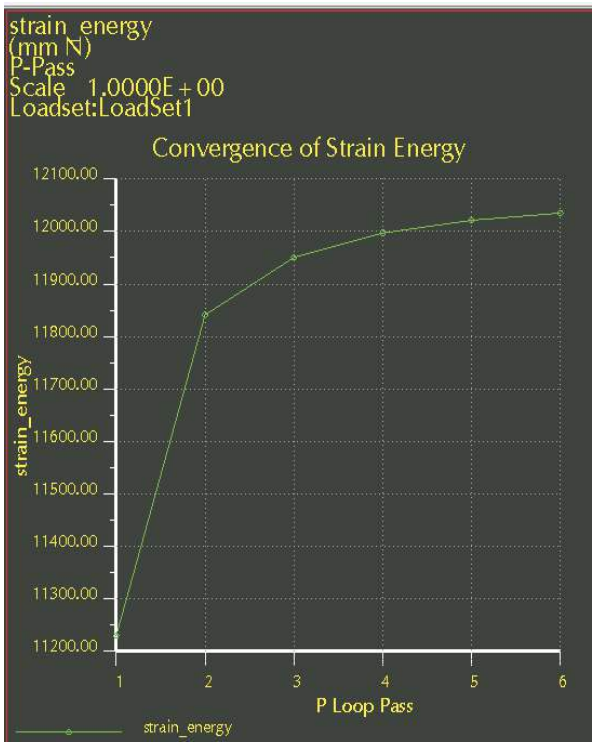


Figure 11: Convergence Test in MECHANICA using Strain Energy

S/N	NAME	Default Meshing		Refined Meshing	
		Value	Convergence (%)	Value	Convergence (%)
1	Maximum Displacement Magnitude (mm)	1.22129e-01	0.1	1.22028e-01	0.0
	Maximum X Displacement over Model (mm)	-3.0504e-03	0.2	2.58718e-03	0.0
3	Maximum Y Displacement over Model (mm)	1.22108e-01	0.1	1.22022e-01	0.0
4	Maximum Z Displacement over Model (mm)	2.87922e-03	5.0	2.75565e-03	4.1
5	Maximum Von Mises Stress (N/mm^2)	1.5307e+03	2.7	1.4851e+03	12.7
6	Maximum XX Stress Component (N/mm^2)	6.3655e+02	12.1	1.1555e+03	18.8
7	Maximum XY Stress Component (N/mm^2)	4.3221e+02	0.6	7.1483e+02	15.9
8	Maximum XZ Stress Component (N/mm^2)	1.9253e+02	11.3	-2.0816e+02	8.6
9	Maximum YY Stress Component (N/mm^2)	1.6322e+03	5.4	1.7433e+03	14.5
10	Maximum YZ Stress Component (N/mm^2)	-6.5061e+02	0.7	6.1835e+02	15.5
11	Maximum ZZ Stress Component (N/mm^2)	7.0775e+02	0.4	9.3754e+02	18.3
12	Points	72		618	
13	Edges	302		3265	
14	Faces	401		4899	
15	Elements	170		2251	
16	Total Elapsed Time (s)	19.96		144.93	
17	Total CPU Time (s)	20.30		153.50	
18	Maximum Memory Usage (KB)	203375		1627923	
19	Working Directory Disk Usage (KB)	47104		118784	

Table 2: Model Summary for Design Study on "Steel Analysis" using Pro Mechanica

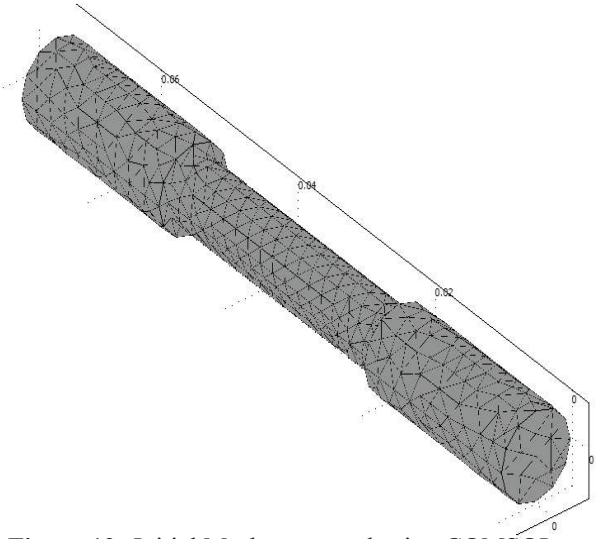


Figure 12: Initial Mesh generated using COMSOL Multiphysics (consisting of 3115 elements)

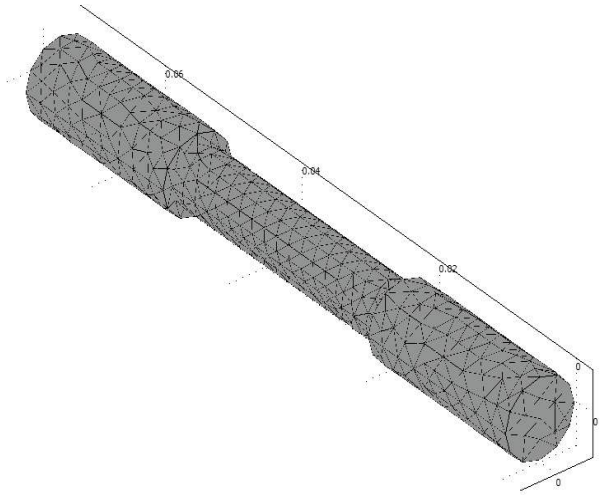
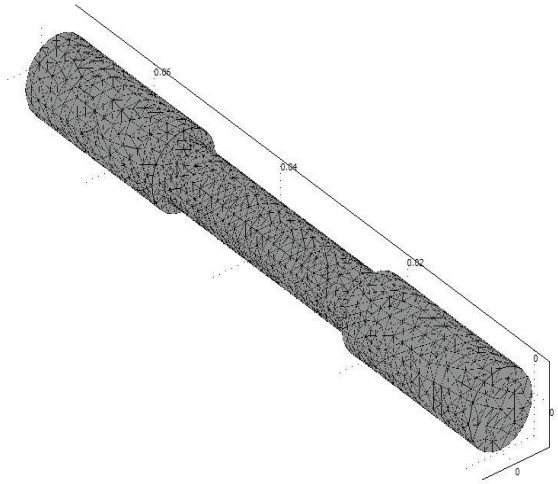


Figure 13: First Mesh Refinement using COMSOL Multiphysics (consisting of 11167 elements)



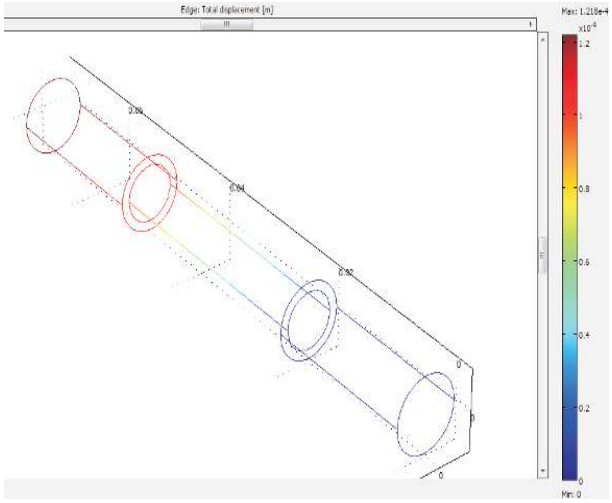


Figure 20: Solution obtained for the Edge Total Displacement using second mesh refinement in COMSOL [in m]

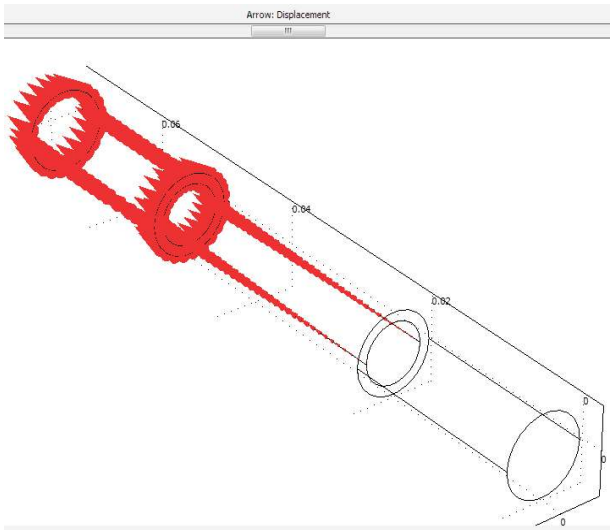


Figure 21: Solution obtained for the Arrow Displacement using second mesh refinement in COMSOL

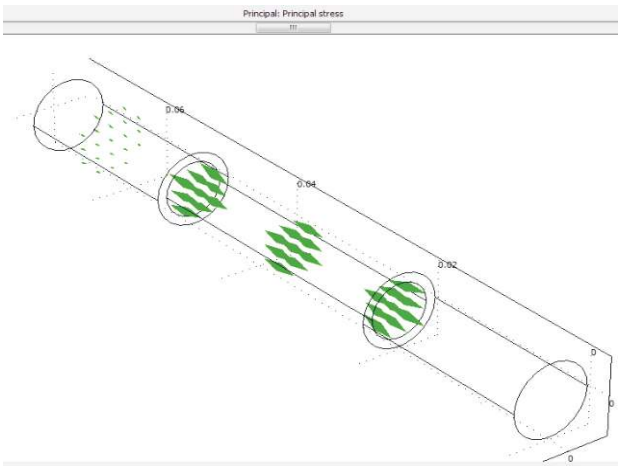


Figure 22: Solution obtained for the Principal Stress using second mesh refinement in COMSOL

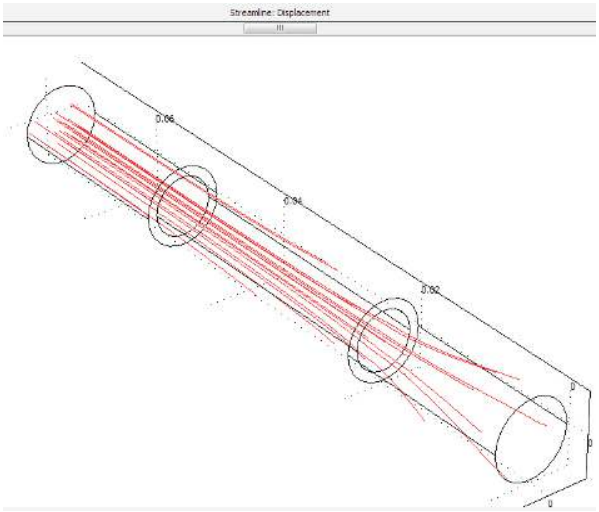


Figure 23: Solution obtained for the Streamline Displacement using second mesh refinement in COMSOL

China electrode weldment	260.5
FED electrode Weldment	244.8
Oerlikon electrode weldment	204.1

Table 3: Hardness values obtained using micro hardness tester

Test Piece	ST	S1	S2	S3	S4
Actual Young Modulus (MPa)	199948	13205.52	17277.61	14922.29	14124.77
Actual Deformation (mm)		8.13337	1.71669	-	0.17487
Actual Tensile Stress at Yield (MPa)		642.28	355.19	-	19.15
Displacement using MECHANICA (mm)	0.1221	1.849	1.413	1.072	0.9904
Displacement using COMSOL (mm)	0.1218	0.1845	0.7716	0.1417	1.254
Von Mises Stress using MECHANICA (MPa)	612.4	612.4	612.4	401.3	350.8
Von Mises Stress using COMSOL (MPa)	610	610	350	500	420

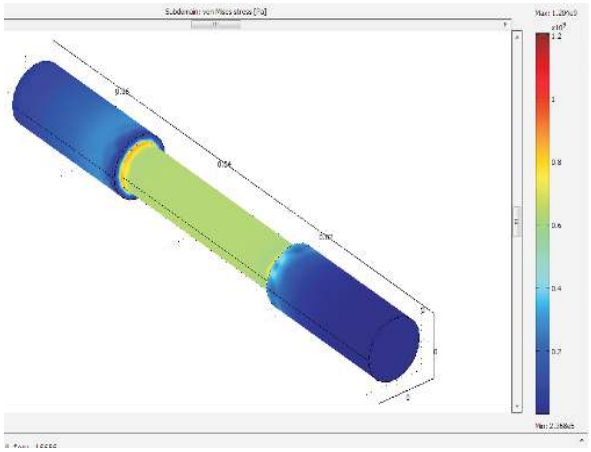


Figure 14: Solution obtained for the Sub-domain Von Mises Stress using initial mesh generated in COMSOL in Pa (Degrees of freedom = 16,656; Solution time = 2.127s)

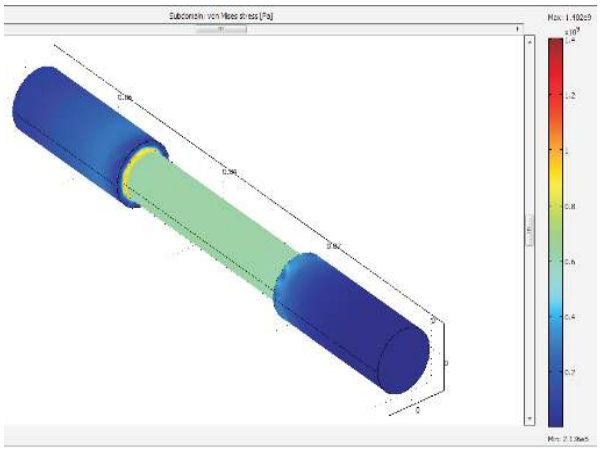


Figure 15: Solution obtained for the Sub-domain Von Mises Stress using first mesh refinement in COMSOL [in Pa] (Degrees of freedom = 51,696; Solution time = 8.394s)

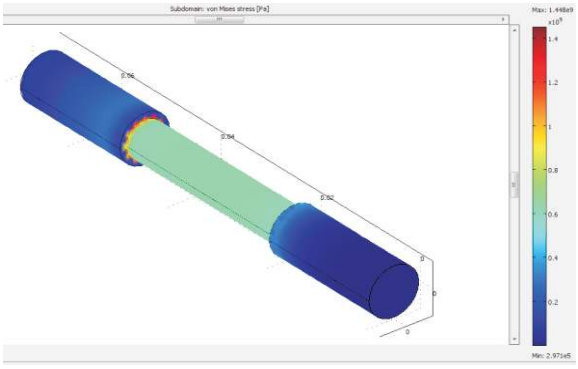


Figure 16: Solution obtained for the Sub-domain Von Mises Stress using second mesh refinement in COMSOL [in Pa] (Degrees of freedom = 154,050; Solution time = 80.811s)

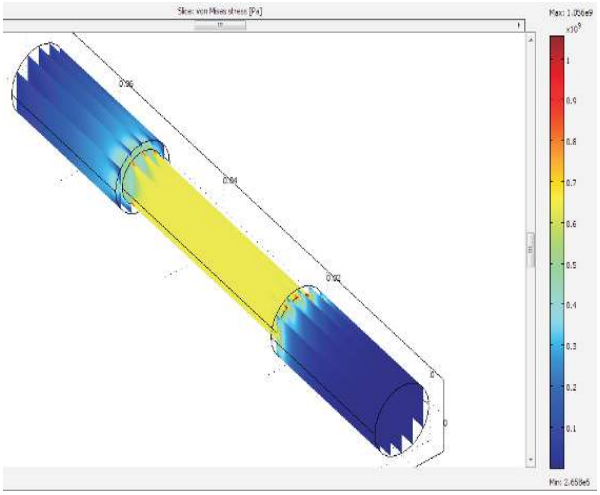


Figure 17: Solution obtained for the Slice Von Mises Stress using second mesh refinement in COMSOL [in Pa]

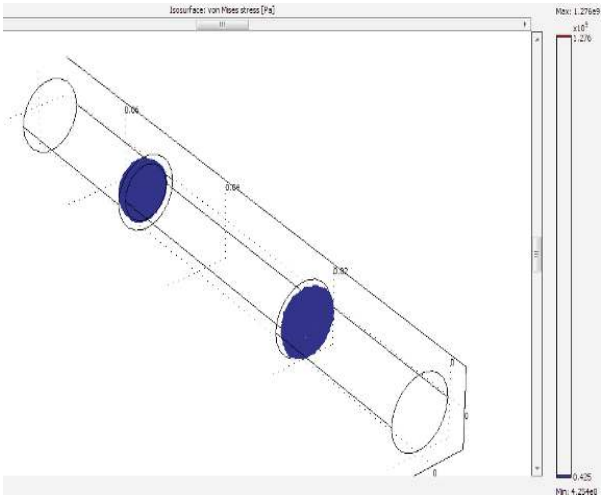


Figure 18: Solution obtained for the Isosurface Von Mises Stress using second mesh refinement in COMSOL [in Pa]

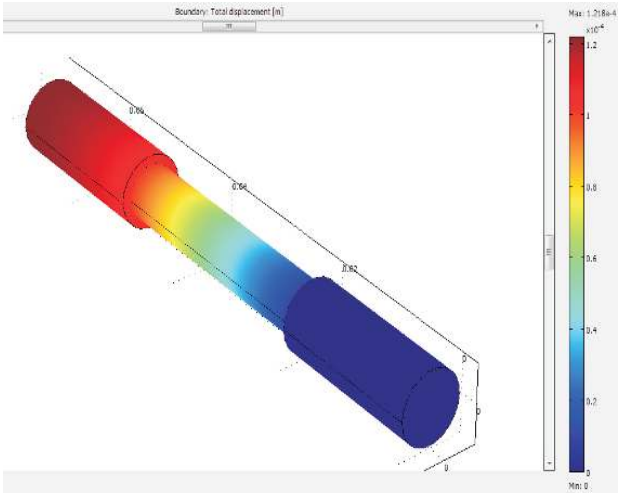


Figure 19: Solution obtained for the Boundary Total Displacement using second mesh refinement in

FINITE ELEMENT ANALYSIS OF THERMOELASTIC CONTACT PROBLEM OF DISC BRAKE WITH FRICTIONAL HEAT GENERATION.

*Moses Omolayo PETINRIN; John Ogheneortega OJI
Prototype Engineering Development Institute
(National Agency for Science and Engineering Infrastructure)
Ilesa, Osun State, Nigeria
*layopet01@yahoo.com

Abstract
This work models the heat generation and dissipation in a disc brake during braking and the following release period. The model simulates the braking action by investigating both the thermal and elastic actions occurring during the friction between the two sliding surfaces, represented by the maximum temperature on the contact surface. Brake pad and disc were selected, and parameters set to certain values from existing literatures. Three dimensional thermomechanical analysis model of the disc brake system was created, and governing dynamics and heat equations described. Comparison was also made of the selected pad material (aramid) with that of asbestos to ascertain its viability as an effective substitute and to improve conceptual designs. The verification and application of the simulation software showed that the models and technique adopted in this work are efficient and appropriate for numerical simulation of brake disc which could be employed to guarantee safety and durability of the braking system.

Keywords: thermoelastic behaviour, heat generation, thermomechanical analysis, finite element analysis, COMSOL Multiphysics.

Introduction

Repetitive braking of the vehicle leads to heat generation during each braking event. The resulting rise in temperatures has very significant role in the performance of the braking system. Problems such as premature wear of brake pads and thermal cracking of brake discs are attributed to high temperatures. Consequently controlling the temperature profiles and thermo-mechanical stresses are critical to proper functioning of the braking system [1].

The friction heat generated between two sliding bodies causes thermoelastic deformation which alters the contact pressure distribution. This coupled thermo-mechanical process is referred to as frictionally-excited thermoelastic instability (TEI) [2]. According to Altuzarra *et al.* [3], if the sliding speed is high, the resulting thermo-mechanical feedback is unstable, leading to the development of non-uniform contact pressure and local high temperature with important gradients called 'hot spots'. The formation of such localized hot spots is accompanied by high local stresses that can lead to material degradation and eventual failure [4]. Also, the hot spots can be a source of undesirable frictional vibrations, known in the automotive disc brake community as 'hot roughness' or 'hot judder' [5].

Eltoukhy *et al.* [6], studied the influence of the material properties on the thermoelastic behaviour and compared different types of brake disk materials found in the literature.

In this study, fully coupled thermoelastic instability problem for a disc brake system would be analysed. Thermal and mechanical model for the disc brake would be generated and solved using Comsol Multiphysics developed base on the finite element principle. COMSOL Multiphysics is a powerful interactive environment for modelling and solving all kinds of scientific and engineering problems based on partial differential equations (PDEs) [7].

A comparison of two different brake pads (white asbestos and Kevlar 29 aramid fibre) is performed on grey cast iron disc. This is to find the thermoelastic effects of those pads on the brake disc and to ascertain the viability of aramid fibre as a good substitute for asbestos, because asbestos pad releases toxic dust into the environment [8].

Wear action takes place during the braking process, resulting from the friction between the disc brake and the pad, is assumed to be so small and thus to be neglected in the analysis.

Theoretical Background

Considering a car of mass, m moving with an initial velocity, v_1. Its velocity reduces to v_2 by applying the brake. Therefore, the change in kinetic energy, E of the moving car can be expressed as

$$E = \frac{1}{2} m(v_1^2 - v_2^2) \qquad (1)$$

Assuming the car is not climbing or descending a hill, this makes the potential energy that can be developed by the car to be zero. Also, neglecting drag and other losses outside the brakes, and no skidding of the car tyres on the road surface, the energy absorbed by the braking system of the car is equivalent to change in its kinetic energy [9]. The brakes' retardation power, *P* is given by the time derivative of the car's kinetic energy.

$$P = -\frac{d}{dt}\left(\frac{mv^2}{2}\right) \qquad (2)$$

$$= -mv\frac{dv}{dt}$$

$$P = -mR^2\omega(t) \propto \qquad (3)$$

Here *R* equals the wheel radius, *w* is the angular velocity, and α is the angular acceleration.

The workdone per unit time by friction at the interfaces between of each of the car four brake discs and the brake pad can be determined by the product of the friction force and the disc's velocity. This work equals the brake's retardation power when integrated over the surface area of the eight pads (two pads per brake disc) and is given as

$$P = 8F_f\omega(t)\iint rdA \qquad (4)$$

From equations (3) and (4), the frictional force per unit area, F_f of the pad surface can be determined as

$$F_f = -\frac{mR^2\alpha}{8r_mA} \qquad (5)$$

Where A is the pad's contact are a and r is the distance between the cent re of the disc and the pad's centre of mass.

During the braking action, the kinetic energy produced at the wheel is transformed into heat energy, therefore, from equation (4) the heat generated per unit c ontact area , Q at time *t* and the distance *r* from the disc centre for one disc pad's surface becomes

$$Q = F_fr\omega(t) \qquad (6)$$

The angular velocity can be defined as

$$\omega(t) = \omega_0 + \alpha t$$

The governing heat equation [10], for the transient thermal analysis is

$$\rho C_p\frac{\partial T}{\partial t} + v.\nabla T = k\nabla^2T + Q \qquad (7)$$

The energy abs orbed by the brake and transformed into heat must be dissipated to the surrounding air in order to avoid excessive temperature rise of the brake lining.

The heat dissipated, q_d by from the disc surface to the surrounding air by convection and radiation may be estimated by

$$q_d = h(T - T_0) + \varepsilon\sigma(T^4 - T_0^4) \qquad (8)$$

The coefficient of heat transfer, h can be determined from Nusselt Number, Nu as a function of the car's speed, v [11].

$$Nu = 0.037Re^{0.8}Pr^{0.33} \qquad (9)$$

$$h = \frac{Nuk}{d} \qquad (10)$$

Where

$$Re = \frac{\rho vd}{\mu} \qquad (11)$$

$$Pr = \frac{C_p\mu}{k} \qquad (12)$$

From equations (8) to (12), T is the temperature, T_0 is the ambient temperature, ε is the material's emissivity, and σ is the Stefan-Boltzmann constant. While d represents the disc diameter, k is the thermal conductivity, ρ is th e density, C_p is the specific heat capacity and μ is the dynamic viscosity of the ambient air.

The invariant form of the dynamic equilibrium equation [12, 13], for the deformation caused by the thermal stress can be expressed as

$$\nabla.\sigma + F = \rho\frac{\partial^2u}{\partial t^2} \qquad (13)$$

For homogeneous, isotropic, and elastic material, the constitutive equation is

$$\sigma = E(\epsilon - \epsilon_0) + \sigma_0 \qquad (14)$$

Assuming there no prestress, σ_0, the self - strain due to thermal expansion in the material is

$$\epsilon_0 = \alpha_T\Delta T \qquad (15)$$

Where 4s, and interval of 1.0 between 6.0s and 12.0s
Figure 2 represents the change in car velocity during the braking process, and the time period of the different phases of braking, dragging, and release.
The developed finite element analysis model (Figure 3) contains a total of 10813 elements, 18736 nodes and 74944 degrees of freedom, while the time step used during the numerical computation was 0.01s. The initial temperature used during the simulation was set as 303K (30 ºC).

Results and Discussion
The finite element model was solved using COMSOL Multiphysics, the properties of the brake materials (aramid fibre, white asbestos and grey cast iron) with the thermophysical properties of air are listed in Table 1. The solution times for both the thermal and mechanical analyses of the aramid fibre and white asbestos (pad materials) on grey cast iron (brake disc) are 24 minutes, 46 seconds and 25 minutes, 20 seconds, respectively. The two analyses were carried out on a computer with Dua-Core 2.0GHz processor and 2GB RAM.
Figure 4 presents the temperature produced and distribution in the brake disc module, with aramid fibre as pad material, at time steps of 0.1s, 2.0s, 2.8s and 12.0s. It can be shown that the localized temperature hot spots were generated on the contact surfaces due to the rubbing action.
The comparison between the temperature distributions (after integrating the thermal load on the rubbing surface) produced during and after the braking processes on the rubbing surface of one of the two pads for the two brake pad materials under the same operating conditions is shown in Figure 5. From the figure, it shows that with asbestos, as pad material, showed a better thermal behaviour with grey cast iron disc during and after the braking processes, for the maximum temperature and the temperature distribution produced. Also, the temperature distributions increased from initial value to maximum at 3s and decreased after the braking action because heat has been dissipated out of the surface through conduction, convection and radiation.
Temperatures computed in the thermal analysis are introduced as thermal loads in the structural analysis, the result for the Von Mises stress distribution, with aramid fibre as pad material, at time step of 2.8s is shown in Figure 6. Also, the comparison between the Von Mises stress distributions produced during and after the braking processes on the rubbing surface of one of the two pads for the two brake pad materials under the same operating conditions is shown in Figure 7. From the figure, stress generated with aramid fibre by thermal load on the contact surface is more than that of the asbestos. The maximum deformations obtained on the grey cast iron from the structural analysis are approximately 243μm and 238μm for aramid fibre and asbestos respectively. These values are close to 200μm got by Eltoukhy *et al.* from different geometry, material and conditions.

Conclusion
A finite element model of the brake disc and two pads were created and thermo-mechanical behaviours developed between the pads and disc during the braking period were investigated using COMSOL Multiphysics. Also, under the same braking conditions, comparisons were made between asbestos and aramid pads. The results obtained show that the selected software package (COMSOL Multiphysics) for the analysis is effective and appropriate for modelling of all kinds of scientific and engineering problems based on partial differential equations. With the already established damaging impact of asbestos to health and the environment, aramid fibre pad proved to be a good substitute for asbestos, because the differences in the results obtained during the braking period and the subsequent brake-release period are insignificant.

References
[1] Chavan P. and Apte A. (2007) "**Axisymmetric Analysis of Bolted Disc Brake Assembly to Evaluate Thermal Stresses",** *Abaqus India Regional Users' Meet, pp. 1-7*

[2] Lee K. J. and Barber J. R., (1994) "An Experimental Investigation of Frictionally-Excited Thermoelastic Instability in Automotive Disk Brakes under a Drag Brake Application", *Journal of Tribology*, Vol. 116, pp. 409-414.

[3] Altuzarra O; Amezua E; Aviles R. and Hernandez A., (2002) "Judder Vibration in Disc Brakes Excited by Thermoelastic Instability", *Engineering Computations*, Vol. 19, no. 4, pp. 411-430.

[4] Jang Y. H. and Ahn S. H., (2007) "Frictionally-Excited Thermoelastic Instability in functionally Graded Material", *Wear*, Vol.262, pp. 1102-1112.

[5] Yi B. Y., Barber J. R. and Zagrodzki P., (2000) "Eigen Value Solution of Thermoelastic Instability Problems using Fourier Reduction", *Proceedings of the Royal Society of London*, Vol.456, pp. 2799-282.

[6] Eltoukhy M., Asfour S., M. Almakky M. and Huang C., (2006) "**Thermoelastic Instability in Disk Brakes: Simulation of the Heat Generation Problem",** Proceedings of the COMSOL Users Conference, Boston

[7] COMSOL (2007), *COMSOL Multiphysics User's Guide*; Copyright 1994-2007, COMSOL

[8] Wikipedia, Brake pad, Wikipedia Foundation Inc; 2010, Retrieved 10th July, 2010 from http://en.wikipedia.org/wiki/Brake_pad

[9] Khurmi R.S. and Gupta J.K. (2005), *A Textbook of Machine Design*, 14th edition, Eurasia Publishing House (PVT.) Ltd, **Ram Nagar, New Delhi**

[10] Kreith F. and Bohn M. S. (1993), *Principles of Heat Transfer*, 5th edition, West Publishing Company, St. Paul

[11] Coulson J.M. and Richardson J.F., "Fluid flow, Heat Transfer and Mass Transfer", (2006) Chemical Engineering, Vol. 1, 6th edition, Butterworth-Heinemann, Imprint of Elsevier, Indian Reprint.

[12] Liu G. R. and Quek S. S. (2003), *The Finite Element Method: A Practical Course*, 1st edition, Elsevier Science, Burlington

[13] Fenner R. T. (1975), *Finite Element Methods for engineers*, 1st edition, The Macmillan Press, London and Basingstoke

[14] Granta (2008), *Granta CES Edupack*, CES Selector Version 4.8.0, Granta Design Ltd.

Table 1: The Brake Materials Properties and Thermophysical Properties of Air

Material Properties	Pad (Kevlar 29 Aramid Fiber)	Pad (White Asbestos)	Disc (Gray Cast Iron, BS grade 180)	Air
Thermal Conductivity (W/mK)	0.25	4	53.5	0.02559
Density (kg/m^3)	1440	2500	7100	1.1388
Linear Expansion Coefficient (K^{-1})	-3.3×10^{-6}	4.25×10^{-6}	12×10^{-6}	-
Specific Heat Capacity (J/kgK)	1400	1060	385	1.0127
Emissivity	0.82	0.82	0.27	-
Modulus of Elasticity (Pa)	7.1×10^{10}	1.65×10^{11}	1.06×10^{11}	-
Poisson Ratio	0.36	0.28	0.24	-
Dynamic Viscosity (Ns/m^2)				1.855×10^{-5}

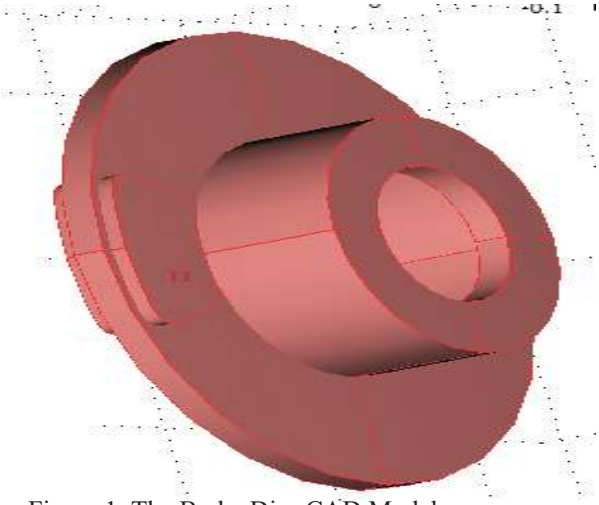


Figure 1: The Brake Disc CAD Model

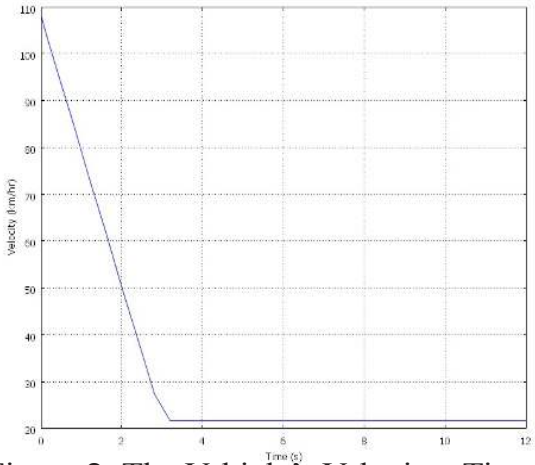


Figure 2: The Vehicle's Velocity Time - Graph

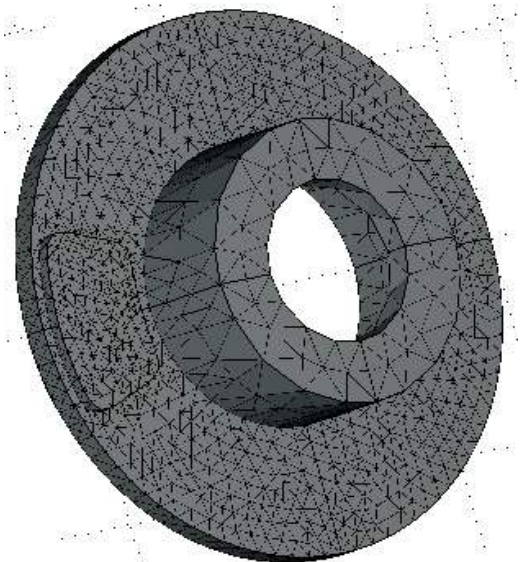
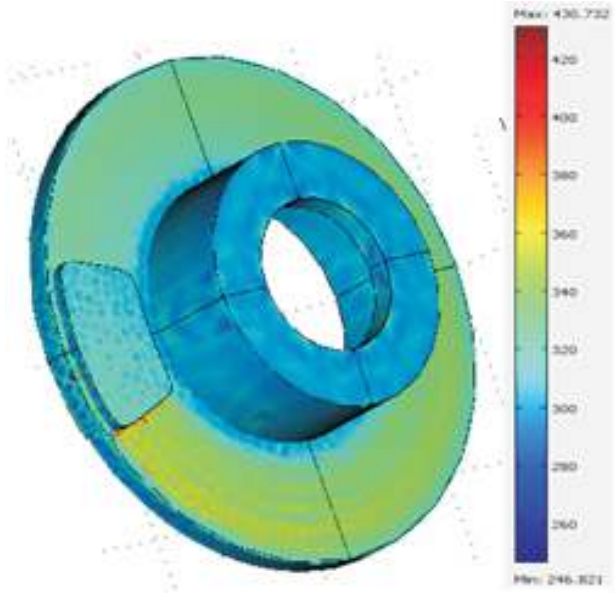
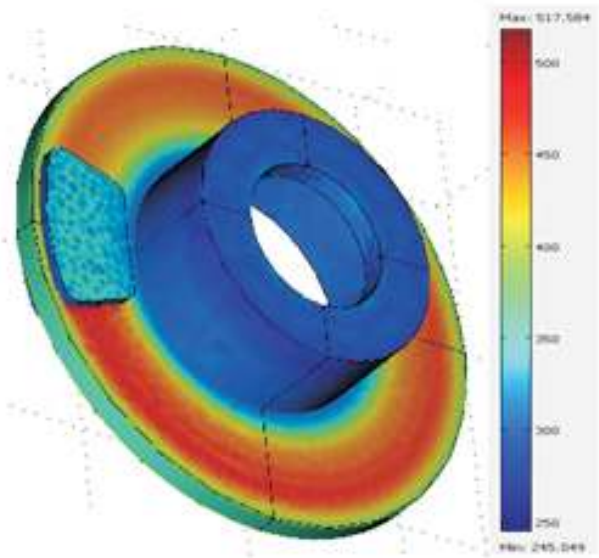


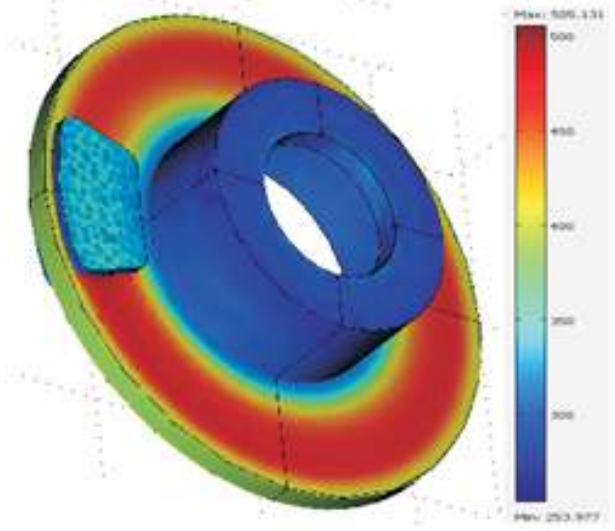
Figure 2: The Vehicle's Velocity-Time Graph



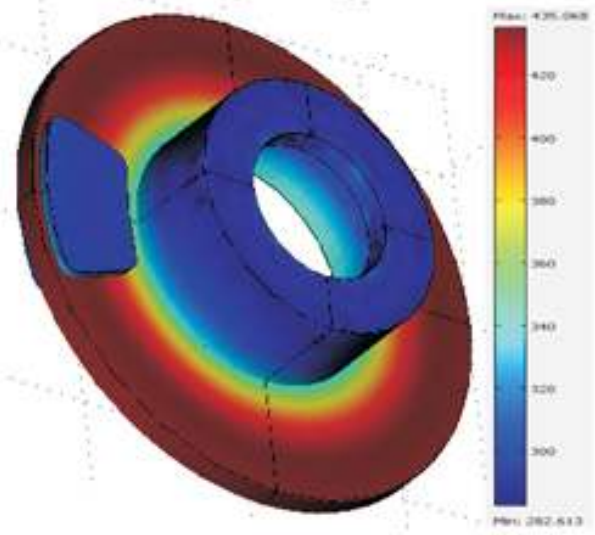
(a) at time = 0.1s



(b) at time = 2.0s



(c) at time = 2.8s



(d) at time = 12.0s

Figure 4: The Temperature distribution at time steps 0.1s, 2.0s, 2.8s and 12.0s

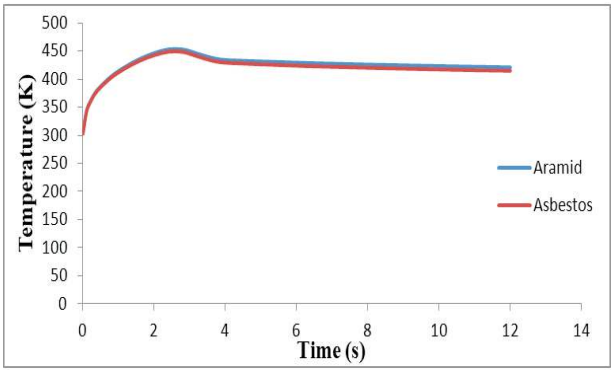


Figure 5: Temperature Distribution Produced with the Brake Disc

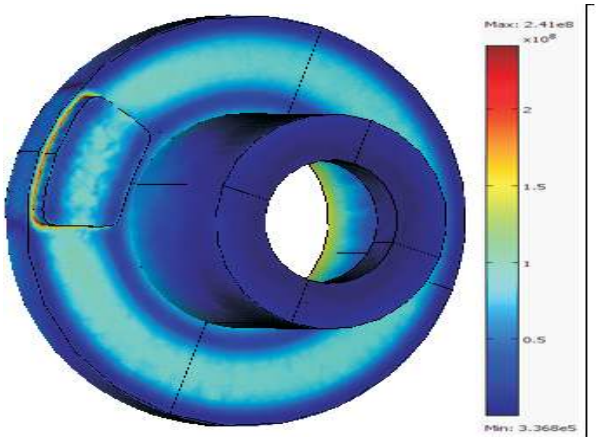


Figure 6: The Stress distribution at Time Step 2.8s

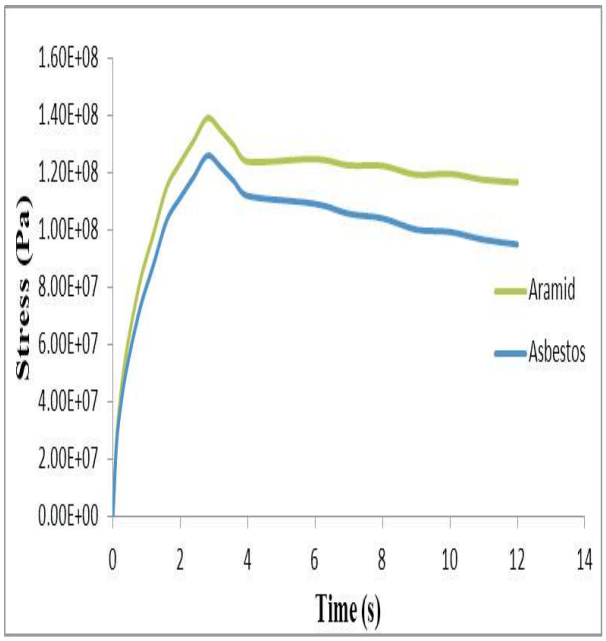


Figure 7: Stress Distribution Produced with the Brake Disc

2011
TECHNICAL PAPERS

EFFECTS OF WATER TEMPERATURE ON THE HARDNESS AND TOUGHNESS OF WATER QUENCHED MEDIUM CARBON STEEL

***A.A. Alabi, A.I. Obi and Magani S.S**
Department of Mechanical Engineering, Ahmadu Bello University, Zaria, Kaduna State, Nigeria
*Corresponding Author: abdulmm2001@hotmail.com,aaalabi@abu.edu.ng

ABSTRACT
The effects of water temperature on the hardness and impact strength of water quenched medium carbon steel was studied. Samples of two different steel, 0.3 wt % C and 0.4 wt % C, were heated to 900 °C and quenched in water at temperatures ranging from 35 °C (room temperature) to 95 °C. The results showed that the high brittleness and low impact strength (toughness) which are two major defects that mostly characterized water quenched steels were reduced by up to 18% and over 50 % respectively simply by raising the water temperature to 95 °C before quenching.

Keywords: Water quenched temperature, Thermal Diffusivity, Hardness, Toughness

Introduction

Water quenching is probably the oldest heat treatment process used by man to harden steel. It can be described as the rapid cooling of metal from the solution treating temperature, usually in the range of 845°C to 870°C for steels. Quenching is usually performed in order to prevent ferrite or pearlite precipitation and facilitate the formation of martensite or bainite, [1] . In the hardened condition, steel should have 100% martensite to attain maximum yield strength,[3]. The severity of water makes the hardened steels brittle and in some cases developed internal cracks thus limiting their engineering application. These shortcomings of water quenched steels have almost made the phrase 'water quenched and tempered' a form of heat treatment, since all water quenched steel are tempered. With tempering, the properties of quench steel could be modified to decrease hardness and increase ductility and impact strength,[3]. Another way to minimized distortion in dimensions and cracking during quenching was to minimize the temperature differences between different areas of a part (or sample). This often requires the use of oil or aqueous polymer solutions to moderate the heat transferred during quenching, [1]. Researchers have shown that mineral and vegetable oils could compete favorably with water as steel quenchant producing similar hardness with higher impact strength,[7]. Neem seed oil and engine oil have also been proven to be good quenchants for plain carbon steel and ductile cast iron. They gave hardness values close to those of water quenched samples while their impact strength were higher,[11]. The use of bitumen as a suitable quenching medium has also been reported. The results obtained by quenching medium carbon steel in hot bitumen was compared with those of water quenched steel tempered at different temperatures. Quenching in bitumen gave better toughness and tensile properties while the hardness values were almost the same,[6,8]. The report on bitumen stated that the experiments were carried out in a fume cupboard due to the health hazard involved in the inhalation of bitumen fume and fire safety related issues. The works on vegetable oils, neem seed oil, engine oil and other mineral oils made little or no mention of the health and safety hazards involved in working with the oils as quenchants,[4]. Water is the cheapest, most abundant and safest of all the media used in the hardening of plain carbon steel. Therefore, it becomes imperative to explore all the thermodynamic properties of water with a view to overcoming the defects in water quenched plain carbon steel. This work is aimed at investigating the effect of water temperature on the hardness and toughness of water quenched medium carbon steel.

Materials and Methods

The steel samples used for the study are from Delta Steel Rolling Mill, Nigeria. There chemical composition is shown in Table 1.The quenchant used is water.

The equipment used include: Lathe machine, electric water heater, electric furnace, Rockwell hardness machine, Hounsfield balanced impact tester, Hounsfield notching machine and Hounsfield tensometer.

Thirty five test piece were machined from each of sample A (0.33%C) and sample B (0.42%C) for hardness, impact and tensile test.

Seven cylindrical test pieces of dimension Φ10mm × 10mm , from each sample ,were machined, grind and polished for digital Rockwell hardness test. Fourteen test pieces of dimension Φ8mm × 45 mm with a V notch 1.9 mm deep, 45° tapered from its root was made at the centre of each impact test piece. Another fourteen test pieces of gauge length dimension of Φ4.8mm ×25 mm [10] were machined from each sample for the tensile test.

The samples were normalized, and then austenitized in batches at 900°C for one hour. Each batch, comprising two impact, one hardness and two tensile test piece, was then quenched in water at temperatures of 35°C, 50 °C, 65 °C, 80°C and 95 °C.

To determine the minimum amount of water required to satisfactorily quenched the steel samples without rising the water temperature by more than 1°C, the first law of thermodynamic was applied

Mass of an impact test sample, M_1 = 17.82g
Mass of a tensile test sample, M_2 = 6.59g
Mass of a hardness test sample, M_3 = 6.20g
Mass of water required for quenching operation, M_w
SHC of steel, C_s = 0.42 J/ gK
SHC of water, C_w = 4.2 J/ gK
Temperature of test pieces from furnace, T_1= 900°C
Initial Temperature of water, T_2 = 35°C
Final temperature of mixture, T_3 = 36°C
Total mass of pieces in one batch, M
$M = 2*M_1 + 2*M_2 + M_3 = 55.02g$
Assuming no heat is lost to the surrounding, from the first law of thermodynamics, heat gained by the quenching medium is equal to the lost by the test pieces [9].

$$MC_s (T_1 - T_3) = M_w C_w (T_3 - T_2) \quad \ldots\ldots. 1$$

$$55.02 * 0.42 * (900-36) = M_{w1} * 4.2 * (36-35)$$

$$M_w = 4753.73g$$

But volume = mass/density
Using density of water as 1gcm^{-3}
Hence, the volume of water needed to quench the 1st batch was 4.76 litres.
Similarly, the volume of water required to quench the 2nd batch at T_2= 50°C was 4.68 litres. While the volume of water required to quench the 3rd, 4th and 5th batches at initial temperature 65°C, 80°C and 95°C respectively were 4.6, 4.52 and 4.43 litres respectively.
The actual volume of water used for quenching each batch was the calculated volume plus two litres. The mixture was stirred continuously for 3 minutes then allowed to cold to room temperature.
The as-quenched pieces were subjected to the hardness, impact and tensile test.

The Rockwell hardness testing machine on the "A" scale was used to determine the hardness values. The samples were properly flattened and polished before the diamond indenter was brought in contact with the test piece.

The impact test was conducted on the Hounsfield balanced impact machine. The hammer was moved out of position by raising the pawl release lever. The inner tup was lifted to the right while the outer tup was moved upward to the left. The test piece was then inserted into the slot in the inner tup by pulling the notch register backward and ensuring that the V notch was actually engaged. The hammer was then threw over smartly and the reading taken by observing the pointer.

The tensile test was conducted on the Hounsfield Tensometer. The test piece were firmly held in the chucks of the machine. A continuous load was manually applied while the load-extension curve was traced on a graph attached to the drum. The percentage elongation and percentage reduction of area were measured using gauges,[10]

Results and Discussion

The chemical composition of the sample A and sample B are shown in Table 1.

The hardness values of the different water quenched conditions for both samples are illustrated in Figure 1. The hardness value of sample B is higher than the corresponding hardness value of sample A for all the five temperatures. This might be due to the fact that the percentage of carbon in sample B is higher [5]. The highest hardness values of 72.6 HRC and 81.3 HRC for sample A and sample B respectively was attained at the water temperature of 65 °C. While the lowest hardness values for both samples were recorded at 95 °C. This may mean that thermal diffusivity of the steels in water was highest at 65°C and lowest at 95°C, [2] .
The impact strength fluctuates as quenching medium temperature increased from the assumed room temperature of 35 °C to the pre-boiling temperature of 95 °C as shown in Figure 2. The toughness of the sample A is higher than that of sample B. This is likely due to the lower carbon content of sample A [5]. The highest impact energy of 46.69J and 40.12J recorded for sample A and sample B respectively at quenching medium temperature of 95 °C confirmed that the thermal diffusivity of the steels in water was least at this temperature,[2]. This implies that it took a longer time for the heat in the steels to flow out to the surroundings, thereby creating room for the hard martensitic structure initially formed in the core of the steels to be slightly tempered. Since tempering always increase the toughness of water quenched steel, [5]

Figure 3, Figure 4 and Figure 5 show the results of tensile strength, percentage elongation and percentage reduction in area respectively for sample A and sample B. Looking at the high values of the percentage elongation and percentage reduction in area, one could argue that the best tensile properties for both samples was achieved at the quenching temperature of 95 °C. This may not also be unconnected to the low thermal diffusivity of the steels in water at 95 °C.

Conclusion
From the results of the study the following conclusion can be drawn.

1. The toughness of water quenched medium carbon steels can be greatly improved with only slight decrease in hardness by raising the temperature of the water to 95 °C
2. Where hardness is the targeted property of a water quenched steel, the best results would be achieved by quenching at 65 °C
3. Water quenching can be used to achieve better mechanical properties for plain carbon steels without wasting additional energy tempering or quenching in some hazardous and expensive oils.

References

1. Bates, C.E. and Totten, G.E. (1992): Quench Severity Effects on the As-quenched Hardness of Selected Alloy Steels. Heat Treatment of Metals, vol.2, p.45-48
2. Paschkis. V and Stolz Jr, G. (1956): Quenching as a Heat Transfer Problem. Journal of Metals, pp. 1074- 1075
3. Htun, M.S., Kyaw, S.T. and Lwin, K.T. (2008): Effect of Heat Treatment on Microstructures and Mechanical Properties of Spring Steel. Journal of Metals, Materials and Minerals. Vol.18, No.2 pp. 191-197
4. **Stephen, L. G.(2003): Metalworking Fluids: Oil Mist and Beyond.** *Applied Occupational and Environmental Hygiene, Vol.*18 pp.818–824
5. Raymond, A. H. (1993). Engineering Metallurgy, Part II. Edward Arnold, London. 6th Edition. pp. 240-283
6. Alabi, A.A.(2009): Improving the Mechanical Properties of Bicycle Axle Using Bitumen Treatment. MSc. Thesis, Department of Mechanical Engineering, Ahmadu Bello University, Zaria, pp. 28-33
7. Ndaliman, M. B. (2006). An Assessment of Mechanical properties of Medium Carbon Steel under Different Quenching Medium. AU J.T. 10(2): pp. 100-104 http://www.journalTechV10N2_aticle06.pdf Retrieved June 14th, 2008
8. Ause, T. (2007). Evaluation of Hot Bitumen Bath as a Quenching Medium for Austempering of Steels and Ductile Cast Iron. Ph. D. Seminar, Department of Materials and Metallurgical Engineering, Ahmadu Bello University, Zaria, Nigeria.
9. Eastop, T.D. and McConkey, A. (1993). Applied Thermodynamics for Engineering Technologies. Longman Group, UK Ltd. Pp 16
10. Vernon J. (1992).Testing of Materials. Macmillan Education Ltd, London.pp.35-37
11. Hassan, S.B., Agboola, J. B., Aigbodion, V.S. and Williams, E.J. (2011): Hardening Characteristics of Plain Carbon Steel and Ductile Cast Iron Nsing neem Oil as Quenchant. Journal of Minerals and Eaterials Characterization and engineering, vol. 10, No. 2, pp. 161-172

Table 1: Chemical Composition of the Steel Samples

	Sample A (wt. %)	Sample B (wt. %)
C	0.32	0.42
Mn	0.68	0.53
Si	0.24	0.17
P	0.032	0.031
S	0.04	0.048
Cr	0.17	0.18
Ni	0.12	0.11
Cu	0.30	0.32
V	0.003	0.003
Al	0.46	0.40
Sn	0.024	0.021
Ti	0.001	0.001

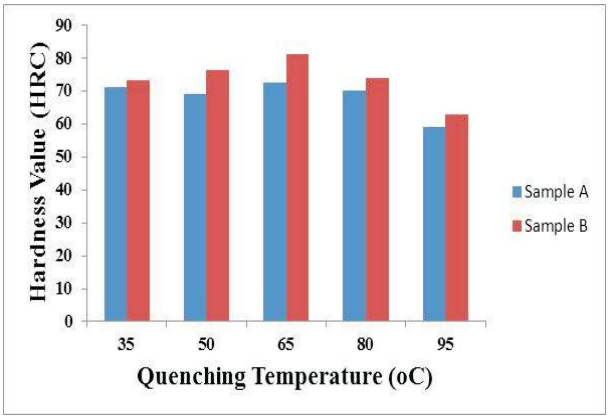


Figure 1: Effect of Quenching Temperature on the Hardness of Steel Samples

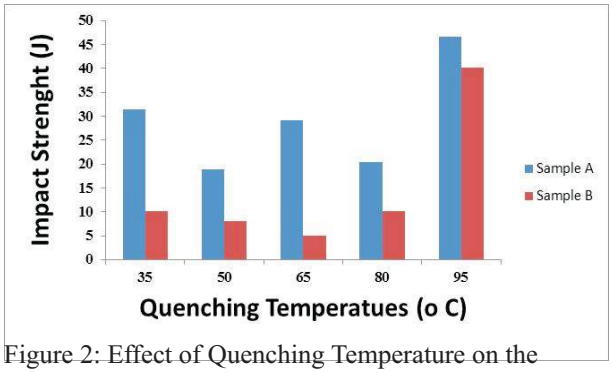


Figure 2: Effect of Quenching Temperature on the Impact Strength of Steel Sample

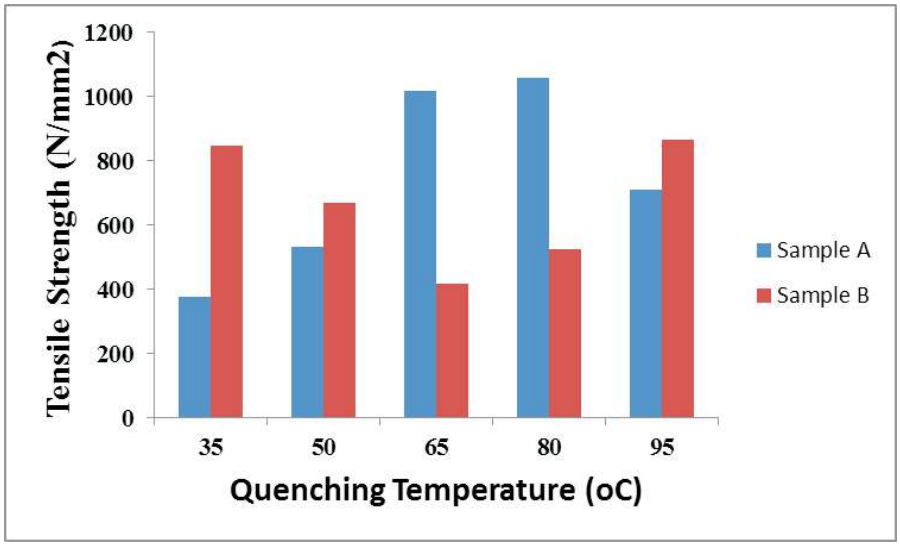


Figure 3: Effect of Quenching Temperature on the Tensile Strength of Steel Samples

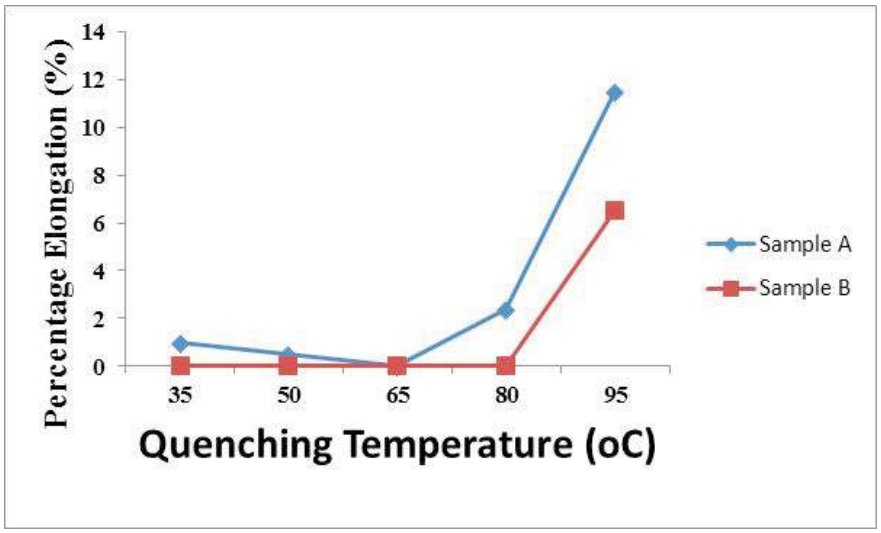


Figure 4: Effect of Quenching Temperature on the % Elongation of Steel Samples

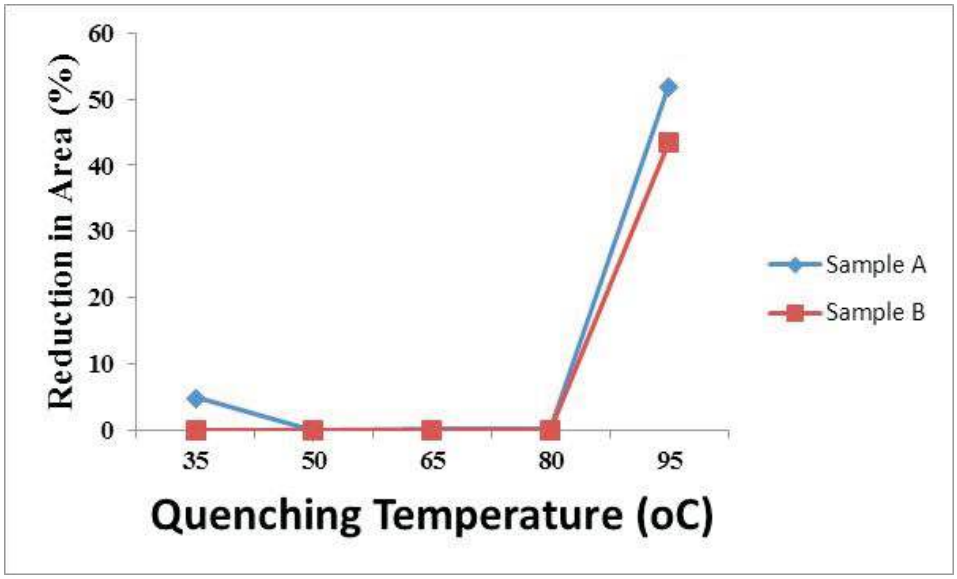


Figure 5: Effect of Quenching Temperature on the % reduction in area of steel samples

THE INFLUENCE OF CARBURIZING VARIABLES ON THE MECHANICAL PROPERTIES OF AISI 1034 (2-D APPROACH)

[1]Adegbola A. A. [1]Adegbenjo. O.A, [1]Olaiya K. A [2]Omotoyibo.J.A, [2]Olaniran O
[1]Department of Mechanical Engineering, The Polytechnic, Ibadan
[2]Federal University of Technology, Akure, Nigeria
(kunleade2002@yahoo.com)

ABSTRACT
The significance of the mechanical properties in metallic components such as, heavy duty industrial gear, brake disc, rolling mill gear, linkage and more cannot be over-emphasized. Industrial machines fail as a result of in appropriate selection and treatment thereby resulting into our Nigeria's industrial comatose. To this end, AISI 1034 Steel was treated with Snail shell and Wood Charcoal respectively at a maximum of 1100°C. The carburization process decreases the hardness value of samples carburized with Wood Charcoal with increase in carburizing temperature. The carburization treatment followed by the water quenching and tempering at 350°C strongly influenced the Ultimate Tensile Strength and Young's Modulus of Elasticity of AISI 1034. The Optimum combination of mechanical properties was achieved with samples carburized with Snail Shell. It could be suggested that samples carburized with Snail Shell will perform better in service than samples carburized with Wood Charcoal when carburized at the same carburizing time and temperature. The process was supported mathematically when the radius *(the ruling section)* is inversely proportional to the diffusion rate.

Keywords: Snail Shell, Wood Charcoal, Carburizing Temperature, Carburizing Time, Modeling

1.0 INTRODUCTION

Carburizing is a heat treatment process aimed at increasing the surface hardness and wear resistance of components which are required to perform good impact strength and resistance to wear in service [1] Basically, the process is based on the theory of thermal absorption and diffusion of carbon atoms into steel. The process is usually done at an elevated` temperature with a chemical agent such as solid or liquid salt that can provide adequate quantity of atomic carbon for the diffusion and absorption process. A broad range of metals that can be carburized includes steel, Nickel and alloys [2]Typical component that are subjected to this treatment are gears, spindles shafts, cams, levers, steering parts, distribution gears, etc.

Pack carburizing is one of the methods in the carburizing, process. It is the earliest application in carburizing, where parts were simply placed in a suitable container and covered with a thick layer of carbon powder. The process is done by packing the component in a solid carburizing compound in a suitable container and heating it slowly in a furnace to attain a temperature of 900^0C and above [3]. Although it is very effective in introducing carbon, this method was exceedingly slow and as the demand for greater production grew, a development of new process was established. This includes vacuum carburizing and plasma carburizing. Another recent development in carburizing is fluidized bed furnace which can provide much faster rate of carburizing compared to the conventional process [4]All of these processes perform better mechanical properties and higher hardness to component than conventional carburizing. Before this, many studies were found focusing on hardness, wear resistance and microstructural properties of carburizing low carbon steel [5]. In this research, the tensile strength, hardness and microstructural analysis of the steel (AISI 1034) is studied.

The carburizing process were discovered by early blacksmiths to increase the strength, surface hardness and enhanced wear resistance of agricultural tools such as scythes, axes and weapon such as swards. All these tools were found to have carburized layer. At that time, the process was done by *leave hot* forged in the hot coals followed by quenching in water and would harden the surface layers. Later processes involved putting such implements into cast iron boxes with charcoal and bone ash. These were heated to "red hot" ($\approx 900^0$C) and left for several hours depending on the layer required. Then, they were quenched and tempered at 300^oC [2,6].

Cooling the forged tool in water *(quenching)* forms martensite which is due to trapped carbon atoms that do not have time to diffuse out of the crystal structure. [5,6,7,8]. In order to make the tools useful they have to be re – heated to a lower temperature than that used for forging temperature. This tempers the steel and reducing the hardness, also improves its toughness. This causes a big increase in the surface hardness, enhanced wear and fatigue resistance. Basically, the carbon content of the case and its depth is controlled by the carburizing time and temperature.

Carbon and other element act as a hardening agent preventing dislocations in the iron atom crystal lattice from sliding past one another. The amount of alloying elements and their presence in the steel can control the quality in terms of hardness ductility, and tensile strength of the resulting steel. Steel with increased carbon content can be made harder and stronger than iron, but is also more brittle .Though steel had been produced by various inefficient methods long before the *Renaissance*, its use

became more common after more efficient production methods were devised in the 17th century. Further refinements in the process, such as basic oxygen steel making, lowered the cost of production while increasing the quality of the metal. Today, steel is one of the most common materials in the world and is a major component in buildings, tools, automobiles, and appliances [9].

1.1 RESEARCH PROBLEM

The use of inappropriate carburizing media had led to the failure of some engineering component [7,8].This could be attributed to poor selection of materials, inability to determine the performance of different carburizing media on the mechanical properties of steel, inability to determine microstructure of steel, and inappropriate heat treatment process[9,10,11].

All of these were as a result of lack of evaluating the performance of different carburizing media capable of improving the wear resistance of engineering components.

Table3.1: Spectrochemical analysis result of the control sample (0.34% carbon ϕ12mm)

Element	**C**	**Si**	**S**	P	**Mn**	**Ni**	**Cr**	**Mo**
% Composition	0.3398	0.2003	0.0529	0.0542	0.7021	0.1168	0.1331	0.0206
Element	**V**	**Cu**	**W**	**As**	**Sn**	**Co**	**Al**	**Pb**
% Composition	0.0032	0.3035	0.0033	0.0055	0.0303	0.0106	0.0020	0.0012
Element	**Ca**	**Zn**	**Fe**					
% Composition	0.0004	0.0042	98.0159					

© Courtesy of Universal Steels, Industrial Estate, Ogba, Ikeja, Lagos, Nigeria, 2011.

2.0 OBJECTIVE OF THE RESEARCH

i. To evaluate the performance of different carburizing media on the mechanical properties of steel.
ii. Determination of microstructure of the steel before and after carburizing.
iii. To examine the effects of heat and mass transfer on the diffusion rate.

3.0 MATERIALS AND METHODS

The materials used for this research work is medium carbon steel (AISI/SAE 1034, 12mm) with the chemical composition shown in Table 3.1. The material was sourced from *Universal Steel Company Ogba Industrial Estate*, Ikeja Lagos).

3.1 MATERIAL SELECTION

Series of materials were searched to enhance the good success of this research work but medium carbon steel was selected due to its sterling qualities and characteristics displayed during fabrications. These are machinability and malleability.

3.2 EXPERIMENTAL TECHNIQUES

Fourteen samples of 1034 steel were machined to standard test sample sizes of tensile test. This was done according to AS_TM's specification on standard tensile sample dimension (Fig.3.1). Twelve samples were carburized and the remaining two were reserved as a control sample.

The prepared test samples were embedded in the carbonaceous material vis-à-vis Wood Charcoal and Snail Shell with small quantity of Barium Carbonate as an energizer in a steel pot which was then tightly sealed with clay cover to prevent the CO from escaping and prevent unwanted furnace gas from entering the steel pot during heating. The furnace temperature was adjusted to the required temperature (*900, 1000 and 1100^{0}C for each stage respectively*) and the loaded steel pot was charged into the furnace .When the furnace temperature reaches the required carburizing time (i.e. 2hr for 1100^{0}c, 3hr for 1000^{0}c and 4hr for 900^{0}c for each media), it was then held at the temperature for 15 – 30minute. After the material was soaked for a specified period, the steel pot was removed from the furnace and the material was quenched in water (which was initially at the ambient atmospheric temperature).

Six of the carburized test samples were then tempered at a temperature of 3500c for 2hrs, and then cooled in air. After the cycles of heat treatment, the test samples were subjected to tensile test, hardness test and metallographic test. Finally, the material was mounted to the microscopes which automatically examine the microstructure of the materials and the cameras attached to the microscope take the picture of the structure.

3.4 MATHEMATICAL MODELING

NOTATION

dB - Breadth change
q - Quantity of heat rate
k - Thermal conductivity
A - Area of the material
$\frac{dT}{dx}$ - Change in temperature with length at x axis
$\frac{dT}{dy}$ - Change in temperature with length at y axis
$\frac{dT}{dz}$ - Change in temperature with length at z axis

dz

T	-	Temperature
du	-	Change in internal energy
dQ	-	Quantity of heat change
dw	-	width change
M	-	Material mass
Cp	-	Specific heat capacity
V	-	Void Fraction

ASSUMPTIONS

The material is homogeneous and isotropic

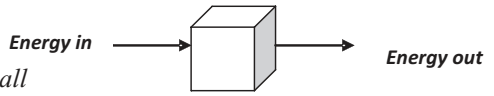
The furnace is a perfectly closed system

The material has negligible void fraction

The material obey hook's law

The material is of constant specific heat

Since the heat transfer process is purely condition, let the pictorial view of the material be represented in Fig. 3.7 Let us consider an elemental body $\mathbf{d}_B$, with $\mathbf{d}_x$, $\mathbf{d}_y$, $\mathbf{d}_z$ as its coordinate dimension. Using energy balance equation:



Recall

Fouriers law of conduction

$q = -kA\left[\frac{\partial T}{\partial x}\right]$ for one dimension

and $q = -KA\left[\frac{\partial T}{\partial x} + \frac{\partial T}{\partial y} + \frac{\partial T}{\partial z}\right]$

$q = -KA\,T$ ---------- (1)

Where $= \partial/\partial x + \partial/\partial y + \partial/\partial z$

Energy in left face + heat generated within element = change in internal energy + energy conducted out of right surface. Energy in left face $= -KA\frac{\partial T}{\partial x}$

Energy generated in element = qAdx

Change in internal energy, du

Recall, **dQ = du + dw** – *first law of thermodynamic*

$du = dQ - dw$, *for* $dw \approx 0$

$du = dQ = MC_p dT$

Recall $\rho = M/V$, $M = \rho V$

:. $du = dQ = \rho VC\,dT$

Since V is a function of void

i.e. $V = 1 - \varepsilon$

$$du = (1 - \varepsilon)\,l\,Cp\frac{\partial T}{\partial t}$$

=> Combining all terms

$$\left(-KA\frac{\partial T}{\partial x} + qAdx\right) = lCA\frac{dT}{dx}dx - AK\frac{dT}{dx} + \frac{\partial}{\partial x}\left[K\frac{\partial T}{\partial x}\right]$$

$$\Rightarrow \frac{\partial}{\partial x}\left[K\frac{\partial T}{\partial x}\right] + q^0 = lC\frac{\partial T}{\partial t}$$

$$\frac{\partial}{\partial x}\left[K\frac{\partial T}{dx}\right] + \frac{\partial}{\partial y}\left[K\frac{\partial T}{\partial y}\right] + \frac{\partial}{\partial y}\left[K\frac{T}{\partial 2}\right] + q^0 = lc\frac{\partial T}{\partial x}\frac{\partial T}{\partial t}$$

$$\Rightarrow \frac{\partial^2 T}{\partial x^2}\left(+\frac{\partial^2 T}{\partial y^2}\right) + \frac{\partial^2 y}{\partial x^2} + q^0 = lC\frac{\partial T}{\partial t}$$

For cylindrical coordinate

$$\frac{\partial T}{\partial t} + \frac{1}{r}\frac{\partial T}{\partial r} + \frac{1}{^2 r}\frac{\partial T}{\partial \phi^2} + \frac{\partial T}{\partial z^2} + \frac{q^0}{K} = \frac{1}{\propto}\frac{\partial T}{\partial t}$$

For simplification

$\frac{\partial^2 T}{dr} + \frac{1}{r}\left[\frac{\partial T}{\partial r}\right] = 0$ (for steady state and no internal heat generation)

$$\frac{\partial^2 T}{\partial r^2} + \frac{1}{r}\left[\frac{\partial T}{\partial r}\right] = 0 \text{ ----------(3)}$$

$$\frac{\partial^2 T}{\partial r^2} + \frac{1}{r}\left[\frac{\partial T}{\partial r}\right] = 0$$

Let $T(r) = l^{mr}$

$\partial T(r) = M^{mr}\ell$

$\frac{\partial^2 T}{\partial r^2}(r) = M^2 l^{mr}$

$M^2 l\,mr = +\frac{1}{r} Ml^{mr} = 0$

$M^2 + \frac{M}{r} = 0$

$M(M + 1/r) = 0$

$M \phi 0$

$T(r) = l^{-r}$

Using taylor series

$l^{-r} = 1 - r + \frac{r^2}{2!} + \frac{r^3}{3!} + \frac{r^4}{4!} - \frac{r^5}{5!} + \text{----------}$

$T(r) = l^{-r}$

SOURCE CODE/COMPUTATION

```
Using System;
Using System Collections Generic;
Class calculate
Public static void Main
Double temp, radius, a radius1;

Console Write Line ("Enter Radius @ start:\t");
Radius = Convert To Double (Console. Read Line)
Console Write Line ("Enter Radius @ End:\t");
radius1 = Convert to Double (Console Read Line);
For (a = radius; a<=radius1; a +=0.01)
Temp = System Math Exp (1 / a);
Console Write Line ("{0}\t\t\t{1}", a, temp);
Console Read Line;The programme was test-run to obtain curve in Fig.(4.18)
```

REFERENCES

[1] Majumbera D (1989), ISD Ints, Vol. 29, Pp 524-28

[2] Mahat K.A (2007), Time and Temperature effects on Fracture Properties of Carburized low Carbon Steel. University Tenknikal Kebangsaan Malaysia

[3] Ashby, Michael F,David R. H. Jones (1992) *Engineering Materials 2*,Oxford: Pergamon Press. ISBN 0-08-032532-7

[4] Gupta, G.S, Chaudhuri, A. and Vasanth Kumari P. (2002): Mater. Science.Technology, 2002, Vol. 18, Pp 1188-94

[5] Qadeer K, A (1972), *The effect of morphology on the strength of copper-based martensites,*, 1, **1** (1 ed.), Leuven, Belgium: A.Q. Khan, University of Leuven, Belgium, pp. 300

[6] BongartzK., W.J. Quadakkers, R. Svhulten, and H. Nickel: Metal Trans. A, (1989), Vol. 20A, Pp. 1021-27

[7] Adegbola. A.A (2004) , "Performance and Evaluation of different Carburizing Media"Arrhenius Approach" March 2005, The Engineer, Journal of the Faculty of Engineering, The Polytechnic, Ibadan, Vol III, Pp57-59

[8] Adegbola A.A (2005), Basic Material Properties and Application. Debo Prints (Ibadan).Primer Edition, Pp3-5,ISBN978-37652-0-X

[9] Goldstein J.I and A.E Moren: metal. Trans. A, (1978), vol. 9A, Pp. 1515-25

[10] Hultgreen A. J. Iron Steel Inst., 1951, Pp. 245-57

[11] Stickels C. A (1989), Metal. Trans. B, , Vol. 20B, Pp 535-46



Fig.3. 1: Standard tensile

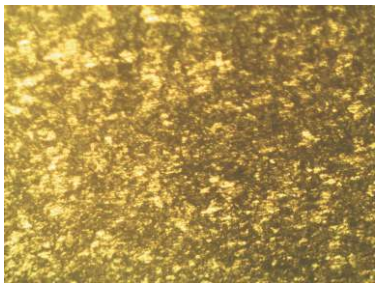


Fig.3.2:1034 steel of ferrite + cementite (as received)

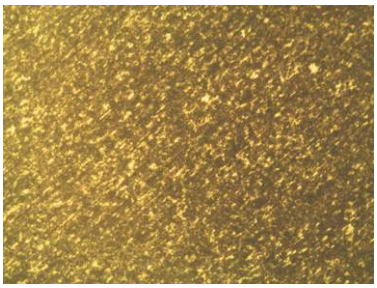


Fig.34:1034 steel carburized with SS at 900^0c for 4hrs and tempered for 2hrs X100mag

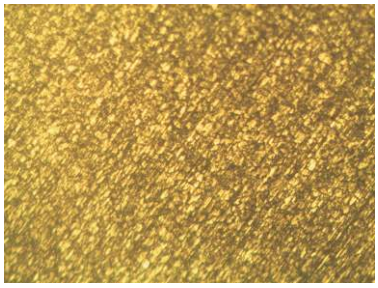


Fig 3.3:1034 steel carburized with SS at 1100°C X100mag

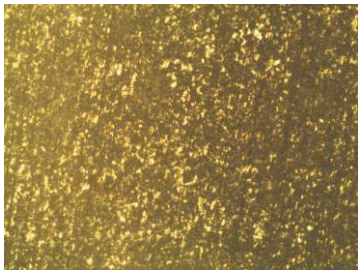


Fig. 3.5:1034 steel carburized with SS at 1000^0 C for 3hrs X100mag

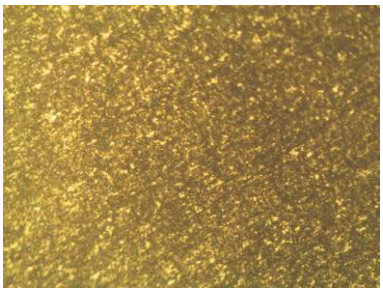


Fig 3.6:1034 steel carburized with WC at 1000^{0}c for 4hrs X100mag

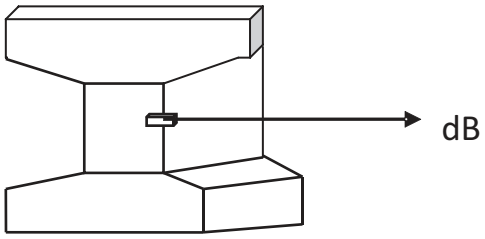


Fig. 3.7: Elemental Body

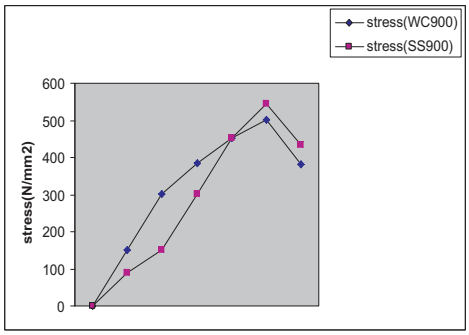


Fig.4.1: Stress variations (N/mm^2) for carbonaceous materials at 900°C for 4Hours

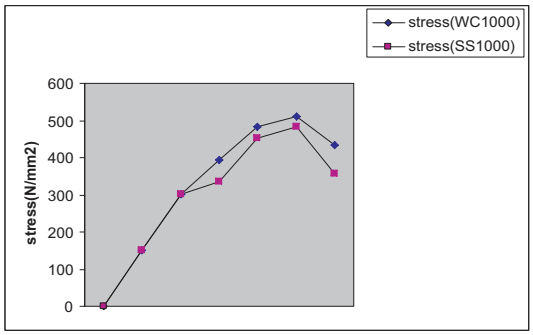


Fig.4.2: Stress variations (N/mm^2) for carbonaceous materials at 1000°C for 3hour

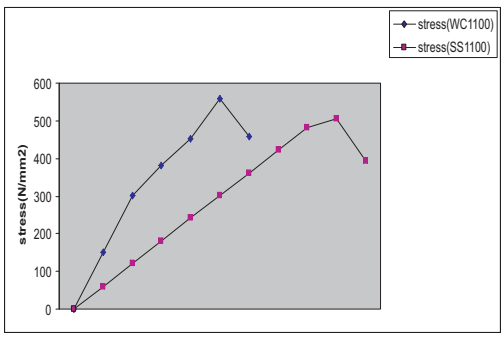


Fig. 4.3: Stress variations (N/mm^2) for Carbonaceous materials at 900°C for 4 Hrs and tempered for 2h

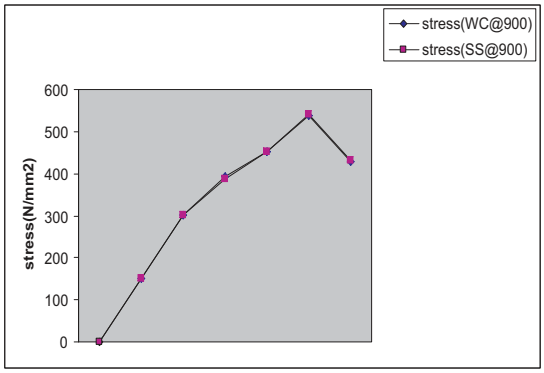


Fig.4.4: Stress variations (N/mm^2) for materials Carbonaceous at 900°C for 4Hrs and tempered for 2hrs

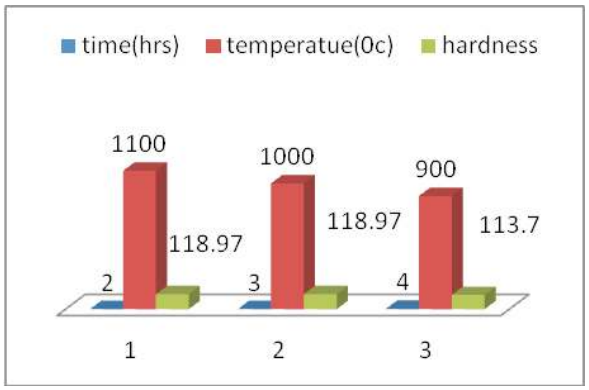


Fig. 4.5: Variation of Temperature, Hardness and Time of sample carburized with Snail Shell

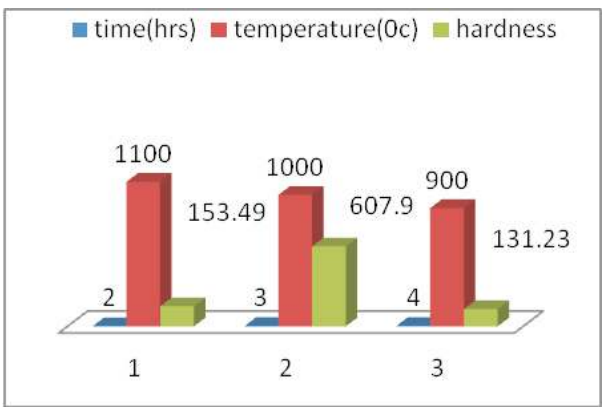


Fig 4.6: Variation of Temperature, Hardness and Time of sample carburized with Wood Charcoal

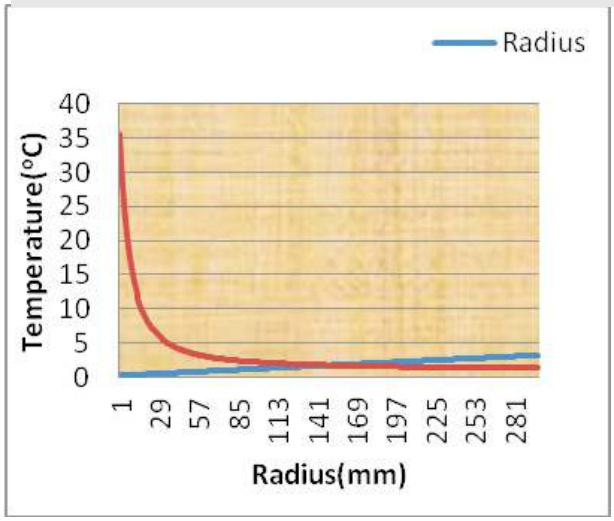


Fig. 4.7: Variation of Radius (mm) against Temperature (°C) across the section of the Steel

EFFECT OF STARCH ON THE MOULD CHARACTERISTICS OF NGWO FOUNDRY SAND

[1]Nwonye E.I., [2]Odo J.U.
[1]Scientific Equipment Development Institute Enugu
[2]Nnamdi Azikiwe University, Awka
Emails: emmanuel_nwonye@yahoo.com, odoju@yahoo.com

ABSTRACT
This research examined the mould characteristics of Ngwo foundry sand, such as the moisture content, bulk density, flowability, permeability, shatter index, green compression strength, green shear strength, dry compression strength, dry shear strength, hot compression strengths at various temperatures ranging from 600^{0}C to 1500^{0}C, hot shear strength at temperatures mentioned above, thermal linear expansion at temperatures from 100^{0}C to 900^{0}C, and in addition, refractoriness of the foundry sand was determined at temperatures ranging from 200^{0}C to 1500^{0}C. This work also characterized the said foundry sand to ascertain its chemical composition, and also investigated the effect of starch addition on the properties of the sand under the temperature conditions mentioned above. The experimental research results show that Ngwo foundry sand is good for casting, while Practical casting trials carried out showed excellent surface finish.

INTRODUCTION

Ngwo foundry sand is scattered all over Ngwo in Enugu State of Nigeria. The Foundry sand is rounded fine-grained, red colour, naturally bounded sand containing 10.68% of clay. It is a foundry sand with medium size GFN of 58%, low fines (1.2%), low coarse grains of 7.87% and a size distribution of 4-sieves (160 microns) [1].

Ngwo foundry sand has been in use for about 30 years in local foundry industries in Enugu State and later in Abakaliki, Awka and their environs for casting aluminum cooking utensil, radiator fans and other simple shape aluminum products. This had been done without the knowledge of its mould characteristics such as bulk density, flowability, permeability and shatter index under green state of the mould. The mechanical strength under varying thermal conditions such as green, dry and hot strength (compression and shear), thermal linear expansion, chemical analysis and refractoriness of the sand mould at varying elevated temperatures had not been conducted on this foundry sand.

The purpose of this work is to determine the mould characteristic of Ngwo foundry sand, as well as the effect of starch on its moulding characteristics and emphasize its acceptance, specification and application in the foundry industries.

Also, it seeks to equip the researchers of foundry materials with information for future development and adaptation of Ngwo foundry sand for use in Nigeria foundries.

RESEARCH METHODOLOGY

MATERIALS

The equipment used for this were hand rammer, small hand foundry shovel, sand rammer, flowability meter, speedy moisture tester, anvil, strength testing machine and heat treatment furnace[2][3].

Table 1.0: Experimental Trial Table

Exp.	A	B	C	D	E	F
Sand %	97	96	95	94	93	92
Water %	3	4	5	6	7	8
Bulk ρ, (g/cm^3)	1.75	1.69	1.70	1.68	1.72	1.75

SAND MOULD SAMPLE PREPARATION

Mould sample preparation for moisture content, bulk density, flowability permeability, shatter index, green, dry and hot strength tests, refractoriness and thermal linear expansion tests were made for the following experiments in the Table 1:1.

Table 1.1 : Material Quantity for the Experiments

Exp.	Materials	Sand-kg	Additive kg
1	Sand/Starch	5.0	0.1
2	Sand/Starch	5.0	0.5
3	Sand	5.0	Nil

The sand from the site was collected, sieved and placed in an oven until a temperature of about 105°C to remove all the water adsorbed. After this, the sand water mixture for each of these experiments A to F on Table 1.0 above was thoroughly prepared using a mixer. Experimental trials of the various sand mixture ratios were carried out as shown in Table 1.0. Experiment D in Table 1.0, produced the specimen with the desired quality; non sticking, without crack at the initial temperature rise, desirable bulk density e.t.c. This mixture was adopted for making cylindrical standard mould specimens of 50mm x 63mm size for the purposes of this analysis.

BULK DENSITY OF THE GREEN SAND MOULD

The bulk density of the sand was found to be 1.68g/cm^3 as shown in table 2.0. The density is good for casting both

ferrous and non ferrous metals [6]. The good bulk density is as a result of good compaction, moisture content and fine grain structure. This means the mould walls will resist molten metal penetration on pouring [11].

MOISTURE CONTENT TEST

A representative sand mixture sample weighed on the balance of the speedy moisture tester was placed in a special container to which a calibrated scale is attached. Two spoon measures of powder calcium carbide were added, covered up and shaken first for two minutes with the calibrated side of the container turned down, and then shaken again for a minute with the calibrated side of the container turned upwards this time.

The moisture content was read directly from calibrated scale on the instrument [2][4].

FLOWABILITY TEST

The standard specimen in the tube was placed in position in a rammer machine for the fourth blow, after having done the first three blows. A weight of 6.35 kg of the rammer was used to give the fourth blow of the rammer head on the specimen, which was followed by the fifth blow. The movement that occurred between the fourth and fifth blow was taken from scales of values assigned to this movement with zero travel corresponding to maximum flowability [5][6].

PERMEABILITY TEST

The test specimen of 50mm x 63mm size still in specimen holder was fixed on the permeability tester. Water, mercury oil, and air, under constant pressure were caused to flow through a large orifice (1.5mm) into the specimen. The permeability number was read directly on the calibrated scale of the machine [6].

SHATTER TEST

Test specimens of 50mm x 63smm size for each of the Experiments 1, 2 and 3 were made and each ejected from its tubular mould by means of a triping post and allowed to fall through a height of 9m to the steel anvil respectively. The fragments were collected in a 12.5mm mesh sieve. The shatter index was determined as the percentage of the total weight retained on the sieve [7].

GREEN STRENGTH TEST

Green standard mould specimens of 50mm x 63mm size for each of the Experiments 1, 2 and 3 were fixed on strength testing machine one after the other using compression holding device. A uniformly increasing load was applied to each of the specimens until it was crushed. The reading on the scale at which each of the specimens was crushed was read as the green compression strength of the specimen [8].

GREEN SHEAR STRENGTH

Green standard mould specimens of 50mm x 63mm size for each of the Experiments 1, 2 and 3 were fixed on a strength testing machine one after the other using a shear holding device. A uniformly increasing load was applied to the specimen until it fractured and crumbled. The reading on the scale at crumble point was noted as the green shear strength [10].

DRY STRENGTH TEST

Green test specimens of 50mm x 63 mm size for the experiments 1, 2 and 3 were dried one after the other at 110^0C and held for about 10 minutes. The specimens were then allowed to cool to temperature 30^0C one after the other. The specimens were then mounted each on the strength testing machine one after the other with a compression holding device and a uniformly increasing load was applied to each of them until they cracked and crumbled. The readings of the scale were read as dry compression strength[10].

DRY SHEAR STRENGTH TEST

The procedures as recorded above in dry strength test were followed except that the compression holding device was replaced with a shear holding device and the readings on the scale at which failure occurred were read and recorded as the dry shear strengths[9].

HOT STRENGTH TEST

Test specimens of 50mm x 63mm size for the Experiments 1, 2 and 3 were heated in a heat treatment furnace to the following temperatures 550^0C, 900^0C, 1300^0C, and 1500^0C, with each of the specimens subjected to each of the temperatures and allowed for two minutes soaking time. Each hot specimen was positioned and held on the strength testing machine holding device one after the other and a uniformly increasing load was applied to each specimen until the specimen cracked and crumbled. The points on the scale at which each specimen crumbled were read as their hot compression strengths respectively [8].

HOT SHEAR STRENGTH TEST

The same equipment, materials and procedures were used but with a change of compression strength holding device to shear strength holding device. The points on the scale at which the specimen cracked and fractured were read as hot shear strengths respectively [10].

THERMAL EXPANSION TEST

Test specimens of 50mm x 63smm size for the Experiments 1, 2 and 3 were heated in a heat treatment furnace to temperatures ranging from 100^0C to 900^0C respectively. Each of the heated specimens was measured with height gauge immediately each was removed from the furnace at the respective temperatures. The linear thermal expansion [9] of each specimen was calculated and recorded using the equation below:

$$\alpha = \frac{L_1 - L_0}{L_o} \times 100$$

REFRACTORINESS DETERMINATION

Test specimens of 50mm x 63mm size were heated in a heat treatment furnace to the following temperatures: 200^0C, 300^0C, 400^0C, 500^0C, 600^0C, 700^0C, 800^0C, 900^0C, 1000^0C, 1100^0C, 1200^0C, 1300^0C, 1400^0C, 1500^0C, for a soaking time of two hours. The specimens were observed one after the other for the following signs: cracks, changes in colour, collapse and distortion [11].

TABLE 1.1: Ngwo Foundry Sand Chemical Oxide Composition

Constituent	Value (%)
SiO_2	89.8
Al_2O_3	4.70
Fe_2O_3	3.98
CaO	0.30
MgO	0.30
SO_3	0.09
Na_2O	0.40
K_2O	0.25
Mn_2O_3	0.02
TOTAL	99.84

RESULTS AND DISCUSSIONS

MOISTURE CONTENT TEST RESULT

The moisture content of Ngwo foundry sand was found to vary from 6.58% to 6.92% as shown on Table 2.0. This amount of moisture content of naturally clay bonded sand is acceptable since it did not exceed the 8% maximum moisture content accepted in naturally clay bonded sand [4].

TABLE 2.0: Some Mould Characteristics Of Ngwo Foundry Sand

CHARACTERISTICS	VALUE
Moisture content	6.58%-6.92%
Bulk Density	1.68g/cm^3
Flowabilty	75%
Permeability	80%
Shatter index	76%

PERMEABILITY TEST

Ngwo foundry sand in the green condition has a permeability of 80% and 89% at temperature of 1500^{0}C as indicated in Tables 2.3 and 2.4 resulting from Experiment 3 (sand without additive). The values of permeability as indicated on the tables 2.1 and 2.2 are good for casting ferrous metals, since, the range of permeability required is between 40% and 120%[6]. This implies that the Ngwo foundry sand will allow the escape of considerable quantities of vapour and gases from the mould when pouring molten metal and this is indication of possibility of obtaining casting without blow holes and also with good finish.

SHATTER INDEX TEST

The shatter index value of Ngwo foundry sand in the green condition is obtained as 76% but increased further to 83% at 1300^{0}C before dropping to 60% at 1500^{0}C, while the various tests carried out in Experiments 1-3 as indicated in Tables 2.1- 2.3 as well as 2.5. The values of shatter index fall within the mouldable range of 50% and 85% recommended for moulding sand [12], which indicates that the sand is tough enough to aid lifting during pattern removal.

GREEN STRENGTH TEST

The green compression strength of each of the foundry sand specimens was read from the scale in Experiments 1-3 as indicated on the Tables 2.1-2.3 above, as well as on Table 2.6 below. The fine grain nature of the sand with very low dust and clay content as well as favourable moisture content contributed to the high green strength value of 0.92kg/cm^2 for 100% sand sample. The resultant green compression strength value is above the 0.32kg/cm^2 and 0.45kg/cm^2 acceptable range of green strength for non ferrous casting and also falls within the range of recommended 0.48kg/cm^2 and 1.2kg/cm^2 green compression strength required for ferrous castings [6].
A look at the Tables above other than Table 3, indicates that samples in Experiments 1(sand/starch 5kg: 0.1kg) sample and 2 (sand/starch 5kg: 0.5kg)sample, can serve the purposes of mould for casting both ferrous and non ferrous metals and alloys.

This implies that the green sand mould has the capacity to resist turbulent reactions of the molten metal in the mould, prevent erosion of the mould cavity walls and also reduce metal penetration into the mould walls provided that the mould is not broken[1].

TABLE 2.6: GREEN STRENGTH OF SAMPLES

Experiment	Green Strength (kg/cm^2)
1: Sand/starch(5kg:0.1kg)	0.53
2:Sand/Starch(5kg:0.5kg)	0.48
3:Sand Sample only	0.92

DRY STRENGTH TEST

The dry compression strength of each of the specimens is as shown above in Tables 2.1-2.3 and below in Table 2.7. This implies that samples in Experiments 1: Sand/starch (5kg: 0.1kg), and 2: Sand/Starch (5kg: 0.5kg), recorded higher dry strength values than the control sample in Experiment 3. These strength values are above the acceptable minimum value of 2kg/cm^2 for dry compression strength of foundry sand [6, 7].

The resultant strength is due to proper ramming of the sand. These values are adequate in a situation where a day is required in making the moulds, while the casting will be done the next day.

TABLE 2.7: DRY STRENGTH OF SAMPLES

Experiment	Dry Strength (kg/cm^2)
1	4.28
2	4.12
3	4.07

HOT STRENGTH TEST

The hot compression strength test results for each of the specimens in Experiments 1-3 at various temperatures starting from 110°C, 550°C, 900°C, 1300°C and 1500°C are as shown in Tables 2.1-2.3 above and in Table 2.8 below.
It was observed that the control sample in Experiment 3: Sand Sample only had the highest hot strength values at all the temperatures. The samples in Experiment 1: Sand/starch (5kg: 0.1kg) at 550^{0}C recorded the lowest value of hot strength.

REFRACTORINESS

The refractoriness by differential heating method of the various sand samples in terms of their resistance to crack appearance and propagation at high temperatures are indicated in Table 2.9 below.

FLOWABILITY TEST

Control sample of foundry sand in Experiment3 has a flowability of 75% as shown in Tables 2.1-2.3 and 2.10. This high flowability enhances the achievement of uniform density on compaction while the samples in Experiment 1: Sand/Starch (5kg:0.5kg) showed a reduced flowability of 65% minimum requirement for moulding sand [4].

TABLE 2.10: FLOWABILITY OF SAMPLES

Experiment	Flowability (%)
1: Sand/starch(5kg:0.1kg)	65
2:Sand/Starch(5kg:0.5kg)	62
3:Sand Sample only	75

The Figures 1-3 on the graphical representation of the strength of various samples versus temperature reveal a sharp rise in strength or steep slope between temperatures 100^{0}C and 200^{0}C. This is because the energy supplied to the samples in the form of heat is utilized in the fusion of the sand particles. At a temperature of 1200^{0}C, the Ngwo foundry sand samples have their highest strength values. This is partly due to the existence of sand in the form of tridymite, which is about the strongest allotropic form of silica and also because there is a minimal expansion (0.047%) of the sand grains. However, this high strength value begins to decrease in each of the experiments after 1200^{0}C as shown on the respective graphs in the figures above. It is also noticed from the figures 1-3 that none of the various additives was able to improve on the hot strength of moulding sand sample. Furthermore at 1500^{0}C, there is another transformation to crystobalite with a significant volume change which is partly responsible for the reduction in hot strength values of the sand samples.

DISCUSSION

The graphs in Figures 4 and 5 indicate closely linear representations as well as a negligible slopes respectively which show a minimal expansions or percentage volume change on transformation from quartz to tridymite and crystobalite during heating. While the graph in Figure 6 show a sharp rise in gradient between temperatures 1300^{0}C and 1500^{0}C, this indicates a significant expansion or volume change on transformation from tridymite to crystobalite.

The thermal linear expansion of the specimen in experiment 3 involving only sand sample at 900^{0}C which is 0.88% can give high resistance to penetration of molten metal into the mould, as there will be fewer cracks on the mould. In addition, there is going to be good dimensional accuracy for both ferrous and non-ferrous castings, since the required range of linear expansion of 0.84% to 1.00% at 900^{0}C is met [4,5,13,14]. Silica, however, undergoes allotropic transformation during which there is a change in volume resulting in cracks in the mould and disintegration of the sand grains [2].

NGWO FOUNDRY SAND REFRACTORINESS TEST

The sand in experiment 3 involving only sand sample did not show any remarkable change in colour until after 500^{0}C. But on reaching 600^{0}C, the sand mould turned to brick red in colour which was due to phase change from alpha quartz beta quartz[12]. It is worthy of note that the sand mould did not show any sign of cracks and this was because of high bulk density of the sand mould. At 800^{0}C, the colour changed to dark orange without cracks. While at 900^{0}C, the colour became lighter and no crack was noticed.

Between 1000^{0}C and 1300^{0}C, the sand became bright orange without crack initiation. At 1400^{0}C, slight cracks were noticed, this was due to volume change accompanying the transformation of sand from beta quartz to tridymite and the colour started to darken. At 1500^{0}C, pronounced cracks and tendency to crumble was observed resulting from massive volume change due to transformation from tridymite to crystobalite. But, it is worthy of note from the graphs of figures 1 and 2 that starch as an additive can enhanced the reduction in volume changes at transformation temperatures. This implies that even at 1400^{0}C, casting made from the sand mould blended with additives such as starch will have a smooth surface finish and good dimensional accuracy.

REFERENCES

[1] EMDI Akure Engineering Materials Journal (2006). Vol. 1, pp.27.

[2] American Foundrymen's Society hand book. *Alternative Utilization of Spent Foundry Sand*. Vol. 2, pp.12-15 (1989).

[3] Procter C.E., Conway A. Kempes Engineers year book 7th Edition pp. 599-606(1969).

[4] Foundry sand technology handbook, 9th edition. pp. 3-7 (2002).

[5] Nwajagu C.O. Foundry theory and practice. pp 78-79,57-67(1999).

[6] John R.B. FESECO Foundryman`s handbook. Feseco Internation LTD Birmingham 12th edition, pp.12-18(2004).

[7] Middleton, M.N., Scrata P. Alternatives to silica for mould production. Chemical Binder Foundries Birmingham, England (1976).

[8] Nwankwo A.I. Foundry sand Technology paper presented at the National workshop on Foundry sand Technology at National Metallurgical Development Centre Jos (1983).

[9]. Morgan J.H., Ivers J., Coleman J.D. The mechanics of sand preparation conference paper (1969).

[10] Javed S. and Lovell C. W. *Use of Foundry Sand in Highway Construction*, Department of Civil Engineering, Purdue University, USA, pp34-45 (1996).

[11] Johnson, C. K. “Phenols in Foundry Waste

Sand," *Modern Casting*. American Foundrymen's Society(1981).

[12] Clyde Sanders A. Foundry sand practice 6th edition, pp. 352-378(2001).

[13] Marienbah C.A. Technology of foundry Practice, Vol. 5. pp. 23-67 (2000).

[14] Journal of Raw Materials Research and Development Council, Maitama Abuja, on research efforts in Nigeria, Vol. 2, pp.12-20(2003).

[15] FOSECO Casting defects and Foundry practice issue. Vol 1.pp. 2-6 (1968).

[16] Ajayi J.A. Defects due to sand casting, paper presented at National workshop on Foundry sand Technology in Jos, pp15-19 (1993).

TABLE 2.1: EXPERIMENT 1: MIXTURE OF 5KG NGWO FOUNDRY SAND AND 0.1KG STARCH ADDITIVE

Xter	RT	110°C	550°C	900°C	1300°C	1500°C
P	54%	58%	62%	70%	75%	77%
S/I	82%	84%	88%	90%	91%	91%
G/S	0.53 kg/cm^2	—	—	—	—	—
Dry/S	—	4.28 kg/cm^2	—	—	—	—
Hot/S kg/cm^2	—	—	4.80	6.76	7.92	5.82
R	No crack	No crack	No crack	No crack	Slight crack	Visible crack
F	65%	—	—	—	—	—
E	—	0.06%	0.59%	0.63%	0.69%	0.74%

TABLE 2.2: EXPERIMENT 2: MIXTURE OF 5kg NGWO FOUNDRY SAND AND 0.5kg STARCH ADDITIVE

Xter	Room Temp.	110^{0}C	550^{0}C	900^{0}C	1300^{0}C	1500^{0}C
P	50%	56%	59%	64%	67%	71%
S/I	85%	87%	90%	93%	93%	93%
G/S	0.48 kg/cm^2	_	_	_	_	_
Dry/S	_	4.12 kg/cm^2	_	_	_	_
Hot/S kg/cm^2	_	_	4.62 kg/cm^2	6.28 kg/cm^2	7.21 kg/cm^2	5.26 kg/cm^2
R	No crack	No crack	No crack	No crack	No crack	Slight crack
F	62%	_	_	_	_	_
E	_	0.04%	0.61%	0.65%	0.71%	0.73%

TABLE 2.3: EXPERIMENT 3: 5kg NGWO FOUNDRY SAND, WITHOUT ADDITIVE

Xter/T	R T.	110^{0}C	550^{0}C	900^{0}C	1300^{0}C	1500^{0}C
P	80%	82%	84%	85%	85%	89%
S/I	76%	78%	80%	83%	83%	60%
G/S kg/ cm^2	0.92	_	_	_	_	_
Dry/S kg/cm^2		4.07	_	_	_	_
Hot/S kg/cm^2	_	_	6.42	8.40	8.96	6.05
R	No crack	No crack	No crack	No crack	Light crack	Heavycr ack
F	75%	_	_	_	_	_
E	_	0.10 %	0.75%	0.88%	0.89%	1.20%

NOTE: R-Refractoriness, F-Flowability, E-expansion, G/S-Green Strength, S-Strength, Exp.-Experiment, T-Temperature, P-Permeability, RT-Room Temperature, Xter-Characteristics

TABLE 2.9: REFRACTORINESS OF SAMPLES AT VARIOUS TEMPERATURES

Experiment /Temp.	110^{0}C	550^{0}C	900^{0}C	1300^{0}C	1500^{0}C
1	No crack	No crack	No crack	Little crack	Pronoun ced crack
2	No crack	No crack	No crack	No crack	Little crack
3	No crack	No crack	No crack	Little crack	Heavy crack

TABLE 2.4: PERMEABILITY OF SAMPLES AT VARIOUS TEMPERATURES

P/T	R T.	110^{0}C	550^{0}C	900^{0}C	1300^{0}C	1500^{0}C
1	54%	58%	62%	70%	75%	77%
2	50%	56%	59%	64%	67%	71%
3	80%	82%	84%	85%	85%	89%

TABLE 2.8: HOT STRENGTH OF SAMPLES AT VARIOUS TEMPERATURES

Hot/S-T	550^{0}C	900^{0}C	1300^0 C	1500^0 C
1	4.08	6.76	7.92	5.82
2	4.62	6.28	7.21	5.26
3	6.42	8.40	8.96	6.05

TABLE 2.5: SHATTER INDEX OF SAMPLES AT VARIOUS TEMPERATURES

S/I % - T	RT	110°C	550°C	900°C	1300°C	1500 °C
1	82%	84%	88%	90%	91%	91%
2	85%	87%	90%	93%	93%	93%
3	76%	78%	80%	83%	83%	60%

ANALYSIS OF THE GRAPHS OF STRENGTH VERSUS TEMPERATURE OF VARIOUS SAMPLES

Figure 1: plot of Strength V temperature in Experiment 3

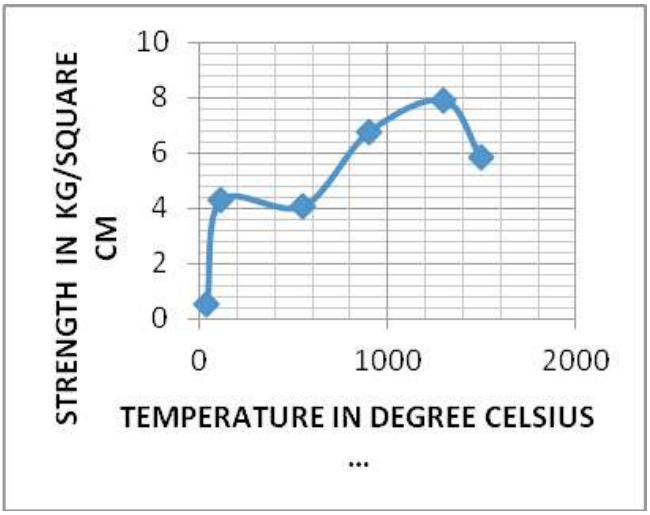


Figure 2: plot of Strength V temperature in Experiment 2

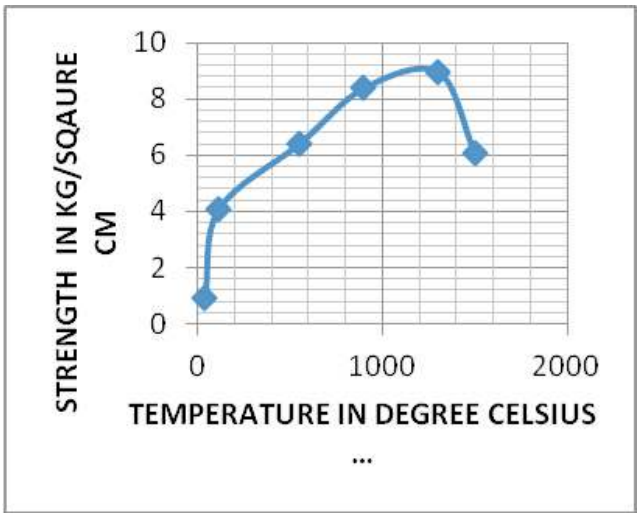
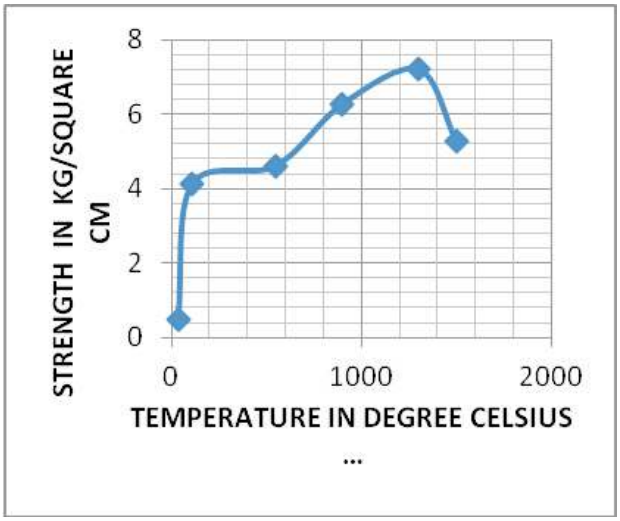


Figure4: plot of Expansion V temperature in Experiment 1



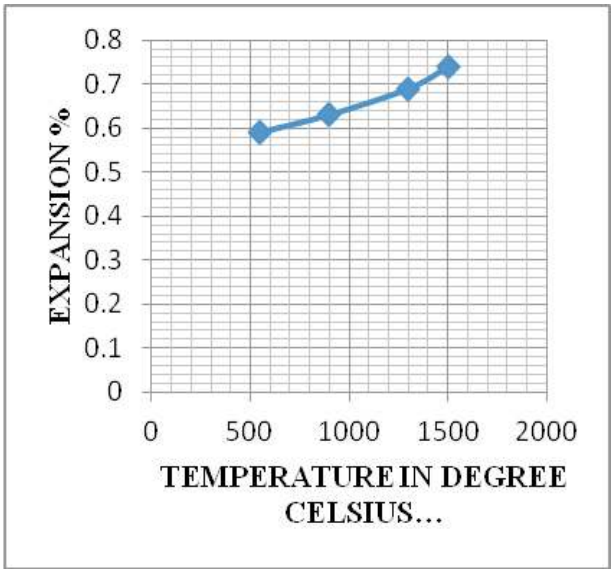


Figure5: plot of Expansion V temperature in Experiment 3

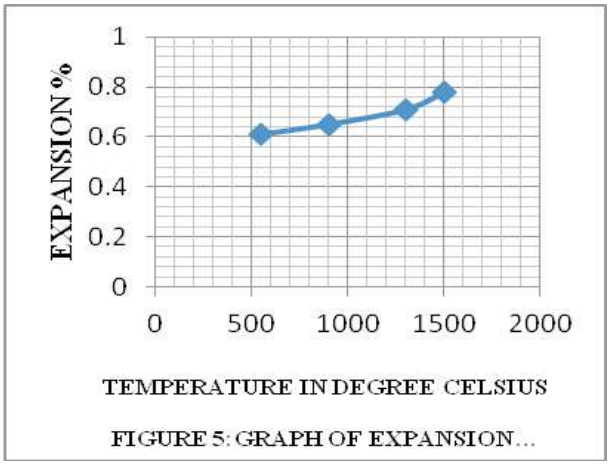
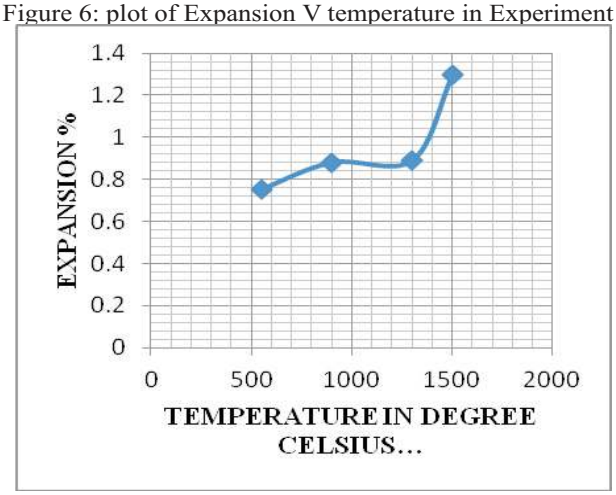


FIGURE 5: GRAPH OF EXPANSION...

Figure 6: plot of Expansion V temperature in Experiment 2



THERMAL LINEAR EXPANSION TEST RESULTS

TABLE 2.11: EXPANSION % OF VARIOUS SAND SAMPLES.

T Exp.	110^{0}C	550^{0}C	900^{0}C	1300^{0}C	1500^{0}C
	EXPANSION IN %				
1	0.06	0.59	0.63	0.69	0.74
2	0.04	0.61	0.65	0.71	0.78
3	0.10	0.75	0.88	0.89	1.20

EVALUATION OF THE INHIBITIVE PROPERTIES OF BLACK CREAM ON DUCTILE IRON

Ibegbulam, C.M; Olowonubi, J.A; Aigbogun, O.J; Olunlade, B.A and Ukoba, O.K
Engineering Materials Development Institute, Akure
c_m_ibe@yahoo.com

ABSTRACT
This work investigated the ability of black cream (PKO) to act as an inhibitor using ductile iron as a case study. This work was carried out in three (3) different media; fresh water (H_2O), brackish (NaCl), and basic (NaOH) solutions. It was carried out for 10weeks and readings were read every 2weeks. Initial weight was taken in order to ascertain the weight loss of the DI pieces. The results showed that a greater weight loss was obtained in the control set up than in the inhibited for all the media except NaOH solutions which showed sign of weight gain from the range of 0.001-0.659g for 10weeks. However, the above denotes that black cream can be a good corrosion inhibitor for ductile iron and the essence of this work is to reduce corrosion to the barest minimum and deterioration of oil pipes, oil well pumps, water and sewer lines, automotive components, high way diesel trucks, among others.

1.0 INTRODUCTION

Ductile iron is not a single material but is part of a group of materials which can be produced to have a wide range of properties through control of the microstructure. The common defining characteristics of this group of materials are the morphological structure of the graphite. In ductile irons, the graphite is in the form of spherical nodules rather than flakes as in grey iron, thus inhibiting the creation of cracks and providing the enhanced ductility that gives the alloy its name. In addition, black cream or palm kernel oil as it's generally known, is edible plant oil derived from kernel of the oil palm Elaeis guineensis. Palm oil is found in the fleshy portion of the fruit (mesocarp), whereas as palm kernel oil is found in the kernel or the seed. Palm oil is naturally reddish in colour because it contains a high amount of *betacarotene.* Palm oil, palm kernel oil and coconut oil are three of the few highly saturated vegetable fats. Palm oil is semi-solid at room temperatures. Palm oil contains several saturated and unsaturated fats in the forms of glyceryl laurate. Furthermore, like all vegetable oils, palm oil does not contain
cholesterol. Palm oil is common cooking ingredient in the tropicalbelt of Africa, Southeast Asia and parts of Brazil. Its increasing use is in the commercial food industry in other parts of the world is buoyed by its lower cost and the high oxidative stability of the refined product when used for frying. The use of palm oil in food products is often the focus of environmental activist groups [1].

2.0 MATERIALS & METHOD

2.1 *Materials*

The materials for this experiment include ductile iron materials, sodium hydroxide solution, sodium chloride solution, tap water, palm kernel oil (PKO), masking, tape, thread, electronic weighing balance, acetone ,cotton wool, razor blade, plastic bowls, abrasive paper, nylon hand gloves etc.

2.2 Materials Preparation

The experimental ductile iron was cut to a round shape of 14mm diameter for all the various set ups with the use of an electric saw. Furthermore, surfaces of the various samples were ground in order to expose it to the different corrosion environment. Adequate grinding and polishing was done using abrasive papers of grits 60, 120, 180 240, 280, 320, 400, 600, 800 and then the polishing was done with an emerald cloth. However, in order to prevent rapid corrosion, acetone and cotton wool were used to clean and cover the surfaces of these ductile materials. Also the specimens/materials were weighed carefully on an analytical three decimal electronic weighing balance. On taking the reading of each specimen it is inserted inside a nylon sachet and closed. After weighing and packaging, the whole samples were stored in desiccators in readiness for the immersion test.

2.3 Experimental Procedure

Experimentation involves immersion of the specimens in the environment and retrieving at specified durations and checking the weight loss in grams.
After preparation of the NaCl and NaOH solutions, a quantity of about fifty centiliters (50cl) were measured out using the graduated plastic bowl and purred inside the plastic bowls and labeled with the aid of the polymeric twine (thread) each specimen is tied and suspended from the plastic lid. However, the specimens were dipped into the palm kernel oil (PKO) and immediately immersed in the environments. Each specimen was suspended such that the exposed surface is totally immersed in the solution without touching either the side or bottom of the container and at an equal distance from each other. For each bowl was suspended (immersed) five specimens labeled and covered. And finally the suspended coupons are immersed simultaneously and the time of immersion noted.
After 14days or 2weeks a specimen is retrieved from each of the bowl/environment, washed gently and properly in water dried with a cotton wool and dipped in acetone to remove every moisture and oxygen. Thereafter, each of the dried specimens was carefully weighed on the

electronic weighing balance and the weight loss recorded.

3.0 RESULT AND ANALYSIS

Corrosion rate:

The results of various tests are presented in the tables 1 – 6 ined using

$$Corrosion\ rate = \frac{weight\ loss}{area} \times time$$

Where,
CR = corrosion rate
W = weight loss in grams (g)
A = Total exposed surface area (cm^2)
T = exposure time (day)

3.1 Calculation of Total Exposed Surface Area

For a circular surface;
Therefore, $=3.142\times0.7^2cm$
$=1.540gcm^2$

4.0 CONCLUSION

The rate of corrosion of ductile iron in an uninhibited fresh water, brackish (NaCl) and basic (NaOH) environments was generally obvious in comparison to the inhibited set up and it is therefore enhanced by the solutions. Generally, the corrosion rate of ductile iron in the environment above declines with the introduction of black cream (PKO). The extent of the declination depends on their concentrations.

5.0 REFERENCES



Figure 1: Electronic Weighing Balance

1. Wikipedia, 2011
2. E.E Oguzie, B.N Okolue, C.E Ogukwe, A.I Onuchukwu; Studies on the Inhibition action of methylene blue dye on aluminum corrosion in KOH solution; Journal of Corrosion Science and Technology; (1.1, 2004); Pages 88-91
3. E.E Ebenso, U.J Ekpe, S.Umoren, Ekerefe Jackson, O.K Abiola, N.C Oforka, S. Martinez; Corrosion Inhibition studies on some plants extract on aluminum in acid medium; Journal of Corrosion Science and Technology; (1.1, 2004)
4. Ibitoye S.A and Yoande, A.O; (1.1.2006); The effect of Nitrite and Chromate Inhibitors on Corrosion of 6063Al in 0.1M HCl acid environment; NSE Technical Transaction; Vol 41; No 1, Jan-Mar 2006; Pages 23-35
5. Umoru L.E, Onike A., Ige O.O; (4.23.2005); Glucose as a Corrosion Inhibitor for an Aluminum alloy in 0.1M NaOH; NSE Technical Transaction; Vol 40; No 4, Oct-Dec 2005; Pages 45-52

6.0 GRAPHS

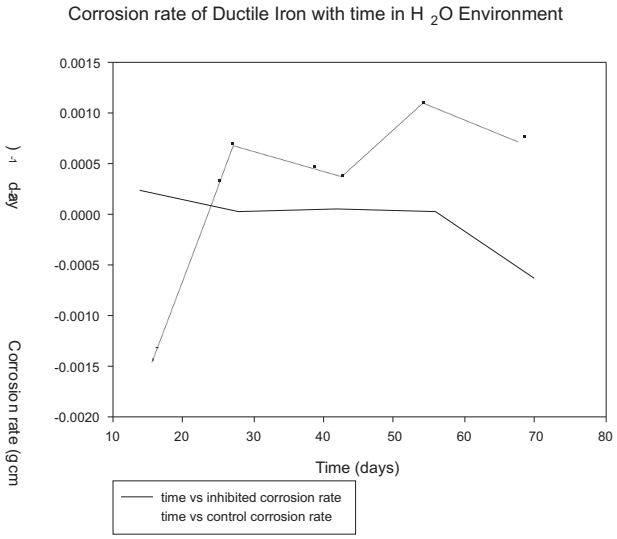


Figure 2: Corrosion rate of Ductile Iron with time in H 2O environment

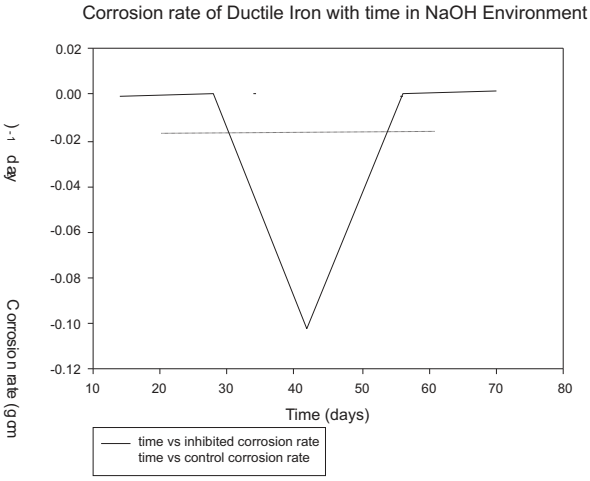


Figure 3: Corrosion rate of Ductile Iron with time in NaOH environment

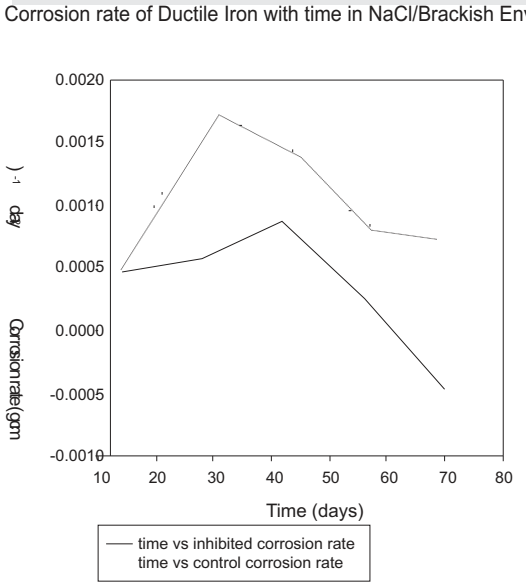


Figure 4: Corrosion rate of Ductile Iron with time in NaCl/Brackish environment

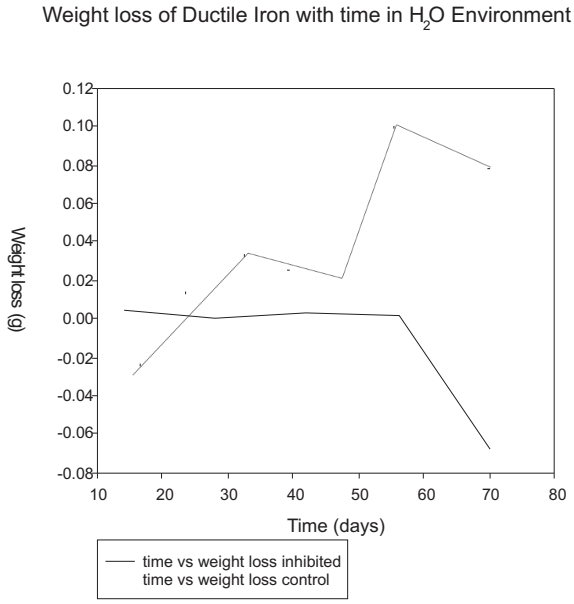


Figure 5: Weight loss of Ductile Iron with time in H_2O environment

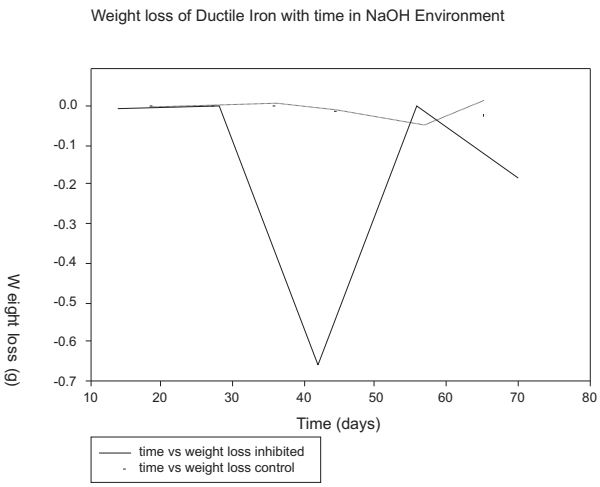


Figure 6: Weight loss of Ductile Iron with time in NaOH environment

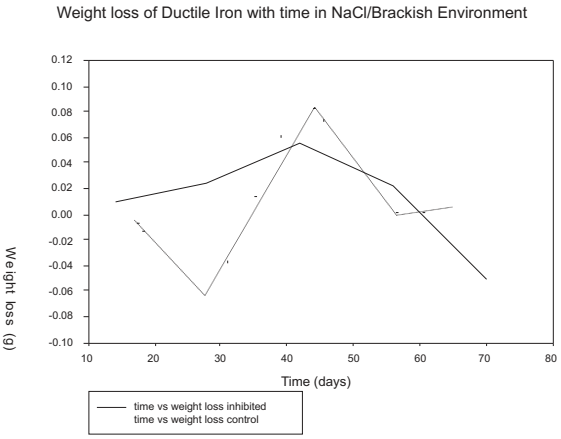


Figure 7: Weight loss of Ductile Iron with time in NaCl/Brackish environment

6.1 TABLE OF VALUES

Table 1: **H_2O ENVIRONMENT UNINHIBITED (CONTROL)**

LABEL	INITIAL MASS (g)	FINAL MASS (g)	WEIGHT LOSS (g	CORROSION RATE ($gcm^{-2}hr^{-1}$)	TIME (Hrs)
A	23.404	23.442	-0.038	0.00176	14
B	8.589	8.551	0.038	0.00088	28
C	15.310	15.288	0.022	0.00034	42
D	24.077	23.973	0.104	0.00121	56
E	22.378	22.300	0.078	0.00072	70

Table 2: **H_2O ENVIRONMENT INHIBITED**

LABEL	INITIAL MASS (g)	FINAL MASS (g)	WEIGHT LOSS (g	CORROSION RATE ($gcm^{-2}hr^{-1}$)	TIME (Hrs)
F	20.630	20.625	0.005	0.00023	14
G	13.628	13.627	0.001	0.00003	28
H	22.957	22.954	0.003	0.00005	42
I	30.649	30.647	0.002	0.00002	56
J	27.341	27.409	-0.068	0.00063	70

Table 3: **NaOH ENVIRONMENT UNINHIBITED (CONTROL)**

LABEL	INITIAL MASS (g)	FINAL MASS (g)	WEIGHT LOSS (g	CORROSION RATE ($gcm^{-2}hr^{-1}$)	TIME (Hrs)
K	20.165	20.168	-0.003	-0.00014	14
L	10.813	10.814	-0.001	-0.00002	28
M	18.885	18.892	-0.007	-0.00011	42
N	19.110	19.166	-0.056	-0.00065	56
O	29.763	29.772	-0.009	-0.00008	70

Table 4: **NaOH ENVIRONMENT INHIBITED**

LABEL	INITIAL MASS (g)	FINAL MASS (g)	WEIGHT LOSS (g	CORROSION RATE ($gcm^{-2}hr^{-1}$)	TIME (Hrs)
P	20.892	20.901	-0.009	-0.00042	14
Q	18.914	18.915	-0.001	-0.00003	28
R	16.141	16.800	-0.659	-0.01019	42
S	19.826	19.831	-0.005	-0.00006	56
T	24.060	24.246	-0.186	-0.00173	70

Table 5: **NaCl/BRACKISH ENVIRONMENT UNINHIBITED (CONTROL)**

LABEL	INITIAL MASS (g)	FINAL MASS (g)	WEIGHT LOSS (g	CORROSION RATE ($gcm^{-2}hr^{-1}$)	TIME (Hrs)
U	13.026	13.010	0.016	0.00046	14
V	17.271	17.346	0.075	0.00174	28
W	20.460	20.362	0.098	0.00152	42
X	18.565	18.492	0.073	0.00085	56
Y	26.024	25.949	0.075	0.00070	70

Table 6: **NaCl/BRACKISH ENVIRONMENT INHIBITED**

LABEL	INITIAL MASS (g)	FINAL MASS (g)	WEIGHT LOSS (g	CORROSION RATE ($gcm^{-2}hr^{-1}$)	TIME (Hrs)
U_2	11.413	11.403	0.010	0.00046	14
V_2	8.810	8.785	0.025	0.00058	28
W_2	27.217	27.161	0.056	0.00087	42
X_2	19.741	19.719	0.022	0.00026	56
Y_2	17.636	17.687	0.051	0.00047	70

COAL PROCESSING IN THE COKE OVEN AND BY PRODUCT PLANT OF THE AJAOKUTA STEEL COMPANY LIMITED

OCHERI C.[1], AGBOOLA, J.B[2]
Foundry Shop, Ajaokuta Steel Company Limited, Ajaokuta, Kogi State[1]
Department of Mechanical Engineering
Federal University of Technology, Minna, Niger State[4]
E-mail:ocheri4c@yahoo.com

ABSTRACT
Coal is an organic fossil fuel that has seen formed over a long period of time in million years. It can be subjected to high temperature and high pressure and it is also associated with the task of forming mineral matters. The Ajaokuta Coke Oven and by Product Plant, consist of three section, they are Coal Handling Plant, Coke Oven Plant and Equipment. The presentation is to discuss methods of coal processing, coal as source of energy for the operation of the Coke Oven Plant; types of coal needed for the operation of the plant, some problems associated to non- coking coal and methods of coals selection were discussed. The roles and functions of coal as source of energy for the operation in the Blast furnace were brought to the fore, process of coal blend charge preparation and other parameters that will make the coal effective and efficient for the purpose of energy generation for the operation of the Coke Oven and by product plant were also emphasized.
Key Words: *Coal, Coke Oven, By Product, Energy and Blast furnace*

INTRODUCTION

The Coke Oven and By Product Plant of the Ajaokuta Steel Company Limited, consist of three units namely Coal Handling Plant (CHP) Coke Oven Plant (COP) Equipment The equipment section or unit takes care of the manufacture, electrical, mechanical and refractory units.

Coke oven & By-product Plant has a capacity of 0.44 MTPA of gross coke from each battery. There is a provision for two batteries, out of which one is already built. The second battery is planned to be commissioned subsequently and would increase the installed capacity to 0.88 MTPA.

The Battery 1 (waiting commissioning) has wet quenching facility for Coke and Battery 2 will have Coke Dry Cooling Plant (CDCP).

Table below summarizes the specifications of the batteriesCoal is a readily combustible black or brownish-black sedimentary rock. The harder forms, such as anthracite coal, can be regarded as metamorphic rock because of later exposure to elevated temperature and pressure. It is composed primarily of carbon along with variable quantities of other elements, chiefly sulfur, hydrogen, oxygen and nitrogen.

Coal was formed from plant remains that were protected by water and mud against oxidization and biodegradation, thus trapping atmospheric carbon in the ground. Over time, the chemical and physical properties of the remains are changed by geological action to create a solid material.

Coal, a fossil fuel, is the largest source of energy for the generation of electricity worldwide, as well as one of the largest worldwide source of carbon dioxide emissions. Gross carbon dioxide emissions from coal usage are slightly more than those from petroleum and about double the amount from natural gas. Coal is extracted from the ground by mining, either underground or in open pits. The classification of coal is generally based on the content of volatiles. However, the exact classification varies between countries

2.0 Source of Coal

The Coal Handling Plant takes care of the preparation of coal into blend in order to be used. Coal is the major source of fuel used in the converter, and other important furnaces e.g Coke Oven battery. The coals are prepared in order to become useable coke in the Blast furnace.

Coal is an organic fossil fuel that has been formed over a long period of time in million years. It can be subjected to high temperature and high pressure and it also associate with the ash forming mineral matter.

3.0 Coal can be divided into two groups:-

Coking coal and Non –coking Coal

(a)The Coking Coal: These are coals when heated to a temperature of 350 -500°C, it often undergo plasticity transient stage and they are fixed together to form a semicoal of porous permeable structure. Upon heating to high temperature of about 1000°C the coals become strong.

(b) Non- Coking Coal: Does not often undergo permeable plasticity transient when it is being
heated to high temperature. The transformation start from vegetable matter when they subjected to either high or low temperature it turns to brown coal –lignite- sub-bismuthmious coal high volatile-bismultmious medium volatile bismuthmiuos low volatile bismultmious anthrasite.

But from peat sub-bismultious this coal are called non –coking coal which ,include anthrasite , which always increase with increase in temperature. Hydrogen and oxygen decreases with increase in temperature.

3.1 Types of Coal

Coal is in abundant in former U.S.S.R , China, U.S.A. South Africa , South America (Columba)

The greatest of them all are the USA , but Germany and Poland are the greatest exporters of coal. In Nigeria, we can get coal in Enugu , Enyi Okapio, Oropa , Okaba ,Idah , Aluze and Lafia /Obi , but all of them have high sulphur content , moisture content and ash content.

3.2 Problems of Non –Coking Coal

The coals in Nigeria have high sulphur content, high ashes content and they have mineable problem, they also have weak floor. The coal found in Lafia / Obi could have been used in the Coke Oven in Ajaokuta Steel Company Limited or in Nigeria , but due to the hazard it cause to miners and the sulphur content which can only be reduced by blending.

Although various tests have been carried out in the hope of using some Nigeria coal in the steel plant, but so far, the efforts have proved abortive.

3.3 Selection of coking coal

Properties of coal

(i) Extarogenous
(ii) Moisture content decrease
(iii) Expansion

The medium violate are the prime coal used in the coke oven, coking coal is raw materials used in the Coke Oven Battery.

Factors that affects selection of coal

(i) Violate matter
(ii) Plasticity
(iii) Dilatation
(iv) Chemical parameter like ashes content and sulphur content.
(v) Pectrographic analysis to determine the

reflectors and macerals composition of the coal when this is combine it enable you to get a blend that is a prime coal.

Reasons for Coal selection

(i) High volatile –bisthmus
(ii) Lot of gases are released
(iii) It becomes porous
(iv) The coal will not be strong
(v) Poor expansion and contraction

Low volatile bisthmious

(a)High pressure on the wall of the oven will crush the wall

(b)Moderate expansion and contraction

This is done so that the coke oven battery will not be damaged by the coal, so that the coke battery will be used for a long time. The volatile matter content 27.7 - 30.3 sulphur content of the coal blend must be max of 1%

Function of coal in the Blast Furnace.

(i) It provides energy for endothermic chemical reaction
(ii) It acts as a reducing agent for converting of iron oxide to metallic iron
(iii) It acts as a porous permeable bed
(iv) Support for burden.

3.4 Transportation of Coal

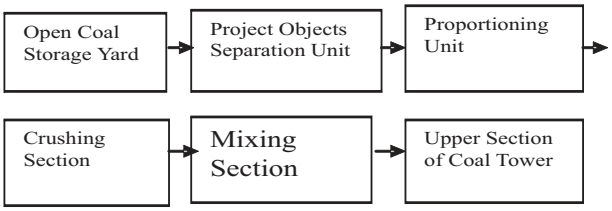
This is being done either by rail from Olle port, the coal are transported to the Coal Handling Plant of the Ajaokuta Steel Company Limited. The coking coal arrives the port from various countries e.g. U.S.A. , Australia , Germany , and Canada and transportation by standard rail of Ajaokuta Steel Company Limited.

They are transported on wagon to an open coal storage yard, the open storage yard ie equipped with stockings and reclaiming machine.

The stocking machine is used in the dumping of coal in heaps, while the reclaiming machine is used to make the coal to be homogenous; this reclaiming machine has nine buckets for homogenous process. The storage yard has the working capacity of 150,000 tonnes and the total capacity of 298,000 tonnes.

Some industries like the cement, steel companies, paper companies and the port authorities' uses coal for the generating of their machine..

3.4.1 Preparation of Coal Blends Charge.



The target of coal handling plant is to prepare trouble free homogeneous coal blend charge which is required to operate efficiently in the Coke Oven Battery.

Target: Coal will be delivered to the stock yard by open belt conveyor, discharging wagon, the stock yard is equipped with two universal machines, the stacker and the reclaiming machines.

The stacking machines are used for dumping of coal in the stock yard in the form of piles, while the reclaiming machines with buckets are used to remove the coal from the stock yard. The process of the removing of coal by the reclaiming machine is done by averaging of individual coal by making it homogeneous. The distance between the stacker must not be less than 1mm.

The coal is taken from the storage yard by the stacking and reclaiming machine in accordance. Coal should not be stored for a long period in the stock yard because it will loss its values or disintegrate due to oxidation reaction that might have taken place.

The properties of calorific valve are formed as a result of oxidation. The following changes are being observed.

(a)Decrease in calorific value

(b)Decrease in carbon and hydrogen content

(c) Increase in oxygen content

(d)Reduction in size

Coal from the stock yard are been processed in the foreign object separation units. In this unit there are electromagnetic separators. In this unit, there is a screen which is used to assist in the sieving of electromagnetic materials and the rotary screen for the removing of non – metallic inclusions that are greater than 100mm.

After the foreign objects have been removed the coals are sent by the feed conveyors to the proportioning sections. The proportioning section is made up of sixteen (16) bins or silos which is arranged in two rolls and eight

(8) , each having a capacity of 800 tonnes and there is are electric feeders with a continuous action process, consisting of electric feeder in lamina form.

Blending of the coal occurs in the underline reversible belt conveyor, each technology grade having not less than two bins or silos they are allocated in order to improve the technology and for maximum coal blend charge.

The coal must be cleaned so that it will not damage the electric vibration feeder and also the magnetic separator. From the proportioning section the charge of defined composition is transported to the crushing section by the aid of belt conveyor, this section is equipped with three (3) reversible hammer crushers. The capacity of each of the hammer is 150 tonnes/ hr for soft coal procession, while hard coal hammer is 300 tonnes/hr, the third hammer is always a stand by hammer.

The size control of each, coal grade is achieved by adjusting gap between the rotary hammer and the crusher and also by changing the size of the hammer rolls. The final product will be 85% and the size is between 0-3mm, while the over sized coals are returned for recycle. After crushing the following components are added to the coal blend charge.

(i)Spend solar oil from Naphthalene , from the recovery section,

(ii)Sludge

The charge is transported by the belt conveyor to the mixing section. The mixing section ie equipped with two mixing machine, one in operation and the other is always stand -by; they both have the capacity of 600 tonnes /hr each. Vigorous mixing must be done by the mixing machine in order to produce homogeneous blend, that will not cause explosion in the Coke Oven Battery for all the coal. i.e volatile , medium and low violate coal must be made to a blend coal charge.

4.0 Problems Associated with Coal

If the low volatile coal is concentrated in one place it develops high pressure and it can cause damage to the oven wall by (cracking).

Similarly, if the high volatile coal is also concentrated in one place, excess fluid or by product will be formed, this can cause explosion to the Coke Oven Battery. The coal blend charge must be conformed to the following specification with the Ajaokuta Steel Company Limited (ASCL).

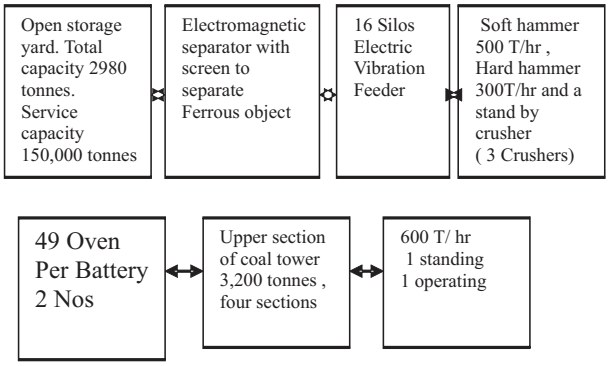
Moisture content 5-9%
Ash content -10% max
Violate matter 27.7-30.3% (dry ash free)
Sulphur content 1% max.
The vertical shrinkage 5-7%

The coal is sent to the final stage which is the upper section of the coal tower consists of four(4) sections having a total capacity of 3,200 tonnes, each sections is equipped at the lower part with three rows of the discharged upper tower , correspond to the number of the coal charging car bin.

The belt conveyor transports the coal to the storage as well as conveying the prepared charge to the coal lower which is equipped with automatic spectaculars for determining the ash, moisture and sulphur content, this is for the purpose of quality control. The whole coal handling operates on a shift of 17½ working hours per day.

The imported coal must not be more than three (3) months in the storage yard, while the local coal must not be more than one (1) month.

5.0 PROCESSION OF COAL LINK



5.1 Coking Processes

The Coke Oven Battery is a narrow Chamber with 50 heating walls and 49 ovens, these ovens are used for carburizing of coal in large amount. The general arrangement for the operation of the Coke Oven is with various accessories. The coke ovens withstand the serve temperature incurred in its use and the gas remain light, even after the great expansion during heating up.

The Ovens are built of refractory bricks with venting walls between the Coke Oven operate intermittently, but each Oven is started and stopped at different times. So that the operation of the entire block continuously produce gas of good average composition. A charge of finely crushed coal is dropped from the charging car through the charging holes (usually three through generalized flow).

In the top and into the Oven, where the walls are approximately at (2000°f) .The surface of the coal in the Oven is leveled by the pushing car and the charging holes are then recovered. Heating is carried out and the charge left in the Oven until it is completely coked and the evolution of violate matter has ceased.

The Coke Oven is operated to make the best quality furnace coke for steel mill and no longer to make a large volume of high grade coal tar or gas. At the end of the coking time

(Approximately 17 hours) the doors at the pusher side of the Oven are opened and the entire red-hot mass is pushed out in less than a minute by a ram electrically driven through the oven from end to end.

The coke falls into a quenching car which holds the charge from one Oven. This is later driven to the quenching section for quenching either by dry quenching or wet quenching method.

(a) **Coke Quenching**

In this section, after the coke has been heated in the Coke Oven Battery to a certain temperature or hours it will be ready for push and these are dumped on the quenching car or coke car, depending on the type of cooling that is to be done.

(b) Wet Quenching

The hot coke are spread on quenching car , the quenching car is driven to the quenching tower where water is being poured on the red-hot coke for 2 minutes and the water is then poured on the coke and drained off through a channel made for the purpose. Later the coke are taken to a place where they are been spread on the floor for drying.

Advantages

(a)Simple to handle
(b) It saves time
(c) Equipment are easy installed and operated

Disadvantages

(i) Heat of the coke is lost
(ii) It causes environmental pollution
(ii)The quality of the coke is reduced (disintegrated)

(c) **Dry Quenching**

This type of drying takes place in the cooling chamber. When the coke has being heated to a certain temperature (1000-2000°c), the cokes are discharged and it is being dumped on the coke car, this is taken to the cooling chamber. In the cooling chamber, an inert gas is introduced into the cooling chamber in order to remove the oxygen content. The inert gas is mainly Nitrogen (N_2). The time of cooling in the chamber is from two hours and above.

Advantages

(i) The heat produced by the coke is utilized
(ii) Pollution is less
(iii) The quality of the coke is better than that of the wet cooling quality.

Disadvantages

(i)The equipment are costly and it is difficult to install
(ii)The process is difficult (operation)
(iii)The time of operation involved is more
(iv) It requires more personnel.

5.2 Sizing of Coke

When the coke has been cooled (either by the wet or dry cooling method) the sizing of the coke must be done and this will lead to screening. Screening is generally done on relatively coarse materials as the efficiency decrease rapidly with fine materials, but in the case of the Ajaokuta Steel Company Limited, the size required after screening is between 0-3mm.

5.3 Purpose of screening

in the coke industries:-

(i)To prevent the entry of under size coke into the crushing machine, so thereby increasing their capacity and efficiency,
(ii)To prevent oversized coke from passing to the next stage in closed circuit fine crushing and grinding operations,
(iii)To prepare a closely sized feed to contain gravity concentration process,
(iv) To produce a closely sized and also an end product this is importantly used in the sintering process of blast furnace use,

At the Coke Oven Battery of the Steel plant, there are two types of screening that is being used.

(a)**The jigging table method**: when the coke has been cooled the coke are now being put on the jigging table where it shaken due to vibration , the particles movement depends on sizes, the bigger one will be dropped first , until the smaller ones drop.

(b)**Sieve band**: when the cokes are put into the sieve band, due to vibration and shaking method, the coke will be dropping into stages where by the bigger ones will be on the top of the sieve bag, while the particles between 0-3mm and some dust particles are dropped at the bottom of the sieve band.

And these dust particles are sent to the sintering plant unit, which will be processed to form blend. The particles between 30-60mm are sent to the blast furnace, some of the oversized particles or materials are sent for recirculation.

5.4 Parameter of the Coke Oven Battery

It has an alternative arrangement heating wall and oven. It has 49 ovens per battery and 50 heating walls or chambers. The Coke Oven Battery has a height of 5.5 mm and width of 410mm. It has two stand pipe and one stack chimney oven. It also has three charging holes, all these factors makes up under this set type.

5.5 Coke Oven Machines

(i)**The charging car:** This is a car used for the charging of coke in the oven, this is being operated with a mechanism which helps to open and close the charging hole.
(ii)**Pusher car:** This is a car used in the leveling of coal in the oven, it has pushing bar mechanism and pusher car which are used for cleaning'
(iii)**Coke side:** This is where machines are being used to collect the coke to the quenching tower (eg) the coke car, quenching car and the door extractors.
(iv)**Electric locomotive engine:** It is driven by an electric mechanism
(v)**Coke car:** It is used for the drying of coke by taking it to the quenching or cooling chamber.
(vi)**Quenching car:** This is a car which is used for the cooling of coke by the means of spreading water on the coke in the quenching car at least for 2 minutes and it has a mechanism for draining out the water that has been poured on the coke. This is later driven to a place where the coke are been spread on the ground before taking the coke for sizing
(vii)**Coke guide:** This is used to prevent the coke from falling off, washing, burning of cables or causing of accident in the workshop.

5.6 Type of coke

There are many types of coke but the important one is the metallurgical coke.

Properties of Coke

(i)It must have low sulphur, ash and moisture content.
(ii)Coke must be rough, light and must remain after it has been heated.

Uses of Coke

(iii)It is used as a reducing agent of iron ore in the blast furnace
(iv)It is used as a source of fuel in the blast furnace.

6.0 Process of Chemical Recovery

The gaseous mixture leaving the oven is made up of permanent gases which form the final purified coke-oven coal gas for fuel, accompanied by

condensable water vapour far and light oil, with solid particles of coal dust.

The gas is passed from the main into the primary condenser and cooler at a temperature of about 74°C, and the gas are cooled to 29.4°C by a mean of water. The gas is conducted to an exhauster which comprises it. The gas rises to a temperature of 120°f; the gas is passed to the final tar extractor where tar is thrown out by impingement of gas jet against metal surface.

The gas carries three-fourth of the ammonia and some quantity of the light oil originally present which it is left in the Oven. The gas is led to the saturator or separator which contains a solution of 5-10% of H_2S and the ammonia is absorbed with the formation of solid and crystalline ammonium sulfate. The saturator is a lead-lined, closed vessel where the gas is fed in by a separated distributor under earth the surface of acid liquid. The acid concentration is maintained by the addition of 60°C surface acid and the temperature is kept at 140°f by the heater and the heat of neutralization.

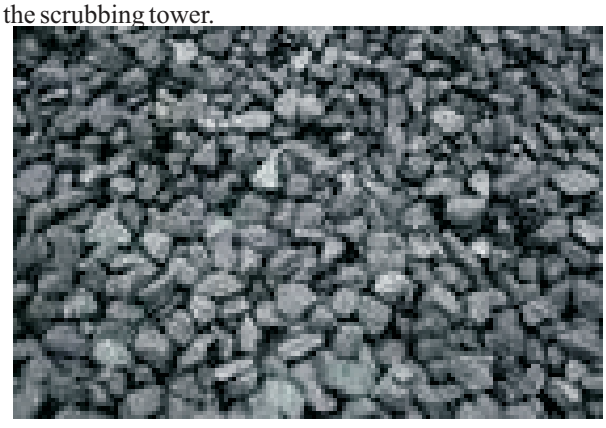
The crystalline ammonia sulfate is removed from the bottom of the saturator by a centrifugal pump and drained on the table where another liquid run back to the saturator. The gas will now move to the final coolers or condenser at 140°f, where it is scrubbed with water unit and its temperature is 75°f .

During the cooling some Naphthalene and hydrogen sulphate separates and it carries along with it the waste water and recovered it. The gas is been passed into the light oil or benzol scrubber, which is circulated at about 75°f as the absorbent medium a heavy fraction of petroleum is called straw oil or (coal –tar oil) ,when the straw oil is been sprayed into the top of the adsorption tower the gas will flow up through the tower.

The straw oil absorb about 2-3 % of its weight of light oil and remove efficiency of about 95% of the light oil vapour in the gas .The rich straw oil are being warned in the heat exchanger of vapour from the light hot oil .

Debenzolized oil flow out from the light hot oil that passes into the stripping column. The straw oil, which flow downward, is brought to direct contact with live straw oil both the vapour of the light oil and the steam are passed off and upward from the still through the heat exchanger into the condenser and separator.

The straw oil, or stripped is returned through the heat exchanger to the scrubber. The far oil is re-sent in order to separate tar from water. The gas after being stripped off its ammonia and light oil has the sulfur removed in purifying boxes which contain iron oxide in the scrubbing tower.



Picture 1: shows Coking Coal



Picture 2: shows the Coke oven Plant of the Ajaokuta Steel Company Limited



Picture 3: shows the Coke Oven Batteries

REFERENCES

1. Project Report: Ajaokuta steel company limited detailed Project Report (DPR) Vol. IV on Personnel

2. Company Report: Ajaokuta steel company limited detailed Project Report (DPR) Vol. I part II Explanatory Note.

3. Project Report: Ajaokuta steel company limited Detailed Project Report (DPR) Vol. V Repair shop, List of Equipment.

4. Evaluation Report of Ajaokuta steel company limited by Voest-Alhine Industrial Service GmbH Linz / Austria 1997

5. Project Report: Investment Profile of Ajaokuta steel company limited, March 1990

6. Status Report and Business Plan for Ajaokuta steel company limited April 1999.

7. Wakawa M.B.(1994) Strategies for the sustaining of optimal Capacity Utilization of the Ajaokuta steel company limited, Processing of the Nigerian

metallurgical Society (NMS) November 30th - December 3rd 1994.pg 19-25

8. Chukukere E.U.(1986) Steel Industries- Strategies for National Development, A paper delivered at 1986 Annual Conference of Nigerian Metallurgical Society. Pg 31-42

9. Alhaji Magaji Inuwa (1986) A welcome address delivered by the General Manager/Chief Executive, Ajaokuta steel company at 1986 Annual Conference of Nigerian Metallurgical Society. Pg 7-9

10. Ajaokuta Steel Company Limited: Diary 1987

11. Abubakar Sadiqi – (2002 "Under the Auspices of steel Week in Nigeria at Ajaokuta Steel Company Limited "A paper presented at Steel week on 9- 13 the April 2002

Description	Specifications
No. of Batteries	2
Ovens per battery	49
Length of oven (mm)	15040
Avg. width of oven (mm)	410
Height of oven (mm)	5500
Effective volume (m^3)	30.3
Distance between ovens (mm)	1260

Volatility	Percentage	Characteristic
High violate	(gas Coals) 35 - 45%	Coke able foamy sponge pronouns
Medium violate	(fat Coals) 26 - 35%	Coke able highly solid dense
Medium violate	(Coking coals) 18-22%	Coke able good coke
Low violate	(Low coking coal) 15-26%	Shrink less than other
Low violate	(Non- Coking coal< 15%	Shrink less than other

Table 1: shows the types of coal and where they can be found in Nigeria in respect to the world

INFLUENCE OF HAMMER MILL OPERATING PARAMETERS ON GRINDING ENERGY REQUIREMENT OF TWO HARD NUT SHELLS

[a]Kayode, O. and [b]Koya, O.A.
[a] Department of Mechanical Engineering, Osun State University, Osogbo, Nigeria.
[b] Department of Mechanical Engineering, Obafemi Awolowo University, Ile-Ife, Nigeria.
E-mail of Corresponding author: adeolakunle@yahoo.com

ABSTRACT
The paper reports on energy required in comminution of Palm Kernel Shells (PKS) and Coconut Shells (CNS), for production of organic friction materials and as primary fuel in improved combustion technologies. Clean PKS and CNS, respectively at 7.12% and 6.47 % moisture content (w.b), were ground using an instrumented hammer mill. Comminution energy for each shell type was measured at shaft speeds of 1200, 1600, and 2000 rpm; screen sizes of 3, 5 and 10 mm and feed rates of 2 and 4 kg/min for PKS, 1.5 and 3 kg/mm for CNS. Based on the results obtained, the energy requirement increased with increasing shaft speed while it decreased with increase in screen size and feed rate. The effective specific energy for PKS increased by 37% from 3.36 ± 2.14 kJ/kg as hammer mill speed increased from 1200 to 2000 rpm. For CNS, effective specific energy increased by 45% from 5.80 ± 3.15 kj/kg for the same conditions. The effective specific energy for PKS decreased by 5.50 kJ/kg (81.3%) from 6.77 ±3.19 kJ/kg for screen size increasing from 3 to 10 mm. The effective specific energy for CNS decreased by 7.79 kJ/kg (71.9%) from 10.85 ± 5.33 kJ/kg for the screen size increasing from 3 to 10 mm. The effective specific energy also decreased by 35% and 39% for PKS and CNS respectively, with an increase in mass feed rate from 2 – 4 kg/min and 1.5 – 3 kg/min for PKS and CNS, respectively. Gross specific energy is significantly affected by all the three parameters while only feed rate and screen size have effect on effective specific energy. On the average CNS milling consumed more energy than PKS for identical milling conditions.
Keywords: *Hammer mill, Grinding energy, Comminution, Palm Kernel Shell, Coconut Shell, Bio-mass fuel, Frictional material*

1. INTRODUCTION

Biomass such as Palm Kernel Shell (PKS) and Coconut Shells (CNS) generally considered as agro-wastes are now finding applications as alternative fuel sources to depletable fossil fuel and as replacement for toxic industrial raw materials. PKS are recovered as a by-product in the processing of oil palm fruits which yields palm oil and palm kernels; while, CNS is a byproduct derived in the process of producing copra, the dried meat of the coconut fruit. Current pattern of world energy consumption is not sustainable due to environmental implications such as problem of global warming, pollution and depletion of the non renewable reserves of fossil fuel. Hence, attention had been turned to the renewable biomass as alternative sources of fuel [1-4]. Biomass is the fourth largest source of energy world-wide and account for about 35 percent of energy consumption in the developing countries [5]. Fluidized bed combustion (FBC) represents one of the most important developments in combustion technology in the last 50 years [5]. The merit of FBC lies in its ability to burn multiple fuels of diverse origin, biomass inclusive. This also includes fuels which are difficult to burn using other technologies. Moreover, FBC possesses relatively high efficiency and has low nitric oxide emission. [5-7]. Another trend in the utilization of agricultural waste such as PKS and CNS is as substitute for existing industrial raw material found to be environmentally degrading, costly or unrecyclable. Recently, research on the use of PKS in the manufacture of friction lining material suggests that PKS could be a possible replacement for asbestos, which is carcinogenic [8, 9].

The form in which CNS and PKS are utilized in these applications requires a machine that can pulverize them efficiently and economically to the required particle size range. Typical fuel particle size for FBC range from 1.4 to a maximum of 50mm [10-14] while *in the production of an experimental brake pad, [8] reported using PKS particle passing 125 µm sieve while [9] used ground PKS of less than 0.1 mm particle size.* Such reduced particles sizes can be achieved by fine grinders (e.g. hammer mill, disc refiner, roller mill, chain mill). However, hammer mills have achieved greater merit because of their ability to finely grind a greater variety of materials than any other machine [15]. It is also one of the most commonly used industrial grinder for agro-materials size reduction, because the equipment is capable of producing what is often termed in the industry as a satisfactory grind [16].

Hammer mills accomplish size reduction by impacting a slow moving target, such as a cereal grain, with a rapidly moving hammer. The target has little or no momentum (low kinetic energy), whereas the hammer tip is travelling at a minimum of 4,880 m/min and perhaps in excess of 7,015 m/min (with the attendant high kinetic energy). The transfer of energy that results from this collision fractures the material into many pieces. Because impact is the primary force used in a hammer mill to reduce particle size, anything that increases the chance of a collision between a hammer and a target, increases the magnitude of the collision (i.e. shaft speed and feed rate of material into machine), or improves material take-away (i.e. hammer mill screen design), would be advantageous to

particle size reduction.

Performance of a grinding device is often measured in terms of its energy requirement, and resulting particle size distribution of the product. In this regard, appropriate combination of machine operation parameters is central to the reduction of fines during milling. Whilst prediction information on particles size distribution and energy consumption is significant in the optimisation of the comminution process, there are no available data in the literature on CNS and PKS. The intent in this work therfore was to investigate how the relevant machine based parameters influence energy consumption in the comminution of PKS and CNS**; since energy costs may be a significant factor in their economical application.**

2. MATERIALS AND METHODS

Feedstock Acquisition and Preparation

Palm kernel shells samples were obtained from a palm oil processing mill in the Teaching and Research Farm of Obafemi Awolowo University in Ile-Ife, Nigeria. The CNS samples were obtained from Badagry area of Lagos State, Nigeria. Following the acquisition, both samples were manually sorted to remove stones, pieces of metals and other foreign matter that may affect experimental results. The moisture contents of PKS and CNS samples in percentage wet basis prior to experimental comminution were determined using the oven method.

The Instrumented Hammer Mill

Figure 1 shows the schematic diagram of the experimental set up that was made up of the following components: a pilot scale hammer mill, digital clamp ammeter and AC voltmeter.The hammer mill had a rotor diameter of 150 mm with fifteen swinging hammers in three sets, loosely bolted to its periphery. The length, breadth and the thickness of each hammer were 90, 25 and 10 mm, respectively. The mill's barrel has a width of 180 mm and diameter, 400 mm. Three interchangeable classifying screens with 3, 5 and 10 mm holes' diameters were designed to be mounted in-turn in an arc of about 180^0 of sector at the lower portion of the barrel. The screen whole configuration was in-line. Blade clearance of 15 mm between hammers and screen was used.

The hammer mill was powered by a 3-phase AC motor (BBC Brown Bovery: MEUC 100L2, France) with rated power of 3 kW and 2870 revolutions per minute. The motor powered the mill via a V-groove pulley and belt drive system. The hammer mill was provided with cone pulley system consisting of three pulleys designed in such a way as to give shaft speed of 1200, 1600 and 2000 revolutions per minute for the mill when coupled with the motor's pulleys. The corresponding tip speeds for the hammers were 20.11, 26.81, and 33.51 m/s. These speeds were within the range of commercial milling of agricultural produce using hammer mills [17]. The clamp ammeter (Steren Clamp Digital Multitester: MUL-100, China) with accuracy of 0.8% ±2% was used to measure current consumed by the motor at an interval of every 10 seconds during comminution. The AC source voltage was measured using Mastech Digital Muiltimeter (MAS 838). The voltage was also recorded, simultaneously with current, for an interval of 10 seconds for each time the experimental runs lasted. The power consumed was calculated using the average values for current and voltage from each experimental run using Eqn. 1;

$$P = (\sqrt{3}).\eta.F.I.V \quad \ldots \quad \ldots \quad \ldots \quad (1)$$

where, P is the power in Watts, η is the motor efficiency (given as 0.8 on the motor data plate), F is the power factor (given as $\cos \varphi = 0.88$), I is the current in Amperes and V is AC voltage in Volts. Similar approach was employed by [17] in determining power consumed in the hammer mill communiution of poplar chips, pine chips, and pine bark. Before the experimental runs, the initial no-load power consumption at the different speeds of 1200, 1600 and 2000 rpm hammer mill shaft speed were determined and recorded. Gross specific energy consumed was determined by dividing gross power consumed by the mass feed rate, while the effective specific energy (that is, energy that may be assumed to reach the feedstock for grinding) was calculated by subtracting the no-load power from gross power and dividing the result by mass feed rate.

Machine Feed Rate

The maximum mass feed rate to the mill for each of PKS and CNS was determined in a pre-test to determine the feeding rate, which may not result in chocking. The maximum feed rates for PKS and CNS obtained were 4 kg/min and 3 kg/min, respectively. Two levels of feed rates were then used for each material: 2 and 4 kg/min for PKS and 1.5 and 3 kg/min for CNS. The mass of feedstock required per minute for each run was measured and divided into six equal portions and gradually fed manually at an interval of 10 seconds each. Each experimental run lasted for an average of one minute.

Design of Experiment

The operating (independent) variables were: the hammer mill shafts speeds (N) in rev/min, Screen size (D), and feed-rates (F) in kg/min. The experiment was designed as a full factorial experimental designed. A total of 18 runs each (3x3x2) were carried out for PKS and CNS making a total of 36 experimental runs.

1. RESULT AND DISCUSSION

Idle Power Consumption

The idle (no-load) power consumption of the hammer mill increased by 0.266kW (43.2%) from 0.615 kW at 1200 rpm to 0.881 kW at 2000 rpm (Fig 2). The increase in power was due mainly to the increasing speed with only marginal change in torque (4.21 - 4.89 Nm).

Effect of Shaft Speeds on Specific Energy

The moisture contents of the PKS and the CNS, at the time of the experiments, were 7.12% and 6.47% (wet basis), respectively. The mean gross specific energy of PKS increased by 42% from 17.19 ± 6.76 kJ/kg with an increase in speed from 1200 to 2000 rpm for all screen sizes (3-10 mm) (Fig.3). For CNS the gross specific energy increased by 44% from 24.23 ± 9.09 kJ/kg with an increase in speed from 1200 to 2000 rpm for all screen

sizes (Fig.4).

The effective specific energy for PKS increased by 37% from 3.36 ± 2.14 kJ/kg as hammer mill speed increased from 1200 to 2000 rpm for all screen sizes. For CNS, effective specific energy increased by 45% from 5.80 ± 3.15kj/kg for the same conditions.

The increase in gross specific energy observed for both CNS and PKS was due, mainly, to increase in idle power of hammer mill as speed increases, while initial average particle size, which is relatively larger for CNS than that of PKS, was responsible for both the higher values obtain for mean effective specific energy and percentage increase in the case of CNS. According to Kick's theory, the greater the ratio of feed size to product size (reduction ratio) the more the energy requires in comminution [18].

Effect of Screen Sizes on Specific Energy

The gross specific energy for PKS decreased by 23.6% from 23.37 ± 7.08 kJ/kg for screen size increasing from 3 – 10 mm at all speeds (Fig.5), while the gross specific energy for CNS decreased by 23.6% from 32.98 ± 9.12 kJ/kg for screen size increasing from 3-10 mm for all hammer mill shaft speeds (Fig.6).

The effective specific energy for PKS decreased by 5.50 kJ/kg (81.3%) from 6.77 ±3.19 kJ/kg for screen size decreasing from 3 to 10 mm. The effective specific energy for CNS decreased by 7.79 kJ/kg (71.9%) from 10.85 ± 5.33 kJ/kg for the screen size decreasing from 3 to 10 mm.

For a given screen size, with an initial impact of hammer on a particle, the particle breaks into pieces with sized ones exiting the screen. The shells which were bigger than the screen holes are subjected to further impacts to become small enough to pass through the screen, consequently, more energy is consumed in breaking the particle until they are able to pass through the screen holes. With increase in screen hole diameter, the percentage of material particles exiting the holes after the initial impacts increased accordingly. With rapid removal of materials from grinding chamber, the requirement for further reduction with minimised with consequent reduction in energy consumption.

Effect of Feed-Rates on Specific Energy

Gross specific energy decrease by 47% and 48% with an increase in mass feed rate from 2 – 4 kg/min and 1.5 – 3 kg/min for PKS and CNS, respectively. The effective specific energy also decreased by 35% and 39% for PKS and CNS respectively, for the same conditions. Decrease in both gross and effective specific energy with feed rates was attributed to crushing of larger quantity of materials in unit time, and increased energy utilization by distributing feedstock all along the full length of the hammer mill rotor. Thus, higher feed rate appeared to favour lesser specific energy consumption.

Significant test of parameters shows that all the three parameters (shaft speed, screen size and feed rate) have significant effect (at 99% confidence level) on gross specific energy; while for effective specific energy only screen size and feed rate had significant effect at 99 and 95%, respectively, for both shells.

2. CONCLUSIONS

Gross specific energy increases with increase in speed, reduction in screen size and reduction in feed rate. The effective specific energy decreases with increase in feed rate and screen size, and increases with increase in speed. On the average CNS milling consumed more energy than PKS for identical milling conditions.

3. ACKNOWLEDGEMENTS

The authors would like to thank the National Mathematical Centre and the Raw Materials Research and Development Council, Abuja, Nigeria, under the 2009 grant for Mathematical Modeling of Processing Equipment, as well as the Osun State University, Osogbo, Nigeria, for providing supports in the execution of this work

4. REFERENCES

[1] Finney, K.N., Sharifi, V.N. and Swithenbank, J. (2009): 'Combustion of spent mushroom compost and coal tailing pellets in a fluidised bed' *Renewable Energy*, 34 : 860-868

[2] Kuti, O.A. (2007): 'Impact of charred palm kernel shell on the calorific value of composite sawdust briquettes'. *Journal of Engineering and Applied Science,* 2(1): 62-65.

[3] Dit, M. (2005): 'Palm kernel shell is more than biomass for alternative fuel after 2005'Extract of PIPOC 2007: Proceedings of Chemistry and Technology Conference (Published Information).

[4] Ghani, W.A.W., Moghadam, R.A., Mohdsalleh, M.A. and Alias, A.A. (2009): 'Air gasification of agricultural wastes in a fluidized bed gasifier: Hydrogen production performance'. *Energy*, 2: 258-268.

[5] Battacharya, S.C. (1998): 'State of the art of biomass combustion'. *Energy Sources,* 20: 113 –135.

[6] Ravelli, S., Perdichizzi, A. and Barigozzi, G. (2007): 'Description, applications and numerical modelling of bubbling fluidized bed combustion in waste-to-energy plants'. *Progress in Energy and Combustion Science*, 34: 224-253.

[7] Fujimura, H., Oshita, T. and Naruse, K. (2001): 'Fluidized-bed gasification and slagging combustion system'. Paper Presented at the IT3 Conference, May 14-18 (2001), Philadelphia, USA.

[8] Ibhadode, A.O.A., and Dagwa, I.M. (2008): 'Development of asbestos–free friction lining material from palm kernel shell'. *Journal of the Brazilian Society of Mechanical Science and Engineering.* April-June 2008,(2) : 166 – 173.

[9] Fono, T.R. (2009): 'A study on the use of palm kernel shell as friction material in automotive brake pads and linings'. Unpublished M.Sc. Thesis, Department of Mechanical Engineering, Obafemi Awolowo University, Ile-Ife.

[10] Yan Cao, Yang Wang, Riley, J.T., and Pan, W. (2006): 'A Novel Biomass Air Gasification Process for Producing Tar-Free Higher Heating Value Fuel Gas'. *Fuel Processing Technology,* 87 : 343 - 353

[11] Patumsawad, S. (2001): **'Fluidised bed combustion of oil palm solid waste'** Waste Incineration Research Center (WIRC), Department of Mechanical Engineering, King Mongku'sInstitute of Technology, North Bangkok, Thailand.

[12] La Nauze, R.D. (1987): 'A review of the fluidized bed combustion of biomass'. *Journal of the Institute of Energy :* 66-76

[13] Eswaraiah, C., Gupta, A., Nagarajan, R., Rajavel, M. and Nandakumar, K. (2008): 'Minimization of fines generation in size reduction of coals by impact Crusher'. *Fuel Processing Technology*, 89: 704-714.www.aciar.gov.au/node/10355, Retrieved 2009-05-30.

[14] Adio, S. A. and Asere, A. A. (2009): 'A study of thermal and emission characteristics of a coconut shells in a fluidized bed combustors'.Procedings of 22nd Annual General Meeting and International Conference of the Nigeria Institute of Mechanical Engineers, 215-219

[15] Scholten, R. L., and McEllhiney, R.R., (1985): 'The effects of prebreaking in hammer mill particle size reduction'. ASAE Paper No. 85-3542. St. Joseph, Mich.

[16] Koch, K. (2002): 'Hammer Mills and Roller Mills'. MF-2048, *Feed Manufacturing*, Kansas State University.

[17] Esteben, L.S. and Carrasco, J.E. (2006): 'Evaluation of different strategies for pulverization of forest biomass' *Powder Technology*, 166 : 139-151

[18] Earle, R.L. (1983): Unit Operations in Food Processing: published by NZIFST (2010 reprint).

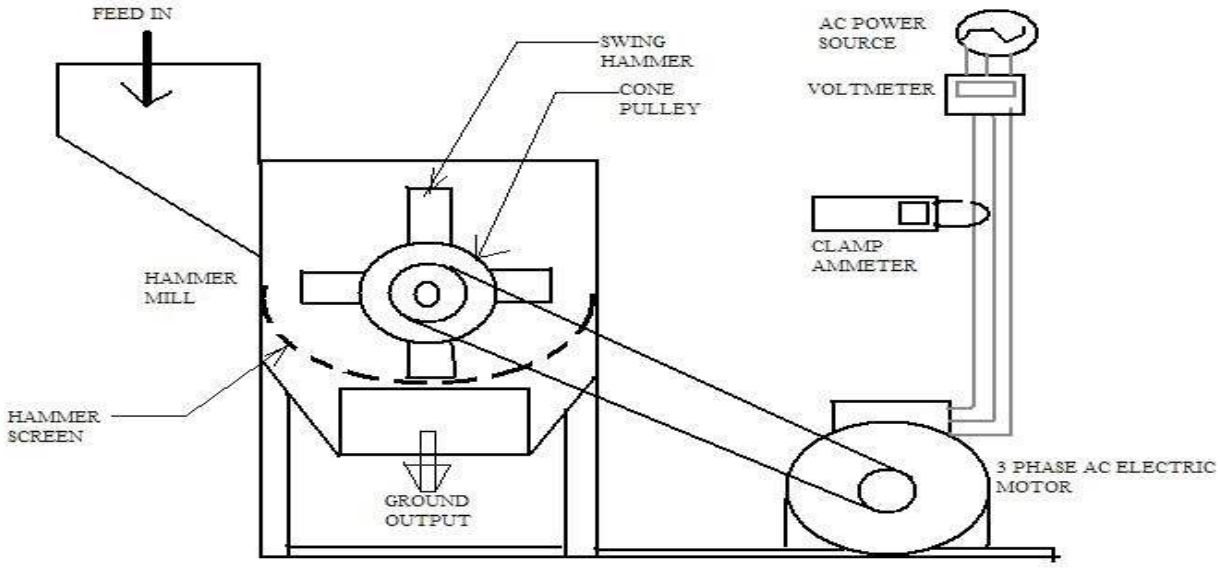


Fig.1. Schematic Diagram of Experimental Set

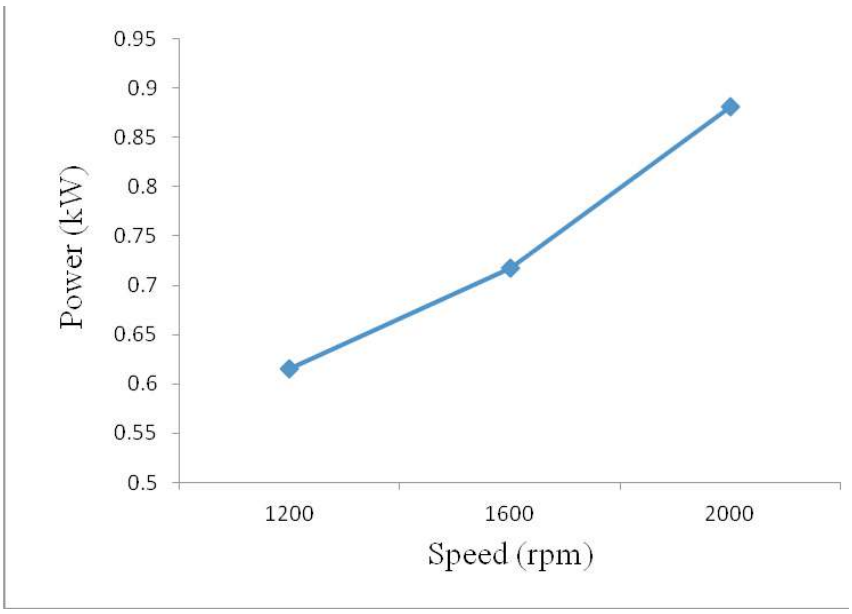


Fig.2: Idle power consumption of hammer mill with speed

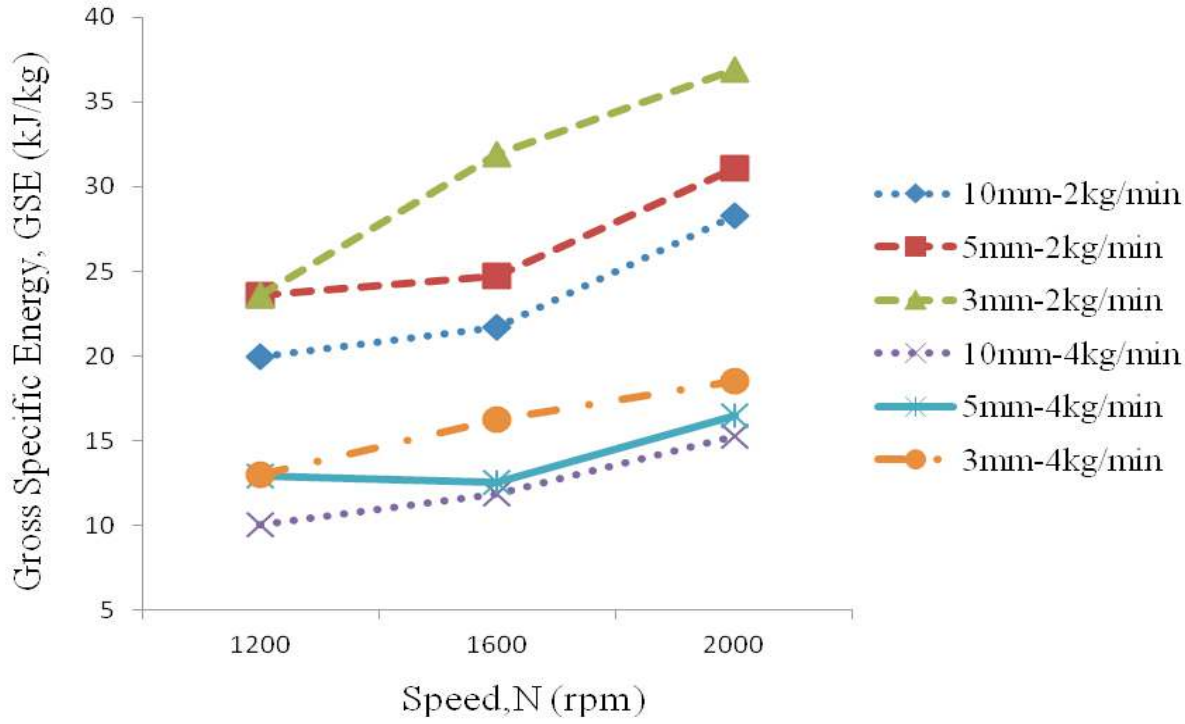


Fig 3 Gross specific energy of PKS with hammer mill speed against screen size and at different mass feed rates.

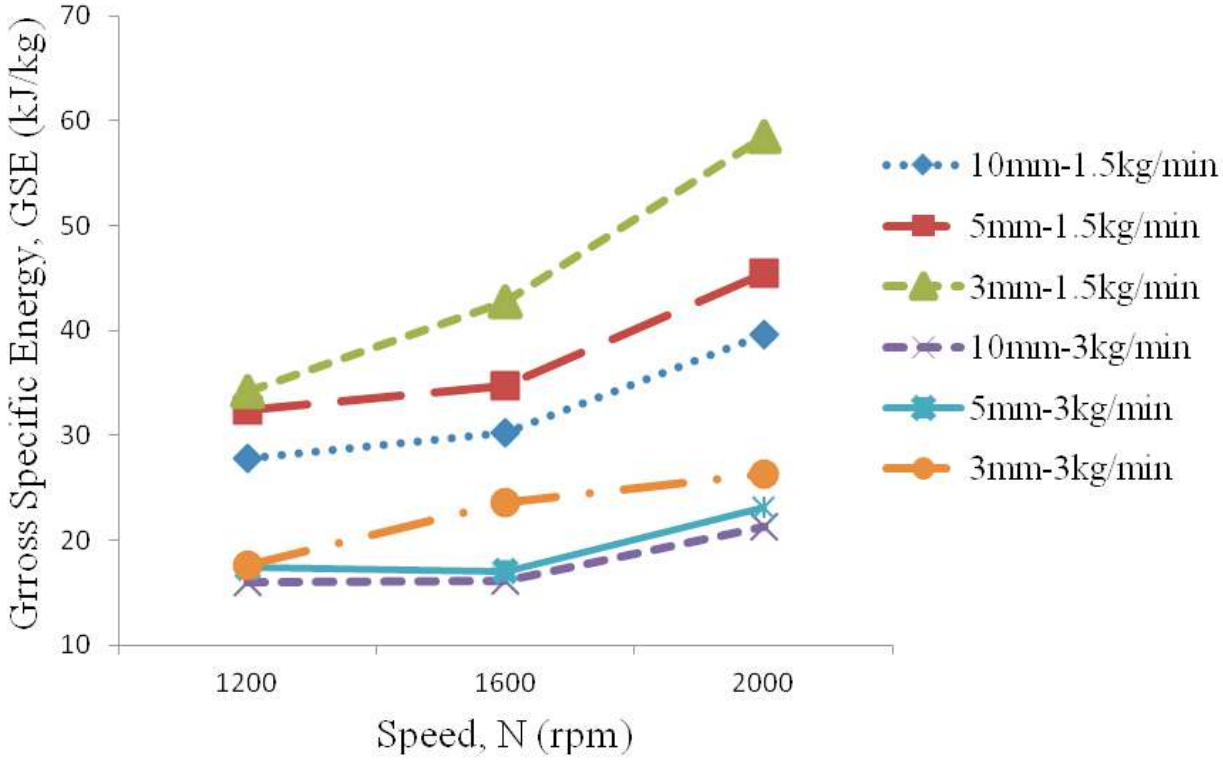


Fig 4 Gross specific energy of CNS with hammer mill speed against screen size and at different mass feed rates.

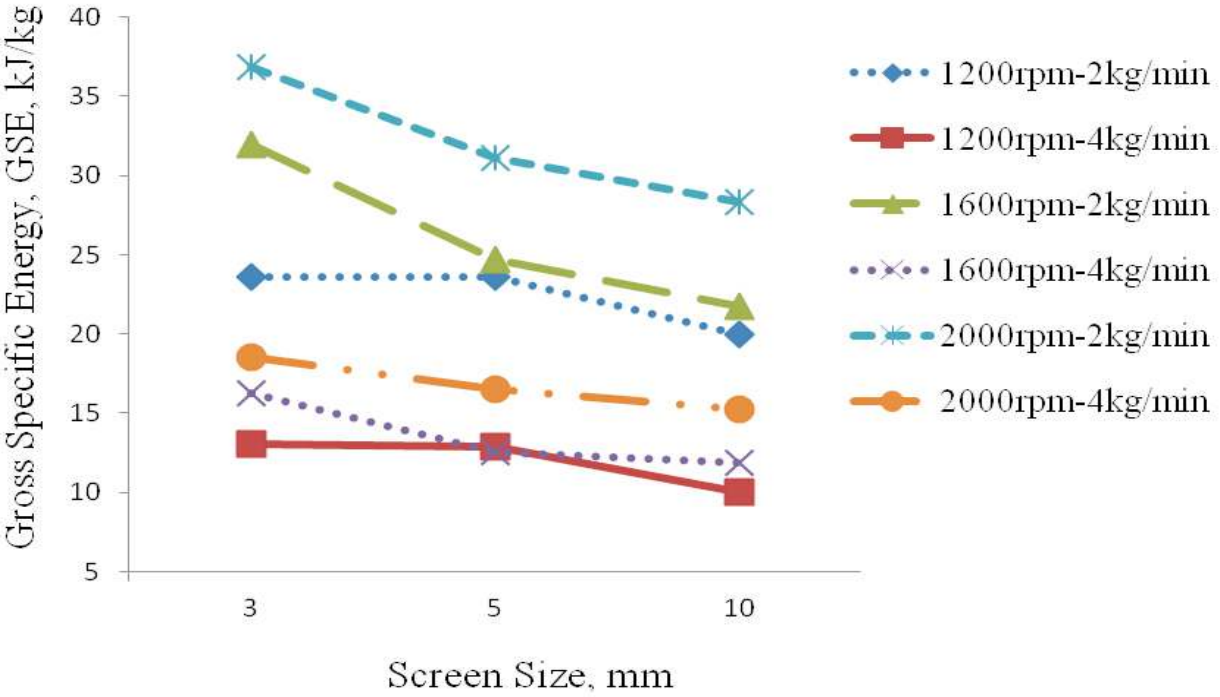


Fig 5 Gross specific energy of PKS with hammer mill screen size against speed and at different mass feed rates

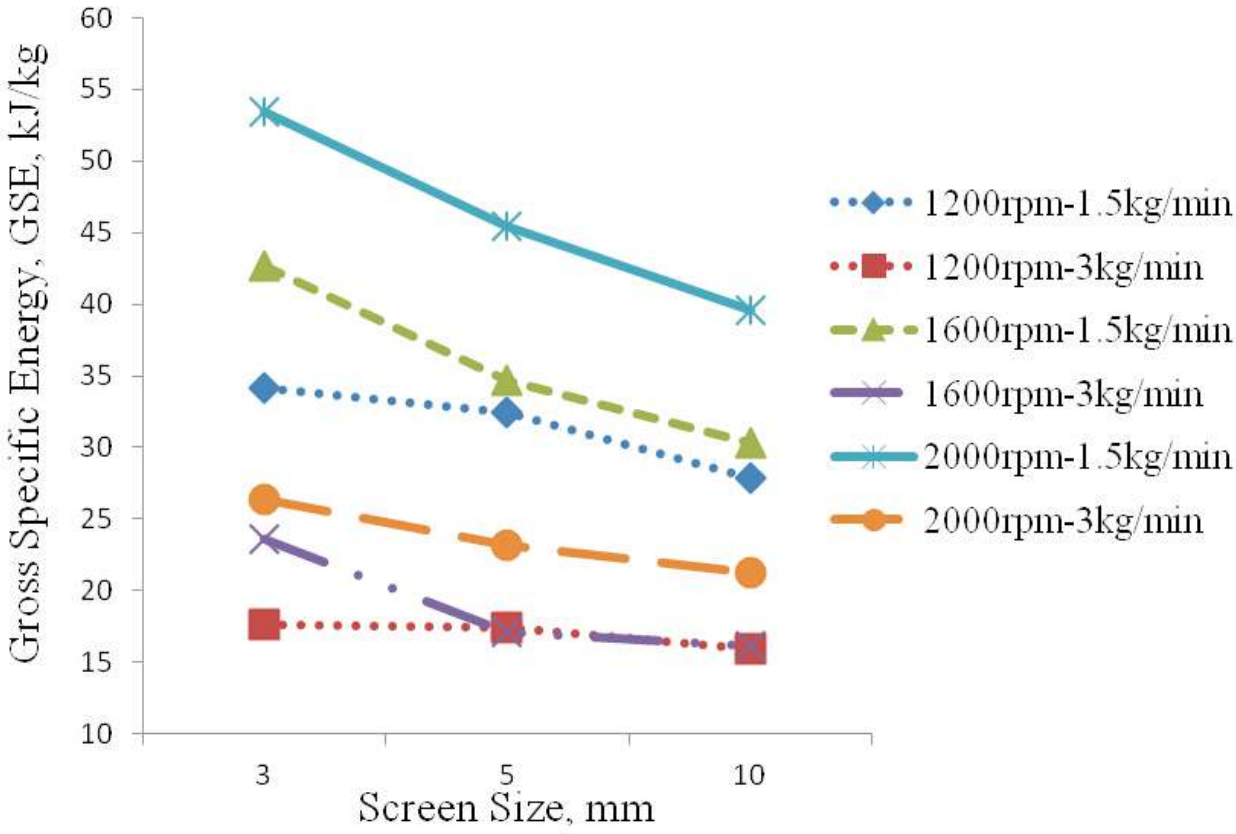


Fig 6 Gross specific energy of CNS with hammer mill screen size against speed and at different mass feed rates

MECHATRONICS FOR SUSTAINABLE ENVIRONMENT AND NATIONAL DEVELOPMENT

[1,2]Onipede B.O., [1,3]Omole F.O, [1,4]Oji J.O., [1,5]Adetunji A. R.
[1]Prototype Engineering Development Institute Ilesa, Osun State
(National Agency for Science and Engineering Infrastructure, NASENI. FCT Abuja)
[2]Dept. of Computer Science and Engineering, Obafemi Awolowo University, (OAU) Ile-Ife
[3]Dept. of Electrical and Electronics Engineering, Obafemi Awolowo University, Ile-Ife
[4]Dept. of Mechanical Engineering, Federal University of Technology, Akure
[5]Dept. of Materials Science and Engineering, Obafemi Awolowo University, (OAU) Ile-Ife
deleonipede@gmail.com

ABSTRACT

The processes, equipment, and systems used for design and production ranging from automobiles to computer chips are undergoing dramatic changes in response to new customer needs, competitive challenges, and emerging technologies. Recent advances in information systems, business practices, engineering techniques, manufacturing and material science enable companies to produce new and better products more quickly and at a much lower cost than before. This paper discusses the general mechatronics concepts as an option to improve the series of operations and processes that transforms industrial materials from their raw state into finished parts or products including the prospects and fields of application in a developing country like Nigeria. It concludes by highlighting the need for mechatronics for sustainable environment and national development which will continue to expand as the global demand for cost-effective product design and manufacturing accelerates.

Keywords: *Mechatronics, Process, Materials, Manufacturing and Development*

1. INTRODUCTION

Manufacturing is the strength of any industrialized nation. Although large segments of the population may be employed in service industries, it is manufacturing that produces the wealth of a nation [1]. The processes, equipment, and systems used in design and manufacturing from automobiles to computer chips are undergoing dramatic changes in response to new customer needs, competitive challenges, and emerging technologies. The situation in Nigeria is that all of our production processes are still based on conventional methods of operation. Recent advances in information systems, business practices, engineering techniques, and manufacturing science now enable companies to produce new and better products more quickly and at a much lower cost than ever before. This makes it increasingly difficult for underdeveloped nations to get into the game of quality material and production processing.

Mechatronics and the use of automation systems such as Factory automation, Process automation, Robotics and Computer Numeric Controlled (CNC) machines have spread rapidly during the last decade. Most of the machine tools in modern manufacturing industry are computer controlled. With the use of these technologies, products can now be made better, faster and cheaper and no manufacturer can afford to do otherwise, else such a manufacturer will produce goods that are not globally competitive. Nigerian products largely do not meet international standards. Nigerian graduates are trained on conventional manufacturing technologies giving rise to inadequate capacity in advanced manufacturing technology systems, both in equipment and personnel.

This paper aims to do two things. First, to present the general mechatronics concepts as an option to improve the series of operations and processes that transforms industrial materials from their raw state into finished parts or products including the prospects and fields of application in a developing country like Nigeria. It then highlights the need for mechatronics for sustainable environment and national development which will continue to expand as the global demand for cost-effective product design and manufacturing accelerates.

2. GENERAL CONCEPT OF MECHTRONICS

The original definition for Mechatronics was done by **[14]** in this way: *The word Mechatronics is composed of 'mecha' from mechanism and 'tronics' from electronics. In other words, technologies and developed products will be incorporating electronics more and more into mechanisms, intimately and organically, and making it impossible to tell where one ends and the other begins.* The definition of mechatronics continued to evolve after [14] suggested the original definition. One often quoted definition of mechatronics was presented by [3] in 1996. In their words, mechatronics is defined as the synergistic integration of mechanical engineering, with electronics and intelligent computer control in the design and manufacturing of industrial products and processes. That same year, another definition was suggested by [4]. They said "Mechatronics is the application of complex decision making to the operation of physical systems". Yet another definition due to [5] appeared in 1997 who opined that mechatronics is a methodology used for the optimal design of electromechanical products. More recently, we find the suggestion by [7] who said: A

mechatronic system is not just a marriage of electrical and mechanical systems and is more than just a control system; it is a complete integration of all of them. All of these definitions and statements about mechatronics are accurate and informative, yet each one in and of itself fails to capture the totality of mechatronics. Despite continuing efforts to define mechatronics, to classify mechatronic products, a consensus opinion on an all-encompassing description of "what is mechatronics" is yet to be made [6].

The concept of Mechatronics has evolved since its first definition [14], and now includes a broader concept than just mechanisms and electronics. A representative definition is stated thus: *Mechatronics is the synergistic combination of precision mechanical engineering, electronic control and systems thinking in the design of products and manufacturing processes. It relates to the design of systems, devices and products aimed at achieving an optimal balance between basic mechanical structure and its overall control (figure 3).* This representative definition gives rise to requirement for more study in this field in order to establish the specific areas that are covered by the term "mechatronics". As a result, the study of mechatronic systems can be divided into the following areas of specialty [6]:

1. Physical Systems Modelling
2. Sensors and Actuators
3. Signals and Systems
4. Computers and Logic Systems
5. Software and Data Acquisition

Even though many people believe that the presence of mechanical, electrical, electronic components, and computers make a system mechatronics, others do not feel the same as there is nothing wrong with the individual identity [6]. Hence, the term mechatronics should be used to represent a different meaning, namely, a design philosophy, where mechanical, electrical, electronics components, and IT should be considered together in the design stage itself to obtain a compact, efficient, and economic product rather than designing the components separately. However, as the field of mechatronics develops, the list of relevant topics associated with the area will most certainly expand.

Ways of Integration

Figure 1 shows a general scheme of a classical mechanical-electronic system. Such systems resulted from adding available sensors, actuators, and analog or digital controllers to mechanical components. The limits of this approach were given by the lack of suitable sensors and actuators, the unsatisfactory life time under rough operating conditions (acceleration, temperature, and contamination), the large space requirements, the required cables, and relatively slow data processing [6]. With increasing improvements in miniaturization, robustness, and computing power of microelectronic components, one can now put more emphasis on electronics in the design of a mechatronic system. More autonomous systems can be envisioned, such as capsuled units with touchless signal transfer or bus connections, and robust microelectronics.

The integration within a mechatronic system can be performed through the integration of components and through the integration of information processing.

Integration of Components (Hardware)

The integration of components (hardware integration) results from designing the mechatronic system as an overall system and imbedding the sensors, actuators, and microcomputers into the mechanical process, as seen in Figure 2. This spatial integration may be limited to the process and sensor, or to the process and actuator. Microcomputers can be integrated with the actuator, the process or sensor, or can be arranged at several places. Integrated sensors and microcomputers lead to *smart sensors*, and integrated actuators and microcomputers lead to *smart actuators*. For larger systems, bus connections will replace cables. Hence, there are several possibilities to build up an integrated overall system by proper integration of the hardware [5, 6].

Integration of Information Processing (Software)

The integration of information processing (software integration) is mostly based on advanced control functions. Besides a basic feed forward and feedback control, an additional influence may take place through the process knowledge and corresponding online information processing (Figure 2).

This means a processing of available signals at higher levels, including the solution of tasks like supervision with fault diagnosis, optimization, and general process management. The respective problem solutions result in real-time algorithms which must be adapted to the mechanical process properties, expressed by mathematical models in the form of static characteristics, or differential equations [6]. Therefore, a *knowledge base* is required; comprising methods for design and information gaining, process models, and performance criteria. In this way, the mechanical parts are governed in various ways through higher level information processing with intelligent properties, possibly including learning, thus forming integration by process-adapted software [5].

3. PROSPECTS OF MECHATRONICS FOR NIGERIA

Mechatronics was born into Nigeria a few years ago. This technology has produced many new products and provided powerful ways of improving the efficiency of the products used in daily life. Currently, there is no doubt about the importance of mechatronics in the drive of Nigeria towards sustainable environment and national development. For Nigeria, there are many prospects for mechatronics application. The mechatronic systems installed in industries are installed by foreigners. In some cases, these systems are non-functional due to the absence of proper technology to handle them.

In the power industry, the need for mechtronics is not far-fetched. Power plants include measurement and control systems integrated into the entire plant. Most of the plants use costly mechatronics systems which require proper handling by qualified personnel. These systems and invariably the power industry can be improved to become a stable and country wide architecture which in turn helps to tackle the problem of power supply in Nigeria. The textile industries in Nigeria are almost moribund. These are partly due to the fact that most of these industries

employ manual processes which are very rigid for incorporating mechatronics. Others involve automated systems which are not integrated. With mechatronics, these systems can be combined to produce a total manufacturing process.

The influence of mechatronics on the evolution of agriculture, and how it is becoming the primary element of future cultivating habits is quite evident. Nigeria must embrace the elements of mechatronics, such as sensors, that play a vital role in farms for fertilizing, seeding, cropping, cleaning, and monitoring of vegetation. Currently, there exist sensors in use of detecting colour, alcohol levels for ripeness, ambient light levels, moisture levels and hazardous levels of chemicals including pesticides [8].

There are many systems in the existing world that require a synergy of these expertise areas including systems in automotive, aerospace, medical, materials processing, manufacturing and consumer products application sectors [9]. Other application areas may include chemical industries, oil and gas, miscellaneous product design, e.t.c.

Benefits of Mechatronics to National Development

Mechatronic techniques are vital to the work of such manufacturing industries as consumer products, defence systems and aerospace, automotive, health care, and materials processing [11].

Manufacturers that harness the best practices of mechatronics can achieve significant benefits. Best-in-class manufacturers are more able to reach their targets for development costs, product revenue, and product quality, and to hit their product launch dates. Such manufacturers can typically also add more features and functions reduce the size, weight and cost of their products and improve their overall efficiency. The use of mechatronics also enables these companies to leverage adaptive control and diagnostics to improve reliability and reduce maintenance costs and to customise or upgrade products by reprogramming embedded firmware [13].

In addition, a mechatronics-based approach mitigates risk and solves common design challenges such as the slow, serial machine design process, poor communication between machine designers and customers and risky physical machine testing. Mechatronics is a major driver of differentiating innovation and can help manufacturers achieve competitive edge [12].

4. CONCLUSION

The need for mechatronics will continue to expand as the global demand for cost-effective product design and manufacturing accelerates. The ongoing "virtualization" of the mechanical elements of design will demand that computer-based modelling, simulation, and control remain deeply ingrained in the life-cycle management of mechatronic systems. Industrial processes involving mechatronics are already been found in the more developed of the developing countries and they have applied mechatronics in many industries (e.g. textile, food, metalworking industries etc.). For Nigeria, the need for mechatronics as a tool to aid her sustainable environment and national development drive can not be over stated so that the nation can enjoy the numerous benefits of mechatronics.

5. REFERENCES

[1] Kyura, N. and Oho, H., (1996): "Mechatronics—an industrial perspective," *IEEE/ASME Transactions on Mechatronics,* Vol.1, No. 1, pp. 10–15.

[2] Mori, T., (1969): "Mechatronics," Yasakawa Internal Trademark Application Memo 21.131.01, July 12.

[3] Harshama, F., Tomizuka, M., Fukuda, T., (1996): "Mechatronics—what is it, why, and how?—an editorial," *IEEE/ASME Transactions on Mechatronics,* Vol. 1, No. 1, pp. 1–4.

[4] Auslander, D. M., Kempf, C. J., (1996): *Mechatronics: Mechanical System Interfacing,* Prentice-Hall, Upper Saddle River, NJ.

[5] Shetty, D. and Kolk, R. A., (1997): *Mechatronic System Design,* PWS Publishing Company, Boston, MA,.

[6] Robert H. B., (2002): ***The Mechatronics Handbook,*** CRC Press LLC, Washington, D.C.,

[7] Bolton, W., (1999): *Mechatronics: Electrical Control Systems in Mechanical and Electrical Engineering, 2nd Ed.,* Addison-Wesley Longman, Harlow, England.

[8] Lior H., , David B., (2003): http://www.google.com/patents?hl=en&lr=&vid=USPATAPP10083343&id=04eCAAAAEBAJ&oi=fnd&dq=robotic+arms+that+cultivate+the+roots+of+plants+and+rotating+mechanisms+to+Seed Issue date; Jan 21

[9] http://www.synthesis.org/Mechatronics-Workshop/by_title.htmlFig

[10] http://www.unido.org/en/doc/12363

[11] http://www.engineersgarage.com/articles/mechatronics

[12] http://findarticles.com/p/articles/mi_qa3739/is_201101/ai_n57036111

[13] www.engineeringcapacity.com/comment-and-analysis101/digital-approach-drives-competitive-edge

[14] www.chameleonproject.eu/index.php?option=com_content&view=article&id=77&Itemid=79

FIGURES

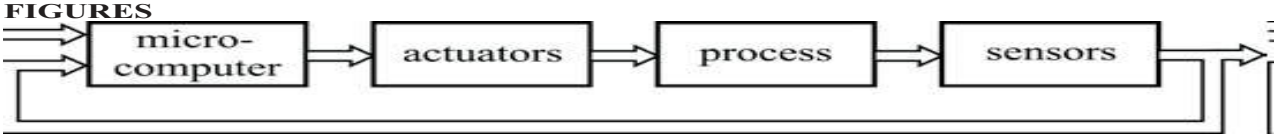


Figure 1: General scheme of a (classical) mechanical-electronic system

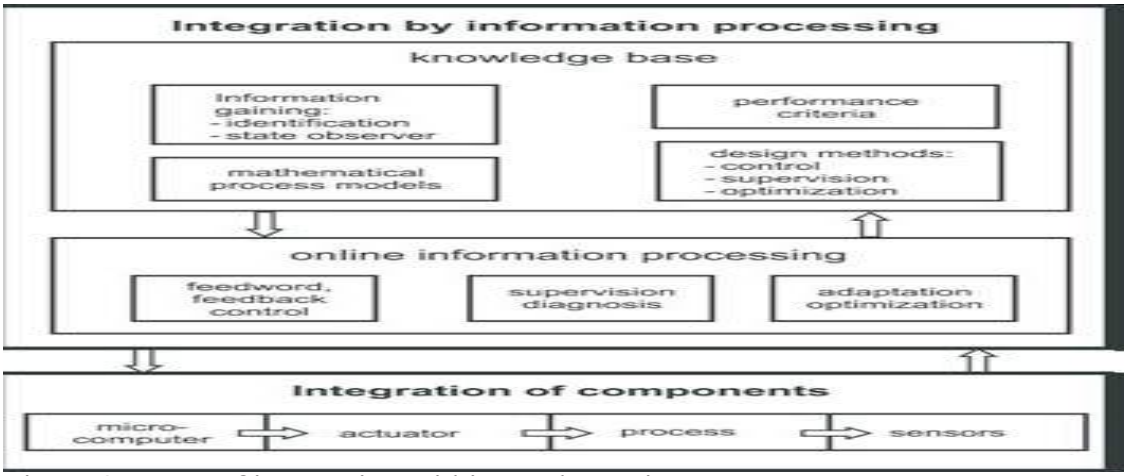


Figure 2: Ways of integration within mechatronic systems.

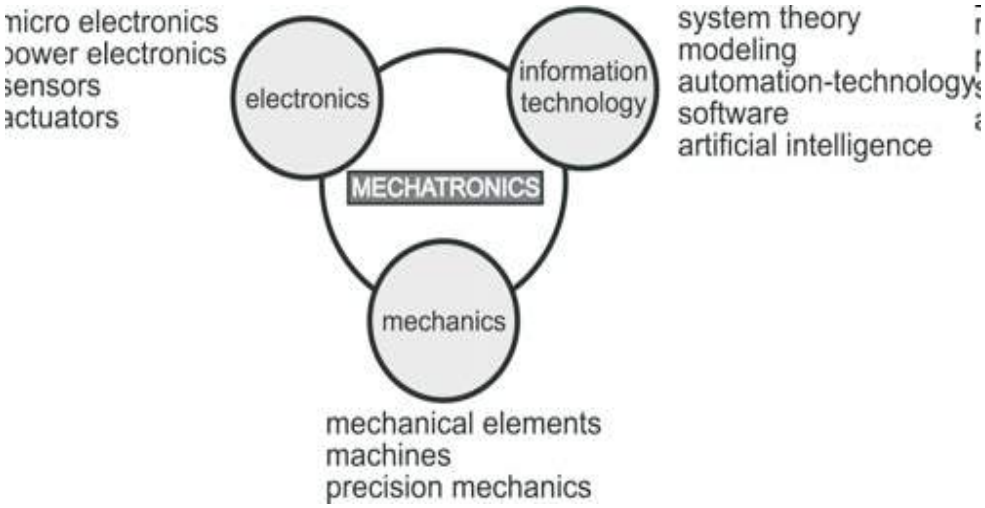


Figure 3: Mechatronics: Synergetic integration of different disciplines

DESIGN OF A COMPRESSION BASED HAND OPERATED BRICK MOULDING MACHINE

[1,2]Yakubu A.M., [1,2]Oji J.O., [1]Ogar M.O., [1,2]Oduola M.O., [1,3]Adetunji A. R.
[1]Prototype Engineering Development Institute Ilesa, Osun State
(National Agency for Science and Engineering Infrastructure, NASENI. FCT Abuja)
[2]Department of Mechanical Engineering, Federal University of Technology, Akure
[3]Department of Materials Science and Engineering,
Obafemi Awolowo University, (OAU) Ile-Ife
yakmoji79@yahoo.com

ABSTRACT
The need for shelter has greatly increased owing to an increase in population, urbanization, and industrialization. With the apparent failure of bricks in the form of cracks and in recent times the collapse of buildings and structures, it is evident that brick/cement blocks produced with conventional hand-moulding machines do not possess sufficient strength due to lack of proper bonding of aggregates mainly cement and sand even though they gain more strength upon production by curing over a period of time. This work presents the design of a compression based hand operated brick moulding machine to fundamentally possess sufficient strength than the conventional hand brick moulding machine. Generally, the weight of the platform imposes constraint on the effort required for both compression and ejection of the mould. This design ensured that a lesser weight of platform is achieved to still meet the quality requirements of modern buildings. From the result of the design analysis, it can be shown that the weight of the press platform, volume of mix in the hopper, stress on the resting rod, maximum bending moment, and theoretical efficiency are 15kg, 5175cm^3, 109.9KN/m^2, 1.35Nm, and 72% respectively. The machine is designed such that component parts can be easily developed, assembled, disassembled, and maintained.
Keywords*: brick, brick moulding machine, maximum bending moment, cracks, mechanical advantage, theoretical efficiency.*

INTRODUCTION

In recent times, with the apparent failure of bricks in the form of cracks and collapse of buildings and structures, it is evident that brick/cement blocks produced with conventional moulding machine do not possess sufficient strength. This is largely due to lack of proper bonding of aggregates mainly cement and sand even though they gain more strength upon production by soaking with water over a period of time According to [2], the quality of bricks
is determined by the reliability and efficiency of the brick machine, which will determine how strong the structure is, and consequently the maintenance cost of the said structure. Maintenance in simple terms is defined as all operations that are conducted on a system in order to retain its components and keep it in good working condition [3]. Maintenance operations are categorized as corrective preventive and scheduled maintenance operations. All these maintenance operations have to be explored for effective and efficient quality assessment of brick production [4].
A brick can be defined as a rectangular block of clay baked by the sun or in a kiln (an enclosed chamber in which heat is produced to fire, burn or dry materials), which is used as a building material or a paving material [5]). It is realized [6] that over the last 3 ½ decades machines for brick making were mainly intuition based backed up by general past mechanical design experience since this machines proved to be functionally feasible and economically viable. The popularity of hydraulic machinery is due to the very large amount of power that can be transferred through small tubes and flexible hoses, and the high power density and wide array of actuators that can make use of this power [7] and [8].
However, the energy considerations and the high costs associated with purchase and maintenance of hydraulic equipment have compelled most brick and block manufacturers to use mud blocks in place of the traditional burnt bricks. Generally, bricks are moulded hand by hand, but there is the need for a machine which would result in easier, faster and cheaper means of producing high compression bricks. Bricks are generally subjected to the tests such as water absorption, shape and size, compressive strength, hardness, efflorescence, soundness, and warpage tests to find out their suitability for construction work. Brick moulding machines come in different designs, types, shapes and sizes, but this work considers a simple hand operated brick moulding machine which uses compression as a basis to ensure proper bonding of constituents which make up the brick in order to meet the strength and quality requirements of modern buildings.

1. DESIGN ANALYSIS

The design criteria and selection of unit

In this design, the need is clearly defined, that is to make a machine that will improve the efficiency of the brick/block produced by the conventional machines. Factors that influence the design of this machine are essentially cost consideration and the availability of raw materials.

Design of Hopper Volume

Since the machine was designed for small and medium scale users, the hopper was designed in conformity with these dimensions.

$$\text{Hopper Volume} = lxbxh \quad \ldots\ldots\ldots\ldots (1)$$

Where;

l= length of the brick;

b=width of the brick;

h=height of the brick

Mass of the mix,

$$M_i = \text{density x volume} = \rho_m x V \quad \ldots\ldots\ldots\ldots (2)$$

Where;

ρ_m=Density of mix (kg/m^3)

V= Volume of the mix (m^3)

Load = fresh brick + weight of press platform assembly..... (3)

Stress (σ) on the resting rod [fulcrum]

This results from the application of forces. It is the total internal resistance in the member divided by its cross-sectional area, sometimes called the intensity of stress with unit in N/m^2 or KN/ m^2.

Mathematically [11],

$$\text{Stress } \sigma = {}^{P}/_{A} \quad \ldots\ldots\ldots\ldots\ldots\ldots\ldots\ldots\ldots\ldots (4)$$

Where,

P = Force or load acting on rod

Cross-sectional area, $A = \pi r^2$ .....(5)

r= radius of the rod (mm)

Bending Mo$\frac{M}{I} = \frac{\sigma}{Y} = \frac{E}{r}$**n** ..... (6)

The bending I rie shaft given by [11] is written as;

Where;

I_m = moment of inertia of the cross-section about the neutral axis,

M = bending moment acting at the given section,

σ= bending stress

E = young modulus of the material

r = radius of curvature

Y = distance from natural axis to the extreme fibre,

$$M = {}^{I_m \sigma}/_{Y} \quad \ldots\ldots\ldots\ldots\ldots\ldots\ldots\ldots\ldots\ldots (7)$$

Where;

$$I_m = {}^{\pi d4}/_{64} \quad \ldots\ldots\ldots\ldots\ldots\ldots\ldots\ldots\ldots\ldots (8)$$

Y= radius of the rod.

Design of the Frame of the Machine

The density of the material is given by [11] the equation:

$$\rho \frac{M_m}{V} \quad \ldots\ldots\ldots\ldots\ldots\ldots\ldots\ldots\ldots\ldots\ldots\ldots\ldots\ldots (9)$$

Where:

ρ = density of the material

M_m = mass of the material, (kg);

V = volume of the material, (m^3).

Design consideration for Mould and Brick

The brick designed for this work is an interlocking brick such that the laying does not require mortar; it just needs to be aligned together. The mould was designed such that the shape of the brick has slots and protrusion. The brick is shown in Figure 3

.

Compression of the bricks

On an average, the force produced by a man is approximately 200N [12], if he works continuously. Therefore human force may be used for a process if the power requirement is at maximum of 200N. If process power requirement is more than 200N and if the process can be of an intermittent nature without affecting the end product, a machine system can be developed that stores the energy.

Compression force: (figure 1)

$$Wh \times x = Pc \times y \quad \ldots\ldots\ldots\ldots\ldots\ldots\ldots\ldots\ldots\ldots (10)$$

$$P_c = \frac{Wh \times x}{y} \quad \ldots\ldots\ldots\ldots\ldots\ldots\ldots\ldots\ldots\ldots (11)$$

Where:

P_c= The compressive force.

W_h= Average human effort (N),

x= distance move by human effort (mm),

y= distance move by load (mm)

Force of Ejection , $P\varepsilon$: (figure 2)

This is given by;

$$Wh \times y = P\varepsilon \times x \quad \ldots\ldots\ldots\ldots\ldots\ldots\ldots\ldots (12)$$

$$P\varepsilon = \frac{Wh \times y}{x} \quad \ldots\ldots\ldots\ldots\ldots\ldots\ldots\ldots (13)$$

Efficiency of the machine, E_{mech}

$$Emech = \frac{\text{load} \times \text{distance moved by load}}{\text{Effort} \times \text{distance moved by effort}} \times 100 \ldots (14)$$

1. CONCLUSION

The conclusion is drawn based on the design and fabrication of the compression based hand operated brick moulding machine. The machine is portable, simple, and is designed in such a way that it can be easily transported from one building site to another, by carefully selection of durable and locally sourced raw materials for its fabrications. Work is in progress to obtain results of the performance evaluation of the machine. Also compressive strength test of the moulded samples will be carried out using standardized test procedures to compare the values with those of other literatures.

2. REFERENCES

[1] Yakubu A.M. et. al. (2003): design of a manually operated brick moulding machine. ND project Department of Mechanical Engineering. Federal Polytechnic Ida. Kogi State, Nigeria

[2] Mogaji P. B. (2011): Development and Performance Evaluation of Hydraulic Brick Moulding Machine. *Assumption University Journal of Technology Technical Report* 14(4): 308-312

[3] Meshkat, L., Dugan, J.B., Andrews, J. (2001): Maintenance modelling for computer-based systems.

Proceedings of the Institution of Mechanical Engineers, Part E: Journal of Process Mechanical Engineering 215(3): 221-31, August.
[4] Agbamu, E.A. (1999): Plant service and maintenance. 2nd ed., Joeseg Associates, Benin City, Edo State, Nigeria, pp. 28-30.
[5] Karnopp, D.C., Margolis, D.L., Rosenberg, R.C. (1990): System dynamics: A unified approach. John Wiley & Sons, Inc., New York, NY, USA, pp. 45-7.
[6] Modak J. P., Moghe, S. D. (1998): "Design & Development of a Human Powered Machine for the Manufacture of Line-flyash-sand Bricks" Human Power Vol. 13, pp 3-8 , *Journal of International Human Powered Vehicle Association*, U.S.A.
[7] Wolansky, W.D., Akers, A. (1988): Modern hydraulics: The basics at work. Merrill's series in mechanical and civil technology. Merrill Publishing Co., Columbus, OH, USA, Amalgam Publishing Co., San Diego
[8] Akers, A., Gassman, M., and Smith, R. (2006): Hydraulic power system analysis. CRC Press, Taylor and Francis Group, Boca Raton, FL, USA, pp. 23-34.
[9] Irtwange, (1998): In "postgraduate experience in the practice of mechanical, industrial and production engineering" by Ogundola Jide. A report submitted in partial fulfillment of the requirement for registration as an engineer of the Council for the Regulation of Engineering in Nigeria (COREN) May, 2011.
[10] Stapanoff (1969): In "postgraduate experience in the practice of mechanical, industrial and production engineering" by Ogundola Jide. A report submitted in partial fulfillment of the requirement for registration as an engineer of the Council for the Regulation of Engineering in Nigeria (COREN) May, 2011
[11] Khurmi R.S., Gupta J.K. (2005), *A Textbook of Machine Design*, 14th edition, Eurasia Publishing House (PVT.) Ltd, **Ram Nagar, New Delhi**
[12] Murell K. F.H., (1965): "Ergonomics, Man in His Working Environment", Chapman and Hall Ltd., London.

FIGURES

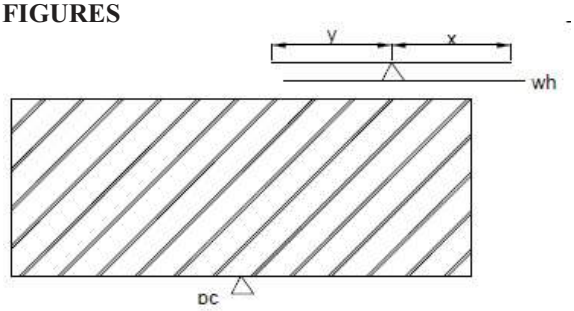


Figure 1: compression of brick

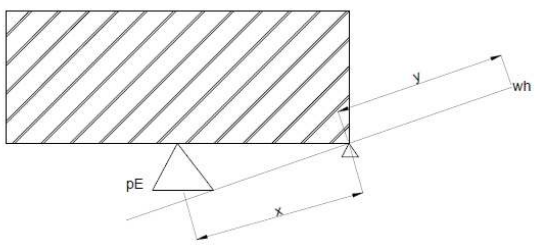


Figure 2: Ejection of brick

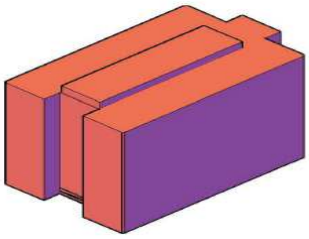


Figure 3: produced brick

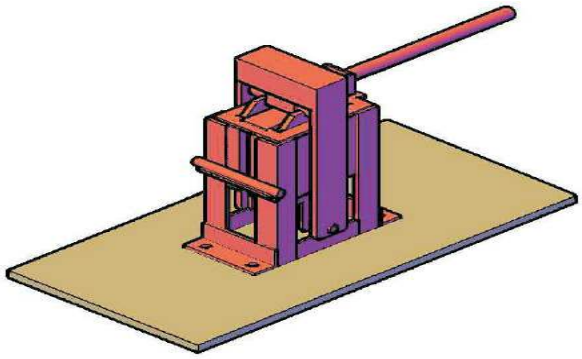


Figure 4: Machine assembly

TABLE

Results of design Calculation

NAME	ABBREVATION	VALUE
Stress on the resting rod	σ	109.9 KN/m^2
Force or load acting on rod	P	215.82N
Cross-sectional area of the rod	A	0.00196375 m^2
Force of Ejection of the mould	$P\varepsilon$	0.405 KN
The compressive force on the mould	P_c	0.654KN
Average human effort	W_h	200 N
Distance move by human effort	x	355mm
Distance move by load	y	240mm
Mass of the machine frame	M_m	40kg
Density of Mild steel	ρ	7800Kg /m^3

Maximum bending moment on the rod	M	1.35N m
Theoretical Mechanical Efficiency of machine	E_{mech}	72%
Length of the brick	l	23cm
Width of the brick	b	15cm
Height of the brick	h	15cm
Density of the mix	ρ_m	1350kg /m^3
Mass of the mix	M_i	7kg
Weight of press platform	W_p	15kg
Moment of Inertia of the rod	I_m	3.06E-07m^4
diameter o Rod	d	50mm
Young modulus of the material	E	200MN /m^2

A STUDY OF THE SOLVENT EXTRACTION OF TANTALUM(V) FROM AQUEOUS SULPHATE/FLUORIDE COLUMBITE LEACH USING TRIOCTYL AMINE IN MIBK

O. Sanda[1*], E. A. Taiwo[2] and G. A. Osinkolu[1]

[1]Centre for Energy Research and Development, Obafemi Awolowo University, Ile-Ife, Nigeria [2]Department of Chemical Engineering, Obafemi Awolowo University, Ile-Ife, Nigeria.
[*]osanda@cerd.gov.ng

ABSTRACT
Columbite with a combined Ta-Nb content of 35 % was leached using 20 M hydrofluoric acid. The acidity of the leach was adjusted with sulphuric acid and the tantalum-niobium content was extracted using methyl isobutyl ketone (MIBK) and trioctyl amine (TOA), with kerosene and xylene as diluents. The effect of pH and diluent type were investigated. Both tantalum and niobium were extracted to different extents, with greater degree of extraction observed for tantalum. Stripping and precipitation of the extracted species was performed using 30 % V/V ammonia solution. It was found that for systems involving TOA as extractant, kerosene proved to be a better diluent than xylene. Synergism was observed with respect to niobium extraction when solution of TOA in MIBK was used as the extractant. From studies carried out, it can be deduced that in stagewise separation of tantalum and niobium from the ore digest, the number of extraction stages can be greatly reduced using a TOA – MIBK blend in place of MIBK or TOA only.

1.0. INTRODUCTION

Liquid–liquid extraction is currently the most effective and the only practical way of separating tantalum and niobium to obtain high purity products such as oxides or complex fluorides that are used as precursors for the production of pure metal powders, carbides, and other products. The industrial process involved in the extraction of tantalum uses methyl isobutyl ketone (MIBK) as the extractant, although the other use of other solvents such as octanol [1,2] **and tertiary amines [3]** have been reported. Most these are however, built around single solvent systems which are usually multistage operations with large solvent inventory.

Various investigations on the extraction of metal values from their ores using a blend of organic solvents have been carried out by different researchers. The extraction of zinc and cadmium from chloride solution by mixtures of a primary amine and Bis(2,4,4-trimethylpentyl) phosphinic acid (CYANEX 272) was studied by Jia et al [4]. The synergistic effect was observed for the extraction of zinc while no synergistic effect for cadmium, which makes it possible to separate zinc and cadmium with the solvent mixture. The synergistic solvent extraction of thorium (IV) and uranium (VI) was investigated by Meera and Reddy [5] using mixtures of para-substituted 1-phenyl-3-methyl-4-aroyl-5-pyrazolones and crown ethers. Similar work was also done on lanthanoids [6, 7, 8] alkaline earth metals [9, 10], vanadium [11] and copper [12].

So far, most of the documented works on tantalum extraction have been based on single solvent systems. Most documentation on synergistic solvent extraction systems showed that extraction of the desired substances is greatly enhanced when a mixture of solvents is used and since many of the solvents used in the separation of uranium and rare earths also extract tantalum, it would be desirable to investigate synergism in solvent extraction with respect to tantalum. This work examines the possibility of a synergistic solvent extraction system for tantalum/niobium separation using MIBK and trioctyl amine (TOA) as the extractants with the purpose of reducing the number of extraction stages required for this separation to take place.

2.0. MATERIALS AND METHODS

The columbite used for this investigation was sourced from Wambe-Nassarawa field in Nassarawa State of Nigeria. Hydrofluoric acid (40 % v/v), sulphuric acid (98 % v/v), ammonia (SG 0.880), methyl isobutyl ketone (MIBK) and xylene were obtained from BDH Chemicals while trioctyl amine (TOA) was obtained from Sigma-Aldrich. All chemicals used are of analytical grade and were used without further purification. The kerosene used was however, obtained from a fuel station in Ile-Ife, Nigeria and distilled before use. Due to the corrosive action of hydrofluoric acid on glass, polypropylene containers were used as reaction and storage vessels in this work.

2.1. Preparation of the Aqueous Phase

The aqueous phase was prepared by dissolving 200 g of pulverized tantalite in 600 ml of 20 mol.dm^{-3} hydrofluoric acid in a thick walled polypropylene bottle immersed in a water bath maintained at 90 $^{\circ}$C for five hours. The reaction vessel was shaken at 15 – minute intervals while the dissolution process lasted. After five hours, the leach solution was decanted, further heated for 1 h to expel

most of the hydrofluoric acid present in the leach solution, made up to 5 litres and stored in polypropylene bottles.

Prior extraction, the leach medium was acidified with sulphuric acid such that the concentration of the sulphuric acid present varied from 0 – 5 mol.dm^{-3}, while the concentration of HF was maintained at 1.5 mol.dm^{-3}.

2.2. Preparation of the Organic Phase

The organic phase was prepared using methyl isobutyl ketone (MIBK) and tri octyl amine (TOA) as extractants. Kerosene and xylene were used as diluents. The organic phases were classified as S_1, S_2, S_3 and S_4 as shown in table 1.

2.3. Solvent Extraction of Tantalum

The solvent extraction stage was carried out at room temperature which throughout the duration of the experiment was found to be 28±2 °C. For each extraction step, 100 ml of the leach solution (the aqueous phase) and 100 ml the solvent were put in a polypropylene bottle and shaken for 20 minutes using a mechanical shaker set at 450 oscillations per minute. The mixture was later transferred to a polypropylene separating funnel where it was allowed to settle for 30 minutes, after which the raffinate was drained off. The tantalum content in the raffinate was then determined by UV-visible spectrophotometry using the methods of Marczenko and Balcerzak [13], and the tantalum value in the organic phase determined by difference.

2.4. Tantalum Recovery

The extracts obtained from the solvent extraction carried out on the leach solution prepared for tantalum recovery were shaken with 50 ml of 30 % (v/v) ammonia solution to precipitate the loaded metal species. The precipitates obtained were washed in distilled water to remove excess ammonia, dried at 110°C in an oven for 4 h, calcined in a muffle furnace at 800°C for 3 h, allowed to cool and weighed.

PIXE analysis was done on the samples obtained using 2.5 MeV protons from the 1.7 MV Tandem Accelerator at CERD, Obafemi awolowo University, Ile-Ife, Nigeria. For each run, the charge and the current were 0.5 μC and 0.26 nA respectively. All spectra obtained were analysed using the Gupixwin software (version 2.1).

3.0. RESULTS

3.1. Elemental Composition of the ore used

The PIXE spectrum shown in Fig. 1 shows the major constituents of the ore to be silicon (8.82 %), iron (10.74 %), tantalum (6.80 %), niobium (28.90 %), titanium (3.75%), tungsten (2.61 %) and manganese (4.72%), with, potassium, zirconium, vanadium, nickel, zinc, strontium, and ytterbium occurring in traces. The result of the elemental analysis is presented in Table 2.

3.2. Effect of Diluents

Comparing the performance of the two diluents used, it was found that the extraction of tantalum did better with kerosene as the diluent as shown in Fig. 2. Replacing the diluents with MIBK, the extraction of tantalum was found to improve (Fig. 2).

3.3. PIXE Analysis of Precipitates

Apart from tantalum, other components of the aqueous phase were found to have been extracted into the organic phase in varying degrees. The solid products derived from the extractions involving solvents $\mathbf{S_1}$ - $\mathbf{S_4}$ have been denoted $\mathbf{X_1} - \mathbf{X_4}$ respectively, and the results of the PIXE analysis carried out on the extracts are shown in figures 3 – 6.

The elemental composition of the ore leach, as well as those of solid products $X_1 - X_4$ are presented in table 3:

For the solvent systems studied, the distribution coefficients, as well as the tantalum separation factor (ratios of the distribution coefficients for tantalum and other elements extracted along with it) for an ore leach containing 4M H_2SO_4 and 1.5M HF are presented in tables 4 and 5 respectively.

3.4. Comparison of Extraction Systems

Suppose the solvent systems described were to be used in a continuous extraction operation which removes 99 % of the tantalum present in the leach. If the leach is considered to be dilute, the partition coefficients for the extracted species (presented in table 4) are needed in the determination of the minimum number of extraction stages required for the extraction of 99 % Ta using either crosscurrent or countercurrent systems.

3.4.1. Crosscurrent extraction system

If it is desired that fresh solvent be used in each stage, then a crosscurrent extraction system may be used. For crosscurrent system of solvent extraction, the theoretical number of stages (N) for the desired degree of extraction

$$N = \frac{\ln\left(\frac{x_a}{x_b}\right)}{\ln(1+E)} \qquad \text{---------- (1)}$$

where x_a and x_b are the initial and final concentrations of the substance to be extracted in the aqueous phase. E is the extraction factor which is given as:

$$E = \left(\frac{V_o}{V_a}\right) k_D \qquad \text{---------- (2)}$$

Using crosscurrent extraction system to effect the extraction of 99 % of the tantalum present in the leach with solvent ratio $\frac{V_o}{V_a} = 1.0$

the theoretical number of extraction stages is shown in table 6.

1.1.1. Countercurrent extraction system

If it is assumed that the distribution coefficient for any given system does not change much with changes in concentration of the extracted specie, then the relationship between the concentration of the extracted specie in both phases and the number of theoretical stages is given by Kremser equation shown below:

$$N = \frac{\ln\left[\left(\frac{x_a - \frac{y_b}{k_D}}{x_b - \frac{y_b}{k_D}}\right)\left(1 - \frac{1}{E}\right) + \frac{1}{E}\right]}{\ln E} \quad \text{--- (3)}$$

Where x_a and x_b are the initial and final solute concentration in the aqueous phase, y_b is the initial concentration of the substance to be extracted in the organic phase and k_D is the distribution coefficient for the extracted specie in the system under study.

For infinite number of countercurrent extraction stages, the minimum extraction factor E_{min} is given by

$$E_{min} = \left(\frac{V_o}{V_a}\right)_{min} k_D \quad \text{------ (4)}$$

where $\left(\frac{V_o}{V_a}\right)_{min} = \frac{x_a - x_b}{y_a - (x_b^*)k_D}$ ------- (5)

For countercurrent systems, the first task is to determine the minimum solvent rate $\left(\frac{V_o}{V_a}\right)_{min}$ required for an infinite number of stages. The minimum solvent ratio, is calculated for the systems under consideration using the equation below and is presented in table 7.

Using a solvent ratio of 3 (since this is slightly higher than the highest $\left(\frac{V_o}{V_a}\right)_{min}$ for tantalum as presented in table 7) along with the K_D values in table 5, the theoretical number of extraction stages was calculated and the results presented in table 8.

1.0. CONCLUSION

The extraction ability of TOA for tantalum is dependent on the type of diluent used. TOA – kerosene systems was found to give a better extraction kinetics for tantalum, compared with TOA – xylene systems, implying that the cost of extracting tantalum using TOA can be reduced using a relatively inexpensive diluent such as kerosene.

Extraction using MIBK, though adopted industrially as the method of choice for tantalum/niobium extraction and separation, can be improved on using a blend of TOA and MIBK as the extractant. For multi – stage extraction processes, fewer number of stages translates to lower operation costs. The synergistic effect of the TOA – MIBK system improves on the extraction efficiency and reduces the number of extraction stages, making it a recommended alternative for the traditional MIBK –based systems.

REFERENCES

[1] Mayorov V. G. and Nikolaev A. I. (2002) Tantalum (V) and niobium (V) extraction by octanol. Hydrometallurgy 66(1-3), 77-83

[2] Agulyansky A., Agulyansky L. and Travkin V. F. (2004) Liquid-liquid extraction of tantalum with 2-octanol. Chemical Engineering and Processing 43, 1231-1237

[3] El Hussaini O. M. and Rice N. M (2004) Liquid-liquid extraction of niobium and tantalum from aqueous sulphate/fluoride solutions by a tertiary amine. Hydrometallurgy, 72, 259-267

[4] Jia Q., Liao W., Li D. and Niu C. (2003) Synergistic extraction of lanthanum(III) from chloride medium by mixtures of 1-phenyl-3-methyl-4-benzoyl-pyrazalone-5 and triisobutylphosphine sulphide. Analytica Chimica Acta, 477(2-3), 251-256

[5] Meera R. and Reddy M. L. P. (2004) Para-Substituted 1-Phenyl-3-methyl-4-aroyl-5-pyrazolones as Chelating Agents for the Synergistic Extraction of Thorium(IV) and Uranium(VI) in the Presence of Various Crown Ethers. Solvent Extraction and Ion Exchange, 22(5), 761 - 789

[6] Ensor D. D. and Reynolds P. S. (1989) The use of crown ethers as synergistic extraction agents for trivalent lanthanides. Journal of the Less Common Metals 149, 287-290

[7] Pavithran R., Varma R. L. and Reddy M. P. (2003) Synergistic Solvent Extraction of Trivalent Lanthanoids with Mixtures of 1-Phenyl-3-methyl-4-pivaloyl-5-pyrazolone and Crown Ethers. Solvent Extraction and Ion Exchange, 21(6), 797 - 813

[8] Reddy K. J., Kumar J. R., Reddy A. V. and Reddy M. L. P. (2006) Synergistic Extraction of Zirconium(IV) and Hafnium(IV) with 4-Acylbis(1-phenyl-3-methyl-5-pyrazolones) in the Presence of Neutral Organophosphorus Extractants. Solvent Extraction and Ion Exchange, 24(3), 419 - 432

[9] McAlister D. R., Chiarizia R., Dietz M. L., Herlinger A. W. and Zalupski P. R. (2002) Extraction of alkaline earth and actinide cations by mixtures of di(2-ethylhexyl) alkylenediphosphonic acids and neutral synergists. Solvent Extraction and Ion Exchange, 20(4), 447 - 469

[10] Chiarizia R., McAlister D. R. and Herlinger A. W. (2003) Composition of the Organic Phase Species in the Synergistic Extraction of Sr2+ by Mixtures of Di(2-Ethylhexyl) Alkylenediphosphonic Acids and Dicyclohexano-18-crown-6. Solvent Extraction and Ion Exchange, 21(2), 171 - 197

[11] Remya P. N., Pavithran R. and Reddy M. L. P. (2005) Effect of Polymethylene Chain Length of 4-Acyl bis(1-phenyl-3-methyl-5-pyrazolones) on the Extraction of Vanadium(V): Synergistic Effect with Neutral Organophosphorus Extractants. Solvent Extraction and Ion Exchange, 23(4), 501 - 518

[12] Torkestani K., Blinova O., Arichi J., Goetz-Grandmont G. J. and Brunette J. P. (1996) Synergistic extraction of copper (II) and other divalent metals with 3-phenyl-4-acylisoxazol-5-ones and 1-phenyl-3-methyl-4-acylpyrazol-5-ones in the presence of tri-n-octylphosphine oxide in toluene. Solvent Extraction and Ion Exchange, 14(6), 1037 - 1056

[13] Marczenko Z. and Balcerzak M. (2000) Separation, preconcentration, and spectrophotometry in inorganic analysis. Elsevier BV, Amsterdam.

Table 1: Composition of the Solvents Considered for Study

Solvent	Composition
S_1	Pure MIBK
S_2	20g/L TOA in xylene
S_3	20g/L TOA in kerosene

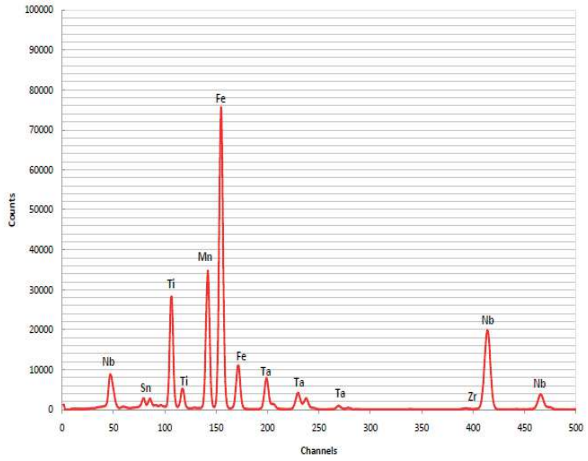


Figure 1: PIXE spectrum of the columbite showing the major elements present

Table 2: Elemental composition of the columbite used

Element	Concentration
Si	8.8251 wt. %
K	404 ppm
Ca	0.1000
Ti	3.7534
Mn	4.7241
Fe	10.7369
Ni	26 ppm
Zn	260 ppm
Sr	85 ppm
Y	17 ppm
Zr	0.2655 wt. %
Nb	28.8984 wt. %
Sn	0.9315 wt. %
Ta	6.7994 wt. %
W	2.6137 wt. %
U	0.7777 wt. %

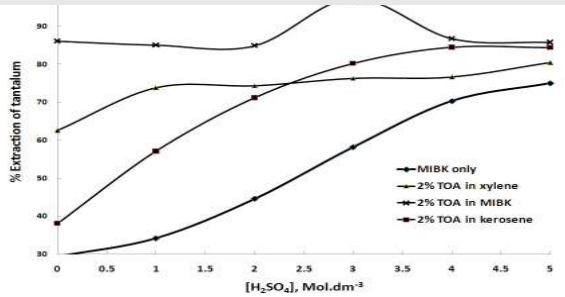


Figure 2: Effect of diluents on the extraction of tantalum using TOA

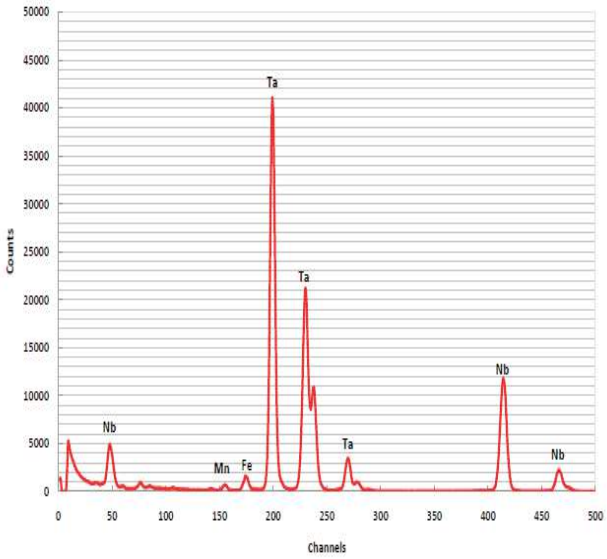


Figure 3: PIXE spectrum of product X_1

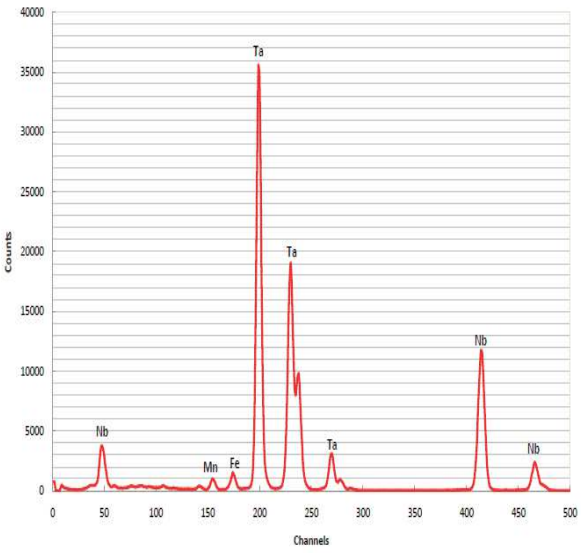


Figure 4: PIXE spectrum of product X_2

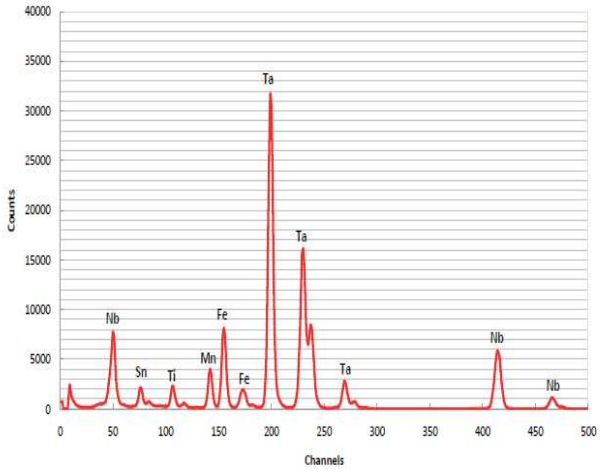


Figure 5: PIXE spectrum of product X_3

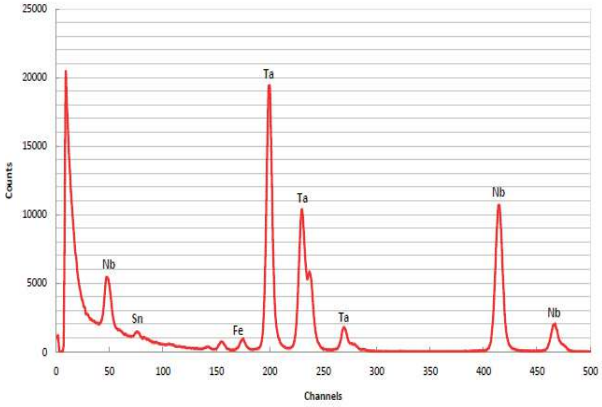


Figure 6: PIXE spectrum of product X_4

Table 3: Elemental composition of the ore leach and the extraction products obtained ([H_2SO_4] = 4 M, [HF] = 1.5 M)

Extracts	Elemental composition (wt %)							
	Zr	Ti	Sn	Mn	Fe	Ta	Zn	Nb
Ore leach	0.407	5.333	3.252	5.162	16.270	38.407	0.0155	15.105
X1	0.0218	0.063	3.585	0.087	0.0191	57.386	0.0125	21.477
X2	0.0210	0.048	4.354	0.194	0.0385	56.270	0.0133	22.668
X3	0.0200	0.841	5.494	1.385	0.2847	60.152	0.0121	14.574
X4	0.0029	0.157	4.658	0.099	0.0322	44.523	0.0121	34.405

Table 4: Distribution coefficients of the various elements present in the leach

Elements	X01	X02	X03	X04
Zr	0.3269	0.1223	0.1220	0.0300
Ti	0.0055	0.0019	0.0361	0.0120
Sn	1.0311	0.3954	0.5946	1.3680
Mn	0.0078	0.0080	0.0629	0.0078
Fe	0.0054	0.0050	0.0402	0.0080
Ta	2.2048	0.4493	0.5283	0.8779
Zn	0.5899	0.2210	0.2073	0.4618
Nb	1.8958	0.4653	0.2706	11.2764

Table 5: Separation factors for the major elements extracted with respect to tantalum

Elements	X1	X2	X3	X4
Zr	6.74	3.67	4.33	29.27
Ti	403.48	233.85	14.65	70.02
Sn	2.14	1.14	0.89	0.61
Mn	282.45	56.03	8.40	107.65
Fe	405.01	89.40	13.15	104.38
Ta	1.00	1.00	1.00	1.00
Zn	3.74	2.03	2.55	1.90
Nb	1.16	0.97	1.95	0.08

Table 6: Theoretical number of stages for the extraction of 99 % Ta along with other accompanying elements using crosscurrent extraction system $\left(\frac{V_o}{V_a} = 1.0\right)$

Solvent	Theoretical number of stages (N) required for 99 % Ta extraction	% Extraction of accompanying elements after N stages							
		Zr	Ti	Sn	Mn	Fe	Ta	Zn	Nb
S_1	4.0	67.32	2.15	93.93	3.03	2.11	99.00	84.01	98.51
S_2	12.4	76.11	2.33	98.40	9.42	6.00	99.00	91.61	99.13
S_3	10.9	71.34	31.96	99.37	48.43	34.81	99.00	87.07	92.57
S_4	7.3	19.43	8.35	99.82	5.52	5.66	99.00	93.76	>99.99

Table 7: Minimum $\left(\frac{V_o}{V_a}\right)$ required for the extraction of 99 % of the tantalum or niobium content in the feed

Solvent	k_D for Ta	k_D for Nb	$\left(\frac{V_o}{V_a}\right)_{min}$ for Ta	$\left(\frac{V_o}{V_a}\right)_{min}$ for Nb
S_1	2.20	1.90	0.449	0.522
S_2	0.45	0.47	2.203	2.128
S_3	0.53	0.27	1.874	3.659
S_4	0.88	11.28	1.128	0.088

Table 8: Theoretical number of stages for the extraction of 99 % Ta along with other accompanying elements using countercurrent extraction system $\left(\frac{V_o}{V_a} = 3.0\right)$

Solvent	Theoretical number of stages (N) required for 99 % Ta extraction	% Extraction of accompanying elements after N stages							
		Zr	Ti	Sn	Mn	Fe	Ta	Zn	Nb
S_1	2.4	69.48	1.65	95.14	2.34	1.62	99.00	86.67	98.61
S_2	11.0	36.69	0.57	97.24	2.40	1.50	99.00	66.05	99.26
S_3	7.9	36.59	10.83	99.54	18.87	12.06	99.00	61.62	77.67
S_4	4.3	9.00	3.60	99.82	2.34	2.40	99.00	91.57	>99.99

POTENTIALS OF UKWA TREE (*sterculia setigera)* AS A SOURCE OF RAW MATERIAL FOR PULP AND PAPER MAKING

[1]Anyanwu, B.U, [2]Olokode, O.S, [3]Aiyedun, P.O, [4]Oyeleke Y.T.
[1-4] University of Agriculture, Abeokuta. Mechanical Engineering Department.
engr_olokode@yahoo.com

ABSTRACT
The fiber and physical characteristics of Ukwa trunk *(Sterculia setigera),* a tropical hardwood specie and also an agricultural residue were investigated. The Ukwa trunk was sourced locally and then debarked. Thereafter, the debarked trunk was chopped into chips of average lengths ranging from 0.3cm to 0.6cm. These chips were gathered and then measured into weights in grammes of 100's. Variable percentage (20%, 40%, 60%, 80%) concentrations of sodium hydroxide (NaOH) were used to pulp different specimens of chips of fixed weights (100g), at a constant time of two (2) hours. The resultant pulps were bleached with 100ml of hydrogen peroxide, H_2O_2 and 5 spoon full of titanium oxide, TiO_4 to improved its brightness. Fiber characteristics and other physical properties of the pulps were obtained and hand-made writing papers were made from these pulps. Finally, different tests in accordance with the Technical Association of Pulp and Paper Industry (TAPPI), U.S.A were carried on the resultant papers and their results compared to those obtained in commercial writing papers. The results compares favourably with those stipulated by TAPPI (1990) and with properties of machine produced commercial writing papers available in Nigeria.

Keywords: Ukwa tree, Pulp, Paper making, Handmade, Fiber, Ash.

INTRODUCTION

The forest Industries subsection of the third world forestry congress, held in Helsinki, Finland, 1949, recommended that in order to enthrone sustainable wood-based forest Industry, there should be an urgent need to widen the sources of potential wood-based fibrous raw materials for Pulp and Paper Industries, by experimenting with tropical hardwood in pulp and paper making [2, 5 and 7].

However, available records indicate that the supply of industrial hardwood is far short of demand in Nigeria (World Bank, 1992). Harvesting pressures on forest in order to meet industrial demand, has in the past resulted in cutting above the Annual Allowable Cut (AAC) and consequent environmental degradation [8 and 9].

Ukwa tree (Sterculia setigera) is a tropical horticultural hardwood species widely grown for its fruits in Sub-Saharan Africa. The tree is widely grown in the rainforest and savanna vegetation belts if Nigeria. It grows to merchantable height, 23m force bole. The wood fibrous raw materials, had at best only been used for fire wood and often burnt, and ashes incorporated into ingredients for local soap making. In view of the wide spread planting of this species, finding an efficient industrial outlet for the fiber, will be an appropriate technology. Available records are that Nigeria's capacity to meet her industrial fivers needs by the year 2010 will be in serious jeopardy unless alternative fiber sources and sustainable industrial wood management is enthroned [3 and 6].

The use of woody and/or agricultural residue for meeting the fiber needs of the wood-based composite Industry is widely practiced [6 and 10].

However, the technical property requirements for optimal and efficient production will vary depending on industry and it's because of this that it is essential to carry out empirical study to understand the characteristics of a particular timber/lignocelluloses species. This is because wide variabilities are known to exist between different parts of same species. There is therefore a compelling need to understudy the potentials of Ukwa trunk, an agricultural residue, as an industrial fiber source.

MATERIALS AND METHOD EXPERIMENTS

The experiment was carried out in two (2) stages stated thus:

- Determination of the fiber and physical characteristics of the pulp and then noting the optimal pulping conditions using variable sodium hydroxide (NaOH) concentrations.
- Production of hand made paper from the resultant pulp.

Determination of the fiber and physical characteristics of the pulp and then noting the optimal pulping conditions using variable sodium hydroxide [NaOH] concentrations.

- Apparatus used
- Automated Optical Analyzer
- Electric Weighing Balance
- Oven
- Dessicator
- Earthen ware pot
- Measuring cylinder [cm]
- Test specimen
- Silicate dish
- Mortar and pestle
- Stirrer
- 100ml Beaker

- Plastic Bucket
- Pressing Iron
- Calico material i.e. white absorbent cloth

Reagents Used

- Nitric Acid, this was used during ashing to peed up the reaction and burn off organic matters quickly.
- Sodium Hydroxide pellets, used during the pulping
- Hydrogen peroxide, H_2O_2 used to bleach the pulp.
- Titanium oxide, TiO_4, used to improve the whiteness of the pulp
- Water, H_2O.

PULPING OF SPECIMEN

0.2g of sodium hydroxide, NaOH, pellets were dissolved in 100mL of water in a beaker, to produce 20% of NaOH concentration.

A fixed sample (100g) of specimen was properly fed into and earthen ware pot and 20% NaOH concentration was added to it and stirred. The mixture was then placed on a hot plate at 100^0C and allowed to digest fully. The time taken for this was 2 hours. It was recorded and kept fixed for other variations of NaOH concentrations. The pulp obtained (slightly brownish in colour) was bleached by adding 100mL hydrogen peroxide, H_2O_2, and about five (5) spoon-full of titanium oxide, TiO_4, in a plastic bucket. This whole mixture was then left for 24 hours to enhance proper brightness of the pulp, the bleached pulp was then washed with about seven (7) liters of water in a bucket.

These procedures were repeated for 40%, 60% and 80% NaOH concentration.

Finally, the yield percent of the pulp obtained was calculated using the relations.

$$Pulp\ yield = \frac{Weight\ of\ oven\ dry\ pulp}{Weight\ of\ oven\ dry\ specimen}$$

FIBER CHARACTERISTICS OR FIBER LENGTH OF PULP.

A sample of the pulp specimen derived from 20% NaOH was dropped on the slide of an Automated Optical Analyzer. It was then viewed from the microscope attached in the analyzer. The length of the fiber in the pulp was then read – off from the scale provided in the analyzer. This value was then recorded. The same procedures were carried out for samples of pulp made from 40%, 60% and 80% NaOH concentrations, and their corresponding fiber lengths recorded respectively.

DETERMINATION OF MOISTURE CONTENTS

A fixed weight of pulps specimen derived from 20% NaOH concentration was oven dried at 105 ± 2^0C in ventilated oven for 24 hours. At the end of this period, the dried oven pulp was quickly weighed and returned to the oven until two consecutive readings indicated no further weight loss. This was taken as the oven dry weight of the pulp specimen.

The moisture content in percentage was then calculated from the relation below:

$$MC(\%) = \frac{W_w - W_d}{W_d} \times 100$$

Where, MC = Moisture content

W_w = Initial weight of the Pulp specimen

W_d = Oven dry weight of the pulp

These whole procedures were repeated for the same weight of pulp specimen derived from 40%, 60% and 80% NaOH concentrations, respectively.

DETERMINATION OF THE ASH CONTENTS OF SPECIMENS

In doing this, a given weight of the specimen derived from 20% NaOH concentration, oven dried; was placed on a weighted empty silicate dish and then reweighed. 5mL nitric acid was added to the specimen (this helped to bring the specimen into ash by burning off the organic matters). This whole arrangement was then placed in a oven at temperature of 105^oC for about 2 hours, until it was completely ashed. It was then removed from the oven and allowed to cool undisturbed over a 24 hours period. The ash content was then calculated from the expression.

$$Ash\ Content(\%) = \frac{B_1}{B_2} \times 100$$

Where B_1 = Weight of Ash and B_2 = Weight of Oven Dry Specimen

These procedures were repeated for pulp specimens derived from 40%, 60% and 80% NaOH concentrations respectively.

DETERMINATION OF SPECIFIC GRAVITY OF PULPS SPECIMEN

A give weight of the pulp specimen derived from 20% NaOH concentration was first oven dried. This was done by placing the specimen in an oven at about 100^oC for 3 hours and weighed at specific intervals until its weight became constant. The specimen was t hen removed from the oven, cooled in a desiccators and weighed. The volume of the specimen was determined by Archimedes principle, that is, a small sample of the over dry specimen was weighed. Water was poured into a measuring cylinder and the volume rerecorded. The oven dried specimen was then added to the water and the extent to which the level of water increased was recorded. The density of the oven dry specimen was then obtained from the relation:-

$$\rho_{OVEN\ DRY\ SPECIMEN} = \frac{Weight\ of\ oven\ dry\ specimen}{Volume\ of\ oven\ dry\ specimen}$$

Finally, the specific gravity of the specimen was obtained from the relation below:-

$$G = \frac{\rho_{OVEN\ DRY\ SPECIMEN}}{\rho_{WATER}}$$

Where $\rho = density$

$G = Specific\ gravity$

These procedures were then repeated for pulp specimens derived from 40%, 60% and 80% NaOH concentrations respectively.

PRODUCTION OF HANDMADE PAPER

- **Bleaching and Sizing:**

As reported earlier during the pulping process, 100ml of hydrogen peroxide was added to the unbleached pulp in a plastic bucket and left for about 24hours. Lignin is the dominating source of color in the unbleached pulp, but on bleaching, the lignin and other discoloring substances were brightened or removed. The bleached pulp was later washed with about 7litres of water in a bucket until it is neutral to litmus. The color of the bleached pulp becomes whitish

- **Binder:**

6g of commercial starch was made from 20% sodium hydroxide solution. These was then added to the bleached pulps

- **Screening:**

The pulp mixture was poured on a handkerchief placed on a tray. The handkerchief was carefully raised up, stretching it properly to see that pulp fills every space for proper interlocking of the cellulose fiber.

- **Pressing & Calendaring:**

The pulp on the handkerchief was covered with an absorbent calico cloth and placed on a plank ready for pressing with blocks, after which it was kept under the sun to dry up. Finally, the paper was calendared using a pressing iron to achieve smoothness.

- **Product Testing:**

Three physical property test were carried on the handmade papers produced and these were done in accordance with the procedures stipulated by the Technical Association of Pulp and Paper Industry (TAPPI, 1990) USA. The test includes caliper/thickness test, burst strength and moisture absorption tests. The tests were carried on each sheet of papers produced from the resultant pulps of 20%, 40%, 60% and 80% NaOH concentrations. The results were finally compared with that of commercial papers.

RESULT AND DISCUSSIONS

The Results are presented in tables 1 to 8

Discussions:

From table1 it can be seen that pulp yield (a property which gives the relative return of pulp compared to the raw chips used, wt/wt basis) increase as NaOH decreases and vice versa. This is in keeping with the range reported in the literature for semi-chemical pulps, [4, and 10]. It is pertinent to note that the pulp yield is a function of paper thickness produced. The more the pulp, the thicker the paper [2].

Considering table 2, the mean fiber length as reported is within the range of hardwoods. The fiber lengths as reported represent the average of twenty fiber measurement selected at random. The variable fiber lengths with concentrations of NaOH used is not sustained by any scientific facts or theory. However, one possible explanation is that out of inexperience, the random selection of chips from the trunk was not effective and thus error emanating from growth related of variability in trees was introduced.

From table 3, it could be observe that there were variations in the moisture contents of the specimen for the various concentration of NaOH. As the concentration of NaOH increases, the percentage moisture content also increases. The mean ash contents for the pulps produced using different NaOH concentrations is presented in table 4. From the table, there is a marginal decrease in ash content as the concentration of the chemical used in pulping increases. One possible explanation is that lignin and other peptic substances removed from the middle lamellae/ primary wall tends to contain more of the earthy substances. On closer observation, however, it does appear that the average ash content recorded is above the average reported for wood and lignocelluloses materials. One possible explanation is the carbonization process was incomplete and thus, the recorded ash content contains some other impurities. However, it is not unusual to record deviations away from average and thus, further work is required to determine conclusively the average ash content of *sterculia setigera* (ukwa trunk).

Table 6,7 and 8 shows the test results and it can be seen that when compared to those of commercial papers, the optimal pulping conditions were achieved at NaOH concentrations range of between 40% and 60%.

CONCLUSION AND RECOMMENDATION

The study has shown that pulp and paper could be produced from ukwa trunk (*sterculia setigera*) a tropical hardwood species and an agricultural residue. The quality of pulp and paper produced, especially by the 40% and 60% NaOH concentrations gave technical properties that are close to that of commercial pulps and papers.

Additionally, pulps produced from a process as used in this study will be suitable for production of commercial writing papers, corrugated boards, fiber boards and some industrial paper.

RECOMMENDATION

Based on the findings, on the course of the project work and having produced good quality hand-made papers from indigenous ukwa tree, we here by recommend that:

Farmers should be encouraged to plant this species of trees to ensure the quantities of its supply for industrial paper productions, even when other hardwood species fall in quantities.

REFERENCES

1. Anichukwu R.C. IT Report on Pulp and Paper and making at Nigeria Paper Mill Jebba, 1990.
2. Anon, (1955), The Dictionary of Paper, 3rd Edition. American Paper and Pulp Association, U.S.A.
3. Anon (1971) TAPPI T20505 71, Forming Hand Sheets for Physical Tests of Pulp
4. Cassey J.P (1980) Pulp and Paper Chemistry and Chemical Technology, 2nd Edition, pp 985 – 989.
5. Miller K.T, Consulting Engineers World Straw Conference, Eugen Oregun 1975
6. Nnabuife E.L.C and Ikwueze W.O. (1993) Paper Recycling, Nigeria Scene four "p" News, Volume 5.
7. Schniewind A.P. (1989). Concise Encyclopedia of Wood and Woode based methods, 354 pp.
8. Shenwood P.M (1983). Project Evaluation in the

Paper Industry Pulp and Paper Magazine, Canada.
9. Timmell, T.E. (1988). Encyclopedia of Material Sciece and Engineering, Volume 7 (T-Z) (pg 5403-5408), U.S.A..
10. Onuorah O.E. (2001). Preliminary Investigation of the Potential of Six Nigerian Grown Hardwood Species as sources of fiber for the Pulp and Paper Industry (Journal of Agricultural Technology (JAT).

Table 1. Percentage Pulp Yields of Specimen.

NaOH(%) concentration	Weight of oven dry pulp (g)	Weight of oven dry specimen (g)	Pulp yield (%)
20	64	100	64
40	62	100	62
60	61	100	61
80	58	100	58

The table above represents the average percentage pulp yields obtained from pulping the specimen (ukwa trunk) using different NaOH Concentrations.

Table 2: Mean fiber lengths obtained from specimen, pulped at different NaOH concentrations.

NaOH(%) concentrations	Fiber length (cm)
20	0.58
40	0.58
60	0.59
80	0.60

Table 3: Moisture Contents of Specimen pulped at different NaOH concentrations.

NaOH(%) concentrations	Initial weight of pulp Ww (g)	Oven dry weight Wd (g)	Moisture content (%)
20	115	103	11.65
40	115	102	12.75
60	115	101	13.86
80	115	100	15.00

Table 4: Ash Contents of Oven Dry specimen as pulped under various NaOH concentrations.

NaOH(%) concentrations	Weight of Ash (g)	Weight of oven dry specimen (g)	Ash Content (%)
20	17.0	100	17.0
40	15.5	100	15.5
60	14.0	100	14.0
80	12.0	100	12.0

Table 5: Specific Gravity of Specimen, pulped at different NaOH concentrations

NaOH (%) conc.	Density of oven dry specimen (g/cm^3)	Density of water (g/cm^3)	Specific gravity
20	0.29	1.00	0.29
40	0.28	1.00	0.28
60	0.28	1.00	0.28
80	0.27	1.00	0.27

Tests Results:

Table 6: Mean caliper/thickness of handmade paper obtained from various NaOH concentrations.

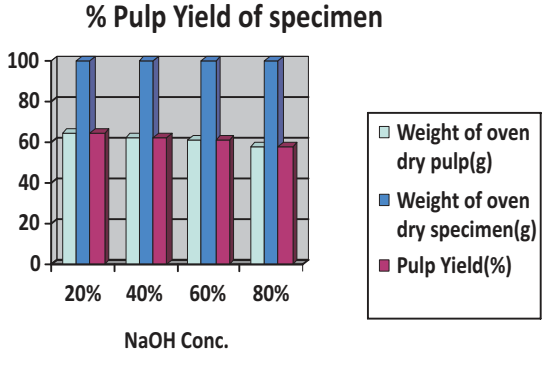
NaOH(%) concentrations	Thickness (mm)
20	0.40
40	0.30
60	0.19
80	0.10
Commercial paper	0.25

Table 7: Burst Strength of handmade paper obtained from various NaOH concentrations.

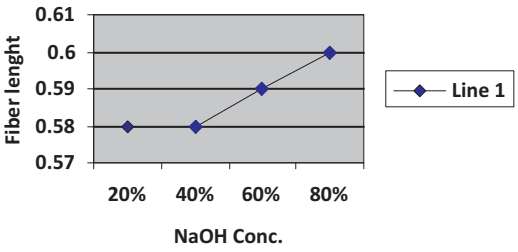
NaOH(%) concentrations	Burst Strength (Nm^{-2})
20	4.89
40	3.89
60	3.20
80	2.10
Commercial paper	3.60

Table 8: Moisture absorption of handmade paper obtained from various NaOH concentrations.

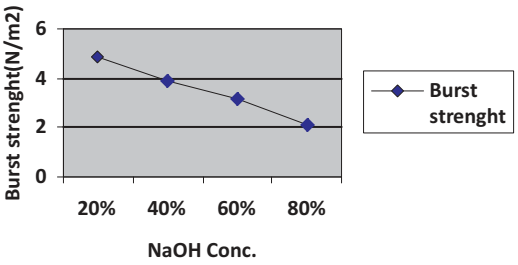
NaOH(%) concentrations	Moisture Absorption (g)
20	0.04
40	0.09
60	0.14
80	0.20
Commercial paper	0.12



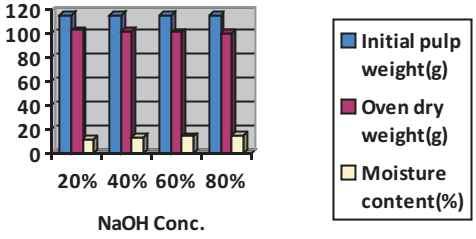
Mean Fiber lenghts



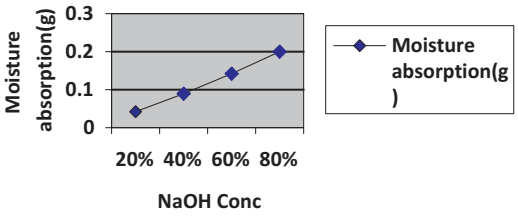
Burst strenght of handmade paper



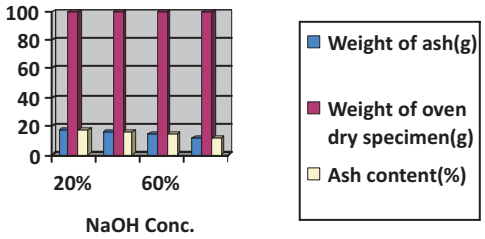
Moisture contents of specimen



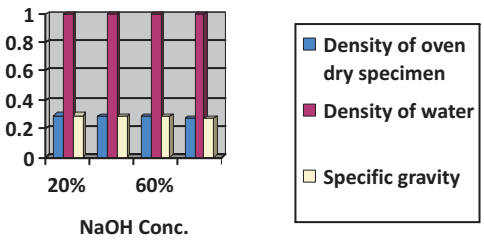
Moisture absorption of handmade paper



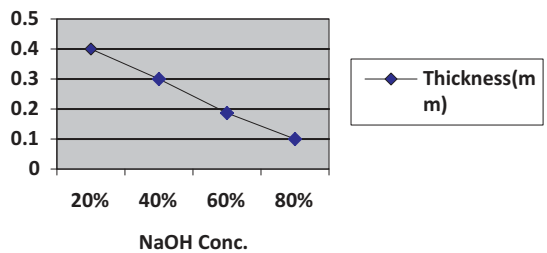
Ash contents of oven dry specimen



Specific Gravity of Specimen



Mean caliper thickness



SYNTHESIS AND COMPARATIVE ANALYSIS OF SAMPLES OF DYE SENSITIZED SOLAR CELLS USING TIO_2 FILMS

Nwanya A. C.[1], Ezema F.I.[2] and Oparaku O.U[1].
1 National Centre for Energy Research and Development, University of Nigeria, Nsukka.
2 Department of Physics and Astronomy, University of Nigeria, Nsukka
Corresponding author: chinweasum@yahoo.com

ABSTRACT
TiO_2 films were prepared on FTO glass using the sol-gel process, the chemical bath deposition method and the slot coating of P-25 Degussa TiO_2 powder for fabrication of samples of dye-sensitized solar cells. Ruthenium red dye R2751 and dye extracts from jathropha and orange citrus leaves were used for the sensitization. $TiCl_3$ was used as a precursor in the sol gel and CBD methods. The chemical, structural, morphology and optical properties of the TiO_2 were investigated using energy Dispersive Spectrum EDS, X-ray diffraction XRD, UV-Visible-Infrared spectroscopy and Scanning Electron Microscopy SEM. The XRD analysis showed a mixture of anatase and rutile phases of TiO_2 in both the slot coated and the CBD deposited films while that of the sol gel was predominantly anatase. The calculated crystallite sizes were in the nanometer range. The morphology of the films showed that they were porous and homogenous. That of the slot coated showed a flower-like structure. The band gap energies determined from the methods were between 3.22-3.62eV. The slot coated TiO_2 with jathropha leaf dye extract showed the highest overall efficiency of 1.26% with open circuit voltage of 350mv, short circuit current of 65.5 μA and a fill factor of 0.55.

Key words: TiO_2, sol-gel, chemical bath deposition, solar cell efficiency.

1.0 Introduction

Titanium dioxide TiO_2 is a wide band gap n- type semiconductor that has received a wide range of attention due to its chemical and optical properties. It finds applications in various fields of science and technology. TiO_2 is used in photo catalysis [1-3], photovoltaic devices [4-6], sensors [7-8], water treatment and in batteries [9]. TiO_2 exists in both crystalline and amorphous forms and mainly exists in three crystalline polymorphs, namely, anatase, rutile and brookite. Anatase and rutile have a tetragonal structure, whereas brookite has an orthorhombic structure. The densities are 3.89g/cm^3, 4.26g/cm^3 and 4.13g/cm^3 for anatase rutile and brookite respectively [10,11]. It is generally accepted that the properties of TiO_2 thin film depend on their microstructure, morphology, porosity and crystallinity and these depends on the method of preparation. Nanocrystalline TiO_2 film can be prepared through the sol gel route [6, 12-13], chemical bath deposition method [14, 15], vapour deposition [10,16-18], SILAR method [19] and by pyrolysis [7,20]

Photovoltaic (PV) energy is known to be one of the cleanest energy sources with a very small carbon footprint. However, owing to the high cost of conventional solar cells, which are mainly based on Si, PV electricity is not competitive for large scale power production. Dye-sensitized solar cells (DSSCs) are attractive low cost PV cells and can be made by using a rather simple solution processing technique in simple laboratory. Typically, DSSCs are composed of a dye-adsorbed nano-porous TiO_2 layer on a fluorine-doped tin-oxide (FTO) glass substrate, redox electrolytes and a counter electrode [21-26]. The nano size TiO_2 colloids used for DSSC are sintered on a transparent conducting substrate. The sintering process forms electrical contact between the various colloids and between the colloids and the substrate [27]. It has been shown that the efficiency of DSSC depends significantly on the properties of the nanostructured TiO_2 electrodes. The surface area of the film determines the dye uptake, the pore size distribution affects the ion diffusion, the particle size distribution determines the optical properties and the electron percolation depends on the interconnection of the TiO_2 particles [28]. Hence it can be said that the art of preparing high efficient DSSC is the art of controlling the properties of the TiO_2 electrode. In this work TiO_2 electrode was prepared using the sol gel dip coating, chemical bath deposition and the slot coating methods. The prepared films were used for the fabrication of samples of DSSCs.

2.0 Experimental Details

Three methods were used to deposit the TiO_2 electrode and they are:

2.1. Slot Coating Method using commercially available Titanium (IV) Powder.

The colloidal TiO_2 paste was prepared using TiO_2 powder P25 Degussa based on the procedure described by Greg and Gratzel [29]. 6g of the aggregated powder was ground in a mortar and while grinding, 10ml of very dilute acetic acid with PH 3-4 in deionizer water was added in drops of 1ml to prevent re-aggregation of the particles. After a colloidal suspension is obtained, few drops of Triton X-100 surfactant were added. Adhesive tape is applied on the conductive side of the fluorine doped tin oxide substrate FTO that has been cleaned to

mask a strip of about 1mm on each side. Few drops of the TiO_2 suspension was applied on one edge of the substrate near the tape and a clean glass rod was used to slide the paste uniformly on the FTO. After the deposition the tape was carefully removed and the plate was allowed to dry for a few minutes at room temperature. This was then sintered at 400^{0}C in an oven for 45minutes.

2.2. Chemical Bath Deposition Method

5ml of 1M NaOH solution was put in a beaker containing 5ml of deionised water. 3ml of $TiCl_3$ (analytical grade) was gradually added to the solution while being stirred on a magnetic stirrer. After the addition of the $TiCl_3$ the entire solution was further stirred for about ten minutes. The FTO which has being cleaned as previously discussed is now immersed fully into the solution. The film is allowed to deposit on the substrate for 24 hours at room temperature. After which the substrate is brought out rinsed with deionised water and sintered at 400^{0}C for 1 hour. The chemical reactions are as shown below:

$$Ti^{3+} + 3OH^- \longrightarrow Ti(OH)_3 \quad 1$$

$$Ti(OH)_3 + OH^- \longrightarrow TiO_2 + 2H_2O \quad 2$$

It was noticed that longer stay of the substrate in the solution gave a thicker deposition. Also the pH of the resultant solution is found to play vital role during film deposition hence the pH was maintained at 3.5 with the drop wise addition of NaOH solution at room temperature.

2.3 Sol-Gel method

1M NaOH was dissolved in 50ml of ethanol solution to which of 5ml of acetic acid has been added. The mixture was stirred vigorously on a magnetic stirrer at 65^{0}C for 3hrs. 7ml of $TiCl_3$ was added dropwise to the solution while the stirring is on. It was observed that the each drop of $TiCl_3$ changes the sol to ash colour and then to white with continued stirring. Previously cleaned and taped FTO glass as described above is dipped into the solution. A gel film was formed on the FTO. This was left for a few minutes in the open air to dry and then sintered at a temperature of 100^{0}C for 30mins. This was brought out and rinsed with deionised water and annealed again for 1hour at 400^{0}C. The concentration ratio of $TiCl_3$ and acetic acid was altered to see the effects on the deposited film. The stirring time was also changed but the sol manufactured due to the method described above was used to produce coating on the substrate. The flow chart for the processes is as shown in figure 1.

2.4 Extraction of natural dye and synthetic dye Preparation and Sensitization

The dye sensitization of the electrodes was done using natural and in-organic dyes. The natural dyes used were extracted from the leaves of two plants viz; jatropha and orange citrus. Jatropha seeds have been used in the production of bio fuels hence the motive to use its leaves is to ascertain whether the leaves are good candidate for natural dye for DSSC while the use of orange citrus was to confirm what other authors have done. The extraction procedure is described below.

Fresh leaves obtained from the aforementioned plants were put in a cup. Boiling water was poured into the cup until it covers the sample leaves for 30 seconds to 1minute. The leaves were removed from the water and dried with paper towel. Boiling water kills the cells and destroys the enzymes which can promote chlorophyll degradation. It also breaks chloroplasts which makes chlorophyll extraction easier. The petioles and central veins were removed from the leaves because these parts of leaf do not contain a lot of pigments. The leaves were cut into small pieces and spread evenly on a foil and put in the oven for 20 minutes at 40^{0}C. The dry leaves pieces were ground and the powder was put in a test tube with tight lid and a few milliliters of ethanol were added. The lid is closed and shaken. This was left for 24hrs in a dark cupboard and then is centrifuged. The centrifuged solution was now poured into another test tube and the lid was opened for some minutes for some of the solvent to evaporate. The remaining plant pigment was now stored in a dark cupboard ready for use.

Inorganic dye used is ruthenium red dye R2751 $[(NH_3)_5RuORu(NH_3)_4ORu(NH_3)5]Cl_5$ obtained from Sigma-Aldrich company Germany. 3x 10^{-4} M solution of the synthetic dye was prepared by dissolving 10mg of the dry ruthenium dye powder in 25ml of methanol and stirring until no traces of solid dye are visible. The result was a dark purple solution which was stored in a non transparent bottle. The staining of the above prepared TiO_2 electrodes was done by heating the electrodes again to about a temperature of about 60^{0}C in the oven and immersed immediately into the already prepared dye solution. This is done in order to remove any water possibly deposited from the ambient air to the TiO_2 films. The TiO_2 electrodes were kept in the dye solution in the dark for about 24hrs. The stained electrodes looked yellowish green in the case of the natural dye but purple red in the case of the ruthenium dyes.

2.4 Electrolytes

0.5M Potassium iodide KI was mixed with 0.05M iodine I_2 in acetonitrile. This was done by putting 0.127g of I_2 and 0.83g of KI in 10ml of acetonitrile. The mixture was stirred until all the solid has dissolved. The solution was stored in a dropper bottle for further use.

2.5 Counter Electrode

The counter electrode used is FTO coated with carbon. The conductive side of the FTO was cleaned as previously described and then coated with graphite. This was heated for a few minutes at 300^{0}C in the oven. This was done so that the carbon will spread evenly on the FTO.

2.6 Assembling the Cell

The stained TiO_2 electrodes and the graphite coated counter electrode were assembled by placing the electrodes a little offset opposite to each other to expose contact areas for alligator clips and by pressing them together with binder clips. Few drops of the electrolyte were added to edge of the plate and by capillary action it travels between the two plates. Any excess electrolyte was removed from the edges of the cell with a tissue paper dampened with ethanol.

3.0 Results and discussion
The results are discussed below:

3.1 Energy-dispersive X-ray spectroscopy (EDS)
Energy Dispersive X-Ray Spectroscopy (EDS) is a chemical analytical technique used for the elemental analysis or chemical characterization of a sample. The chemical compositions of the deposited TiO_2 were determined by X-Ray Energy Dispersion spectroscopy (EDS). Figures 2 (a-c) shows the EDS data of CBD, sol gel and slot coated deposited TiO_2. The CBD spectrum shows the peaks of Ti and O. The presence of chlorine emanates from the precursor used and is typical for chloride type of precursors [17], while the other elements seen are due to the FTO glass used. Table 1 show the percentage weight and atomic percent of the chemical composition of the deposited film from sol gel and slot coated TiO_2. From the table, it is seen that carbon constituted about 12.15% in the sol gel deposited film while the atomic ratio of Oxygen to Titanium is 2.12: which is nearly that of TiO_2, with the difference remaining within the range of experimental error. The atomic percent of chlorine is 6.72 which is within the 3.3-7.5 range typical for chloride precursors [17, 29]. The chemical composition of the slot coated TiO_2 show a high percentage of carbon. This could be due to the surfactant Triton X 100 added. The ratio of oxygen to titanium is 3.01. Though this ratio is higher than the TiO_2 stoichiometric value, it still suggests a predominant presence of titanium dioxide. All the EDS spectra show the characteristic x-ray energy level of titanium (K_α=4.510KeV and K_β=4.931KeV) and oxygen (K_α = 0.523KeV) [30].

Table 1: Chemical Composition of the deposited TiO_2

Sol gel			Slot coating			CBD		
Element	Weight %	Atomic %	Element	Weight %	Atomic %	Element	Weight %	Atomic %
C	12.57	12.15	C	36.53	38.31	C	8.95	9.15
O	35.55	47.04	O	46.54	46.20	O	36.28	48.16
Na	11.96	11.02	Sn	0.69	0.09	Na	10.66	9.92
Al	1.17	0.92	Cl	0.09	0.04	Al	1.04	1.89
Cl	11.25	6.72	Ti	16.15	15.35	Cl	13.52	6.75
Ti	27.50	22.15	Total	100.0		Ti	29.58	24.15
Total	100.0					Total		100

3.2 X-ray Diffraction (XRD)
The crystal structure and the phases present in the TiO_2 film was determined using XRD. The crystal grain size was estimated using Schererr equation:

$$D = \frac{K\lambda}{\beta \cos\theta} \qquad 3$$

Where K is a dimensionless constant often called the shape factor with a value of 0.9, λ is the wavelength of the x-ray radiation, β is the full width at half maximum (FWHM) of the diffraction peak and 2θ is the diffraction angle in degrees. Figures 3 (a-c) show the X-ray diffraction patterns of the TiO_2 deposited by the three methods. The diffraction intensity was measured at 0.5^0 incidence angle in the 2θ range between 10^0 and 120^0 with a step size of 0.01^0. The CBD spectrum shows a mixture of rutile and anatase phases. Two sharp diffraction peaks of the anatase phase (004 and 204) corresponding to 2θ = 37.7, and 65.5 respectively, and two sharp peaks of rutile phase (110 and 105) corresponding to 2θ =26.5 and 52.5 respectively, were observed. The multiphase of anatase and rutile structure was obtained in comparison with the Joint Committee on Powder Diffraction Standards (JCPDS) Card File No. 21-1272 and 21-1276. The average crystallite size calculated using Scherer's equation for the various peaks were between 246-96.9nm. The XRD pattern of the sol gel deposited TiO_2 shows diffraction peaks at 2θ = 25.46, 55.12 43.275 and 63.04. These correspond to three anatase phases; 101 (2θ = 25.46), 211 (2θ= 55.12) and 204 (2θ= 63.04). The peak due to 43.275 and 41.9 could not be identified. It could possibly be due to the FTO substrate. XRD pattern of slot coated TiO_2 shows a mixture of anatase and rutile phase structure. Four sharp diffraction peaks of the anatase phase (101, 004, 200, and 204) corresponding to 2θ = 25.3, 37.7, 48.0 and 65.5 respectively, and two sharp peaks of rutile phase (110 and 105) corresponding to 2θ =27.3 and 53.4 respectively, were observed. This is in agreement with literature, [2, 31]. Other peaks are due to the FTO substrate. The average crystallite sizes calculated were between 344-97 nm.

4.3 Scanning Electron Micrograph (SEM)
The surface morphology of the deposited films was studied using SEM. Figures 4 (a-c) show the SEM image of CBD, sol gel deposited and slot coated TiO_2 respectively. The SEM image of CBD shows that the coating is porous homogenous and closely packed with no gaps between the coatings. The image of the sol–gel deposited TiO_2 shows soft and small agglomerates with irregular structure while the image of the slot coated TiO_2 shows a smooth coating with a nano-flower-like

structure.

3.4 Optical Studies

The optical properties of the films deposited on the FTO substrates were examined for their absorbance and transmittance at normal incident by using a UV-Visible spectrophotometer. The absorbance was measured normally in the wavelength range of 200–1100 nm.

Band gap was determined by applying Tauc's law. $(\alpha h\nu)^n$ is plotted against (hν) and then the linear part of the curve was extrapolated to $(\alpha h\nu)^n = 0$ [32, 33]. The relationship between the absorption coefficient α and incident photon energy (hν) is written as:

$$(\alpha h\nu)^n = A(h\nu - E_g) \qquad 6$$

Where: α is the absorption coefficient, (hν) is the photon energy, A is a constant which does not depend on photon energy, E_g - band gap energy, n is a constant, which depends on the type of transition.

For indirect allowed transition n = ½, while for direct transitions n = 2.

Figures 5a- show the absorbance spectra of TiO_2 prepared by the three methods while figure 5b shows a plot of $(\alpha h\nu)^2$ vs. (hν). The absorbance spectra show absorption edges of 385nm for CBD, 370nm for Slot coating and 365nm for Sol gel method. This agrees with what some authors have done and shows that TiO_2 absorb in the ultraviolet region and can be used as a UV sensor. Yang et al [34], obtained an absorption edge at 387nm while Sonawane et al [35] obtained an edge at 307nm. The sol gel method and slot coated showed some peak broadening at 485nm and 475nm respectively. These peaks observed in the visible range might not be as a result absorption by TiO_2 film but might be as a result of wave interference because TiO_2 been a white substance does not absorb in the visible spectrum. None of such peaks was observed for the CBD method. The optical absorption coefficients α were determined from the relative transmission and the sample thickness using equation 7:

$$\text{Absorption coefficient } \alpha = \frac{\ln\left(\frac{1}{T}\right)}{x} \qquad 7$$

The obtained values for energy band gaps for TiO_2 films determined by plotting $(\alpha h\nu)^2$ vs. (hν) are presented in Table 2 below.

Table 2. Values for energy band gap for direct transition

Sample	Eg determined by applying Tauc's law for direct band gap (eV)
CBD	3.53
Sol gel	3.45
Slot Coating	3.20

The obtained values for energy band gaps for TiO_2 films determined by plotting $(\alpha h\nu)^2$ vs. (hν) for direct band gap are 3.53eV, 3.45eV and 3.20eV for CBD, sol gel and slot coating respectively The value for slot coating corresponds to anatase phase of the TiO_2. The average literature values for absorption and corresponding band gap energy for bulk anatase TiO_2 is $\lambda = 385$ nm and $E = 3.2$ eV [36-39]. The E_g value obtained for Sol gel and CBD gave a higher value than what was obtained in most publications although Yang et al [34] obtained a value of 3.4 eV for TiO_2 deposited on glass substrate while Lei et al [37] obtained a value of 3.5eV for TiO_2 sol calcined at 100°C. Mechiakh et al [40] obtained values of 3.7ev and 3.5ev for TiO_2 film calcined at 400°C and 450°c respectively. The increase in the optical band gap may be as a result of the grain size being very small.

UV-Vis spectroscopy of the extracted natural dyes is shown in figure 6a. Figure 6(b) shows the TiO_2 films stained with Jathropha dye extract while fig 6(c) shows TiO_2 films stained with orange dye extract. Figure 6(d) shows TiO_2 films stained with R2751 dye. It was observed that the orange dye extract had absorption peaks at 600nm and 850nm corresponding to absorbance values of 1.791and 0.577 respectively while the jathropha dye extract had peaks at 350nm, 650nm and 850nm corresponding to absorbance values of 1.66, 1.231 and 0.671 respectively. These show that the extracts absorbs strongly in the visible region especially in the red region. No blue peak was observed in contrast to what authors who have extracted chlorophyll obtained. Steel et al obtained a blue peak at 425nm and a red peak at 660nm while Gleue [41] obtained a blue peak at 405nm and a red peak at 627nm. Lai et al [42] obtained a blue peak at 430nm and a red peak at 670nm. This shows that different chlorophyll associated with different plants have different spectra. This may be because the pigments are modified by their local protein environment or because the accessory pigments have intrinsically different absorption spectra form [42].

When stained with the jathropha dye extract, the sol gel prepared TiO_2 had no observable peak absorption but had higher absorbance value than the other methods over the same wavelength range. The CBD prepared TiO_2 stained with the jathropha dye showed peak absorptions at 380nm and 675nm corresponding to absorbance values of 2.263 and 1.294 respectively while the slot coated method had a peak at 465nm at an absorbance value of 2.522.

When stained with the orange dye extract the sol gel method showed small peaks at 615nm and 800nm with absorbance values of 1.267 and 1.218 respectively while the slot coated showed a peak at 445nm corresponding to absorbance of 2.699. In all the stained TiO_2, the absorption edge shifted to the visible region showing strong absorption in the visible region.

Table 3: Summary of the efficiencies of the cells

	Voc (mv)	Isc (mA)	ff	%	Voc (mv)	Isc (μA)	ff	%	Voc (mv)	Isc (mA)	ff	%
Sol gel	100	0.034	0.43	0.15	-	-	-	-	211.5	0.011	0.71	0.16
CBD	80	0.018	0.55	0.08	210	0.78	0.37	0.06	180	0.026	0.21	0.01
Slot Coating	70	0.3	0.20	0.4	350	65.5	0.55	1.26	310	0.114	0.30	1.06

3.5. Current- Voltage (I-V) Characteristics

A standard solar simulator of light intensity 1000W/m^2, spectral distribution AM 1.5 global standard solar spectrum and temperature is 25°C was used the solar simulation. The sample sizes of the solar cells

characterized were typically (1.5x1.5) cm^2. Figures 7(a-c) shows the I-V curve in the dark while figure 8 (a-c) shows the illuminated curve of the ruthenium red sensitized cells. The dark I–V curves in the dark indicate good junction rectification properties.

The open circuit voltage, Voc, short circuit current Isc, were determined from the illuminated I-V curves while the fill factor FF and the overall efficiencies η of the solar cells were calculated using equations 9 and 10 respectively. The results are as tabulated below.

$$FF = \frac{V_{PP}..I_{PP}}{V_{oc}..I_{sc}} \qquad 8$$

$$\eta = \frac{P_{\max}}{P_{light}} = \frac{V_{PP}.I_{PP}}{P_{light}} \qquad 9$$

The results show that the the slot coated TiO_2 gave the highest efficiency using the the three dyes. With the ruthenium red it gave an efficiency of 0.4% while with jathropha and orange dye extract an efficiency of 1.26% and 1.06% were obtained respectively. This is comparable with what other authors have obtained. Guterrez-Taste et al [5], obtained an efficiency of 1.8% with N3 ruthenium dye and platinum counter electrode using the commercial Degussa P25 TiO_2 powder mixed with water soluble titanium (IV) cis ammonium hydroxide prepared by the slot coating method. Huizhi et al [43] prepared DSSC using Ti-nanoxide paste deposited by the slot coating method with platinum counter electrodes and obtained efficiencies between 0.17-1.17% using various natural dyes and efficiency of 6.11% using N719 dye. Smestad and Gratzel [44], obtained efficiencies between 0.5-1.0% using anthocyanin and chlorophyll dye on TiO_2 synthesized by the slot coating method. Lai et al [42] prepared DSSC loaded with gold nano particles, sensitized with chlorophyll using P-25TiO_2 Degussa powder and obtained an efficiency of 0.705%. Ozuomba et al [45] prepared 1.0% efficient DSSC using chlorin dye extracted from bahama grass on Ti-nanoxide.

The CBD deposited TiO_2 gave the lowest efficiency with the three dyes. This may be attributed to the non availability of bonds between the dye and TiO_2 molecules through which electrons can transport from the excited dye molecules to the TiO_2 film or to the poor adhesion of TiO_2 on FTO glass [15]. Similar method used by Zhu et al [14] gave an open-circuit voltage of 0.63 V and a short-circuit current of 7.02 mA/cm^2.

The sol gel method gave comparatively better results than the CBD method although the efficiency was still lower that what was obtained in the literature. The sol gel method with jathropha only gave noise. Liu et al [6], synthesized TiO_2 by sol gel process using $TiCl_4$ precursor and obtained an efficiency of 0.99% for the DSSC fabricated with it using platinum counter electrode and N3 ruthenium dye. Jin Y.S. et al [4] obtained efficiencies in the range of 0.74-1.57% using TiO_2 synthesized with titanium (IV) isopropoxide at different concentrations using N719 ruthenium dye.

The low efficiency of the sol gel and the CBD could also be attributed to the use of $TiCl_3$ precursor. The presence of chlorine in the semiconductor could aid in the degradation of the dye, hence affecting the spectral response to the radiation. The quantity of dye adsorbed by each cell could not be ascertained as this also plays a vital role in the amount of radiation absorbed and consequently in the overall efficiency of the cell. Another factor that contributed to the low efficiency of all the cells is the use of carbon counter electrode. All the referred works made use of platinum counter electrodes, but we couldn't lay our hands on platinum because it is scarce.

4.0 Conclusion

In DSSC TiO_2 is the key component in determining the device efficiency. Hence in this study TiO_2 was prepared by the slot coating using Degussa P25 powder, the CBD and the Sol gel methods. The chemical, structural, morphological and optical properties of the TiO_2 were investigated using Energy Dispersive Spectroscopy EDS, X-ray diffraction XRD, Scanning Electron Microscopy SEM and UV-Visible-Infrared spectroscopy respectively. The chemical composition of all the TiO_2 showed the presence of titanium and oxygen in a proportion that indicated the presence of TiO_2. The XRD analysis showed a mixture of anatase and rutile phases of TiO_2 in both the slot coated and the CBD deposited films while that of the sol gel was predominantly anatase. The calculated crystallite sizes were in the nanometer range. The morphology of the films showed that they were porous and homogenous. That of the slot coated showed a flower-like structure. The band gap energies determined from the methods were between 3.20-3.53ev. The TiO_2 also showed absorption in the ultraviolet spectrum but when coated with the dyes, the absorption shifted to the visible region. The prepared TiO_2 were used to assemble DSSC using red ruthenium dye and dye extracts from jathropha leafs and orange citrus leafs. The electrolyte used was potassium iodine and iodine in acetonitrile solvent and the counter electrode was FTO substrates coated with carbon. The slot coated TiO_2 with jathropha leaf dye extract showed the highest overall efficiency of 1.26%. This means that jathropha, apart from its applications in the production of biofuels, the leaves are a good source of natural dye in the fabrication of DSSC.

References

1. N. S. Begum. H.M. Farveez Ahmed, Bull. Mater. Sci., 31, 1, (2008) 43.
2. A. Karami, *J. Iran. Chem. Soc.,* 7, Suppl.9 (2010) S154
3. D.A.H. Hanaor, G. Triani, C.C. Sorrel, Surface and Coatings Technology, 205, 12 (2011) 3658.
4. Y.S Jin, K.H. Kim, H.W. Choi, Journal of the Korean Physical Society, 57, 4, (2010) 1049
5. D. Guterrez-Taste, I. Zumenta, E. Vigil, X. Domennech, M. A. Hermadez-Fenolosa, A. A. Esteve Jose, Journal of Photochem and

Photobiology A: Chem 175, (2005) 165.

6. Y.C Liu, Y.F. Lu, Y.Z. Zeng, C.H. Liao, J.C.Chung, T.Y. Wei, International Journal of energy (2011) Article ID 619069.

7. Photo R.N Goyal., D. Kaur, A.K. Pandey, ***The Open Chemical and Biomedical Methods Journal, 3,*** (2010) **115.**

8. Z.R. Ismagilov, L.T. Tsykoza, N.V. Shikina, V.F. Zarytova, V.V. Zinoviev, S.N. Zagrebelnyi, Russian Chemical Reviews, 78, 9, (2009)

9. M.A. Lazar, J.K. Tadvani, W.S. Tung, L. Lopez, W.A. Daoud, Materials Science and Engineering **12** (2010) 012017 .

10. O. Carp, C.L. Huisman, A. Reller Progress in solid state chemistry, 32, 1-2, (2004) 33.

11. U. Diebold Surface Sciences Reports, 48, 5-8, (2003) 53

12. L. Kavan, B. O'Regan, A. Kay M. Gratzel. J. Electroanalytical. Chem., 346, (1993) 291

13. Y. Li**,** J. Hagen**, W. , P.** Otschik **D.** Haarer, Solar Energy Materials and Solar Cells, 56, 2. (1998) 167

14. H. Zhu, J. Yang, S. Feng, M. Liu, J. Zhang, G. Li Applied Physics A: Materials Science and Processing, (2011) 10.1007/s00339-011-6513-y

15. I. Zumeta**, J.A.** Ayllón**, B.** González, **X.** Domenech, **E.**Vigil, Solar Energy Materials and Solar Cells, 93, 10 **(2009)** 1728-1732.

16. R. S. Rawat, V. Aggarwal, M. Hassan, P. Lee, S. V. Springham, T. L. Tan, S. Lee, Applied surface science, (2008) 2932.

17. J. Kowalski, A. Sobczyk-Guzenda, H. Szymanowski, M. Gazicki-Lipman, Journal of Achievements in Materials and Manufacturing Engineering 37/2**(2009)** 298.

18. M. L. Hitchman and F. Tian, Journal of Electroanalytical Chemistry, 538-539, (2002) 165

19. U.M. Patil, K. V. Gurav, O-S. Joo, C.D. Lokhande, Journal of Alloys and Compounds, 478, 1-2 (2009) 711.

20. L. Kavan, M. Gratzel, **Electrochimica Acta, 4, 5,** (1995) **648.**

21. B. O'Regan M. Grätzel *Nature* **353**, (1991) 737.

22. F. Linda., H. Amy, K. Shanks K, P. Bruecken, W. Goates, Institute for Chemical Education Madison, WI (2008).

23. M. Gratzel, JR. Durrant. In Mary D Archer & Arthur J (eds) series on photo conversion of solar energy 3: (2008) 503.

24. M. Gratzel, J of Photochemistry and photobiology A; chemistry 164 (2004) 1.

25. C. Longo, M. De Paoli, Journal of the Brazilian Chemical Society **J. Braz. Chem. Soc., 14, 6, (2003) 889.**

26. S. Ito, T.N. Murakami, P. Comte, P. Liska, C. Gratzel, MK. Nazeeruddin, M. Gratzel, Thin solid Films, 515, 140, (2008) 4613.

27. P.S. Greg, M. Gratzel, Journal of Chemical Education 75 (1998) 752.

28. C.J. Barbe, Journal of America Ceramic Society, 80 12, (1997) 3157.

29. A. Sobczyk-Guzenda**, M.** Gazicki-Lipman**, H.** Szymanowski**, J. Kowalski, P.** Wojciechowski**, T.** Halamus, A. Tracz, Thin film Solids. 517, 18, **(2009)** 5409.

30. H. Ninsonti, S. Sangsrichan, W. Kangwansupamonkon, S. Phanichphant, P. Pookmanee, Journal of Microscopy Society of Thailand, 23, 1, (2009) 91.

31. D.Guterrez-Taste, Doctoral thesis submitted to the department de quimica de la Universitat autonoma de Barcelona. (2008).

32. A. Molea V. Popescu, Optoelectronics And Advanced Materials – Rapid Communications 5, 3, (2011) 242.

33. R. Zallen M. P. Moret, Solid communications 137 (2006) 154

34. H. Yang, X. Zhang, Q. Tao, A. Tang, Journal Of Optoelectronics And Advanced Materials 9, 8, (2007) 2493.

35. R.S. Sonawane , S. G. Hegde, M.K. Dongare, Materials chemistry and physics 77(2002) 744.

36. F. Gordillo-Delgado, K. Villa-Gomez, Superficies y 24, 1, (2011) 20.

37. G. Lei, X. Mingxia, F. Haibo, Thin Solid Films, 515 (2007) 3414.

38. K. Kalyanasundaram, M. Gratzel Coordination Chemistry Reviews, 177 (1998) 347.

39. F. Gordillo-Delgado, K. Villa-Gomez, Microelectronics Journal 39, 11, (2008) 1333.

40. R. Mechiak, B.N. Sedrine. B.J. Naceur, R.

Chtourou, Surface and Coatings Technology 206, 2-3, (2011) 243.

41. D.A. Gleue (2011) available at http://teachers.usd497.org/agleue/index.html assessed 12/07/11

42. W.H. Lai, Y.H. Su, L.G. Toeh, M.N. Hon, Journal of Photochemistry and Photobiology A: Chemistry. 195 (2008) 307.

43. Z. Huizhi, W. Liqiong, G. Yurong, M. Tingli, Journal of Photochemistry and Photobiology A: Chemistry. 219 (2011) 188.

44. G.P. Smestad, M. Gratzel, Journal of Chemical Education,75 (1998) 752

45. J.O. Ozuomba, A.J. Ekpunobi, P.I. Ekwo, Chalcogenide Letters, 8, 3, (2011) 155.

Figure captions

Figure : Flow chart for preparing titanium dioxide sol gel on FTO
Figure 2 : EDS spectrum of (a) CBD deposited TiO_2 (b) sol gel deposited TiO_2 (c) slot coated TiO_2
Figure 3: XRD pattern of (a) CBD deposited TiO_2 (b) sol gel deposited TiO_2 (c) slot coated TiO_2
Figure 4 :SEM image of(a) CBD deposited TiO_2 at 2000 magnification (b) sol gel deposited TiO_2 at 500magnification (c) slot coated TiO_2 at 2000 magnification

Figure 5(a) Absorbance spectra of the TiO_2 films (b) The plot of $(ahv)^2$ vs. (hv)
Figure 6: (a) Absorbance spectra of Jathropha and Orange extract, (b) TiO_2 films stained with Jathropha dye extract, and (c) TiO_2 films stained with orange dye extract. (d) TiO_2 films stained with R2751 dye
Figure 7: I-V curves in the dark for (a) cell sensitized with ruthenium dye (b) jathropha leaf extract, (c) orange leaf extract.

Figure 8: Illuminated I-V curve of the solar cells sensitized with ruthenium red dye (a) sol gel, (b) slot coating, and © CBD

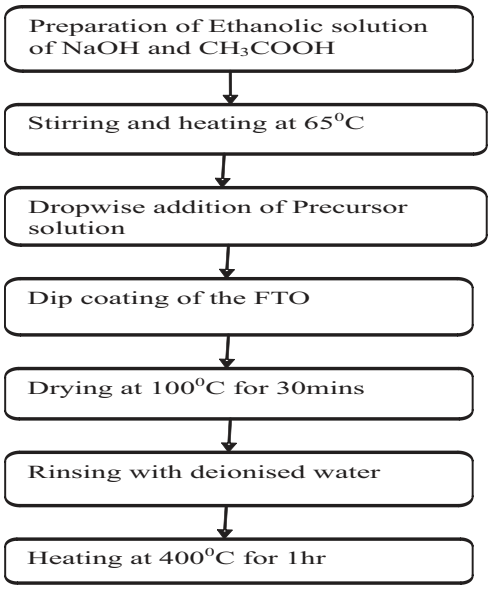


Figure 1

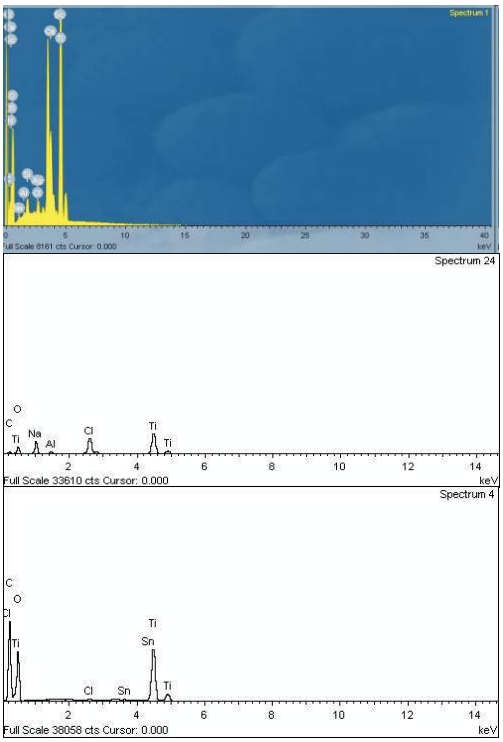
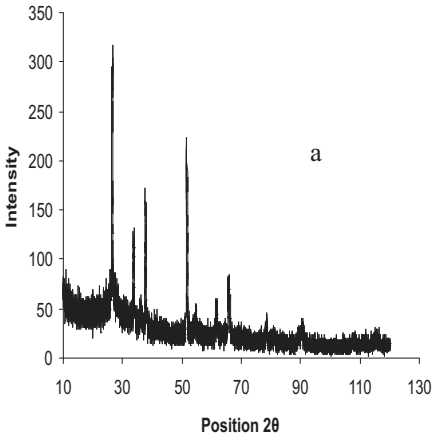
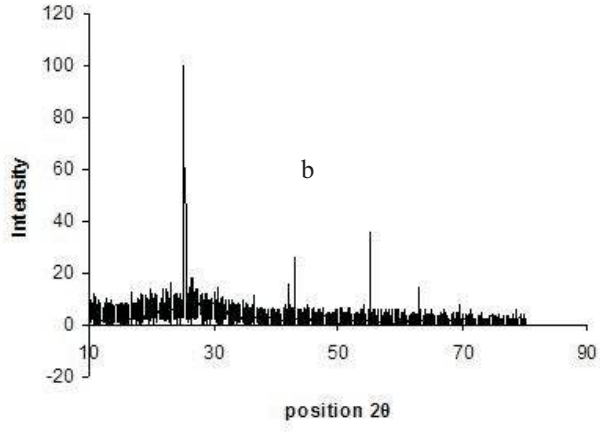


Figure 2





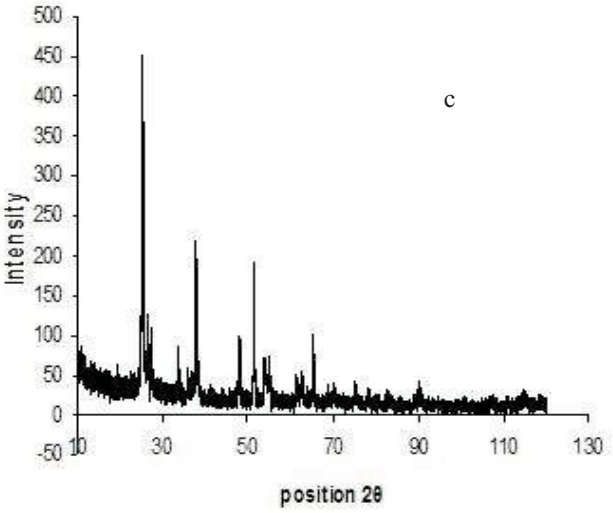
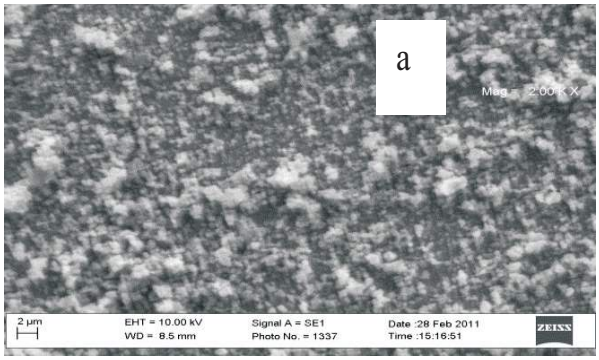


Figure 3



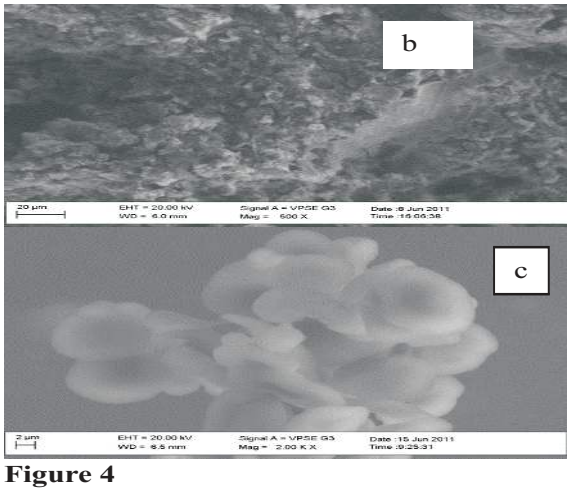
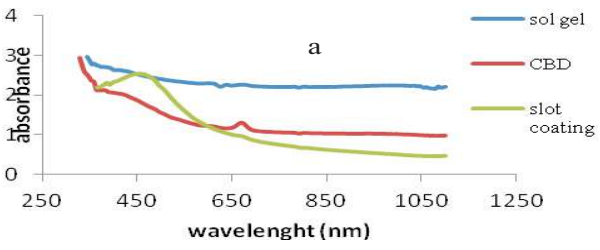


Figure 4



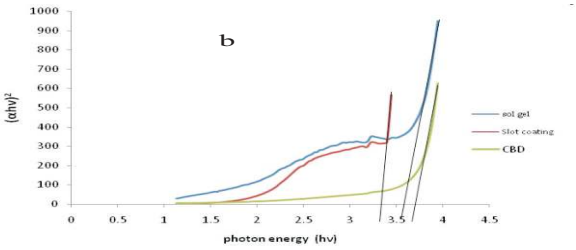


Figure 5

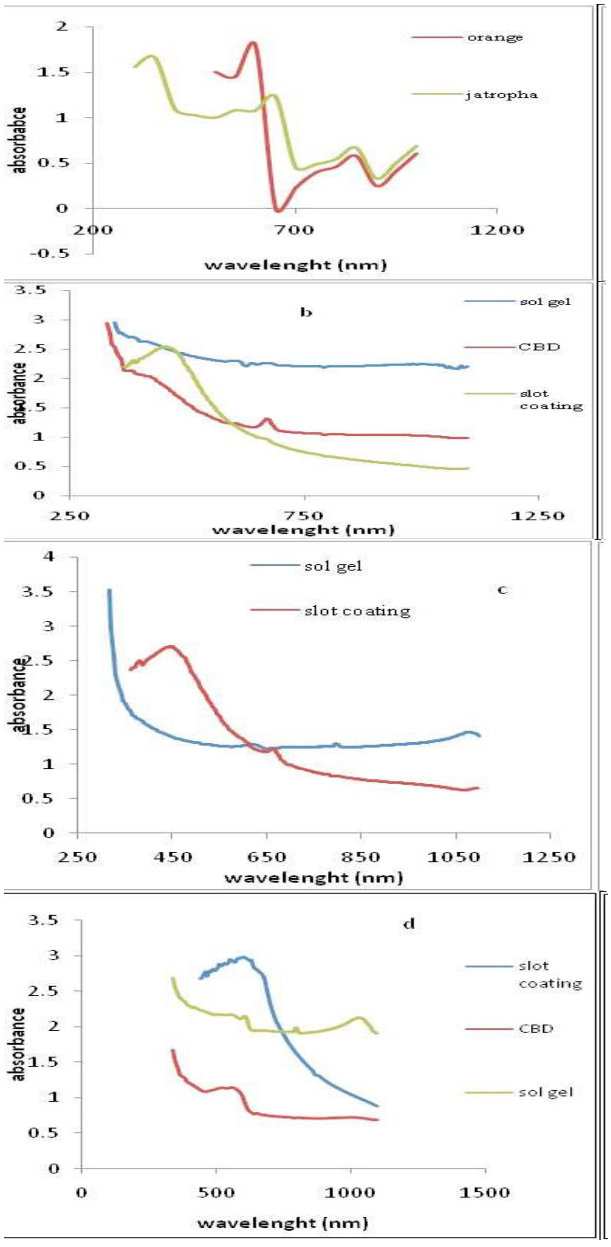


Figure 6

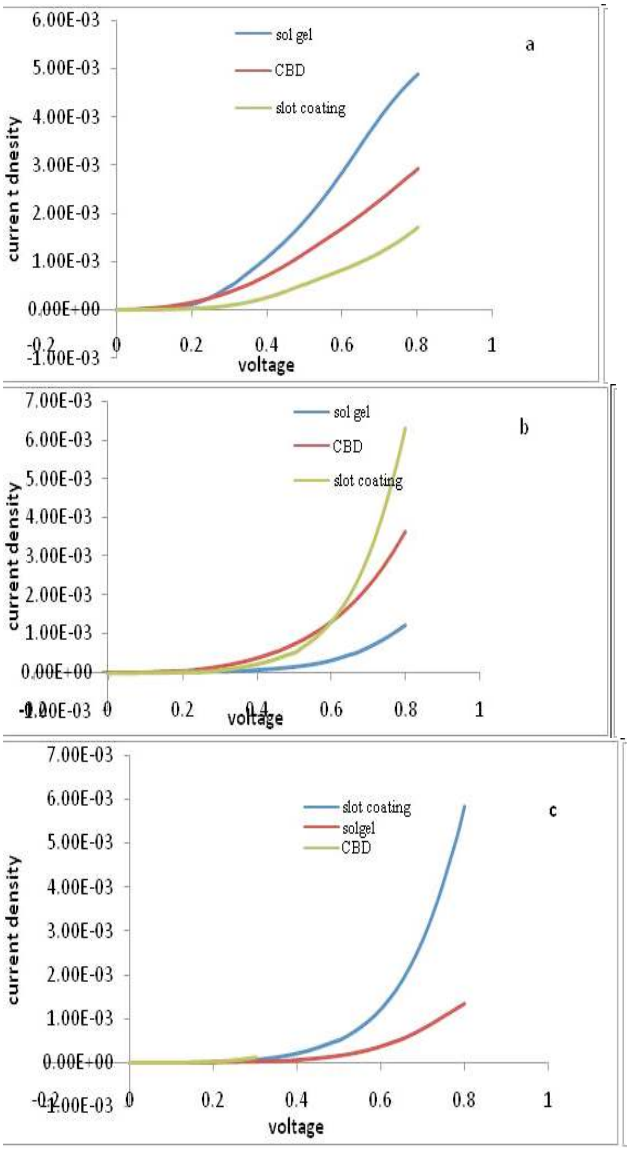


Figure 7

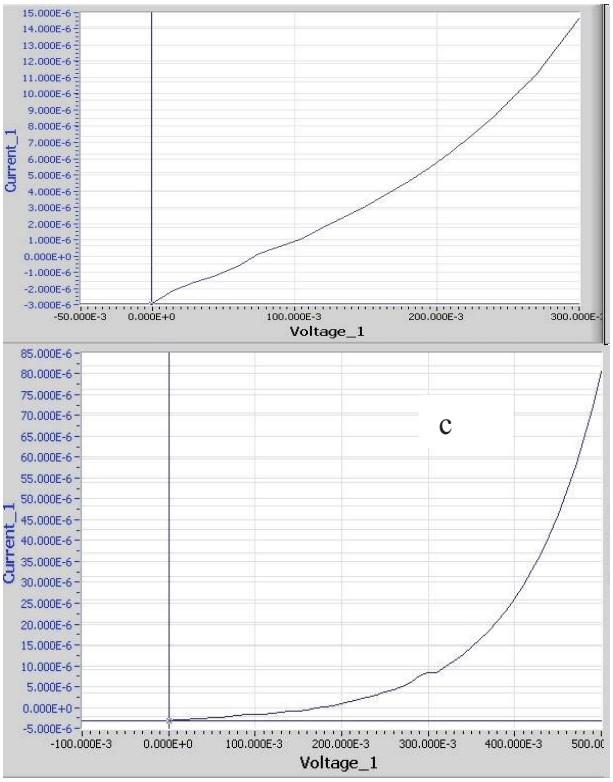
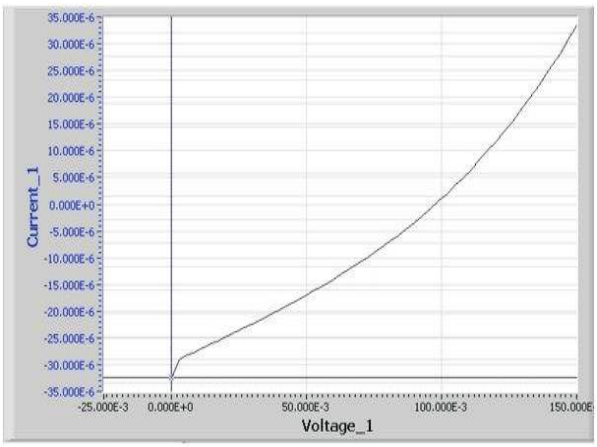


Figure 8



CHARACTERIZATION OF VACUUM THERMALLY DEPOSITED ALUMINIUM ZINC NANO THIN FILM

O.R.ADETUNJI [1]; P.O.AIYEDUN[2]; T.A.AROWOLO [3] ; O.J.ALAMU [4]
[1&2]Mechanical Engineering Department, Universty of Agriculture, P.M.B.2240,Abeokuta
[3]Environmental Management and Toxicology Department, Universty of Agriculture, P.M.B.2240, Abeokuta, Ogun State, Nigeria
[4]Mechanical Engineering Department, Osun State Universty Oshogbo, Osun State, Nigeria.
E-mail; adetunjiolayide@yahoo.co.uk

ABSTRACT
Vacuum thermal evaporation technique was employed in depositing thin film of aluminium, mixture of aluminium and zinc, on microscopic glass and steel substrates using Edwaed 090-10-895 B Auto 306 vacuum coating system. Characterization of Aluminium Zinc Nano thin films produced were done using Dektak Stylus Profilers, Four-Point Probe Restivity Measurement, and Uv-Vis Spectrometer, Scanning Electron Microscope[SEM] and Energy Dispersive X-ray[EDAX].The reflectance of nano thin films of Aluminium and Zinc produced increased with increase in wavelength. The transmittance of 100% Aluminium thin films on glass substrate was low within wavelength of 350 and 500 nm.The absorbance of 100% Aluminium, 100% Zinc and 50% Aluminium and Zinc are satisfactory within wavelength of 350 to 500 nm. The electrical resistance was low for 100% Aluminium thin films which correspond to high conductivity. The principal element of the thin films is indicated by the peaks of the graphs produced by EDAX. The reflectance of nano thin films of Aluminium and Zinc produced increased with increase in wavelength. The electrical characteristics of Aluminium film can facilitate its use as do pant in some solar cell's film for better performance and enhanced conversion efficiency

Keywords: Aluminium, Zinc, Thin, Films, Electrical, Characteristics

INTRODUCTION

Nano materials have a characteristic length scale less than about a hundred nanometers. The length scale could be a particle diameter, grain size, layer thickness, or width of a conducting line on an electronic chip [1]. These nano materials have technological applications in catalysts and pigments. The large surface area to volume ratio increases the chemical activity [3]. Cost advantage in fabricating catalysts from nano materials properties improve through preparing them as nanostructures [4]. For example, sintering temperature can be decreased and plasticity increased of single-phase structural ceramics by reducing the grain size to several nanometers [2].

Aluminium which is one of the elements of Group IIIA has been increasingly used to dope materials for effective conductivity. At temperature of 1472 K, typical value for the average grain size of face centred cubic metal like Aluminium is 22 nm [Koch, 1993]5

Aluminium is being employed in doping thin films so as to achieve highly conductive thin films and other associated improved electrical properties of the films. Thin film is a layer of material deposition whose thickness is of the order of a given wavelength of electromagnetic radiation. In making zinc nano particles, oxygen had the tendency of causing the particles to clump and form agglomerates approximately 0.5 μm in size [Eversole and Broida, 1974].6

The main objective of this research work is to examine electrical and optical properties of zinc aluminum nano thin film.

MATERIALS AND METHODS

Laboratory grade of Aluminium wire and Zinc flakes were used. Aluminium deposition was carried out. Zinc deposition was also carried out by weighing small pieces on Mettler weighing balance. Proportions of both aluminium and zinc were also done in the same method.

The process began by switching on recirculating water chiller attached to the evaporator. The coater (Fig.6) is switched on and the process of creating vacuum in the backing line initiated. Once the desired vacuum is achieved in the backing line, the deposition chamber is vent. The chamber is opened and the substrate is mounted. The evaporant (aluminium, zinc and mixture) is put in the crucible. The deposition chamber is closed and rough vacuum is done.

The fine vacuum is started, about 1.5litres of liquid nitrogen is poured. Once the required vacuum is achieved (better than 10^{-6} Torr). The evaporation power supply is switched on gradually. The power was increased until the desired evaporation rate is achieved. The shutter is opened. Once the desired thickness (from Monitor) is achieved, the shutter is closed and evaporator power switched off.

The system is vent. The sample is removed. The steps are repeated for next deposition otherwise the vacuum is created in the system; the system is sealed and shut down. Once the system is in standby mode, it is switched off from the control panel and the main utility line is turned off.

Optical characterization

The thin films coated on glass substrates were characterized on ultra violet spectrometer for reflectance and transmittance. Eight samples of thin films of aluminium, zinc and different proportion of both aluminium and zinc were analyzed. The results obtained

are contained in tables 1-8 and figures1-5.
The sixteen thin films produced (glass slides and steel substrates) were tested for electrical resistivity. The results obtained were contained in tables in section four.

Scanning Electron Microscopy (SEM) for thin Films.
The samples were prepared for SEM analysis by cutting into 10mm x 10mm. Each of the glass slide samples were mounted on the machine. They were scanned and the best resolution taken on the monitor.

Energy Dispersive X ray (EDX) for thin films on glass slides.
The prepared samples for SEM analysis were also run for EDX analysis to confirm the elements in the thin films.
The sixteen thin films produced (glass slides and steel substrates) were tested for electrical resistivity. The results obtained were contained in tables in section four.

RESULTS AND DISCUSSION
Optical Properties of Aluminium and Zinc Nano thin films
The results of reflectance (R) and Transmittance (T) Data measured with spectrometer serial number: 0708067S1

Table1 Reflectance and Transmittance of Al -Zn Nano thin film (Al-50%)

S/N	Wavelength (nm)	R (%)	T (%)
1	350	12.35	12.46
2	400	16.12	11.89
3	500	25.23	10.70
4	600	30.91	9.93
5	700	24.67	9.52
6	800	37.88	9.69
7	900	41.54	10.50
8	1000	47.32	10.31
9	1100	70.60	8.54

The reflectance and transmittance obtained for the Al-Zn (50%) film on glass slide was 12.35% and 12.46% respectively at wavelength of 350 nm. As the wavelength increased to 600 nm, the reflectance increased to 30.91 % while reflectance decreased to 9.93 %. Transparency depends on amount of light absorbed and backscattered light is collected as reflected light by the integrating sphere. A can be simply be computed as A=1- T-R. The highest value of reflectance got was 70.60% with corresponding lowest of 8.54 %.

Table 2 Reflectance and Transmittance of Al -Zn Nano thin film (Al 100%)

S/N	Wavelength (nm)	R (%)	T (%)
1	350	40	0.059
2	400	46	0.000
3	500	55	0.007
4	600	33	0.023
5	700	25	0.015
6	800	50	0.051
7	900	62	0.047
8	1000	70	0.000
9	1100	81	0.000

The reflectance of pure aluminium thin film on glass ranged from 40 % to 81 % while the transmittance values were low. The reflectance of zinc thin film on glass slide ranged from 13 % to 68 % within a wavelength of 350 nm to 1100 nm while the transmittance were very low from 0.37 % to 3.56 %.

Table 3 Reflectance and Transmittance of Al -Zn Nano thin film (Zn-100%)

S/N	Wavelength (nm)	R (%)	T (%)
1	350	13	0.37
2	400	21	0.41
3	500	46	0.36
4	600	58	0.32
5	700	61	0.28
6	800	60	0.33
7	900	60	0.80
8	1000	68	2.35
9	1100	68	3.56

Table 4 Reflectance and Transmi ttance of Al-Zn Nano thin film (Al-30%)

S/N	Wavelength (nm)	R (%)	T (%)
1	350	12	0
2	400	19	0
3	500	42	0.041
4	600	59	0.129
5	700	76	0.117
6	800	89	0.161
7	900	96	0.705
8	1000	102	0.709
9	1100	106	0.00

The reflectance of 30 % Aluminium and 70 % Zinc improved from 12 % to 106 % at higher wavelength of 1100 nm but the transmittance was very low.

Table 5: Reflectance and Tran smittance of Al - Zn Nano thin fim (Al-70%)

S/N	Wavelength (nm)	R (%)	T (%)
1	350	25	11
2	400	32	12
3	500	50	13
4	600	58	15
5	700	60	16
6	800	66	17
7	900	64	19
8	1000	69	20
9	1100	56	22

The reflectance of 70 % Aluminium and 30 % Zinc thin film on glass slide rose from 25 % to 56 % while the transmittance rose from 11 % to 22 % as wavetength increased from 350 nm to 1100 nm.

Table 6: Reflectance and Transmittance of Al - Zn Nano thin film (Al-36%)

S/N	Wave length (nm)	R (%)	T (%)
1	350	25	11
2	400	32	12
3	500	50	13
4	600	58	13
5	700	60	16
6	800	66	17
7	900	64	19
8	1000	59	20
9	1100	55	22

The reflectance of 36 % Aluminium and 64 % Zinc rose from 25 % to 55 % while transmittance increased from 11 % to 22 %. As wavelrngth increased from 350 nm to 1100 nm.

Table 7 Reflectanc e and Transmittance of Al - Zn Nano thin film (Al-64%)

S/N	Wave length (nm)	R (%)	T (%)
1	350	12	14
2	400	19	13
3	500	42	12.5
4	600	59	14
5	700	76	16
6	800	89	16.8
7	900	96	17.6
8	1000	102	18
9	1100	106	19

The reflectance of 64 % Aluminium and 36 % Zinc thin film on glass slide increased from 12 % to 106 % while transmittance rose from 14 % to 19 % as wavelength moved from 350 nm to 1100 nm.

Table 8 Reflectance and Transmittance of Al -Zn Nano thin film (Al-45%)

S/N	Wave length (nm)	R(%)	T (%)
1	350	63	25
2	400	67	32
3	500	75	50
4	600	81	58
5	700	86	60
6	800	88	66
7	900	90	64
8	1000	92	69
9	1100	98	56

Both reflectance and transmittance improved considerably with 45 % Aluminium and 55 % Zinc thin film on glass slide when subjected to optical analysis. This is a good sample where both properties are desirable.

Reflectance and Transmittance of Al-Zn Nano thin film.

The reflectance of 100% aluminium thin film on glass substrate increased from 40 % to 55 % between a wavelength of 350 and 500 nm. This is later decreased to 25 % at wavelength of 700 nm. As wavelength increased further the reflectance increased from 25 % to 81 % at wavelength of 1100 nm. However, the transmittance remained very low for this consideration. For the 100 % zinc thin film, the reflectance is slightly lower within same wavelengths considered, transmittance is also low. The absorbance of the thin film which is given by 1-R-T is okay for 100 % Aluminium, 100 % Zinc and 50 % Aluminium and Zinc within wavelength of 350 to 500 nm.

Electrical Properties of AL-Zn Nano thin films. The resistance of the thin films as measured by four point probe revealed low resistivities for 100 % aluminium thin film with corresponding high conductivities. Conductivities of 9.283 E9/Ωm of 100% Al, 4.295 E8/ Ωm for 100 % Zn and 2.078 E 7/ Ωm for 50 % Al, 50 % Zn. The conductivity for 100 % Al on Steel substrate got was -8.82 E12/ Ωm. The advantage of this conductivity value can be utilized to facilitate the conductivity of the doped materials for enhanced performance and improved conversion efficiency. Some earlier reporters like Amusan et al. (2010) agreed on these findings.

Surface Texture Analysis: The results obtained from Dektak Stylus Profilers for the nano thin films showed values for R_p which is the peak values anR_v the lowest values. The Surface profiler employed for the research scans with the following parameters: Stylus Radius 12.5 μm, length of scan coverage of 1000 μm, D uration of scan is 60 sec, Resolution of 0.056 μm per sample, Force of 3.0 mg, Measurement range of 6.5 μm and the profile covering hills and valleys. The maximum peak to valley is obtained from sum of R_p and R_v.These values are contained in table 33 as illustrated by figures 1 to 5. R_a and R_z which measures the waviness and average height between peaks and valleys. From the results contained in table 1 to 8, best result was got for G3(45%Al,55%Zn) with R_z of 960 while worse result was got for S1(100%Al on steel substrate) due to surface roughness. The values of R_z are contained in table 7.

Surface Morphology from Scanning Electron Microscope

Figures 3 & 4 showed the image of 100 % aluminium thin film on glass substrate, the image of 100 % zinc thin film on glass.

Energy Dispersive X ray

The principal elements in the thin film are showed by the peak of the graph (Figure 5).

CONCLUSION

The reflectance of nano thin films of Aluminium and Zinc produced increased with increase in wavelength.

There is specific range of length on the film which gives the uniform, uncontaminated surface film. The four point probe technique provides the resistivities at various points on thin film surface. The electrical characteristics of Aluminium film can facilitate its use as do pant in some solar cell's film for better performance and enhanced conversion efficiency.

REFERENCES

1.Amusan,J.A, Olayinka A.S, Nwambo, Y.P, Alayande,S.O, Ojuh,O.D, James C.C, Ibiyemi,A,

Adetunji,O.R ,Fagbulu,A. and Ayinde,W.B (2010) Electrical Characterization of Vacuum Thermally Deposited Aluminium Thin Film Research Journal of Applied Sciences 5(2) pp 96-100.
2.Okoli, D.N,Okeke G.C and Ekpunobi A.J 2010. "Optical Properties of Chemical Bath Deposited Ag2S Thin Films". *Pacific Journal of Science and Technology*. 11(1):411-415.

3.Yang and Luzzi (2009) Nanotechnology Microsoft Encarta DVD Redmond WA Microsoft Corporation.

4.Zebaze Kana M.G, Centurioni E, Iencinella D and Summonte C (2006). Influence of the Sputtering System's Vacuum Level on the Properties of Indium Tin Oxide Films Elsevier Thin Solid Films 500 pp 203-208.

5 Eversole J.D. and Broida H.P (1974) Zinc particles Journal of Applied Physics.

6 Koch C.C 1993 Nanostructural Matter

7 Bein T 1992 Supramolecular Architecture; Synthetic Control in Thin Films and Solids (ACS Symposium Series 499) (Washington, DC; American Chemical Society).

8 Knozinger H 1991 Fundamental Aspects of Heterogeneous Catalysis Studied by particle Beams ed H H Brongersma and Ravansanten (New York; Plenum) p7

9 Munday J.S and Cotton RJ 1990 Chemistry and Physics of Solid Surfaces VII ed New York Springer p 347.

10 Munday JS, Cotton RJ and Rath BB 1993 Synthesis, Processing, and Modelling of Advanced Materials Brookfield p149

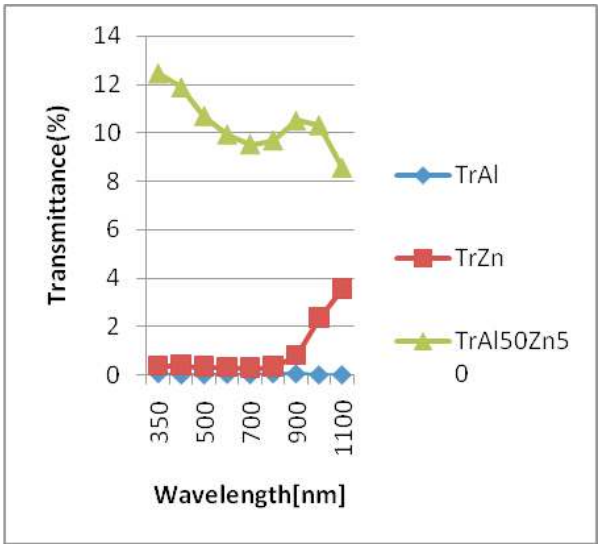


Fig.1 Reflectance of nano thin films againstwavelength

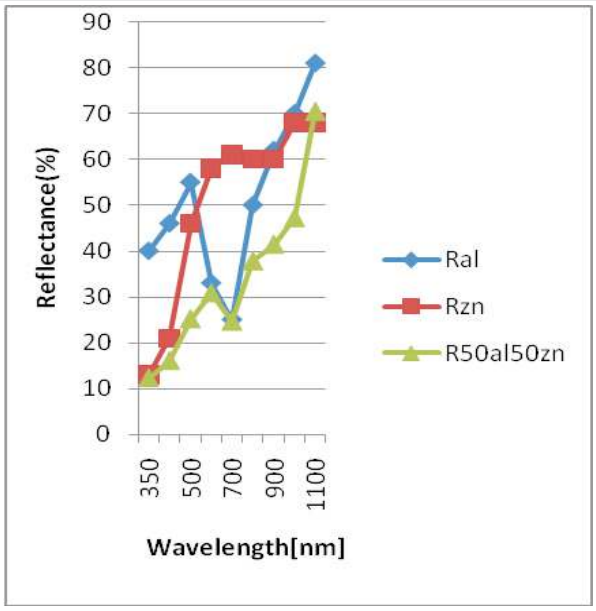


Fig.2 Transmittance of nanothin films against wavelength.

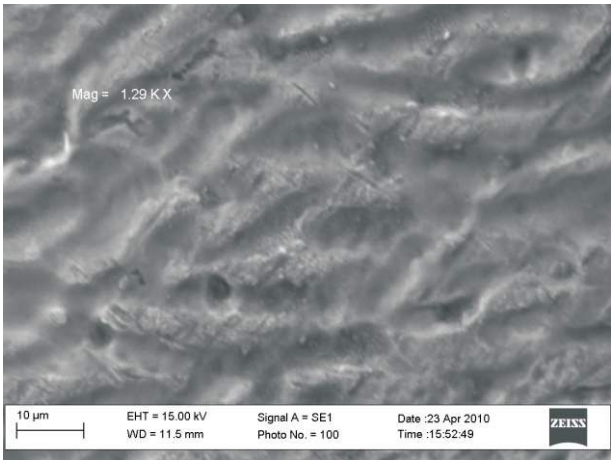


Fig.3 SEM for 100% Al thin film on glass



Fig.4 SEM for 100% Zn

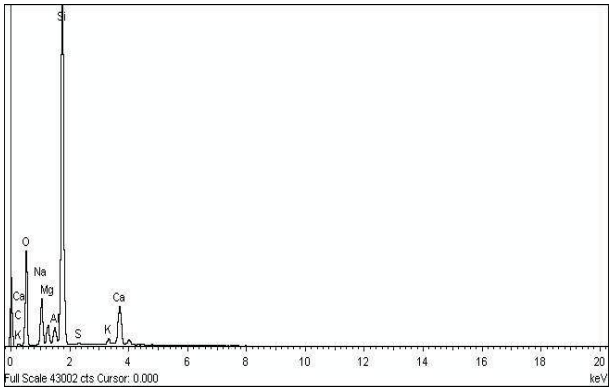


Fig.5 EDAX plot of 100% Al thin film on glass

INVESTIGATION ON PROPERTIES OF RECYCLED ACRYLONITRILE-BUTADIENE-STYRENE (ABS) FROM DIFFERENT FRIDGE BRANDS

A.O. Aroke*, A. S. Ahmed and B.O. Aderemi
Department of Chemical Engineering, Ahmadu Bello University Zaria
*Corresponding author: e-mail: kenlamin@yahoo.com

ABSTRACT

Acrylonitrile-butadie-styrene (ABS) is a strategic material with useful engineering applications including the internal wall lining of refrigerators. Properties of recycled acrylonitrile-butadiene-styrene (ABS) from different brands of discarded refrigerators were investigated in this work. Solvent method of recycling was adopted at room temperature. Tetrahydrofuran (THF) was found to be the most suitable solvent; it has solubility parameter of 9.79 cal/cm^3 which was close to the solubility parameter of Acrylonitrile-butadiene-styrene (ABS) of 9.4cal/cm^3. FTIR analysis indicated presence of ABS in materials recycled from all the refrigerator brands. However, the recycled ABS from Matsui fridge was found to have mechanical properties closest of the virgin ABS, with tensile strength, modulus of elasticity, flexural strength of 31.66MPa, 1021MPa, 60.18MPa respectively, as compared to the virgin ABS tensile strength, modulus of elasticity, flexural strength of 48.3 MPa, 1312MPa, 65.75MPa respectively. The recycled ABS can be used directly for appliances production or as blend with other polymer materials.

Keywords: Acrylonitrile Butadiene Styrene, Solubility parameter, Used refrigerators, Mechanical properties, Tetrahydrofuran

1.0 Introduction

The large waste emanating from electronics and electrical appliances has been attributed to rapid technological development [1]. Acrlonitrile-butadiene-styrene (ABS) is an engineering thermoplastic that is widely used in many practical aspects, such as in electronics and electrical appliances because of their good mechanical, low density and thermal properties and the demand for the production increases from year to year [2, 3, 4]. ABS is used for refrigerators insulation because they are not readily attacked by fluorocarbon unlike impact polystyrene, thereby making ABS one of the largest polymer components of refrigerator [1, 5]. However, these materials are discarded into the environment after their service life which constitutes environmental menace.

Recycling of polymeric materials has attracted a lot of interest in the society and this method has been applied severally to the recovery of ABS and other polymer materials from different electrical and electronic appliances. The use of selective depressants for the separation of ABS and high impact polystyrene (HIPS) has been investigated [6]. Arnold et al [1] also recycled ABS and high impact polystyrene from waste computer equipment.

Four main approaches to polymer recycling has been identified [7], these are: primary recycling, secondary recycling, tertiary or chemical recycling and quaternary recycling. A new method based on dissolution of polymers is being developed [8]. This new method involves size reducing polymers and treating it with appropriate solvent, filtering the solution to remove any insoluble contaminants and additives and the polymer then recovered by evaporation and drying. Effect of dissolution-based recycling on the degradation and mechanical properties of ABS has been investigated [9]. Limonene (oil produced from the skin of citrus fruits such as orange) is known to dissolve expanded high impacts polystyrene using a solid/liquid ratio of 1/10 at a temperature of 40°C over a period of 90 min. [10].

It has been established that successful dissolution of a polymer in a solvent has to do with selection of a proper solvent. The theory of solubility parameter is one way of identifying which polymer will dissolve in what solvent, it has been reported that a polymer is expected to be soluble in a solvent if δ_1-δ_2 is less than 1.7-2.0 [8].

In this work, the dissolution method of polymer recycling was used to recover ABS from used refrigerator brands using the theory of solubility parameter to determine the suitable solvent for the dissolution and the mechanical properties of the recovered ABS from these different sources studied.

2.0 Experimental

2.1 ABS Waste collection

The fridge which consists of metals and polymers were dismantled manually to remove the metals from the polymers. The inner lining which is rich in the ABS containing materials was stripped out.

The sorted waste ABS containing material was washed thoroughly with detergent to remove all dirt and paper labels then rinsed with water and spread to dry.

The dried materials were cut into flakes with an average dimension of about 2 – 4 mm with a sharp knife. This stage of size reduction was done to enhance the dissolution of the ABS materials.

2.2 Dissolution process

The dissolution process involves dissolving the waste into a suitable solvent and this was determined by evaluating the difference in solubility parameter of the solvent and the polymer. Three different solvents were

tested and tetrahydrofuran (THF) was found to be the best. Therefore, the dissolution was carried out using THF in a fume cupboard. 75g of the ABS material was weighed and poured into the beaker, 300ml of THF was measured and poured into the beaker at room temperature and pressure condition for 1 hr, and the mixture was stirred intermittently to homogenize the mixture.

2.2.1 Filtration

The stirred mixture of the acrylonitrile-butadiene-styrene (ABS) containing material was poured into the Buchner funnel of the filtration set up; it takes about 5 -10 mins to separate the filtrate and the residue. The filtrate was material containing the ABS and the residue which was made up of the insoluble contaminants and the additives.

2.3 Sample preparation

The mould was cleaned with a piece of cloth to remove all adhered particles and then coated with petroleum jelly, which served as a releasing agent for easy removal of the sample from the mould after drying. The filtrate was poured into the mould and allowed to stay for 2 days for the solvent to evaporate. The dried sample was removed from the mould and was further dried in an oven at a temperature of 80°C for three hours in order to avoid possible moisture degradation reaction and complete the removal of the remaining solvent [12]. The sample was weighed and the weight recorded.

2.3.1 Compression

The dried material was cut into flakes and poured into a metallic mould covered with Aluminium plate. This was inserted into an electrically heated Moore hand operated compression moulding machine which was pre- heated for 10 mins. The pressure was 10 tons at a temperature of about 160-170 ^{o}C. This was monitored for 5min after which the mould was removed from the compression moulding machine and left to cool for 5min at an ambient conditions. The sample was then removed from the mould and cut into test sizes. The same steps from section 2.2-2.3 were repeated for samples from other fridge brands.

2 .3.2 Testing of the samples

Tests were conducted for the recycled and virgin ABS. The cut samples were subjected to various tests.

2.3.2.1 Tensile test

The specimen was cut into dumb bell shape to aid grip at each end. ASTM D638M dimension was adopted. A gradually increasing load was applied to the specimen and the machine automatically plotted the load versus the extension values.

3.0 Results and discussion

Polymers generally do not dissolve in all organic solvents, to this effect the choice of solvent has to be made and this is simplified using solubility parameter. Usually a solvent is suitable for the dissolution of a selected polymer if the solubility parameter values for both are very close e.g. 1.7 -2.0cal/cm^3 [3]. The solubility parameter of ABS was evaluated to be 9.49cal/cm^3 and that of other solvents were also evaluated to compare for choice of solvent. The difference in solubility parameter of ABS and that of THF calculated as 9.79cal/cm^3 was found to fall in the range suggested by literature. Therefore, THF was chosen as the solvent and others discarded.

The chemical composition and structure of polymers after reprocessing can change due to a chemical reaction giving rise to a new product or remain unchanged [11]. These changes can be identified by different types of analysis. The presence of a functional group in a polymeric material is usually revealed by fourier transform infrared (FTIRS) spectra [12].

The spectra of recycled ABS from Matsui fridge was observed that acrylonitrile (C=N) has absorbance peak of 2252cm^{-1}, the benzene ring which is associated with polystyrene, has peak of 697.29-756.12 cm^{-1}, the =CH_2 bond is observed at a bend vibration and a range of 908.5cm^{-1} CH_2 is observed at a bend rocking vibration with symmetric type and a range of 1448.59cm^{-1} However there are other functional groups such as C-C which is observed as a bond stretch vibration with the range of 1189cm^{-1}.

the essence of the Fourier transform infra red (FTIR) analysis was to establish the presence of ABS in the samples. From the peak values therefore, it is evident that there are presence of acrylonitrile, butadiene and styrene functional groups as revealed by the spectral. This confirms the presence of ABS in the samples. The Tec fridge had its own acrylonitrile peak (C=N) at the range of 2240-2305 cm^{-1} ,the aromatic ring peak is at 739.73cm^{-1} and 1446.66 cm^{-1}, the CH_2 has a bend rocking at 1446.66 cm^{-1} ,C=C is observed as a stretch at 1600.01 cm^{-1}, at 3056.31 cm^{-1} $CH_2C(SP^2)$-H is seen.

3.1 Mechanical and physical properties of ABS from different sources

Table 1 the mechanical properties of recycled and virgin ABS obtained experimentally.

The results indicated that recycled ABS from Bauchnect fridge and Matsui fridge had the highest tensile strength while recycled ABS from Fides, Tec, had almost the same tensile strength. Probably, this difference in tensile properties of the recycled ABS may have resulted from the different grades of ABS that are available for the manufacture of fridges and also the application purposes [5]. The wide difference in tensile Properties of recycled ABS as observed in, Matsui fridge and their counterpart Fides, Tec and Bauchnect fridge may have resulted probably from the initial grades of ABS used for their manufacture. However the effect of aging cannot be ruled out. This is because it has been established that aging result into the degradation of poly butadiene components of the ABS and this could affect the overall properties [13, 14]. Previous service life and application conditions also have been established to affect properties achievable from

recycled materials [15, 13]. The tensile properties obtained for all the recycled ABS is less than the experimentally determined values and also the literature values. For the experimentally determined value of the virgin ABS that is lower than the literature value, this could be attributed to the effect of recycling because polymer generally can lose some additives or anti oxidant when in contact with solvent and this can accelerate changes in properties during the recycling process[10].

For the modulus of elasticity (MOE) Matsui fridge had the highest value, while Bauchnect and Tec fridge have very close values, the fides fridge has the least values. The reason for this trend can not be readily explained, but on a general note the reasons advanced for the tensile strength may hold in this case. However, for the flexural strength also known as modulus of rupture(MOR) the values for all the sample are very close but still lower than the experimentally determined value of virgin ABS but they all fall within the literature values [3]. For the elongation at break Matsui fridge has the highest value very close to the experimentally determined values of ABS which fall within the literature value while the values obtained for Tec and Bauchnect fridge are lower than the literature value. Some variation between samples was noticed but it was not generally great as the standard deviation of the test were mostly less than 10%.

Table 2 presents the water absorption and the density of the recycled and virgin ABS.

The virgin ABS has water absorption of about 1.6 % higher than the literature value of 0.3%. The recycled ABS from Bauchnet fridge and Tec Fridge has water absorption higher than the virgin ABS and reported literature value. This could be as a result of presence of impurities that could not be removed completely. The Fides fridge and Matsui fridge has low water absorption relative to the virgin ABS and reported value. Probably the type of impurities present in this recycled from the fridges are not susceptible to water absorption.

The density of Bauchnet fridge which is 1.03/cm^3 is very close to the experimentally determined value of virgin ABS that is 1.04g/cm^3 and both fell within the literature values of 1.02-1.04g/cm^3. However the values obtained for both Fides and Tec fridges are 1.06g/cm^3 and 1.07g/cm^3 respectively and are above both higher than experimentally determined ABS and literature values while the value for matsui Fridge is 1.01g/cm^{3}and is lower than both literature and the experimentally determined ABS values, these deviations could be attributed to absorption of solvent or other causes such as presence of and the of some other impurities.

Changes in density of a specimen may be due to changes in crystallinity, loss of plasticizer, absorption of solvent, or to other causes [16].
Polymers generally do not dissolve in all organic solvents, to this effect the choice of solvent has to be made and this is simplified using solubility parameter. Usually a solvent is suitable for the dissolution of a selected polymer if the solubility parameter values for both are very close e.g. 1.7 -2.0 [3]. One of the most suitable solvent for the dissolution of acrylonitrilre-butadiene-styrene(ABS) is Tetrahydrofuran(THF). The solubility parameter for ABS is 9.49cal/cm^3 while that of THF is 9.79cal/cm^3.

Conclusions

The following conclusions can be drawn from the investigations carried out in this work

Acrylonitrile-butadiene-styrene (ABS) was successfully recycled from used refrigerator material.

Tetrahydrofuran (THF) was found to be the best solvent that can dissolve acrylonitrile-butadiene-styrene (ABS) from waste refrigerator material at room temperature.

The mechanical properties of the recycled ABS were quite low when compared to virgin ABS. The mechanical properties of recycled ABS from Matsui had closest values to the virgin ABS.

The physical properties for all the recycled acrylonitrile-butadiene-styrene agrees with the values obtained for the virgin ABS.

References

[1]. Brennan L.B, Isaac D.H, Arnold J.C (2002), Recycling of Acrylonitrile-butadiene-styrene and High-Impact Polystyrene from Waste Computer Equipment, Journal of Applied Polymer science vol.86,572-578

[2]. Dewen Dong, Shigeru Tasaki, Satoru Aikawa, Shingo Kamiyo, Norihiro Inagagaki, Youji Inouc (2001) Thermal Degradation of Acrylonitrile-butadiene-styrene Terpolymer in bean-oil. Polymer Degradation and stability 73, 319-326

[3]. Robert O.Ebewele (2000) polymer Science and Technology CRC Press Florida U.S.A Pg 433-434

[4].Antal Boldizar,Kenneth moller (2003) Degradation of ABS during repeated processing and accelerated ageing, Polymer degradation and stability 81, 359-366

[5]. Basdekis C.H (1964) ABS plastics Reinhold publishing corporation U.S.A pg 107

[6]. Pascoe R.D (2004), The use of selective depressant for the separation of ABS and HIPS by froth flotation, material Engineering 18, 233-237

[7].Papaspyrides C.D, Poulakis J.G,In :Salmone J.C editor(1996), Polymeric materials encyclopedia,volume set: recycling, plastics. New York: CRC press Inc, pg 7403

[8]. Arostegui .A, Sarrionanda.M, Aurrekoetxea.J, Urrutibeascoa .I (2006), Effect of dissolution-based recycling on the mechanical properties of acrylonitrile-butadiene-styrene copolymer, polymer Degradation and

stability91, 2768-27746.
[9]. Pascoe R.D. (2003) Physical separation of plastics. In: Dhir, R.K. Newlands, M.D., Halliday, J.E editors (2003), Recycling and reuse of waste materials.Thomas Teflords, pg 173-188

[10] John Burke in Craig Johnson editor (1984), Solubility Parameter: Theory and application, appeared in the AIC Book and paper Group Annual, vol3, 13-58

[11]. Bastida .S, Marieta . C, Eguiazabal. J. I, Nazabal.J (1995), Effects of reprocessing on the nature and properties of SAN. Eur polymer Journal 31, 643-6

[12].Arnold J.C, Alston .S, Holder .A, (2009), Void formation due to gas evolution during recycling of acrylonitrile-butadiene-styrene (ABS) from Waste Electrical and Electronic Equipment (WEEE) Polymer Degradation and Stability 94, 693-700

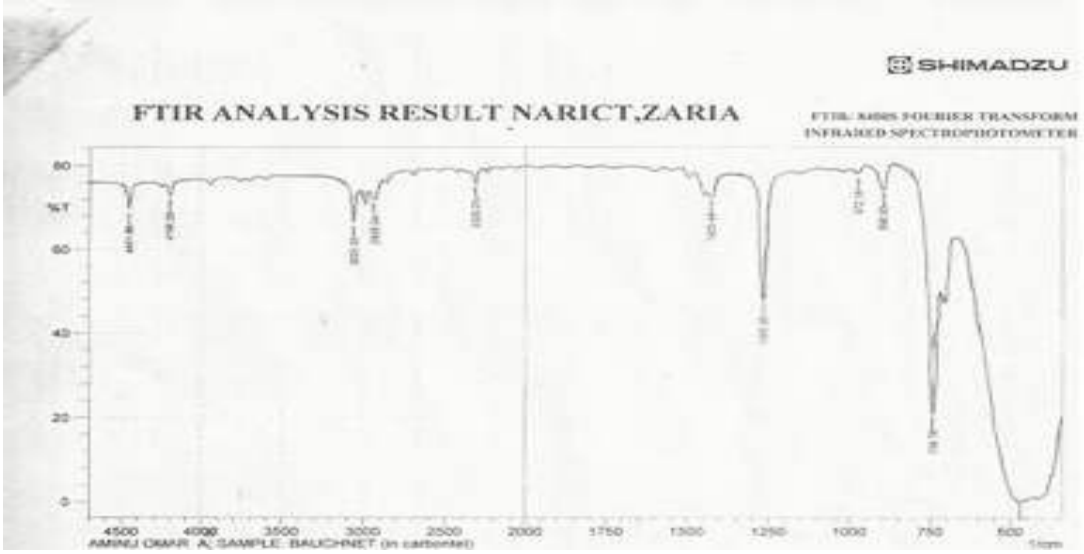
[13] Boldizar.A, Keneth.M (2003), Degradation of ABS during repeated processing and accelerated ageing, Polymer Degradation and stability, 359-366

[14]. Tiganis B.E, Burn L.S, Davis. P, Hill A.J, (2002), Thermal degradation of Acrylonitrile-butadiene-styrene (ABS) blends.polymer degradation and stability76; 425-434

[15] Vilplana.F,Ribes-Greus.A, Karlsson .S (2007), Analytical strategies for the quality assessment of recycled High-impact polystyrene: a combination of thermal analysis, vibrational spectroscopy , and chromatography, Anal chim acta 604, 18-28

[16] ASTM Standards and Literature References for Composite Materials (1987),1st edn





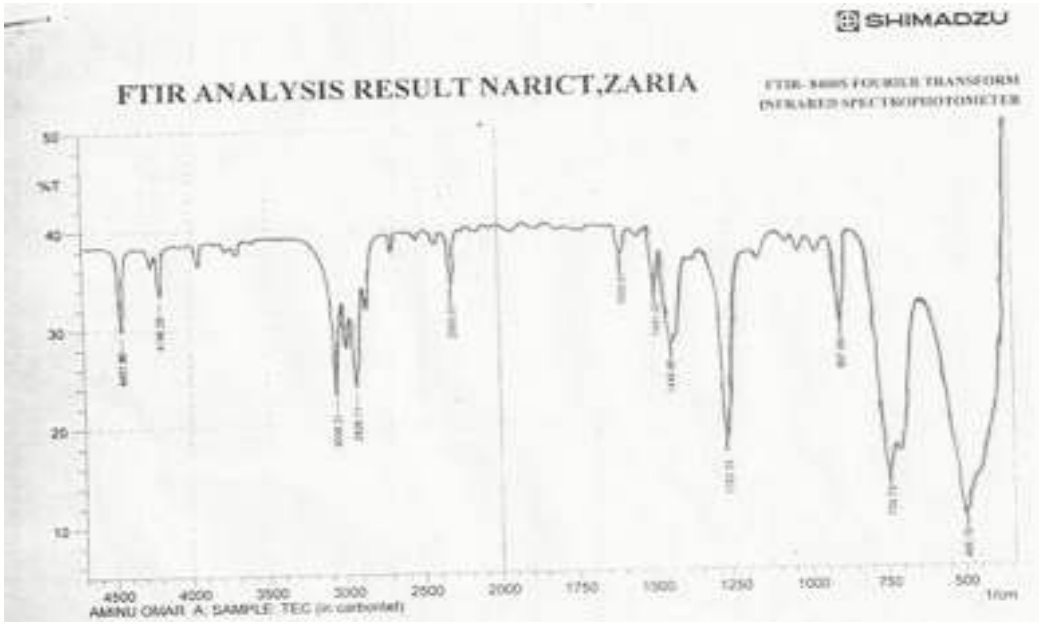


Figure 1: Sample FTIR spectra of the recycled ABS (A) Matsui Fridge, (B) Bauchnet Fridge and (C) Tec Fridge

Table 1: Mechanical properties of recycled and virgin ABS

materials	Tensile strength (Mpa)	Modulus of elasticity (MOE) (Mpa)	Flexural strength (Mpa)	Elongation (%)
Fides Fridge	30.89	820	57.5	4.11
Tec fridge	27.63	925	51.2	3.71
Matsui fridge	31.66	1021	60.18	4.8
Bauchnet fridge	29.71	935	55.25	4.4
Virgin ABS	48.3	1312	65.75	13.37

Table 2: Physical properties of recycled and virgin ABS

Materials	Density (g/cm^3)	Water absorption (%)
Fides fridge	1.06	0.2569
Tec fridge	1.07	0.3934
Matsui fridge	1.01	0.2625
Bauchnet fridge	1.03	0.3211
Virgin ABS	1.04	0.3048

EFFECT OF *DELIGNIFIED* NATIVE *BAMBOO (BAMBUSA VULGARIS) CELLULOSIC* –G-POLY (ACRYLONITRILE) ON THE GROWTH OF OKRO (*ABELMOSCHUS ESCULENTUS)* SEEDLINGS

L. O. Ekebafe*[1], M.O.Ekebafe[2], S.O. Ugbesia[1], J.A. Idiaghe[1]
[1]Polymer technology department, Auchi Polytechnic, P.M.B. 13, Auchi, Nigeria
[2]Department of Chemistry, Nigerian Institute for Oil Palm Research, P.M.B. 1030, Benin
*Corresponding author e-mail: lawekebafe@gmail.com

ABSTRACT
Graft copolymers of bamboo cellulosic and acrylonitrile were synthesized in aqueous solution using ceric ammonium ion as the initiator. Saponification of grafted copolymer was done by reaction with sodium hydroxide followed by methanol precipitation. The grafting was confirmed using FTIR and characterized in terms of %GE, %G, % add-on, water retention value and free polymer. Soil samples collected were prepared and analyzed for physico-chemical properties in the laboratory using standard techniques. The growth of the okro seedlings in the hydrogel –soil mixture in which the seedlings have been planted were measured as a function of hydrogel loading and compared with the values obtained in the control in which hydrogel was not added. The hydrogel showed good improvement in soil properties more as a soil conditioner. The results of the soil-hydrogel analysis at a monthly interval showed that there was increase in the growth of the okro seedlings compared to the control.
KEYWORDS: Hydrogel, soil, cassava starch, acrylonitrile, maize

INTRODUCTION

One of the most active areas in scientific research is the development of new and exciting materials for a wide variety of applications. Superabsorbent polymers (SAPs) or hydrogels are loosely cross-linked, three-dimensional networks of flexible polymer chains that carry dissociated, ionic functional groups. They are basically the materials that can absorb fluids of greater than 15 times their own dried weight, either under load or without load, such as water, electrolyte solution, synthetic urine, brines, biological fluids such as urine sweat, and blood, [1]

Relatively few or no data are available in the literature on the effect of hydrogel on the physico-chemical properties of soil supporting crop production in developing countries. The present communication describes the investigation of the influence of delignified bamboo cellulosic -g-P(AN) on physio-chemical properties of soil supporting the growth of okro seedlings in Nigeria, by varying the loading concentration of the hydrogel while keeping soil load constant.

MATERIALS AND METHODS

Materials

Bamboo culms were obtained from Igieduma village, along Benin –Auchi Expressway, Edo State, Nigeria, **the soil used was obtained from a farm site at Auchi Polytechnic, Auchi, Edo State and okro seedlings obtained from Igbe market, Auchi, Nigeria.** Acrylonitrile (AN) was supplied by B.D.H. as reagent grade and was distilled under reduced pressure and stored in the dark at 5 ◦C before use, ceric ammonium nitrate and other reagents used were of analytical grade and supplied by BDH, England.

Preparation of the Bamboo Cellulosic material

Matured bamboo culms were harvested and cut into small strips with saw blade. The strip material was grounded in the mill. The material was then placed in a shaker with sieves to pass through a 425-µm mesh sieve yet retained on a 250-µm mesh sieve. The resulting material was placed in glass jars labeled with appropriate designation for the analysis.

The delignified cellulosic was isolated using the method described by Brendel O. et al [2]

Characterization of the Bamboo Culms and soil

The bamboo culms were characterized in terms of the lignin content, determined according to ASTM D1106-56 [3] . Holocellulose content, determined using the method described in ASTM 1104-56 [4]. Ash content, determined as described in ASTM D1102-84. [5] Hemicellulose content and cellulose content, determined according to ASTM D1103-60 [6]. The results are as presented in Table 1.

The soil samples were characterized as follows: Bulk density was measured by core method, [7] Soil pH was measured in 1:1 soil-water ratio [8], Soil organic carbon was estimated by combustion at 840°C,[9], while total nitrogen was obtained by microkjeldahl method. Cation exchange capacity was measured using ammonium acetate leaching at pH 7.0,[10] Available phosphorus was determined by Olsen method,[11] and soil heavy metal content was determined using the AAS. The results are as presented in Table 2.

Synthesis of Graft Copolymers

The grafting reaction was carried out under nitrogen atmosphere in a flask equipped with a nitrogen inlet immersed in a constant temperature water bath. Solution of ceric ammonium nitrate (CAN) of varied concentrations were prepared by dissolving the required molar concentration of CAN salt in 1% nitric acid. In a typical reaction, 1 g cellulosic was immersed in 30 ml

solution of 20 mmol/L CAN for 30 mins followed by addition of a mixture of 20 ml toluene and 12.5 mol/AGU acrylonitrile,[12]. The grafting reaction was carried out for 3 h at 40°C under stirring. At the end of reaction, mixture was washed with distilled water, subsequently with methanol, filtered and the product was dried in the vacuum oven at 60°C for 4 days. The dried product was divided into two equal portions, one portion treated with dimethylformamide for 48 h to remove the free polymer (FP)/homopolymer (polyacrylonitrile). The grafted cellulose was dried for 4 days to obtain a constant weight. The percent graft yield (%G) and percent grafting efficiency (%GE) were calculated on an oven dry weight of cellulose from the increased weight of cellulose after grafting. Results are as presented in Tables 2, 3

Alkaline Saponification

A suspension of 1.0 g of cellulose –g-poly (AN) copolymer in 9ml, 0.7M NaOH was introduced in a weighing bottle and mixed well. The bottle (loosely stoppered to permit escape of ammonia) was then placed in an electric oven at 95°C for desired time to complete the saponification. The mixture was dispersed in 200mL methanol using electric blender for 5 min and then poured into an excess of ethanol. The precipitate was washed with slightly acidified ethanol (ethanol with few drops of acetic acid) until pH 8, then filtered and dried at 60°C for 3 h.

Characterization of bamboo cellulosic-g-P(AN) copolymer hydrogel

The grafted copolymer hydrogel was characterized in terms of %GE, %G, % add-on, water retention value and free polymer, [13]. Swelling of hydrogel was measured by the free swelling method, [14] and expressed as a water retention value (WRV) calculated in grams of water per grams of dry polymer.

Infrared analysis

IR spectra of ungrafted and grafted cellulose were recorded on an ABB Bomem MB-100 FTIR spectrophotometer and as presented in the spectral sheet in Figure 1.

Soil - Hydrogel mixing procedure

Measured quantities of the hydrogel (0, 3.0, 6.0, 9.0, 12.0g by weight) were thoroughly mixed with 2kg of soil each and designated as W_0, W_1, to W_5, placed in containers. Okro seedlings (a widely-used vegetable plant with high water requirements) were planted in the center of each container. The soil was irrigated with water and the volume of water required to saturate the soil to field capacity was recorded. Subsequent irrigations were applied, the amount of water required to attain field capacity was recorded.

Data Analysis

In all, 5 treatments per set (Hydrogel, 4 concentrations and one control) were replicated and arranged in complete randomized block design with five containers per treatment. Biometric data on height, and leaf population of the experimental plants were recorded at bi-weekly intervals. The total amount of water used for irrigation was determined upon completion of the study. Data were analyzed by Analysis of Variance (ANOVA). The results are as presented in Table 4 and 5.

RESULTS AND DISCUSSION

Characteristics of the bamboo culms and Cellulose yield

Table 1 shows the Characteristics of the Bamboo culms and the extractive cellulose yield.

In general, the alpha-cellulose content in bamboo is 40-50%, which is consistent with the reported cellulose content of softwoods (40-52%) and hardwoods (38-56%). Alpha-cellulose is the main source of the mechanical properties of bamboo and wood, [15]. Holocellulose include alpha-cellulose and hemicellulose. Approximately 40-55% of the dry substance in bamboo is alpha-cellulose.

Grafting characteristics

The results of the percent graft levels and graft efficiencies shows that graft copolymers formation is most likely due to combination of growing homopolymer chains with the radicals formed on the substrate,[16]. It has been established that the extent of graft copolymer formation depend on the amount of monomer complexed [17]

The water absorption (WRV) of the grafted copolymer gave high water absorption of 379 g g^{-1}. A careful study of the reaction indicates that grafting is associated with the homopolymer formation and that saponification converts the same grafted poly (AN) chain and homopoly(AN) chain with cyano group (-C=N) as the main group to both amide ($-CONH_2$) and carboxylate (-COONa) groups. The nitrile groups of PAN were converted to a mixture of hydrophilic carboxamide and carboxylate groups during alkaline hydrolysis, followed by in situ cross-linking of the grafted PAN chains. More PAN led to more carboxamide and carboxylate groups being generated.

IR characterization

The FTIR spectra of the cellulosic material derived from bamboo *(Bambusa vulgaris)* and the optimized grafted sample (%G 167.3, %GE 93) were recorded. In the FTIR spectra of the optimized sample of grafted cellulose, besides the typical signals of cellulose backbone (υOH 3414 cm^{-1}, υCH 1431 cm^{-1}, υCOC 1059 cm^{-1}, υβ-linkage 890 cm^{-1}), the characteristic absorption bands at 2245 cm^{-1}, for the nitrile group (–CN) introduced and 2926 cm^{-1} (characteristic for $–CH_2$ group) with increased intensity were observed, which shows that grafting of acrylonitrile has occurred.

Physico-chemical characteristics of the experimental soil before planting

Textural analysis in table 2 showed the preponderance of sand fraction (69.22%), followed by clay (16.38%), then silt (14.40%), thus classifying the soil as sandy loam soil, [18] this is corroborated by the soil bulk density (1.33g/cm^3) which is an index of the textural nature of the soil. The slightly alkaline pH of 8.0 recorded for the soil

is within the range of agricultural soils. The pH of soil influences ion-pair formation, solubility of organic matter, as well as surface charge of Fe, Mn and Al- oxides, organic matter and clay edges, [19].

Influence on the Growth of okro seedlings, Water Retention and Physicochemical properties of the soil

Sandy soils which are coarse-textured, are light soils and are easier to till, they drain better, and are warm. Crop production on sandy soil requires frequent irrigation to make up for its poor water holding capacity. Thus the idea of applying hydrogel therefore is to increase the water holding capacity of the soil as to reduce the frequency of irrigation and its cost implication. The capacity of hydrophilic polymers to provide water to plants depends on the proportion of water held by the polymer that is easily available to plants, the pressure the soil exerts on the polymers, the presence of soluble salts and the ability of the hydrogel to make use of gravitational water, water which is usually not available to plants, as well as capillary water, [20]

Table 5, Figure 2 and Figure 3 show the growth of the okro seedlings in terms of height and leaf number of the plant. The table and figures reveal consistent increase in growth and leaf number, which is expected based on the availability of soil nutrients and water. The results show that there are significant effects of irrigation regime on the height and leaf number. The height and leaf number increases from W_0 to W_5 due to the ability of the soil to make water available to the plant. The control did not show comparable increase in the height and leaf number of the plant.

CONCLUSION

The main aim of this work is to gauge the influence of bamboo cellulosic-g-P(AN) hydrogel on the growth of okro seedlings in Nigeria, as well as the water holding capacity of the hydrogel-soil mix, under farming condition typical to developing countries.

The results indicate that there is an improvement in the ability of the soil to hold water by reason of the introduction of the hydrogel, thus, this could become cost effective in irrigation of farmlands in Africa. These results are of interest for the development of hydrogel-based technologies for solving the problem of agriculture and water conservation management in sub-Saharan Africa.

REFERENCES

1. Zohuriaan-Mehr MJ, PourJavadi (2003). New Polysaccharides -gcopolymers: Synthesis and Thermal Characteristics. Polym. Adv.Technol. 14: 508-516

2. O. Brendel,P.P.M. Iannetta, and D. Stewart. *Phytochem. Analy.*, **11**:7–10, (2000).
3. ASTM D1106-96 " Standard Test Method for Acid-Insoluble Lignin in Wood," ASTM International, West Conshohocken, PA, 2007, www.astm.org.
4. ASTM D1104-56 Method of Test for Holocellulose in Wood ,ASTM International, West Conshohocken, PA, 1978, www.astm.org.
5. ASTM D1102-84: Standard Test Method for Ash in Wood ,ASTM International, West Conshohocken, PA, 2007, www.astm.org.
6. ASTM D1103-60 Method of Test for Alpha-Cellulose in Wood, ASTM International, West Conshohocken, PA, 1977, www.astm.org.
7. Grossman, R.B., T.G Ranches. (2002); Bulk Density and linear extensibility in: Dane J.H. Topp. G.C.(eds) Methods of soil analysis, part 4 physical methods. Soil Sci. Am. Book series No. 5 ASA and SSSA. Madison WT; 201-228

8. Hendershot, W.H. H. Lalande, M. Duqyette (1993): Soil reaction and exchangeable acidity in; carte M.R. (ED) Soil sampling and methods of analysis. Can. Soc. Soil sci. Lweis publisher London, 141-145.
9. Wang, D. D.W. Anderson (1998): Direct measurement of organic carbon content in soils by leco CR-12 carbon analyzer. Commun. Soil sci. plant Anal., 29:15-21
10. Rhoades J.D. (1982): Cation Exchange Capacity in; page A.I. Miller R.H. Keeney D.R. (eds) Methods of soil analysis part 2 American Soc. Agro. Madison W.I. pp. 149-158
11. Emteryd O. (1989) :Chemical and physical analysis of inorganic nutrients in plants soil water and air stencil no. Uppsala Swedish University of Agricultural Sciences.
12. Pourjavadi A, Zohuriaan-Mehr MJ, Ghaempoori SN, Hossenzadh H (2007). Modified CMC. V. Synthesis and superswelling behaviour of hydrolysed CMC-g-PAN Hydrogel. J. Appl. Polym. Sci. 103: 877 – 883.
13. Lanthong ,P; R. Nuisin b, S. Kiatkamjornwong Graft copolymerization, characterization, and degradation of cassava starch-g-acrylamide/itaconic acid superabsorbents Carbohydrate Polymers 66 (2006) 229–245
14. Weaver, M.O; R.R.Montgomery, L.O. Mitler, V.E.Seina, G.F.Fanta, and W.M. Doena, A practical process for the preparation of super slurper, a starch-Based polymer with a large capacity to absorb water, De Sark. Jabrg. 1977 12 S. 410-421
15. Scurlock, J.M.O; D.C. Dayton, and B. Hames: Biomass and Bioenergy. 2000, 229-244.
16. Ogbeifun D.E. and Okieimen F.E.(2009): Synthesis, Characterization and Flocculation properties of Gum Arabic-g-Acrylamide copolymer. J. Nig. Ints.Prod. Engrs. Vol. 11 pp. 278-288
17. Jideonwo A, Okieimen FE (2000). Graft copolymerization of methylacrylate onto gum Arabic, Niger. J. Appl. Sci. 18: 109 -114.
18. Soil Survey Staff, (1998). Keys to Soil Taxonomy (8th. Ed.), USDA-NRCS, Center Technology Evaluation Report TE- 98-01, 37.
19. Tokalioglu, S.; Kartal, S.; Gültekin, A., (2006). Investigation of heavy-metal uptake by vegetables growing in contaminated soils using the modified BCR sequential extraction
20. Pritchard James J. and Quinn James J.(1983)Terra-Sorb, A Water management Tool for World crop production. Industrial services internation, inc.

Table 1 Characteristics of the Bamboo culms and the extractive cellulose yield

Ash (%)	Lignin (%)	Hemicellulose (%)	Cellulose (%)	Holocellulose (%)	Cellulose yield (%)
1.95	21.26	24.44	47.51	71.95	62.46

Table 2: Result of physic -chemical characterization of the soil sample before planting

Analytical characteristics	**Results**
Particle size distribution	%Clay 16.38 % Silt 14.40 %Sand 69.22
pH	8.0±0.01
Bulk Density(g/cm^3)	1.33±0.02
Soil organic carbon, g/kg	0.544±0.05
Total Nitrogen, g/kg	0.048±0.002
Cation exchange capacity,mg/kg	286.02±0.92
Available Phosphorus, mg/kg	5.889±0.150
Sodium content, mg/kg	7.18±0.07

Table 2: Result of physic -chemical characterization of the soil sample before planting

Potassium content, mg/kg	2.70±0.05
Magnesium content, mg/kg	67.63±0.25
Calcium content, mg/kg	208.51±0.55
Lead (mg/Kg)	0.05
Cadmium (mg/Kg)	ND
Arsenic(mg/Kg)	ND
Copper (mg/Kg)	0.002
Total acidity	0.2

ND = Not Detected

Table 3: Characteristics of the grafted copolymer

Characteristics	**Results**
Water retention value (g/g)	379
Grafting Efficiency (%)	93.52
Grafting Yield (%)	167.89
Add-on percentage	60.33
Free Polymer (%)	15.67
pH	8.0

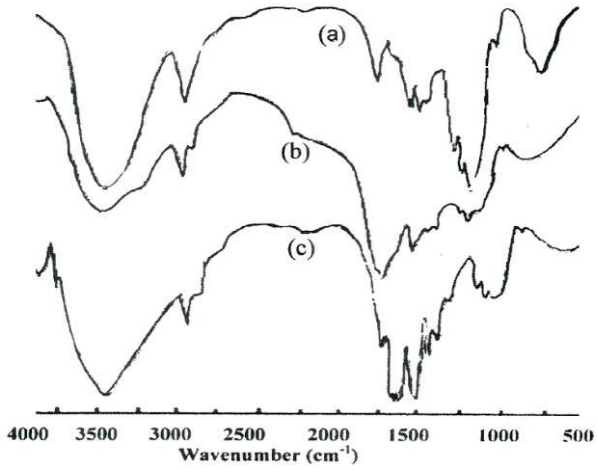


Figure 1: IR spectra of ungrafted (a), grafted (b) and hydrolyzed grafted (c) bamboo cellulosic

Table 4: water used by zea may in polymer amended soil

Soil/poly. Conc.	Water 2 weeks	Applied to 4 weeks	Soil(ml) 6 weeks
W_1	500	240	190
W_2	540	260	210
W_3	580	288	225
W_4	620	315	238
W_5	740	342	262

Table 5: Biometric observations of the okro seedlings showing the height and leaf number

Control (W1) BIWEEK	Ht (cm)	LN	W2	Ht (cm)	LN	W3	Ht (cm)	LN	W4	Ht (cm)	LN	W5	Ht (cm)	LN
2	8.5	2		10.1	2		11.1	2		12.6	3		17.3	4
4	9.5	2		10.5	4		11.5	4		13.6	6		17.9	6
6	10.1	2		11.1	4		11.8	6		15.1	8		19.3	8
8	10.5	3		11.8	4		12.5	8		15.8	8		20.5	10

Ht=Height, LN = Leaf Nu **mber**

DEVELOPMENT AND APPLICABILITY OF SYNTHETIC POLYMERIC MATERIALS FOR CORROSION INHIBITION; A SUSTAINABLE TECHNOLOGY FOR PIPELINES AND ALLIED STRUCTURES INTEGRITY

C. I. Nwoye[1*], J. U. Odo[1], E. O. Obidiegwu[2], and C. C. Ugwuegbu[3]
*[1]Department of Metallurgical and Materials Engineering, Nnamdi Azikiwe University, Awka.
[2]Department of Metallurgical and Materials Engineering, University of Lagos.
[3]Department of Materials and Metallurgical Engineering, Federal University of Technology, Owerri.
*Corresponding author: chikeyn@yahoo.com

Abstract
The development and applicability of synthetic polymeric materials for corrosion inhibition have been appraised in terms of their sustainability as a growing technology for pipeline and allied structure integrity. Polymer synthesis were reviewed and found to be classified into laboratory synthesis, which are generally divided into step-growth polymerization and chain-growth polymerization as well as biological synthesis which are sub classified into polysaccharides, polypeptides, and polynucleotides. A critical review of polymeric coatings shows they are classified into inert, inhibitive and sacrificial coating. The types of polymeric coating were also reviewed with particular reference to pipeline and allied structure protection. A review of the progress recorded in terms of advancement in the development of polymer for corrosion protection revealed that 3356 GP, ***Elasti-Liner***, fiberglass or flake filled reinforces epoxy novolac, vinyl ester and polyester, phenolics, baked phenolics, epoxy phenolics, epoxies and aliphatic polyketones have all been tested and certified highly resistant to severely corrosive environment even at a temperature up to 400^0F. A mathematical analysis to determine the condition for high pipeline and allied structure integrity indicates that the pipeline and allied structure integrity (P_i) is directly proportional to the inhibitor efficiency E_i.

Keywords: Development, Application, Synthetic Polymer, Corrosion Inhibition, Pipeline

INTRODUCTION

The word ***polymer*** is derived from the Greek words *πολύ- - poly-* meaning "many"; and *μέρος - meros* meaning "part" [1]. The term was coined in 1833 by Jöns Jacob Berzelius, although his definition of a polymer was quite different from the modern definition.

Historical development

From 1811, Henri Braconnot did pioneering work in derivative cellulose compounds,

perhaps the earliest important work in polymer science. The development of vulcanization later in the nineteenth century improved the durability of the natural polymer rubber, signifying the first popularized semi-synthetic polymer. In 1907 Leo Baekeland created the first completely synthetic polymer, bakelite, by reacting phenol and formaldehyde at precisely controlled temperature and pressure. Bakelite was then publicly introduced in 1909.

Despite significant advances in synthesis and characterization of polymers, a correct understanding of polymer molecular structure did not emerge until the 1920s. Before then, scientists believed that polymers were clusters of small molecules (called colloids), without definite molecular weights, held together by an unknown force, a concept known as association theory. In 1922, Hermann Staudinger proposed that polymers consisted of long chains of atoms held together by covalent bonds, an idea which did not gain wide acceptance for over a decade and for which Staudinger was ultimately awarded the Nobel Prize. Work by Wallace Carothers in the 1920s also demonstrated that polymers could be synthesized rationally from their constituent monomers. An important contribution to synthetic polymer science was made by the Italian chemist Giulio Natta and the German chemist Karl Ziegler, who won the Nobel Prize in Chemistry in 1963 for the development of the Ziegler-Natta catalyst. Further recognition of the importance of polymers came

with the award of the Nobel Prize in Chemistry in 1974 to Paul Flory, [1] whose extensive work on polymers included the kinetics of step-growth polymerization and of addition polymerization, chain transfer, excluded volume, the Flory-Huggins solution theory, and the Flory convention.

Synthetic polymer materials such as nylon, polyethylene, Teflon, and silicone have formed the basis for a burgeoning polymer industry. These years have also shown significant developments in rational polymer synthesis. Most commercially important polymers today are entirely synthetic and produced in high volume on appropriately scaled organic synthetic techniques. Synthetic polymers today find application in nearly every industry and area of life. Polymers are widely used as adhesives and lubricants, as well as structural components for products ranging from children's toys to aircraft. They have been employed in a variety of biomedical applications ranging from implantable devices to controlled drug delivery. Polymers such as poly(methyl methacrylate) find application as photo resist materials used in semiconductor manufacturing and low-k dielectrics for use in high-performance microprocessors and computer screens. Recently, polymers have also been employed as flexible substrates in the development of organic light-emitting diodes for electronic display.

POLYMER SYNTHESIS

Polymerization is the process of combining many small molecules known as monomers into a covalently bonded chain [2]. During the polymerization process, some chemical groups may be lost from each monomer. This is the case, for example, in the polymerization of PET polyester. The monomers are terephthalic acid (HOOC-C_6H_4-COOH) and ethylene glycol (HO-CH_2-CH_2-OH) but the repeating unit is -OC-C_6H_4-COO-CH_2-CH_2-O-, which corresponds to the combination of the two monomers with the loss of two water molecules. The distinct piece of each monomer that is incorporated into the polymer is known as a repeat unit or monomer residue.

Laboratory synthesis

Laboratory synthetic methods are generally divided into two categories, step-growth polymerization and chain-growth polymerization. [2] The essential difference between the two is that in chain growth polymerization, monomers are added to the chain one at a time only, whereas in step-growth polymerization chains of monomers may combine with one another directly. However, some newer methods such as plasma polymerization do not fit neatly into either category. Synthetic polymerization reactions may be carried out with or without a catalyst. Laboratory synthesis of biopolymers, especially of proteins, is an area of intensive research.

Biological synthesis

There are three main classes of biopolymers: polysaccharides, polypeptides, and polynucleotides [2]. In living cells, they may be synthesized by enzyme-mediated processes, such as the formation of DNA catalyzed by DNA polymerase. The synthesis of proteins involves multiple enzyme-mediated processes to transcribe genetic information from the DNA to RNA and subsequently translate that information to synthesize the specified protein from amino acids. The protein may be modified further following translation in order to provide appropriate structure and functioning.

APPLICATION OF SYNTHETIC POLYMERIC MATERIALS FOR CORROSION PROTECTION

Corrosion of Pipelines and Allied Structures

Report [3] has shown that one of the major causes of pipeline defects around the world is corrosion. Studies [4-7] have shown that the most commonly used material for petroleum pipelines is mild steel because of its strength, ductility, weldability and amenability to heat treatment for varying mechanical properties. Mild steel has been reported [8] to corrodes easily because oxide formed on exposure to air readily breaks down and in the presence of moisture, not repaired and so a reaction between iron (Fe), moisture (H_2O), and oxygen (O_2), takes place to form rust as shown in equation (1):

$$4Fe + 2H_2O + 3O_2 = 2Fe_2O_3.H_2O \qquad (1)$$

$Fe_2O_3.H_2O$ is the rust, and usually unprotected, hence the corrosion process goes unimpeded [9].

Studies [10] have shown that development and application of synthetic polymeric materials as coatings on pipelines and allied structures opens up a new frontier for achieving pipeline and allied structures integrity. There is a growing need to appropriately tackle and combat corrosion on oil pipelines and allied facilities as shown in Figs 1 and 2 and suppress or inhibit processes that could promote further corrosion on these facilities in order to obviate the occurrence of ruptures resulting to fire out break and devastating environmental pollution as well as loss of money through oil spillage in addition to fuel scarcity, harsh economic meltdown and enormous casualties on the part of oil field workers.

The role of synthetic polymeric coatings is essentially to insulate the metal from the external medium and so prevent the formation of microcells on the metal surface. The efficiency of these coatings is directly related to the degree to which it interposes itself between the environment and the structure hence reducing attack by the environment [10].

Research [12] has shown that good functioning of a coating depends on its adhesiveness rate to the metal surface. Initial adhesiveness and its durability in the contact conditions are among those factors that enhance coating efficiency in long term. The rate of Initial adhesiveness has a high relationship with coating movement and surface wetness by this movement in the course of applying the coating and also with cleanliness and preparedness of pipe surface. The durability and permanence of adhesiveness depends on coating

properties including its resistance to moisture penetration.

POLYMERIC COATINGS

Classification of Polymeric Coatings

Polymeric coatings can be classified [13] into;

(a) Inert coating; which restricts contact between the structure and the environment
(b) Inhibitive coating; which releases substance that are inhibitive of attack on the structure
(c) Sacrificial coating; which produces electric current that protects the structure

Types of Polymeric Coatings

The various polymeric coatings used for combating corrosion [13] includes: Epoxy high build 6450, epoxy primer red 6151, catalytically-cured, high solids content epoxy. Polyester resins reinforced with embedded fiberglass mats, epoxy-phenolic resins, catalytically cured epoxy-phenolic, aluminum pigmented alkyd resin.

Polymeric Coatings for Pipelines

The major polymeric coatings used for pipelines are epoxy high build 6450 and catalytically-cured, high solids content epoxy [13].

***Epoxy High Build 6450*:** This coating was found [13] to have excellent resistance to abrasion and to fresh, salt water, non oxidizing acids and alkalis, oils and many chemicals. It is ideal as a build coat or finish for structural steelwork in aggressive environments. It is also used in onshore operation as lining for concrete and steel tanks, portable water tanks, external tankage, pipeline, harbour and shore installations, high performance structural steel, chemical plants, food processing industries. This coating can be applied by airless spray (with tip size range: 0.43-0.53 mm and tip pressure: 1600-2300psi) or using rollers.

Catalytically-cured, high solids content epoxy: This is used for primarily for maintenance coating of all steel surfaces in the splash zone area of marine structures that are not otherwise protected [13]. Typical applications are in secondary structural bracing, pipe and piping, pipeline risers, hangers, ladders and other attachment that can be applied under water and to concrete. The recommended coating for onshore buried pipe at above/below ground transitions in areas of drifting sand. The recommended coating above ground pipe subjected to direct seawater splash and spray in beach areas.

NEWLY DEVELOPED ADVANCED POLYMERIC MATERIALS FOR CORROSION INHIBITION

A newly developed polymeric material [14] for corrosion protection such 3356 GP gives outstanding performance characteristics which includes; very high adhesion to a wide variety of substrates, (over steel, concrete or old coatings), high temperature stability to 250ºF, low temperature flexibility, with high elongation of 40% to 60%, thermal cycling stability, low embedment stress, very low molecular moisture permeability (implying 3356 GP is hydrophobic i.e. it rejects water) and high corrosion resistance to a wide variety of organic and inorganic acids and caustics including bleaches and some solvents at the widest range of operating temperatures. It also combines many advantages of rubbers and elastomers in a single high performance polymer material that is resilient, ductile and not damaged from external forces placing the system in tension. Developed as a Railcar lining, 3356 GP is ideally suited as a coating for splash & spill or full time immersion in railcars, over the road tank trucks and storage/processing tanks. Many additional uses will include sump and trench lining and flooring systems where 3356 GP properties are desired. It (3356 GP) may also be reinforced with glass fiber, Kevlar® I or other CCSI recommended reinforcing material to build a "laminate structure" providing a tougher lining or floor system.

The polymeric coating (3356 GP) is 96% solids and is easily installed by airless spray, plural component, or roll and brush, to piers, decks, offshore structures and waste treatment areas, crude oil and refined product storage and handling. It resists skydrol and hydraulic fluids and a myriad of potent chemicals such as 100% adipic acid, an organic acid, at temperatures ranging to a maximum of 210ºF (98.8ºC).

A recent breakthrough in polymer chemistry is the development of an elastomeric polymer [15]. This product is called ***Elasti-Liner*** from KCC Corrosion Control. ***Elasti-Liner*** possesses excellent elongation and tensile properties while having chemical resistance equal to or superior to the rigid and thermoplastic polymers available to date [15]. The new polymer system is spray, roller, or squeegee applied over prepared concrete, or even cracked but well-bonded lining materials, in two or three successive coats. Upon cure, the most widely used version of the polymer possesses about 235% elongation and resists immersion of unlimited duration in aggressive aqueous chemistry. ***Elasti-Liner Joint*** is a truly unique innovation in crack and joint sealing. The key component of the ***Elasti-Liner Joint*** is a premolded version of ***Elasti-Liner.*** This 5" wide material is supplied in rolls of 50 lineal feet. It is chemically adhered to various substrates including concrete, polymer or steel. EL joints provide protection over concrete with up to 1/4" of dynamic movement of the substrate. This can be used over true expansion or isolation joints within that range [15].

Thermoset polymer systems have also been applied for corrosion protection. These include fiberglass or flake filled reinforces epoxy novolac, vinyl ester and polyester [15].

Heresite has developed [16] other high temperature resistant linings that will resist the corrosive effects of most commodities. These linings include phenolics, epoxy phenolics, and epoxies. These polymeric materials can extend the service life of tanks in trailers and protect the purity of the product being hauled. Baking phenolic and air-drying phenolic coatings have been used for many years to protect fans, blowers, fume hoods, dampers, grills duct work etc. from corrosion. Baking phenolic coatings are used for severely corrosive environments or where operating temperatures exceed 150°F. Also, they

are used to provide protection against abrasion. These polymeric coatings can protect all types of finned tube coils used for oil, water, air, gas and process cooling (and heating), as well as large condensing coils against damaging environments. The baking phenolic coating from Heresite will withstand operating temperatures up to 400°F. However, this does vary depending upon the products in the environment. Wheel balance normally is not disturbed because the coating is applied in thin, uniform, multiple coats. The baked phenolic coating is considered as being spark resistant and as such is suitable for exposure to explosive gases and dusts. Also, the coatings do not support combustion. Excessive temperature will char the coating, but the coating will not burn. The baked phenolic coatings will withstand exposure to practically all corrosive atmospheres with the exception of strong alkalis such as potassium and sodium hydroxide, strong oxidizers such as aqua regia and wet bromine, chlorine and fluorine in concentrations greater than 100ppm. Baked phenolic coatings from Heresite are also used to provide protection against abrasion. These polymeric coatings can protect all types of finned tube coils used for oil, water, air, gas and process cooling (and heating), as well as large condensing coils against damaging environments. The coating has effectively demonstrated its value in protecting heat transfer coils from corrosive attack, and appreciably increasing equipment service life. The excellent chemical and temperature resistance coupled with the good heat transfer properties of the Heresite coating have resulted in outstanding performance.

The coatings have been found [16] to offer an economical alternative to the use of special metals for corrosive environments. For example, aluminum fin coils coated with Heresite are more economical than copper fin coils. Special metal casing materials are unnecessary since the Heresite coating is applied to the casing, as well as to the finned tubes. Additionally, Heresite coated aluminum fins will resist attack from most cleaning agents more successfully than copper fin coils. It is noted that the Heresite coating is applied to both plate fin coils, as well as spiral wound tubing.

Alternating aliphatic polyketones are a new family of engineering thermoplastics whose molecular chains are linear, perfectly alternating carbon monoxide and alpha olefin structures, possessing a unique combination of mechanical strength, barrier properties, wear resistance and chemical resistance [17]. Specifically, these semi-crystalline polymers maintain dimensional stability and mechanical strength in corrosive hydrocarbon environments at elevated temperatures. These qualities make PK well suited for horizontal pipe liners, inner barrier layers in coilable composite tubing and downhole tubing and casing liners.

Pipe liners produced from extrusion grades of alternating aliphatic polyketones have found [17] to maintain dimensional stability under demanding conditions, including elevated temperatures and harsh chemical environments. These performance properties make alternating aliphatic polyketones well suited for many industrial, oil and gas corrosion control applications, particularly for use as a liner material. Field trials and laboratory evaluations have demonstrated that alternating aliphatic polyketone pipe liners can be spooled, hot-plate welded and inserted into steel host pipelines with either diameter reduction or diameter expansion. Measurements of tensile properties and sample dimensions after exposure to hydrocarbons at elevated temperatures, permeability, explosive decompression, and slurry abrasion all indicate that alternating aliphatic polyketones are suitable for oilfield pipe liners, reinforced composite and flexible piping.

Properties of Good Polymeric Coating

Successful studies [12] carried out to determine the properties of good polymeric coating shows that they must be:

(1) Resistant against water and moisture which if absorbed, results in weight increase and electrical resistant reduction.

(2) Resistant against variable pressures which often results from the presence of gravel, movement of soil due to moisture and also other existing particles in the soil.

(3) Resistant against bacteria and mushrooms which can attack different materials and cause their extinction.

(4) Resistant against water capillary effect which can cause water penetration and invariably separation of coating from steel.

(5) Suitable with temperature variations. Variation in temperature can result to differential rate of steel expansion and coating.

(6) Resistant against being dissolved.

(7) Resistant against absorbing soil: Soil may absorb some materials. Clay, silica gel, charcoal and some other combinations have the absorbing property. Soil always is completely in the contact with coating and absorption of some elements from coating by the soil may make coating fragile, perforated or reduce its resistance against soil.

(8) Resistant against mechanical damages resulting from stresses during installation or storage.

Layers of Coating

It has been found]12[that coating systems have their own advantages and limitations, and this brings about preferment of a particular one over another in most conditions

First layer

Epoxy powders used in three-layered coatings is classified in two different groups. The first group has primer property and the second group has coating quality. These two materials have remarkable differences in application, temperature and thickness; there is a tendency in industries to use epoxies with coating quality. Time is a sensitive and critical factor in creating adhesive and polyethylene layers. First the adhesive develops a very strong chemical bond with chemical groups in epoxy powder which is uncured. During application of epoxy, the viscosity of the coating should be moderate so as to allow a good flow and complete wetting of metal surface.

Second layer
Second layer polymer creates adhesiveness between layers 1 and 3 and must be compatible with both layers. Minimum thickness must be from 160-200 micron. Thickness may increase or reduce according to the mutual agreement with customer but minimum thickness must be investigated safely.

Third layer
Polyethylene coating must be formed in this layer. Thickness must be uniform in all through the pipe and minimum general thickness must be acceptable. Three-layered poly ethylene is one of the coatings with high efficiency, although it seems that it is used in the field in a very limited extent compared with other coatings. Three-layered poly ethylene coating includes epoxy, adhesive and poly ethylene. Any of the layers provides coating with properties to lengthen its efficiency for a long term. Epoxy layer has a very good adhesiveness due to its transverse bonds and has a very high resistance against corrosion and oxygen penetration. But it is vulnerable to the mechanical hit when storing and line performance. Poly ethylene layer is a very good protection to prevent physical damages. A main problem with this coating is that poly ethylene does not have adhesiveness with the metal and for this reason an adhesive layer being a kind of reduced polymer is used for pasting poly ethylene to epoxy [12].

ASSURANCE OF PIPELINES AND ALLIED STRUCTURES INTEGRITY THROUGH APPLICATION OF POLYMERIC COATINGS
The integrity of pipelines and allied structures is dependent on the susceptibility of the steel materials involved to corrosion attack. This implies that any measure aimed at reducing corrosion attack on the pipelines and allied structure is geared towards achieving or maintaining integrity
. A critical review of the performance tendencies of polymeric materials for corrosion inhibition [12-17] has shown that the polymeric materials can give a very high level of protection against corrosion most especially when a three layer coating system is used (even though it is costly). This is because the first layer gives a very strong chemical bond with the metal surface, hence impervious to water and chemicals. The second layer is compatible with the first and third layer, hence sealing-up any opening while the third layer seals-off any smallest opening left. This way the metal surfaces coated with polymeric materials are completely cut-off from the corrosive environment.

Condition for Pipeline and Allied Structure Integrity
The mathematical expression for evaluating the efficiency of corrosion inhibitors [10] is given by;

$$E_i = \frac{R_o - \left(\frac{R_i}{R_o} \times 100\right)}{} \qquad (2)$$

Where
E_i = Inhibitor Efficiency (%)
R_i = Corrosion Rate in the presence of Inhibitor (mm/yr)
R_o = Corrosion Rate in the absence of Inhibitor (mm/yr)

It therefore follows (from equation (2)) that any inhibitor that can completely prevent corrosion has efficiency E_i = 100%. And so the pipeline and allied structure integrity equals 100% because there exist no corrosion. This implies that R_i from equation (2) = 0. Based on the foregoing, if the inhibitor cannot give a complete protection from corrosion, $R_i > 0$, and so $E_i < 100\%$. Therefore usage of polymeric materials such as aliphatic polyketones, baked phenolic etc. which have been tested and certified highly resistant to corrosion in all severely corrosive environments can significantly reduce the value of R_i very close to zero, thereby raising highly the inhibitor efficiency and invariably the pipeline integrity and service life.

Based on the forgoing, pipeline and allied structure integrity and inhibitor efficiency can be related mathematically as;

$$P_i \alpha E_i \qquad (3)$$

$$P_i = K E_i \qquad (4)$$

Where
P_i = Pipeline and allied structure integrity
K = Constant of proportionality

References

1 . http://nobelprize.org/nobel_prizes/chemistry/ aureates /1974/. Retrieved 27 September 2010.
2. Sperling, L. H. (Leslie Howard) (2006). *Introduction to physical polymer science*. Hoboken, N.J.: Wiley. p.10 ISBN 0-471-70606-X.
3. Callister, W.D. Jr. (1997), "Materials Science and Engineering, An Introduction", Fourth Edition, John Willey and Sons, USA
4. Smith, W.F. and Hashemi, J. (2006), "Foundations of Material Science and Engineering", Fourth Edition, McGraw-Hill, New York
5. **Abdul Hameed A. (2005),** "Evaluation of

Quality of Steels Produced Locally" B.Eng. Thesis, Department of Mechanical Engineering, University of Ilorin, Ilorin, Nigeria
6. Bolton, W. (1994), "Engineering Materials Technology", 2nd Ed, B. H Newness Ltd., Oxford, London, England
7. Davies, D. J. and Oelmann, L. A. (1983), "The Structure, Properties and Heat Treatment of Metals", First Ed., Pitman Publishing New Zealand Ltd, Wellington, England
8. Badmos, A.Y. and Ajimotokan, H.A. (2009) "The Corrosion of Mild Steel in Orange Juice Environment", Technical Report No: 2009-02, Department of Mechanical Engineering, University of Ilorin, Nigeria, 8.
9. BISRA (1965), "The Corrosion Resistance of Stainless Steel", British Steel Corporation Corrosion Prevention Booklet No. 2, 02-03
10. Ijomah, M. N. C. (1991). Elements of Corrosion and Protection Theory, Auto-Century Publishing Company Limited 1st Edition, Enugu, Nigeria
11. Anyakwo, C. N. (2007). Corrosion of Surface Facilities of an Industrial concern in the Niger Delta area of Nigeria splashed by produced water. J. Eng & Appl. Sc., 3, 57-60.
12. Amir, S., and Soroush, Z. **(2011). An Analysis of Polyethylene Coating Corrosion in Oil and Gas Pipelines** Journal of American Science 7(1):1032-1036
13. NNPC Field Hand Book, RGS 2300.
14. http://chemicalcontainment.com/kcc_tank_liners.html
15. http://chemicalcontainment.com/membranes.html
16. http://chemicalcontainment.com/heresite_info.htm
17. James, C. K., and Cary, V. (2000). Polyketone Polymers: A New Liner Material for Corrosion Control in Oil and Gas Industry. CORROSION 2000, March 26 - 31, 2000, Orlando, Fl

Appendix

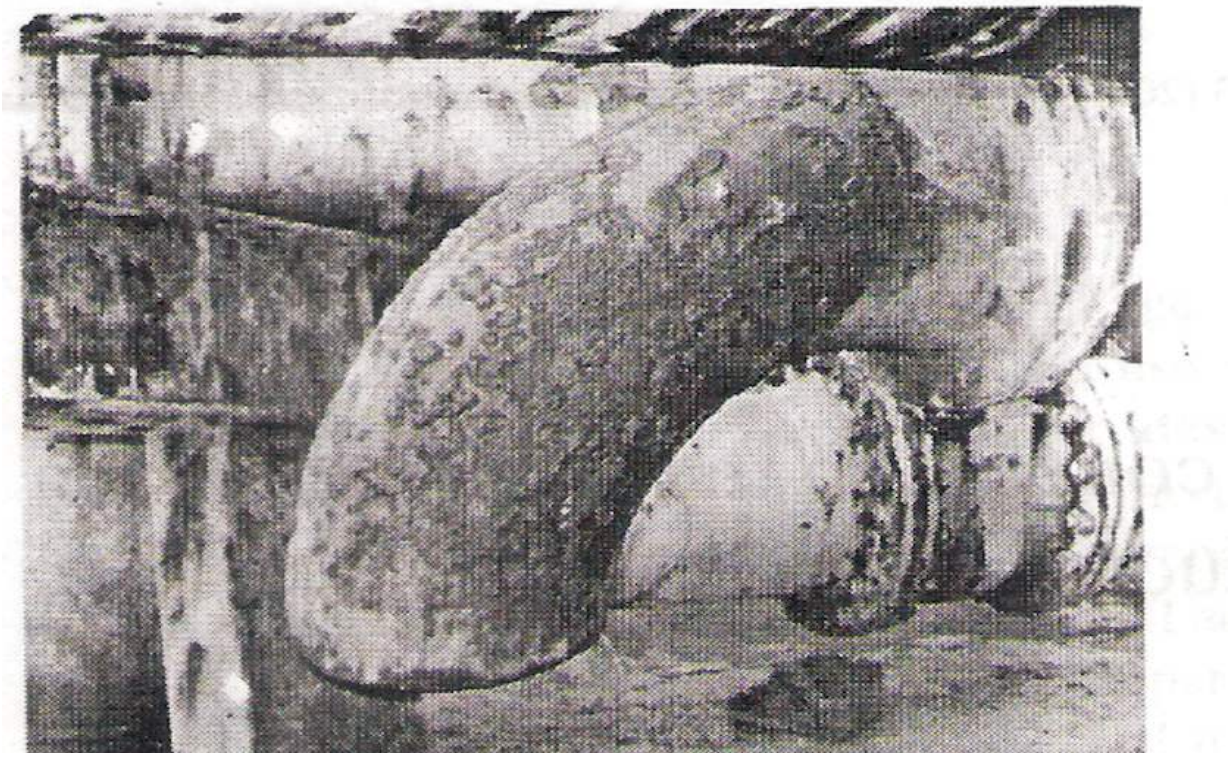


Fig. 1: Pipeline corrosion in a flow station [11

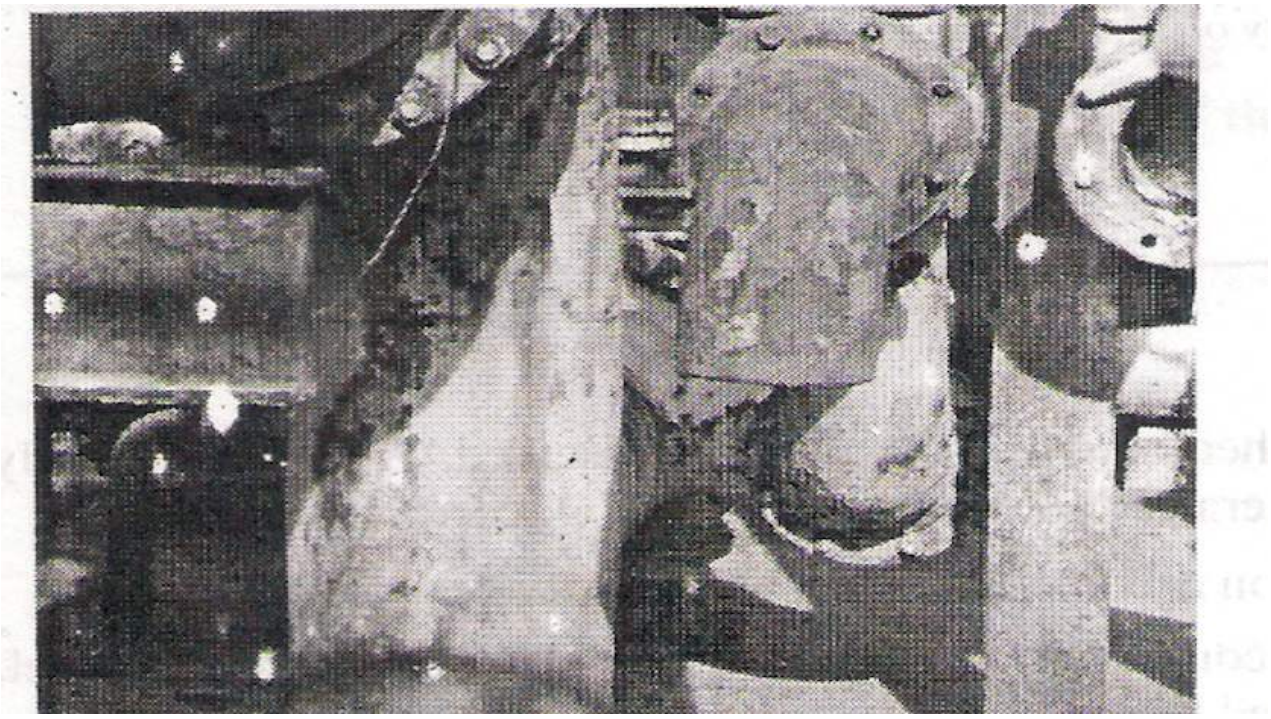


Fig. 2: Pipeline corrosion in a refinery [11]

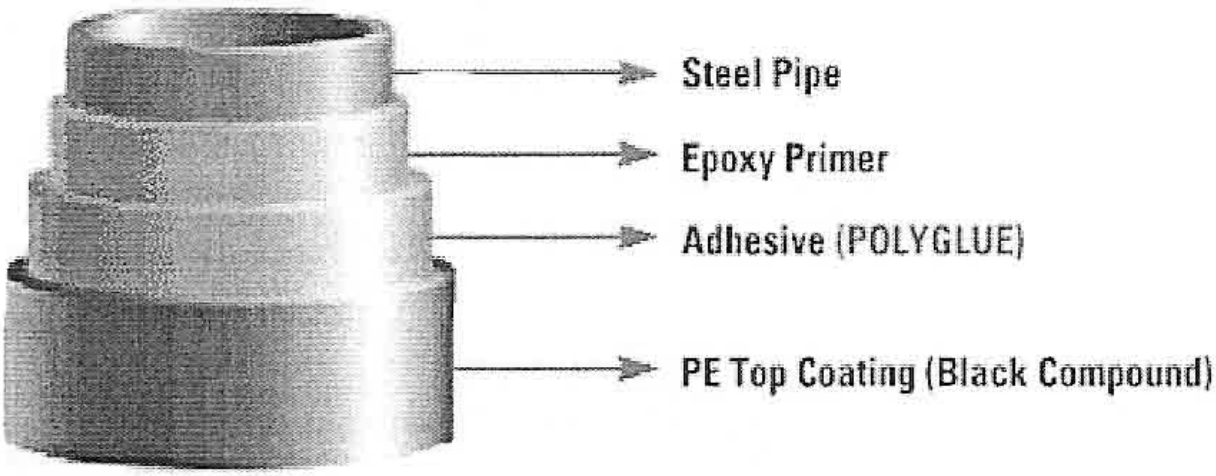


Fig. 3: Corroded blower [16]



Fig. 5: A view of steel pipe with three folds cover]12[.

DETERMINATION OF FLAMMABILITY PROPERTIES OF ACETALDEHYDE HOMO-POLYMER

Nsikak S. A., Edward O., Bashir I., Nkechinyere N. E., Uduak-Obong I., Martins K. U.
National Research Institute of Chemical Technology, Zaria, Kaduna
ikem404umi@yahoo.com

ABSTRACT
Polymers, depending on the specie-composition, can either be self-extinguishing or non-extinguishing. This work presents the physico- chemical characterization of acetaldehyde as a polymer. Analysis like: Limiting oxygen index (LOI), flame spread, ignition temperature, rate of heat release, smoke density were carried out and the results obtained for LOI as; Acetal polyoxy-methylene(16), Polyethylene(18), polystyrene(18), nylon 66,(24) and polychloroprene (26) shows the status of acetaldehyde as non-extinguishing polymer material because they all have LOI values lower than 27% which is the minimum value for homo-polymer to burn in air under normal condition and also found to be highly flammable polymer. The characterisation process opens a window for the quick assessment and identification of polymer as one of the two categories for application in end use area where material flammability is of utmost importance.

KEYWORDS: Limiting Oxygen Index (LOI), Flame Spread, Ignition Temperature, Smoke Density, and Rate of Heat Release.

INTRODUCTION

In the world of polymer engineering and science, more researches are still being conducted in order to source for more polymers of highly rated and physical properties that could substitute the existing ones. Homo-polyacetaldehyde has been found to be one of the new existing polymers [3].
Nevertheless, organic polymers provide one of the most versatile groups of materials and find widespread use as plastics, fibres, rubbers, adhesive, coating, etc. Many common polymers are used as plastics, which including; polystyrene, polyethylene and polyvinyl chloride. They soften sufficiently at about 100^0C not to be use in many loads bearing application, this is because of their low density, high specific stiffness and strength, especially when used as the basic for fibre reinforced composite material. This has led to their use in transportation, especially aerospace and deep space vehicles where weight savings is of vital importance in so many aspects of life.

Moreover, it is obvious to say that flame retardants are necessary for polymers to alter the combustion process or to reduce the flammability of the polymers so that they can satisfy the specification for heat application. There are several strategies for effective flame retardants which include the halogenated and non-halogenated flame retardant.
Halogenated flame retardants are based on halogens family compounds such as chlorine, bromine and this system offers the advantages of lower loadings to achieve the desired level of flame retardant. Also presence of halogen in polymers produces the most dramatic increase in Limiting Oxygen Index (LOI) hence decrease flammability.
In the case of non-halogenated flame retardants, it is not from halogens compound family e.g. Ammonium phosphate and Magnesium hydroxide, the required loadings is high, say up to 605 of flame retardant [2].
The above mentioned halogens types must be taken into consideration during application.

Properties of Acetaldehyde;
Acetaldehyde, sometimes known as ethanal, is an organic chemical compound with the molecular formula C_2H_4O, molar mass 44.05gmol-1, boiling point of 20.2^oc, melting point of -123.5^0c and density of $0.788gcm^{-3}$. It is a flammable liquid with a fruity smell. In the chemical industry, acetaldehyde is used as an intermediate in the production of acetic acid, certain esters, and a number of other chemicals like; acetic acid, chloral, silvering mirrors; hardening gelatine fibres; denaturing alcohol; and in the manufacture of disinfectants, dyes, drugs, explosives, flavourings, phenolic and urea resins, rubber accelerators and antioxidants, varnishes, and yeast [1].

Property of polymers;
The term polymer denotes a molecule made up of some simpler units (monomers) capable of building up to form large macromolecules. The term macromolecules used to present large molecules of complex structure; therefore polymer since the later carries with the notation of simple repeating units. An example of natural occurring macromolecules is INSULIN, a protein hormone that is produced in the pancreas.
Polymers may be of light weight, corrosion resistant, crystalline, resistant to chemical or solvent attack, strong and rigid, electrical insulator may be relatively moderate, tensile strength and are suitable for use at high temperature [8].

Uses of Polymer;
Polymers are used for so many applications such as toys, home appliances, structural and decorative items, coating, paint, adhesive, automobile tyres, packaging,

etc).
Homo-polymers formed by repeating monomer units that are identical as shown below.
n M----M-M-M-M-EM (M) n-2M
(E.g. of homopolymer)
Homopolymers may and do contain irregularities in minor amounts at the ends of branch junction. Examples of homo-polymer are poly-ethylene and poly (hexamethylene).

COPOLYMER:
This is the polymer that can be obtained from mixture of two or more monomer units to form polymeric products. The polymer chain will carry some structure as two or more monomer unit combined together [10] e.g. acetal, polycarbonate.

POLYMER ADDITIVES
These are materials or chemicals added to polymers in order to change the end property or properties of the polymer products. In some industries there are so many additives such as:

- Lubricants
- Flame retardants
- Stabilizers
- Antioxidants
- Fillers
- Colorants
- Plasticizers
- Reinforces
- Processing aids
- Impact modifiers

These are used for various purposes and also designed and formulated to meet particular requirements and in a sense, these may be regarded as specialties.
The additives may be mixed with the polymer before processing by a variety of techniques such as dry blending, extrusion, compounding and some other methods [7].

Flame Retardant
They are chemicals that are added to polymer to alter the combustion process in some way. During that process in the absence of oxygen this is called pyrolysis, while in the presence of oxygen; it is called oxidative pyrolysis or thermal oxidation [8].

Classes of Flame Retardant

- Organo-chlorine compounds
- Organobromine compounds
- Organophosphorous compounds
- Boron compound, etc

Flame retardants are necessary to reduce the flammability of polymers so that they can satisfy the specification for electrical applications, transportation and for building construction [11].

MATERIALS AND METHOD
The given sample homopoly-acetaldehyde was cut into five different sizes and each size was weighed with the use of beam balance and recorded. Then each sample was exposed to flame (Bunsen burner) through the help of the tripod stand with the clamp, and after few seconds the sample ignited and burned in a satisfactory manner while the source of ignition (burner) was off immediately when it was ignited and the sample continue to burn for few seconds and later stopped. The following parameters were determined: Combustion Time was recorded by the use of stop watch, Smoke Density, Flammable Component was weighed and recorded by the use of beam balance, while the Flame Spread was measured by the use of meter rule and the Flame Area was calculated by the use of formula $\pi D/2$ cm^2 and also Limiting Oxygen Index was determined by the used of appropriate formula written below. Eventually the above mentioned parameters were the factors to determine polymer as either Self-extinguishing or Non-extinguishing products. The results of these parameters are tabulated on the down page.

Limited Oxygen Index
This is the simple, most widely used test of polymer flammability. It is the amount or percentage of oxygen, in an oxygen-nitrogen mixture, required to maintain burning after the removal of the ignition source under specified condition. But in normal conditions air contains 21% of oxygen and almost all the flammable polymers have an oxygen index in excess of 21%. Certainly, the limiting oxygen index of self-extinguishing is after taken as 27% and not 21% (which is the volume concentration of oxygen in the air). But in my experimental work, the polymer sample was not self-extinguishing because after removing the ignition source, it stopped burning after some few seconds and also from the reading, the LOI values in each of the sample were less than 27%. Mathematically:

$$\% \text{ LOI} = \frac{\text{Mole } O_2}{O_2 + \text{Mole } N_2} \times 100$$

Smoke Density
It is the amount or the rate at which smoke has been emitted when the burnt polymer was in the air. The trapped smoke was weighed by the use of beam balance. And the reading was recorded.

$$\text{Smoke Density} = \frac{\text{Weight of smoke}}{\text{Area Occupied}}$$

Rate of Heat Released
This is the rate or amount of heat released by the burnt polymer during the burning process. Eventually, polymers having higher rates of heat release, the same property being the same will also tend to produce more smoke and combustion gases in a fire [10], since surrounding products will be ignited only if they are rapidly reached by a sufficient amount of heat.

$$Q = mcP\Delta T$$

Flame Spread

This is another important parameter in which the readings were obtained by the use of meter rule to measure the height or length of the flame with the use of digital camera to capture the flame image during the burning process.

RESULTS AND DISCUSSION

The results of flammability properties of homopoly-acetaldehyde is tabulated into sample A and sample B raw data and shown as in the appendix.

The tabulated result of various raw reading parameter in table 1 and 2 such as weight of polymer, weight of residues, flammable component, smoke trapped, combustion time, flame spread, flame area were all important raw data in flammability properties measurement of homopoly-acetaldehyde. The above stated parameters lead to another derived parameter called flammability properties of homopoly-acetaldehyde. The parameters are flammable volatile density, LOI, smoke density, rate of heat release, were all aimed to determine the polymer samples as either self-extinguishing or non-extinguishing products.

From the readings gotten from LOI parameter, it is obvious to say that the polymer was highly inflammable but it was not self-extinguishing polymer because the LOI values were less than 27%.

For the rate of heat released, it indicated that the higher the flammable volatile values, the higher the amount or values of the heat release and in the same way the lower the weight of flammable volatile, the lower the rate of the heat released. But the polymer was highly inflammable.

In the case of smoke density, the amount of smoke trapped depends on the weight of the flammable volatile and the rate of heat supplied to the polymer. It was observe that the higher the rate of heat supply and weight of flammable volatile, the higher the amount of smoke trapped. The same thing was applicable to the rate of lowness. Generally, the experimental results indicate that the polymer was highly flammable but was not self-extinguishing.

CONCLUSION

General conclusions regarding the flammability of individual polymers can be drawn from the common example of limiting oxygen index. Homopolyacetal polymers are all flammable but, as the hetero-atom content increases, so flammability decrease.

Further work is required to define the test specimen and test conditions for certain materials and products and to establish both value and limitation of test data for specification purposes. In view of the non-steady state burning behaviour of many materials and the effects of chemicals and physical changes, the relevance of test sample behaviour to real life fire should be considered.

It is obvious to say that, the characterization process opens a window for the quick assessment and identification of polymers products as one of the two categories for application in end use climatic areas where material flammability is of utmost importance.

RECOMMENDATIONS

The cone calorimeter should be used as main test methods because it can measure a variety of fundamental properties of burning of polymer.

REFRENCES

1. Adkins, H., and Nissen, B.H. (1941); Acetal Organic Syntheses, Collected Volume 1, p.1.
2. Retrieved August 15, 2007. Chemicals in the environment; Acetaldehyde (Cas no.75-07).
3. Ferdinard R. (1983)"principles of polymer system", MC Craw Aill, New York, second edition p.1; pp.13 18,33-43,pp.72-80;45-55.
4. Flame retardant "92 by the plastics and rubber institute pp:36-44,pp130-150,p.184,pp.230-289.
5. Hirscher, M.M. How to measure smoke obscuration in the manner relevant to fire hazard assessment. Use of heat release calorimetric test equipment J fire Science, 1991, 93 183-220.
6.http://www.epa.gov/chemfact/f_acetal.txtm
7. Natural Chemical Inspectorate, Stockholm, Sweden, 1990, 452-453
8. Odian G.G (1999) "Principles of Polymerization" John Wiley and Sons, Canada, third edition pp.353-358, pp.452-456.
9. Office of Pollution Prevention and Toxics, Chemical Summary for Acetaldehyde. Retrieved August 15, 2007.
10. Polymer additives, Blends and composites by temperature p ix; pp252-253, pp257-261.Thomas, P.H. Int. Cont "FIRE; control the heat reduce the hazard," fire research station, October 24-25, 1988 London.
11. Smoking (2006). Encyclopædia Britannica. Accessed 27 October 2006.

TABLE I: Raw data for the combustion of homopolyacetaldehyde Sample A.

	Weight of polymer(g)	Weight of residues(g)	Flammable component(g)	Smoke trapped(g)	Combustion time (sec)	Flame spread (m70m)	Flame area (cm^2)	Time before combustion (sec)
1.	2.2	0.5	1.7	0.3	50	70	7.86	20
2.	2.1	0.5	1.6	0.2	50	70	7.86	20
3.	2.2	0.2	2.0	0.2	60	70	7.86	30
4.	1.1	0.5	0.6	0.1	20	70	7.86	10
5.	1.1	0.3	0.8	0.2	25	70	7.86	12
Total	8.7	2.0	6.7	1.0	205	350	12.86	92

TABLE 2: Raw data for the combustion of homopolyacetaldehyde sample B

<	Weight of polymer(g)	Weight of residues(g)	Flammable component(g)	Smoke trapped(g)	Combustion time (sec)	Flame spread (m70m)	Flame area (cm^2)	Time before combustion (sec)
1.	2.6	0.8	1.8	0.2	55	70	7.86	25
2.	1.3	0.8	0.5	0.3	15	70	7.86	5
3.	2.1	0.7	1.4	0.2	40	70	7.86	18
4.	2.0	0.9	1.1	0.2	30	70	7.86	15
5.	2.0	0.8	1.2	0.1	35	70	7.86	17
Total	10	4.0	6.0	1.0	175	350	12.86	80

Table 3: Flammability properties of homoploymer of acetaldehyde, Sample A

Sample	Flammability volatile (g)	LOI (%)	Smoke density (g/m^2)	Rate of heat release (kj/s)	Flammable volatile (moles)
1.	1.4	20.39	0.000098	198.80	0.00077
2.	1.4	20.39	0.000098	198.80	0.00077
3.	1.8	21.10	0.000126	255.61	0.00099
4.	0.5	20.33	0.000036	24.09	0.00028
5.	0.6	21.00	0.00004	36.92	0.00033

Table 4: Flammability properties of homopolyacetaldehyde, Sample B

Sample	Flammability volatile (g)	LOI (%)	Smoke density (g/m^2)	Rate of heat release (kj/s)	Flammable volatile (moles)
1.	1.6	20.97	0.0000116	234.95	0.00091
2.	0.2	21.00	0.000014	4.73	0.00011
3.	1.2	21.00	0.000087	128.75	0.00068
4.	0.9	21.03	0.000065	65.84	0.00051
5.	1.1	21.00	0.000079	96.05	0.00062

PRODUCTION OF SILICON SLURRY AS A HIGH TEMPERATURE PROTECTIVE COATING FOR MILD STEEL IN A SALT ADMIXTURE

1,2 Liadi, A. A., 1Taiwo, A. T., 1Akinluwade, K. J; and 1,3Adetunji, A. R.
1Prototype Engineering Development Institute (PEDI), Ilesa, Nigeria
2Department of Materials Science, Corrosion and Protection Centre, University of Manchester, UK
3Department of Materials Science and Engineering, O.A.U., Ile-Ife, Nigeria
***Correspondence author**: abiodunliadi@yahoo.com*

ABSTRACT
This work undertakes production of relatively inexpensive, thick overlay coatings intended to reduce oxidation, hot corrosion, and erosion-corrosion in high-temperature oxidizing environments. The coating is meant for prevention of corrosion of mild steel in a salt admixture of 8.2% NaCl, 10.5% KCl, 17.7% Na2CO3 and 63.6% Na2SO4 at 750 °C — a service environment similar to that found in Kraft recovery boilers used in paper and pulp industry. A silicon-rich diffusion coating was formed by the vapour-slurry method. The slurry consisted of silicon powder and ammonium chloride in an aqueous cellulose lacquer. After exposure in the furnace of the substrate coated with the slurry, microscopy examination of the substrate was carried out and results showed appreciable protection ideally suited for high temperature service environment.

***Keywords**: vapour-slurry method, cellulose lacquer, overlay coatings, Kraft recovery boiler, hotcorrosion*

INTRODUCTION

Hot corrosion can be defined as hightemperature corrosion of a metallic material by molten salt deposits. As there is a need to increase the efficiency of equipment at high temperatures, there is also a corresponding need to improve the corrosion and high-temperature degradation resistance of the materials that will enable better performance of equipment at higher temperatures and pressure.

The salt usually comes from combustion of impure fuels or the environment e.g. salt spray. The salt or deposit, as it is sometimes called, makes the formation of a protective scale difficult for the material. The major corrosive contaminants found in deposits include chlorine, sulphur and potassium. Chemical reactions alsooccur between the salt and the protective oxide resulting in a breakdown of the oxide scale especially when the salt deposit becomes molten.

Salt chemistry and electrochemistry both contribute to the hot-corrosion mechanism. Hot corrosion replaces the protective oxide on a material with a non-protective oxide. It can severely reduce the service life, sometimes leading to catastrophic failures, although regular and careful inspections could reduce that likelihood considerably.

Ways to reduce hot corrosion incidence include reducing the sulphur content of the fuel used in an engine, not exceeding the first melting temperature of the deposit (salt) or the use of a coating, which provides a barrier between the material and the aggressive atmosphere.

LITERATURE REVIEW

Hot corrosion is a combination of oxidation and reactions with sodium, sulphur and other contaminants present, either in the environment or in the fuel [1]. It produces a non-protective oxide on the metallic material surface in place of the normal protective oxide of aluminium or chromium. It is sometimes called deposit corrosion as the salts first deposit on the metallic material surface and then turn to liquid melt, either of their own or by forming complex mixtures of salt [2]. Additionally it is also known as molten-salt corrosion or hot-salt corrosion.

Rapid degradation can occur if the processtemperature is above the salt melting point.

Some solid salt deposits can limit access of gas to a metal surface, but are not corrosive. Some salts involved in hot corrosion are sulphates, carbonates, hydroxides, chlorides and nitrates.

The occurrence of sulphur in fossil fuels causes high-temperature corrosion problems in some industries, in which these materials are used e.g. superheaters and other heat exchangers, gas turbines, carbon baking furnaces and coal gasification systems [3, 4]. Other factors such as moisture also contribute to hot corrosion. "The use of alkali nitrates in heat transfer and storage media reduces the life of containment materials due to continuous oxidation. The presence of moisture in such systems enhances the hot corrosion reaction and materials failure occurs in short duration. Therefore, moisture appears to be a main contaminant in molten salt systems that affect the oxidation reaction to certain extent [5]." Oxidation rate of the metals is greatly enhanced by cathodic process catalyzed by the presence of moisture [6].

For hot-corrosion to occur, a liquid (usually sulphate) deposit is required on the surface of components. The formation of this deposit depends on trace metal species (e.g. sodium, potassium, lead, zinc compounds) in the gas streams and other reactive gas species [e.g. sulphur dioxide (SO_2), sulphur trioxide (SO_3), HCl]. "The rates of corrosion will depend (among other factors) on the rate of deposit formation, deposit composition, temperature and

the surrounding environment.
Hot-corrosion occurs in several environments e.g. severe attack occurs in metallic materials at high temperature (600-800°C) corrosive atmospheres existing in industrial waste incinerators particularly when the chlorine content in the waste is high, the corrosion phenomena are more close to molten salts interactions than to gaseous corrosion [7]. Gas turbines encounter high-temperature oxidation, low-temperature hot corrosion and high temperature hot corrosion in high-temperature attacks [8].

The addition of either K_2SO_4 to a Na_2SO_4 deposit or Na_2SO_4 to a K_2SO_4 deposit brought about an enhanced corrosion rate of iron-base alloys. "In hot corrosion, iron (including other metals) takes part in the anodic oxidation reaction to form Fe^{2+} ions, some of which are further oxidized to Fe^{3+} in the compact oxide layer. In the melt, O2 and $S_2O^{2-}7$, mainly the latter, participate in the cathodic reaction on the surface of the compact oxide layer, and O^{2-} ions produced are incorporated into the oxide lattice and combined with Fe3+ to form Fe_2O_3 [9]".
In that way, the compact oxide layer grows. SO2, even $SO^{2-}4$, from the cathodic reaction could penetrate the compact oxide layer through cracks and pores, thereby leading to the formation of sulphides at the metal/oxide interface and also within the oxide layer. The fast growth of the compact oxide layer can be linked to the easy diffusion of cations along short-circuit paths of sulphides. In the eutectic melt, Fe3+ ions may also participate in the cathodic reaction. The Fe2+ product ions and those from the anodic reaction are dissolved in the melt transport and get oxidized in the melt near the melt/gas interface, causing Fe2O3 particles to precipitate.

Liquid salt deposits destroy protective oxide films, as the protective oxide dissolves the corrosion rate increases. Dissolution of the oxide is caused by the fluxing of salts. Pure Na2SO4 melts at 884°C, but when other salts such as NaCl, $NiSO_4$ etc are present its melting point is lowered [10].

Hot-corrosion in recovery boilers
Black liquor recovery boilers operating with the Kraft process are used in the pulp and paper industries and are critical components of the mills. Steam is generated from the boilers and is utilized for process applications and power generation. Occurrence of corrosion makes the recovery boiler operate less than optimal conditions and causes down-time in order to address maintenance issues which make the recovery of energy from the burning of the organic components of black liquor less efficient than desired.

As there is a need to increase the efficiency of Kraft black liquor recovery boiler, there is also a corresponding need to improve the corrosion and high temperature degradation resistance of the boiler tubes that will enable better performance at higher temperatures and pressure. A way of increasing the efficiency is by increasing the steam values of the boiler but this increases the corrosiveness of the fireside deposits the boiler forms. Most boilers have a steam temperature of
around 480-490°C with a few exceptions of 500°C. Steam temperatures of above 500°C may
cause severe corrosion in a fairly short time span. This steam temperature of about 500°C is
similar to the steel material temperature in the superheater region of a recovery boiler which is
540°C which further coincides with the temperature range at which the salt deposits starts to melt. Table 1 is the composition and first melting temperature (FMT) of a deposit found in a superheater region of a black liquor recovery boiler.

Table 1: Composition & FMT of superheater deposits [11].

Chemical Composition (wt. %)					FMT (°C)
Na	K	Cl	CO3	So4	
30.5	5.5	1.4	9.8	52.9	547

Black liquor recovery boilers are designed to recover as much as inorganic salt and heat content of the spent pulping liquor. The inorganic salt-forming elements are mainly sodium and sulphur with chlorine and potassium as the major salt-forming impurity elements [12].

Four major corrosion mechanisms are indentified in the superheater area of recovery boilers: active oxidation, high-temperature oxidation, hot-corrosion and sulphidation [13].
These could be present individually or as a combination of two or more different mechanisms. Active oxidation and hightemperature are usually present in oxidizing conditions, unlike sulphidation that requires reducing conditions. Hot-corrosion may occur in both oxidizing and reducing conditions. Hotcorrosion is linked to deposit properties, which is caused by the black liquor composition. A way to limit material loss from hot-corrosion is to keep the metallic materials temperature below the FMT of the deposits.
Some hot-corrosion in a Kraft black liquor recovery boiler is shown in Fig. 1.

Protective coatings
High-temperature coatings are used to protect structural alloys and to prolong service life of hot-section components of gas turbines and some energy systems operating in aggressive environments which are exposed to attack by oxidation, sulphidising, carburising, chloridation, erosion or molten salt corrosion. The need to protect materials has resulted in a wide variety of corrosion-resistant coatings which are applied by a number of different processes, and are specific for different applications and corrosive environments [15].
Coatings are mostly based on aluminium and chromium, which both form protective films of tenacious refractory oxide. These films are effectively self-sealing and since the ionic mobilities of chromium aluminium within the films are low, oxidation rates beneath the film are also very low.
Large, manipulation equipment and expensive vacuum

chambers are required in methods for physical vapour deposition (sputtering, evaporation, etc) of surface coatings. These PVD processes are widely used in the thin-film electronics applications; they are not ideally suited for the production of relatively inexpensive, thick overlay coatings intended to reduce oxidation, hot corrosion, and erosion in high-temperature oxidizing environments.

High-temperature coatings are designed to form protective alumina, chromia or silica scales.

Increases in operating temperatures combined with a reduction in fuel and environmental quality and a decrease in inherent corrosion resistance of superalloy in exchange for better mechanical properties, has led to the need for coatings to protect hot-section components.

Metals and alloys degradation by hightemperature oxidation can be easily reduced by the application of appropriate coatings containing chromium, aluminium or silicon [16].

Requirements of a protective coating

i. Ability to form an effective barrier between the substrate being protected and the environment.
ii. Free of pores, flaws or other defects which may allow penetration of oxygen or other aggressive gases.
iii. Adherence to the substrate
iv. Development of a protective oxide scale
v. High compatibility with the thermomechanical properties of the substrate alloy

EXPERIMENTAL PROCEDURE

Slurry preparation and application: the slurry consisted of silicon and ammonium chloride, xanthan gum and sodium bicarbonate powders, hydroxy propyl cellulose binder and de-ionised water carrier. The slurry preparation involved dissolving 2.5g of hydroxy propyl cellulose (binder) in 100ml of de-ionised water (carrier) by the use of a magnetic stirrer for 3 hours until the binder dissolved then left overnight to disperse the air bubbles. 50g of the solution (carrier + binder) was mixed with 44g of NH4Cl and 6g of Si with a magnetic stirrer for about 18 hours to form a slurry.

Since, the slurry was thin, xanthan gum (thickener) was added. The slurry was made alkaline by adding sodium bicarbonate. A litmus paper was used to determine when to stop the addition at a pH of 11. This would make the steel not corrode by giving it a passive film. The substrates were initially ground on 600 grit silicon carbide papers, degreased in ethanol and measured. The slurry was applied as a single layer on a side of each substrate with a small size paint brush. The substrates were then placed in an oven at 75? C overnight to evaporate the water carrier.

Substrate and slurry heat-treatment: The specimens after slurry application were heattreated at 750°C for 5 hours for diffusion to occur according to the following reaction: $4NH_4Cl(S) + Si(S) \rightarrow SiCl_4 + 4NH_3 + 2H_2(g)$.

After heat-treatment, the coupons were cooled to room temperature in the heat-treatment furnace by switching it off, then removed and cleaned off with a hard bristle brush, then ultrasonically cleaned in ethanol.

RESULTS AND DISCUSSION

Fig. 3 shows diffusion in the adhered residue on the substrate surface. It shows a compound containing both silicon and iron. The figure below shows evidence of protection from hot-corrosion by the slurry. A one-sided coated specimen was put in the furnace in molten salt for 12 hours. The result showed that less corrosion occur on the coated side.

CONCLUSION

? The salt composition is 8.2% NaCl, 10.5% KCl, 17.7% Na2CO3 and 63.6% Na2SO4.
? The slurry composed of 50g of the lacquer (hydroxy propyl dissolved in de-ionised water) mixed with 44g of NH4Cl and 6g of Si.
? The silicon coating residue on the substrate showed diffusion occurred.
? The silicon coating protected the substrate.

REFERENCES

1. Tretheway K. R. and Chamberlain J. (1995). Corrosion for Science and Engineering, 2nd ed. Longman, Singapore.
2. Khanna A. S. (2002). Introduction to High Temperature Oxidation and Corrosion, ASM International, Materials Park, OH, U.S.A.
3. Natesan K. (1982), High Temperature Corrosion, R.A. Rapp Ed. NACE, Houston, p.336.
4. Stringer J. (1990), High Temperature Oxidation and Sulphidation Processes,
J.D. Embury Ed. (Pergamon, New York) p. 257.
5. Singh I. B. (2004). 'Influence of Moisture on the Hot Corrosion of Metals in Nitrate and Sulfate Melts'.Materials Science Forum, Vols. 461-464, pp 927-932.
6. Singh I. B. (1995 & 2003): Corros. Sci. Vol. 37, p.1981; and Vol. 45, p. 2285.
7. Devisme F., Flament T., Mulet J. C., Prebende C. and Martigneaux J. L. (1993).
8. 'Coating behaviour for materials of industrial waste incinerators and heat exchangers in high temperature corrosive atmospheres'. Journal de Physique IV, 3, 771 – 778.
9. Bernstein H. L. (1993). 'Practical aspects of material data bases and expert systems for high-temperature corrosion and coatings in gas turbines'. Journal de Physique IV, 3, 1001 – 1012.
10. Zhang Y. and Weitao Wu. (1993). 'Summary of studies on hot corrosion of iron-based alloys by sodium sulfate in 02/S02/S03 environment'. Journal de Physique IV, 3, 319 – 326.
11. Keiser J. R., Kish J. R., Singbeil D. L. (2010). Recovery boiler superheater corrosion field study, CORROSION 2010, March 14 - 18, NACE International, Houston, Tx.
12. Makipaa M. and Oksa M. (2001), Superheater Tube Corrosion in Changing Operation Conditions in Recovery Boilers, CORROSION 2001, March 11 - 16, NACE International,

Houston, Tx.
13. Salmenija K. (Dr.), Superheater corrosion in modern recover boilers, Metsa-Botnia, Finland.
14. Bob Prescott (Dr.), Corrosion and Protection Centre, University of Manchester, 2010.
15. Komornicki, S. and Streiff, R. (1993). 'Relational data structure of the coating database from the "Coatings & High Temperature Corrosion Data Bank"'. Journal de Physique IV, 3, 1013 – 1021.
16. Zhang Y.S., Li X.M., Cao T.L., Shih S.T. (1992). Corros. Sci. Prot. Tech. 4 pp. 9

FIGURES



(i)



(ii)

Fig. 1: (i) ash deposits on support between superheater tubes (ii) example of corrosion in U-bend in superheater [14]



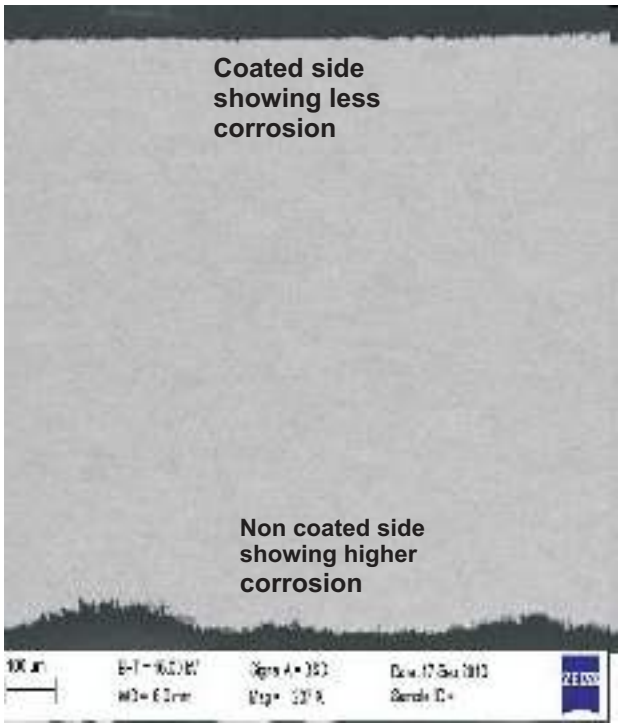
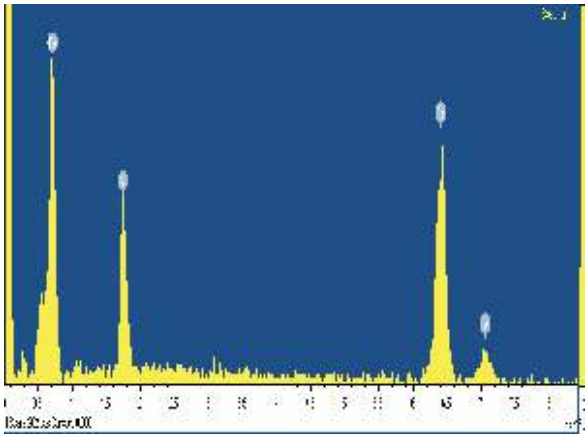


Fig. 3: Electron micrograph of cross section of mild steel substrate with a single slurry layer of 6 wt% Si, 44 wt% NH4Cl heat-treated at 750°C for 5 hours after exposure in a salt mixture of 8.2 NaCl, 10.5 KCl, 17.7 Na2CO3 and 63.6%

Na2SO4 at 640 □ 6C for 12 hours showing evidence of protection.



Element	Weight %	Atomic %
Si K	12.46	22.06
Fe K	87.54	77.94
Totals	100.00	

(iii)

Fig. 2: (i) SEM (ii) EDX (iii) composition at Spectrum no. 1 of mild steel substrate with a single slurry layer containing 6 wt% Si, 44wt% NH4Cl after 750°C heat-treatment for 5 hours.
Fig. 3: Electron micrograph of cross section of mild steel substrate with a single slurry layer of 6 wt% Si, 44 wt% NH4Cl heat-treated at 750°C for 5 hours after exposure in a salt mixture of 8.2 NaCl, 10.5 KCl, 17.7 Na2CO3 and 63.6% Na2SO4 at 640 □ 6 for 12 hours showing evidence of protection

PRODUCTION OF PARTICLEBOARD FROM SUGARCANE BARK, BAGASSE AND THEIR COMPOSITE

[1] Muhammed Tijani ISA*, [1], AbdulAziz ATTA, [1]Baba ABDUL, [1] Tajudeen Kolawole BELLO and [2], Shuaibu Adajine YUSUF
[1]Department of Chemical Engineering, Ahmadu Bello University, Zaria
[2] Kaduna Refinery and Petrochemical Company Kaduna
*Corresponding author: mtisaz@yahoo.com or mtisa@abu.edu.ng

ABSTRACT

Particleboards were produced from sugar cane bark, bagasse and the combination of equal proportion of both using urea formaldehyde as binder. Particle sizes of 1.7mm, 4mm and 8mm were used to study the effect of particle sizes on the properties of the particleboards produced. The particleboards were produced at temperature of 160°C, pressure of 12.5MPa and press time of 10 minutes. The particleboards produced were tested for thickness swell, water absorption and tensile strength. Tensile strength of 8.20MN/m^2, 8.38MN/m^2 and 9.45MN/m^2 were obtained for particle sizes of 8mm, 4mm and 1.7mm respectively for the particle board produced from the sugar cane bark. This was 1.16, 1.16 and 1.26 times respectively higher than corresponding particle sizes of particle board obtained from bagasse and 1.11, 1.11 and 1.18 times higher than for the combination of both. Thickness swell of 7.33%, 4.93% and 2.78% were obtained for particle sizes of 8mm, 4mm and 1.7mm respectively for the particleboard obtained from sugar cane bark. These values were better than 11.29%, 8.73% and 5.92% obtained for the bagasse and 9.38%, 6.43% and 4.41% for the combination of both. The water absorption was obtained as 71.97%, 58.31% and 32.39% for particle sizes of 8mm, 4mm and 1.7mm respectively for the particleboard produced from the sugar cane bark. These results indicated that the properties of the particleboard increases with decrease in the particle size, the board from the sugar cane bark had the best properties and the particleboard obtained from the combination of both had properties better than that produced from bagasse only.

Key words: Particle board, Binder, Sugar cane, Properties

1.0 Introduction

Particle board is a composition board largely made up of dry wood fibers and particles of different geometry and sizes. The particles are usually blended with binder and treated in a hot press to form a board [1]. Particle boards are ideal for applications such as wall units, TV cabinets, shelving, toys and cup boards. They provide the most economical option for general indoor building requirements [2]. Wood particles such as sawdust, planer shaving, and such other waste generated by wood users are the primary raw materials for the formation of particle board. Agricultural waste such as corn stalks, cotton stalks, rice husks bagasse sunflower hulls etc are other sources of raw materials for the production of particle boards [1-7]. The binder may be synthetic thermosetting resins such as phenol, melamine and urea formaldehyde or naturally occurring resins which includes tannin or lignin, starches, thermoplastics etc [8].

Bagasse is the biomass remaining after the sugarcane stalks are crushed to extract their juice. The baggasse and sugarcane bark contain high content of lignocellulosic fibers, lower lignin and higher hemicellulose compared with wood [9]. Similar to other agricultural residues, the waxy layer on the outer surface of the sugarcane bark has a significant impact on the bondabilty when with urea or phenol formaldehyde resins [10].

There is need for maximum utilization of available resources and reduction of waste this calls for waste recovery and recycling for economic enhancement. With the current initiative to produce ethanol from sugarcane as an alternative source of fuel, sugarcane and waste such as bagasse and sugarcane bark are expected to increase. These "wastes" can serve as feed stock for the production of other useful product such as particle board thereby reducing environmental pollution, create employment and increase product availability.

The strength and the applicability of a particle board is dependent on a number of factors, while previous works dwell on the effect of moisture content, pressure, temperature and setting time, little has been reported on the effect of particle size as it affects the physical and mechanical properties of particle board from bagasse and sugarcane bark.

Therefore this work focused on the production of particle board from bagasse, sugarcane bark and the combination of both using urea formaldehyde as binder and the effect of particle size studied.

2.0 Experimental

Sugarcane bark and bagasse were collected from sites where these materials were dumped and were

beneficiated by the removal of dirt and unwanted materials. The beneficiated raw materials were dried in the oven at temperature of 60°C for 3hrs to remove water moisture. Grinder with specification Ski 1.1kW, Nr 20204, 220Volts; Retsch K: G HAAN made in West Germany was used to grind the sugarcane bark and the bagasse. The ground raw materials were sieved into particle sizes of 8mm, 4mm and 1.7mm using sieve manufactured by Twente wire weaving co. Hengello, Holland.

Particle board was produced from the sugarcane bark by combining with urea formaldehyde on ratio 2:1. In this work, 40g of the sugarcane bark was combined with 20g of the urea formaldehyde. The two items were mixed together and spread on a metal plate (mold) which was covered with aluminum foil that was folded to enclose the particles between the two metal plates. The metal plates with the content were placed on hydraulic press with specification D288, pressure 0-40ton on 4" diameter ram, temperature 0-200°C which was heated to temperature of 160°C and pressure load of 10tons was applied for 10 minutes. The procedure was adopted for each of the particle sizes for the sugarcane bark and the bagasse. The same procedure above was used to produce particle board from mixture of 20g of bagasse and 20g of sugarcane bark using 20g of urea formaldehyde. Several samples were formed from each of the particle sizes and from the sugarcane back, bagasse and the mixture of both.

Thickness swell test was conducted by soaking 2cm by 2cm of each of the boards formed in water for 24 hours. The thickness of the board before and after soaking was determined and the difference in thickness was expressed as ratio of the original thickness as percentage. Standard test method was adopted for the tensile strength after the sample was cut into dumbbell shape.

$$TS = \frac{L_1 - L_0}{L_0} X100\%$$

……..1

Where TS is thickness swell, L_1 is the thickness of board after immersion in water and L_0 is thickness before immersion.

$$WA = \frac{W_1 - W_0}{W_0} X100\%$$

…….2

Where WA is water absorbed, W_1 is the weight before immersion in water and W_0 is the weight before immersion in water.

$$UTS = \frac{Maximumload}{Cross\,\sec tionalarea}$$

3

Where UTS is ultimate tensile strength

$$MOR = \frac{3PL}{2bd^2}$$

……4

Where MOR is modulus of rupture, P is the breaking load, L, span length, b, width and d, thickness.

3.0 Results and Discussions

The average of the results of test carried out on five samples for each particle size are shown in figures below for bagasse, sugarcane bark and combination of both (mixed). Figure 1-4 represent effect of particle size on properties of particle boards investigated in this work.

The result presented in Figure 1 and Figure 2 indicated that the sugar cane bark particle board had better moisture properties because it had the lowest value of thickness swell and water absorption. This implied that the particle board made from sugarcane back probably will have better dimensional stability when exposed to moisture or used in humid environment than the one from bagasse and the mixture of the two. Also, the result indicated that the composite of the sugarcane bark and bagasse had a better water absorption and thickness swell than that of bagasse only. These properties were found to improve with decrease in particle sizes of the materials used for the particle board, with the values for example in the bagasse particle were 48.66%, 70.73% and 84.08% for particle size of 1.7mm, 4mm and 8mm respectively. This kind of trend was exhibited by the sugarcane bark and composites of the bagasse and sugarcane bark particle boards. Probably reduced particle size caused higher packing of particles during compression resulting to reduced pore spaces available for water to penetrate.

The tensile strength and the modulus of rupture as indicated in Figure 3 and Figure 4 respectively, indicated that the particle from the sugarcane bark would withstand more stress than the boards made from bagasse and the combination of sugarcane bark and bagasse. The particle board made from bagasse showed the least stress bearing capability and the composite bearing more stress than bagasse particle board. It was also indicated that these properties improved with decrease in particle sizes studied.

In general, this observation of properties improvement as particle sizes decrease may be attributed to the fact that reduced particle size caused increase in surface area and therefore exposed them to temperature, proper mixing and caused increase in bondability of the particles. Increase in bondability definitely would cause increase in molecular interaction between the particles and the binder, then resulting to better mechanical properties of particle board of smaller particle size.

Conclusion

Particle boards were produced from sugarcane bark, bagasse and the combination of the two. The effect of particle size on water absorption, thickness swell, tensile strength and modulus of rupture was studied.
The result showed that the particle board from sugarcane bark had better properties than those from bagasse and the composite, while the composite had better property than

that of bagasse only.
The properties were found to improve with decrease in particle sizes studied in this work; increase in molecular interaction as a result of decrease in size was suggested to have been responsible.

Acknowledgement

The authors wish to thank the Department of Chemistry Ahmadu Bello University Zaria Nigeria and Department of Mechanical Engineering Federal Polytechnic Kaduna Nigeria for allowing the use of their compression machine and Characterization of the samples respectively.

References

1. Xiaoqun M. O., Jie H., Susan S. X., Jo, A. R., *Compression and tensile strength of low-density straw-protein particleboard*, Industrial crops and products, 2001, 14, p. 1-9

2. Parker P., *A summary report on building materials produced from wheat straw*, Inorg. Bonded wood fiber comp. material, 1997,5, 47-48

3. Mehmet H. A., Hulya K., Ibrahim B., Ahmat T., *Properties of cotton carpel-based particleboards*, Industrial crops and products, 2005, 22, p. 141-149

4. Hulya K., Gokay N., *Producing composite particleboard from kenaf (Hibiscus Cannabinus L.) stalks*, Industrial crops and products, 2006, 24, p. 177-180

5. Turreda L. D., Bagasse, wood and wood-bagasse particleboards bonded with urea formaldehyde and polyvinyl isocynate adhesives, USDA Technol. J., 1983, 8, 3, p. 66-79

6. Sampathrajan A., Vijayaraghavan N. C., Swaminathan K. R., *Mechanical and thermal properties of particleboards made from farm residues*, Bioresources technology, 1992, 40, 3, p.249-251

7. Nemli G., Kalaycioglu H., Alp H., *Suitability of date palm (phoenix dactyliferia) branches for particleboard production*, Holz als Roh-und 2001, 59, 411

8. Zucaro J., Reen R., *The second forest: filling the wood source gap while creating the environmental performance borad of the 21st century developing composites from wheat straw*, In: Proceeding of the 29 th international symposium of Washington State University on particleboard/composite materials, 1995, p.225-231

9. Rowell R. M., *Composites from agri-based resources*, In: Proceedings, N0. 7286, the use of recycled wood and paper in building applications Forest Products Society Madison WI, 1996, P.217-222

10. Han G. K., Umemura S. K., Kajita H., *Improvement mechanism of bondability in UF-bonded reed and wheat straw boards by silane coupling agent and extraction treatment*, J. wood sci., 1999, 45, 4, p.299-305

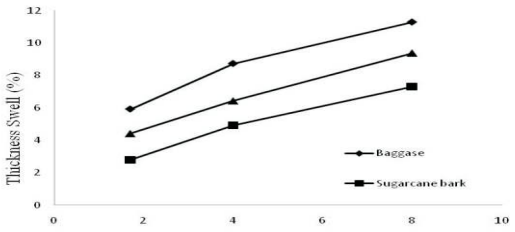


Figure 1: Effect of Particle Size on Thickness Swell

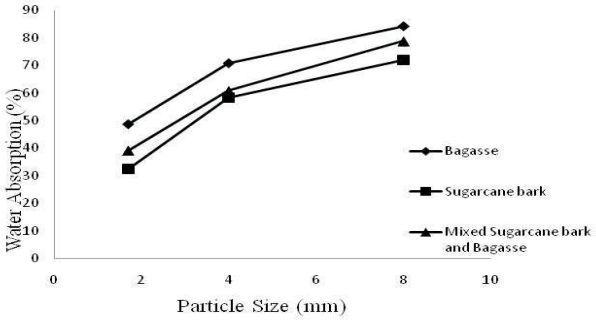


Figure 2: Effect of Particle Size on Water Absorption

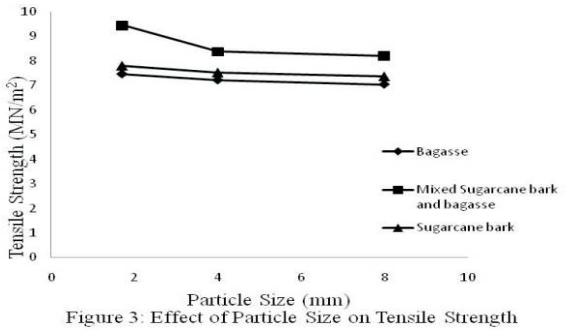


Figure 3: Effect of Particle Size on Tensile Strength

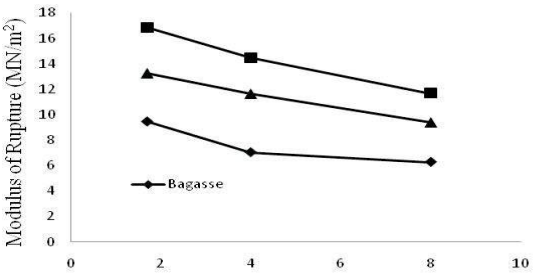


Figure 4: Effect of Particle Size on Modulus of Ruputre

EFFECT OF DIOCTYL PHTHALATE ON THE PROPERTIES OF UNSATURATED POLYESTER RESIN

M. T. Isa *[a], A. S. Ahmed [a], B. O. Aderemi [a], R. M. Taib [b], I. A. Mohammed-Dabo[a]
[a] Department of Chemical Engineering, Ahmadu Bello University, Zaria Nigeria
[b] School of Materials and Mineral Resources, University of Sains Malaysia, 14300, Nibong Tebal Penang, Malaysia
*Corresponding Author
e-mail: mtisaz@yahoo.com, mtisa@abu.edu.ng

Abstract
The effect of plasticization of unsaturated polyester resin using dioctyl phthalate was investigated. The advantage of the exothermic curing reaction of unsaturated polyester and close solubility parameter of the two materials were taken without further addition of external heat. The plasticized and un-plasticized polyester were characterized for impact strength, tensile strength, modulus of elongation, modulus of rupture and thermal stability. The results of the tests indicated that the impact strength of the plasticized polyester increased over the un-plasticized polyester by 48% at dioctyl phthalate content of 5 wt%. The modulus of elasticity, tensile strength and modulus of rupture decreased generally with increase in content of dioctyl phthalate (DOP). However, the elongation increased generally with increase in DOP content. The thermogravimetric analysis (TGA) indicated that 5 wt% DOP plasticized polyester was more thermally stable than the neat resin and other modified samples.
Key words: Unsaturated polyester, Plasticizers, Thermogravimetric analysis (TGA), Charpy impact

1.0 Introduction

Unsaturated polyesters belong to thermosetting class of polymer family with wide use as matrix in fiber composite materials. These resins have wide application due to relative low cost, ease of processing, excellent chemical resistance [1-2]. However, unsaturated polyester resins are brittle and have poor resistance to crack propagation [3]. Polymer modification has been identified as less costly and can be readily achieved than through synthesis of new polymer [4], and works on polymer modification have been widely reported [1-2, 5-14].

The use of epoxy as modifier for unsaturated polyester (UP) resins have been reported widely [2, 11-14] and also the use of reactive rubbers have been reported [15-16]. Diketogluconic acid and salt formation between amine and carboxy groups was used to modify UP [17]. The use of 2-hydoxy ethyl methacrylate and 2, 3- epoxy propyl methacrylate was also reported to have been used as modifier for UP [18]. Few studies are available on the use of low molecular weight additives such as DOP [1]. In the works where DOP was used, high temperature mixing of the unsaturated polyester and DOP was adopted. Meanwhile, the ester inter unit is polar and therefore good combination of UP and DOP is expected [4] and more so, the difference solubility parameters of the two compounds evaluated from data presented by Burke [19] and Leonardo [20], falls within the range given in Ebewele [4] for polymer to be expected to be soluble in a solvent.

The aim of this present work is to take advantage of close the solubility parameters of the compounds and the exothermic reaction nature of the curing process of unsaturated polyester, where temperature generated is usually very high to mix the compounds without any external sources of heat. In addition to investigate the mechanical, thermal and structural changes of the polyester resin using this processing method.

2.0 Experimental

2.1 Formulation and curing of test samples

The mould was cleaned with foam to remove all adhered particles and then coated with petroleum jelly which served as release agent for easy removal of the moulded samples from the mould. Polymer mix was then prepared by measuring 150ml of unsaturated polyester resin and weighed into a plastic cup and 2 wt% of initiator (methyl ethyl ketone) was added and stirred for 3 minutes, after which 2 wt% of cobalt accelerator was then added and stirred for another 2 minutes. The polyester mix was poured into the prepared mould until 4mm mark was reached. The content of the mould was allowed to cure for 24 hours in a fume cupboard, after which it was removed and transferred to an oven to post cure at temperature of 60°C for 3 hours. The same procedure was adopted to produce samples for Charpy impact and modulus of rupture tests, the polyester mix was poured until 8mm mark was reached.

The samples so prepared above were considered unmodified samples. The modified samples were

prepared by the addition of 5 wt% of dioctyl phthalate (DOP) to 150ml of unsaturated polyester resin and stirred for 10 minutes, 2 wt% of initiator was added stirred for 3 minutes, followed by the addition of 2 wt% of cobalt accelerator and stirred for another 2 minutes. The same procedure used for the preparation of the unmodified samples was then adopted. Other samples were produced using 10, 15, and 20 wt% DOP respectively.

2.2 Characterization of Polyester Samples

2.2.1 Mechanical test of samples

The tensile test was conducted on moulded samples by cutting the samples into dumb bell shape according to ASTM D638M. Axial torsion system universal testing machine (Bi-05-172) was used to generate the stress-strain data at strain rate of 5mm/min. The tensile strength, elongation at break and modulus of elasticity (MOE) were obtained from the stress-strain curve. The flexural test was conducted by preparing the test samples according to ASTM D790M at strain rate of 5mm/min with the same test machine used for the tensile test. The maximum breaking load was obtained and used to calculate the modulus of rupture (MOR) as depicted in Equation 1.

$$MOR = \frac{3PL}{2bd^2} \quad \ldots\ldots\ldots\ldots\ldots\ldots\ldots\ldots\ 1$$

MOR is the modulus of rupture, P is the breaking load, L is the span length, b is the width and d the depth.

The Charpy impact test was conducted based on ASTM D256. The variance of the impact tester was to enable the determination of the correction factor to the energy required to break the material and this was determined to be 0.10 J. Hammer with potential energy of 7.5 J was used to impact the samples and the absorbed energy was recorded. This was used to calculate the Charpy impact energy.

2.2.2 Thermal analysis of samples

Thermal gravimetry analysis (TGA) was carried out using approximately 25mg of the sample. The sample was placed in a sample holder in a pre-calibrated Perker Elmer testing machine (TGA 6) and heated at the rate of 10°C/min under nitrogen flow of 20.0ml/min for a temperature range of 30°C- 900°C. The weight loss was obtained with respect to temperature.

3.0 Results and Discussions

The impact strength of the modified unsaturated polyester resin increased by 48% over the neat polyester resin as indicated in Fgure1. It was highest at 5% DOP content after which it dropped to lowest value at DOP content of 20%. The trend depicted conforms to that reported Bakar and Djaider [1] where DOP and tricresyl phosphate (TCP) were used to modify unsaturated polyester.

It was observed Bakar and Djaider [1] that the impact strength of the modified resin at 5% DOP and 5% TCP increased by 65% and 55% respectively over the neat resin. The same trend was observed by Cherian et al [2], where epoxied phenolic novalac (EPN) was used to modify unsaturated polyester resin, with attendant increase of over 100% in impact strength. Probably the difference in the percentage increment observed in this work and previous works probably was due to difference in processing technique adopted in this work. In this work, additional source of heat was not used whereas in previous works additional source of heat was used.

The flexural strength as represented by the modulus of rupture (MOR) [21], was observed to decrease with increase in dioctyl phthtalate (DOP) content (Figure 2).

The neat resin has MOR higher than the modified resin at all DOP contents. This could be as a result of solvency effect of the plasticizer which results in separating polymer molecules, hence reduces intermolecular attraction between polymer molecules [4].

The tensile strength decreases with increase in DOP content, with the neat resin having higher strength than modified resin at all the DOP contents investigated, as shown in Figure 3. This decrease indicates the softening of the tested samples by the plasticizer, indicating high molecular mobility within the polymer chain [1, 4].

The elongation at break of the modified resin increases over the neat resin up till 10% DOP content after which it dropped Figure 4 referred. This observation is in consonant with that of [1] who reported increase of elongation at break up till 5% DOP after which there was decline. In another work, where epoxidised phenolic novalac (EPN) was used instead of DOP [2] similar reported increase in elongation at break up till 7.5% was reported. It was expected that increase in plasticizer content should cause loose packing of the polymer chains, therefore higher elongation.

The moduli of the plasticized resins are lower than that of the neat resin, Figure 5. The moduli fell within the literature range of 2-4 GN/m^2 [22]. This reflects the capacity of the modified resins to absorb energy and provide a higher degree of molecular flexibility [2]. The moduli generally decreased with increase in DOP content and the reason advanced for the observation in the tensile strength could be applied in this case too.

The result of the thermal gravimetric analysis (TGA) showed that the 5% DOP plasticized resin has better thermal stability than the neat polyester. Meanwhile, the neat polyester resin has higher thermal stability than other plasticized resin beyond 5%. At plasticizer content beyond 5%, increased matrix weakening obviously resulted in accelerated resin degradation. There were only marginal differences when the thermal stability at higher plasticizers content was compared to one other.

Conclusions

Unsaturated polyester was modified with dioctyl phthalate (DOP) without external heat source in this work.

Impact property and elongation at break of unsaturated polyester increased with increase in DOP content at 5wt% and 10wt% over the neat resin by 48 and 38 % respectively before they started to drop. The flexural strength (MOR) and modulus of elasticity (MOE) generally decreased with increase in DOP content within the same DOP content.

The addition of DOP reduced the thermal stability of

unsaturated polyester resin except at 5wt% DOP content. The neat resin had a weight loss of 90% at 436°C, while the unsaturated polyester with 5 wt% DOP had a weight loss of 90% at 468°C.

References

[1] M. Bakar, F, Djaider, Effect of plasticizers content on the mechanical properties of unsaturated polyester resin, journal of thermoplastic composite materials 20 (2007) 53-64

[2] A. Benny Cherian, Lity Alen Varghese, Eby Thomas Thachil, Epoxy modified unsaturated polyester hybrid networks, European polymer journal 43 (2007) 1460-1469[3] Bryson J. A., "Plastic material", (1999), Butterworths Heinemann, Oxford

[4] R. O. Ebewele, "Polymer science and technology", (1996), CRC press LLC, Florida USA

[5] N. Bicak, D. C. Sherrington, H. Bulbul, Vinylamine polymer via chemical modification of PVC, European polymer journal 37 (2001) 801-805

[6] Balakrishnan B., Kumar, D. S., Yoshida, Y., Jayakrishnan A., Chemical modification of poly (vinyl chloride) using poly (ethylene glycol) to improve blood compatibility, Biomaterials, 26 (2005) 3495-502

[7] Kruglova, V. A., Dobrynina, L. M., Vereshchagin, L. I., Synthesis of N- vinylazole polymers via chemical modification of poly (vinyl halides), Polymer sci. Ser A 49 (2007) 407-11

[8] Rahul M. Rasal, Amol V. Janorkar, Douglas E. Hirt, Poly (lactic acid) modifications, progress in polymer science 35 (2010) 338-356

[9] Mehdi Borghei, Abdolreza Karbassi, Shahrzad Khoramnejadian, Abdrasoul Oromiehie, Micro biodegradable potato starch based low density polyethylene, African journal of biotechnology 26 (2010) 9, 4075-4080

[10] Wong W., Horfall I., Champion S. M., Watson C. H., The effect of matrix type on the ballistic and mechanical performance of E-glass composite armour, 19th International symposium of ballistics, 7-11 May 2001, Interlaken, Switzerland

[11] Shaker Z. G., Browne R. M., Stretz H. A., Cassidy P. E., Blanda M. T., Epoxy toughened unsaturated polyester interpenetrating networks, Journal applied polymer sci. 84 (2002), 2283-6

[12] Cherian A. Benny, Thachil Eby Thomas, Epoxidised phenolic novalac: a novel modifier for unsaturated polyester resin, Journal applied polymer sci. 1 (2006) 100, 457- 65

[13] Lin Mu- Shih, Liu Chia- Cheng, LEE Chen-Tze, Toughened interpenetrating polymer network materials based on unsaturated polyester and epoxy, Journal applied polymer sci. 72 (1999) 4, 585-92

[14] Park S. J., Park W. B., Lee J. R., Roles of unsaturated polyester in the epoxy matrix system, Polymer journal 31 (1999) 1, 28-31

[15] Malinconico M., Martuscelli E., Ragosta G., Volpe M. G., Rubber modification of polyester resins, 2-Impact behaviour and morphology, International journal of polymeric materials 11 (1987) 317-331

[16] Crosbie G. A., Phillips M. G., Toughening of polyester resins by rubber modification, Journal of materials science 20 (1985) 1, 182-192

[17] Yuen-Yuen Chiu, Reiko Saito, Li James Lee, Modification of unsaturated polyester resins for viscosity control, Polymer 37 (1996) 11, 2179-2190

[18] Sharifah H. Aziz, Martin P. Ansell, Simon J. Clarke, Simon R. Pantery, Modified polyester resins for natural fibre composites, Composites science and technology 65 (2005) 525-535

[19] John Burke, Solubility parameters: Theory and application, appeared in AIC book and paper group annual 3 (1984) 13-58

[20] Leonardo G. Krauskopf, Prediction of plasticizer solvency using Hasen solubility parameters, Journal of vinyl and additive technology 5 (1999) 2, 101-106

[21] ASTM, "Literature Reference for Composite Materials" 1st edition, ASTM International (1987), West Conshohocken

[22] Hull, D. and Clyne, T. W., "An Introduction to Composites Materials" (1996) 2nd edition Cambridge University, Press, Pg 133-211

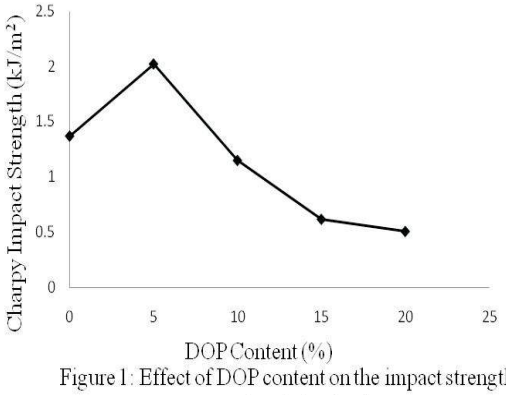


Figure 1: Effect of DOP content on the impact strength of unsaturated polyester

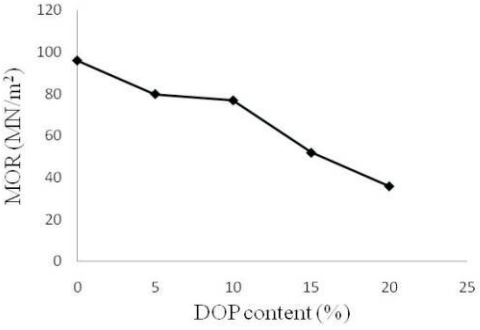


Figure 2: Effect of DOP content on MOR of unsaturated polyester

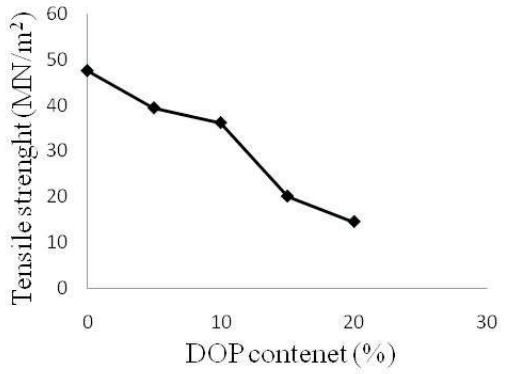


Figure 3: Effect of DOP content on Tensile strenght of unsaturated polyester

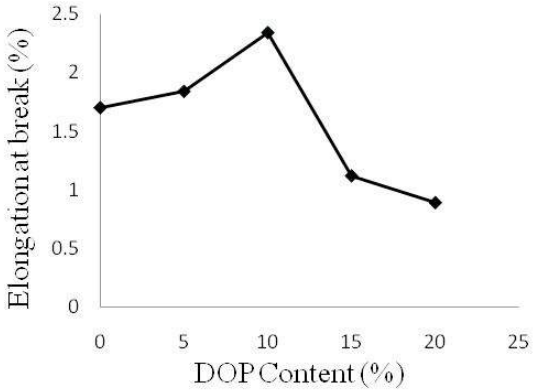


Figure 4: Effect of DOP content on elongation at break of unsaturated polyester

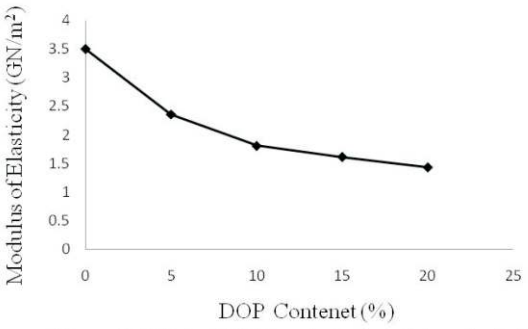


Figure 5: Effect of DOP content on modulus of elasticity of unsaturated polyester

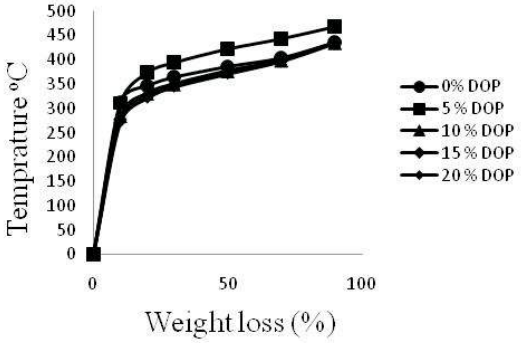


Figure 6: Effect of DOP content on thermal stability of unsaturated polyester

PRODUCTION OF CARBON NANOTUBES CNTS USING ALCOHOL CATALYTIC CHEMICAL VAPOUR DEPOSITION (ACCVD) TECHNIQUE: A REVIEW

Adewuyi B. O. and Aladejebi O. A.
Department of Metallurgical and Materials Engineering, The Federal University of Technology, Akure, P M B 704, Ondo State, Nigeria

ABSTRACT
The mass production of high purity Carbon Nanotubes CNTs at cheaper rate is becoming the most important factor in the application point of view and most industries today are opting for the Chemical Vapour Deposition CVD technique. The CVD method is the most suitable synthesis method in terms of product quality and quantity. This is due to its flexibility, inexpensive, energy efficient, simple and low cost of fabrication, and ability to produce CNTs in large quantity. This paper reviewed the production of CNTs using the Alcohol Catalytic Chemical Vapour Deposition ACCVD technique with emphasis on the influence of hydrocarbon, reaction temperatures, catalyst and substrate materials on the growth of CNTs.

Keyword: Carbon nanotubes CNTs, Alcohol Catalytic Chemical Vapour Deposition ACCVD

1.0 INTRODUCTION

Carbon in its various forms can be referred to as soot, diamond, graphite, coke, Buckey Balls, carbon nanotubes and Fullerenes. Carbon nanotubes (CNTs) are allotropes of carbon with a cylindrical nanostructure, also referred to as sheets of graphite rolled into tubes and possess excellent properties due to their symmetric structure [1]. They are broadly classified into single-walled carbon nanotubes (SWNTs) and multi-walled carbon nanotubes (MWNTs). CNTs possess exceptional properties and wide range applications as a result of their high strength, stiffness, thermal and electrical conductivity [2], CNTs are designated as attractive material in applications range from nanoelectronics [3], sensors [4], ultracapacitors [5], and field emitters to composites [6]. Reliable growth techniques capable of yielding high-purity material in desirable quantities are critical to realize CNTs potential applications. A number of technological advancements in the field of agriculture, electronics, medicine, aerospace, power, to automobiles can be traced to the applications of CNTs. CNTs can be produced by electric arc discharge method [7], chemical vapour deposition method [8], pulsed laser vaporization technique [9], and high-pressure carbon monoxide conversion (HiPCO) process [10].

In pulse laser vaporization and arc discharge methods, although high quality materials can be produced, the high temperature employed for evaporating the carbon atoms from solid carbon sources (over 2700°C) make them difficult to scale up the process in a cost-effective way. Also, arc discharge and pulse laser vaporization methods produce CNTs as powder samples in bundles while CVD offers synthesis of CNTs on substrates [11, 12] as well as in powder form. Additionally, using CVD the diameter length and orientation of CNTs can be effectively controlled.

Hence, chemical vapour decomposition (CVD) method is the most suitable synthesis method in terms of product quality and quantity [11, 12, 13]. This is due to its flexibility, inexpensive, energy efficient, simple and low cost of fabrication, to uniformly deposit thin films of materials, even onto nonuniform shapes and ability to produce CNTs in large quantity. The CVD method is currently the best hope for large-scale production of SWNTs. CVD processes can be used to deposit a wide range of conducting, semiconducting, and insulating materials [13].

2.0 PRODUCTION PROCESS OF CARBON NANOTUBES CNTs THROUGH ALCOHOL CATALYTIC CHEMICAL VAPOUR DEPOSITION TECHNIQUE (ACCVD)

The prerequisite for successful CNTs synthesis is the proper selection of carbon-containing precursor compound, catalyst (e.g. metal nanoparticles and support material), and suitable experimental conditions such as temperature, residence time in the reaction zone and flow conditions. The production of CNTs by CVD method is a 3-step processes that involves the preparation of the catalyst, synthesis of CNTs and purification of the as-produced CNTs. The process involves passing a hydrocarbon vapour (typically for 15-60 minutes) through a tube furnace in which a catalyst material is present at sufficiently high temperature (600-1200°C) to decompose the hydrocarbon. CNTs grow over the catalyst and are collected upon cooling the system to room temperature.

According to Afolabi and co-worker [14] "the catalyst is loaded into a refractory container at room temperatures and placed in the reactor that is heated at a controlled rate. Nitrogen gas will be introduced into the reactor to flow over the catalyst, followed by the introduction of C_2H_2 gas at a controlled rate. After about 60mins of reaction time, the flow of C_2H_2 gas will be stopped and the reactor is left to cool to room temperatures under a continuous flow of nitrogen gas also at a controlled rate". The amount of CNTs synthesized can be calculated by measuring the weight of the container and its content, the difference in

weight will be recorded as weight of the synthesized CNTs.

The production of carbon nanotubes CNTs using Chemical Vapour Deposition CVD technique is usually associated with impurities such as the catalyst support materials and non-CNT inclusions. The impurities can be effectively removed by purifying the as-synthesized CNTs in a mixture of concentrated HNO_3 and H_2SO_4 solutions. This purification technique is known as the acid treatment method. This method is very effective in purifying as-produced CNTs. It causes no damage to the CNTs structure and also promotes the formation of functional groups [14, 15].

2.1 THE INFLUENCE OF HYDROCARBON ON THE GROWTH OF CNTS

Hydrocarbon serves as carbon-source for the synthesis of CNTs. Commonly used carbon sources include methane, ethylene, hexane, ethanol, naphthalene, carbon monoxide, carbon dioxide, acetylene, and benzene. In the case of a liquid hydrocarbon (benzene, alcohol, *etc*.), the liquid is heated in a flask and an inert gas purged through it to carry the vapour into the reaction furnace. The vaporization of a solid hydrocarbon (camphor, naphthalene, *etc*.) can be conveniently achieved in another furnace at low temperature before the main, high temperature reaction furnace. MWNTs are easier to grow from most hydrocarbons than SWNTs, which can only be grown from selected hydrocarbons (*e.g*. CO, CH_4, *etc.)* that have a reasonable stability in the temperature range of 900-1200°C which favours the production of SWNTs [16].

2.2 THE INFLUENCE OF REACTION TEMPERATURE ON THE GROWTH OF CNTS

Generally, low-temperature (600-900°C) CVD reaction yields MWNTs, whereas a higher temperature (900-1200°C) reaction favours SWNT growth, indicating that SWNTs have a higher energy of formation- presumably owing to their small diameters, which results in high curvature and high strain energy. This could explain why MWNTs are easier to grow from most hydrocarbons than SWNTs, which can only be grown from selected hydrocarbons. Common efficient precursors of MWNTs (*e.g*. acetylene, benzene, *etc*.) are unstable at higher temperatures and lead to the deposition of large amounts of carbonaceous compounds other than CNTs [16].

2.3 THE INFLUENCE OF CATALYST MATERIALS ON THE GROWTH OF CNTS

The catalyst material may be solid, liquid, or gas and can be placed inside the furnace or fed from outside. When the substrate-catalyst interaction is strong, a CNT grows up with the catalyst particle rooted at its base (known as the 'base growth mode'). When the substrate-catalyst interaction is weak, the catalyst particle is lifted up by the growing CNT and continues to promote CNT growth at its tip (the 'tip growth mode'). The growth model of the catalyst material is based on a strong interaction between the metals and the support which produced a good yield of CNTs. Formation of SWNTs or MWNTs is governed by the size of the catalyst particle. Broadly speaking, when the particle size is a few nanometers, SWNTs form, whereas particles a few tens of nanometers wide favour MWNT formation.

The growth of CNTs is catalyzed by transition metals. The metals such as Fe, Co, Ni or their combination are most commonly used for CNT growth, since the phase diagram of carbon and these metals suggests finite solubility of carbon in these transition metals at high temperatures. On saturation the carbon precipitates out. This leads to the formation of CNTs under the growth mechanism. It is remarkable that transition metals have proven to be efficient catalysts not only in CVD but also in arc-discharge and laser methods. This indicates that these apparently different methods might have a common growth mechanism for CNTs, which is not yet clear. The catalyst particle size has been found to dictate the tube diameter. Hence, metal nanoparticles of controlled size can be used to grow CNTs of controlled diameter. Therefore, catalyst materials such as solid organometallocenes which liberate nanometal particles in-situ are used to catalyze CNTs growth. Thin films of catalyst coated onto various substrates have also proved successful in achieving uniform CNT deposits [16].

2.4 THE INFLUENCE OF SUBSTRATE MATERIALS ON THE GROWTH OF CNTS

The material, morphology, and textural properties of the substrate greatly affect the yield and quality of the resulting CNTs. Substrates such as silica, quartz, alumina and zeolite are mostly used. Zeolite support with catalysts in their nanopores has resulted in significantly higher yields of CNTs with a narrow diameter distribution. Alumina materials are reported to be better catalyst supports than silica owing to their strong metal-support interaction, which allows high metal dispersion and thus, a high density of catalytic sites [16].

4.0 CONCLUSION

The production of high purity CNTs using ACCVD technique was reviewed. The preparation of the catalyst, synthesis of CNTs and purification of the as-synthesized CNTs are important steps in the production of high purity and quality CNTs. The main parameters for CNTs growth in CVD are the hydrocarbon, reaction temperatures, catalyst and substrate materials, as mentioned by various researchers; they determine the type of CNTs produced and also influence the synthesis of large quantity and high purity CNTs.

REFERENCES

1. Barros E. B., Jorio A., and Jorio A., "Review on the Symmetry-Related Properties of Carbon Nanotubes" Physics Reports, 431, 6, 261–302, 2006.
2. Wang Z. L., Poncharal P., and De Heer W. A., "Measuring Physical and Mechanical Properties of Individual Carbon Nanotubes by in situ TEM," Journal of Physics and Chemistry of Solids, 61, 7, 1025–1030, 2000.
3. Tsukagoshi K., Yoneya N., Uryu S., Aoyagi Y., Kanda A., Ootuka Y., and Alphenaar B. W., "Carbon Nanotube Devices for Nanoelectronics," Physica B, 323, 1–4,

107–114, 2002.

4. Rivas G. A., Rubianes M. D., and Rubianes M. D., "Carbon Nanotubes for Electrochemical Biosensing," Talanta, 74, 3, 291–307, 2007.
5. Adewuyi B., Olaniran O., and Olaseinde A., "Research and development in Nanotechnology – Application and Implication of The New Technology of The Society- Review, Proceedings of Annual Conference of IRDI Research and Development Network, 2, 7, 80, 2007.
6. Ajayan P. M., and Zhou O. Z., "Application of Carbon Nanotubes", Department of Materials Science and Engineering, Renesselar Polytechnic Institutes, Troy, USA, 391-418, 2001.
7. Iijima S., "Helical Microtubules of Graphitic Carbon," Nature, 354, 6348, 56–58, 1991.
8. José-Yacamán M., Miki-Yoshida M., Rendón L., and Santiesteban J. G., "Catalytic Growth of Carbon Microtubules with Fullerene Structure," Applied Physics Letters, 62, 2, 202–204, 1993.
9. Guo T., Nikolaev P., Thess A., Colbert D. T., and Smalley R. E., "Catalytic Growth of Single-Walled Nanotubes by Laser Vaporization," Chemical Physics Letters, 243, 1-2, 49–54, 1995.
10. Nikolaev P., Bronikowski M. J., Bradley R. K., Rohmund F., Colbert D. T., Smith K. A., and Smalley R E., "Gas-Phase Catalytic Growth of Single-Walled Carbon Nanotubes from Carbon Monoxide". Chemical Physics Letters, 313, 91–97, 1999.
11. Zheng B., Li Y., and Liu J., "CVD Synthesis and Purification of Single-Walled Carbon Nanotubes on Aerogel-Supported Catalyst," Applied Physics A, 74, 3, 345–348, 2002.
12. Ward J. W., Wei B. Q, and Ajayan P. M., "Substrate Effects on The Growth of Carbon Nanotubes by Thermal Decomposition of Methane," Chemical Physics Letters, 376, 5-6, 717–725, 2003
13. Baddour C. E. and C. Briens C., "Carbon Nanotube Synthesis: A Review," International Journal of Chemical Reactor Engineering, 3, 2005.
14. Afolabi A, Abdulkareem A, Mhlanga S, and Iyuke S, Synthesis and Purification of Bi-Metallic Catalyzed Carbon Nanotubes in a Horizontal CVD Reactor, Journal of Experimental Nanoscience, 2009.
15. Ajayan P. M., Ebbesen T. W., Ichihashi T., Iijima S., Tanigaki K., and Hiura H., "Opening Carbon Nanotubes with Oxygen and Implications for Filling". Nature, 362, 522, 1993.
16. Sivakumar V. M., Abdul Rahman M., Ahmad Zuhairi A., and Siang-Piao C., Role of Reaction and Factors of Carbon Nanotubes Growth in Chemical Vapour Decomposition Process Using Methane—A Highlight, Journal of Nanomaterials, 395191, 11, 2010

THE USE OF OPERATIONAL AMPLIFIER IN PROVIDING SAFETY FOR ELECTRONIC DEVICES

OLUYAMO S.S. and OLUSOLA O.I.
Department of Physics, Federal University of Technology P. M. B. 704, Akure
E-mail: olajideibk@yahoo.com & oluyamos@yahoo.com

Abstract
Operational amplifiers commonly referred to as Op-Amp find a wide application and usage in electronics, control and instrumentation circuits. The use of this device in ensuring the longevity of electronic systems is discussed in this paper. Equipment such as automatic voltage regulators, automatic inverter systems and so on make use of OP-Amp to provide safety for the entire components that make up the device. In this work, the Op-Amp is used to provide overload and no load indication. A low and high battery level indication when in used and while undergoing charging process is ensured respectively; this however elongates the life-span of the battery. With the aid of an external shutdown circuit arrangement, the entire system can be shut down after given a prior warning alarm about all the conditions earlier mentioned above.
Keywords: Op-Amp, battery, Electronic Devices, Inverter.

INTRODUCTION

An operational amplifier ("OP-Amp") is a DC-coupled high-gain electronic voltage amplifier with a differential input, and usually, a single ended output. An OP-Amp produces an output voltage that is typically hundreds of thousands times larger than the voltage difference between its input terminals **[1]**. Operational amplifiers are important building blocks for a wide range of electronic circuits. They had their origins in analog computers where they were used in many linear, non linear and frequency-dependent circuits. Their popularity in circuit design largely stems from the fact that characteristics of the final Op-Amp circuits with negative feedback (such as their gain) are set by external components with little dependence on temperature changes and manufacturing variations in the Op-Amp itself.

Op-Amps are among the most widely used electronic devices today, being used in a vast array of consumer, industrial, and scientific devices. The Op-Amp is one type of differential amplifier. Other types of differential amplifier include the instrumentation amplifier (usually built from three Op-Amps), the isolation amplifier (similar to the instrumentation amplifier, but with tolerance to common-mode voltages, and negative feedback amplifier (usually built from one or more Op-Amps and a resistive feedback network **[4]**. A standard Op-Amp has a minimum of five pins for its operation; this is shown in figure 1. The basic pins are: V_+ (non-inverting input), V_- (inverting input), and V_{out} (output), V_{S+} (positive power supply and V_{S-} (negative power supply)

The amplifier's differential inputs consist of a V_+ input and a V_- input, and ideally the Op-Amp amplifies only the difference in voltage between the two, which is called the differential input voltage. The output voltage of the op-amp is given by equation 1

$$V_{out} = (V_+ - V_-) A_{OL} \qquad (1)$$

Where V_+ is the voltage at the non-inverting terminal, V_- is the voltage at the inverting terminal and A_{OL} is the open-loop gain of the amplifier (the term "open-loop" refers to the absence of a feedback loop from the output to the input). Without negative feedback, and perhaps with positive feedback for regeneration, an Op-Amp acts as a comparator **[6]**.

Op-Amp as a Comparator

In electronics, a comparator is a device that compares two voltages or currents and switches its output to indicate which is larger. They are commonly used in devices such as analog-to-digital converters (ADCs), relaxation oscillator, null detectors, zero-crossing detectors, level shifter and so on. In theory, a standard op-amp operating in open-loop configuration (without negative feedback) may be used as a low-performance comparator **[2]**. When the non-inverting input (V_+) is at a higher voltage than the inverting input (V-), the high gain of the op-amp causes the output to saturate at the highest positive voltage it can output. When the non-inverting input (V_+) drops below the inverting input (V-), the output saturates at the most negative voltage it can output. The Op-Amp's output voltage is limited by the supply voltage.

A dedicated voltage comparator will generally be faster than a general-purpose operational amplifier pressed into service as a comparator. A dedicated voltage comparator may also contain additional features such as an accurate, internal voltage reference, an adjustable hysteresis and a clock gated input **[3]**. A dedicated voltage comparator chip such as LM339 and LM324 is designed to interface with a digital logic interface (to a TTL or a CMOS). The output is a binary state often used to interface real world signals to digital circuit. Operational Amplifier plays a big role in the Pulse Width Modulated (PWM) based inverter system; the Op-Amp is used as a comparator in the inverter circuit. In this design, Op-Amp LM324 is used as a voltage comparator in the inverter circuit. The LM 324N is a quad two input Op-Amp. Four different Op-Amps in the LM324N can be used for four different works. Each of the Op-Amps in the LM324N IC package has three pins; two for input and one for output. Out of the two input pins, one is called inverting (-) input and the other is called non-inverting (+) input.

Non-Inverting Input (+)

If the input given to this pin is less than the input given to the inverting input pin, then the Op-Amp output will be low. If the input given to this pin is more than the input given to the inverting input pin, then the Op-Amp output will be high. In summary, if the input to the non-inverting pin is low, the output will be low and if the input is high, the output will be high.

Inverting Input (-)

If the input given to this pin is less than the input given to the non-inverting input pin, then the Op-Amp output will be high. If the input given to this pin is more than the input given to the non-inverting input pin, then the output of the Op-Amp will be low. The output will be reverse of the input at the inverting pin; that is, if the input to the inverting pin is low, the output will be high and vice versa **[5]**.

It can therefore be seen that the Op-Amp output depends on the value of the signal at its input pins. This property of the Op-Amp makes it useful as a comparator in inverter circuit **[7]**. Op-Amps in the inverter receive a fixed reference voltage at its one input pin and the other input pin is given the value to be checked. When the value to be checked differ from the reference voltage, the Op-Amp output will go low or high. This output is used to provide audio/visual indication about the conditions of the protective circuit or to shutdown the inverter. In this paper, Op-Amp is used to provide safety for an inverter system; this is achieved by using Op-Amp to design a no load indication circuit, a low battery indicator circuit and an overload detection circuit. With the Op-Amp circuit arrangement, a visual indication is given when any of the conditions earlier mentioned is detected and with an external shutdown arrangement; the inverter system can be shut down after given a prior warning alarm about all the conditions given above.

NO LOAD SHUTDOWN SECTION

When the inverter is working in battery mode and no load is connected at the inverter output, or if the load at its output is switched off, the inverter senses this and automatically switches off itself. This type of protective circuit as shown in figure 2 is essential to protect the inverter from unnecessarily discharging the battery.

How the "No load" is sensed

Source (S) of the MOSFETs at the inverter output is grounded through a shunt. According to Manahar 2004, different polarity of 0V is generated at this shunt, based on the load connected to the inverter output. When no load is connected at the inverter output, the shunt shows negative 0V, and when proper load is connected to the output, the shunt shows positive 0V. The negative 0V is used by the no-load shutdown circuit.

No Load Shutdown Circuit.

The No-load shutdown section uses two Op-Amps using Pin-1, 2, 3, and 8, 9, 10 of IC1, transistors T3 and T4. Pin-2, 3, 9 and 10 are input pins of Op-Amp while Pin-1 and 8 are output pins.

Working Principle

Pin-3 of IC1 receives positive 0V, through R12. Pin-2 of IC1 receives voltage from shunt, through R20 and R18. When no load is connected at output, negative 0V reach pin-2 of IC1 and positive 0V reach pin-3. This results in high output at output pin-1 of IC1. High output at pin-1, turns on the Light Emitting Diode D10 connected to that pin. This indicates that inverter is on, but no load is connected at its output.

High output at pin-1 is given to pin-10 of IC1 through R3 and D5. Capacitor C1 at pin-10 will slowly increase the voltage at this pin. Pin-9 of IC1 receives +5V regulated supply from an external source. As C1 charges, voltage at pin-10 increases; when the voltage at pin-10 becomes higher than the voltage at pin-9, a high voltage (10V) is output from output pin-8. This high output is given to the base of T3, through R34, D11 and D10.

High voltage at the base of T3, switch on the transistor and a 0V is output from its collector. This 0V reach the pin-1 and 5 of another IC2 called NAND gate (CD4011), IC2 is a Quad 2 input NAND gate. Pin-1 and 5 are input pins of two of the NAND gates inside the IC package. When pin-1 and 5 receive 0V, output pins 10 and 11 of the NAND gate will stop the output of MOS drive voltage. With the absence of the MOS drive signal from IC2, the MOSFETs in the output section will stop functioning. This will stop the output at the inverter output socket, that is, the inverter shuts down. The shutdown circuit comprises of pin-8, 9 and 10 of Op-Amp (IC1), transistors T3, T4 and the circuit arrangement of IC2; this is shown in fig. 3.

No-Load Indication.

High voltage at pin-8 of IC1 is given through R8, to the following.

- LED D8, through R2
- Buzzer, through D1and R1

This will switch on the LED D8 and buzzer will sound, indicating no-load condition.

Attaching load when Inverter is in no-load condition.

During the no-load shutdown condition, when a load is connected to the inverter output socket, a positive 0V develops at the output section of MOSFETs source. This results in a positive 0V at pin-2 of IC1. When positive 0V reach pin-2 and 3 of IC1, 0V is output from its pin-1. This will stop the voltage at pin-10 from increasing and a continuous low voltage is produced from its output pin-8. This results finally in normal operation of the inverter.

LOW BATTERY SHUTDOWN SECTION

To protect the battery- a device that serves as input to the inverter system- and to ensure a longer life span of the battery, a low battery detector/shutdown circuit is used. When the battery discharge to a preset level, the low-battery shutdown section sounds the buzzer for sometime and then automatically shuts down the inverter. When a 12V battery reaches 10V, it is considered completely discharged **[5]**. Once the battery is discharged to 10V, it requires charging before it can be used. The inverter system therefore automatically shuts down itself when the battery voltage reaches 10V to

protect the battery from getting damaged.

Low Battery Shutdown Circuit

Low battery shutdown circuit consists of Op-Amp made of pin-5, 6 and 7 of IC1. Pin-5 of IC1 receives +5V regulated supply as reference voltage from an external source. Pin-6 receives battery supply through the potential divider R16 and R17. Pin-7 is output pin.

Working Principle

When the battery has enough charge, the voltage at pin-6 is higher than the voltage at pin-5. For example, when the battery is fully charged (13.5V), pin-6 has around 8.7V, as the battery gets discharged to around 12V; the voltage at pin-6 reduces to about 7.2V. As the battery gets discharged, the voltage at pin-6 gets further reduced. When the voltage at pin-6 becomes a little higher than the voltage at pin-5, output pin-7 will output a high signal (around 8.5V).

High output at pin-7 of IC1 will reach the following through R7:

- Low battery indicator LED D9, through R4
- Positive terminal of buzzer through D2 and R1
- Pin-10 of ICI through R5, D3 and R9.

High voltage at D9 and buzzer will turn on the LED and starts sounding the buzzer. This alerts the user about low-battery shutdown. Turning on of LED D9 and sounding of buzzer indicate that the battery has reached 10V level, but low-battery shutdown has not yet taken place. High voltage at pin-7 of IC1 reaches pin-10 of IC1, through R5, D3 and R9. This repeats the whole process of inverter shutdown which was explained in the no-load shutdown section. Voltages at the various pins were measured, recorded and tabulated under different conditions of the battery level. Table 1 shows the voltage at various pin points of IC1 before the low-battery shutdown occurs

Table1: Voltage at various points b efore low-battery shutdown.

PIN	VOLTAGE
5	5.0V
6	8.7V
7	0V
8	0V
9	5.0V
10	0V

It should be noted that pin-6 of IC1 receives 8.7V only when the inverter battery is fully charged, that is the battery voltage will indicate around 13.5V. As the battery voltage reduces, the voltage at pin-6 also gets reduced. Table 2 shows the voltages when the low-battery starts sounding while table 3 shows the voltages after the low-battery shutdown occurs.

Table2: Voltages when the Low-Battery Buzzer starts sounding..

PIN	VOLTAGE
5	5.0V
6	4.0V
7	8.5V
8	0V
9	5.0V
10	0V

Table 3: Voltages after the Low -Battery Shutdown

PIN	VOLTAGE
5	5.0V
6	4.8V
7	8.5V
8	10.5V
9	5.0V
10	5.1V

OVERLOAD SHUTDOWN SECTION

If a load higher than the inverter capacity is connected at the inverter output, the MOSFETs at the output, and the output mains transformer could get damaged **[5]**. To protect the inverter from this situation, an overload shutdown section is used in the inverter. This section protects the inverter mains transformer and MOSFETs by switching off the inverter output. When the overload occur, the inverter does not switch off immediately; it indicates this condition by lighting an overload Light Emitting Diode (LED) and sounding buzzer before shutting down the inverter.

Overload Circuit

Overload shutdown section uses two Op-Amps using Pin-12, 13, 14, and 8, 9, 10 of IC1, transistors T4 and T3.

Working Principle

Load sensing voltage is given to the pin-12 of IC1 from source of MOSFETs, through R20, R18. Pin-13 of IC1 receives a constant reference voltage, through R14, R15 and overload adjustment preset VR1. The value of reference voltage at pin-13 of IC1 is around 0.05V; this value can be increased / decreased by VR1. According to **Phillip et al, 2002,** a 500VA/12V inverter should be set for overload cut at 300W. When a 300W load is connected to the inverter, pin-12 of IC1 receives around 0.03V from the MOSFETs source. When more than 300W load is connected to the inverter, this results in 0.04V at pin-12 of IC1.

When the load is further increased, a point is reached when the voltage at pin-12 of IC1 becomes a little higher than the voltage at pin-13. This results in a high output (around 5.5V) at pin-14 of IC1. High output at pin-14 is given to pin-10 of IC1 as input, through R10 and D7. A high voltage at pin-10 results in high voltage (around 8V) from the output pin-8 of IC1. High voltage at pin-8 of IC1 repeats the whole process of inverter shutdown which was explained in the no-load shutdown section.

CONCLUSION

The use of an Op-Amp to provide safety for electronic device is very vital as it ensures the longevity of the electronic systems. The incorporation of Op-Amp inside an inverter system has a lot of advantages over the ones that does not have the Op-Amp feature. The Op-Amp design discussed in this paper does not only ensure the safety of the inverter system; it also ensures that all the peripherals, battery for example, used with the inverter system are protected from damage that could result from overuse.

REFERENCES

[1] Horowitz, P. and Hill, W. 1989. The Art of Electronics. Cambridge University Press, Cambridge, pp. 176-180, 284-285.

[2] Jung, W.G. 2004. OP Amp Applications Handbook. Newness, pp. 777-779.

[3] Stout, D.F. 1976. Handbook of Operational Amplifier Circuit Design. Mc Graw-Hill, pp.1-11.

[4] Malmstadt, E. 1981. Electronics and Instrumentation for Scientists. The Benjamin/Cummings Publishing Company Inc., pp.108–110.

[5] Manahar, L. 2004. Modern Uninterrupted Power Supply – Introduction, Servicing and Troubleshooting. B.P.B publication, New Delhi, India. pp. 23-48.

[6] Phillip, A. and Douglas, H. 2002. *CMOS Analog Circuit Design*, Oxford University Press, Oxford, pp.55-58.

[7] Rogenmoser, R. and Kaeslin, H. 1997. The impact of transistor sizing on power efficiency in submicron CMOS circuits. Solid-State Circuits, IEEE Journal 32 (7), pp. 1142–1145.

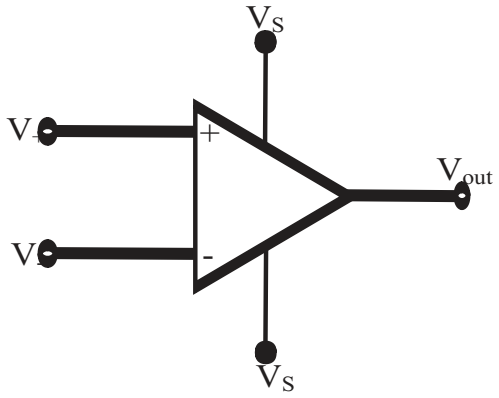
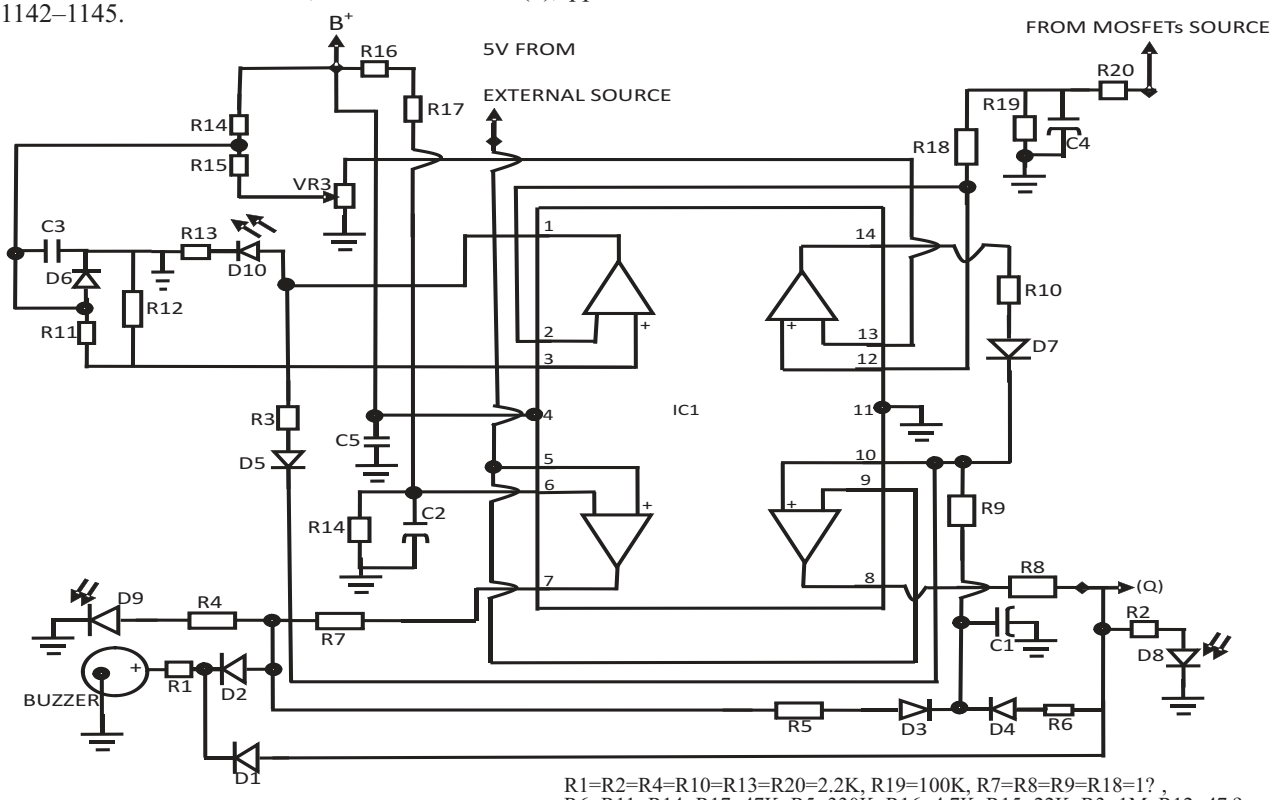
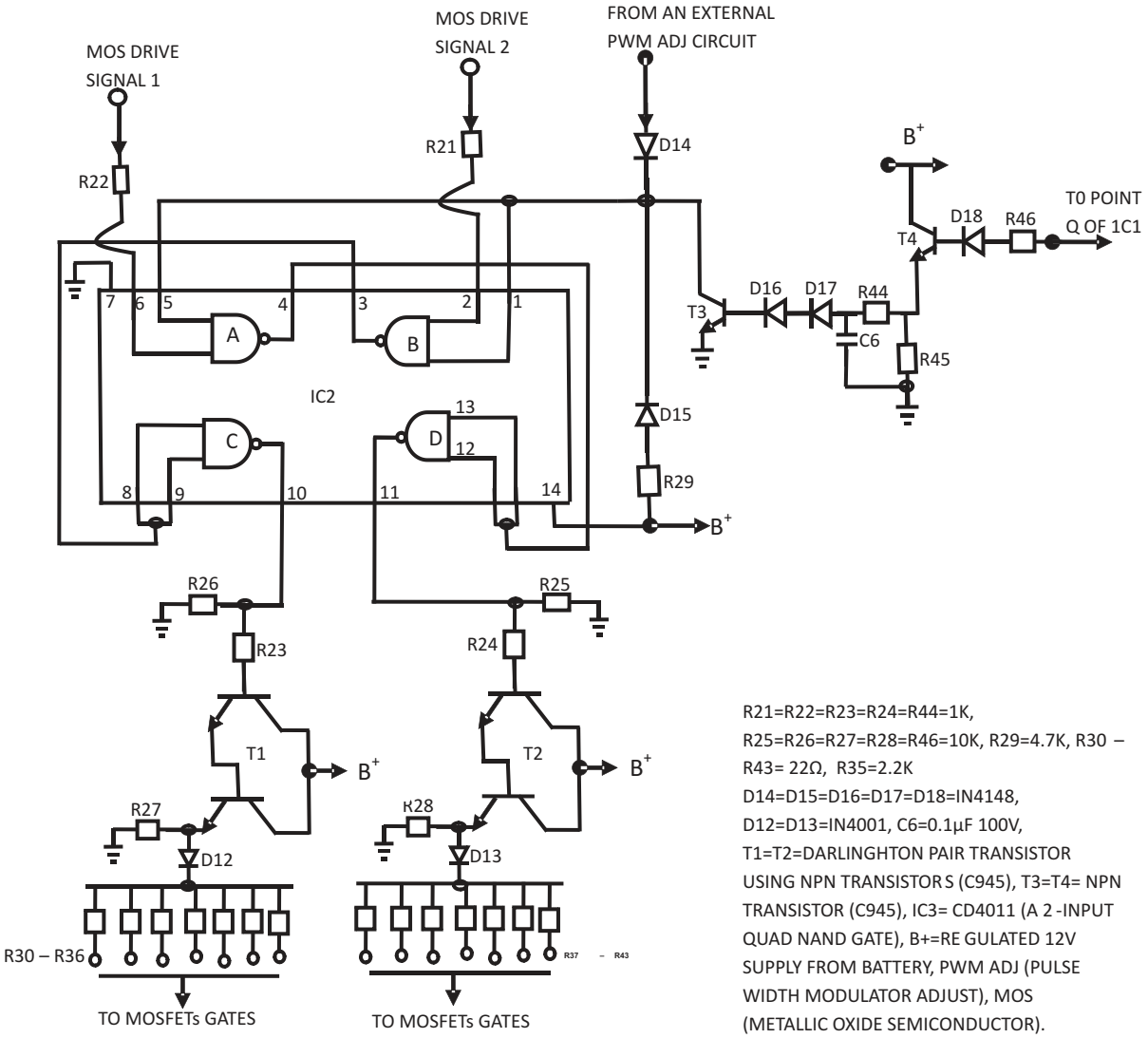


Fig. 1: Circuit symbol for an Op-Amp



R1=R2=R4=R10=R13=R20=2.2K, R19=100K, R7=R8=R9=R18=1? , R6=R11=R14=R17=47K, R5=330K, R16=4.7K, R15=22K, R3=1M, R12=47 ? D1=D2=D3=D4=D5=D6=D7=IN4148, D8=OVERLOAD/SHUTDOWN LIGHT EMITTING DIODE (LED) INDICATOR, D9=LOW BATTERY LED INDICATOR, D10=NO-LOAD LED INDICATOR, C1=47µF 50V, C2=10µF 50V, C3=0.22µF 100V,C4=100µF 50V, C5=0.1µF 100V, IC1=LM324 (QUAD OPERATIONAL AMPLIFIER) , VR3 (OVERLOAD ADJUSTMENT PRESET) =4.7K, B+=REGULATED 12V SUPPLY FROM BATTER.

FIGURE 2: PROTECTIVE CIRCUIT USING OP -AMP



R21=R22=R23=R24=R44=1K, R25=R26=R27=R28=R46=10K, R29=4.7K, R30 – R43= 22Ω, R35=2.2K
D14=D15=D16=D17=D18=IN4148, D12=D13=IN4001, C6=0.1µF 100V, T1=T2=DARLINGHTON PAIR TRANSISTOR USING NPN TRANSISTOR S (C945), T3=T4= NPN TRANSISTOR (C945), IC3= CD4011 (A 2 -INPUT QUAD NAND GATE), B+=RE GULATED 12V SUPPLY FROM BATTERY, PWM ADJ (PULSE WIDTH MODULATOR ADJUST), MOS (METALLIC OXIDE SEMICONDUCTOR).

FIGURE 3: SHUTDOWN CIRCUITRY USING NAND GATE AND MOS DRIVER SECTION

BASE AND PRECIOUS METAL VALUES IN END-OF-LIFE ELECTRONICS

OGUNNIYI I. O.
Metallurgical and Materials Engineering, Federal University Of Technology, Akure, Nigeria
mrolatunji@yahoo.com

ABSTRACT
Many naturally occurring deposits of base and precious metals assay far less in the metal values compared with that contained in end of life electronics appliances, particularly the printed circuit board components in these devices. This fact is brought to the fore in this paper with a compilation of metal assays of printed circuit boards from various works. The assays are discussed along with those of known mines. Various processing techniques for recovery of these valuables are briefly addressed, compared to the rather hazardous manners this material stream is being presently managed in many cities and suburban communities. The paper basically aims at continuous awareness creation for the cyclic material use culture, so that increasing proportion of the populace can start seeing items normally considered waste as valuable materials that can be economically processed. Cleaner environment, economic enterprise, responsible material use and development in material processing practice and research are all possible spin-off within this view.
Keywords: precious metals, base metals, waste electronics, resource recovery, environment

1 INTRODUCTION

End-of-life (eol) electronics, commonly referred to as waste in electrical and electronic equipment (WEEE) piles up faster than ever. Central unit in this WEEE stream are the printed circuit board (PCB). PCB mechanically supports and electrically connects electronic components by using conductive copper pathways, called traces, which are etched from copper sheets laminated onto a non-conductive substrate [1]. Record rate of accumulation of the PCB were in the region of fractions or multiples of a million tons per annum in countries such Taiwan, South Africa, USA, UK and Nigeria [2 – 8]. There have been more recent focus in the media on e-waste accumulation at the computer village, Ikeja, Lagos, Nigeria, while all over the country are scatters of e-waste already at the end of their service lives. It is common to see CRT monitors by the road side; indicators of a need for a functional channel of disposing such goods, functional in the economic sense and in being environmentally benign.

Although, these items contain high material values that make them economically attractive for processing as a secondary material resource, although they contain a lot of hazardous substances that should conform to strict disposal guidelines, still they lie around; end up in water ways and in the green fields. As a technical campaign, this brief will expand on the valuable content of the PCBs in eol electronics, processing options, and better handling practices, towards promoting cyclic material use, cleaner environment, economic enterprise, and development in material processing practice and research.

2 COMPOSITION OF PCB AS A SECONDARY MATERIALS RESOURCE

Being a multi-component unit, PCB composition analysis is demanding in terms of sample preparation and appropriate analytical techniques. X-ray fluorescence, inductively coupled plasma optical emission spectroscopy and inductively coupled plasma mass spectroscopy have been used in combination and preferably recommended by the author [9]. Other techniques such as atomic absorption spectroscopy, X-ray diffraction, infra-red spectroscopy, fire assay and thermal analyses, have been mentioned by other workers and in reviews [10]. Table 1 shows a compilation of metallic content of the PCB from various workers.

The data for each element in Table 1, can be seen to vary across the different compositions. This is expected as PCB material make-up continues to change with technology over time. In essence, a typical PCB composition must be carefully defined. Anyhow, the typical metallic values in PCB can be seen to include valuable base and precious metals in appreciable proportions comparable or even better than those of the natural deposits of these metals. Gold, for instance, at 40 g/t assay in vaal reefs in South Africa represent good grade deposits [11]. Whereas, copper assays in copper porphyry deposit economically mined can be lower than 2 % [12], the least copper assays in the Table 1 is 10 %. Platinum and palladium, in natural deposits are typically at 10 g/ton run of mine head grade.

When high grades spikes are found in some deposits, it is not the order. Such is the Colossus Mineral Inc recent hit of a behemoth gold-PGM intercept in Serra Pelada, in the mineral prolific Carajas region, Para State, Brazil [13]. At some spots were remarkably high grades of gold and record grades of platinum and palladium over significant widths: 7.30 m at 1494.7 g/t gold, 516.6 g/t platinum, and 558.90 g/t palladium; 70.70 m at 53.59 g/t gold, 20.77 g/t platinum and 31.30 g/t palladium. However, the underground operation will have to decline some 3500 m

to access the orebody. That is where the table turns. PCB values on the other hand come only for the pick; with zero mining cost, yet loaded with the values. At the current prices of $3.50 per pound of copper, $30.80, $1640, $1510 and $616 per troy ounce silver, gold, platinum and palladium, respectively, the material-economic value of the PCB is obvious [14, 15]. A conservative estimate, by the author, of only gold and copper values in eol PCB in Nigeria is ? 5 billion per annum.

However, with the ever stiffer criteria to make technology available at cheaper prices, quantity of precious metal values per unit PCB/device is reducing. With development in surface technology, coatings can be only a few tens of nanometers, without compromising the required functionality in comparison with thicker coatings of earlier technology. Precision etching also has led to thinner and narrower traces. These translate to lower assays of the metal values in a PCB. Recovering the precious values from this waste stream is also becoming more demanding, likeable to recovery of values from leaner orebodies. The enormity of appliances produced and used in recent times, however, translates to increasing quantity of precious values in the resulting end of life electronics stream. This implies that though the value is getting leaner, the reserve is rising continuously. In essence, secondary resources processing potentially regenerates its reserves, unlike primary resources processing that depletes natural reserves irreversibly. The pointer here is that secondary resources processing is the hope of sustaining the material demand level of the global pace of manufacturing and development. This submission implicitly makes two demands: increased attention to resource recovery from waste stream, and the need to handle end of life stream more responsibly. The two issues need to be expounded.

3 PROCESSING TECHNIQUES

Processing of eol PCB to recover the material value dates back to more than three decades in the industrialised communities. In the 1970s, the predominant method of recovery of metals from electronic scrap was via the blast furnace in conjunction with secondary copper/lead smelter [16]. Early in the 1980s, some physical processing stages were employed to preconcentrate the values. Figure 1 shows a multi-component REE (radio-electronics equipment) physical processing flowsheet [17]. Scrap REE has now taken on the WEEE nomenclature.

Features of this processing included differentiated disassembly (more recently referred to as selective disassembly), cryogenic cooling and crushing, airflow classification, stages of magnetic separations and, finally, magneto-hydrostatic separation (MHS). The magneto-hydrostatic separation density was first set to 2000 kg/m^3 (2 g/cm^3), then to 3000 kg/m^3. This will cause non-metallic stuff to be floated first, followed by aluminum in the second stage, while copper, lead and tin were in the sink product. In more recent times, the full complement of extensive physical processing, hydrometallurgical and pyrometallurgical techniques are used to maximise resource recovery from the WEEE stream. Table 2 summarises the various e-waste treatment approaches, with the pros and cons of each method.

4 RESPONSIBLE HANDLING

In some industrially backward communities, eol electronics is still treated as waste. End-of-life electronics end in municipal waste piles en route to some dung hills. Apart from the valuable materials that are irretrievably dispersed, there have been pressures from environmental point of views on responsible handling of eol electronics. Lead, mercury, cadmium, hexavalent chromium and polychlorinated biphenyl are among the six materials declared hazardous in the RoHS (Restriction on Hazardous Substances) directives [18]. All these can be found on a single populated PCB. Polychlorinated biphenyl is found in some capacitors. Lead, cadmium, chromium and mercury are usually concentrated in batteries. Mercury is also found in relays and switches, while cadmium can also be found in some surface-mounted chip resistors, infrared detectors and semiconductors. These hazardous contents can leach into the environment when eol PCB are not disposed in safe manners. From the two sides of environmental protection and high resource recovery, responsible handling of eol electronics is obviously imperative in any community. Responsible handling can be summarised under two headings: standard collection system and standard processing.

4.1 Standard Collection System: In material conscious communities, standard collection system entails selective disposal, take back policy, return rebates, among others [2]. Selective disposal entails dropping waste items in labelled bins. Bins are labelled based on material types that can be dropped inside them. A set of bins labelled for polymers, metals and papers, are put together around offices, street corners and at waste processing facilities. These bins are for regular non-hazardous household municipal wastes. For electronics wastes such as eol PCBs, batteries, and waste with hazardous contents, take back policy are employed. Consumers drop their wastes at designated centres maintained by the original manufacturers of such items. The return rebate is a way of encouraging consumer to return their waste. On car batteries, for instance, consumers have about 25 % off the price of a new one when they come with the old. The collection system ensure material content of wastes gets back to manufacturers, and back to the material cycle. Cyclic material use is ensured and there no useless wastes or hazards

In many developing communities, there are no such system, hence all the pollution and the litters. Government policies do not reflect knowledge of these standard practices. Original equipment manufacturers easily sneak or shy away from their take back responsibility. For instance, battery manufacturers in Nigeria do not promote any return rebate, yet they are aware of the international standards guiding their trade, about disposal of lead bearing devices. Communities pile up a dung hill of plastics, papers, metals, fabrics, etc., and burn the heap in open air time and again. Many of the cities litter itself, line its street with wastes stuffed in big plastic bags, and give ugly pictures of urban jungles.

4.2 Standard Processing: PCB processing for

resource recovery must conform to high safety standards. As Table 2 indicates, the pyro route is known for releasing harmful off gases, containing dioxins and furans, from the thermal decomposition of organics in the PCB [19]. The hydrometallurgical processing can also be hazardous, such as the manual aqua regia leaching of gold plaiting from edge connectors reported in small scale backhouse practices in mainland China [4]. Generally, PCB being so multi-component, its processing can be very hazardous on the health of the human operators in short and long term.

Apart from safety threats, poor recovery on many of the valuables will lowers overall resource recovery when the processing route is not comprehensively thought out. A good recommendation in this regard is that PCB processing must start out from a comprehensive physical processing operation to produce clean material fractions or concentrates, which can feed the hydrometallurgical or pyrometallurgical alternatives. However, considering the huge capital and the large scale of operation for the type of smelters that are ideal for the non-ferrous fraction from PCB physical processing, it can be recommended that hydrometallurgical processing will be the route to explore in technologically challenged communities. After comminution, eddy current and electrostatics separation, impure anodes casts or bags can be made directly from the non-ferrous fraction to produce high purity copper cathodes while noble values can be recovered from the anodic slimes.

5 RECOMMENDATIONS

While government formulate and enforce progressive policies, the people must be resolved to move forward. Communities can start by separately collecting paper, plastic, metal and biodegradable wastes in separate labelled bins. The biodegradables can be fetched and deposited in the green spaces. It will recondition the soil. The heap of papers, plastic and metal with no biodegradable organic content will not stink, until appropriate material processing. Some commercial activities will naturally spring up around the stark of resources. A paper company far away will readily bring a truck to a township to pack a heap of waste paper not mixed with diapers, stinking mess of food leftovers, etc. Meanwhile, need driven research efforts into secondary resource processing should be intensified. With community and research efforts in place, policy and fund assistance from government towards executing suggestions on more technical waste handling, research and industry will have a smooth ride. This is the version of the bottom-up approach in national development that will surely work in this regard. A quick fix waste commission, institute, centre or agency may fail due to lack of requisite culture and/or norms. Rather, a national orientation (employing relevant agencies) towards the standard practice of selective disposal of waste (described) can be a very good starting point.

6 CONCLUSION

End of life electronics contains highly valuable base and precious metal content, concentrated in the printed circuit boards. Gold, platinum now hover around $ 1500 per troy ounce, while eol PCB assays well above many natural deposits of this precious metals. Standard waste collection system which entails selective disposal, take back policy, return rebates are necessary to ensure this material values return to the material cycle. There is an economic advantage to it, while the city cleans up itself. A lot depends on what the community want to be – developed or backward. Some national orientation can be very appropriate to sell the standard waste collection practice and the cyclic material use culture. The requisite know how for processing this stream of material is purely a metallurgical engineering business. Here is a wide need driven research and development space. The community, the research and development institutions, and the government are all critical in this concept.

REFERENCES

[1] www.wikipedia.com

[2] Kang Hai-Yong and Schoenung J. M., 2005. Electronic waste recyling: A review of US infrastructure and technology options. *Resources, Conservation and Recycling*, Vol. 45, pp. 368 – 400.

[3] Shuey, S.A., Vildal, E.E. and Taylor, P.R., 2006. Pyrometallurgical processing of electronic waste', *SME Annual Meeting*, March 2006, St. Louis, MO.

[4] Goosey, M. and Kellner, R., 2003. Recycling technologies for the treatment of end of life printed circuit boards (PCBs). *Circuit World*, v. 29, pp. 33 – 37, 2003.

[5] Lee Ching-Hwa, Chang-Tang Chang, Kuo-Shuh Fan and Tien-Chin Chang, 2004. An overview of recycling and treatment of scrap computers. *J. Hazardous Matls.*, B114, pp. 93 – 100.

[6] Lee Ching-Hwa, Ssu-Li Chang, King-Min Wang and Lih-Chyi Wen, 2000. Management of scrap computer recycling in Taiwan. *J. of Hazardous Matls.*, Vol. A73, pp. 209 - 220.

[7] Mackay, T., 2004. Where do PCs go to die? *PC Format*, August, pp. 16 – 20.

[8] Laurie, J. Flynn, 2005. Poor nations are littered with old PC's, *New York Times*, Oct. 24, 2005.

[9] Ogunniyi, I. O., Vermaak, M.K.G. and Groot, D. R., 2009: Chemical composition and liberation characterization of printed circuit board comminution fines for beneficiation investigations. *Waste Management*, 29, pp 2140 – 2146, 2009.
http://dx.doi.org/10.1016/j.wasman.2009.03.004

[10] Li Jihanzi, Puneet S, Zong G, Hong-Chao Z., 2004. Printed circuit board recycling: a state of the art survey. *IEEE Transaction on Electronics Packaging Manufacturing*, Vol. 27/1, pp. 33 – 42.

[11] SAIMM, 1987. The extractive metallurgy of gold in South Africa. South African Institute of Mining and Metallurgy, Monograph Series M7. G. G. Stanley, ed. Vol. 1.

[12] Wills, B. A. and Napier-Munn, T. J., 2006. Mineral Processing Technology. 7ed. Elsevier, Great Britain.

[13] www.colossusminerals.com

[14] www.horizonmetal.com

[15] www.metalprices.com

[16] Sum, E. Y. L., 1991. The recovery of metals from electronic scrap, *Journal of the Minerals Metals and Materials Society*, Vol. 43/4, pp. 53 – 60.

[17] Kravchenko, N.D., Dubinskii, Y. M. and Krichevskii,

V.I., 1983. Processing scrap of radio-electronic equipment. *The Soviet Journal of Non-ferrous Metals (Tsvetnye Metally)* Vol. 24, pp. 100-101.

[18] **Directive 2002/95/EC of the European parliament and of the council on the restriction of the use of certain hazardous substances in electrical and electronic equipment;** *Official Journal of the European Union* l37/19 EN 13.2.2003.

[19] D'Silva K., 2004. Brominated organic micropollutants – igniting the flame retardants issue. *Critical Reviews in Environmental Sc. and Tech*, vol. 34, pp. 141 – 207.

[20] Zhao, Y., Wen, X., Li, B., and Tao, D., 2004. Recovery of copper from printed circuit boards', *Minerals and Metall. Processing*, Vol. 21, No. 2, pp. 99 – 102.

[21] Zhang, S. and Forssberg, E., 1997. Electronic scrap characterizaton for materials recycling. *J. of Waste Management and Resource Recovery*, Vol. 3, pp. 157 – 167.

[22] Kim, B., Lee, J., Seo, S., Park, Y. and Sohn, H., 2004. A process for extracting precious metals from spent printed circuit boards and automobile catalysts, *JOM*, Vol. 56, No. 12, pp. 55-58.

[23] Iji, M. and Yokoyama, S., 1997. Recycling of printed wiring boards with mounted electronic components. *Circuit World*, Vol 23/3, pp. 10 – 15.

[24] Patent Application, WO 6006/013568 A3, 2006. Recovery of precious metals scrap by hydrometallurgical processing.

Table 1: Composition of some metallic values in PCB (Wt. %)

Cu	Al	Pb	Zn	Ni	Fe	Sn	Sb	Au/ppm	Pt/ppm	Ag/ppm	Pd/ppm	Ref.
20	2	2	1	2	8	4	0.4	1000	-	2000	50	[3]
26.8	4.7	--	1.5	0.47	5.3	1	0.06	80	-	3300	-	[20]
10	7	1.2	1.6	0.85	--	--	--	280	-	110	-	[21]
15.6	--	1.35	0.16	0.28	1.4	3.24	--	420	-	1240	10	[22]
22	--	1.55	--	0.32	3.6	2.6	--	350	--	--	--	[23]
17.85	4.78	4.19	2.17	1.63	2	5.28	--	350	4.6	1300	250	[24]
23.47	1.33	0.99	1.51	2.35	1.22	1.54	--	570	30	3301	294	[9]

Table 2: A comparison of general WEEE treatment approaches

Treatment Approach	Operation	Merits	Demerits
Landfilling	Direct dumping of cl assified wastes in landfills	A means of disposal; at least removes physical junks	Leaching of hazardous constituents; wasteful disposal of otherwise huge material resources.
Hydro-metallurgy	A secondary processing, entailing leaching and winning.	Gives hi gh purity product; can handle small tonnages of feed supply	Preconcentration is important on complexity of the leaching and winning. Treatment of secondary effluent streams
Pyro-metallurgy	Smelting in furnaces, giving three products: noble metals report t o molten metal phase, metal with more stable oxides report to slag phase, while metals with high vapor pressure will be collected from the vapor phase. Each product further treated separately.	Little feed preparation: sizing, removal of hazardous components - mercury bearing, capacitors.	Require consistent high grade and quantity of feed; dedicated plant highly capital intensive; feasible where there are existing facilities which accepts e - waste as secondary feed materials; recovers zero value for plastic constituents; off -gas treatment; facilities not available in many parts of the world.
Physical Processing	Applied mineral processing: comminution and separation of constituent materials by exploring variations in physical properties.	Already relevant in feed preparation for hydro or pyro routes; handling of varying feed constituents; amenable for low or high scale operation; least impact on the environment.	Dust handling in aggressive grinding for total liberation; possible precious metal losses; noise; not very clean fractions.

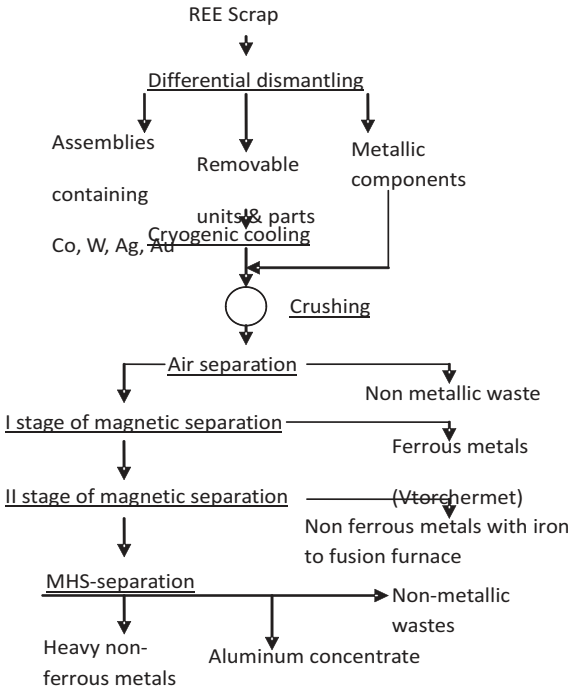


Figure 1: Flowsheet for reprocessing of multicomponent REE scrap [17]

POTENTIAL APPLICATIONS OF CARBON NANOTUBES CNTS: A REVIEW

Adewuyi B. O. and Aladejebi O. A.
Department of Metallurgical and Materials Engineering, The Federal University of Technology, Akure, P M B 704, Ondo State, Nigeria

ABSTRACT
Many potential applications have been proposed for carbon nanotubes, including conductive and high-strength composites; energy storage and energy conversion devices; sensors; field emission displays and radiation sources; hydrogen storage media; and nanometer-sized semiconductor devices, probes, and interconnect. Some of these applications are now realized in products. This paper reviewed the application of carbon nanotubes both in the present and future, and also highlighted the possible challenges facing the application of carbon nanotubes CNTs.

Keyword: Carbon nanotubes CNTs, potential application

1.0 INTRODUCTION
Since the discovery of carbon nanotubes CNTs in 1991 by Iijima [1], it has become one of the most commonly mentioned building blocks of nanotechnology. Independent of the outcome of the ongoing races to exploit nanotubes in applications, CNTs have provided possibilities in nanotechnology that were not conceived in the past. Nanotechnologies of the future in many areas will build on the advances that have been made for CNTs. CNTs are designated as attractive material in applications range from nanoelectronics [2], sensors [3], ultracapacitors [4], and field emitters to composites [5]. A number of technological advancements ranging from agriculture, electronics, medicine, aerospace, power, automobiles, construction, to nanotechnology can be traced to the applications of CNTs [6,7].
CNTs are widely classified into single-walled nanotubes SWNTs and multi-walled nanotubes MWNTs. SWNTs are extremely flexible; it can be bent into an arc with a radius of curvature as small as 20nm.
Nanotubes have an extremely high Young's Modulus (1500-5000GPa) [8,9,10].

Nanotubes also have notable electrical properties that are directly related to their unique quantum mechanical structure. CNTs possess exceptional properties and wide range applications [5,11], as a result of their high strength, stiffness, thermal and electrical conductivity [5,12,13].

2.0 APPLICATION OF CARBON NANOTUBES
CNTs possess the needed combination of properties that are superior to available materials, these make them right materials to be used in service applications where new functionality and enhance performances are required. CNTs have found potential applications in various fields.

2.1 ELECTROCHEMICAL DEVICES
Supercapacitors with carbon nanotubes electrodes can be used for applications that require much higher power capabilities than batteries and much higher storage capacities than ordinary capacitors, such as hybrid electric vehicles that can provide rapid acceleration and store braking energy electrically. The use of nanotubes as electrodes in lithium batteries is a possibility because of the high reversible component of storage capacity at high discharge rates [5,13].

2.2 FIELD EMISSION DEVICES
Industrial and academic research activity on electronic devices has shown that CNTs can be use as field emission electron sources for flat panel displays, lamps, gas discharge tubes providing surge protection, and x-ray and microwave generators. Carbon nanotubes have the right combination of properties – nanometer size, diameter, structural integrity, high electrical conductivity, and chemical stability – that makes it good electron emitters [5,13].

2.3 ENERGY STORAGE
Carbon nanotubes are being considered for energy production and storage. Graphite, carbonaceous materials and carbon fiber electrodes have been used for decades in fuel cells, battery and several other electrochemical applications. Nanotubes are special because they have small dimensions, a smooth surface topology, and perfect surface specificity, since only the basal graphite planes are exposed in their structure. The rate of electron transfer at carbon electrodes ultimately determines the efficiency of fuel cells and this depends on various factors, such as the structure and morphology of the carbon material used in the electrodes [5,13]

2.4 FILLED COMPOSITES
The mechanical behaviour of carbon nanotubes is exciting since nanotubes are seen as the “ultimate” carbon fiber ever made. The traditional carbon fibers have about fifty times the specific strength of steel and are excellent load-bearing reinforcements in composites.

Nanotubes should then be ideal candidates for structural applications. Carbon fibers have been used as reinforcements in high strength, light weight, high performance composites; one can typically find these in a range of products ranging from expensive tennis rackets to spacecraft and aircraft body parts. There are certain advantages that have been realized in using carbon nanotubes for structural polymer (e.g., epoxy) composites. Nanotube reinforcements will increase the toughness of the composites by absorbing energy during their highly flexible elastic behaviour. Nanotubes would also offer multi-functionality, such as increased electrical conduction. Nanotubes will also offer better performance during compressive loading in comparison to traditional carbon fibers due to their flexibility and low propensity for carbon nanotubes to fracture under compressive loads [5,9,13]

2.5 NANOPROBES AND SENSORS

The small and uniform dimensions of the nanotubes produce some interesting applications. With extremely small sizes, high conductivity, high mechanical strength and flexibility, nanotubes may ultimately become indispensable in their use as nanoprobes. One could think of such probes as being used in a variety of applications, such as high resolution imaging, nano-lithography, nanoelectrodes, drug delivery, sensors and field emitters. Since nanotube tips can be selectively modified chemically through the attachment of functional groups, nanotubes can also be used as molecular probes, with potential applications in chemistry and biology [5,13].

2.6 MEDICINE

Nanotubes and other fullerenes may one day serve as transportation molecules for a variety of drugs and therapeutic compounds. Certain molecules can either be attached to the exterior of fullerenes or carried within the closed-cage structure. In the future, buckyballs might be able to attack diseases such as HIV by carrying drugs directly to the virus [14]. The open cage of a carbon nanotube might carry biological agents to individual cells in the body, like a targeted, nanometer-sized test-tube. Potentially, nanotubes could be used as probes for atomic force microscopes in the task of identifying chemical characteristics of individual genes [13,15].

2.7 CONSTRUCTION OF MOLECULAR-SCALE STRUCTURES AND NANOMACHINES

Nanotechnology is a new and exciting field, just beginning to unfold. Accepted in theory, nanotechnology promises to revolutionize the daily lives of every man woman and child on earth. One of the major obstacles yet to be hurdled in the quest for the inevitable development of atomic-sized machines and structures is the availability and suitability of construction materials. Nanotubes appear to have the most potential in overcoming this obstacle [13].

2.8 SPRINGS AND BEARINGS

Experiments conducted at the University of California, Berkeley in July of 2000, revealed that concentrically configured nanotubes demonstrate mechanical properties akin to both springs and bearings. When two tubes are arranged coaxially, one inside of the other, they can be made to rotate independently with no signs of friction or wear. The concentrically configured tubes also can move axially, up and down, like a collapsible telescope. Again, this linear movement shows no signs of wear of fatigue. Thus, these coaxially arranged nanotubes operate as linear and rotational bearings. The Van der Wals forces that "lubricate" the surfaces of the tubes also exert small forces that serve to retract the inner tube back into the outer tube when it is pulled in a linear direction. This allows the telescoping nanotubes to behave like tiny springs [13,16].

2.9 GEARS

The symmetry and shape of fullerene molecules and nanotubes make them perfect candidates for the construction of nano-scale gears [13].

2.10 VELCRO

The common loop-and-hook configuration of Velcro could be mimicked at the atomic level by using nanotubes. The ultra-high temperature resistance and super strength of nanotube Velcro would make them extremely powerful fasteners. Nano Velcro could be used to manufacture anything – from shuttles to micro-robots – and would require the same force necessary to form diamond to pull the two sides apart." [17]

2.11 FILMS AND COATINGS

Buckyballs can be combined with various elements such as silicon and thermally treated to create coatings and layers for surfaces. These films and coatings impart a variety of electrical, mechanical, and optical properties to the host materials they are used to bind and cover. For example, nanotubes can be added to plastic parts allowing them to be electrified, thus facilitating better adhesion of paint. Such a process has already been successfully implemented by General Motors [13, 15].

2.12 MICROELECTRONICS AND COMPUTING

By far the most intriguing and abundant applications for nanotubes and fullerenes lie in the field of microelectronics and computing. Numerous applications ranging from molecular wire conductors to flat panel displays, to nanotransistors are currently being envisioned by scientists on every continent. Today, although we are at the dawn of this new technology, scientists have proven that it is possible to build entire nanometer-scaled circuits that consist of switches, memory, and conducting paths entirely out of nanotubes [13].

3.0 THE FUTURE APPLICATION OF CARBON NANOTUBES

The success of nanotechnology based on carbon nanotubes will depend on improvements in the mechanical properties of nanotubes sheets and fibers with a high surface area by increasing nanotubes alignment and the binding between nanotubes.

The small size of nanostructures hampers the applications of the well-established testing and

measurement techniques, thus new methods and approaches must be developed for their synthesis, property characterization and device fabrication which are different from the conventional engineering technique. Due to the small sizes of nanomaterials, their characterization may be different from that of large-size bulk materials. The most exciting research in characterization is how to measure the physical or chemical properties of individual nanostructures, which is critical in developing new nanomaterials and exploring their unique and novel applications.

Nanotube cost, polydispersity in nanotube type, and limitations in processing and assembly methods are important barriers for some applications of CNTs. If CNTs were not so expensive and if there were a commercial need, one could make nanotube sheets with similar methods (and at a similar scale) to those used to make ordinary paper [5].

4.0 CONCLUSION

The potential applications of carbon nanotubes CNTs in various discipline was reviewed. The properties of nanotubes are certainly amazing; but even more remarkable are the countless applications that may be possible when these newly discovered materials are integrated into mainstream products. The application of CNTs has been linked to the excellent and promising properties exhibited by CNTs; which makes it a potential building block that will serve as a motivating factor for more rigorous research to solving real world problems in the field of nanotechnology and its related discipline for a more sustainable future. However, the difficulties encountered in the applications of CNTS will be solved with further research.

REFERENCES

2. Iijima S., "Helical Microtubules of Graphitic Carbon". Nature; 354: 56-58, 1991.
3. Tsukagoshi K., Yoneya N., Uryu S., Aoyagi Y., Kanda A., Ootuka Y., and Alphenaar B. W., "Carbon Nanotube Devices for Nanoelectronics," Physica B, 323, 1–4, 107–114, 2002.
4. Rivas G. A., Rubianes M. D., and Rubianes M. D., "Carbon Nanotubes for Electrochemical Biosensing," Talanta, 74, 3, 291–307, 2007.
5. Adewuyi B., Olaniran O., and Olaseinde A., "Research and Development in Nanotechnology – Application and Implication of The New Technology of The Society-Review, Proceedings of Annual Conference of IRDI Research and Development Network, 2, 7, 80, 2007.
5. Ajayan P. M., and Zhou O. Z., "Application of Carbon Nanotubes", Department of Materials Science and Engineering, Renesselar Polytechnic Institutes, Troy, USA, 391-418, 2001.
6. Zhou O., Shimoda H., Gao. B., Soojin O., Fleming L., and Yue G., "Fabrication, Integration, and Properties of Macroscopic Structures of Carbon Nanotubes" Account of Chemical Research, 35, 1045, 2002.
7. Heer W. A., "Nanotubes and the Pursuit of Applications" Material Research Society Bulletin, 29, 281, 2004.
8. Harris P. J., Carbon Nanotubes and Related Structures, Cambridge Press, 1999.
9. Dresselhaus M. S., Dresselhaus G., and Ecklund P. C., "Science of Fullerenes and Carbon Nanotubes", Academic Press, New York, 1996.
10. McBridge S. W., "Synthesis of Carbon Nanotubes by Chemical Vapour Deposition", College of William and Mary in Virginia, Williamsburg, Virginia, 2001.
11. Zhang M., Fang S., Zakhidov A. A., Lee S. B., Aliev A. E., Williams C. D., Atkinson K. R. and Baughman R. H., "Strong, Transparent, Multifunctional, Carbon Nanotubes Sheets". Science, 309, 1215, 2005.
12. Wang Z. L., Poncharal P., and De Heer W. A., "Measuring Physical and Mechanical Properties of Individual Carbon Nanotubes by in situ TEM," Journal of Physics and Chemistry of Solids, 61, 7, 1025–1030, 2001.
13. Rosso M. A., "Origin, Properties and Applications of Carbon Nanotubes and Fullerenes, Advanced Materials and Processes, California State University, 2001.
14. Hogan H., "Buckyballs: Making Full Use of Fullerenes" Westech. 1998.
15. Avouris A, P and Collins, Philip G., "Nanotubes for Electronics" Scientific American, 2001.
16. "UC Berkeley Physicists Create Tiny Bearings and Springs Out of Carbon Nanotubes for Use in Microsopic Machines." (AScribe Newswire, July 25, 2000)
17. "Nanotubes Hold Promise for Grounbreaking Technological Change in Products for TVs to Computer Memory to Velcro" (Ascribe Newswire, February 29, 2000)

CORRELATION BETWEEN STRUCTURAL AND OPTICAL PROPERTIES OF PVA/TIO$_2$ NANOCOMPOSITES

[1*]AHMED, T. O., [*]AKUSU, P. O., [#]ALU, N.,[*]ISMAILA, A. & [*]SHIGA, Y. A.
[*]Materials Science Section, Department of Physics, Ahmadu Bello University, Zaria, Nigeria.
[#]Physics Advanced Laboratory, Sheda Science & Technology Complex, Abuja, Nigeria.

Correspondence: tajahmol@yahoo.co.uk

ABSTRACT
Polyvinyl alcohol/titanium (IV) oxide (PVA/TiO_2) nanocomposites have been produced via a two-stage reaction involving the synthesis of TiO_2 Nanoparticles (Nps) from titanium (IV) chloride employing sol-gel technique and subsequent mixing of TiO_2 Nps with PVA dissolved in water boiled at 110°C. The TiO_2 Nps was characterized using SEM-EDS system for its purity and size. The analysis revealed that the TiO_2 Nps have sizes in the range of 25-40nm and of 99.9% purity. Furthermore, the PVA/TiO_2 nanocomposites were found to be tough and transparent with the TiO_2 Nps evenly dispersed in the host polymer matrix. Subsequently, the PVA/TiO2 nanocomposites were characterized by FTIR, Mechanical tests and UV-Vis Spectrophotometry for possible structural modification, toughness and its suitability for UV absorption and filtering.

Keywords: TiO_2 Nanoparticles, Polymer Nanocomposites, Structure, Toughness, UV absorption/filtering.

INTRODUCTION

In the last few decades, conventional polymer composites reinforced by micrometer-scale fillers have seen myriad of applications in automobile, construction, electronics, and consumer products. In comparison to the pristine polymer, polymer composites possess enhanced properties like higher strength and stiffness at the cost of toughness which is directly linked to optical transparency [1]. Recently, polymer nanocomposites developed by incorporating nanosized fillers into pristine polymers have proffered a way to ameliorate the precincts of traditional counterparts. This conceptual fact contradicts the current theories of micromechanics by Jordan in 2005 [2], which supported the size independence of fillers on the properties of polymer composites. The small size of fillers (less than 100 nm) in polymer nanocomposites could bring about dramatic phenomena leading to novel properties for specialized applications if the degree of interfacial interactions between the polymer and filler phase are well controlled and monitored [3].

To realize the novel properties of polymer nanocomposites, synthetic methods which have effect on controlling particle size distribution, dispersion, and interfacial interactions are critical. Despite numerous challenges, considerable research efforts have been made to develop appropriate synthetic techniques for making good polymer nanocomposites but creating one universal technique for developing polymer nanocomposites is impossible due to the physiochemical differences between each system [4]. Nevertheless, a number of polymer nanocomposites based on layered silicate have been recently commercialized, such as the polyimide-clay nanocomposites pioneered by Toyota in 1993 and polypropene-clay nanocomposites by General motors in 2002. The study by Mohan et al., (1996), on intercalated polystyrene/layered silicates nanocomposites revealed that the intercalated hybrid resembles the pristine organosilicate in appearance except that it showed voids where it is localized in the unannealed mixture [5]. Lee et al., (2001) carried out studies on the effect of acrylonitrile content on the gallery height of intercalated clay/poly (styrene-co-acrylonitrile), but there was a limit to increase in the gallery height with increase in acrylonitrile [6]. In 2007, Pegoretti and his co-workers found that the relative stiffness in HDPE/modified clay nanocomposites produced via melt intercalation increases with the addition of clay [7]. A novel heat-sealing performance across the broadest possible temperature range was achieved using polymer blend consisting of polyethylene and ethylene vinyl acetate reinforced by Montmorillonite [8].

Due to the high refractive index and high degree of transparency to UV radiation of nanosized TiO_2 coupled with its low cost, non-toxicity and chemical inertness, a lot of attention is drawn to explore these novel properties in hybridization of polymer materials [9]. In order to explore these aforementioned properties, Feng (2006) studied the effect of TiO_2 nanoparticles on the polystyrene matrix produced **via *In-situ* Polymerization** and concluded that the dispersion (20-50nm size) of TiO_2 into polystyrene matrix gave rise to improved optical properties making the hybrid polymer a potentially active transparent UV filters [10]. In this work, TiO_2 Nanoparticles (Nps) was synthesized from titanium (IV) chloride employing sol-gel technique and subsequently blended with dissolved PVA employing solution mixing technique. The hybrid PVA/TiO_2 nanocomposites were characterized by FTIR, Mechanical tests and UV-Vis Spectrophotometry for possible structural modification, toughness and its suitability for UV absorption and

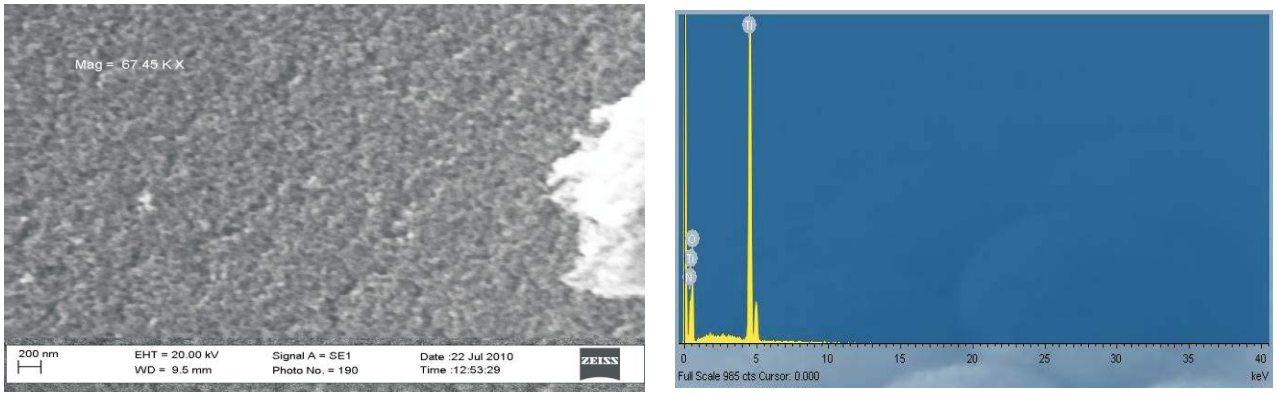
filtering.

EXPERIMENTAL

Polyvinyl alcohol/titanium (IV) oxide (PVA/TiO_2) nanocomposites were produced via a two-stage reaction involving the synthesis of TiO_2 Nanoparticles (Nps) from titanium (IV) chloride employing sol-gel technique and subsequent mixing of TiO_2 Nps with PVA dissolved in water boiled at 110°C via one-pot reaction. The TiO_2 Nps was characterized using SEM-EDS system for its purity and size. The mixing of the TiO_2 Nps with PVA was possible because PVA is hydrophilic. Four samples of PVA/TiO_2 nanocomposites containing 1-4% of TiO_2 Nps were produced. The samples were oven dried at 150°C for 7hrs and subsequently hot pressed at a temperature close to the melting point of PVA in order to produce flat, uniform thin samples. Rectangular shaped samples of PVA/TiO_2 nanocomposites were made and labeled S1, S2, S3, and S4 which contain 1-4% of TiO_2 Nps respectively. These samples were subjected to FTIR measurements, UV-Vis spectroscopy and mechanical tests. The samples were subjected to mechanical tests in order to determine their strengths and toughness. The samples were analyzed by a FTIR spectroscopy in transmission mode without KBr. The spectra were recorded in the frequency range from 350 to 4600 cm^{-1}, after 25 scans, with resolution of 2cm^{-1}. The positions and intensities of the IR bands were processed with Spectral Analysis software. The ultraviolet and visible spectroscopic study was carried out with a spectrophotometer in a wavelength range of 200 to 900 nm.

RESULTS AND DISCUSION

Surface morphology of TiO_2 NPs was observed by scanning electron microscope and the microstructure and EDS spectra of the TiO_2 NPs are given in Figs. 1(a) and (b). The morphology of TiO_2 particles is such that the particles are closely packed together and spherical in shape. The particle size is in the range of 25-40nm, which makes TiO_2 very transparent and suitable for this research. Figure 1b shows the EDS spectra for the TiO2 NPs with characteristic X-ray energies ranging from 0-10keV. Qualitatively, the peak intensity for Ti is much stronger than the peak intensities for nitrogen and oxygen and quantitative analytic results show that the relative concentration of nitrogen and oxygen are minute reflecting that the Ti is the component of TiO2 NPs with concentration greater than 99%.



(a) (b)

Figure 1: (a) Surface morphology and (b) EDS of TiO_2 NPs.

The FTIR spectra of the four samples of PVA/TiO_2 nanocomposites containing 1-4% of TiO_2 Nps given in Figs. 2(a)-(d), were recorded periodically to find out if the TiO_2 NPs was embedded in the PVA matrix and chemically bonded to polymer chains. It is a known fact that the fundamental vibrations of solids (finger prints) are localized in the low frequency region (<1200 cm^{-1}) of the midrange (400 to 4000 cm^{-1}) IR spectrum and that the Ti-O bond is clearly located in the range from 400 to 900 cm^{-1}[11]. The spectral of PVA/ TiO2 nanocomposites is almost a combination of the spectra of PVA and TiO_2 NPs, showing typical absorptions for PVA with characteristic O-H, C=O, and C-H stretching bands at > 3600-1600cm-1, the peaks slightly above 1600cm-1 and below 1500cm-1 indicate vinyl group and the significant absorption below 500 cm-1 represents Ti-O band of TiO2, which indicates the TiO2 NPs are located in the PVA matrix of the nanocomposites. These observations are in good agreement with the works reported in the literature [10, 12, 13].

From Fig. 1(a)-(d), it can be seen that the pure PVA peaks are represented by O-H stretching vibrations of intermolecular hydrogen bonds between 3614.72cm-1 and 3426.66cm-1, stretching vibrations of conjugated triple bonds in the frequency range 2175cm-1 - 2150.70cm-1 and the peaks at 1643.41cm-1, 1642.44cm-1, 1448.59cm-1 and 1439.91cm-1 indicate vinyl groups which act as functional sites for further bonding with Ti. The C=O vibration bands at 1736.96cm-1, 1729.24cm-1, 1718.63cm-1 and1642.44cm-1 come from the formation of the hydrogen bonds between the carbonyl groups of PVA and the hydroxyl groups on TiO2 surface. Below 500cm-1 in the spectra for the four samples, the significant absorption bands represent Ti-O bonds.

The mechanical tests revealed that the PVA/TiO2 nanocomposites samples have very high tensile strengths ranging from to and implies that the hybrid polymer composites are tough with elastic

modulus having values in the range to . The PVA/TiO2 nanocomposites with 4% TiO2 loading has the lowest tensile strength of while the sample with 2% TiO2 loading has the highest tensile strength of

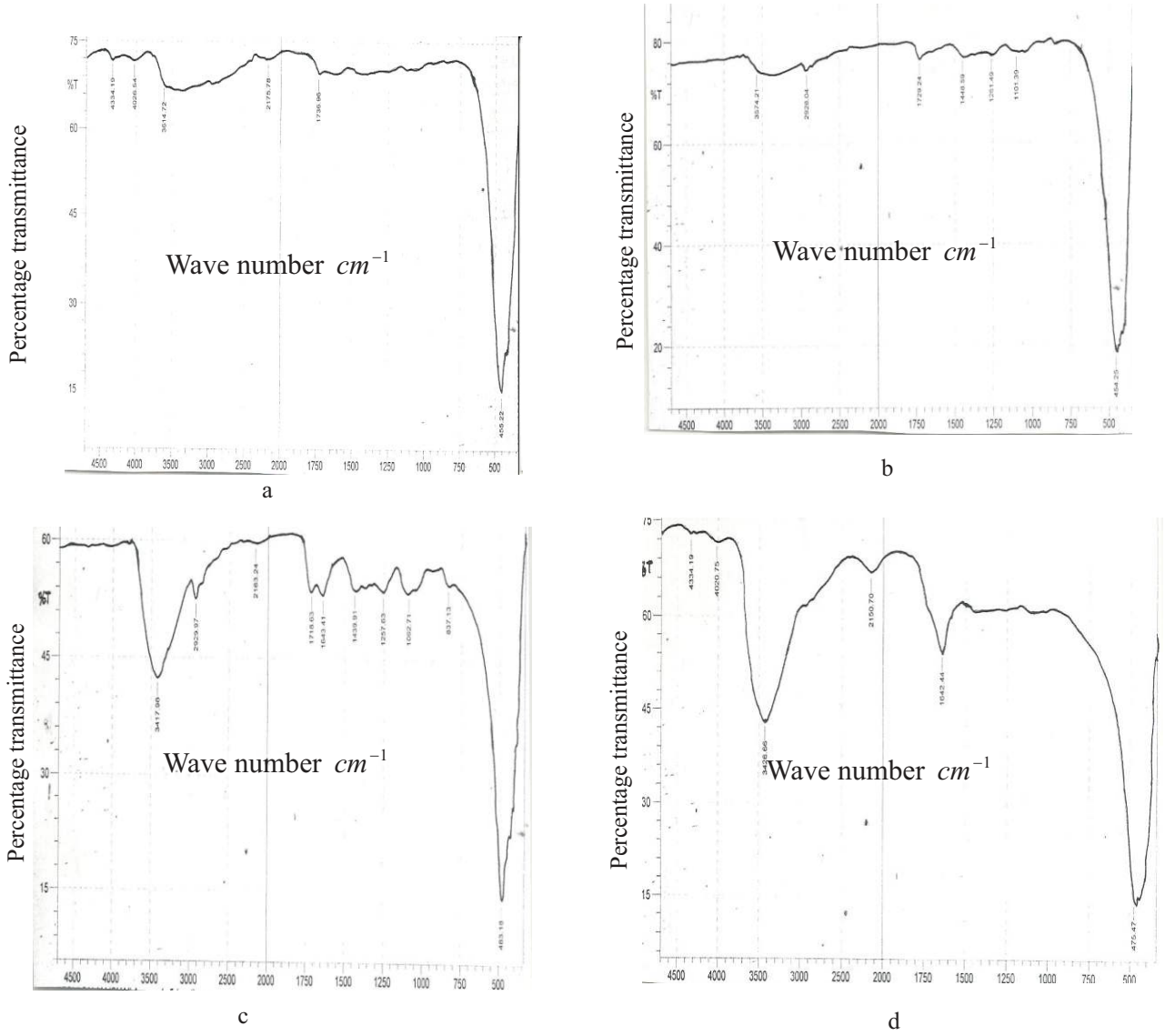


Figure 2: FTIR Spectra of PVA/TiO_2 Nanocomposites containing: (a) 1% of TiO_2 (b) 2% of TiO_2 (c) 3% of TiO_2 and (d) 4% of TiO_2

The samples were scanned in the UV-Visible range of wavelength 200nm-900nm, in order to study the optical properties of the nanocomposites. The UV-Vis spectra of PVA/TiO_2 nanocomposites containing 1- 4% of TiO_2 respectively, are presented in Figures 3(a)-(d). Small values of absorbances at the visible and UV region were observed for PVA/TiO_2 film, which implies reasonable transparency but no ability of filtering out UV light. However, relatively strong absorbance in the UV region and small absorbance at the visible region were observed, which also connotes that the PVA/TiO_2 nanocomposites containing 1% and 3% TiO_2 possess dual optical properties of visual transparency and UV filters close to the visual wavelengths. With the further addition of TiO_2, the sample containing 4% TiO_2, appeared opaque to eye observation and had significant absorbance in the visible region. At this level (4%), the performance of the material as a visually transparent UV filter was reduced.

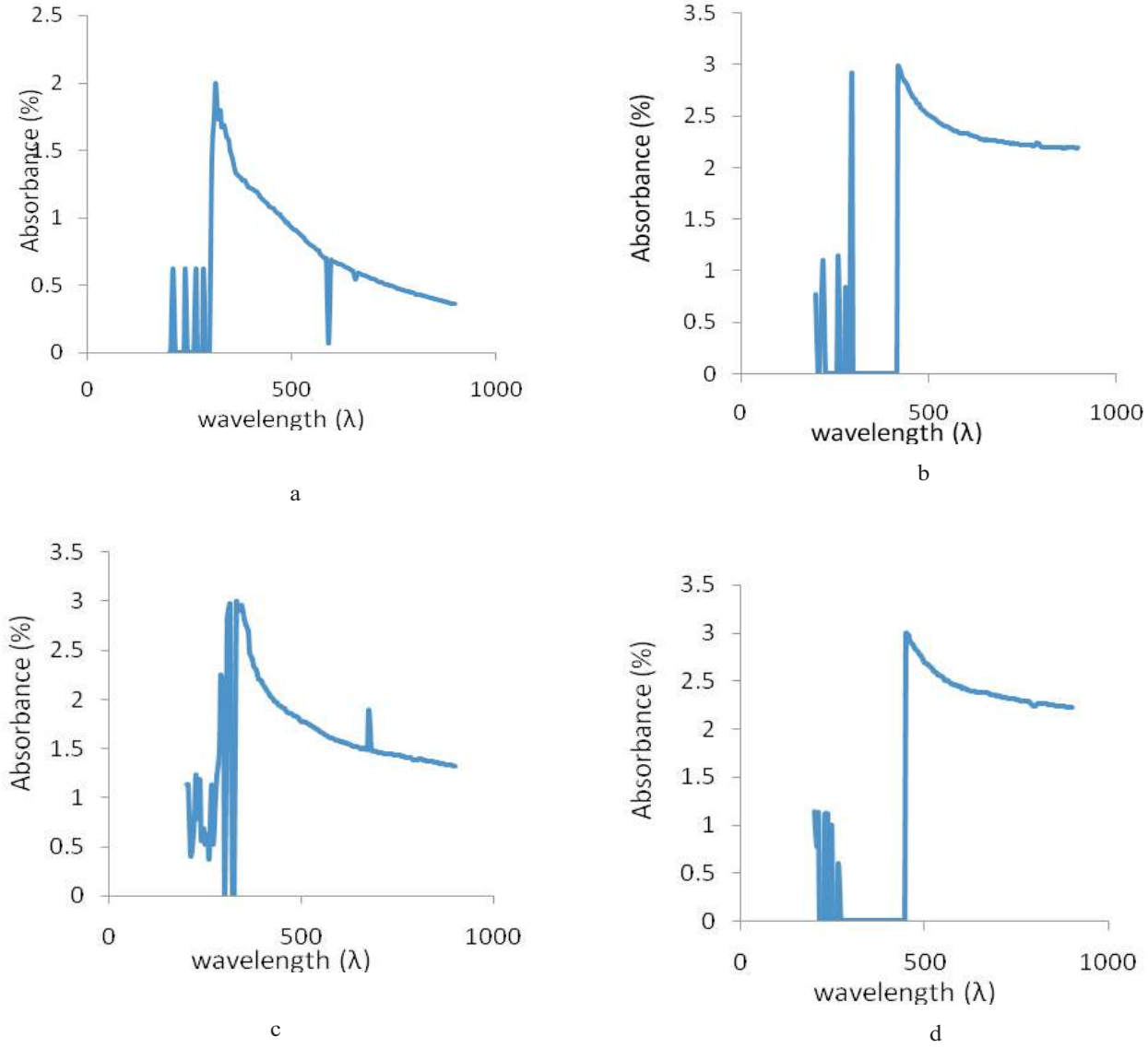


Figure 3: UV-Vis Spectra of PVA/TiO_2 Nanocomposites containing: (a) 1% of TiO_2 (b) 2% of TiO_2 (c) 3% of TiO_2 and (d) 4% of TiO_2

CONCLUSION

The solution mixing technique has been employed to develop PVA/TiO_2 hybrid nanocomposites which have the polymer chains covalently bonded onto the TiO_2 NPs. Integrated characterization techniques, such as SEM, EDS, FTIR, UV-Vis and strength test, were employed to study the behaviour of the PVA/TiO_2 hybrid nanocomposites. It was observed that the developed PVA/TiO_2 hybrid nanocomposites are very tough with high elastic modulus and could act as visually transparent UV filters. FTIR spectroscopy revealed that the TiO_2 NPs was embedded in the PVA matrix and chemically bonded to polymer chains.

Characterization with SEM-EDS showed that the TiO_2 powders are nanocrystalline in structure are very transparent with particles size in the range of 25-40nm. The FTIR spectroscopy revealed that existence of strong interfacial interaction between PVA and TiO_2 NPs as the pristine polymer matrix are uniformly interspersed with TiO_2 NPs showing strong absorption bands for the polymer and the TiO_2 NPs. Finally, UV-Vis spectroscopy confirmed that the dispersion of TiO2 particles at nanoscale level resulted to improved optical properties for the polymer nanocomposites.

REFERENCES

[1] Rosoff, M. (2002). Nano-Surface Chemistry, Marcel Dekker Inc., New York.

[2] Jordan, J., Jacob, K.I., Tannenbaum, R., Sharaf, M.A. and Jasiuk, I. (2005). Experimental Trends in Polymer Nanocomposites: A Review. J. of Mat. Sci. & Eng., (A). 393, 1-11.

[3] Chandra, A., Turng, L. S., Gopalan, P., Rowell, R.M. and Gong, S. (2008). Study of Utilizing Thin Polymer Surface Coating on Nanoparticles for Melt Compounding Polycarbonate/Alumina Nanocomposites and their Optical Properties. Composite Science and Technology, 68, 768-

776.

[4] Berta, M., Lindsay, C., Pans, G. and Camino, G. (2006). Effect of Chemical Structure on Combustion and Thermal Behaviour of Polyurethane Elastomer Layered Silicate Nanocomposites. Polym. Degrad. Stabil., 91, 1179-1191.

[5] Mohan, S., Lauren, N.C., Surya, S.G. and Karen, I.W. (1996). Melt Intercalation of Polystyrene in Layered Silicates. J. of Polym. Sci.,: part B: Polym Physics, Vol. 34,, 1433-1449.

[6] Lee, S.S., Lee, C.S, Kim, M.H., Kwak, S.Y., Park, M., Lim, S., Choe, C.R. and Kim, J. (2001). Specific Interaction Governing the Melt Intercalation of Clay with Pol (Styrene-co—acrylonitrile) Copolymers, J. of Polym. Sci: Part B: Polym. Physics, Vol. 39, 2430-2435.

[7] Pegoretti, A., Dorigato, A., and Penati, . (2007). A Tensile Mechanical Response of Polyethylene-Clay Nanocomposites, express Polymer Letters, Vol. 1. No 3, 123-131.

[8] Manias, E., Zhang, J. and Huh, J.Y. (2009). Polyehylene Nanocomposite Heat Selants with Versatile Peelable Character. Macromol, Rapid Commun., 30, 17-23.

[9] Evora, V.M.F. and Shukla, A. (2003). Fabrication, Characterization and Dynamic Behaviour of Polyester-TiO2 Nanocomposites. Mater. Sci. Eng. (A). 361, 358-366.

[10] Feng, L. (2006). Preparation and Characterization of Polymer TiO_2 nanocomposites via in-situ Polymerization. Master of Applied Science in Chemical Engineering Thesis Presented to the University of waterloo, Ontario Canada.

[11] Morterra, C.; Magnacca, G.(1996). *Catal. Today*, 27, 497.

[12] Rong, Y.; Chen, H. Z.; Wu, G.; Wang, M. (2005). *Mater. Chem. Physics.* 91, 370.

[13] Chen, G.; Liu, S; Zhang, S.; Qi, Z. (2000). *Macromol. Rapid Commun*., 21, 746.

INFLUENCE OF THE SPUTTERING PRESSURE ON THE OPTICAL CHARACTERISTICS OF TIN_X/TIO_XN_Y THIN FILMS PREPARED VIA REACTIVE MAGNETRON SPUTTERING

E. Ajenifuja, A. Y. Fasasi, G. A. Osinkolu
Centre for Energy Research and Development, Obafemi Awolowo University, Ile-Ife, Nigeria.
E-mail: emmanuelaje@yahoo.com, eajenifuja@cerd.gov.ng

Abstract

In the sputtering deposition technique, the sputtering pressure is usually a function of the inert working gas pressure and the reactive gas pressure depending on the kind of deposition (reactive and non-reactive). Within the context of this work, coloured films based on single layered titanium nitride were synthesized by varying the sputtering pressure (S-Pr), thereby using low (0.80Pa), intermediate (3.40-5.33Pa) and high (11.33Pa) S-Pr. The deposited films possessed colour that ranged from dark blue characteristic of oxygen-rich titanium nitride (Ti-N_y-O_x) films to reflective golden yellow reminiscent of low oxygen content TiN_x films. Studies on the optical properties were carried out using UV-Visible Spectrophotometry. Characterization results showed variation in the optical properties of the film depending on the deposition sputtering pressure. High sputtering pressure is shown to be beneficial to the formation of oxygen- deficient TiN_x thin films with relatively higher bandgap compared to films deposited under lower sputtering pressure.

Keywords: Titanium Nitride, Magnetron, Sputtering, Bandgap, UV-Visible

1. Introduction

Titanium nitride is a widely-known material, which exhibits excellent mechanical properties such as high hardness, high wear resistance, low electrical resistivity, high chemical and thermal stability, and interesting optical properties, the colours varying from gold to dark brown. Titanium nitride have been applied in areas such as abrasion resistant coatings on tool steels, decorative coatings in architecture, diffusion barrier layers in semiconductor devices and flat panel displays [1-3].

Titanium nitride films are usually found to contain a trace amount of oxygen as impurities, and the amount of oxygen strongly depends on the deposition conditions used. The deposition of TiN_x and TiO_xN_y films by sputtering has important specific advantages such as low levels of impurities and easy control of deposition rate just by varying the deposition conditions. Based on this premise, it can be assumed that progressive layers of different materials can be obtained on a suitable substrate in a single experimental session. Great efforts have been expended to realized better films quality especially to meet the current technological realities and expectations, therefore numerous studies have been tailored towards the understanding of the effects of process parameters such as sputtering power, substrate temperature [4], rapid thermal annealing [9], sputtering gas, reactive gas pressures and sputtering pressure [5, 6, 7] on other oxides, metallic and ceramic thin films. We present the report on the deposition of TiNx/ TiOxNy thin films with the primary focus on the sputtering deposition pressure effects on the film formation, the optical and micro-structural characteristics of deposited thin films. These properties are however found to be strongly dependent on the sputtering pressure.

2. Materials and Methods

2.1 Deposition Procedure

The films were deposited on glass substrates by DC magnetron sputtering with DC power kept constant at 200W. The sputtering cathode with titanium target in place with the dark anode shield is shown in Fig. 1. The substrate was cleaned by rinsing sequentially with the following; methanol, acetone, de-ionized water and finally in 20% HNO_3 to remove dust and oily layer on the surface and then finally dried using nitrogen gas. For the plasma generation, high purity argon was used and the sputtering target was circular 99.99% pure Ti (50.8 mm in diameter and 5 mm in thickness) fixed at an angle of around 45 degree relative to static substrate platform with an indirect cooling system. In all the depositions, after reaching a base vacuum of 1.33E-3 Pa, the deposition chamber was filled with pure argon after which the reactive nitrogen was introduced up to the chamber pressure parameter required for a particular deposition. However, before starting the deposition, the targets were pre-sputtered in high purity argon gas plasma for average time of 5 min prior to the introduction of the reactive nitrogen gas. The uniform base pressure and other process parameters employed for all depositions are as stated in Table 1.

2.2 Characterization Details

The equipment used for the X-ray diffraction analysis was MD-10 Precision Mini X-Ray Diffractometer with 2 theta angle between 16° and 72° by using CuK_α radiation. Scanning electron microscopy instrument (Carl Zeiss MA-10 SEM) equipped with energy dispersive spectroscopy (EDS) facility was used to study the surface morphology and the microstructure of the films at an acceleration voltage of 20 kV. UV-Visible Thermo Scientific Helios Omega machine was used to obtain the

transmittance data of all the films. The acquired data was used to generate the normalized transmittance to have a better picture of films transmittance in visible regime and most significantly for absorption edge shift evaluation. *The study of the thickness in the nanometer range and the surface topography of the films were carried out using Dektak 150 surface stylus profiler.*

3. Results and Discussion

3.1 Optical Characteristics

The films deposited at high and intermediate sputtering pressures *hsp*, *msp1* and *msp2* showed a reflective golden colour characteristic of TiN_x, while sample *lsp* deposited at low sputtering pressure possessed dark blue colour characteristic of oxygen-rich titanium nitride (Ti-N_x-O_y). The percentage and normalized optical transmittance spectra of the TiNx films prepared at varying sputtering pressures are shown in Figs. 2 and 3 respectively. Obviously the optical transmittance is low in the visible region for the low sputtering pressure prepared sample (lsp) and increased from 10.05% to 97.52% with the increase of sputtering pressure from 0.80Pa to 11.53Pa respectively. The optical transmittance of the films prepared at low sputtering pressure of 0.80Pa was low probably due to the formation of sub-stoichiometric TiN_xO_y film with characterization of the dark blue colour due to the combination of the oxygen ion with the reactive nitrogen gas and titanium. The oxygen ions may have originated from two sources, residual air in the deposition chamber or impurity component from the reactive gas. In addition, the presence of non-reactive titanium along with TiN_xO_y phase could act as scattering centers of light and thus the decrease in the transmittance of the film deposited at low sputtering pressure. Afterwards as the sputtering pressure increased to within the range 3.40Pa and 11.33Pa with the consequent increase in the nitrogen partial pressure, the transmittance of the films increased since most of the nitrogen vacancies tends to disappear and hence the composition of the films approached that of TiN_x. The films prepared at higher sputtering pressure between 3.40Pa and 11.33Pa possessed high transmittance (89.14% to 97.52%) in the visible region and towards the near infrared region with reflective golden colour indicating stoichiometric titanium nitride behaviour. Zhou Ji-Cheng et al [9] also observed that with the increase of sputtering pressure, the surface roughness of the films decreases, which reduces the scattering effects on the visible light. Under the condition of high sputtering pressure with relative higher concentration of nitrogen gas, with bombardment of the target surface by some nitrogen ions, the nitride films deposited were formed not only from direct combination between titanium and nitrogen, but also from titanium nitride generated at the target surface. This was shown from the visual observation of the target after the deposition.

On the transmission bands of the films, Jeyanchandra et al. [8] observed that the broadness of the visible transmission band and the transmittance of the TiN_x films increased with an increase in the N_2 concentration. Sample *lsp* deposited under the low sputtering pressure condition (0.80Pa) with relatively lower nitrogen concentration exhibited a narrower transmission band in the visible region followed by a sharp dip towards the near infrared, while TiN_x film samples prepared at high and intermediate sputtering pressure possessed higher and broader transmission band with a slight dip towards the near infrared. The transmittance band shifted towards higher wavelength with increase in the thickness of the films. Durusoy et al. [10] reported that a narrow transmission band in the wavelength region 300-600nm and a low transmittance towards higher wavelength region are typical of TiN films.

3.2 Bandgap Analysis

The optical absorption coefficient of the films was determined from transmission data where the reflection loses were taken into account. While, the optical bandgap of the film was evaluated from the plot of $(\alpha hv)^2$ versus photon energy (hv) using the Tauc's relation (equation 1) [11].

$$(ahv) = B(hv - E_g)^r \quad (1)$$

Where B is a parameter that depends on the transition probability Eg is the optical bandgap energy of the material, hv is the photon energy and r is an index that characterizes the optical absorption process. For this work, r is equal to ½ for direct allowed transition. Figs. 4 and 5 show the bandgap energies for the films deposited at high sputtering pressure (11.33Pa), intermediate sputtering pressure (3.40Pa and 5.33Pa) and low sputtering pressure (0.80Pa) respectively. From the figures, it shows that sample lsp possessed the lowest gap energy of 3.75eV, while films deposited at high and intermediate sputtering pressure possess a common value of bandgap energy (3.78eV). Large bandgap from 3.70 to 4.50eV have been reported for non-stoichiometric TiNx films ($0.2 \leq x \leq 0.5$) by Kuppuswamy et al. [12]. The difference in the bandgap energies (Table 2) is a pointer to the fact that there is a compositional change in the material based on the deposition pressure. The thin films prepared at sputtering pressures 3.40Pa, 5.33Pa and 11.33Pa, as shown in Fig. 4, all have a common bandgap energy, which indicated a strong connection between the films in term of their composition. The extinction coefficients (k plots) of the films prepared at varying sputtering pressures are shown in Fig. 6 with the inset figure showing the closer observation of the films prepared at high sputtering pressure. The films exhibited minimum extinction coefficient values within the range of 450nm – 550nm. On the average, the extinction coefficient of the films decreased with the increase of sputtering pressure. As stated earlier, it shows that the scattering centre concentration decreases with the sputtering pressure due to the reduction in the roughness and the crystallites size of the films as the sputtering pressure increases.

4. Conclusion

In this work, TiNx thin films with distinctive optical and microstructural characteristics were deposited on glass substrates by DC reactive sputtering technique using 99.99% pure titanium as the target material and laboratory grade N2 as the reactive gas. It is observed that

low sputtering pressure (0.80Pa) favours the formation of oxygen-rich TiNx (Ti-O-N phase) films as shown from their unique colour, while high sputtering pressure (3.40-11.33Pa) enhances the formation of typical reflective golden yellow titanium nitride with unique ITO-like properties (large bandgap, low UV transmission, dipped IR transmission) which could make them to be suitable as optical pass filters, UV detectors, hot mirrors etc.

REFERENCES

[1] B. Rauschenbach, J. W. Gerlach, Cryst. Res. Technol. 35 (6-7) 675-688 (2000)

[2] T. S. Yeh, J. M. Wu, L. J. Hu, Thin Solid Films 516, 7294-7298 (2008)

[3] J. E. Sundgren, H. T. G. Hentzell, J. Vac. Sci. Technol., A4 2259 – 2279 (1986)

[4] K. Vasu, M. Ghanashyam Krishna, K. A. Padmanabhan, Applied Surface Science, 257 3069 – 3074 (2011)

[5] Young-Soon Kim, Young-chulpark, S. G. Ansari, Jeong – Young Lee, Byung – Soo Lee, Hyung- Shik Shin, Surface and Coatings Technology 173 299–308 (2003)

[6] Pengtao Gao, L. J. Meng, M. P. dos Santos, V. Teixeira, M. Andritschky, Applied Surface Science 173 84-90 (2001)

[7] V. Nirupama, K.P. Gunasekhar, B. Sreedhar, S. Uthana, Current Applied Physics 10 272-278 (2010)

[8] Y. L. Jeyachandran, Sa. K. Narayandass, D. Mangalaraj, Sami Areva and J. A. Mielczarski, Material Science and Engineering A 445-446 223-236 (2007)

[9] Zhou Ji-cheng, Luo Di-tian, Li You-Zhen and Liu Zheng, Trans. Nonferrous Met. Soc. China 19 359 – 363 (2009)

[10] Durusoy, H.Z. and Duyar, O. and Aydinli, A. and Ay, F., Vacuum, 70 (1). pp. 21-28 (2003)

[11] J. Tauc, R. Grigorovici, and A. Vancu, Phys. Status Solidi 15, 627 (1966)

[12] T. N. Kuppuswamy, P. Anantha, K. Ghanashyam, A. P. Mamidipudi, K. N. Sri-Rama and A. P. Mangalampalli, US Patent Application Publication, US 2010/0323205 A1 (2010)



Fig. 1 Sputtering cathode with the titanium target installed and the dark anode shield

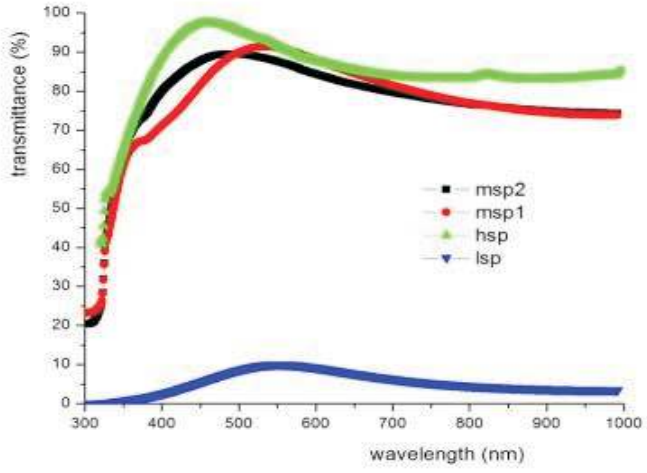


Fig. 2: % Transmittance for high, intermediate and low S-Pr films.

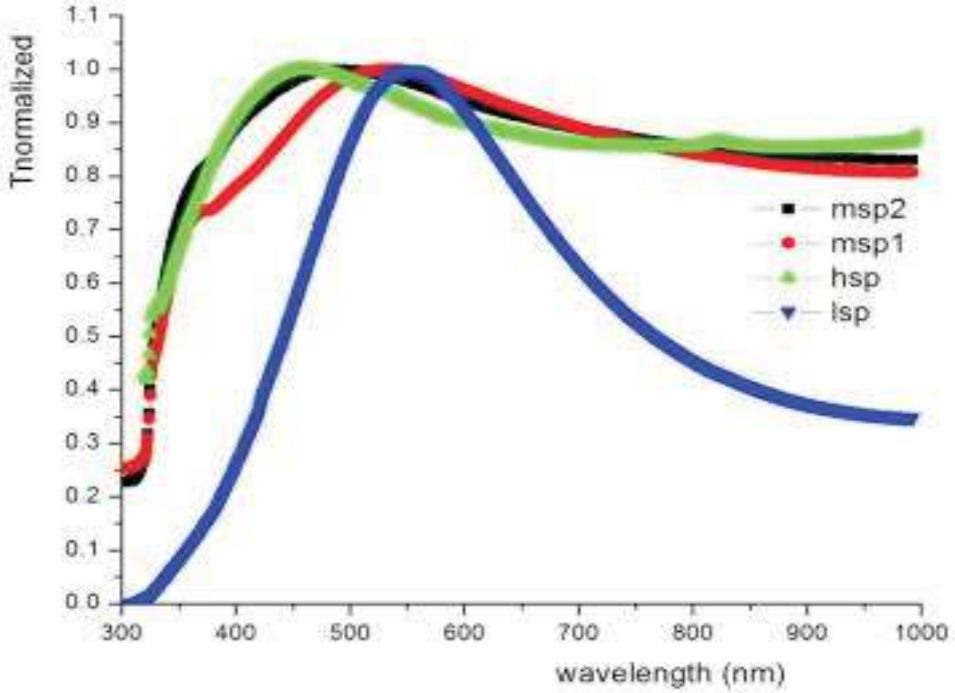


Fig. 3: Normalize Transmittance for high, intermediate and low S-Pr films

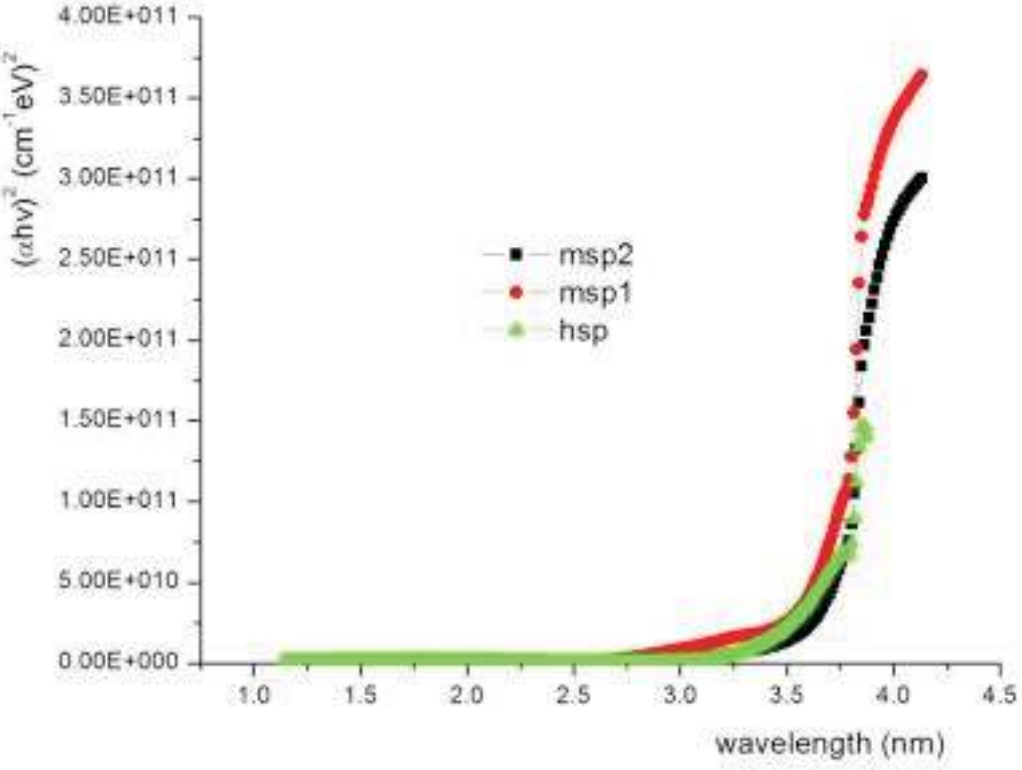


Fig. 4: Bandgap energy for high and intermediate S-Pr deposited films

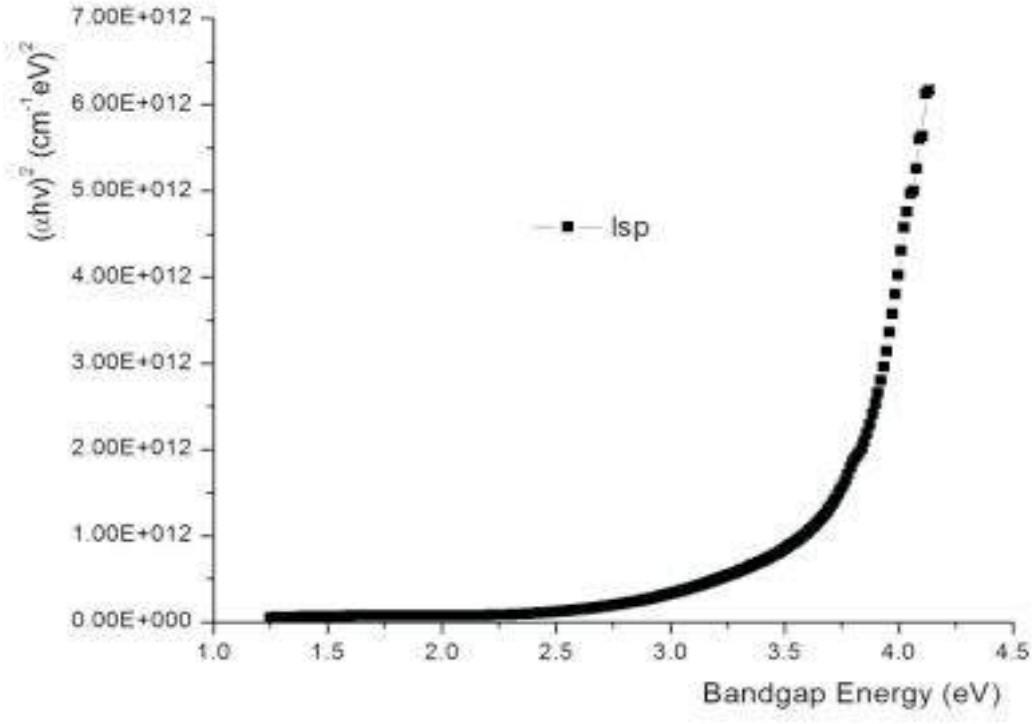


Fig. 5 : Bandgap energy for low S -Pr deposited films.

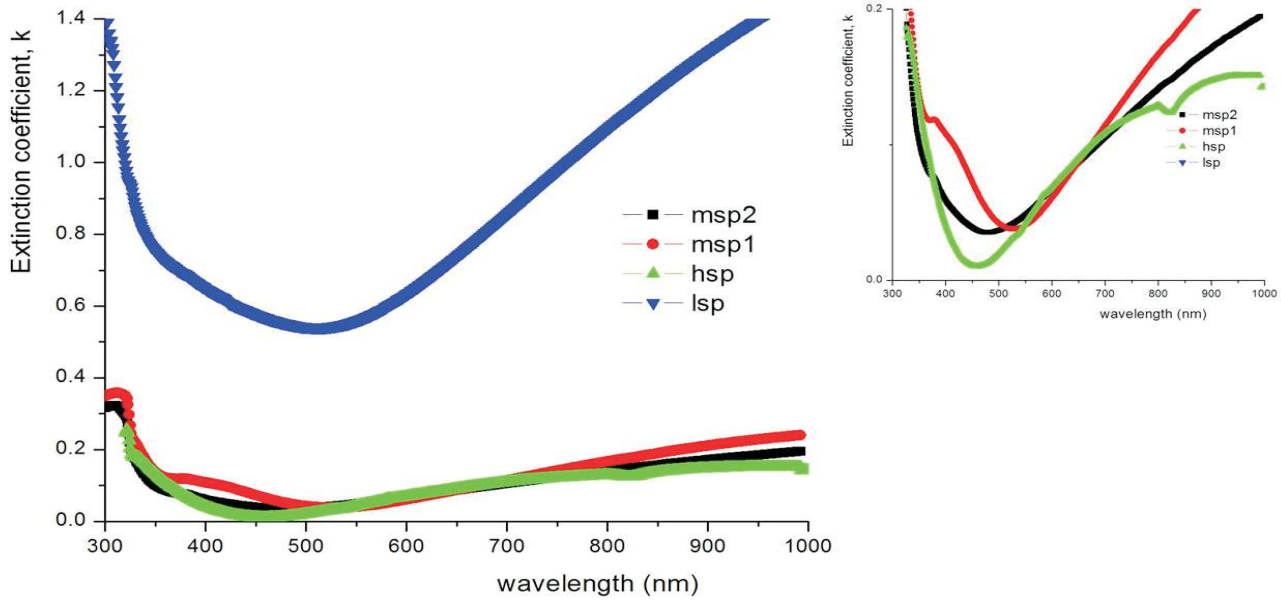


Fig. 6: Extinction coefficient for intermediate, low and high S-Pr deposited films

Parameters	Values
Target	Ti
Sputtering Gas	Ar
Reactive Gas	N_2
Sputtering Power	200W
Deposition Time	10 minutes
Base Pressure	1.33×10^{-3} Pa
Sputtering Pressure	0.80 - 11.33 Pa
Substrate	Glass slide
Substrate-Target	150mm

Table 1: Sputtering Parameters for TiN_x/TiO_xN_y thin films

Sample	Thickness (nm)	Sputtering Pressure (Pa)	Dep. Time (min)	Peak Transmit. (%)	Bandgap Energy (eV)
lsp	180	0.80	10	10.03	3.75
msp2	120	3.40	10	89.14	3.78
msp1	100	5.33	10	91.21	3.78
hsp	90	11.33	10	97.52	3.78

Table 2: Optical properties of TiN_x/ TiO_xN_y films with varied sputtering pressure

COMPARATIVE ANALYSIS OF CORROSION IN DIFFERENT ALUMINIUM PLATES CONCENTRATION OF LIME SOLUTIONS

[1]Owoeye, F.T., [2]Olokode, O.S., [3]Aiyedun, P.O.
[1,2,3], University of Agriculture, Abeokuta. Mechanical Engineering Department

ABSTRACT
Aluminum samples were cut into 5x5mm pieces using four lime solutions with different molarities varying 0.5, 1.0, 1.5, and 2.0 were analyzed. Sixteen samples of aluminum plates were produced from each thickness which was further sub divided into four thicknesses (0.3 mm, 0.6 mm, 0.9 mm and 1.2 mm). Each group was then immersed into different solutions of lime for different time intervals. The samples were first weighed before and after immersion with a Miller weight balance. Weight losses were calculated for all samples. The corrosion rate of 8.250 mm/yr was obtained for the 0.3 mm sample of aluminum at 72 hours while the rate of corrosion decreased to 1.295 mm/yr at 288 hours. The photo micrographs of the aluminum samples both soaked and un-soaked were taken. It was observed that corrosion rates of the aluminum samples decreased with increase in thickness while the rates of corrosion decreased with time of immersion.
Keywords: corrosion, weight loss, Al, lime water, aluminu, aluminium, $Ca(OH)_2$, hydrated lime

INTRODUCTION

Comparative analysis of corrosion behaviour in different aluminum plates concentration of the solutions has continued to attract considerable attention because of the many application of the metal. Aluminium relies on the formation of a compact, adherent passive oxide film for its corrosion immunity in various environments. This surface film is amphoteric and dissolves substantially when the metal is exposed to high concentrations of acids or bases [7, 9]. Aluminum compounds have proven to be useful for thousands of years. Around 5,000 B.C., Persian potters made their strongest vessels from clay that contained aluminum oxide. Ancient Egyptians and Babylonians used aluminum compounds apart not only for making vessels but also for cosmetics, fabric dyes, and medicines. However, it was not until the early nineteenth century that aluminum was identified as an element and isolated as a pure metal. Aluminum compounds occur in aluminum types of clay, but the ore that is most useful for producing pure aluminum is bauxite. Bauxite consists of 45.60% aluminum oxide, along with various impurities such as sand, iron and other metals.

Aluminum metal is a soft, lightweight, malleable metal with an appearance varying from silvery to dull gray, depending on the surface roughness. Its light in weight and its flexibility has made it a good material for domestic use in making cooking utensils and others items such as containers, appliances, and building materials [4].

As a result of the good thermal and mechanical properties, aluminum is often used in making cooking pots. Aluminum pots have a rounded-bottom shape that provides good thermal efficiency. It has much better hear-transfer characteristics and provides an improved and uniform thermal dispersion into the substance being cooked. This has actually helped and attributed important economic considerations, where fuel is both scarce and expensive.

Calcium hydroxide is also known as hydrated lime, slaked lime, lime water, and calcium hydrate [6]. Certain properties of calcium hydroxide which are crystals or soft, odorless granules or powder are: 1) it has a slightly bitter, alkaline taste [2]; 2) it readily absorbs carbon II oxide from air, forming calcium oxide and it is slightly soluble in water; 3) a solution of lime water is a medium to strong base, and reacts violently with acids; and 4) It attacks many metals in the presence of water forming flammable explosive hydrogen gas. Calcium hydroxide is used as liming in agriculture, particularly when a rapid change in pH is needed and majorly in water treatment. Calcium hydroxide dissolves in water to form Ca^{++} and OH^{-}. Aluminum has a special reaction that is called amphoteric which exhibits both acidic and basic reactions. Aluminum loses its electrons by reacting with the dissolved ions of calcium hydroxide and this attack leads to reduction in weight of the aluminum cooking pot termed corrosion. Corrosion means the breaking down of essential properties in a material due to chemical reactions with its surroundings and the loss of electrons of aluminum metal react with water and oxygen. The corrosion can be generally concentrated locally to form pits and cracks, or it can extend across a wide area to produce general deterioration [8].

The major percentage of domestic (kitchen and restaurant) utensils used today is made up of aluminum. The question then arises as to how durable are these aluminum utensils are related to incessant replacement due to perforations and wear caused by corrosion. Since aluminum cooking pots are common household utensils for cooking, the study of its reaction with lime (calcium hydroxide) is of importance as reactions occur between the cooking pots and water or soup which is major source of lime contacts.

The investigation of the durability of aluminum plates in lime water is the broad objective of this study. As a result of the problems mentioned above, the specific objectives of the study are:

- ✓ To investigate the corrosion rates of aluminum at different times of immersion and different pH levels of lime

- ✓ To examine the corrosion rate of different thickness of aluminum plate in the solution of lime
- ✓ To investigate the effect of temperature on the pitting of aluminum cooking pots
- ✓ To investigate the effect of different concentrations of lime solution on corrosion rates of aluminum.

MATERIALS AND METHODS

The four thicknesses of aluminum specimens used for the study were been obtained from the Aluminium Rolling Mills Sango- Otta, Ogun State, Nigeria in form of flat sheets. The two aluminum cooking pots used were made from Aluminium Rolling Mills with 1.5 mm thickness, diameter of 153 mm and a height of 84 mm.

Sixteen (16) different 5mm x5mm were cut from each of the four thicknesses, making a total of sixty- four (64) samples. These samples were cut from the parent materials with the help of shears, while a steel rule and scriber were used for the dimensioning.

EXPERIMENTAL PROCEDURES

The four different concentrations of lime solutions [calcium hydroxide, Ca (OH_2)] were prepared from Chemistry Department's Laboratory, University of Agriculture, Abeokuta. The four different concentrations of lime were prepared with distilled water a week before starting the experiment. These solutions were stored in four different plastic kegs. The four lime concentrations were 0.5 molar, 1.0 molar, 1.5 molar and 2.0 molar. Each of the measured samples was inserted into the identified plastic containers and different concentrations of lime were been poured as each was labeled. The chemical compositions of each of the four different thicknesses of aluminum samples were analyzed by a Quatometer/Metal Analyzer from the Quality Control Department of Aluminium Rolling Mills Sango-Otta. These compositions are shown in Table 1 with aluminum thickness of 0.3mm, 0.6mm, 0.9 mm, and 1.2mm. The total surface area of the samples exposed was 5mm x 5mm (25 mm^2). The sixteen sub-samples from each of the four samples were first weighed as the initial weights by mean of weigh balance. The weighed samples were inserted into each of the separate plastic containers. The first numbered one to sixteen plastic containers contained the same aluminum thickness of 0.3mm. The first sixteen plastic containers were then divided into four groups with four plastic containers in a group. In each of the four groups different concentrations of lime solutions were poured. The pH values of each of the four solutions and the initial temperature were determined by using pH meter and thermometer. These were repeated for other samples making a total of sixty- four (64) samples.

The aluminum cooking pot was filled with 0.5 molar concentration of lime solution (calcium hydroxide) with a pH of 12.55. The pot filled with lime solution was placed on a heater. This was boiled to 100°C, as measured by a thermometer and was held for another 30 minutes (until the pot boiled dried).

The pot was then soaked in water for some days in order to wash and remove the lime that had reacted with the pot during the heating process. This could not be removed by detergent, due to aluminum oxide being formed. A 6 molar solution of hydrochloric acid (HCl) was added which remove all of the attack of the lime solution.

One sample was taken out from each of the four a single sample. Each sample of the four concentrations of lime solutions was timely labeled. The first 3 days (72 hours), the samples were removed by using tongs. The aluminum samples were firstly washed with distilled water in order to remove the un-dissolved lime attached to the samples. The samples were then cleaned with tissue paper, rinsed with acetone solution, dried under a ceiling fan and re-weighed for the final weight. An electronic digital weighing balance of 100g and of four decimal places was used for measuring both initial and final weight of the samples.

After some days of soaking the cooking pot with 2.0 molar lime solutions, the pot developed many pitting corrosion spots. Since the pitting was relatively great, a square 5mm x 5mm portion was dimensioned, within the covered area. The number of pits was counted and this was calculated in response to the total surface area of the experimental pot

RESULTS AND DISCUSSION

The analysis exhibited that 1.2mm thickness of aluminum has the highest percentage of aluminum purity while the least is 0.9mm thickness.

The first 72 hours of all the samples in respective of the lime concentrations and samples thickness have the highest corrosion rates compared to the longest duration of 288 hours. The tables also showed that the corrosion rates of the same sample that is, the same thickness depended majorly on the level of lime concentrations. The corroding medium of 2 g/dm^3 (molarity) has the highest corrosion rate compared to the lower lime solutions.

The graphs (Figures 1 to 3) showed the corrosion rate against time of immersion in different concentration of lime solutions (molarities). The sample that was immersed in highest molarity had the highest corrosion rate due to high level of the aggressive interaction between the aluminum samples and the molarity.

From Table 3, the weight loss per area showed a decreasing trend with immersion time.The highest value was observed for 1.2mm aluminum plate at 72 hours of immersion while the lowest value was obtained for 0.3 mm aluminum at an immersion time of 288 hours.

From table3, Aluminum samples of 0.3mm thickness showed the highest corrosion rate compared to other thicknesses. Pitting of an aluminum cooking pot was observed when soaked in lime solution and the pot heated to 1000C and held for 30 minutes.

The corrosion rates of all of the samples decreased drastically with increase in period (duration) of immersion in respect of thickness and the concentration of the corroding medium (molarities).

Both the level of lime concentrations and the thickness of the samples played a significant role in the level of corrosion rate. For example, a sample of 0.3 mm

thickness has the highest corrosion rate of 0.6875 mm/yr been immersed in 0.5 g/dm3 of lime solution while the sample immersed in 2.0g/dm3 of lime solution had an highest corrosion rate of 1.2980 mm/yr which has a difference of 0.4730mm/yr as shown in Table 2.

The first 72 hours of the corrosion rate of 0.3mm is 0.8250 mm/yr while the corrosion rate of 1.2 mm sample immersed in the same corroding medium (molarity) has a corrosion rate of 0.3926mm/yr.

CONCLUSION

The results obtained from this study indicate the negative but significant effect of lime solution (calcium hydroxide [CaOH2] on aluminum plates. The general reaction is known as corrosion effect which led to a reduction in the weight and thickness of aluminum cooking pots.

The highest corrosion rate of all the aluminum samples were observed in the first three days (72 hours) of immersion while the lowest was in the last 12 days (288 hours). The corrosion rate was also observed at the highest concentration of calcium hydroxide (2.0g/dm^3) and the lowest pH value.

The thinnest of the aluminum samples also gave the highest corrosion rate while the thickest aluminum sample (1.2mm thickness) gave the least corrosion rate.

REFERENCES

[1[Asai. 2000. *Aluminium, Corrosion Engineering, 2nd Edition*. McGraw-Hill: New York, NY.

[2] Bidavari, K. 1986. "Calcium Hydroxide Production". Calcium Company of American. U.S. Pat iv(4):5- 11.

[3] Brian, M. and J.E.R. McDonagh. 2003. "Medical Problems of Today". *Nature of Disease Journal* (London). Vol 2.

[4] Fontana, M.G. 1986. *Corrosion Engineering, 3rd Edition*. McGraw-Hill: New York, NY.

[5] Loretta, H. 1999. *Manufacture of Aluminium, The History of Fluorine, Fluoride and Fluoridation*.

[6]Hardy. 2001. "Lime Water, Lime Burns". *Journal of the National organic Standard Board*. ix:52.

[7] Hurlen T., Lian H., Odegard O. and Valand T. (1984). Corrosion and passive behaviour of Aluminium in weakly acid solution. Electrochim. Acta., 29:579-585.

[8] Oddo and John. 1992. "Aluminium, Nature's Building Block". *An A-Z guide to the Elements.* Oxford University Press: Oxford, UK.

[9] Oguzie E (2007). Corrosion inhibition of Aluminium in acidic and alkaline media Sansevieria trifacciata extract. Corros. Sci., 49:1527-1539

Table1: Chemical compositions of Aluminium plates.

Al Plates	**Fe**	**Si**	**Mn**	**Cu**	**Ti**	**Al**
0.3mm	0.561	0.155	0.023	0.012	0.006	99.19
0.6mm	0.493	0.194	0.005	0.004	0.150	99.27
0.9mm	0.454	0.183	0.032	0.035	0.011	99.17
1.2mm	0.397	0.221	0.011	0.011	0.016	99.32

Table2: The pH value of Lime solutions

Lime(g/dm3)	**pH 0 HR**	**pH 72 HRS**	**pH 144 HRS**	**pH 216 HRS**	**pH 288 HRS**
0.5	12.68	12.64	12.62	12.59	12.58
1.0	12.66	12.6	12.65	12.61	12.6
1.5	12.58	12.55	12.65	12.6	12.6
2.0	12.57	12.54	12.64	12.6	12.58

Table3: Corrosion Rates of Aluminium Plates (mm/yr).

Lime (g/dm3)	**Al plates(mm)**	**CR 72HR 3DY**	**CR144 HR 6DY**	**CR 216HR 9DY**	**CR 288HR 12DY**
0.5	0.3	8.2500	3.3672	2.4084	1.2948
1.0		10.3848	4.2744	3.1056	1.8300
1.5		11.2044	1.9260	1.4424	0.1140
2.0		12.9804	1.6764	0.8196	1.4904
0.5	0.6	8.6568	4.9452	3.3900	2.1552
1.0		8.6388	2.7300	2.4864	1.9308
1.5		9.5760	3.7716	2.8524	2.1360
2.0		11.0544	3.1392	2.1924	1.7328
0.5	0.9	5.1264	5.2956	3.5316	2.6520
1.0		5.4480	3.9132	2.0796	2.0544
1.5		9.1368	4.2744	2.9220	2.2620
2.0		11.5356	2.1744	2.1324	1.7748
0.5	1.2	3.9264	6.4128	4.4160	3.3816
1.0		5.9616	3.8820	3.4992	2.8896
1.5		7.6812	5.1960	3.5280	2.8668
2.0		8.6172	3.8676	2.6784	2.0988

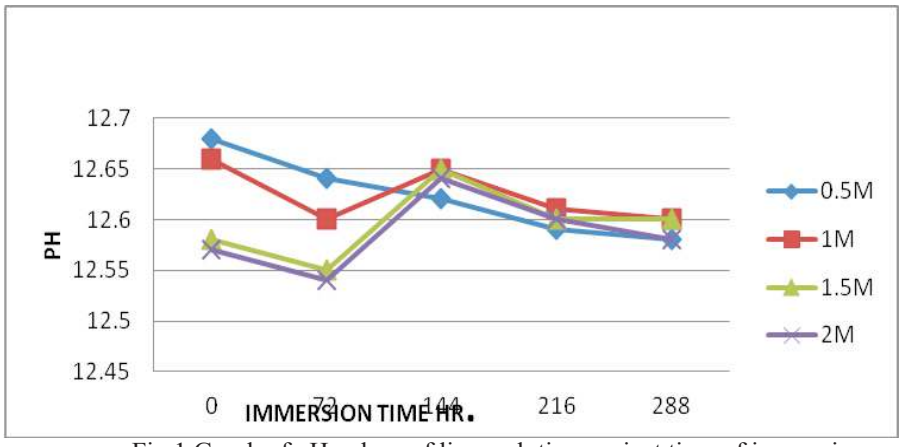


Fig.1 Graph of pH values of lime solution against time of immersion

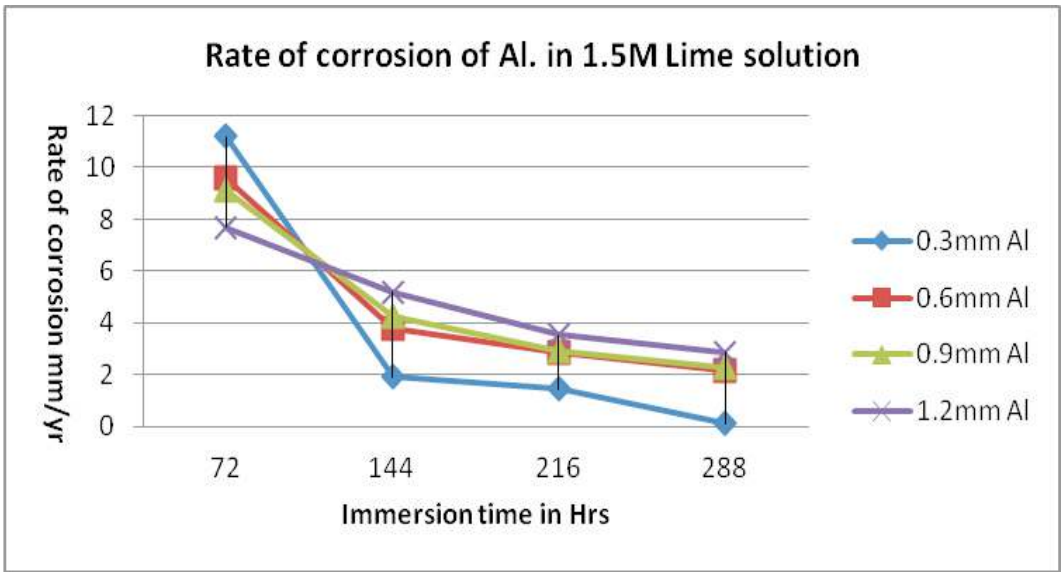


Fig.2 Graph rate of corrosion of Aluminium (Al) against time of immersion

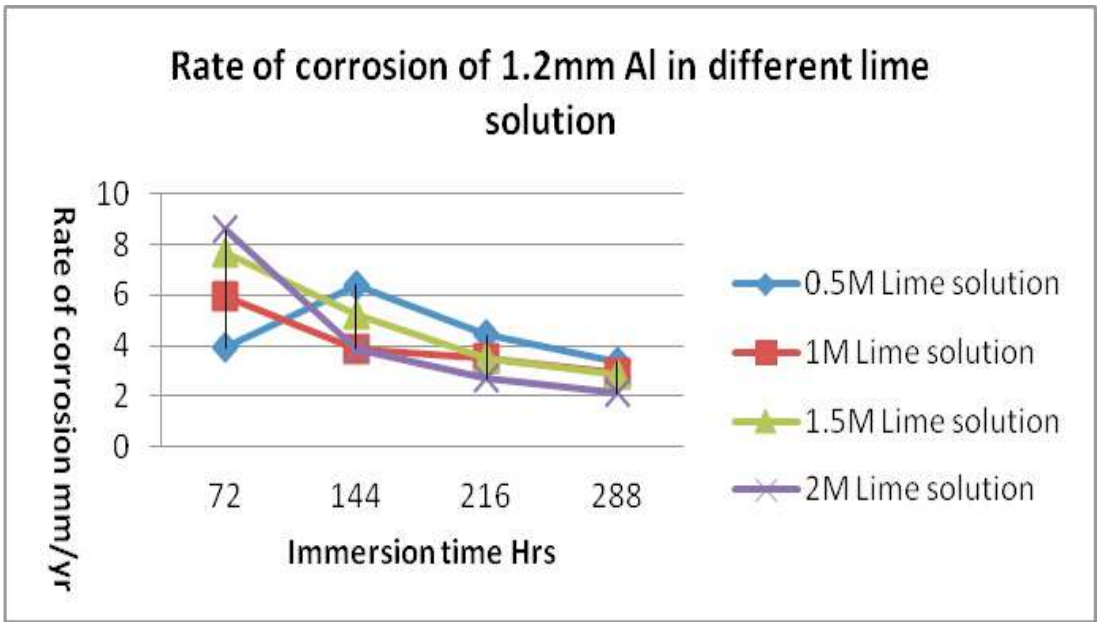


Fig.3 Graph of rate of corrosion of 1.2mm Aluminium in different lime solution against time of immersion



Plate 1: Initial state of SEM 0.6mm Al
Mx400,2% Nitric acid and 98% Ethyl Alcohol.



Plate 2: Immersed SEM 0.6mm of Al
Mx400,2% Nitric acid and 98% Ethyl Alcohol.



Plate 3: Immersed SEM 0.9mm of Al
Mx400,2% Nitric acid and 98% Ethyl Alcohol



Plate 4: Immersed SEM 1.2mm of Al
Mx400,2% Nitric acid and 98% Ethyl Alcohol

EFFECTS OF CHEMICAL ADDITIVES ON THE HYDRATION BEHAVIOUR OF CEMENT COMPOSITES FROM *CALAMUS* AND *LACCOSPERMA* CANES

Adefisan, O.O and Olorunnisola, A.O.
femiadefisan@yahoo.co.uk, femiadefisan@hotmail.com
Department of Agricultural and Environmental Engineering, Faculty of Technology, University of Ibadan, Nigeria

Abstract
The effects of Calcium Chloride ($CaCl_2$) and Magnesium Chloride ($MgCl_2$) on the maximum hydration temperature (T_{max}), setting time (t_{max}) and Time ratio (t_R) of *Calamus deerratus* and *Laccosperma secundiflorum* particles mixed with Portland cement was investigated. Particles of rattan canes were mixed with cement, water and chemical additives. Hydration tests were performed in thermally sealed thermos flasks while hydration parameters: T_{max} and t_{max} were measured after 24 hrs. The t_{max}, T_{max} and t_R ranged between 25.7 to 26.5hrs, 43.1 to 46.6^{0}C and 3.6 to 3.7 respectively without pre-treatment and were between 7.4 to 23.1 hrs, 49.3 to 65.7^{0}C and 1.0 to 3.0 respectively when pre-treated with chemical additives. Findings showed that untreated rattans generally inhibited cement setting probably due to inherent sugar content. Particles of *Laccosperma* canes inhibited cement setting more than those of the *Calamus* canes. The addition of both $CaCl_2$ and $MgCl_2$ significantly improved the T_{max} but reduced the t_{max} and t_R of the rattan-cement mixes. Addition of $CaCl_2$ enhanced the hydration behaviour of the rattan composites more than $MgCl_2$.

Keywords: *Calamus deerratus*, *Laccosperma secundiflorum*, cement composite, hydration behaviour, chemical additives.

Introduction

Rattans are spiny climbing plants belonging to the palm family known as *Calamoidea*. There are about 600 rattan species distributed in the tropical and sub-tropical regions of the world. Four genera namely *Laccosperma, Calamus, Eremospatha* and *Oncocalamus* are endemic to Nigeria with *Calamus deerratus* representing the largest available species while *Laccosperma secundiflorum* species are used for skeletal structures of baskets and furniture (Liese, 2002; Lucas and Dahunsi, 2004). Although the primary use of rattan canes are largely for basketry and furniture works, yet they are now gaining prominence as furnish for cement bonded composites (CBC) production due to their availability and accessibility (Olorunnisola, 2005; Olorunnisola *et al*., 2005; Olorunnisola, 2008; Olorunnisola and Adefisan, 2008). Olorunnisola and Adefisan (2002) noted the usefulness of mixed rattan furniture waste for the production of low stressed internal building components while cement bonded composites made from *L. secundiflorum* particles were found to possess adequate dimensional stability for outdoor applications (Olorunnisola, 2005).

Furthermore, since different rattan canes exhibit different physical and mechanical properties (Dahunsi, 2000) which may affect CBC production, it is necessary to investigate the compatibility of different rattan canes for CBC manufacturing. A major limitation in rattan cement composites production is the inherent sugar which may likely affect rattan-cement interactions (Dahunsi, 2000; Adefisan and Olorunnisola, 2007). Pre-treatment measures such as the application of chemical accelerators may be incorporated into the composite mixes to enhance the formation of strong crystalline bonds by increasing the hydration temperature and reducing the setting times (Ramachandran, 1994; Soriano *et al*., 1998). Semple and Evans (2002) noted the accelerating effects of chlorides in cement composite mixes. It was found that the addition of calcium chloride enhanced the hydration temperature and reduced the setting time. However, different chemical additives have diverse accelerating effects when incorporated in cement composites production (Semple and Evans, 2002). Therefore, the effect of different chemical accelerators on the hydration behaviour of rattan-cement mixes should be explored.

This work examines the compatibility of different rattan species namely *Calamus deerratus* and *Laccosperma secundiflorum* with cement and the effects of calcium chloride ($CaCl_2$) and magnesium chloride ($MgCl_2$) on the hydration characteristics of rattan cement mixes using the hydration test approach.

Material and Methods

Material preparation

Matured stems of *Calamus deerratus* and *Laccosperma secundiflorum* canes were harvested from Gambari Forest Reserve Ibadan, Oyo state, Nigeria. These were identified through comparison with stocks kept in the herbarium of the Department of Botany and Microbiology, University of Ibadan. The harvested canes were converted into billets of about 6 cm and hammer milled. The milled particles were collected and sieved

using a set of 1.18 mm, 0.85 mm and 0.60 mm sieves. Particles that passed through the 0.85 mm sieve and were retained in the 0.60 mm sieve were collected, air dried to 10% moisture content and separated into two portions i.e. those to be used 'as is' and those to be subjected to chemical pre-treatments.

Hydration Test

For the hydration tests, 15g of the rattan particles, 200g of ordinary Portland cement and 93ml of de-ionized water were mixed in a polyethylene bag to form homogeneous slurry as in Adefisan and Olorunnisola (2007). The neat cement was mixed with 90 mL of de-ionised water. Calcium chloride ($CaCl_2$) and magnesium chloride ($MgCl_2$) used as chemical accelerators, were added by dissolving in the de-ionised water at two concentration levels, i.e. 0 and 3% (by weight of cement). The tests were performed in a set of well insulated thermos flasks. Temperature rise was monitored for 27 hours using a T-type thermocouple. Three replicates of each mixture were prepared. The compatibility of *C. deerratus* and *L. secundiflorum* with cement was assessed using the compatibility indices shown in Table 1.

Results and Discussion

The results of the hydration tests are shown in Table 2 and depicted in Fig 1.

Setting time of Rattan-Cement Composites

The setting time of the rattan-cement composites are presented in Table 2. The setting time of the rattan composites without pre-treatment ranged from 25.7 to 26.5hrs. Based on the classification of Hofstrand *et al.* 1984, the untreated rattan particles are unsuitable for CBC production having t_{max} greater than 15hrs. The addition of chemical additives improved the t_{max} of the rattan-cement mixes. Composites pre-treated with $CaCl_2$ had between 56 to 72% improvement in setting time compared with 10 to 58% for $MgCl_2$ treated composites. What this suggests is that chemical additives rendered the inhibitory substances present in rattan particles inactive and enhanced compatibility of rattan particles with cement. This observation is in line with those of Semple and Evans (2002) that the application of chemical additives to wood-cement mixes remove / reduce cement inhibitors and enhance the hydration behaviour.

Also, while the application of different chemical additives did not have significant influence on the t_{max} of the *Calamus* composites, $CaCl_2$ was more effective than $MgCl_2$ in reducing the setting times of the *Laccosperma* composites. What this indicates is that particles of the *Laccosperma* canes inhibited cement setting more than *Calamus* (Table 3) due to higher sugar content (Dahunsi, 2000). The higher reactivity of calcium over magnesium (Bodner and Pardue, 1999) may have resulted in the ability of $CaCl_2$ to overcome the inhibitory effects of sugars and extractives in the cement mixes than $MgCl_2$.

Table 1: Compatibility Assessment Schemes

S / No.	Parameters	Classification Index	Reference
1	Time to Maximum Temperature (t_{max})	Suitable (<15hr) Unsuitable (> 20hr)	Hofstrand *et al.* 1984
		Suitable ($T_{max} > 60^0C$)	
2	Maximum Hydration Temperature	Intermediately Suitable (T_{max} = 50 - 60^0C) Unsuitable ($T_{max} < 50^0C$)	Sandermann and Kohler, 1964
3	Time Ratio (t_R): Ratio of setting time of wood- cement composite to neat cement i.e. $t_R = t_{WC} / t_{NC}$	$1 \leq t_R \geq 1.5$ (Suitable) $1.5 < t_R \geq 2.0$ (Acceptable) $t_R > 2.0$ (Inhibitory)	Olorunnisola, 2008

Table 2: Hydration Parameters of Rattan-Cement Composites

Pre-treatments	Hydration Parameters: Maximum Temperature (T_{max})	Setting Time (t_{max})	Time Ratio (t_R)
	Calamus deerratus		
None	46.6^{BC}	26.5^{A}	3.7^{A}
3% $CaCl_2$	65.7^{A}	7.4^{B}	1.0^{C}
3% $MgCl_2$	62.8^{A}	11.1^{B}	1.4^{C}
	Laccosperma secundiflorum		
None	43.1^{C}	25.7^{A}	3.6^{AB}
3% $CaCl_2$	60.9^{A}	11.3^{B}	1.6^{C}
3% $MgCl_2$	49.3^{B}	23.1^{A}	3.0^{B}

*Means with the same letters are not statistically different

Table 3: Duncan's Multiple Comparison of the Effect of Chemical Additives, Additive Concentration and Species on the Hydration Parameters of Rattan-Composites

Factors	Hydration Parameters: T_{max}	t_{max}	t_R
Additive Concentration			
0%	44.9^{B}	26.1^{A}	3.6^{A}
3%	59.7^{A}	13.2^{B}	1.7^{B}
Chemical Additives			
$CaCl_2$	54.1^{A}	17.3^{B}	2.5^{B}
$MgCl_2$	50.4^{B}	21.6^{B}	2.9^{A}
Species			
Calamus	55.4^{A}	17.9^{B}	2.5^{B}
Laccosperma	49.1^{B}	21.5^{A}	2.9^{A}

*Means with the same letters are not statistically different

Maximum Hydration Temperature of Rattan-Cement Composites

The maximum hydration temperatures (T_{max}) attained by the rattan composites without pre-treatment ranged between 43.1 to 46.6^{0}C. Based on the Sandermann and Kohler (1964) classification, the untreated rattans are again unsuitable for CBC production. The addition of chemical additives to the rattan-cement mixes however resulted in 12 to 29% increment in T_{max} (Table 2). Composites pre-treated with $CaCl_2$ had higher T_{max} than those treated with $MgCl_2$. The application of $MgCl_2$ did not significantly improve the T_{max} of the *Laccosperma*-cement mixes in relation to the *Calamus* composites. What the foregoing suggests is that chemical additives removed / reduced the cement inhibitors present in the rattan-cement mixes and enhanced the hydration temperature in line with the observations of Ramachandran, (1994); Soriano *et al*., (1998) and Semple and Evans (2002).

However, while calcium chloride seemed to perform better as a chemical accelerator for the rattan-cement mixes than $MgCl_2$ due to the higher reactivity of calcium over magnesium (Bodner and Pardue, 1999), particles of the *Laccosperma* canes inhibited cement setting more than those of the *Calamus* (Table 3). Again, higher sugar content of the *Laccosperma* canes (Dahunsi, 2000) may have retarded the T_{max} of the *Laccosperma* composites in comparison with those of the *Calamus* composites.

Time Ratio Indices of Rattan-cement Composites

The time ratio index (t_R) of the rattan-cement mixes are shown in Table 2. The t_R ranged from 3.6 to 3.7 for the rattan composites without pre-treatment and from

1.0 to 3.0 when treated with chemical additives. Based on Olorunnisola (2008) classification, the untreated rattans are again unsuitable for CBC production having a t_R greater than 2.0. Pre-treating the rattan composites with chemical additives generally improved the t_R indices and hence the compatibility of the rattan canes with cement.

The application of $CaCl_2$ improved the t_R indices of the rattan-cement composites more than $MgCl_2$ (Tables 2 and 3). As shown in Table 2, whereas rattan-composites pre-treated with $CaCl_2$ had t_R indices that ranged between "Acceptable to Suitable" for CBC production, *Laccosperma*-composites treated with $MgCl_2$ strongly inhibited cement setting. What this implies is that $CaCl_2$ again improved the compatibility of rattan canes with cement than $MgCl_2$. Hence, $CaCl_2$ can be regarded as a better chemical additive than $MgCl_2$ in the production of rattan-cement composites. Particles extracted from the *Laccosperma* canes again inhibited cement setting more than those of the *Calamus*.

Conclusions

The following can be deduced from this work:

(i) The untreated particles of *Calamus deerratus* and *Laccosperma secundiflorum* canes are not compatible with cement.

(ii) Particles extracted from the *Laccosperma* canes inhibited cement setting more than those of the *Calamus* canes.

(iii) The addition of chemical additives enhanced the compatibility of the rattan particles when mixed with cement.

(iv) Calcium chloride improved the hydration behaviour of the rattan cement composites more than magnesium chloride.

References

Adefisan, O.O and Olorunnisola A.O. 2007. Compatibility of rattan particles with ordinary Portland cement. *Journal of Applied Science Engineering and Technology* 1 (1): 61-71.

Bodner, G.M and Pardue, H.L. 1999. *Chemistry and experimental science*. Second edition New York. John Wiley. 316-317

Dahunsi, B.I.O. 2000. The Properties and potentials application of rattan canes as reinforcement materials in concrete. Ph.D. Thesis. Department of Agricultural Engineering. University of Ibadan.

Hofstrand, A.A., Moslemi, A.A. and Gracia, J.F. 1984. "Curing characteristics of wood particles from nine rocky mountains species mixed with Portland cement". *Forest Products Journal* 34(2): 57 - 61.

Liese, W. 2002. Challenges and Constraints in Rattan Processing and Utilization. In. J. Dransfield, F.O. Tesoro and N. Manokaran eds. Non-Wood Forest Products 14. Rattan Current Research Issues and Prospects for Conservation and Sustainable Development. P. 35 – 42. F.A.O., Rome.

Lucas, E.B. and Dahunsi, B.I.O. 2004 Characteristics of three western nigerian rattan species in relation to their utilisation as construction material. *Journal of Bamboo and Rattan* 3(1):45-56

Olorunnisola, A.O. 2005 Dimensional stability of cement-bonded composites boards from rattan cane particles. *Journal of Bamboo and Rattan* 4.2:173-182

Olorunnisola, A.O. Pitman, A. and Mansfield-William, H. 2005. Hydration characteristics of cement–bonded composites made from rattan cane and coconut husk. *Journal of Bamboo and Rattan* 4.2:193-201

Olorunnisola, A.O. 2008. Effects of pre-treatment of rattan (*Laccosperma secundiflorum*) on the hydration of Portland cement and the development of a new compatibility index. *Cement and Concrete Composites* 30.1:37-43

Ramachandran, V.S. 1994. Accelerators. In: Ramachandran, V.S ed., *Concrete Admixtures Handbook*: Properties, Science and Technology. Noyes Publications, New Jersey, 54-115.

Sandermann, W. and Kohler, R. 1964. Studies on mineral-bonded wood materials. IV. A short test of the aptitudes of woods for cement-bonded materials. Holzforschung: 1853–9.

Semple, K and Evans, P.D. 2002. Screening of Inorganic Additives for ameliorating the inhibition of hydration of Portland cement by heartwood of Acacia mangium. In: Evans, P.D. (ed.) wood-Cement Composites in Asia-Pacific region. Proceeding of a Workshop held at Rydges Hotel, Canberra, Australia 10 December, 2000. p 29-39

Soriano, F.P. Eusebio, D.A.; Cabangon, R.J.; Alcachupas, P.L.and Evans, P.D. 1998. The Effect of wood-cement ratio and cement setting accelerator on the properties of wood-wool cement board made from Acacia mangium. Willd: In:Turnbull, J.W.,Crompton, H.R. and Pinyopusarek, K.,eds. Recent devolpment in Acacia Planting. Proceeding of an International Workshop 27-30 October 1997 Hanoi, ACIAR Canberra,353-358

Sunderland, T.C.H. 2001, Rattan research and use in west and central Africa. *Unasylva* 205, Vol. 52. F.A.O., Rome, P. 18 – 26.

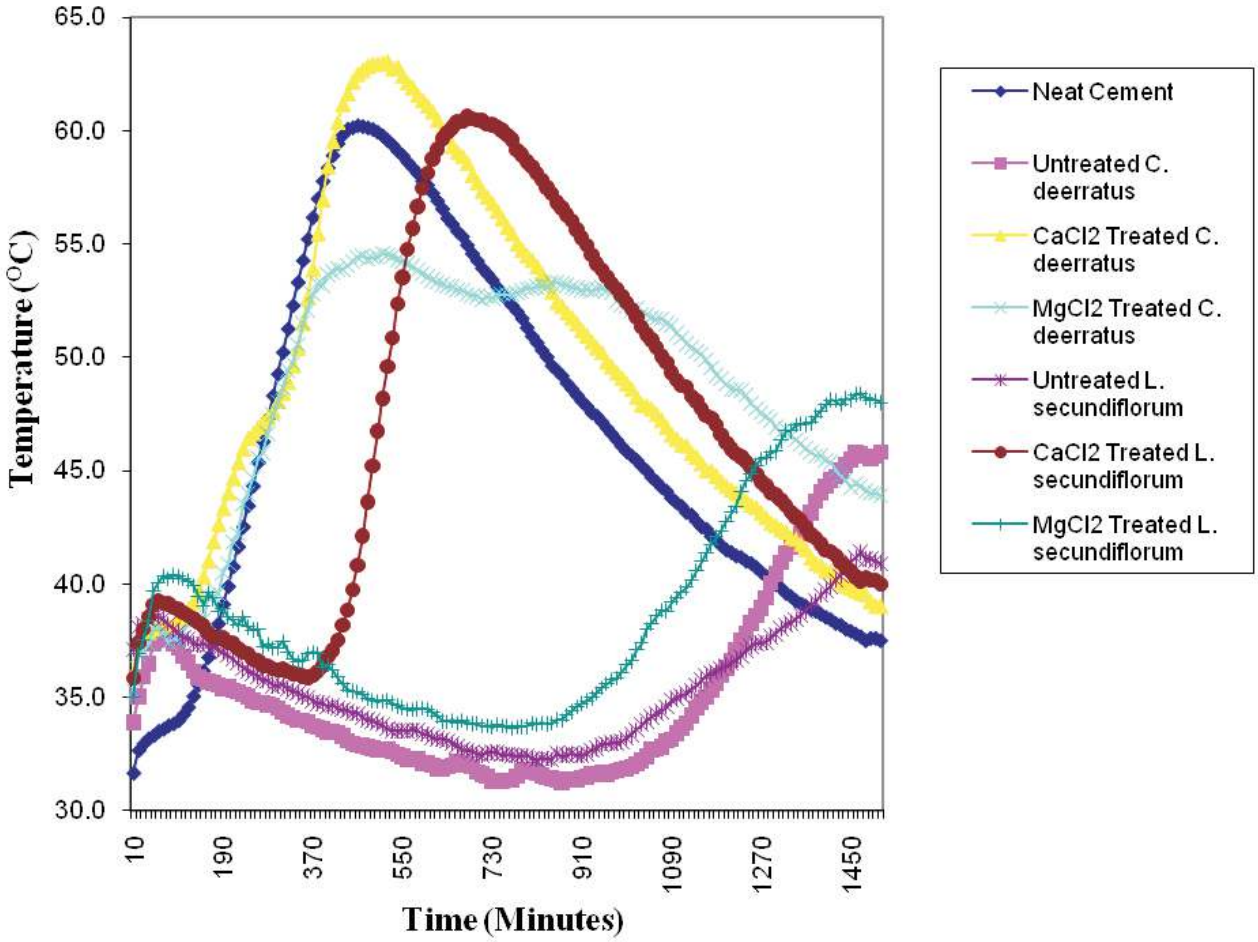


Fig 1: Hydration Behaviour of *C. deerratus* and *L. secundiflorum* Cement Mixes

PROCESS OF SINTER PRODUCTION FOR USE IN THE BLAST FURNACE OF THE AJAOKUTA STEEL COMPANY LIMITED

OCHERI C.[1], OYELARAN O.A[2] & BARNABAS A.[3] AGBOOLA, J.B[4] AJI DANIEL [5]
Foundry Shop, Ajaokuta Steel Company Limited, Ajaokuta, Kogi State[1]
Hydraulic Equipment, Development Institute, Kano [2]
Department of Metallurgical & Materials Engineering, Federal University of Technology Akure[3]
Department of Mechanical Engineering, Federal University of Technology, Minna ,Niger State[4]
Department of Metallurgical Engineering, Federal Polytechnic Idah[5]
E-mail:ocheri4c@yahoo.com

ABSTRACT
The Sintering Plant of the Ajaokuta Steel Company Limited comprises of the following sections, the Sinter mix preparation, Sinter production and Auxiliaries. Iron ore concentrates come from the raw material handling unit and they are charged directly to the stock bin building for proportioning, while limestone comes from the raw material handling unit and goes to the limestone / fuel grinding building where they are crushed with the hammer. The materials are sized at the handling unit and processed to a range of 0-80 mm these materials were further proportioned to the size of 0-30mm , but any materials with a size of +3mm and above will be sent for re-crushing. This paper further high lights the process of sinter production, their uses in the Blast furnace operations and Steel making processes.
Keywords: Process, Sinter Production, raw materials and Blast furnace

1.0 INTRODUTION

Process of sinter production in the Sintering Plant of the Ajaokuta Steel Company Limited . Iron ore concentrate comes from the raw material handling unit and it is charge directly to the stock bin building for proportioning while limestone comes from the raw material handling unit it goes to the limestone /fuel grinding building so that it can be crushed with the hammer crusher.

From the raw material handling unit the size of the material will be about 0-80mm , so that when it is being proportioned the size will be reduced to 0-3 mm . But any material that have the size of + 3mm above will be taken for re-crushing.

The size of coke in the coke storage yard is between 0- 30mm and when the coke is pre –crushed the size will now be 0-12 mm, this crushing usually takes place in the fuel pre-crushing units with the aid of the hammer crusher and later the coke of 0-12mm are sent to the limestone / fuel grinding building and limestone are also sent to this same unit for grinding and the coke and the limestone are also sent to this same unit for grinding and the coke and the limestone are both sent to the stock bin or proportioning unit and the size of both the coke and limestone must be from 0-3mm.

In the stock bin building the materials i.e coke , limestone and iron ore concentrate are both made into proportion with the aid of the electric vibration feeder. In the batching bin the iron ore concentrate are first laid , followed by limestone and the last to be drop is coke and with the aid of the battery containing a belt conveyor , the three materials are taken to the primary mixing drum where about 5-6% of water is added to the materials and a proper mixing is done in this area.

In the pelletizing drum about 8-10% of water is added to the material after they have been mixed properly and bentonite of about 1 % is added as bond.

This will make the pellet to be strong and it should not be too large when it is been heated in the reducing of gas . It can lead to break-down in the furnace . The pallets are used as feed for electric steel making.

In the Sintering unit there are six ovens for heating and the ovens are lined with brick to maintain the temperature to 100°C and there are 28 vacuum chambers to allow air to the oven.

At the end of the discharging end of the machine , the whole materials are poured into the jaw crusher and after the lump has being crushed the materials are screened and the undersize materials of 0-5mm are gotten as sinter returns for re-circulating . But the materials of +5mm are poured into the drum cooler. There are six cooling drums for the purpose of cooling the sinters . There is a double roll crusher that will crush the material to 0-15mm , 0-25mm for Blast furnace use.

2.0 SINTERING PLANT.

The sintering plant comprises of the following sections.

1) Sinter mix preparation section.
11) Sinter production section.
111) Auxiliaries.

2.1 Sinter mix preparation section comprises of the following facilities set-up and their brief characteristics;
(a) Fuel preliminary crushing building; (b)Limestone crushing, screening, and fuel grinding building (unit 8.70);
(c) Stock bins build
(d) Primary mixing building;
(e) Sintering building;
(f) Process gas cleaning plant.

The stock bins building are intended for receiving and proportioning of all the stock components:
(i)Fuel at 1300t/hr.
(ii) Limestones are crushed at 150 t/hr.

(iii)Sinter return 750 t/hr.

Fe- bearing materials and fluxes enter the sintering plant at the junction tower 75. Fe-bearing materials are stocked in the first three bunkers in the stock bins building for further processing. The fluxes (limestone and dolomite) screen 0-3mm size fraction is delivered to the next two bifurcated bunkers in the stock bins building. The coke breeze (0-3mm, 95%) is delivered to one bifurcated bunker in the stock bins building. The stocked materials are proportioned as designed with the aid of disc and electro-vibro feedings and weighing belt on to the conveyor belt. The proportioned materials are delivered to the primary mixing drum and en-route at the entrance of the drum; sinter returns (size 0-8mm) are proportioned. The composites are then home-generously mixed and discharged in the palletizing are delivered to the sintering building

2.3 Sintering unit to protect the life span of the machines.

Electrostatic filler is used to clean the gas, the exhauster is stationed to create vacuum and it will also suck the wasted gas. The dust catcher will collect all the dropped particles , and it will send the particles to the atmosphere through the stack. The air collected from the sintering area is drawn by the aided of powerful fans through the chimney or stack. The heavier particles are treated in the control air cleaning station.

In the screening dept the materials are been screened with the vibration screen in order to make it to the required size.

The qualities of a good sinter:-

(a)A good sinter should be strong but capable of being crushed to its required size with generating a large quantity of fire .

(b)It should be chemically reactive

(c)Permeable to gases and of large specific surface

.

3.0 SINTER PRODUCTION SECTION

The palletizing drum, 4200mm diameter, 24,000mm in length, is used for the final mixing, moistening and palletizing after which the materials is charged into a bin over the sintering machine by a shuttle distributor by a will feeder it is evenly placed on the sintering machine pallet grates over the hearth layer materials.

The Sintering machine has a total suction area of 360 square metre ; the Sintering area being 300m^2 and that for the sinter preliminary cooling amounting to 60m^2 . The Sintering machine working surface is 4.0 m wide and 90m long. The machine is equipped with 150 pallets whose motion speed can be controlled within 1 to 6m / min.

The Sintering machine is equipped with an elongated hearth. The ignition temperature is 1200 - 1300°C, but in the heat treatment zone the temperature in the hearth gradually lower to 750°C. The total gaseous fuel consumption is taken as 12,000 kcal/ton of sinter. 30 gas suction vacuum chambers are installed on the sintering machine. Waste gases from the sintering area are forced away by two fans with a total capacity of 24,000 cum/ min, the rarefaction making 1350WG and temperature 150°C.

From the sintering machine, sinter coke goes into a single roll foot crusher (sinter) and then on to a self –balance screen with a 3000 x 6400 mm grate area where 0-8 mm size return is separated from the sinter coke.

The sinter return cooling by water takes place in a drum cooler. The remaining bulk of the sinter shall be cooled on straight line cooler with a working area of 315 sq.m. The cooler is equipped with eight 27, 500 m^3/ hr . Fans which blow the air through the sinter layer, 750mm high, the air pressure being 395 mm WG.

The cooling bed motion speed can be controlled within 1 to 3 m / min.

The cooled sinter goes to a self –balance screen, 8, 3000 mm x 64, 000mm for separation of +40mm size. This size goes to two –roll crushers , 9 , add together with –40mm size is delivered to the screening department where the sinter in the screening department , separate into :-

(a) sinter of size + 25 mm, 8-15 mm

(b) hearth layer of size 15-25mm

(c) return of size , 0.8mm

By belt conveyors, the good sinter is delivered to the iron making plant, hearth layer to the sintering building return to the batching bins in the primary mixing building.

Gas from the sintering machine caking zone is delivered to the (3) three electrostatic precipitator in the process gas cleaning plant where the dust content is reduced to not more than 100mg/ cu. m.



Picture 1 : shows the stacking machine with nine buckets



Picture 2: shows the operation process in the sintering plant



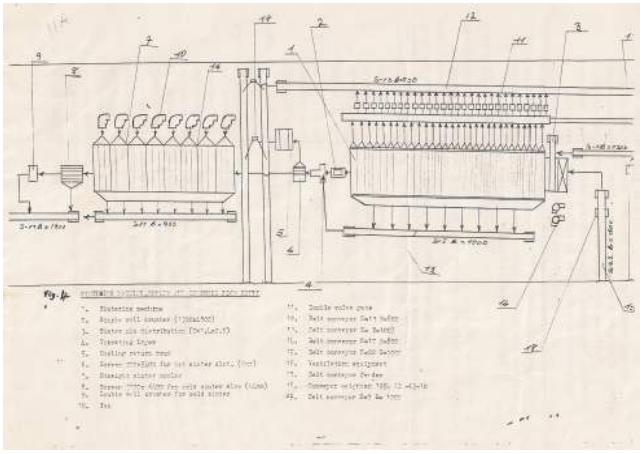
Picture 3 : shows the transportation of processed Sinters to the Blast Furnace.



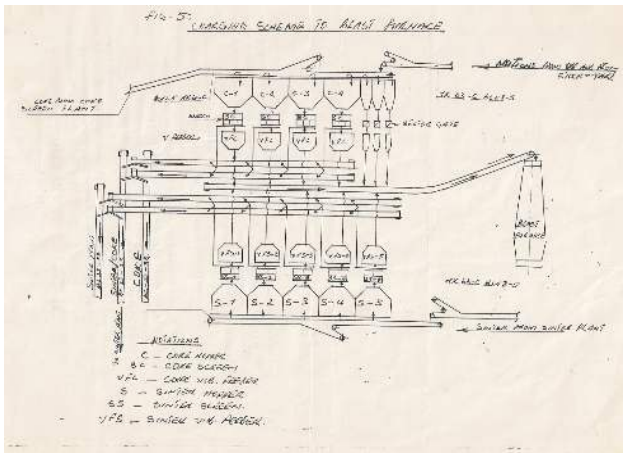
Picture 4: shows the transfer of processed sinters through conveyor belts en-route to the Blast Furnace

S/N	Description	Iron Ore Concentrate	Scale	Flux	Sludge of Gas Cleaning Plant		MN	Limestone	Dolomite
1	Total Iron , Fe	63.0	72.20	46.10	48.60	56.80	1.40	0.15	0.20
2	Mn	-	0.41	0.34	0.71	-	28.5	-	-
3	P	0.03	0.004	0.022	0.03	0.087	0.18	0.013	0.013
4	S	0.004	0.021	0.40	0.11	0.08	0.06	0.052	-
5	Fe_2O_3	88.90	46.14	54.14	59.29	59.0	2.0	0.21	0.28
6	FeO	1.0	51.10	10.60	9.09	20.0	-	-	-
7	MnO_2	-	-	-	1.12		41.20	-	-
8	MnO	Trace	0.53	0.44	0.12	1.50	5.2	-	0.005
9	SiO_2	0.80	0.42	9.10	7.49	2.50	30.0	1.81	4.07
10	Alumina (AlO_3)	0.80	0.09	1.10	0.87	0.60	2.0	0.31	0.26
11	Calcium oxide , CaO	0.15	0.07	8.11	10.09	15.0	4.20	53.0	31.02
12	Magnesium oxide	Traces	0.09	0.49	1.73	1.0	0.50	0.64	20.76
13	Titanium oxide , TiO_3	0.06	-	-	0.04	-	-	0.02	Trace
14	Diphosphorus penoxide	0.07	0.01	0.05	0.07	0.20	0.42	0.03	0.03
15	Alkali	-	0.20	0.55	-	-	-	0.09	-
16	Carbon C	-	0.90	11.62	-	-	-	-	-
17	Ignition Loss	0.21	0.40	3.34	9.97	-	14.33	43.76	43.58
18	Sulphur Trioxide	0.01	0.05	0.10	0.02	0.20	0.15	0.13	-

Table 1. CHEMICAL ANALYSIS OF RAW AND MAIN MATERIALS FOR SINTER MANUFACTURE – SINTER –MIX COMPONENT



Picture 5: Shows the Sinter Machine, Cooler and Crushing Flow sheet



Picture 6: Shows the Charging Scheme to Blast Furnace.(Sinters and other bulk materials)

In Conclusion:

The main operation of the process scheme of the sinter production ensure proper control of the physical and chemical properties of the sinter. These schemes include

(i)Solid fuel (Coke) , Limestone and dolomite preparation

(ii)Sinter –mix components proportioning

(iii)Sinter –mix blending , moistening and pelletizing (secondary mixing) till optimum size

(iv)Sinter-mix and bed material laying on sintering machine

(v)Sinter-mix ignition

(vi)Sinter-mix caking and process gas cleaning

(vii)Hot sinter-mix crushing and screening with hot returns separation

(viii)Return and sinter cooling

(ix)Crushing of sinter lumps with size over 40mm and sinter screening with separation of return bed materials and prepared sinter

(x)Prepared sinter removal

(xi)Preparation of the sinter gives good permeability: The gas permeability depends upon the size of the particles. Coarser the grains, more is the permeability but if the grains are excessively coarse, the sinter quality becomes poor. Addition of certain amount (6-8%) of moisture improves the permeability quality, quality and sizes fraction of fuel.

Ash content increases the gangue content in the sinter and the volatile material sublimates and decreases the porosity. Fine size of fuel will lead to increase is vertical speed of sintering resulting in decrease in the time of sintering and significant improvement in the sinter quality. The consumption of fuel also decreases.

REFERENCES

1. Company Report: Ajaokuta steel company limited Detailed Project Report (DPR) Vol. I part II Explanatory Note.

2. Project Report: Investment Profile of Ajaokuta steel company limited, March 1990

3. Status Report and Business Plan for Ajaokuta steel company limited April 1999. Pg 58-60

4. Wakawa M.B (1994). Strategies for the sustaining of optimal Capacity Utilization of the Ajaokuta steel company limited, Processing of the Nigerian metallurgical Society (NMS) November 30th - December 3rd 1994.pg 19-25

5."The Role of Metallurgical Industry in the Nigerian Economic Development " A proceeding of Nigerian Metallurgical Society (NMS) 4th Annual Conference Held at ASCL 29th – 31st October 1986.

6. Ajaokuta Steel Company Limited: Diary 1987

7. Okonji, P.O (1995) "Steel: Path to Economic Diversification Proceedings", NMS, 13, 1995 PP 11 – 16.

8. S.K. Oni (Major) Steel in Defence, Proceedings, NMS Seminar, NIPSS, Kuru, 1988, pp 8-9

9. Banji Oyeleran Tenuche(1994) "The Steel Industry in Nigeria": CAL TOP Publications Nigeria Ltd 1994 pp 52

CHARACTERIZATION OF UGWU-OGBA CLAY DEPOSIT FOR FURNACE REFRACTORY PRODUCTION

[+]Odo, J.U., [*]Agbo, A.O., [+]Nwoye C.I and [+]Adinna, B.O+ Nnamdi Azikiwe University, Awka, Anambra State
*Enugu State University of Science and Technology Enugu.e-mail: odojus@yahoo.com, alfredagbo@yahoo.com.

Abstract
Characterizations of Ugwu-Ogba clay deposit have been carried out with a view of finding its usefulness in furnace refractory production and other industrial applications. The chemical analysis was carried out using Atomic Absorption Spectrometer (AAS) and Ultra-Violet Visible Range Spectroscopy (UV-VIS). Particle size analysis and other physical properties tests such as porosity, shrinkage, water absorption, modulus of rupture, cold crushing strength, refractoriness, moisture content, plasticity and thermal shock resistance were carried out using international accepted standard techniques. The result of the chemical analysis indicates that the clay is composed of silica, SiO_2 (56.50%), alumina, Al_2O_3 (31.32%) calcium oxide, CaO (2.25%), iron oxide, Fe_2O_3 (0.32%); magnesium oxide, MgO (1.54%); titanium oxide, TiO_2 (0.87%); sodium oxide, Na_2O (1.60%); potassium oxide, K_2O (1.70%) and other chemical compounds as trace. The results of the physical properties tests conducted at firing temperatures of 900°C, 1000°C, 1100°C and 1200°C respectively indicated as follows: porosity, 12.18; shrinkage, 13.35; bulk density, 2.34; percentage water absorption, 6.65, modulus of rupture, 91.30kg/cm^2; apparent density, 2.62mm^2, and cold crushing strength, 13.85 kN/mm^2 at 1200°C with an estimated refractoriness of 1680°C. The clay deposit therefore can be used for the production of refractory bricks for linings of furnaces for ferrous and non-ferrous metals, low melting point alloys, reheating furnaces, kilns, ladles and other foundry and heating equipment(s) that require medium duty refractory bricks. As a result of its low iron oxide, and Titania contents, the clay has whitish colour and can be used by paint, ceramics, and chalk, pharmaceutical and paper making industries.

1. Introduction

Nigerian is blessed with abundant natural resources of which clay is one of them. For a country to be developed technologically, most of her natural resources have to be identified and harnessed for proper usage. In Nigeria most of her solid minerals of which clay is part are yet to be identified, harnessed and put to proper use, hence this research work. Clay refractories are mainly produced from clay that has alumina, (Al_2O_3) and silica, (SiO_2) contents between 18 - 44% and 50 -70% respectively. Clay minerals are the fine-gained components of geological materials, occurring mostly as particles with a phyllosilicate or sheet structure with diameters ranging from a few microns to a few hundred of a micron. They tend to have large surface areas, often high cation exchange capacities, high adsorption capacities and some have swelling properties, all of these characteristics make clays fascinating materials for study and gave them properties which are important from many view points, academic, and applied. Most of the common clay minerals belong to the following groups: kaolinite serpentine, pyrophillite-talc, smectite, vermiculite, mica, chlorite and sepiolite- palygorskite[2]

Refractories are materials which can withstand high temperatures normally above 1580°C and the physical and chemical action of molten metal, slag and gases in furnace without deformation, failure or change in composition under their own weight [6,7]. A large number of major industries are dependent on high temperature processes and therefore are dependent on heat-resisting structures of some sort. Refractories are of major importance to them and constitute a key production input. Prominent among this industries with heavy refractories demand are the metallurgical, cement, and oil industries boiler, bake ovens, galvanizing pot, incinerators of various designs and others [8,9]. The bulk of the refractories for these industries in Nigeria are present imported. This situation needs to be addressed for the nation's dream of vision 20,2020 to be realized.

2. Materials and Method

The clay sample used for this work was collected from Ugwu-Ogba clay deposit, Ebor Nwenye-Ani, Eha Alumona in Nsukka Local Government Area of Enugu State. The clay sample was collected from five different locations of the deposit and mixed together by pounding process. The mixture was dried, pulverized, sieved and stored in a decicator for various tests.

The chemical analysis of the clay was carried out using Atomic Absorption Spectrometer (AAS) and Ultraviolent Visible Range Spectroscopy (UV-VIS). The result is presented in Table 3.1. The physical properties tests carried out include: plasticity and plasticity ratio;

moisture content; dry, fried and total shrinkage; modulus of rupture (MOR); water absorption; apparent porosity; apparent density; bulk density; cold crushing strength; thermal shock resistance, loss on ignition and refractoriness. For each of the tests, five (5) specimens were used and the average taken and recorded.

Plasticity and plasticity ratio

Five (5) specimens were produced using cylindrical mould and a plastomer used in deforming them.

$$\text{Modulus of plasticity} = \frac{x_1}{y_1}$$

$$\text{Plasticity ratio} = \frac{x_2}{y_2}$$

Where x_1 = original height of deforming load.

x_1 = deformed height of load

x_2 = Original height of sample

y_2= deformed height of sample

Moisture content: Five cylindrical specimens (1.5cm dia. x 10cm length) were weighed green and their weight noted. They were then dried in air for two weeks and later oven dried at a temperature of 110oC for twenty four hours. The dry weight of the specimens was measured and recorded.

$$\text{Moisture Content} = \frac{W_w - d_w}{W_w} \times \frac{100}{1}$$

Where: W_w = wet weight

d_w = dry weight.

Green, Dry and Fired Strength: Five rectangular specimens (1.5 x 3.5cm) were taken and recorded. They were oven dried for two days and a rupture testing machine (CBR-California Bearing Ratio) used to test for the strength at green, dry and fired state. The fired strength was tested after firing the specimens to temperatures of; 900oC, 1000oC, 1100oC and 1200oC respectively.

$$\text{Modulus of Rupture: } \frac{3pl}{2bh} \text{ or } \frac{8\,pl}{\pi d^2}$$

Where: p = applied load (kg)

l = distance between supports, constant (em)

b = width of the specimen at the point of rupture (cm)

h = height of the specimen at the point of rupture

d = diameter of the cylindrical specimen

Apparent porosity, water absorption, Apparent and bulk density tests: Rectangular specimens (5cm x 7cm) were prepared and their weight noted. They were dried for two weeks, oven dried and their new weight recorded. They were fired to temperatures of 900oC, 1000oC, 1100oC and 1200oC respectively. Their weights at each stage of firing were taken. The fired specimens were soaked in water for twenty-four hours and the weight noted. They

- Apparent porosity $= \frac{S_w - F_w}{S_w - S_{sw}} \times \frac{100}{1}$
- Water absorption $= \frac{S_{sw} - F_w}{F_w} \times \frac{100}{1}$
- Apparent density $= \frac{F_w}{F_w - S_{sw}}$
- Bulk density $= \frac{F_w - dl}{S_w - S_{sw}}$

Where: S_w = Soaked weight

F_w = Fired weight

S_{sw} = Suspended weight

dl = Density of water.

Linear, dry and fired shrinkage: Rectangular specimens (5cm x 7cm) were produced and marked at 5cm lengths. Temperatures of heating ranges were inscribed on the specimens to be fired. They were dried in air for two weeks and oven dried for forty eight hours. The change in the 5cm length mark was measured. They were then fired to temperatures of 900°C 1000°C, 1100°C and 1200°C respectively and the change in the 5cm length mark noted at each stage/temperature.

a. Dry Shrinkage (%) $= \frac{wl - dl}{wl} \times \frac{100}{1}$

b. Fired Shrinkage (%) $= \frac{dl - fl}{dl} \times \frac{100}{1}$

Where wl = wet length, cm

dl = dry length, cm

f1 = fired length, cm

Permeability to air: Five specimens were prepared using standard specifications of 5.08cm diameter and 5.08cm length/height. They were dried in air for twenty-four hours and oven dried for twelve hours. They were completely sealed by the sides and the lower surface exposed to an orifice in a permeability meter. The permeability meter was filled with 2000cm3 of water and a bell jar put in place. The orifice was opened and the time taken for the 2000cm3 of water to displace equal volume of air through the specimens taken. The pressure difference between the surfaces was measured by a manometer.

$$P = \frac{vxh}{pxAxt} \text{ or } \frac{vh}{pAt}$$

Where: P = Permeability number.

v = Volume or air passed through the specimen (m^3)

h = height of specimen.

A = cross-sectional area of the specimen.

p = pressure head under which the air has passed in cm^3 of water.

t = time of flow in seconds.

$$\text{or } P = \frac{30072}{pxt} \text{ or } \frac{30072}{pt}$$

Thermal shock resistance: The test was carried out using 50mm x 50mm specimens. They were inserted into a muffle furnace and heated to 900^{0}C and held for 10 minutes. They were removed quickly from the furnace, placed on fire bricks and allowed to cool for 10 minutes. After the 10 minutes cooling, they were then returned to the furnace and the process repeated for 30 cycles. They were seen at the end of the 30 cycle not to have deformed or cracked.

Refractoriness: Pyrometric cone equivalent test was used to determine refractoriness. Specimens with 50mm pyramid height and 15mm rectangular base were used. They were put inside a refractory plague with two Seeger cones of 12 and 13 and oven dried at 110°C. The temperature equivalents for the two Seeger cones were 1337°C and 1349°C respectively. They were put in a furnace and temperature raised at the rate of 100°C per-minute until the two Seeger cones bent over level with the base. Upon observation, it was noted that the specimens had not deformed at all let alone melting. The firing was continued until temperature of 1400°C was attained, yet the specimens remained under-formed.
The refractoriness was estimated using Shuen's formular[11].

Refractoriness, K (^{o}C) = $\frac{360 + 2.2Al_2O_3 + RO}{0.228}$

Where, Al_2O_3 = % alumina in the clay
RO = sum of all other oxides be sides silica
360, 0.228 = constants.

Cold crushing strength (C.C.S.): Specimens of 76.2mm cube were moulded, and dried for three weeks for proper diffusion of the internally held water. They were fired slowly to a temperature of 2000C and held for six hours before rising to temperature of 900oC 1000oC, 1100oC, and 1200oC respectively. They were held for six hours at the various temperature ranges before cooling to room temperature and storing in a decicator. They were placed in a compressive tester and load was applied axially until fracture occurred and load at fracture was recorded.
C.C.S. (N/m2) =

Loss on ignition: 50g of the clay sample was oven dried at 110oC and cooled in a desicator. A porcelain crucible with weight (m1) was used. The dried sample was put inside the crucible and the weight of the crucible and the sample noted (m2). The crucible with its content was put into a muffle furnace, fired/heated to a temperature of 900oC and held for three hours. The crucible and its content were cooled in a desicator and then re-weighed (m3).

$$\text{L.O.I.} = \frac{m_2 - m_3}{m_2 - m_1} x \frac{100}{1}$$

3. Results and Discussions.
The result of granulometric particle size analysis of the clay as shown in Table 3.1 indicated that the clay has fine particle < 5.0mm of about 62% and fairly coarse particles of about 38% respectively. This indicates that the clay is siliceous with fairly large sized particles. This property of a clay material is very important because it affects other properties such as plasticity, percentage water absorption shrinkage, strength, porosity, density, etc.
The chemical composition of Ugwu-Ogba clay deposit as indicated in Table 3.2 above showed that the clay has: 56.50% SiO2, 31.32% Al2O3, 0.32% Fe2O3, 0.87% TiO2, 2.25% CaO, 1.54% MgO, 1.60% Na2O, 1.70% K2O, and 5.52%, loss on ignition (L.O.I) as it constituents matter. From the result, the clay has a characteristics composition of fire clay refractories of semi-acid class with general composition range of 18 – 44% Al2O3 and 50 – 80% SiO2. The alumina and silica contents of: 31.32% and 56.50% fall within the range of high duty fire-clay refractories of 25 – 38% Al2O3 and 57 – 70% SiO2 respectively. The percentages of all other oxides of the clay except TiO2 fall within the specified standard [1,8]. The clay could therefore be used for important applications such as in rotary kiln lining, roofs of electric steel making furnaces, soaking pits, heat-treatment furnaces and other areas where medium and low duty fire-clays bricks could not be used because of spalling influences and rapid temperatures changes[1,11].

The estimated refractoriness of the clay was 1680oC using Shuen's formular [12]. The estimated refractoriness of Ugwu-Ogba clay fell with the pyrometric Seger cone of 31. Also the sintering point of above 1400oC is a good indication that the clay is of high refractory class and can be used where medium and high temperatures are required for melting of non-ferrous metals and their alloys, treatment of steels and their alloys, melting of cast irons and alloyed cast irons, etc

[The results of the physical properties of Ugwu-Ogba clay deposit as shown in Tables 3.3 and 3.4 indicate that the transverse strength/modulus of rupture, porosity, cold crushing strength, shrinkage and density fall within the International Standard Organization (ISO) specifications for aluminosilicate refractories of the fire-clay class[2,4]. The shrinkage and density strength were seen to increase with the increase in firing temperature while porosity and percentage water absorption decreased with increase in the firing temperature. The higher a clay material is fired, the more it looses its absorbed moisture and constitutional water, thereby leading to increased shrinkage and reduced porosity. Also at higher temperatures, the low melting point constituents of the clay body tend to melt, oxidize and fuse to the highly refractory constituents thereby closing the pores and leading to the formation of a denser body and increased strength due to strong bond formation. The more a clay body shrinks, the less porous it becomes hence the denser. Also as the clay body is fired to higher temperatures, the closer to its sintering point, the low melting point constituents of the body melts, oxidizes, fuse and some even evaporates to the air, thereby reducing porosity and increasing density and total shrinkage [4,7,11].

The clay is a plastic clay from the results of modulus of plasticity (3.25) and plasticity ratio of (1.25 : 1) as shown in Table 3.4. Because of the inherent white colour of this clay, the clay can find applications in the paper, ceramics, paint and pharmaceuticals industries.

4. Conclusions and Recommendations

Ugwu – Ogba clay deposit from the chemical analysis carried out is an alumino-silicate refractory of semi-acid fire-clay class. The clay could therefore be used in the production of alumino-silicate refractory for lining of furnaces for non-ferrous metals production, soaking pits, ovens, ladles and heat-treatment furnaces for steel and its alloys. As a result of the characteristics white colour of the clay, the clay can be used by the paper, paint, chalk, ceramics and pharmaceutical industries.

The clay deposit if exploited, harnessed and utilized can help in the nation's quest for rapid industrial, technological, and economic development. This will lead to social and economic growth of the large teeming population of Nigerian citizens.

The federal, state and local government and the private sectors are therefore requested to take keen interest in the solid minerals' development since the country is abundantly blessed with them. This will go a long way in achieving the aims and objectives of vision 20, 2020.

Reference

1. Harbion Walker Refractories Company. (1979). Modern Refractory Practice. 4th Edition. Pittsburgh, Pennsyivania USA.
2 . http://www.webref.org/geology/c/c/aymineral s.html
3 . http://minerals.usgs.gov/minerals/pubs/comm odity/days/.
4. Odo, J.U and Okorie, B.A. (2001). Eha-Alumona Clay – An indigenous raw material for refractory industries, proceeding of the conference on new products and technologies for small and medium scale enterprises (SME). Benin-City Nigeria.
5. Nnuka E.E and Okunonye, P.A. (1991). Industrial potentials of Ukpor clay.
6. Proceedings of NMS, Owvian – Aladja, Warri Nigeria.
7. Odo, J.U and Neife S.I. (2002). Effect of additives on some refractory properties of Enugu fire-clay, proceedings of NIMACON, EMDI, Akure, Nigeria
8. Ogo, D.U.I., Ette, A.O and Nnuka, E.E. (2003). Production of an alumina silicate refractory similar in using linear programming. Proceedings of NMS, Ajaokuta, Nigeria.
9. Felix Singer and Sonja .S. Singer (1989). Industrial ceramics. Chapman and Hall, New York, USA.
10. Nnuka E.E. and Enejor, C. (2001). Characterization of Nahuta clay for industrial and commercial application. NSE Technical Transactions Vol. 2. No3
11. Krivandin, V.A and Markov, B.L (1980). Metallurgical furnaces. MIR Publishers. Moscow
12. Odo, J.U, Nnamchi, P.S. and Nnuka, E.E (2009). Development of aluminosilicate refractories from blends of two local clays. NMS Proceedings of 26th Annual Conference and AGM.
13. Eochvaron, S. etal. (1977). Technology of Silicate Materials. Engineering Press, Sofia Bulgaria.

Table 3.1. Granulometric particle size analysis.

Size (mm)	Quantity, %
5.0 – 2.0	22
2.0 – 0.5	16
0.5 – 0.1	27
<0.1	35

Table 3.2 Chemical composition analysis.

Oxides	SiO_2	Al_2O_3	Fe_2O_3	TiO_2	CaO	MgO	Na_2O	K_2O	L.O.I
Composition (%)	56.50	31.32	0.32	0.87	2.25	1.54	1.60	1.70	5.52

Table 3.3 Physical properties tests at temperatures of 900°C, 1000°C, 1100°C and 1200°C.

Property /Temperature °C	**900°C**	**1000°C**	**1100°C**	**1200°C**
Fired shrinkage (%)	2.01	3.20	4.00	4.50
Total shrinkage (%)	8.12	10.65	11.78	13.35
Apparent porosity (%)	24.96	21.39	15.30	12.18
Apparent density (g/cm^3)	2.37	2.45	2.50	2.62
Bulk density (g/cm^3)	1.24	1.89	2.27	2.45
Water absorption (%)	12.43	10.70	7.87	6.65
Transverse strength (T.S)/modulus of rupture (MOR) (Kgf/cm^2)	52.68	74.61	79.85	91.30
Cold crushing strength (C.C.S.) KN/mm^2	7.25	9.40	11.15	13.85

Table 3.4 Other physical properties.

Property	Quality
Modulus of plasticity	3.25
Plasticity ratio	1.25 : 1
Thermal shock resistance	30
Permeability number	58.24
Green strength (Kgf/cm^2)	25.21
Moisture content (%)	22.45
Sintering point °C	>1400 °C
Estimated Refractoriness	1680°C
Green Colour	White

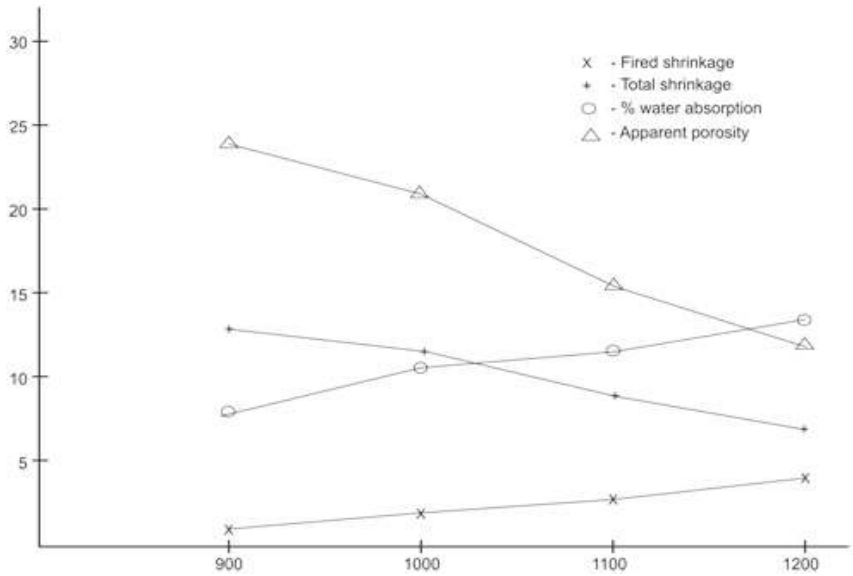


Figure 3.1 Fired shrinkage, total shrinkage, porosity and percentage water absorption against firing temperatures.

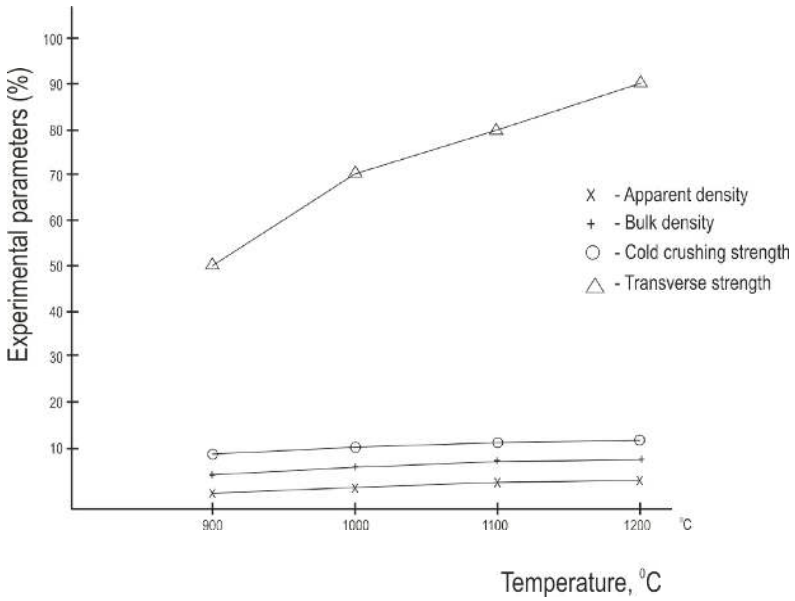


Figure 3.2. Relationship between bulk density, apparent density, transverse strength and cold crushing strength and firing temperature.

MICROBIAL CORROSION OF MILD AND MEDIUM CARBON STEELS

J. E. O. Ovri, S. I., Okeahialam, and O. O. Onyemaobi
Department of Materials and Metallurgical Engineering, Federal University of Technology, Owerri, Nigeria.

Abstract
The role of bacteria in the corrosion of mild and medium carbon steels is reported. The steels were exposed to anaerobic and aerobic, and fresh water (control) environments. The corrosion rates were evaluated at intervals of seven days for a period of 42 days using weight loss and electrochemical methods. The corroded specimens were visually examined and majorities were found to have undergone general corrosion in the three environments (aerobic, anaerobic, and fresh water). The mild steel was found to corrode more than the medium carbon steel in anaerobic environment – mild steel: 6.43 x 10-4 mpy and -0.93mV, due to limited available oxygen whilst it had -0.89mV in aerobic and -0.77mV in the fresh water. The medium carbon steel had 5.30 x 10-4 mpy and -0.91mV in anaerobic: -0.84mV in aerobic and -0.74mV in Freshwater.
Keywords: Anaerobic and aerobic bacteria, corrosion rates, weight loss, electro-chemical method, general corrosion.

Introduction

Corrosion due to the activities of micro-organisms is referred to as microbial corrosion. These organisms are involved in the corrosion process by the virtue of the growth and metabolic actions and their presence often provide concentration cells in the structure where they are present, whereby some areas in the structure are anodic to the rest. These bacteria are therefore classified into two-those that require oxygen in their metabolic and growth processes often referred to as aerobic bacteria and those that carry out their activities in the absence of oxygen often referred to as anaerobic[1]. These bacteria are active in stagnant water mainly at bottom of tanks, the soil, freshwater, seawater and air.

The mere detection of sulphur reducing bacteria (SRB) does not constitute a problem but what is important is the number of micro-organisms of the relevant types generated. It has been observed that under favourable conditions, bacteria can multiply every 10 - 60 minutes in their metabolic and growth process up to 2.8 x 1014 organisms which lead to the corrosion and biodeterioration of materials. However, this growth and reproduction process is generally reduced after the first bloom since conditions progressively become inhibitory; predators become evident [1]. These organisms thrived in medium with pH values between 0 and 11, temperature between 0 and 80oC (30 and 180F) and under the pressure of up to 103MPa (15ksi). The activities of bacteria are affected by the availability of nutrient e.g. phosphate, nitrogen, and presence of toxic substances (oxygen for sulphate reducers, chlorine, biocides).

SRB is the most important group of bacteria associated with this form of corrosion and it is widely believed that all microbial- induced failures are due to its activities. SRB are anaerobic and heterotrophic i.e. they obtain their energy from organic nutrients.

Their respiratory utilizes sulphate, which is abundant in fresh water, sea water and soils and often results in the formation of hydrogen sulphide. This hydrogen sulphide appears as H2S (in the dissolved or gaseous form).HS- ions, S2- ions or metal sulphides, or a combination of these according to the prevailing conditions.

The SRB in the presence of organic materials is oxidized to form the sulphide.

$4H2 + S2\text{-}O4 = S2- + 4H2O$…… (1)

The sulphide is highly corrosive to most engineering materials. The most commonly encountered SRB is Desulfovibrio. In the industrial process plant, a wide range of bacteria such as seudomonas and Falvo bacterium exist. These can secret large amount of organic material under both aerobic and oxygen free (anaerobic) conditions.

The petroleum industry has been plagued by the activities of bacteria (SRB) because it handles large volumes of deaerated water from underground reservoirs.

Aerobic bacteria grow due to the assimilation of CO2, by using the energy derived from the oxidation of sulphur, sulphate, thiocynate, and trio and tetraathionate for their growth. These are chemolithotrophs or authotrophs i.e the ability to grow on CO2 as opposed to chemo-organtrophs whose energy for growth is from organic materials.

The aerobes that cause this type of corrosion are the bacillus of which thiobacillus and thio-oxidans are examples.They are generally found in sulphur-bearing organic waste product, in soil and water with low pH in the immediate vicinity. The thiobacilli oxidizes the elemental sulphur to produce sulphric acid as shown in the reaction below:

$2S + 3O2 + 2H2O = 2H2SO4$ ……...(2)

The present study was undertaken to quantitatively determine the corrosion of mild and medium carbon steels in aerobic and anaerobic conditions.

3.0 MATERIALS AND METHODS

3.1 Materials:

The mild and medium carbon steels were obtained from Delta steel Company Limited, Ovwian-Aladja, Delta State. They were forms of rods of diameter of 12mm and were cut to coupons of nominal dimensions of 73 x 22 x 5mm using a hacksaw blade. All cut edges were grinded to produce a good surface, finishing with emery cloths of different grades. A hole of diameter 7.0mm was drilled on

the steel coupons to enhance their ease of suspension in the different media. The chemical compositions of the steels as supplied by the manufacturer are given in Table 3.1.

3.2 Preparation of the Environments

Three environments were used in this research, viz: Anaerobic sulphur reducing bacteria, Aerobic sulphur reducing bacteria, and Fresh water (control).

3.2.1.Preparation of Bacterial Environment

5g of sulphur was measured and buried in the soil for seven days. The sulphur powder mixed with soil sample was collected after seven days. Then, 1g of the soil was weighed and serially diluted. Nutrient agar medium was prepared by mixing the compositions in Table 3.2 and was added to 1g of sulphur and allowed to solidify. 0.1ml of the fifth serially diluted soil sample was pipette on the nutrient agar plate. It was spread with a spreader and incubated anaerobically. The bacterial of the genera Desulphurvibrio was isolated from anaerobic incubation.

3.3. Experimental Procedure

3.3.1. Corrosion Rate Measurement

The corrosion rate of the coupons was monitored by total immersion/weight loss technique and electropotential methods. The coupons were cleaned and dried in acetone before immersion.

The initial weights of the coupons were taken with a digital electronic weighing machine (contech) to the nearest 0.001g and were noted. The samples were then totally exposed to the environments containing aerobic and anaerobic sulphur reducing bacteria.

Suspension was done with the aid of a rubber thread which passes through the hole in each coupon. The initial electro-potential of each of the coupons was taken using the copper/copper sulphate (Cu/CuSO4) reference electrode connected to a digital multi-meter of the model DT 9205, and the results were noted. A coupon was removed from each media each week till
the end of the experiment.

The coupons were removed from the environments at interval of seven days. The oxide film formed on the surface of the coupons were examined visually, brushed with a sponge in running tap water and then dipped in acetone and then dried.

3.4. Visual Examination

Samples were carefully examined visually during each monitoring day with the aim of identifying: The type of substances or the nature of the oxide scales on the surface of the specimens; The type of corrosion occurring; and any changes in the colour of the corrosion products.

3.5. Chemical Test

Chemical test was carried out to indicate the type of corrosion. This was done by gently scrapping the corroding surface and putting it in a test tube. Concentrated hydrochloric acid (HCl) was then added to it. The mixture was heated in a gas burner.

3.6. Bacteria Concentration and pH of the Environment

The bacteria concentrations in colony forming units per milliliter (cfu/ml) were taken at an interval of seven days for a period of six weeks using colony counter. Bacterial concentration increases with exposure time (days).

The pH of the environment was taken along each time potential readings were taken. The pH readings were made using a pH meter (MAC Type).

4.0 EXPERIMENTAL RESULTS

4.1 Weight Loss

The corrosion behaviour of mild and medium carbon steels in aerobic, anaerobic environments and in fresh water which serves as a control was studied by monitoring the electro-potential and weight loss of the specimens at intervals of seven days. The results of the weight losses of the steel coupons were converted to corrosion rate in penetration per year and are given in Table 4.1 and plotted in Figures 4.1 - 4.5.

4.2: CORROSION RATE

The corrosion rates of steels using weight loss method in the various environments were calculated using theformula [2].

$CR = 534W/DAT$

Where, CR= corrosion rate in mill per year (mpy)

W= weight loss in grams (g)

D= Density of steel (g/cm3)

A= Total surface area (cm2)

T= Exposure Time in hours (hrs)

The results are given in column 2 of Table 4.1 for each week.

Details of calculation are shown in appendix A.

4.3 POTENTIAL MEASUREMENT

The corrosion rate measurement was made using the electrical properties of a corroding system. For a corroding system the electrical potential and consequently the current and resistance are affected [2].

Using Ohm's law i.e.

$V = IR$

Where V = Potential in voltage

R = Resistance in ohms

I = Current in Amperes

The voltage decreases as the resistance increases due to the corrosion product formed on the steel surface.

Hence, the lower the potentials, the more the corrosion is.

4.4 CHEMICAL TEST RESULT

A colourless gas with a rotten egg odour evolved with a black residue of iron II chloride. The rotten egg odour of H2S indicated that SRB is responsible for the corrosion.

$2HCl + FeS = H2S + FeCl2$ ---------- (4.1)

4.5 VISUAL EXAMINATION

The steel samples exposed to the various environments were examined visually. General
(uniform) corrosion and pitting were observed for all the steel samples exposed to aerobic, anaerobic and the control.

5.0 DISCUSSION OF RESULTS

The corrosion rate of mild steel and medium carbon steels depends on several corrosion parameters such as chemical composition, surface finish, and pH.

Anaerobic, aerobic and fresh water contain corrosion inducing ions such OH- and SO4 2-. Therefore these environments are considered aggressive and toxic to most engineering materials including steel.

Relating between laboratory test, chemical analysis, and visual examination, the results of the investigation are discussed under the following headings: weight loss of sample, and corrosion rates measurement.

5.1 WEIGHT LOSS OF SAMPLES

Figure 4.1 shows the weight loss of the steel samples as a function of the environment and exposure time (days). Mild steel and medium carbon steel were found to corrode in different environment containing SRB investigated, and this was evidenced by the decrease in the original weight (weight loss).

Mild steel has the highest weight loss in all the environments investigated; recorded (156mg) in anaerobic, (130mg) in aerobic environment and (82mg) in the control. As could be seen in Table 4.1 and Fig 4.1, the weight loss of mild steel coupons in all the environments increased within the first 28 days. This observation was attributed to the fact that the rate of a chemical reaction increases with time [3].

However, between the 35th and 42nd days of the investigation, mild steel in all the environments showed a sharp decrease in weight loss with time. This behaviour could be explained from the concept of passivation [4].

Medium carbon steel has the least weight loss, recorded (136mg) in anaerobic, (98mg) in aerobic environment and (76mg) in the control. It was generally observed (Table 4.1 and Fig 4.1) that the weight loss of medium carbon steel coupons in all the environments increased with time in the first 28 days. Also, between the 35th and 42nd day of the investigation, medium carbon steel in all the environments showed sharp decrease in weight loss with time. These observations are attributed to the same behaviour reported for mild steel above.

The higher weight losses associated with anaerobic environment was partly due to the high rate of permeability and diffusion of corrosion-inducing agents such as OH- and SO4 2- ions through the protective barrier oxide film formed, while in aerobic environment the rate of permeability and diffusion of these corrosion-inducing ions is slow. The presence of SO42- ion which is reduced by SRB to produce H2S, ferrous sulphide and other corrosion products can be illustrated in the following equations:

Electrolytic dissolution of water

$8H2O = 8OH- + 8H+$ ----------(5.0.4)

Anodic reaction

$4Fe = 4Fe2+ + 8e-$ ----------(5.0.5)

Cathodic Reaction

$8H+ + 8e- = 8H2$ ----------(5.0.6)

Cathodic Deplorization by Bacteria

$SO4\ 2- + 8H2 = S2- + 4H2O$ ----------(5.0.7)

Corrosion Product

$Fe2+ + S2- = FeS$ ----------(5.0.8)

Corrosion Product

$3Fe2+ + 6OH- = 3Fe(OH)2$ ----------(5.0.9)

Overall Reaction becomes

$4Fe + SO4\ 2- + 4H2O = FeS + 3Fe(OH)2 + 2(OH)-$ ---(5.1.0)

The corrosion products such as Fes and 3Fe(OH)2 do not form protective layers as discussed earlier, hence continuation in the corrosion process.

5.2. CORROSION RATE MEASUREMENT

Weight Loss Method:

The corrosion rate was higher for mild steel, followed by the medium carbon steel. It was generally observed (Figure 4.2) that corrosion rate decreases with exposure times in all the environments. This experimentally observed behaviour was due to the formation of an impermeable protective oxide film on the surface of the steel. In this state, the steel is said to be passive [1, 2], and does not corrode easily.

Mild steel corroded more than medium carbon steel in the first 28 days due to high rate of permeability of corrosion inducing agents such as OH- and SO42- , while after 28 days the aggressive ions in the various environments could not be absorbed by the protective oxide film, hence the decrease in the corrosion rate with higher exposure times for all the environments studied.

Electro-Chemical Method:

The plot of the electrode potentials with exposure times of the steel coupons in all the environments investigated is given in Figure 4.2. It was observed that the electrode potential of the steel exposed to all the environments decreased with time during the first 28 days of the investigation and later increased till the end of the study. The electrode potential (voltage) decreased as resistance increased due to corrosion product formed on the steel surface [2]. Hence, the lower the potential, the more the corrosion.

Mild steel in anaerobic environment recorded the highest decrease in electrode potential in the first 28 days of the study. It had initial potential of -0.47(mV) in the first day and -0.93(mV) in the 28 days. This decrease in electrode potential shows increase in corrosion rate and weight loss. However, a sharp increase in electrode potential occurred from the 35th to the 42nd days (-0.86mV to -0.85mV), showing a decrease in the corrosion rate. This effect is similar to all results obtained for mild steel in aerobic and the control environment.

Medium carbon steel in anaerobic environment was next after the mild steel. It had -0.66(mV) in the first day and -0.91(mV) in the 28th day which is an indication of increase in corrosion rate. However, the electrode potential increased from -0.83mV to -0.82mV in the 35th to 42nd days respectively, showing decrease in corrosion rate and weight loss. This effect is similar to all results obtained for medium carbon steels in aerobic environment and the control.

The observed increase in electrode potential after 28 days of the test was attributed to the concept of passivity. This was caused by the formation of protective oxide film on the surface of the steels. Due to chemical, physical and electronic properties of these oxide films, metal dissolution is lowered resulting to the decrease in corrosion rate. The mild steel in anaerobic environment exhibited lowest electrode potential (highest negative

potentials) indicating both high weight losses and corrosion rate, followed by aerobic and the control respectively.
The results are in qualitative agreement with those reported by Owate, et al [5] for the corrosion of mild and high carbon steels.

The pH
The pH decreased in the first 28 days indicating high corrosion rate and weight loss. It could be seen in Figure 4.6 that weight loss increased as the pH is decreased (lowered) making the environment more acidic and consequently more corrosive. However, between the 35th and 42nd days, the pH increased.
This is due to the presence of protective oxide film that passivate the steel surface. The passivity of steel is reduced as the pH is increased [2].

6.0 CONCLUSION
The following conclusion can be drawn from this investigation: (1) Mild steel was observed to be more

corrosive in all the environments (6.43×10-4 mpy). This

is due to the high rate of permeability of corrosion inducing agents such as OH- and SO42-. This was

followed by medium carbon steel (5.30×10-4 mpy) with

low rate of diffusion of the corrosion inducing agents.
(2) General (uniform) corrosion was observed for mild and medium carbon steels in all the environments investigated.
(3) The passivity of the steels is reduced as the pH is lowered.
(4) It has been shown that corrosion rate tends to decrease with increasing carbon content.
(5) Based on these results, medium carbon steel is suggested for use in oil industries when the environment contains SRB.

REFERENCES
[1] J. O. Borode And A.N Okpala: "Effect of carbon content and Inhibitors on Corrosion of Steels" Nig Corr. Journ. Vol 2 Sept. (1999) 106-110.
[2] J. E. O Ovri: "The Corrosion of Steel Reinforcements in Concrete in Acidic and Fresh Water Environment" Nig. Corr. Journ. Vol.1, No.1, sept. (1998) 1-10.
[3] E. Osarolube, et al: "Corrosion Behaviour of Mild and High Carbon Steel in Various Acidic Media" Sci. Res. & Essay Vol. 3 (6) (June, 2008) 224-228.
[4] Donald R. Askland & Pradeep .P. Phile "The Science and Engineering of Materials" Nelson, Canada (2006) 805-828.
[5] I. O. Owate et al: "Corrosion Behaviour of Mild and High Carbon Steels in various Acidic Media". Scientific Research and Essay Vol. 3(6) June, 2008. 224-228.

APPENDIX A
The total surface area (A) of the rectangular steel coupons used in the investigation was calculated using the following relationship.

$A = 2[LW + LH + WH] - 2(\_d2/4)$

Where, A = Total surface area of coupons (cm2)
L = Length (cm) = 7.30cm
W = Width (cm) = 2.20cm
H = Thickness = 0.5cm
D = Diameter of holes (cm) = 0.7cm
$A = 2[7.3 \times 2.2 + 7.3 \times 0.5 + 2.2 \times 0.5] - (3.142 \times (0.7)\, 2/4)$
$= 2[16.06 + 3.65 + 1.10] - 2(0.385) = 40.85cm2$
The corrosion rate (CR) is calculated using the relationship.
C.R = 534W/DAT
W = Weight loss (g)
D = Density of metal (g/cm3)
A = Total surface area of coupons (cm2)
T = Exposure Time (hrs)
C.R (Control 7days mcs) =
$534 \times 0.030 / 7.87 \times 40.85 \times 168 = 16.02 / 54010.24$
$= 2.94 \times 10\text{-}4$ mpy
C.R (Control 7 days ms) = $534 \times 0.042/7.87 \times 40.85 \times 168 = 4.15 \times 10\text{-}4$ mpy.

Table 3.1: Chemical Composition of the Steels as Supplied by the Manufacturer.

Steel Grade	C	Si	Mn	Cu	P	S	Cr	Ni	Sn	Fe
MS	0.18	0.23	0.80	0.20	0.03	0.04	0.05	0.55	0.02	Bal
MCS	0.40	0.25	0.52	0.05	0.03	0.02	-	-	-	bal

Key: MS = Mild Steel, MCS = Medium Carbon Steel

Table 3.2: Composition of Nutrient Algae Used for the Preparation of the Bacterial Environment.

Compound	Nacl	$MgSO_47H_20$	KCl	KH_2PO_4	Na_2HPO_4	$NaNO_3$	Agar
Composition	10g	0.3g	0.29g	0.83g	1.25g	0.42g	12.5g

Table 4.1: Weight loss (g), Corrosion rate (mpy) and potential (mV) in various environments.

	Weight Loss Method														Electrode Potential Method						
	0 day		7 days		14 days		21 days		28 days		35 days		42 days		0 days	7 days	14 days	21 days	28 days	35 days	42 days
	Wt Loss (g)	CR (mpy)	Wt Loss (g)	CR (mpy)	Wt Loss (g)	CR (mpy)	Wt Loss (g)	CR (mpy)	Wt Loss (g)	CR (mpy)	Wt Loss (g)	CR (mpy)	Wt Loss (g)	CR (mpy)	EP (mV)	EP (mV)	EP (mV)	EP (mV)	EP (mV)	EP (mV)	EP (mV)
Control MCS	0.00	0.00	0.030	2.94	0.051	2.50	0.076	2.35	0.076	1.86	0.076	1.49	0.074	1.21	-0.47	-0.65	-0.70	-0.74	-0.74	-0.72	-0.73
Control MS	0.00	0.00	0.042	4.15	0.069	3.41	0.076	2.60	0.082	2.03	0.080	1.58	0.078	1.29	-0.55	-0.67	-0.73	-0.76	-0.77	-0.74	-0.74
Anaerobic MCS	0.00	0.00	0.054	05.30	0.088	4.31	0.125	4.08	0.136	3.33	0.132	2.59	0.128	2.09	-0.66	-0.77	-0.83	-0.90	-0.91	-0.83	-0.82
Anaerobic MS	0.00	0.00	0.065	6.43	0.098	4.84	0.140	4.61	0.152	3.76	0.150	2.95	0.140	2.31	-0.70	-0.83	-0.87	-0.95	-0.93	-0.86	-0.85
Aerobic MCS	0.00	0.00	0.49	5.00	0.076	3.72	0.089	2.91	0.098	2.40	0.083	1.76	0.085	1.40	-0.54	-0.70	0.77	-0.82	-0.84	-0.76	-0.75
Aerobic MS	0.00	0.00	0.053	5.24	0.084	4.15	0.105	3.46	0.130	3.21	0.120	2.37	0.116	1.91	-0.62	-0.75	-0.81	-0.88	-0.89	-0.79	-0.79

Key: Envt. - Environment Wt. Loss - Weight Loss C.R - Corrosion Rate Ep - Electro potential

TABLE 4.2: Results for pH Measurement in Anaerobic, Aerobic and the Control Environments.

Environment	pH 0-day	7-day	14-day	21-day	28-day	35-day	42-day
Control	6.90	6.72	6.40	5.78	5.78	6.32	6.80
Anaerobic	6.80	6.05	5.50	5.00	4.50	5.50	6.00
Aerobic	6.85	6.40	6.35	5.25	5.00	6.00	5.85

Table 4.3: Results of Bacterial Concentration of Anaerobic and Aerobic Environments.

Bac.Conc	0-day	7-day	14-day	21-day	28-day	35-day	42-day
Anaerobic (cfu/ml)	300	350	400	450	500	530	550
Aerobic (cfu/ml)	200	250	300	350	380	400	450

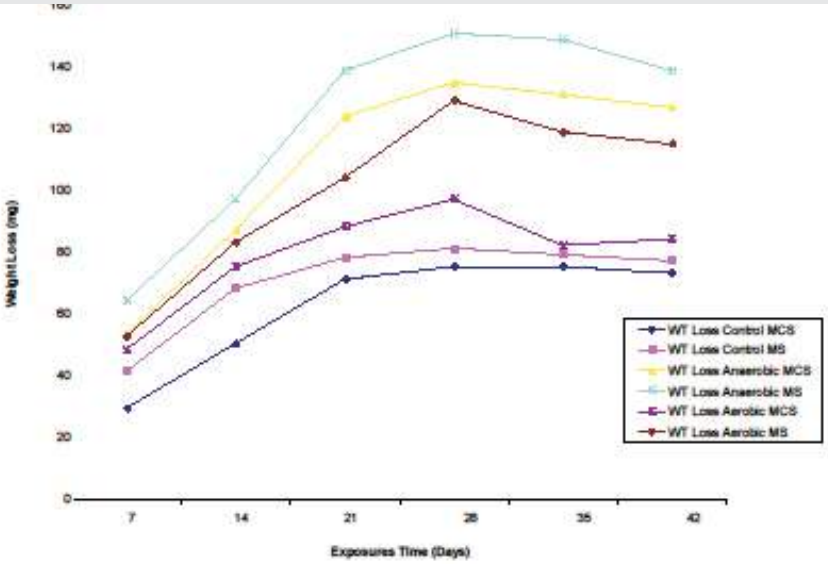


Fig. 4.1 variation of Weight Loss in (mg) with Exposure time in (days) for steel coupons exposed to Aerobic, Anaerobic and Control.

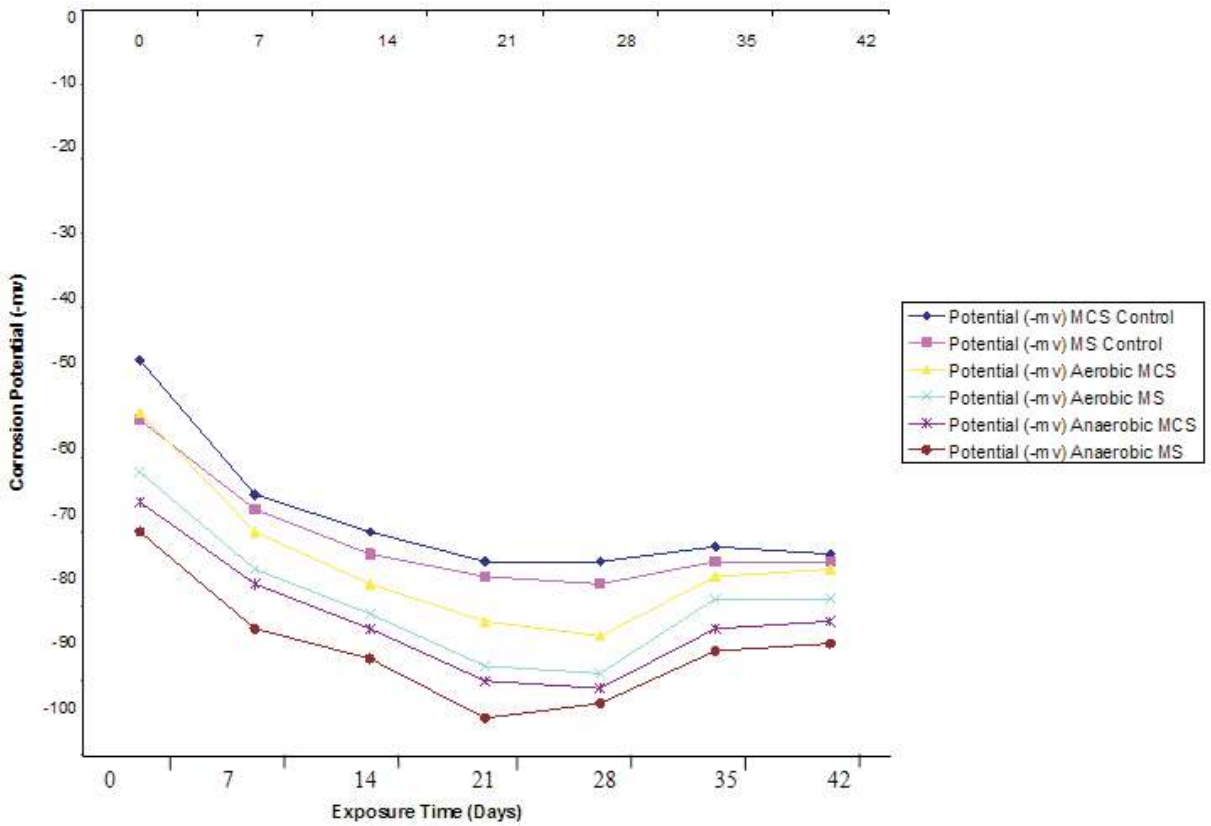


Fig. 4.2 Variation of Potential (-mV) with Exposure Time with (days) for Steel Coupons exposed to Aerobic, Anaerobic and Control.

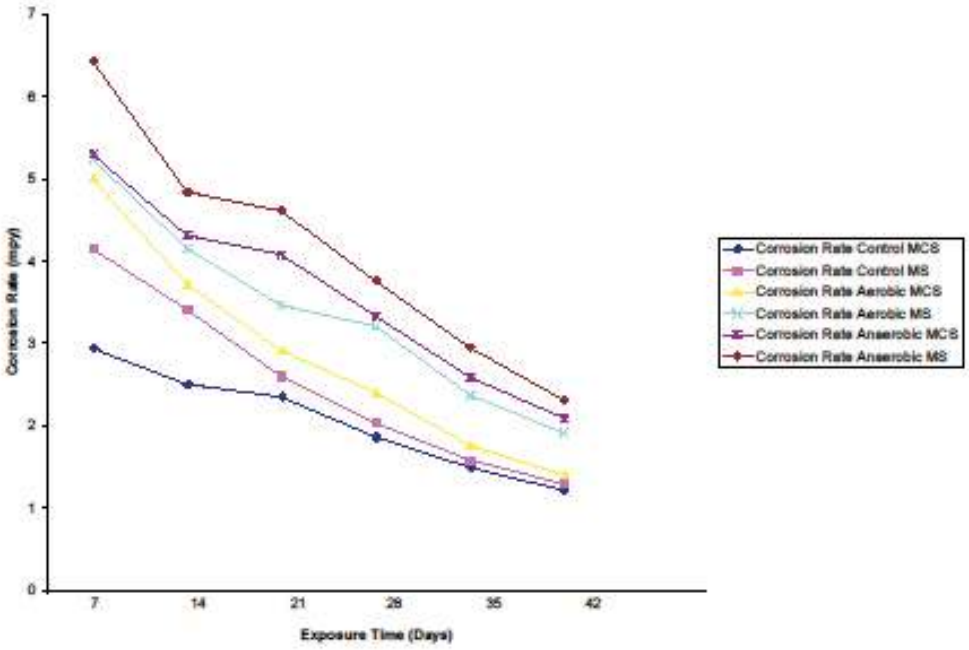


Fig. 4.3 Variation of Corrosion rate in (mpy) with Exposure Time (days) for Steel Coupons exposed to Aerobic, Anaerobic and Control.

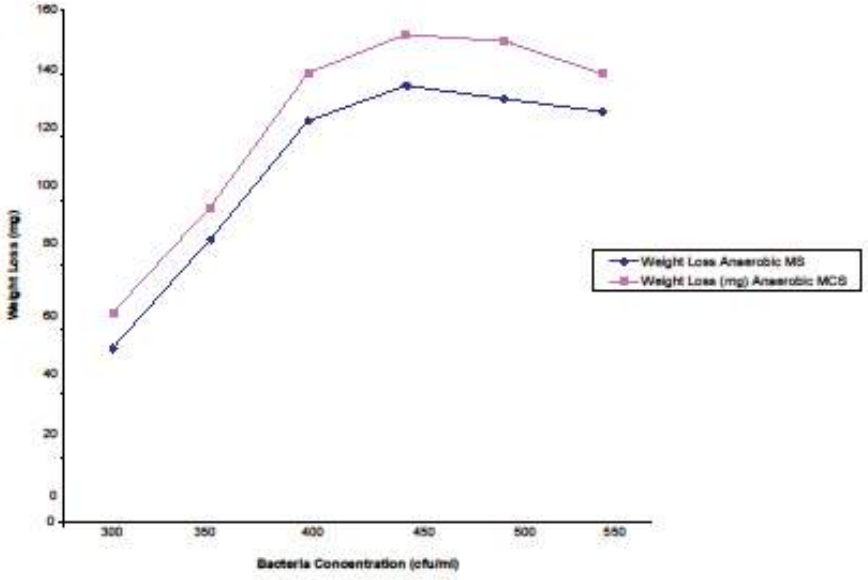


Fig. 4.4 Variation of Weight Loss in (mg) with Bacteria concentration (cfu/ml) for Steel Coupons exposed to anaerobic environment

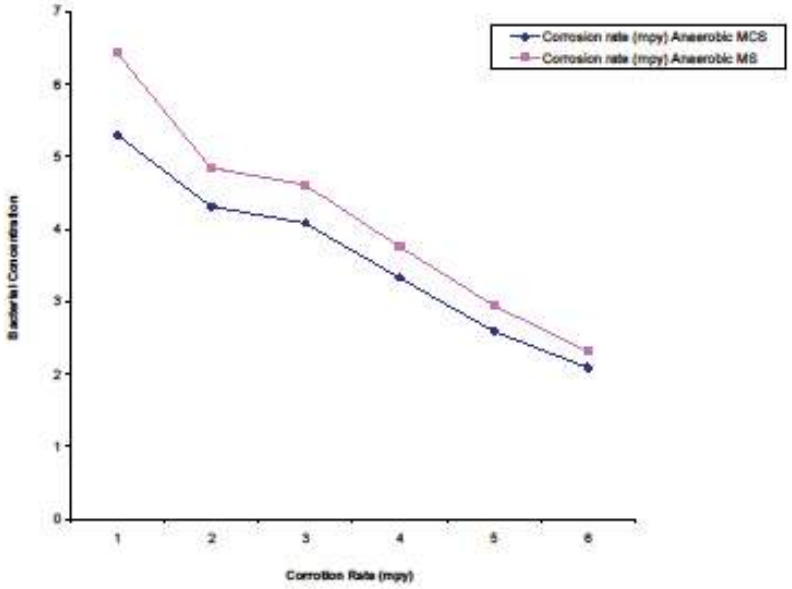


Fig. 4.5: Variation of Bacterial Concentration with Corrosion rate for Steel Coupons exposed to anaerobic environment.

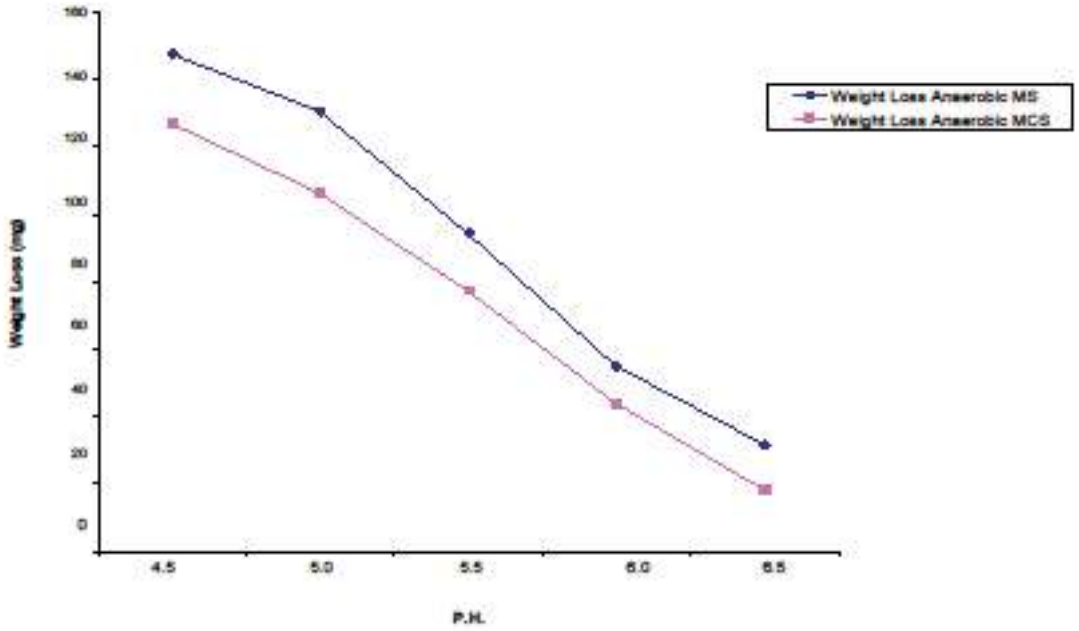


Fig. 4.6: Variation of Weight Loss with pH for Steel Coupons exposed to anaerobic environment.

UTILIZATION OF SOLAR ENERGY FOR POWER GENERATION IN NIGERIA

[1]Oji J.O., [2]Nosa I., [1]Aliu T.O., [1]Petinrin M.O., [1]Odejobi O.A., [1,3]Adetunji A. R.
[1]Prototype Engineering Development Institute Ilesa, Osun State
(National Agency for Science and Engineering Infrastructure, NASENI. FCT Abuja)
[2]Department of Mechanical Engineering, University of Ibadan, Oyo State
[3]Department of Materials Science and Engineering,
Obafemi Awolowo University, (OAU) Ile-Ife
ojiortega@yahoo.com

ABSTRACT
This study presents the viabilities for power generation in Nigeria through the utilization of the sun's energy. Solar-thermal and photovoltaic options were discussed. It highlights the basic science for the design and selection of components for successfully harnessing solar power. Requirements for solar panel placement and orientation were also highlighted. It emphasizes that the knowledge and experience gained in solar energy as an abundant and convenient energy source, can play a role in steering the nation toward a permanent and sustainable development. The energy demand in Nigeria far outweighs the supply which is epileptic in nature. The acute electricity supply hinders the country's development notwithstanding the availability of vast natural resources in the country. Our ability to continue the trend for affordable energy will be severely tested in the coming decades, as evidenced by the widening trade imbalance, collapse of big manufacturing companies, sharp increase in the cost of doing business just to mention but a few. It is the issue of utilizing the sun's silent, inexhaustible, and non-polluting resource for power generation in Nigeria that this work addresses; hence it is the long-range review of the energy problem.

Key Words: *solar energy, energy crisis and demand,* ***power generation*** *technologies, solar-thermal conversion, solar electric (photovoltaic) conversion, panel placement and orientation.*

1. INTRODUCTION

The Earth as a resource system has a limited capacity for supporting a growing human population with an intensive exchange of materials and energy with its environment, hence the need for a growing awareness to achieve a more sustainable societal use of materials [1]. The earth receives energy directly from the sun. It is silent, inexhaustible, and non-polluting [2].

The utilization of solar energy depends on its availability and appropriate technology [3]. The idea of using the sun's power has held scientist in its grips for centuries [4]. Also, for most of its evolution, mankind relied for its sources of energy on constantly replenished materials. Throughout the early phase of human development, the availability of the readily renewable sources of energy was a key constraint and affected the size and distribution of populations [5], [25].

The sun's power reaching the earth is typically about $1000W/m^2$. The total amount of energy that the earth receives daily is $1353W/m^2$ [6]. Some 4million of tons of the sun's matter will continue to be changed into energy every second [7].The sun is the most readily and widely available Renewable energy source capable of meeting the energy needs of whole world. It can provide more power than any fossil fuel on the planet [8]. The solar radiation arrives at the earth at a maximum flux density of about $1kw/m^2$ in wave length of band between 0.3 and 2.5μm.This is called short wave radiation and it includes visible spectrum. For habited areas received fluxes vary widely from about 3 to $30MJ/m^2/day$, depending on place, time and weather. The quality of radiation is characterised by the photon energy of around 2eV as determined by 6000K surface temperature of the sun [9].

Solar panels are made up of solar cell which is an array of photovoltaic cells (PV). Any type of equipment used to convert sunlight into energy is considered solar cell or panels. The technology behind Solar panels has varied widely throughout the five or six decades and while solar cells were the true origin of modern solar panels, today researchers are shifting to new platform and approaches to gathering energy from sunlight which including crafting Solar cells from Silicon semiconductor configured to trap and convert sun energy which are coated in an antireflective coating and contained under a glass cover plate to protect the cell from the elements [10].

In the 1950s General Pearson, Calvin Fuller and Daryl Chaplain (of Bells Laboratories) discovered how well silicon worked as a semi-conductor. Silicon is what solar cells and panels are generally made up of today [11]. An ambiguous study has been made of using a solar satellite which is continuously in direct sunlight to collect the energy, convert into electricity and direct a microwave beam to a receiver on earth where it would be reconverted to electricity [2]. However, the cost of such a scheme is likely to prohibit its realization.

2. ENERGY DEMAND, CRISIS, AND UTILIZATION IN NIGERIA

The Nigerian economy can be disaggregated into industry, transport, commercial, household, and agricultural sectors, with the household sector

dominating energy consumption [12] and [13]. The energy consuming activities in the household sector still remain mainly cooking, lighting, and operations of electrical appliances (i.e., non-substitutable electricity). The percentage distribution of the total final consumption in 1989 in this sector and in terms of the major energy carriers is Kerosene (13%), Electricity (4%), LPG (1%), and Wood/Others (82%) [13].

Nigeria's economy face deepening challenges: a widening trade imbalance, growing competition from developed countries, a collapse of big manufacturing companies, and a sharp increase in the cost of doing business, all owing basically to energy and its related infrastructural costs. Energy demand far outweighs the supply which is epileptic in nature. It is still pertinent to note that our energy consumption is projected to grow geometrically (figure 1) while our ability to sustain our growth through energy generation, transmission and distribution continues to dwindle (Figure 2). Our capability to continue the trend for affordable energy will be severely tested in the coming decades.

Figure 3 shows the variation of the total radiation per square meter per day throughout the year in some cities of the country. The average total radiation received per day at the northern cities of Kano, Zaria, and Kaduna is more than that of the southern cities of Ibadan, Lagos and Nsukka. Furthermore, at each of these cities the total radiation varies significantly with the period of the year. For example, the total radiation received per day on a $1m^2$ surface at Ibadan varies from 16MJ in January to 22MJ in May. Under the same period at Kano the total radiation received varies from 33MJ to 37MJ par day on the same surface. Using this as a benchmark, it can be seen that even the minimum harnessible power in any part of the country is more than that required for powering an average 3- bed room flat and 2-room apartment using low-power consuming appliances (Table 1 and Table 2). The need for harnessing this renewable energy supply is apparent as fossil fuels (especially oil) become increasingly expensive, population increases, and each individual presses for a higher standard of living in terms of material goods, especially in rural and developing regions.

3. POWER GENERATION TECHNOLOGIES

Power generation is the process of converting energy from an available source to electrical energy in a form that is suitable for distribution, consumption and storage. Solar energy can be used to generate power in two ways; solar-thermal conversion and solar electric (photovoltaic) conversion.

Solar-thermal conversion

Solar-thermal is the heating of fluids to produce steam to drive turbines for large-scale centralized generation (figure 4). Like solar cells, solar thermal systems, also called concentrated solar power (CSP), use solar energy to produce electricity, but in a different way. Most solar thermal systems use a solar collector with a mirrored surface to focus sunlight onto a receiver that heats a liquid. The super-heated liquid is used to make steam to produce electricity in the same way that coal plants do. Albeit, the Renewable Electricity Action Program (REAP) of the Federal Ministry of Power and Steel (2006) published by the International Centre for Energy, Environment and Development did not cover this aspect of power generation [14].

Solar electric (photovoltaic) conversion.

Solar-electric (photovoltaic) conversion is the direct conversion of sunlight in to electricity through a photocell. This could be in a centralized or decentralized fashion. Solar-electric (Photovoltaic) technologies convert sunlight directly into electrical power. Photovoltaic system is made up of a balance of system (BOS), which consists of mounting structures for modules, power conditioning equipment, tracking structures, concentrator systems and storage devices. Photovoltaic conversion could be small scale for stand-alone systems or large scale connected to national grid (figure 5).

PV cells also have one or more electric field that acts to force electrons freed by light absorption to flow in a certain direction. This flow of electrons is the current, and by placing metal contacts on the top and bottom of the PV cell, we can draw that current off for external use say, to power a calculator. This current, together with the cell's voltage (which is a result of its built-in electric fields), defines the power (or wattage) that the solar cell can produce [15].

PV modules are integrated into systems designed for specific applications. The components added to the module constitute the “balance of system” or BOS. Balance of system components can be classified into four categories [16].

Deep cycle battery - store electricity to provide energy on demand at night or on overcast days. They are designed to be discharged and then re-charged hundreds or thousands of times.

Inverters - required to convert the Direct current (DC) power produced by the PV module into Alternating current (AC) power.

Charge Controller - A charge controller monitors the battery's state-of-charge to insure that when the battery needs charge current it gets it, and also insures the battery isn't over charged.

Structure - required to mount or install the PV modules and other components.

Not all systems will require all these components. Some systems also require other components which are not strictly related to photovoltaic [17].

Solar Panel Placement and Orientation

Solar panels should also be inclined at an angle as close to the area's latitude as possible to absorb the maximum amount of energy year-round. A different orientation and/or inclination could be used if you want to maximize energy production for the morning or afternoon, and/or the summer or winter. The modules should never be shaded by near trees or buildings, no matter the time of day or the time of year. In a PV module, if even just one of its cells is shaded, power production can be significantly reduced.

Optimally, the angle of the panels is set to provide the most exposure to direct sunlight. The caveat is that the optimum angle which depends on latitude, as the sun's height in the daytime sky will be different for all. To determine the optimum angle for solar panel, the following instructions are generally adhered to [24].

1. Calculate latitude using a global positioning system, GPS, map an Atlas or even from Google Earth, and it creates an easy to read sun map with key information such as the number of hours of sunshine, its intensity and so on. This will be used to calculate the optimum angle
2. Add 15 to the calculated latitude (This is the rule of thumb for even production throughout the year).
3. Adjustment on solar panel's mounting system. Ratchet systems can be installed to raise or lower the angle or panel can be adjusted manually.

Challenges

According to [18], some of the factors militating against the growth of the Solar – PV and concurrently solar thermal Industry in Nigeria include:

(a) Financial constraints: A basic barrier to the development of solar energy technology in Nigeria as a developing country lies in high initial costs and long payback times.

(b) Technological incapability: Though the technologies for harnessing solar energy are being developed in Nigeria, most components have to be imported which further pushes the investment costs higher.

(c) General absence of comprehensive National Energy Policy: There was virtually no comprehensive energy policy in Nigeria until very recently. Only sub-sectorial policies relating to energy exist.

(d) Low level of Public Awareness: The level of awareness about the immense socio-economic and environmental benefits derivable from solar energy is very low in Nigeria.

4. Recommendations

For effective and efficient utilization of solar electricity in Nigeria, the following recommendations will be useful-

a) More research into the techno-economies involving the initial and subsequent costs of solar plants and their power efficiencies is encouraged.
b) Government should subsidize the cost of importation of Renewable Energy Technologies (RET) most especially solar PV to bring down the high cost in Nigeria.
c) Private individuals and organisations should be encouraged by appropriate authorities to invest in solar technologies in the country.
d) Consequently, the wide chasm between research bodies (universities, polytechnics and research institutes) and manufacturing industries must be bridged.
e) Government should create more awareness on the advantages derivable from Renewable Energy Technologies (RET) such as solar technologies.
f) Government can also consider placing restrictions on the importation of generators because of its adverse effects on the environment even as the global community gear towards clean (green) energies.
g) Funding of solar technology researches and development initiatives in our Universities, Polytechnics and Research Institutes so as to develop solar PVs with increased efficiency that will be adaptable to our environment is advocated. Such pilot schemes are seriously undertaken at the National Agency for Science and Engineering Infrastructure, NASENI, FCT Abuja and the Prototype Engineering Development Institute Ilesa, Osun State. The National Energy Research Centres at the University of Nigeria, Nsukka, the Obafemi Awolowo University, Ile-Ife and Usmanu Danfodiyo University, Sokoto, also provide a valuable source of solar radiation and other climatic information. Less consistently collected are data from some tertiary institutions nationwide, where individual energy researchers work on various energy projects.

Conclusion

This paper focuses on the maximization of the sun's energy supply for generating optimum power. It has presented the viabilities for power generation in Nigeria by the utilization of the sun's energy through solar-thermal or photovoltaic technologies. The basic science for the design and selection of solar components as well as panel placement and orientation were highlighted. The future of solar electricity is brighter than before. Solar energy is free- it needs no fuel and produces no waste or pollution. It is only recently that mankind turned to the large scale exploitation of new, and non-renewable sources of energy and those sources have made possible the advance of industrial revolution and large increase in populations. It is clear however, that because of the finite magnitude of these sources, this phase of human development is transitory and the era of extensive dependence on finite fossil energy resources will appear as a brief episode.

References

[1]Karlsson, S. (1999): "Closing the Technospheric Flows of Toxic Metals: Modelling Lead Losses from a Lead-Acid Battery System for Sweden". Journal of Industrial Ecology. Vol 3, no1. © Copyright 1999 by the Massachusetts Institute of Technology and Yale University.

[2]Eastop T.D., McConkey A. (2002): Applied Thermodynamics for Engineering Technologists. Fifth Edition. Pearson Education (Singapore) Pte. Ltd., Indian Branch. Patparganj, India. P 697

[3] Nasir, A. (2001): A Technology for Helping to Alleviate the Energy Problems; Solar Energy for Cooking and Power generation. paper presented at the 3rd annual Engineering Conference of Federal University of Technology, Minna, Nigeria

[4]Bradley, D. (1995): Plants point the way to renewable energy. New Sci.121: 8.

[5] Sambo, A.S. (2001): "Renewable Energy

Technology for National Development: Status, Prospects and Policy Directions". Proceedings of the Annual General Meeting of the Nigerian Society of Engineers. Bauchi branch. Bauchi State, Nigeria.

[6] Hoff, E.; and Cheney, M. (2000): The Idea of Low Cost Photovoltaic. Energy J. 93: 17.

[7] David, K., Hare, G. (1983): Applied Solar energy. Butterworths Litho Preparation Department.Primted by Cambridge University Press, Cambridge, England.

[8] Rochell, M.S. (2010): The History of Solar power today. http://enzinearticles.com Retrieved February 23rd, 2011

[9] John W. T., Anthony D. W. (1987): Renewable energy resources, University Press Cambridge, England.

[10]Jonathan, G. (2010): A brief History of Solar Power. http://eziniearticles.com Retrieved February 20th, 2011

[11]Clark, A. (2010): The history of solar energy-It is longer than you may think. http://ezinearticles.com February 23rd, 2011

[12]Akinbami, J.F.K. (2001): "Renewable Energy Resources and Technologies in Nigeria: Present Situation, Future Prospects and Policy Framework". Mitigation and Adaptation Strategies for Global Change. 6:155-181. Kluwer Academic Publishers: Holland, The Netherlands.

[13]Oladosu, G.A. and Adegbuluge, A.O. (1994): "Nigeria's Energy Sector: Issues and Supply/Demand Frontiers". Energy Policy. 22(6): 538-549

[14]Federal Ministry of Power and Steel, (2006): Renewable Electricity Action Program (REAP) published by the International Centre for Energy, Environment and Development. www.iceednigeria.org

[15]Agrafiotis, C. (2005): "Solar water splitting for hydrogen production with monolithic reactors". Solar Energy 79 (4): 409–421.

[16]Owolabi I.E (2008): "Solar Photovoltaic power technology: Prospects and challenges for socioeconomic empowerment in Nigeria". Technical Paper presented to the Nigerian Society of Engineers (NSE) Ado-Ekiti branch. Pg 3-5.

[17]Ogunleye, I.O., Awogbemi, O. (2011): Constraints to the use of solar photovoltaic as a sustainable power source in Nigeria American Journal Of Scientific And Industrial Research Vol. 2(1): 11-16

[18]Chendo, M.A.C. (2002): "Factors Militating Against the Growth of the Solar – PV Industry in Nigeria and their Removal". Nigeria Journal of Renewable Energy. 10(1&2):151 – 158.

[19] Sambo, A.S. (2008): "Matching Electricity Supply with Demand in Nigeria", International Association for Energy Economics.

[20]Iwayemi, A. (2008): "Nigeria's Dual Energy Problems: Policy Issues and Challenges". International Association for Energy Economics, pp 17-21.

[21]Bamiro, O.A. et al, (1999): Introductory Technology for Schools and Colleges. Book 3.Evans Brothers (Nigerian Publishers) limited.

[22]Green, M.A. (1982): Solar Cells Operating Principles, Technology and Systems Application. Prentice Hall, Eaglewood Cliff, NJ, USA.

[23]Abdulkarim H.T.(2010): Techno-Economic Analysis of Solar Energy for Electric Power Generation in Nigeria. Department of Electrical/Electronics College of Education, Minna, Niger State, Nigeria. (Untitled Journal Publication Vol. 8(4): 215-221

[24]Hankins, M. (1995): Solar Electric systems for Africa. Commonwealth Science Council. Marlborough house. Pall mall, London.

[25]Sambo, A.S. (2001): "Renewable Energy Technology for National Development: Energy Crisis in Nigeria. The Way Foward". Proceedings of the Annual General Meeting of the Nigerian Society of Engineers. Bauchi branch. Bauchi State,Nigeria.

[26]Becker et al, (2000): Solar Thermal Power Plants prepared for the EUREC-Agency drafted version with status of May 03,2000.

FIGURES

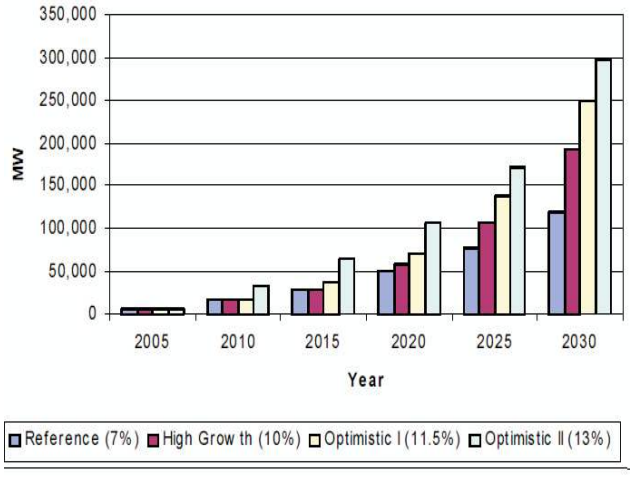


Figure 1: Electricity Demand Projection in Nigeria. Source: [19]

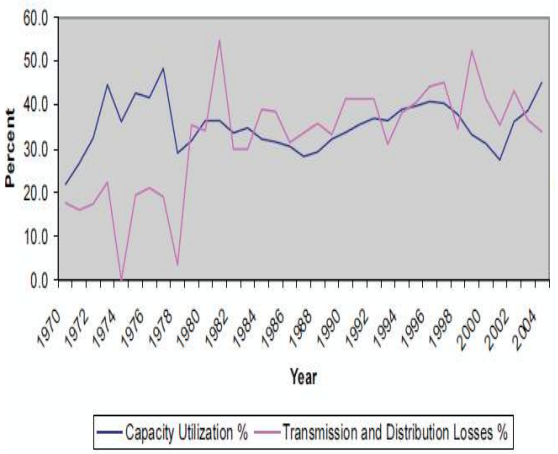


Figure 2: Indicator of Electricity Crisis in Nigeria 1970 to 2004. Source: [20]

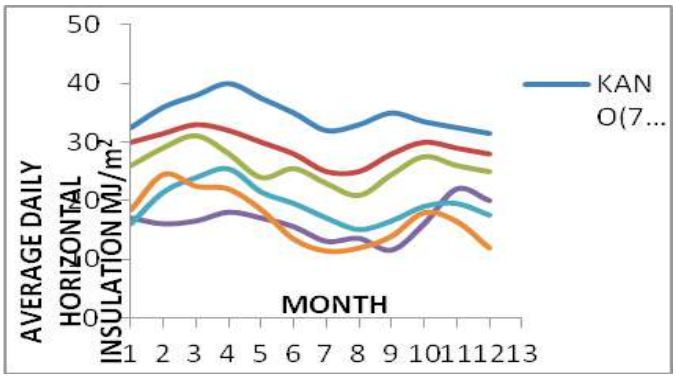


Figure 3: Variation of daily total radiation in some Nigerian cities. Souce: [21]

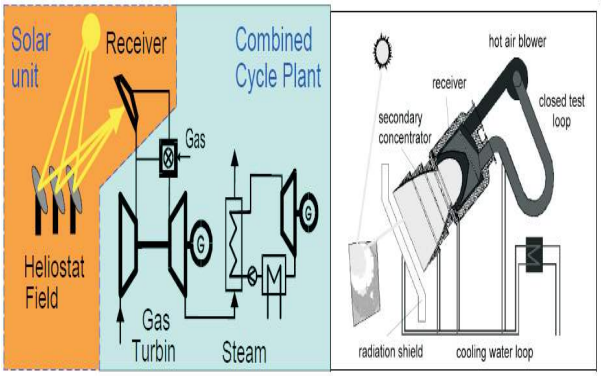


Figure 4: The REFOS-receiver for testing at the Plataforma Solar de Almería. Source: [26]

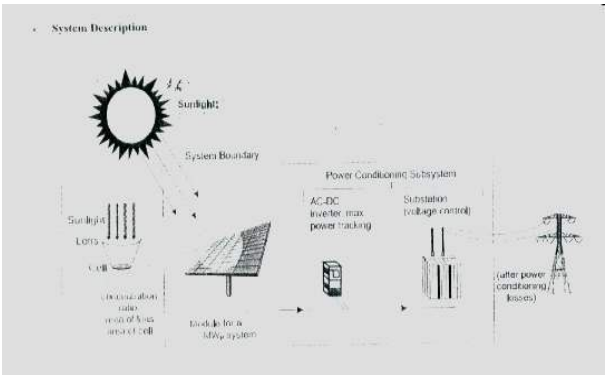


Figure 5: Schematic of a large-scale photovoltaic system. Source: [22]

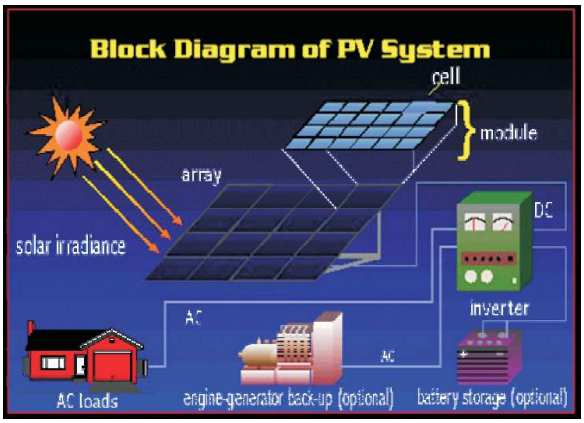


Figure 6: Schematic of small-scale Photovoltaic System. Source: **[23]**

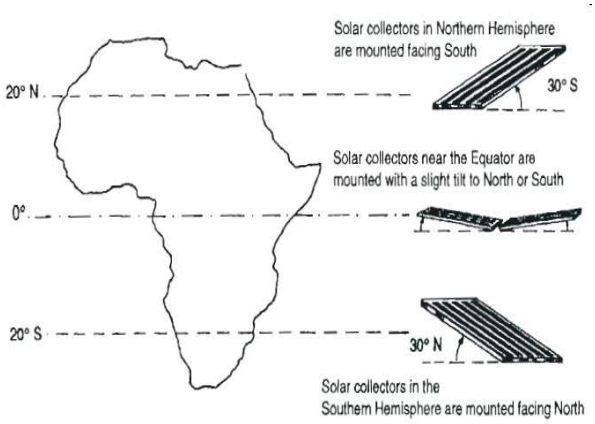


Figure 7: Mounting angles for fixed solar collectors. Source: [24]

S/N	APPLIANCE	POWER (W-h)	QTY	TOTAL POWER (W-h)
1	Light	20	10	200
2	Fan	100	4	400
3	TV	58	2	116
4	Home theatre	95	1	95
5	Fridge	850	1	850
6	Air conditioner	750	1	750
8	Miscellaneous	100	-	100
TOTAL POWER REQUIRED 2511W-h or 2.511KWh Note: 1J/sec=1 Watts				

Table 1: Power estimate for an average 3-bedroom flat in Nigeria

Table 2: Power estimate for an average 2-room apartment in Nigeria

S/N	APPLIANCE	POWER (W-h)	QTY	TOTAL POWER (W-h)
1	Light	20	4	80
2	Fan	80	2	160
3	TV	58	2	116
4	Fridge	500	1	500
6	Miscellaneous	100	-	100
TOTAL POWER REQUIRED 956W-h or 0.956KWh Note: 1J/sec=1 Watts				

COMPARATIVE STUDY OF CORROSION SENSITIVITY OF SELECTED FERROUS METALS IN CRUDE OIL

Ogundare,O., Momoh, I.M., Akinribide, O.J., *Adetunji, A.R., [+]Olusunle, S.O.O. and [+]Adewoye, O.O.
Engineering Materials Development Institute, Akure
*Prototype Engineering Development Institute, Ilesa
[+]National Agency for Science and Engineering Infrastructure, Abuja
Corresponding Author: suppiedee@yahoo.com

Abstract

Corrosion characteristic of selected ferrous metal samples (plain and alloyed ductile iron, low carbon steel and austenitic stainless steel) in crude oil was investigated using weight loss method. The microstructures of the coupons were taken before and after corrosion test. It was observed that all the materials experience gain in weight within the first 10 days in the medium. This weight gain is attributed to the formation of hard and passive phases which acted as strong protective barriers to corrosion. It was also observed that the rate of corrosion decreased with increase in the number of days of exposure for all the coupons, this may be probably due to the deposition of corrosion products that tend to shield the corroding surface from further corrosion attack, there by depressing the rate of corrosion. This result shows that despite initial low corrosion resistance of plain ductile iron, it can still be considered, alongside other materials, for application in pipelines and storage facilities for crude oil.

Keywords: Corrosion, agitation, ductile iron, Austenitic Stainless Steel, Mild steel and crude oil.

1. INTRODUCTION

Ferrous materials which include steels and cast irons of various compositions have all demonstrated their usefulness in structural (e.g. residential buildings, bridges etc) and domestic applications. Its relevance in pipelines cannot be over-emphasized considering its vast use in the oil sector. Ferrous materials have gain prevalence over many other materials in the aforementioned applications. This unique noticeable prevalence has been attributed, among others, to spring from its response to harsh corrosive conditions/environments along with appreciable mechanical properties.

Ductile iron or nodular cast iron or spheroid-graphite (SG) cast iron contains nodules of graphite embedded in a matrix of ferrite or pearlite or both, the graphite separates out as nodules from iron during solidification because of the additives like magnesium (Mg) and Silicon (Si) introduced into the molten iron before casting. These nodules act as crack arresters thereby improving the mechanical properties of ductile iron. Its corrosion resistance has been attributed to the formation of a thin passive barrier film of hydrated oxides of silicon on the metal surface. The film develops with time due to the dissolution of iron from the metal matrix leaving behind silicon which hydrates due to the presence of moisture. The passive hydrated silicon film is thought to bridge over and form an impervious barrier layer on a fine grained high silicon cast iron with spheroidal graphite areas much more readily than on a high silicon cast iron with coarse graphite flakes [1].

Corrosion, which has been conveniently classified according to the manner in which it manifest itself [2] is regularly encountered in the chemical, petrochemical, oil, and food processing industries; in the air, sea, rail, and road transportation; in conventional and nuclear power generation station; in buildings and construction industries; in agriculture and in numerous domestic applications.

Passivity is the loss of chemical reactivity, under particular environmental conditions, by some active metals and alloys. It is the result of the formation of a highly protected but thin and sometimes invisible film on the surface of a metal or an alloy that makes its soluble potential more noble. This, however, does not take into consideration the position of the metal in the electrochemical series. This is, among others, the function of most corrosion resistance alloying elements (e.g. chromium, nickel, vanadium etc) in metals [3].

Since metals and alloys form the essential basis for modern technological civilization, the harmful repercussions are extremely wide spread and diverse; the problem of metallic corrosion is one of significant proportions; in economic terms, it has been estimated that approximately 5% of an industrialized nation's income is spent on corrosion prevention and the maintenance or replacement of products lost or contaminated as a result of corrosion reactions. Therefore the need arise to examine their corrosion behavior so as to reduce or even stop their corrosion [2].

[4] Investigated the stress corrosion behavior of low and medium carbon steels in agro- fluids and discovered that low carbon steel in both media exhibit high corrosion

resistance due to the low amount of carbon content.

Nigeria, as an oil producing nation, needs to intensify research in the area of ferrous metal applications. In order to assess and evaluate the life-span of the materials employed in such transportation and storage, this research has embarked on the comparative study of various selected materials in mildly agitated crude oil.

2. MATERIALS AND METHOD

Materials and Equipment

The materials used in this experiment include mild steel, austenitic stainless steel; plain ductile iron and alloyed ductile irons were produced from EMR 100 rotary furnace at Engineering Materials Development Institute Akure and crude oil obtained from the oil field. Equipment used for the experiment are bench vice, Digital analytical balance, Atomic Absorption Spectrophotometer (AAS), Instron tensile testing machine, micro-hardness tester, Buehler mounting press, grinding and polishing machines. The composition of the crude oil is shown in table 1.

Composition (%)	C	Si	P	Mn	S	Mo	Mg	Co	Al	Cu	Ni	Cr	Nb	Fe
Plain D.I	3.60	2.00	0.007	0.300	0.010	0.014	0.05	-	-	-	-	-	-	Bal.
Ni – D.I	3.72	1.98	0.005	0.220	0.011	0.012	0.07	-	-	-	0.90	-	-	Bal.
Cr –D.I	3.97	2.01	0.008	0.233	0.010	0.016	0.10	-	-	-	-	0.8	-	Bal.
Ni/Cr – D.I	3.51	2.12	0.004	0.150	0.008	0.020	0.07	-	-	-	0.36	0.90	-	Bal.
Mild Steel	0.117	0.033	0.0258	0.011	0.014	0.014	-	0.005	0.59	0.055	0.19	-	-	Bal.
ASS	0.08	0.75	0.045	2.00	0.030	2.50	-	-	-	-	8.0	18.0	0.1	Bal.

Table 2: Chemical composition of the selected ferrous metals

Methods

Sample preparation: The as-cast and as-received samples were machined to a specific preferred corrosion configuration. It was further ground and polished after which the hardness values were determined with the aid of a micro-hardness tester.

Microstructural Examination:

Metallographic samples were cut from the coupons before immersion. The cut samples were then mounted in Bakelite, impregnated emery paper (60-2400 grits) sizes were used to grind the samples, and then polished, etched and the photomicrographs were taken after 56 days of immersion in crude oil for comparison.

Corrosion Test: After machining, the coupons were cleaned, weighed and stored in a dessicator before suspending it in crude oil with the aid of threads at room temperature of 27^0C. Each test coupon was exposed for a total period of 56 days with seven weight measurements taken at an interval of 7 days. The average corrosion rates of the coupons, measured in mg/mm^2/yr were determined using the following established relation [5, 6, 7, 8 and 9].

Weight Loss/corrosion Rate: The weight losses of the coupons were determined by finding the difference between the original weights of the coupons and the new weights after each withdrawal.

1. RESULTS AND DISCUSSION

Results

The results are has shown in Table 3

Discussion

Figure 1 shows the hardness values of the selected ferrous materials. The materials were observed to possess a relatively high hardness property (see figure 1) indicating that all of them have adequate strength to withstand the stress posed by floating crude oil.

Figure 2 shows the corrosion behavior of the materials and interestingly shows that the majority has high corrosion resistance property in crude oil. The corrosion deposit observed in the microstructure was in a regular orientation (fig. 3a) which could be inferred from the directionality of the slip plane with respect to the manufacturing process. All the immersed samples experience an increase in corrosion rate between first 8 – 10 days. This is attributed to the formation of hard and passive phases which acted as strong protective barriers to corrosion.

However, after the tenth day measurement, It was also observed that the rate of corrosion gradually decreases with increase in the number of days of exposure time for all the coupons, this may be probably due to the deposition of corrosion products that tend to shield the corroding surface from further corrosion attack, there by depressing the rate of corrosion. This observation is similar to the findings of [1] who investigated the corrosion characteristics of vanadium alloyed ductile iron. Surprisingly, mild steel was observed to have the lowest corrosion rate because it is the least susceptible to crude oil attack. This observation supports the report of [5] who worked extensively on corrosion in petroleum pipelines.

The presence of chromium and nickel in the alloyed ductile iron and silicon in mild steel forced the reactive ions (anodic potential) to become passive on reacting with the sulphide or oxides in the crude oil (to form e.g. silicon oxide) and hence, stops further attack. This phenomenon is indicated by the predominant dark phase on their respective micrographs (fig. 3a, c, d and e). The breaking –up and the reformation of the thin film (especially in nickel alloyed ductile iron) may be due to environmental alterations like concentration, temperature, velocity of agitation.

However, plain ductile iron shows a noticeably high corrosion rate due to vicious attack on the surface resulting in pitting corrosion as shown in the micrograph (fig. 4f). Thus; this would be the least recommended metal for application in crude oil from corrosion viewpoint.

2. CONCLUSION

1. The rate of corrosion decreased with increase in the number of days of exposure for all the coupons.
2. Plain ductile iron shows the lowest corrosion resistance in mildly agitated crude oil.

5. REFERENCES

[1]. Aigbodion, V.S., Mohammed, O.Y., Yakubu, S.I. and Agunsoye, J.O. 2007. **Corrosion Characteristics of Vanadium Alloyed Ductile Cast Iron in Nitric Acid.** Journal of Applied Sciences Research, 4(10): 1267-1271.

[2]. William D. Calister Jr. 2003. Materials Science and Engineering : An Introduction. John Wiley & Sons, Inc. New York.

[3]. Khana O.P. 2009. Materials Science and Metallurgy; Dhanpet Rai and Sons Publication, New Delhi.

[4]. **Afolabi A.S. 2007. Corrosion and Stress Corrosion Behaviors of Low and Medium Carbon Steels in Agro-Fluid** Journal of Practices and Technologies, Issue 10. Pp. 55-66.

[5]. Badmos, A.Y, Ajimotakan, H.A and Emmanuel, E.O. 2009. Corrosion in Petroleum Pipelines. New York Science Journal 2(5): 36 - 40.

[6]. Lawal, A.I. 2005. Corrosion of Carbon Steel in Natural and Packed Orange Juice. B. Eng. Thesis, Department of Mechanical Engineering, University of Ilorin, Nigeria

[7]. Osarolube, E., Owate, I.O. and Oforka, N.C. 2004. The Influence of Acidity Concentrations on Corrosion of Copper and Zinc. Journal of Corrosion Science and Technology, 1(1): 66-69.

[8]. Ovri, J. E. and Ofeke, T.B. 1998. The Corrosion of Mild Steel in Marine Environment. Journal of Science Engineering Technology, 5(2): 1117-1129

[9]. Gregory, O. W. 2004. Corrosion Resistance of Copper and Brass in Various Media. Journal of Corrosion Science and Technology, 1(1): 58-60.

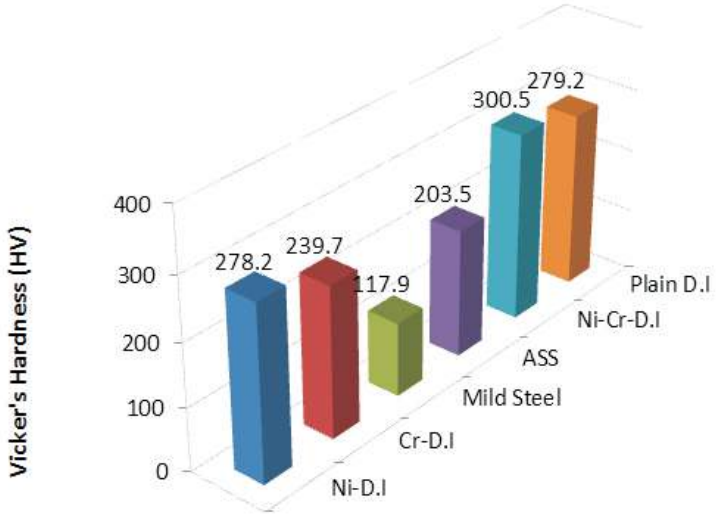


Fig. 1: graph showing the hardness properties of some selected ferrous

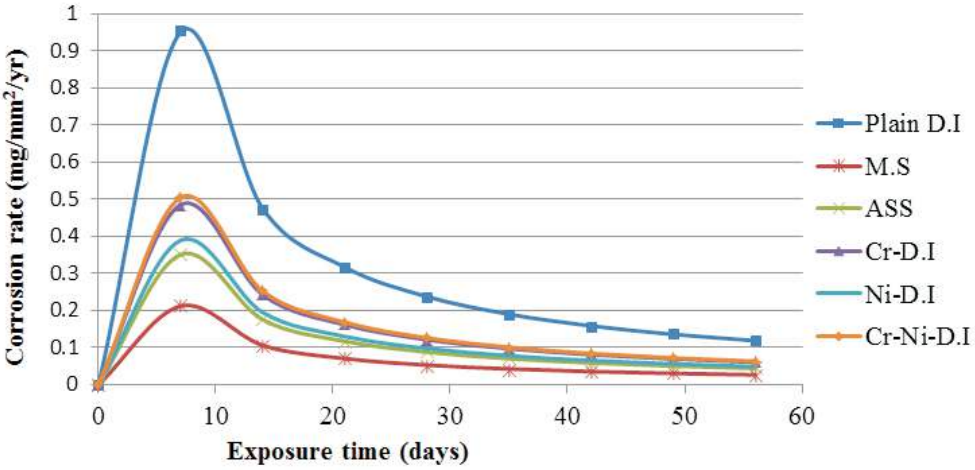


Fig. 2: combined graph showing the corrosion behavior of ductile irons of various compositions, Mild steel and Austenitic Stainless Steel with respect to each other subjected to corrosion in crude

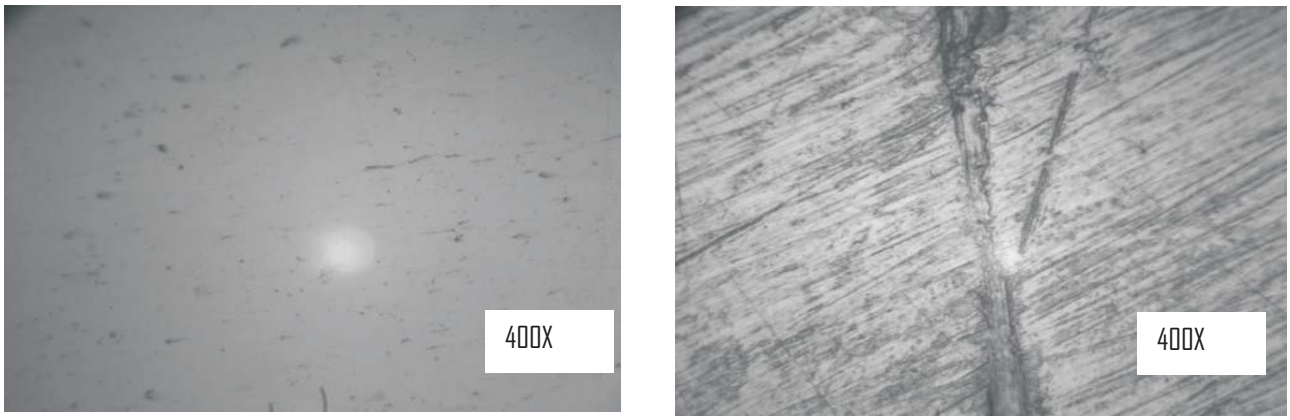


Fig. 3a: Microstructure of Austenitic Stainless Steel (a) before corrosion (LHS) and (b) after 56 days in crude oil (RHS).

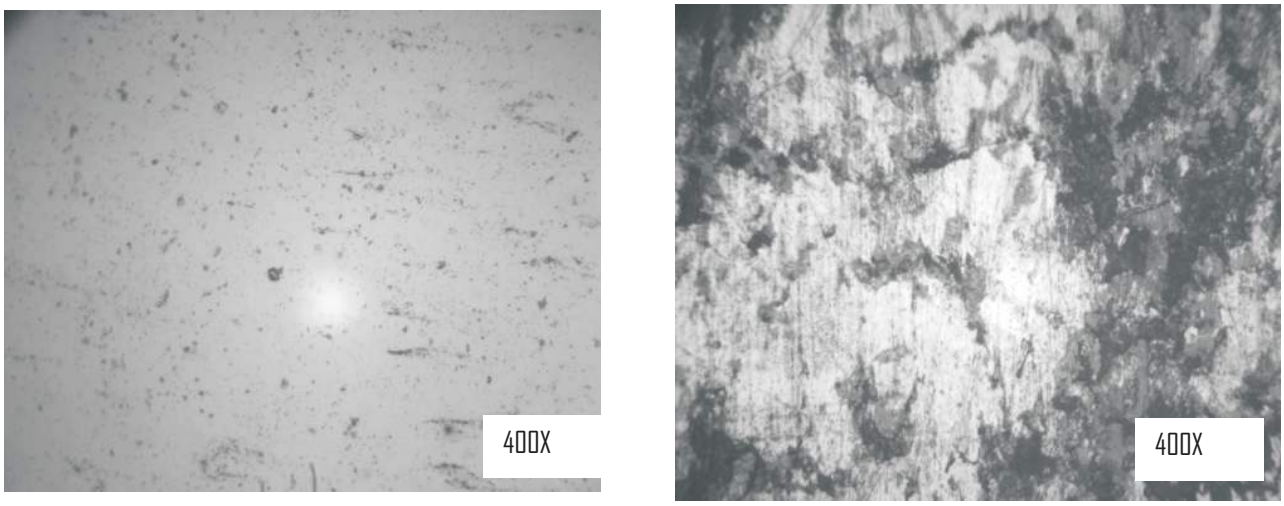


Fig. 3b: Microstructure of Mild Steel (a) before corrosion (LHS) and (b) after 56 days in crude oil (RHS).

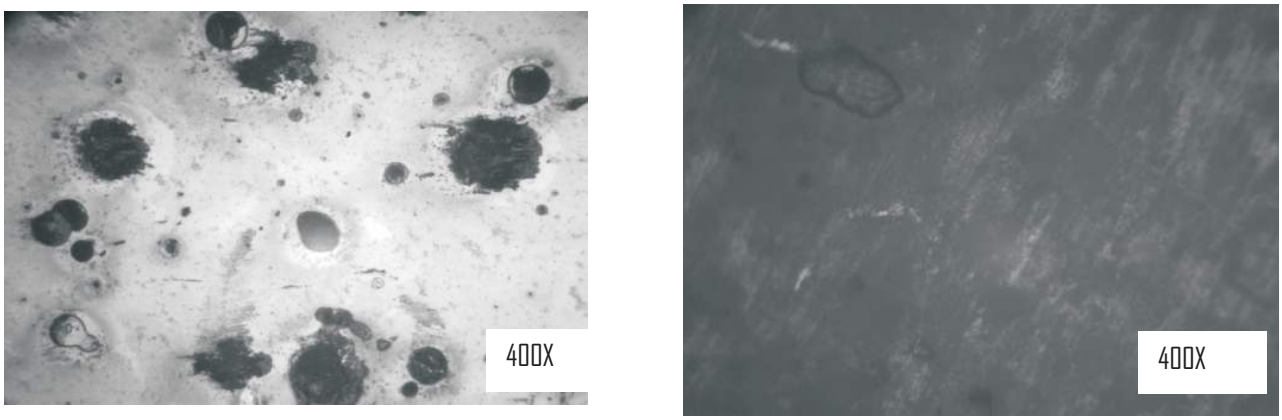


Fig. 3c: Microstructure of Chromium Alloyed Ductile Iron (a) before corrosion (LHS) and (b) after 56 days in crude oil (RHS).

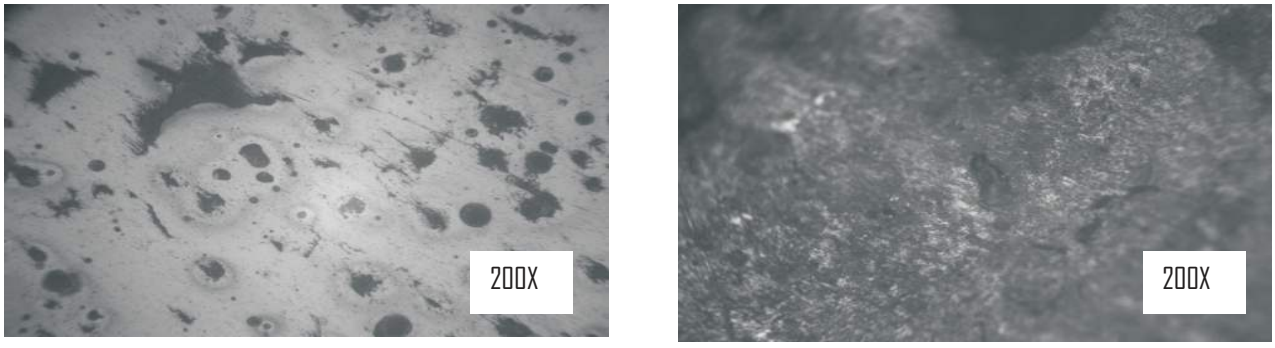


Fig.3d: Microstructure of Nickel Alloyed Ductile Iron (a) before corrosion (LHS) and (b) after 56 days in crude oil (RHS).

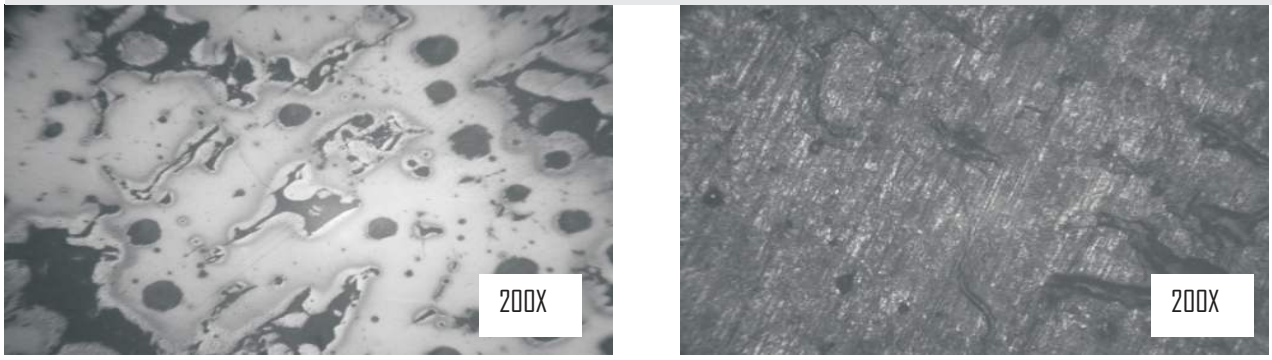


Fig.3e: Microstructure of Nickel – Chromium Alloyed Ductile Iron (a) before corrosion (LHS) and (b) after 56 days in crude oil (RHS).

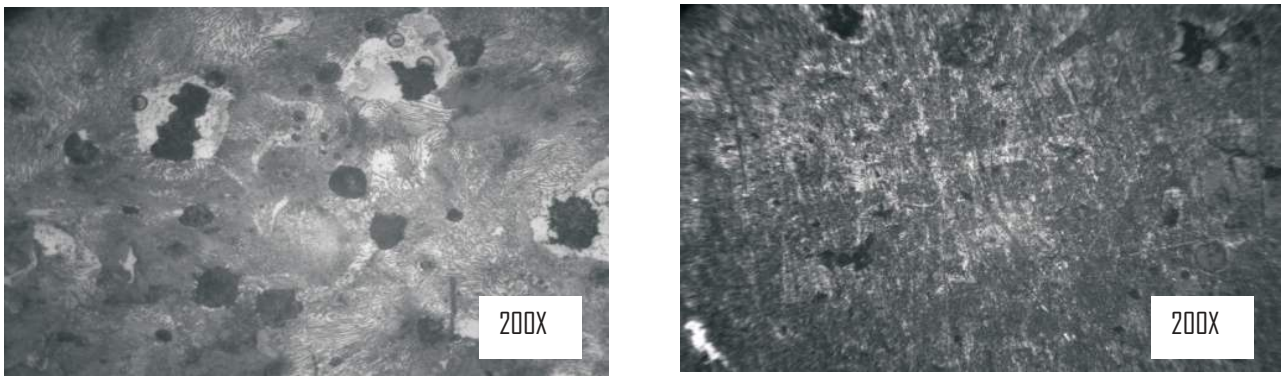


Fig.3f: Microstructure of Plain Ductile Iron (a) before corrosion (LHS) and (b) after 56 days in crude oil (RHS).

Table 1: Compositional Analysis for the Crude oil

CONTENT	CONCENTRATION (ppm)	AMOUNT (%)
Iron	0.3105	0.000776
Copper	0.2331	0.000583
Nickel	0.05678	0.00142
Sulphur	1863.85	0.1863
Carbon (in hydrocarbon)	1340	46.8

Table 3: Vicker's hardness values of the selected ferrous metals

Materials	Hardness values (HV)
Ni-DI	278.2
Cr-DI	239.7
Mild steel	117.9
ASS	203.5
Ni-Cr-DI	300.5
Plain DI	279.2

DEVELOPMENT OF ERGONOMIC CABINET FOR DISABLE PERSON

*Ukoba, O.K; Olunlade, B.A; Olubayode, S.A; Idowu, A.S; Aigbogun, O.J; and Oyegunwa, O.A
Engineering Materials Development Institute, Akure
*E-mail: ukobaking@yahoo.com

ABSTRACT
Physically challenged persons are found everywhere in the society but the difficulties experienced in the course of performing personal duties either in the office or house chores on their own has become a source of concern to all sundry. This necessitated the need to design a cabinet that can be accessible and within the reach of these group of individuals. Using anthropometric data of disabled army personnel (since it cut across individuals of different race), a mobile cabinet (that can be used either domestically or in the office) was designed and simulated to reduce the difficulty experienced by these individuals. The cabinet consists of one step with different segment and can travel up and down using a push-button to control the movement.
Keyword: Disable person, mobile cabinet, analysis, ergonomics

INTRODUCTION

According to Encarta, 2009 disability is said to make somebody unable to perform the activities needed to earn a living or carry out the basic tasks of daily life without difficulty.
A comprehensive study was conducted on U.S. Army personnel (Gordon et al., 1989). Although over 200 dimensions were measured on a group of 9,000 ethnically diverse soldiers. The result is shown in table below. According to 234next (2011) there are over 19millions living with disability in Nigeria. They 234next (2011) also stated that this group of person complain that they are not consider when constructing public structures and buildings and the likes.
Ergonomics is the scientific discipline which concerned with the understanding of the interactions among humans and other elements of a system, and the profession that applies theory principles, data, and methods to design in order to improve human well-being and optimize overall system performance (International Ergonomics Association, 2000). The objectives of ergonomics are those of achieving functional effectiveness of whatever, physical equipment or facilities people use and of maintaining or enhancing human welfare or well-being (such as health, safety, and satisfaction) by appropriate design of equipment, facilities and environments (Adekoya, 1999).

GOALS OF ERGONOMICS: the goal of ergonomics is to reduce stress and eliminate injuries and disorders associated with the overuse of muscles, bad postures, and repeated tasks. This is accomplished by designing.
DOMAIN OF ERGONOMICS: Derived from the Greek ergon (work) and nomos (laws) to denote the scientific of work, ergonomics is a discipline, which now applies to all aspects of human activity. The domains are:·

* Physical Ergonomics: it is concerned with human anatomical, anthropometric, physiological and biomechanical characteristics as they relate to physical activity. The relevant topics include working postures, materials handling, repetitive movements, work – related musculoskeletal disorders, workplace layout, safety and health.

· Cognitive Ergonomics: it is concerned with mental processes, such as perception, memory, reasoning, and motor response, as they affect interactions among humans and other system. The relevant topics include mental workload, decision-making, skilled performance, human – computer interaction, human reliability, work stress and training as these may relate to human – system design.

· Organizational Ergonomics: it is concerned with the optimization of sociotechnical systems, including their organizational structures, policies, and processes. The relevant topic include communication, crew resource management, work design, design of working times, teamwork, participatory design , community ergonomics, cooperative work, new work paradigms, organizational culture, virtual organizations, telework, and quality management.

Moving
Users will move around in their environment to file papers, the space in a cubicle or desk area should allow the chair to move around easily (Ukoba, 2010). Also, a wheelchair may need to turn around or move in the office space, requiring a 60" diameter turning radius and at least 36" of passage width.

MATERIALS AND METHOD
Anthropometrics data of physically challenged persons were used as the input data for this design. Also, the weight of a breakable plate was used to simulate how

much weight it can carry. The down chamber measures 3,500 by 650 mm while the top chamber (mobile part) measures 2280 by 650mm. the top chamber can travel a distance of 430mm up and down.

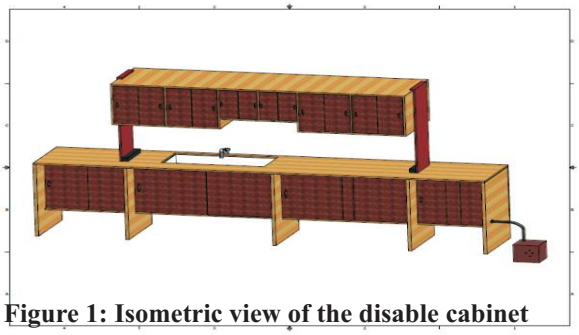


Figure 1: Isometric view of the disable cabinet

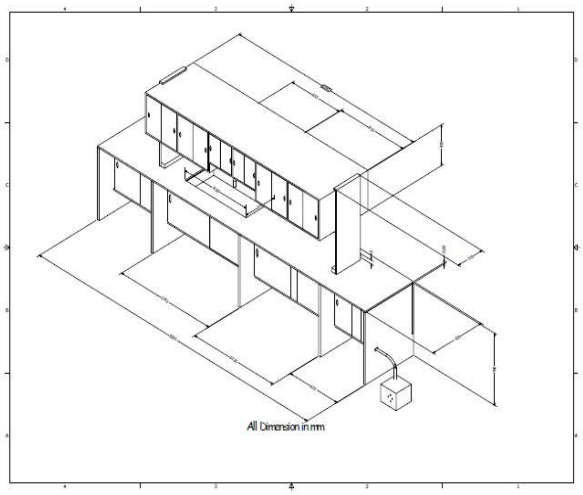


Fig 2: wire frame Isometric view showing the dimensions of the cabinet

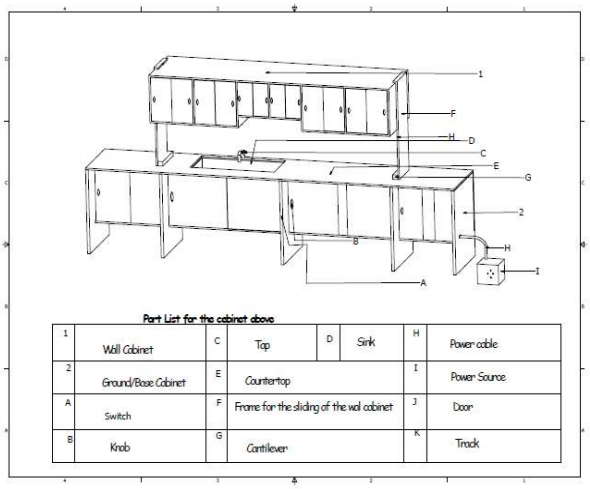


Fig 3: The cabinet showing the part list

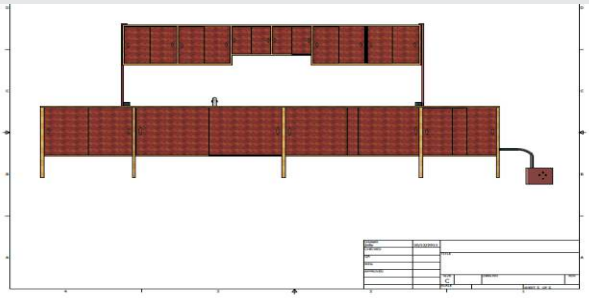


Fig 4: Front view of the disable cabinet

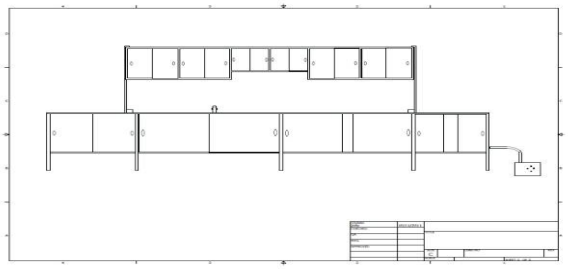


Fig 5: Wire frame Front view of the disable cabinet

Sitting

Knowing what parameters to design for while the user is seated can help increase the comfort of the user. Common seated anthropometric measurements can be seen in the Figure below:

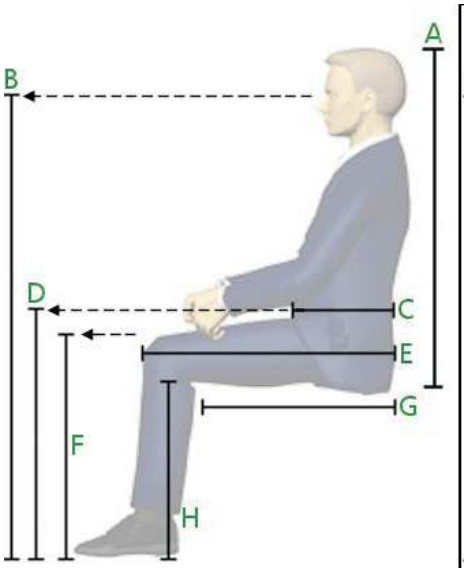


Fig 6: Sitting position

Table 1: Values for 5th to 95th percentile males and females in the seated position used in designing seating. Use Figure 3 for visualization. Data from BIFMA Ergonomics Guidelines, 2002. All measurements are in inches.

MEASUREMENT	LETTER	FEMALE	MALE	OVERALL RANGE
Sitting Height	A	31.3" - 35.8"	33.6" – 38.3"	31.3" – 38.3"
Sitting Eye Height	B	42.6" – 48.8"	46.3" – 52.6"	42.6" – 52.6"
Waist Depth	C	7.3" – 10.7"	7.8" – 11.4"	7.3" – 11.4"
Thigh Clearance	D	21.0" – 24.5"	23.0" – 26.8"	21.0" – 26.8"
Buttock-to-Knee	E	21.3" – 25.2"	22.4" – 26.3"	21.3 – 26.3"
Knee Height	F	19.8" – 23.2"	21.4" – 25.0"	19.8" – 28.0"
Seat Length/Depth	G	16.9" – 20.4"	17.7" – 21.1"	16.9" – 21.1"
Popliteal Height	H	15.0" – 18.1"	16.7" – 19.9"	15.0" – 19.9"
Seat Width	Not shown	14.5" – 18.0"	13.9" – 17.2"	13.9" – 18.0"

TABLE 2: Coefficients of Variation (CV) for Selected Anthropometric Dimensions. Samples of Persons with Disabilities and U.S. Army Males

Dimension	Persons with Disabilities			Army	Difference
	Min and Max CV	No. of Studies	Average CV		
Mass-Weight	5.5-20.4	7	11.1	14.1	-3.0
Stature-Sitting	2.9-8.3	6	6.6	3.9[2]	2.7
Shoulder Height, Sitting	6.9-11.0	4	9.3	5.0	4.3
Elbow-Rest Height	12.7-29.2	6	20.0	11.8	8.2
Thigh Clearance	18.3-33.0	4	22.7	7.5	15.2
Shoulder Width	4.6-8.9	5	6.8	4.5[3]	2.3
Elbow-Elbow Breadth	4.4-13.4	5	8.7	8.0[4]	0.7
Popliteal Height	7.9-10.2	4	8.9	5.7	3.2
Buttock-Knee Length	5.4-8.0	2	6.7	4.9	1.8
Buttock-Popliteal Length	7.0-10.4	4	8.6	5.3	3.3
Hip Breadth	7.8-25.8	4	14.4	5.9	8.5

TABLE 3: Male and Female arm length

Male arm length(thumbtip reach)	Female arm length(thumbtip reach)
up to 29"	up to 26.5"
30 – 32"	28.5 – 29.5"
over 34"	over 31"

Analysis result:

Below is the analysis result carried out on the disable cabinet. A force of 13,328N (equivalent of about 42 ceramic plates or 12 reams of A4 papers) was used to simulate the process on the disable cabinet.

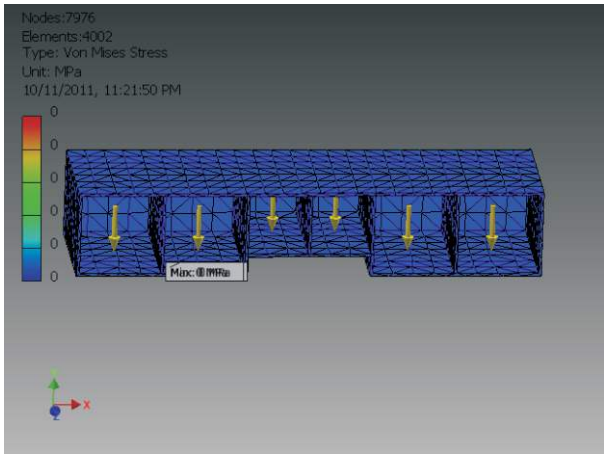


Fig 7: Von mises stress analysis of the cabinet

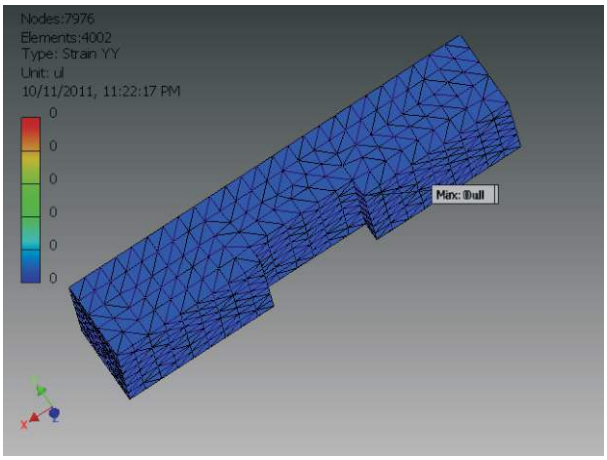


Fig 8: strain YY analysis of the cabinet

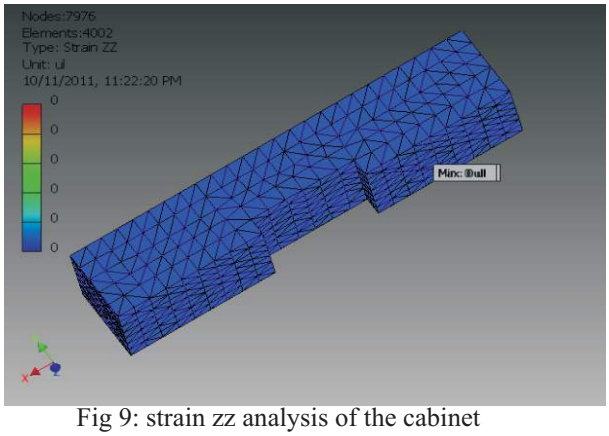


Fig 9: strain zz analysis of the cabinet

Material(s)

Name		
General	Mass Density	0.56 g/cm^3
	Yield Strength	46.6 MPa
	Ultimate Tensile Strength	5.5 MPa
Stress	Young's Modulus	9.3 GPa
	Poisson's Ratio	0.35 ul
	Shear Modulus	3.44444 GPa
Stress Thermal	Expansion Coefficient	0.0000049 ul/c
	Thermal Conductivity	0.14 W/(m K)
	Specific Heat	1200 J/(kg c)

Operating conditions

Force:1

Load Type	Force
Magnitude	13328.000 N
Vector X	0.000 N
Vector Y	-13328.000 N
Vector Z	0.000 N

Results

Reaction Force and Moment on Constraints

Constraint Name	Reaction Force		Reaction Moment	
	Magnitude	Component (X,Y,Z)	Magnitude	Component (X,Y,Z)
Fixed Constraint :1	0 N	0 N	0 N m	0 N m
		0 N		0 N m
		0 N		0 N m
Fixed Constraint :2	13328 N	0 N	51.7433 N m	-51.7433 N m
		13328 N		0 N m
		0 N		0 N m
Fixed Constraint :3	0 N	0 N	0 N m	0 N m
		0 N		0 N m
		0 N		0 N m

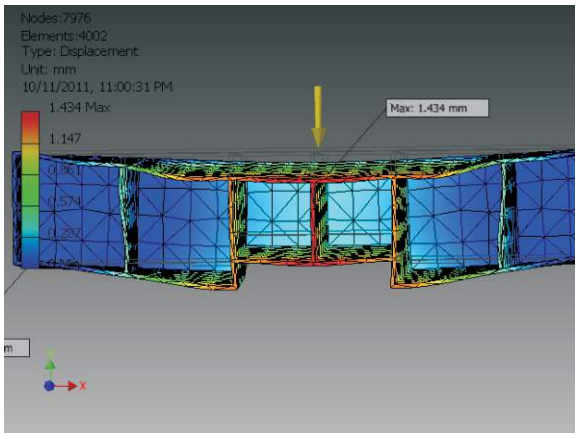


Fig 10: Displacement analysis of the cabinet

Greater than 13328N

Result Summary

Name	Minimum	Maximum
Volume	80779500 mm^3	
Mass	45.2365 kg	
Von Mises Stress	0.00028153 MPa	5.68435 MPa
1st Principal Stress	-2.04856 MPa	6.07253 MPa
3rd Principal Stress	-7.24623 MPa	2.09922 MPa
Displacement	0 mm	1.43436 mm
Safety Factor	8.19795 ul	15 ul
Stress XX	-7.00481 MPa	5.94567 MPa
Stress XY	-1.18826 MPa	1.18851 MPa
Stress XZ	-0.786259 MPa	0.770319 MPa
Stress YY	-2.58363 MPa	2.53153 MPa
Stress YZ	-0.705772 MPa	0.468993 MPa
Stress ZZ	-2.74986 MPa	2.34185 MPa
X Displacement	-0.140215 mm	0.136602 mm
Y Displacement	-1.41131 mm	0.000585282 mm
Z Displacement	-0.300056 mm	0.264274 mm
Equivalent Strain	0.0000000306873 ul	0.000560468 ul
1st Principal Strain	-0.00000480522 ul	0.000497601 ul
3rd Principal Strain	-0.000625758 ul	0.0000257028 ul
Strain XX	-0.000613933 ul	0.000490472 ul
Strain XY	-0.000172489 ul	0.000172526 ul
Strain XZ	-0.000114134 ul	0.00011182 ul
Strain YY	-0.00021965 ul	0.000211056 ul
Strain YZ	-0.000102451 ul	0.0000680796 ul

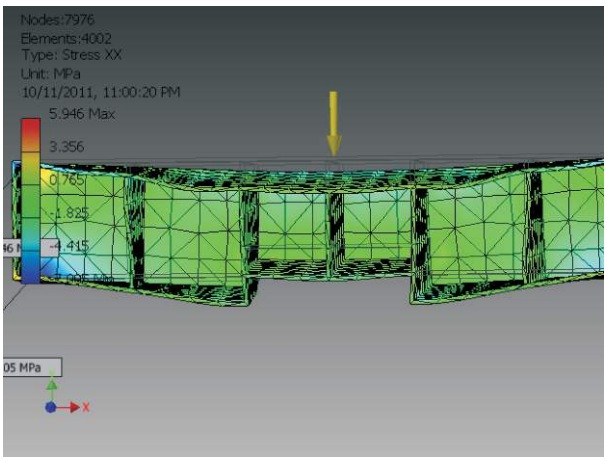


Fig 11: strain XX analysis of the cabinet

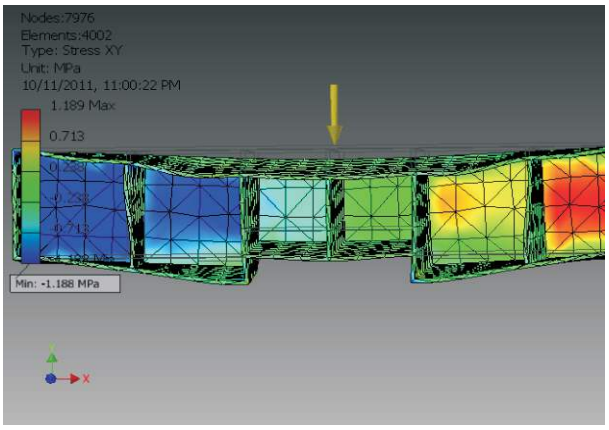


Fig 12: stress XY analysis of the cabinet

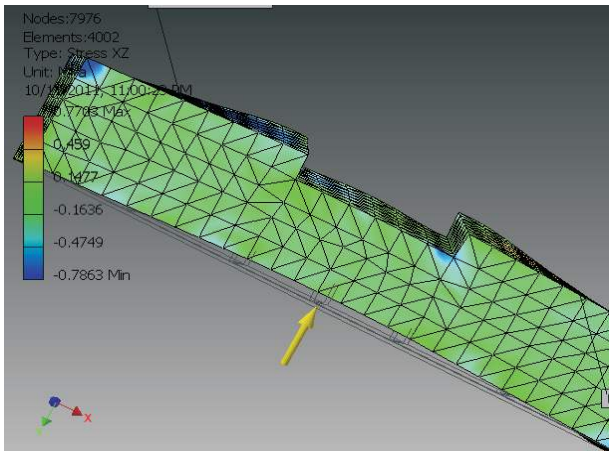


Fig 13: stress XZ analysis of the cabinet

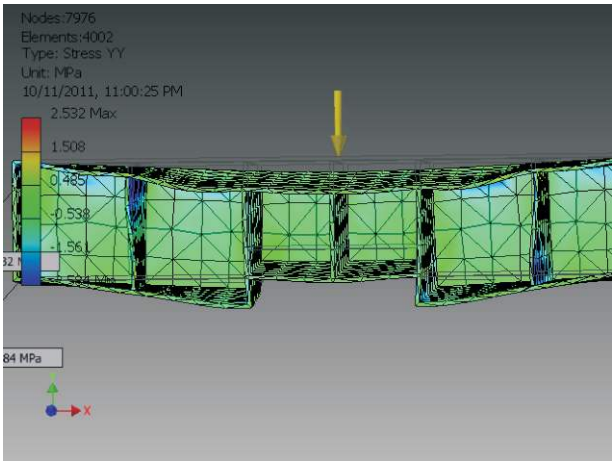


Fig 14: stress YY analysis of the cabinet

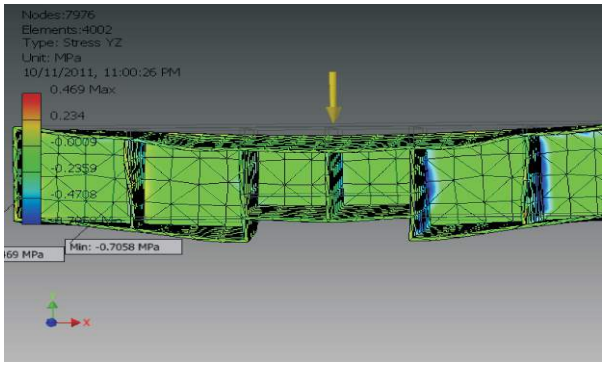


Fig 15: stress YZ analysis of the cabinet

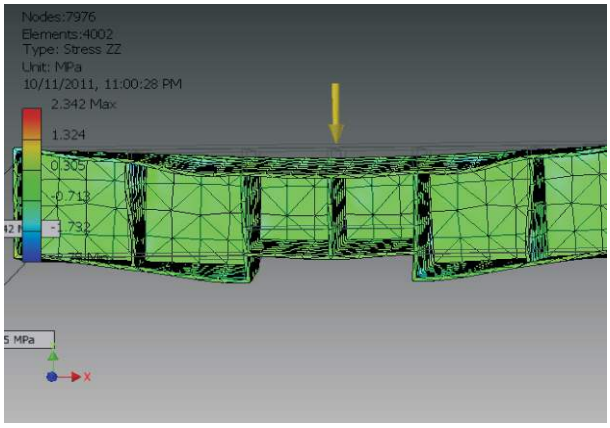


Fig 16: stress ZZ analysis of the cabinet

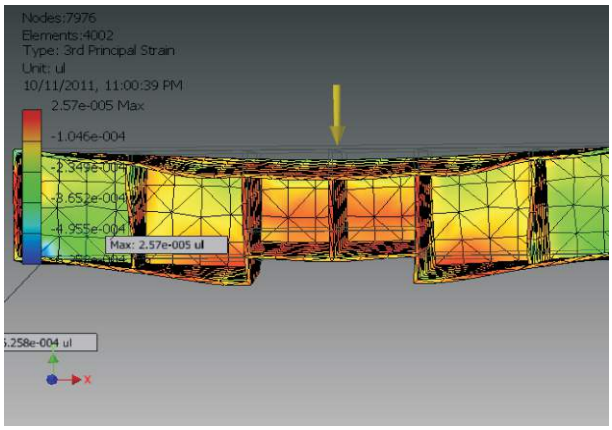


Fig 17: 3rd principal stress analysis of the cabinet

CONCLUSION/RECOMMENDATION

The cabinet has a down chamber measurement of 3,500 by 650 mm while the top chamber (mobile part) measures 2280 by 650mm. the top chamber can travel a distance of 430mm up and down.

The cabinet can carry a load to the tune of 13,380N (ie about 42 ceramic plates or 12 reams of paper) which was further confirmed from the analysis ran on the cabinet. With this work, the problem encountered by the physically challenged person in the society especially Nigeria when filing documents or doing house/kitchen chores independent will be a thing of the past.

We therefore recommend both the public and private sector to have this kind of cabinet in their offices and include it when designing and building a house that might be use by physically challenged individuals.

ACKNOWLEDGEMENT

The authors wish to thank everyone that contributed to this work especially authors that their references were used and establishments where their equipments were used.

REFERENCE

1. Adekoya LO, 1999, Human factor in Engineering Design. *Paper presented at the 1st National Engineering Design Conference organized by National Agency for Science and Engineering Infrastructure (NASENI), Nigeria Society of Engineers (NSE) and Council for the Regulation of Engineering in Nigeria (COREN), Abuja, Nigeria*
2. Allwell Okpi (2011). No city for disable persons. 234Next publishers, Lagos Nigeria.
3. Gordon CC, Bradtmiller B, Clauser CE, Churchill T, McConville JT, Tebbetts I, and Walker RA (1989) *1987-1988 Anthropometric Survey of U.S. Army Personnel: Methods and Summary Statistics.* Technical Report (TR-89-044). U.S. Army Natick Research, Development and Engineering Center, Natick, MA.
4. International Ergonomics association. What is Ergonomics website. Retrieved 6 December 2010.
5. Microsoft® Encarta® (2009). Disable. 1993-2008 Microsoft Corporation.
6. Ukoba, O.K (2010). Ergonomic Evaluation of SAAT building in Federal University Technology Akure. Paper presented as term paper for Human Factor (Ergonomics) seminar to Dr S. Peter of Mechanical Engineering department of FUTA, Nigeria

EFFECT OF SUBMERGED ARC WELDING ON CORROSION SENSITIVITY OF DUCTILE IRON

[1]Akinribide, O.J., [1]Oyelami, A.T., [1]Ogundare, O., [2]Olaosebikan, F., [1]Momoh, I.M.
Engineering Materials Development Institute, Akure.
[2]Department of Metallurgical and Materials Engineering, University of Benin
Email: akinribideojo@yahoo.com

ABSTRACT
In this work, the effect of submerged arc welding on the corrosion sensitivity of ductile iron in brackish environment was investigated. The parameters used in assessing the effect of corrosion of welded ductile iron subjected to brackish environment are the mass loss before and after immersion, equations for the correlation coefficients, and microstructure. Throughout the 42 days of exposure, the highest corrosion rate of 0.25mg/mm^2/yr was achieved for welded ductile iron compared to unwelded ductile iron with highest corrosion rate of 2.85mg/mm^2/yr after 7 days of the exposure time. Generally, it was observed that the mass loss decreases as the days of exposure increases in all the samples. However, their corresponding regression coefficients from the line equations shows that the welded sample III and unwedded sample I possess the best trend of (R^2=0.993 and 0.998) with the closest approximation to unity. This singularly made the two samples possess the most consistent decrease in mass loss and corrosion rate. The microstructure of the welded ductile iron before subjecting it into corrosion revealed some random distribution of graphite flakes in a ferrite matrix at weldment zone, while the envelopment of graphite nodules with ferrite shell at the HAZ of the welded DI Microstructures of welded ductile iron using different weld configurations after subjecting it to corrosion showed sparsely distributed flakes of graphite and intricate distribution of the carbon precipitates at the weldment zone while graphite nodules distribution of various sizes were observed at the HAZ.
Keywords: Ductile Iron, Submerged Arc Welding, Corrosion, brackish, HAZ.

1.0 INTRODUCTION

Ductile iron is not a single material, but a family of versatile cast irons exhibiting a wide range of properties which are obtained through microstructure control [6]. The most important and distinguishing microstructural feature of ductile irons is the presence of graphite nodules which act as crack-arresters and give ductile iron ductility and toughness superior to all other cast irons, and equal to many cast and forged steels [1]. The matrix in which the graphite nodules are dispersed plays significant roles in determining both corrosion properties and mechanical properties.

Matrix control, obtained in ductile irons either as-cast through a combination of composition and process control, or through heat treatment, gives the designer the option of selecting the grade of ductile iron which provides the most suitable combination of properties [4]. [5] Proposed the numerous, successful uses of ductile iron in critical components in all sectors of industry highlight its versatility and suggest many additional applications.

Ductile iron, also called nodular cast iron, is of graphite nodule structures in a matrix that could be ferritic, pearlitic, both (i.e ferritic-pearlitic), bainitic (which is strong and tough grade) or martensitic which is a strong and hard phase [9]. Ductile iron and steel are similar metallurgically; the main difference is carbon and silicon content of the materials. The nominal composition in mass fraction for unalloyed ductile iron is 3.1 to 3.9 percent carbon, 2.1 to 2.8 percent silicon, and less than 1 percent of other elements (chromium, nickel, molybdenum, and others) with the balance iron. It is the shape and distribution of the nodular carbon within the iron matrix that imparts the desired properties.

Nodule count has the following effects on microstructure, which can significantly influence both corrosion and mechanical properties of ductile iron:

1. Nodule count influences the pearlite content of as-cast ductile iron.
2. Matrix homogeneity is influenced by nodule count.
3. Nodule count affects graphite size and shape of ductile iron [4]

However, in order to increase the use of ductile cast iron as a material for industrial applications, this research focused on the effect of corrosion sensitivity of submerged arc-welded ductile iron using mild steel electrode.

2.0 MATERIALS AND METHOD

2.1 MATERIALS

The materials used in the course of this project include the ductile iron from the rotary furnace EMR 100 EMDI, mild steel electrode procured for the joining of the pairs of samples separately. The chemical composition indicates 93.52%Fe, 3.6%C, 2.5%Si, 0.007%P, 0.3%Mn, 0.01%S, 0.014%Mo, 0.05%Mg; other materials used are 2% Nital etchant solution, Acetone, consumable welding electrode. Also, commercial NaCl was procured and prepared to preselected molarity for the corrosion studies.

2.2 EQUIPMENT

The equipments used are welding machine, medium size lathe machine, Instron universal testing machine, Leco Microhardness Tester LM 700AT; Beuhler Grinding and

Polishing Machines and Optical Daheng Software-Driven Microscope No. 70290

2.3 METHOD

Machining: The Ductile Iron was machined to a standard tensile test configuration of gauge length 30mm, diameter 5.5mm. A minor-sector-like configuration specimen was also cut for the microstructural examinations. The specimens were drilled to different sizes using various sizes of drill bits to various diameters and depths (Table 1).

Welding: The drilled specimen was subsequently filled with weld using commercially available consumable electrodes. One among the tensile samples was cut into two and welded together before subjecting them to tensile evaluation.

Micrographs: The test specimens were examined using a metallurgical microscope to evaluate the degree of distribution of the phase and the matrix. Prior to this, the specimen was grit blasted with grinding papers of various grits (ranging between 60µm - 1200µm) and later polished with an emery cloth. The mirror-like surface was enhanced by the use of a diamond suspension of 1 µm. it was later etched by swabbing with 2% Nital solution before taking the photomicrograph of the specimen in a Daheng – software driven microscope.

3. RESULTS AND DISCUSION

The results are has shown in Figure 3, 4 and 5

EFFECT OF WELDING ON THE CORROSION RATE OF WELDED AND UNWELDED DUCTILE IRON IN BRACKISH ENVIRONMENT

From figure 3, it was observed that the corrosion rate of unwelded ductile iron rose sharply from the beginning to 2.85mg/mm^2/yr and gradually decreases until it begins to maintain a steady rate. In the same vein, the welded ductile iron rose sharply from the beginning to 0.35mg/mm^2/yr rate of corrosion and decrease gradually until it begins to maintain a constant rate of corrosion similar to unwelded ductile iron, all within 7 days of exposure time in brackish environment. From this illustration, it was observed that the unwelded ductile iron corroded more than the welded ductile iron.

EFFECT OF CORROSION ON THE MICROSTRUCTURE OF WELDED AND UNWELDED DUCTILE IRON

Figures 4a and 4b show the microstructures of unwelded ductile iron immersed in brackish environment at magnifications of 200 and 400. It was observed that sparsely distributed graphite nodules enveloped the ferrite shells. After exposure to brackish environment, the structure revealed some pearlite at the nodules which later were covered with corrosion products on almost the entire surface

Figures 4c and 4d show the micrographs of unwelded DI immersed in brackish environment at magnifications of 200 and 400. It revealed sparsely distributed graphite nodules at grain boundaries covered with corrosion products which are rod-like but the nodules are still in place.

Figures 4e and 4f show the microstructures of unwelded ductile iron immersed in brackish environment at magnifications of 200 and 400. It shows the distribution of graphite nodules scattered within the matrix but covered with black dots of corrosion products.

Figures 4g and 4i show the micrographs of unwelded ductile iron immersed in brackish environment at magnifications 200 and 400. It can be observed that the distribution of graphite nodules on the grain boundaries with some corrosion product.

Figures 5a and 5b show the microstructures of 13.8 mm depth and 8.7 mm diameter of welded ductile iron immersed in brackish environment at magnifications of 200 and 400. It revealed some pearlite and chilled carbide at the weldment and the heat affected zones enveloped with pitting form of corrosion product on almost the entire surface.

Figures 5c and 5d revealed the microstructure of heat affected zones and fusion zone of ductile iron welded immersed in brackish environment at a depth and diameter of 11mm and 12mm respectively at magnifications of 200 and 400. It was observed that the graphite nodules in the ferrite shell were covered with corrosion product, but the nodules are still in place.

Figures 5e and 5f show the microstructure of random distribution of graphite in a ferrite matrix at the weldment zone of welded ductile iron immersed in brackish environment with 14.6mm depth and 13mm diameter. It was observed that the random distribution of the fine ferrite at the matrix later transformed to coarse pearlite covered with some little corrosion product.

4. CONCLUSION

In the present research, the effect of corrosion on the weldment, heat affected zones and microstructure analysis of welded ductile iron was investigated using a consumable electrode in a SAW. From the results, it was observed that there was a significant increase in corrosion rate and mass loss of welded samples as time progressed. A fine graphite nodules was observed in the micrographs attacked by pitting corrosion at the weldment / fusion and heat affected zones, which pose a serious challenge to the strength of ductile iron in brackish environment.

5. REFERENCES

[1] Armentani .E, Esposito .R, Sepe .R (2007):The Effect of Thermal Properties and Weld Efficiency on Residual stresses in welding. Journal of Achievements in Materials and Manufacturing Engineering,Vol 20:319-322.

[2] Bipin K.S, Tewari S.P, Jyoti. P (2010): **A Review on Effect of arc Welding Parameters on Mechanical Behaviour of Ferrous metals/alloys.** International Journal of Engineering Science and Technology. Vol. 2(5), 2010, 1425-1432.

Corrosion control data for engineers,meeting held in august, 2011.

[3] Datta .S, Sundar .M, Bandyopadhyay .A, Nandi .G, Pal P.K, Roy .S.C (2005): Effect of Electrode Stick out on Quality and Performance of Submerged Arc Weldment Experimental and Statistical Analyses, International Conference on Mechanical Engineering , Volume AM39:1- 6.

[4] Ductile iron society meeting 26-28-2011,ductile iron data for Engineers (part 1),2011.

[5] Keshav P, Dwivedi D.K (2008): Microstructure and Tensile Properties of Submerged Arc Welded 1.25Cr-0.5Mo Steel Joints, Journal of Materials and Manufacturing Processes, Vol. 23: 463-468.

[6] Wen S.W, Hilton .P and Farrugia .D. C. J (2001): Finite Element Modeling of a Submerged Arc Welding Process. Journal of Materials Processing Technology, Vol. 119: 203-209.

[8] Viano, D.M.; Ahmed, N.U.; Schumann, G.O. (2000): Influence of Heat Input and Travel Speed on Microstructure and Mechanical Properties of Double Tandem Submerged Arc High Strength Low Alloy Steel Weldments. Journal of Science and Technology of Welding and Joining, Vol.5 :26-34..

[9] Yongyutph .P, Ghoshp .K, Guptaa .C, Patwardha .K, Satya .P (1992): Influence of Macro/Microstructure on the Toughness of'All Weld' Multipass Submerged Arc Welded C-Mn Steel Deposits, ISIJ International. Vol.32: 771-778.

FIGURES



Fig 1 :Shows the welded and unwelded samples
us



Fig.2:Shows the welded and unwelded samples immersed in brackish environment

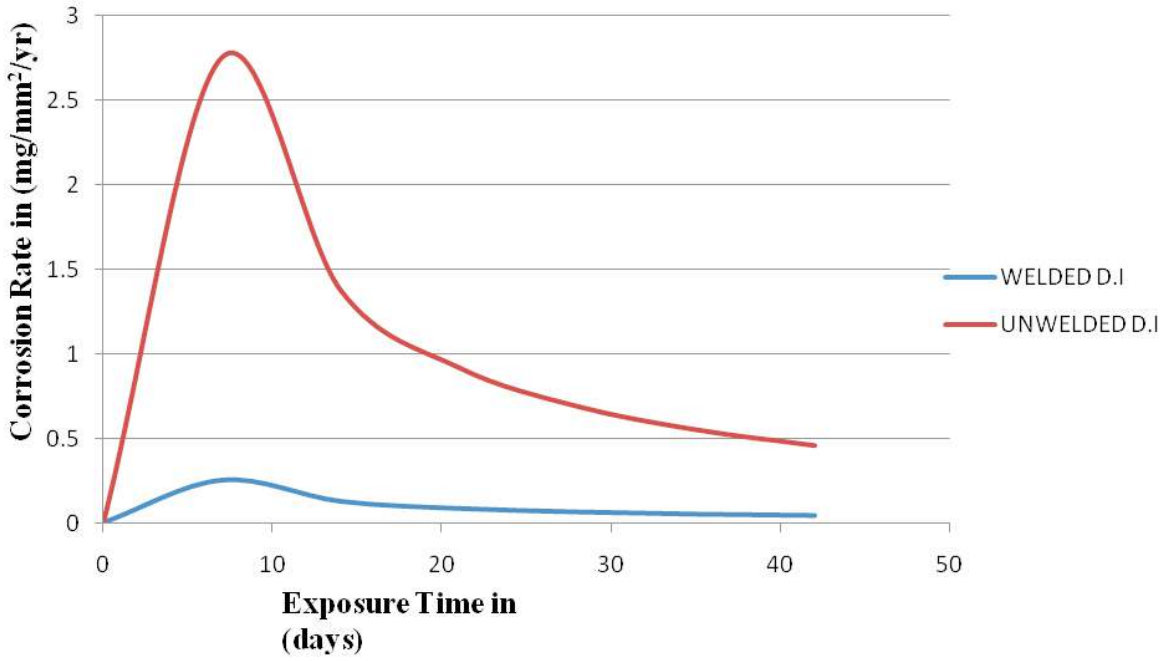


Fig 3: COMPARISON OF WELDED AND UNWELDED DUCTILE IRON IN BRACKISH ENVIRONMENT



Fig.4a: Unwelded ductile iron showing sparsely graphite nodules enveloped with ferrite shell. (400X)



Fig.4b: 13.8mm depth and 8.7mm diameter welded D.I showing the weldment, revealing graphite flakes emanating from the effect of the welding. (400X)



Fig. 4c: Welded D.I showing the HAZ revealing a densely distribution of the carbon in the form of graphite. (400X).

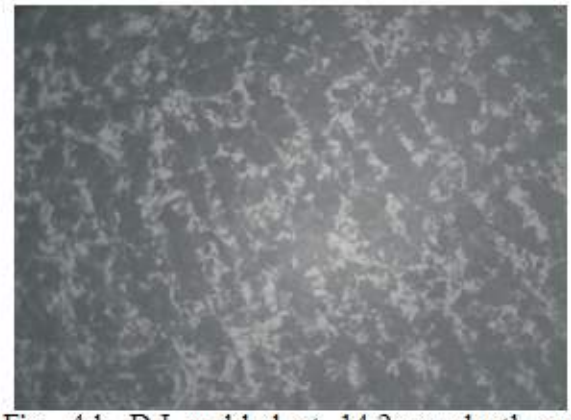


Fig. 4d: D.I welded at 14.2mm depth and 10.4mm diameter revealing densely populated graphite at the fusion zone. (400X).

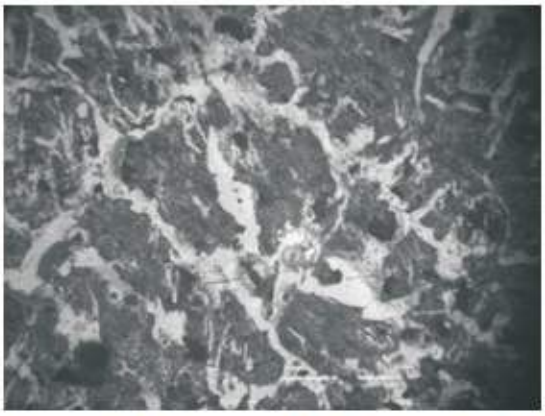


Fig. 4e: D.I welded at 14.2mm depth and 10.4mm diameter revealing sparsely distributed coarse graphite structure at the HAZ. (400X).



Fig. 4f: Weldment zone of a D.I welded at 11mm depth and 12mm diameter showing the distribution of graphite within the matrix. (400X).



Fig. 4g: HAZ of a D.I welded at a depth and diameter of 11mm and 12mm respectively showing the envelopment of graphite nodules with ferrite shell. (400X).

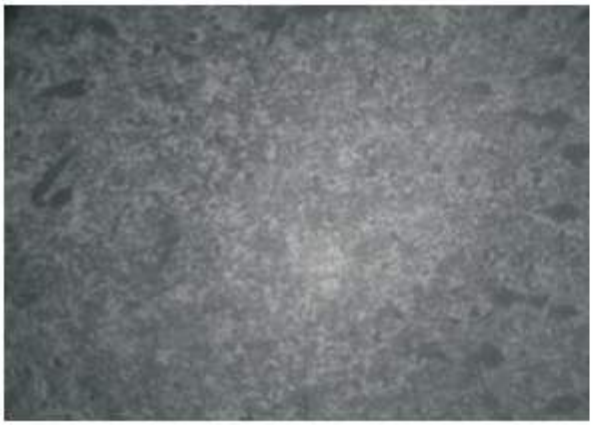


Fig. 4h: Random distribution of graphite in a ferrite matrix at the weldment zone of a D.I welded to 14.6mm depth and 13mm diameter (400 X).



Fig. 4i: HAZ showing the distribution of graphite in a D.I welded at 14.6mm depth and 13mm diameter (400X).

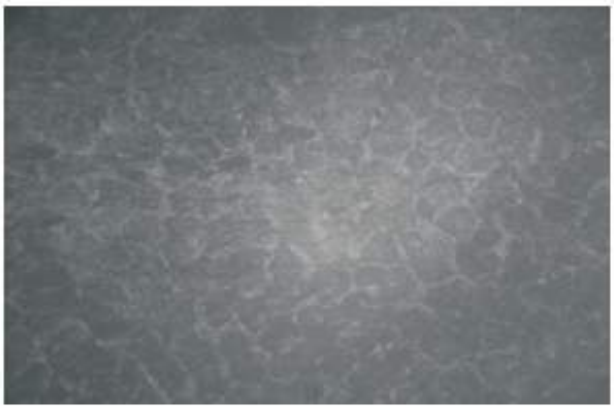
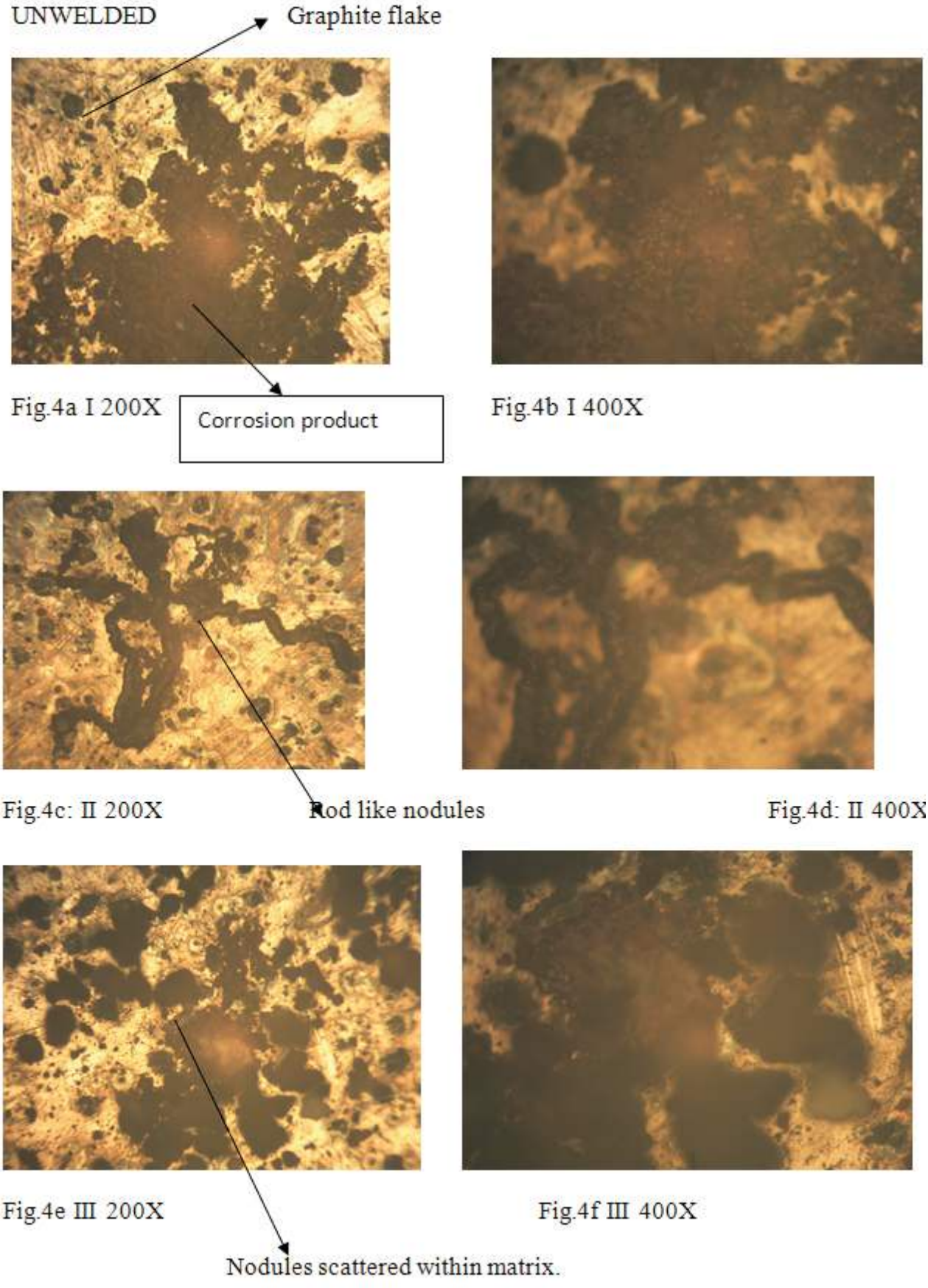


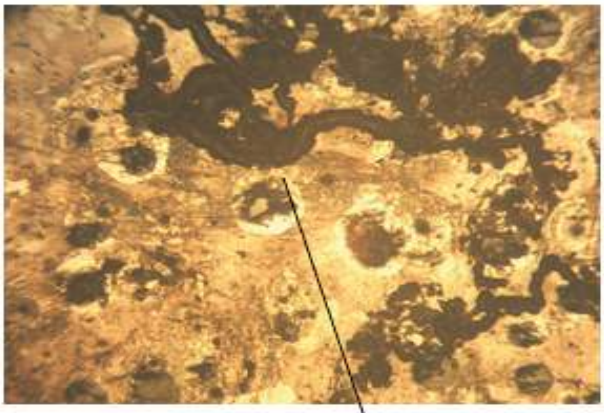
Fig. 4j: Distribution of graphite showing the grain boundaries within the matrix at the weldment zone of a D.I welded to 14.0mm depth and 16mm diameter. (400X).



Fig. 4k: HAZ showing the distribution of graphite in a D.I welded at 14.0mm depth and 16mm diameter. (400X).

Fig 4: Microstructures of welded ductile iron using different weld configurations before subjecting it to corrosion





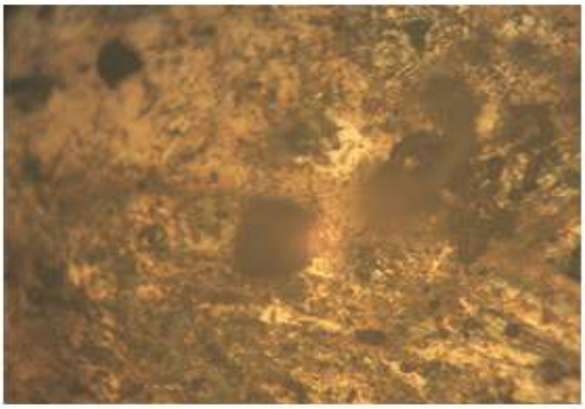
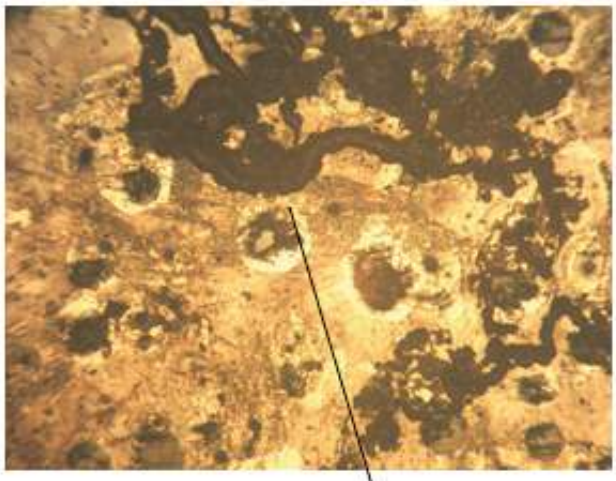


Fig.4g: IV 200X Nodules within grain boundaries Fig.4h: IV 400X



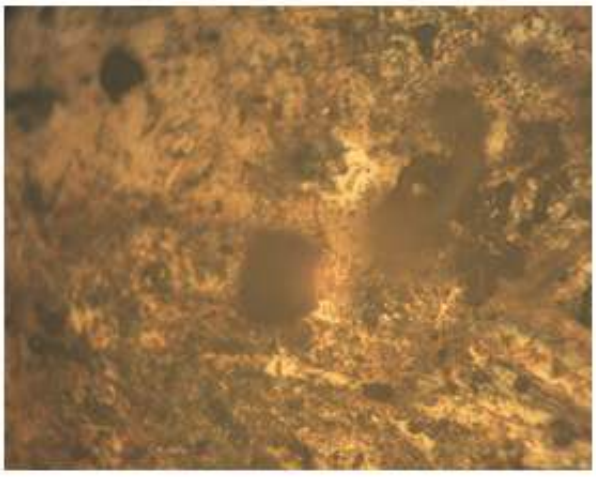
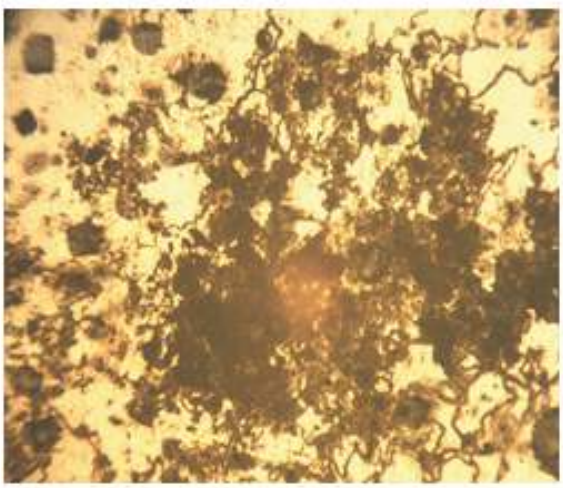


Fig.4g: IV 200X Nodules within grain boundaries Fig.4h: IV 400X



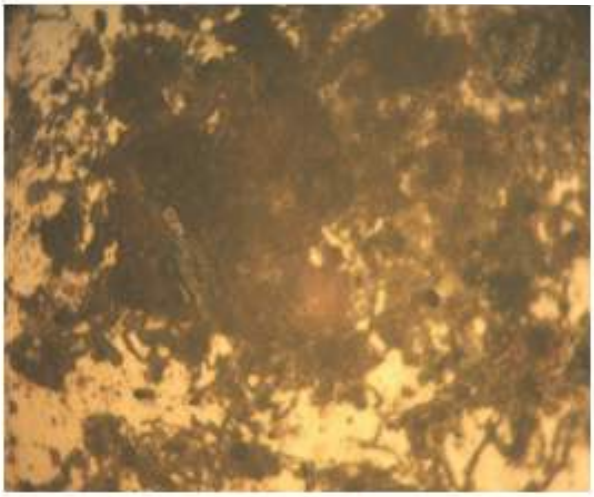


Fig.4i V 200X Fig.4j V 400X

Fig 4: Microstructure of Unwelded Ductile Iron after Immersed in Brackish Environment.

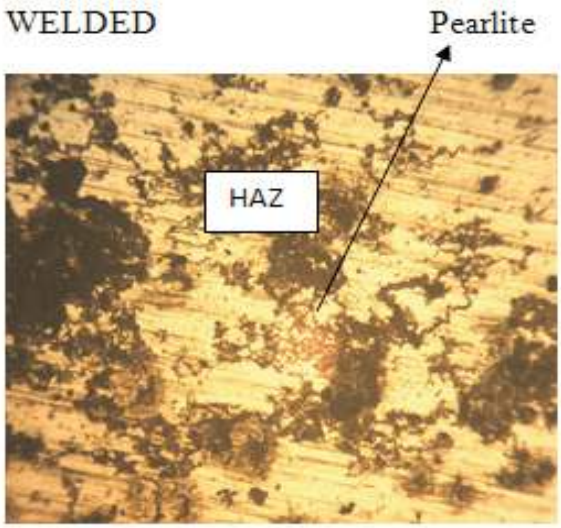


Fig.5a I 200X

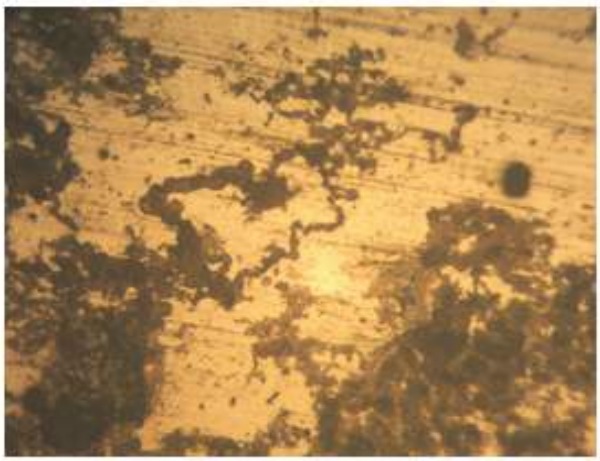


Fig.5b I 400X



Fig5c.:II 200X

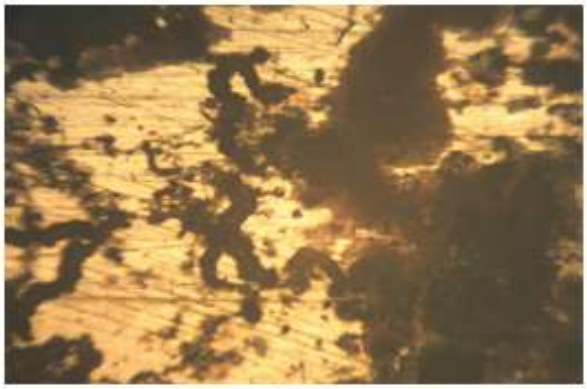


fig.5d II 400X

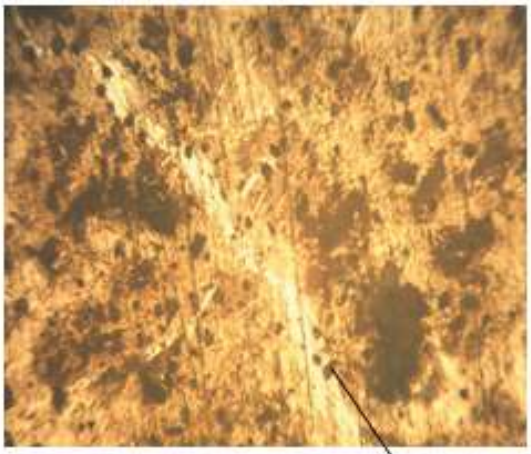


Fig.5e: IV 200X

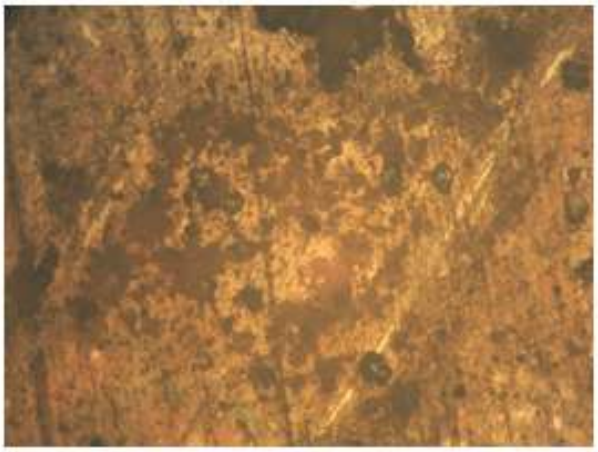


Fig.5f: IV 400X

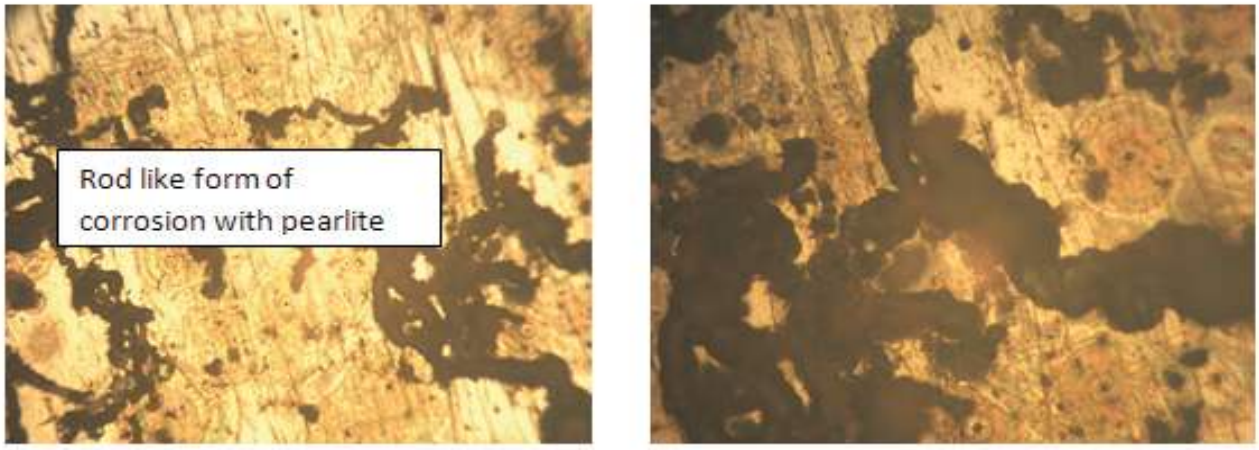


Fig.5g V 200X Fig.5h V 400X

Fig 5:Microstructure of Welded Ductile Iron after Immersed in Brackish Environment

TABLES

Table1:Sample's welding configuration

S/N	Description	Depth (mm) of the drill	Diameter (mm) of the drill
1	I	13.8	8.7
2	II	14.2	10.4
3	III	11.0	12.0
4	IIII	14.6	13.0
5	IIIII	10.0	16.0

Days	I	II	III	IIII	IIIII	tensile
0	69.440	52.651	46.398	63.162	60.998	20.891
7	69.412	52.635	46.382	63.146	60.995	20.852
14	69.375	52.601	46.350	63.122	60.969	20.833
21	69.338	52.575	46.315	63.110	60.942	20.809
28	69.308	52.545	46.295	63.077	60.894	20.788
35	69.273	52.522	46.259	63.058	60.870	20.766
42	69.035	52.354	46.108	62.856	60.668	20.675

PROGRAMMING AND COMMUNICATION IN FACTORY AUTOMATION USING PROGRAMMABLE LOGIC CONTROLLER

*Oyelami, A.T. and Ogunkoya, A.K.

Engineering Materials Development Institute, Km4 Ondo Road, P.M.B 611 Akure, Nigeria
*atoyelami@yahoo.com

ABSTRACT
Automatic control, automation and mechatronics all aim at, however having a somewhat different focus, the solution to control and supervision of problems arising in simple applications as well as extremely complex systems. This paper therefore attempts to review the modus operandi of **Programmable Logic Controller** which can be described as the heart of modern automation technology. In the past humans were the main methods for controlling a system. More recently electricity has been used for control and early electrical control was based on relays. These relays allow power to be switched on and off without a mechanical switch. It is common to use relays to make simple logical control decisions. The development of low cost computer has brought the most recent revolution, the Programmable Logic Controller (PLC). PLC or programmable controller is a digital computer used for automation of electromechanical processes. PLCs are used in many industries and machines, such as packaging and semiconductor machines. Unlike general-purpose computers, the PLC is designed for multiple inputs and output arrangements, extended temperature ranges, immunity to electrical noise, and resistance to vibration and impact. Programs to control machine operation are typically stored in battery-backed or non-volatile memory. A PLC is an example of a real time system since output results must be produced in response to input conditions within a bounded time, otherwise unintended operation will result.

Keyword: Automatic Control, Automation, Mechatronics, Programmable Logic Controller, Relays

1. INTRODUCTION

Mechatronics, automatic control, and automation and all aim at, however having a somewhat different focus, the solution to control and supervision of problems arising in simple applications as well as extremely complex systems [6]. Mechatronics are often understood by the synthesis of electronics, computers and mechanics while in automation, principles for the synthesis and analysis of computerized systems for control and supervision are studied [2].

The programmable logic controller has made a significant contribution to factory automation [5]. Earlier automation systems had to use thousands of individual relays and cam timers, but all of the relays and timers within a factory system can often be replaced with a single programmable logic controller [2]. Today, programmable logic controllers deliver a wide range of functionality, including basic relay control, motion control, process control, and complex networking, as well as being used in Distributed Control Systems [4].

Digital signals yield an "on" or "off" signal, which the programmable logic controller sees as Boolean values. Analog signals may also be used, from devices such as volume controls, and these analog signals are seen by the programmable logic controller as floating point values. There are several different types of interfaces that are used when people need to interact with the programmable logic controller to configure it or work with it [5]. This may take the form of simple lights or switches or text displays, or for more complex systems, a computer of Web interface on a computer running a Supervisory Control and Data Acquisition (SCADA) system [1].

2. OVERVIEW OF AUTOMATION

Mechatronics

Mechatronics could be defined as the synergistic combination of mechanical engineering, electronics engineering and software engineering (or informatics); and this makes handling of automated and networked systems possible [7]. Mechatronics is the perfect tool to transfer the know-how of the interfaces between the single technologies of; mechanical engineering; electronics engineering and informatics engineering [3] as illustrated in figure 1.The basic trainings required for the full understanding and application of Mechatronics are; Mechanics, Electrics/Electronics, Pneumatics, Hydraulics, Sensorics, Controllers, Robotics, Computer Aided Design /Computer Aided Manufacturing /Computer Numerically Control and Information Technology [1]. The technological parts which mechatronics handles are Factory automation and Process automation.

Factory Automation in the Industry

Factory automation is the handling of specific solid workpieces through-out the production steps of industrial processes. Specific workpieces imply that in each step of the process, the shape, dimension, colour, and orientation of the material are known and clearly defined so that the devices are designed according to those definitions [4]. **In the scope of industrialization, factory automation is a step beyond mechanization, while mechanization**

provided human operators with machinery to assist them with the muscular requirements of work, automation greatly decreases the need for human sensory and mental requirements as well [8].

Process Automation in the Industry

Process Automation deals with the handling of all flowing materials, such as fluids, gas or powdery material, processes i.e. the production, transportation, treatment and disposal [4]. Mostly closed loop controllers are used within the Process Technology to control pressure, level, flow, temperature, ph-level and ratio/mixture. Process automation is applicable in various industrial sectors such as; Water and waste water treatment; Petrol and Petrochemical Industry; Pharmaceutical and cosmetical Industry; Agro Industries – Food, Wood, Textile, Leather; Power generation and Recycling among others.

Programmable Logic Controller (PLC)

A programmable logic controller (PLC) or programmable controller is a digital computer used for automation of electromechanical processes, such as control of machinery on factory assembly lines [5]. The main difference from other computers is that PLCs are armored for severe conditions (such as dust, moisture, heat, cold) and have the facility for extensive input/output (I/O) arrangement which connect the PLC to sensors and actuators. On the actuator side, PLCs operate electric motors, pneumatic or hydraulic cylinders, magnetic relays, solenoids, or analog outputs. The input/output arrangements may be built into a simple PLC, or the PLC may have external I/O modules attached to a computer network that plugs into the PLC.

Importance of Programmable Logic Controller (PLC)

Programmable Logic Control is important because all production processes go through a fixed repetitive sequence of operations that involve logical steps and decisions [3]. A PLC is used to control, time and regulate sequence. Originally, a logical control system was "hard-wired" using electronic relays, timers and logical units. Once a "hard-wired" logic system had been constructed and a machining schedule was altered for another type of product, the logic control system had to be manually rewired for the new application, this was inflexible and time consuming [1]. It restricted the production scheduling of a factory and made changing of products difficult. It is however easy to perform switching, time delays and logic in computer programs. A computer program is also easy to change when the control problem changes and allows many more logical functions than are possible with hardwired logic controls. The microcomputer based PLC is a robust, reliable instrument with many functions and features.

From figure 2, the PLC has four main units namely:

a) The Programmable Memory – the instructions for the logical control sequence are stored here

b) The Data Memory – the status of switches, interlocks, past values of data and other working data are stored here

c) The output devices – these are hardware/software drivers for the industrial process actuators, such as solenoid switches, motors and valves

d) The input devices – these are hardware/software drivers for the industrial process sensors such as switch status sensors, proximity detectors, interlock settings etc

e) In addition to these, the PLC has a programming unit. This is either a special module, a PC connected to the PLC by the serial link or both

Programmable Logic Controller (PLC) Connections

I. From figure 3,when a process is controlled by a PLC it uses inputs from sensors to make decisions and update outputs to drive actuators, as shown in Figure 3. The process is a real process that will change over time.

II. Actuators will drive the system to new states (or modes of operation). This means that the controller is limited by the sensors available, if an input is not available, the controller will have no way to detect a condition.

Initial Programmable Logic Controller (PLC) Programming Language

I. The original programming language of PLC is Ladder Logic. The reason is because ladder logic was developed to mimic relay logic which used to be configured through "hard-wired" using electronic relays, timers and logical units.

II. The decision to use the relay logic diagrams was a strategic one. By selecting ladder logic as the main programming method, the amount of retraining needed for engineers and trades people was greatly reduced**.**

Complete Programmable Logic Controller (PLC) Programming Languages

The languages consist of two textual and two graphical versions as shown in figure 4:

a. Textual: Instruction List (IL), Structured Text (ST)

b. Graphical: Ladder Diagram (LD) and Function Block Diagram (FBD)

All the four languages are interlinked. They provide a common suite, with a link to existing experience. In this way they also provide a communication tool, combining people of different background. The choice of programming language is dependent on: the programmers' background; the problem at hand; the level of describing the problem; the structure of the control

system and the interface to other people / departments.

Programming with Function Block Diagram (FBD)

A function block diagram is a diagram that describes a function between input variables and output variables. It also described as a set of elementary blocks. Input and output variables are connected to blocks by connection lines. An output of a block may also be connected to an input of another block. Inputs and outputs of the blocks are wired together with connection lines, or links. Single lines may be used to connect two logical points of the diagram:

a. An input variable and an input of a block

b. An output of a block and an input of another block

c. An output of a block and an output variable

Overview of Bit Logic Instructions

Bit logic instructions work with two digits, 1 and 0. These two digits form the base of a number system called the binary system [5]. The two digits 1 and 0 are called binary digits or bits. In conjunction with AND, OR, XOR and outputs, a 1 stands for logical YES and a 0 for logical NO. The bit logic instructions interpret signal states of 1 and 0 and combine them according to Boolean logic. These combinations produce a result of 1 or 0 that is called the "result of logic operation" (RLO). There are bit logic instructions to perform the following functions:

a. AND, OR and Exclusive OR: these instructions check the signal state and produce a result that is either copied to the RLO bit or combined with it.

b. AND-before-OR Logic Operation and OR-before-AND Logic Operation

c. Assign and Midline Output. these instructions assign the RLO or store it temporarily

Result of Logic Operation (RLO)

The following instructions react to an RLO of 1:

a. S : Set Output

b. R : Reset Output

c. SR : Set Reset Flip Flop

d. RS : Reset Set Flip Flop

Other instructions react to a positive or negative edge transition to perform the following functions:

a. N : Negative RLO Edge Detection

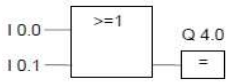
b. P : Positive RLO Edge Detection

c. NEG : Address Negative Edge Detection

d. POS : Address Positive Edge Detection

Bit Logic Instructions

a. >=1 : OR Logic Operation



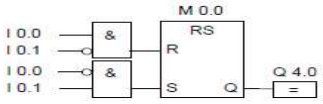
b. & : AND Logic Operation



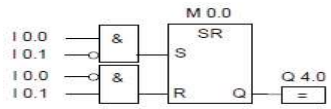
c. XOR : Exclusive OR Logic Operation



d. RS : Reset_Set Flip Flop



e. SR : Set Reset Flip Flop



CONCLUSIONS

The role of Manufacturing in the development of a nation cannot be overemphasized; factory automation systems monitor the process and production flow in a manufacturing or industrial environment. This makes process, production and manufacturing engineering more precise thereby improving the quality of goods product and enhances production time thereby reducing wastage of resources. The expertise in the area of automation is limited in Nigeria therefore; Research in this area needs to be encouraged in order to develop our manufacturing sector in Nigeria.

REFERENCES

[1] Henry Lieberman, Computer-Aided Design of user Interface by Example, Media Laboratory, Massachusetts Institute of Technology (MIT), 20 Ames st. 320G Cambridge, MA 02139(USA)

[2] Innovation (2006) Didactic, a publication of Festo Didactic GmbH & Co. KG, D-73770 Denkendorf

[3] Wolfgang Eckart (2008), Festo Didactic Training Manual Festo Didactic GmbH & Co. KG, D-73770 Denkendorf.

[4] Wolfgang Eckart and Festo Didactic GmbH & Co. KG (2008) Mechatronics Teachware: Handling description MPS Separating station, Festo Didactic GmbH & Co. KG, D-73770 Denkendorf

[5] Wikipedia, the free encyclopaedia, Programmable logic controller, retrieved on the 29th of May 2009

[6] http://www.mehatronics.rpi.edu/index.htm

[7] http://www.mechatropolis.com/defualt.asp

[8] http://www.mechtronics.uwaterloo.ca.

APPENDIX

CASE STUDY: PROGRAMMING OF A SORTING WORK STATION



The steps involved in programming the Sorting PLC are as highlighted below:

Step1: The Symbol Table

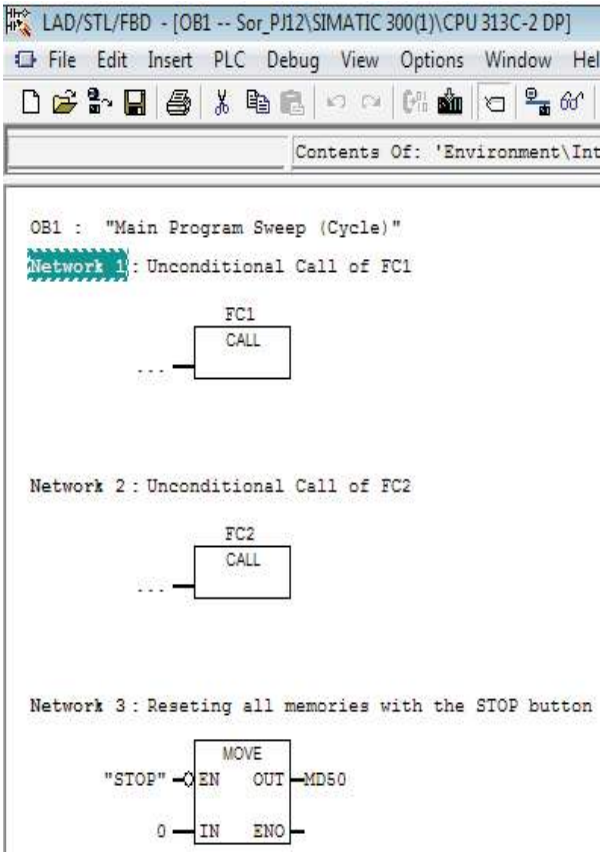
Symbol Editor - [ST Program(1) (Symbols) -- Practice1\SIMATIC 300(1)\CPU 313C-2 DP]

Symbol Table Edit Insert View Options Window Help

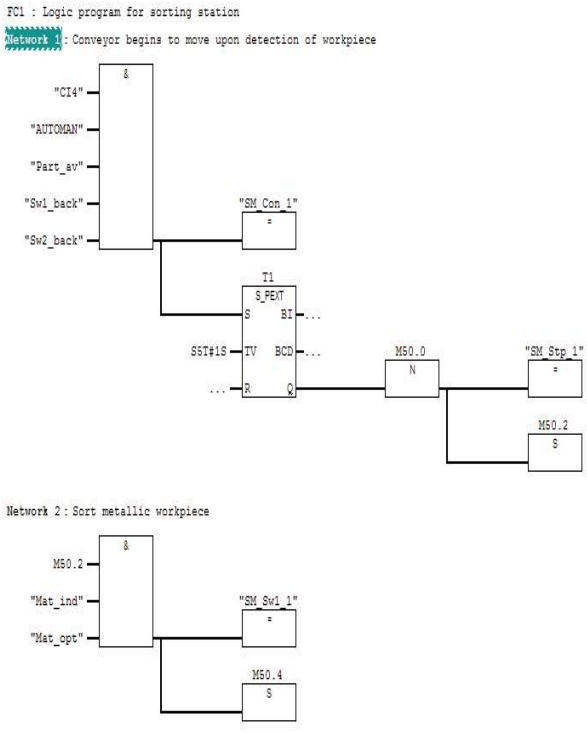
All Symbols

	Status	Symbol	Address	Data type	Comment
1		AUTOMAN	I 125.2	BOOL	Switch automatic and manual cycle
2		CI4	I 125.4	BOOL	Communication input from Handling Station
3		Conveyor	Q 124.0	BOOL	Start the conveyor motor
4		CQ4	Q 125.4	BOOL	Communication Output from the handling station
5		L_Q1	Q 125.2	BOOL	Light no. 1 special function
6		L_Q2	Q 125.3	BOOL	Light no. 2 special function
7		L_RESET	Q 125.1	BOOL	Light inside the Reset button
8		L_START	Q 125.0	BOOL	Light inside the Start button
9		Mat_ind	I 124.1	BOOL	Inductive sensor for material check
1		Mat_opt	I 124.2	BOOL	Optical sensor for material check
1		Part_av	I 124.0	BOOL	Workpiece is available
1		Previous	Q 124.7	BOOL	Light barrier to the previous station
1		RESET	I 125.3	BOOL	Reset button
1		RM_Con_1	M 2.0	BOOL	Reset memory for the conveyor motor for the 1st time
1		RM_Con_2	M 2.2	BOOL	Reset memory for the conveyor motor for the 2nd time
1		RM_Con_3	M 2.4	BOOL	Reset memory for the conveyor motor for the 3rd time
1		RM_CQ4_1	M 38.0	BOOL	Reset memory for the Communication Output for the 1st time
1		RM_CQ4_2	M 38.2	BOOL	Reset memory for the Communication Output for the 2nd time
1		RM_CQ4_3	M 38.4	BOOL	Reset memory for the Communication Output for the 3rd time
2		RM_LQ1_1	M 30.0	BOOL	Reset memory for the Light inside the Light 1 special function for the 1st time
2		RM_LQ1_2	M 30.2	BOOL	Reset memory for the Light inside the Light 1 special function for the 2nd time
2		RM_LQ1_3	M 30.4	BOOL	Reset memory for the Light inside the Light 1 special function for the 3rd time
2		RM_LQ2_1	M 34.0	BOOL	Reset memory for the Light inside the Light 2 special function for the 1st time
2		RM_LQ2_2	M 34.2	BOOL	Reset memory for the Light inside the Light 2 special function for the 2nd time
2		RM_LQ2_3	M 34.4	BOOL	Reset memory for the Light inside the Light 2 special function for the 3rd time
2		RM_LRS_1	M 26.0	BOOL	Reset memory for the Light inside the Reset button for the 1st time
2		RM_LRS_2	M 26.2	BOOL	Reset memory for the Light inside the Reset button for the 2nd time

Step2: Organization Block (OB)

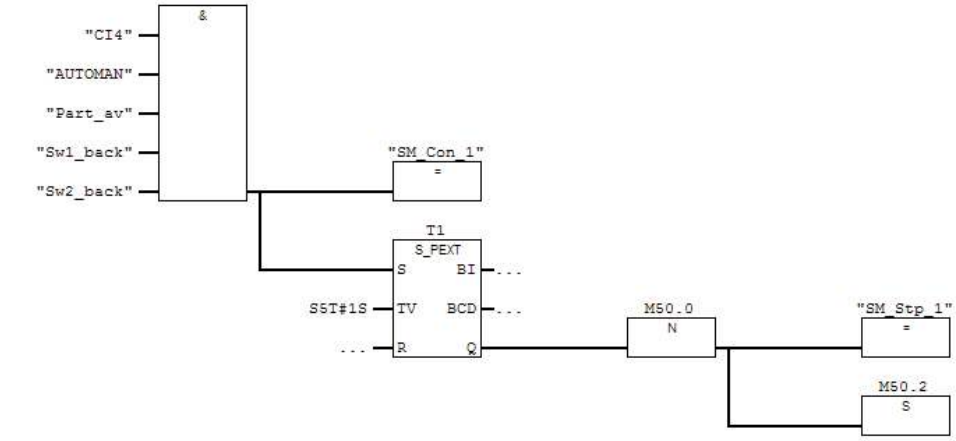


Step3: Function Fc1

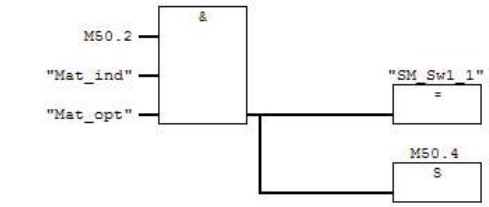


Step 4: Functional Fc2

```
FC1 : Logic program for sorting station
Network 1: Conveyor begins to move upon detection of workpiece
```




```
Network 2 : Sort metallic workpiece
```



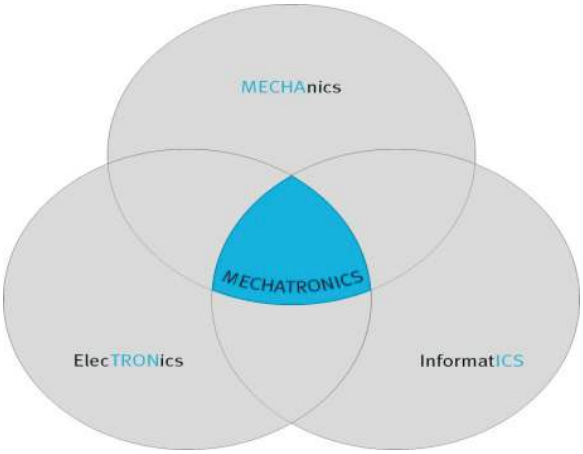


Figure1: Mechatronics Interface Between single Technologies

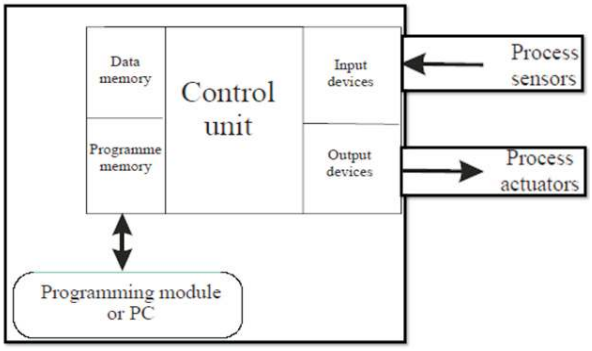


Figure2: Basic structure of a Programmable Logic Controller (PLC)

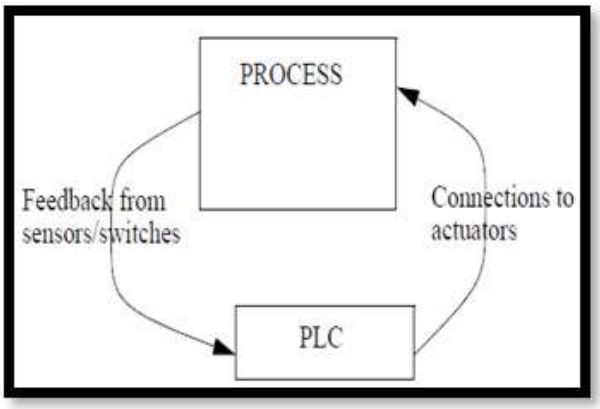


Figure 3: The Separation of Controller and Process

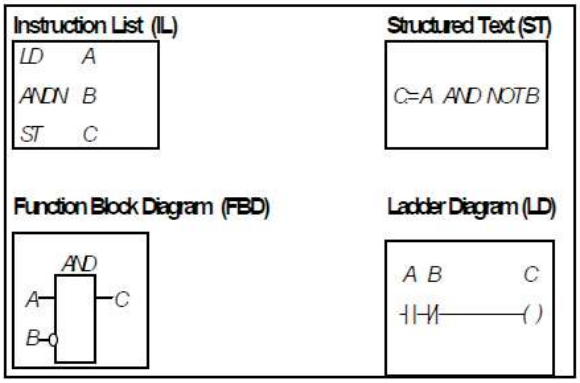


Figure4: Types of Programmable Logic Controller **(PLC) Programming Languages**

EFFECT OF SUBMERGED ARC WELDING ON MECHANICAL PROPERTIES AND MICROSTRUCTURES OF DUCTILE IRON

Momoh, I.M, Oyelami, A.T., Ogundare, O., Akinribide, O.J, and *Olaosebikan, F.
Engineering Materials Development Institute, Akure.
*Dept. of Metallurgical and Materials Engineering, University of Benin.
Email: mondayitopa@yahoo.com

ABSTRACT
In this research, ductile cast iron of composition 93.52%Fe, 3.6%C, 2.5%Si, 0.007%P, 0.3%Mn, 0.01%S, 0.014%Mo, 0.05%Mg produced in EMDI was machined, drilled, and subjected to Submerged Arc Welding (SAW) using a consumable electrodes. Six (6) samples of different configurations (diameter ranging from 8.7mm - 16.0mm and depth 10mm – 14.6mm) were taken into consideration for comparison including the unwelded sample that served as the control. The hardness, tensile property was examined and the micrographs analyzed. It was observed that the fusion zone of the welded sample exhibit a high hardness property of 525.2HV (welded sample I) and the HAZ has a peak hardness value of 486.7HV (welded sample IIIII) with reference to the control sample that has 354.6HV. The tensile property examined in the welded sample indicates a less UTS value of 102.1N/mm^2 in comparison to the control sample having 539.8 N/mm^2. The microstructure shows more graphite nodules enveloped with ferrite shells which does contributed to the enhancement of the mechanical properties considered.
Keywords: *Weld Fusion Zone, HAZ, Graphite Nodule, Weld Cracks.*

1. INTRODUCTION

Ductile iron, also called nodular cast iron, is of graphite nodule structures in a matrix that could be ferritic, pearlitic, both (i.e ferritic-pearlitic), bainitic (strong and tough) or martensitic (strong and hard) phase. The even distribution in ductile iron and the variation of the matrix structures have caused the mechanical properties of ductile iron to vary widely and have made them applicable in a wide range of industrial applications.

Ductile cast iron has a very high tensile strength and hardness. It also exhibits unique microstructures depending on the chemical composition of the cast iron, the cooling rates in production and heat treatment processes of the cast iron. Ductile iron and steel are similar metallurgically; the main difference is the carbon and silicon content of the materials. The nominal composition in mass fraction for unalloyed ductile iron is 3.1 to 3.9 percent carbon, 2.1 to 2.8 percent silicon, and less than 1 percent of other elements (chromium, nickel, molybdenum, and others) with the balance as iron – the base metal, it is the shape and distribution of the nodular carbon within the iron matrix that imparts the desired mechanical properties.

The weldability of engineering material is usually considered to be the production of a fusion welds in a manner such that the weldment does not contain injurious imperfections (more commonly described as defects when they detrimentally affect the metallurgical structure, properties and subsequent manufacturing operations). The advantages of welding, as a joining process include high joint efficiency, simple set up, flexibility and low fabrication costs [1]. Because of its high reliability, deep penetration, smooth finish and high productivity, submerged arc welding (SAW) has become a natural choice in industries for fabrication. As it is well known, the residual stresses have a strong influence on weld deformation, fatigue strength, fracture toughness and buckling strength [1, 5 and 7]. As such, SAW has been considered a very productive welding process over the years [2]. Some of the factors that determine the quality of weld are voltage, current, stick out, wire feed rate, welding speed or travel, etc. [3]

[4] While describing the Microstructure and Tensile Properties of Submerged Arc Welding in engineering materials concluded that the increase in the heat input affects the proportions of different micro constituents both in the weld fusion and heat affected zone (HAZ). He also observed that the tensile strength (UTS, YS) decreases with increase in heat input [4]. [6] discussed the influence of heat input and travel speed on microstructure and mechanical properties of double tandem submerged arc welding and concluded that increase in heat input results in a decrease in cooling rate and the widths of the different zones of the HAZ increase steadily with the increase in heat input [6]. Lots more has been researched on in the enhancement of the properties of welded ferrous material.

However, in order to expand the scope of use of ductile cast iron as a material for industrial applications, this research focus on the study of the mechanical properties of arc-welded locally produced ductile cast iron using a consumable electrode.

2. MATERIALS AND METHOD

Materials and Equipment

In the course of this research, the materials used in include: ductile iron – sourced from the foundry department of Engineering Materials Development Institute (EMDI), Akure; the chemical composition indicates 93.52%Fe, 3.6%C, 2.5%Si, 0.007%P, 0.3%Mn, 0.01%S, 0.014%Mo, 0.05%Mg; other materials used are 2% Nital etchant solution, Acetone, consumable welding electrode. The equipments used are welding machine, medium size lathe machine, Instron universal testing machine, Leco Microhardness Tester

LM 700AT; Buehler Grinding and Polishing Machines and Optical Daheng software driven microscope No. 702907.

Methods

The Ductile Iron was machined to a standard tensile test configuration and a minor sector-like configuration for hardness and microstructure evaluation. The minor sector-like samples was drilled to different sizes using various sizes of drill bits to different diameters and depths (Table 1). The drilled samples were subsequently filled with weld using commercially available consumable electrodes. One among the tensile samples was cut into two and welded together before subjecting them to tensile evaluation. A load of 490.3MN (50kg) was applied on each of the samples over a dwelling time of 10 seconds to evaluate the effect of weld on the hardness property of the specimen. A minimum of two specimens per treatment was tested for confirmation. The tensile property was also evaluated by carrying out uniaxial tensile test on the prepared samples at a strain rate of 10^{-3}/sec under a room temperature. Microstructural analysis was thereafter taken using a metallurgical microscope to evaluate the degree of distribution of the phase and the matrix. Prior to this, the samples were grinded with grinding papers of various grits (ranging between 60μm - 1200μm) and later polished with emery cloth of superfine grit. The mirror-like surface was enhanced by the use of a diamond suspension of 1 μm. it was later etched by swabbing with 2% Nital solution before taking the photomicrograph of the specimen in a Daheng – software driven microscope.

3. RESULTS AND DISCUSSION

Hardness

Figure 2 presents the Hardness values of the welded and the unwelded ductile iron of various geometries (diameter and depth of drill). It was observed that all welded specimens exhibited higher hardness values at the weld fusion zone than the control sample thus indicating a better hardness property of a welded ductile iron despite the choice of electrode used. The lower hardness value exhibited by sample III in the Heat Affected Zone could be as a result of the crack introduced during welding.

Tensile Property

Figure 1 shows the tensile configuration of the specimen. The tensile stress – strain results, when subjected to a uniaxial tensile test in Instron universal Machine at room temperature, is as shown in figure 3. The result of the control specimen (upper) and the welded sample (lower) when observed shows that the unwelded sample, which served as control, has a higher UTS value of 535 MPa and strain-to-fracture of 0.28 while the welded D.I sample has UTS value of 100 MPa and strain at 0.52. This unusual lower UTS value of the welded specimen could be attributed to inadequate joint geometry and crack initiation inherited from welding.

Micrographs

The effects of the welding on the microstructure are shown in figure 4. Observation shows that a fine graphite nodules ware formed at the welded fusion zones of some of the samples (fig 4b,d,f,h,j) while a uniformly distributed graphite flakes is formed in weld fusion zone of figure 4b giving proof for its unique high hardness values. The heat-affected zones (fig 4e,i,k) shows a coarse graphite nodules with sparsely distributed graphite flakes (fig 4c) thus justifying its relatively lesser hardness values in comparison to the weld fusion zones.

4. CONCLUSION

In the present research, the mechanical properties and microstructure analysis of welded ductile iron was investigated using a consumable electrode in a SAW. From the results, it was observed that there was a significant increase in the hardness property of the welded samples while maintaining its continuous yield in comparison with the unwelded specimen. A fine graphite nodules was observed in the micrographs at the weld fusion zones, Thus indicating that a better mechanical properties could be attain in ductile iron when subjected to SAW using a consumable electrode.

5. REFERENCES

[1] Armentani .E, Esposito .R, Sepe .R (2007): The Effect of Thermal Properties and Weld Efficiency on Residual stresses in welding. Journal of Achievements in Materials and Manufacturing Engineering,Vol 20:319-322.

[2] Bipin K.S, Tewari S.P, Jyoti. P (2010): A Review on Effect of arc Welding Parameters on Mechanical Behaviour of Ferrous metals/alloys. International Journal of Engineering Science and Technology. Vol. 2(5), 2010, 1425-1432.

[3] Datta .S, Sundar .M, Bandyopadhyay .A, Nandi .G, Pal P.K, Roy .S.C (2005): Effect of Electrode Stick out on Quality and Performance of Submerged Arc Weldment Experimental and Statistical Analyses, International Conference on Mechanical Engineering , Volume AM39:1- 6.

[4] Keshav P, Dwivedi D.K (2008): Microstructure and Tensile Properties of Submerged Arc Welded 1.25Cr-0.5Mo Steel Joints, Journal of Materials and Manufacturing Processes, Vol. 23: 463-468.

[5] Wen S.W, Hilton .P and Farrugia .D. C. J (2001): Finite Element Modeling of a Submerged Arc Welding Process. Journal of Materials Processing Technology, Vol. 119: 203-209.

[6] Viano, D.M.; Ahmed, N.U.; Schumann, G.O. (2000): Influence of Heat Input and Travel Speed on Microstructure and Mechanical Properties of Double Tandem Submerged Arc High Strength Low Alloy Steel Weldments. Journal of Science and Technology of Welding and Joining, Vol. 5 :26-34..

[7] Yongyutph .P, Ghoshp .K, Guptaa .C, Patwardha .K, Satya .P (1992): Influence of Macro/Microstructure on the Toughness of 'All Weld' Multipass Submerged Arc Welded C-Mn Steel Deposits, ISIJ International. Vol.32: 771-778.

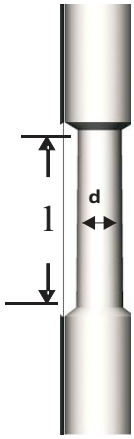


Fig. 1: Tensile Test Configuration



Plate 1: Tensile pieces for the experiment

Table 1: Specimen's Welding Configuration

S/N	Description	Depth (mm) of the drill	Diameter (mm) of the drill
1	I	13.8	8.7
2	II	14.2	10.4
3	III	11.0	12.0
4	IIII	14.6	13.0
5	IIIII	10.0	16.0

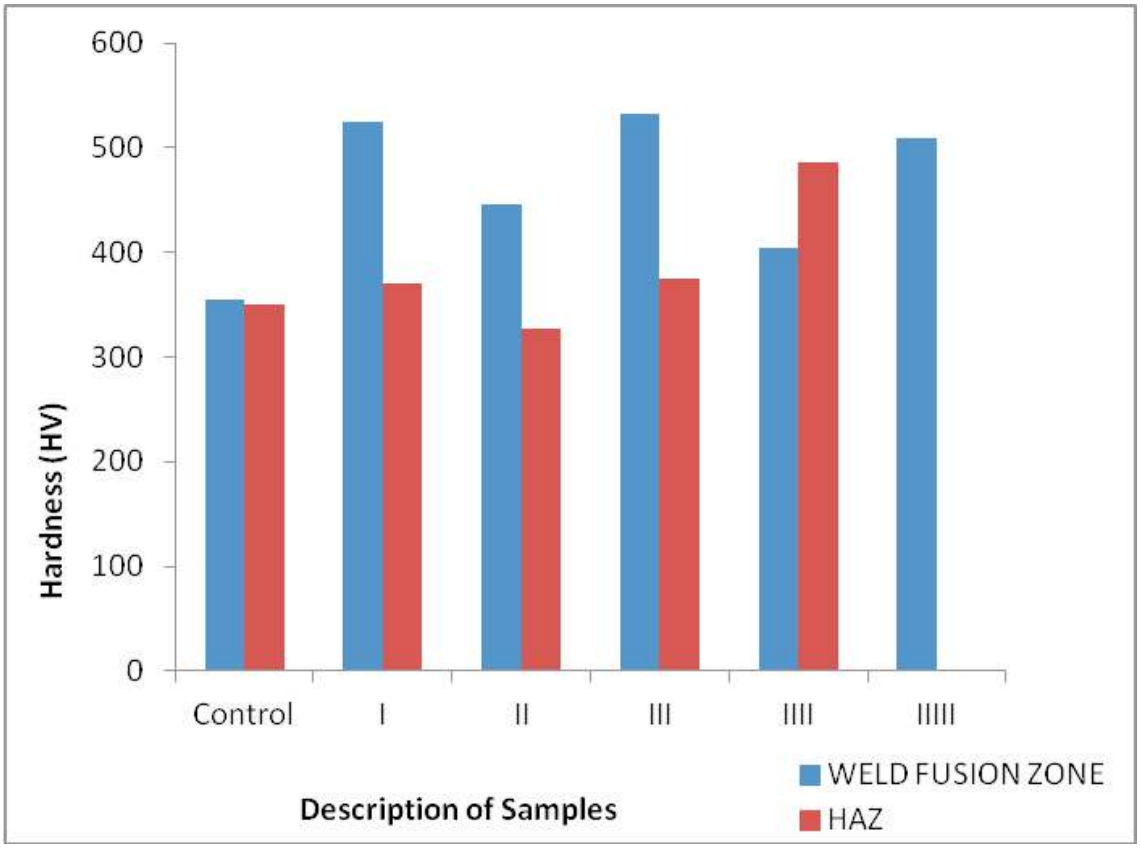


Fig. 2: Effects of SAW on Ductile Iron.

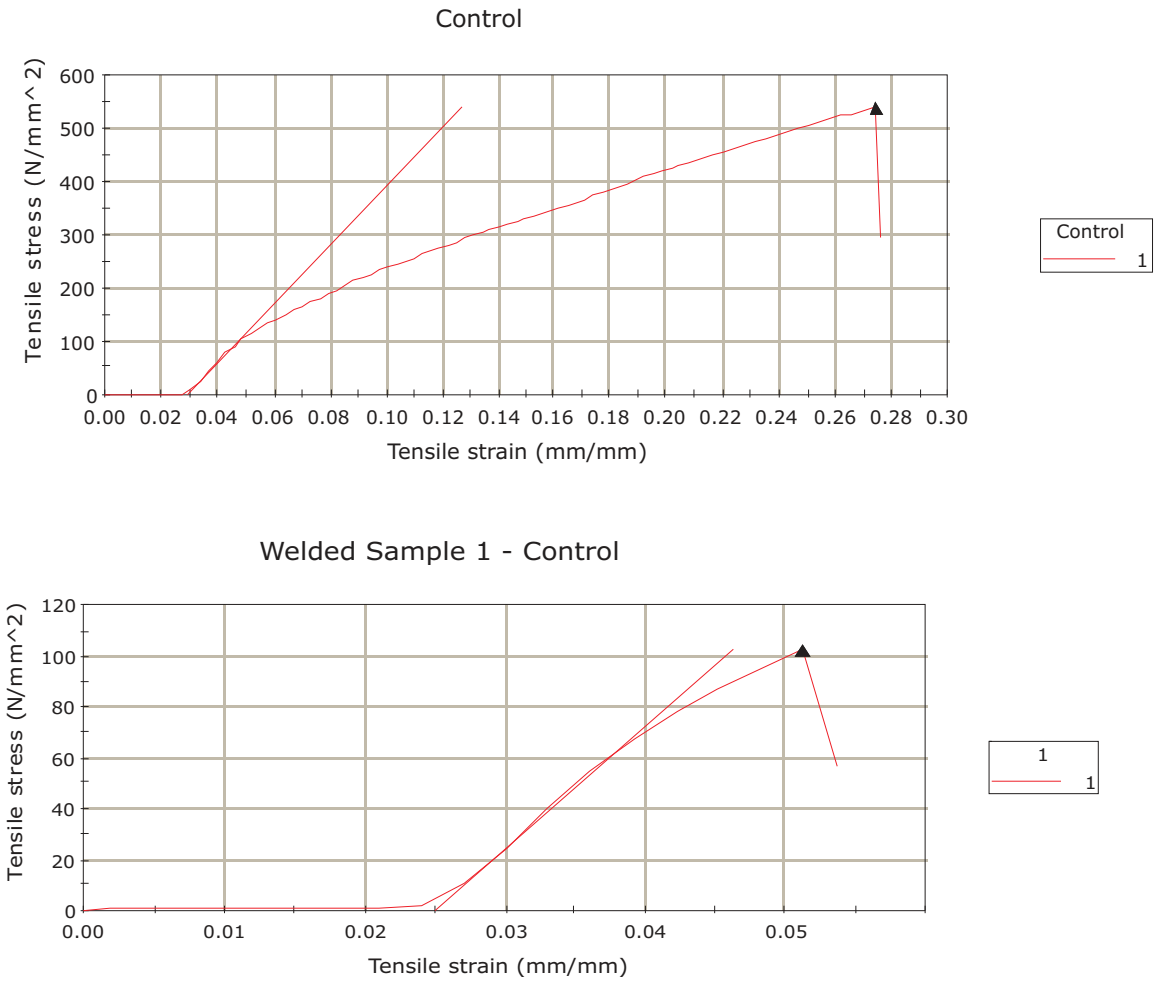


Fig. 3: Tensile result of the unwelded ductile cast iron (upper) and the welded sample (lower).

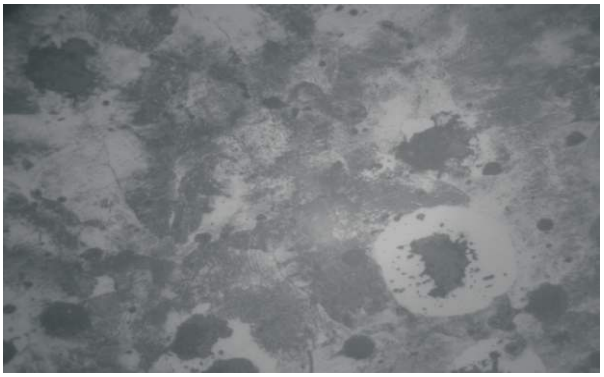


Fig.4a: Unwelded ductile iron showing sparsely graphite nodules enveloped with ferrite shell. (400X)



Fig.4b: 13.8mm depth and 8.7mm diameter welded D.I showing the weldment, revealing graphite flakes emanating from the effect of the welding. (400X)

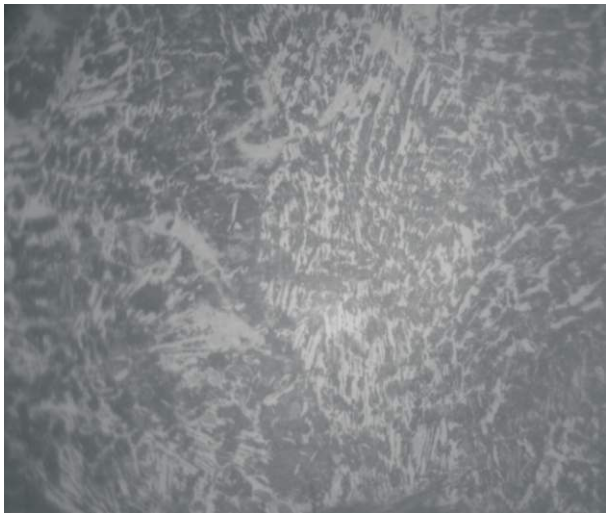


Fig. 4c: Welded D.I showing the HAZ revealing a densely distribution of the carbon in the form of graphite. (400X).

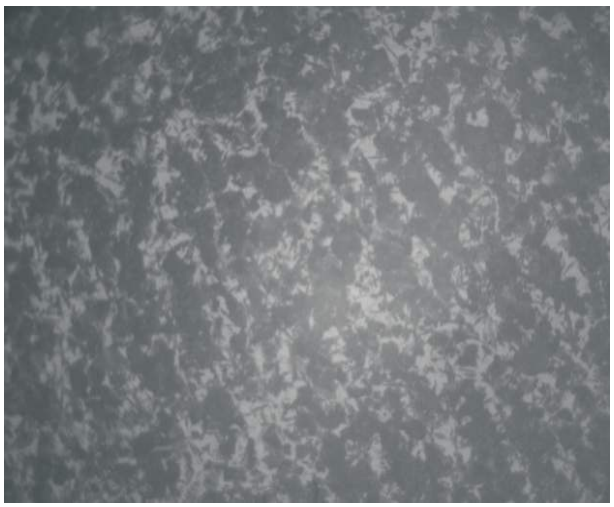


Fig. 4d: D.I welded at 14.2mm depth and 10.4mm diameter revealing densely populated graphite at the fusion zone. (400X).

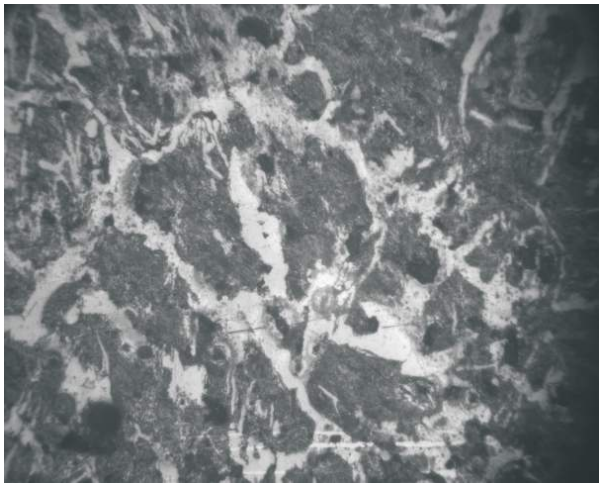


Fig. 4e: D.I welded at 14.2mm depth and 10.4mm diameter revealing sparsely distributed coarse graphite structure at the HAZ. (400X).

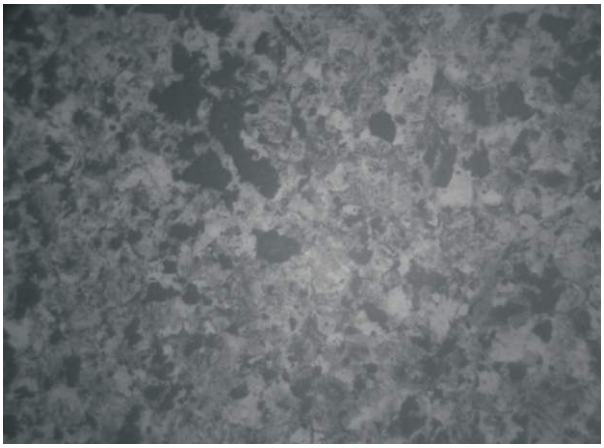


Fig. 4f: Weldment zone of a D.I welded at 11mm depth and 12mm diameter showing the distribution of graphite within the matrix with some sparsely distributed weld defects. (400X).

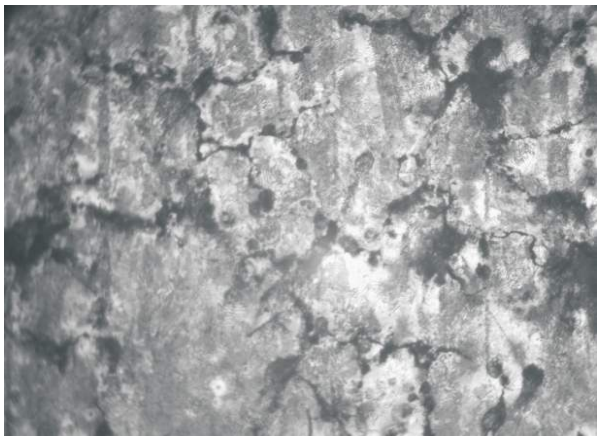


Fig. 4g: HAZ of a D.I welded at a depth and diameter of 11mm and 12mm respectively showing the formation of weld cracks in the matrix. (400X).

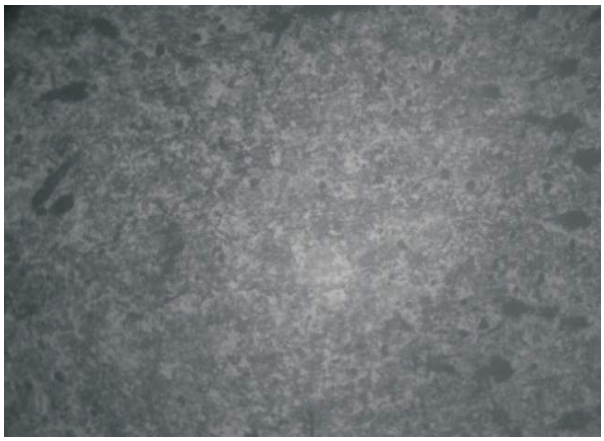


Fig. 4h: Random distribution of fine graphite nodules in a ferrite matrix at the weld fusion zone of a D.I welded to 14.6mm depth and 13mm diameter (400 X).

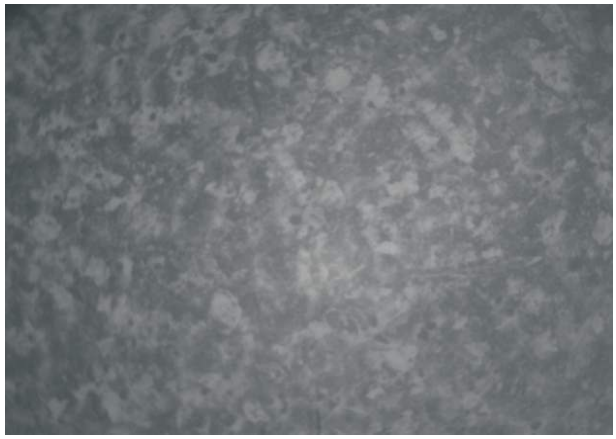


Fig. 4i: HAZ showing the distribution of coarse graphite in a D.I welded at 14.6mm depth and 13mm diameter (400X).

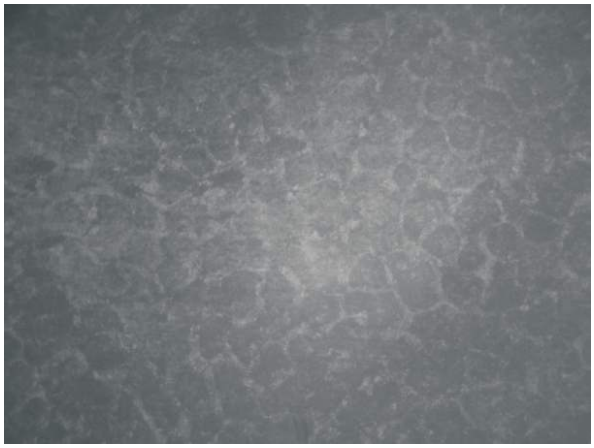


Fig. 4j: Distribution of graphite showing the grain boundaries within the matrix at the weldment zone of a D.I welded to 14.0mm depth and 16mm diameter. (400X).

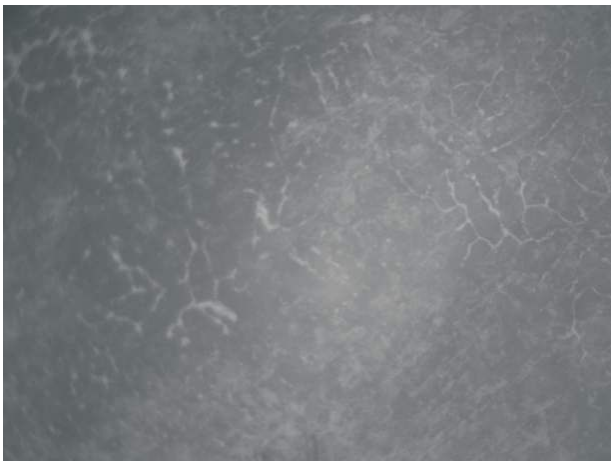


Fig. 4k: HAZ showing the distribution of graphite in a D.I welded at 14.0mm depth and 16mm diameter.(400X).

Fig. 4a – k: Microstructures of welded ductile iron using different weld configurations before subjecting it to corrosion

CATHODIC PROTECTION SOFTWARE DESIGN USING SLOPE PARAMETER APPROACH

J. E. O. Ovri, Tini E. Umoh

Department of Material and Metallurgical Engineering,
Federal University of Technology, Owerri, Imo State, Nigeria
jimvri@yahoo.com

ABSTRACT
This software was developed to reduce cathodic protection (cp) design to data inputting, and allowing the corrosion engineer to focus on more creative aspect of the design process, rather than the harrowing computation. The software also incorporate within It, a linear optimisation module, allowing key design parameters like anode spacing to be optimise base on a given set of parameters. The software was developed in VB.NET and c++ programming language. The designed and developed software was validated using, a 2000 metre fusion bonded epoxy (FBE) coated, medium carbon steel pipe in sub tropical sea water using Al-Zn-In alloy bracelets (anodes). The results obtain were: (I) Driving potential of 0.3V. (II) The average current demand of 5.48A (III) Final anode current output of 1.156A. (IV) A total anode mass of 853.572Kg. (V) A total of 17 anodes, each weighing 50Kg. (VI) Anode spacing (centre to centre) of 117.155m. To confirm the validity of the result obtained using the software, the same variables were calculated manually and high correlations were obtained for all variables.

Keywords: Cathodic Protection, Attenuation, Slope Parameter Approach, VB.NET, C+++ programming language.

INTRODUCTION

There are numerous computational approaches to cathodic protection design of which the boundary element model (BEM) is the most recent development. The BEM approach design gives a good characterization of the potential field about a surface, but however; fails at providing key information relevant to anode or anode array optimization. In addition, the BEM approach failed at incorporating the metallic return path components. This metallic return path component dictates Potential and current distribution between anodes on one - dimensional systems like pipelines [1] [2]. The BEM fails as a design concept, for designing CP systems for long thin structure like pipelines.

On the other hand, the slope parameter approach provides a linear relationship between anode potential, cathode potential and cathode current density at any point during the polarization process, as such, reducing the design process to finding a single polarization curve that will be used in the CP design, with the necessary correction for attenuation [3][4][5].

Modelling cathodic protection

The interdependence of corrosion variables is a setback on accurately modelling a corrosion system. Model gives a current understanding of reality; it provides a method of simplifying design and repair[6][7]. Numerical modelling provides an avenue for optimising design and repairs, also models provide a safe opportunity for test and trial by providing a "virtual" test environment. Scientific models can take many shapes and forms, but they all seek to characterize response variables through relationships with appropriate factors[8][9]. The two basic models are the mathematical or theoretical models and the statistical or empirical models.

A typical cathodic model will involve three components namely; the structure – cathode, anode, and the environment. The relationship between these components can be established by the slope parameter equation. As such the software algorithm will focus on solving these two linear equations (equation 3 and equation 6)[9].

$= IR$ ---------- 1

$= \frac{\Phi_c - \Phi_a}{R_t}$ ---------- 2

$= (R_t \cdot A_c) \cdot i_c + \phi_a$ ---------- 3

, =closed circuit structure potential, $\mathbf{R_t}$ = total circuit resistance, $\mathbf{\Phi_a}$ = close circui t anode potential, i_a= anode current output, A_c = structure surface area, $\mathbf{i_c}$ = structure current demand, $s = R_t . A_c$ =slope Parameter. This projects a linear interdependence between $\mathbf{\Phi_c}$ and $\mathbf{i_c}$, with $R_t . A_c$ as the slope, with the vertical intercept ϕ_a provided $\mathbf{R_t}$, A_c, and $\mathbf{\Phi_a}$ are constant for the time

$= \frac{R_a \cdot A_c}{N}$ ---------- 4

Where, N is the number of anodes. In estimating the weight of anode needed to protect a structure the combination of the modified Faraday's law expression for design of galvanic CP system -equation 5 and equation 4, yields the unified design equation[10][11]

$= \frac{i_m \cdot A_c \cdot T}{u \cdot C \cdot w}$ ---------- 5

$\cdot w = i_m \cdot T \cdot k \cdot S$ ---------- 6

In the equation above, C is the anode current capacity, T is design life of the structure, w is weight of individual anode, u is the utilization factor, R_a is anode resistance, and k is the anode consumption rate (the inverse of C). The slope parameter method defines in practical terms the principle of "rapid polarization" The impress current CP design is solve by using the relationship

$= s.i_c + \phi_{a(sq)}$ ----------7

Where $\phi_{a(sq)}$ is the potential that would have to be realized by the galvanic anode if it were to provide the same current as an impressed current one $\phi_{a(ic)}$, for this it has been shown;

$= \phi_{a(sq)} + (-\phi_c) + \mathrm{v_m}$ ----------8

Where v is the rec tifier voltage and $\mathbf{v_m}$ sums any other voltage drops in the circuit (lead wires etc).

SOFTWARE IMPLEMENTATION

A model was developed base on the interaction of these three components. A total of four classes were used to model the CP design process, three of the classes defines the key corrosion process and the fourth defines a means to identify and control the other three components.

SOFTWARE TESTING

The table below shows the list of all the necessary design parameters used to design the CP system for the 2000 metres Medium Carbon Steel gas line, in sub tropical sea water using Al-Zn-In type bracelet anode, the values adopted here are typical values stipulated by NACE RP 01607, or DNV – RP – B405: 2005[12]. Other values used will be reference appropriately.

VALIDATION OF RESULT

To validate the result generated by the software, the design was done manually, shows the values obtained, whilst the procedure for the calculation is given in the Appendix A

Manual Computation

DRIVING POTENTIAL

E)drivingpotential $= E_{cathode} - E_{anode}$

athode $= -0.80V$

node $= -1.10V$

$= -0.80 - (-1.10)$

$= 0.3V$

Software generated value = 0.30 Volts

ANODE RESISTANCE

Anode resistance for Bracelets anodes;

$$\text{node} = \frac{0.315\rho}{\sqrt{A}}$$

densityofthemedia) = 0.30;

radiusofanode) = 0.15; L(lengthofanode) =; 0.5;

Anode surface area) $= 2 \times \pi \times R_{anode} \times$

ode

$$\text{Anode surface area})_{initial} = 2 \times \pi \times R_{anode} \times l_{anode}$$

$$\text{Anode surface area})_{initial} = 2 \times \pi \times 0.15 \times 0.5$$

$$\text{Anode surface area})_{initial} = 0.471m^2$$

$$\text{node,initial} = \frac{0.315\rho}{\sqrt{A}}$$

$$\text{node,initial} = \frac{0.315 \times 0.3}{\sqrt{0.471}}$$

$$\text{node,initial} = 0.137 \text{ Ohms}$$

The $R_{anode,final}$ will be the anode resistance at 85% utilization factor at this stage the anode length and the radius will change hence the resistance, so the length of the anode at this stage will be;(in this formula it is assume that length red uction corresponding to 10% of the net anode mass/volume reduction occurs when the anode has been consumed to its utilization factor)[13]

$$\text{nal} = L_{initial} - (0.1 \times u \times L_{initial})$$

$$\text{nal} = 0.5 - (0.1 \times 0.85 \times 0.5)$$

$$\text{nal} = 0.458m$$

itial(initiallenghtofanode) =0.5;

itial(initialradiusofanode) = 0.15

nal(finallengthofanodeat 85%

ilizationfactor) = 0.458m

ore(anodecoreradius) = 0.01 m

nsity(densityofanode) = 2750kg/m^3

utilizationfactor) = 0.85

(anodeunitmass) = 50kg

;

$$\text{nal} = \sqrt{\frac{m \times (1-u)}{\pi \times \text{density} \times L_{final}} + (r_{core})^2}$$

$$\text{nal} = \sqrt{\frac{50 \times (1-0.85)}{\pi \times 2750 \times 0.46} + (0.01)^2}$$

$$\text{nal} = 0.04354 \text{ m}$$

nal(finalradiusofanodeat 85%

ilizationfactor) = 0.04354 m

$$\text{Anode surface area})_{final} = 2 \times \pi \times 0.04354 \times 0.46$$

$$\text{Anode surface area})_{final} = 0.126m^2$$

$$\text{node,final} = \frac{0.315 \times 0.3}{\sqrt{0.126}}$$

$$\text{node,final} = 0.267 \text{ Ohms}$$

ANODE CURRENT OUTPUT

$$\text{nodecurrentoutput}) = \frac{E_{cathode} - E_{anode}}{R_{anode}}$$

$$\text{nodecurrentoutput})_{initial} = \frac{\Delta E}{R_{anode(initial)}}$$

$$\text{nodecurrentoutput})_{initial} = \frac{0.3}{0.137}$$

$$\text{nodecurrentoutput})_{initial} = 2.19A$$

$= 0.30$Volts;

$$_{node,initial} = 0.137 \text{ ohms}$$

$$_{node,final} = 0.267 \text{ A}$$

$$_{nodecurrentoutput)final} = \frac{0.3}{0.267}$$

$$_{nodecurrentoutput)_{final}} = 1.123 \text{ A}$$

CURRENT DENSITY DEMAND

$$_{urrentdensitydemand)} = A_{cathode} \times I_{currentdensity} \times f$$

$$_{urrentdensitydemand)initial} = A_{cathode} \times I_{(currentdensity)initial} \times f_{initial}$$

$$_{athode} = 2 \times \pi \times R_{cathode} \times L_{cathode}$$

$$_{athode} = 2 \times \pi \times 0.15 \times 2000$$

$$_{athode} = 1884.96 \text{ m}^2$$

$$_{urrentdensitydemand)initial} = 1884.96 \times 0.06 \times 0.05$$

$$_{urrentdensitydemand)initial} = 5.655 \text{ A}$$

$$_{urrentdensitydemand)final} = A_{cathode} \times I_{(currentdensity)final} \times f_{final}$$

$$_{urrentdensitydemand)final} = 1884.96 \times 0.04 \times 0.07$$

$$_{urrentdensitydemand)final} = 5.28 \text{ A}$$

$$_{urrentdensitydemand)average} \frac{(currentdensitydemand)initial + I_{(currentdensitydemand)final}}{2}$$

$$_{urrentdensitydemand)average} \frac{5.655 + 5.28}{2}$$

$$_{urrentdensitydemand)average} = 5.468 \text{ A}$$

TOTAL ANODE MASS

$$_{otalanodemass} = \frac{I_{cathode,av} \times T \times 8760}{u \times \varepsilon}$$

$$_{otalanodemass} = \frac{5.468 \times 20 \times 8760}{0.85 \times 1320}$$

$$_{otalanodemass} = 853.83 \text{ Kg}$$

$$_{nodenumber} = \frac{M_{totalanodemass}}{M_{anodemas}}$$

ANODE NUMBER

$$_{nodenumber} = \frac{853.83}{50}$$

$$_{nodenumber} = 17.01$$

ANODE SPACING

$$_{anodespacing)} = \frac{L_{cathode}}{N_{anodenumber}}$$

$$_{anodespacing)} = \frac{2000}{17.01}$$

$$_{anodespacing)} = 117.58 \text{ m}$$

POTENTIAL CHECK

The CP design to be effective the potential must be more negative that -0.80

$$_{athode} = E_{anode} - \left(R_{anode,final} \times I_{(anodecurrentoutput)_{final}}\right)$$

$$_{athode} = -1.1 - (0.267 \times 5.28)$$

$$_{athode} = -2.51 \text{ V}$$

CURRENT TEST

$$_{nodecurrentoutput)_{final}} \times N_{anodenumber} \geq I_{(currentdensitydemand)final}$$

$$_{nodecurrentoutput)_{final}} \times N_{anodenumber} \geq I_{(currentdensitydemand)final}$$

$$123 \times 17 \geq 5.28$$

$$.091 \geq 5.28$$

ANODE LIFE TEST

Life test at end of 20 year assuming the pipeline is on a constant initial current of 2.19 A

$$_{e\ test} = \frac{M \times u \times \varepsilon}{\frac{\Delta E}{R} \times 8760}$$

$$_{stlife} = \frac{853.83 \times 1320 \times 0.85}{2.19 \times 8760}$$

$$_{stlife} = 499 \text{ years}.$$

CONCLUSION

The software designed and developed has been found to be workable, and released as window compatible software. The following conclusion could be drawn from the software design:

1) A driving potential of 0.3V.

2) An average current demand of 5.468 Amps was obtained for the software for a 20 years cathodic protection for medium carbon steel.

3) It has been shown that a total mass of 853.573 Kg of anode of Al-Zn-In will be required to give a 20 years cathodic protection to a medium carbon steel pipeline using an anode current output of 1.156 Amps and 17 anodes equally spaced along the length of the pipeline.

4) The result obtained such as potential, current and designed life tests has showed that the designed software can be used for predicting cathodic protection system design variables.

The core CPDEx class had in it other unimplemented interfaces for anode retrofit, current survey and potential survey. It is believed that future work on CP design software or software design on interpretation of pipeline survey data will involve improving on this core classes or implementing the interfaces of the core CPDEx classes.

The survey class can implement a SCADA corrosion system base on off-the-shelf technology using DPN3

protocol. Also, the survey class can interface geo - spatial data with corrosion data thereby enhancing real time pipeline integrity monitoring decision, maintenance, and even security surveillance of pipeline systems.

REFERENCES

[1]**R. A. Adey, C. A. Bebbia and S. M. Niku (**2003)**.***Application of Boundary Elemenets in Corrosion Engineering.* 34, manchester : JCSE, Vol. 8.

[2]**S. Aoki, K. Amaya, A. Nakayama, and A. Nishikawa (1998).***Elimination of Error from Nonuniform Current Distribution in Polarization Measurement by Boundary Element Inverse AnalysisBoundary Element Inverse Analysis.*259–264., houston : Corrosion, Vol. 54.

[3]**Lysogorski, W. H.Hartt and D. K. (2003).** *A Comprehensive Review of The Slope Parameter Based Approach To Cathodic Protection Design And Analysis.* 21, Dania Beach,Forida : JSCE, Vol. 8.

[4] **W.H. Hartt, P.Pierson (1998).** *Application of the Slope Parameter Approach to Cathodic Protection Design of Conductor Arrays on Offshore Structures.* Houston : NACE Annual conference, 98728.

[5]**D. W. Townley (2003).** *Boundary Elemenet Modeling of Galvanic Anode Cathodic Protection Using The Design Slope Method.* 23, Manchester : JSCE, Vol. 9.

[6]**Roberge, R. Pierre (1999)***Handbook of Corrosion Engineering.* new york : McGraw-Hill. ISBN 0-07-076516-2.

[7]**F. Brichau, J. Deconinck, and T. Driesens (1996).** *Modeling of Underground Cathodic.* 480–488, houston : Corrosion, Vol. 52.

[8]**Qiu, Chenchen (2003).***Model for Interpretation of Pipeline Survey Data (Ph.D Dissertation).* Gainesville : University of Florida.

[9]**Fagan, J.Waber and B. (1956).** *Mathematical Studies on Galvanic Corrosion.* 103, s.l. : Journal of the Electrochemical Society, Vols. 64–72.

[10]**D. W. Townley (1997).** *Unified Design Equation for Offshore Cathodic Protection.* HOUSTON : NACE, 97473.

[11]**A. Meillier (2004).** *A Review of Galvanic Anode Cathodic Protection Design.* 32, Manchester : JSCE, Vol. 8.

[12]**Det Norske Veritas (2005).***Recommended Practice DNV -RP-B401:Cathodic Protection Design.* Hovik : Det Norske Veritas, January.

Appendix A

Manual Computation

DRIVING POTENTIAL

$$E)driving potential = E_{cathode} - E_{anode}$$

$$_{athode} = -0.80V$$

$$_{node} = -1.10V$$

$$= -0.80 - (-1.10)$$

$$= 0.3V$$

Software generated value = 0.30 Volts

ANODE RESISTANCE

Anode resistance for Bracelets anodes;

$$_{node} = \frac{0.315\rho}{\sqrt{A}}$$

$$density of the media) = 0.30;$$

$$radius of anode) = 0.15; \quad L(length of anode) =;$$

0.5;

$$\text{Anode surface area}) = 2 \times \pi \times R_{anode} \times$$

$$_{ode}$$

$$\text{Anode surface area})_{initial} = 2 \times \pi \times R_{anode} \times l_{anode}$$

$$\text{Anode surface area})_{initial} = 2 \times \pi \times 0.15 \times 0.5$$

$$\text{Anode surface area})_{initial} = 0.471\text{m}^2$$

$$_{node,initial} = \frac{0.315\rho}{\sqrt{A}}$$

$$_{node,initial} = \frac{0.315 \times 0.3}{\sqrt{0.471}}$$

$$_{node,initial} = 0.137 \text{ Ohms}$$

The $R_{anode,final}$ will be the anode resistance at 85% utilization factor at this stage the anode length and the radius will change hence the resistance, so the length of the anode at this stage will be;(in this formula it is assume that length reduction corresponding to 10% of the net anode mass/volume reduction occurs when the anode has been consumed to its utilization factor)[13]

$$_{inal} = L_{initial} - (0.1 \times u \times L_{initial})$$

$$_{inal} = 0.5 - (0.1 \times 0.85 \times 0.5)$$

$$_{inal} = 0.458\text{m}$$

$$_{nitial}(initial lenght of anode) = 0.5;$$

$$_{itial}(initial radius of anode) = 0.15$$

$$_{inal}(final length of anode at 85\%$$

$$ilization factor) = 0.458\text{m}$$

$$_{re}(anode core radius) = 0.01 \text{ m};$$

$$nsity(density of anode) = 2750 kg/\text{m}^3$$

$$utilization factor) = 0.85;$$

$$(anode unit mass) = 50\text{kg}$$

$$_{inal} = \sqrt{\frac{m \times (1-u)}{\pi \times density \times L_{final}} + (r_{core})^2}$$

$$_{nal} = \sqrt{\frac{50 \times (1 - 0.85)}{\pi \times 2750 \times 0.46} + (0.01)^2}$$

$_{nal} = 0.04354$ m

$_{nal}(final radius of anode at 85\%$
$ilization factor) = 0.04354$ m

$$\text{Anode surface area})_{final} = 2 \times \pi \times 0.04354 \times 0.46$$
$$\text{Anode surface area})_{final} = 0.126 m^2$$
$$_{node,final} = \frac{0.315 \times 0.3}{\sqrt{0.126}}$$
$$_{node,final} = 0.267 \text{ Ohms}$$

ANODE CURRENT OUTPUT

$$anodecurrentoutput) = \frac{E_{cathode} - E_{anode}}{R_{anode}}$$
$$nodecurrentoutput)_{initial} = \frac{\Delta E}{R_{anode(initial)}}$$
$$nodecurrentoutput)_{initial} = \frac{0.3}{0.137}$$
$$nodecurrentoutput)_{initial} = 2.19A$$

$= 0.30$Volts;

$_{node,initial} = 0.137\ ohms$;

$_{node,final} = 0.267\ A$

$$nodecurrentoutput)final = \frac{0.3}{0.267}$$
$$nodecurrentoutput)_{final} = 1.123\ A$$

CURRENT DENSITY DEMAND

$$urrentdensitydemand) = A_{cathode} \times I_{currentdensity} \times f$$
$$urrentdensitydemand)initial = A_{cathode} \times I_{(currentdensity)initial} \times f_{initial}$$
$$athode = 2 \times \pi \times R_{cathode} \times L_{cathode}$$
$$athode = 2 \times \pi \times 0.15 \times 2000$$
$$athode = 1884.96\ m^2$$
$$urrentdensitydemand)initial = 1884.96 \times 0.06 \times 0.05$$
$$urrentdensitydemand)initial = 5.655 \text{ A}$$
$$urrentdensitydemand)final = A_{cathode} \times I_{(currentdensity)final} \times f_{final}$$
$$urrentdensitydemand)final = 1884.96 \times 0.04 \times 0.07$$
$$urrentdensitydemand)final = 5.28\ A$$
$$\frac{urrentdensitydemand)average}{(currentdensitydemand)initial + I_{(currentdensitydemand)final}}{2}$$
$$urrentdensitydemand)average = \frac{5.655 + 5.28}{2}$$
$$urrentdensitydemand)average = 5.468 \text{ A}$$

TOTAL ANODE MASS

$$otalanodemass = \frac{I_{cathode,av} \times T \times 8760}{u \times \varepsilon}$$
$$otalanodemass = \frac{5.468 \times 20 \times 8760}{0.85 \times 1320}$$
$$otalanodemass = 853.83\ Kg$$
$$nodenumber = \frac{M_{totalanodemass}}{M_{anodemas}}$$

ANODE NUMBER

$$nodenumber = \frac{853.83}{50}$$
$$nodenumber = 17.01$$

ANODE SPACING

$$nodespacing) = \frac{L_{cathode}}{N_{anodenumber}}$$
$$nodespacing) = \frac{2000}{17.01}$$
$$nodespacing) = 117.58 \text{ m}$$

POTENTIAL CHECK

The CP design to be effective the potential must be more negative that -0.80

$$athode = E_{anode} - \left(R_{anode,final} \times I_{(anodecurrentoutput)_{final}}\right)$$
$$athode = -1.1 - (0.267 \times 5.28)$$
$$athode = -2.51 \text{ V}$$

CURRENT TEST

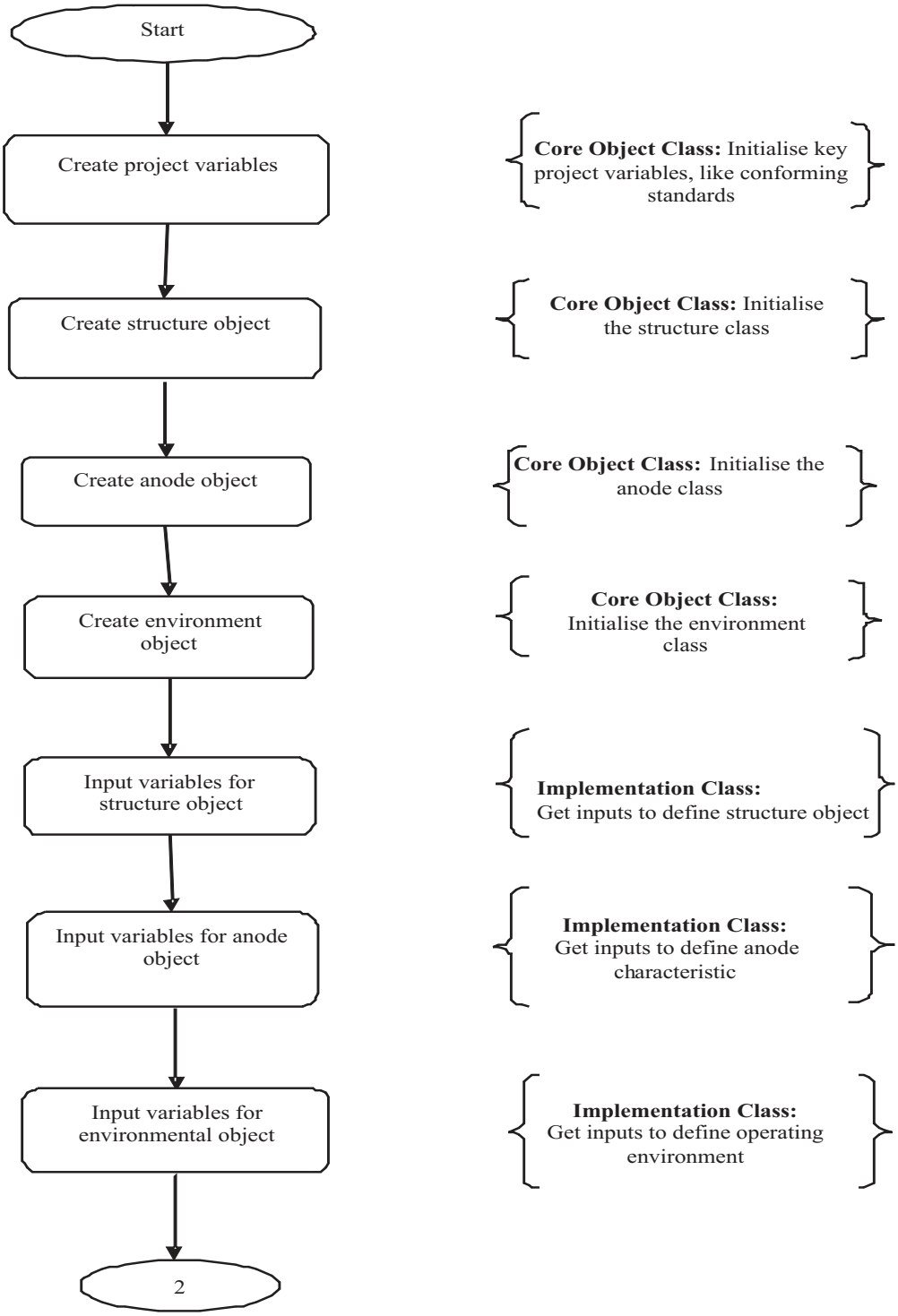
$$nodecurrentoutput)_{final} \times N_{anodenumber} \geq I_{(currentdensitydemand)final}$$
$$nodecurrentoutput)_{final} \times N_{anodenumber} \geq I_{(currentdensitydemand)final}$$
$$123 \times 17 \geq 5.28$$
$$.091 \geq 5.28$$

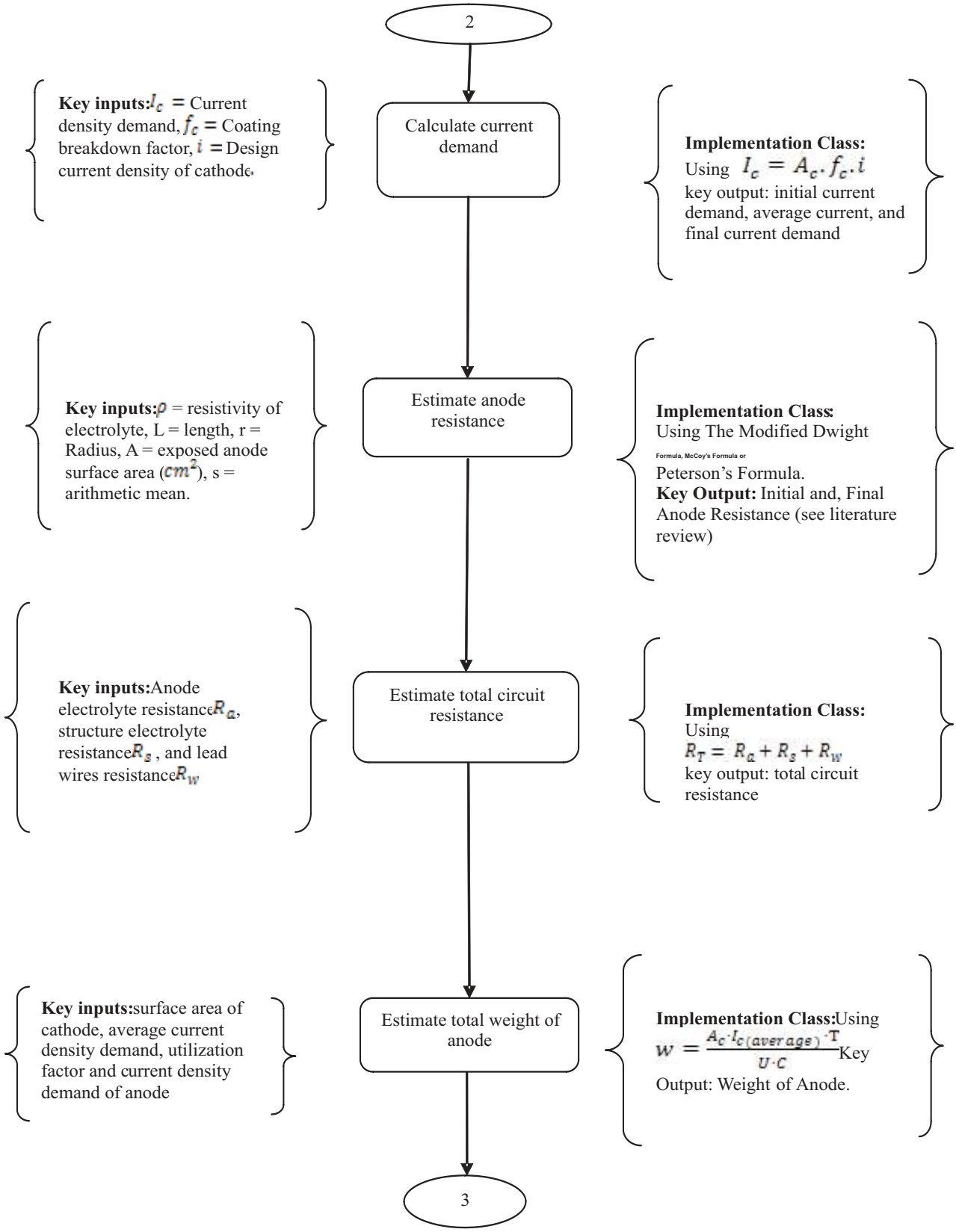
ANODE LIFE TEST

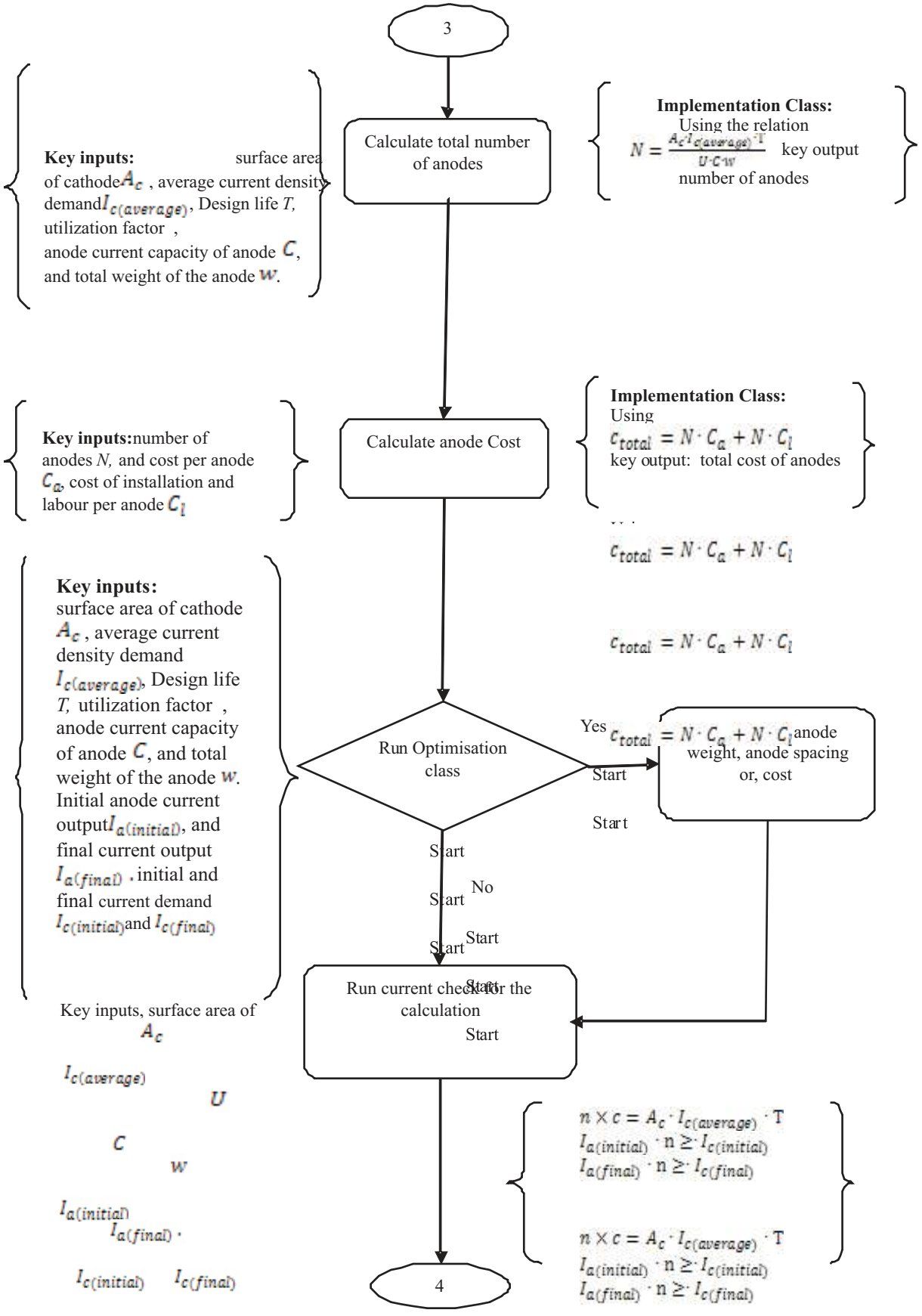
Life test at end of 20 year assuming the pipeline is on a constant initial current of 2.19 A

$$e\ test = \frac{M \times u \times \varepsilon}{\frac{\Delta E}{R} \times 8760}$$
$$stlife = \frac{853.83 \times 1320 \times 0.85}{2.19 \times 8760}$$
$$stlife = 499 \text{ years.}$$

PROGRAM FLOW CHART




2
Key inputs: I_c = Current density demand, f_c = Coating breakdown factor, i = Design current density of cathode.
Calculate current demand
Implementation Class: Using $I_c = A_c . f_c . i$ key output: initial current demand, average current, and final current demand
Key inputs: ρ = resistivity of electrolyte, L = length, r = Radius, A = exposed anode surface area (cm^2), s = arithmetic mean.
Estimate anode resistance
Implementation Class: Using The Modified Dwight Formula, McCoy's Formula or Peterson's Formula. Key Output: Initial and, Final Anode Resistance (see literature review)
Key inputs: Anode electrolyte resistance R_a, structure electrolyte resistance R_s, and lead wires resistance R_w
Estimate total circuit resistance
Implementation Class: Using $R_T = R_a + R_s + R_w$ key output: total circuit resistance
Key inputs: surface area of cathode, average current density demand, utilization factor and current density demand of anode
Estimate total weight of anode
Implementation Class: Using $W = \frac{A_c \cdot I_{c(average)} \cdot T}{U \cdot C}$ Key Output: Weight of Anode.
3


3
Calculate total number of anodes
Key inputs: surface area of cathode A_c , average current density demand $I_{c(average)}$, Design life T, utilization factor , anode current capacity of anode C, and total weight of the anode w.
Implementation Class: Using the relation $N = \frac{A_c \cdot I_{c(average)} \cdot T}{U \cdot C \cdot W}$ key output number of anodes
Calculate anode Cost
Key inputs: number of anodes N, and cost per anode C_a, cost of installation and labour per anode C_l
Implementation Class: Using $c_{total} = N \cdot C_a + N \cdot C_l$ key output: total cost of anodes
$c_{total} = N \cdot C_a + N \cdot C_l$
$c_{total} = N \cdot C_a + N \cdot C_l$
Key inputs: surface area of cathode A_c , average current density demand $I_{c(average)}$, Design life T, utilization factor , anode current capacity of anode C, and total weight of the anode w. Initial anode current output $I_{a(initial)}$, and final current output $I_{a(final)}$, initial and final current demand $I_{c(initial)}$ and $I_{c(final)}$
Run Optimisation class
Yes
$c_{total} = N \cdot C_a + N \cdot C_l$ anode weight, anode spacing or, cost
Start
Start
Start
No
Start
Start
Start
Run current check for the calculation
Start
Key inputs, surface area of A_c
$I_{c(average)}$
U
C
w
$I_{a(initial)}$
$I_{a(final)}$,
$I_{c(initial)}$ $I_{c(final)}$
$n \times c = A_c \cdot I_{c(average)} \cdot T$
$I_{a(initial)} \cdot n \geq I_{c(initial)}$
$I_{a(final)} \cdot n \geq I_{c(final)}$
$n \times c = A_c \cdot I_{c(average)} \cdot T$
$I_{a(initial)} \cdot n \geq I_{c(initial)}$
$I_{a(final)} \cdot n \geq I_{c(final)}$
4

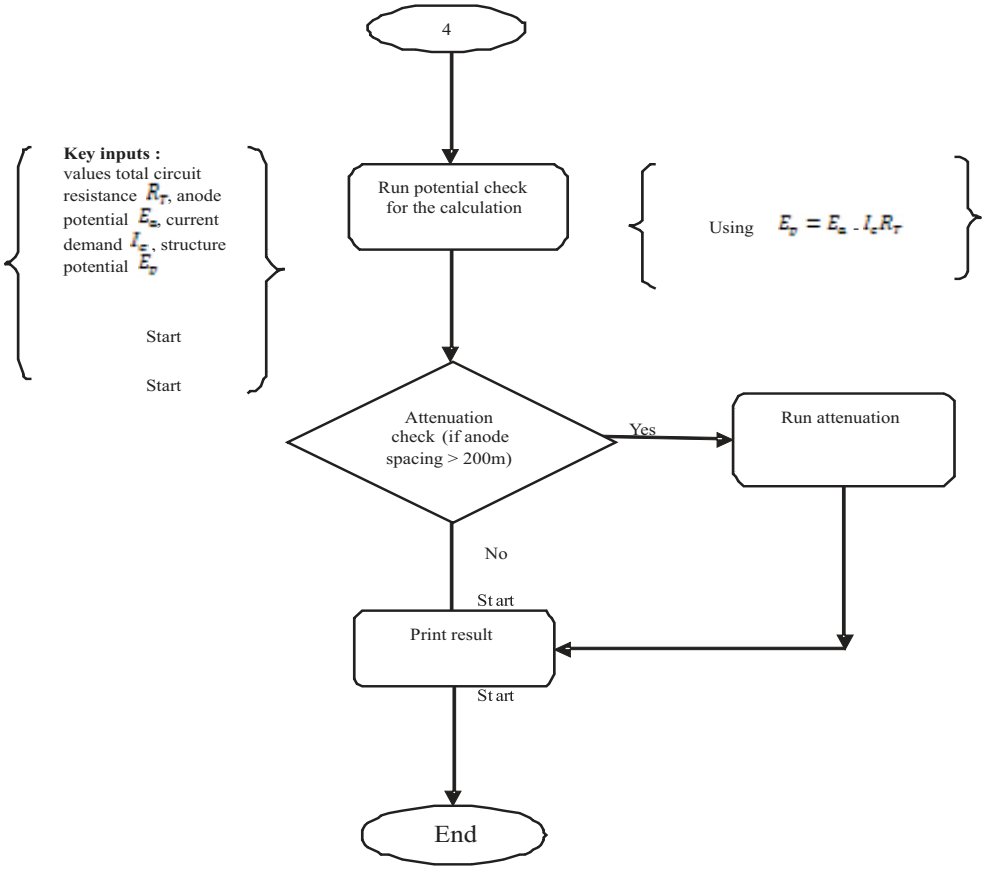


Table 1:Table Indicating General Property Values.

PARAMETER	VALUE
Project Type	CP Design
CP Type	Galvanic Anode System
Conforming Standard	Best Practice

Table 2: Table Indicating General Structure Property Values.

DESIGN PARAMETER	TYPICAL VALUE
Structure	Pipe
Shape	Cylindrical
Length	2000 m (1.24 miles)
Outer Diameter	0.3 m (300 mm)
Inner Diameter	0.28 m
Material Type	Medium carbon Steel
Specification	
Standard Reference Cell	$Ag/AgNO_3$
Potential	-0.85 V
Coating Type	FBE
Coating Resistance	10 Ohm-m
Coating Break Down Factor(Initial)	5%
Coating Break Down Factor(Final)	7%
Resistivity	1.8E-7 Ohm-m

Table 1: Table Indicating General Environment Property Values.

DESIGN PARAMETER	TYPICAL VALUE
Climate	Sub Tropical
Environment Type	Water
Sub Type	Sea Water
pH	8
Resistivity	0.30 Ohm-m
Depth	30m
Temperature	25^0C
Current Density (Initial)	0.06 A/m^2
Current Density (Average)	0.05 A/m^2
Current Density (Final)	0.04A/m^2
Lead Wires Resistance	-

Table : Table Indicating General Anode Property Values.

Table 2

DESIGN PARAMETER	TYPICAL VALUE
Anode Shape	Cylindrical
Anode Type	Short Slender
Length	0.5m (50cm)
Stand Off	0.3m (30cm)
Outer Radius	0.15m (15 cm)
Core Radius	0.01 m (1 cm)
Density	1320 kg/m^3
Alloy Type	Al-Zn-In
Close Circuit Potential	-1.10 V
Electrochemical Capacity	2670 A-hr/kg
Utilization Factor	85%
Mass per Anode	50 kg
Anode Cost	1200 Niara
Installation Cost	7000 Niara

Table : Snapshot of the General Property Form.

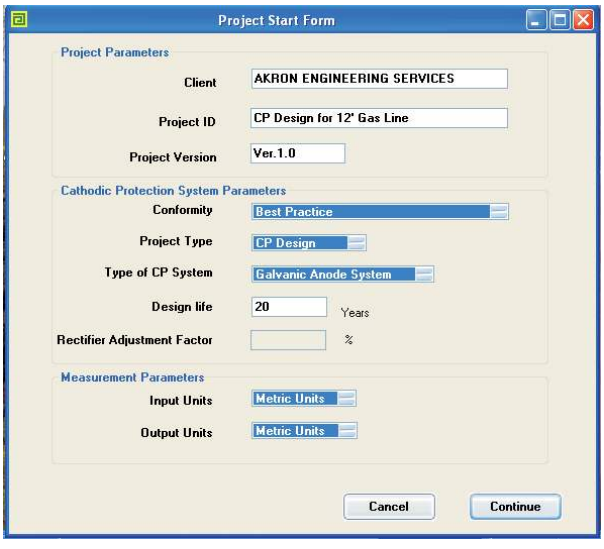


Table : Snapshot of the Structure Property Form.

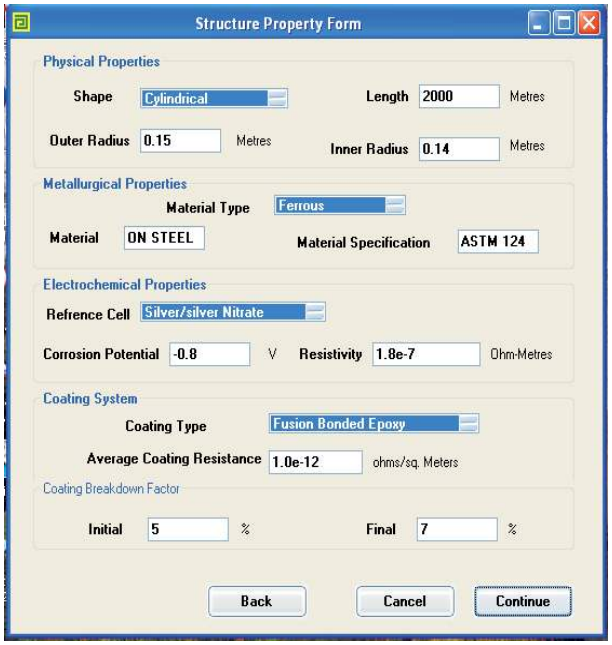


Table : Snapshot of the Environment Property Form.

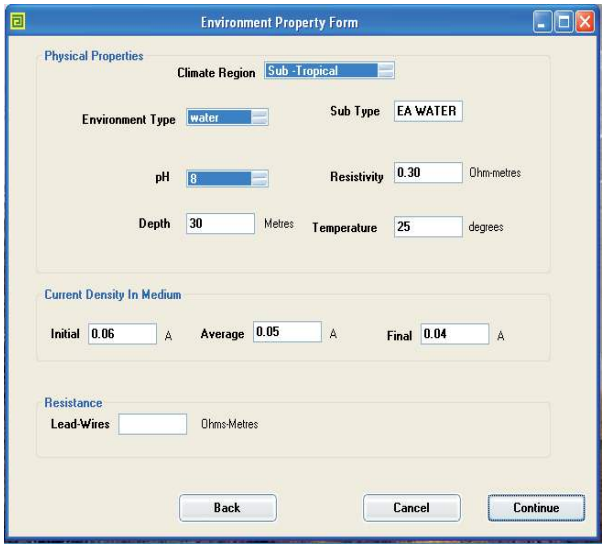
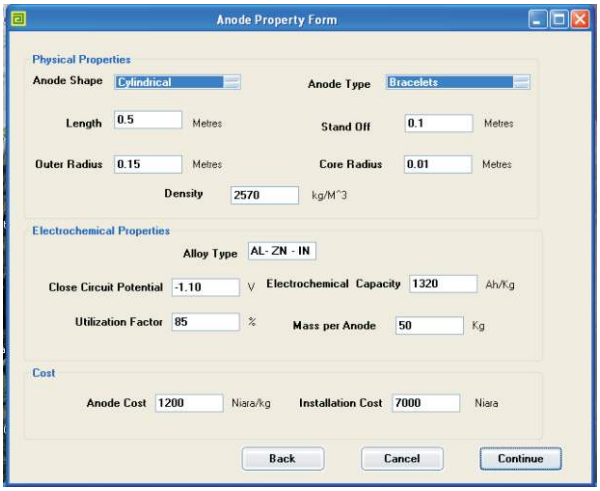


Table : Snapshot of the Anode Property Form.



SOFTWARE VALIDATION

Table : Snapshot of the Calculation Preview Property Form.



Table : Snapshot of the Result Property Form.

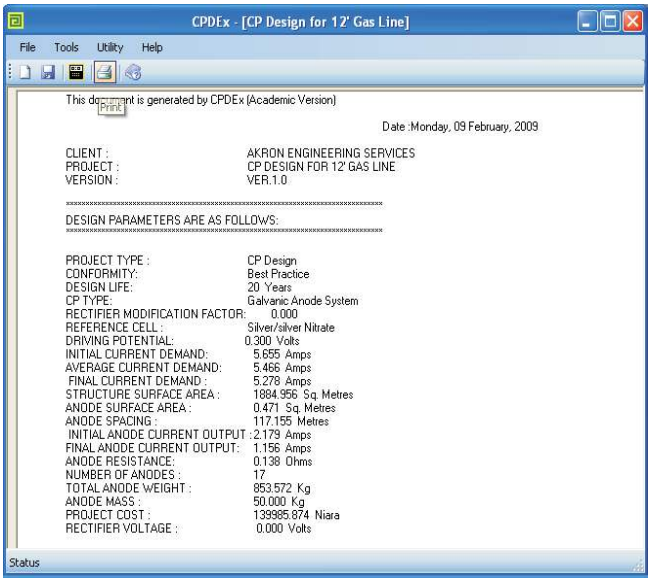


Table : Table Indicating the Result of the Key CP Design Parameters Values as Generated from the Software.

DESIGN PARAMETER	VALUE
Driving Potential	0.300 Volts
Initial Current Demand	5.655 Amps
Average Current Demand	5.466 Amps
Final Current Demand	5.278 Amps
Structure Surface Area	1884.956 Sq.m^2
Anode Spacing	117.155 m
Initial Anode Current	2.179 Amps
Final Anode Current	1.156 Amps
Anode Resistance(Initial)	0.138 Ohms
Number Of Anodes	17
Total Anode Weight	853.572 kg
Multiple Anode Factor	16.954
Anode Adjustment Current	36.947 Amps

Table :Table Comparing Software Generated Result to the Manually Calculated Result

VARIABLE	SOFTWARE GENERATED VALUE	MANUALLY CALCULATED VALUE
Driving Potential	0.3 Volts	0.3 Volts
Initial Current Demand	5.655 Amps	5.655 Amps
Final Current Demand	5.278 Amps	5.28 Amps
Initial Anode Resistance	0.138 Ohms	0.137 Ohms
Final Anode Resistance	0.259 Ohms	0.267 Ohms
Anode Current Output (Initial)	2.179 Amps	2.19 Amps
Anode Current Output (Final)	1.156 Amps	1.123 Amps
Anode Spacing	117.155 m	177.58 m
Anode Number	17	17.01
Total Anode Mass	853.572 Kg	853.83 Kg
Total Surface Area Of Cathode	1884.956 Sq. meters	1884.96 Sq. meters
Anode Surface Area	0.471 Sq. meters	0.471 Sq. meters

CORRELATION BETWEEN STRUCTURAL AND OPTICAL PROPERTIES OF PVA/TIO$_2$ NANOCOMPOSITES

[1*]AHMED, T. O., [*]AKUSU, P. O., [#]ALU, N.,[*]ISMAILA, A. & [*]SHIGA, Y. A.
[*]Materials Science Section, Department of Physics, Ahmadu Bello University, Zaria, Nigeria.
[#]Physics Advanced Laboratory, Sheda Science & Technology Complex, Abuja, Nigeria.
Correspondence: tajahmol@yahoo.co.uk

ABSTRACT
Polyvinyl alcohol/titanium (IV) oxide (PVA/TiO_2) nanocomposite have been produced via a two-stage reaction involving the synthesis of TiO_2 Nanoparticles (Nps) from titanium (IV) chloride employing sol-gel technique and subsequent mixing of TiO_2 Nps with PVA dissolved in water boiled at 110°C. The TiO_2 Nps was characterized using SEM-EDS system for its purity and size. The analysis revealed that the TiO_2 Nps have sizes in the range of 25-40nm and of 99.9% purity. Furthermore, the PVA/TiO_2 nanocomposites were found to be tough and transparent with the TiO_2 Nps evenly dispersed in the host polymer matrix. Subsequently, the PVA/TiO2 nanocomposites were characterized by FTIR, Mechanical tests and UV-Vis Spectrophotometry for possible structural modification, toughness and its suitability for UV absorption and filtering.

Keywords: TiO_2 Nanoparticles, Polymer Nanocomposites, Structure, Toughness, UV absorption/filtering.

INTRODUCTION

In the last few decades, conventional polymer composites reinforced by micrometer-scale fillers have seen myriad of applications in automobile, construction, electronics, and consumer products. In comparison to the pristine polymer, polymer composites possess enhanced properties like higher strength and stiffness at the cost of toughness which is directly linked to optical transparency [1]. Recently, polymer nanocomposites developed by incorporating nanosized fillers into pristine polymers have proffered a way to ameliorate the precincts of traditional counterparts. This conceptual fact contradicts the current theories of micromechanics by Jordan in 2005 [2], which supported the size independence of fillers on the properties of polymer composites. The small size of fillers (less than 100 nm) in polymer nanocomposites could bring about dramatic phenomena leading to novel properties for specialized applications if the degree of interfacial interactions between the polymer and filler phase are well controlled and monitored [3].

To realize the novel properties of polymer nanocomposites, synthetic methods which have effect on controlling particle size distribution, dispersion, and interfacial interactions are critical. Despite numerous challenges, considerable research efforts have been made to develop appropriate synthetic techniques for making good polymer nanocomposites but creating one universal technique for developing polymer nanocomposites is impossible due to the physiochemical differences between each system [4]. Nevertheless, a number of polymer nanocomposites based on layered silicate have been recently commercialized, such as the polyimide-clay nanocomposites pioneered by Toyota in 1993 and polypropene-clay nanocomposites by General motors in 2002. The study by Mohan and his co-workers, on intercalated polystyrene/layered silicates nanocomposites revealed that the intercalated hybrid resembles the pristine organosilicate in appearance except that it showed voids where it is localized in the unannealed mixture [5]. In 2001 studies were carried out on the effect of acrylonitrile content on the gallery height of intercalated clay/poly (styrene-co-acrylonitrile), but there was a limit to increase in the gallery height with increase in acrylonitrile [6]. In 2007, Pegoretti and his co-workers found that the relative stiffness in HDPE/modified clay nanocomposites produced via melt intercalation increases with the addition of clay [7]. A novel heat-sealing performance across the broadest possible temperature range was achieved using polymer blend consisting of polyethylene and ethylene vinyl acetate reinforced by Montmorillonite [8]. Due to the high refractive index and high degree of transparency to UV radiation of nanosized TiO_2 coupled with its low cost, non-toxicity and chemical inertness, a lot of attention is drawn to explore these novel properties in hybridization of polymer materials [9]. In order to explore these aforementioned properties, Feng (2006) studied the effect of TiO_2 nanoparticles on the polystyrene matrix produced **via *In-situ* Polymerization** and concluded that the dispersion (20-50nm size) of TiO_2 into polystyrene matrix gave rise to improved optical properties making the hybrid polymer a potentially active transparent UV filters [10]. In this work, TiO_2 Nanoparticles (Nps) was synthesized from titanium (IV) chloride employing sol-gel technique and subsequently blended with dissolved PVA employing solution mixing technique. The hybrid PVA/TiO_2 nanocomposites were characterized by FTIR, Mechanical tests and UV-Vis Spectrophotometry for possible structural modification, toughness and its suitability for UV absorption and filtering.

EXPERIMENTAL

Polyvinyl alcohol/titanium (IV) oxide (PVA/TiO_2) nanocomposites were produced via a two-stage reaction involving the synthesis of TiO_2

Nanoparticles (Nps) from titanium (IV) chloride employing sol-gel technique and subsequent mixing of TiO_2 Nps with PVA dissolved in water boiled at 110°C via one-pot reaction. The TiO_2 Nps was characterized using SEM-EDS system for its purity and size. The mixing of the TiO_2 Nps with PVA was possible because PVA is hydrophilic. Four samples of PVA/TiO_2 nanocomposites containing 1-4% of TiO_2 Nps were produced. The samples were oven dried at 150°C for 7hrs and subsequently hot pressed at a temperature close to the melting point of PVA in order to produce flat, uniform thin samples. Rectangular shaped samples of PVA/TiO_2 nanocomposites were made and labeled S1, S2, S3, and S4 which contain 1-4% of TiO_2 Nps respectively. These samples were subjected to FTIR measurements, UV-Vis spectroscopy and mechanical tests. The samples were subjected to mechanical tests in order to determine their strengths and toughness. The samples were analyzed by a FTIR spectroscopy in transmission mode without KBr. The spectra were recorded in the frequency range from 350 to 4600 cm^{-1}, after 25 scans, with resolution of $2cm^{-1}$. The positions and intensities of the IR bands were processed with Spectral Analysis software. The ultraviolet and visible spectroscopic study was carried out with a spectrophotometer in a wavelength range of 200 to 900 nm.

RESULTS AND DISCUSION

Surface morphology of TiO_2 NPs was observed by scanning electron microscope and the microstructure and EDS spectra of the TiO_2 NPs are given in Figs. 1(a) and (b). The morphology of TiO_2 particles is such that the particles are closely packed together and spherical in shape. The particle size is in the range of 25-40nm, which makes TiO_2 very transparent and suitable for this research. Figure 1b shows the EDS spectra for the TiO2 NPs with characteristic X-ray energies ranging from 0-10keV. Qualitatively, the peak intensity for Ti is much stronger than the peak intensities for nitrogen and oxygen and quantitative analytic results show that the relative concentration of nitrogen and oxygen are minute reflecting that the Ti is the major component of TiO_2 NPs with concentration greater than 99%.

The FTIR spectra of the four samples of PVA/TiO_2 nanocomposites containing 1-4% of TiO_2 Nps given in Figs. 2(a)-(d), were recorded periodically to find out if the TiO_2

Nps was embedded in the PVA matrix and chemically bonded to polymer chains. It is a known fact that the fundamental vibrations of solids (finger prints) are localized in the low frequency region (<1200 cm^{-1}) of the midrange (400 to 4000 cm^{-1}) IR spectrum and that the Ti-O bond is clearly located in the range from 400 to 900 cm^{-1}[11]. The spectral of PVA/ TiO2 nanocomposites is almost a combination of the spectra of PVA and TiO_2 NPs, showing typical absorptions for PVA with characteristic O-H, C=O, $C \equiv C$ and C-H stretching bands at > 3600-1600 cm-1, the peaks slightly above 1600cm-1 and below 1500cm-1 indicate vinyl group and the significant absorption below 500 cm-1 represents Ti-O band of TiO2, which indicates the TiO2 NPs are located in the PVA matrix of the nanocomposites. These observations are in good agreement with the works reported in the literature [10, 12, 13].

From Fig. 2(a)-(d), it can be seen that the pure PVA peaks are represented by O-H stretching vibrations of intermolecular hydrogen bonds between 3614.72cm-1 and3426.66cm-1, stretching vibrations of conjugated triple bonds in the frequency range 2175cm-1 - 2150.70cm-1 and the peaks at 1643.41cm-1, 1642.44cm-1, 1448.59cm-1 and 1439.91cm-1 indicate vinyl groups which act as functional sites for further bonding with Ti. The C=O vibration bands at 1736.96cm-1, 1729.24cm-1, 1718.63cm-1 and1642.44cm-1 come from the formation of the hydrogen bonds between the carbonyl groups of PVA and the hydroxyl groups on TiO2 surface. Below 500cm-1 in the spectra for the four samples, the significant absorption bands represent Ti-O bonds.

The mechanical tests revealed that the PVA/TiO2 nanocomposites samples have very high tensile strengths ranging from $0.689 \times 10^5\ Pa$ to $34.443 \times 10^5\ Pa$ and it implies that the hybrid polymer composites are tough with elastic modulus having values in the range

The PVA/TiO2 nanocomposites with 4% TiO2 loading had the lowest tensile strength of $34.443 \times 10^5\ Pa$
$0.689 \times 10^5\ Pa$

while the sample with 2% TiO2 loading had the highest tensile strength of $1.296 \times 10^6\ Pa$ to $28.703 \times 10^6\ Pa$.

The samples were scanned in the UV-Visible range of wavelength 200nm-900nm, in order to study the optical properties of the nanocomposites. The UV-Vis spectra of PVA/TiO2 nanocomposites containing 1- 4% of TiO2 respectively, are presented in Figures 3(a)-(d). Small values of absorbances at the visible and UV region were observed for PVA/TiO2 film, which implies reasonable transparency but no ability of filtering out UV light. However, relatively strong absorbance in the UV region and small absorbance at the visible region were observed, which also connotes that the PVA/TiO2 nanocomposites containing 1% and 3% TiO2 possess dual optical properties of visual transparency and

UV filters close to the visual wavelengths. With the further addition of TiO2, the sample containing 4% TiO2, appeared opaque to eye observation and had significant absorbance in the visible region. At this level (4%), the performance of the material as a visually transparent UV filter was reduced.

The FTIR spectroscopy revealed that existence of strong interfacial interaction between PVA and TiO2 NPs as the pristine polymer matrix are uniformly interspersed with TiO2 NPs showing strong absorption bands for the polymer and the TiO2 NPs. Finally, UV-Vis spectroscopy confirmed that the dispersion of TiO2 particles at nanoscale level resulted to improved optical properties for the polymer nanocomposites.

CONCLUSION

The solution mixing technique has been employed to develop PVA/TiO2 hybrid nanocomposites which have the polymer chains covalently bonded onto the TiO2 NPs. Integrated characterization techniques, such as SEM, EDS, FTIR, UV-Vis and strength test, were employed to

study the behaviour of the PVA/TiO2 hybrid nanocomposites. It was observed that the developed PVA/TiO2 hybrid nanocomposites are very tough with high elastic modulus and could act as visually transparent UV filters. FTIR spectroscopy revealed that the TiO2 NPs was embedded in the PVA matrix and chemically bonded to polymer chains. Characterization with SEM-EDS showed that the TiO2 powders are nanocrystalline in structure and are very transparent with particles size in the range of 25-40nm.

REFERENCES

[1] Rosoff, M. (2002). Nano-Surface Chemistry. Marcel Dekker Inc., New York.

[2] Jordan, J., Jacob, K.I., Tannenbaum, R., Sharaf, M.A. and Jasiuk, I. (2005). Experimental Trends in Polymer Nanocomposites: A Review. J. of Mat. Sci. & Eng., (A). 393, 1-11.

[3] Chandra, A., Turng, L. S., Gopalan, P., Rowell, R.M. and Gong, S. (2008). Study of Utilizing Thin Polymer Surface Coating on Nanoparticles for Melt Compounding polycarbonate/Alumina Nanocomposites and their Optical Properties. Composite Science and Technology, 68, 768-776.

[4] Berta, M., Lindsay, C., Pans, G. and Camino, G. (2006). Effect of Chemical Structure on Combustion and Thermal Behaviour of Polyurethane Elastomer Layered Silicate Nanocomposites. Polym. Degrad. Stabil., 91, 1179-1191.

[5] Mohan, S., Lauren, N.C., Surya, S.G. and Karen, I.W. (1996). Melt Intercalation of Polystyrene in Layered Silicates. J. of Polym. Sci.,: part B: Polym Physics, Vol. 34,, 1433-1449.

[6] Lee, S.S., Lee, C.S, Kim, M.H., Kwak, S.Y., Park, M., Lim, S., Choe, C.R. and Kim, J. (2001). Specific Interaction Governing the Melt Intercalation of Clay with Pol (Styrene-co—acrylonitrile) Copolymers. J. of Polym. Sci: Part B: Polym. Physics, Vol. 39, 2430-2435.

[7] Pegoretti, A., Dorigato, A., and Penati, (2007). A Tensile Mechanical Response of Polyethylene-Clay Nanocomposites, express Polymer Letters, Vol. 1. No 3, 123-131.

[8] Manias, E., Zhang, J. and Huh, J.Y. (2009). Polyethylene Nanocomposite Heat Sealants with Versatile Peelable Character. Macromol, Rapid Commun., 30, 17-23.

[9] Evora, V.M.F. and Shukla, A. (2003). Fabrication, Characterization and Dynamic Behaviour of Polyester-TiO2 Nanocomposites. Mater. Sci. Eng. (A). 361, 358-366.

[10] Feng, L. (2006). Preparation and Characterization of Polymer TiO2 nanocomposites via in-situ Polymerization. Master of Applied Science in Chemical Engineering Thesis Presented to the University of waterloo, Ontario Canada.

[11] Morterra, C.; Magnacca, G.(1996). Catal. Today, 27, 497.

[12] Rong, Y.; Chen, H. Z.; Wu, G.; Wang, M. (2005). Mater. Chem. Physics. 91, 370.

[13] Chen, G.; Liu, S; Zhang, S.; Qi, Z. (2000). Macromol. Rapid Commun., 21, 746.

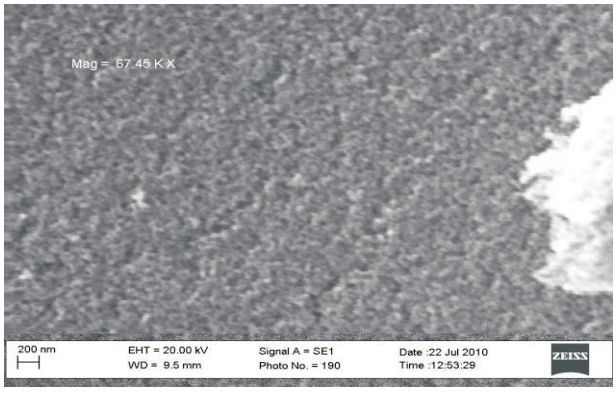
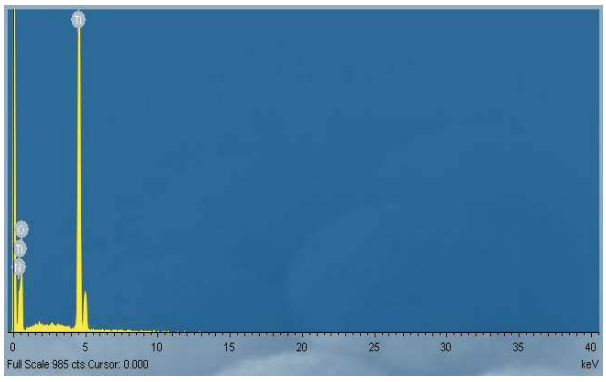


Fig 1 (a)



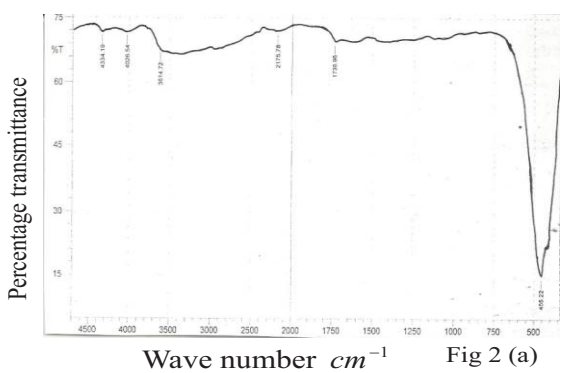


Fig 2 (a)

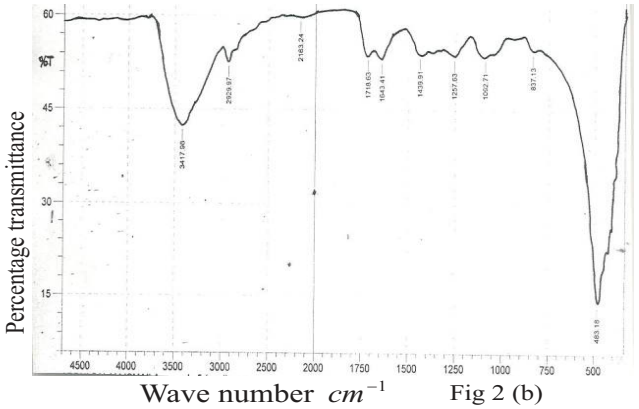
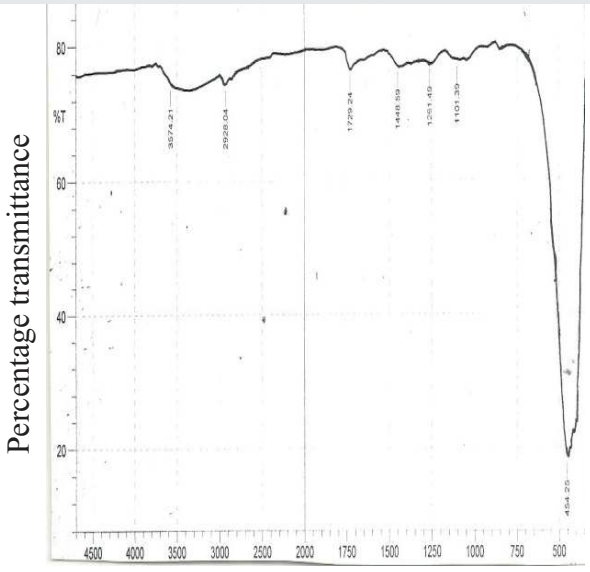


Fig 2 (b)



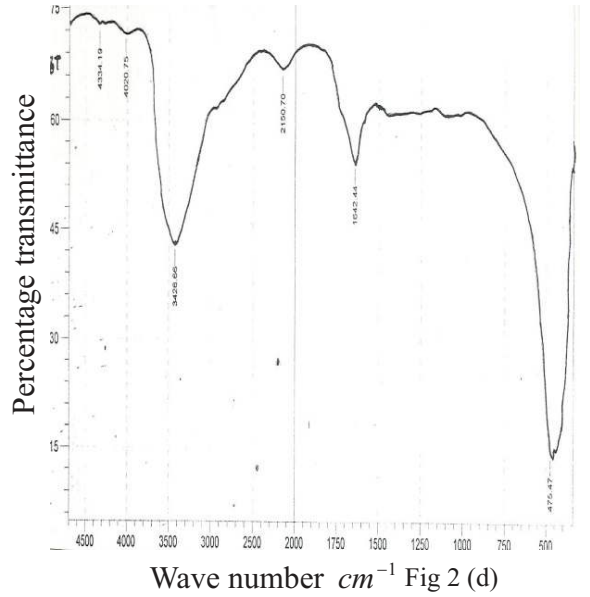
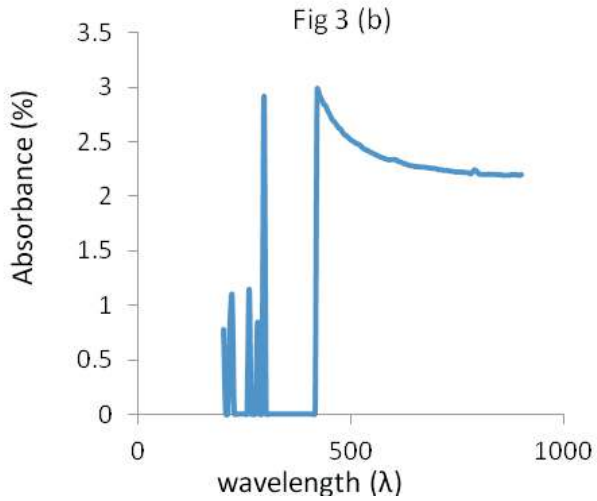
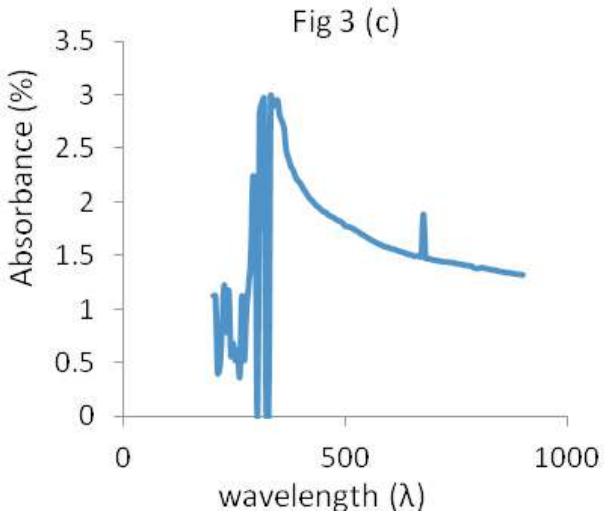


Figure 2: FTIR Spectra of PVA/TiO_2 Nanocomposites containing: (a) 1% of TiO_2 2% of TiO_2 (c) 3% of TiO_2 and (d) 4% of TiO_2





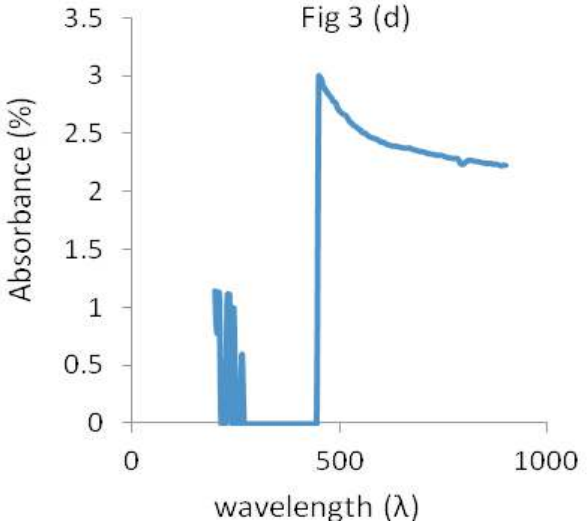


Figure 3: UV-Vis Spectra of PVA/TiO_2 Nanocomposites containing: (a) 1% of TiO_2 (b) 2% of TiO_2 (c) 3% of TiO_2 and (d) 4% of TiO_2

PREPARATION OF NANO- TIO_2 THIN FILM USING SPIN COATING METHOD

*Daniyan, A.A.,[1, 2] Umoru, L.E[1]., and Olunlade, B.A[2].
[1]**Department of Materials Science and Engineering,** Obafemi Awolowo University, Ile Ife.
[2]Engineering Materials Development Institute, Akure.
*E-mail: daniyanayodele@yahoo.com

ABSTRACT
This work presents the preparation of TiO_2 thin film on empty glass and ITO glass by spin coating method. Highly transparent titanium oxide thin films were prepared on empty glass and Indium Tin Oxide (ITO) from a titanium (III) chloride precursor. The Optical absorption and transmission of the film prepared from both the synthesised and the commercially available TiO_2 were measured with the UV- Visible Spectrophotometer. A sharp absorption edge of the TiO_2 film was observed. The estimated energy band gap for the film of the commercially available sample is larger than that of the synthesised one.
Keywords: Titanium oxide, ITO, spin coating, absorption, band gap

1. Introduction

Nanotechnology is a part of science and technology that is about the control of matter on the atomic and molecular scale - this means things that are about 100 nanometers or smaller. Nanotechnology includes making products that use these small parts, such as electronic devices, catalysts, and sensors etc. Some of the most current research and development work are in the area of functional Nanotechnology. This term describes applications in which material nanostructures are used to produce optical electronics or magnetic properties. [1]

Titanium dioxide, also known as titanium (IV) oxide or Titania, is the naturally occurring oxide of titanium, chemical formula TiO_2. It has a wide range of applications, from paint to sunscreen to food colouring. Titanium dioxide (TiO_2) has attracted significant attention from researchers because of the many interesting physical and chemical properties that make it suitable for a variety of applications. For instance, TiO_2 has high corrosion resistance and chemical stability and an excellent optical transparency in the visible and near infrared regions, as well as a high refractive index that makes it useful for anti-reflection coatings in optical devices [2] .It has been used mostly as a pigment in paints, sunscreens, ointments toothpaste e.t.c. Therefore, this work seeks to investigate the structural and the optical properties of synthesized nano- TiO_2 for opto-electronics application.

Recently, titanium oxide (TiO_2) thin films have emerged as one of the most promising oxide materials owing to their optical, electrical and photo electrochemical properties.

Many studies on TiO_2 thin films formed by conventional and advanced sol–gel processes have been reported.

As far as we know, however, previous studies indicate that the properties of TiO_2 films appear to strongly depend on the process conditions and starting materials used in the processes, many researchers have used sol–gel method to synthesise, For instance, in 2001, [3] worked on the research topic, Synthesis of nano rutile TiO_2 powder at low temperature by sol-gel method using $Ti(OC_4H_9)_4$ & HNO_3 and obtained mean particle size of about 50nm after calcination at 600°C in rutile phase. Similarly, [4] researched into the photocatalytic activity of nano-sized TiO_2 powders by sol –gel method, using TTIP and $EtOH/H_2O$ solution. The results obtained were anatase (75.1%) and brookite (24.9%) phases at 400°C. The particle size obtained were 7.9nm and 7.4nm respectively. Likewise, [5] also studied the 'Preparation and characterization of nano – TiO_2powder by sol-gel method' and yielded a mean size of about 10nm after calcinations. By similar method,[6]investigated the 'Microstructure control of thermally stable TiO_2 obtained by hydrothermal process' The result gotten were; Hydrothermally treated TiO_2 nanoparticles at pH 3 were 13 and 34nm in average diameter after calcinations at 600 and 800°C. Hydrothermally treated TiO_2nanoparticles at pH 2 were 11 and 26nm in average diameter after calcinations at 600°C and 800°C. Furthermore, by sol gel route, [7] studied on the synthesis, characterization of nano- TiO_2 The results obtained were; 5 to 10nm in diameter after calcination at 400°C, in pure anatase phase, anatase (53.4%) and rutile (46.6%) phase after calcinations at 600°C and the particle size were 22.6nm and 29.3nm respectively. 46.2nm in diameter after calcinations at 800°C, in pure rutile phase.

2. Experimental procedure

(A) Synthesis of TiO_2 (rutile)

5 grams of chitosan powder was poured into a vessel containing 100 ml of deionized water and 5 ml of acetic acid. The mixture was stirred for 6 h at 90 °C, and finally cooled naturally to room temperature. 10 grams of this as-synthesized chitosan solution was added dropwise into a vessel containing 40 ml of acetone and 4 ml of $TiCl_3$ solution, and then the vessel was covered with parafilm and left at room temperature for 2 weeks. The resulting white deposit was immersed in water to dissolve the chitosan, and then the suspension was centrifuged and washed several times with deionized water and ethanol. Finally, the powder was dried at 60 °C [8].

(B) Preparation of TiO_2 thin film

A commercially available TiO_2 powder was gotten to comparatively study the synthesised TiO_2 powder sample.

The commercially available TiO_2 powder and the synthesized TiO_2 and were used to prepare TiO_2 thin film on both empty glass substrate and Indium Tin Oxide (ITO) coated glass substrate using Spin coater. Prior to the preparation of TiO_2 thin film, the glass substrate and the Indium Tin Oxide (ITO) coated glass substrate used were cut and ultrasonically cleaned by degreasing with acetone, methanol, rinsed in iso – propanol, kept in staining jar and allow to dry in vacuum oven.

5 mg of commercially available powder of TiO_2 and synthesized sample were thoroughly mixed with 5ml of Polyethylene Oxide (PEO) solution. The resulting colloidal solution was spin coated on glass substrate and ITO at 1500rpm. The thickness of the film were measured using the weight differential method [9]

3. Results and discussion

The results are shown in Figure 1- 11 and Table 1.

X-ray diffraction (XRD) pattern (radiation used: CuKα) of both the synthesized and commercially available powder samples are shown in Figures 1 and 2 (from the diffraction pattern). There are appreciable similarities in their structures, which show that the two samples are of similar material. The d-values of synthesized sample obtained in this work are in agreement with the standard d-values of rutile structure with error of about ±1. The average particle sizes of Figure 1 and 2 were calculated using Sherrer's equation. Sherrer's equation is as follows:

$$D = 0.9\lambda / \beta\cos\theta \qquad (1)$$

Where λ is the wavelength of X-ray (0.1540nm), β is the full-width at half- maximum of the peak (in radian), and the θ is the Bragg's angle of the X-ray diffraction peaks.

The sharp diffraction peaks indicated the polycrystallinity of the TiO2 powder. The broadening of some peaks observed on the synthesised sample, according to [15], the broadening could be as a result of smaller crystals. Other causes of broadening are; instruments used and synthesis temperature of the powder [16]. The broadening could be improved by calcination [17].The little shift observed in the diffraction peaks that correspond to the main peak of the synthesised samples could be caused by particle size variation [18]. Also, the correlation between the values of diffraction angles of the synthesized sample with the commercially available one with respect to the standard value of diffraction angles of rutile structure obtained by the XRD machine (Table 1) shows that the two powder samples are of the same material. Hence, the structure further confirmed the sample synthesised to be rutile.

The particle size, 15.9 nm obtained from the synthesised sample was smaller than the commercially available one (26.7 nm) and much more smaller than 50 nm, the result obtained by [3] who used Sol gel method from Ti(OC4H9)4 precursor .

The optical transmission spectra of the films, for both the synthesized and the commercially available samples in figure 5 indicate that the synthesized TiO2 possessed higher transmission in the visible region of the spectrum than the commercially available one. This can be traced to the particle size difference between the two samples. That is, the synthesized sample is of smaller size.

Figure 6 and 7 indicated that the coated thin films showed excellent transparency, about 100% over 285 and 1085nm for the empty glass and 85% (high transparency) for the ITO glass substrate, in the visible – light region of the spectrum. More so, it was shown that, the difference observed on the film deposited on the ITO glass is slight, compared to the one on the empty glass, which is very sharp. That is, the transmittance spectrum of nano TiO2 coating on ITO substrate was quite similar to that of bare substrates. To measure the energy band gap from the absorption spectra, a graph of α2 versus E (eV) is plotted as shown in Figure 8 – 11.

$$\alpha = \frac{1}{d}\ln\left(\frac{1}{T}\right) \qquad (2)$$

Where d is film's thickness and T is transmittance.

The linear extrapolation of the plot to energy axis gives the value of the energy band gap of the film. The value obtained for the synthesized sample was 3.95 eV which agrees to 3.75eV obtained by [10] and comparable to 3.98 eV obtained from the commercially available sample. The estimated value of the band gap for the film is larger than for the for TiO2 bulk solid (3.3 eV). It was assumed, according to [11] that the increase in the band gap is due to the quantum size effect (QSE), which occurs for semiconductor particles below 100 nm. Also, this could also be inferred from the increment, 4.28eV and 4.30eV observed respectively on the ITO films. These results are also in agreement with the values reported by [12, 13, 10 and 14].

4. Conclusion

The optical behaviour of the films was investigated at room temperature. It has been found that all the films were highly transparent; they showed high transmission in the visible region of the spectrum, which reveals relatively high surface smoothness without abnormal grain growth. The analysis of the spectra also showed that

the film has an estimated energy band gap of 3.95eV on the empty glass and 4.28eV on ITO substrate.

References

1. Adewoye, O. O., (2007) Advances in Engineering Materials Development. In:Proceedings of Nigeria Materials Congress (NIMACON 2007). Held at Centre for Energy, Research and Development (CERD), Obafemi Awolowo University, Ile-Ife, Pp. 118-122.
2. Shan, C.X, Hou, X. and Choy, K. (2008) "Corrosion resistance of TiO2 films grown on stainless steel by atomic layer deposition". Surf. Coat. Tech. 202, Pp. 2399-2402.
3. Tang, Z. L., Zhang, J. Y., Cheng Z and Zhang, Z. T. (2001) "Synthesis of Rutile TiO2 at low Temperature" Mater. Chem. Phys.,Vol. 77, Pp 314.
4. Yu, J. C., Yu, J. G., Zhang, L. Z and Ho, W. K. (2002) "Photocatalytic activity of nano-sized TiO2 powders by sol –gel method, using titanium tetraisopropoxide and EtOH/H2O solution." J. Photochemistry. Photobiology. A: Chem., Vol. 148, Pp. 263.
5. Li, Y. Z, Lee, N. H., Lee, E. G Song J. S. and. Kim, S. (2004) "Preparation and characterization of nano – TiO2powder by sol-gel method" J. Chem. Phys. Lett., Vol. 389, Pp.124.
6. Ruiz, A. M. . Sakai, G. Cornet, A. Shimanoe, K. Morante, J. R and Yamazoe, N. (2004) "Microstructure control of thermally stable TiO2 obtained by hydrothermal process." Sens. Actuators., B 103, Pp. 312.
7. Qiu S. and Kalita, S. (2006) "Synthesis and characterization of nano- TiO2" J. Mater. Sci. Eng. A, Vol. 327, Pp. 435-436,
8. Chen, S.F., Li, J.P., Qian,K., Xu, W.P., Lu, Y., Huang, W.X., Yu, S.H. (2010) "Large Scale Photochemical Synthesis of M@TiO2 Nano composites

(M = Ag, Pd, Au, Pt) and Their Optical Properties, CO Oxidation Performance, and Antibacterial" Effect.www.springerlink.com. Accessed on 29th September 2010.

9. Choi J. Y, K. Kim, Yoo J. and Kim D., (1998) "Properties of Cadmium Sulphide Films Deposited by Chemical Bath Deposition with Ultrasonication", Solar Energy Vol.64, Pp. 41-47.
10. Kim ,B.H., Ahn, J.H., Jeong, J.H., Jeon, Y.S., Jeon, K.O., , Hwang, K.S., (2006) "Preparation of TiO2 thin film on SiO2 glass by a spin coating–pyrolysis process." Ceramics International, Vol 32, Pp. 223–225.
11. Ito, S., Chen, P., Comte, P., Khaja, M., Nazeeruddin, K., Liska .P., Pe´chy, P., and Gra¨tzel, M. (2007) Fabrication of Screen-Printing Pastes From TiO2 Powders for Dye-Sensitized Solar Cells, Progress In Photovoltaics: Research And Applications, Published Online In Wiley InterScience (www.interscience.wiley.com)
12. Addamo, M., Augugliaro, V. Paola., A., García-López, E., Loddo, V., Marcì, G., Palmisano, L. (2008) "Photocatalytic thin films of TiO2 formed by a sol–gel process using titanium tetraisopropoxide as the precursor". Thin Solid. Films.Vol. 516, Pp. 3802–3807.
13. Ito,S., Takeuchi, T., Katayama,T., Sugiyama,M., Matsuda, M., Kitamura,T., Wada,Y., and Yanagida,S.(2003) "Conductive and Transparent Multilayer Films for Low-Temperature-Sintered Mesoporous TiO2 Electrodeof Dye-Sensitized Solar Cells". Chem. Mater. Vol. 15, Pp.2824-2828
14. Raghupathi, P.S., George, J and.Menon, C.S. (2005) "The Effect of Deposition Rate on Electrical, Optical and Structural Properties of ITO Thin Films". E-Journal of Chemistry Vol. 2, No. 8, Pp 171-177.
15. Reddy, D. S., Reddy, D. R., Reddy, B. K., Reddy, A.M., Gunasekhar, K. R. and Reddy, P.S. (2007) "Annealing effect on physical properties of thermally evaporated MnS nanocrystalline films" Journal of Optoelectronics And Advanced Materials Vol. 9, No. 7, Pp. 2019 - 2022
16. Wahi, R.K., Liu, Y., Falkner, J.C. and Colvin, V.L., (2006) " Solvothermal synthesis and characterization of anatase TiO2 nanocrystals with ultrahigh surface area" Journal of colloid and interface science. Vol. 302, Pp. 530–536.
17. Addamo, M., Augugliaro, V. Paola., A., García-López, E., Loddo, V., Marcì, G. and Palmisano, L. (2007) "Photocatalytic thin films of TiO2 formed by a sol–gel process using titanium tetraisopropoxide as the precursor". Thin Solid Films. Vol. 516, Pp. 3802–3807.
18. Kim, B.H., Ahn, J.H., Jeong, J.H., Jeon, Y.S., Jeon, K.O. and Hwang, K.S., (2006) ' Preparation of TiO2 thin film on SiO2 glass by a spin coating–pyrolysis process'. Ceramics International. Vol. 32 Pp. 223–225.

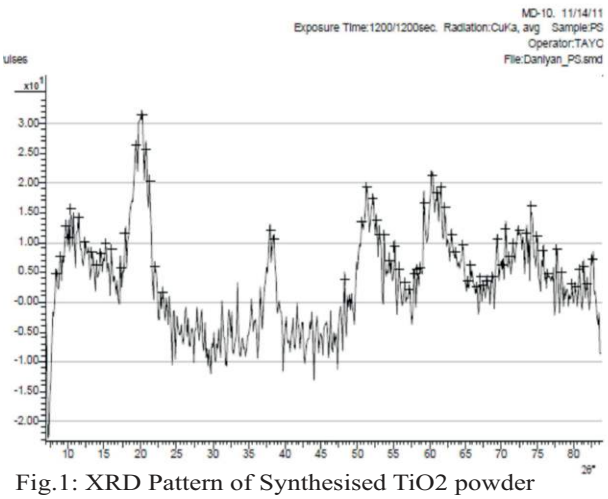


Fig.1: XRD Pattern of Synthesised TiO2 powder

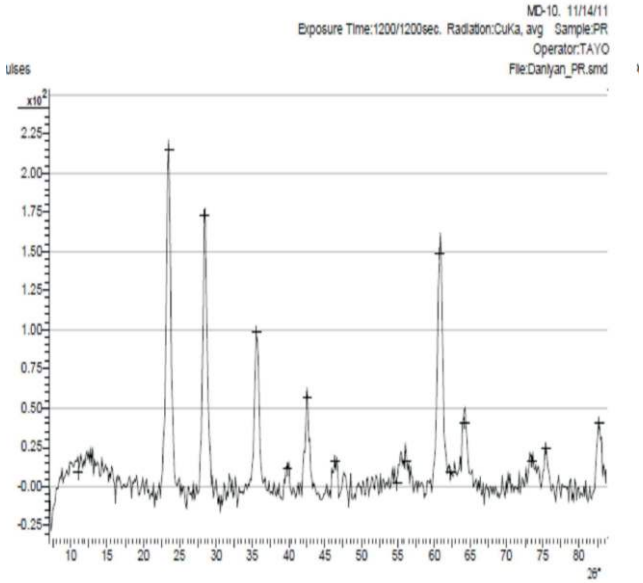


Fig. 2: XRD Pattern of the commercially available TiO_2 powder

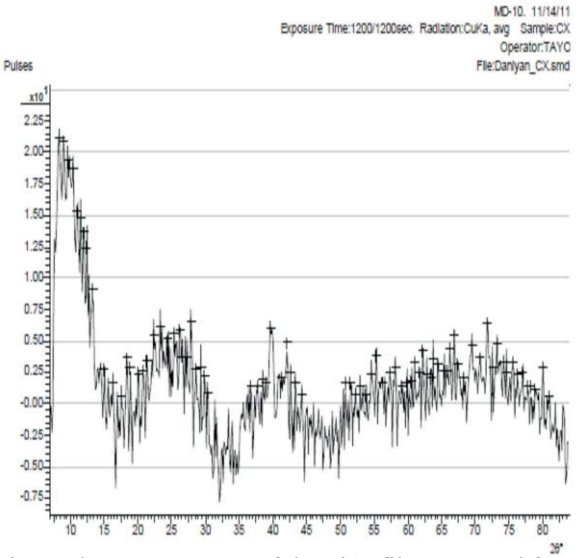


Fig.3: The XRD Pattern of the TiO_2 film prepared from synthesised TiO_2 powder

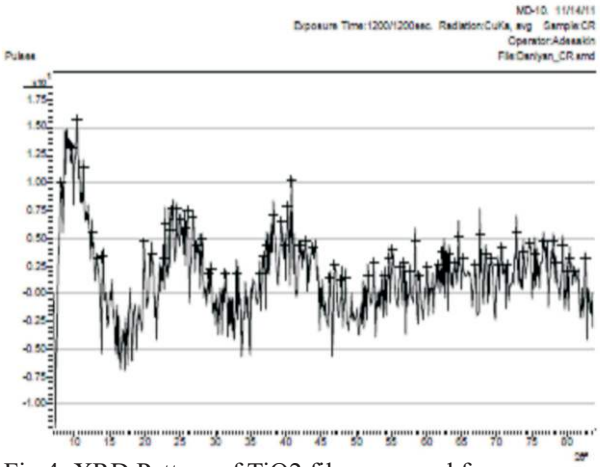


Fig.4: XRD Pattern of TiO2 film prepared from commercially available TiO2 powder.

Table 1: Diffraction angles of the synthesized (S 2?°) Commercially available TiO2 powder (R 2?) and the

S 2θ°	R 2θ	STD 2θ°	h k l
22.99	23.39	27.45	1 1 0
38.47	35.53	39.19	2 0 0
52.63	42.50	54.32	2 1 1
63.75	64.17	64.04	3 1 0
82.45	82.60	82.34	3 2 1

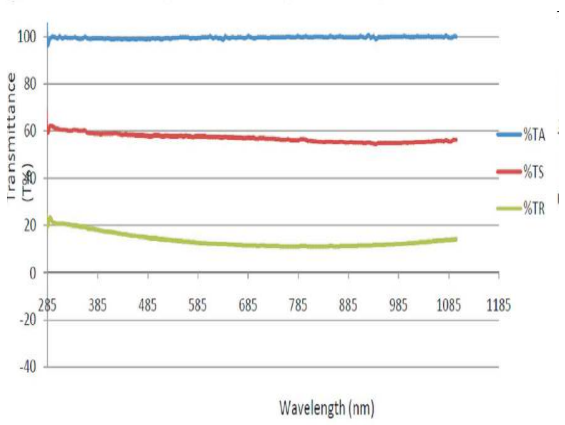


Fig. 5: Optical transmittance plot of the PEO solution, synthesized and commercially available TiO_2

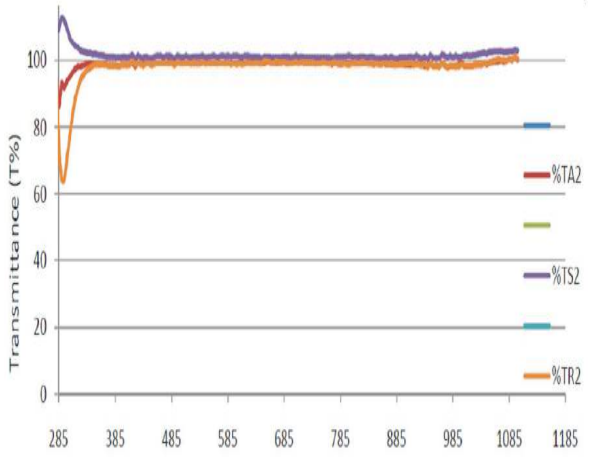


Fig. 6: Optical transmittance plot of the PEO, the synthesized and commercially available TiO_2 film

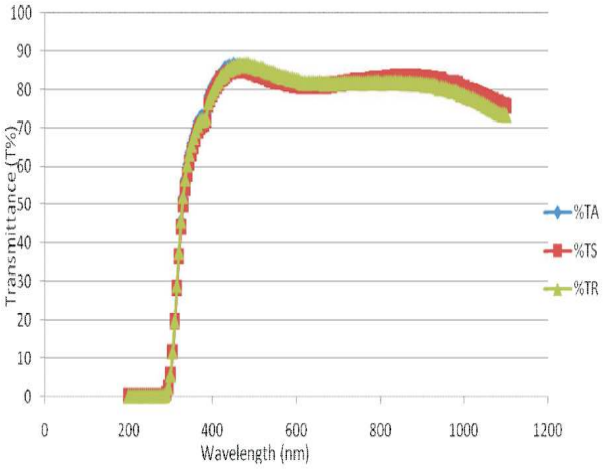


Fig. 7: Optical transmittance plot of the PEO, synthesized and commercially available TiO_2 film on ITO glass

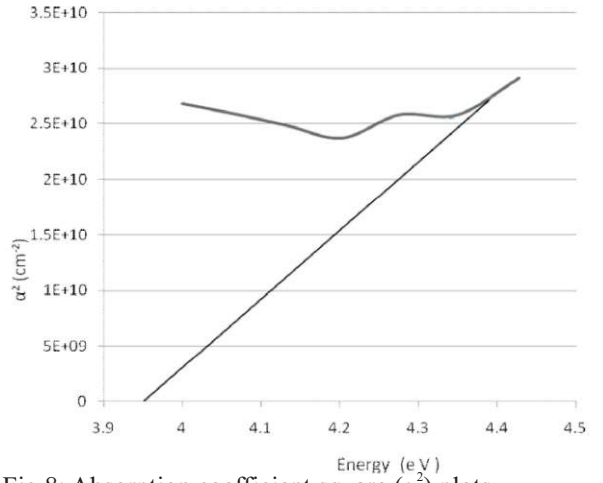


Fig.8: Absorption coefficient square (α^2) plots of the synthesized TiO_2 on empty glass

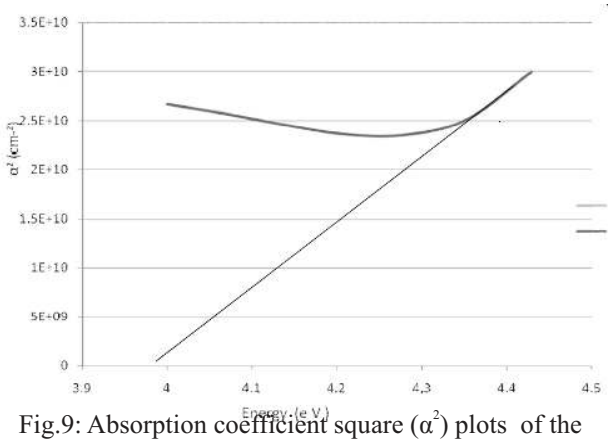


Fig.9: Absorption coefficient square (α^2) plots of the commercially available TiO_2 on empty glass

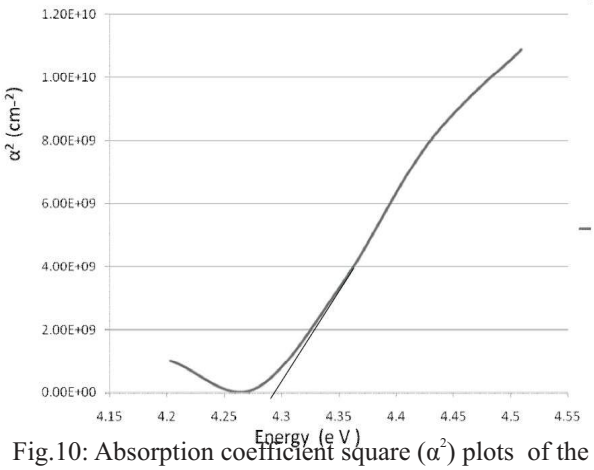


Fig.10: Absorption coefficient square (α^2) plots of the synthesized TiO_2 on ITO glass

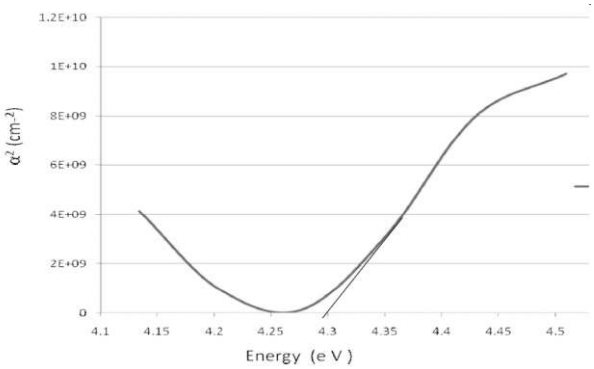


Fig.11: Absorption coefficient square (α^2) plots of the commercially available TiO_2 on ITO glass

INFLUENCE OF THE SPUTTERING PRESSURE ON THE OPTICAL CHARACTERISTICS OF TIN_X/TIO_XN_Y THIN FILMS PREPARED VIA REACTIVE MAGNETRON SPUTTERING

E. Ajenifuja, A. Y. Fasasi, G. A. Osinkolu
Centre for Energy Research and Development, Obafemi Awolowo University, Ile-Ife, Nigeria.
E-mail: emmanuelaje@yahoo.com, eajenifuja@cerd.gov.ng

Abstract

In the sputtering deposition technique, the sputtering pressure is usually a function of the inert working gas pressure and the reactive gas pressure depending on the kind of deposition (reactive and non-reactive). Within the context of this work, coloured films based on single layered titanium nitride were synthesized by varying the sputtering pressure (S-Pr), thereby using low (0.80Pa), intermediate (3.40-5.33Pa) and high (11.33Pa) S-Pr. The deposited films possessed colour that ranged from dark blue characteristic of oxygen-rich titanium nitride (Ti-N_y-O_x) films to reflective golden yellow reminiscent of low oxygen content TiN_x films. Studies on the optical properties were carried out using UV-Visible Spectrophotometry. Characterization results showed variation in the optical properties of the film depending on the deposition sputtering pressure. High sputtering pressure is shown to be beneficial to the formation of oxygen- deficient TiN_x thin films with relatively higher bandgap compared to films deposited under lower sputtering pressure.

Keywords: Titanium Nitride, Magnetron, Sputtering, Bandgap, UV-Visible

. Introduction

Titanium nitride is a widely-known material, which exhibits excellent mechanical properties such as high hardness, high wear resistance, low electrical resistivity, high chemical and thermal stability, and interesting optical properties, the colours varying from gold to dark brown. Titanium nitride have been applied in areas such as abrasion resistant coatings on tool steels, decorative coatings in architecture, diffusion barrier layers in semiconductor devices and flat panel displays [1-3].

Titanium nitride films are usually found to contain a trace amount of oxygen as impurities, and the amount of oxygen strongly depends on the deposition conditions used. The deposition of TiN_x and TiO_xN_y films by sputtering has important specific advantages such as low levels of impurities and easy control of deposition rate just by varying the deposition conditions. Based on this premise, it can be assumed that progressive layers of different materials can be obtained on a suitable substrate in a single experimental session. Great efforts have been expended to realized better films quality especially to meet the current technological realities and expectations, therefore numerous studies have been tailored towards the understanding of the effects of process parameters such as sputtering power, substrate temperature [4], rapid thermal annealing [9], sputtering gas, reactive gas pressures and sputtering pressure [5, 6, 7] on other oxides, metallic and ceramic thin films. We present the report on the deposition of TiNx/ TiOxNy thin films with the primary focus on the sputtering deposition pressure effects on the film formation, the optical and micro-structural characteristics of deposited thin films. These properties are however found to be strongly dependent on the sputtering pressure.

2. Materials and Methods

2.1 Deposition Procedure

The films were deposited on glass substrates by DC magnetron sputtering with DC power kept constant at 200W. The sputtering cathode with titanium target in place with the dark anode shield is shown in Fig. 1. The substrate was cleaned by rinsing sequentially with the following; methanol, acetone, de-ionized water and finally in 20% HNO_3 to remove dust and oily layer on the surface and then finally dried using nitrogen gas. For the plasma generation, high purity argon was used and the sputtering target was circular 99.99% pure Ti (50.8 mm in diameter and 5 mm in thickness) fixed at an angle of around 45 degree relative to static substrate platform with an indirect cooling system. In all the depositions, after reaching a base vacuum of 1.33E-3 Pa, the deposition chamber was filled with pure argon after which the reactive nitrogen was introduced up to the chamber pressure parameter required for a particular deposition. However, before starting the deposition, the targets were pre-sputtered in high purity argon gas plasma for average time of 5 min prior to the introduction of the reactive nitrogen gas. The uniform base pressure and other process parameters employed for all depositions are as stated in Table 1.

2.2 Characterization Details

The equipment used for the X-ray diffraction analysis was MD-10 Precision Mini X-Ray Diffractometer with 2 theta angle between 16° and 72° by using CuK_α radiation. Scanning electron microscopy instrument (Carl Zeiss MA-10 SEM) equipped with energy dispersive spectroscopy (EDS) facility was used to study the surface

morphology and the microstructure of the films at an acceleration voltage of 20 kV. UV-Visible Thermo Scientific Helios Omega machine was used to obtain the transmittance data of all the films. The acquired data was used to generate the normalized transmittance to have a better picture of films transmittance in visible regime and most significantly for absorption edge shift evaluation. *The study of the thickness in the nanometer range and the surface topography of the films were carried out using Dektak 150 surface stylus profiler.*

3. Results and Discussion

3.1 Optical Characteristics

The films deposited at high and intermediate sputtering pressures *hsp*, *msp1* and *msp2* showed a reflective golden colour characteristic of TiN_x, while sample *lsp* deposited at low sputtering pressure possessed dark blue colour characteristic of oxygen-rich titanium nitride (Ti-N_x-O_y). The percentage and normalized optical transmittance spectra of the TiNx films prepared at varying sputtering pressures are shown in Figs. 2 and 3 respectively. Obviously the optical transmittance is low in the visible region for the low sputtering pressure prepared sample (lsp) and increased from 10.05% to 97.52% with the increase of sputtering pressure from 0.80Pa to 11.53Pa respectively. The optical transmittance of the films prepared at low sputtering pressure of 0.80Pa was low probably due to the formation of sub-stoichiometric TiN_xO_y film with characterization of the dark blue colour due to the combination of the oxygen ion with the reactive nitrogen gas and titanium. The oxygen ions may have originated from two sources, residual air in the deposition chamber or impurity component from the reactive gas. In addition, the presence of non-reactive titanium along with TiN_xO_y phase could act as scattering centers of light and thus the decrease in the transmittance of the film deposited at low sputtering pressure. Afterwards as the sputtering pressure increased to within the range 3.40Pa and 11.33Pa with the consequent increase in the nitrogen partial pressure, the transmittance of the films increased since most of the nitrogen vacancies tends to disappear and hence the composition of the films approached that of TiN_x. The films prepared at higher sputtering pressure between 3.40Pa and 11.33Pa possessed high transmittance (89.14% to 97.52%) in the visible region and towards the near infrared region with reflective golden colour indicating stoichiometric titanium nitride behaviour. Zhou Ji-Cheng et al [9] also observed that with the increase of sputtering pressure, the surface roughness of the films decreases, which reduces the scattering effects on the visible light. Under the condition of high sputtering pressure with relative higher concentration of nitrogen gas, with bombardment of the target surface by some nitrogen ions, the nitride films deposited were formed not only from direct combination between titanium and nitrogen, but also from titanium nitride generated at the target surface. This was shown from the visual observation of the target after the deposition.

On the transmission bands of the films, Jeyanchandra et al., [8] observed that the broadness of the visible transmission band and the transmittance of the TiN_x films increased with an increase in the N_2 concentration. Sample *lsp* deposited under the low sputtering pressure condition (0.80Pa) with relatively lower nitrogen concentration exhibited a narrower transmission band in the visible region followed by a sharp dip towards the near infrared, while TiN_x film samples prepared at high and intermediate sputtering pressure possessed higher and broader transmission band with a slight dip towards the near infrared. The transmittance band shifted towards higher wavelength with increase in the thickness of the films. Durusoy et al. [10] reported that a narrow transmission band in the wavelength region 300-600nm and a low transmittance towards higher wavelength region are typical of TiN films.

3.2 Bandgap Analysis

Th[illegible]cient of the films was det[illegible]smission data where the reflection loses were taken into account. While, the optical bandgap of the film was evaluated from the plot of $(\alpha hv)^2$ versus photon energy (hv) using the Tauc's relation (equation 1) [11].

$$(ahv) = B(hv - E_g)^r \quad (1)$$

Where B is a parameter that depends on the transition probability Eg is the optical bandgap energy of the material, hv is the photon energy and r is an index that characterizes the optical absorption process. For this work, r is equal to ½ for direct allowed transition. Figs. 4 and 5 show the bandgap energies for the films deposited at high sputtering pressure (11.33Pa), intermediate sputtering pressure (3.40Pa and 5.33Pa) and low sputtering pressure (0.80Pa) respectively. From the figures, it shows that sample lsp possessed the lowest gap energy of 3.75eV, while films deposited at high and intermediate sputtering pressure possess a common value of bandgap energy (3.78eV). Large bandgap from 3.70 to 4.50eV have been reported for non-stoichiometric TiNx films ($0.2 \leq x \leq 0.5$) by Kuppuswamy et al. [12]. The difference in the bandgap energies (Table 2) is a pointer to the fact that there is a compositional change in the material based on the deposition pressure. The thin films prepared at sputtering pressures 3.40Pa, 5.33Pa and 11.33Pa, as shown in Fig. 4, all have a common bandgap energy, which indicated a strong connection between the films in term of their composition. The extinction coefficients (k plots) of the films prepared at varying sputtering pressures are shown in Fig. 6 with the inset figure showing the closer observation of the films prepared at high sputtering pressure. The films exhibited minimum extinction coefficient values within the range of 450nm – 550nm. On the average, the extinction coefficient of the films decreased with the increase of sputtering pressure. As stated earlier, it shows that the scattering centre concentration decreases with the sputtering pressure due to the reduction in the roughness and the crystallites size of the films as the sputtering pressure increases.

4. Conclusion

In this work, TiNx thin films with distinctive optical and microstructural characteristics were deposited on glass

substrates by DC reactive sputtering technique using 99.99% pure titanium as the target material and laboratory grade N2 as the reactive gas. It is observed that low sputtering pressure (0.80Pa) favours the formation of oxygen-rich TiNx (Ti-O-N phase) films as shown from their unique colour, while high sputtering pressure (3.40-11.33Pa) enhances the formation of typical reflective golden yellow titanium nitride with unique ITO-like properties (large bandgap, low UV transmission, dipped IR transmission) which could make them to be suitable as optical pass filters, UV detectors, hot mirrors etc.

References

[1] B. Rauschenbach, J. W. Gerlach, Cryst. Res. Technol. 35 (6-7) 675-688 (2000)

[2] T. S. Yeh, J. M. Wu, L. J. Hu, Thin Solid Films 516, 7294-7298 (2008)

[3] J. E. Sundgren, H. T. G. Hentzell, J. Vac. Sci. Technol., A4 2259 – 2279 (1986)

[4] K. Vasu, M. Ghanashyam Krishna, K. A. Padmanabhan, Applied Surface Science, 257 3069 – 3074 (2011)

[5] Young-Soon Kim, Young-chulpark, S. G. Ansari, Jeong – Young Lee, Byung – Soo Lee, Hyung- Shik Shin, Surface and Coatings Technology 173 299–308 (2003)

[6] Pengtao Gao, L. J. Meng, M. P. dos Santos, V. Teixeira, M. Andritschky, Applied Surface Science 173 84-90 (2001)

[7] V. Nirupama, K.P. Gunasekhar, B. Sreedhar, S. Uthana, Current Applied Physics 10 272-278 (2010)

[8] Y. L. Jeyachandran, Sa. K. Narayandass, D. Mangalaraj, Sami Areva and J. A. Mielczarski, Material Science and Engineering A 445-446 223-236 (2007)

[9] Zhou Ji-cheng, Luo Di-tian, Li You-Zhen and Liu Zheng, Trans. Nonferrous Met. Soc. China 19 359 – 363 (2009)

[10] Durusoy, H.Z. and Duyar, O. and Aydinli, A. and Ay, F., Vacuum, 70 (1). pp. 21-28 (2003)

[11] J. Tauc, R. Grigorovici, and A. Vancu, Phys. Status Solidi 15, 627 (1966)

[12] T. N. Kuppuswamy, P. Anantha, K. Ghanashyam, A. P. Mamidipudi, K. N. Sri-Rama and A. P. Mangalampalli, US Patent Application Publication, US 2010/0323205 A1 (2010)



Fig. 1 Sputtering cathode with the titanium target installed and the dark anode shield

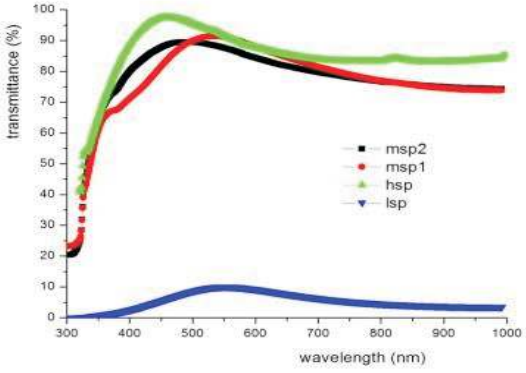


Fig. 2: % Transmittance for high, intermediate and low S-Pr films.

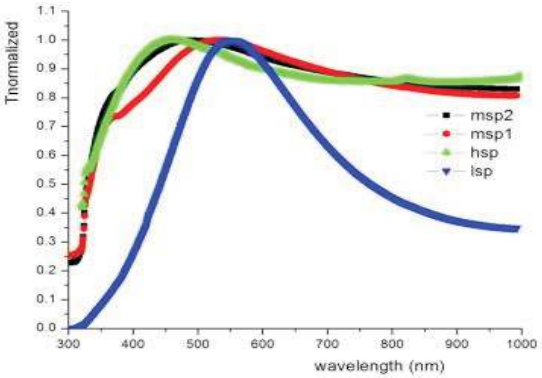


Fig. 3: Normalize Transmittance for high, intermediate and low S-Pr films

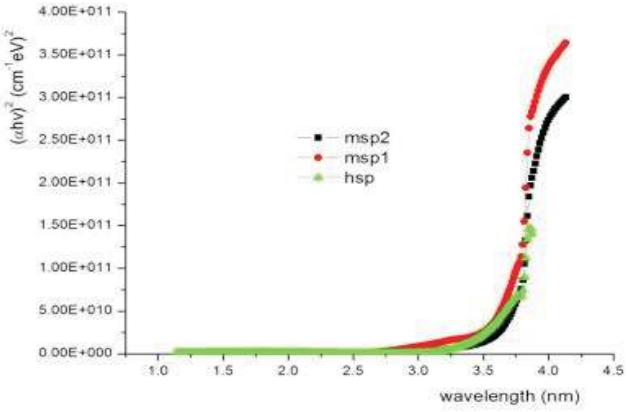


Fig. 4: Bandgap energy for high and intermediate S-Pr deposited films

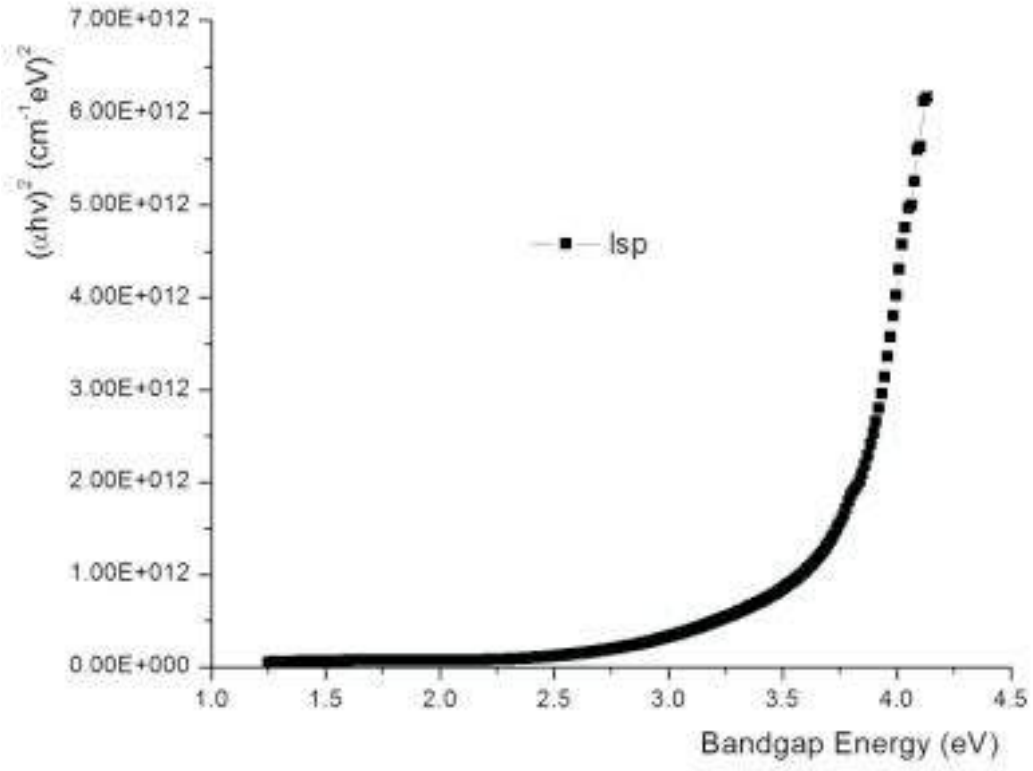


Fig. 5: Bandgap energy for low S-Pr deposited films.

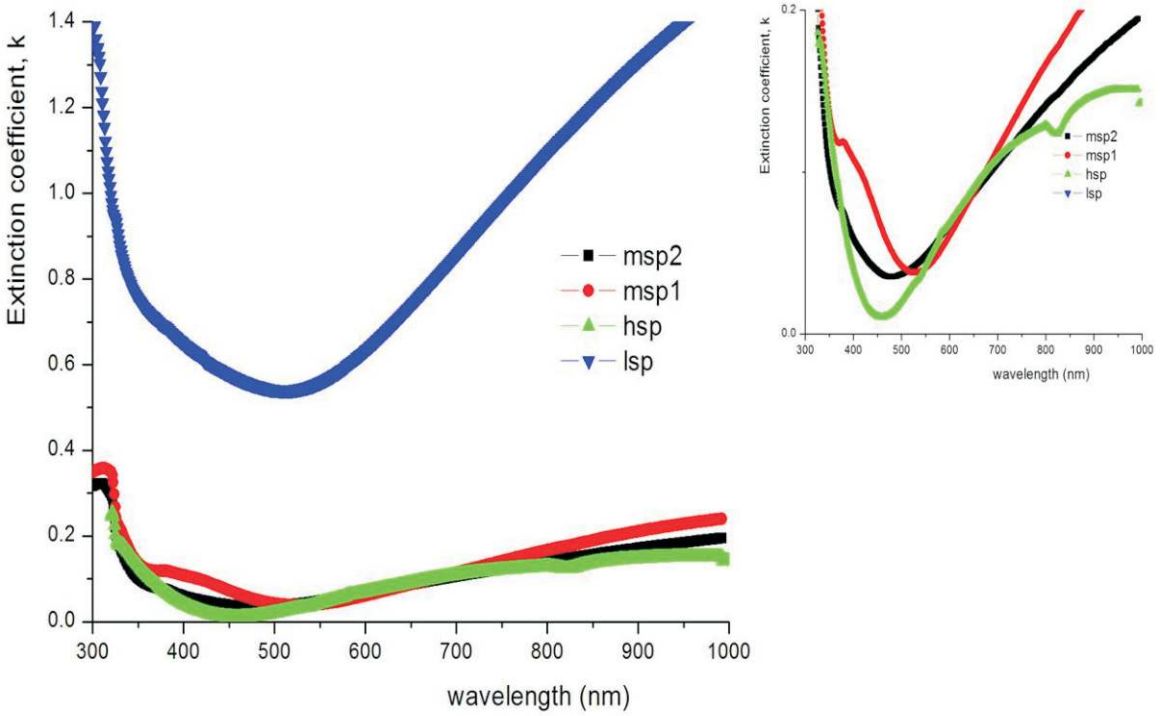


Fig. 6: Extinction coefficient for intermediate, low and high S-Pr deposited fill

Parameters	Values
Target	Ti
Sputtering Gas	Ar
Reactive Gas	N_2
Sputtering Power	200W
Deposition Time	10 minutes
Base Pressure	1.33×10^{-3} Pa
Sputtering Pressure	0.80 - 11.33 Pa
Substrate	Glass slide
Substrate-Target	150mm

Table 1: Sputtering Parameters for TiN_x/TiO_xN_y thin films

Sample	Thickness (nm)	Sputtering Pressure (Pa)	Dep. Time (min)	Peak Transmit. (%)	Bandgap Energy (eV)
Lsp	180	0.80	10	10.03	3.75
msp2	120	3.40	10	89.14	3.78
msp1	100	5.33	10	91.21	3.78
Hsp	90	11.33	10	97.52	3.78

Table 2: Optical properties of TiN_x/ TiO_xN_y films with varied sputtering pressure

PHYSICOCHEMICAL CHARACTERIZATION OF CRUDE OIL SAMPLES FROM SELECTED OIL FIELDS IN NIGERIA

[1,2]Ikutegbe, C. A.; [3]Edoga, M. O.; [1,4]Akinluwade, K. J. and [1,4]Adetunji, A. R.
[1]Prototype Engineering Development Institute (PEDI), Ilesa
[2]Department of Chemical Engineering Obafemi Awolowo University (OAU), Ile-Ife
[3]Department of Chemical Engineering Federal University of Technology, Minna
[4]Department of Materials Science and Engineering Obafemi Awolowo University Ile-Ife
Correspondence Author: charlesakay@gmail.com

ABSTRACT
This study was carried out to determine the physicochemical properties of some selected Nigerian Crude Oils. Crude oil samples tested were collected from the Imiringi oil well and Nembe oil well. The properties tested for include sulphur content, pour point, flash point, specific gravity (S.G), American petroleum institute gravity (^{0}API), viscosity, carbon residue, basic sediment and water (BS&W), ash content, sand content, reid vapour pressure, salt content, asphalt content, total acid number and metals in crude. Results obtained from comparative analysis of the characterization factor (K) showed that the Imiringi crude oil (K=12.29) is parraffinic while that of Nembe (K=10.80) is napthanic. Both crudes however, belong to the class of high-grade crude oil with high API gravity (low sulphur content) in the range 21—45 ^{0}API as the acceptable range for light crudes in Nigeria.

Keywords: crude oil, physicochemical properties, characterization factor (K), naptha, paraffin

Introduction

Crude oil is a naturally occurring liquid found in formations in the earth consisting of a complex mixture of hydrocarbons (mostly alkanes) of various lengths. The approximate length range is C_5H_{12} to $C_{18}H_{38}$. Any shorter hydrocarbons are considered natural gas or natural gas liquids, while long-chain hydrocarbons are more viscous, and the longest chains are paraffin wax. In its naturally occurring form, it may contain other nonmetallic elements such as sulfur, oxygen, and nitrogen. It is usually black or dark brown (although it may be yellowish or even greenish) but varies greatly in appearance, depending on its composition. [1] ***Nigeria is the largest oil producer in Africa.*** (Nigeria had 35.9 billion barrels of proven oil reserves as of January 2006. The Nigerian government plans to expand its proven reserves to 40 billion barrels by 2010. The majority of reserves are found along the country's Niger River Delta, with the majority of oil located in approximately 250 small (i.e., less than 50 million barrels each) fields. However, at least 200 other fields contain undisclosed reserves. [2]**.** One widely accepted postulate is that petroleum is generated by the decomposition of the remains of some certain aquatic organisms (marine algae) and animals, deposited in layers. Subsequently on the sea bed for a very long period of time say (400 to 500million years). The inorganic origin of petroleum has also been taken into consideration, but such a theory seems to be much less possible. As far as the organic origin is concerned, it postulates that organisms forming residues after death were deposited for a very long period of time on the sea bed and covered by layers of mud and other sediments. [3] In this regard, such environmental conditions of high temperature and pressure, low dissolved oxygen concentration results in decaying process that forms oil and gas. However, oil fields with different characteristics can exist because it is originated through some different geological and physical phenomenon. [4] Known reserves of petroleum are typically estimated at around 1.2 trillion barrels without oil sands, or 3.74 trillion barrels with oil sands. However, oil production from oil sands is currently severely limited. [5]

Composition of Crude Oil

The chemical composition of crude varies between regions and even within the same geologic formation. No two batches of crude oil are chemically identical. Crude oil is categorized based on the molecular weight distribution of their constituents, and distinctions are made between light, medium, and heavy crude oil. The density ranges from 0.800g/cm^3 to almost 1.000g/cm^3. Generally, crude oil is inflammable in ambient conditions and its odor can also vary from very pleasant aromatic odor in the case of some light crude oil to strongly unpleasant garlic smell, usually associated with sulphur derivatives. [6]

METHODOLOGY

Description of Kolo Creek Oil Field and Nembe Creek Oil Field

Kolo creek oil field

Kolo Creek oil field is a 5X10km size, faulted, rollover structure with the E2.O reservoir as the main oil bearing sand. It is located on the eastern part of Bayelsa state in a community known as Imiringi, about 10km from Yenagoa the state capital. It lies on land reclaimed from the natural swamp and it is accessible by road, but only by water and air. Since its commissioning, it has been in full

operation by Shell petroleum development company (SPDC). The crude oil from "well E2- ox", enters the manifold through a 2x4 inch flow line from the Kolo creek oil field to the flow station situated at Imiringi a community in Bayelsa State. The Kolo creek flow station has a production capacity of 25,000bbl/d, and its crude has a trade name called "Bonny light"

Nembe creek field

Nembe creek oil field is a remote and predominantly mangrove swamp area with numerous creeks and rivers located at the eastern bank of the St. Nicholas River in the Nembe local government area of Bayelsa State, in the Niger Delta region of Nigeria. It has four crude oil flow stations; I, II, III, and IV each for Nembe creek I, Nembe creek II, Nembe creek III and Nembe creek IV respectively. Access is available only by helicopter or boat which created logistic difficulties. It is being operated by Shell Petroleum Development Company (SPDC). The crude oil from "well 42" gets to piping manifold via a 12 inch flow line from the Nembe creek oil field to the Nembe crude oil flow station. The Nembe creek flow station has the largest production capacity of 120,000bbl/d. Also has a trade name 'Bonny light'.

Procurement of Crude Oil Samples

Samples for the test analysis were taken from the samples withdrawal point at the manifolds of Kolo creek flow station and Nembe creek flow station respectively. At each of the manifold, the valve belonging to a particular well is gradually opened for samples to be collected. Here, the samples collected are in there raw form and not pretreated form. Also, the samples have not been mixed with crude oil gotten from other similar oil wells within same field linked via flow lines to the manifold. During collection, a 1 litre 'Ragolis' bottle was used in order to get enough sample for the proper conduction of test and to obtain accurate results. The analysis of the parameters was carried out in the laboratory according to the set standards for crude oil analysis by the American Society for Testing and Materials (ASTM) and Institute of Petroleum (IP). The analysis was carried out in the Petroleum Analysis Laboratory (PAL) and Science Laboratory Technology. (SLT), both of Petroleum Training Institute (PTI) Effurun

Measurement of sulphur content in crude oil using sulphur analyzer. [ASTM D1266]

Procedure: The sulphur analyzer (Figure 3) was switched on and left to age for about 1800 seconds (30 minutes during which the time and date (year, month and day) were set). The instrument was then calibrated using different sulphur content of standards values. Hence the samples were poured in one after the other in the sample pot of the instrument and depressing the bottom of their corresponding number of counts display. The calibration process took about 300 seconds each (total time is 900 seconds) at the end of which the measuring light shone, indicating that the instrument is ready for measurement. The sample was then measured or poured into the sample cell to mark and covered with cellophane (seal). The cell and its contents were then slotted into the sample pot of the sulphur analyzer with the cellophane side facing downwards. After 200 seconds the instrument then displayed and printed out both the corresponding amount and the average weight of sulphur present in the sample results.

Measurement of pour point of crude oil [ASTM D97]

Procedure: The automatic tester (Figure 2) was switched on. The crude oil sample was left in the laboratory for 24 hours in order to attain laboratory temperature and after which it was poured carefully into test jar up to 30ml mark. The test jar was then covered tightly with the cork carrying the test thermometer up to the point where the bulb of thermometer was 3mm below the surface of the crude oil sample. After the initial temperature has been recorded, the test jar was placed in the jacket in a vertically upright position inside the pour point apparatus and the top covered properly. The method of operation of the pour (automatic tester): Point apparatus is that of the American standard of testing and materials ASTMD 97, which an expected pour point value was keyed into the (automatic tester) pour point apparatus. The test jacket title when the temperature of the crude oil was observed to be 9°C close to the expected pour point (estimated as a multiple of 3°C). At every 3°C change in temperature, the test jacket was observed to till until a point is reached at which the crude oil showed no movement when the test jar was removed and held in a horizontal position for 5seconds, the printer prints the result of the initial reading test temperature.

Measurement of flash point using pensky – martens closed up apparatus [ASTM D93].

Procedure: Using the pensky-martens closed cup tester, the inner cup of the tester was cleaned using a cleaning solvent such as toluene or acetone to remove any solvent which had been used previously. The cup was then filled to at least 85% of the total volume capacity with crude oil sample, the thermometer placed, the lid closed, and the test flame heated and adjusted for every nine

(9) degree rise in temperature. A mechanism which controls the shutter was operated so that the test flame burner is lowered into the vapor space in 0.5 second and quickly raised to its high position. The temperature on the thermometer at the time the test flame ignites shows a distinct flash that is recorded as the flash point.

Measurement of specific gravity/American petroleum institute (API) gravity of crude oil [ASTM D1298]

Procedure: The measuring cylinder (100ml) was washed with water and soap after which it was rinsed with the crude oil sample and placed on a workbench to ensure that it stood erectly (vertically) in a free location from contact (Figure 1). Crude oil sample was transferred into the clean measuring cylinder without splashing to avoid minimum evaporation of the lower boiling point constituent until it got to 90ml mark of the measuring cylinder. Air bubbles formed at the surface of the sample were removed by touching them with a piece of clean filter paper before the hydrometer was inserted.. When the hydrometer starts floating freely on the surface of the sample without touching the wall of the measuring cylinder, the reading

for specific gravity was taken and recorded on the stem of the hydrometer. The temperature of the sample was also taken and recorded by inserting a thermometer.

Measurement of carbon residue [ASTM D198]
Procedure: The porcelain crucible was first weighed empty, after which 10grams of crude oil sample was poured into the crucible; the crucible and the content (crude oil sample) were together weighed and recorded. The porcelain crucible was lowered into the centre of the skid more crucible. Both crucibles were introduced into a large iron crucible that was covered at the bottom at about 10mm layers of sand. The skid more crucible and iron crucible were covered but the cover of the latter loosely fitted so that the free exit of vapour can be allowed. On the tripod stand, the triangle nicnihrome wire was placed on it, the insulator and the crucibles covered with an iron hood (chimney) and a high strong heat from the meter type gas burner was applied for five minutes and smoke was seen above the chimney and this smoke was ignited immediately for the purpose of burning the vapor by tilting burner carefully to one side. This process was done repeatedly for about 13 minutes until no blue flame was seen (i.e. until the vapor cease to burn). After this stage, the heat was maintained for another 7minutes to ensure total burning. At the end of the specified heating period, the test crucible containing the carbon residue was collected in a desiccator and weighed.

Measurement of viscosity of crude oil using an automated viscometer [ASTM D445]
Procedure: The automated viscometer apparatus (Figure 4) was switched on and the viscometer bath temperature was elevated/set at 210°F (98.9°C). An appropriate clean and dry u-tube viscometer was selected for use. The crude oil sample was first poured into a beaker and hence into the reservoir arm of the u-tube viscometer with the oil to the 30ml mark while the working arm was closed. The suction pump was used to aid the movement of the oil upwards inside the capillary tube just above the upper mark of the u-tube viscometer. On opening the working arm of the u-tube viscometer, the oil starts flowing downwards. The time of flow from the upper mark to the lower mark of the working arm of the u-tube viscometer was taken and recorded.

Measurement of basic sediment and water in crude oil by centrifuge method [ASTM D96]
Procedure: The centrifuge tubes were properly washed, cleaned and dried with clean water, soap and a very clean rag. The manual centrifuge apparatus was positioned on a work bench with its stand clamped to the bench. The samples were properly mixed to give a homogenous mixture for each sample, before they were poured into each of the 0ml centrifuge tube to the 10ml mark. The tubes containing the samples were placed in opposite direction inside the centrifuge tube holder of the apparatus. Care was taken to ensure they were fitted properly to avoid accident while spinning. With the use of the hand crank, the machine was centrifuge at 500rpm (revolution per minute) for 10 minutes, then, the hand crank was removed leaving/allowing the centrifuge jacket and allowed to settle down, in order to ensure proper separation of fractions of crude oil, sediments and water. From the graduated body of the centrifuge tubes, readings of different fractions were taken and recorded.

Measurement of ash content in crude oil [ASTM D482]
Procedure: Evaporation of the sample was done at a temperature range of 700 to 800°C and allowed to cool to room temperature in a container. And was weighed to the nearest 0.1mg. The sample was weighed into the evaporating dish, which was with flame maintaining the temperature at which the sample continues to burn at a uniform and moderate rate, leaving only ash and carbon when burning cease. The residue was heated in the muffle furnace with temperature at 775 + 25°C until all carbonaceous material had disappeared. The dish was cooled to room temperature in a porcelain dish and weighed to the nearest 0.1mg

Measurement of sand content in crude oil using sieve analysis [ASTM D98]
Procedure: The apparatus were properly cleaned with shellite and dried with acetone. The sample of crude oil was measured out and poured into the big beaker through the sieve, with a continuous stirring. The shellite and acetone were used to wash and dry sample after every 6 sieving. The sand sample that remained on the sieve was dried for about an hour and then it was brushed into a 50ml beaker via a funnel. The samples were weighed in the mettle's balance and the results was used to calculate for the sand content in the two various sample treated.

Measurement of vapor pressure of crude oil using Reid method [ASTM D323]
Procedure: The apparatus was connected to a mains and the switch on. The temperature of the water bath was raised to 37.8°C and was kept constant by the thermostat which regulates the temperature of the water bath. The sample chamber was filled to the brine with the crude oil sample. The sample chamber containing the crude oil sample was then chilled between 0°C and 1°C. On the other hand the air chamber was connected to a coupling hose and immersed into the heated water bath for 10minutes so that it assumes a temperature similar to that of the water bath. Hence, the sample chamber was connected with the air chamber inside the water bath and titled to about 45 degrees. The sample chamber of the bomb was observed to turn such that pressure developed was transported via the coupling hose to the transducer which transmitted and displayed the readings.

Measurement of salt content in crude D3230]
Procedure: Firstly, the instrument was calibrated, (blank check). This was done by pouring 10ml of neutral oil into a 100ml glass stopper graduated cylinder. Then 40ml of xylene was added, the mixture was shaken thoroughly. Hence, 50ml of mixed alcohol was also added and the solution transferred into a test beaker, an electrode was placed, the analyzer was pressed (on) to "READ" position, this records the milliameter reading (BLANK). After this, 10ml of neutral oil was replaced with 10ml of crude oil sample with addition of 50ml of mixed alcohol

and 40ml of xylene, thoroughly mixed and was allowed to stand for about 5 minutes. Then the mixture was poured into a test beaker and electrode inserted. The switch was turned from "CALIBRATION" switch to "HIGH" position, then to READ position. The blank millimeter reading mass hence subtracted from the sample reading to have a true reading. The true reading obtained was checked to determine the salt content in parts-per thousand barrels (P.T.B).

Measurement of asphaltene content [ASTM D128]

Procedure: 10g of the test portion of the crude oil sample was taken and mixed with 300mL heptane and the mixture heated in a flask for 60minutes under reflux, and the precipitated asphaltenes, waxy substances, and inorganic materials were collected on a filter paper. This was achieved by allowing the flask and its contents at the end of thisperiod to cool, the flask properly corked with a stopper and stored in a dark cupboard for 90 to 150minutes. The waxy substances were removed by washing with hot heptane in an extractor. After removal of the waxy substances, the asphaltenes was separated from the inorganic material by dissolution in hot toluene, hence evaporating the extracted solvent and the asphaltenes weighed.

Measurement of total acid number using an automatic titrator [ASTM D974]

procedure: The sample was dissolved in 100mL of the titration solvent (a mixture of toluene and isopropyl alcohol) containing small amount of water and was titrated potentiometrically with KOH using a glass indicator and two calomel reference electrodes. The meter readings automatically determine the end point of the titrating solution. The values were displaced and printed out by a printer connected to the titrator. Note that the procedure requires 15 to 20 minutes to perform and the degree of accuracy of the automatic titrator is 0.02mg KOH/gram of crude oil.

Measurement of metals in crude oil [ASTMD3831]

Procedure : The atomic absorption spectrometer was switched on and left to initiate, after which it was calibrated to the expected range of values of the metals that were expected to be found in the crude oil sample. The crude oil sa[illegible]ed with a diluent, and the diluted sample [illegible]o the beaker and placed under the machine, where a tiny pipe was inserted into it. The machine was allowed to run the test for minutes, after which a sound was made by the machine, the result displayed on the machine's digital screen and the result printed out from the printer. The result showed the metals that were present in the samples were nickel, vanadium,iron and copper in their right amounts.

Measurement of characterization factor (k-factor)

This provides a method for determining the characterization factor (k). It is calculated from the relation.

$$K = \frac{\sqrt[3]{T\ X\ 460}}{S}$$

Where,
K = characterization factor
S = specific gravity at 60oF (15oC)
T = the average boiling point at atmospheric pressure

Discussion

From the test analysis conducted, the API gravities were 42.40API and 30.10API for Kolo creek oil field sample and Nembe creek oil field sample respectively. This indicates that both crude oil samples from Kolo creek and Nembe creek are light crude oil. According to the result (Table 1), it can be seen that Kolo creek crude oil sample has a better API gravity which is an indication that it is lighter than Nembe Creek crude oil sample with 30.10API. API and Specific gravity are essential parameters because they help in determining the commercial value of crude oil. Also they can be used by petroleum engineers to determine flow efficiency or viscosity of crude oil. As such, heavy crude with high viscosity is expected to have low API gravity. For pipelines, carrying heavy crude, with known API gravity, appropriate diluents is added at regular distances to facilitate its flow.

The viscosity was carried out at a temperature of 2100F, and at the end of the test analysis, the result of the viscosities of Kolo creek crude oil sample and Nembe creek crude oil sample were 0.925cSt and 2.282cSt respectively, which shows that Nembe creek crude oil sample, offers more resistance or opposition to flow of the product (sample) under same condition of temperature. Hence, it can be said that Kolo creek crude oil would flow better in regions where the temperature is up to 2100F. Viscosity, pour point and flash point are very important service parameters in that they are all temperature dependent. Viscosity of crude oil has an inverse relationship with the API gravity. The higher the viscosity (as in the case for heavy crudes), the lower the API gravity. This parameter is essential to a petroleum engineer in that highly viscous crudes flows better in regions with high temperatures.

After the test analysis carried out on crude oil samples from Kolo creek and Nembe creek, the pour point gotten were 160C and 230C respectively. This means that the pour point for both samples is high but the latter being higher. At any given temperature below these pour points for respective crude oil samples, they will not flow any longer. In relative terms, Kolo creek crude oil sample has a better pour point value of 160C. Pour point being the lowest temperature at which crude oil will resist to flow, this information is very essential to a petroleum engineer because most of the crude oil produced in fields are being exported to other regions of low temperatures.

The test analysis carried out on the crude oil samples reveals that crude oil samples from Kolo creek has a flash point of 820F and crude oil sample from Nembe creek has a flash point of 2920F. This means that Kolo creek crude is highly flammable in relative terms. Hence, such routine check is important during handling, transportation and storage of these samples. Flash point is an essential safety parameter because it is used by engineers to assess the overall flammability hazard of crude oil.

From the result obtained from the test analysis carried out, it was understood that, the calculated sulplur content was 0.03wt% and 0.05wt% for Kolo creek sample and Nembe

creek samples respectively, and this gives a clear indication that both crude oil samples contains very low sulphur content. Hence, both crude oil are placed under the class of sweet crudes. Note that in terms of quality, Kolo creek crude oil sample is a better choice in the crude oil market because of its lower sulphur content. Sulphur content is a parameter of interest to a petroleum engineer. Its presence in crude oil poses problems of corrosion to refining equipment, difficulties during processing; an example is desulphurization of crude oil. And due to its environmental unfriendliness. As a result of these, crudes acceptability in both the local and international market is highly dependent on whether crude oil is sweet (sulphur content < 0.5wt %) or sour (sulphur content > 0.5wt %).

At the end of the test analysis, the percentage of the carbon residue in the crude oil samples from Kolo creek and Nembe creek were 1.14% and 1.73% respectively. And this shows that, the percentage of carbon residue is low when compared with other crudes in the assays presented in this paper.

The Reid vapour pressure test analysis was carried out at a temperature of 37.80C and the result obtained were 4PSI and 1PSI for Kolo creek and Nembe creek crude oils samples respectively. Hence, it can be seen that the amount of volatile matters present in Nembe creek crude oil is less than that in Kolo creek and as such, both crude oil should be handled with care with more attention given to Kolo creek crude oil. From the test analysis carried out, it can be gathered that, the amount or percentage of basic sediments and water for both crude oil samples were 1.5% and 3.5% respectively. This is an indication that both crudes have exceeded the maximum allowable percentage of 1%. Hence, both Kolo creek crude oil and that of Nembe posses a high percentage of basic sediment and water, as such they would have to undergo pretreatment. However, Kolo creek crude oil has a better BS&W value and should be the preferred choice.

The characterization factor (K - factor) for both crudes was determined by calculations. The K – factor gotten were 12.29 and 10.80 for Kolo creek crude oil sample and Nembe creek crude oil sample respectively. This results show that Kolo creek crude oil sample with K – factor of 12.29 is a paraffin based crude and Nembe creek crude oil sample with K – factor of 10.80, is a naphthanic based crude. Characterization factor (K), which is dependent on the average boiling point and specific gravity, was determined from a correlation chart. For the crude oil samples tested, Kolo creek sample is paraffinic based while Nembe creek sample is naphthanic based.

Knowledge of asphalt content present in crude oil is essential to a petroleum engineer due to problems encountered during storage and handling.

Reference

[1] Williams C. Lyons. (1996); "Standard Handbook of Petroleum and Natural Gas Engineering" Gulf professional publishing – volume 2

[2] United States Energy Information Administration, Country Information on Nigeria. URL://www.eia.doe.gov/emeu/cabs/nigeria.htm.

[3] Speight G. J. (1999); Applied Energy Technology Series, Petroleum chemistry and Refining Edited by: New York.

[4] Charles M.E (1973); "Origin and Refining of Petroleum", Gulf Publishing Company. Houston Texas. Society of petroleum engineers

[5] Brandley H.B. (2003); Petroleum Engineering Handbook Society of Petroleum Engineers.

[6] Erith and Rasma (1974); "Chemistry and Technology of Petroleum and Gas". Oxford and IBH Publishing Co.P.V.I Ltd.

[7] Annual Book of ASTM Standards (2003); Section Five. Petroleum Products Lubricants and Fossil Fuels. Volume 05.1 Petroleum Products and Lubricants (1): D56 – D3230

FIGURES



Figure 1: Centrifuge Apparatus

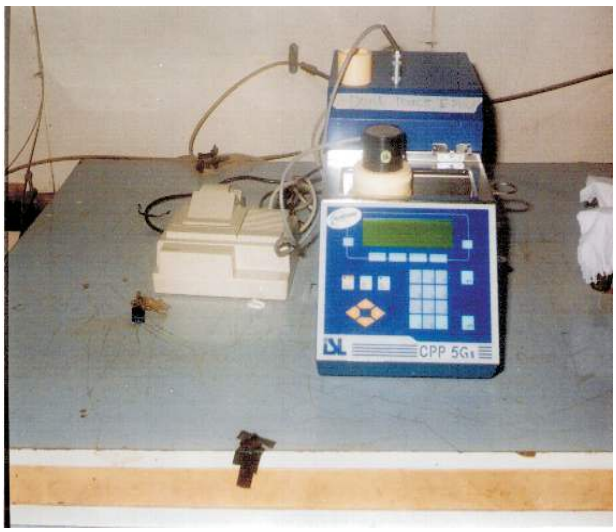


Figure 2: Automated Pour Point Apparatus

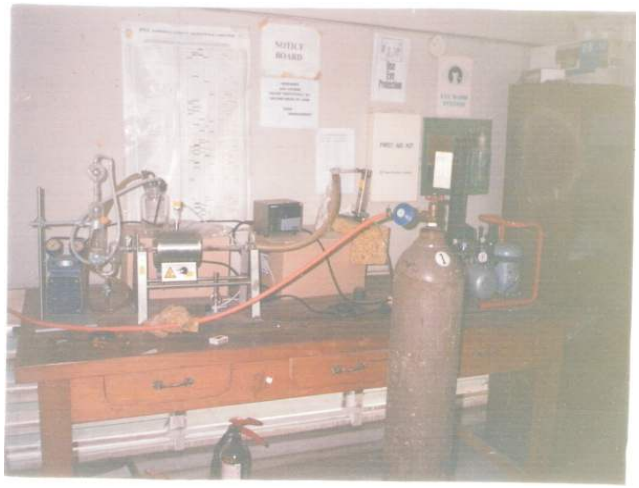


Figure 3: Sulphur Analyzer Apparatus



Figure 4: Automated Viscometer

RESULTS

Physicochemical properties

Table 1: Assay on crude oil from Kolo and Nembe oil wells

Parameters	Samples		Primary ASTM Test Method
	Kolo creek (E2 – OX WELL)	Nembe Creek (WELL 42)	
API	42.4	30.1	D1298
Specific gravity	0.8139	0.8756	D1298
Viscosity (CST @210°F)	0.925	2.282	D445
Flash point °F/°C			D93
Pour point °F/°C			D97
BS & W (Vol. %)	1.5	3.5	D96
Reid vapor pressure (PSI @37.8°C)	4	1	D323
Coradson carbon residue (wt%)	1.14	1.73	D198
Salt in crude	0.03	0.04	D3230
Sulphur content wt%	0.03	0.05	D1266
Sand content	1.72	4.73	
Total and number	0.49	0.61	D974
Asphalt content (wt %)	1.25	2.05	D128

LEVITATION UNDERCOOLING AND PATHWAY SELECTION OF NI BASED TERNARY EUTECTIC ALLOYS

O. E. Femi[1], C. S. Tiwary[1], S. Kashyap[1], G. Phanikumar[2] and K. Chattopadhyay[1]
[1] Department of Materials Engineering, India institute of science, Bangalore- 560012, India
[2] Department of Metallurgy and Materials Engineering, India Institute of Technology Madras Chennai-600036, India.
Email: foluemm@gmail.com

ABSTRACT
The microstructural evolution of regular binary eutectic alloys has been extensively studied both experimentally and theoretically by several investigators leading to a detailed understanding of the eutectic solidification. However, less is understood about ternary eutectics alloy. The pathways of microstructure evolution in ternary eutectic and near eutectic alloys are more complex. The understanding of the process of phase selection under non-equilibrium conditions for these alloys is limited.
We have used Electromagnetic levitation to achieve different undercooling in Ni based ternary alloys. Levitated droplet technique allows us to reduce the number of heterogeneous nucleation site significantly thereby promoting undercooling by delaying the process of crystal nucleation. Using electromagnetic levitation under argon atmosphere, we report the solidification behavior and evolution of multiphase microstructure in nickel based ternary eutectics. We show that a maximum undercooling of 27K could be achieved during processing. The details of the current levitation technique used in the present investigation together with the results obtained will be presented.

Introduction

Rapid solidification processing of undercooled alloy melts has been extensively studied for the production of novel structures and composites. The main emphasis of the processing techniques is heat removal from the melt subsequently leading to studies of structural evolution and phase selection of the undercooled melts.
Example of this techniques includes splat, quenching melt spinning, laser surface melting, powder atomization, sputtering and containerless techniques (Electromagnetic levitation and drop tube) [Fig 1].
Electromagnetic Levitation offers a unique advantage in that the container wall effects on the purity of the sample as well as on the heterogamous nucleation of the undercooled melts can be eliminated. By this technique, R. Abbaschan and M, D Lipschutz reports the undercooling and rapid solidification of processing of Nb-Si alloy with variety of metastable effects [1]. Yongchang Liu reports the lamellar spacing and mechanical property of undercooled Ti-45Al-2Cr-2Nb with a fully lamellar at 1273K for hr [2].

2. Experimental Method

Ni based alloy with composition Ni-68%atm Ti-12%atm and Zr-20%atm as shown in the phase diagram Fig[2] weighing about 1g and 10mm in diameter was prepared by arc melting. Electromagnetic Levitation facility [Fig 3] was used to perform undercooling experiment as it gives an extra benefit that freely suspended drops are not only accessible for direct diagnostics but also for external manipulation of the crystallization process. The Lavitation coil, together with the sample was placed in an ultra-high vacuum chamber which was then evacuated to a pressure of 10^{-6} mbar.
The sample is processed within the levitation coil which is connected to a high frequency generator. The sample is placed on an alumina crucible placed upside down as shown in [Fig 3] and heated up by the eddy current resulting from the surrounding coils. To achieve maximum undercooling $\Delta T_{m,}$ as soon as the sample levitate the alumina crucible was removed from the bottom of the sample. Successive heating and cooling were repeated for atleast six times. At each cycle, the sample was heated above the melting temperature by 300K and held for 3-5minute and cooled by helium gas flow together with decreasing the power of the high frequency generator.

3. Result and Discussions

We have used electromagnetic levitation to achieve undercooling in a Ni based ternary alloy. Undercooled melt corresponds to a non-equilibrium state. The melt at this state has choices of solidification pathways.
It is well know that solidification is initiated by nucleation process followed by a subsequent growth process. Eutectic growth involves the nucleation and a mutual growth of two or more solid phases from one liquid phase [3]. Recent works shows that the coupled growth theory of regular eutectic growth only applies to small undercooling [3].The catalytic potency of heterogeneous nucleation sites and its nucleation kinetics are the underlying factor to which the degree of undercooling of a melt depends. With this in mind, there are two alternatives to achieve undercooling in a melt which are (a) to eliminate these nucleation sites and (b) rapid cooling to kinetically bypass these heterogeneous nucleations. Melt wall surface are the major sites for heterogeneous nucleation electromagnetic levitation technique is very useful in promoting undercooling as contact of melt with substrate is avoided.
We report an undercooling of 27K as shown in the cooling curve obtain by the two color pyrometer and

subsequent analysis [Fig 3] the pyrometer has an accuracy of ±3°C. Comparing the microstructure obtain with the use of FEI Quanta 2020 Scanning Electron Microscopy(SEM) with a thermionic gun there is a remarkable changes in the micrograph as you go from Ascast to the highest undercooling achieved[Fig 4a-c]. Using JOEL Electron Probe Micro Analysis (EPMA) machine the composition of the phase was determined. The EPMA compositional analysis shows a shift in the starting composition which could probably be due to the fact that both Zr and Ti are Oxygen getter at high temperature and as a result of losses that may have result during melting due to the small weight. Wavelength Dispersive X-ray (WDX) of the undercooled sample gives resultant composition as shown in table [1].

4. Conclusion

The microstructure reveals a dramatic change in the length scale of the Ascast and undercool sample because there is a power law relationship between undercooling and λ. Our result shows that the Ni-68%at, Ti-12%atm and Zr-20%atm alloy can be undercooled by levitation Techniques. A maximum repeatable undercooling of 27K below the melting point of 1260°C could be achieved in our experiment. A typical cooling curve obtained by using a two color pyrometer (accuracy ±3°C) is shown in fig [4].

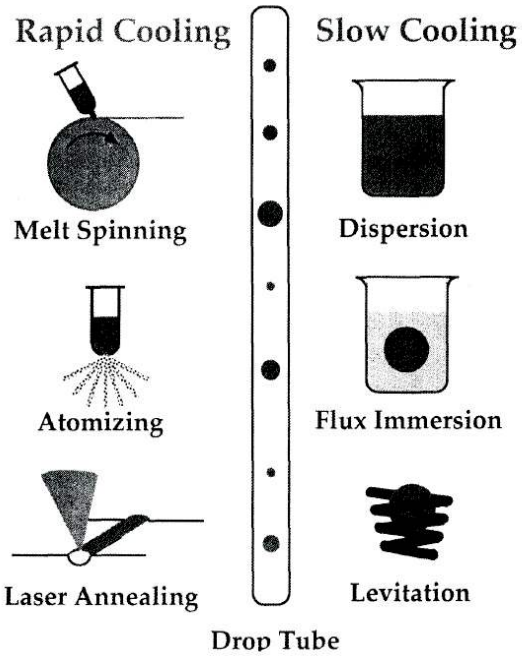


Fig1 Rapid solidification technique

In order to study the effect of undercooling on the microstructure, we have carried out detailed microstructural studies using a scanning electron microscope (FEI make Quanta 2020). Fig [5a] shows a typical as cast microstructure. The X-ray pattern obtained from the sample shown in Fig [6] indicate the presence of four phases namely, Ni_3 (Ti, Zr), Ni_5 (Zr, Ti), Ni_7Zr_2 and a ternary Ni-Ti-Zr phase. The Ni_3 (Ti, Zr) and Ni_5 (Zr,Ti) form eutectic structure while the two other phases grow dendritically as primary phases. On undercooling no new phases appear. However, the Ternary phase fraction reduces significantly. The eutectic also exhibits a much coarser morphology. A detail composition analysis using a field emission EMPA indicate that undercooling leads to a change in solubility of eutectic phases. Our result indicates an increase in the length in the length scale of overall microstructure on undercooling. This strongly suggests a strong effect of recalescence on the overall development of microstructure.

5 References

[1] R. Abbachian, M.D Lipchitz, Material Science and Engineering A226-228 (1997) 13-12.
[2] Yongchang Liu, Materials letters 57(2003) 2262-2266.
[3] Dieter .M. Herlach, Materials science and Engineering R12 (1994) 177-272.

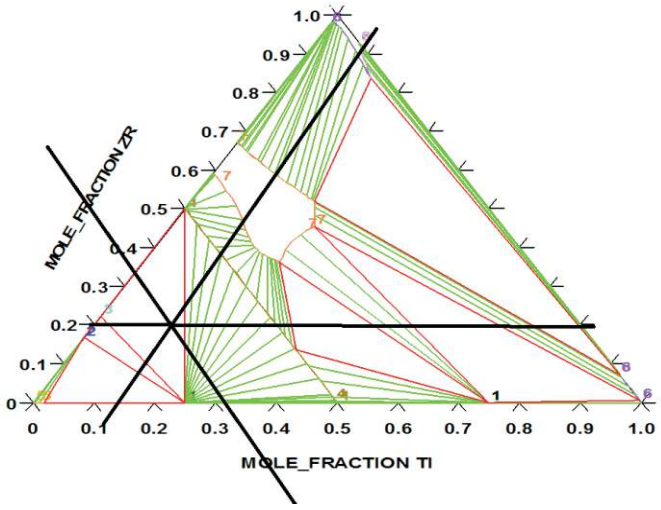


Fig 2 Phase diagram showing starting composition

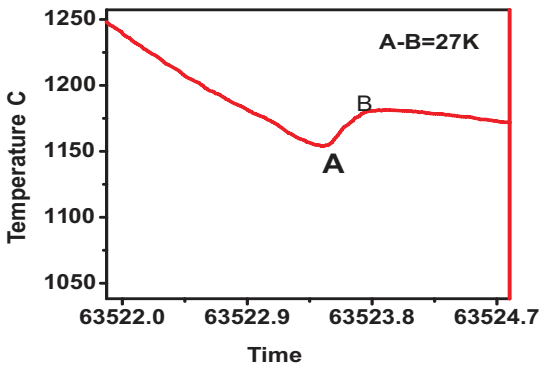
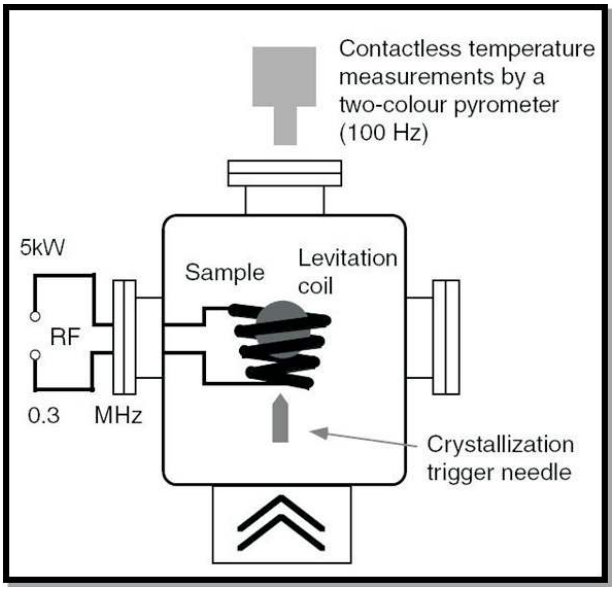


Fig [4] cooling curve



Fig[3] chamber of Electromagnetic facility showing the sample and levitation coil

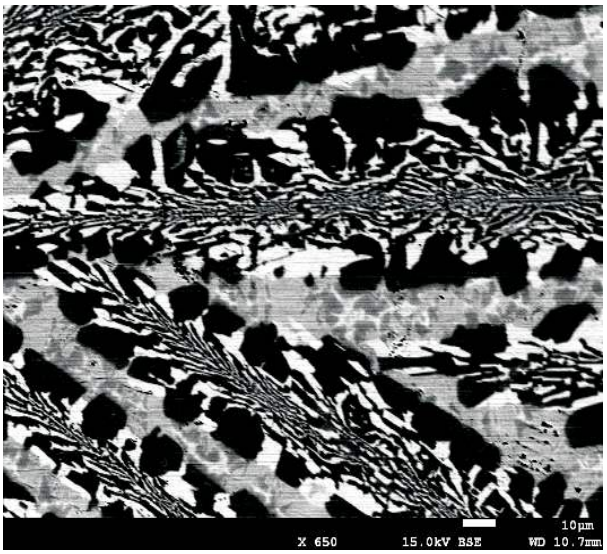


Fig [5a] ascast

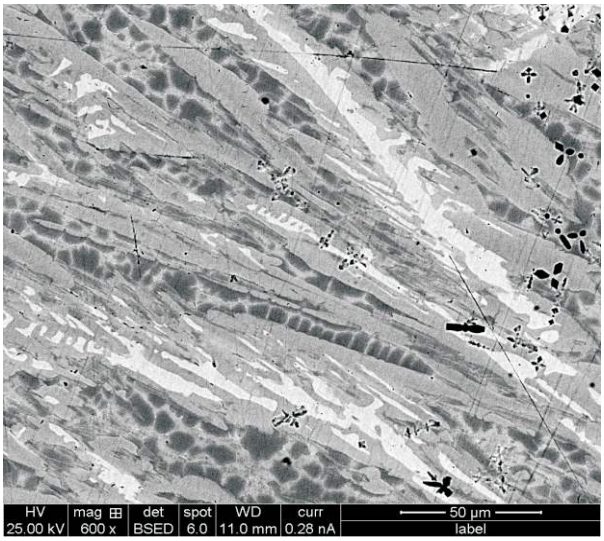


Fig [5b] undercooled sample

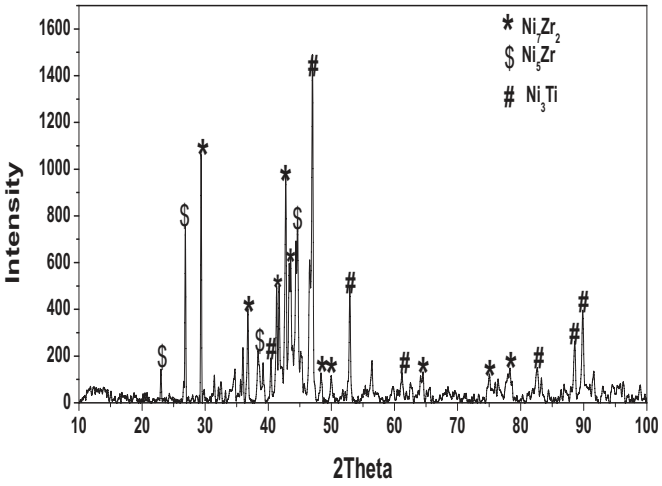


Fig [6] X-ray pattern showing different phases

Phase present	Composition
Overall	Ni-73%atm, Ti -13.62%atm and Zr - 12.25%atm
Dark phase	74%atm Ni, 18%atm Ti and 7%atm Zr
Lamellas	76%atm Ni and 20%atm Zr and 3%atm Ti
Gray phase	65%atm Ni, 19%atm Ti and 15atm Zr

Table [1] EPMA composition analysis

ADSORPTION OF NICKEL NITRATE ON KANKARA KAOLIN

Edomwonyi-Otu L.C*, Ogabor O. S, Idowu A.O, Bawa, G. S
Chemical Engineering Department, Ahmadu Bello University, Zaria, Nigeria
***Corresponding Author:** Email address: osas1law@yahoo.com

ABSTRACT
Kankara kaolin was used as an adsorbent to remove nickel nitrate from aqueous solutions. The factors that usually affect adsorption studied included temperature, stirring speed, contact time, adsorbate and adsorbent concentration and pH. The removal efficiency of 97.68% and 3.92% was obtained for concentrations of 9.5mg/l and 177mg/l respectively at the following operating conditions a pH of 2, stirring speed of 300rpm, temperature of 40°C, contact time of 200minutes, mass of adsorbent 0.5g/100ml of $NiNO_3$ solution, and pH of 2, temperature of 50°C, stirring speed of 400rpm, contact time of 150minutes and mass of adsorbent of 3g/100ml respectively. The factors studied all showed remarkable influence on the adsorption efficiency of Kankara kaolinite. The surface area of the Kankara kaolinite used was measured to be 9.1217m^2/g and a pore radius of 25nm.

1.0 INTRODUCTION

Pollution by heavy metals is serious and complex since they can bio-accumulate to higher levels in biota and being poisonous. Wastewater containing heavy metal contaminants needs treatment system that can remove these contaminants effectively. These types of waste come from, electroplating processes and mining waste. Heavy metals can be removed by several ways, e.g, precipitation and sorption by various media. The choice of which depends upon the type and concentration of both sorptive material and sorbent employed, as well as their costs. (Harvey and Chantawong, 2001).

The literature reports countless studies on heavy metal removal from waters and effluents, including chemical precipitation, physical treatment, such as ion exchange, solvent extraction and adsorption. However due to the high maintenance and import costs of chemicals or conventional adsorbents, some methods have become unsustainable. (Viera et al, 2010).

Nickel is a heavy metal applied extensively to our life and wastewater dissolved or dispersed with Ni(II) is harmful due to vomiting, chest pain, and shortness of breath (Hong et al, 2004). Nickel is a silvery white metal that takes on a high polish. It is hard, malleable, ductile, somewhat ferromagnetic, and a fair conductor of heat and electricity. It resists corrosion even at high temperatures and for this

reason, it is used in gas turbines and rocket engines. Some nickel compounds can cause cancer if the dust is inhaled, and some individuals are allergic to contact with the metal. Nickel cannot be avoided because we take in some nickel compounds with our diet, and it is an essential element for such plants as the navy bean, which is used for baked beans. (Wikipedia.org).
Adsorption is a process through which a substance in a fluid phase moves to accomodate on the interface between that phase (adsorbed) and a seperate solid phase (adsorbent). This phenomenon is driven by the available surface area (including pores), pore sizes, concentration of the adsorbate (in its various forms e.g vapour pressure), prevailing temperature and the forces among the molecules of the adsorbent and adsorbate. (Adefila et al, 2003). Some adsorbent that have been used and reported in several studies includes alumina, bentonite clay, biosorbents, kaolinites etc (Quintel et al, 2008; Devidal et al, 1996; Vimonses et al, 2009).

Advantages of using Kankara kaolinite as an adsorbent is because of its properties which includes good specific surface area, excellent physical, chemical stability, its pore size, and a number of other structural and surface properties. Although Kankara kaolin has been found to be a good adsorbent its efficacy in adsorption of nickel ions has not been studied.
The aim of this paper is to determine the adsorption efficiency of Kankara kaolin (obtained from Kankara village in Katsina State) in the the removal of nickel nitrate from aqueous solution and to determine the effect of some operating conditions,specifically PH, conentration of metal ion solution, temperature, amount of adsorbate, and stirring speed on the percentage removal of the nickel nitrate solution. Kinetic models were also tested to identify the adsorption mechanisms.

2.0 MATERIALS AND METHODS

2.0 Kankara kaolin
Kankara kaolin was obtained from Kankara village in katsina state without any chemical treatment. It was calcined at 50

$$\% = (C_i - C_e) \times \frac{100}{C1} \quad \text{.....(1)}$$

$$q = (C_i - C_e) \times \frac{V}{m} \quad \text{.....(2)}$$

where C_i is the initial nickel nitrate concentration (mg/l), C_e is the concentration of nickel nitrate at adsorption equilibruim (mg/l). V is the volume of the nickel nitrate solution (ml), and m is the mass of the adsorbent (g/100ml) of the adsorbate.

3.0RESULTS AND DISCUSSION

Kaolinite clay	BET surface area (m^2/g)	Pore volume (cm^3/g)	Pore size (nm)
Raw	7.9541	0.05410	24.56000
Calcined	9.1217	0.05922	25.57349

From table 1, an increase in the surface area (7.9541 to 9.1217) as well as pore volume and size is observed when Kaolinite clay is calcined. The replacement of Na^+ cations with Ni^{2+} cations led to an increase in the lamellar interplanar distance of the clay, which may account for the increase in the surface area of the clay following the nickel adsorption process (Viera et al, 2010).

3.1 Effect of temperature

Figure 1 Illustrates the percentage removal of nickel nitrate on Kankara kaolin as a function of temperature.The temperature range is between 30 - 75

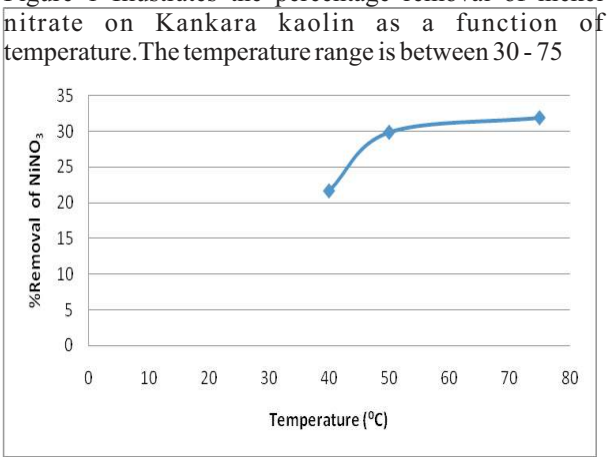


Figure1 : Effect of temperature on percentage removal.It is well known that temperature is an additional factor greatly influencing any sorption process.(Hamissa et al, 2010). Since adsorbent is porous in nature and possibilities of diffusion of adsorbate cannot be ruled out therefore, increase in the sorption with the rise of temperature may be diffusion controlled hence a rise in temperature favours the adsorbate transport within the pores (Manjeet et al, 2009). The adsorption of nickel nitrate into the kaolin pores was observed to increases with increase in temperature which conforms to literature.

3.2: Effect of pH on the adsorption of nickel nitrate on Kankara kaolin

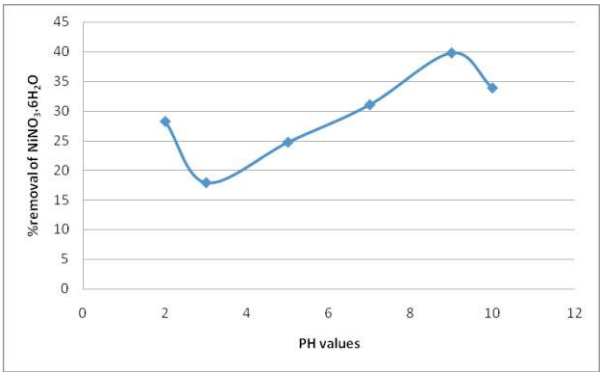


Figure 2: pH effect on percentage removal of nickel nitrate on Kankara kaolin.

The adsorption of nickel nitrate increases with an increase in pH values.Both adsorbent surface metal binding sites as well as metal chemistry in solution are influenced by solution pH. At low pH values, metal cations and protons compete for binding sites on adsorbent surface which results in lower uptake of metal. It has been suggested that at highly acidic condition, adsorbent surface ligands would be closely associated with H_3O^+ that restricts access to ligands by metal ions as a result of repulsive forces. It is to be expected that with increase in pH values, more and more ligands having negative charge would be exposed which result in increase in attraction of positively charged metal ions .In addition at higher pH the lower binding is attributed to reduced solubility of the metal and its precipitation (Manjeet et al, 2009).

3.3: Effect of stirring speed on the adsorption of nickel nitrate on Kankara kaolin

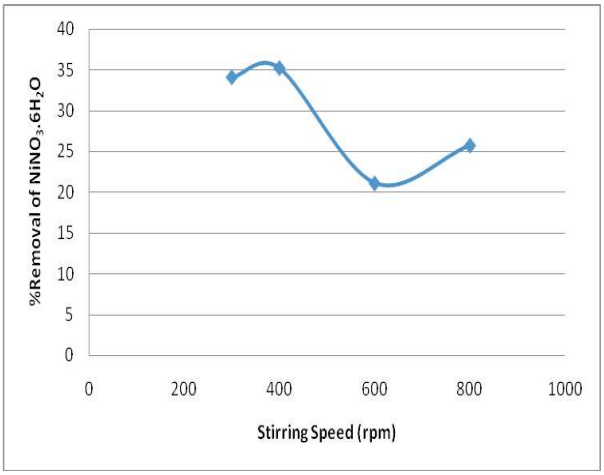


Figure 3: showing effect of stirring speed on percentage removal.

Stirring speed favours the adsorption of nickel nitrate by kankara kaolin because the stirring helps to increase the diffusion of the nickel nitrate into the Kankara kaolin pores. In this experiment it has been observed that a very high stirring speed will push the molecules of the nickel nitrate away from the Kankara kaolin instead of adsorbing it. Therefore a higher percentage removal was observed between stirring speeds of 300 and 400rpm.

3.5 Effect of adsorbent amount nickel nitrate by Kankara kaolin

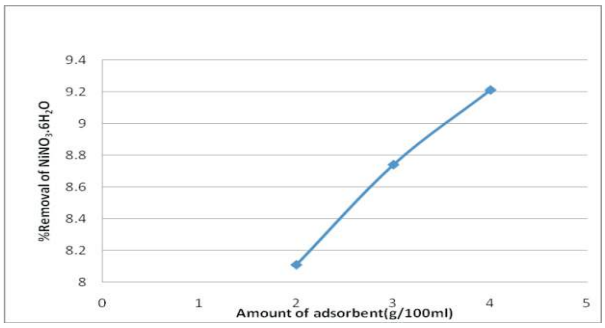


Figure 5:Effect of amount of adsorbent(g/100ml) on adsorbate solution.

An increase in the percentage removal is noted as the amount of clay used increases. This is expected because at a fixed initial concentration of sorbate the increase in adsorbent amount provides a larger surface area or adsorptive sites.Although the absorbed amount per unit mass of adsorbent decreases.This was observed for 85mg/l of nickel nitrate solution. The decrease in the adsorbed amount per unit mass of adsorbent is a generally observed behaviour. It has been reported by many researchers. This may be attributed to two reasons:

- A large adsorbent amount effectively reduces the unsaturation of the adsorption sites and correspondingly, the number of such sites per unit mass comes down resulting in comparatively less adsoption at higher adsorbent amount.
- Higher adsorbent amount creates particle aggregation , resulting in a decrease in the total surface area and an increase in the diffusional path length both of which contribute to decrease in amount adsorbed per unit mass.(Vieira et al, 2010).

3.6: Effect of Contact time on the adsorption of Nickel nitrate on Kankara Kaolin

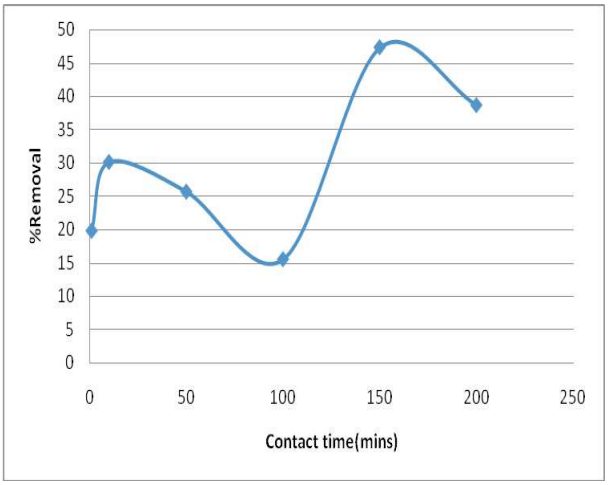


Figure 6: effect of contact time on percentage removal.

Although contact time has a positive effect on adsorption of nickel nitrate into Kankara Kaolin when all the kaolin pores are saturated even if the contact time is increased to a hundred times the smallest time it may not have a significant effect on the adsorption of the nickel nitrate.This accounts for the reason why some high contact times have a low percentage removal as shown in figure 5 above. Also the experiments were carried out at different conditions such as temperature, stirring speed, pH and adsorbent amounts.

3.7: Effect of Adsorbate amount on the adsorption of Nickel nitrate on Kankara Kaolin

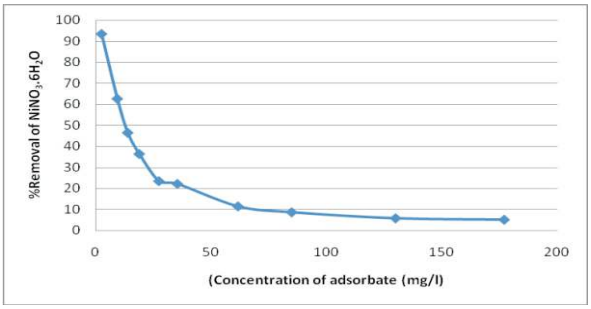


Figure 7: Effect of adsorbate on percentage removal of nickel nitrate.

High adsorption occurred at very low concentrations of nickel nitrate (2.66mg/l and 9.5mg/l). The reason is because with the initial solution at low concentration, the ratio between number of ions and number of adaptive sites available is small.

3.0 CONCLUSIONS

Kankara kaolin was used as an adsorbent to remove nickel nitrate from aqueous solutions. The removal efficiency of 97.68% and 3.92% was obtained for concentrations of 9.5mg/l and 177mg/l respectively at the following operating conditions a pH of 2, stirring speed of 300rpm, temperature of 40^{0}C, contact time of 200minutes, mass of adsorbent 0.5g/100ml of $NiNO_3$ solution and pH of 2, temperature of 50^{0}C, stirring speed of 400rpm, contact time of 150minutes and mass of adsorbent of 3g/100ml.

REFERENCES

1. C. J. Miranda-Trevino, A.C. Coles, (2003). Kaolinite properties, structure and influence of metal retention on pH. Faculty of Engineering and Applied Science, Memorial University of Newfoundland, St. John's, Newfoundland, Canada. Vol 23, pp133 -139
2. R.E. Grim, (1968). Clay Mineralogy. McGraw-Hill, New York.
3. S.S. Adefila, B.O. Aderemi, O.A Ajayi and

D.A. Baderin, (2003). Comperative surface area determination using water adsorption method, Vol 11, pp88-94.

4. N.W. Harvey and V. Chantawaog, (2001). Adsorption of heavy metals by ball clay: their compatition and selectivity. Vol 5, pp79
5. V. Vimonses, S. Lei, B. Jin, C. Saint, (2009). Kinetic study and eqilibruim isotherm analysis of Congo Red adsorption by clay materials. Vol 148, pp354-361.
6. N. Selvaraju, S. Pushpavanam, (2009). Adsorption Characteristics on sand and brick beds. Vol 147, pp130-138.
7. A. Menyar, B. Hamissa, A. Lodi, M. Seffen, E. Finoccho, R. Botter, A. Converti, (2010). Sorption of Cd(II) and Pb(II) from agave americana fibers. Vol 159, pp67-74
8. C. Quintel, Z. Rocha, B. Silva, B. Fonseca, H. Figueiredo, T. Tavares. (2008). Removal of Cd(II),Cr(VI),Fe(III), and Ni(II) from Aqueous Solutions by an E. coli Biofilm Supported on Kaolin. IBB-Institute of Biotechnology and Bioengineering, Center of Bioengineering, University of Minho, Campus of de Gualtar 4710-057 Braga purtugal.
9. http://www.wikipedia,the free encyclopedia.(Date accessed 17/06/2011)

CORROSION PERFORMANCE OF ALUMINIUM ZINC ALLOY COATED STEEL IN CASSAVA JUICE, MAIZE PULP AND SEA WATER SOLUTION

O.R.ADETUNJI [1]; P.O.AIYEDUN[2]; T.A.AROWOLO [3] ; O.J.ALAMU [4]
1 & 2 Mechanical Engineering Department, Universty of Agriculture, P.M.B.2240,Abeokuta
3 : Environmental Management and Toxicology Department, Universty of Agriculture, P.M.B.2240, Abeokuta, Ogun State, Nigeria
4: Mechanical Engineering Department, Osun State Universty Oshogbo, Osun State, Nigeria.
E-mail; adetunjiolayide@yahoo.co.uk

ABSTRACT
This study was carried out to investigate and evaluate the corrosion performance of aluminium zinc alloy coated steel sheet in three different media (cassava juice, maize pulp and sea water).The samples were prepared for the study by cutting into 5cm x 5cm. the soaking media were also prepared by extracting cassava juice from cassava tubers and maize pulp from maize grains. Sea water solution was got from bar beach (Atlantic ocean).The weight loss of each sample for specific periods of immersion (72, 144, 216, 288, 360 and 432 hours) was determined on average of two samples exposed under the same condition and test media in different container. The findings showed that cassava fluid had highest corrosion rate of the samples, followed by maize pulp and sea water. Also, pH of cassava fluid is more acidic, while that of maize pulp and sea water increased from acidity to neutral. Corrosion rates of samples in cassava fluid and maize pulp showed an increasing trend with time but later decreased, while that of sea water showed a decreasing trend.

Keywords: Aluminium, Zinc, Coating, Steel, Corrosion, Media

INTRODUCTIONAluminum is one of the most abundant elements in the earth crust, but, owing to its high affinity for oxygen, it cannot be reduced to the metallic state by reduction with carbon and carbon monoxide, as is the case with many metallic oxides [1]. Aluminum may be alloyed with a number of elements to produce a series of useful engineering materials. [2]. The principal heat treatable alloys are those of the following systems: Aluminum Zinc (Al -Zn), aluminum cooper nickel (Al-Cu-Ni), aluminum magnesium silicon (Al-Mg-Si), aluminum zinc copper (Al-Zn-Cu) and aluminum lithium (Al-Li). Those various alloys types respond to age hardening or precipitation hardening treatments.

A 55% A1-Zn alloy coated steel is comprised of 55% aluminum, 43.5% zinc and 1.5% silicon. Although the corrosion performance is mostly related to the aluminum zinc alloy, the addition of approximation 1.5% silicon is vital. The primary purpose of the silicon is to control the growth of a brittle intermetallic layer that would otherwise form during manufacturing of the product.[5].

The effects of fluid squeeze from cassava tuber on the corrosive behaviour of Al-Zn coated steel were investigated. The researchers equally carried out develop models to show that the correlation coefficient between the experimental values of corrosion rates and predicted values was high [4].

The corrosion evaluation of aluminum alloy coated steel, galvanized steel, cast iron and stainless steel in cassava juice was studied.The finding was that the aluminum alloy and the stainless steel were resistance to corrosion in cassava juice, the galvanized steel offered resistance but the dissolution of the zinc coating was apparently high initially the grey cast iron corroded badly in the juice showing general corrosion resulting from the anodic dissolution of the test specimen by interfacial reaction[3].

MATERIALS AND METHODS

Aluminium zinc alloy coated steel sheet samples (Al-Zn), cassava juice (undiluted cassava fluid), maize pulp, sea water, plastic containers, distilled water, paper tape, plastic bowls,
pH meter, sensitive weighing balance, bench shearing machine.

Aluminum zinc coated steel sheet samples sourced from Kolorkote Otta has thickness of 0.5mm.

The cassava fluid was sourced by grinding pilled cassava tubers and squeezing out the fluid using clean white cloth sieve. Sea water solution was got from bar beach at Lagos-state.

The plastic containers were first washed with detergent, rinsed in distilled water and were cleaned and allow to dry for hours.

Each of the measured samples was inserted into identified plastic containers, cassava juice was poured to cover the samples, maize fluid was poured to cover the sample and salt water solution was poured to cover the sample.

The sourced samples were cut into sizes 50mm by 50mm using a shearing machine, scriber, steel rule and engineer's try square. The cut samples were forty eight pieces of the same thickness.

The samples were weighed and recorded before and after immersed into testing fluid using sensitive weighing balance.

Each weighed samples was separated and fully immersed into a plastic containers filled with testing media and then covered.

RESULTS AND DISCUSSION

The results obtained are contained in tables 1 to 3. The weight loss per surface area of aluminium zinc alloy coated steel sheet in cassava juice with reference to time of immersion had an averagely increasing trend (table 1). Due to acidic nature of the cassava juice as shown by pH values recorded which causes dissolution of aluminium zinc alloy coated steel sheet in contact with it. The relationship is further shown in figure 1

The corrosion intensity (corrosion rates) of aluminium zinc alloy coated steel sheet with reference to time of immersion had an averagely increasing trend to certain level before it decreased (Table 1). This resulted from the fermentation process of cassava juice with time.

The weight loss per surface area of the samples in maize pulp with reference to time of immersion had an averagely increasing trend (table 2). the pH of the maize pulp decreases from acidity to neutral over the time of immersion that implies that the maize pulp had less aggressive on the protective sample (figure 2) the relationship between weight loss per surface area and time of immersion are shown (figure 3)

Comparative study between pH values Al-Zn in cassava fluid, maize pulp and sea water with reference to time of immersion. Comparatively, as shown in Figure 2, the pH values of Al-Zn in cassava fluid increased in acidity over a period of immersion. The pH values of Al-Zn in maize pulp and sea water reduced in acidity over a period of immersion. This implies that cassava fluid had highest impact on the tested samples than maize pulp and sea water over a period of immersion. Figure 4 showed the scanning electron microscope photograph of Aluzinc sample in cassava fluid for twelve days.

CONCLUSION

From experiments carried out in this study and the results obtained, the followings can be concluded.

The zinc aluminium coated steel sheets (Aluzinc) investigated showed higher corrosion rates when immersed in cassava juice compared with lower rates in maize pulp and seawater.

The corrosion rates of Aluzinc in cassava fluid showed an initial increase up till 216 hours of immersion and decreased thereafter.

The rates of corrosion of Aluzinc in maize pulp and seawater were very low proving its suitability in such environment.

REFERENCES

1. John, T.A. 1999. Introduction to Engineering Materials, 3rd Ed. ELBS. pp 195-197.

2 .Kameya (1989) Hot Dip Zinc Aluminium Alloy Coated Steel Sheet, Process for producing the same and prepainted steel sheet, World Intellectual Property Organization.

3. Loto, C.A (1992) Pitting and Crevice Corrosion Susceptibility of Super Austenitic Stainless Steels in Sea Water Conference Proceedings of Corrosion Nigeria, pp 65-77.

4.Jekayinfa, S.O, Waheed, M.A, Adebiyi, K.A and Adebiyi, F.T (2005). Effect of cassava fluid on Corrosion Performance of Mild steel. Anti-corrosion Methods and Materials, Emerald Group Publishing Limited, vol. 52(5) pp 286-292.

5. Townsend, H.E and Meitzner C.F. (1983) Corrosion Resistance of Zinc/4% Aluminium and Zinc/ 54% Aluminium Castings, Materials Performance, 22(1), 54; Journal of the Metal Finishing Institute of Japan, 34(3), pp 1-3 ;

Table 1 Average Corrosion rates and weight loss/surface area of Aluzinc in Cassava juice

Time (hrs)	Wd (g	Area (m^2)	WL (g/m^2)	PH	CR (mm/yr)
72	0.0280	0.0025	1.1547	3.5433±0.0058	0.1750±0.0181
144	0.0714	0.0025	22.7600±9.0084	3.6700±0.0173	0.2237±0.0224
216	0.1132	0.0025	45.2667±2.18	3.6967±0.0551	0.2362±0.0114
	0.1407	0.0025	56.2800±1.3804	3.8500±0.00	0.2202±0.0054
360	0.1719	0.0025	68.7600±1.7004	3.8733±0.0058	0.2152±0.0054
432	0.1781	0.0025	71.2400±6.4800	3.7870±0.0234	0.1858±0.0169

Table 2 Average result of Samples in Maize Pulp

hr	Wd(g)	Area (m^2)	AWL (gm^2)	PH	CR (mm/yr)
72	0.0030	0.0025		4.9800±1.2384	0.0184±0.01455
144	0.0010	0.0025	0.3200±0.06928	6.1500±0.0866	0.0025±0.00052
216	0.0015	0.0025	0.6000±0.000	6.4200±0.1559	0.0031±0.00
288	0.0035	0.0025	1.4000±0.08314	5.8900±1.2759	0.0055±0.00191
360	0.0044	0.0025	1.7600±0.6235	5.5900±1.2529	0.0055±0.00191
432	0.0034	0.0025	1.3500±0.1848	7.2200±0.1501±	0.0035±0.00052

Table 3 Average result of Samples in Sea Water

Time (hr)	Wd (g)	Area (m^2)	AWL (g/m^2)	PH	Cr (mm/yr)
72	0.0009	0.0025	0.3600±0.1600	6.7300±0.1562	0.0056±0.0025
144	0.00053	0.0025	0.2133±0.0231	6.9033±0.07506	0.0017±0.00017
216	0.00053	0.0025	0.2133±0.1405	7.0200±0.0265	0.0011±0.00754
288	0.00025	0.00025	0.0800±0.0400	7.2233±0.0751	0.0004±0.00015
360	0.010	0.0025	0.4133±0.2411	6.7033±0.1674	0.0013±0.00075
432	0.0125	0.0025	0.6533±0.2663	7.0833±0.0153	0.0013±0.0012

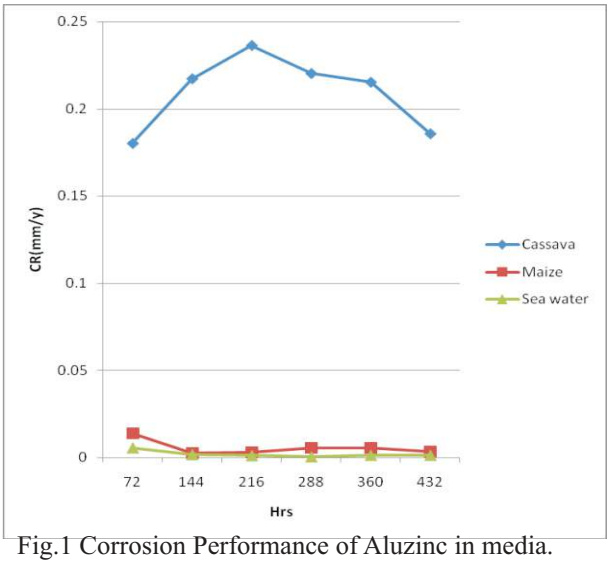


Fig.1 Corrosion Performance of Aluzinc in media.

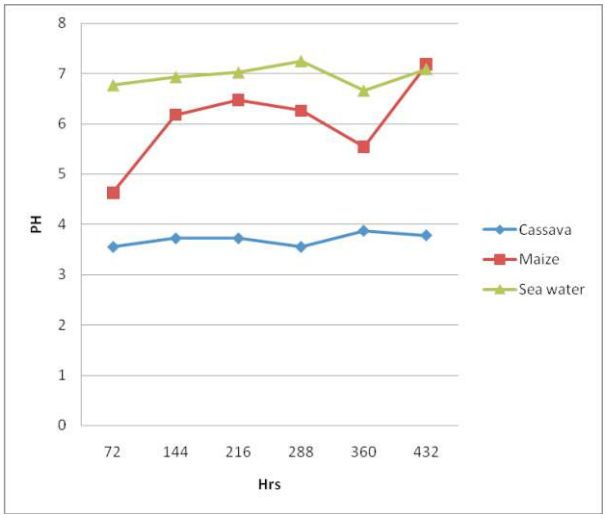


Fig.2 pH of media against immersion time

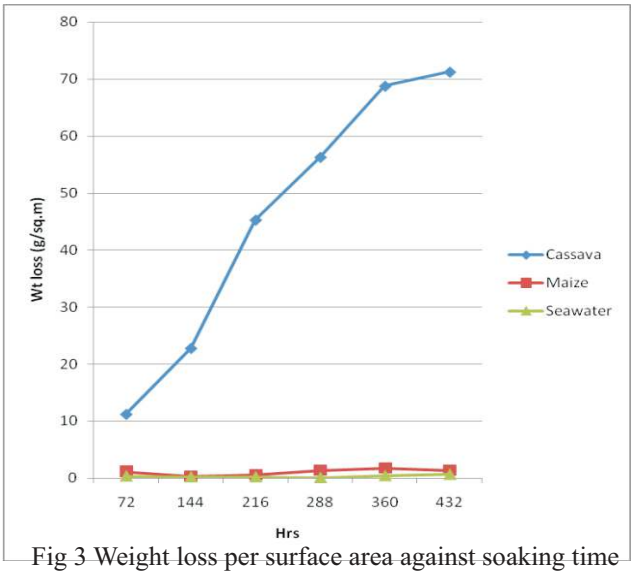


Fig 3 Weight loss per surface area against soaking time

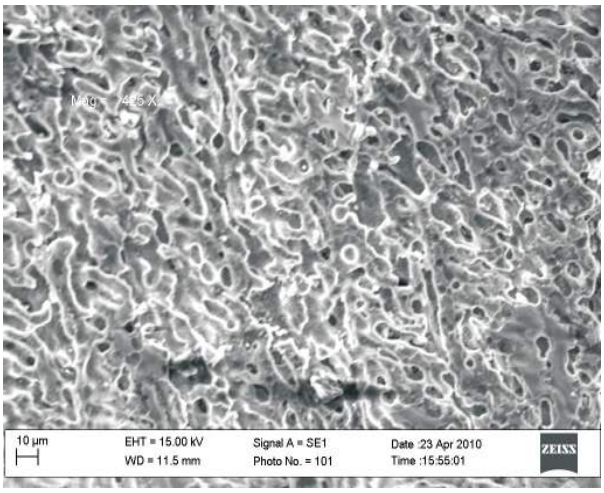


Fig. 4 SEM for Aluzinc soaked in cassava fluid for 12 days

BASE AND PRECIOUS METAL VALUES IN END-OF-LIFE ELECTRONICS

OGUNNIYI I. O.
Metallurgical And Materials Engineering,Federal University Of Technology, Akure
mrolatunji@yahoo.com

ABSTRACT
Many naturally occurring deposits of base and precious metals assay far less in base and precious metal values compared with that contained in end of life electronics appliances, particularly the printed circuit board components in these devices. This fact is brought to the fore in this paper with a compilation of metal assays of printed circuit boards from various works. The assays are discussed along with those of known mines. Various processing techniques for recovery of these valuables are briefly addressed, compared to the rather hazardous manners this material stream is being presently managed in many cities and suburban communities. The paper basically aims at continuous awareness creation for the cyclic material use culture, so that increasing proportion of the populace can start seeing items normally considered waste as valuable materials that can be economically processed. Cleaner environment, economic enterprise, responsible material use and development in material processing practice and research are all possible spin-off within this view.
Keywords: precious metals, base metals, waste electronics, resource recovery, environment

INTRODUCTION

End-of-life (eol) electronics, commonly referred to as waste in electrical and electronic equipment (WEEE) piles up faster than ever. Central unit in this WEEE stream are the printed circuit board (PCB). PCB mechanically supports and electrically connects electronic components by using conductive copper pathways, called traces, which are etched from copper sheets laminated onto a non-conductive substrate [1]. Populated PCBs have mounted components, while unpopulated ones comprise of only reinforced resin and printed copper wiring laminate. PCBs are found in almost all electronic applications, spanning personal computers, telecommunication equipment, hospital equipment, cellphones and various consumer electronics. Rapid advances in technological innovations result in a high rate of obsolescence of electronc devices, leading to large tonnages of PCB going into the WEEE stream. In the United States of America (USA), for personal computers (PC) alone, 63 million units was estimated to be obsolete in 2005 [2]. At about 0.75 kg PCB per PC unit or 2.75 % by weight, and one PC unit with monitor weighing about 27.5kg [3], the huge tonnage of materials this translates to can be appreciated. In the UK, about 50 000 tons of waste PCBs are generated *per annum* [4]. Of these, about 40 000 tons are populated PCBs, and 10 000 tons are unpopulated or associated boards manufacturing scrap. The estimate for 2006 was 100500 tons [3]. A year 2000 review in Taiwan claims about 300 000 scrap PC units per annum, and this had risen to 700 000 by 2004 [5,6]. Intel South Africa, an original equipment manufacturer (OEM), has been in business for 35 years and has sold more than one billion CPUs. Although, with generally few statistics, more than 500 000 PC units were reported dumped per year [7]. Large undocumented accumulation, or scatters, of PCBs occur around the world, much due to shipment of used PC to developing countries. A 2005 British Broadcasting Corporation (BBC) report, focused on Nigeria, claimed that about 400 000 used computers are imported to Nigeria monthly. Almost 75 % of these cannot be used, cannot be repaired economically or resold [8].There have been more recent focus in the media on e-waste accumulation at the computer village, Ikeja, Lagos, Nigeria, while all over the country are scatters of e-waste already at the end of their service lives. It is common to see CRT monitors by the road side; indicators of a need for a functional channel of disposing such goods, functional in the economic sense and in being environmentally benign. Although, these items contain high material values that make them economically attractive for processing as a secondary material resource, although they contain a lot of hazardous substances that should conform to strict disposal guidelines, still they lie around; end up in water ways and in the green fields. As a technical campaign, this brief will expand on the valuable content of the PCBs in eol electronics, processing options, and better handling practices, towards promoting cyclic material use, cleaner environment, economic enterprise, and development in material processing practice and research.

1 COMPOSITION OF PCB AS A SECONDARY MATERIALS RESOURCE

Being a multi-component unit makes PCB chemical composition analysis very demanding in terms of sample preparation and appropriate analytical techniques. Inductively coupled plasma optical emission spectroscopy, inductively coupled plasma mass spectroscopy, and x-ray fluorescence have been used in combination and preferably recommended by the author [9]. Other techniques such as atomic absorption spectroscopy, X-ray diffraction, infra-red spectroscopy, fire assay and thermal analyses, have been mentioned by other workers and in reviews [10]. Table 1 shows a

compilation of metallic content of the PCB from various workers.

The data for each element in Table 1, can be seen to vary across the different compositions. This is expected as PCB material make-up continues to change with technology over time. In essence, a typical PCB composition must be carefully defined. Anyhow, the typical metallic values in PCB can be seen to include valuable base and precious metals in appreciable proportions comparable or even better than those of the natural deposits of these metals. Gold, for instance, at 40 g/t assay in vaal reefs in South Africa represent good grade deposits [11]. Whereas, copper assays in copper porphyry deposit economically mined can be lower than 2 % [12], the least copper assays in the Table 1 is 10 %. Platinum and palladium, in natural deposits are typically at 10 g/ton run of mine head grade.

When high grades spikes are found in some deposits it is not the order. Such is the Colossus Mineral Inc recent hit of a behemoth gold-PGM intercept in Serra Pelada, in the mineral prolific Carajas region, Para State, Brazil [13]. At some spots were remarkably high grades of gold and record grades of platinum and palladium over significant widths: 7.30 m at 1494.7 g/t gold, 516.6 g/t platinum, and 558.90 g/t palladium; 70.70 m at 53.59 g/t gold, 20.77 g/t platinum and 31.30 g/t palladium. However, the underground operation will have to decline some 3500 m to access the orebody. That is where the table turns. PCB values on the other hand come only for the pick; with zero mining cost, yet loaded with the values. At the current prices of $3.50 per pound of copper, $30.80, $1640, $1510 and $616 per troy ounce silver, gold, platinum and palladium, respectively, the material-economic value of the PCB is obvious [14, 15].

However, with the ever stiffer criteria to make technology available at cheaper prices, quantity of precious metal values per unit PCB/device is reducing. With development in surface technology, coatings can be only a few tens of nanometers, without compromising the required functionality in comparison with thicker coatings of earlier technology. Precision etching also has led to thinner and narrower traces. These translate to lower assays of the metal values in a PCB. Recovering the precious values from this waste stream is also becoming more demanding, likeable to recovery of values from leaner orebodies. The enormity of appliances produced and used in recent times, however, translates to increasing quantity of precious values in the resulting end of life electronics stream. This implies that though the value is getting leaner, the reserve is rising continuously. In essence, secondary resources processing potentially regenerates its reserves, unlike primary resources processing that depletes natural reserves irreversibly. The pointer here is that secondary resources processing is the hope of sustaining the material demand level of the global pace of manufacturing and development. This submission implicitly makes two demands: increased attention to resource recovery from waste stream, and the need to handle end of life stream more responsibly. The two issues need to be expounded.

2 PROCESSING TECHNIQUES

The metal values in eol PCB has been recognised for long and many approaches have been adopted towards recovering these values back to the material cycle. Processing of eol PCB to recover the material value dates back to more than three decades in the industrialised communities. In the 1970s, the predominant method of recovery of metals from electronic scrap was via the blast furnace in conjunction with secondary copper/lead smelter [16]. Early in the 1980s, some physical processing stages were employed to preconcentrate the values. Figure 1 shows a multi-component REE (radio-electronics equipment) physical processing flowsheet [17]. Scrap REE has now taken on the WEEE nomenclature.

Features of this processing included differentiated disassembly (more recently referred to as selective disassembly), cryogenic cooling and crushing, airflow classification, stages of magnetic separations and, finally, magneto-hydrostatic separation (MHS). The magneto-hydrostatic separation density was first set to 2000 kg/m^3 (2 g/cm^3), then to 3000 kg/m^3. This will cause non-metallic stuff to be floated first, followed by aluminum in the second stage, while copper, lead and tin were in the sink product. In more recent times, the full complement of extensive physical processing, hydrometallurgical and pyrometallurgical techniques are used to maximise resource recovery from eol PCBs, and WEEE stream in general. Table 2 summarises the various e-waste treatment approaches, with the pros and cons of each method. It is interesting to note the landfilling approach in the table.

3 RESPONSIBLE HANDLING

With all the alternative approaches for valuable resource recovery from eol electronics, in some industrially backward communities, it is still treated as waste. End-of-life electronics end in municipal waste piles en route to some dung hills. Apart from the valuable materials that are irretrievably dispersed, there have been pressures from environmental point of views on responsible handling of eol electronics. Lead, mercury, cadmium, hexavalent chromium and polychlorinated biphenyl are among the six materials declared hazardous in the RoHS (Restriction on Hazardous Substances) directives [18]. All these can be found on a single populated PCB. Polychlorinated biphenyl is found in some capacitors. Lead, cadmium, chromium and mercury are usually concentrated in batteries. Mercury is also found in relays and switches, while cadmium can also be found in some surface-mounted chip resistors, infrared detectors and semiconductors. These hazardous contents can leach into the environment when eol PCB are not disposed in safe manners. From the two sides of environmental protection and high resource recovery, responsible handling of eol electronics is obviously imperative in any community.

Responsible handling can be summarised under two headings: standard collection system and standard processing.

4.1 Standard Collection System: In material conscious communities, standard collection system entails selective disposal, take back policy, return rebates,

among others [2]. Selective disposal entails dropping waste items in labelled bins. Bins are labelled based on material types that can be dropped inside them. A set of bins labelled for polymers, metals and papers, are put together around offices, street corners and at waste processing facilities. These bins are for regular non-hazardous household municipal wastes. For electronics wastes such as eol PCBs, batteries, and waste with hazardous contents, take back policy are employed. Consumers drop their wastes at designated centres maintained by the original manufacturers of such items. The return rebate is a way of encouraging consumer to return their waste. On car accumulators, for instance, consumers have about 25 % off the price of a new one when they come with the old. The collection system ensure material content of wastes gets back to manufacturers, and back to the material cycle. Cyclic material use is ensured and there no useless wastes or hazards. The social effect is obvious: good material stewardship and clean communities.

In many developing communities, there are no such system, hence all the pollution and the litters. Government policies do not reflect knowledge of these standard practices. Original equipment manufacturers easily sneak or shy away from their take back responsibility. For instance, battery manufacturers in Nigeria do not promote any return rebate, yet they are aware of the international standards guiding their trade, about disposal of lead bearing devices. Communities pile up a dung hill of plastics, papers, metals, fabrics, etc., and burn the heap in open air time and again. Many of the cities litter itself, line its street with wastes stuffed in big plastic bags, and give ugly pictures of urban jungles. When there is no law, there is no sin.

4.2 Standard Processing: PCB processing for resource recovery must conform to high safety standards. As Table 2 indicates, the pyro route is known for releasing harmful off gases, containing dioxins and furans, from the thermal decomposition of organics in the PCB [19]. The hydrometallurgical processing can also be hazardous, such as the manual aqua regia leaching of gold plaiting from edge connectors reported in small scale backhouse practices in mainland China [4]. Generally, PCB being so multi-component, its processing can be very hazardous on the health of the human operators in short and long term.

Apart from safety threats, poor recovery on many of the valuables will lowers overall resource recovery when the processing route is not comprehensively thought out. A good recommendation in this regard is that PCB processing must start out from a comprehensive physical processing operation to produce clean material fractions or concentrates, which can feed the hydrometallurgical or pyrometallurgical alternatives. However, considering the huge capital and the large scale of operation for the type of smelters that are ideal for the non-ferrous fraction from PCB physical processing, it can be recommended that hydrometallurgical processing will be the route to explore in technologically challenged communities. After comminution, eddy current and electrostatics separation, impure anodes casts or bags can be made directly from the non-ferrous fraction to produce high purity copper cathodes while noble values can be recovered from the anodic slimes.

4 REALITIES AND RECOMMENDATIONS

Practice can forever remain a whole world away from the theory. 'Easier said than done' goes the saying. Suggestions, recommendations, policies are mere rhetoric in a communities where people do not face the fact that duties of everyone will never be done by anyone until someone actually steps out to do it. While a good government should be able to formulate and enforce progressive policies, people must actually be resolved to move forward. The urge to make something, rather than buy something, the urge to process materials, is the beginning of creativity, industrialization and national development. A lot depends on what the community wants to be – developed or backward.

Communities can start by separately collecting paper, plastic, metal and biodegradable wastes in separate labelled bins. The biodegradables can be fetched and deposited in the green spaces. It will recondition the soil. The heap of papers, plastic and metal with no biodegradable organic content will not stink, until appropriate material processing. Some commercial activities will naturally spring up around the stark of resources. A paper company far away will readily bring a truck to a township to pack a heap of waste paper not mixed with diapers, stinking mess of food leftovers, etc. Meanwhile, need driven research efforts into secondary resource processing should be intensified. With community and research efforts in place, policy and fund assistance from government towards executing suggestions on more technical waste handling, research and industry will have a smooth ride. This is the version of the bottom-up approach in national development that will surely work in this regard. A quick fix political waste commission, institute, centre or agency may fail due to lack of requisite grass root culture and/or norms. It is worse off when the structures multiply and replicate one another actually for political assuaging or 'cake'. Rather, a national orientation (employing relevant agencies) towards the standard practice of selective disposal of waste (described) can be a very good starting point. Commercial activities around waste processing, research, and improved policies, should normally follow.

5 CONCLUSION

End of life electronics contains highly valuable base and precious metal content, concentrated in the printed circuit boards. Gold, platinum now hover around $ 1500 per troy ounce, while eol PCB assays well above many natural deposits of this precious metals. Standard waste collection system which entails selective disposal, take back policy, return rebates are necessary to ensure this material values return to the material cycle. There is an economic advantage to it, while the city cleans up itself. A lot depends on what the community want to be – developed or backward. Some national orientation can be very appropriate to sell the standard waste collection practice and the cyclic material use culture. The requisite know how for processing this stream of material is purely a metallurgical engineering business. Here is a wide need

driven research and development space. The community, the research and development institutions, and the government are all joined in this suit.

REFERENCES

[1] www.wikipedia.com

[2] Kang Hai-Yong and Schoenung J. M., 2005. Electronic waste recyling: A review of US infrastructure and technology options. *Resources, Conservation and Recycling*, Vol. 45, pp. 368 – 400.

[3] Shuey, S.A., Vildal, E.E. and Taylor, P.R., 2006. Pyrometallurgical processing of electronic waste', *SME Annual Meeting*, March 2006, St. Louis, MO.

[4] Goosey, M. and Kellner, R., 2003. Recycling technologies for the treatment of end of life printed circuit boards (PCBs). *Circuit World*, v. 29, pp. 33 – 37, 2003.

[5] Lee Ching-Hwa, Chang-Tang Chang, Kuo-Shuh Fan and Tien-Chin Chang, 2004. An overview of recycling and treatment of scrap computers. *J. Hazardous Matls.*, B114, pp. 93 – 100.

[6] Lee Ching-Hwa, Ssu-Li Chang, King-Min Wang and Lih-Chyi Wen, 2000. Management of scrap computer recycling in Taiwan. *J. of Hazardous Matls.*, Vol. A73, pp. 209 - 220.

[7] Mackay, T., 2004. Where do PCs go to die? *PC Format*, August, pp. 16 – 20.

[8] Laurie, J. Flynn, 2005. Poor nations are littered with old PC's, *New York Times*, Oct. 24, 2005.

[9] Ogunniyi, I. O., Vermaak, M.K.G. and Groot, D. R., 2009: Chemical composition and liberation characterization of printed circuit board comminution fines for beneficiation investigations. *Waste Management*, 29, pp 2140 – 2146, 2009.
http://dx.doi.org/10.1016/j.wasman.2009.03.004

Table 1: Metallic values in PCB (Wt. %)

Metals	% [3]	% [20]	% [21]	% [22] *	% [23]	% [24]	% [9]
Cu	20	26.8	10	15.6	22	17.85	23.47
Al	2	4.7	7	--	--	4.78	1.33
Pb	2	--	1.2	1.35	1.55	4.19	0.99
Zn	1	1.5	1.6	0.16	--	2.17	1.51
Ni	2	0.47	0.85	0.28	0.32	1.63	2.35
Fe	8	5.3	--	1.4	3.6	2.0	1.22
Sn	4	1.0	--	3.24	2.6	5.28	1.54
Sb	0.4	0.06	--	--	--	--	--
Au/ppm	1000	80	280	420	350	350	570
Pt/ppm	-	-	-	-	--	4.6	30
Ag/ppm	2000	3300	110	1240	--	1300	3301
Pd/ppm	50	-	-	10	--	250	294

[10] Li Jihanzi, Puneet S, Zong G, Hong-Chao Z., 2004. Printed circuit board recycling: a state of the art survey. *IEEE Transaction on Electronics Packaging Manufacturing*, Vol. 27/1, pp. 33 – 42.

[11] SAIMM, 1987. The extractive metallurgy of gold in South Africa. South African Institute of Mining and Metallurgy, Monograph Series M7. G. G. Stanley, ed. Vol. 1.

[12] Wills, B. A. and Napier-Munn, T. J., 2006. Mineral Processing Technology. 7ed. Elsevier, Great Britain.

[13] www.colossusminerals.com

[14] www.horizonmetal.com

[15] www.metalprices.com

[16] Sum, E. Y. L., 1991. The recovery of metals from electronic scrap, *Journal of the Minerals Metals and Materials Society*, Vol. 43/4, pp. 53 – 60.

[17] Kravchenko, N.D., Dubinskii, Y. M. and Krichevskii, V.I., 1983. Processing scrap of radio-electronic equipment. *The Soviet Journal of Non-ferrous Metals (Tsvetnye Metally)* Vol. 24, pp. 100-101.

[18] **Directive 2002/95/EC of the European parliament and of the council on the restriction of the use of certain hazardous substances in electrical and electronic equipment;** *Official Journal of the European Union* l37/19 EN 13.2.2003.

[19] D'Silva K., 2004. Brominated organic micropollutants – igniting the flame retardants issue. *Critical Reviews in Environmental Sc. and Tech*, vol. 34, pp. 141 – 207.

[20] Zhao, Y., Wen, X., Li, B., and Tao, D., 2004. Recovery of copper from printed circuit boards', *Minerals and Metall. Processing*, Vol. 21, No. 2, pp. 99 – 102.

[21] Zhang, S. and Forssberg, E., 1997. Electronic scrap characterizaton for materials recycling. *J. of Waste Management and Resource Recovery*, Vol. 3, pp. 157 – 167.

[22] Kim, B., Lee, J., Seo, S., Park, Y. and Sohn, H., 2004. A process for extracting precious metals from spent printed circuit boards and automobile catalysts, *JOM*, Vol. 56, No. 12, pp. 55-58.

[23] Iji, M. and Yokoyama, S., 1997. Recycling of printed wiring boards with mounted electronic components. *Circuit World*, Vol 23/3, pp. 10 – 15.

[24] Patent Application, WO 6006/013568 A3, 2006. Recovery of precious metals scrap by hydrometallurgical processing, February.

Table 2: A comparison of general WEEE treatment approaches

Treatment Approach	Operation	Merits	Demerits
Landfilling	Direct dumping of classified wastes in landfills	A means of disposal; at least removes physical junks	Leaching of hazardous constituents; wasteful disposal of otherwise huge material resources.
Hydro-metallurgy	A secondary processing, entailing leaching and winning.	Gives high purity product; can handle small tonnages of feed supply	Preconcentration is important on complexity of the leaching and winning. Treatment of secondary effluent streams
Pyro-metallurgy	Smelting in furnaces, giving three products: noble metals report to molten metal phase, metal with more stable oxides report to slag phase, while metals with high vapor pressure will be collected from the vapor phase. Each product further treated separately.	Little feed preparation: sizing, removal of hazardous components - mercury bearing, capacitors.	Require consistent high grade and quantity of feed; dedicated plan t highly capital intensive; feasible where there are existing facilities which accepts e - waste as secondary feed materials; recovers zero value for plastic constituents; off -gas treatment; facilities not available in many parts of the world.
Physical Processing	Applied mineral processing: comminution and separation of constituent materials by exploring variations in physical properties.	Already relevant in feed preparation for hydro or pyro routes; handling of varying feed constituents; amenable for low or high scale operation; least impact on the environment.	Dust handling in aggressive grinding for total liberation; possible precious metal losses; noise; not very clean fractions.

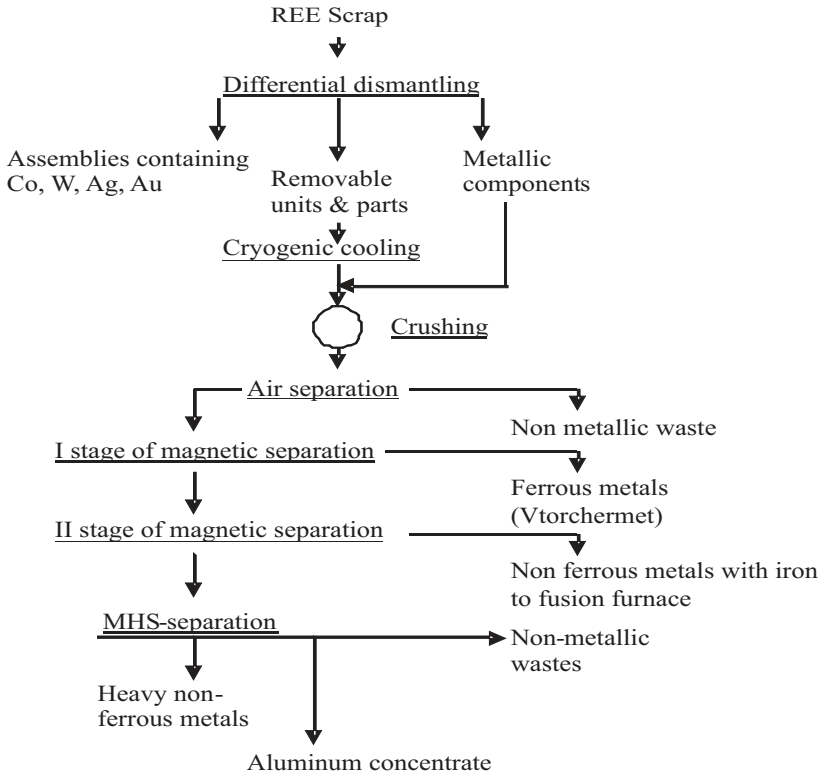


Figure 1: Flowsheet for reprocessing of multicomponent REE scrap [17]

DETERMINATION OF SILICON IN AMORPHOUS SILICA USING MOLYBDENUM BLUE METHOD

ADEEYINWO, C.E,[1] *OKORIE, N. N.[2] and OLUNLADE, B. E.[3]
[1,2] Department of Chemistry, Federal University of Technology Akure.
[2, 3] Engineering Materials Development Institute.
* Correspondence *to: ngoigbo@yahoo.com*

ABSTRACT
The determination of silicon (silica) using the molybdenum blue reaction was studied. The UV-Visible spectrophotometer scanning for the silicon molybdenum blue reaction was studied between 400nm and 800nm using Jenway 6405. The instrumental analytical procedure applied consists of four basic parts: the sample pretreatment, the instrument adjustment, the calibration and measurement and the calculations. The instrument was optimized using standard solution of $KMnO_4$ with Normal calibration method applied. The performance characteristics of the spectrophotometer at a wavelength of maximum abortion λ_{max} of 825 ± 5nm for the silicon-molybdenum blue analysis are presented. The procedure was applied to amorphous silica produced from glass sand and results presented.

Key words: Molybdenum blue reaction, Performance characteristic, Instrument optimization, Silicon.

INTRODUCTION

Silicon analysis is of importance in environmental and industrial type monitoring application. Its presence in material is usually estimated by calorimetric (spectrophotometric) method (1). The overall high concentration and strong tendency to form stable silicides with many element, silicon represents a very important material (as impurity) in high purity materials. For similar reason, its determination at trace levels is difficult (2).

A very sensitive method in which silicomolybdic acid is formed and then reduced to molybdenum blue is now been used for the determination of silicon in trace amounts in materials e.g. sea water, potable water, biological samples and other materials. Several procedures have been published for the determination of silicon in different materials using the molybdenum blue method as reported in literature {1,3,4,10,5,7,]. The variations can be seen in the sample dissolution, conditions of the silicomolybdic complex formation and reduction, reducing agents and other reagents.

The molybdenum Blue Silicon method in conjunction with a UV-visible spectrophotometer is a standard analytical method [1][9] with AOAC approval[8]. It is easy, especially after reducing the yellow molybdic acid to the blue thus forming a stable complex that allows for sample analysis and direct determination [1].

Methods suitable for detailed description in an analytical procedure are either non-instrumental or makes use of instruments that are easily adjustable. Methods for the determination of trace amounts of analyte, lack the necessary sensitivity that must be replaced by relative methods of analysis. This typically involves the measurement of a physical properly that through comparison with known reference solution is then converted to a value for the concentration of the component to be determined in the sample [10].

UV/visible spectrophotometer is a good example of a relative method of analysis. It requires an instrumental adjustment (optimization) that can be easily described and is usually not very critical consequently; the measured absorbance is nearly independent of the instrument used. Remaining minor variations between different instruments can usually be accounted for in the calibration graph prepared from reference solutions [10].

Molybdenum Blue method

The acidification of solutions having molybdate ion and silicate form a yellow crystalline precipitate known as molybdosilicate (silicomolybdic acid) [11] [3] [7]. When there is selective reduction of the silicomolybdate ion, by reducing agents such as ascorbic acid [3], tin (ii) chloride [], hydrazinum sulphate [I] 1-amino-2-napthol-4sulphonic acid[7] and others, a blue colour is produced due to Molybdenum Blue of uncertain composition.

The intensity of the blue colour is proportional to the amount of silicate initially incorporated into the heteropoly acid. [I].This is the basis for the use of the Molybdenum blue method in quantitative and qualitative analytical technique [4].

This is peculiar to hetero atoms whose ion forms heteropoly acids such as tungstate, Phosphate, germante and arsenate. These heteropoly acids may be present as interferences and must be suppressed by introducing masking agents such as oxalic acid, citric acid and tartaric acid [5][15].

This work presents the determination of the silicon in the amorphous silica produced from glass sand and characterized by a metallurgical microscope, XRD & EDXRF [12]. Considering the fact that, a standard analytical method is needed for the determination, it was subjected to the silica-molybdenum blue reaction using ascorbic acid as the reducing agent and analysed using the UV-visible spectrophotometer. The UV-visible

spectrophotometer (Jenway 6405 model) was optimized using KM_nO_4 as a standard carried out with the normal calibration method [13].

MATERIALS AND METHOD

Safety

The MSDS for the detailed information and safety precautions for all the chemical reagents used in addition to the appropriate safety sections in the instrument manual was reviewed and applied.

Reagents

1. Silicon Standard Solution, commercial AAS Standard. (10 $m_g dm^{-1}$)
   10ml of 1000 $m_g dm^{-3}$ of commercial AAS silicon Standard diluted in 100cm. standard flask - 100$m_g d_m^{-3}$ with silicon-free deionized water.
   10ml of 100$m_g dm^{-1}$ diluted in 100cm standard flask -To get 10 $m_g dm^{-3}$
   Stored in a polyethylene container.
2. Acidified Molybdate Solution
   8.000g of Analytical Reagent Ammonium Molybdate, $(NH_4)_6Mo_7O_{24}$:$4H_2O$ was dissolved in 1M HCL diluted to 00ml with the 1M HCL. This solution is to be prepared fresh daily.
3. Ascorbic acid Solution (0.04 $moldm^{-3}$)
   0.7000g of Analytical Reagent, Ascorbic acid was dissolved in deionized water and diluted in 100ml
4. Oxalic acid solution (5% $^m/_v$)
   5.00g of Analytical reagent, oxalic acid was dissolved in deionized water and diluted to 100 ml.
5. Glycerin solution (1% $^v/_v$)
   1ml of Analytical reagent, glycerin was diluted with deionized water and diluted to 100ml.
6. Amorphous silica sample. Production and pre-treatment [14]

Apparatus/Instrument

UV/visible spectrophotometer, (Jenway 6405 model)
1cm quartz cell and a wavelength range of 190 – 1100nm.

Procedure

All reagents having silicon was stored in a polyethylene container.
All glassware was treated with acid to avoid introduction of silicon.
All reagents were prepared using silicon-free deionized water.
Blank solution: The blank solution was prepared by pipetting 1ml of acidified ammonium molybdate solution, 5ml of oxalic acid solution. 1ml of 0.04m ascorbic acid, 1ml of 1% ($^v/_v$) glycerin and made up to mark in a 100ml standard flask with silicon-free deionized water.
Standard working solutions: silicon molybdenum blue mixtures containing 0.1, 0.2, 0.4, 0.6, 0.8, 1.0 $m_g dm^{-3}$ of the standard silicon stock solution was made by diliution method after pipetting appropriate aliquot of the stock for a 5 $m_g dm^{-3}$concentration and reacting with other reagents as in the blank.

Scanning of the spectrophotometer with silicomolybdenum reaction. [Determination of λ_{max}].

6ml (0.6 $m_g dm^{-3}$) standard silicon stock solution was taken into a 100ml standard volumetric flask. 3ml of acidified ammonium molybdate (yellow) was added. After 5mins, 5ml oxalic acid, 1ml of 0.04m ascorbic acid,and 1ml of 1% glycerin solutions were added one after the other. The mixture was made up to 100ml mark with deionized water and immediately transferred into a polyethylene container and left for 20mins for blue colour development.
The mixture was introduced into a 1cm quart curette of the spectrophotometer and scanned between 400-800nm. The blank solution was used to establish a baseline in the instrument. A fit of absorbance against wavelength gave the spectrum of the reaction. Fig. 1.

Spectrophotometric determination of silicon in amorphous silica using molybdenum blue reaction.

0.1g of the silica was weighed accurately into a porcelain crucible in a fume hood. 1ml of water and 2mls of hydrofluoric acid (HF) was introduced into the sample. The mixture was allowed until dissolved (adapted from Vogel). 3ml of acidified ammonium molybdate (yellow) was added for every 0.6$mgdm^{-3}$ of the dissolved sample. After 5mins, 5ml oxalic acid and 1ml of 1% glycerin solutions were added one after the other. The mixture was made up to 100ml mark with deionized water and immediately transferred into a polyethylene container and left for 20mins for blue colour development.
The absorbance of the sample was measured at 825 ± 5nm against a reagent blank sample. The corresponding silicon concentration of the amorphous silica sample was deduced from the calibration curve by interpolation.

RESULT

The absorption spectrum for the molybdenum blue reaction showed maximum absorption (λ_{max}) at 825 ± 5nm (Fig. 1).The scanning of the instrument gave standard results as shown in Table 1. Fig.2 graphically illustrates this data.
A linear correlation was obtained between concentration and absorbance giving a linear range of 0.00 - 2.00 $m_g dm^{-3}$. The slope of the calibration curve was determined to give the sensitivity of the instrument for silicon determination as 0.438AU $m_g^{-1}dm$, with a molar absorptivity of 3.540×10^{-7} AU $mol^{-1}dm^3cm^{-1}$.
The detection limit is calculated by analyzing a 0.4 $m_g dm^{-3}$ standard and reagent blank 8 times. Using 3 times the standard deviations D_L = (n, 3s.d) confident limit, giving a detection limit of 0.002 $m_g dm^{-3}$ [1]. The concentrations of

the standards were chosen such that their absorbances bracketed the absorbances of the sample. By interpolation, the concentration of the sample with absorbances 0.427 AU and 0.219 AU gave 0.99 $m_g dm^{-3}$ and 0.49 $m_g dm^{-3}$ respectively.

DISCUSSION

The wavelength of maximum absorption (λ_{max}) was taken as 825 ± 5nm. This was because the absorption peaks for the reaction appeared for some reaction mainly between 820 - 830nm and average was taken.

It was also observed that with different Ammonium molybdate $(NH_4)_6MO_7O_{24}4H_2O$ having different assays, different points of maximum absorption can be obtained e.g. Fisher product gave 815nm and AVIS chemical gave 825 ±5 nm. All of it appeared within reported ranges. It changes colour and throws down precipitate after 1 or 2days and so must be prepared fresh before use daily.

Preparations of the standard solution of the molybdenum blue are better done by dilution method. This is due to the fact that the absorbance is subject to variations which could be caused by pH considerations and colloidal formations when direct preparations are made.

CONCLUSION

The UV/visible spectrophotometer determination of silicon using the molybdenum blue reaction provides a standard method of confirming the presence of silicon in materials.

An analyst must optimize his instrument and check its performance before use.

This work has provided more literature for silicon determination and given a good understanding and behavior of the Ammonium molybdate produced by different sources.

REFERECES

1. Liberatore P A“ Cintra 10e- Enhanced sensitivity from 600 – 1200nm, Analysis of phosphorus to sub ppb-levels” GBC scientific application notes – UV Visible ,pg 35 - 39
2. Hornung M. and Krivan V (1997) “Determination of silicon in biological tissue by electrothermal Atomic Absorption Spectrometry using slurry sampling of original and pre- ashed samples” Journal of Analytical Atomic spectrometry Vol. 12 pg 1123 - 1130
3. Adeeyinwo C. E and Adesina K. (2002) “Performance characteristic of visible spectrophotometer in Analyzing silicon” Journal of Applied Sciences 5(4), p 3139 – 3147
4. Molybdenum Blue – Wikipedia , the free Encyclopedia
5. Armstrong F. A. J (1951) “The determination of silicate in sea water” Journals of marine biological association of the United Kingdom. Vol 30 No 1
6. Hioki et al (1997) “On – line determination of dissolved silica in seawater by exclusion chromatography in combination with inductively coupled plasma mass spectrometry” Anal chemistry, volume 69 issue (1) pg 21 – 24
7. Rajkovic D (1997) “Spectrophotometric determination of traces of silicon as molybdenum blue in uranium dioxide” Freseuieus' journal of analytical chemistry , volume 225, Number 3, pg 190 – 194
8. Dyck et al (2000) “Spectrometric determination of silicon in food and biological samples and interlaboratory trial” Journal Anal. Spectrom, 2000. 15, p735- 741.
9. Lim P. G. (2005), “Total silica Analysis using a double beam Atomic Absorption Spectrophotometer” Proceedings world Geothermal Congress, Anataly, Turkey ,24- 29 .
10. Van dalen H. P. J and Galam Leo De (1981) “formulation of analytical procedures involving flame atomic - Absorption Spectrometry” Analyst, Vol 106 pg 695 – 701
11. Mondal J. K. and Kundun D (2009) “Spectrometric determination of trace silica in water after enrichment on polyuerethene foam and complexation with Rhodamine B” EJAC, Eurasian j.anal chemistry. 4(1) pg 46 – 52
12. Adeeyinwo C. E. and Okorie N. N. (2010) “Characterisation of the silica produced at different Eutectics through and in –house crucible furnace” NIMACON proceedings 2010.
13. Adeeyinwo, C. E., **et** al “Basic Calibration of UV/visible spectrophotometer using $kMnO_4$ as standard” Chemical Society of Nigeria CSN p proceedings 2010 pg 411 - 415
14. Adeeyinwo C. E. and Okorie N. N. (2008) “Design and Construction of an “in – house” crucible furnace for the production of glass systems at different eutectics”. As presented at NIMACON 2008.

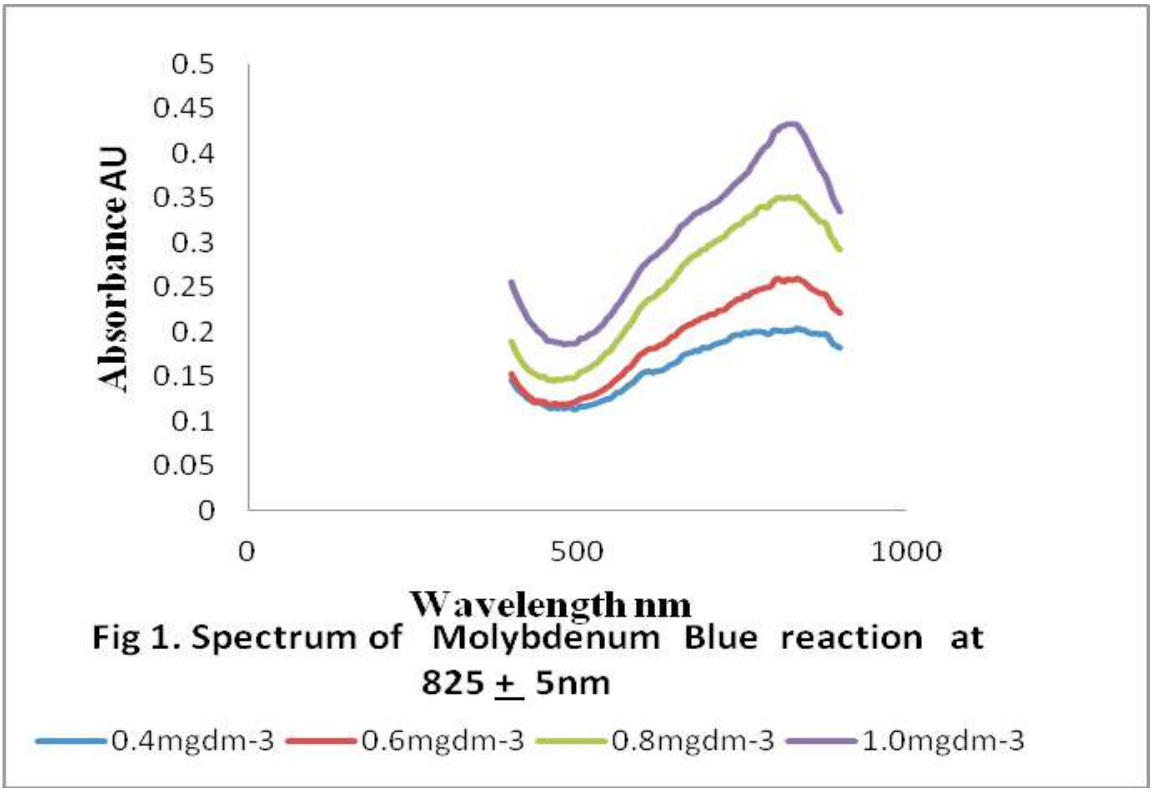


Fig 1. Spectrum of Molybdenum Blue reaction at 825 ± 5nm

Table1. Normal Calibration Data for Standard results at 825 ± 5nm

S/N	Absorbance (AU)	Concentration ($m_g dm^{-3}$)
1	0.0	0.0
2	0.027	0.1
3	0.141	0.2
4	0.201	0.4
5	0.258	0.6
6	0.350	0.8
7	0.433	1
8	0.520	1.2
9	0.606	1.4
10	0.693	1.6
11	0.866	2.0
12	0.930	4.0
13	0.970	6.0

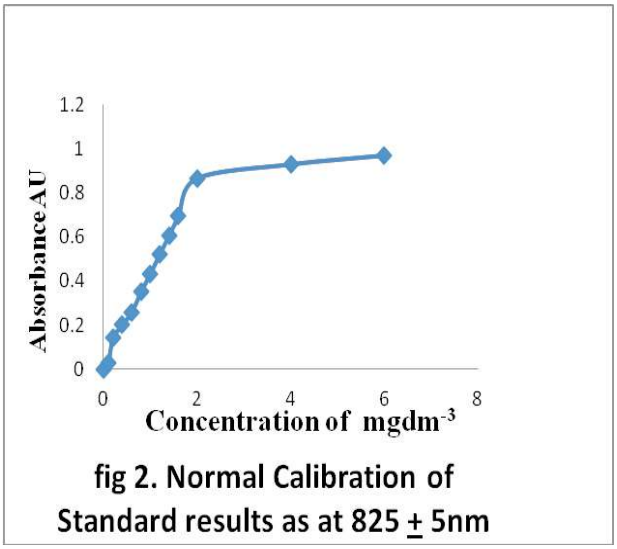


fig 2. Normal Calibration of Standard results as at 825 ± 5nm

SYNTHESIS OF NANOPOROUS SILICA MEMBRANE FROM CORN HOB ASH (ZEA MAYS) BY SOL-GEL METHOD

OGUNFOWOKAN. A.O., Ezenwafor. T. C and Imosili. P
Department of Chemistry, Faculty of Science, Obafemi Awolowo University, Ile – Ife
Engineering Materials Development Institute Akure, Nigeria.
Author of correspondence, email: marrisconso@yahoo.com

Abstract
The research is focused on the production of nanoporous Silica from corn-hob ash and studying on the effect of nanostructuring on the crystal sizes of the obtained silica for industrial application. Corn-cob obtained was **ashed at 700°C, in Muffle furnace for 2 hours and e**xtraction was carried out using 1M NaOH. The template Cetyltrimethylammonium Chloride (CTMACL) which serves as surfactant in the sol-gel process was used for nanostructuring and porosity generation of the extracted silica. The bulk and nanostructured silica was analyzed using X-ray diffractometer (XRD), UV-visible spectrophotometer and Optical Microscope for symmetry, average particle size, pore size and average crystal size determination. The percentage yield of silica obtained from the corn cob was 55.2%, silica of different symmetry was observed on the bulk and the nanostructured silica. Significant changes in value of the average particle and crystal sizes were observed on both the bulk and nanostuctured silica, clearly indicating the effect of nanostructuring. The average pore size values obtained shows that the novel silica is mesoporous and within the nano-range, hence will enhance the application efficiency especially in the membrane industry.
Key words: Silica, Nanostructuring, X-ray Diffractometer, Corn cob ash.

1.0. Introduction

Research interest is gradually moving towards the area of nanotechnology which is increasingly attracting scientific curiosity owing to the new potentials uses of particles in nanometer range. In the frame work of rapid development of nanoscience and nanotechnology, the domain of nanostructured materials is attracting more and more researchers, both in academic and industrial. Nanomaterials are implicated in several domains such as chemistry, electronics, high density magnetic recording media, sensors and biotechnology. This is, in part, due to their novel material properties that differ from both the isolated atoms and the bulk phase.

An crucial challenge in materials research is now the design of perfect nanometer-scale crystallites (in size and shape) identically replicated in boundless quantities in a state that can be manipulated and that act as pure macromolecular substances. The essential first step in the study of their physical properties and the use of nanomaterial in various technologies is their production.

Though silica is highly abundant in nature and its application versatile, the call for ecological challenges has given it a serious concern in converting and re-engineering waste around us to overcome the global environmental problems. Corn hob is one of the common agricultural waste that is found in all part of the world. The high content of silica in corn hob approximately 65% has made it a viable raw material for silica production. The amorphous nature of the corn hob silica makes it extractable at lower temperature.

For years, research has been going on in applying densified method containing homogenously arranged ultra fine particles in the development of concrete with high strength. Some research work has been carried out in the area of application of corn cob ash to improve the properties of the materials. Raheema A.A etal (2010) in their work, studied the effect of Corn cob ash on cement concrete. Their report indicated improvement in the strength of the concrete and this was attributed to the presence of silica in the corn cob ash. In all this research, no report has been given on nanosructuring of silica from the corn cob ash for other industrial applications or its application on concrete at the nano level. The objective of this work is to produce nanoporous silica from corn hob ash and check the effect of nanostructuring on the crystal size of the obtained silica.

2.0. MATERIALS AND METHODS

2.1. Materials

Corn cobs obtained from maize sellers in Akure, Ondo State was washed, dried in the sun and ovum at temperature of 100°C for 3hrs. The dried sample was ashed at 700°C, in Muffle furnace for 2 hours.

2.2. Extraction of pure silica from the Corn cob ash

Ten grams of corn hob Ash (CHA) sample were stirred in 100mL of 1M sodium hydroxide solution ($NaOH_{(aq)}$). The content was poured into conical flask, place in water bath and left to boil for 1hr at the temperature of 100°C. The solution was filtered and the residue washed with boiled de-ionized water. The filtrate was left to cool down. A 3M hydrochloric acid was used to reduce the filtrate to pH of 8.The filtrate which formed a zero gel was left to age for 18hrs, the gel was separated with de-ionized water, centrifuged and decanted. The content was poured inside crucible and dried in the ovum for 12hrs at the temperature of 70°C.The solid crystals obtained was washed with de-ionized water and dried in

the ovum at 100°C. The obtained silica was investigated along with commercial silica using UV- Visible spectrometer, X-ray Diffractometer (XRD) and Optical microscope respectively.

2.3. Synthesis of Nanoporous Silica

The 10% of extracted silica and 30% of Cetyltrimethylammonium chloride (CTMACl) was weighed out and stirred into 1000mL beaker containing 60 mL of de-ionized water. The solution was maintained to pH of 10 using ammonia. The contents in the beaker were stirred for 48hrs at room temperature with the aid of magnetic stirrer. The contents after stirring was filtered, the residue dried and calcine in muffle furnace at 550°C for 5hrs.The obtained residue which is the nanoporous silica was stored in the container for characterization.

2.4. Characterization of the Extracted silica and Nanoporous Silica

2.4.1. Morphology and particle size

The morphology and average particle size of both extracted silica and nanostructed silica was inspected by AP2000 MTI Optical Microscope (Diagnostic Instruments Inc.). The sample was compacted on a spherical sample holder and mounted on the Direct Image Projection optical microscope equipped with microscope to video camera couplers. The photographs of the samples were taken at 100magnifications. The micrographs were analyzed using IMAGEJ software to obtain the 3D graphical imaging of the surface of the silica. Quantitative estimates of the average particle size of the silica were obtained by performing section analysis and particle size estimations of the micrographs.

2.4.2. Phase analysis, Crystal size and pore size

Radicon X-Ray Diffractometer (MD10 with software, $CuK_{\alpha 1}$ radiation of wavelength of 1.54178nm, 2θ ranges from 11^0 - 76^0) was used. The pore size was determined using the value of the interplenary distance (d) at 2?° in Scherrer equation to determine the phase analysis and pore size.

The particle size of the analyzed sample was determined from XRD by Shearer's equation. Sherrer's equation (ZnS nano-particles by Nagalingam).

$$N = \frac{K\lambda}{\beta} COS\theta \quad \text{.....(6)}$$

where; k= constant (0.9),
N= Crystal size
λ =wavelength
β= Full Width at Half Maximum
θ = Angle

3.0. RESULT AND DISCUSSION

3.1. Percentage Yield of Silica:

The percentage yield of Silica obtained was 55.2%. Silica obtained from these wastes gave a higher yield which is in correlation with what A.A Rahaeem etal, (2010) and Mohamed A. El- Sayed, (2006) obtained in their study; 66.38%. The marked difference which was observed when compare the yield of extracted Silica could be associated with geographical location.

3.2. Cetyltrimethylammonium chloride (CTMACl) effects the synthesis of nanoporous Silica

The morphology, particle size, pore size and crystal size of silica after nanostucturing was investigated by the optical microscope and X- ray diffractometer. Cetyltrimethylammonium chloride (CTMACl) has a serious effect as showed by the obtained results below.

Figures 1 & 2 represent the Micrographs of raw Silica extracted from alkaline medium before and after Nanostructuring. Before Nanostructuring, it presented modules of Strand having average particle size of 6790nm while after Nanostructuring; it presented aggregates of crystals with particle size of 305nm

This is observed in the synthesis as the crystal size determination is presented using Scherrer's equation as stated in equation one, the nanostructured silica gave average crystal size of 2.47nm against 9.96nm which is the average crystal size before nanostructuring.

Average Pore size value of the nanosilica obtained was 5.26nm proved to be mesoporous based on IUPAC specification (i.e. Mesoporous materials 2–50-nm pores).

Fig.5 represents the spectrum of the silica extract obtained from the ash of corn cob using 1MNaOH. Several peaks were also obtained having three major peaks at 2? angles 25.45o, 59.31o, and 63.23o respectively. Angle 59.31o and 63.23o represents silica having lattice constant of a= 14.24, b= 20.14, c= 8.4 with indication for orthorhombic structure (JCPDS card no; 44-1394). A figure 6 shows the spectrum of the nanostructured silica from the corn hob, the major peaks is at 2?o of 50.76o, 67.09o and 67.33o. The angle at 50.76o and 67.09o is associated with silica having lattice constant a = 13.603, c = 8.277 connected to hexagonal structure (JCPDS card no; 45 – 0131) with the last angle 67.33o associated with silica also having lattice constant of a = 14.24, b= 20.14, c = 8.4 with the indication of orthorhombic structure (JCPDS card no; 44- 1394)

TABLE 1: Average Particle size (Grain Size)

Sample	Silica Extract (in nanometer)	Nanostructured Silica (in nanometer)
CHB	6790	305

TABLE 2: Average Crystal size Determination

Sample	Silica Extract (in nanometer)	Nanostructured Silica (in nanometer)
CHB	9.96	2.47

TABLE 3: Average Pore size Determination

Sample	Pore size (in nanometer)	Inference
CHB	5.26	Mesopore

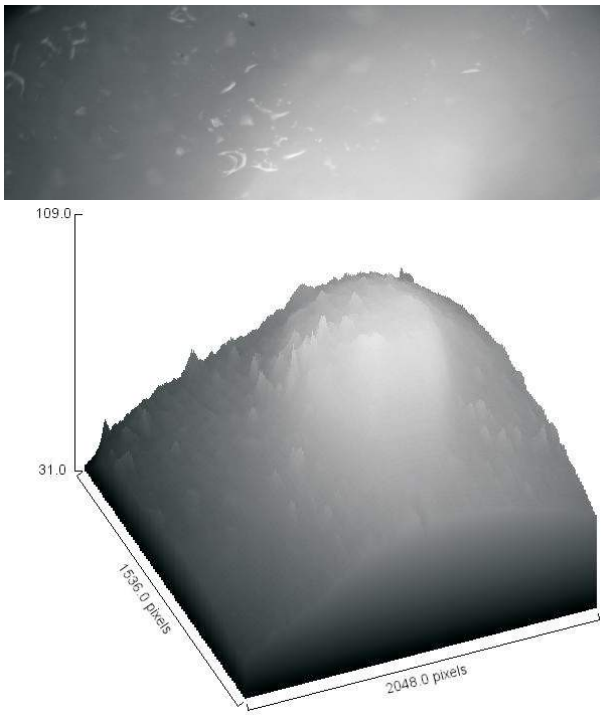


Fig. 1a: Micrograph of raw Silica
Fig. 1b: Surface plot of raw Silica

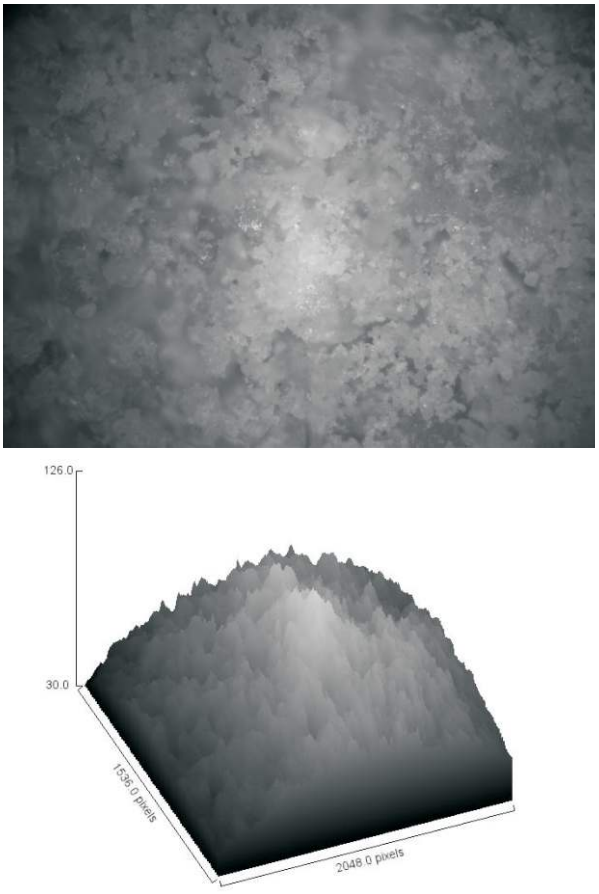


Fig. 2a: Micrograph of nanostructured Silica
Fig. 2b: Surface plot of nanostructured Silica

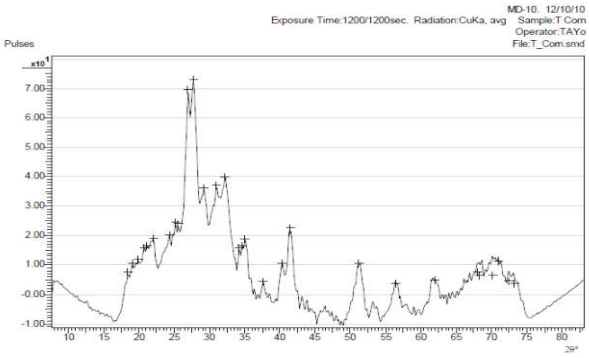


Fig.3: Corn cob ash

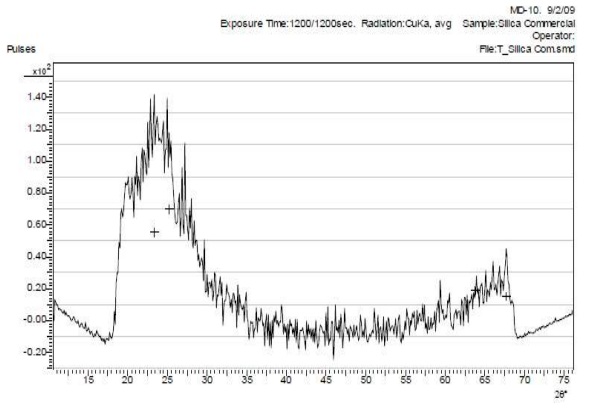


Fig.4 : Commercial Silica

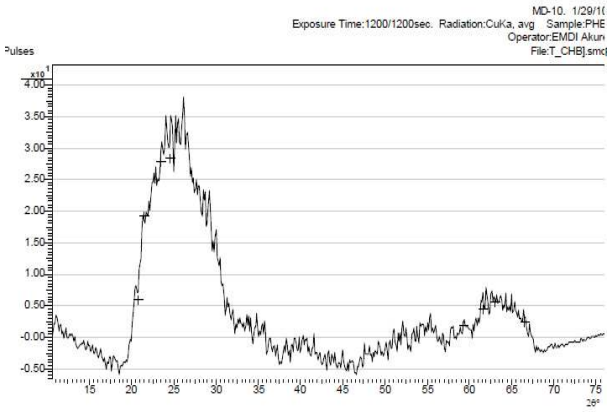


Fig.5: Extracted Silica from Corn hob using 1MNaOH

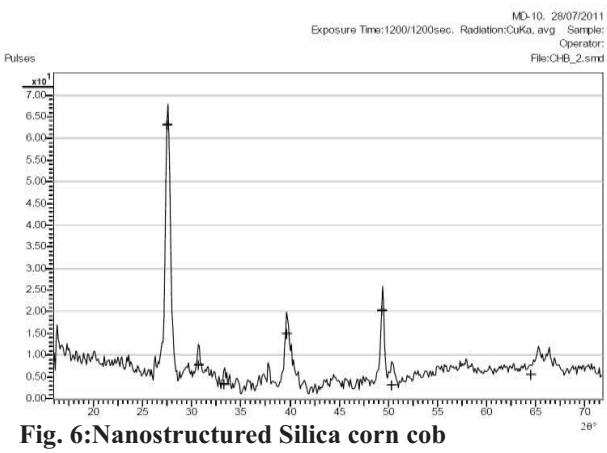


Fig. 6:Nanostructured Silica corn cob

The X- ray diffractometer showed a strong band peaks between 25° and 28°.These strong bands are the characteristics of amorphous SiO_2

CONCLUSION

The percentage yield result ascertained the high concentration of Silica in the corn-hob, indicating that the waste contains reasonable amount of silica which can be extracted for industrial application. The optical micrograph and the surface plot showed the effect of nanostructuring on the particle size of the silica. The pore size value showed that the nanostructured silica obtained is mesoporous. The X- ray result ascertained that silica extracted was of different symmetry and crystal sizes which changed after nanostructuring. The obtained result supports the fact that the rheology and properties of materials is affected by nanostructing, affecting the technological application.

Reference

1 Binici H., Zengin H. Zengin G., H. Kaplan and Yucegok F., (2009) Resistance to Sodium Sulphate attack of Plain and Blended Cement containing Corncob ash and ground granulated blast Furnace Slag, *Academic Journals,* **4(2)**, 098 – 106.

2 Dare. E.O and Bello A. O (2009) Extraction of Nanosilica from Bagasse Ash. Unpublished Undergraduate project.

3 Edelstein. A.S and Cammarata. R.C. (1996) Nanomaterials: Synthesis, Properties and Applications, Institute of Physics United Kingdom

4 Gleiter H, (1995), Nanostructured Materials: State of Curt and Perspectives, ***Nanostructured Materials*****, 6, 03 – 14**

5 Jutzi P.and Schubert U. (2003), Silicon Chemistry: From the atom to Extended Systems, Wiley

6 Keely W.M. 1(966), Simple Techniques for the Determination of Surface Area Using XRD .*Analytical Chemistry Journal of America Chemical Society*, 38(1), 147 – 148

7 Lu G.O., "Nanoporous Materials – An Overview" World Scientific Publishing C Company Nov. 2004 **Nanocomposite Materials,** ***Chemistry Material,*** **13, 3151 – 3168.**

8 Raheem**a A.A., Oyebisi S.O., Akintayo S.Oand Oyniran M.I (**2010) **Effects of Admixtures on the Properties of Corn Cob Ash Cement Concrete,** *Leonardo Electronic Journal of Practices and Technologies*,**16**, 13-20

9 Smarsly.B.,(2002), Nanoporous Materials ***Journals of Nanoscience and Nanotechnology*** **2, 6, 581- 612.**

10 Wall G. C. and Brown J. C.,(1987), Determination of Pore size Distribution from Sorption isotherms Application of percolation *Theory Journal of Colloid and Interface Science*, **120,** 218 – 223.

11 Wikipedia, Maize, *from online the free encyclopedia,* Retrieved 2011-8-29.

12 H.L.Tuller, 2002



Fig A: Maize Plant with corn



Fig B: Corn Cob

THE USE OF OPERATIONAL AMPLIFIER IN PROVIDING SAFETY FOR ELECTRONIC DEVICES

Oluyamo S.S., Ogunjo S.T., Oluwasusi, F.F.,
Department of Physics, Federal University of Technology, Akure
ogunjosam@yahoo.com

Abstract
Operational amplifiers commonly referred to as Op-Amp find a wide application and usage in electronics, control and instrumentation circuits. The use of this device in ensuring the longevity of electronic systems is discussed in this paper. Equipment such as automatic voltage regulators, automatic inverter systems and so on make use of OP-Amp to provide safety for the entire components that make up the device. In this work, the Op-Amp is used to provide overload and no load indication. A low and high battery level indication when in used and while undergoing charging process is ensured respectively; this however elongates the life-span of the battery. With the aid of an external shutdown circuit arrangement, the entire system can be shut down after given a prior warning alarm about all the conditions earlier mentioned above.
Keywords: Op-Amp, battery, Electronic Devices, Inverter.

INTRODUCTION

An operational amplifier ("OP-Amp") is a DC-coupled high-gain electronic voltage amplifier with a differential input, and usually, a single ended output. An OP-Amp produces an output voltage that is typically hundreds of thousands times larger than the voltage difference between its input terminals **[1]**. Operational amplifiers are important building blocks for a wide range of electronic circuits. They had their origins in analog computers where they were used in many linear, non linear and frequency-dependent circuits. Their popularity in circuit design largely stems from the fact that characteristics of the final Op-Amp circuits with negative feedback (such as their gain) are set by external components with little dependence on temperature changes and manufacturing variations in the Op-Amp itself.

Op-Amps are among the most widely used electronic devices today, being used in a vast array of consumer, industrial, and scientific devices. The Op-Amp is one type of differential amplifier. Other types of differential amplifier include the instrumentation amplifier (usually built from three Op-Amps), the isolation amplifier (similar to the instrumentation amplifier, but with tolerance to common-mode voltages, and negative feedback amplifier (usually built from one or more Op-Amps and a resistive feedback network **[4]**. A standard Op-Amp has a minimum of five pins for its operation; this is shown in figure 1. The basic pins are: V_+ (non-inverting input), V_- (inverting input), and V_{out} (output), V_{S+} (positive power supply and V_{S-} (negative power supply)

The amplifier's differential inputs consist of a V_+ input and a V_- input, and ideally the Op-Amp amplifies only the difference in voltage between the two, which is called the differential input voltage. The output voltage of the op-amp is given by equation 1

$$V_{out} = (V_+ - V_-) A_{OL} \qquad (1)$$

Where V_+ is the voltage at the non-inverting terminal, V_- is the voltage at the inverting terminal and A_{OL} is the open-loop gain of the amplifier (the term "open-loop" refers to the absence of a feedback loop from the output to the input). Without negative feedback, and perhaps with positive feedback for regeneration, an Op-Amp acts as a comparator **[6]**.

Op-Amp as a Comparator

In electronics, a comparator is a device that compares two voltages or currents and switches its output to indicate which is larger. They are commonly used in devices such as analog-to-digital converters (ADCs), relaxation oscillator, null detectors, zero-crossing detectors, level shifter and so on. In theory, a standard op-amp operating in open-loop configuration (without negative feedback) may be used as a low-performance comparator **[2]**. When the non-inverting input (V_+) is at a higher voltage than the inverting input (V-), the high gain of the op-amp causes the output to saturate at the highest positive voltage it can output. When the non-inverting input (V_+) drops below the inverting input (V-), the output saturates at the most negative voltage it can output. The Op-Amp's output voltage is limited by the supply voltage.

A dedicated voltage comparator will generally be faster than a general-purpose operational amplifier pressed into service as a comparator. A dedicated voltage comparator may also contain additional features such as an accurate, internal voltage reference, an adjustable hysteresis and a clock gated input **[3]**. A dedicated voltage comparator chip such as LM339 and LM324 is designed to interface with a digital logic interface (to a TTL or a CMOS). The output is a binary state often used to interface real world signals to digital circuit. Operational Amplifier plays a big role in the Pulse Width Modulated (PWM) based inverter system; the Op-Amp is used as a comparator in the inverter circuit. In this design, Op-Amp LM324 is used as a voltage comparator in the inverter

circuit. The LM 324N is a quad two input Op-Amp. Four different Op-Amps in the LM324N can be used for four different works. Each of the Op-Amps in the LM324N IC package has three pins; two for input and one for output. Out of the two input pins, one is called inverting (-) input and the other is called non-inverting (+) input.

Non-Inverting Input (+)

If the input given to this pin is less than the input given to the inverting input pin, then the Op-Amp output will be low. If the input given to this pin is more than the input given to the inverting input pin, then the Op-Amp output will be high. In summary, if the input to the non-inverting pin is low, the output will be low and if the input is high, the output will be high.

Inverting Input (-)

If the input given to this pin is less than the input given to the non-inverting input pin, then the Op-Amp output will be high. If the input given to this pin is more than the input given to the non-inverting input pin, then the output of the Op-Amp will be low. The output will be reverse of the input at the inverting pin; that is, if the input to the inverting pin is low, the output will be high and vice versa **[5]**.

It can therefore be seen that the Op-Amp output depends on the value of the signal at its input pins. This property of the Op-Amp makes it useful as a comparator in inverter circuit **[7]**. Op-Amps in the inverter receive a fixed reference voltage at its one input pin and the other input pin is given the value to be checked. When the value to be checked differ from the reference voltage, the Op-Amp output will go low or high. This output is used to provide audio/visual indication about the conditions of the protective circuit or to shutdown the inverter. In this paper, Op-Amp is used to provide safety for an inverter system; this is achieved by using Op-Amp to design a no load indication circuit, a low battery indicator circuit and an overload detection circuit. With the Op-Amp circuit arrangement, a visual indication is given when any of the conditions earlier mentioned is detected and with an external shutdown arrangement; the inverter system can be shut down after given a prior warning alarm about all the conditions given above.

NO LOAD SHUTDOWN SECTION

When the inverter is working in battery mode and no load is connected at the inverter output, or if the load at its output is switched off, the inverter senses this and automatically switches off itself. This type of protective circuit as shown in figure 2 is essential to protect the inverter from unnecessarily discharging the battery.

How the "No load" is sensed

Source (S) of the MOSFETs at the inverter output is grounded through a shunt. According to Manahar 2004, different polarity of 0V is generated at this shunt, based on the load connected to the inverter output. When no load is connected at the inverter output, the shunt shows negative 0V, and when proper load is connected to the output, the shunt shows positive 0V. The negative 0V is used by the no-load shutdown circuit.

No Load Shutdown Circuit.

The No-load shutdown section uses two Op-Amps using Pin-1, 2, 3, and 8, 9, 10 of IC1, transistors T3 and T4. Pin-2, 3, 9 and 10 are input pins of Op-Amp while Pin-1 and 8 are output pins.

Working Principle

Pin-3 of IC1 receives positive 0V, through R12. Pin-2 of IC1 receives voltage from shunt, through R20 and R18. When no load is connected at output, negative 0V reach pin-2 of IC1 and positive 0V reach pin-3. This results in high output at output pin-1 of IC1. High output at pin-1, turns on the Light Emitting Diode D10 connected to that pin. This indicates that inverter is on, but no load is connected at its output.

High output at pin-1 is given to pin-10 of IC1 through R3 and D5. Capacitor C1 at pin-10 will slowly increase the voltage at this pin. Pin-9 of IC1 receives +5V regulated supply from an external source. As C1 charges, voltage at pin-10 increases; when the voltage at pin-10 becomes higher than the voltage at pin-9, a high voltage (10V) is output from output pin-8. This high output is given to the base of T3, through R34, D11 and D10.

High voltage at the base of T3, switch on the transistor and a 0V is output from its collector. This 0V reach the pin-1 and 5 of another IC2 called NAND gate (CD4011), IC2 is a Quad 2 input NAND gate. Pin-1 and 5 are input pins of two of the NAND gates inside the IC package. When pin-1 and 5 receive 0V, output pins 10 and 11 of the NAND gate will stop the output of MOS drive voltage. With the absence of the MOS drive signal from IC2, the MOSFETs in the output section will stop functioning. This will stop the output at the inverter output socket, that is, the inverter shuts down. The shutdown circuit comprises of pin-8, 9 and 10 of Op-Amp (IC1), transistors T3, T4 and the circuit arrangement of IC2; this is shown in fig. 3.

No-Load Indication.

High voltage at pin-8 of IC1 is given through R8, to the following.

- LED D8, through R2
- Buzzer, through D1and R1

This will switch on the LED D8 and buzzer will sound, indicating no-load condition.

Attaching load when Inverter is in no-load condition.

During the no-load shutdown condition, when a load is connected to the inverter output socket, a positive 0V develops at the output section of MOSFETs source. This results in a positive 0V at pin-2 of IC1. When positive 0V reach pin-2 and 3 of IC1, 0V is output from its pin-1. This will stop the voltage at pin-10 from increasing and a continuous low voltage is produced from its output pin-8. This results finally in normal operation of the inverter.

LOW BATTERY SHUTDOWN SECTION

To protect the battery- a device that serves as input to the inverter system- and to ensure a longer life

span of the battery, a low battery detector/shutdown circuit is used. When the battery discharge to a preset level, the low-battery shutdown section sounds the buzzer for sometime and then automatically shuts down the inverter. When a 12V battery reaches 10V, it is considered completely discharged **[5]**. Once the battery is discharged to 10V, it requires charging before it can be used. The inverter system therefore automatically shuts down itself when the battery voltage reaches 10V to protect the battery from getting damaged.

Low Battery Shutdown Circuit

Low battery shutdown circuit consists of Op-Amp made of pin-5, 6 and 7 of IC1. Pin-5 of IC1 receives +5V regulated supply as reference voltage from an external source. Pin-6 receives battery supply through the potential divider R16 and R17. Pin-7 is output pin.

Working Principle

When the battery has enough charge, the voltage at pin-6 is higher than the voltage at pin-5. For example, when the battery is fully charged (13.5V), pin-6 has around 8.7V, as the battery gets discharged to around 12V; the voltage at pin-6 reduces to about 7.2V. As the battery gets discharged, the voltage at pin-6 gets further reduced. When the voltage at pin-6 becomes a little higher than the voltage at pin-5, output pin-7 will output a high signal (around 8.5V).

High output at pin-7 of IC1 will reach the following through R7:

- Low battery indicator LED D9, through R4
- Positive terminal of buzzer through D2 and R1
- Pin-10 of ICI through R5, D3 and R9.

High voltage at D9 and buzzer will turn on the LED and starts sounding the buzzer. This alerts the user about low-battery shutdown. Turning on of LED D9 and sounding of buzzer indicate that the battery has reached 10V level, but low-battery shutdown has not yet taken place. High voltage at pin-7 of IC1 reaches pin-10 of IC1, through R5, D3 and R9. This repeats the whole process of inverter shutdown which was explained in the no-load shutdown section. Voltages at the various pins were measured,

PIN	VOLTAGE
5	5.0V
6	8.7V
7	0V
8	0V
9	5.0V
10	0V

It should be noted that pin-6 of IC1 receives 8.7V only when the inverter battery is fully charged, that is the battery voltage will indicate around 13.5V. As the battery voltage reduces, the voltage at pin-6 also gets reduced. Table 2 shows the voltages when the low-battery starts sounding while table 3 shows the voltages after the low-battery shutdown occurs.

Table2: Voltages when the Low-Battery Buzzer starts sounding.

PIN	VOLTAGE
5	5.0V
6	4.0V
7	8.5V
8	0V
9	5.0V
10	0V

Table 3: Voltages after the Low-Battery Shutdown

PIN	VOLTAGE
5	5.0V
6	4.8V
7	8.5V
8	10.5V
9	5.0V
10	5.1V

OVERLOAD SHUTDOWN SECTION

If a load higher than the inverter capacity is connected at the inverter output, the MOSFETs at the output, and the output mains transformer could get damaged **[5]**. To protect the inverter from this situation, an overload shutdown section is used in the inverter. This section protects the inverter mains transformer and MOSFETs by switching off the inverter output. When the overload occur, the inverter does not switch off immediately; it indicates this condition by lighting an overload Light Emitting Diode (LED) and sounding buzzer before shutting down the inverter.

Overload Circuit

Overload shutdown section uses two Op-Amps using Pin-12, 13, 14, and 8, 9, 10 of IC1, transistors T4 and T3.

Working Principle

Load sensing voltage is given to the pin-12 of IC1 from source of MOSFETs, through R20, R18. Pin-13 of IC1 receives a constant reference voltage, through R14, R15 and overload adjustment preset VR1. The value of reference voltage at pin-13 of IC1 is around 0.05V; this value can be increased / decreased by VR1. According to **Phillip et al, 2002,** a 500VA/12V inverter should be set for overload cut at 300W. When a 300W load is connected to the inverter, pin-12 of IC1 receives around 0.03V from the MOSFETs source. When more than 300W load is connected to the inverter, this results in 0.04V at pin-12 of IC1.

When the load is further increased, a point is reached when the voltage at pin-12 of IC1 becomes a little higher than the voltage at pin-13. This results in a high output (around 5.5V) at pin-14 of IC1. High output at pin-14 is given to pin-10 of IC1 as input, through R10 and D7. A high voltage at pin-10 results in high voltage (around 8V) from the output pin-8 of IC1. High voltage at pin-8 of IC1 repeats the whole process of inverter shutdown which was explained in the no-load shutdown section.

CONCLUSION

The use of an Op-Amp to provide safety for electronic device is very vital as it ensures the longevity of the electronic systems. The incorporation of Op-Amp inside an inverter system has a lot of advantages over the ones that does not have the Op-Amp feature. The Op-Amp design discussed in this paper does not only ensure the safety of the inverter system; it also ensures that all the peripherals, battery for example, used with the inverter system are protected from damage that could result from overuse.

REFERENCES

[1] Horowitz, P. and Hill, W. 1989. The Art of Electronics. Cambridge University Press, Cambridge, pp. 176-180, 284-285.

[2] Jung, W.G. 2004. OP Amp Applications Handbook. Newness, pp. 777-779.

[3] Stout, D.F. 1976. Handbook of Operational Amplifier Circuit Design. Mc Graw-Hill, pp.1-11.

[4] Malmstadt, E. 1981. Electronics and Instrumentation for Scientists. The Benjamin/Cummings Publishing Company Inc., pp.108–110.

[5] Manahar, L. 2004. Modern Uninterrupted Power Supply – Introduction, Servicing and Troubleshooting. B.P.B publication, New Delhi, India. pp. 23-48.

[6] Phillip, A. and Douglas, H. 2002. *CMOS Analog Circuit Design*, Oxford University Press, Oxford, pp.55-58.

[7] Rogenmoser, R. and Kaeslin, H. 1997. The impact of transistor sizing on power efficiency in submicron CMOS circuits. Solid-State Circuits, IEEE Journal 32 (7), pp. 1142–1145.

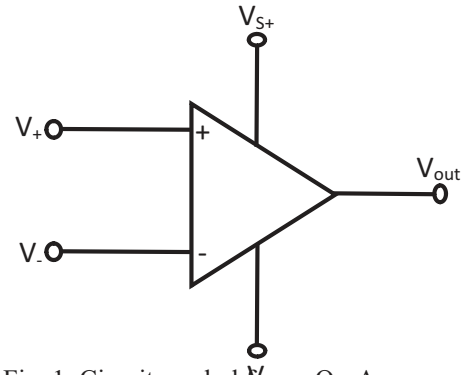
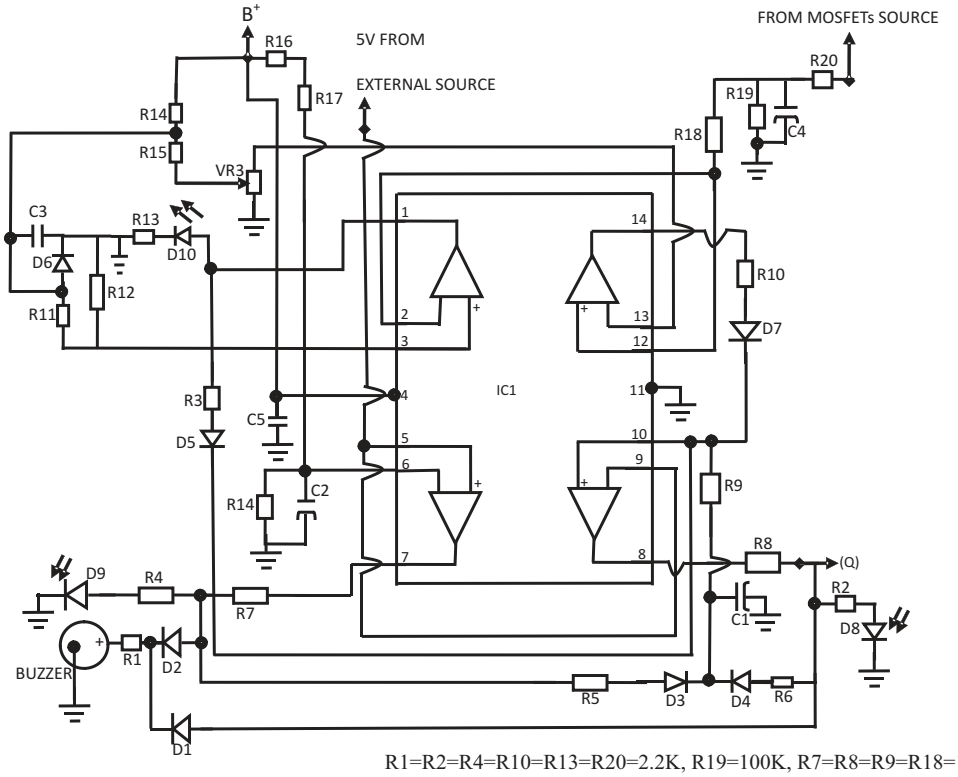
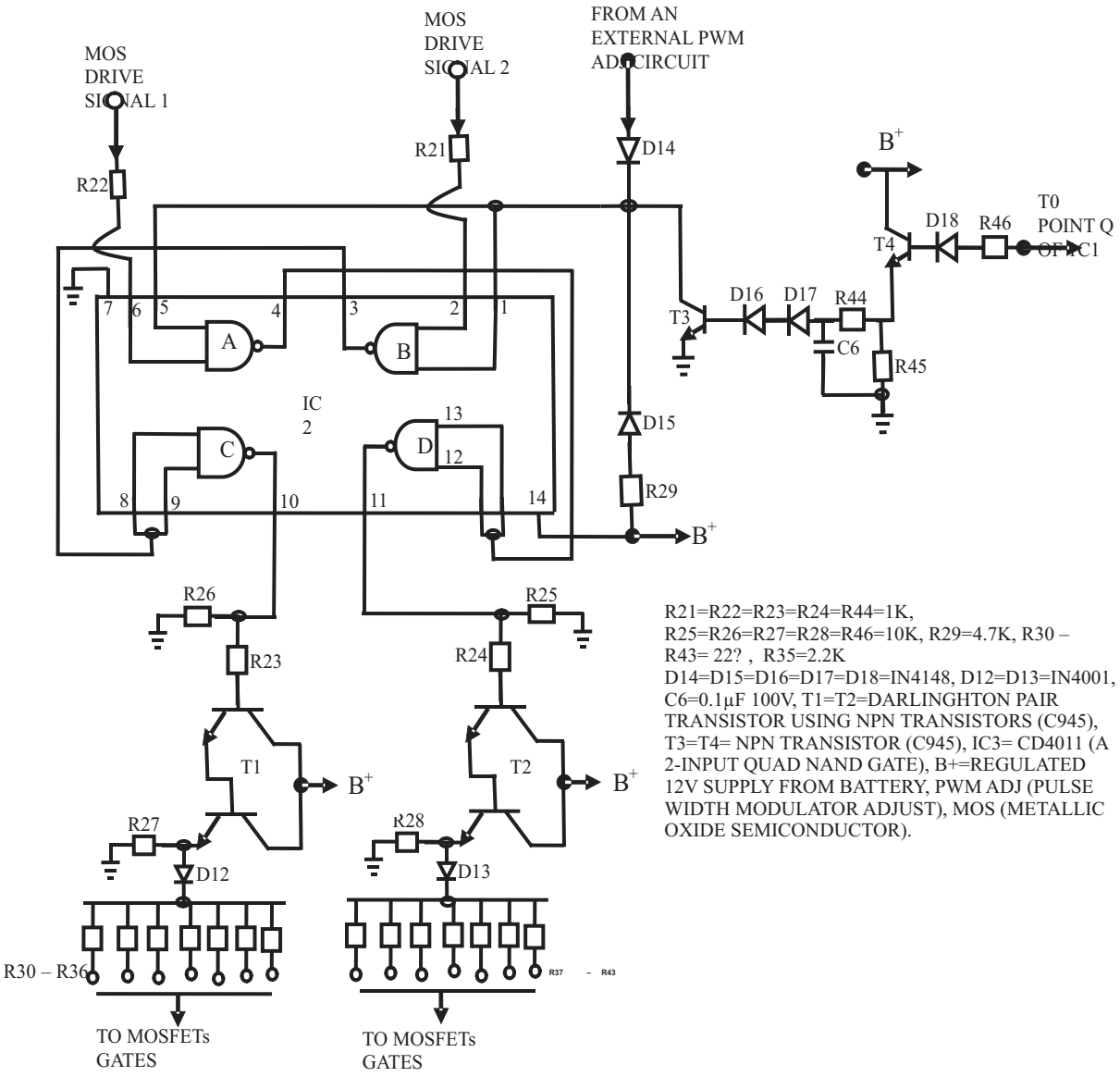


Fig. 1: Circuit symbol for an Op-Amp.



R1=R2=R4=R10=R13=R20=2.2K, R19=100K, R7=R8=R9=R18=1? , R6=R11=R14=R17=47K, R5=330K, R16=4.7K, R15=22K, R3=1M, R12=47 ? D1=D2=D3=D4=D5=D6=D7=IN4148, D8=OVERLOAD/SHUTDOWN LIGHT EMITTING DIODE (LED) INDICATOR, D9=LOW BATTERY LED INDICATOR, D10=NO-LOAD LED INDICATOR, C1=47µF 50V, C2=10µF 50V, C3=0.22µF 100V,C4=100µF 50V, C5=0.1µF 100V, IC1=LM324 (QUAD OPERATIONAL AMPLIFIER) , VR3 (OVERLOAD ADJUSTMENT PRESET) =4.7K, B+=REGULATED 12V SUPPLY FROM BATTER.

FIGURE 2: PROTECTIVE CIRCUIT USING OP -AMP



R21=R22=R23=R24=R44=1K, R25=R26=R27=R28=R46=10K, R29=4.7K, R30 – R43= 22? , R35=2.2K
D14=D15=D16=D17=D18=IN4148, D12=D13=IN4001, C6=0.1µF 100V, T1=T2=DARLINGHTON PAIR TRANSISTOR USING NPN TRANSISTORS (C945), T3=T4= NPN TRANSISTOR (C945), IC3= CD4011 (A 2-INPUT QUAD NAND GATE), B+=REGULATED 12V SUPPLY FROM BATTERY, PWM ADJ (PULSE WIDTH MODULATOR ADJUST), MOS (METALLIC OXIDE SEMICONDUCTOR).

FIGURE 3: SHUTDOWN CIRCUITRY USING NAND GATE AND MOS DRIVER SECTION

PRODUCTION OF *BAMBOO-LAM FROM* FLAT BAMBOO STRIP PREPARED FROM *BAMBUSA VULGARIS SCHRAD*

Adewole A. N.[1] **and Olayiwola H. O.**[2]
[1&2] Department of Agricultural and Environmental
Faculty of Technology, University of Ibadan, Oyo State, Nigeria
[1]E-mail: dabukyo@yahoo.com or an.adewole@mail.ui.edu.ng

ABSTRACT
This study addressed the problem of producing bamboo-lam from flat strips prepared from Bambusa vulgaris Schrad. Such bamboo-lam is suitable for making bamboo-based products for interior use. Bambusa vulgaris samples were sourced from 4 years old stock, at the time of harvest, from within the University of Ibadan, Oyo State, Nigeria. The harvested matured culms were reduced to 780mm long each with a minimum diameter and wall thickness of 30mm and 5mm respectively. The short culms were split, rough planed to remove nodal protrusion and green epidermal layer before soaked in hydrogen peroxide treated hot water for 24 hours to improve strips resilience to insect and fungal attack. The dried strips were dressed, glued, cured and finished to produce bamboo-lam. For the flat bamboo strips produced, the percentage recovery index (RI) after splitting was 75% and reduced to between 50 – 57% after surface planed. Untreated strip was prone to attack while soaking in hot hydrogen peroxide treated water for 24 hours improved their resilience to degradation and insect attack. The dimensions, percentage RI and durability of strips produced from Bambusa vulgaris thus depend on its culm features, handling skill, equipment and treatment. Bamboo laminates of width 25 x (5 – 8) mm were produced from the flat bamboo strips produced. This study has been able to produce durable bamboo strips and laminates from Bambusa vulgaris Schrad using common carpentry tools and machines. The bamboo-lam produced is suitable for manufacturing bamboo-based products for interior use.

Keywords: Bambusa vulgaris Schrad**,** Strips Preparation, Durability, Bamboo laminate

1.0 INTRODUCTION

Excessive timber harvest has caused a marked reduction in the supply of wood. This is due in part to the increasing demand of wood as a result of rapid population growth [1]. The extent of reduction is currently affecting wood position as a prime choice among conventional raw materials for varying applications. A significant contributor to the swaying of interest away from over dependence on wood is its escalating cost that has greatly reduces its affordability to all. In order to circumvent wood scarcity problem via abolition of over dependence for its sustainability, concerted efforts have been directed at re-engineering wood waste and other tree products to produce engineered wood-based products [2]. The 21st century appears to be witnessing a growing consensus to tap into potentials of Non-Timber Forest Products (NTFPs) that are also lignocellulosic materials **[3,4,5,6]**. The need to exploit NTFPs stemmed from the current drive to eradicate poverty and extreme hunger through expansion of employment opportunities particularly to the rural dwellers and low income earners.

From among the commonest NTFPs, bamboo and rattan potentials have made them to be most favoured. One of such potentials is availability in multiple varieties in many countries. Nigeria is also blessed with numerous species of bamboo and rattan [7] and their abundance was attested to by [8 and 9]. However, bamboo seems to have overriding advantages, enshrine in its versatility, over rattan. Bamboo a multifaceted non-timber plant is reported to have emerged as a valuable wood substitute for cushioning the pressure on wood raw material supply in the last 15-20 years [10]. And that the development of bamboo resources and industries worldwide promotes rural livelihood, economic and environmental growth, mitigates deforestation and illegal logging, prevents soil degradation and restores degraded lands [11]. With modern processing techniques, many of which are still quite new in Nigeria, bamboo can be transformed into many products that compete directly with wood products in price and performance.

1.1 Bamboo: Genera, Species and Uses

Bamboo is a group of woody perennial grasses in the true grass family *Poaceae* having 91 genera with over 1,000 species. It varies in size from small annuals to giant timber bamboo, a fastest growing woody plant in the world which sometimes grows up to 38.1-50.8 mm/hr [12]. One of the commonest genera is *Bambusa* and it has 85 species that are all clumper save Bambusa *ventricosa, the clumper*/**runner /extinct status of which was yet to be verified**. Among *Bambusa genera* is *vulgaris* that consists of 4 species: the *Bambusa vulgaris Schrad, Bambusa vulgaris* Vittata, *Bambusa vulgaris* Wamin and *Bambusa vulgaris* Wamin Striata. The Bambusa *vulgaris* in general attained maximum height of 15.24m and 101.6mm diameter. It grows generally in the tropics with lots of branches and its new shoots appear in late fall. Some varieties of *Bambusa vulgaris* have been used in many countries of the world for food, gardening,

furniture, light structures and erosion control [12].

Some studies have buttressed the availability of ***Bambusa vulgaris*** **Schrad in** abundance **[13,14,]** in various parts of Nigeria while its strength adequacy, versatility and beauty in both natural and finished states had been reported by [15,16,17]. Up till now, ***Bambusa vulgaris*** **Schrad** culm is still been used in round in Nigeria. However, there are challenges in using *Bambusa vulgaris* Schrad in round form. The challenges are inherent in the culm's physical and chemical properties [4]. The culm has high sugar content that made it highly susceptible to insect attack and other biodegrading agents [16] while the hollow structure limits its use in the round form due to problems associated with jointing induced by discontinuity in the formation of its fibres as a consequence of numerous nodes and internodes.However, the round culm can be processed into strips with reduced starch content so as to enhance its durability [10]. Furthermore, the conversion of round culm into flat strips will further enhance its versatility and adaptability for producing modern bamboo-based products at cottage level.

Apart from these reasons, timber remains the major source of attraction to Nigerian forest exploiters and the over-dependency on timber has being the bane sustaining timber resource in the country. The development had encouraged the use of wood from hitherto fruit trees [18,8] for various end uses. The global consensus on the negative impacts of deforestation on climate change is promoting development of alternative raw material from numerous NTFPs to complement wood in various applications. This is belief to have mitigating capacity for over-dependency on timber while it will also ensure wood utilization sustainability. Therefore adaptation of appropriate technology for manufacturing bamboo-based products represents a step to unlocking the abundant bamboo supply and its effective utilization. This work is limited to the production of bamboo-lam from processed flat bamboo strips from bamboo species grown in the University of Ibadan.

2.0 MATERIALS AND METHODS

The bamboo species utilized for this study was harvested from the University of Ibadan premises. The species and age of the bambusa stock from where the samples were harvested had earlier been identified by [19]. The species used is *Bambusa vulgaris* Schrad while the age at the time of harvest was 4 years. There are four main stages involved in the production of bamboo-lam as shown in Figure 1 (Appendix I). Matured culms with minimum diameter and wall thickness of 30mm and 5mm respectively were harvested. The culms were reduced into 780mm length before splitting on circular saw. The strips were rough planned to remove both the nodal protrusion and green epidermal layer. The planned strips were later soaked in treated hot water for 24 hours to improve strips resilience to insect and fungal attack before drying. The dried stripes were prefinished, glued, cured and finished to produce bamboo-lam.

3.0 RESULTS AND DISCUSSION

Quite a number of challenges were encountered when harvesting the bamboo culms used for this study. The *Bambusa vulgaris* Schrad being a clustered type poses some difficult to access the matured culms. The traditional cut and withdrawal method used was time consuming and tedious. The details of the *Bambusa vulgaris* Schrad harvested for the study is presented next.

3.1 Bamboo and Its Strip Characteristics

The characteristics of the *Bambusa vulgaris* Schrad used for the study is presented in Table 1. Maximum stripe length of 760 mm was produced with single nodal point. The dimension conforms to the minimum acceptable dimension recommended for stripe to be used for structural purposes [20, 21]. From length 780 mm lengths, the details of the **Laminate Recovery Index (LRI) a**fter both splitting and rough planning are presented in Table 2.

Table 1: Statistics of the Harvested Culms

Parameters	Values (range)
Age	3 – 4 years
Internode (length)	360 – 380mm
Moisture content	Fresh (? 42%)
Culm circumference	240 – 270mm
Inner culm diameter	60 – 70mm
Culm thickness	10 – 14mm

Four stripes each were produced from each length with average width of 35mm before planning and 25mm wide after planning. Thus the LRI of the stripes from Bambusa vulgaris Schrad was 75%. Variation in culm curvature markedly reduces the recovery index after planening. It was observed that the wider the strip the greater the curvature and the higher the resulting material wasted.

Laminate Recovery Index (LRI) after Splitting	
Parameters	**Values**
No of short culms	12
Total no of strips	96
Recovered lam. (38 – 43cm)	72
	75
Recovered laminates (%)	25
Wasted laminates (%)	
Laminate Recovery Index (LRI) after Planning	
Parameters	**Values**
Thickness before planing	10 – 14mm
Thickness after planing	5 – 8mm
Percentage recovered	50 – 57 %

Table 2: Laminate Recovery Index (LRI) after Splitting and Planning

3.2 Strip Treatment for Durability

Bamboo is highly susceptible to deterioration due to its high sugar content [22]. Within the first week after harvesting, infestation was noticed on the unprocessed culms (Plate 1). This could be due to insipient attacks before harvesting or mere direct contact with bare ground. After six weeks of abandonment in the workshop in contact with floor as shown in Plate 2, there has been considerate deterioration by powder post beetle. The split bamboo also becomes infested on surface after three days and the rate of



Plate 1: Unprocessed Bamboo Infested



Plate 2: level of Infestation after 6weeks

infestation increases in the order presented in Table 3. The increase in the rate of infestation after splitting may be attributed to the exposed sections of the epithelial layer which is soft and rich in sugar content. The planning of the epithelial section of the inner part further exposes it to unrestricted access by agent of bio-deterioration to infest the strips. But the condition changes after **boiling the strips in hydrogen peroxide treated water for 24 hours.** This action appears to preserve the strips against bio-deteriorating agents as none of the strips is attacked after four weeks of drying. The strips are dried with air for four weeks. The average maximum moisture content of the *Bamusa vulgaris* Schrad samples used for the study is 93.4% and this agrees with the range of values quoted for the base moisture

Table 4: Rate of Strip Infestation

Parameters	Value (days)
After harvesting	7
After splitting	3
After planening	2
After boiling	Not available

content of cultivated Bambusa vulgaris Schrad by [22]. The strip was air dried as shown in Plate 3 under ambient temperature 29 ± 50 and 65± 50 % relative



Plate 3: Air Drying Process **of the Strips**

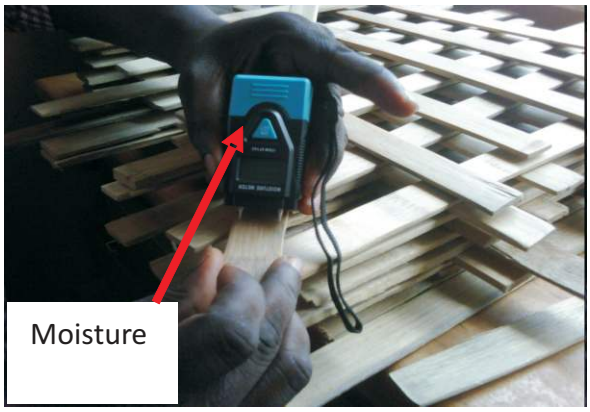


Plate 4: Drying Strips Moisture Content Monitoring

humidity while the rate of drying of the samples were monitored using the moisture meter shown in Plate 4.

3.3 Bamboo-lam Production

The final product created from the dried B. vulgaris strips are two sizes of bamboo-lam: 300x300x15mm and 450x60x35mm. An unfinished sample of the bamboo-lam is shown in Plate 5. The two sizes of bamboo-lam produced can be used as raw material in the manufacturing of decoration and novel items, chair's rails, stretchers and seat, other furniture parts and mixed bamboo furniture.



Plate 5: Unfinished Bamboo-lam

4.0 CONCLUSION AND RECOMMENDATION

The use of newer bamboo products like laminated furniture, bamboo ply among others is at present not common in our society. This is due to the notion that bamboo products are not durable and are only meant for temporary applications. Specifically in Nigeria, production of bamboo modern products is thought of as been difficult to attainable due to wide perception that high technical knowhow and sophisticated machineries are required to process bamboo to these products. This study has been able to produce bamboo laminates from *Bambusa vulgaris* Schrad using common carpentry tools and machines. Bamboo havesting with crude tools is tedious and time consuming. The characteristics of the laminates depend on the features of the harvested culms while soaking of the bamboo strip in hot water treated with hydrogen peroxide for 24 hours improved the resilience of bamboo strips to deterioration and insect attack. The bamboo-lam produced is durable and can sufficiently be used to complement wood in the production of furniture, interior decoration, novel and structural items.

Based on the observations recorded during the study, it is advisable to stalk bamboo vertically in a less humid place while waiting to begin its processing to reduce rate of infestation. Appropriate splitting and planning machines will reduce time required for processing and increase maximum recovery index. Also there is need to develop further means of harvesting bamboo.

REFERENCES

1.INBAR, 1996. "Bamboo mat board: a new bamboo-based building material from India". International Network for Bamboo and Rattan, International Development Research Center, Regional Office for South Asia; New Delhi; India

[2] Clemons, Craig. 2002. Wood-plastic composites in the United States: the interfacing of two industries. Forest Prod. J. 52(6): 10.18.

[3] Eric Boa, 1995. "Knowing bamboo, knowing people" Bamboo People and The Environment, Vol. 4: Socio-economics and Culture. INBAR Technical Report No.08, pg: 40-44.

[4] Zhang BinYuan and Jiang JingYan 2001. "The Bamboo Furniture Making Unit" Transfer of Technology Model (TOTEM). 30pp

[5] Aiyeloja, Adedapo Ayo and Ajewole, Opeyemi Isaac 2006. "Non-timber forest products' marketing in Nigeria. A case study of Osun state". Educational Research and Reviews Vol. 1 (2), pp. 52-58, www.academicjournals.org/ERR

[6] Thammincha, S. 1987. "Role of bamboo in rural development and socio-economics". In Rao, AX; Dhanarajan, G.; Sastry, C.B. ed., Recent Research on Bamboo. Proceedings of the International Bamboo Workshop, Hangzhou, China, 6-14 October 1985. Chinese Academy of Forestry, Beijing, China; International Development Research Centre, Ottawa, Canada. pp. 359-365.

[7] Redhead, J.F. 1971. "Timber Resources of Nigeria". Nigerian Journal of Forestry, 1 (1):7–11.

[8] Adewole A.N., Onilude A. M. 2011. "An Overview of Rattan Distribution in Four States in South-South Part of Nigeria *(Akwa-Ibom, Balyesa, Cross-Rivers and River States)*". World Rural Observations 2011;3(2) http://www.sciencepub.net/rural

[9] Ogunjinmi A.A., Ijeomah H.M. and Aiyeloja A.A., 2009. "Socio-Economic Importance of Bamboo (*Bambusa Vulgaris*) in Borgu Local Government Area of Niger State, Nigeria". Journal of Sustainable Development in Africa (Volume 10, No.4, 2009) ISSN:1520-5509. Clarion University of Pennsylvania, Clarion, Pennsylvania.

[10] INBAR, 2010."Bamboo and Climate Change Mitigation". International Network for Bamboo and Rattan, Technical Report No. 32. pg 1-30.

[11] Lou Yiping **2011. Bamboo and Climate Change Mitigation. Sourced from** INBAR. Downloaded from http://www.inbar.int/show.asp?NewsID=373 on July 3rd 2011.

[12] Wikipeadia 2011. Bamboo Species. Accessed on 13th July, 2011 via http://en.wikipedia.org/wiki/Bamboo_species

[13] FAO and **INBAR** 2005. Global Forest Resources Assessment Update: Nigeria Country Report On Bamboo Resources. **Working Paper 127** by **Forestry Department sponsored through collaborative effort of Food and Agriculture Organization (FAO) of the United Nations**

and International Network for Bamboo and Rattan (INBAR) in Rome in 2006. 16Pgs.

[14] Onilude, M. A. 2006. Potential of Bamboo as Raw Material for Wood-based Industries. A paper presented at Raw Material Research and Development Council (RMRDC) of Nigerian, organized Workshop in Ikeja Lagos State. 10pp

[15] Farrelly David 1984. The Book of Bamboo: A Comprehensive Guide to This Remarkable Plant, Its Uses, and Its History.Published by Amazon, USA First Edition 895 pgs.

[16] Yang Yuming and Xue Jiru 1998. Bamboo resources and their utilization in China. Proceedings of training course cum workshop organized by INBAR, IPGRI and the Government of Japan. 10-17 May 1998, Kunming and Xishuanbanna, Yunnan, China.

[17] Sattar, M.A. 1995."Traditional Bamboo Housing in Asia: Present Status and Future Prospects", In Bamboo, People and the Environment. Proceedings of the Vth International Bamboo Workshop and the IV International Bamboo Congress, Ubud, Bali, Indonesia 19-22pp.

[18] Adewole A. N. and Ajibi A. B., 2010. **"Evaluation of wood properties of *c. albidum* tree grown in Akinyele Local Government Area of Ibadan**

APPENDIX I

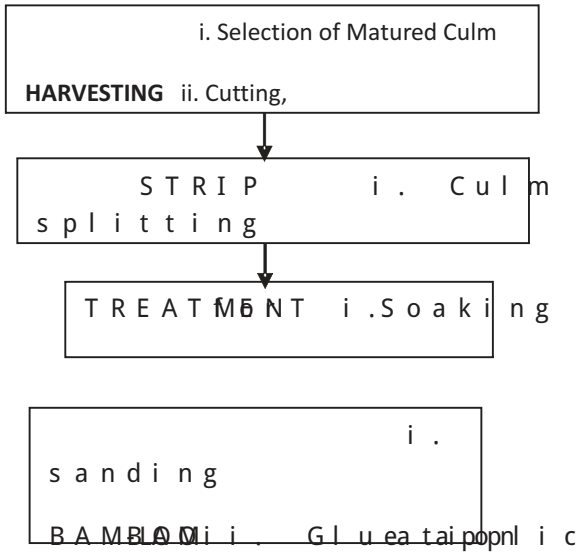


Fig 1: Flow Process for Producing Bamboo-lam

in relation to its utilization".*3rd International Conference on* Engineering Research and Development (ICERD2010) Benin City, Nigeria, 7th - 9th September 2010.

[19] Olayiwola H.O., 2008. "Production and testing of bamboo-cement composites." Unpublished project work, submitted to the Department of Agricultural and Environmental Engineering, Faculty of Technology, University of Ibadan.

[20] Janssen J.A. Jules 1995. "Building with Bamboo: A Handbook". Published by Amazon, USA First Edition 650 pgs.

[21] UNIDO, 2008. "Raw Materials and Tools for Woven Bamboo Applications". A Cottage Manual Published by United Nations Industrial Development Organisation.

[22] Lionel Jayanetti, (2003): "Bamboo in Construction -Status and Potential". Proceedings of International Workshop on Bamboo Industrial Utilization. Sponsored by International Network for Bamboo and Rattan; Hosted by Hubei Provincial Government & Xianning Municipal Government October 2003.

[23] Wahab. R; Mohamed A, Mustafa M T and Hassan A. 2009. Physical Characteristics and Anatomical Properties of Cultivated Bamboo (Bambusa vulgaris Schrad.) Culms. Journal of Biological Sciences 9(7); 753-759.

COMPARATIVE STUDY OF *THEVETIA PERUVIANA* AND *JATROPHA CURCAS* SEED OILS AS FEEDSTOCK FOR GREASE PRODUCTION

[1]Olisakwe, H.C., [2]Tuleun, L.T., [3] Eloka-Eboka, A.C.
[1, 2, 3] Mechanical Engineering Department, University of Agriculture, Makurdi, Nigeria
Corresponding author: Eloka-Eboka, A.C., fatherfounder@yahoo.com, +234-8067915670

Abstract:
Thevetia peruviana and *Jatropha curcas* seed oils were investigated as feed stocks for grease production. Seven different blends of *Thevetia peruviana* and *Jatropha curcas* seed oil were used for this research. The seeds were obtained locally and oven dried until a constant weight was obtained, *Thevetia peruviana* seeds had 3.91 % moisture content while *Jatropha curcas* seeds had 2.93 % moisture content. The oils were thereafter extracted. *Thevetia peruviana* seeds were found to have 58.5 % oil content while *Jatropha curcas* seeds had 54.6 % oil content. The Chemo-physical tests of the oils indicated that the density of the oils were the same (908.7 kg/m^3), and the flash point of *Thevetia peruviana* seed oil was 168°C while that of *Jatropha curcas* seed oil was 122°C; the viscosity at 100°C for both oils fell within the range of 7.2 - 7.9 cSt for 400 pale oil 400p, which is of petroleum origin. The viscosity index values for both oils were very high, hence very stable. *Jatropha curcas* oil had a viscosity index of 214 and *Thevetia peruviana* oil had 202. The grease was produced by cooking a calculated quantity of base oil and lithium stearate in a pot at 200°C with continuous stirring for 30 minutes, the reaction was allowed to cool to 85°C before sodium thiosulphate and calcium sulphonate additives were added to the reactor; further milling was maintained to yield a homogeneous product (lithium stearate grease) which were taken for analysis. Five classes of grease were produced from each oil blend; all the grease samples produced, showed no significant difference at 95 % confidence level among blends, but showed a significant difference among the grease compositions. The viscosity temperature coefficient for all the grease samples was very low, this means that all the oil blends and grease compositions were very suitable for the production of semi-solid lubricant (grease). *Thevetia peruviana* and *Jatropha curcas* seed oil and it blends were found to be suitable for the production of different grades of bio-degradable grease and can effectively substitute 400 pale oil 400p grade of fossil origin for grease production.

1. Introduction

Most engineering components fail as a result of the failure or loss of the properties of the lubricants used, this loss of properties is primarily due to high temperature and pressure they are subjected to. There is also high level of environmental pollution and degradation causing the much talked about global warming, economic meltdown, mutation and ecological extinction. The use of fossil fuel and petro-chemical based lubricant are the major contributors of these problems because of the high emission of carbon and sulphur based oxide. The development and formulation of bio-based grease and products will checkmate these problems. Lubricants exist in the three states of matter; gas, liquid and solid. Any material capable of preventing and controlling wear and tear between contacting surfaces is a lubricant [4]. Gaseous lubricants include air and neon. Liquid lubricants include: engine oil, gear oil and water based emulsion used as cutting fluids in metal working operations. Lubricants can also be classed as semi-solid/ solid which are made by the dispersion of a thickening agent in a liquid lubricant. Grease can be seen as a fine dispersion of an oil insoluble thickening agent, usually soap in a fluid. Lubricant is basically oil. The soap is made up of fatty acid, saponified with alkali which can be hydrated lime, caustic soda, lithium hydroxide or aluminum hydroxide. The type of soap used depends on the conditions in which the grease is to be used. Bio based semi solid lubricants intends to substitute petrochemical based grease because the long carbon chains present in the bio oils can be broken down naturally to simpler carbon chains of harmless compounds and the fatty acids are used by microorganisms as a source of energy.

The thrust of this work is to make use of bio-based oils to produce grease of comparative efficiency with those made of synthetic oils. *Thevetia peruviana* oil is obtained from *thevetia peruviana* seed; the plant is a dicotyledon which belongs to the family of *aponaceae*, it is a composite ever green shrub, it has a milky sap, it is native to West-indies, Mexico and Brazil, it is known as Yellow Oleander [8]. The plant is perennial, a shrub reaching 3 to 3.9 metres contains about 60-64 % oil on dry matter basis. The plant produces white latex (sap) that is highly poisonous, the seed is also poisonous. The plant thrives very well in all the climatic and vegetation belts of Nigeria, readily found in all the states: Rivers, Sokoto, Borno, Benue, Kwara, etc. [9]. *Thevetia peruviana* oil is not edible; it maintains its properties at 220 ^{0}C, which makes it an important choice for engineering base oil [7] while *Jatropha curcas* is a drought resistant, perennial plant, growing well in marginal /poor soil. It is easy to establish, grows relatively quickly, producing seeds for

50 years. The oil can be combusted as fuel without being refined. It is a small tree or shrub with smooth gray bark, which exudes a whitish colored, watery, latex when cut, it is poisonous.

Extensive research has been made on *Thevetia peruviana* seed oil, the oil was studied for its thermal stability, the oil was heated to 180, 200 and 220 ^{0}C over a period of 15 hours and there was no significant difference in the five parameters (iodine value, acid value, peroxy values, saponification value, and amount of polar compounds) studied. The study proved that the seed oil would be stable to heat at those temperatures. This property also justifies the use of the seed oil in the making of lubricants and grease [8]. In this study, research and emphasis have been focused on the suitability and properties of grease produced from *Thevetia peruviana* and *Jatropha curcas* seed oils. Works have been recorded for the use of other biodegradable oils for the production of greases. The works of Awoyale *et al.* [2] reported the successful production and utilization of black date oil as biodegradable lubricant.

2. Materials and Methods

Thevetia peruviana and *Jatropha curcas* seeds were locally collected from Makurdi town, Benue State of Nigeria. The seeds obtained from the fruits and capsules were washed and oven-dried at 100°C at an hourly interval until a constant weight was obtained. The moisture-free seeds were ground using a grinding machine and oil extracted from it using Soxhlet apparatus. The rotary evaporator was used to recover the solvent (n-hexane). *Thevetia peruviana* seed oils and *Jatropha curcas* seed oils have similar extraction processes. The moisture – free *Thevetia peruviana* seeds were ground with a grinding machine. The finely ground grain were put into the thimble in an extraction chamber of sohxlet apparatus. Two hundred millilitres (200 ml) of normal hexane was charged into the round bottom flask (500 ml) of the Soxhlet apparatus and mounted in the heating mantle of the apparatus and was heated to between 65-100°C in order to prevent loss of hexane vapour because the boiling point of n-hexane is 69°C. The evaporating n-hexane was condensed into the thimble by the condenser where it leached the oil out of the paste. The extracted oil was taken for analysis and characterization at A-Z Petroleum Products Limited Nnewi, Anambra state of Nigeria for densities, flash points, pour points, kinematic viscosities, appearance/colours, viscosity indexes, and cloud points. These are some of the parameters with which base oils are identified as recommended by National Lubricating Grease Institute (NLGI) and American Oil Analytical Chemists [1].

The extracted oils were blended into seven grades and labeled A,B,C,D,E,F and G at the proportions of 100:0, 0:100, 20:80, 80:20, 40:60, 60:40 and 50:50 respectively (See Table 1). Each blend of oil was used to produce five grease types with different thickener and additive composition. Thirty five grease samples were produced and characterized at A-Z Petroleum Product Limited, Nnewi, Nigeria. Mechanical application was carried out using the counting gears of a fuel dispensing machine and the bearing of a simple grinding engine. Each blend was used to produce grease with same empirical composition of components as shown in Table 2.

2.1 Preparation of Thickening Agents and production of grease

Thickening agents' preparation is carried out by saponification reaction which is a process of reacting fatty acids with metals/metallic hydroxides to produce soap and water at a temperature of about 160°C. The water produced as a by-product of the reaction is evaporated due to very high reacting temperature of the mixture. The soap produced under this manner is referred to as thickening agent in the lubrication industry. In this study, the thickening agent used was lithuim stearate (lithuim soap) which is a simple soap.

Formulation of five different samples of grease was done in accordance to NLGI specifications for each oil blend. For each sample, proportions of base oil and lithium stearate (thickening agent) were varied. Table 3 shows the different proportions of components of the samples of the grease produced. Different quantities of additives were added to these formulations. The base oil and lithium stearate mixtures were cooked at temperature 200°C with continuous stirring. The mixtures were reacted with respect to the proportions as shown in Table 3 while Table 2 shows the empirical composition of the basic components of the developed grease samples. From literature the combination of sodium thiosulphate (0.5 – 6 %), calcium sulphate (0.2 – 3 %) and 1,2,3-benzotrizole (0.2 – 3 %) is an ideal composition of additives for grease production. But for the purpose of this research, only sodium thiosulphate and calcium sulphonate were used as additives at the ratio of 7: 3 as 1,2,3-benzotrizole was not commercially available.

The mixture of the base oil and the lithium stearate after being thoroughly cooked and blend for 30 minutes at 200°C was allowed to cool to 85°C before the additive was added to the blend; the mixture was continuously stirred until the temperature reached room temperature of 35°C. At room temperature, further milling of the mixture was done until a homogenous substance was obtained. The homogeneous substance obtained was the lithium stearate grease which was then taken for further analysis and characterization.

2.2 Analysis and characterization of grease

The analysis and characterization of the developed grease samples were based on ASTM specifications. The analysis carried out included, the cone penetration consistency test (ASTM D-217), dropping point of lubricating grease over wide temperature range test (ASTM D-2265), copper strip corrosion test (ASTM D-130) and apparent viscosity (ASTM D1092). The Equation for the dropping point test is DP = ODP+ ((BT – ODP)/3) (7)

Where: DP - dropping point; ODP - Thermometer reading when first drop reaches the bottom of the test tube; and BT - block temperature when the drop falls.

3.0 Results and Discussion

Tables 4 and 5 are the percentage moisture content and the percentage oil yields of the two oil seeds studied, the moisture content of *Thevetia peruviana* seeds (3.91%) is higher than that of *Jatropha curcas* seeds (2.93 %). The

difference could be as a result of the thick shell covering the nuts and the size of the seeds. Also the moisture contents of seeds are influenced by time of harvest, duration of exposure to sun drying and maturity of the seeds before harvesting/plucking. The percentage oil yield is higher in *Thevetia peruviana* seeds than in *Jatropha curcas* seeds, *Thevetia peruviana* seeds oil yield was found to be 58.5 %, a value lower than the expected value of 64 % as presented by Ibiyemi et al.[8]. Jatropha curcas seeds oil yield stood at 54.6 %, this value is also lower than the expected of 63 %. Tables 6 presents the results of the chemo-physical properties of *Thevetia peruviana and Jatropha curcas* seed oils; the density of the two seed oils were the same 908.7 kg/m^3. The flash point of *Thevetia peruviana* seed oils (168 ^{0}C) was higher than that of *Jatropha curcas* seed oils (122 ^{0}C). It means that *Jatropha curcas* is more volatile than *Thevetia peruviana*. Oil with very high flash point can withstand high temperature operations and safe for handling and haulage. However it is of limited significance as far as grease lubrication is concerned because the additives, thickeners, viscosity improvers play a major part in increasing or reducing the flash point of the lubricant (Spencer, 2002). The pour point of *Jatropha curcas* seed oils (-5 ^{0}C) was lower than that of *Thevetia peruviana* seed oils (8 ^{0}C). This suggests that *Jatropha curcas* oil can withstand extreme cold condition more than *Thevetia peruviana* oil; this is an indication that *Jatropha curcas* seed oils will thrive better in temperate region and can transverse across regions without been affected by cold climates unlike *Thevetia peruviana*. It will have an easier start up than the later (Spencer, 2002). The kinematic viscosity at 100 ^{0}C for *Thevetia peruviana* seed oils (7.84 c.St) was higher than that of *Jatropha curcas* seed oils (7.23 c.St), it means that *Thevetia peruviana* seed oils resist flow more than *Jatropha curcas.* The low value of kinematic viscosity of *Jatropha curcas*, justifies its unsaturated nature and its ability to be combusted as fuel without been refined in a simple diesel engine [10]. The kinematic viscosity at 100 ^{0}C for both *Thevetia peruviana* seed oils (7.84 c.St) and *Jatropha curcas* seed oils (7.23 c.St) fell within the range (7.2 - 7.9 c.St) for kinematic viscosity of 400 pale oil 400p which is one of the grades of lubricating base oil derived from petroleum origins as shown in Table 8.

Viscosity index of *Jatropha curcas* seed oil is 214 which is higher than that of *Thevetia peruviana* (202). A low number indicates oil which changes viscosity rapidly with temperature, whereas, a high number indicates oil which changes viscosity little when heated or cooled; for both oils the viscosity indexes were very high [3], which means that both seed oils are very stable with temperature fluctuations, *Jatropha curcas* seed oils is more stable. A lubricant should change its viscosity as little as possible so that it is not too thick when cold thereby making start-up to be very difficult and not too thin when hot, thereby running off the surface [5], [12]. The viscosity index of 400 pale oil 400p is 75; this base oil is of fossil origin. The brightness and clarity of both seed oils were superb.

5. Conclusion and Recommendation

The results of the analysis clearly shows that all the oil blends are suitable for the production of different grades of bio-degradable grease. The produced samples of grease are non corrosive, hence it can be used in different material surfaces and engineering application. The seed oil content of both *Thevetia peruviana* and *Jatropha curcas* are relatively high. The grease produced did not have any significant difference in the quality among the blends. From the data and results obtained, grease samples of pure *Jatropha curcas* base oil has the highest dropping point, it can withstand higher operating temperatures and hence the best grease blends. The quantity of additives in the grease is best between 5 – 4 % of the total mass of grease. The dropping point temperature of these grease produced met the regular grease standards (80 – 200 ^{0}C).The viscosity temperature coefficient for all the grease samples are very low and the viscosity index of both seed oils are very high, this means that all the oil blends and grease compositions are very suitable for the production of semi-solid lubricant (grease), The use of these products in engineering application was also successful. *Thevetia peruviana* and *Jatropha curcas* seed oils can be used to substitute 400 pale oil 400p grade (petroleum base) for grease production. The two seed oils studied can therefore be registered as natural sources of bio lubricants which no doubt will find uses in aquatic Engineering and other applications. The indispensability of their application in the modern demands for bio based products can no longer be ignored as the urgent needs for technological shift from fossil fuels continue to be an imperative.

References

[1] Analytical testing services, Inc. U.S.A (2009) (web master @ we test it.com) A.O.A.C (1984). Official Methods of Analysis 14th edition AOAC Washington DC

[2] Awoyale, A.A., Odubuyi, O.A. and Eloka-Eboka, A.C. (2011). Production and Testing of biodegradable grease from Black-date (Canarium Sweinfurthii) Oil. *Journal of Innovative Research in Engineering and Science* 2(4). pp. 223 - 233.

[3] Bennett, E. (2004). New Greasepro, Exonmobil News Letter April 2004 Edition.

[4] Benton, W. (1982). The new encyclopedia Britannica, Encyclopedia Britannica Inc. USA Volume VI, pages 693-694, Volume XI pp. 169-171.

[5] Canakci, M. and J. Vangerpen (2003) A pilot plant to produce biodiesel from high free fatty acid feed stocks. Trans. ASAE volume 46 (4) pp. 945-954

[6] Grolier, I. (1994). Encyclopedia Americana, Grolier Inc. USA Volume 17, pp 210-223.

[7] Ibiyemi, S. A. (2008). Thevetia Plant Economic Potential, Chemistry's Key Position (Unpublished) pp 3 - 34.

[8] Ibiyemi, S. A., Bako S.S, Fadipe V.O, and Akinremi, O. O. (2002). Variation in Oil Composition of Thevetia Perviana Fruit Seeds. *Journal Applied Science Environment Management* 6(2) pp 61-65.

[9] Ibiyemi, S. A., S. S. Bako, G. O. Ojokuku and V. O. Fadipe (1995). *Journal American Oil Chemical Society* 72(6) pp 745-747.

Table 1: Empirical composition of components of developed grease

Sample	Baseoil (g)	Stearic acid (g)	Lithium hydroxide (g)	Water evaporated (g)	Additive (g)	Total (g)
1.	300	78.344	6.624	4.968	20	400
2.	284	97.93	8.28	6.21	16	400
3.	264	117.516	9.936	7.452	16	400
4.	252	137.102	11.592	8.694	8	400
5.	228	156.688	13.248	9.936	12	400

Table 2: Proportions of Components of Grease Samples

Sample	Lithium Stearate (g)	Base oil (g)	Additive (g)	Total (g)
i.	80=20%	300=75%	20=5%	400
ii.	100=25%	284=71%	16=4%	400
iii.	120=30%	264=66%	16=4%	400
iv.	140=35%	252=63%	8=2%	400
v.	160=40%	228=57%	12=3%	400

Table 4: Chemo- physical Properties of *Jatropha curcas* and *Thevetia peruviana* Seed oils

Properties	Test methods	*Jatropha curcas*	*Thevetia peruviana*
Density (km/m^3)	ASTM D1298	908.7	908.7
Flash point (^0C)	ASTM D92	122	168
Kinematic Viscosity at 40^0 C (cSt)	ASTM D445	30.59	35.47
At 100 ^0C (cSt)	ASTM D445	7.23	7.84
Viscosity Index	ASTM D2270	214	202

Table 5: Percentage Oil Extracts

	Jatropha curcas	*Thevetia peruviana*
Qty of seeds used (kg)	10.7	10.8
Qyt of oil extracted (kg)	5.85	6.32
Oil yield (%)	54.67	6.32

EFFECTS OF EGGSHELL ON THE MICROSTRUCTURES AND PROPERTIES OF AL-CU-MG/EGGSHELL PARTICULATE COMPOSITES

Hassan .S. B and Aigbodion.V.S
Dept. of Metallurgical and Materials Engineering, Ahmadu Bello University, Zaria
hassbolaji@yahoo.com, **aigbodionv@yahoo.com**

Abstract
The effects of eggshell particles on the microstructures and properties of Al-Cu-Mg/eggshell particulate composites have been studied. A total of 2-12wt%eggshell particles were added. The microstructures of the Al-Cu-Mg/eggshell particulate composites produced were examined by SEM/EDS. The physical and mechanical properties measured included: density, tensile strength, hardness values and impact energy. The results revealed that the tensile strength increased by 8.16% at 12wt% uncarbonized eggshell and 14.28% at 12wt% carbonized eggshell, the hardness values increased by 10.01% at 12wt% uncarbonized eggshell and 25.4% at 12wt% carbonized eggshell with decreased in the density by 6.50% at 12wt% uncarbonized eggshell and 7.4% at 12wt% carbonized eggshell. The impact energy decreased by 23.5% at 12wt% uncarbonized eggshell and 24.67% at 12wt% carbonized eggshell particles respectively. These increases in strength and hardness values are attributed to the distribution of hard phases of the eggshell particles in the ductile Al-Cu-Mg alloy matrix. These results showed that using the carbonized eggshell as reinforcement in the Al-Cu-Mg alloy gives better physical and mechanical properties as compared to uncarbonized eggshell particles and that better properties are achievable by addition of both uncarbonized and carbonized eggshell to Al-Cu-Mg alloy. Hence addition of eggshell particles up to 12wt% can be used as a low cost reinforcement for the production of metal matrix composites for engineering applications.
Keywords: Eggshell, Metal matrix composite, Mechanical and Physical properties

INTRODUCTION

Metal-matrix composites (MMCs) have emerged as a class of materials capable of advanced structural, aerospace, automotive, electronic, thermal management and wear applications. The performance advantage of metal matrix composites is their tailored mechanical, physical, and thermal properties that include low density, high specific strength, high specific modulus, high thermal conductivity, high abrasion and wear resistance. In general, the reduced weight and improved strength and stiffness of the MMCs are achieved with various monolithic matrix materials[1-2].

In recent years there has been an increasing interest in composites containing low density and low cost reinforcements. Among various discontinuous dispersoids eggshell [3] could be one of the most inexpensive reinforcement available in large quantities as solid waste. Hence, composites with eggshell as reinforcement are likely to overcome the cost barrier for wide spread applications in automotive and small engine applications. It is therefore expected that the incorporation of eggshell particles in aluminium alloy will promote yet another use of this low-cost waste and thereby, reducing the cost of aluminium products. The eggshell waste is basically consisted of calcium carbonate in the form of calcite ($CaCO_3$). The eggshell waste powder consists of porous irregular particles, whose size ranges from 2 to 900μm Previous research has showed that the eggshell solid waste in form of powder can be regarded as an interested raw material for manufacture of single-fired ceramic wall tile materials [3].

The ever-increasing demand for low cost reinforcement stimulated the interest towards production and utilization of using bye-products from industry as reinforcement since they are readily available or are naturally renewable at affordable cost. Aigbodion[4] have used Kankara clay(alumino-silicate) in reinforcing Al-Si alloy, Bienia et al[5] used fly ash in reinforcement of aluminium matrix, Naresh[2], worked on the development and characterization of metal matrix composite using red mud an industrial waste for wear resistant applications, they all reported good dispersion and recovery of the particles in the composites castings. It is in the light of the foregoing researches that investigation into the possibility of using eggshell in metal matrix particulate composite for engineering applications was motivated. The present investigation has been focused on the utilization of abundantly available eggshell in useful manner by dispersing it into aluminium to produce composites by stir casting method.

2. EXPERIMENTAL PROCEDURE

2.1 Materials/Equipment

The eggshell used in this work was obtained from local tea seller around Samaru area of Zaria in Kaduna-State, Nigeria(see Plate 1), High purity aluminum electrical wires obtained from Northern Cable Company

NOCACO (Kaduna), Nigeria, copper, magnesium , Moulding box silica sand, Bentonite were purchasing from chemical shop in Kaduna, Nigeria.



Plate 1: Photograph of eggshell

The equipment used in this study included: Pyrometer, mechanical stirrer, crucible, electrical resistance furnace, Rockwell hardness tester, Charpy impact machine, Tinus Olsen tensile machine, Scanning electron microscope (SEM) with e n e r g y dispersive X-ray spectroscopy (EDS)

2.2 Method

The eggshell was dried and grinded into eggshell powder (uncarbonized particles)(see Plate 2), the powder particles was packed in a graphite crucible and fired in electric resistance furnace at temperature of 1200oC to form eggshell ash(carbonized particles)(see Plate 3). The particle size analysis of the eggshell particles was carried out in accordance with BS1377:1990[6]. About 100g of the eggshell particles was placed unto a set of sieves arranged in descending order of fineness and shaken for 15minutes which is the recommended time to achieve



Plate 2: Photograph of eggshell particles uncarbonized



Plate 3: Photograph of eggshell particles carbonized

The composite used in this study was Al-Cu-Mg/Eggshell particles composite containing 2-12 wt% eggshell particles (Uncarbonized and Carbonized) at interval of 2wt%. The samples were produced using the double stir-casting method [1, 6] by keeping the percentage of copper and magnesium constant (3.7%Cu and 1.4%Mg) according to the recommended standard to produce alloy of type A2009. A control sample without the eggshell particles was also produced. A preheated sand mould was used to produce cast bars. After casting, the samples were machined into tensile, impact and hardness test samples for the purpose of determining the mechanical properties.

The microstructure and the chemical compositions of the phases present in the eggshell particles and composite test samples were studied using a JEOL JSM 5900LV Scanning Electron Microscope equipped with an Oxford INCA™ Energy Dispersive Spectroscopy (EDS) system. The basic method of determining the density of a sample by measuring the mass and volume of the sample was used. The density of the sample was then estimated from the formula given below:

$$Density = \frac{Mass}{Volume} \quad \text{———}$$

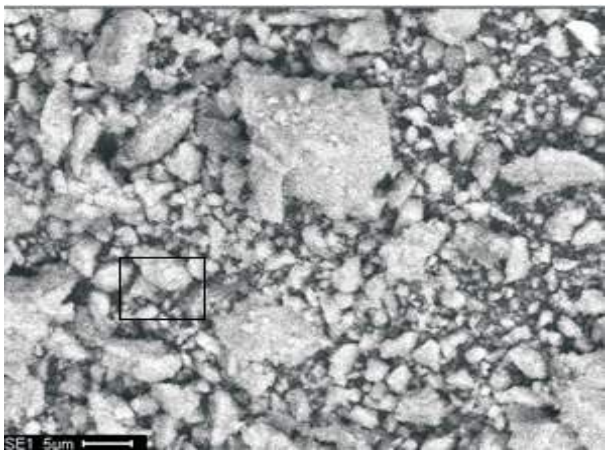
The hardness values of the samples were determined (ASTM E18-79) using the Rockwell hardness tester on "F" scale (Frank Well test Rockwell Hardness Tester, model 38506) with 1.56mm steel ball indenter, minor load of 10kg, and major load of 100kg and hardness value of 101.2HRF as the standard block[7-8].

The tensile properties of the as-cast composites sample were conducted on Tinus-Olsen tensile testing machine with a strain rate of 2x10-3S-1. The test pieces were machined to the standard shape and dimensions as specified by the American Society for testing and Materials.

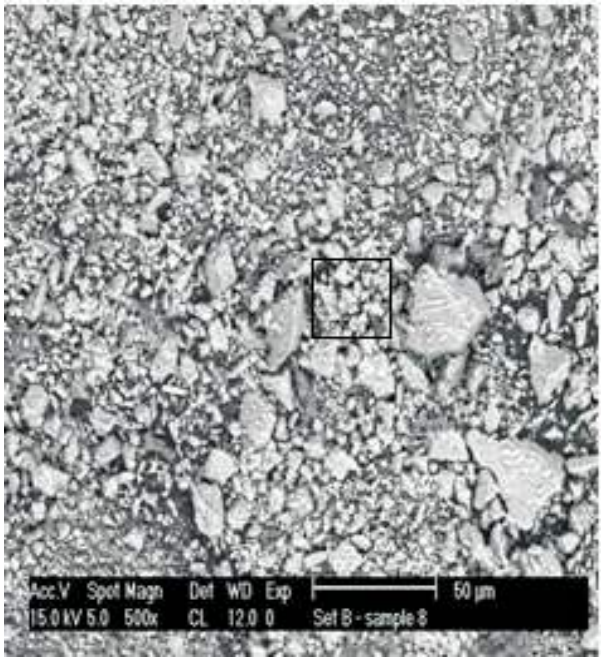
The impact test of the as-cast composites sample was conducted using a fully instrumented Avery Denison test machine. Charpy impact tests were conducted on notched samples. Standard square impact test sample measuring 75 x 10 x 10 mm with notch depth of 2 mm and a notch tip radius of 0. 02 mm at angle of 45o was used[1, 6].

3.0 RESULTS AND DISCUSSION

The microstructure of the eggshell particle (Uncarbonized and Carbonized) reveals that the size and shape of the particles vary; however, they consist of porous irregular shape particles. The EDS of the eggshell particles reveals that the particles contain Ca, Si, O, C, Mg (see Micrographs 1-2). These elements confirm that, the eggshell particles consists of calcium carbonate in the form of calcite (CaCO3), carbon in graphite form, silica etc. These analyses are in par with others analysis of reinforcement used by other authors [3, 7-8].

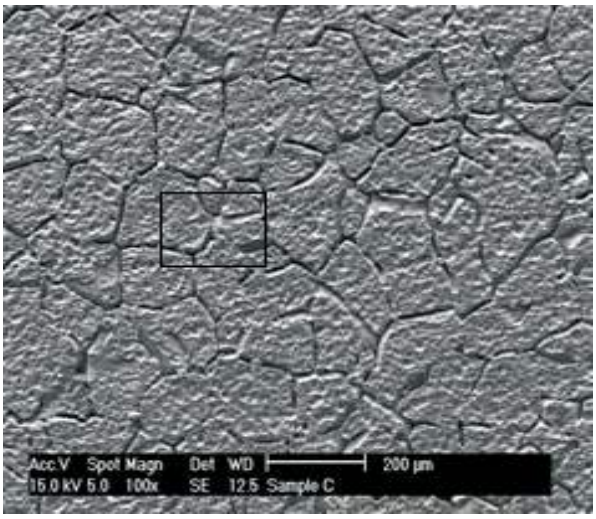


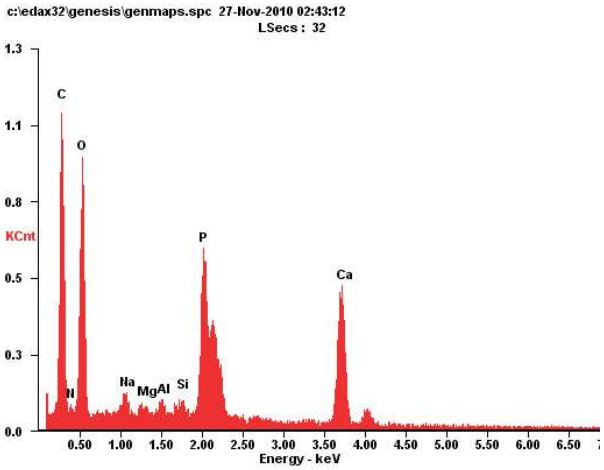
Micrograph 1: SEM/EDS Microstructure of the carbonized eggshell particles

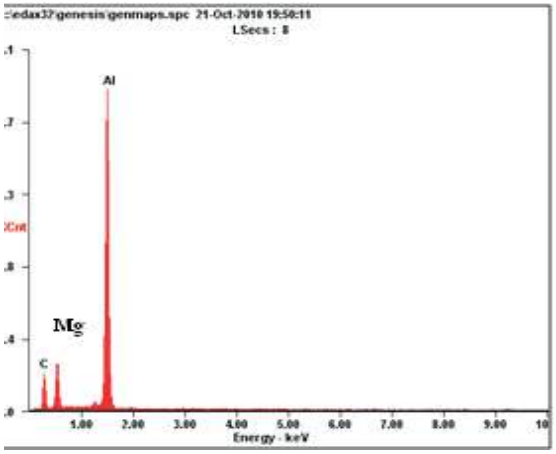


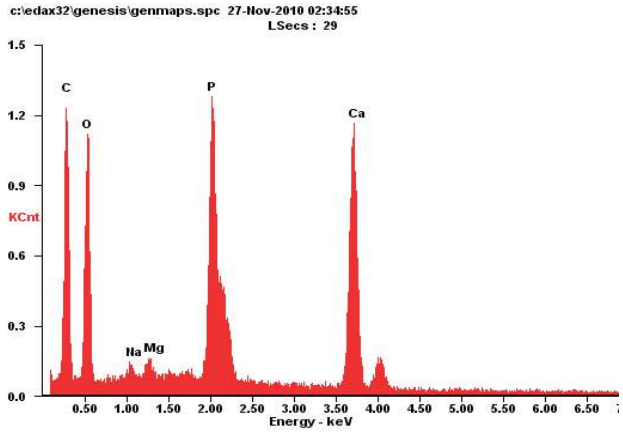
Micrograph 2: SEM/EDS Microstructure of the carbonized eggshell particles

The microstructure of the unreinforced Al–Cu-Mg alloy is shown in Micrograph 3. The structure reveals the eutectic phase containing Cu_3Al_2, Al_6CuMg_4 in α-aluminum matrix[6]. In the Al-Cu-Mg alloy, Cu and Mg are present both in solid solution as well in precipitated form as Cu_3Al_2 and Al_6CuMg_4 phase both in the grain and along the grain boundaries (see Micrograph 3).





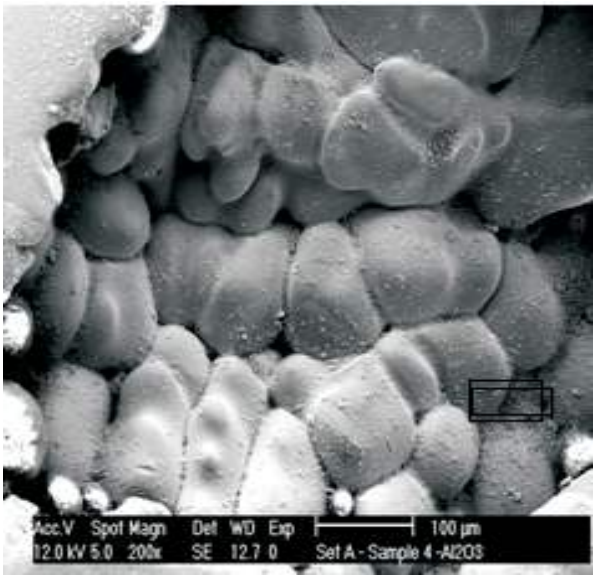




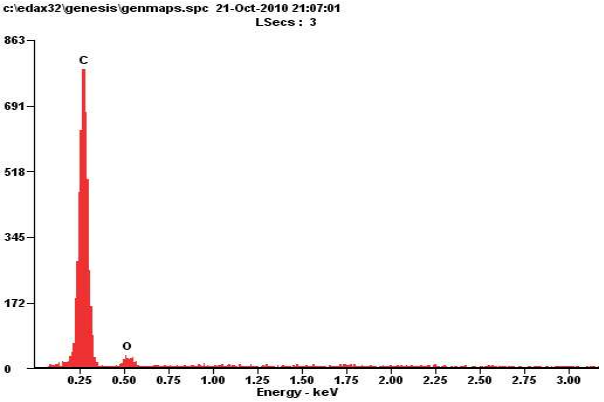
Micrograph 3: SEM/EDS Microstructure of Al-Cu-Mg alloy

Micrographs 4-7 show the microstructure of the reinforced alloy with eggshell particle additions. The microstructure reveals that there are reasonably uniform distributions of eggshell particles in the metal matrix. The ceramic phase is shown as dark phase, while the metal phase is white (see Micrographs 4-7). The distribution of eggshell particles is influenced by good wettability of the eggshell particles by the molten metal and good interfacial bonding between particles and matrix material. Good retention of the eggshell particles was clearly seen in the microstructures of the composites. The eggshell particles are well distributed along the grain boundaries of the microstructures of the composites.

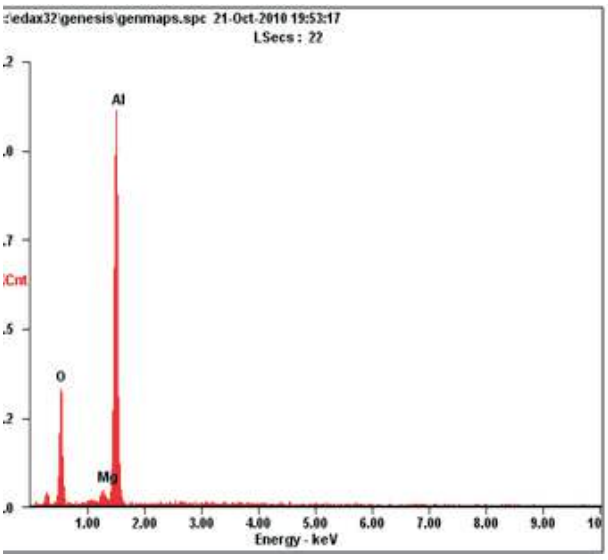
It should be noteworthy, that the grain size of the matrix alloy is somewhat larger than that of the composites. Micrographs 4-7, clearly reveal minimal micro porosities in the casting. No clustering of reinforcements was observed in the matrix, and the dispersion of eggshell particles was seen to be almost uniform. No gap is observed between the particle and matrix and reinforcing materials are seen well bonded with the matrix.



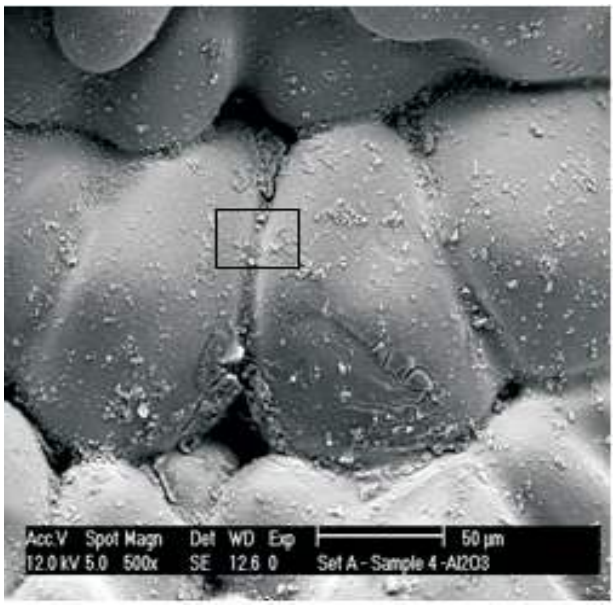
Micrograph 4: SEM/EDS Microstructure of 2wt% uncarbonized eggshell particles reinforced Al-Cu-Mg alloy



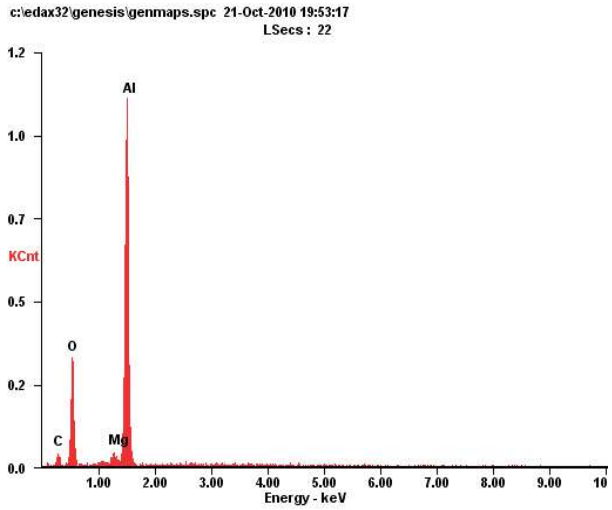


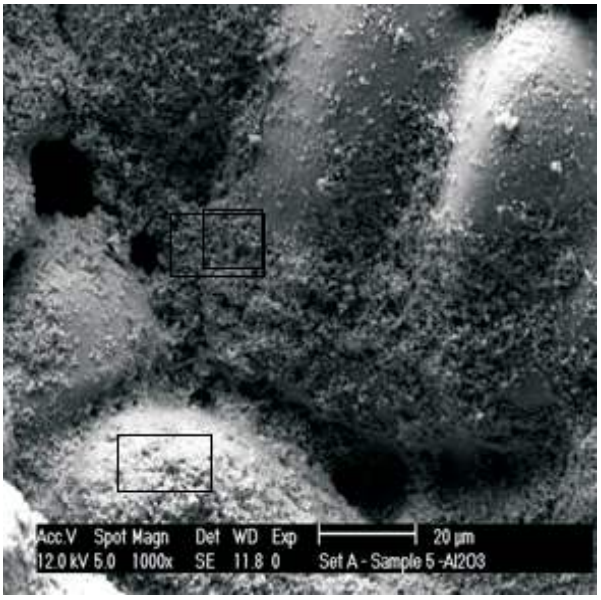


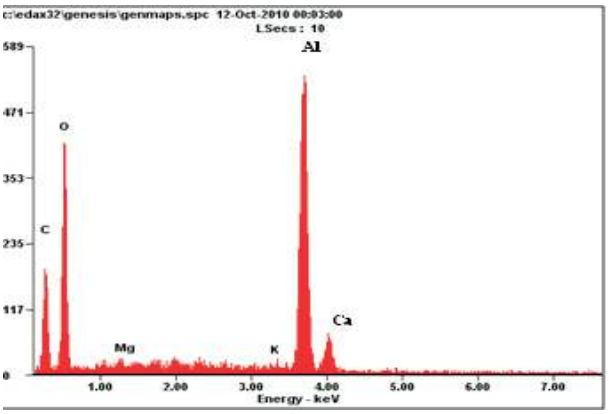
Micrograph 5: SEM/EDS Microstructure of 2wt% carbonized eggshell particles reinforced Al-Cu-Mg alloy



Micrograph 6: SEM/EDS Microstructure of 8wt% uncarbonized eggshell particles reinforced Al-Cu-Mg alloy







Micrograph 7: SEM/EDS Microstructure of 8wt% carbonized eggshell particles reinforced Al-Cu-Mg alloy

The Al-Cu-Mg alloy reveals the presence of α - A l , Cu and Mg as evident from the EDS spectra (see Micrograph 3). From the EDS analysis of the composites material (see Micrographs 4-7) there is indication of some possible chemical reaction between aluminum melt and eggshell particles which led to the release of Si, Na, O and Ca e.t.c in the composites, since the eggshell particles consist of C , SiO_2, and $CaCO_3$ a s t h e major constituents(see Micrographs 1-2). These constituents react with Al and Cu present in the molten matrix alloy depending on the kinetics of reactions. It should be noted that the presence of the carbonized eggshell particles result in a much smaller grain size in the cast composites compared to uncarbonized eggshell cast composites. This could be attributed to the much fineness and smaller particles of carbonized eggshell than uncarbonized eggshell particles (see Micrographs 1-2).

The density decreased with increasing percentage additions of eggshell particles (see Figure. 1). The density of uncarbonized and carbonized eggshell particles were 2.47 and 1.98g/cm^3 respectively. The overall density of Al-Cu-Mg/egg shell particulate composites decreased with wt% additions of eggshell particles e.g the density of the composites decreased from 2.78g/cm^3 at 0wt% to 2.57g/cm^3 and 2.50g/cm^3 at 12wt% for uncarbonized and carbonized eggshell particles respectively. This shows that composites with light weight can be made with eggshell. This is in agreement with the earlier work of Aigbodion[6] and Rajan et al[7].

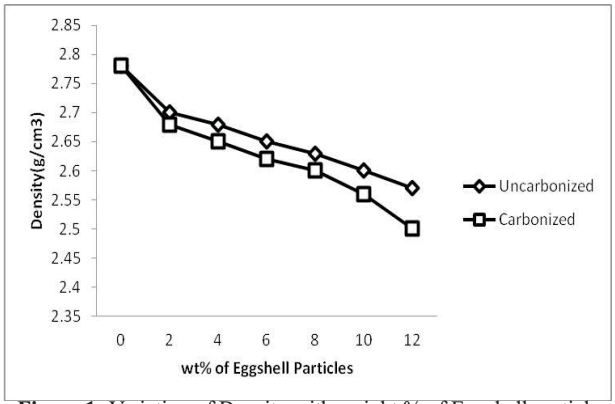


Figure 1: Variation of Density with weight % of Eggshell particles

The hardness values increased as the weight percentage of eggshell particles addition increased in the Al-Cu-Mg alloy(see Figure 2). For example the hardness values increased from 59.12HRF at 0wt% to 65.41HRF at 12wt% for uncarbonized eggshell particles and 74.17HRF at 12wt% for carbonized eggshell particles respectively. These increaments are attributed to increase of the weight percentage of hard and brittle phase of the eggshell particles in the Al-Cu-Mg alloy. This hardness of the eggshell particles are obtained from the $CaCO_3$, C and SiO_2 of the chemical made up of the particles. Also the presence of eggshell particles in the Al-Cu-Mg alloy increases the dislocation density at the particles-matrix interfaces. This is as a results of differences in coefficient of thermal expansion (CTE) between the hard and brittle reinforced particles and soft and ductile metal matrix which results to elastic and plastic incompatibility between the matrix and the reinforcement [1, 6-8].

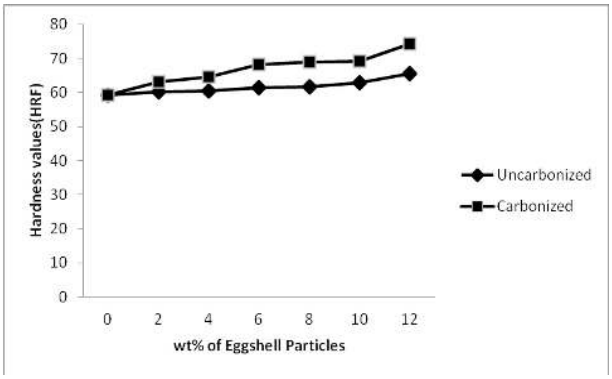


Figure 2: Variation of Hardness values with weight % of Eggshell particles

The tensile strength increased with increasing percentage of eggshell particles in the Al-Cu-Mg alloy (see Figure 3). For example the tensile strength increased from 98.28N/mm^2 at 0wt% to 106.79N/mm^2 and 112.84N/mm^2 for uncarbonized and carbonized eggshell particles respectively. The increases in tensile strength with percent eggshell particles additions due to the formation of nearly uniform distribution of eggshell particles in the Al-Cu-Mg alloy matrix [7]. By dispersion of eggshell particles in a soft ductile Al-Cu-Mg alloy matrix results in improvement in strength [4]. And improvement in tensile strength may be due to the matrix strengthening that might have occurred following a reduction in composite grain size and the generation of a high dislocation density in the matrix as a result of difference in coefficient of thermal expansion between matrix and reinforcements [5-9]. Wettability is one of the dominating factors to ensure good bonding between the matrix and reinforcement [8]. A good bonding between reinforcement and soft aluminium matrix favors an enhancement of the ultimate tensile strength of the composite [9].

It is found that the addition of eggshell particles has significant effect on the tensile properties. The addition of the eggshell particles increases strength mainly by the load transfer from matrix to the reinforcement due to the differences in the elastic constants. It is noteworthy, that the composites with carbonized eggshell particles has a higher tensile strength than the composites with uncarbonized eggshell particles, this is attributed to the much fineness particles of the carbonized eggshell particles which resulted in more uniform distribution in the microstructures of the Al-Cu-Mg/carbonized eggshell particulate composites. Hence, the more grain sizes/particles in the microstructures of the composites, the more obstacles to dislocation movement which resulted to a higher strength of Al-Cu-Mg/ carbonized eggshell particulate composites than that of Al-Cu-Mg/ uncarbonized eggshell particulate composites.

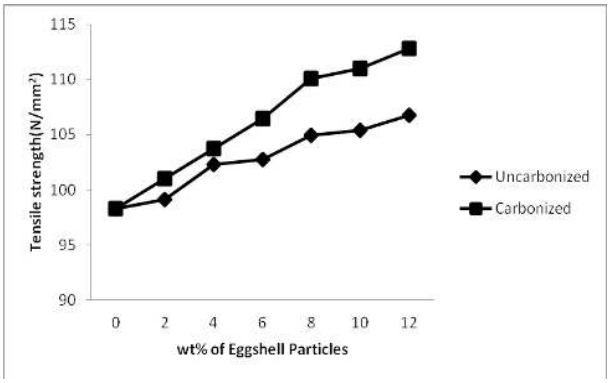


Figure 3: Variation of tensile strength with weight % of eggshell particles

The impact energy decreases as the percent eggshell particles addition increases in the composites(see Figure 4). The brittle nature of the reinforcing materials (eggshell) plays a significant role in degrading the impact energy of the composites. On the other hand, as can be suggested from the impact test, the elastic behavior of the matrix proportionately varies with the addition of the eggshell particles. As the loading of eggshell particles increases, the ability of the composites to absorb impact energy decreases since there is less ratio of the matrix to particles. However the results obtained are remained within the standard level[9].

However, the properties obtained with Al-Cu-Mg/ carbonized eggshell particulate composites showed higher values than Al-Cu-Mg/uncarbonized eggshell particulate composites; this can also be attributed to the volatile matters and moisture that are given off during carbonization. This may also account for the poor distribution and dispersion of the uncarbonized eggshell particles in the Al-Cu-Mg alloy matrix resulting in weak-particles-matrix interaction [7]. This poor particles dispersion will reduce the particles-matrix interaction and consequently decreases the ability of the uncarbonized eggshell to restrain gross deformation of the Al-Cu-Mg matrix.

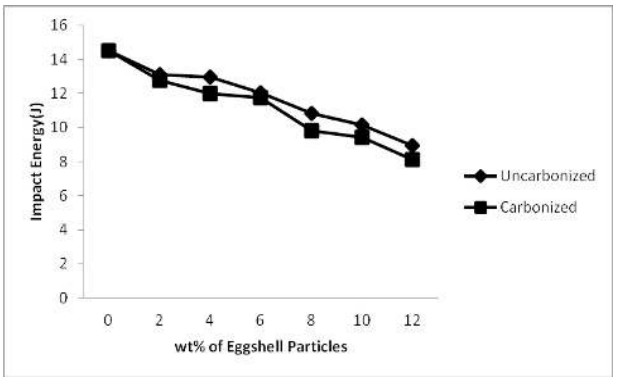


Figure 4: Variation of Impact strength with weight % of Eggshell particles

CONCLUSIONS

From the results and discussion in this work, the following conclusions can be drawn:

1. Eggshell particles were successfully incorporated in Al-Cu-Mg alloy by using stir casting technique.
2. Microstructure analysis shows the uniform distribution of eggshell particles in the aluminium alloy. The microstructure also revealed good retention of carbonized eggshell particles in the matrix.
3. The uniform distribution of the eggshell particles in the microstructure of the composites is the major factor responsible for the improvement in the mechanical properties.
4. The addition of eggshell particles reinforcement to Al-Cu-Mg alloy increased the tensile strength, the hardness value of the Al-Cu-Mg/Eggshell particulate composites with slightly reduction in impact energy.
5. The increase in strength and hardness was as a result of the increases in the amount of the hard eggshell phase in the ductile metal phase which leads to increase in dislocation density at the matrix-particle interphase.
6. Incorporation of eggshell particles in aluminium matrix can lead to the production of low cost aluminium composites with improved hardness and strength. These composites can find applications in automotive components like pistons, cylinder liners and connecting rods as well as applications where light weight materials are required with good stiffness and strength.

References

[1] Aigbodion V.S. & Hassan .S.B(2007): Effects of silicon carbide reinforcement on Microstructure and properties of cast Al-Si-Fe/SiC particulate composites, Journal of Materials Science and Engineering A, 447: 355-360.

[2]Naresh P(2006): Development and characterization of metal matrix composite using red Mud an industrial waste for wear resistant applications, PHD thesis Department of Mechanical Engineering, National Institute of Technology Rourkela -769 008 (India), January, pp23-34.

[3]Kin, J. Puri, V.M. and Anantheswaran, R.C. (1995): "Measurement of Eggshell Thermal-Mechanical Properties". American Society of Agricultural and Biological Engineering Retrieved Sept. 05, 2010

[4] Aigbodion .V.S (2007): Particulate-strengthened of Al-Si alloy/alumino-silicate composite materials science and Engineering A **460-461**, 574-578.

[5]Bienia J, Walczak .M, Surowska, B, Sobczaka J (2003): Microstructure and corrosion behaviour of aluminum fly ash composites, Journal of Optoelectronics and Advanced Materials, **5**, No. 2,493 – 502.

[6] Aigbodion. V.S(2010): Potential of using Bagasse ash particle in Metal Matrix Composite, PhD Dissertation, Department of Metallurgical and Materials Engineering, Ahmadu Bello University, Samaru, Zaria, Nigeria(2010), pp 34-50.

[7] Rajan T.P.D, Pillai R.M, Pai B.C., Satyanarayana K.G, Rohatgi, P.K (2007): Fabrication and characterization of Al–7Si–0.35Mg/fly ash metal matrix composites processed by different stir casting routes, Composites Science and Technology, 67, 3369–3377.

[8]Siva Prasad. D and Rama Krishna. A(2011): **Production and Mechanical Properties of A356.2 /RHA Composites,** International Journal of Advanced Science and Technology Vol. 33, 51-58

[9]Arun Kumar M. B and Swamy R. P(2011): Evaluation of Mechanical Properties of Al6061, Flyash And E-Glass Fiber Reinforced Hybrid Metal Matrix Composites, ARPN Journal of Engineering and Applied Sciences, VOL. 6, NO. 5, 40- 4.

EFFECT OF FIBRE EXTRACTION AND CHEMICAL TREATMENT ON THE TENSILE PROPERTIES OF SISAL FIBRE REINFORCED POLYPROPYLENE COMPOSITES

Oladele I.O [1,3], Omotoyinbo J.A [1,3]., Adewuyi B.O [1,3]., Adewara J.O.T [1,3]., and Kavishe F. P.L.[2,3]
[1]Department of Metallurgical and Materials Engineering, Federal University of Technology, Akure.
[2]Department of Metallurgical and Minning Engineering, University of Namibia.
[3]African Materials Science and Engineering Network.

Abstract
The influence of fibre extraction and chemical treatment on the tensile properties of sisal fibre reinforced polypropylene composites was investigated in this study. Sisal fibre for the reinforcement was extracted by soil retting after which it was chemically treated with 1 M of KOH, NaCl, HCl and Ethanol respectively. Both treated and untreated sisal fibre were characterised and used for the reinforcement of homopolymer and copolymer polypropylene. The composites were produced by compression moulding technique while the tensile test was carried out on the samples using Instron Universal Tensile Testing Machine. Scanning Electron Microscope was used to study both the fibre surface morphology before they are used for the reinforcement and the fractured surface of the composites after the test. From the results, it was observed that soil retting can be used for the extraction of sisal fibre and, chemical treatment can be used to enhance the tensile properties of the fibre as well as the composites produced.
Keywords: chemical treatment, tensile properties, sisal fibre, polypropylene.

1. Introduction

There has been a growing interest in utilizing natural fibres as reinforcement in polymer composite for making low cost construction materials in recent years [1]. Natural fibres are prospective reinforcing materials and their use until now has been more traditional than technical.

Due to the relatively high cost of synthetic fibres such as, glass, plastic, carbon and Kevlar used in fibre reinforced composites, and the health hazards of asbestos fibres, it has become necessary to explore natural fibres. Natural fibres are produced from renewable resources, are biodegradable and relatively inexpensive compared to the traditionally used synthetic fibres. Fibres of this type, for instance, hemp and flax, are successfully used as packaging material, interior panels in vehicles, and building components, among others. Also, natural fibres like banana, sisal, hemp and flax, jute, coconut, local fibres and oil palm [2-8] have attracted scientists and technologists for applications in consumer goods, low-cost housing and other civil structures.

Sisal (Agave sisalana) is a plant that yields stiff fibres traditionally used for rope and twine. It is usually extracted by a process known as decortications. One difficulty that has prevented the use of natural fibres is lack of good adhesion with the polymeric matrix. In particular, the large moisture absorption by natural fibres in hydrophobic matrix adversely affects adhesion and leads to premature ageing by degradation and loss of strength [9].

There are, however, several separation of fibre processing techniques such as mechanical or chemical pulping, whereby lignin is degraded and dissolved, leaving most of the cellulose and hemicelluloses in the form of fibres. This generally has an important effect on both mechanical and chemical properties of the fibres. This work was carried out to study the effect of extraction method and chemical treatment on the tensile properties of sisal fibre reinforced polypropylene composites.

2. Materials and Method

2.1. Materials

The materials that were used are sisal leaves, distilled water, potassium hydroxide (KOH), hydrogen chloride (HCl), sodium chloride (NaCl) and ethanol.

2.2. Equipment

Weighing balance, shaker water bath, beakers, furnace, crucible, instron universal tensile testing machine.

2.3. Method

2.3.1 Extraction of the Sisal Fibre

The sisal fibre used was obtained from the plant leaves by soil retting. This was carried out by cutting the leaves and buried under ground for 15 days so as to allow fermentation to take place. For the reaction to proceed naturally, the leaves were buried close to stream of water and are watered daily. The fermented leaves were washed after which they were sun dried.

2.3.2. Chemical Treatment

Combinations of chemicals and mechanical treatments were carried out on different samples while some was left as untreated sample that serves as control. The treatment was carried out by weighing out 60g of sisal fibre into which 1.0M each of KOH, HCl, NaCl and Ethanol was

added in a solution of 450ml inside shaker water bath maintained at 50ºC for 4 hours respectively. The treated samples were washed thoroughly with water and finally washed with distilled water. Five fibre samples were obtained including the untreated sample.

2.3.3. Production of Composites

To produce the composites, tensile test mould of 3mm thick was used. The filled mould was placed inside the compression moulding machine maintained at 190 ºC and 15 tons for 15 minutes followed by air cooling.

2.3.4 Determination of the Tensile Properties of the Materials

Tensile test was carried out on the samples using Instron Universal Tensile Testing Machine in accordance to ASTM D638. To carry out the test, sample was fixed at the edges of the upper and the lower grip of the machine and the test commenced. As the test piece is being extended, graph is being plotted automatically and important tensile properties data were generated.

3. Results and Discussion

3.1 Variation of the Constituents with Chemical Treatments of the Sisal Fibre

The results of the constituents of the different sisal fibre samples were as shown in Figure1.

3.2 Discussion

During chemical treatments, constituent like hemicelluloses was hydrolyzed by the action of alkaline solutions whereas lignin was removed using sodium chloride and hydrogen chloride. To improve and achieve an acceptable dispersion level in the solution, mechanical homogenization with shaker water bath was also used for all samples at elevated temperature.

The treatments contributed to the removal of hemicelluloses and lignin contents as shown Figure 1. The resistance to extraction with alkaline of the sugars that are the main constituents of hemicelluloses is due to the association between xyloglucan and cellulose that is very strong. Xyloglucan probably binds not only to the surface of cellulose microfibrils, but it can also be entrapped within the microfibrils [10]. Xylans, xyloglucans and glucomannans are all able to bind onto cellulose fibrils in a manner similar to the interchain bonding of cellulose itself.

The bonding nature between the fibre and the matrix depends on the atomic arrangement, chemical properties of the fibre and the chemical constitution of polymeric matrix. However, in the natural fibre composite, cellulose is the principal coupling agent in the polymer/fibre bonding. On the other hand, lignin acts as an obstruction to the coupling agent diffusion, preventing good adhesion [11].

From the results, common trend was observed for cellulose and hemicelluloses in which higher retention of the constituents was observed in the following order; KOH, NaCl, HCl and Ethanol respectively except for lignin where higher retention was observed for Ethanol treated sample more than HCl treated sample. However, for ash and PH, similar trend was also observed in terms of retention in the following order; KOH, Ethanol, NaCl, and HCl respectively.

3.2.1 Variation of Tensile Properties with Chemical Treatments of the Sisal Fibre

The results of the tensile properties obtained were shown in Figures 2-5.

3.2.2 Response of the Fibres to Strain.

The response of fibres to the strain at break was shown in Figure 3. The results showed that sample treated with 1 M KOH has the best strain at break property of 0.0850mm/mm followed by the untreated sample with a value of 0.0773mm/mm and sample treated with 1 M NaCl with a value of 0.0731mm/mm respectively. This shows that these samples can withstand the load generating the stress that will cause the materials to fail for longer period before they will break. The breaking load is the load that brings about material failure, [12].

3.2.3. Response of the Fibres to Breaking Stress

The results in Figure 4 revealed the response of the fibres to the breaking stress. It was observed that **sample treated with 1 M KOH with a value of 672.4**9 MPa followed by sample treated with1 M NaCl with a value of 345.94 MPa and Ethanol with a value of 264.20 MPa gave the best breaking stress property. This show that these samples are likely to fail if loaded beyond these values. Breaking load is the load that brings about the failure of a material.

3.2.4. Response of the Fibres to Ultimate Tensile Strength (UTS).

The result in Figure 5 revealed the response of the fibres to the ultimate tensile strength (UTS) property. It was observed that sample treated with 1 M KOH with a value of 1130MPa followed by sample treated with1 M NaCl with a value of 900MPa and Ethanol with a value of 800 MPa gave the best UTS property. Ultimate tensile strength is the maximum stress a material can withstand before it will fail.

3.2.5. Response of the Composites to Young's Modulus of Elasticity.

Figure 6 show the response of the Young's Modulus of Elasticity against the various samples. Young's Modulus of Elasticity is the property of material that measures its stiffness. From the result, it was observed that 1 M KOH treated sample in homopolymer 3wt% fibre fraction gave the best Young's Modulus of Elasticity value of 831 MPa followed by 5wt% fibre fraction of the same sample with a value of 795 MPa and 5wt% fibre fraction of sample treated with 1 M NaCl with a value of 789 MPa.

3.2.6. Response of the Composites to Ultimate Tensile Strength (UTS).

The Ultimate Tensile Strength (UTS) property of the different composites was shown in Figure 7. From the graph, it was observed that, the unreinforced homopolymer has the best UTS value of 33.88 MPa followed by 1 M KOH treated sample in homopolymer 3wt% fibre fraction with a value of 32.70 MPa and 1 M Ethanol treated sample in homopolymer 3wt% fibre fraction with a value of 32.33 MPa respectively.

The yield stress at 0.2 % for the composites was shown in Figure 8. Yield stress is defined as the stress at which a

material will undergo an increase in strain at a constant stress. At this point, the microstructure of the material will be distorted, that is, there will be a change at the microstructural level. From the graph, it was observed that, the untreated sample **in homopolymer 3wt% fibre** fraction with a value of 14.877 MPa followed by 1 M NaCl treated sample in homopolymer 5wt% fibre fraction with a value of 14.802 MPa and 1 M Ethanol treated sample in copolymer 3wt% fibre fraction with a value of 13.740 MPa respectively gave the best yield strength property.

Figure 9 show the variation of the stress at break against samples for the composites. From the graph, it was observed that, 1 M KOH treated sample in homopolymer 3wt% fibre fraction with a value of 29.678 MPa followed by unreinforced homopolymer polypropylene material with a value of 28.634 MPa and 1 M Ethanol treated sample in homopolymer 3wt% fibre fraction with a value of 28.486 MPa respectively having the best strength at break. The stress at break is a measure of the breaking strength of a material, which is the amount of strength the material can withstand before it will fail.

The strain at peak of a material is the maximum strain the material can withstand before failure. Figure 10 show the strain at peak for the samples. From the graph, it was observed that, the unreinforced homopolymer has the best strain at peak value of 13.834 MPa followed by 1 M HCl treated sample in copolymer 3wt% fibre fraction with a value of 13.291 MPa and 1 M KOH treated sample in copolymer 5wt% fibre fraction with a value of 12.497 MPa respectively.

The strain at which a material will break is known as the strain at break. Figure 11 reveal the strain at break for the samples. From the graph, it was observed that, the unreinforced copolymer has the best strain at break value of 226.133 MPa followed by 1 M NaCl treated sample in copolymer 5wt% fibre fraction with a value of 40.614 MPa and untreated sample in copolymer 5wt% fibre fraction with a value of 38.422 MPa respectively.

Plates a-e show the SEM of the untreated and treated sisal fibres. It was observed that the treatment affect the surface morphology of the fibres due to the removal of some lignin and hemicelluloses that bind the cellulose together. The treatment was able to expose the cellulose that is actually needed for the reinforcement, thereby enhancing the bonding between the fibre and the matrix.

Plates f-i show the SEM for the fractured surfaces for the composites. It was observed that the fibres were more wetted in homopolymer than in copolymer and, hence, better properties were achieved in homopolymer matrix than in copolymer. This was the reason for the results that was obtained where the properties were more enhanced in homopolymer matrix than in copolymer.

4. Conclusion

The effect of extraction technique and chemical treatment on the chemical constituents and the tensile properties of sisal fibre and sisal fibre reinforced polypropylene have been studied and from the results, it was observed that;

- Soil retting can be used to extract sisal fibre with good tensile properties.
- Chemical treatment can be used to enhance the properties of the extracted sisal fibre. The result of the treatment show that, 1 M KOH followed by 1M NaCl treatment enhanced the tensile properties of the fibre and hence, the properties of the ensuing polypropylene composites.
- The properties (Young's Modulus of Elasticity, Ultimate Tensile Strength, 0.2% yield strength and stress at break) of the homopolymer composites were better enhanced compared to the copolymer samples.

Acknowledgement

Carnegie-IAS Regional Initiative in Science and Education (RISE), African Materials Science and Engineering Network (AMSEN), Science Initiative Group (SIG) and Federal University of Technology Akure (FUTA).

References

1. Rai, M., Jaisingh, M. P.(1986) Advances in Building and Construction Materials. Roorkee: Central Building Research Institute.
2. Idicula M., Malhota S.K., Joseph K., Thomas S., (2005), Dynamic Mechanical Analysis of Randomly Oriented Intimately mixed Short Banana/Sisal Hybrid Fibre Reinforced Polyester Composites, Composites Science and Technology, 67(7-8), pp 1077-1087.
3.Jacob M., Thomas S., Varughea K.T., (2004), Mechanical Properties of Sisal/Oil Palm Hybrid Fibre Reinforced Natural Rubber Composites, Composites Science and Technology, 64, pp 955-965.
4. Hautala M., Pasila A., Pirila J., (2004),Use of Hemp and Flax in Composite Manufacture: a search for new production methods, Composite Part A, 35, pp 11-16.
5.Chand N., Dwivedi U.K., (2006),Effect of Coupling Agent on Abrasive Wear Behaviour of Chopped Jute Fibre-Reinforced Polypropylene Composites, Composites Science and Technology, 261, pp1057-1063.
6. Brahmakumar M., Pavithran C., Pillai R.M., (2005),Coconut Fibre Reinforced Polyethylene Composites: effect of natural waxy surface layer of the fibre on fibre/matrix interfacial bonding and strength of composites, Material Processing Technology , 65(3-4),pp 563-569.
7. Oladele,I.O. and Adewuyi B.O. (2008) Development of Automobile Gaskets fromLocal Fibres, Journal of Science and Technology, Vol 28 No 3, p152-157.
8. Yousif B.F.,EL-Tayeb N.S.M.,(2007), The Effect of Oil Palm Fibres as Reinforcement on Tribological Performance of Polyester Composites, Surface Review Letter, Composites Science and Technology, 14(6), pp 1-8.
9. Khalil H.P.S.A., Rozman H.D.,(2000),Rice-Husk Polyester Composites:The Effect of Chemical Modification of Rice Husk on the Mechanical and Dimensional StabilityProperties, Polymer Plastic

and Technology Engineering, 39, 757-781.
10. Habibi,Y., Heux,L., Mahrouz, M.and Vignon,M.R. (2008) Morphological and Structural Study of Seed Pericarp of Opuntia Ficus- Indica prickly Pear Fruits.

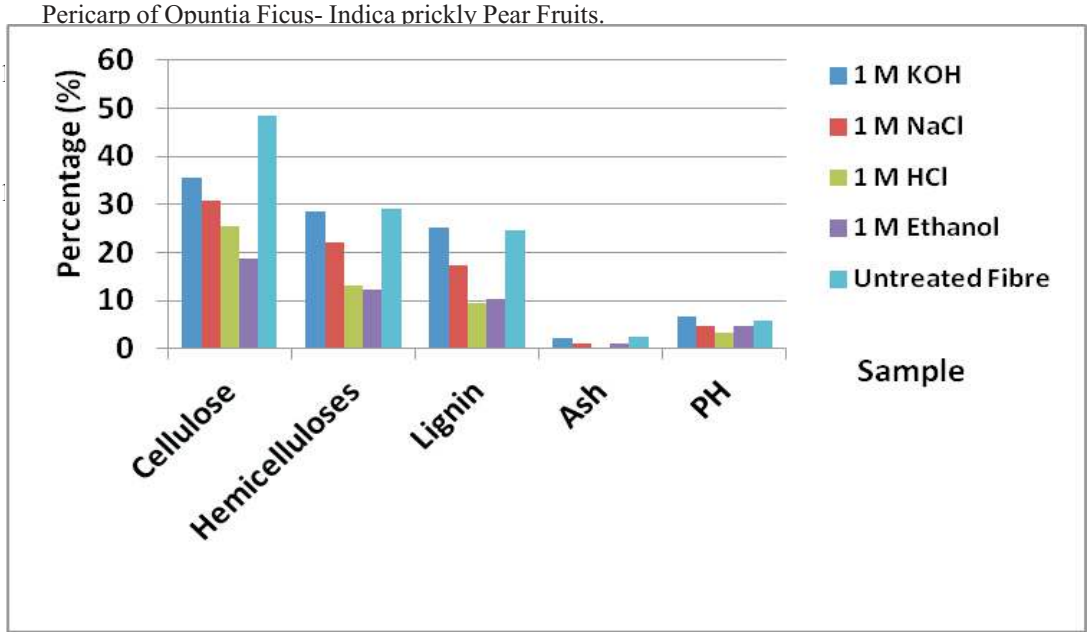


Figure 1: Variation of Percentage Sisal Fibre Constituents and PH Values for both Treated and Untreated Sisal Fibres.

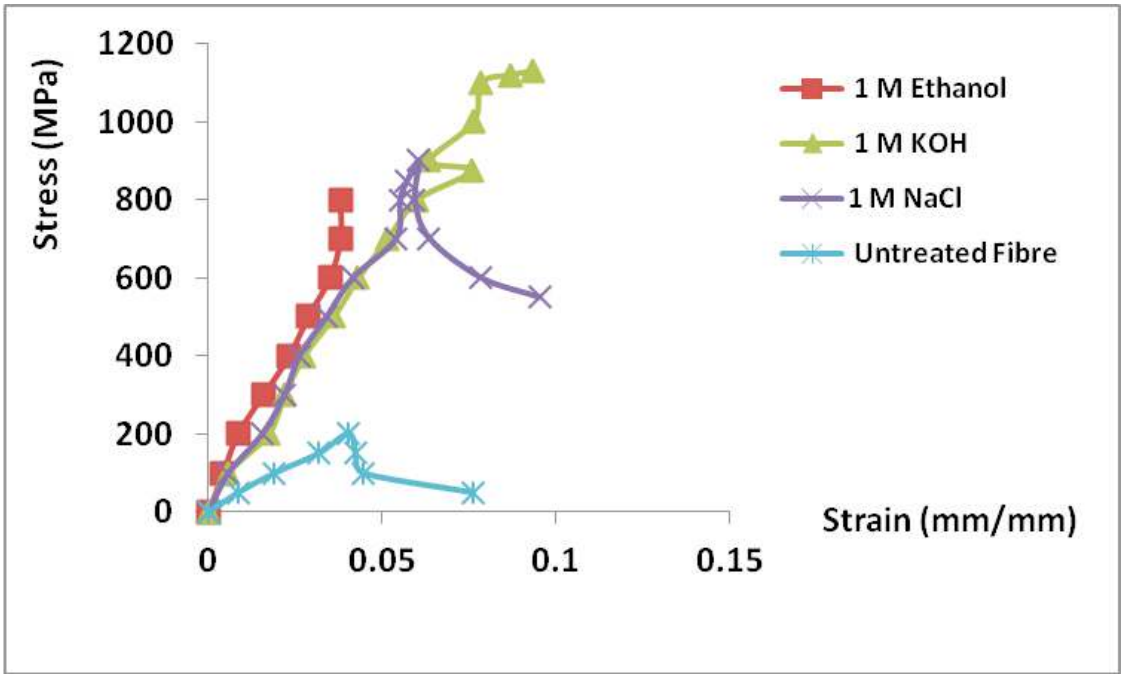


Figure 2: Variation of Stress against Strain for Treated and Untreated Sisal Fibres.

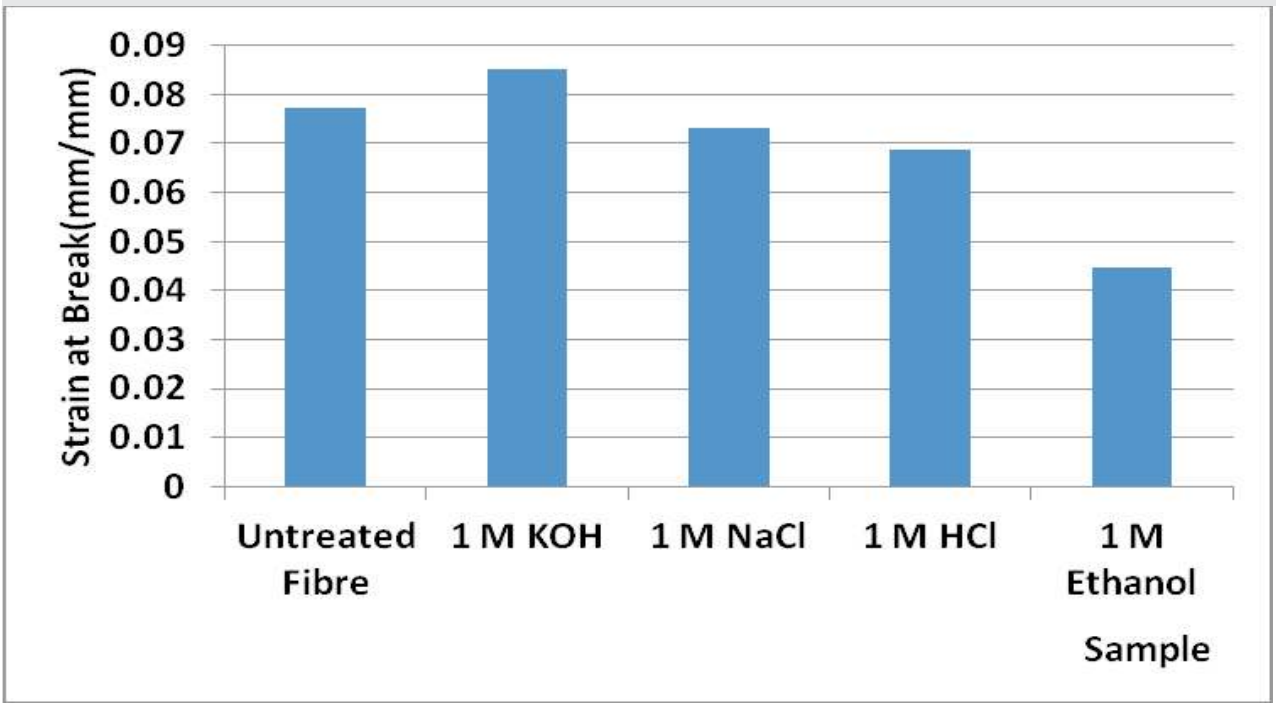


Figure 3: Variation of Strain at Break against Sample for Treated and Untreated Sisal Fibres.

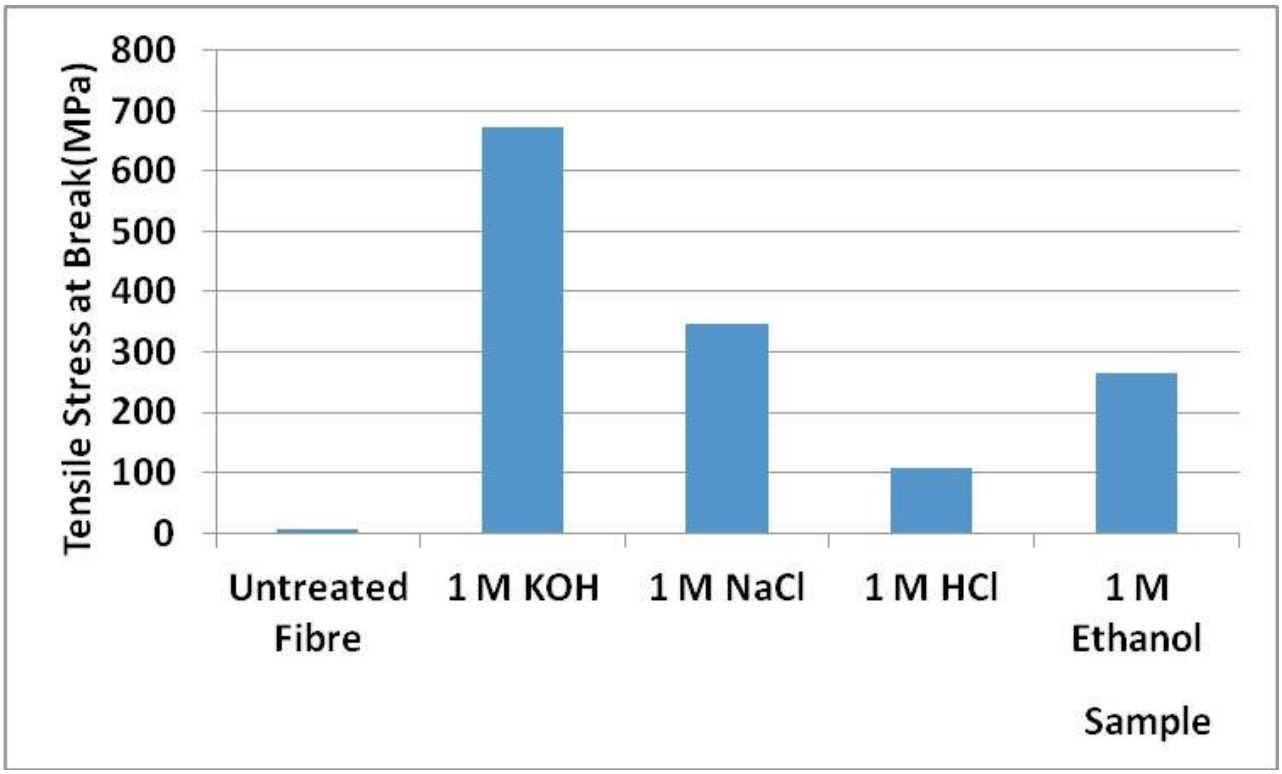


Figure 4: Variation of Tensile Stress at Break against Sample for Treated and Untreated Sisal Fibres.

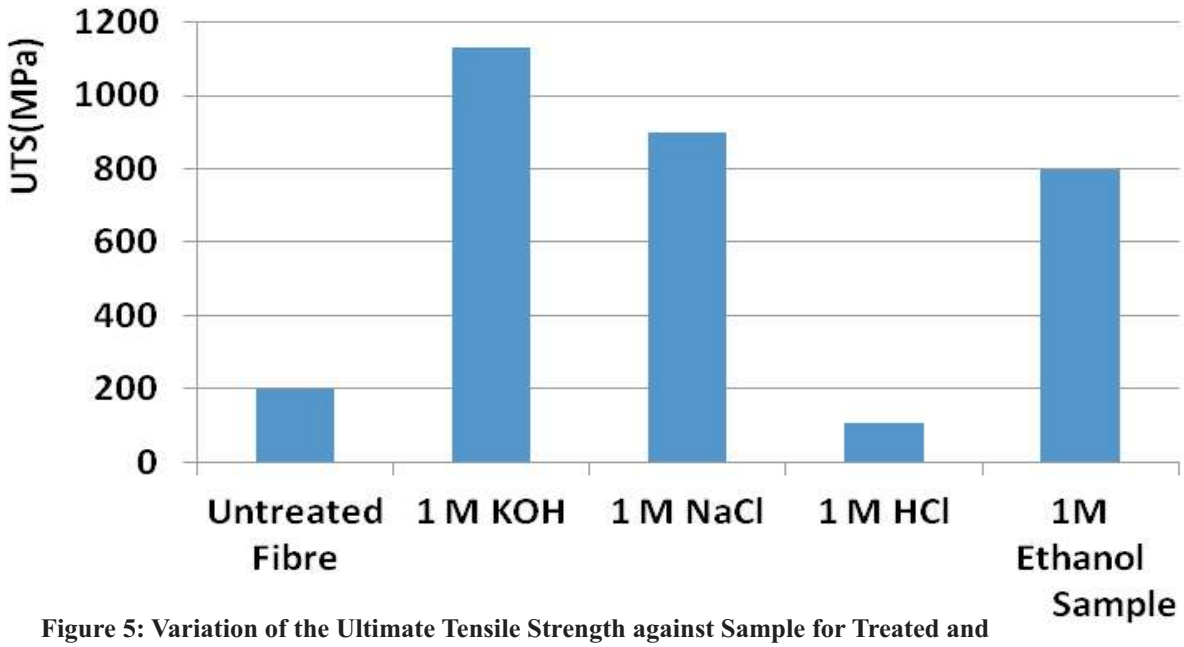


Figure 5: Variation of the Ultimate Tensile Strength against Sample for Treated and Untreated Sisal Fibres.

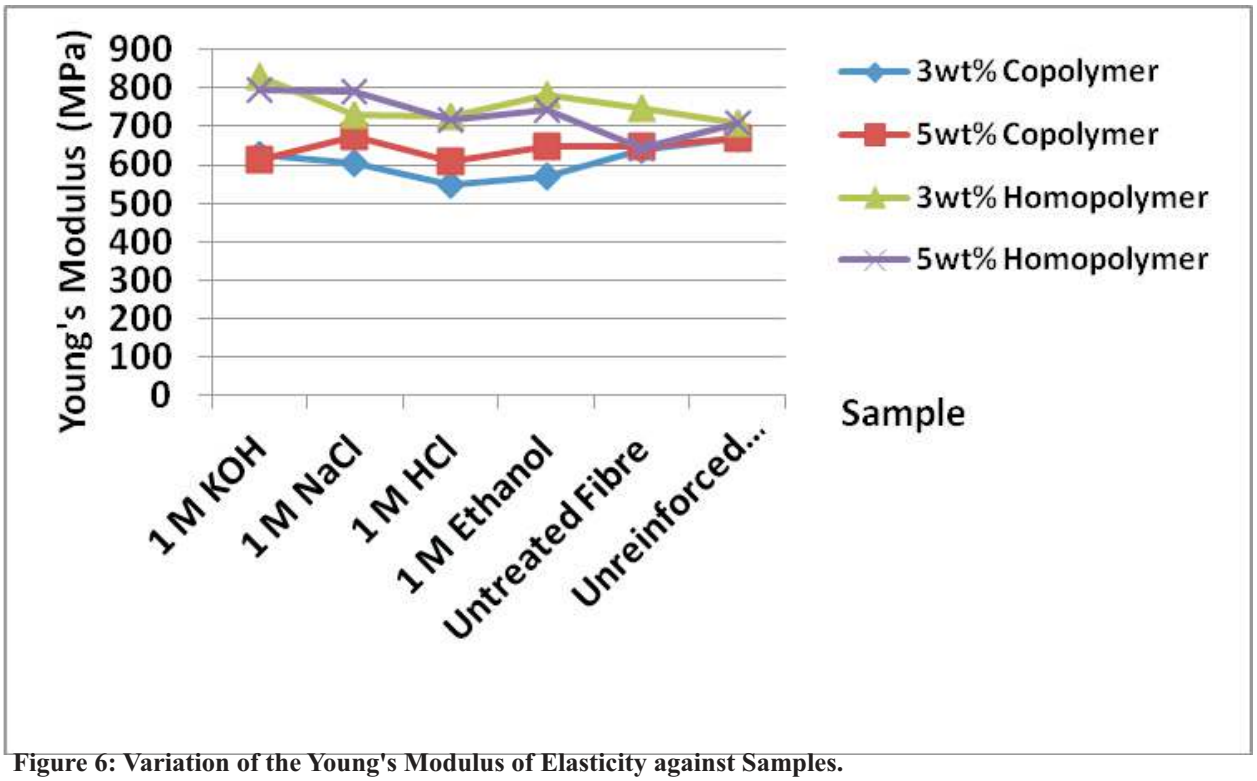


Figure 6: Variation of the Young's Modulus of Elasticity against Samples.

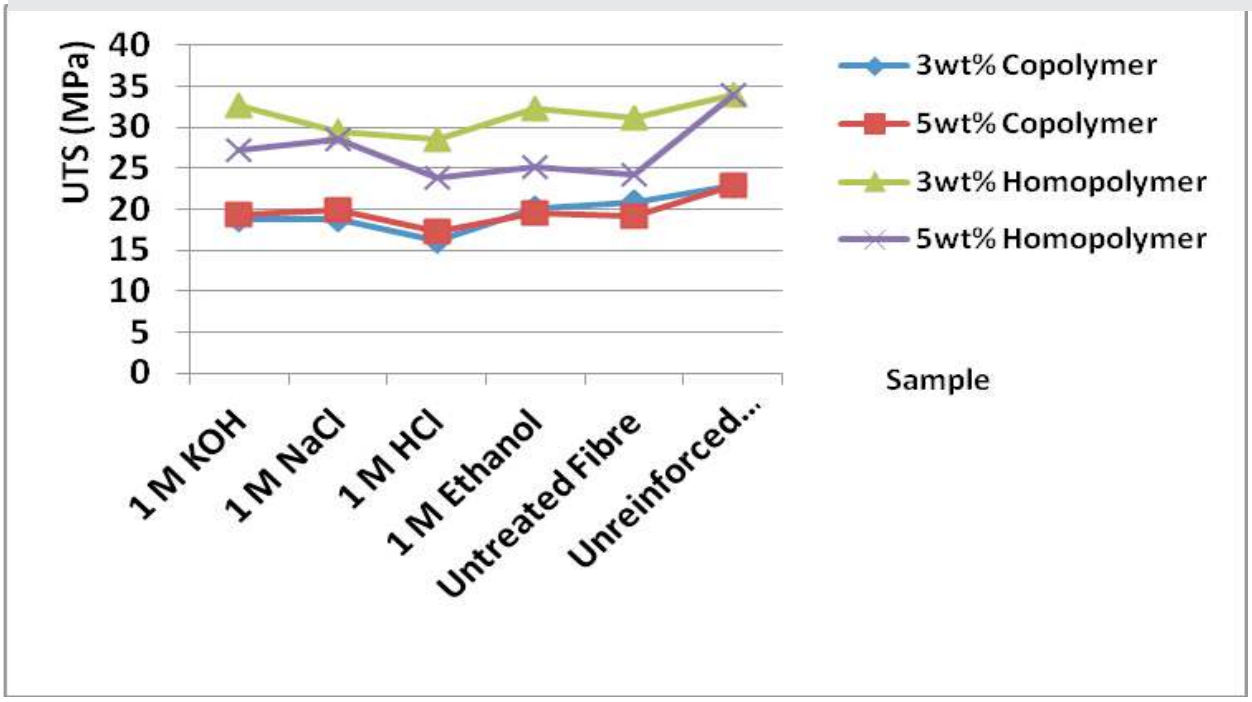


Figure 7: Variation of the Ultimate Tensile Strength against Samples.

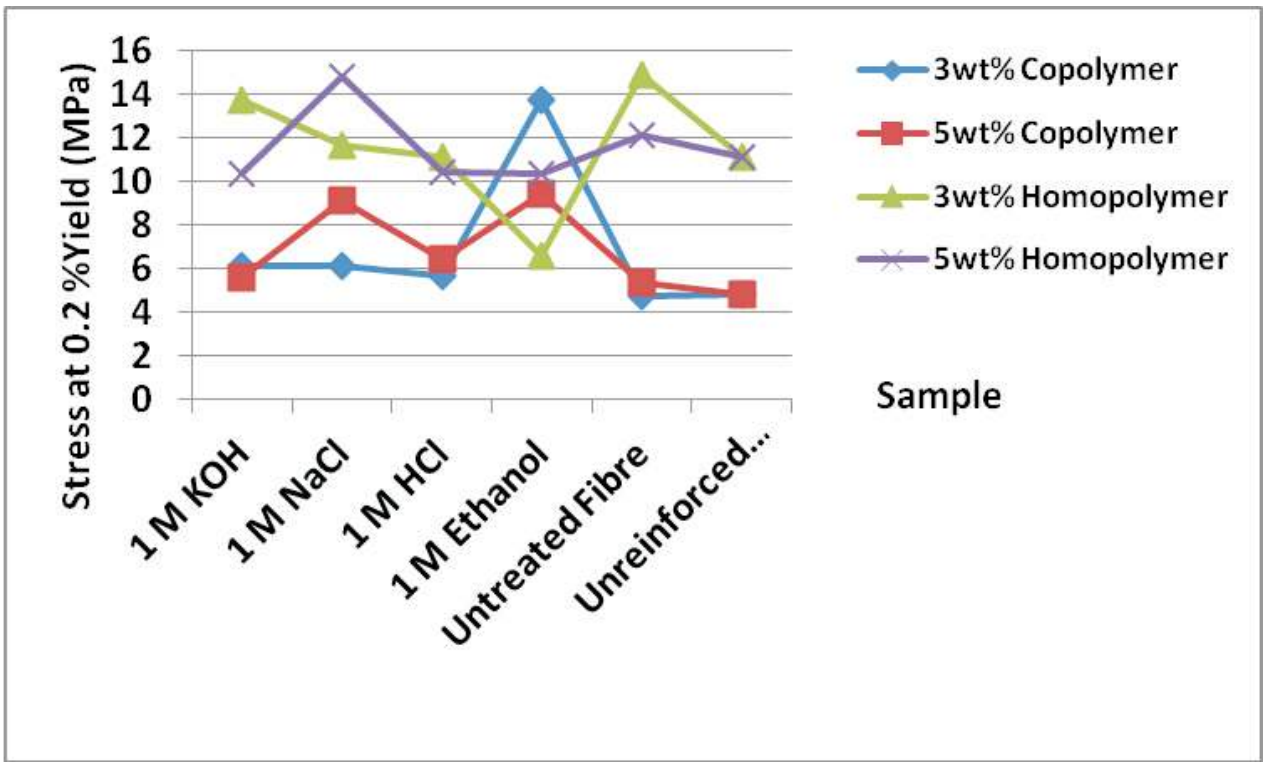


Figure 8: Variation of the Stress at 0.2 % Yield against Samples.

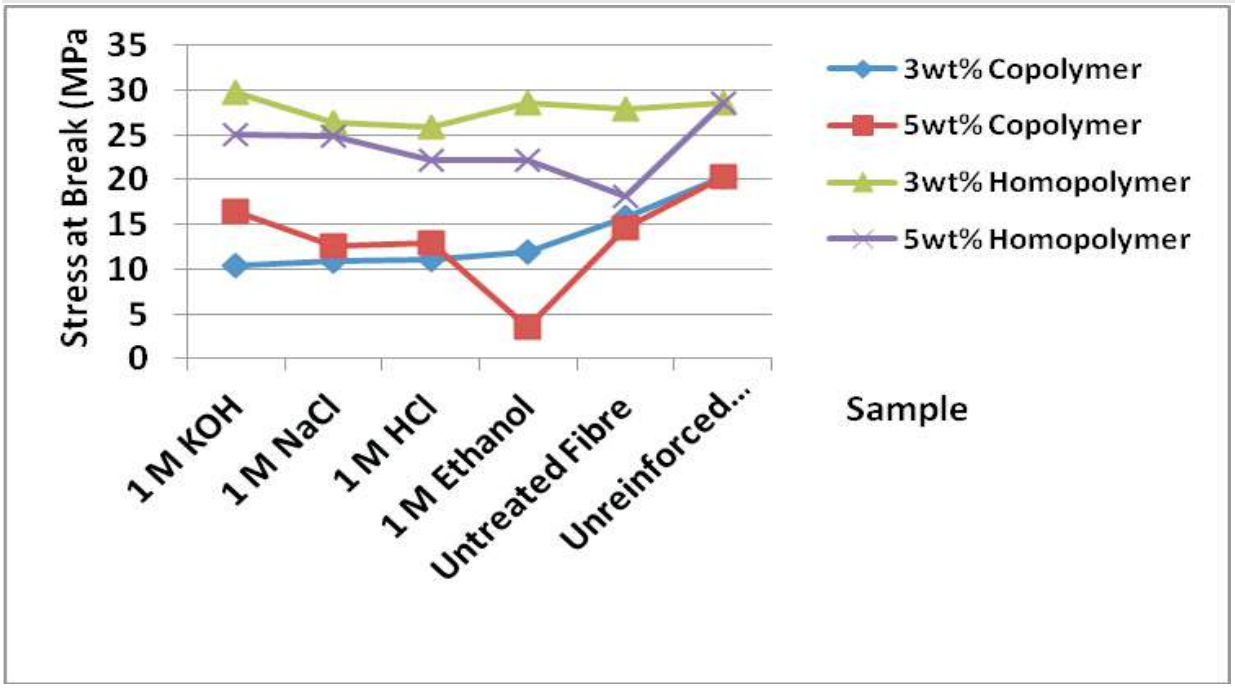


Figure 9: Variation of the Stress at Break against Samples.

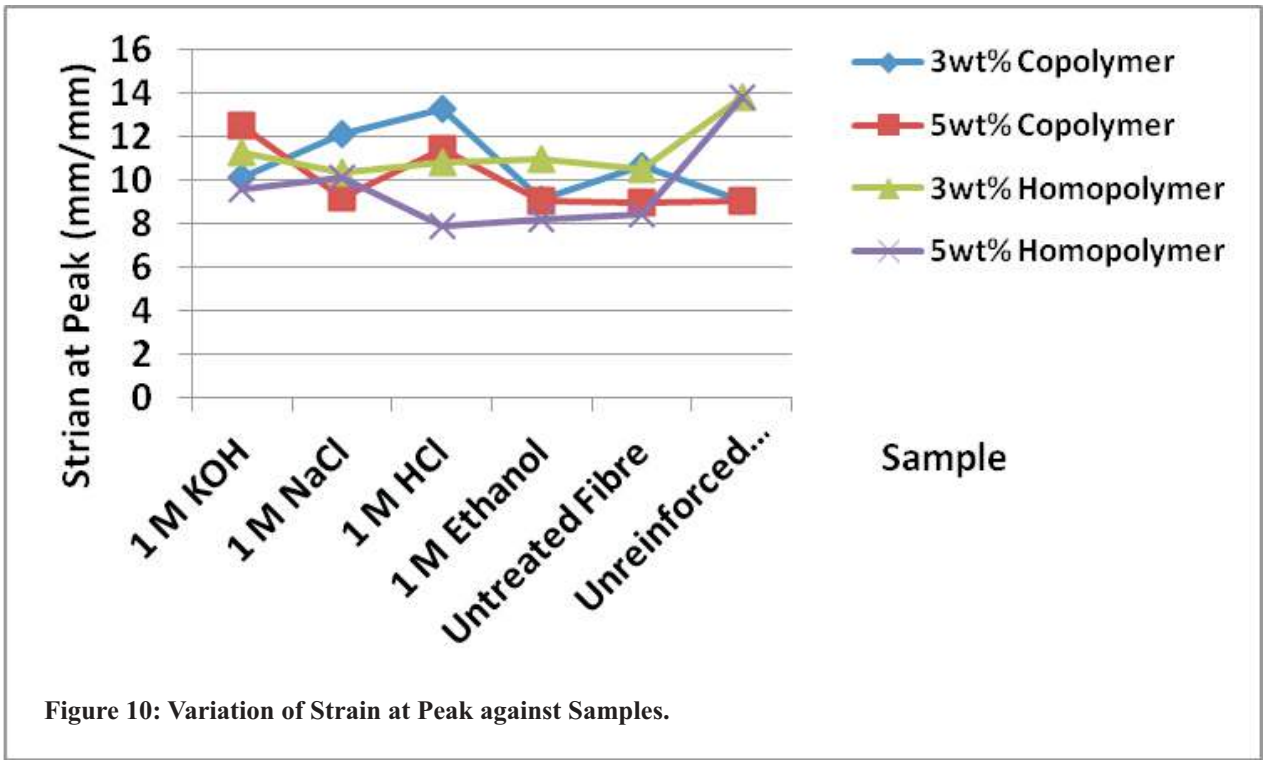


Figure 10: Variation of Strain at Peak against Samples.

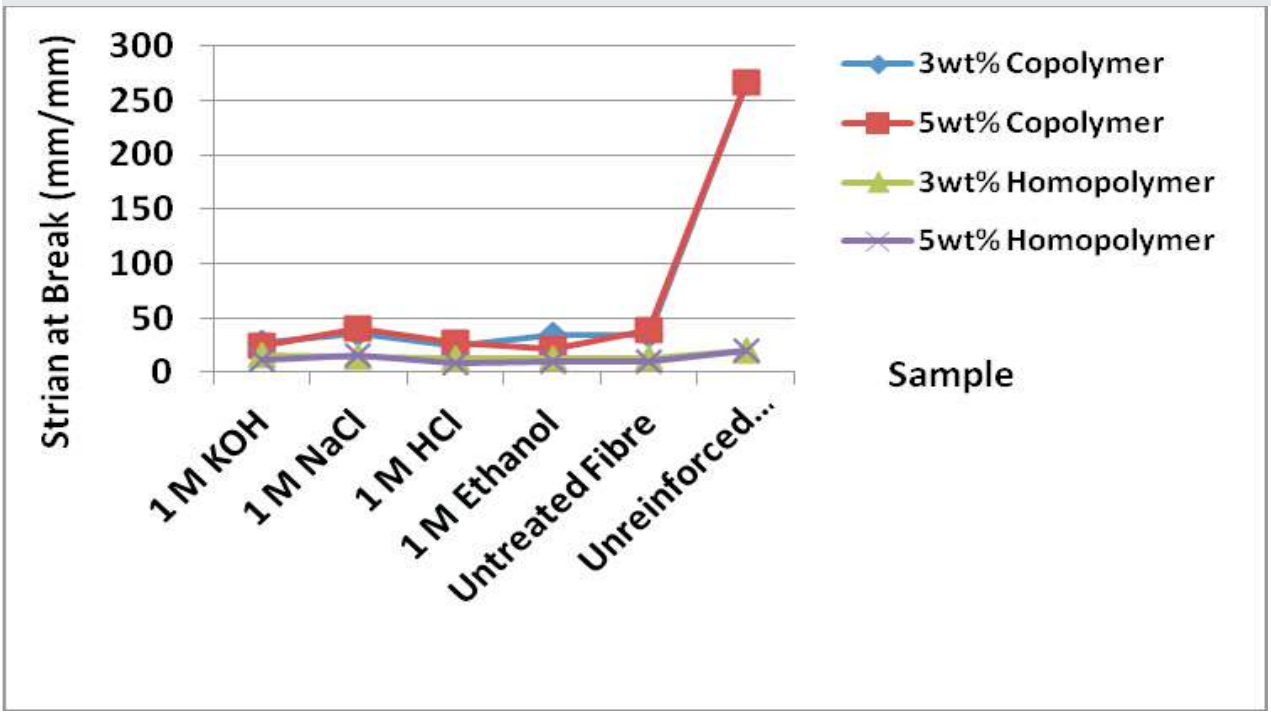
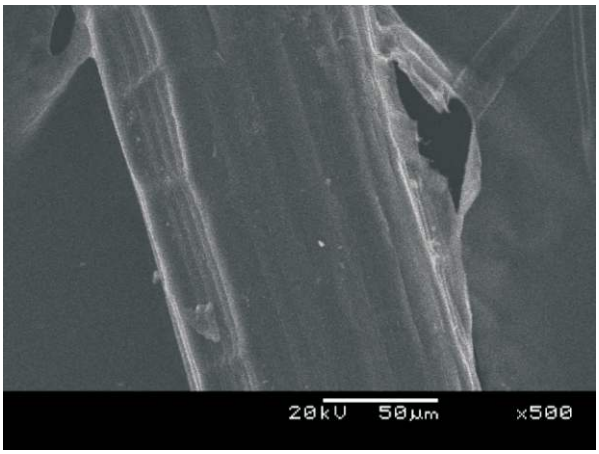
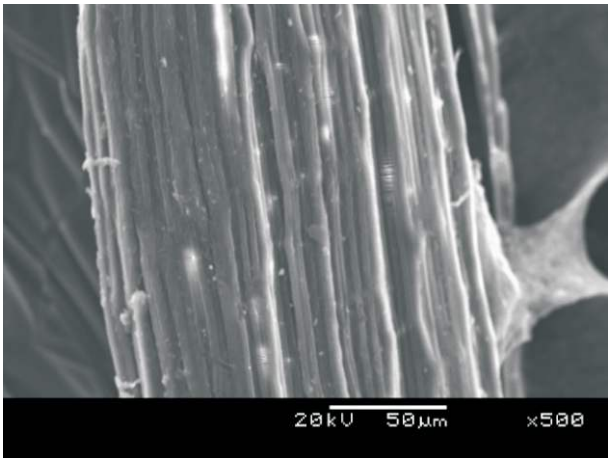


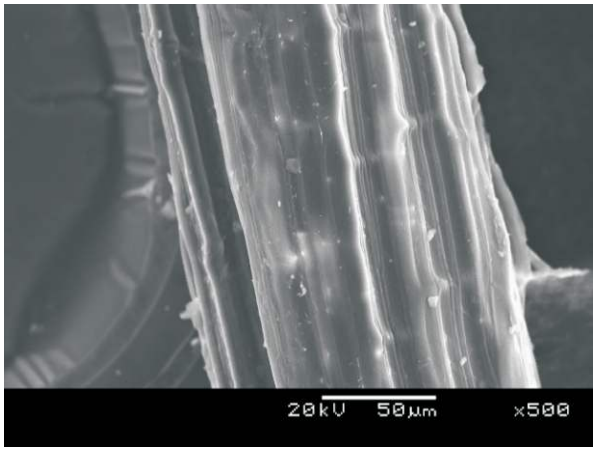
Figure 11: Variation of Strain at Break against Samples.



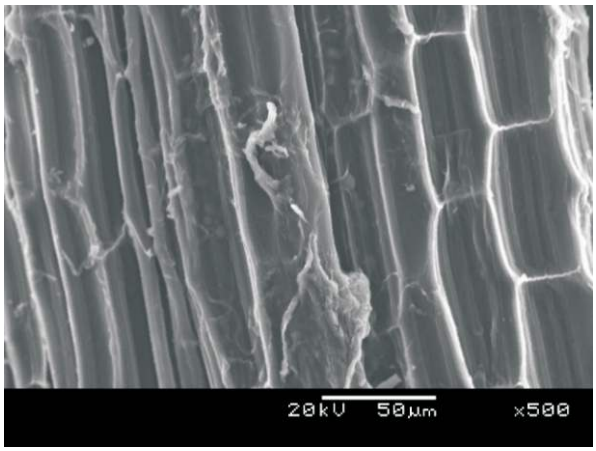
(a) Untreated Sisal Fibre



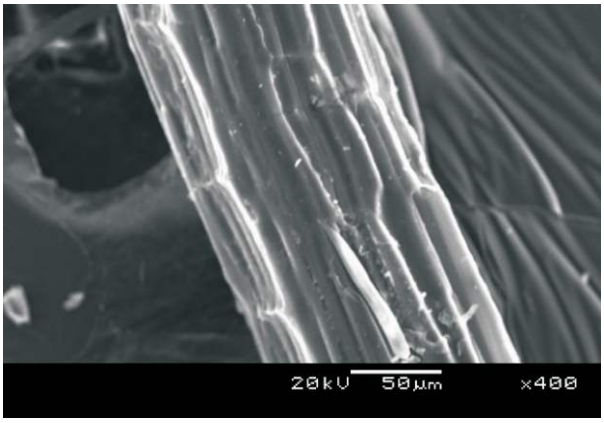
(b) 1 M KOH Treated Sample



© 1 M NaCl Treated Sample



(d) Plate 4. 1 M HCl Treated Sample



(e) 1 M Ethanol Treated Sample

Plates (a-e). SEM of the Untreated and Treated Sisal Fibres.

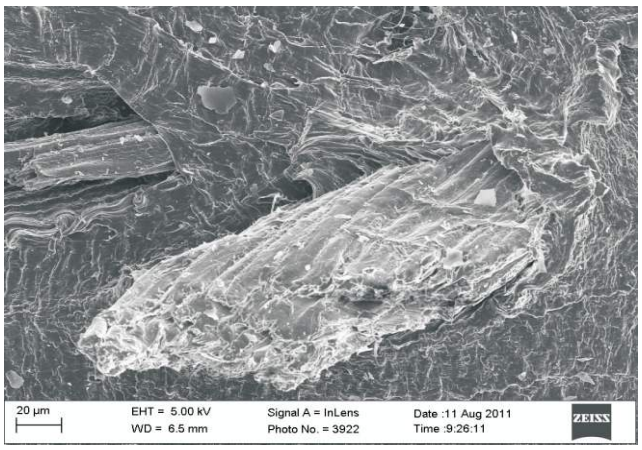


Plate f. SEM of the Fractured of surface of Copolymer Reinforced with Untreated Sisal Fibre

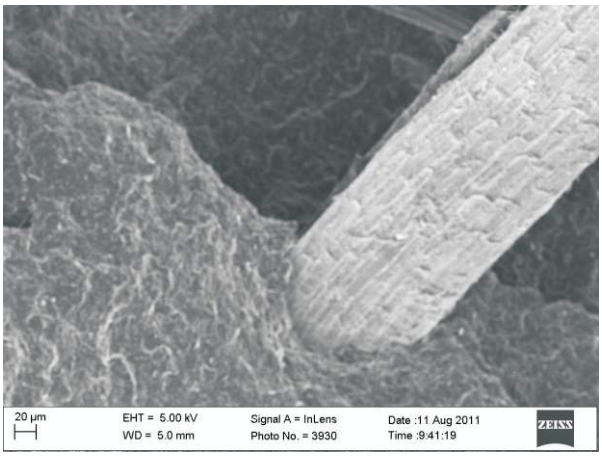


Plate g. SEM of the Fractured of surface of Copolymer Reinforced with Treated Sisal Fibre.

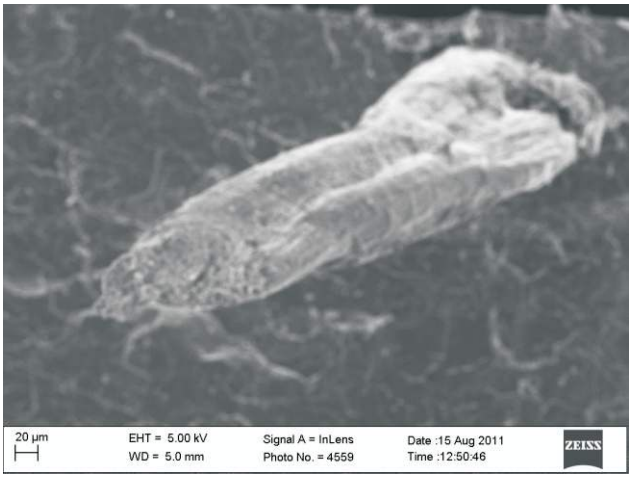


Plate i. SEM of the Fractured of surface of Homopolymer Reinforced with Treated Sisal Fibre.

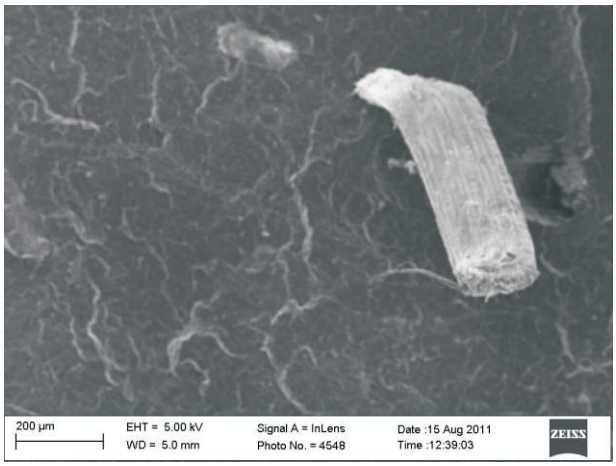


Plate h. SEM of the Fractured of surface of Homopolymer Reinforced with Untreated Sisal Fibre.

MODEL FOR ANALYSIS AND PREDICTION OF ETHANOL PRODUCTION BASED ON TREATMENT TEMPERATURE AND MICROBIAL GROWTH DURING BIODEGRADATION OF SUGAR CANE MOLASSES

C. I. Nwoye*[1], J. U. Odo[1], B. C. Chukwudi[2] and C. N. Mbah[3]
[1]Department of Metallurgical and Materials Engineering, Nnamdi Azikiwe University, Awka.
[2]Department of Mechanical Engineering, Imo State University, Owerri.
[3]Department of Metallurgical and Materials Engineering, Enugu State University of Science & Technology, Enugu.
*Corresponding author: chikeyn@yahoo.com

Abstract

This paper presents a model for analysis and prediction of ethanol yield during biodegradation of sugar cane molasses. The model expressed as;

$$\alpha = 5.4247 \ln\beta - 0.0477\gamma^2 + 2.9656\gamma - 35.8559$$

shows that ethanol produced during the process is principally dependent on the treatment temperature and the growth of microbes attacking the substrate. The computational analysis of results generated indicates that ethanol production per unit temperature rise during the process are 15.3889 and 17.3578% /^{0}C as obtained from experiment and derived model respectively. Similarly, ethanol production per unit growth of microbes are – 0.1847 and – 0.2083 % $(O.D)^{-1}$ as obtained from experiment and derived model respectively. The graphical analysis showing very close alignment of curves from both experimental and model-predicted results, indicate 0.9438 and 0.9902 as the correlations between concentration of ethanol yield and treatment temperature as obtained from experiment and derived model respectively. Similarly, 0.9891 and 0.9894 are the correlations between concentration of ethanol yield and the microbial growth as obtained from experiment and derived model respectively. Statistical analysis of the results indicate that the variance and standard deviation as obtained from experiment and derived model are 8.1440 and 2.8538 as well as 7.4053 and 2.7213 respectively, indicating proximate agreement. Deviational analysis indicates that the maximum deviation of the model-predicted ethanol yield from the corresponding experimental value is less than 12%. The validity of the model was found to be rooted on the expression $0.3372(\alpha + 35.8547) = 1.8292\ln\beta - 0.0161\gamma^2 + \gamma$ where both sides of the expression are correspondingly approximately equal.

Keywords: Model, Analysis, Prediction, Ethanol Production, Sugar Cane Molasses.

Introduction

In recent times, research [1] has shown that biologically produced alcohols, most commonly ethanol, and less commonly propanol and butanol, are used as fuel for energizing vehicles.

The usefulness of ethanol in diversifying energy sources for transportation has lead to studies [2] on micro-organisms such as yeast which has been found to produce alcohol with particular reference to *Saccharomyces cerevisiae*. Ethanol production from molasses using *Saccharomyces cerevisiae* and *Zymomonas mobilis* yeast was found [2] to produce more ethanol at sugar concentration above 15% (v/v), hence ethanol tolerant.

Various studies [3-8] have been put forward on the production of bio-ethanol from several sources, but only a very few research [9-11] studied optimization of ethanol production from sugar cane using yeast cells (*Saccharomyces cerevisiae*). Maximum ethanol production was obtained at a temperature range 28-30°C [17]. This result is in agreement with most previous studies on *Saccharomyces cerevisiae*. Maximum ethanol production using Saccharomyces cerevisiae has also been reported in past researches [9-16] to occur between 48 to 84 hours. Furthermore, a recent report [17] shows that maximum ethanol production was obtained at 30°C, pH 6, 35% sugar cane molasses as fermentation medium, 1% corn steep liquor, 1ml of 1 O.D. YEPD broth and shaking rate at 200 rpm.

During ethanol production, temperature tolerance was found [12] to depend upon the sugar concentration of the medium based on the fact that fermentation of molasses at 35°C was possible when sugar concentration was 20%(w/v), while no fermentation occurs when sugar concentration was 22%(w/v).

It was observed that the concentration of yeast increases with the yield of bio-ethanol up to specific point and then it starts to decrease [16]. Furthermore, increased final ethanol concentration was achieved on adding excess assimilable nitrogen to the batch ethanol fermentations by

Saccharomyces cerevisiae [18].

The validity of any derived model could be established [19] through any one or more of the routes or techniques known as 4th Degree Model Validity Test Technique (4th DMVTT), following the testing of results generated from comparative evaluation between data from experiment and derived model. This is attributed to the fact that the mapping pattern of the associated values gives a persistent level of values congruency, proximity and disparity ones any particular route indicates a degree of validity in relative comparison with experimental data.

The aim of this work is to derive a model for analysis and prediction of ethanol production during biodegradation of sugar cane molasses.

Bioethanol Production Process Analysis

During the process, the solid phase (wastes) was assumed to be stationary, containing some un-reacted sugar cane molasses remaining in the prepared waste. Very high gravity ethanol fermentation [17] was used as screening method. Ethanol was produced by the action of micro organisms (yeast); *Saccharomyces cerevisiae* and enzymes through fermentation of sugars under anaerobic condition.

Materials and Methods

Different concentrations of molasses were prepared as fermentation medium in 250 ml Erlenmeyer flasks, each inoculated with yeast culture, and incubated in a shaking incubator. Details of the experimental procedure and associated process conditions are as stated in the past report[17].

Model Formulation

Experimental data obtained from research work [17] were used for this work. Computational analysis of the experimental data [17] shown in Table 1, gave rise to Table 2 which indicate that;

$$N(\alpha + Cs) \approx S \ln\beta - Ne\ \gamma 2 + \gamma \quad (1)$$

Introducing the values of N, Cs, S, and Ne into equation (1) reduces it to;

$$0.3372(\alpha + 35.8547) = 1.8292 \ln\beta - 0.0161\gamma 2 + \gamma \quad (2)$$

$$0.3372\alpha + 12.0906 = 1.8292 \ln\beta - 0.0161\gamma 2 + \gamma \quad (3)$$

$$0.3372\alpha = 1.8292 \ln\beta - 0.0161\gamma 2 + \gamma - 12.0906 \quad (4)$$

$$\alpha = 1.8292\left[\frac{\ln\beta - 0.0161\gamma^2 + \gamma - 12.0906}{0.3372}\right] \quad (5)$$

$$\alpha = 5.4247 \ln\beta - 0.0477\gamma^2 + 2.9656\gamma - 35.8559 \quad (6)$$

Where

- (β) = Growth of microbes (O.D)
- (α) = Ethanol yield concentration (%)
- N = 0.3372; coefficient of ethanol production (determined using C-NIKBRAN [20]
- (γ) = Treatment temperature (^{0}C)
- N_e = 0.0161; Microbe - substrate interaction factor (determined using C-NIKBRAN [20])
- S = 1.8292; Microbe- ethanol interaction factor (determined using C-NIKBRAN [20])
- C_s =35.8547; Microbial Growth-Temperature relativity (determined using C-NIKBRAN [20])

Different concentrations of molasses were prepared as fermentation medium in 250 ml Erlenmeyer flasks, each inoculated with yeast culture, and incubated in a shaking incubator. Details of the experimental procedure and associated process conditions are as stated in the past report[17].

Boundary and Initial Condition

Consider sugar cane molasses of required consistency (in Erlenmeyer flasks) interacting with microbes *(Saccharomyces cerevisiae)*. The flask's atmosphere is not contaminated i.e (free of unwanted gases, dusts and other micro organisms). Range of microbial growth (measured by Optical Density (O.D.) at wavelength 600 nm) used: 0.80-1.56 (O.D.). Range of treatment temperature used: 25- 40 ^{0}C. Mass of wastes used, resident time, treatment temperature, and other process conditions are as stated in the experimental technique [17].

The boundary conditions are: anaerobic atmosphere to enhance the action *Saccharomyces cerevisiae* on the wastes (since the flask was air-tight closed). At the bottom of the particles, a zero gradient for the gas scalar are assumed and also for the gas phase at the top of the waste particles. The microbial treated waste is stationary. The sides of the waste particles are taken to be symmetries.

Results and Discussion

The derived model is equation (6). The computational analysis of Table 1 gave rise to Table 2

Model Validation

The validity of the model was found to be rooted in equation (2) where both sides of the equation are correspondingly approximately equal. Table 2 also agrees with equation (2) following the values of 0.3372 (α + 35.8547) and 1.8292 $\ln\beta - 0.0161\gamma^2 + \gamma$ evaluated from the experimental results in Table 1. In addition, the derived model was validated by comparing the ethanol yield evaluated by the model and that obtained from the experiment [17]. This was done using the 4th Degree Model Validity Test Techniques (4th DMVTT); computational, graphical, statistical and deviational analysis [19]

Computational Analysis

A computational analysis of the experimental and model-predicted ethanol yield was carried to ascertain the degree of validity of the derived model. This was done by comparing ethanol yield per unit treatment temperature as well as growth of microbe obtained by calculations involving experimental results, and model-predicted results obtained directly from the model.

Ethanol yield per unit temperature rise (E_T % /(^{0}C)) was calculated from the equation;

A plot of ethanol yield against treatment temperature as in Fig. 1 using experimental results in Table 1, gives a slope, S = - 0.1847 % /(^{0}C) on substituting the points (25, 8.17) and (40, 5.4) for (γ_1, α_1) and (γ_2, α_2) respectively into the mathematical expression;

$$E_T = S = \Delta\alpha/\Delta\gamma \qquad (7)$$

which is detailed as

$$S = \alpha_2 - \alpha_1/\ \gamma_2 - \gamma_1 \qquad (8)$$

Where

$\Delta\alpha$ = Change in the ethanol yield α_2, α_1 at two temperature values γ_2, γ_1. This is the ethanol yield per unit temperature during the actual experimental process. Also similar plot (as in Fig. 2) gives a slope S = - 0.2083 % /(^{0}C) using model-predicted results and substituting the associated points (25, 8.3620) and (40, 5.2376) for (γ_1, α_1) and (γ_2, α_2) respectively into equation (8). This is the model-predicted ethanol yield per unit temperature rise during the process. These two values of the ethanol yield per unit temperature rise also indicate proximate agreement.

Ethanol yield per unit growth of microbe E_g (% /O.D) was calculated from the equation;

$$E_g = \alpha/\beta \qquad (9)$$

Therefore, a plot of ethanol yield against microbial growth as in Fig. 3 using experimental results in Table 1, gives a slope, S at points (0.98, 8.17) and (0.8, 5.4) following their substitution into the mathematical expression;

$$E_g = S = \Delta\alpha/\Delta\beta \qquad (10)$$

Equation (10) is detailed as

$$S = \alpha_2 - \alpha_1/\ \beta_2 - \beta_1 \qquad (11)$$

Where

$\Delta\alpha$ = Change in the ethanol yield α_2, α_1 at two growth values of the microbes β_2, β_1. Considering the points (0.98, 8.17) and (0.8, 5.4) for (β_1, α_1) and (β_2, α_2) respectively, and substituting them into equation (11), gives the slope as 15.3889 % (O.D.)$^{-1}$ which is the ethanol yield per unit growth of microbes during the actual experimental process. Also similar plot (as in Fig. 4) using model-predicted results gives a slope. Considering points (0.98, 8.3620) and (0.8, 5.2376) for (β_1, α_1) and (β_2, α_2) respectively and substituting them into equation (11) gives the value of slope, S as 17.3578 % (O.D.)$^{-1}$. This is the model-predicted ethanol yield per unit growth of microbes. A comparison of these two values of the ethanol yield per unit growth of microbes shows proximate agreement and hence validity of the model.

Graphical Analysis

Comparison of ethanol yield per unit temperature rise during the biodegradation process **as obtained from experiment [17]** and derived model the purpose of validity testing is achieved by considering the R^2 values (coefficient of determination). The values of the correlation coefficient, R calculated from the equation;

$$R = \sqrt{R^2} \qquad (12)$$

using the R-squared values (coefficient of determination) from Figs. 1 and 2 show better *correlation; 0.9902 for the derived model than for the experiment [17]; 0.9438 respectively between the ethanol yield and treatment temperature. Similarly,* Figs. 3 and 4 indicate better *correlation; 0.9894 for predicted values (from derived model) than for the experiment [17]; 0.9891 between the ethanol yield and microbial growth respectively.* This is also clear indication that the model predicts accurate and reliable ethanol yield which are in proximate agreement with values from actual the experiment [17], hence confirming the validity of the derived model.

Comparative graphical analysis of Figs. 5 and 6 shows very close alignment of the curves from the experiment (ExD) and model-predicted (MoD) for ethanol yield per unit temperature and growth of microbes respectively. Furthermore, the degree of alignment of these curves is indicative of the proximate agreement between both experimental and model-predicted ethanol yield. This invariably indicates validity of the model.

Statistical Analysis

The model was also validated statistically by comparing the values of the variance and standard deviation evaluated from experimental and model-predicted data. The variance V is given by

$$V = \frac{\sum(x - x_a)^2}{\sum n} \quad [21] \qquad (13)$$

Furthermore, standard deviation is given by

$$SD = [V]^{1/2} \quad [21] \qquad (14)$$

Substituting equation (13) into equation (14) reduces it to;

$$SD = \sum\left(\frac{(x - x_a)^2}{\sum n}\right)^{1/2} \qquad (15)$$

$$x_a = x_1\left(\frac{+ x_2 + x_3 + x_{4..}}{\sum n}\right) \qquad (16)$$

Where
SD = Standard deviation
V = Variance
x = Variables representing ethanol yield
xa = Arithmetic mean (evaluated as average ethanol yield using experimental data, [17] and model-predicted data
n = Number of samples

Standard deviation and variance as obtained from experiment [17]

Substituting the values of $\sum n$ and $\sum (x-xa)2$ from Table 3 into equations (13) and (15), where xa = 9.788 (as calculated from equation (16)) gives variance and standard deviation as 8.1440 and 2.8538 respectively.

Standard deviation and variance as predicted by derived model

Also substituting the values of $\sum n$ and $\sum (x-xa)2$ from Table 4 into equations (13) and (15), where xa = 9.8163 (as calculated from equation (16)) gives variance and standard deviation as 7.4053 and 2.7213 respectively. The proximity of values of the standard deviation and variance (Table 5) as obtained from experiment [17] and derived model indicates agreement and validity for the model.

Deviational Analysis

Comparative analysis of ethanol yield from experiment [17] and derived model revealed insignificant deviations on the part of the model-predicted values relative to values obtained from the experiment. This is attributed to the fact that the surface properties of the waste material and the physiochemical interactions between the waste material and the microbes (under the influence of the treatment temperature) which were found to have played vital roles during the process [17] were not considered during the model formulation. This necessitated the introduction of correction factor, to bring the model-predicted ethanol yield to those of the corresponding experimental values.

Deviation (Dv) of model-predicted ethanol yield from that of the experiment [17] is given by

$$Dv = \frac{Mv - Ev}{Ev} \times 100 \qquad (17)$$

Correction factor (Cr) is the negative of the deviation i.e

$$Cr = -Dv \qquad (18)$$

Therefore

$$Cr = -\left(\frac{Mv - Ev}{Ev} \times 100\right) \qquad (19)$$

Where
Mv = Model-predicted ethanol yield (%)
Ev = Ethanol yield from obtained from experiment (%)
Cr = Correction factor (%)
Dv = Deviation (%)

Introduction of the corresponding values of Cr from equation (18) into the model gives exactly the corresponding experimental ethanol yield.

Comparative analysis of Figs. 7-9 show that the maximum deviation of the mode-predicted ethanol yield from the corresponding experimental values is less than 12% and quite within the acceptable deviation limit of experimental results. These figures show that least and highest magnitudes of deviation of the model-predicted ethanol yield (from the corresponding experimental values) are +2.35 and +11.40 % which corresponds to ethanol yields: 8.3620 and 10.7613 %, treatment temperature 25 and 35 as well as microbial growth: 0.98 and 1.26 (O.D.) respectively.

Analysis of Figs. 7-12 indicates that the orientation of the curve in Figs. 10-12 is opposite those of the deviation of model-predicted ethanol yield in Figs. 7-9. This is because correction factor is the negative of the deviation as shown in equations (17) and (18). It is believed that the correction factor takes care of the effects of the surface properties of the waste material and the physiochemical interaction between the waste material and the microbes which (affected experimental results) were not considered during the model formulation. Figs. 10-12 indicate that the least and highest magnitudes of correction factor to the model-predicted ethanol yield are -2.35 and -11.40 % which also corresponds to ethanol yields: 8.3620 and 10.7613 %, treatment temperature 25 and 35 as well as microbial growth: 0.98 and 1.26 (O.D.) respectively.

It is also important to state that the signs preceding the values of deviation and correction factors only signify deficit or surplus. The actual values are the magnitudes.

Conclusion

The model gives an analysis and prediction of the ethanol yield based on the treatment temperature and microbial growth during the biodegradation of sugar cane molasses. The ethanol productions per unit temperature rise during the process are 15.3889 and 17.3578% / 0C as obtained from experiment and derived model respectively. Similarly, ethanol productions per unit growth of microbes are – 0.1847 and – 0.2083 % (O.D)-1 as obtained from experiment and derived model respectively. The graphical analysis showing very close alignment of curves from both experimental and model-predicted results, indicate 0.9438 and 0.9902 as the correlations between concentration of ethanol yield and treatment temperature as obtained from experiment and derived model respectively. Similarly, 0.9891 and 0.9894 are the correlations between concentration of ethanol yield and the microbial growth as obtained from experiment and derived model respectively. Statistical analysis of the results indicate that the variance and

standard deviation as obtained from experiment and derived model are 8.1440 and 2.8538 as well as 7.4053 and 2.7213 respectively, indicating proximate agreement. Deviational analysis indicates that the maximum deviation of the model-predicted ethanol yield from the corresponding experimental value is less than 12%. The validity of the model was found to be rooted on the expression $0.3372\ (\alpha + 35.8547) = 1.8292\ \ln \beta - 0.0161\ \gamma 2 + \gamma$ where both sides of the expression are correspondingly approximately equal.

References

[1] Onuoha, C. (2008). Biofuel Energy, Federal University of Technology, Owerri, Nigeria, Term Paper, 12-34.

[2]Mike, K., and Kevin, K., (2006). Specific yeasts developed for modern ethanol production. Sugar industry, 131: 753-758.

[3]Dale, B. E, (1987). Lignocellulose conversion and the future of fermentation biotechnology. TIBTECH, 5: 287-291.

[4]Ferrari, M. D., Neirotti, E., Albornoz, C., and Saucedo, E., (1992). Ethanol production from eucalyptus wood hemicellulose hydrolysis by Pichia stipitis. Biotechnol. Bioeng, 40: 753-759.

[5]Nigam, J. N. (1999). Continuous ethanol production from pineapple cannery waste. J. of Biotechnol, 72: 197-202.

[6]Olsson, L., and Hahn, H. B. (1996). Fermentation of lignocellulosic hydrolysis's for ethanol production. Enzyme Microb. Technol, 18: 312-331.

[7]Beatriz, P. A., Mats, G., and Guido, Z. (2005). Pretreatment of barley husk for bio-ethanol production. J. of Chemical Technology and Biotechnology, 80: 85-91.

[8]Martin, C., Lopez, Y., Plasencia, Y., and Hernandez., (2006). Characterization of agricultural and agro-industrial residues as raw materials for ethanol production. Chem.Biochem.Eng, 20 (4): 443-447.

[9]Doelle, H. W., and Greenfield, P .F. (1985). The production of ethanol from sucrose using zymomonas mobilis. Appl. Microbial. Biotecnol, 22: 405-410.

[10]Huertaz, D. H., Cacho, C. L., and Bernard, L. (1991). Fermentation of sugarcane juice and blackstrap molasses by zymomonas mobilis. J. Agric. Univ.P.R, 75(1): 43-50.

[11]De Vasconcelos, J. N., Lopes, C. E., and de França, F. P. (1998). Yeast immobilization on cane stalks for fermentation. International Sugar J, 100(1190): 73-75.

[12]Morimura, S, Ling, Z. Y. and Kida, K. (1997). Ethanol production by repeated batch fermentation at high temperature in a molasses medium containing a high concentration of total sugar by thermotolerant flocculating yeast with improved salt tolerance. J Ferment Bioeng, 83: 271-274.

[13]Agrawal, P. K., Kumar, S., and Kumar, S. (1998). Studies on alcohol production from sugarcane juice, sugarcane molasses, sugarbeet juice and sugarbeet molasses, Saccharomyces cerevisiae NSI-113. Proceedings of the 60th Annual Convention of the Sugar Technologists Association of India, Shimla, India.

[14]Kadambini, G. (2006). Process optimization for the production of ethanol via fermentation. Department of biotechnology and environmental sciences, Thapar institute of Eng & Technology (Deemed University).

[15]Brooks, A. A. (2008). Ethanol production potential of local yeast strains isolated from ripe banana peels. African Journal of Biotechnology, 7 (20): 3749-3752.

[16]Sivakumar, V., Shanmugam, P., Sridhar, R., and Venkatesan, S. (2010). Production of Bio-ethanol from Sugar Molasses Using Saccharomyces Cerevisiae. Modern applied science 3(8): 32-37.

[17]Osman, M. E., Khattab, O. H., Hammad, I. A., El-Hussieny, N. I. (2011).Optimization of Bio-Fuel Production by Saccharomyces cerevisiae Isolated from Sugar Cane Bagasse. Journal of American Science 2011;7(5):485-492.

[18]Petra, B., Daniela, S., Iveta, S., Jaroslava, P., and Zoltan, D. (1999). Improvement of very high gravity ethanol fermentation by media supplementation using Saccharomyces cerevisiae. Biotechnology Letters, 21: 337–341.

[19]Nwoye, C. I., Onyedika. G. O., and Ugwuegbu, C. C. Model Development for the Prediction of Methane Gas Yield during Microbial Treatment of Fruit Wastes. JMME (in press)

[20]Nwoye, C. I. (2008). Data Analytical Memory; C-NIKBRAN

[21]Nwosu, K. H. (1992). Advanced Statistical Analysis, AJEK Publishers, Enugu, 34-38.

Table 1: Variation of ethanol yield concentration with inoculum size and microbial growth [17]

(α)	(γ)	(β)
8.17	25	0.98
12.76	28	1.54
12.95	30	1.56
9.66	35	1.26
5.4	40	0.80

Table 2: Variation of 0.3372(α + 35.8547) with 1.8289 ln β - 0.0161 γ2 + γ

0.3372(α +35.8547)	1.8289 ln β - 0.0161 γ^2
14.8451	+ γ 14.9006
16.3929	16.1673
16.4569	16.3233
15.3476	15.7002
13.9111	13.8319

Table 3: Variation of (x-xa) with (x-xa)2

Table 4: Variation of (x -xa) with (x -xa)^2

n (Mod)	$(x-x_a)$	(x
1	-1.4543	2.1150
1	2.3101	5.3366
1	2.7780	7.7173
1	0.9450	0.8930
1	-4.5787	20.9645

? n = 5 ? $(x-x_a)^2$ = 37.0264

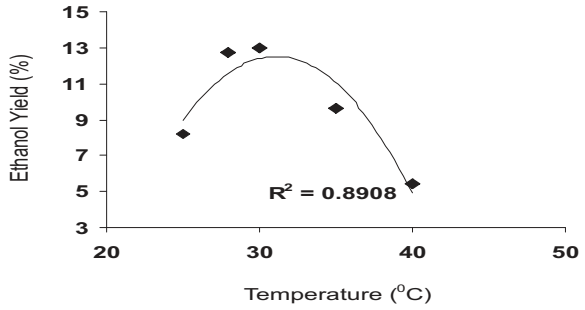


Fig. 1: Coefficient of determination between concentration of ethanol yield and treatment temperature as obtained from the experiment [17].

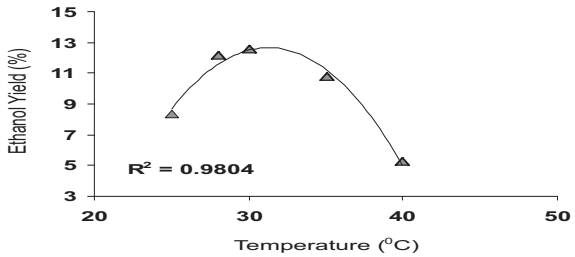


Fig. 2: Coefficient of determination between concentration of ethanol yield and treatment temperature as evaluated by derived model

	Experiment [17]	Model
SD	2.8538	2.7213
V	8.1440	7.4053

n (Exp)	$(x-x_a)$	$(x-x_a)^2$
1	-1.6180	2.6179
1	2.9720	8.8328
1	3.1620	9.9982
1	-0.1280	0.0164
1	-4.3880	16.2545

∑n = 5 ∑(x-xa)2 = 37.7198

Table 5: Comparison of standard deviation (SD) and variance (V) from experimenta l and model-predicted results

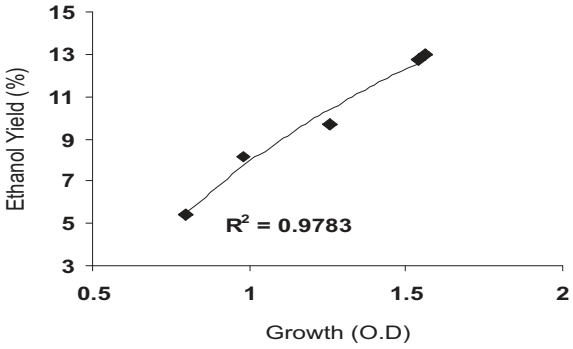


Fig. 3: Coefficient of determination between concentration of ethanol yield and microbial growth as obtained from the experiment [17].

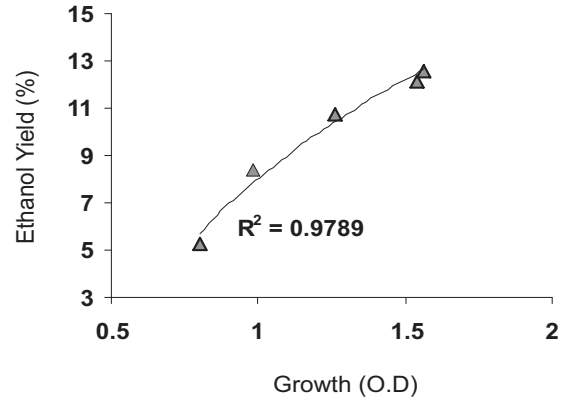


Fig. 4: Coefficient of determination between concentration of ethanol yield and microbial growth as evaluated by derived model

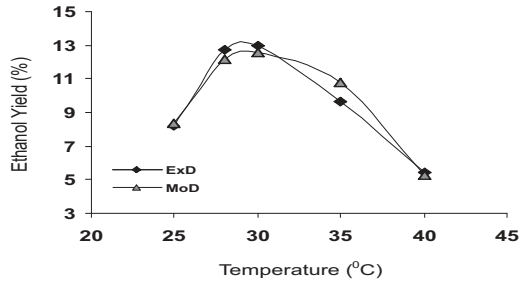


Fig. 5: Comparison of the ethanol yield per unit treatment temperature as obtained from experiment [17] and derived model.

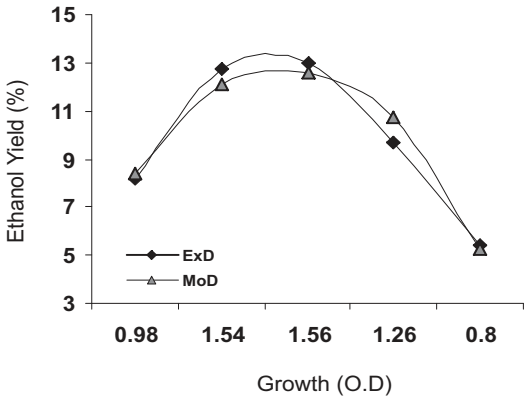


Fig. 6: Comparison of the ethanol yield per unit growth of microbes as obtained from experiment [17] and derived model.

Fig. 8: Variation of deviation (of model-predicted ethanol yield) with treatment temperature

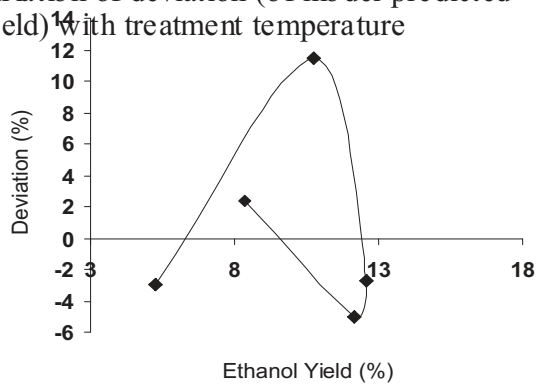


Fig. 7: Variation of model-predicted ethanol yield with its associated deviation from experimental values

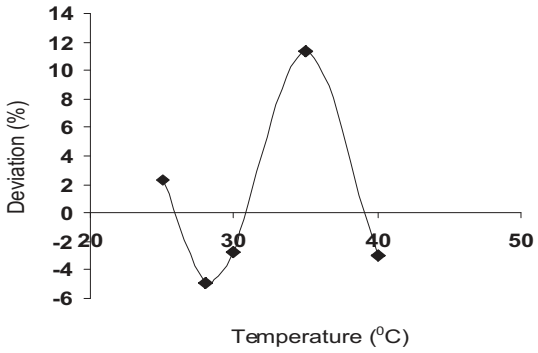


Fig. 8: Variation of deviation (of model-predicted ethanol yield) with treatment temperature

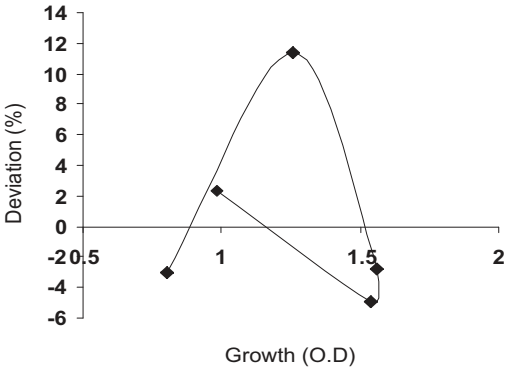


Fig. 9: Variation of deviation (of model-predicted ethanol yield) with microbial growth

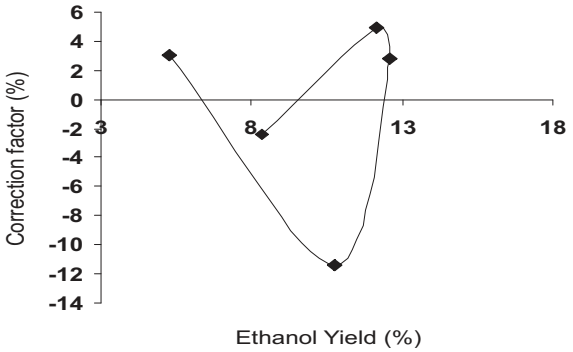


Fig. 10: Variation of correction factor (to model-predicted ethanol yield) with ethanol yield

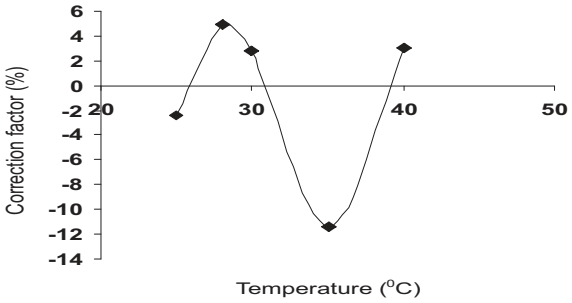


Fig. 11: Variation of correction factor (to model-predicted ethanol yield) with treatment temperature

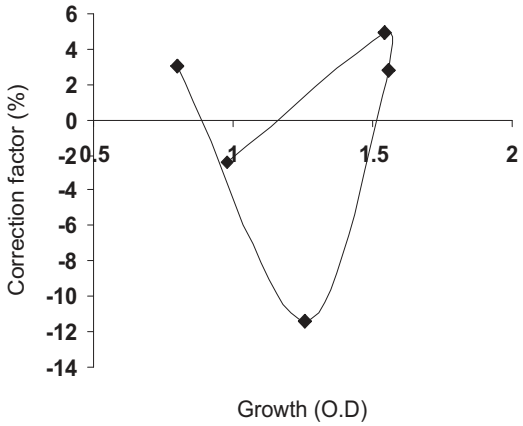


Fig. 12: Variation of correction factor (to model-predicted ethanol yield) with microbial growth

VIRTUAL REALITY AS A TOOL FOR REDUCING ROAD DESIGN/CONSTRUCTION COST

Laseinde, O. T.1 and Adejuyigbe, S.B.2
1,2Mechanical Engineering Department, College of Engineering, FUNAAB, Abeokuta
1famefresh@gmail.com

Abstract
A large fraction of the country's annual budget is expended on Road infrastructure of which a huge sum goes to modifications, maintenance, repairs and reconstruction caused by design flaws preventable by a thorough application of engineering approaches such as Virtual Reality. Virtual Reality (VR) refers to a technology which is capable of shifting a subject into a different environment without physically moving it. To this end, the perceived environment is associated with the desired Virtual Environment and not with the physical one.The paper evaluates the use of VR for effective roadway and drainage designs. It assessed possible traffic and unforeseen road activities caused by climate changes, human factors, past project history and other factors which are sometimes not factored into the original design of roads. Finite analysis method was used in developing a dynamic 3-Dimensional road framework using a VR platform useful for evaluating detailed structure of roadways and its environment. It further evaluated internationally accepted best practices which proactively checkmate design flaws, hence reducing cost of road maintenance. The study concluded with recommendations as a panacea to cutting down road construction cost.

Keywords: Virtual Reality, Road design, Construction, Road Cost

INTRODUCTION

Nigeria is one of the largest countries in Africa with the widest expanse of road network; the high level of population plying these roads presents certain challenges for its transportation system [2]. In a nationwide survey conducted by the Federal Ministry of Works on Trunk 'A' roads [5], the report showed vast dilapidation and it concluded that the state of Nigerian roads has remained poor for a number of reasons that include; faulty designs, poor drainage, poor funding, excessive traffic loading and inadequate roadway maintenance.

There are several reasons identified as causes of road problems but this paper focuses more on the common design errors which often end up in a total redesign of roads, drainages and bridges.

Huge sums of money have been sunk into road development in Nigeria within the past ten years. The road network is currently estimated at about 194,000 kilometres, with the Federal Government being responsible for about 17 percent, State Governments 16 percent and local Governments 67 percent [4]. However, these roads have been plagued by a number of problems, with the major ones being faulty designs, inadequate drainage system and poor maintenance culture, which have significantly reduced the utility of the roads. There are potholes, washing away of pavements and fallen bridges along most Nigerian roads. As stated by the Federal Ministry of Works & Housing, the annual loss due to bad roads is valued at N80 billion, while additional vehicle operating cost resulting from bad roads is valued at N53.8 billion, bringing the total loss per annum to N133.8 billion. This figure does not take into account the man-hour losses in traffic due to bad roads and other emotional and physical trauma experienced by road users and the colossal loss in productivity. Road maintenance falls primary into 4 categories namely: routine, recurrent, Periodic and emergency/special maintenance [1]. The general observation within the last 15 years shows that Billions of Naira is continually being budgeted for emergency/special repairs. Using a cause-effect approach, we observed that one major reason for this situation is the poor design approved and implemented in the construction of the roads in the past. To that effect, much funds is continually expended to manage a situation which should actually undergo a thorough revamp/redesign.

The need to provide a proper road system had long been recognized by governments, especially as a means of ensuring reasonable contacts within and between human settlements, as well as providing the channels for the evacuation of produce, so as to boost external trade [4]. Consequently, it has been suggested that in the face of dwindling funds, consideration should be given to appropriate and relevant costs saving road designs. Kent [6] identified three distinct stages in road development levels as; 1- provision of access; 2- provision of additional capacity; and 3-increase of operational efficiency. It was asserted that developing countries will not usually be at stage three; indeed most will be at the first stage with stage three design standards often leading to uneconomical and technically inappropriate designs.

Hence, in the situation of these types of circumstances, road developers/maintaining agents should adopt cheaper means of design evaluation for construction and maintenance of these vast infrastructures across the

country. One of such easily adaptable engineering options is Virtual Reality, a field under Artificial Intelligence (AI). This approach helps to quickly evaluate, project and forecast possible challenges which may emerge due to poor designs. It is also useful for formulating better road designs and effective drainage system using turbulence analysis of the worst possible envisaged condition of hydro flow along various drainage portions in order to avoid erosion and future road damages.

LITERATURE REVIEW

Road designs are achieved by the use of a variety of Computer Aided Design applications. The list of such cannot be exhausted as several applications utilized by designers cuts across the need of various project, the design approach of each firm and the desired means of interpretation of each design concept.

The growing and ever increasing capability of design applications has made it possible to virtually determine a lot of details as regard road development. Such details include: road life span, erosion prone spots based on the design, effect of bend and road features on automobiles/drivers, possible accident prone areas, turbulence/hydro flow analysis based on water level/weather conditions and previous statistics and Several other details to mention but a few.

For the Government to get the best value for its money spent on roads, it should keep abreast with current technologies. These design evaluation/validation techniques are often neglected by even some established construction firms hence, leading to a breakdown in road infrastructures within a short time. This paper do not focus on material used for road construction, rather emphasis is purely on the design/construction methodology.

METHODOLOGY

Effective roadways void of design errors can be achieved through some of the commercial road design applications available. Road designing has gone far beyond the conventional use of 2 Dimensional (2D) applications to 3D applications. Road analysis and testing can be achieved using these 3D platforms. One of such viable and effective application is Civil Visualization 3D, a commercial software by Autodesk which cost far below many of the proprietary road design software's available. We were able to test some existing roads using this application. A case study was carried out on a major driveway of the University of Agric Abeokuta (Ceremonial road) using 3D Visualization (AutoCAD Civil 3D 2011) in combination with a hydro flow analyzing software called Gambit. We desired to build a 3D world using Virtual Reality. A world we can walk/drive through, alter and manipulate as desired.

We commenced by capturing the plan view of the campus using Google map as shown in Figure 1 below.



Fig1: Google map satellite view of the campus using auto measuring tool.

We utilized the free map system available to public viewers because the research was mainly for findings and not advanced situations such as defense and security. The map was plotted electronically to get the precise road details. These approach eliminated the time and energy involved in measuring each individual feature along the road though for validation purpose, measurement can be physically taken. We designed the straight sections of the road using finite element modeling approach and went further to design the road bends using the corridor model, a method used for achieving smooth bends in 3D civilization as shown in figure2 below.

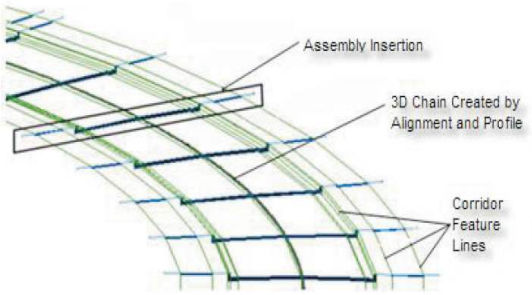


Figure2: A 3D Chain represents an alignment and profile which control the horizontal and vertical aspects of the road

Corridors are arguably the most powerful and sophisticated objects in AutoCAD Civil 3D 2011. To create a corridor, an alignment, profile, and assembly are combined to form a 3-Dimensional representation of a linear feature such as a road or channel.

Together the alignment and profile create a 3D Chain (Figure3) with the alignment providing the horizontal aspect (x and y) and the profile providing the vertical aspect (z/elevation). The assembly, which represents the cross-sectional shape of the road, is inserted along this 3D path at user-specified increments. Similar points on the assembly insertions are connected using corridor feature lines—establishing the edges of the 3D model in the longitudinal direction. The corridor model served as the "backbone" of the design and from it many useful forms of information were derived. For example, surfaces can be derived from the corridor representing finished ground or any number of underlying surfaces.

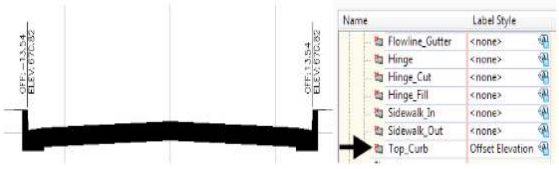


Figure 3: This example shows Top_Curb codes being used to label cross sections. Offsets and elevations are automatically derived from the corridor model and conform to company or jurisdictional as sidewalks, curb, and lanes.

We further designed a replica of the road using another software application by the same company, 3Dstudio max. On completing the road designs, we designed all the road elements along the road namely: speed humps, road signs, road divider, road markings, drainage system, horticultural features and general street lighting systems. All these elements were designed from concept using the aforementioned applications. We were able to achieve a model which took care of the material used for surfacing the road from the sand, lateral to the final coal tar surface. Details are shown in figure 3. We then designed a car using a 3rd party plug-in which we used to test the effect of the road features on the driver and passengers when approaching bends and speed humps at various speeds. We further tried to validate the accuracy of the speed humps across the road by evaluating the effective braking distance to zero as shown in Table2.
Other road features such as the light illumination were also determined across the road. The results from the real source were also compared with the simulated data using Virtual Reality. Further analyses carried out are not within the scope of this discussion.

4. RESULTS

Table 1: Dimensions of road elements along UNAAB Ceremonial road as evaluated from the developed VR model

S/No	Data Description	Result (Metres)
1	Distance between the campus gate & the end of Ceremonial road	1,330
2	Width of road	7.133
3	Drainage depth	0.79
4	Drainage width	0.66
5	Drainage side walls	0.15
6	Average size of orifice channelling water off the road to drainage	0.15
7	Average distance of trees from drainage	5.5
8	Average space interval between road middle markings	5.89
9	Road markings width (Broken lines)	0.14
10	Road markings length (Broken lines)	2.79
11	Average space between street light poles	30.94
12	Space of divider between entry and exit roads	5.334 (17.5ft)
13	Depth of central drainage sump	3.048 (10ft)
14	Speed hump length	7 (22.97ft)
15	Speed hump width	0.406 (16")
16	Speed hump height	0.0635 (2.5")

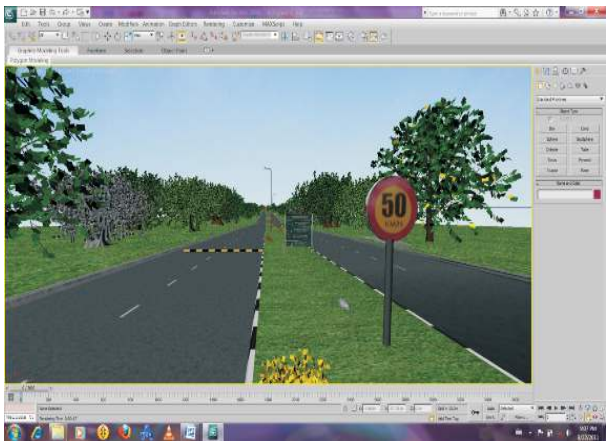


Figure 4.a: 3D scene showing road sign



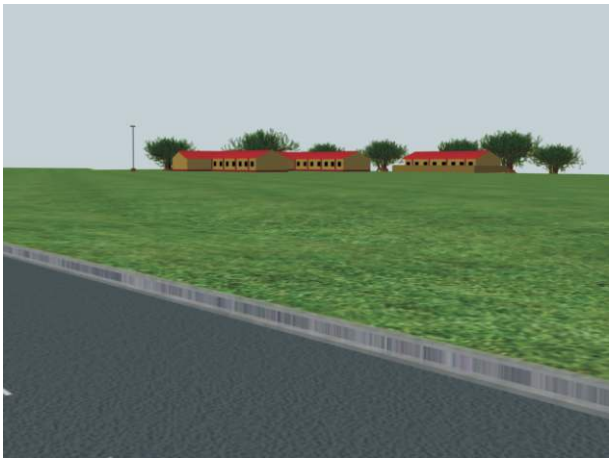
4b: Scene showing road side board



4c: scene focused on road divider



4d: drainage system



e: buildings beside the road/land topography

Table 2: Times and Distances for barking to zero from various speeds

Hump arrangement within UNAAB Ceremonial road(driving into campus)	Starting Speed (Km/h)	Top Speed (km/h)	Top Speed (m/s)	Time to brake (sec)	(X) Distance to brake (m)
1st-2nd hump	0	40	11.11	9	18.9
2nd-3rd hump	5	50	13.89	12	22.69
3rd-4th hump	10	35	9.72	8	13.76
4th-5th hump	15	45	12.50	11	16.50

Times and Distances for barking to zero from various speeds with little impact on the driver and passengers when the simulated car weighing (1,850kg) is loaded with an additional 300kg assumed to be equally spread on all part of the car shock. It is assumed that the car is moving at a constant speed when the signage is identified and an average braking deceleration of $2m/s^{2}$. these was achieved through the use of the timeline functionality of 3Ds max.

The effective breaking distance x was calculated,

Using $x = vt - \frac{1}{2}at^2$ Where a=deceleration and V=velocity

DISCUSSION

From the design, we were able to identify various portions within the road way which had the possibility of retaining water. The prototype design is dynamic in nature hence; we can easily alter parameters in order to evaluate better options to the original model. The developed model is in 3D hence, we walked and drove through with the sense of actually being on the road. Based on our results from the application of Gambit software (hydro flow analysis), neglecting other environmental factors, we realized that considering the terrain features, the specified drainage depth/height spanning over a distance of 1kilometer can effectively retain over 40,000 cubic m of water in event of the blockage of the water exit channel. This in clear terms explains that it will take quite some hours of continuous heavy rains before experiencing flooding of the tarred road. Based on this evaluation using the fluent analysis embedded within Gambit software, flooding may not be a possible threat to the road.

We went further to examine the elevation data of the road in order to identify possible terrain features which may lead to the road being eroded from its edges. Using Google map, we were able to acquire some of the elevation data needed thereby eliminating the high cost of manual measurement in the preliminary stage of the research hence, terrain visualization through these approach cannot be ignored in road design. Real time data obtainable from the paid platform can drastically cut down the time and resources expended for terrain study in the preliminary stage of road projects. Table 1 shows some of the data captured using this approach.

The required quantity of materials for various portions of the road was also determined from the corridor model used. Poor bill of quantity/need evaluation is a major factor which leads to inconsistent quotation in road projects. With the application of this 3D VR model, it becomes possible to visualize and calculate in details the cost of various elements within the road way. Since we designed the various road elements using finite portions, achieving exact quantity and cost of material becomes possible once the unit cost of a miniaturized fragment of the materials are known.

A road cannot be complete until all the road features are put in place. We carried out a comprehensive road marking as shown in Fig. (4a-b). with this prototype, a comprehensive detail of how to go about marking the road is achieved. The appropriate type and appropriate position for placing the signage's/road humps reduces the cost of manual evaluation of the road. Using VR, all these can be achieved in the comfort of the design room hence, project execution becomes relatively easy. Using the cause-effect approach, we determined the bases for the placement of various objects along the Ceremonial road as shown in Figure 4 (a-e). We determined the accuracy of the driving speed set using data from our VR prototype as shown in Table2. These approach eliminated the cost of physically carrying out tests to determine suitable speed limits.

CONCLUSION

Putting all these measures together, the total cost of designing, constructing and maintaining roads may be reduce drastically based on finite details achieved using Virtual Reality. A relatively cheaper means of achieving cost estimates have been discussed therefore, agencies saddled with the responsibilities of road project management, monitoring and evaluation should explore some of these modern techniques of evaluating terrain visualization and road construction prototyping.

REFERENCES.

[1] Beesley, M.E (1973).Urban Transport: Studies in Economic Policy"

[2] *Ben-Edigbe, J.E. (2005). Influence of Pavement Distress on Roadway Capacity PhD Thesis 1998-2002 University of Strathclyde Library, Glasgow UK*

[3] *Ben-Edigbe, J.E.* **(2010). Bituminous Low Cost Road Initiatives: How Effective?** European Journal of Scientific Research
I SSN 1450-216X Vol.40 No.1 (2010), pp.115 - 124 © EuroJournals Publishing, Inc. 2010
http://www.eurojournals.com/ejsr.htm

[4] CBN (2002). The 11th Annual Conference of Zonal Research Units, June 2002 by the Research Department on Infrastructure Development and Economic Growth in Nigeria.

[5] *Federal Ministry of Works and Housing (FMWH)(1998). National Road Network Assessment for Maintenance Road Maintenance Draft Document, FMWH, Abuja FCT-Nigeria*

[6] Kent, F.J. (1995) .Highway and Traffic Engineering in Developing Countries, Edited by Bent Thangesen. Published by E and FN Spon, London

APPLICATION OF VIRTUAL REALITY (VR) FOR THE PRODUCTION OF SPUR GEARS

Laseinde, O. T.[1] and Adejuyigbe, S.B.[2]
[1,2]Mechanical Engineering Department, College of Engineering, FUNAAB, Abeokuta
[1]famefresh@gmail.com

Abstract
This paper attempts to present the research findings of a study into the production of plastic spur gears using Virtual Reality (VR). It is aimed at developing a functional model and further validating the model for the production of plastic spur gears. Also, it aims at developing Virtual Reality architecture capable of depicting a real life production process of plastic spur gears.
The result obtained shows the construction, modeling and rendering of a complete plastic spur gear manufacturing process. This was achieved using AutoCAD, 3D Studio max, macromedia flash and Q-basic. The results obtained were revalidated by comparing them with manually computed once and the result showed a higher level of accuracy and a faster speed of computation.
In conclusion, Virtual Reality can be applied as a useful teaching tool for the improvement of engineering learning processes especially in areas with limited access to required learning infrastructure.

Keywords: ***Production, Spur Gear, Virtual Reality, CAD, CAM, Plastic mould***

INTRODUCTION

The amazing development in Computer Aided Designing (CAD) within the last three decades has opened up totally new and challenging research areas.
Virtual Reality (VR) has been defined in so many different ways by various authors but summarily, it is seen as the act of simulating a real life event. It is generally agreed that the essence of VR lies with computer-based three-dimensional (3D) environments. Often termed 'worlds', they represent real-world or conceptual environments that can be navigated through, interacted with and updated in real-time. VR is an artificial intelligence tool otherwise called Artificial Reality or Virtual Environment. It involves manipulation of objects using sensor data and real time control.
Another probably more easily understood definition is that VR is a computer generated simulation of a real or imaginary environment (world) with which the user can interact and manipulate [1].
This world may be a CAD model, a scientific simulation or a view into a data base. The user can interact with the world and directly manipulate object within the world. The applications being developed for VR run a wide spectrum, from games to building and business planning. Many applications are worlds that are very similar to our own, like CAD or architectural modeling. Some applications provide ways of viewing from an advantageous perspective not possible with the real world, like scientific simulators, telepresence systems and air traffic control systems [8].
Interaction with the virtual, at least with near real time control of the view point is a critical test for a Virtual Reality. Therefore the specific objective of the research is to develop a design model which can be used for the production of plastic spur gear using input data control.

LITERATURE

VR is a major aspect amongst the five subdivisions of Artificial Intelligence (AI). They are all interrelated depending on their area of application. Virtual Reality can be divided into two basic types - Text based and graphical based. Text based virtual environment are created by two or more networked users in Multi User Domains (MUD) over the internet.
In general, people are more familiar with graphics based Virtual Reality. In graphics-based systems, the virtual environment is created to visually simulate a real or imaginary world. Technically, this environment can be either Two-Dimensional (2D) or Three Dimensional (3D); however 3D environments are more immersive, they are used more frequently to create virtual worlds. These world may either be partially (Semi) immersive or fully immersive.

Head mounted displays, data gloves, special rooms and other devices can be used with graphics-based environments to make them completely immersive giving the users a sense of actually being inside the virtual world. However, these devices are expensive, cumbersome and uncomfortable. The most widely used form of Virtual Reality in use today is desk-top Virtual Reality. In these systems Virtual Reality worlds run on users' desk-top computers and are displayed on a standard monitor and navigated using a mouse or 3-D Space ball with a keyboard.

Most virtual environments meant to be experienced by both general public are presented through the user's computer monitor [4].
It is evident from so many reports however that there has been an early realization of the advantage a simulated graphics work can present but getting it on the format seen and felt had rather been difficult .

RESEARCH DEFINITION

An analysis of the user requirements of the VR application to be developed.

A definition of the objects, textures, animations and sounds that will make up the world
Documentation for the design of the model and how it works within the chosen system
A definition of the platforms which the world will run on
Determining how to develop the software suitable for gear calculations.

ABOUT PLASTIC SPUR GEAR

There are many common applications of VR. They fall into the main categories of training, education, conceptual navigation, simulation, visualization, concept design and entertainment but there is much overlap between these categories. The research aimed at developing a computer generated gear design model which will help the gear moulder by effectively cutting down the time and improve accuracy in the production of plastic gears.
Practically, everything needed to make gears turns up from standard pressure angles to uniform tooth shapes have been handled and can be bought off the shelf. The science of plastic gearing is still in its infancy. Making plastic gears required a willingness to let slip the time tested principles of cutting gears out of metal. Plastic gears can melt at temperatures where metal hardly sweats but plastics gear can also run dry without lubricants .They can be molded in unusual shapes and large enough lots, inexpensively.
Despite many advances in plastics gear technology, users of metal gear haven't begun trading in all their current lots for plastic version. That's not to say making plastics gear is any small matter. The main concern in molding them is that they'll shrink upon cooling, throwing off any chance of obtaining accurate geometry in the final form.
According to Koller et al.[5], direct gear design works ideally for plastic gears because it provides total design flexibility that is not achievable using the traditional gear designing techniques. Direct gear design compensates plastic low strength to the bending stresses, reducing the bending stress concentration, minimizing and balancing specific sliding velocities resulting in maximum efficiency and minimum heat generation.
A big road block to producing a precise plastic gear is the distortion from shrinkage as experienced during the injection molding process. The distortions results in an inconsistent gear tooth profile and low gear accuracy. The generic molding solution cavity correction method was developed for producing the high precision molded gear.
Today's molders go through a number of tool cavity corrections until they get it right just to obtained a high precision part. The shape of a molded part is the result of a combination of factors including the tool geometry, material properties, molding process parameter to mention but a few. These factors are the genetic molding blue print of a part, much like Deoxyribo-Nucleic Acid (DNA); in the genetic blue print of living organism, Genetic molding solution technology is based on the mathematical prediction software which defines the transformation functions between initials cavity profile and the resulting part profile. These methods do not depend on plastic material properties, part shape or molding process parameters. This technology allows going from initial tooling cavity to final tooling cavity in one straight process explained by the software developed. These tools actually deliver:

- Corrected tool cavity geometry for the high precision plastic parts.
- Eliminates the expense of repetitive cavity correction.
- Cuts process development and delivery time.
- Increase precision of molded parts.

BUILDING THE MODEL

The first phase in a successful Virtual Reality project is deciding whether it is in fact the best option to achieving research aims and Objectives. Virtual Reality may not be suitable if the target audience do not have access to the technology needed to view it or lacks the computer skills necessary to manipulate the model. Hence, a well-planned, well-documented and detailed work plan was put in place towards achieving a well-executed VR world [3].

The basic application process was broken down into an Input Processor, a Simulation Process, a Rendering Process, and a World Database. The time required for processing was carefully put into consideration since every delay in response time degrades the feeling of 'presence' and reality of the simulation [7].
The following high level applications were adopted: AutoCAD/Pro Engineer; 3D-Max; Macromedia flash and Q-Basic.
The process design was drafted out using AutoCAD in conjunction with 3D-Studio max. Macromedia flash and Q-Basic were utilized for the final gear parameter calculator.
To start with, Q-Basic was employed for the computation of gear parameters such as Addendum, Dedendum and Diametral Pitch. Macromedia flash software was adopted to facilitate effective interaction and enhance appearance since interactivity is the most important feature that brings out the desired reality in VR [3].
The required formulas, parameters and relationships which would be needed for the process of calculation of plastic spur gears were clearly itemized. These were programmed into the applications backend using Q-basic. It yielded good result but the user interface was not so attractive. As earlier explained, the beauty of every VR work is the users perception towards the application which is directly corresponding to how interactive and how attractive the front end application looks. Further research work eventually led to the use of a better interface which is designed to generate required spur gear calculations.
Three spur gear tooth forms are generally used with pressure angles of 14½, 20, and 25 degrees. The 14½ degree tooth form is being replaced and made obsolete by the 20 and 25 degree forms (Figure1). Figure2 illustrates two meshing gears with description of terms. The larger

pressure angle makes teeth with a much larger base, which makes these teeth much stronger and also allows the production of gears with fewer teeth. Any two gears in mesh with each other must be of the same pressure angle [6]. When gear tooth measurements are to be made with gear tooth calipers, the chordal tooth thickness and the

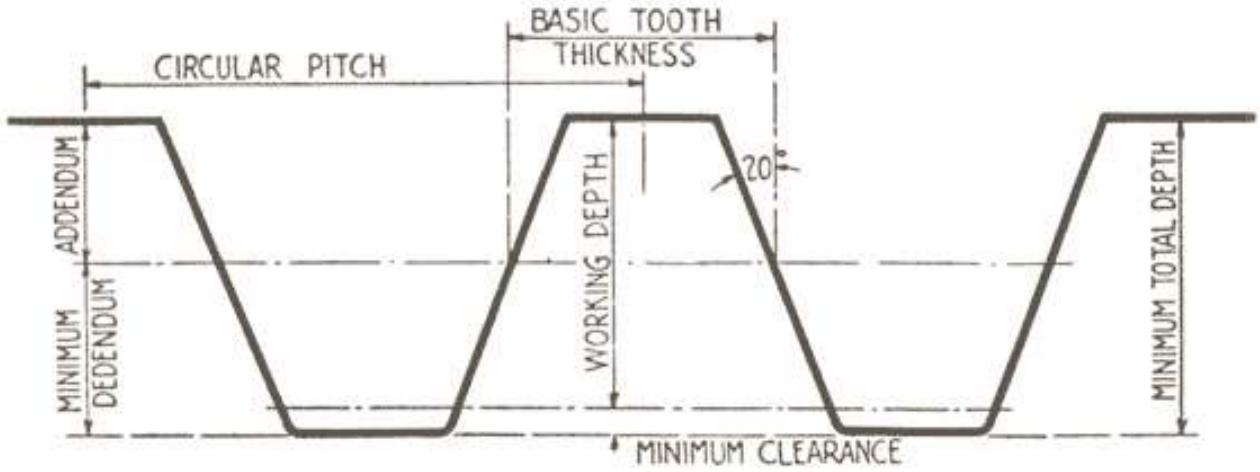


Fig.1- Basic Rack of the 20-Degree Tooth Form (Full depth Involute System) [3].

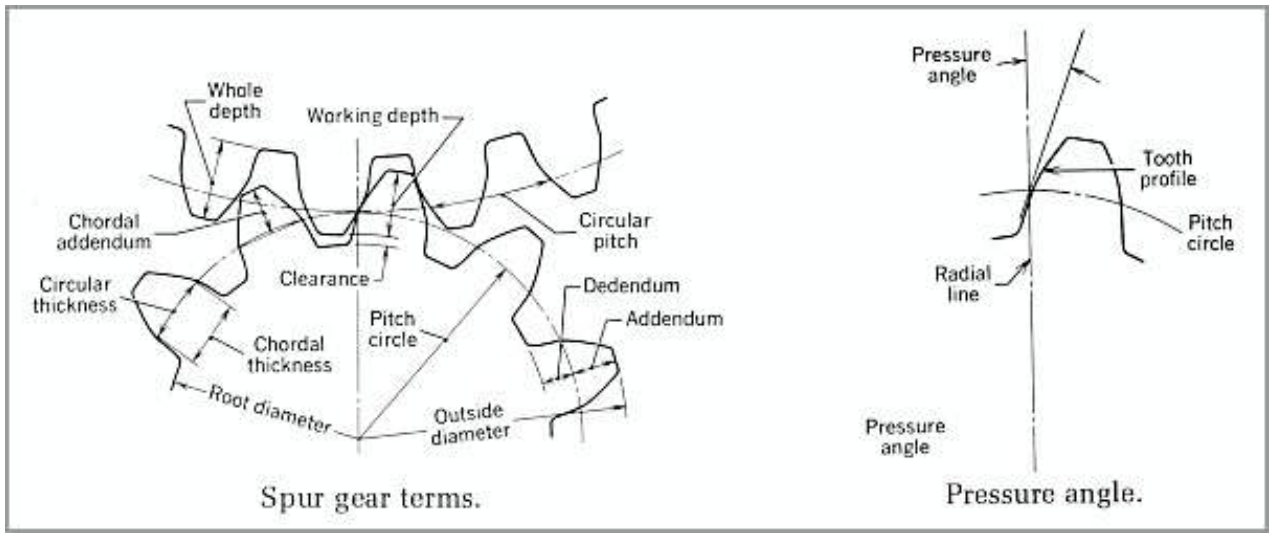


Fig.2- Two meshing Spur Gears with Gear Terms and Pressure Angle Description [3]

COMPUTER MODEL FOR PLASTIC SPUR GEAR CALCULATIONS

A software application was designed capable of generating gear parameters seamlessly. The front end interface is shown in figure 3-5. We named the developed application Gear Lab; which is capable of generating a 3D profile of the gear teeth and also present detailed values of all the gear parameters suitable for producing gear molds when using a modern plastic gear mold making machine called Electric Discharge Machine (EDM).The calculations are for a 20 degree pressure angle spur gear with module 5, 20 teeth and gear ratio 6.

The module, number of teeth and Gear ratio defines the gear features. These were imputed and the results are as presented in Test 1 to 3.

TEST 1

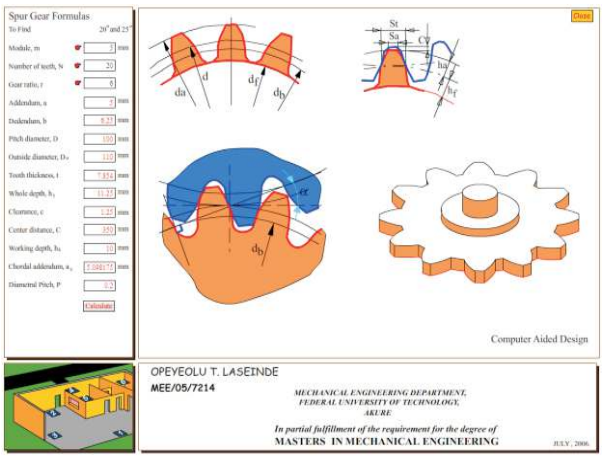


Fig.3: Spur Gear Calculation using Module=5, Number of teeth=20, Gear ratio=6

Author developed software
TEST 2

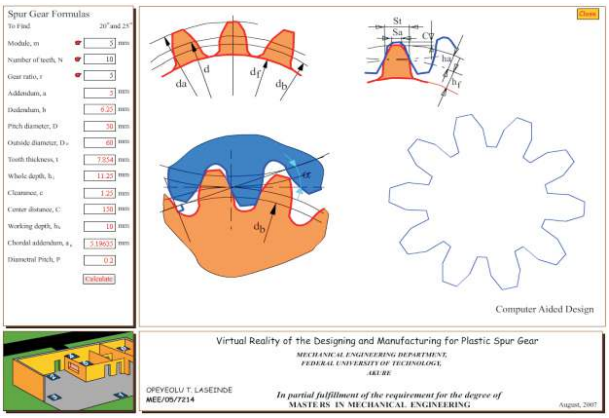


Fig.4: Spur Gear Calculation using Module=5, Number of teeth=10, Gear ratio=5
Author developed software

TEST 3

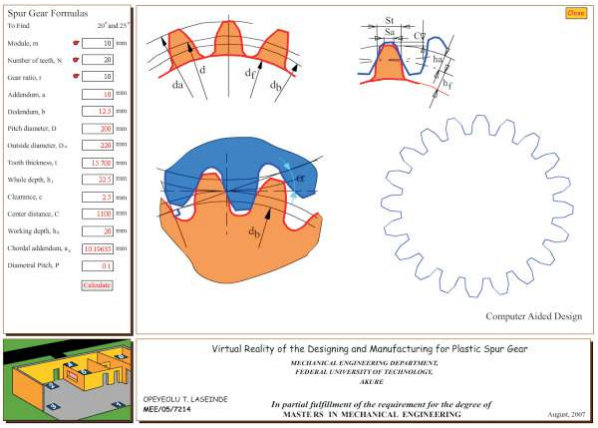


Fig.5: Spur Gear Calculation using Module=10, Number of teeth=20, Gear ratio=10
Author developed software

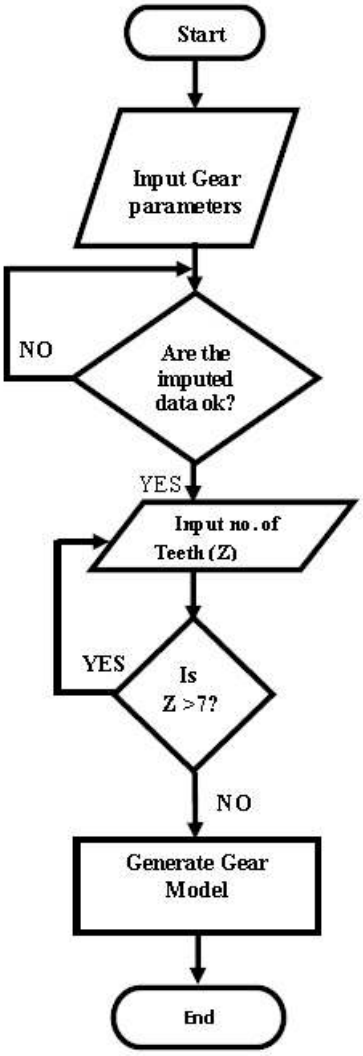


Fig 6: Gear Parameter generation flow Process using Gear Lab.
Author developed

Table 1 below shows the result-comparison between the computer generated model and the manual iteration carried out.

TABLE 1

Parameters	TEST1		TEST2		TEST3	
	Computer Result	Manual Result	Computer Result	Manual Result	Computer Result	Manual Result
Module (M)	5	5	5	5	10	10
No. of teeth (N)	20	20	10	10	20	20
Gear Ratio (r)	6	6	5	5	10	10
addendum (a)	5	5	5	5	10	10
Dedendum(b)	6.25	6.24	6.25	6.25	12.5	12.5
pitch diameter (D)	100	100	50	50	200	200
outside diameter (D_o)	110	110	60	60	220	220
tooth thickness (t)	7.854	7.854	7.854	7.854	15.704	15.704
whole depth (h_t)	11.25	11.2	11.25	11.25	22.5	22.5
Clearance (c)	1.25	1.25	1.25	1.25	2.5	2.5
centre distance (C)	350	350	150	150	1100	1100
working depth (h_k)	10	10	10	10	20	20
chordal addendum (a_c).	5.098175	5.098	5.19635	5.19635	10.19635	10.19635
diametral pitch (P)	0.2	0.2	0.2	0.2	0.1	0.1

DISCUSSION

The aim of VR is to have a simulation in reality. We have been able to develop a computer model for the design of plastic spur gears defining the maximum number of teeth per time as shown in the process flow chart (Fig 6). The gear profile is automatically generated and displayed in 3Dimension for quick reference/prototype. The results obtained have been validated and has shown high level of accuracy and less time to generate desired gear data.

The research has also revealed various techniques of achieving the set goals. Such was discovered when a better user interface was built by integrating Macromedia Flash into the design process compared to the User Interface (UI) achieved at the beginning of the research when Q-Basic was used.

CONCLUSION AND RECOMMENDATION

Haven completed a VR model for plastic spur gear generation, it is possible to apply these same principles in various production processes and as such, make transfer of technology easier, cheaper and quicker. Finally, educators should explore this area of study for developing interactive learning teaching aids.

REFERENCES

[1] Barwick, K., Gray, J. and Roberts D.(1993)- *Virtual Reality in Engineering*, IEE, London.

.

[2] Dudley, D. W. (1984), Handbook of Practical Gear Design, Volume II, Academy press, pp 8-25

[3] Encarnacao, J. and Fruhauf, M.(1994) -Global Information Visualization: the Visualization Challenge for the 21st Century. Academic Press.

[4] Jeffrey, S.(2001)- A Simple Technique for Visualizing Three Dimensional Models in Landscape Contexts , *Internet Archaeology* [on-line]: http://intarch.ac.uk/journal/issue10/jeffrey_index.html.

[5] Koller, D., Lindstrom, P., Ribarsky, W., Hodges, L., Faust, N. and Turner, G. (1995) -Virtual GIS: Gear Technology, in *Proceedings of IEEE Visualization '95 Conference*.

[6] Maryland Metrics, (2002) –Technical data, owing mills, pp 1-3 : htpp://mdmetric.com

[7] Sato, K., Shiratori, N., Nunokawa, H., Kusumi, T. and Syoichi, N.(1997)- A User Interface Metaphor for Distributed Systems, Electronics and Communications in Japan Part III', *Fundamental Electronic Science* 80, Part 11, pp. 82–93.

[8] Teylingen, R. van, Ribarsky, W. and Mast, C. van der (1997)-Virtual Data Visualizer', *IEEE Transactions on Visualization and Computer Graphics*, Vol. 3, No. 1, January–March 1997.

APPLICATION OF OPTIMIZATION AND MATHEMATICAL MODELLING TO RESEARCH & INDUSTRIAL FORMULATION

Idowu G. O. and Okorie N. N.
Engineering Materials Development Institute (EMDI), Akure
Emails: gabrielolufemiidowu@yahoo.com, ***ngoigbo@yahoo.com***

Abstract
This paper considers the general basis of research formulation with emphasis on the nature of data as a dictate for the kind of research formulation and the expecting modelling techniques being employed. Basic data concepts and general surveys of modelling techniques were conducted with the aim of highlighting the place of Mathematical and Optimization modelling for research and industrial applications. This paper discuses the interplay between quantitative observation (experimental/sampling data) and the process of arriving at mathematical construction (population parameters) that characterizes the system property relationship being studied. Some key aspects considered include defining appropriate research objectives, methods for optimizing decision input variables while planning for projects, project experimentation, data collection and resolution of the data. Others include model generation, model feed-back and revision, classifying and publication of the model. In addition, major general and specialized mathematical modelling software are reviewed and criteria for selecting appropriate one for research purpose recommended. This presentation is concluded with a practical demonstration of typical modelling software (especially locally developed ones) to solve some practical problems.

Keywords: *Data concept, Research formulation, Input decision variable optimization, Mathematical model construction*

Introduction

A model is a representation of the reality that captures "the essence" of reality. A photograph is a model of the reality portrayed in the picture. Blood pressure may be used as a model of the health of an individual. A pilot sales campaign may be used to model the response of individuals to a new product. In each case the model captures some aspect of the reality it attempts to represent.

A model only captures certain aspects of reality, for instance a photograph of a person is a model of that individual, but provides little information regarding his or her academic achievement. An equation that predicts annual sales of a particular product is a model of that product, but is of little value if we are interested in the cost of production per unit. Thus, the usefulness of the model is dependent upon the aspect of reality it represents. A useful model is one that captures the proper elements of reality of interest with acceptable accuracy.

Following, survey of modelling software is given but theoretical framework gives a basic background to especially formulating and modelling with the demonstrating software – "Grand Optimizer".

Mathematical Modelling

A mathematical model is an abstract construction that offers the analyst a tool that he can manipulate in his/her analysis of the system under study, without disturbing the system itself. For example, suppose that a mathematical model has been developed to predict annual sales as a function of unit selling price (S). If the production cost per unit (C) is known, total annual profit (P) for any given selling price can easily be calculated as:

$$P = S - C$$

Analytical Modelling Methodology

In general, analytic mathematical solution can be arrived at with either of the following two main classes which are "General Solution" and "General Methodology".

General Solution

This involves formulating a mathematical solution in an abstract form which can be applied directly to solve a particular problem. For example the following equation gives a general polynomial solution.

$$y = \beta_0 + \beta_1 x + \beta_2 x^2 + \ldots, + \beta_k x^k$$

General Methodology.

In general methodology, there is a general procedure that can be applied to solve a specific problem and this method is usually iterative. Examples include the simultaneous linear equations solution methods and many statistical procedures.

Data Concepts

Data based on Risk Level

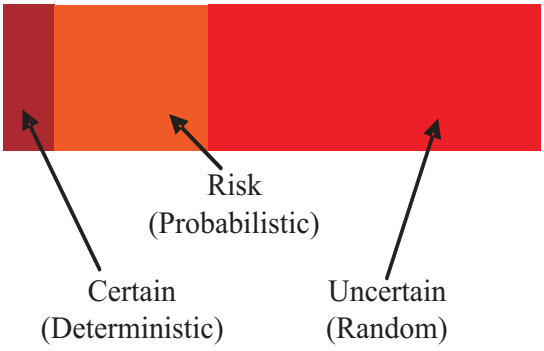
Data collected on an experiment can fall in any of the following three categories.

Certain/Deterministic
Risk/Probabilistic
Uncertain/Random

These classes are rather a spectrum that ranges from

almost certain to absolutely uncertain data.

Data Spectra:



Data based on Continuity/Discretization

Continuous
Discrete/Finite
Dichotomous
Ordinal/Categorical

Nature of modelling objectives

Utility Optimization of Input Decision variables

Mathematical optimization is the branch of computational science that seeks to answer the question `What is best?' for problems in which the quality of any answer can be expressed as a numerical value. Such problems arise in all areas of business, physical, chemical and biological sciences, engineering, architecture, economics, and management.

A mathematical optimization model consists of an objective function and a set of constraints expressed in the form of a system of equations or inequalities.
The problem is formulated as:

$$\text{Maximize / Minimize } Z = \sum_{j=1}^{n} c_j x_j$$

subject to

$$\sum_{i=1}^{m} a_{ij} x_j \le b_i \quad for\ i = 1, 2, \ldots, m$$

$$x_j \ge 0 \quad for\ j = 1, 2, \ldots, n$$

To define those conditions that will lead to the solution of a systems problem, the analyst must first identify a criterion by which the performance of the system can be measured. This criterion is often referred to as the measure of the system performance or the measure of effectiveness. In business applications, the measure of effectiveness is often either cost or profit, while government applications more often are in terms of a benefit-to-cost ratio.

Empirical modeling

Empirical modelling consists of a variety of statistical and mathematical techniques that analyze experimental or historical data so as to detect a mathematical construction for predicting/estimating a response variable given a set of explanatory data or to make predictions about future events. The fundamental of empirical modelling is all about capturing relationships between explanatory variables (xi) and the predicted variable (y) and present it in the form of mathematical expression, i.e. y = f(xi).

Types of Empirical Modelling

Univariate

Univariate model is a mathematical relationship in which the dependent variable is related to only one independent variable. It is of the mathematical form,
y = f(x)

Multivariate

Multivariate model however is a mathematical relationship in which the dependent variable is related to more than one independent variable. It is of the mathematical form,
y = f(x1, x2, …, xn)

Model Search Guide

Many modelling software these days have enriched preset of models from which you can search for model that fit your data. The first attempt to streamline model searching is to have a scatter plot of the data. Using your a priori background at understanding the form of the curve, you may be able to guess the group of model your data belong so you can initially peruse such likely models. For instance, if the scatter plot is cyclic, you may speculate that the data has a sinusoidal pattern, so you can firstly investigate the sinusoidal models.

Selection Criteria for Competing Models

In searching for empirical models, you may have more than one good model that fit your data. The question then arises on how to select the best out of those good ones. Two rules are usually recommended either of which can decide, Occam's razor principle of parsimony and Statistical strength.

Occam Razor Principle of Parsimony

Occam Razor's principle gives precedence to simplicity; of two competing theories, the simplest explanation of an entity is to be preferred. Occam's rule applied to model selection therefore says the simplest of all competing models should be preferred.

Statistical Strength (Goodness of Fit)

You select a performance measure such as standard error, residual sum of errors, standard deviation, bias, or any performance measure of your choice, based on statistical strength of your chosen performance measure, you choose a superior model by comparing the performance measure for each of all competing models (i.e. models of good fit) and pick the model with best performance measure. For instance, if standard error is chosen as performance measure, the model with least Std. Error will be the best model.

Response surface analysis

For some problems, the ultimate goal may not only be to discover a mathematical expression that describe the variables relationship, it may be required to carry out further analysis on the model to determine the data global

optimal. To achieve this, differential, optimization and statistical methods are called into play and this solution procedure is referred to as response surface analysis. Polynomial model is a very versatile model that lends itself to such analysis.

Variable Dropping & Surrogate Analysis

Variable dropping is statistical methods for identifying extraneous and superfluous variables.

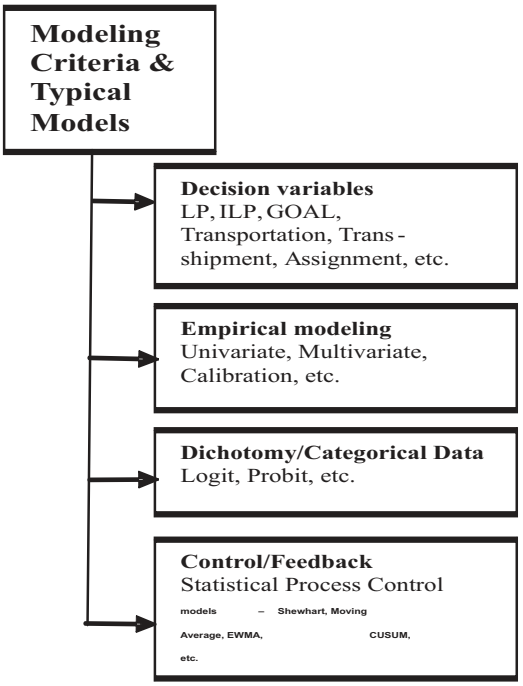
Extraneous Variable
A variable is extraneous when it does not significantly contribute to response variable.

Surrogate Analysis
Surrogate analysis is very important tool to especially industrial researchers. Surrogates are two independent variables/inputs that serve the same purpose in a formulation, that is, either is a close substitute of the other, and thus the experiment is excessively formulated. Surrogate analysis is the process of identifying surrogates. For surrogates to be detected, the problem must be a multivariate problem. Surrogate could be useless when it reveal a situation of mere duplication. However, many industrial researches are carried out purposely to identify surrogates that provide useful industrial applications. For instance, when two different materials are identified as surrogates, it signifies to a design engineer as alternative materials, such that when one becomes unavailable or expensive, the other could be used. To an industrial researcher interested in formulating multiple products, surrogates allow the researcher to formulate three products out of one formulation. One product with the whole combination, another with material B eliminated, and the other with material A eliminated.

System controls/feedbacks
In an attempt to consistently control a system to ensure it is in control, Statistical process control models are usually adopted. Shewhart variable and attribute Control charts and such models as Moving Average (MA), Exponential Weighted Moving Average (EWMA), Cumulative Sum (CUSUM), etc. can be applied

Objectives and Typical Modelling Options
The following chart presents a synoptic of some modelling objectives and the likely type of models usually consider for solving such problems.

Model Chart



Survey of Some Modelling Software

Software Package	Developer	Major Modelling Objectives	Major Application Areas
Microsoft Excel Standard Solver	Frontline Systems, Nevada, USA (www.solver.com)	Input Variable Decision making	Linear Equations & Optimization, Goal Programming, etc.
Premium Solver	Frontline Systems, Nevada, USA (www.solver.com)	- DO-	-DO-
Microsoft Excel Analysis ToolPak	Grey Matter International, Inc., Cambridge, Massachusetts, United States (www.microsoft.com)	Empirical Modelling, Statistical Inferences	Statistical Analysis, Engineering Functions

DataFit	Oakdale Engineering Oakdale, USA (www.curvefitting.com)	Empirical Modelling, Statistical Inferences	Regression and Curve Fitting
SigmaPlot	Systat Software, Inc. California, USA (www.sigmaplot.com)	Empirical modelling, Statistical Inferences	Regression and Curve Fitting, Statistical Analysis
Grand Optimizer	Optisoft Global Resources, Akure, Nigeria (www.optisoftnigeria.com)	Optimization, Empirical Modelling, System Controls and Device Calibration	Linear Equations & Optimization, Regression and Curve Fitting, Device Calibration, Polynomial Roots Finding,
			Statistical Process Control, etc.
Lingo	LINDO Systems Inc, Chicago, USA (www.lindo.com)	Input Variable Decision making	Optimization Modelling
AMPL	AMPL Optimization LLC, Albuquerque, USA (www.ampl.com)	Input Variable Decision making	Optimization Modelling
Igor Pro	*WaveMetrics, Inc., Portland, USA (www.wavemetrics.com)*	Empirical modelling, Statistical Inferences	Scientific Graphing, Data Analysis, Image Processing and Programming
OriginPro	*OriginLab Corporation, Northampton, USA (www.originlab.com)*	Empirical modelling, Statistical Inferences	Scientific Graphing, Data Analysis, Image Processing and Programming
Minitab	*Minitab Inc., Pennsylvania, USA (www.minitab.com)*	Empirical modelling, Statistical Inferences	Regression and Curve Fitting, data Analysis
SAS	*SAS Institute Inc. North Carolina, USA (www.sas.com)*	Empirical modelling, Statistical Inferences	Regression and Curve Fitting, data Analysis
Scientific WorkPlace (SWP)	*MacKichan Software, Inc. Washington, USA (www.mackichan.com)*	Mathematical computation & scientific plotting	Scientific word processing on Microsoft Windows
MatLab	*MathWorks, Natick, Massachusetts, USA (www.mathworks.com)*	MATLAB is a high-level language and interactive computationally environment	Multi-purpose for scientific computing and modelling
A host of modelling packages and many third party Add-In programs to Microsoft Excel that address various particular modelling problems are available on the net.			

Introducing Optisoft Grand Optimizer

Optisoft Grand Optimizer (GO) is a Nigerian based Multi-Solver Add-In program to Microsoft Excel. It may be used to solve Simultaneous Linear Equations, Linear Optimizations, Mathematical Modelling (Curve Fitting, Calibration, Response Surface and Surrogate Analyses), Polynomial Roots and Statistical Quality Control Process problems among others. It is a resourceful Mathematical Modelling tool for research/academic community and invaluable companion to corporate managers.

Demonstrating Examples:

We have formulated the following three examples to demonstrate some modelling applications using a locally developed computer assisted modelling software.

Linear Optimization Example: Minimization LP Example

Ise Takuntakun Construction Company requires a minimum of 10,000 cu. meters of sand and gravel mixture. The mixture must contain not less than 5,000 cu. meters of sand and not more than 6,000 cu. meters of gravel. Materials may be obtained from two sites: 30% of sand and 70% gravel from site 1 at a delivery cost of N5000.00 per cu. meter and 60% sand and 40% gravel from site 2 at a delivery cost of N7000.00 per cu. meter.

Required:
a) Formulate the problem as a LP model
b) Solve using Grand Optimizer

Solutions:

Min $z = 5000\,x_1 + 7000\,x_2$

s. t. $0.3\,x_1 + 0.6\,x_2 \geq 5000$ Sand constra int

$0.7\,x_1 + 0.4\,x_2 \leq 6000$ Gravel Constra int

$x_1 + x_2 \geq 1000$ Total Amount constra int

and $x_1 \geq 0$ $x_2 \geq 0$ Non – negative constra int

Note: x_1 and x_2 represent the amount of materials got from Site 1 and 2 respectively.

Input table:

A3 PROJECT TITLE: Ise Takuntakun Construction Company

	A	B	C	D	E	F
3	**PROJECT TITLE: Ise Takuntakun Construction Company Mix Project**					
4		**Constraints**			**Decision Variables**	
5					**Mat. Site 1**	**Mat. Site 2**
6	**S/No**	**Description**	**Limit**	**Compa rator**	**X_1**	**X_2**
7		Non-negative (i.e. Xj ≥ 0) ?			Yes	Yes
8		Min: Obj. (Z)	0		5000	7000
9	1	Sand	5000	>=	0.3	0.6
10	2	Gravel	6000	<=	0.7	0.4
11	3	Total Amt. Mix.	10000	>=	1	1

Result table:

	A	B	C	D
1	PROJECT TITLE: Ise Takuntakun Construction Company Mix Project Result_1			
2		Description	Solution	
3	S/N	Variable	Value	Reduced Cost
4		Objective: Min.	63333333.33	
5	1	Mat. Site 1 (X1)	3333.333333	3000
6	2	Mat. Site 2 (X2)	6666.666667	6666.666667

Post Optimal Tables:

1	PROJECT TITLE: Ise Takuntakun Construction Company Mix Project Objective Cost/Price Coefficient Sensitivity Analysis_Result 1						
2	Variable		Permissible				
3			Range for Objective Cost/Price Coefficient				
4	S/N	Description	Minimum	Original	Maximum	Decrease	Increment
5	1	Mat. Site 1 (X1)	3500	5000	7000	1500	2000
6	2	Mat. Site 2 (X2)	5000	7000	10000	2000	3000

PROJECT TITLE: Ise Takuntakun Construction Company Mix Project Constraint Limits Sensitivity Analysis_Result 1

12	Variable		Permissible			
13			Range for Constraint Limits			
14	S/N	Description	Minimum	Original	Maximum	Decrease	Increment
15		Sand	4000	5000	6000	1000	1000
16		Gravel	-∞	6000	+∞	-∞	+∞
17		Total Amt. Mix.	8333.33	10000	11000	1666.67	1000

***Univariate Modelling & Response Surface Analysis Example*:**

It has been found that Igbokoda sand is at least 98% silica pure and EMDI Akure has ventured to formulate some Silicate Gels from the sand. The sand starts melting at high temperature of about 1800 º C. To reduce the melting temperature, a certain flux was added at various grams of the flux to per kilogram of the sand as shown in the table below and the corresponding melting temperature.

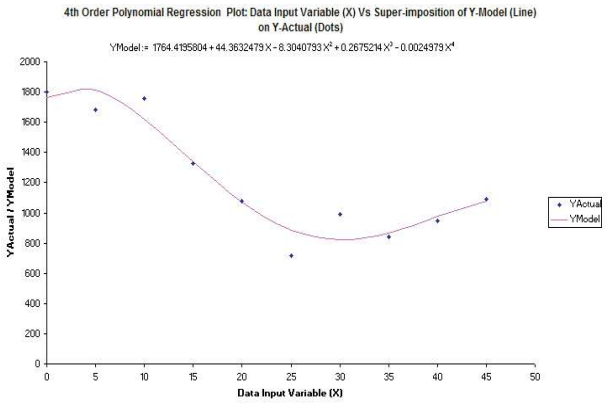
Input table:

	A	B	Q
3	**PROJECT TITLE: My Uni-Variate Mathematical**		
6	**S/No**	**Temp (° C)**	**Flux (g)**
7		**Y-Actual**	**X**
8	1	1800	0
9	2	1680	5
10	3	1760	10
11	4	1330	15
12	5	1080	20
13	6	718	25
14	7	990	30
15	8	840	35
16	9	950	40
17	10	1090	45

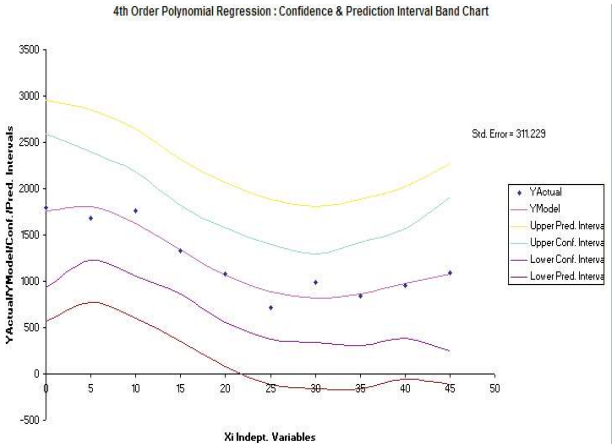
Output table:

	A	B	I	M	N	Q
3	**PROJECT TITLE: My Uni-Variate Mathematical Modeling Project 77 - Polynomial**					
4	**YModel := 1764.41958041958 + 44.3632478632479 X - 8.30407925407925 X^2 + 0.267521367521368 X^3 - 2.4979020979021E-03 X^4**					
6	**S/No**	**Temp (° C)**	**PolyNom Model**	**Standardized Residual of Y-Model**	**Normal Scores of Y-Model**	**Flux (g)**
7		**Y-Actual**				**X**
8	1	1800	1764.42	35.58041958	0.323352294	0
9	2	1680	1810.513	-130.5128205	-0.250458973	5
10	3	1760	1620.186	139.8135198	0.131965206	10
11	4	1330	1337.879	-7.878787879	-0.004942891	15
12	5	1080	1070.559	9.440559441	0.004437398	20
13	6	718	887.7296	-169.7296037	-0.063792435	25
14	7	990	821.4219	168.5780886	0.052785909	30
15	8	840	866.2005	-26.2004662	-0.007030897	35
16	9	950	979.1608	-29.16083916	-0.006846449	40
17	10	1090	1079.93	10.06993007	0.002101401	45

Model curve:



Prediction Band:



	A	B	C	D	E	F	G	H
1	Regression Analysis Output Summary for 4th Order Polynomial Uni-Variate Model							
3	Regession Statistics							
4	Fitted Model	No. of Observations	Residual Sum of Squares	Std. Error	R^2	Adj. R^2	Durbin-Watson	Bias of Estimator
5	rder Polyn	10	96863.5	311.22904	0.931315	0.876367	3.188164463	4.43379E-12
7								
8	Analysis of Variance (ANOVA)							
9	Source	DF	SS	MS	F Stat	p-Value		
10	Regressio	4	1313396	164174.51	16.94906	0.0041		
11	Residual	5	96863.5	96863.515				
12	Total	9	1410260					
13								
14								
15	Regression Table							
16	Variable	Coeff. Value	Std. Error	t - Ratio	p-Value			
17	Constant	1764.42	301.276	5.8564896	0.1077			
18	X	44.36325	104.535	0.4243866	0.7445			
19	X^2	-8.304079	10.2668	-0.808826	0.567			
20	X^3	0.267521	0.35204	0.7599146	0.5863			
21	X^4	-0.002498	0.00388	-0.643828	0.6358			
24	Correlation Matrix							
25		Y	X					
26	Y	1	-0.81037					
27	X	-0.810372	1					

Regression tables:

	A	B	C	D	E
13					
14	Global Optima				
15	Optimum Description	Dependent Variable (Y)	Independent Variable (X)		
16	Maximum of Maxima	1829.8861	3.124610682		
17	Minimum of Minima	821.2224	30.29682988		

Optima Table:

Multivariate & Surrogate Analysis Example: Supermarket Deliveries:

A supermarket manager decides to investigate how long it takes to unload deliveries from truck. An initial consideration of the problem suggests that the unloading time could depend upon both the volume of delivery and the weight of the delivery. In addition, the supermarket has a day shift and a night shift, and the manager suspect that the unloading time may be different for the two shifts. Ten deliveries are selected at random for both the day and night shifts, and the unloading times are measured together with the volumes and weights of deliveries. The data set obtained is shown in the table below. Notice that the two shifts are designated by an indicator variable which takes the 0 for the day shift and 1 for the night shift.

Adapted from: Anthony J. Hater, "Probability & Statistics for Engineers and Scientist", PWS Publishing Company, 1995, p.698.

Input table:

	A	B	P	Q	R
3	PROJECT TITLE: My Multi-Variates Mathematical Modeling				
6	S/No	UnLoadingTime	Vol. (m3)	Wt. (Kg)	Shift (Day - 0/Night - 1)
7		Y-Actual	X1	X2	X3
8	1	48	79	43	0
9	2	42	76	46	0
10	3	44	84	43	0
11	4	33	66	32	0
12	5	53	98	56	0
13	6	58	98	57	0
14	7	52	92	56	0

Output table:

PROJECT TITLE: My Multi-Variates Mathematical Modeling Project 74 - Multiple Linear Regression

YModel := -25.5508100147275 + 0.838247422680412 X1 + 1.37260677466866E-02 X2 + 0.761899852724595 X3

YRevModel := -24.1613648024628 + 0.832820249700701 X1

S/No	UnLoadingTime Y-Actual	Multiple Lin. Reg. Y-Model	Multiple Lin. Reg. Y-Rev. Model	Residual of Y-Model	Residual of Y-RevModel	Standardized Residual of Y-Model	Standardized Residual of Y-RevModel	Vol. (m3) X1	Wt. (Kg) X2	Shift (Day - 0/Night - 1) X3
1	48	41.261	41.6314	6.73904271	6.36856508	0.015204559	0.017130038	79	43	0
2	42	38.7874	39.133	3.21260677	2.86702583	0.007538507	0.008022451	76	46	0
3	44	45.4522	45.7955	-1.4521944	-1.79553617	-0.003080492	-0.004540188	84	43	0
4	33	30.2128	30.8048	2.78724595	2.19522832	0.007523298	0.007062427	66	32	0
5	53	57.3661	57.455	-4.3660972	-4.45501967	-0.007942745	-0.009663018	98	56	0
6	58	57.3798	57.455	0.62017673	0.54498033	0.00112832	0.001182229	98	57	0
7	52	52.3366	52.4581	-0.33661267	-0.45809817	-0.000652518	-0.001058941	92	56	0
8	34	36.1628	36.6345	-2.16284242	-2.63451343	-0.005279764	-0.007666395	73	38	0

Key result interpretation table:

Key Result Interpretation

Result Index	Result Value	Applicable Data	Result Interpretation			Remark
			Hypothesis Testing			
			Null hypothesis (H0): The model does not make a good fit ; Alternative hypothesis (H1): The model makes a good fit			The Null hypothesis (H0) looks implausible, as a result the model appears a good fit for the data population.
pValue	0	All	pvalue is the probability of null hypothesis (H0) being plausble/implausible. (pvalue critical range inferences)			
			0 - 0.01	> 0.01 and <= 0.1	> 0.1	
			Reject H0 /Accept H1	Indeterminate	Accept H0 / Reject H1	
			Autocorrelation Test Parameters			
			d Lower alpha (dLa)	d Upper alpha (dUa)	4 - d	
			1	1.68	2.43830259	
			(i) Positive Autocorrelation Test (Range inferences)			Inconclusive, you probably have some positively serially correlated data
			d < dLa	dLa < d <	d > dUa	
Durbin Watson (d)	1.56163741	Time Series Data	Possitively serially correlated	Inconclusive	NOT positively serially correlated	
			(i) Negative Autocorrelation Test (Range inferences)			
			4 - d < dLa	dLa < 4 - d < dUa	4 - d > dUa	The data does not appear negatively serially correlated
			Negatively serially correlated	Inconclusive	NOT Negatively serially correlated	
			Comparative Analysis of Models' Measure of Goodness			
Std. Error	3.64865246	All	Based on Statistical strength, you choose a superior model by comparing the Std. Errors of all competing models [i.e. models			Alternatively, you may apply Occam's rule of

UnLdgTm_RevLMReg_RvY_Vs_X | UnLdgTm | UnLdgTm_RevLMReg | Un

Conclusion

It has been shown that the more analytical attempt that is made on experimental analysis, the more effective the output result that will be obtained and modelling provides a way to put our systems consistently under control.

References

[1] K. A. Stroud, Engineering Mathematics,Palgrave, 5th Edition, (2001)

[2] Hayter J. Anthony, Probability and Statistics for Engineers and Scientists, PWS Publishing Company, (1996)

[3] Irwin Miller, John E. Freund, Probability and Statistics for Engineers, Prehentice-Hall of India, 3rd Edition 1987

[4] Harvey M. Wagner, Principles of Operations Research, Prehentice-Hall of India, 2nd Edition (1989)

[5] Hamdy A. Taha, John E. Freund, Operations Research: An Introduction, Prehentice-Hall of India, 7th Edition (2002)

[6] Guisseppi A. Forgionne, Quantitative Decision Making, Wadsworth Publishing Company, 7th Edition (1986)

[7] Frederick S. Hillier, Gerald J. Liebarman, Introduction to Operation Research, McGraw-Hill Companies, 7th Edition (2001)

[8] Microsoft Corporation, Visual Basic User's Guide, Automating, Customizing, and Programming in Microsoft Excel with Microsoft Visual Basic programming System, Microsoft Corporation, Application Edition, (1994)

[10] Kaj Madsen,"A Root-Finding Algorithm Based on Newton's Method", Annales Mathematicae et Informaticae 33 (20060 pp. 3 – 13)

[11] Wei Zhu, Zhe-zhao Zeng, and Dong-mei Lin, "An Adaptive Algorithm Finding Multiple of Polynomials", Spring-Verlag Berlin Heideberg, (2008)

[12] Antonio A. Trani and H. Baik, "Applications of Linear Programming – Minimization", 2003

MODEL FOR EVALUATION AND ASSESSMENT OF ENERGY TRANSMISSIVITY BY SOLAR COLLECTOR BASED ON THE REFLECTIVITIES OF BEAM AND DIFFUSED COMPONENTS OF RADIATION

*C. I. Nwoye[1], E. O. Obidiegwu[2],U. C. Nwoye[3], and J. U. Odo[1]
[*1]Department of Metallurgical and Materials Engineering, Nnamdi Azikiwe University, Awka
[2]Department of Metallurgical and Materials Engineering, University of Lagos, Nigeria
[3]Department of Electrical Engineering,Weatherford Nig. Ltd., Port Harcourt, Nigeria

*Email: chikeyn@yahoo.com

Abstract
This paper presents a model for evaluation and prediction of energy transmissivity by solar collector based on the reflectivities of the beam and diffused components of radiation. Computational analysis of the derived model;

$$\alpha = 0.4464e^{-0.2820\beta} + 0.005\ln\gamma + 0.4568$$

indicates that transmissivity per unit reflectivity of the beam component of radiation as obtained from experiment and derived model are – 0.2385 and – 0.2462 respectively. Similarly, transmissivity per unit reflectivity of the diffused component of radiation as obtained from experiment and derived model were evaluated as 0.2897 and 0.2991 respectively. The graphical analysis showing very close alignment of curves from both experimental and model-predicted results indicates 0.9964 and 0.9989 as the correlations between transmissivity and reflectivity of the beam component of radiation as obtained from experiment and derived model respectively. Similarly, 0.9918 and 0.9980 are the correlations between transmissivity and reflectivity of the diffused component of radiation as obtained from experiment and derived model respectively. Statistical analysis of the results indicate that the variance and standard deviation as obtained from experiment and derived model are 1.626×10^{-6} and 1.275×10^{-3} as well as 1.706×10^{-6} and 1.306×10^{-3} respectively. Deviational analysis indicates that the maximum deviation of the model-predicted transmissivity from the corresponding experimental value is less than 0.08%. The validity of the model was found to be rooted on the expression $2.2401\alpha = e^{-0.2820\beta} + 0.0112\ln\gamma + 1.0233$ where both sides of the expression are correspondingly approximately equal.

Keywords: Model, Prediction, Solar Energy Transmissivity, Reflectivities of Radiations.

Introduction

Report [1] has shown that environmental weather condition, sun's radiation on the collector location and the duration of the radiant inflow, the time of the day at which the sun's radiant heat is being collected, the angle of incidence (i.e the angle between the normal to the solar array and a light ray from the sun), the solar distance (i.e the distance of the array from the sun), light transmission losses in cover glasses and cover adhesive are factors which determine the level conversion of sun's radiation to electric and heat energy for domestic and industrial use.

$$\dot{q}_{ab} = (\tau\alpha)I(t) \qquad (1)$$

where τ is the transmittance or transmissivity of the glazing cover.

Transmissivity was found [3] to vary with geographic location due to the variation of solar geometry with location. The research work shows that the transmissivity of a glazing cover is very important in designing and evaluating the performance of solar energy conversion systems.

Successful attempt has been made [4] to determine the transmissivity for the most commonly used glazing surfaces; 3mm transparent glass. This research work was aimed at assessing its performance under the solar geometrical condition of Yola town (Nigeria). The results of the investigation indicate that the performance of the glazing surface is dependent on the magnitude of its transmissivity. An annual mean value of 0.8807 was recorded with a standard deviation of 0.0015. This result imply that plane glass as a glazing surface admits about 88% of the solar radiation incident on it to the absorbing surface.

Earlier work [4] showcases the calculation of transmissivity from associated solar geometrical factors using parametric definitions and computations. However, there was no mathematical relationship which

placed transmissivity of the glazing surface (used for the solar collector) directly dependent on reflectivities of the beam and diffused components of solar radiation.

The aim of this work is to derive a model for evaluation and prediction of energy transmissivity by the solar collector based on reflectivities of the beam and diffused components of solar radiation.

Solar Energy Formation and Radiation

Radiant energy is generated from the sun by combination of hydrogen atoms to form helium. The energy released in this process directly supplies most of the natural energy systems on earth which can be utilized by conversion of the heat to electricity [5].

Materials and Methods

The glazing surface of a solar flat plate collector was positioned at different latitude angles to permit different amount of incident radiations from the sun. Details of the experimental procedure and associated process conditions are as stated in the past report [4].

It has been found [2] that the intensity of solar radiation striking the absorber plate of a flat plate collector depends on the transmission properties of the glazing cover while the rate at which energy is absorbed by a plate per unit area

$$N\alpha = e^{-S\beta} + K \ln\gamma + n \text{ (approximately)} \quad (2)$$

Introducing the values of N, K, n and S and Se into equation (2) reduces it to;

$$2.2401\ \alpha = e^{-0.2820\beta} + 0.0112 \ln\gamma + 1.0233 \quad (3)$$

$$\alpha = \left(\frac{e^{-0.2820\beta} + 0.0112 \ln\gamma + 1.0233}{2.2401} \right) \quad (4)$$

$$\alpha = 0.4464\, e^{-0.2820\beta} + 0.0112 \ln\gamma \left(1.0233 \right) \quad (5)$$

$$\alpha = 0.4464 e^{-0.2820\beta} + 0.005 \ln\gamma + 0.4568 \quad (6)$$

Where

- (β) = Reflectivity of the beam component of the solar radiation
- (γ) = Reflectivity of the diffused component of the solar radiation
- N = 2.2401; Scattering index of incident radiation (determined using C-NIKBRAN [6]
- (α) = Transmissivity
- K = 0.0112; Dust-incident radiation interaction factor (determined using C-NIKBRAN [6]
- S=0.2820; Gas-incident radiation interaction factor (determined using C-NIKBRAN [6]
- n = 1.0233; Water vapour-incident radiation interaction factor (determined using C-NIKBRAN [6]

Boundary and Initial Condition

Consider solar radiations incident to the solar collector positioned at different latitude angles. The amount of incident radiations on the collector is slightly affected by gases, water vapour and dusts in the atmosphere. Range of reflectivites **of** beam and diffused components of solar radiation considered are 0.0417-0.0547 and 0.0277-0.0384 respectively. The environmental weather condition, sun's radiation on the collector location and the duration of the radiant inflow, the time of the day at which the sun's radiant heat is being collected, the angle of incidence (i.e the angle between the normal to the solar array and a light ray from the sun), the solar distance (i.e the distance of the array from the sun), the light transmission losses in cover glasses, cover adhesive and other optical elements and other process conditions are as stated in the experimental technique [4].

The boundary conditions are: All around the collector, a zero gradient for the gas scalar are assumed. Also zero gradients are assumed dusts and water vapour in the atmosphere. The solar collector is stationary during the incidence of the radiation except when moved to a new location (different latitude angles). The sides of the collector are taken to be symmetries.

Results and Discussion

The derived model is equation (6). The computational analysis of Table 1 gave rise to Table 2.

Model Validation

The validity of the model was found to be rooted on equation (3) where both sides of the equation are correspondingly approximately equal. Table 2 also agrees with equation (3) following the values of 2.2401 α *and* $e^{-0.2820\beta}$ + 0.0112 lnγ + *1.0233* evaluated from the experimental results in Table 1. In addition, the derived model was validated by comparing the transmissivity predicted by the model and that obtained from the experiment [4]. This was done using the 4th Degree Model Validity Test Techniques (4th DMVTT); computational, graphical, statistical and deviational analysis [7]

Computational Analysis

Comparative computational analysis of the experimental and model-predicted transmissivity was carried out to ascertain the degree of validity of the derived model. This was done by comparing transmissivity per unit reflectivity of beam component of the solar radiation obtained by calculations involving experimental and model-predicted results obtained directly from the model.

Transmissivity per unit reflectivity of the beam component of radiation α_r

Transmissivity per unit reflectivity of the beam component of radiation α_r was calculated from the equation;

$$\alpha_r = \alpha / \beta \quad (7)$$

Therefore, a plot of transmissivity against reflectivity of the beam component of radiation as in Fig. 1 using experimental results in Table 1, gives a slope, S at points

(0.0417, 0.8821) and (0.0547, 0.8790) following their substitution into the mathematical expression;

$$\alpha_r = \Delta\alpha/\Delta\beta \qquad (8)$$

Equation (8) is detailed as

$$\alpha_r = \alpha_2 - \alpha_1 / \beta_2 - \beta_1 \qquad (9)$$

Where

$\Delta\alpha$ = Change in the transmissivity α_2, α_1 at two reflectivity values β_2, β_1 of the beam component of radiation. Considering the points (0.0417, 0.8821) and (0.0547, 0.8790) for (β_1, α_1) and (β_2, α_2) respectively, and substituting them into equation (9), gives the slope as – 0.2385 which is the transmissivity per unit reflectivity of the beam component of radiation during the actual experimental process. Also similar plot (as in Fig. 2) using model-predicted results gives a slope. Considering points (0.0417, 0.8817) and (0.0547, 0.8785) for (β_1, α_1) and (β_2, α_2) respectively and substituting them into equation (9) gives the value of slope, S as – 0.2462. This is the model-predicted transmissivity per unit reflectivity of the beam component of radiation. A comparison of these two values of the transmissivity per unit reflectivity of the beam component of radiation shows proximate agreement and a high degree of validity of the derived model.

Transmissivity per unit reflectivity of the diffused component of radiation α_d

Transmissivity per unit reflectivity of the diffused component of radiation was calculated from the equation;

$$\alpha_d = \alpha/\gamma \qquad (10)$$

Therefore, a plot of transmissivity against reflectivity of the diffused component of radiation as in Fig. 3 using experimental results in Table 1, gives a slope, S at points (0.0384, 0.8821) and (0.0277, 0.8790) following their substitution into the mathematical expression;

$$\alpha_d = \Delta\alpha/\Delta\gamma \qquad (11)$$

Equation (11) is detailed as

$$\alpha_d = \alpha_2 - \alpha_1 / \gamma_2 - \gamma_1 \qquad (12)$$

Where

$\Delta\alpha$ = Change in the transmissivity α_2, α_1 at two reflectivity values γ_2, γ_1 of the diffused component of radiation. Considering the points (0.0384, 0.8821) and (0.0277, 0.8790) for (α_1, γ_1) and (α_2, γ_2) respectively, and substituting them into equation (12), gives the slope as 0.2897 which is the transmissivity per unit reflectivity of the diffused component of radiation during the actual experimental process. Furthermore, a similar plot (as in Fig. 4) using model-predicted results gives a slope of 0.2991 on considering and substituting into equation (12) points (0.0384, 0.8817) and (0.0277, 0.8785) for (α_1, γ_1) and (α_2, γ_2) respectively. This is the model-predicted transmissivity per unit reflectivity of the diffused component of radiation. These two values of transmissivity per unit reflectivity of the diffused component of radiation indicate proximate agreement.

Graphical Analysis

Graphical analysis for comparison of transmissivity per unit reflectivity of the beam and diffused components of radiation **as obtained from experiment [4]** and derived model for validity testing is achieved by considering the R^2 values (coefficient of determination). The values of the correlation coefficient, R calculated from the equation;

$$R = \sqrt{R2} \qquad (13)$$

using the r-squared values (coefficient of determination) from Figs. 1 and 2 show a better correlation (0.9989) for model-predicted values between transmissivity and reflectivity of the beam component of radiation than that obtained from experimental (0.9964) values. Analysis of Figs. 3 and 4 also show better a correlation (0.9980) for model-predicted values than experimental values (0.9918) between transmissivity and reflectivity of the diffused component of radiation. This is also an indication that the model predicts accurate and reliable transmissivity which are in proximate agreement with values from actual experiment, confirming its validity.

Critical graphical analysis of Figs. 5 and 6 show very close alignment of the curves from both the model-predicted (MoD) and experimental values (ExD) of transmissivity per unit reflectivity of the beam and diffused component of radiation respectively. The degree of alignment of these curves is indicative of the proximate agreement between both experimental and model-predicted transmissivity, hence validity of the model.

Statistical Analysis

Further validation of the model was achieved statistically by comparing the values of the variance and standard deviation evaluated from experimental and model-predicted data.

The variance V is given by

$$V = \frac{\sum (x - x_a)^2 \quad [8]}{\sum n} \qquad (14)$$

Furthermore, standard deviation is given by

$$SD = [V]^{1/2} \quad [8] \qquad (15)$$

Substituting equation (14) into equation (15) reduces it to;

$$SD = \frac{\sum (x - x_a)^{2\ 1/2}}{\sum n} \qquad (16)$$

$$x_a = \frac{x_1 + x_2 + x_3 + x_4 \ldots .}{\sum n} \qquad (17)$$

Where
SD = Standard deviation
V = Variance
x = Variables representing transmissivity
x_a = Arithmetic mean (evaluated as average transmissivity using experimental data, [4] and model-predicted data
n = Number of samples

Standard deviation and variance as obtained from experiment [4]

On substituting the values of $\sum n$ and $\sum (x-x_a)^2$ (Table 3) into equations (14) and (16), where x_a = 0.8806, (as calculated from equation (17)) variance and standard deviation are evaluated as 1.626 x 10^{-6} and 1.275 x10^{-3} respectively.

Standard deviation and variance as predicted by derived model

Similarly, substituting the values of $\sum n$ and $\sum (x-x_a)^2$ (Table 4) into equations (14) and (16), where x_a = 0.8801 (as calculated from equation (17)) gives variance and standard deviation as 1.706 x 10^{-6} and 1.306 x10^{-3} respectively. The proximity of values of the standard deviation and variance as shown in Table 5 as obtained from experiment [4] and derived model indicates agreement and a high level of validity for the derived model.

Deviational Analysis

A comparative analysis of the transmissivity values obtained from experiment [4] and derived model shows very insignificant deviations on the part of the model-predicted values relative to values obtained from the experiment. This is attributed to the fact that the surface properties of the glazing cover material and the physiochemical interactions between the glazing material and gas molecules, water vapour as well as dust (under the influence of the temperature of the sun) which were believed to have played vital roles during the process [4] were not considered during the model formulation. This necessitated the introduction of correction factor, to bring the model-predicted transmissivity to those of the corresponding experimental values.

Deviation (De) of model-predicted transmissivity from that of the experiment [4] is given by

$$De = \left(\frac{P\alpha - E\alpha}{E\alpha} \times 100 \right) \qquad (18)$$

Correction factor (Cn) is the negative of the deviation i.e

$$Cn = -De \qquad (19)$$

Therefore

$$Cn = -\left(\frac{P\alpha - E\alpha}{E\alpha} \right) \times 100 \qquad (20)$$

Where
$P\alpha$ = Model-predicted transmissivity
$\underline{E\alpha}$ = Transmissivity from experiment
Cn = Correction factor (%)
De = Deviation (%)

Introduction of the corresponding values of Cn from equation (20) into the model gives exactly the corresponding experimental transmissivity.

Figs.7-9 show that the maximum deviation of the mode-predicted transmissivity from the corresponding experimental values is less than 0.08% and quite within the acceptable deviation limit of experimental results.

Comparative analysis of Figs. 7-9 shows that the least and highest magnitudes of deviation of the model-predicted transmissivity (from the corresponding experimental values) are -0.0453 and - 0.0794%. This corresponds to transmissivity: 0.8817 and 0.8805; reflectivity of the beam component of radiation: 0.0417 and 0.0466 as well as reflectivity of the diffused component of radiation: 0.0384 and 0.0338 respectively.

It is highly significant to state that deviation is just a measure of the magnitude of model-predicted values *straying way* from experimental data. The preceding sign is just to indicate if the deviation is deficit or surplus.

Comparison of Figs. 7-12 indicates that the orientation of the curves resulting from correction factors is opposite that of the deviation of model-predicted values of transmissivity. This is because correction factor is the negative of the deviation as shown in equations (19) and (20). Figs. 10-12 shows that the least and highest correction factor (to the model-predicted transmissivity) are -0.0453 and - 0.0794% which correspond to transmissivity: 0.8817 and 0.8805; reflectivity of the beam component of radiation: 0.0417 and 0.0466 as well as reflectivity of the diffused component of radiation: 0.0384 and 0.0338 respectively.

Conclusion

The model evaluates and predicts the energy transmissivity by solar collector based on reflectivities of the beam and diffused components of the radiation. *The validity of the model is rooted on the expression* $2.2401\alpha = e^{-0.2820\beta} + 0.0112\ ln\gamma + 1.0233$ *where both sides of the expression are correspondingly approximately equal*. The maximum deviation of the model-predicted transmissivity from the corresponding experimental value is less than 0.08%. Transmissivity per unit reflectivity of the beam component of radiation *as obtained from experiment and derived model are* – 0.2385 *and* – 0.2462 *respectively. Similarly,* transmissivity per unit reflectivity of the diffused component of radiation *as obtained from experiment and derived model were evaluated as 0.2897 and 0.2991 respectively.* The evaluated values of variance and standard deviation as obtained from experiment and derived model are 1.626 x 10^{-6} and 1.275 x 10^{-3} as well as 1.706 x10^{-6} and 1.306 x 10^{-3} respectively.

References

[1] Far Ultraviolet Spectroscopic Explorer, FUSE: Space Based Astronomy, FACT Sheet, NASA, (1999).

[2] Sukhatme, S. P. (1984). Solar Energy: Principles of Thermal Collection and Storage. Tata McGraw-Hill Publishing Company Limited, New Delhi.

[3] Tiwari, G. N. and Suneja, S. (2002). Solar Thermal Engineering System. New Delhi. Arosa Publishing House, p3.

[4] Bello, Y. I., and Dillip, K. D. (2011). Transmissivity of the Glazing Surface of a Solar Flat Plate Collector Based on the Metrological Parameters of Yola, Nigeria. Journal of American Science. 7(1):639-643. (ISSN: 1545-1003).

[5] Garg, H. P. and Prakash, J. (2000). Solar Energy Fundamentals and Application. New Delhi: Tata McGraw-Hill.

[6] Nwoye, C. I., (2008). Data Analytical Memory; C-NIKBRAN

[7] Nwoye, C. I., Onyedika. **G. O., and Ugwuegbu, C. C.** Model Development for the Prediction of Methane Gas Yield during Microbial Treatment of Fruit Wastes. ***JMME*** **(in press)**

[8] Nwosu, K. H., (1992). Advanced Statistical Analysis, AJEK Publishers, Enugu, 34-38.

Table 1: Variation of transmissivity with reflectivities of beam and diffused components of solar radiation [4]

(α)	(β)	(γ)
0.8821	0.0417	0.0384
0.8816	0.0445	0.0358
0.8812	0.0466	0.0338
0.8792	0.0537	0.0281
0.8790	0.0547	0.0277

Table 2: Variation of 2.2401 α *with* $e^{-0.2820\beta}$ + 0.0112 lnγ + *1.0233*

2.2401 α	$e^{-0.2820\beta}$	0.0112 ln γ	1.0233	$e^{-0.2820\beta}$ + 0.0112 ln γ + 1.0233
1.9760	0.9883	-0.0365	1.0233	1.9751
1.9749	0.9876	-0.0373	1.0233	1.9736
1.9740	0.9870	-0.0379	1.0233	1.9724
1.9695	0.9850	-0.0400	1.0233	1.9683
1.9690	0.9847	-0.0402	1.0233	1.9678

n (Exp)	$(x-x_a)$	$(x-x_a)^2$ $(x\ 10^{-4})$
1	0.0015	0.0225
1	0.0010	0.0100
1	0.0006	0.0036
1	-0.0014	0.0196
1	-0.0016	0.0256

Table 3: Variation of $(x-x_a)$ with $(x-x_a)^2$

$\sum n = 5$ $\quad \sum(x-x_a)^2 = 0.0813 \times 10^{-4}$

Table 4: Vari ation of $(x-x_a)$ with $(x-x_a)^2$

$\sum n = 5$ $\quad \sum(x-x_a)^2 = 0.0853 \times 10^{-4}$

Table 5: Comparison of standard deviation (SD) and variance (V) from experimental and model-predicted results

n (Mod)	$(x-x_a)$	$(x-x_a)^2$ $(x\ 10^{-4})$
1	0.0016	0.0256
1	0.0010	0.0100
1	0.0004	0.0016
1	-0.0015	0.0225
1	-0.0016	0.0256

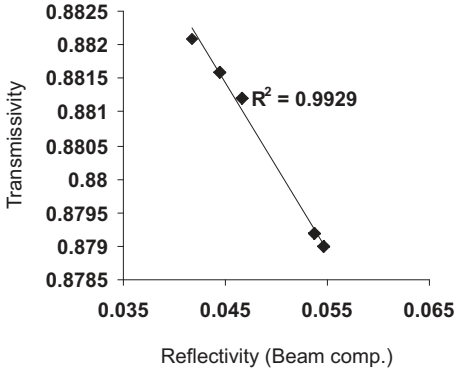


Fig. 1: Coefficient of determination between transmissivity and reflectivity of the beam component of radiation as obtained from the experiment [4]

	Experiment [4]	Model
SD	1.275×10^{-3}	1.306×10^{-3}
V	1.626×10^{-6}	1.706×10^{-6}

2: Coefficient of determination between transmissivity and reflectivity of the beam component of radiation as predicted by derived model

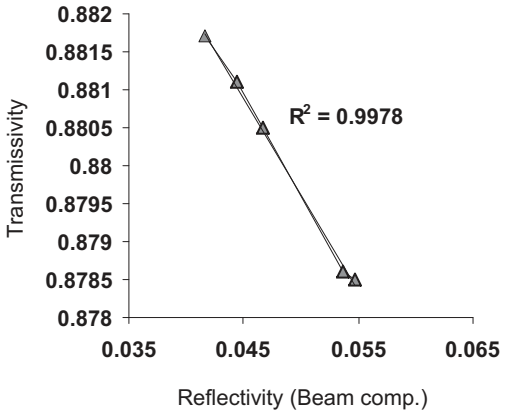


Fig. 3: Coefficient of determination between transmissivity and reflectivity of the diffused component of radiation as obtained from the experiment [4]

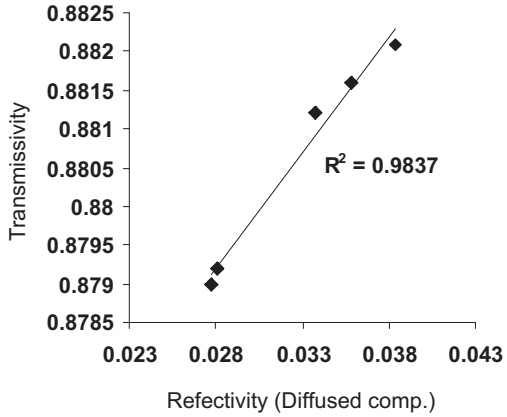


Fig. 4: Coefficient of determination between transmissivity and reflectivity of the diffused component of radiation as predicted by derived model

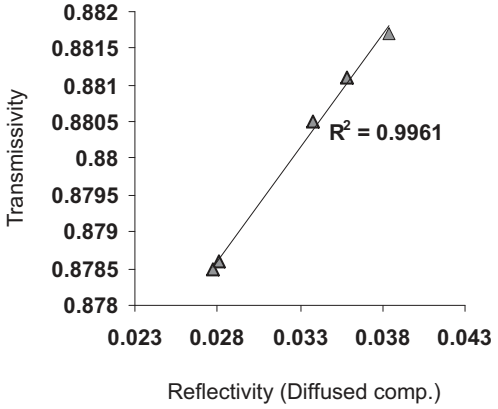


Fig. 5: Comparison of the transmissivity per unit reflectivity of the beam component of radiation as obtained from experiment [4] and derived model.

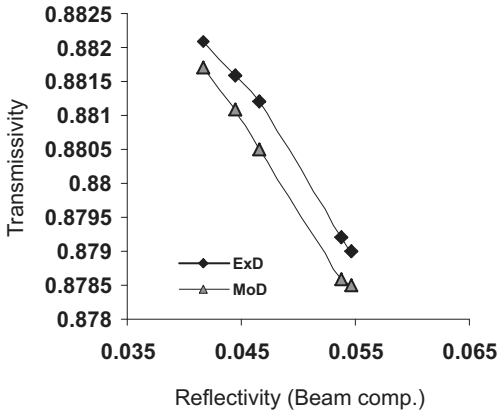


Fig. 6: Comparison of the transmissivity per unit reflectivity of the diffused component of radiation as obtained from experiment [4] and derived model.

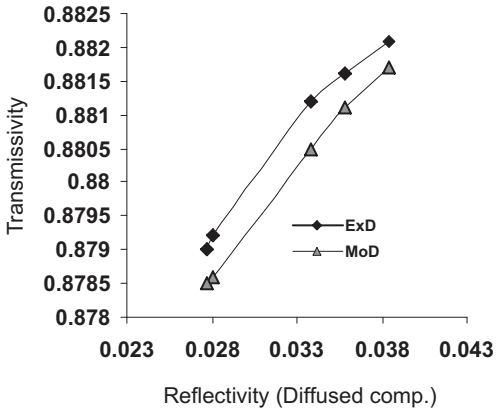


Fig. 7: Variation of model-predicted transmissivity with its associated deviation from experimental values

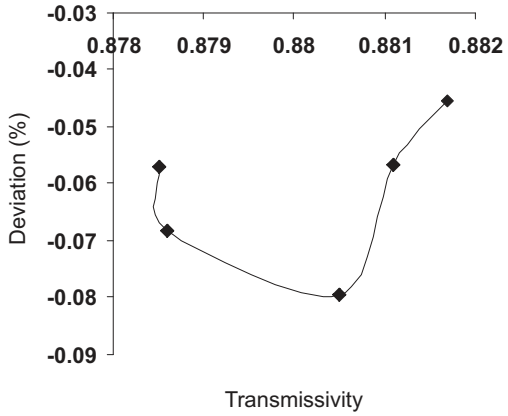


Fig. 8: Variation of deviation (of model-predicted transmissivity) with reflectivity of the beam component of radiation

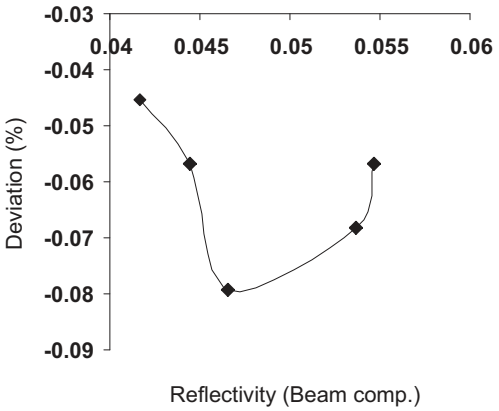


Fig. 9: Variation of deviation (of model-predicted transmissivity) with reflectivity of the diffused component of radiation

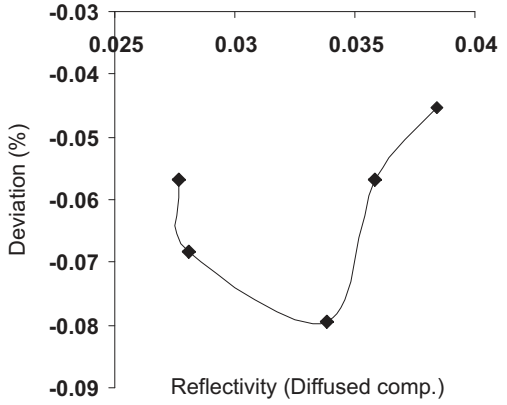


Fig. 10: Variation of model-predicted transmissivity with its associated correction factor

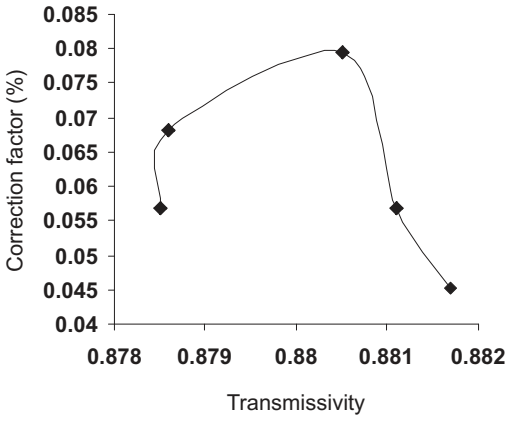


Fig. 11: Variation of correction factor (to model-predicted transmissivity) with the latitude angle of location of the solar collector.

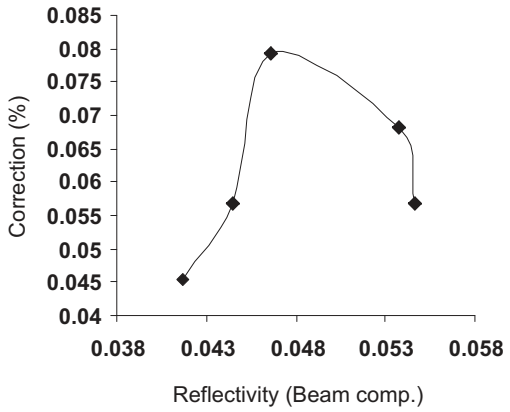
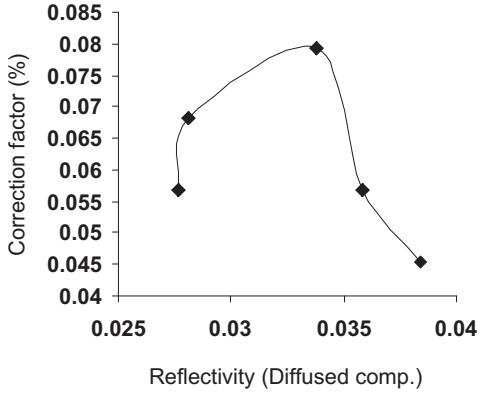


Fig. 12: Variation of correction factor (to model-predicted transmissivity) with the duration of collector exposure.



BIODEGRADABLE METALS FOR BIOMEDICAL APPLICATIONS: A PARADIGM SHIFT IN METALLIC BIOMATERIALS.

[a]C.S. Obayi, [b]B.A. Okorie, [c]D.O.N. Obikwelu, [d]R.E. Njoku, [e]Diego Mantovani.
a, b, c, d Department of Metallurgical and Materials Engineering, University of Nigeria, Nsukka.
[e] Laboratory for Biomaterials and Bioengineering, Department of Mining, Metallurgical and Materials Engineering &University Hospital Research Centre. **Université Laval**, Quebec City, G1K 7P4, Canada
a camillus.obayi@unn.edu.ng **b** bonokorie@yahoo.com **c** daniel.obikwelu@unn.edu.ng
d romanus.njoku@unn.edu.ng, e Diego.Mantovani@gmn.ulaval.ca

ABSTRACT
The practice of using metals and alloys to repair or replace human body parts is established in biomedical applications. Over the years, the paradigm in metallic biomaterial science has been the design, development, and, deployment of permanent medical implants that remain corrosion-resistant and inert once implanted in the human body. Recently, a new approach has emerged that considers metals as degradable, bioactive, and, bioabsorbable biomaterials. Physiological trace elements of iron and magnesium and their alloys have been proposed and investigated as candidates for biodegradable metallic implants because of their essentiality and recognized effect on human metabolism. However, these alloys have not strictly met the vital requirements of sufficient strength and ductility, controlled biocorrosion rate matching tissue healing rate and good biocompatibilities. Iron *has suitable mechanical properties, but* very slow degradation rate *while Magnesium* has limitations of both low strength, and, very rapid degradation rate in physiological media. Many materials' design and development strategies such as selective alloying, electro-deposition, bulk or surface modification and microstructural control are being exploited to overcome these challenges. This paper reviews the current design and evaluation of these two metal alloys as biodegradable implant materials, especially for treating coronary artery disease, the number one cause of death globally.

1.0 Introduction

The practice of using metals and alloys to repair or replace human body parts is established in biomedical applications. Despite the development of assorted biomedical implants made from different biocompatible materials such as polymers, ceramics and composites, metals still account for a substantial percentage of clinically used materials, and, for many applications, they represent the only current viable reconstructive strategy [1]. Metals have remained preferred materials of choice in many load-bearing applications such as total joint replacements and coronary stenting because they possess attributes of strength, stiffness, fracture toughness and fatigue resistance [2, 3, 4]. There are millions of patients who currently have metallic implants and millions more who will need these devices in the near future. Market research indicators put the total US biomedical implant market at about US$27bn, the biocompatible materials market at about US$11bn, the microelectronics medical implant market at about US$12bn, and these markets are increasing at about nine percent per year [5].

Over the years, the paradigm in metallic biomaterial science has been the design, development, and, deployment of permanent medical implants that remain corrosion-resistant and inert once implanted in the human body. This paradigm was anchored on the need to prevent leakage and interference of metallic ions with the human body, which could be toxic and harmful or upset ionic balance of the body. This is because most metallic materials have the intrinsic weakness of being corrodible in aqueous service environments including the human body fluids.

Recently, a new approach has emerged that considers metals as degradable, bioactive, and, bioabsorbable biomaterials. Biodegradable metallic implants, once implanted in the human body are expected to disappear via corrosion after providing temporary mechanical support during the healing process of a diseased or an injured tissue or organ for a certain period of time depending on the application site [6]. They are gradually dissolved, absorbed , and consumed as new tissue is formed or expelled from the body through physiological pathways [7, 8, 9, 10, 11], thereby saving patients the pain and expense of multiple surgery used to implant and then later remove, refit and re-implant the current generation of devices [5]. Repeat surgery increases costs to the health care system and further morbidity to the patient.

Moreover, biodegradable implants may overcome the disadvantages of permanent devices such as prolonged physical irritation and chronic inflammation [12].

The concept of degradable biomaterials is not new because biodegradable materials including polymers has been proposed since 1988 [13]. However, the idea of considering metals as degradable biomaterials is more recent, even though the use of degradable metallic materials (DMMs) for biomedical applications dates back to 1938 when magnesium was used for fixing bone fractures [6, 9]. It has been found that certain metals which consist of physiological trace elements found in the human body such as magnesium (Mg) and iron (Fe) are the promising candidates for this approach [6]. They are essential to human life and their effects on human metabolism are well known [14, 15, 7, 13]. The toxicity of Mg and Fe are relatively low, and , the transport mechanisms for clearance of their degradation products from the human body are relatively understood. The proposed areas of use of this new class of biomaterials in biomedical applications include cardiovascular, orthopaedic and paediatric fields. In cardiovascular applications, the most popular of such degradable implants with temporary functions is a coronary artery stent.

An ideal biodegradable implant made of these alloys should demonstrate an excellent combination of vital requirements of controlled biodegradation matching tissue-healing rate, excellent mechanical properties and biocompatibility. Unfortunately, Mg-and Fe-alloys have certain limitations when considered as degradable implantable materials. The main drawbacks of pure Mg and its alloys are poor corrosion resistance, low elastic modulus (41-45 GPa), and, their limited strength and creep resistance at elevated temperatures [6]. Pure Fe and its alloys, on the other hand, possess outstanding mechanical properties, but their degradation rate is too slow for temporary implant applications.

The current challenges in the design and development of biodegradable metallic implants include: (1) the selection and fabrication of iron-based alloys with an increased but suitable degradation/corrosion rate or magnesium alloys with improved mechanical properties but with reduced corrosion rate to meet the requirements of implant applications; (2) the assessment of the degradation behaviour of these materials which consists of investigation of mechanisms of decomposition and rate via in vitro degradation tests prior to clinical human study; and, (3) the assessment of biocompatibility, or, the tolerance of the surrounding tissues in the presence of degradation products when placed in the human body. This paper reviews the current investigations of these two metal alloys as biodegradable implant materials, especially for treating coronary artery disease, the number one cause of death globally.

2.0 Coronary Artery Disease and Therapy:

Coronary artery disease (CAD), which results from narrowing (stenosis) or total blockage of the coronary artery, has remained the major cause of illness, disability and death globally [16, 17, 18]. According to the World Health Organization (WHO), an estimated 17.1 million people died from various forms of cardiovascular diseases (CVDs) in 2004, representing 29% of all global deaths, and by 2030, almost 23.6 million people will die from CVDs [16]. Of these deaths, an estimated 7.2 million were due to coronary heart disease and 5.7 million were due to stroke. WHO also reported in 2005 that 11% of all deaths due to chronic diseases were caused by CVDs in Nigeria [19].

The main cause of CAD is atherosclerosis-deposit of fatty materials such as cholesterol and lipids on the inner arterial walls, which can build up plaques inside the blood vessel walls leading to restriction or shortage of blood supply to the vital organs of the body such as the heart, brain, kidneys, arms and legs. Metallic coronary stenting is now developed, accepted, and a preferred revascularization method for CAD therapy. A cardiovascular stent is a miniaturized, tubular, wire-mesh structure that is deployed routinely in a stenotic artery following balloon angioplasty. It provides mechanical support to the diseased arterial wall and holds it open or dilated while it remodels and heals, thereby re-establishing vascular lumen, restoring and maintaining reliable and sufficient blood flow conditions within the coronary artery [17, 18]. Prior to the introduction of stenting, percutaneous transluminal coronary angioplasty (PTCA) was one of the main CAD treatment methods used to dilate the vascular lumen, apart from pharmacological therapy and coronary artery bypass graft (CABG) [3].

Metallic stenting has progressed from permanent bare metal stents, made from corrosion resistant alloys, such as stainless steel 316L (SS316L), cobalt (Co)-chromium (Cr) alloys and nickel (Ni)-titanium (Ti) alloys, to drug-eluting stents and currently, biodegradable stents [13, 20, 21]. All these stages were driven by shortcomings observed in medical procedures applied in treating CAD and solutions were anchored on materials' innovation to enhance device performance. For instance, conventional balloon angioplasty, introduced in the 70s, presented two major complications: abrupt vessel closure and restenosis [106]. Permanent bare metal stenting, introduced in 1987 by Sigwart et al [22], prevented abrupt vessel closure and significantly reduced the rate of restenosis, from 60% to 25%. However, bare metal stenting was limited by other clinical complications such as prolonged physical irritation and chronic inflammation due to its permanence in the blood vessel [9], in-stent restenosis [23], and possible release of potential toxic metallic ions through corrosion or wear processes in vivo [24]. Drug-eluting bare metal stents, which combined drug storage and delivery functions and utilized surface coating as a barrier against metal ion leakage, were introduced to treat restenosis caused by proliferation of cells in the stented segment and chronic inflammation, but had the problems of late-stent thrombosis and delayed endothelialization [25].

Metallic biodegradable stent was introduced to fulfill the short-term need of stent in CAD treatment. Clinically it has been found that it takes a period of 6-12 months for the healing (remodeling) process to be completed [26], thus making a permanent stent implant redundant beyond 12 months and continued management of potential long-term complications unnecessary. Biodegradable stent provides temporary mechanical support during the healing process of a diseased artery and it can be gradually dissolved, absorbed and consumed as new tissue is formed or expelled from the body through physiological pathways [7, 8, 9, 10, 11].

3.0 Desirable properties of biodegradable coronary stents and validation.

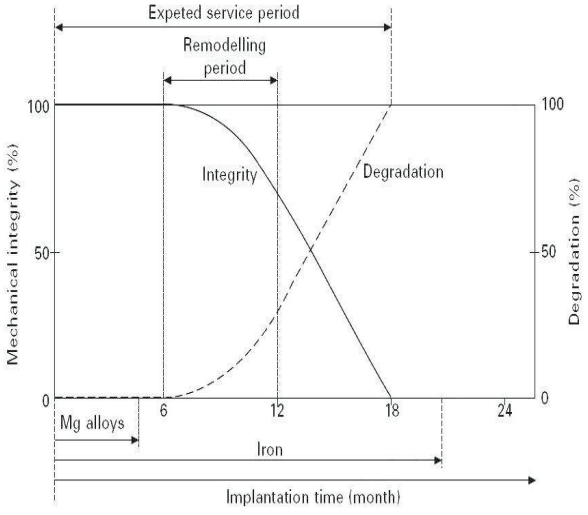
An ideal biodegradable stent should demonstrate an excellent combination of vital requirements of controlled biodegradation, excellent mechanical properties and biocompatibility. Polymers such as poly-L-lactic acid (PLLA) [27, 28], polyglycolic acid/polylactic acid and polycaprolactone[29], which have been investigated as biodegradable biomaterials since 1988, exhibit inferior mechanical properties when compared with metals. Although degradable polymers decompose in the human body after 12-24 months and have good compatibilities, they need to be thicker in order to compete with metals in making miniaturized and load-bearing coronary stents (stent weight --40mg $d = 2-4mm; l = 15-20mm$ that require high strength and ductility. [13, 30].

Currently, stainless steel 316L (SS316L) is the most popular among the corrosion-resistant metallic biomaterials used for long-term application. In developing new biomaterials for stent applications, it is considered as the standard reference for mechanical properties [31]. The mechanical properties of some already implanted degradable metals as compared with SS316L are tabulated below.

Metal and its composition (wt. %)	Density (g/cm^3)	magnetic/ non-magnetic	Yield strength (MPa)	Tensile strength (MPa)	Young's modulus (GPa)	Elongation (%)
SS316L annealed plate [32] Fe, 16 – 18.5Cr, 10 – 14Ni, 2–3Mo, <2Mn, <1Si, <0.03C	8.00	Non-magnetic	190	490	193	40
Iron annealed plate [33] 99.8Fe	7.87	magnetic	150	210	200	40
WE43 magnesium alloy temper T6 [34] Mg, 3.7 – 4.3Y, 2.4 – 4.4Nd, 0.4–1Zr	1.84	Non-magnetic	170	220	44	2

Pure Fe is more suitable for use in coronary stents as its mechanical properties are closer to those of SS316L than Mg alloys. However, unlike most metallic biomaterials, Fe is magnetic, a property which can influence its compatibility with magnetic resonance imaging (MRI), the modern imaging and diagnostic technique. Mg alloys have limited ductility compared to most Fe alloys.

In addition to good mechanical properties, an ideal biodegradable metallic biomaterial should possess controlled degradation behaviour. It should undergo gradual and uniform in vivo degradation that will be completed at the end of vessel remodeling, without releasing toxic substances that can induce negative side effects on the physiology or health of the patient. There should also be a good compromise between degradation and mechanical integrity during in vivo implantation as shown in figure below [31].



A series of in vivo and in vitro tests are employed in understanding and *a*ssessing the degradation behaviour and compatibility of these materials. In vitro degradation tests consist of investigation of mechanisms of decomposition and rate without contact with the cells prior to clinical human study using biological fluids or simulated biological fluids such as Hank's solution. These degradation tests which are the usual laboratory corrosion tests used to screen metals for corrosion prevention and control include immersion test (ASTM G 31) [35], potentiodynamic polarization test (ASTM G 59) [36] and a specialized dynamic immersion test method that approximates the physiological conditions obtainable in coronary arteries [37]. Biocompatibility tests involve the assessment of host response or the tolerance of the surrounding tissues in the presence of degradation products when placed in the human body. A biocompatible biomaterial is should show minimum inflammatory and toxicity reactions both locally and systematically.

4.0 Fe and Mg Alloys: state-of-the-art

4.1 Iron

In the earth's crust, Fe is the second most abundant metallic element after Al [38]. Fe is an essential element for most living organisms. It is a useful component of cytochromes, haemoglobin and myoglobin (oxygen-binding molecules) and many enzymes [39]. It plays significant roles in diverse physiological processes including the transport, storage and activation of molecular oxygen, and DNA synthesis [40, 41]. Fe ions are bound to transferrin (the Fe-transporting protein) during circulation and bound to ferritin (the Fe-storaging protein) when accumulated within cells. Adult men normally have 35 to 45 mg of iron per kilogramme of body weight [42] and Fe-load of blood is as high as 447 mg/L [43]. In a balanced state, 1-2 mg of iron enters and leaves the body each day [39]. Despite the essentiality of iron to life, its excess or deficiency can be deleterious [39].

Fe has the capacity to accept and donate electrons readily; interconverting between ferrous (Fe^{2+}) and ferric (Fe^{3+}) forms in alkaline, high chloride and oxygen-rich environment of physiological fluids leading to the precipitation and deposition of oxides and phosphates. Although, the *in vivo* degradation rate of pure Fe is slow, the mechanism of clearance of its degradation products from the body is relatively known.

Since the pioneering work of Peuster, et al [44] on the use of high purity iron (Fe>99.8%) as biodegradable stent, iron has attracted a quantum of research effort. In vivo investigations have shown that pure iron has outstanding biological performance. It has no organ accumulation of degradation products and no systemic toxicity, no pronounced neointimal proliferation and inflammatory response of the stented vessel [45, 44, 6]. The major limitation of pure iron as the most potential stent material is slow biodegradation rate [45, 44], as it has suitable mechanical properties (high strength, ductility and elastic modulus) close to that of stainless steel SS316L [7], the referred gold standard for stent implants.

Various materials' design strategies have been employed to enhance the degradation rate and biological performance of pure Fe, without compromising its mechanical properties. Such strategies include selective alloying [7, 13, 12, 8, 9, 46, 47], electro-deposition/electroforming [10], bulk or surface modification [48, 49]. Fe alloys produced and investigated as candidate biodegradable materials include antiferromagnetic iron-manganese (Fe-35Mn) alloy [7, 13, 12, 8], ternary iron-manganese-palladium (Fe-10Mn-1Pd) alloy [9], binary Fe alloys [46], ternary iron-manganese-silicon (Fe30Mn6Si) alloy [47] and electroformed iron [10].

4.2 Magnesium

Magnesium (Mg) is the third most abundant metal in the earth's crust, only exceeded by aluminium and iron [50]. It is an exceptionally lightweight metal with a density of 1.74 g/cm^3 [51]. The high strength-to-weight ratio of Mg and its alloys makes them extremely useful in applications requiring lightweight such as the aerospace and transport industries [51]. The major drawbacks of Mg and its alloys for engineering applications are low corrosion resistance in electrolytic, aqueous environments, low elastic modulus (41-45MPa) and their limited strength and creep resistance at elevated temperatures [24]. The global use of Mg was 360,000 tonnes per year in 1998 with a growth rate of 7% per year [24].

Mg ions are present in large amounts in the human body and they are essential to human metabolism and biological mechanisms [51]. It is the fourth most abundant cation in the human body, with an estimated 1 mol of Mg stored in the body of a normal 70 kg adult, with approximately half of the total physiological Mg stored in the bone tissue [53]. Mg is co-factor for numerous metabolic enzymes and stabilizes the structure of Deoxyribonucleic acid (DNA) and ribonucleic acid (RNA) [52]. The level of Mg in normal blood serum ranges between 0.73-1.06 mmol/L. While deficiency of Mg is reported to cause cell membrane dysfunction, an increased incidence of cancer, heart disease and susceptibility to oxidative stress, its excess can lead to muscular paralysis, hypertension, respiratory distress and cardiac arrest [54]. However, the incidence of hyper-magnesium is rare due to its efficient and harmless filtration by the kidneys and excretion in the urine [52].

Due to above positive properties of Mg, it has been considered safe to fabricate Mg for use as implantable biodegradable materials that can be gradually dissolved, consumed or absorbed in the human body. Mg and its alloys have been actively investigated and utilized as a potential biodegradable material for orthopaedic or bone implants. This is because Mg and its alloys have low density and stiffness close to that of natural bone ($\rho = 1.8 - 2g/cm^3, E = 11.7 - 18.2GPa$) [24] and has been reported to support the activation of bone cells. Its low Young's modulus will be beneficial in reducing stress shielding at the bone-implant interface [24].

The unfortunate complication in the potentiality of Mg as a biodegradable metal is that pure Mg corrodes too quickly in the physiological PH (7.4-7.6) and high chloride environment of the physiological system,

loosing mechanical integrity before tissue has sufficiently healed and producing magnesium hydroxide and hydrogen gas in a corrosion process at a rate that is too fast to be dealt with by the host tissue. The overall corrosion reactions of Mg in a high-chloride aqueous physiological environment [24] are as given below:

$$Mg(s) + 2H_2O \rightarrow Mg(OH)_2(s) + H_{2(g)}$$

$$Mg(s) + Cl^-(aq) \rightarrow MgCl_2$$

$$Mg(OH)_2(s) + 2Cl^- \rightarrow MgCl_2$$

In a high chloride environment, magnesium hydroxide which accumulates on the underlying magnesium matrix as a corrosion protective layer reacts with chloride ions to form highly soluble magnesium chloride and hydrogen gas. The formation of $MgCl_2$ causes severe corrosion and can lead to severe pitting corrosion in body fluid where chloride ions are present at levels on the order of 150 mmol/L [24].

Some design strategies such as alloying [170], grain refinement [24], surface protective coating with dicalcium phosphate dehydrate, and, alkali heat treatment, have been used to improve strength, ductility and corrosion resistance of Mg, to obtain nontoxic and biological compatible material. Alloying targets use of alloying elements such as Ca, Zn, Mn, and, a very small amount of rare earth elements that have low toxicity and could be tolerated in the human body and could also retard the biocorrosion of magnesium alloys [55]. Several Mg Alloys have been investigated including Mg-Ca, AE21, AZ91, AM60, LAE442 and WE43. A number of Mg alloy stents such as AE21, WE43 have been investigated in vivo in animals. Absorbable magnesium stents (AMS) containing rare earth metals have been implanted in the lower limb of adult patients [56], in the left pulmonary artery of a preterm baby [57] and in the aorta of a newborn [58].

5.0 Conclusion

The introduction of biodegradable metallic implants is breaking the established paradigm that metallic implants must be corrosion resistant and inert. Physiological trace elements of iron and magnesium and their alloys are candidate materials for biodegradable metallic implants because of their essentiality and recognized effect on human metabolism. However, these alloys have not strictly met all the vital requirements of sufficient strength and ductility, controlled biocorrosion rate matching tissue healing rate and good biocompatibilities. Iron has suitable mechanical properties but very slow degradation rate while Mg has limitations of both low strength and very rapid degradation rate in physiological media. Many materials' design and development strategies such as selective alloying, electro-deposition, bulk or surface modification and microstructural control are being exploited to overcome these challenges and enable the production of biodegradable metallic implants that will satisfy the required specifications of biocompability, biofunctionality, biodurability and biosafety in the short, medium and long term when placed in the body.

References

1. Kohn, D.H., Metals in medical applications. Current Opinion in Solid State and Materials Science, 1998. 3(3): p. 309-316.
2. Metals As Biomaterials edited by Jef A. Helsen and H. Jurgen Breme. John Wiley and Sons, West Sussex, England, 1998.
3. Z. Paszenda. Use of Coronary stents – material and Biophysical Conditions. JAMME, 43(1), pp. 125-135, 2010.
4. Staiger, M.P., Alexis M. Pietak, Jerawala Huadmai, George Dias. Magnesium and its alloys as orthopedic biomaterials: A review. Biomaterials, 2006. 27(9): p. 1728-1734.
5. Yeoheung Yun, Zhongyun Dong, Namheon Lee, Yijun Liu, Dingchuan Xue, Xuefei Guo, Julia Kuhlmann, Amos Doepke, H. Brian Halsall, William Heineman, Surya Sundaramurthy, Mark J. Schulz, , Zhangzhang Yin, Vesselin Shanov, Douglas Hurd, Peter Nagy, Weifeng Li, Curtis Fox. Revolutionizing biodegradable metals. Materialstoday, Vol. 12, Iss.10, 2009, Pp.22-32.
6. Waksman, R.O.N., et al., Short-Term Effects of Biocorrodible Iron Stents in Porcine Coronary Arteries. Journal of Interventional Cardiology, 2008. 21(1): p. 15-20.
7. Hermawan, H., Alamdari, H., D. Mantovani, Dominique Dube, Iron-manganese: new class of metallic degradable biomaterials prepared by powder metallurgy. Powder Metallurgy, 2008. 51(1): p. 38-45.
8. Hermawan, H., et al., Fe-Mn alloys for metallic biodegradable stents: Degradation and cell viability studies. Acta Biomaterialia. 6(5): pp. 1852-1860.
9. Schinhammer, M., Anja c. Hanzi, Jorg F. Loffler, Peter J. Uggowitzer. Design strategy for biodegradable Fe-based alloys for medical applications. Acta Biomaterialia. 2010, 6(5): p. 1705-1713.
10. Moravej, M., et al., Electroformed iron as new biomaterial for degradable stents: Development process and structure-properties relationship. Acta Biomaterialia. 6(5): p. 1726-1735.
11. Song, G., Control of biodegradation of biocompatable magnesium alloys. Corrosion Science, 2007. 49(4): p. 1696-1701.
12. Hermawan, H., D. Dubé, and D. Mantovani, Degradable metallic biomaterials: Design and development of Fe–Mn alloys for stents. Journal of Biomedical Materials Research Part A. 93A(1): p. 1-11.
13. Hermawan, H., D. Dubé, and D. Mantovani, Developments in metallic biodegradable stents. Acta Biomaterialia. 6(5): p. 1693-1697.
14. Lévesque, J., et al., Design of a pseudo-physiological test bench specific to the development of biodegradable metallic biomaterials. Acta Biomaterialia, 2008. 4(2): p. 284-295.
15. Zhu, S., et al., Biocompatibility of pure iron: In vitro assessment of degradation kinetics and cytotoxicity on endothelial cells. Materials Science and

Engineering: C, 2009. 29(5): p. 1589-1592.
16. World Health Organization (WHO). Cardiovascular Diseases (CVDs). Fact Sheet No.317, January, 2011. http://www.who.int/mediacentre/factsheets/fs317/en/. Accessed on 29/03/2011.
17. Murphy, B.P., et al., The Stress–Strain Behavior of Coronary Stent Struts is Size Dependent. Annals of Biomedical Engineering, 2003. 31(6): p. 686-691.
18. ANKUR Raval, Animesh Choubey, Chhaya Engineer, Devesh Kothwala. Development and assessment of 316LVM cardiovascular stents. Materials Science & Engineering A, 2004, 386, pp331-343.
19. World Health Organization (WHO). Reference: http://www.who.int/chp/chronic_disease_report/mediaNIGERIA.pdf. Accessed on 15/08/2011.
20. Elliot J.S., Ajay K., Martin T.R. New Developments in Coronary Stent Technology. J.Interv. Cardiol, 19, 493-9, 2006.
21. Waksman, R., Promise and challenges of bioabsorbable stents. Catheterization and Cardiovascular Interventions, 2007. 70(3): p. 407-414.
22. Sigwart, U., et al., Intravascular Stents to Prevent Occlusion and Re-Stenosis after Transluminal Angioplasty. New England Journal of Medicine, 1987. 316(12): p. 701-706.
23. Hoffmann, R, Mintz GS, Dussaillant GR, Popma AD, Satler LF, Kenneth M. Kent, Jennifer Griffin, Martin B. Leon. Patterns and Mechanisms of In-Stent Restenosis: A Serial Intravascular Ultrasound Study. Circulation, 1996. 94(6): p. 1247-1254.
24. Mark P. Staiger, Alexis M. Pietak, Jerawala Huadmai, George Dias. Magnesium and its alloys as orthopedic biomaterials: a review. Biomaterials 2006; 27: 1728–34.
25. Virmani, R, Farb A, Guagliumi G, Kolodgie FD. Drug-eluting stents: caution and concerns for long-term outcome. Coronary Artery Disease, 2004. 15(6): p. 313-318.
26. Schomig A, Kastrati A, Mudra H, Blasini R, Schuhlen H, Klauss V, et al. Four-year experience with Palmaz-Schatz stenting in coronary angioplasty complicated by dissection with threatened or present vessel closure. Circulation 1994; 90: 2716–24.
27. Stack R.S., Califf R.M., Phillips H.R., Pryor D.B., Quigley P.J., Bauman R.P., Tcheng, J.E., Greenfield, J.C., Jr. Interventional cardiac catheterization at Duke Medical Center. Am. J. Cardiol, 1988; 62: 3F–24F.
28. Tamai H., Igaki K., Kyo E., Kosuga K., Kawashima A., Matsui S., Komori, H., Tsuji, T., Motohara, S., Uchata, H. Initial and 6-month results of biodegradable poly-L-lactic acid coronary stents in humans.Circulation 2000;102:399–404.
29. Van der Giessen W.J., Lincoff A.M., Schwartz R.S., Van Beusekom H.M., Serruys P.W., Holmes D.R. Jr, Ellis, S.G., Topol, E.J. Marked inflammatory sequelae to implantation of biodegradable and nonbiodegradable polymers in porcine coronary arteries.
Circulation 1996; 94: pp. 1690–7.
30. Y.P. Kathuria. The potential of biocompatible metallic stents and preventing restenosis Materials Science and Engineering A 417 (2006) 40–48.
31. H. Hermawan, D. Dube, D. Mantovani. Degradable metallic biomaterials for cardiovascular applications. Wood head Publishing Limited, Cananda, 2010, pp.379-404.
32. ASTM F 138: Standard specification for wrought 18chromium–14nickel–2.5molybdenum stainless steel bar and wire for surgical implants (UNSS31673). West Conshohocken: ASTM International; 2003.
33. Goodfellow Corporation. Iron (Fe)—material information. http://www.goodfellow.com/csp/active/STATIC/A/Iron.HTML (accessed 05/05/2011).
34. ASTM. ASTM B 80: Standard specification for magnesium-alloy sand castings. West Conshohocken: ASTM International; 2001.
35. ASTM G31-99. Standard practice for laboratory immersion corrosion testing of metals. West Conshohocken, ASTM International, 2001.
36. ASTM G59-97 (2003), Standard test method for conducting potentiodynamic polarization resistance measurements, West Conshohocken, PA: ASTM International, 2006.
37. Levesque J, Hermawan H, Dube D, Mantovani D. Design of a pseudophysiological test bench specific to the development of biodegradable metallic biomaterials. Acta Biomater 2008; 4: 284–95.
38. Agung Purnama, Hendra Hermawan, Jacques Couet, Diego Mantovani. Assessing the biocompatibility of degradable metallic materials: State-of-the-art and focus on the potential of genetic regulation. Acta Biomaterialia. 6(5): p. 1800-1807.
39. Andrews NC. Disorders of iron metabolism. N Engl J Med 1999;341:1986–95.
40. Shengfa Zhu, Nan Huang, Li Xua, Yu Zhang, Hengquan Liu, Hong Sun, Yongxiang Leng. Biocompatibility of pure iron: In vitro assessment of degradation kinetics and cytotoxicity on endothelial cells. Materials Science and Engineering C 29 (2009), pp. 1589–1592.
41. Fontcave M, Pierre JL. Iron: metabolism, toxicity and therapy. Biochimie 1993;73:767–73.
42. Bothwell TH, Finch CA. Iron metabolism. Boston: Little, Brown, 1962.
43. Emsley J. The elements. Oxford:
Clarendon Press; 1998
44. Peuster, M., et al., A novel approach to temporary stenting: degradable cardiovascular stents produced from corrodible metalâ€"results 6-18 months after implantation into New Zealand white rabbits. Heart, 2001. 86(5): p. 563-569.
45. Peuster, M., et al., Long-term biocompatibility of a corrodible peripheral iron stent in the porcine descending aorta. Biomaterials, 2006. 27(28): p. 4955-4962.

46. Liu, B. and Y.F. Zheng, Effects of alloying elements (Mn, Co, Al, W, Sn, B, C and S) on biodegradability and in vitro biocompatibility of pure iron. Acta Biomaterialia. 2011. 7(3): p. 1407-1420.
47. Liu, B., Y.F. Zheng, and L. Ruan, In vitro investigation of Fe30Mn6Si shape memory alloy as potential biodegradable metallic material. Materials Letters. 65(3): p. 540-543.
48. F.L. Nie, Y.F. Zheng, S.C. Wei, C. Hu, G. Yang. In vitro Corrosion, Cytotoxicity andHemocmpatibility of Bulk Nanocrystalline Pure Iron. Biomedical Materials, 2010, 5: p.065015.
49. Shengfa Zhu, Nan Huang, Hui Shu, Yanping Wu, Li Xu. Corrosion resistance and blood compatibility of lanthanum ion implanted pure iron by MEVVA. Applied Surface Science, 2009. 256(1): p. 99-104.
50 Yizao Wan, Guangyan Xiong, Honglin Luo, Fang He, Yuan Huang, Xiaoshong Zhou. Preparation and characterization of a new biomedical magnesium-calcium alloy. Materials and Design, 29, pp.2034-2037, 2008.
51.Song G.L., Arrens A. Corrosion mechanisms of magnesium alloys. Adv,Eng.Mater., 1(1), pp. 11-33, 1999.
52. Vormann J. Magnesium nutrition and metabolism. Mol. Aspects Med., 24, pp.27-37, 2003.
53. Wolf H. Cittadini A. Chemistry and biochemistry of magnesium. Mol. Aspects Med., 24, pp.3-9, 2003.
54. Saris NEL. Magnesium: an update on physiological, clinical and analytical aspects. Clin. Chem. Acta, 294, pp. 1-26, 2000.
55. ASTM E8-04, Standard test methods for tension testing of metallic materials. West Conshohocken, PA: ASTM International , 2006.
56. Ong AT, McFadden EP, Regar E, de Jaegere PP, van Domburg RT, Serruys PW. Late angiographic stent thrombosis (LAST) events with drug-eluting stents. J Am Coll Cardiol 2005;45:2088–92.
57. Witte, F., et al., Degradable biomaterials based on magnesium corrosion. Current Opinion in Solid State and Materials Science. 12(2008): p. 63-72.
58. Le´vesque J, Dube´ D, Fiset M, Mantovani D. Investigation of corrosion behaviour of magnesium alloy AM60B-F under pseudo- physiological conditions. Mater Sci Forum 2003; 426-432:pp521–526.

POWDER METALLURGY; AN ALTERNATIVE PROCESS ROUTE FOR DUPLEX STAINLESS STEEL NANOCOMPOSITE - REVIEW

OLANIRAN O.S.[a & b], OLUBAMBI P.A[a & b]. ADEWUYI B.O.[b] AND OLADELE I.O.[b]

a. Department of Chemical and Metallurgical Engineering, Tshwane University of Technology, Pretoria, South Africa

Metallurgical and Materials Engineering Department, Federal University of Technology, Akure, Ondo State.

Emails: dayo525@yahoo.com, tayo_adewuyi@yahoo.com

ABSTRACT

The synthesis of nanomaterials in powder form has been successfully demonstrated in large number of materials, while that of nanostructured materials in bulk form with controlled microstructure and phases poses formidable challenge. Synthesizing nanostructured duplex stainless steels composites is therefore a significant practical challenge and remains largely an area of research interest. Powder metallurgy (PM) technology offers an ability to produce a broader spectrum of alloy compositions with unique properties. The powder metallurgical method offers an efficient technique for the fabrication of metal–ceramic composites and provides a uniform distribution of particulates in the composites. Amongst the various means which the overall properties of powder metallurgy stainless steel components can be improved are: the reinforcement with selected additives while the second is the improvement on sintering techniques. However, these were not unassociated with some challenges which shall be discussed in this work.

Keywords: Powder metallurgy, sintering, nanocomposites, reinforcement and grain growth

INTRODUCTION

Stainless steels are a special class of engineering materials that can be employed in a variety of industrial applications including the oil and gas industries, automotive, pulp and paper plants, chloride containing process fluids, mining and minerals processing industries, and in numerous other chemical industries. They offer a combination of properties, such as corrosion resistance in hot corrosion environments containing chloride ions, mechanical strength and ductility, abrasion resistance and weldability [1]. The various service requirements in many industries however necessitate the development of improved stainless steels with superior properties. Improving the overall properties of stainless steels in turn requires the selection of effective materials development techniques. Available synergistic approaches include the manipulations and modifications of the metallurgical influencing parameters through phase modifications and transformation, microstructural modifications, and control of alloy composition. Apart from the above approaches, the overall improvement of stainless steel properties can be best achieved through the selection of effective production process.

The powder metallurgical method offers an efficient technique for the fabrication of metal–ceramic composites and provides a uniform distribution of particulates in the composites [2]. Amongst the various means which the overall properties of powder metallurgy stainless steel components can be improved, two major approached are very critical. The first is the reinforcement with selected additives while the second is the improvement on sintering techniques. According to Padmavathi et al. [3], there is considerable scope for improving the properties of powder metallurgy components through novel sintering techniques and/or by alloying additives.

The in-situ second-phase grain reinforcement method of improving stainless steel properties has attracted increasing interests owing to the highly thermal stability of the reinforced phase, the highly interfacial strength between matrix and reinforced phase, the widely uniform distribution of reinforced phase in the matrix, and the excellent mechanical property of the grain reinforcement nanocomposite materials [4]. Ceramic particles such as metal oxides, metal carbide, and metal nitrides can be added to improve the mechanical properties. The addition of different ceramic particulates to metal matrix can result in improved stiffness, creep, fatigue and wear resistance [5].

The high strength recorded has been attributed to the nearly equal contribution of solution alloying of the matrix, fine grain hardening as well as dispersed oxide particle hardening. According to Imbaby and Jiang [6], the fabrication of micro components of composite materials offers the possibility of varying the properties for a wide range of applications.

SIGNIFICANCE OF POWDER METALLURGY

Duplex stainless steels have a wide range of engineering applications, mainly in the automotive, figs. 1 and 2, chemical, petrochemical, food, mining and nuclear industries etc, as well as in medical. They can be widely applied as filters in the chemical industries, while in the automotive industry, they are mostly used as ABS rings or temperature control valves, wear resistance materials such as brake, mounting brackets for the rear view mirrors, the tone wheels for the antilock brake systems and also in automotive exhaust applications like exhaust flanges and mounting unit of HEGOS. They also find extensive applications in tools, dies, and wear-and high-

temperature oxidation-resistant component in the chemical and mining industries. However, the usage of duplex stainless steel composites in many industries in South Africa especially the automobile industry as well as chemical and mining industries is very low. The need for advanced researches on the sintered duplex stainless steel parts is therefore very important and urgent. Studying the corrosion/oxidation behaviour of cathodically modified duplex stainless steel is not only of high importance from technological effectiveness perspective alone, but also from the possible cost reductions from the decrease in corrosion/oxidation loss in many industries.

PROBLEMS / CHALLENGES OF PM

The goal of modification of metal part is achieved through the technique that involves appropriate incorporation of ceramic powders and other elements of interest into the metal matrix, a major and critical step therefore, is the appropriate mixing of the metal/ceramic powders prior to powder compaction and difficulty associated with compaction of metalic materials.

MIXING

Upon the selection of appropriate powder and binder system, mixing of the powder and binder are conducted to form the feedstock. Inappropriate mixing method of the varying powders and with binder may lead to inhomogeneity of the resultant feedstock powder. During mixing, insufficient binder may induce incomplete wetting of the powder surface. This is particularly important in nanomaterials since smaller particle size generally demands a larger amount of binder to wet the free. Another challenge during mixing as observed by Wei et al, [7] is possible agglomeration of nanopowders. Thus the ability to prepare well-mixed and homogeneous nanopowders with retained nanograins as feedstock for compaction and sintering is extremely important. When two or more phases are mixed together to produce a nanocomposite, a combination of phases and properties could be obtained. Since nanocomposite exists at a nanoscale, many interfaces may exist between the intermixed solid phases. This is particularly very prominent and present significant challenges during the synthesis of nanostructured materials in bulk form, where the different metallurgical processes occurring at their grain boundaries could fast result in grain growth, and inter-growth of secondary phases. Duplex stainless steels obtained from ferritic and austenitic powders mixtures achieved a sintered microstructure that strongly depends on the balance of initial powders. Care must therefore be taken while mixing because, inappropriate mixture of such phase may impair austenite/ferrite phase balance.

COMPACTION

Despite the global focus on metal matrix nanocomposite, not much attention has been paid to the synthesis of stainless steel nanostructured composite. Amongst the several factors that have so far limited the commercial application of PM stainless steels, the relatively poor compressibility and the abrasive nature of stainless steel powder particles during compaction chiefly poses serious technical challenge [8,9].

SINTERING

The sintering of compact nanopowders especially stainless steel is a very complex process. According to Anselmi-Tamburini et al. [10], sintering of nanopowders to full or nearly full density without appreciable grain growth continues to present a significant practical challenge. Inadequate sintering process or method can result in microstructural coarsening and the formation of undesirable secondary phases that may impair ferrite/austenite targeted properties. It has been observed that high oxide content in stainless steel can be very difficult to reduce during sintering without using very high temperatures, thus leading to distortion [8]. Similarly, improper compaction and sintering technique can lead to the formation of grain growth, coarsening with pores formation within the matrix [11].

High-pressure densification, microwave sintering, shock densification, high-frequency induction heating and magnetic pulse compaction [12 - 15] have been proposed as suitable techniques for improving powder compacting and sintering. However, these fabrication routes can be uneconomical for many applications or can be difficult to apply successfully [8]. A faster heating rate proposed during sintering in conventional furnaces has resulted in thermal gradient within the compacts and caused compact distortion and an inhomogeneous microstructure [3]. There is therefore the need to investigate simple and economical routes for microstructural improvements.

Generally, powder metallurgy stainless steel may sometimes be less resistance to corrosion and wear, as compared to that of their unreinforced matrix, possibly due to the presence of pores (porosity) and the low interaction between matrix and reinforcement [1, 16 -17]. These low interactions may arise from poor bonding between the matrix and the reinforcement due to poor compaction and sintering. Since different constituent phases within duplex stainless steel composites have different thermodynamic properties, possible inbalance between ferrite/austenite phases, as well as between the reinforcement and the matrix, may result in galvanic interaction within the bulk nanocomposite [1]. These could lead to corrosion cell being formed within the nanocomposite matrix and thus promote galvanic and grain boundary corrosion.

SUGGESTED SOLUTIONS

In order to proffer solution to the various metallurgical challenges during the synthesis of duplex stainless steel nanocomposites, several powder mix, unconventional sintering and densification techniques can be adopted to manipulate the structure/composition/processing technique/property consequences of different types/grades of stainless steel, alloying elements and varying reinforcing ceramics starting powders. Proper and adequate mixing and blending of correct proportions of the selected powders with the addition of some alloying elements such as Cr, Ni and Cu, will act as binder as well as promotes corrosion resistance within the matrixes of the duplex stainless steel nanocomposites

developed. The presence of these binding metals can reduce friction of steel powders and thus aid easy compaction. The addition of suitable active cathodes e.g. the PGMs can help in retarding the kinetics of the cathode process, thus enhancing the resistance of the composite to corrosion.

Recently, investigations have shown that spark-plasma sintering (SPS) can be utilized to sinter both monolithic and composite powder compacts much more rapidly than conventional sintering, producing materials with better microstructural, corrosion and mechanical properties [1, 16, 18 - 20]. Since SPS is a short time sintering process where powder particles are compacted by uniaxial processing and heating simultaneously, grain growth can be easily restricted with improved densification through the combine benefit of its rapid sintering [11]. Due to the features of rapid heating, cooling rates and short holding time of the SPS process, the powder compact can be consolidated at relatively lower temperature than in the general methods for the equivalent density of the sintered bulk specimen.

CONCLUSION

Powder metallurgy (PM) components produced from corrosion-resistant alloys are a growing area of PM application, of which stainless steel PM alloys span a variety of industries, including aerospace, automotive, chemical processing, medical, and recreational. Recent progress has also led to the understanding that proper processing and sintering of M stainless steel are critically important factors in achieving corrosion resistance for increasingly demanding applications. In fact, many (if not most) cases of underperforming PM stainless steel parts in terms of corrosion resistance can be traced to metallurgical defects due to improper processing [21]. Therefore, improved understanding of the PM stainless steel processing factors can have important results in terms of corrosion resistance and the extended use of PM technology for its well-known economic value in terms of net shape processing and more efficient material utilization in a large number of applications for the automotive and other industries

REFERENCES

[1] Campos M., Baustita A., Caceres D., Abenojar J., Torralba J.M. (2003), *Study of the interfaces between austenite and ferrite grains in P/M duplex stainless steels*. Journal of the European ceramic society 23, 2813-2819

[2] Chawla, N. and Chawla, K. K. (2006), Metal matrix composites. New York: Springer. Chen, W. and Zhou, J. (2009) Preparation and Characterization of Stainless Steel/TiC Nanocomposite Particles by Ball-milling Method, Journal of Wuhan University of Technology-Mater.38-41

[3] Padmavathi, C., Upadhyaya, A. and Agrawal, D. (2007) *Corrosion behavior of microwave-sintered austenitic stainless steel composites,* Scripta Materialia, 57, 651–654

[4]Chen, W. and Zhou, J. (2009) Preparation and Characterization of Stainless Steel/TiC Nanocomposite Particles by Ball-milling Method, Journal of Wuhan University of Technology-Mater.38-41

[5] Molins, C., Bas,J. A. and Planas, J. (1992) *PM stainless steel: types and their characteristics and applications,* Advances in Powder Metallurgy, 2(5),345–57

[6] Imbaby, M.F. and Jiang, K. (2009) *Fabrication of free standing 316-L stainless steel–Al2O3composite micro machine parts by soft moulding*, Acta Materialia, 57, 4751–4757

[7] Wei, D., Dave, R. and Pfeffer, R (2002), *Mixing and characterization of nanosized powders: An assessment of different techniques,* Journal of Nanoparticle Research, 4,21-41

[8] Menezes, R.R. and Kiminami, R.H.G.A. (2008) Microwave sintering of alumina–zirconia nanocomposites, **J**ournal of Materials Processing Technology, 20 3, 513–517

[9] Robert Aaland (2008), Spark plasma sintering, Ceramic Industry Magazine. May issue.1

[10] Anselmi-Tamburini,U., Garay, J.E. and Munir,Z.A. (2006) *Fast low-temperature consolidation of bulk nanometric ceramic materials,* Scripta Materials, 54, 823–828.

[11] Youngmoo Kim, Kyong Ho Lee, Eun-Pyo Kim, Dong-Ik Cheong, Soon Hyung Hong, (2009), *Fabrication of high temperature oxides dispersion strengthened tungsten composition by spark plasma sintering process,* Int. Journal of Refractory Metals & Hard Materias 27, 842-846

[12] Godlinski, D., Kuntz, M. and Grathwohl, G. (2002) *Transparent alumina with submicrometer grains by float packing and sintering,* Journal of American

[13] Krell, A., Blank, P., Ma, H., Hutzler, T., van Bruggen, M.P.B. and Apetz, R. (2003) *Transparent sintered corundum with high hardness and strength* Journal of American Ceramic Society, 86, 12–18

[14] Kim, S.W. and Khalil, K.A.R. (2006), *High-frequency induction heat sintering of mechanically alloyed alumina–yttria-stabilized zirconia nano-bioceramics*, Journal of American Ceramic Society, 89, 1280–1285

[15] Jiang, D., Hulbert, D.M., Kuntz, J.D., Anselmi-Tamburini, U. and Mukherjee, A.K., (2007) *Spark plasma sintering: a high strain rate low temperature forming tool for ceramics,* Material Science and Engineering. A 463, 89–93

[16] Moral C., Bautista A., Velasco F. (2009), *Aqueous corrosion behavior of sintered stainless steels manufactured from mixes of gas atomized and water atomized powder,.* Corrosion Science 51, 1651-1657

[17] Garcia, C., Martin, F., Blanco, Y., de Tiedra, M.P. and Aparicio, M.L. (2009) *Corrosion behavior of duplex stainless steels sintered in nitrogen,* Corrosion Science, 51, 76–86

[18] Wong, W.L.E. and Gupta, M. (2007), *Development of Mg/Cu nanocomposites using microwave assisted rapid sintering,* Composites Science and Technology 67 (2007) 1541–1552

[19] Agrawal, S., Cheng, J., Guo, R., Bhalla, A. S., Islam, R. A. and Priya, S. (2009 *Magnetoelectric properties of microwave sintered particulate composites*, Materials Letters, 63, 2198–2200

[20] Nawathe, S., Wong, W.L.E. and Gupta, M. (2009).Using microwaves to synthesize pure aluminum and metastable Al/Cu nanocomposites with superior properties. Journal of Materials Processing Technology, 209, 4890–4895

[21] Erhard Klar and Prassan K. Samal, 2007, *Powder Metallurgy Stainless Steels: Processing, Microstructures and Properties*, ASM International, 1-4

[23] www.ssubsteck.com Accessed on 25th September, 2011.



Figure 1a



Figure 1b

Figure 1a: Applications in automotive engines and 1b: Applications for Gear Boxes www.substeck.com

MECHANICAL BEHAVIOUR OF COLD DEFORMED AND SOLUTION HEAT-TREATED ALUMINA REINFORCED AA 6063 METAL MATRIX COMPOSITES

Kenneth Kanayo ALANEME*

Department of Metallurgical and Materials Engineering, Federal University of Technology, Akure, Nigeria
*kalanemek@yahoo.co.uk

ABSTRACT
The mechanical behaviour of cold deformed and solution heat-treated aluminium alloy (6063) - alumina particulate composites was investigated. AA 6063 – Al_2O_3 particulate composites having 6, 9, and 12 volume percent of Al_2O_3 were produced using two step stir casting process. The composites were cold rolled to 20 and 35% deformation before solution heat-treating at 550°C for 1hour cooling rapidly in water. Density measurements were used as a basis of evaluating the percent porosity of the composites; while tensile properties and fracture toughness were utilized to study the mechanical behaviour. It was discovered that the cold rolling and solution heat-treating processes resulted in remarkable reduction in porosity levels in the *AA 6063/Al_2O_{3p} composites (≤2.8 % porosity). A good uniform distribution of the alumina particulates in the matrix of the AA 6063 were also produced.* The tensile strength and yield strength increased with increase in alumina volume percent and degree of cold rolling. The strain to fracture and fracture toughness decreased with increasing volume percent alumina but improved with increase in the degree of cold deformation.
Keywords: stir casting; AA 6063 – Al_2O_3; cold rolling; mechanical behaviour; porosity; solution heat-treatment

1.0 INTRODUCTION

Metal Matrix Composites (MMCs) have become an important class of engineering materials because of the unique properties and higher performance efficiencies they offer over traditional metals and alloys utilized for the same applications [1-2]. Some of the remarkable property combinations of MMCs are high specific strength and stiffness, better high temperature strength and stability in comparison to its base alloy, low thermal coefficient of expansion, and satisfactory levels of corrosion resistance [3-5]. Among MMCs, Aluminium based metal matrix composites have been the most developed and utilized for a wide range of engineering applications [6]. Some of its areas of applications are in the design of components/accessories for use in aerospace technology, defence, electronic heat sinks, solar panel substrates and antenna reflectors, automotive drive shaft fins, explosion engine components, sports among others [7-8].

There have been sustained efforts by materials researchers to develop AMCs using simple, cost-effective, and technically efficient processing techniques. Two step stir casting has been explored to develop AMCs with very encouraging results with regards lowered porosity levels (less than 4 %) achieved. However, in the as-cast or solution heat-treated conditions some of the AMCs do not possess sufficient toughness and mechanical strength even when porosity levels are satisfactory [9]. Recently, there has been interest to develop AMCs based on the use of Aluminium alloy 6063 [9-11]. AA 6063 are conventionally applied for the design of medium strength window and door profiles and other architectural design works [12]. The choice of AA 6063 is informed by its local availability and lower cost of processing. The present research work presented here is aimed at improving the mechanical properties of AA 6063 – alumina composites by adopting cold rolling and solution heat-treatment in combination as a secondary processing stage in the production of the AMCs.

2.0 MATERIALS AND METHODS

2.1 Materials

100 percent chemically pure alumina (Al2O3) particles having particle size of 28µm and Aluminium alloy 6063 (AA 6063) which served as the matrix; were utilized for the production of the composite. The composition of the Aluminium alloy 6063 is shown in Table 1.

2.2 Method

2.2.1 Stir Casting

Charge calculations were utilized to determine the quantities of Aluminium (6063) alloy and alumina (Al2O3) particles required to produce composites having 6, 9, and 12 volume percent alumina. The alumina particles were initially preheated at a temperature of 250oC for 5-10 minutes to help improve wettability with the AA 6063 alloy. The AA 6063 ingots were charged into a gas-fired crucible furnace and heated to a temperature of 750oC ± 30oC (above the liquidus temperature of the alloy) and the liquid alloy was then allowed to cool in the furnace to a semi solid state at a temperature of about 600oC. The preheated alumina was added at this temperature and stirring of the slurry was performed manually for 5-10 minutes. The composite slurry was then superheated to 720oC and a second stirring performed using a mechanical stirrer. The stirring operation was performed at a speed of 300rpm for 10minutes to help improve the distribution of the alumina

particles in the molten AA 6063. The molten composite was then cast into prepared sand moulds. Unreinforced AA 6063 were also prepared by casting for control experimentation.

2.2.2 Cold Rolling and Solution Heat-treatment Processing

The cast composites of 6, 9, and 12 volume percent alumina along with the unreinforced alloy; were subjected to cold deformation using a miniature cold rolling machine. The composites were rolled to 20 and 35 % degrees of deformation using the round orifice of the cold rolling machine before solution heat-treating the samples at 550oC for 1hour cooling rapidly in water. The sample designations for the different temper conditions (as-cast, 20% and 35% cold rolled and solution heat-treated conditions) are presented in Table 2.

2.2.3 Density Measurement

The density measurements were carried out to determine the porosity levels of the composites produced. This was achieved by comparing the experimental and theoretical densities of each volume percent Al2O3 reinforced composite (both for the as-cast and the cold deformed – solution heat-treated conditions). The experimental density of the samples was evaluated by weighing the test samples using a high precision electronic weighing balance with a tolerance of 0.1mg. The measured weighs in each case was divided by the volume of the respective samples. The theoretical density was evaluated by using the rule of mixtures given by:

$$\rho_{AA\ 6063/Al_2O_{3p}} = Vol._{AA\ 6063} \times \rho_{AA\ 6063} + Vol._{Al2O3} \times \rho_{Al2O3} \quad \text{..... (2.1)}$$

Where, $\rho_{AA\ 6063/Al2O3p}$ = Density of Composite, $Vol._{AA\ 6063}$ = Volume fraction of A A 6063, $\rho_{AA\ 6063}$ = Density of A A 6063, $Vol._{Al2O3}$ = Volume fraction Al_2O_3, and ρ_{Al2O3} = Density of Al_2O_3.

The percent porosity of the composites was evaluated using the relations:

$$\%\ porosity = \{(\rho_T - \rho_{EX}) \div \rho_T\} \times 100\% \quad \text{..... (2.2)}$$

Where, ρ_T = Theoretical Density (g/cm^3), ρ_{EX} = Experimental Density (g/cm^3)

2.2.4 Tensile Testing

Room temperature uniaxial tension tests were performed on round tensile samples machined from the unreinforced alloy and the composites with dimensions of 6 mm diameter and 30 mm gauge length. The testing was performed using an instron universal testing machine operated at a constant cross head speed of 1mm/s; and the procedure adopted was in conformity with ASTM E8M - 91 standards [13]. Three repeat tests were performed for each test condition to guarantee reliability of the data generated. The tensile properties evaluated from the stress-strain curves developed from the tension test are - the ultimate tensile strength (σ_u), the 0.2% offset yield strength (σ_y), the strain to fracture (ε_f), and the elastic modulus (E).

2.2.5 Fracture Toughness, K_{IC}

Circumferential notch tensile (CNT) specimens were prepared for the evaluation of fracture toughness in accordance with Alaneme [14]. The CNT specimens were machined with gauge length of 30mm, specimen diameter of 6mm (D), notch diameter of 4.5mm (d) and notch angle of 60°. The specimens were then subjected to tensile loading to fracture using an instron universal testing machine. The fracture load (P_f) obtained from the CNT specimens' load – extension plots were used to evaluate the fracture toughness using the empirical relations by Dieter [15]:

$$K_{1C} = P_f / (D)^{3/2} [1.72(D/d) - 1.27] \quad (2.3)$$

Where, D and d are respectively the specimen diameter and the diameter of the notched section. The validity of the fracture toughness values was evaluated using the relations in accordance with Nath and Das [16]:

$$D \geq (K_{1C} / \sigma_y)^2 \quad (2.4)$$

A minimum of two repeat tests were performed for each treatment condition and the results obtained were taken to be highly consistent if the difference between measured values for a given treatment condition is not more than 2%.

2.2.6 Microstructure

The microstructural investigation was performed using a Zeiss Metallurgical Microscope. The specimens for the optical microscopy were polished using a series of emery papers of grit sizes ranging from 500µm – 1500µm; while fine polishing was performed using polycrystalline diamond suspension of particle sizes ranging from 10µm – 0.5µm with ethanol solvent. The specimens were etched using 1HNO_3: 1HCl solution by swabbing before microstructural examination was performed.

3.0 Results and Discussion

3.1 Microstructure

Figure 1 show optical micrographs for the 9 and12 volume percent Al_2O_3 reinforced AA 6063 composites in the as-cast and 35% cold rolled and solution heat-treated conditions (which are selected as representative microstructures for all the temper conditions for the composites produced). It is observed that the Al_2O_3 particulates are well dispersed in the cold rolled and solution heat-treated condition in comparison to the as-cast condition. This is a clear indicator that the cold rolling and solution heat-treatment processes helped in achieving a homogeneous distribution of the particulates and reduced particle clusters in the composites produced.

3.2 Percent Porosity

The results of the percent porosity of the as-cast, 20% and 35% cold rolled and solution heat-treated AA 6063/Al_2O_{3p} composites are presented in Figure 2. It is observed that the as-cast AA 6063/Al_2O_{3p} composites had the highest porosity levels (1.85-3.78 %) in comparison with the 20% cold rolled and solution heat-treated composites (1.05-2.8 %) and the 35% cold rolled and solution heat-treated composites (0.74-2.0 %). For all temper conditions, it is observed that the percent porosities are less than 4 % which is reported as the maximum permissible porosity level in cast metal matrix composites [11, 17-18]. The percent porosity can be observed to increase with increase in volume percent alumina and decreases with the degree of cold deformation. This is an indication that the cold rolling and solution heat-treating process helps in improving the quality of the cast composites by reducing the percent porosity.

The reduced porosity of the cold deformed and solution heat-treated composites is attributed to the cold rolling process which compresses the composites thereby aiding the collapse of voids, micro-cracks and vacancies in the composite making it more compact and denser [19].

3.3 Mechanical Properties

The variation of ultimate tensile and yield strengths and strain to fracture are presented in Figures 3 - 4. Figure 3 shows clearly that the ultimate tensile and yield strengths of the composites increases with increase in volume percent alumina and extent of cold deformation. The cold rolling and solution heat-treatment helps in achieving a refined and homogeneous structure by removing voids and micro-voids and also helps in redistributing the particulates and second phase particles resulting in considerable elimination of particle clusters and segregation [19-20]. The elimination of a considerable amount of defects in the composite by the cold rolling and solution heat-treatment process helps in enhancing the strain hardening capacity of the composites [20].

The strains to fracture for the composites (Figure 4) are observed to decrease with increase in volume percent alumina but improve slightly with prior cold deformation. The strain to fractures are observed to be within the range of 0.1(10 %) and .215 (21.5%). The increased matrix/particulate interfaces with increase in volume percent alumina leads to an increase in the potential sites for void nucleation or micro-crack formation. The uneven plastic strain at the interface facilitates the nucleation of voids or micro-cracks [21-22]. The reduced porosity of the cold rolled and solution heat-treated composites is largely responsible for the improved strain to fracture of the composites.

The variation of fracture toughness of the composites with increase in Al_2O_3 volume percent is presented in Figure 5. The results were taken to be reliable because the requirement for nominal plain strain condition was met with the specimen diameter of 6mm when the relation $D \geq (K_{1C}/\sigma_y)^2$ [16] was utilized to test for the validity of the K_{1C} values evaluated from the CNT testing. The fracture toughness was observed to decrease with increase in volume percent of Al_2O_3 but improves with degree of cold deformation before solution heat-treatment. The fracture micro-mechanism in particulate reinforced MMCs have been reported to be due to particulate cracking, interfacial cracking or particle debonding [23 - 24].The reduced porosity and considerable elimination of particle clusters in the composites is responsible for the slight improvement in the fracture toughness of the composites. Generally, the fracture toughness values obtained for the composites were found to be comparable to that of Al matrix composites processed under similar conditions [25].

4.0 Conclusion

It was discovered that the cold deformation and solution heat-treating processes resulted in remarkably reduced porosity levels in the AA 6063/Al_2O_{3p} composites ($\leq$ 2.8 %porosity). A good uniform distribution of the alumina particulates in the matrix of the AA 6063 were also produced.The tensile strength and yield strength increased with increase in alumina volume percent and degree of cold deformation. The strain to fracture and fracture toughness decreased with increasing volume percent alumina but improved with increase in the degree of cold deformation.

References

[1] Miracle, DB. Metal Matrix Composites-From Science to technological significance. Composites Sci and Tech 2005; 65(15-16): 2526-2540.

[2] Matthews F L, Rawlings R D. Composites Materials Engineering and Science. London: Chapman and Hall; 1994.

[3] Hashim J, Looney L, Hashim M S J. Metal Matrix Composites Production by the Stir-Casting Method. J Matls Proc Tech 1999; 92-93: 1-7.

[4] Zhou W, Xu Z M. Casting of SiC Reinforced Metal Matrix Composites, J Matls Proc Tech 1997; 63: 358-363.

[5] Ray S. Review: Synthesis of Cast Metal Matrix Particulate Composites, J Matls Sci 1993; 28: 5397-5413.

[6] Surappa M K. Aluminium Matrix Composites: Challenges and Opportunities. Sadhana 2003; 28(1 & 2): 319-334.

[7] Chawla V, Manoj S, Dwivedi D D, Lakhvit S. Development of Aluminium Based SiC Particulate Metal Matrix Composite 2009; J of Minerals & Matls Charac & Eng 2009; 8(6): 455-467.

[8] Veeresh Kumar GB, Rao, CSP, Selvaraj N, Bhagyashekar MS. Studies on Al (6061) and 7075 - Al203 Metal Matrix Composites. J of Minerals & Matls Charac & Eng 2010; 9(1): 43-55.

[9] Alaneme K K and Bodunrin M O. Corrosion Behaviour of Alumina reinforced Al (6063) Metal Matrix Composites, Journal of Minerals, Materials Characterization and Engineering, (2011); USA, (In Press).

[10] Khalifa, T.A. and Mahmoud, T.S. (2009), "Elevated temperature mechanical properties of Al alloy AA6063/SiCp MMCs", Proceedings of

the World Congress on Engineering 2009, Vol.11, July 1-3.

[11] Alaneme K K and Aluko A O. Production and Age – hardening Behaviour of Borax Pre-mixed SiC Reinforced Al-Mg-Si alloy Composites developed by Double Stir Casting Technique, The West Indian Journal of Engineering, Trinidad and Tobago, 2012; Vol. 34, Nos. 1/2, pp 80-85.

[12] Polmear I J. Light Alloys from Traditional Alloys to Nanocrystals, (4th), Butterworth Heinemann, 2006, Oxford.

[13] ASTM E 8M . Standard Test Method for Tension Testing of Metallic Materials (Metric) in Annual Book of ASTM Standards. Philadelphia: ASTM; 1991.

[14] Alaneme, K. K. Fracture Toughness (K_{1C}) Evaluation for Dual Phase low alloy Steels Using Circumferential Notched Tensile (CNT) Specimens, Materials Research, 2011, Vol. 14, No. 2, Pp 155-160.

[15] Dieter G E. Mechanical Metallurgy, SI Metric Ed. Singapore: McGraw- Hill; 1988.

[16] Nath S K, Das U K. Effect of Microstructure and Notches on the Fracture Toughness of Medium Carbon Steel. J Naval Archi & Marine Eng 2006; 3: 15 – 22.

[17] Kok M. Production and Mechanical Properties of Al_2O_3 particle Reinforced 2024 Aluminium Composites, Journal of Materials Processing Technology. Volume 16, 2005, Pp. 381-387.

[18] Prabu, S.B., Karanamoorty, L., Kathiresan, S. and Mohan, B. (2006), "Influence of stirring speed and stirring time on distribution of particulates in cast metal matrix composite", Journal of Materials Processing Technology, Vol.171, No.2, pp.268-273.

[19] Huda Z. Effects of Degrees of Cold Working and Recrystallization on the Microstructure and Hardness of Commercial-Purity Aluminium, European Journal of Scientific Research, 2009, Vol. 26, No. 4, Pp 549-557

[20] Shahani R A and Clyne T W. Recrystallization in Fibrous and Particulate Metal Matrix Composites, Materials Science and Engineering A, 2003, Vol.135, Pp 281 – 285.

[21] Chawla N, Shen Y. Mechanical Behavior of Particle Reinforced Metal Matrix Composites. Advanced Engineering Materials 2001; 3(6): 357 – 370.

[22] Sharma S C, Girish B M, Kamath R, Satish B M. Fractography, Fluidity and Tensile Properties of Aluminium/Hematite Particulate Composites. J Matls Eng & Perf 1999; 8(3) 310 – 314.

[23] Mohammed M. Ranjbaran, Low Fracture Toughness in Al 7191-20%SiCp Aluminium Matrix Composite. European Journal of Scientific Research, Vol. 41, No. 2, 2010, Pp. 261-272.

[24] Mortensen, A. A Review of the Fracture Toughness of Particle Reinforced Aluminium Alloys. Proc Int Conf Fabrication of Particulates Reinforced Metal Composites, Quebec, Canada 1999; 217 – 233.

[25] Milan M T, Bowen P. Tensile and Fracture Toughness Properties of SiCp reinforced al alloys: Effects of Particle Size, Particle volume fraction and matrix strength, Journal of Materials Engineering and Performance 2004; 13(6) 775 – 783.

Table 1: Chemical Composition of the Aluminium Alloy 6063 (AA 6063)

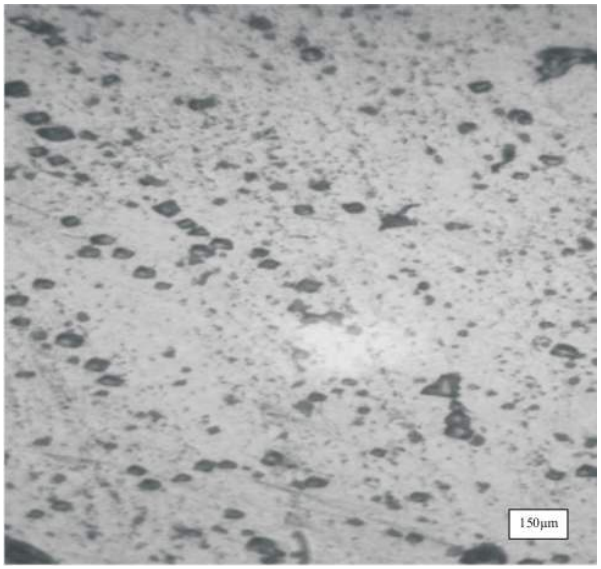
Si	Fe	Cu	Mn	Mg	Zn	Cr	Ti	Al
0.45	0.22	0.02	0.03	0.50	0.02	0.03	0.02	Bal.

Table 2: Sample Designation for the Different Temper Conditions

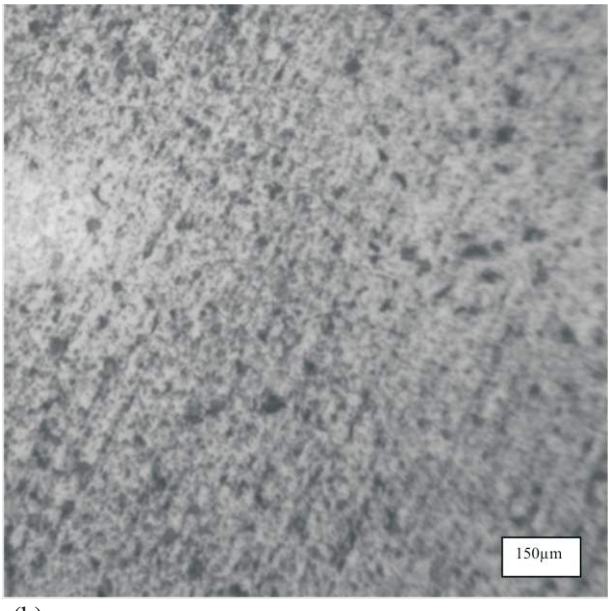
Vol.% alumina	Temper Condition		
	as-cast	20% cold - rolled + solution heat - treated	35% cold - rolled + solution heat - treated
0	A1	A2	A3
6	B1	B2	B3
9	C1	C2	C3
12	D1	D2	D3

Table 2: Sample Designation for the Different Temper Conditions

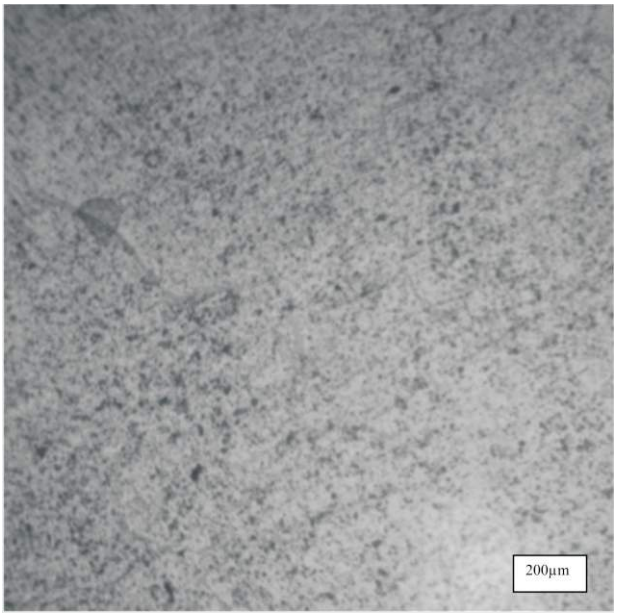
Vol. % alumina	0	6	9
as-cast	A1	B1	C1
20% Cold -rolled + solution heat - treated	A2	B2	C2
25% Cold -rolled + solution heat - treated	A3	B3	C3
35% Cold -rolled + solution heat - treated	A4	B4	C4



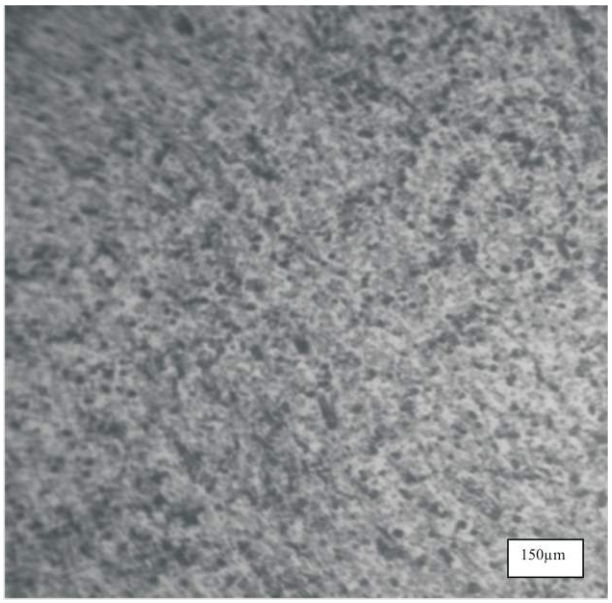
(a)



(b)



©



(d)

Figure 1: Representative Micrographs for (a) as-cast AA 6063 - 9 vol.% Al_2O_3, (b) as-cast AA 6063 – 12 vol.% Al_2O_3, (c) 35% cold-rolled and solution heat-treated AA 6063 - 9 vol.% Al_2O_3, and (d) 35% cold-rolled and solution heat-treated AA 6063 - 12 vol.% Al_2O_3.

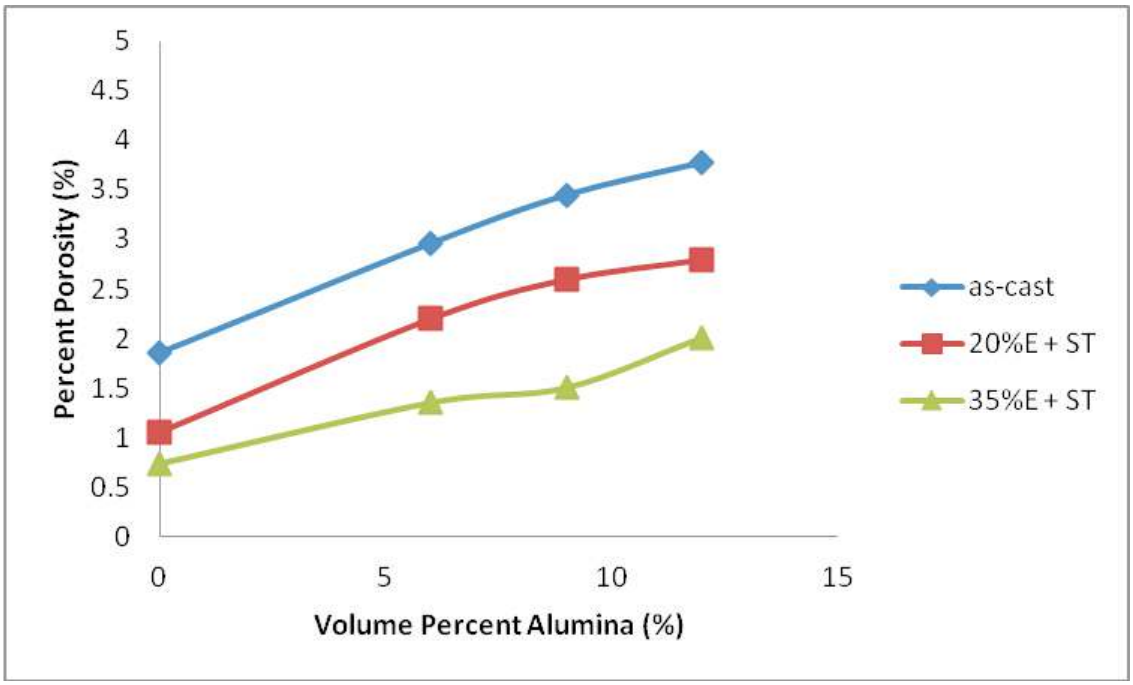


Figure 2: Percent Porosity for the AA 6063 – Al_2O_3 Composites Produced

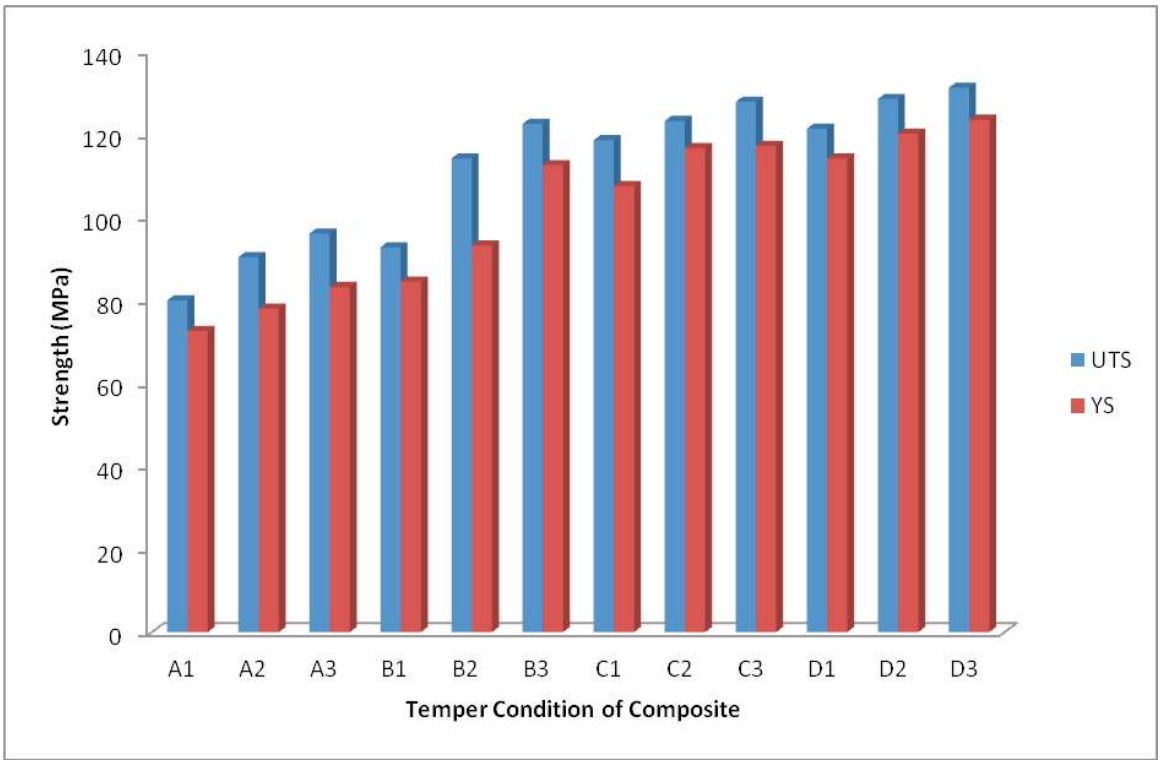


Figure 3: Variation of Ultimate Tensile Strength and Yield Strength for the AA 6063 – Al_2O_3 Composites Produced

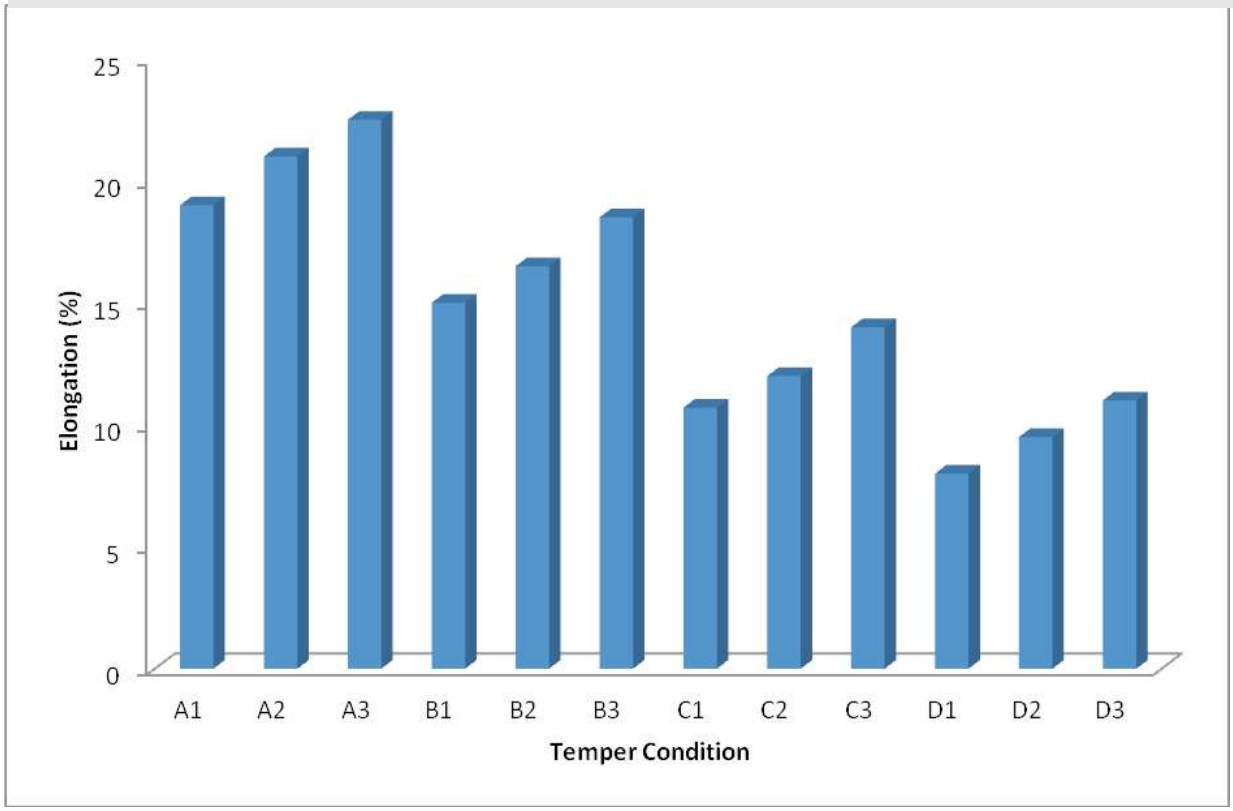


Figure 4: Variation of Percent Elongation for the AA 6063 – Al_2O_3 Composites Produced

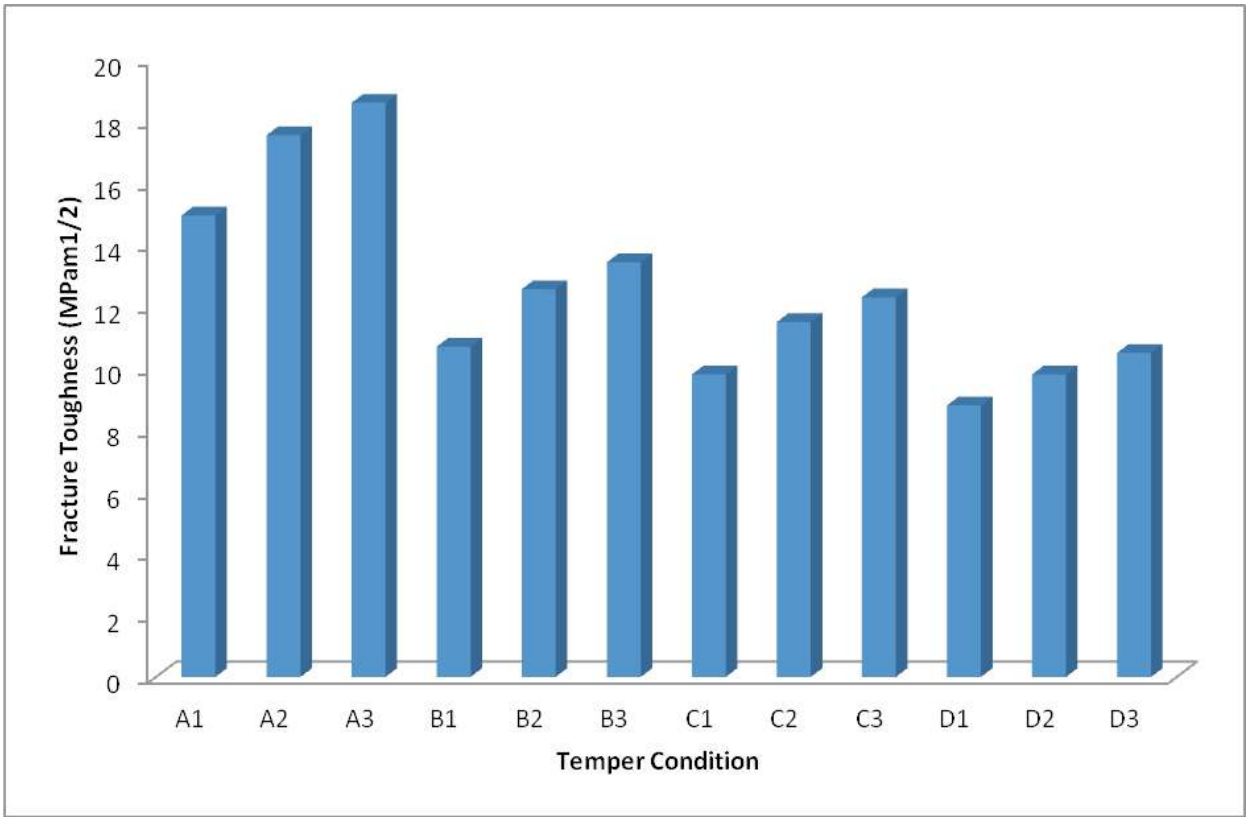


Figure 5: Variation of Fracture Toughness for the AA 6063 – Al_2O_3 Composites Produced

ADSORPTION OF CADMIUM IONS ON KANKARA KAOLIN

Edomwonyi-Otu L.C*, Alonge J. K, Ajiboye O.O, Bawa, G. S
Chemical Engineering Department, Ahmadu Bello University, Zaria
***Corresponding Author:** osas1law@yahoo.com, lcotu@abu.edu.ng

ABSTRACT
Cadmium is known to be very harmful to human health and there has been a cry to reduce the content of this substance with the use of cheap and readily available materials. Adsorption of cadmium ions on Kankara kaolin has therefore been successfully carried out. The effects of cadmium concentration, contact time, stirring speed, clay concentration, pH, and temperature were examined. The result showed that the adsorption capacities on Kankara kaolin increased with cadmium concentration. This adsorbent exhibited a good adsorption potential with high clay concentration, at about 50^{0}C with moderately low speed of 300rpm having maximum efficiency of 91.57% at 10 minutes. The adsorption process followed pseudo first and second order kinetics but best fitted by pseudo second other kinetics. The equilibrium adsorption capacity of cadmium on the kaolin was found to be 20.408mg/g with a rate constant of 0.0022mg min/g. The thermodynamic parameters such as ? H, ? S and ? G were computed from the experimental data obtained in the research as; -30.17kJ/mol, 0.906J/kg and -217kJ/mol respectively. These values described the adsorption process as; exothermic and spontaneous with a decreased degree of randomness and it was a physical adsorption process (physiosorption).
Keywords: Kankara kaolin, cadmium ions, calcinations, spectrophotometer, cadmium concentration, clay concentration, pH, contact time, temperature and stirring speed.

INTRODUCTION

The heavy metal (cadmium) is a highly toxic inorganic pollutant whose emission sources are widely diffused giving rise to a large scale environmental pollution. Environmental regulations define severe limitations on the maximum cadmium concentration in natural bodies as well as on the maximum allowed concentration for waste water discharge. To assure the compliance with these limits, appropriate depuration technologies are usually required. Cadmium ions can be removed by chemical precipitation, ion exchange, adsorption, electrochemical deposition, etc (Letterman, 1999). The values of process parameters such as concentration, pH, temperature stirring speed and time severely affect the equilibrium adsorption capacity of a given sorbent determining a strong variation of the overall efficiency of the process and playing a crucial role in the industrial scale up of adsorption units. The study of adsorption in model aqueous solutions allows a more interesting and reliable analysis of adsorption phenomena and a more meaningful method for the comparison or sorbent sorbents adsorption capacity.

The adsorption is done using Kankara kaolin which is a very common and important mineral having a relatively two layered silicate sheets in structure. Kaolin clay has the formula, $Al_2SiO_5(OH)_4$. In nature, it often associate with impurities like MgO, Fe2O3, CaO, ZnO, etc depending on its source and its location. Kaolin has the ability to adsorb cadmium ions and other heavy metals into its pores which were found to have an average sizes ranging between 2nanometers and 50nanometers with the aid of a transmission electronic material (TEM) (Matusik et al, 1996), the empirical atomic radius of cadmium is about 155picometers (webelements.com, 2011) hence allowing a good number of it to be adsorbed into the kaolin pores depending on the working conditions such as temperature, stirring speed etc.

Due to the heavy metals resulting from sewage, mining processes, industrial wastes etc**.** absorbed by growing plants, dissolved in underground water and flowing streams, causing harm to their consumers, there is need to reduce the content of such substances in waters that are consumed using cheap and readily available materials. Although Kankara kaolin has been found to be a good adsorbent but its efficacy has not been studied the aim of this research work is therefore to adsorb cadmium ions as well as to investigate the effect of process parameters such as concentration, pH, stirring speed and contact time on the adsorption on Kankara kaolin. This is necessary because There have been reported cases of lost lives as a result of pollutions caused by cadmium ions, Kankara kaolin is cheap and abundant and the Knowledge of pollution standards and treatment process are available in open literature.

EXPERIMENTAL PROCEDURE

Calcination of Kankara Kaolin and Determination of Its BET

The Kankara kaolin was grinded and sieved to obtain the desired particle size and placed in the furnace at 500^{0}C for 24 hours[2] (Apreepriya et al, 2006) , in order to increase its mechanical resistance and to eliminate its impurities. The BET for Kankara kaolin was done in South Africa.

Spectrophotometer Calibration

A 100mg/100ml solution of cadmium nitrate (BDH, London) was prepared by dissolving 0.1g of the salt in 100mg of deionised water. This was diluted to get

solutions of different concentrations in order to calibrate the spectrophotometer (Thermo Fisher Scientific Heliot™ Zeta).

The Adsorption Process

1g/L of $Cd(NO_3)_2.6H_20$ (BDH, London) was prepared by dissolving 1g of the salt in 1L of deionised water. This was diluted to obtain the concentrations of 20mg/L, 40mg/L, 60mg/L, 80mg/L, 100mg/L, 120mg/L, 140mg/L and 160mg/L. 100mL of the prepared solutions was measured and adjusted to a desired pH value by adding a buffer solution (H_2SO_4 or NH_3). The solution at its desired pH value was then placed on the heating mantle and allowed to attain the desired temperature after which the desired quantity of Kankara kaolin was added and stirred at the desired speed for a particular time interval, after the which, the mixture was filtered using the high vacuum pump and a Sinta glass filter funnel and the clear solution was transferred into a small bottle for the spectrophotometric analysis.

Spectrophotometric Analysis

The absorbance of the solutions obtained from the adsorption processes were obtained at a wavelength of 340nm using the spectrophotometer. Concentrations of the new solutions were obtained from the absorbance using appropriate equations, the efficiencies were calculated and its variation with the different factors was determined.

RESULTS AND DISCUSION

Determination of BET For The Kankara kaolin

Table1 BET of Kankara kaolin.

BET SURFACE AREA (m^2/g)	PORE VOLUME (cm^3/g)	PORE SIZE (nm)
9.1217	0.051222	25.96991

Effect Cadmium Concentration on Adsorption

The sorption efficiency increases with cadmium concentration rapidly between 20mg/L and 40mg/L to 75% due to diffusion as there is more concentration of the cadmium ions in the solution as seen in figure1. It then increases steadily with intermittent plateaux until an equilibrium state is attained between the cadmium solution and the kaolin at 140mg/L with about 93% efficiency which strongly depends on the clay concentration and other working conditions.

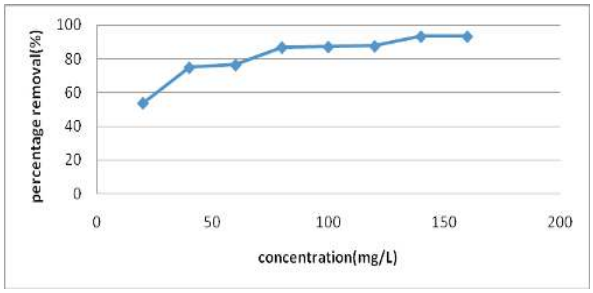
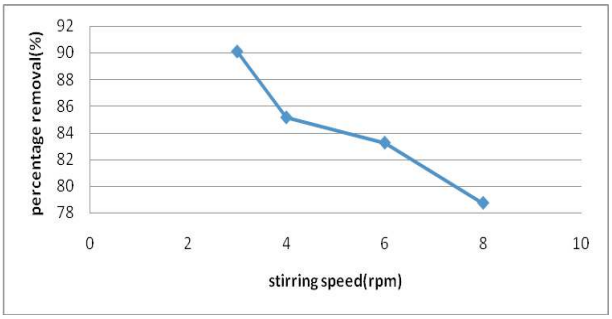


Fig.1 Variation of percentage removal with cadmium concentration

Effect of Contact Time on Adsorption

As shown in figure 2 below, it can be observed that there is a rapid increment in sorption efficiency up to 75% in the first minute. This is an effect of diffusion where the high concentration of cadmium ions in the solution moves into the kaolin pores having a low concentration of the cadmium ions. The efficiency then increases steadily to 91.57% at 10minutes when the kaolin becomes saturated. Then, there is a steady decrease to 83% at 100minutes, since the kaolin pores becomes more concentrated than the mother liquor, the diffusion process is reversed where the cadmium ions moves into the solution. Increment of the efficiency between 100 and 150 minutes and subsequent decrease is principally the effect of diffusion. Maximum adsorption of cadmium ions is obtained at 5minutes using AAF according to a research by Haimssa and his co-workers (2010), this has a faster rate than the process using Kankara kaolin because such fibres may have more adsorption capacity than Kankara kaolin.



From figure4 below, it can be observed that the adsorption efficiency increases rapidly up to 83% with a clay concentration of 2g/100mL because high concentration of clay and with surface area and pore volume of $9.1217m^2/g$ and $0.051222cm^2/g$ respectively (Private communication, 1999) provides adequate sites for adsorption to take place but may have an optimal quantity as seen between 3mg/L and 4mg/L especially when a low concentration of cadmium ions is involved in the process and also depending on other factors such as temperature and speed of stirring.

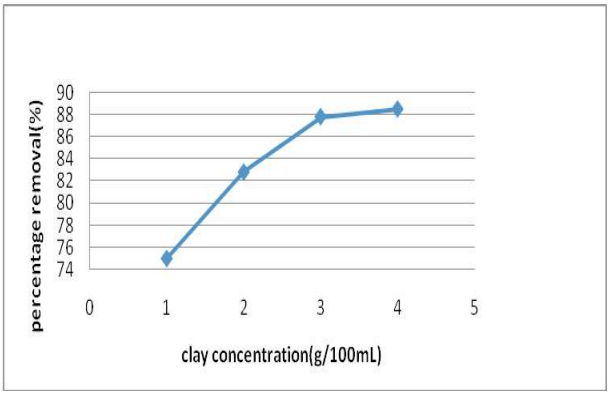


Fig.4 variation of percentage removal with clay concentration

Effect of pH on Adsorption

As seen in figure5 below, it can be observed that the most favourable pH for this process in 3 and 9 with percentage adsorption of 90% and less favourable at a pH of 7 with percentage adsorption of 64%. The percentage of cadmium molecule adsorbed is high at lower pH and can be very low at basic pH values due to precipitation of cadmium hydroxide (Benjamin, 2002), using activated carbon which may have varied characteristics.

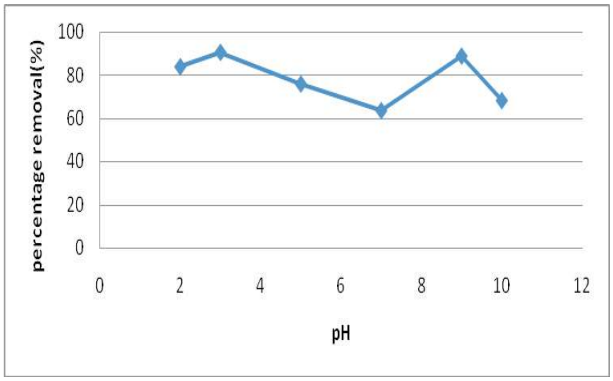


Fig.5 Variation of percentage removal with pH

Effect of Temperature on Adsorption

It can be observed in figure6 below, that adsorption increases rapidly between 30^{0}C and 40^{0}C to about 85.5% this is because the kaolin particle become swollen as the temperature of the medium increases and therefore has the ability to adsorb more of the cadmium ions. It then increased steadily to an optimum of 50^{0}C with an efficiency of 88%, (Private communication). The adsorption efficiency decreases rapidly with very high temperatures as observed between 50^{0}C and 60^{0}C, this is because increase in kinetic energy consequently leading to a high entropy in the medium which causes the kaolin to lose its adsorbed cadmium ions. Also, adsorption is not favoured at very high temperatures due to exothermicity (Benjamin, 2002).

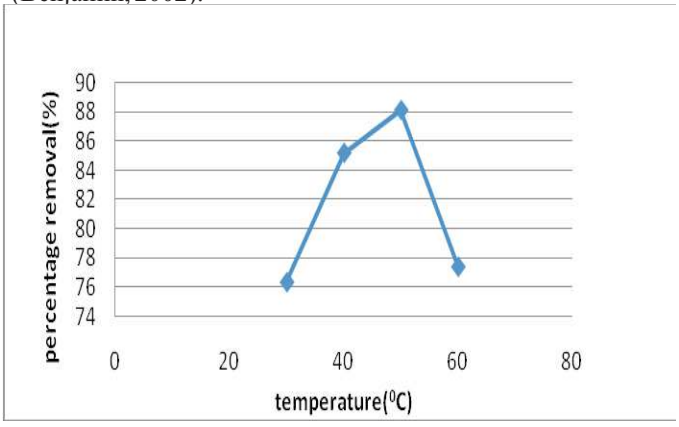


Fig.6 Variation of percentage removal with temperature

ADSORPTION KINETICS

The lagergren equation (Lagergren, 1898) (equation1) was applied assuming pseudo-first-order kinetics where the number of metal ions outnumbers the adsorption sites on clay surface;

$$In(q_e - q) = In(q_e) - k_1/2.303.t \quad \text{----------1}$$

Where q_e and q are the values for the adsorbed amount per unit mass at equilibrium and at any given time, t, (mg/g) and k_1 as the pseudo-first-order adsorption rate constant. The k_1 value can be obtained from the angular coefficient of the straight line obtained by plotting the $In(q_e - q)$ versus t graph and obtained to be 0.00087min^{-1} from fig.7.

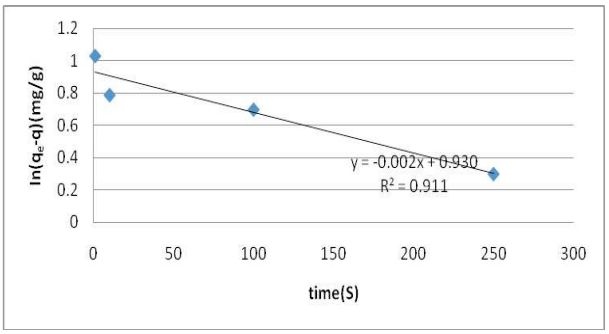


Fig.7; pseudo- first- order kinetics

From figure7, The low rate constant obtained signifies a slow mechanism hence the pseudo-second-order kinetics is tested.

The kinetics was also tested, applying pseudo-second-order model of Ho and McKay based on the sorption capacity of the solid phase and consistent with the chemisorption mechanism described in equation 5.2.

$$t/q = 1/k_2q_e^2 + t/q_e \quad \text{----------2}$$

where $k_2q_e^2$ is described as the initial adsorption rate when t tends to zero. The t/q versus t graph, (figure 8), provides a straight line giving the values of q_e and k_2 from its slope and intercept as 20.408mg/g and 0.00222mg min g^{-1} respectively.

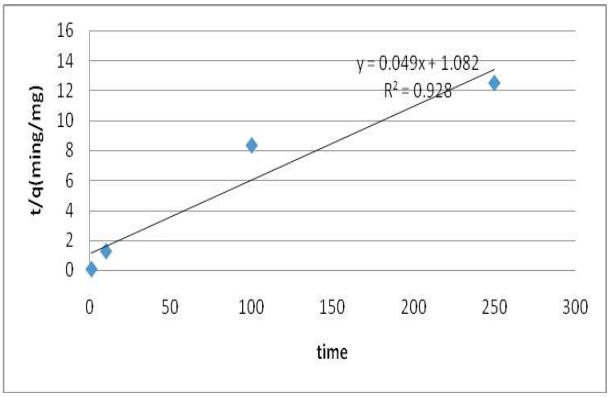


Fig.8; pseudo-second- order kinetics

The rate constant obtained from figure8, given as

0.0022mg min g^{-1} implies a faster mechanism than for the pseudo-first-order, it also has an equilibrium sorption capacity of cadmium on Kankara kaolin of 20.408mg/g.

THERMODYNAMIC PARAMETERS

The thermodynamics parameters for the adsorption process ? H(kJ/mol), ? S(j/kg mol) and ? G(kJ/mol) were evaluated to know whether the process will occur spontaneously or not using thermodynamic equations 3 and 4

$$? G = -RT.In(K_d) \quad \text{----------3}$$

$$In(K_d) = -? G/RT = ? S/R - ? H/RT \quad \text{----------4}$$

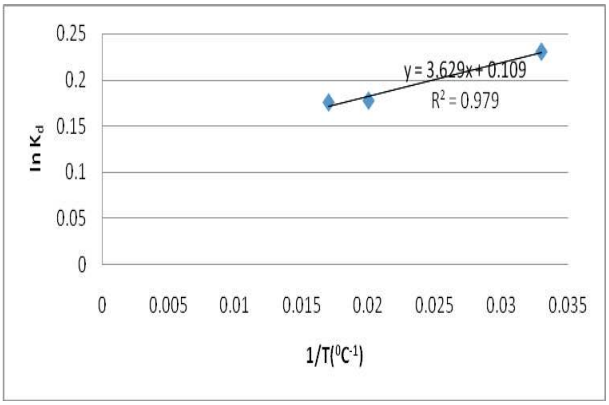


Fig. 9; Thermodynamic parameters

From figure 9, relating the slope and intercept to equations 3 and 4,

? H= -30.17kJ/mol, ? S = 0.906J/kg mol and ? G = -217 kJ/mol.

The enthalpy of -30.17kJ/mol implies an exothermic process of the reaction and also a physiosorption process since it is less than 40kJ/mol (Levenspiel, 2011). The entropy of 0.906J/kg mol indicates a low degree of randomness. Also the Gibbs free energy of -217kJ/ mol obtained indicates a spontaneous adsorption process.

Table5.3; Summary of Kinetics and Thermodynamics Parameters.

Pseudo-first-order kinetics	Pseudo-second-order kinetics	Thermodynamic parameters
K_1 = 0.00087min^{-1}	K_2 = 0.00222mg min g^{-1}	? H= 30.17kJ/mol
q_e = 2.53mg/g	q_e = 20.408mg/g	? S = 0.906J/kg mol
		? G = -217 kJ/mol

The rate equation for the pseudo-first-order kinetics can then be written as;

$$In(2.53 - q) = 0.930 - 0.00037t \quad \text{----------5}$$

And for the pseudo-second- order kinetics;

$$t/q = 1.08 + t/20.408 \quad \text{----------6}$$

CONCLUSIONS

Cadmium adsorption on Kankara kaolin has been investigated under different working conditions including solution pH, temperature, cadmium concentration, time of contact, clay concentration and stirring speed. Results shows that high cadmium concentration, high clay concentration, moderately low stirring speed, allows maximum adsorption, the effect of temperature is coherent with the exothermicity of adsorption hence, moderately high temperature favours adsorption. The ? G is negative at all temperatures indicating that the adsorptions are spontaneous processes. The ? H is also negative showing that the process is exothermic, it is less than 40kK/mol implying that it is a physiosorption process.

REFFRENCES.

1. Ahmed S. And Mustafa S. (2007) Equilibrium and thermodynamic studies of stearic acid adsorption on celtek clay. Serbian journal of chemical society, Vol.94 pp 25-31.
2. Apipreeya K, Phussadee P. and Patnukao P. (2006) Removal of Metal ion from synthetic waste water by activated carbon from eucalyptus camalduensis dehn bark. Books of Proceedings of Conference on Sustainable Energy & Environment. Vol 141 pp 8-9
3. Ernest G. and Blatt, Harvey (1982). Petrology, Igneous, Sedimentary, and Metamorphic rocks San Francisco: W.H. Freeman and Company. Vol.84 pp167-179
4. Octave Levenspiel, (1991) Chemical Reaction Engineering. John Willey and Son, New York, 3rd edition, pp 238-684
5. Vieira M. G, Gimennes M. L, and da Silva M. C. (2010) Sorption Kinetics and Equilibrium For The Removal of Nickel Ion From Aqueous Phase on Calcined Bofe Bentonite Clay. Journal of Harzardous Material, Vol.177, pp 362-371
6. Guem S, Yao B, Adouby K. and Ado G. (2007). Kinetics and Thermodynamics Studies of Lead Adsorption onto Activated Carbon from coconut and Seed Hull of The Palm Tree. International Journal of Environmental Science Technology. Vol.81 pp 11-17.

7

http://www.clays.org/journal/archive/volume%2043/43-2-255.pdf. searched on September 2, 2011

8 . http://www.atsdr.cdc.gov/csem/cadmium/cdcontents.html. searched on September 4, 2011

9. www.wikipedia.org/adsorption, searched on September 2nd, 2011

EVALUATION OF THE COMPRESSIVE STRENGTH OF HYBRID CLAY BRICKS

* O. Azeez, *[1] O. Ogundare, * T.E. Oshodin, O.A. Olasupo, and *B.A. Olunlade
*Engineering Materials Development Institute P.M.B. 611 Akure Nigeria.
National Agency for Science and Engineering Infrastructure P.M.B. 391 Garki Abuja
Email: suppiedee@yahoo.com*[1]

ABSTRACT
This work has presented the evaluation of the compressive strength of hybrid clay bricks from interlocking brick making machine. The mixture of clay and cement at varying proportions was loaded into the mould compartment, mechanically rammed and hydraulically controlled.
The raw clay was sourced from Ilesa and Akure in the south-western part of Nigeria. The results showed that when the cement content was 6%, the highest compressive load and energy at break were obtained in hybrid bricks from both Ilesa and Akure samples. However, the optimum service performance under compressive loading was attained at 6% cement in Ilesa hybrid bricks. Ilesa hybrid bricks possess better reliability and workability under loading than the Akure bricks.
Keywords: Hybrid bricks, compressive strength, clay, cement, interlocking machine.

INTRODUCTION

Clay based material is one of the materials that has been widely used in construction materials instead of wood, sand, concrete and other waste materials. This material is a major compound in clay brick, clay tiles and clay roofing tiles due to its wide-ranging properties, high resistance to atmospheric condition, geochemical purity, and easy access to its deposits near the earth's surface and low price. Fired clay brick (FCB) can be categorized as one of the demolition wastes as most of the unwanted FCB from buildings or houses renovation are being illegally disposed off in most places. The utilization of this type of clay based waste materials would replace the natural aggregates in concrete mixture [1]. Studies related to ancient clay bricks alone deal mainly with physical, chemical, and mineralogical composition [2,3,4], durability and deterioration agents [5] and deterioration modelling [6,7,8] neglecting the mechanical properties.

The compressive strength is a mechanical property used in brick specifications, which has assumed great importance for two reasons. Firstly, with a higher compressive strength, other properties like flexure, resistance to abrasion, etc., also improve. Secondly, while other properties are relatively difficult to evaluate, the compressive strength is easy to determine [9]. Generally, compressive strength decreases with increasing porosity but strength is also influenced by clay composition and firing.

Compression testing is a method for assessing the ability of a material to withstand compressive loads. This test is commonly used as a simple measure of workability of material in service. Materials behave differently in compression than they do in tension so it may be important to perform mechanical tests which simulate the condition the material will experience in actual use. Compression testing is typically carried out on the following materials; Plastics, Foams, Rock, Concrete and Asphalt. It is rarely used to test metals [10]. Compressive strength of Blocks and Bricks is a critical parameter for determining the quality of these materials. The loads and forces acting on these materials while in service are compressive in nature and their ability to withstand such loads and forces without failure is a measure of their reliability [11].

The tasks of inspection and diagnosis of ancient buildings require obtaining a certain number of parameters, which provide information about the properties of the materials, the structural behaviour, or possible defects. Mechanical characterization is a fundamental task for the structural works and safety assessment, where the compression strength is a key parameter in the case of masonry structures. In fact, the compressive strength of masonry in the direction normal to the bed joints has been traditionally regarded as the sole relevant structural material property, at least until the recent introduction of advanced numerical methods for masonry structures [12].

The aim of this research is to evaluate the compressive strength of hybrid bricks from 8-mould interlocking brick making machine

.

MATERIALS AND METHODS

MATERIALS

The samples were collected from certain locations in Ilesa and Akure in South western part of Nigeria. The Ordinary Portland Cement (OPC) was obtained commercially.

METHOD

The clay sample was mixed with water to desired consistency. Ordinary Portland Cement (OPC) was added in different percentages ranging from 0% – 14% putting into consideration the volume of each mould. The OPC was thoroughly mixed with the clay sample for even distribution and homogeneity. The aggregate was loaded into the eight moulds of the interlocking machine. After sometime, the hydrid bricks were hydraulically lifted out of the moulds. The interlocking machine used for this research was the 8- Mould Interlocking Earth Brick Making Machine which was designed, developed and

fabricated at Engineering Materials Development Institute Akure Nigeria. Each sample was left for the first 28 days for proper curing and sufficient strength before compression testing was carried out.

COMPRESSION TESTING PROCEDURE

For the compression test, the specimens were cut from the bricks to be tested in the direction of the moulding or perpendicular to bed joints (see Fig.1), which is the usual loading direction in building elements (e.g., walls and vaults) subjected to dead load. Generally, very small specimens were obtained, with typical cross sections of 30mm x 30 mm and 30mm of height. All specimens were ground using a rectifying machine, so that the loading faces were properly aligned. The test setup for the compression tests was carried out on Instron Universal Tester model 3369 available at the **Engineering Materials Development Institute Akure Nigeria. Its** steel frame was equipped with a compression load cell with a maximum capacity of 50 kN and connected to a software- driven computer system. The steel platens were rectified in order to provide a flat surface. The lower platen has a spherical seat made of tempered steel that allows the initial alignment and accommodation of the specimen, thus facilitating the alignment of the applied load with the centre of the specimen as well as preventing any other unfavourable effect due to geometrical imperfection of the specimen. The Instron software was programmed to capture all data during the course of the test.

RESULTS AND DISCUSSION

Figure 2 shows the bar chart of compressive load at break of hybrid bricks made from Ilesa samples. The mixing of Ordinary Portland Cement (OPC) in different percentages has revealed the different compressive strengths. It was observed that when no cement (0% cement content) was mixed, a compressive strength of 727.91 N was obtained. This shows the fact that the virgin clay sample possesses a reasonable compressive strength. With 4% cement mixed with the clay sample, a compressive load at break (crushing strength) of 481.03 N was obtained. It was observed that when 6% cement was mixed with the clay sample before loading into the interlocking machine, the highest compressive load at break of 2,537 N was obtained. This shows that 6% hybrid bricks will be able to withstand 2537 N before failure under loading. This is because at this percentage, the cement elements were able to penetrate most into the matrix of the clay resulting in strong interlinking and bonding network of the hybrid brick. This means that in service, 6% hybrid bricks will be used under compressive loading up to 2,537 N. Figure 3 shows compressive load at break of hybrid bricks from Akure samples. It was observed that the highest compressive load was obtained at 8% cement ratio and followed by 14% cement ratio. This was closely followed by 6% cement ratio. This is because the cement elements were able to intertwine the network of the clay elements at the highest capacity at 8% cement ratio. This resulted in formation of strong matrix of the hybrid bricks with the same compressive stress values of 1.12 MPa and 1.11 MPa at 6% and 14% cement ratio respectively as shown in figure 4 below.The comparative compressive loads at break of hybrid bricks from both Ilesa and Akure samples are presented in figure 4 above. At a glance, it can be observed that at 0%, 6%, 10% and 12% cement ratios, the compressive resistance of Ilesa Hybrid bricks are better than that of Akure. This may be due to geographical and environmental factors on the virgin clay since that same ordinary Portland cement was mixed.Figure 5 is a bar chart of energy at break of hybrid bricks from Ilesa samples. It shows that energy absorbed (71 J) before failure is greatest at 6% cement ratio. This is to support the highest compressive load at break that also occurred at 6% cement ratio (see Fig. 2 above). In other words, the energy absorbed is directly proportional to the compressive strength characteristics. This is due to high adhesive property between the clay and the cement particles resulting in high resistance to dislocation stress. Figure 6 is a bar chart of energy at break of hybrid bricks from Akure samples. It can be observed that the highest energy absorbed before break of 16 J was at 6% cement ratio.

CONCLUSION

On the strength of the results presented above, it can be concluded that

1. **The optimum service performance under compressive loading was attained at 6% cement in Ilesa hybrid bricks.**
2. **Ilesa hybrid bricks possess better reliability and workability under loading than the Akure bricks.**
3. **Ilesa clay has better binding characteristics and quality than the Akure species.**

REFERENCES

[1] Ummi Kalsum, H.M.N, Mashitah, M.D. and Badorul, A.B. 2008. **Recycling of clay based demolition wastes for the production of concrete block. A paper delivered at** International Conference on Environment (ICENV 2008).

[2] López-Arce, P., Garcia-Guinea, J., Gracia, M., and Obis, J. 2003. "Bricks in historical buildings of Toledo City: Characterization and restoration." Mater. Charact., 50, 59–68.

[3] Cardiano, P., Ioppolo, S., Stefano, C., Pettignano, A., Sergi, S., and Piraino,P. 2004. "Study and characterization of the ancient bricks of Monastery of "San Filippo di Fragalà" in Frazzanó _Sicily_." Anal. Chim. Acta, 519 (1), 103–111.

[4] Pauri, M., Stazi, A., Mastrosanti, F., and D'Orazio, M. (1994). "The decay of ancient building masonry, a case study." Proc., 10th International Brick/Block Masonry Conference Calgary, Canada, 1295–1304.

[5] Wijffels, T., and Nijland, T. G. 2004. "Deterioration of historic brick masonry due to combined gypsum, ettringite and thaumasite: A case study." Proceedings of 13th International Brick/Block Masonry

Conference, Amsterdam, The Netherlands, 809–815.

[6] Cultrone, G., De la Torre, M. J., Sebastian, E. M., Cazalla, O., and Rodriguez-Navarro, C. 2000. "Behavior of brick samples in aggressive environments." Water, Air, Soil Pollution, 119, 191–207.

[7] Binda, L., Baronio, G., and Ferrieri, E. D. _1996a_. "Full-scale models for the calibration of laboratory ageing tests." Proceedings of 7th International Conference on Durability of Building Materials and Components, Stockholm, Sweden, 559–568.

[8] Binda, L., Baronio, G., and Ferrieri, E. D. 1997. "Durability of brick masonry surface treatments to salt crystallization." Proc., 11th International Brick/Block Masonry Conf., Shanghai, China, 732–747.

[9] Adeola, J.O., 1977. A Review of Masonry Block/Brick Types Used for Building in Nigeria. Unpublished M.Eng. Thesis, University of Benin, Benin-City.

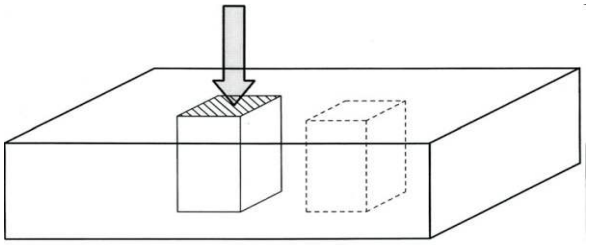


Fig. 1 Schematics showing how specimens were cut from bricks and direction of compression tests

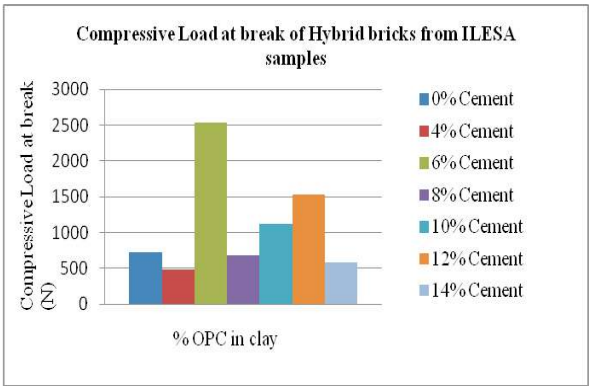


Fig.2 Compressive Load at break of hybrid bricks from Ilesa samples

[10] Bukar, Y. A. 1992. "Benefits of Enhanced Product Quality for Industries like Aluminum, Steel, Auto Mobile and related Industries" been paper presented at the seminar on Strategy for developing Local Raw Materials for Metallurgical and Building Industries.

[11] Hassan, A.B. and Bukar, Y. A. 2009. Design and Fabrication of a Compression Strength Testing Machine for Blocks and Clay Bricks. Leonardo Electronic Journal of Practices and Technologies. 14,142-153.

[12] Francisco Fernandes and Paulo B. Lourenço. 2007. Evaluation of the Compressive Strength of Ancient Clay Bricks Using Microdrilling. Journal of Materials in Civil Engineering, 19(9): 791-800.

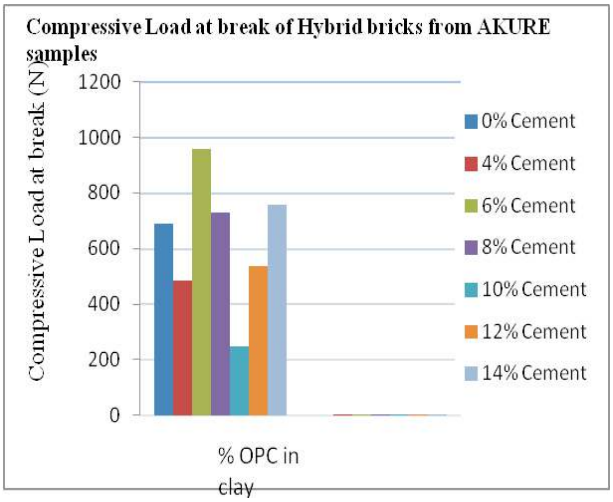


Fig.3 Compressive Load at break of hybrid bricks from Akure samples

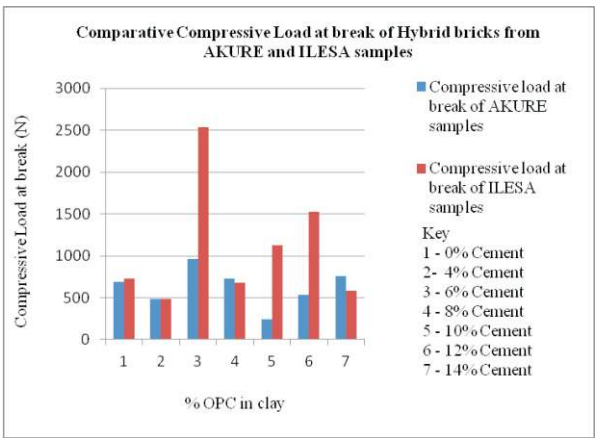


Fig.4 Comparative Compressive Loads at break of hybrid bricks from Ilesa and Akure samples

STUDIES ON THE FIVE (5) SELECTED CLAYS IN ABEOKUTA, NIGERIA

[1]Aiyedun, P.O, [2]Olokode, O.S, [3]Oyeleke Y.T. [4]Lee, W.E, Anyanwu, B.E
[1, 2, 3] University of Agriculture, Abeokuta. Mechanical Engineering Department.
[4]Imperial College, London. Materials Department.
engr_olokode@yahoo.com

ABSTRACT
Clays from five (5) deposits in Abeokuta, South-West Nigeria has been investigated with a view to determine their suitability for various uses. The samples were collected from different commercial centres in Abeokuta namely: Asero 1 (AS1), Fajol (FA), Agba-Akin 1 Onibode 1 (AA1), Ile-Ise Awo 1 (IA1), and Ajebo 1 (AJ1). The clay samples were crushed, pulverized and sieved. Their chemical compositions and X-ray diffraction were determined. The mineralogical characteristics of these samples revealed kaolinite as the principal mineral but other minerals are present in small quantities: illite, quartz, muscovite, microcline, cristoballite, and zeolite. Experimental tests for refractoriness, water absorption, bulk density, linear shrinkage, percentage dry shrinkage, percentage total shrinkage, percentage warpage compressive strength breaking load/flexural tests and crack formation were carried out on each of the five selected clays.
Keyword: clays, kaolin, mineral, bulk density, porosity, shrinkage.

INTRODUCTION

Raw materials used in the traditional ceramics industry can be classified as clay (plastic) and non-clay (non-plastic) minerals. Clays is the chief raw material for many commercial structural ceramics products such as wall tiles, roofing tiles, building bricks, white wares. Chemically, clay minerals are phyllosilicates with ions arranged in parallel planes forming layers G. Brown (1984). Clays occur in deposits of greatly varying nature. No two deposits have exactly the same clay and frequently different samples of clay from the same deposit differ. The geomorphology of the township, Abeokuta and environs is made up of flat topped hills, escapements and lowlands. The hills geologically are the olden granite masses and other rocks such as gneisses and migmatites, commonly referred to as crystalline basement or basement complex. This escapement is of cretaceous age. Alluvial terraces are well dissected by the Ogun and where underlying rock is deeply weathered.

The laterite caps on these rocks resistant to the environ and it is believed that they have contributed largely to the development of the escapements and crestas [3].

According to Kogbe [6], the sedimentary rocks are not well exposed. There is however outcrops of coarse, ill-sorted, clayey brown sandstone occurring at about 200ft. Similarly, these are outcrops of cross bedded femiginious sandstone and pebble sandstone among others in south eastern part of Abeokuta. There are also fallen blocks of conglomerates, consisting of quartz cobbles in a femiginious and cretaceous sandstone matrix.

The basic rocks from which clays are formed are complex aluminosilicates. During the weathering these become hydrolysed, the alkali and alkaline earth ions form soluble salts and are leached out. The remainder consists of hydrated aluminosilicates of varying composition and structure, and free silica. It is the orientation of this predominantly silica structure that gives clay its unique plastic property. Nigeria has appreciable distribution of industries engaged in metal and process industries hence the need for adequate and appropriate raw materials to support their growth. Clay products such as wall tiles, ceramic wares, burnt bricks, roofing and floor tiles are cheaper and durable building materials than cement especially under tropical conditions [7]. An optimum combination of various clays is the essential ingredient in ceramic wall tile compositions, which provides plasticity and green strength during forming stages and contributes substantially to the colour of the fired products depending upon the impurity of oxides present. The formation, structure, mineralogical and other physico-chemical properties of various types of clay minerals are widely studied subject discussed in literatures [1,2,4,5,8]. Two factors are accentuating the development of good refractories using the local raw materials. The first one is the growing number of metallurgical industries that are in dire need of these refractories, while the other factor is the advent of foreign exchange market, a situation that has led to higher and unaffordable cost of procuring the refractory materials needed by these industries. Some of the refractories materials usually employed are fireclay, quartz sand, magnesite, sillimanite, berylia, alumina, chromite, zirconia, boron, nitride, graphite and carbide.

This study investigate the working properties of the Asero, Fajol, Onibode, Ile-Ise Awo, and Ajebo clays deposits in Nigeria with the view to propose other possible uses such as microfilteration membrane in water treatment, food and beverages, chemical engineering and refractory purposes.

MATERIALS AND METHODS RAW MATERIALS

Representative samples of the five (5) different selected clays from Abeokuta in Ogun-State were taken by hand (as received) from five (5) different geological

formations at their respective depths in the pits of Asero 1, Fajol, Onibode 1, Ile-Ise Awo 1, and Ajebo 1.

CHARACTERISATION OF THE FIVE DIFFERENT CLAY DEPOSITS IN ABEOKUTA.

The physical, chemical, mineralogical properties of the natural kaolins from Abeokuta clay was examined in the Materials Laboratory of Imperial College, London.

The results were compared with results published in literature, to ascertain if these five clays are suitable for the manufacturing of floor tiles, ceramics, stoneware and firebricks

Sample Preparation

All the five collected clays, in the form of agglomerated lumps of five (5) kilograms was initially dried at 110C over night for 24 hours, in an oven MOV-112 of Imperial College London, and were grounded in a porcelain mortar and pestle and the resulting fine powder was termed the Un-treated clay.

Chemical Analysis

Chemical analyses of the materials were determined using inductively coupled plasma. Atomic emission microscopy (ICP- Varian Vista-Pro ICP-AEP), where all sample were dried at 110C for eight (8) hours prior to analyses. Samples analysed by fusion with Lithium Barium ($LiBO_2$) into the plasma flame to produce characteristic emission of major and minor elements.

Mineralogical Analysis X-Ray Diffraction (XRD)

Each of these 5 clay samples was dried in an oven, crushed, ground to a fine powder and was determined in the laboratory section of Materials Department, Imperial College London. The mineralogical data were obtained on powdered samples using XRD instrument Phillips PW1700 series automated powder diffractometer using CuK_a radiation at 40 Kv/40mA from $5°<2\theta<85°$ with the step size 0.04 at the counting time of 2 seconds. Both random and oriented powder samples were studied and were compared with International card for diffractometer data (ICDD).

Refractoriness

Each of the five test cones were prepared by mixing clay deposits aggregate with sufficient quantity of water to make the clay plastic and moulded by hand into cone shape. Each clay samples were dried and fired to a temperature of 900^0C in a muffler furnace. Pyrometric cones designed to deform at 1250, 1300, 1350, 1400, 1500^0C were placed round all the samples and the temperature raised to above 1000^0C at 10^0C per min. The heating was discontinued when the test cone bent over and levelled with the base of the disc. The Pyrometric cone equivalent (P.C.E) of each clay samples recorded to the number of standard pyrometric cone corresponding in the time of softening to the test cone.

Pressing

Dry pressing is commonly used to produce ceramic particles thicker than 0.5mm. Stages of dry pressing include: filling of the die, compaction, shaping and ejection.

Approximately 8mm diameter die were pressed using a laboratory hydraulic press Model 15010. The desired pressure applied, 40 MPa was maintained for about 60 seconds to allow for particle rearrangement. Freshly compacted test specimen were measured, weighed, marked for further identification and dried in an oven type MOV 112 at 110°C overnight prior to firing. Dry shrinkage, fired shrinkage and total shrinkage of these samples was determined at various temperatures of 600, 700, 800, 900, 1000, 1100, 1200°C. A micrometer with accuracy of 0.01mm was used to measure the length of the samples directly after pressing, and the length of the dried samples. After firing at specific temperatures, the fired length for each temperature was measured. The formula for the calculation of dry shrinkage is:

$$\% DS = \frac{L_2 - L_3}{L_2} \times 100 \qquad (1)$$

Where, DS = Dry Shrinkage

L_2 = length of sample directly after pressing (mm)

L_3 = length of dry pressed sample (mm)

The formula used for the calculation of the fired shrinkage at each temperature is:

$$\%TS = \frac{L_2 - L_4}{L_2} \times 100 \qquad (2)$$

Where, TS = Total Shrinkage

L2 = length of sample directly after pressing (mm)

L4 = length of fired sample at a specific individual temperature (mm)

Water Absorption

Water absorption measurements were carried out according to British Standard EN 99 (1991). Fired pellets were soaked in boiling water in a beaker, and left to cool down to room temperature still soaked in water. Excess water was removed from the pellets surface using a moistened cloth prior to weighing. The wet weight (Ww) was then measured. Pellets were left drying in an oven at 110C overnight, and the dry weight was measured (Wd). Water absorption (WA) was computed as:

$$WA = \frac{W_w - W_d}{W_d} \times 100 \qquad (3)$$

As boiling water will penetrate open or interconnected pores of the specimen, the higher the water absorption the more porous is the material in terms of that specific type of porosity. Open pores are common in under fired stoneware, where not enough liquid has been produced to close the porosity of the ware on firing. In over fired specimens, gas escaping from inside the ware will create blistering on its surfaces.

Bulk Density

The bulk density of the fired samples was determined by water displacement using Archimedes principle. The experimental set-up allows the weights of the beaker partially filled with water, with and without the pellet immersed in water, to be measured. The difference gives weight of water displacement, according to the Archimedes principle. The weight of water displaced can be easily related to the volume of water displaced, as the density of water is known. The volume of water

immersing in the water using a precision balance. Thus, the bulk density (BD, g/cm³) is given in terms of sample mass (Sm) and the sample volume (Sv) as:

$$BD = \frac{S_m}{S_v} \quad (4)$$

Assuming that the composition of the glassy phase and that of the crystalline materials present in the samples fired at neighbouring firing temperatures, and thus their theoretical density, are very similar, it is then possible to use bulk density measurements to give an idea of the total porosity of the ware. The higher the bulk density, the lower the total porosity.

Linear Shrinkage

Dry-to-fired contraction or linear shrinkage (LS) was determined by measuring the diameter of the dried pellet (Dd) and that of the fired pellet (Df), according to the following equation:

$$LS = \frac{D_d - D_f}{D_d} \times 100 \quad (5)$$

The measurements were made using digital calliper. As the ceramic body densities, it shrinks in all direction. The shrinkage along the disk diameter gave more results than that of the height.

Pressing Moisture

A representative batch of pressed test pieces were weighed (M2), dried at 110°C for 24 hours and then weighted (M1) again. The difference in mass was divided by the initial mass, multiplied by the initial mass, multiplied by the average pressing moisture of the sample is:

$$\%MC = \frac{M_1 - M_2}{M_2} \times 100 \quad (6)$$

Where, MC = moisture content
M1 = weight of the sample after drying
M2 = weight of the sample after pressing.

Thermal shock resistance

Each of the five test specimens of area 0.002m2 and thickness of 0.01m were cut from their respective bricks. A conical flask containing 50ml of water was placed directly above and in contact with specimen. A cork having a thermometer passing through it was used to cork the mouth of the conical flask. The thermometer reads the temperature changes of the water in the flask. The test section was then closed and the initial water temperature was noted. A second thermometer with the aid of a cork was inserted into the stream outlet pipe offset to monitor the stream temperature so as to ensure a constant base temperature of 1000C.

The boiler water outlet valve was closed while 5 litres of water was measured and poured into the boiler. The stream inlet valve, outlet valve and condensate outlet valve were all closed. With the boiler cover remaining opened, the boiler was switched on. Immediately, the water started boiling, the boiler cover was closed, while the steam inlet valve was fully opened with all the remaining valves closed. Timing commenced with the aid of a stopwatch immediately the steam inlet valve was opened.

The testing was timed in each case for 10 minutes and final temperature of the water in the beaker was noted at the end of time. Each specimen was tested (experimented) twice and mean temperature value was obtained. At the end of each experiment, the steam outlet valve was opened to release steam. The water in the boiler was refilled to maintain 5 litres and the experiment was repeated as stated above for the other specimens.

The value of the thermal conductivity, K for each of the specimen was determined using the formula:

$K = 2.303MCL/A[\log(\theta 1 \theta 2)]/\tau$ (7)

Where:
K = Thermal conductivity of the specimen,
T1 = Temperature of steam K.
Ti = Initial temperature of water in conical flask,
T4 = Final temperature of water in conical flask,
τ = Time (s),
A = Specimen area (m2),
M = mass of water in conical flask (Kg)
C = Specific heat capacity of water in conical flask (J/KgK),
L = Thickness of specimen (m),
$\theta 1 = T1 - Ti$,
$\theta 2 = T1 - T4$.

Percentage warpage

Warping is the measurement of curvature (convex or concave) of deviations of material surface from a true plane along the edges or the diagonals. The deviations were measured at the mid-length of an edge or diagonal and expressed as percentage of the length of the edge or diagonal. The diagonal method was used by initially setting a dial indicator to zero at the mid- centre of each of the five clay deposits and later moving the dial indicator to record deviations of points along the drawn diagonal lines on the moulded clay.

The percentage warpage were calculated using equation (8)

$WL/DL \times 100$ (8)

Where, WL is the amount of warpage in mm.
DL is the gauge length or total length of the diagonal.
The recorded percentage warpage is based on average percentage warpage of at least two times of each of the five clay deposits.

Mechanical properties

The mechanical properties, compressive strength and breaking load were conducted using equation 8 and 9 in accordance with ASTM standards for testing structural clay materials.

Compressive strength

Each specimen from the five selected clay deposit was placed on hardened steel plate and load was gradually applied by manually operated hydraulic press through an indenter or load applicator until there was a sign of crack. The compressive test was calculated using equation 9.

$\delta C = W/A$

Where, W- Is the maximum attained (N)
A- Is the area of load allocation
The recorded compressive strength was an average of the two times of each of the five clay selected deposits.

Breaking load/Flexural test

This test method consisted of supporting the tile specimens on the ends of three cylindrical rods, arranged in an equilateral triangle form and applying a load, until it fail. The recorded flexural strength was an average of the two times of each of the fire clay deposits.

REFERENCES

[1] Society. 81(1), 3-20. Carly, W.M. and Senapati, U. (1998). Porcelain Raw Materials, Processing Phase Evolution and Mechanical Behaviour. Journal of American Ceramic

[2] Das, S.K, Dana, K. Singh and Sarka, V. (2005). Shrinkage and Strength Behaviour of Quartzitic and Kaolinitic Clays in Wall tile Composition. Applied Clay Science. 29. Pp 137-143.

[3] Durotoye (1975). Quaternary Sediments in Nigeria. Elizabethan Publishing Co. Nig. Pp. 347-362

[4] Hinkley D.W. (1962). Variability Crystallinity Values among the Kaolin Deposits of the Coastal Plain of Georgia and South Carolina. Proceedings of the 11th National Conference on Clays and Clay Minerals. (Ottawa, Ontario, Canada). Pp. 229-235.

[5] Kingery, W.D. (1976). Introduction to Ceramics. Wiley New York. Pp. 78-79, Pp. 532-540.

[6] Kogbe, C.A (1975). Soil Survey report bulletin. No 46.

[7] Nnuka, E.E, Enejo, C. (2001). Characterization Nahuta Clay for Industrial and Commercial Applications. Nigerian Journal of Engineering and Materials. 2(3), 9-12.

[8] Olgun, A, Erdogan, Y and Zeybek, B. (2005). Development of Ceramic tiles from Coal Fly ash and Tincal ore waste Ceramic International. 31. Pp 153-158.

Results and Discussion

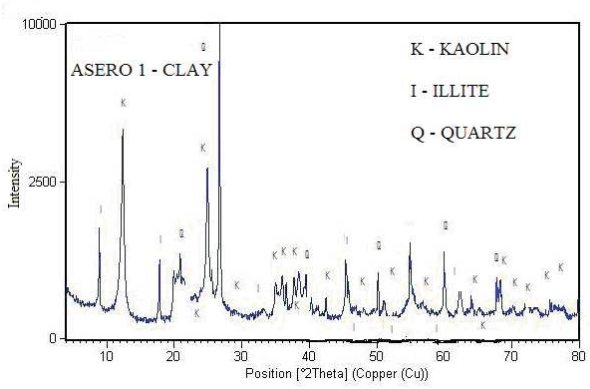


Figure 1: XRD trace of Asero clay

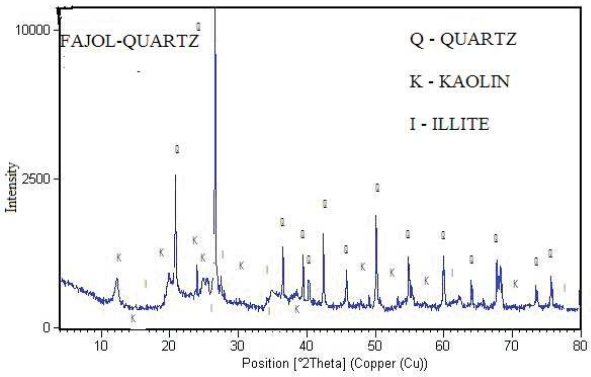


Figure 2: XRD trace of Fajol clay

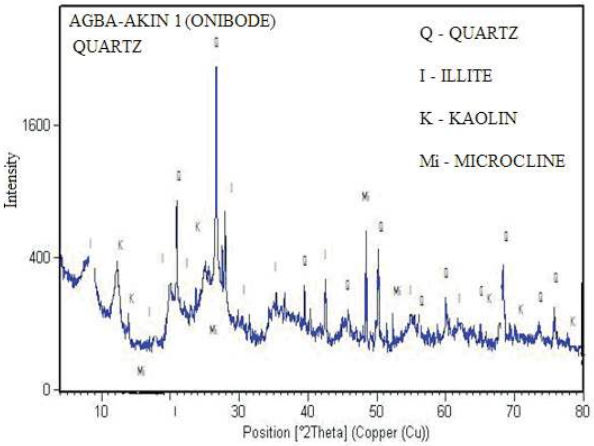


Figure 3: XRD trace of Agba-Akin clay 1

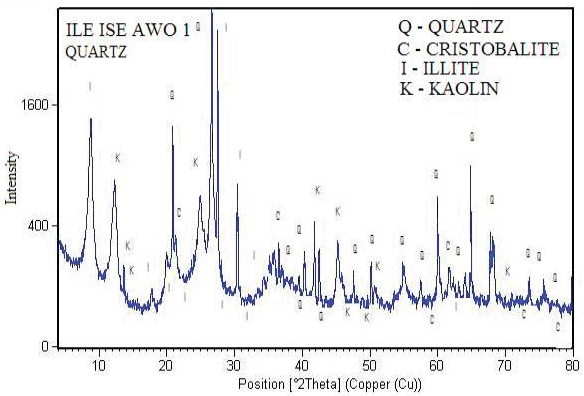


Figure 4: XRD trace of Ile-Ise Awo 1

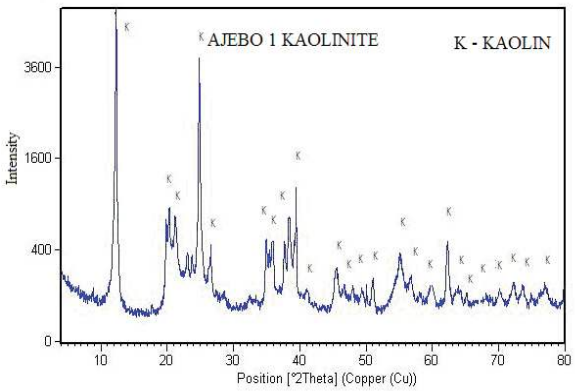


Figure 5: XRD trace of Ajebo 1 clay

Table 1: Chemical Composition of five (5) clays deposits in Abeokuta, Nigeria.
n.d- Not detectable

Raw Materials (RM)	SiO_2	TiO_2	Al_2O_3	Fe_2O_3	MnO	MgO	CaO	Na_2O	K_2O	P_2O_5	LOI
Asero (AS1)	66.8	0.45	21.3	2.94	n.d	0.07	0.08	0.02	0.45	0.06	8.43
Fajol	78.3	0.87	9.1	2.94	0.02	0.31	0.26	0.24	1.01	0.03	6.92
Agba-Akin 1(Onibode) AA1	63.7	0.7	18.7.	5.6	0.02	1.0	1.1	1.9	0.04	0.03	5.89
Ile-Ise Awo 1 (IA1)	67.9	0.6	14.7	5.9	0.03	0.8	0.4	0.49	2.46	0.05	6.67
Ajebo1 (AJ1)	46.4	1.69	34.0	2.49	n.d	0.04	0.02	0.03	0.08	0.04	17.7

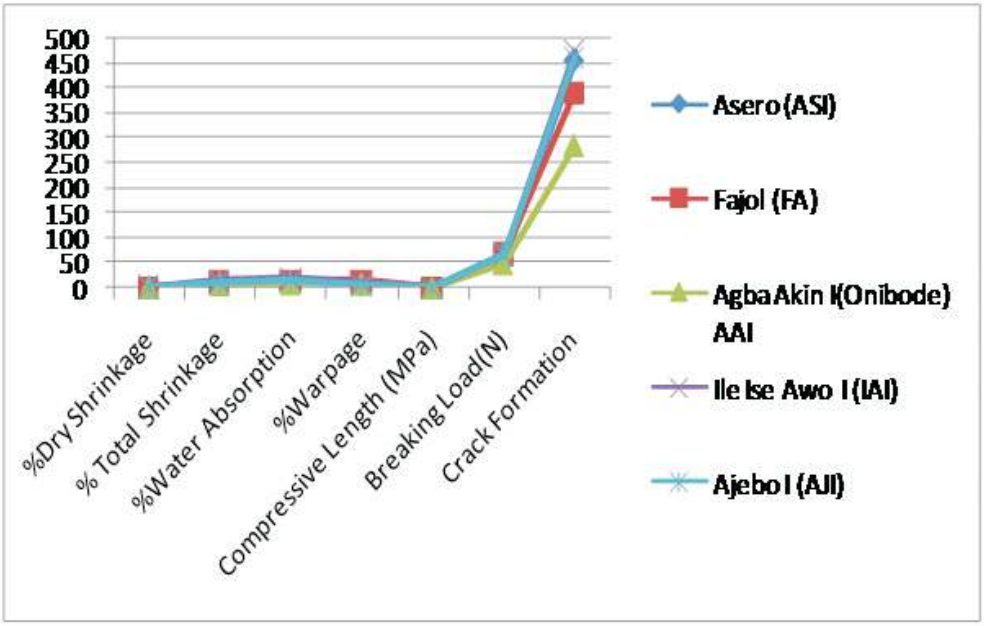


Figure 6: Experimental Physico-Mechanical Properties of the Five Selective Clays in Abeokuta at 1200^{0}C
Table 2 Experimental Physico-Mechanical Properties of the Five Selective Clays in Abeokuta at 1200^{0}C

Clay deposits	**Properties**							
	Bulk density (g/cm^3)	%Dry Shrinkage	% Total Shrinkage	%Water Absorption	%Warpage	Compressive Length (MPa)	Breaking Load (N)	Crack Formation
Asero (ASI)	1.26	9.53	11.91	10.73	1.82	54.53	454.15	No Crack
Fajol (FA)	1.62	12.26	15.61	14.77	2.12	69.17	391.88	No Crack
Agba Akin I(Onibode) AAI	1.24	7.59	9.56	8.24	1.09	49.10	284.60	Slight Crack
Ile Ise Awo I (IAI)	2.46	14.57	18.56	9.94	0.95	65.51	472.50	No Crack
Ajebo I (AJI)	1.79	11.21	14.92	3.34	0.82	67.90	461.83	No Crack

ASTM -Allowable Value for ceramic tiles on sale states the % warpage maximum should not be more than 2.1%, 15% maximum for total shrinkage and % water absorption should not be more than 16% maximum.

ALTERNATIVE PRODUCTION OF XYLANESES USING SAWDUST AND DIFFERENT LOCAL DIGESTIVE BRAN AS SUBSTRATES.

M.I. Alibe, A.S. Magaji, A.M. Sule, B.Inuwa, G. Mohammed, I. A. Suleiman, I. Khalid, M.H. Aliyu
National Research Institute for Chemical Technology (NARICT), PMB 1052, Basawa, Zaria
Email: ibrahim_mstpha@yahoo.com.com

ABSTRACT
Xylanases are a major group of enzymes, mostly produced from microbial fermentation processes, and have wide industrial and biotechnologicalapplications. The production cost of xylanase is the major factor limiting its use, thus indicating the need for low cost production systems for market of this enzyme.
In this study, therefore, sawdust and different local digestive bran of Wheat, Maize, Guinea corn and Millet were investigated as substrates for xylanase production by *Bacillus subtillus*. From the research it was discovered that all the locally digestive bran that was used, were capable of producing xylanase enzyme.
Further research should be done to evaluate the quantity produce by other digestive bran, so that this can serve as a cheap method of producing xylanases using digestive bran which is mostly consider as waste in this part of the world.
Keywords: xylanases, enzymes, sawdust, *Bacillus subtillus*.

INTRODUCTION

Organic wastes from agricultural residues comprise cellulose, hemicellulose and lignin in an average ratio of4:3:3, with hemicellulose being the second most abundant fraction available in nature (Taiz and Honigman, 1976; Abdel-Sater and El-Said, 2001). Xylans, the major portion of the hemicellulose of plant cell walls, are heteropolymers consisting principally of xylose and arabinose (Biely, 1985; Coughlan and Hazlewood, 1993) and is amenable to degradation by different microorganisms, including bacteria, yeasts, and fungi. Several types of enzymes appear to be involved in the degradation of native xylan. Endoxylanases, which attack the linear polyxylose chain in a manner analogous to that of endoglucanase on cellulose, are the most important and have accordingly received the most attention (Sunna and Antranikian, 1997). β-xylosidase hydrolyzes xylobiose and oligosaccharides to complete the conversion of xylan to xylose and probably relieves the end product inhibition of endoxylanase activity (Srinivasan and Rele, 1999; Subramaniyan and Prema, 2000; Chávez et al., 2006).This activity appears to be extracellular in fungi but cellassociated in bacteria, although relatively few of these enzymes have been studied in detail (Esteghlalian et al., 2008). Other enzymes play an important role in the removal of side groups from polymeric xylan to create more sites for subsequent enzymatic hydrolysis and possibly contribute to lignin solubilization by attacking the covalent bonds responsible for the integrity of the lignocarbohydrate matrix (Bachmann and McCarthy, 1991; Contreras et al., 2008). The choice of an appropriate substrate is of great importance for the successful production of xylanases.The substrate not only serves as carbon and energysource, but also provides the necessary inducing compounds for the organism, preferentially for an extended period of time, for an increased overall productivity of the fermentation process (Duff and Murrayh, 1996; Haltrich et al., 1996). Purified xylans are frequently used for small scale experiments and are considered as excellent substrates not only because of high yields of xylanase obtained, but also because they cause a selective induction of xylanase with little or no concomitant cellulose activities (Biswas et al., 1990; Gilbert et al., 1992).However the high cost of xylan and other good substrates has limited their applications for larger-scale production processes, hence, the need to search for cheaper alternatives. Several inexpensive substrates, mainly insoluble lignocellulosic material, such as barley husk, corn cobs, sugarcane bagasse have been used (Camassola and Dillon,2009).Although poorly investigated, the use of soluble sugars for the production of xylanases has been shown to circumvent problems associated with the use of high concentrations of insoluble substrates, such as media viscosity and difficulties with agitation. In addition, xylose, which can be easily obtained from the xylan portion of lignocellulosic material, has been described as an effective inducer of xylanase activity in several organisms (Haltrich et al., 1996). Biotechnological applications of xylanases have broadened markedly since they are now widely employed as supplements in paper manufacturing, animal feeds, biobleaching of pulp and paper, and in the production of bioethanol (Beg et al.,2000; Subramaniyan and Prema, 2000; Techapun et al.,2003). The most important industrial application of xylanase is in the pre-bleaching of Kraft pulp. This allows for a lower consumption of chemicals during the bleaching process, and also results in a brighter product than can be achieved without the enzymatic treatment (Viikari et al., 1994; Ninawe and Kuhad, 2006). Most of the commercial xylanase is produced by microbial fermentation process.

The production cost of xylanase is the major factor preventing its use, thus indicating the need for low cost production systems for market of this enzyme. Therefore, the main objective of this study is to investigate the

potential of cheap raw substrates such as sawdust and digestive bran for the production of xylanases by *Bacillus* sp. The thermo stability and pH stability of the xylanases produced by these organisms on the raw substrates was also investigated to determine their potential industrial applications.

MATERIALS AND METHOD

Organisms and sawdust used in this study

Bacillus subtillus used in this study were obtained from microbiology lab of (NARICT) Basawa Zaria, Kaduna state Nigeria and pure cultures of the *Bacillus subtillus* were preserved on nutrient agar slants and stored at 4°C. Sawdust used in this study was obtained from carpentry workshop in Sabon Gari Zaria, Kaduna State, and Nigeria.The different digestive brans used were obtained from different grains mills in Zaria city Zaria Kaduna.

Preliminary screening for xylanase production

The bacterial strains were inoculated onto modified xylan agar plates, consisting (in g/l): Digestive bran or sawdust, 10.0; yeast extract, 5.0; peptone, 5.0; K2HPO4, 1.0; CaCO3, 2.0; (NH4)2SO4, 2.0 (pH 8.0) (Kapoor et al., 2008) and 1.8% (w/v) bacteriological agar. Pure colonies obtained were tested for xylanase production by flooding plates with 0.1% Congo red for 15 min and destained with 0.1 M NaCl for 30 min (Mamo et al., 2006). The zones of hydrolysis were revealed by finally flooding the plates with 0.5% (v/v) acetic acid. Isolates with clearing zone were considered xylanase positive.

Xylanase production and assay

Erlenmeyer flasks (250 ml) containing 100 ml of modified xylan medium (pH 8.0) were inoculated with 5 ml of standardized cultures (OD of 1 at λ600 nm) and incubated at 35°C in a rotary shaker (200rpm) for 4 days. The cultures were harvested by centrifugation at6000 × g for 5 min and the cell free supernatant was then used as an enzyme source. Xylanase activity was measured by the DNS (3, 5-dinitrosalicylic acid) assay (Miller, 1959), that determines the amount of reducing sugars liberated from oats-spelt xylan (OSX) (5g/l, Sigma) solubilized in phosphate buffer (0.05 M, pH 6.0), according to Bailey et al. (1992). This reaction mixture of an enzyme (100 µl) and a substrate (900 µl) was incubated for 15 min at 50°C, before stopping the reaction by the addition of 1.5 ml DNS solution. The samples were boiled in test tubes for 10 min, cooled under running water for colour stabilization and the optical density was measured at 540 nm. Xylanase activity was determined from a calibration curve constructed with varying concentrations of Dxylose (sigma) and expressed in nkat. One nkat (0.0599 IU) was defined as the amount of enzyme that releases 1 nmol xylose/s, at 50°C.

RESULTS AND DISCUSSION

The results as presented in the table and graph below shows that the different digestive brans used were capable of producing Xylanase at different quantity and time. However, it was observed that sawdust had the highest yield of xylanase production of 39nkat at day one andpeak yield of 46nkat/ml at day two. It was also observed that most of the peak yield was at day two except in the case of wheat which the highest yield (36nkat/ml) was observed on the third day. The production cost of xylanase is the major factor preventing their use, thus indicating the need for low cost production systems for this enzyme (Bae et al., 2008). In this study, different digestive bran and sawdust were used as cheap alternate substrates for the production of xylanase by *Bacillus subtillus*. Sawdust is a material that exhibits a high polarity mainly due to the presence of different oxygen-containing functional groups such as alcohol and ether (Bledzki and Gassan, 1999; Álvarez et al., 2005). The cell walls of sawdust mainly consist of cellulose and lignin, and many hydroxyl groups, such as tannins or other phenolic compounds, which are active ion exchange compounds. The lignin content of hardwoods is usually in the range of 18 to 25%, whereas that of softwoods varies between 25 and 35% (Batzias and Sidiras, 2007).

CONCLUSION AND RECOMMENDATION

In conclusion, for commercial production of xylanase enzymes, the focus should be on the utilization of agro residual wastes along with development of efficient bioprocess strategies to obtain high enzyme titer (Biswas et al., 2010). The alternate substrates investigated in this Study demonstrates a good potential for production of high titre of xylanase by the *Bacillus subtillus*. The present work has shown that sawdust and digestive brans could be considered as a promising material for enzyme production. Overall, the use of sawdust and digestive bran could provide a cheaper alternative for the large-scale production of xylanases, for various industrial applications, compared to oat-spelt and Birchwood xylan currently being used in small scale experiments.

REFERENCES

Abdel-Sater MA, El-Said AHM (2001). Xylan-decomposing fungi and xylanolytic activity in Agricultural and industrial wastes. Int. Biodeterior. Biodegrade, 47: 15-21.

Álvarez P, Blanco C, Santamaría R, Grand M (2005). Lignocelluloses'/pitch based composites.
Composites Part A., 36: 649-657.

Anuradha P, Vijayalakshmi K, Prasanna ND, Sridevi K (2007).Production and properties of alkaline xylanases from *Bacillus* sp.Isolated from sugarcane fields. Curr. Sci., 92: 1283-1286.

Archana A, Satyanarayana T (1997). Xylanase production by thermophilic *Bacillus licheniformis*
A99 in solid-state fermentation. Enzyme Microb. Technol., 21: 12-17.

Asther M, Meunier JC (1990). Increased thermostability of *Bacillus licheniformis* α-amylase in the presence of various additives. Enzyme Microb. Technol., 12: 902-

905.

Bachmann SL, McCarthy AJ (1991). Purification and cooperative activity of enzymes constituting the xylan degrading system of *Thermomonospora fusca*. Appl. Environ. Microbial., 57: 2121-2130.

Bae HJ, Kim HJ, Kim YS (2008). Production of a recombinant xylanase in plants and its potential for pulp biobleaching applications.Bioresour. Technol., 99: 3513-3519.

Bailey M, Biely P, Poutanen K (1992). Interlaboratory testing of methods for assay of xylanase activity. J. Biotechnol., 23: 257-270. Bataillon M, Cardinali APN, Castillon N, Duchiron F (2000).

Purification and characterization of a moderately thermostable xylanase from *Bacillus* sp. strain SPS-0. Enzyme Microb. Technol., 26: 187-192.

Battan B, Sharma J, Dhiman SS, Kuhad RC (2007). Enhanced production of cellulose-free thermostable xylanase by *Bacillus pumilus* ASH and its potential application in paper industry. Enzyme Microb. Technol., 41: 733-739.

Batzias FA, Sidiras DK (2007). Simulation of dye adsorption by beech sawdust as affected by pH. J. Hazard Mater., 14: 668-679. Beg QK, Bhushan B, Kapoor M, Hoondal GS (2000).
Enhanced production of a thermostable xylanase from *Streptomyces* sp. QG-11- 3 and its application in biobleaching of eucalyptus kraft pulp. EnzymeMicrob. Technol., 27: 459-466.

Biely P (1985). Microbial xylanolytic system. Trends Biotechnol., 3: 286-290.

Biswas R, Sahai V, Mishra S, Bisaria VS (2010). Bioprocess strategies for enhanced production of xylanase by *Melanocarpus albomyces* IITD3A on agro-residual extract. J. Biosci. Bioeng., doi:10.1016/j.jbiosc.2010.07.013.

Biswas SR, Jana SC, Mishra AK, Nanda G (1990). Production, purification, and characterization of xylanase from a hyperxylanolytic mutant of *Aspergillus ochraceus.* Biotechnol. Bioeng., 35: 244-251.

Bledzki AK, Gassan J (1999). Composites reinforced with cellulose based fibres. Prog. Polym. Sci., 24: 221-274.Cacais AOG, De Paula Silveira FQ, Filho EXF (2001). Production of xylan degrading enzymes by a *Trichoderma harzianum* strain. Braz. J. Microbiol., 32: 141-143.

Camassola M, Dillon AJP (2009). Biological pretreatment of sugar cane bagasse for the production of cellulases and xylanases by *Penicillium echinulatum*. Ind. Crops Prod., 29: 642 -647.

Chávez R, Bull P, Eyzaguirre J (2006). The xylanolytic enzyme system from the genus *Penicillium*. J. Biotechnol., 123: 413-433.

Contreras LM, Gómez J, Prieto J, Clemente-Jiménez JM, Heras- Vázquez FJL, Rodríguez-Vico F, Blanco FJ, Neira JL (2008). The family 52 β-xylosidase from *Geobacillus stearothermophilus* is a dimer: Structural and biophysical characterization of a glycoside hydrolase. Biochim. Biophys. Acta, 1784: 1924-1934.

Coughlan MP, Hazlewood GP (1993). β-1,4-D-Xylandegrading enzyme systems: Biochemistry,molecular biology and applications. Biotechnol. Appl. Biochem., 17: 259-289.

Duff SJB, Murrayh WD (1996). Bioconversion of forest products, industry waste cellulosics to fuel ethanol: A Review. Bioresour. Technol., 55: 3l-33.

Esteghlalian AR, Kazaoka MM, Lowery BA, Varvak A, Hancock, B Woodward T, Turner JO,Blum DL, Weiner D, Hazlewood GP (2008). Prebleaching of softwood and hardwood pulps by a high performance 752 Afr. J. Microbiol. Res. xylanase belonging to a novel clade of glycosyl hydrolase family 11. Enzyme Microb. Technol., 42: 395-403.

Gessesse A (1998). Purification and properties of two thermostable alkaline xylanases from an alkaliphilic *Bacillus* sp. Appl. Environ. Microbiol., 64: 3533-3535.

Gessesse A, Mamo G (1999). High-level xylanase production by an alkaliphilic *Bacillus* sp. by using solid-state fermentation. Enzyme Microb. Technol., 25: 68-72.

Gilbert M, Breuil C, Saddler JN (1992). Characterization of the enzymes present in the cellulose system of *Thielavia terrestris* 255B. Bioresour. Technol., 39: 147-154.

Haltrich D, Nidetzky B, Kulbe KD, Steiner W, Župančič S (1996). Production of fungal xylanases. Bioresour. Technol., 58: 137-161.

Hidayah A, Mohd AH, Umi Kalsom MS, Norhafizah A, Farinazleen MG, Yoshihito S (2008).Production of bacterial endoglucanase from pretreated oil palm empty fruit bunch by *Bacillus pumilus* EB3. J. Biosci. Bioeng. 06: 231-236.

Joshi C, Khare SK (2010). Utilization of deoiled *Jatropha curcas* seed cake for production of xylanase from thermophilic *Scytalidium thermophilum* Bioresour. Technol., doi:10.1016/j.biortech.2010.08.070. Kapoor M, Nair LM, Kuhad RC (2008). Cost-effective xylanase production from free and immobilized *Bacillus pumilus* strain MK001 and its application in saccharification of *Prosopis juliflora*. Biochem. Eng. J., 38: 88-97.

Liu M, Liu G (2008). Expression of recombinant *Bacillus licheniformis* xylanase A in *Pichia pastoris* and xylooligosaccharides released from xylans by it. Protein Expression Purif., 57: 101-107.

Maheshwari R, Bharadwaj G, Bhat MK (2000). Thermophilic fungi: Their physiology and enzymes. Microbiol. Mol. Biol. Rev., 64: 461-488.

Mamo G, Hatti-Kaul R, Mattiasson B (2006). A thermostable alkaline active endo-ß-1-4xylanase from *Bacillus halodurans* S7: Purification and characterization. Enzyme Microb. Technol., 39: 1492-1498.

Miller L (1959). Use of dinitrosalicylic acid reagent for determination of reducing sugar. Anal. Chem., 31: 426-428.

Nawel B, Said B, Estelle C, Hakim H, Duchiron F (2010). Production and partial characterization of xylanase produced by *Jonesia denitrificans* isolated in Algerian soil. Process Biochem. doi:10.1016/j.procbio.2010.10.003.

Ninawe S, Kuhad RC (2006). Bleaching of wheat straw-rich soda pulp with xylanase from a thermoalkalophilic *Streptomyces cyaneus* SN32. Bioresour. Technol., 97: 2291-2295.

Pham PL, Taillandier P, Delmas M, Strehaiano P (1998). Production of xylanases by *Bacillus polymyxa* using lignocellulosic wastes. Ind. Crops Prod., 7: 195-203.

Pinaga F, Pena JL, Vallés S (1993). Xylanase production by *B. polymyxa*. J. Chem. Technol. Biotechnol., 57: 327-333.

Podar M, Reysenbach A (2006). New opportunities revealed by biotechnological explorations of extremophiles. Curr. Opin. Biotechnol., 17: 250-255.

Prescott M, Harley JP, Klein DA (1996). Microbiology 3rd ed., W. M. C. Brow Publishers, New York, p. 176.

Ramesh M, Lonsame BK (1989). Solid state fermentation for production of higher titers of thermostable alpha-amylase with two peaks for pH optimum by *Bacillus licheniformis* M27. Biotechnol. Lett., 11: 49-52.

Roy N, Belaluddin M (2004). Production and characterization of alkaline xylanases from *Bacillus* sp. isolated from an alkaline soda lake. J. Biol. Sci., 7: 777-781.

Sa´-Pereira P, Costa-Ferreira M, Aires-Barros MR (2002). Enzymatic properties of a neutral endo-1, 3(4) - β -xylanase Xyl II from *Bacillus subtilis*. J. Biotechnol., 94: 265-275.

Shah AK, Sidid SS, Ahmad A, Rele MV (1999). Treatment of bagasse pulp with cellulase-free xylanases from an alkalophilic *Bacillus sp*. Sam-3. Bioresour. Technol., 68: 133-140.

Srinivasan MC, Rele MV (1999). Microbial xylanases for pulp and paper industry. Curr. Sci., 77: 137–42.

PRODUCTION AND UTILIZATION OF CERAMIC GLAZE FROM LOCALLY SOURCED MATERIALS OF NIGERIAN ORIGIN

[1] Eloka-Eboka, A.C.*, [2]Ajiwe, V.I.E, [3] Oshuoha, I.C. and Shima, P.
[1, 3] Mechanical Engineering Department, University of Agriculture, Makurdi, Nigeria
[2] Department of Production Technology, Nnamdi Azikiwe University, Awka, Nigeria
[4] Department of Chemistry, Benue State University, Makurdi, Nigeria.

Corresponding/Presenting author: *Eloka-Eboka, A.C., fatherfounder@yahoo.com, +234-8067915670

Abstract
This work explores the feasibility study of ceramics glaze development and production from locally sourced raw materials of Nigerian origin and their utilization in the production of ceramics products as electrical porcelains, insulators, tiles, tables wares and vases. A classification screening and examination of selected glaze materials were carried out and used to formulate glazes. The produced glazes were then utilized to produce ceramics wares by slip cast and dipping methods. Their apparent porosity, water absorption, firing shrinkage/characteristics, contraction after drying, bulk density, modulus of rupture, acidity, chemical analysis by x-ray fluorescence were carried out on the glaze and wares. Based on a test trial of fifteen formulations, five were investigated closely and two feldspathic glazes were developed. One is of low temperature and leadless, the other is of high temperature containing traces of lead used as a flux. These were found suitable for insulators' production, sanitary wares, tiles, table wares and the other, suitable as electrical insulators respectively due to their high temperature nature. Feldspar was found to play a major role in the quality of the insulators. The glazes produced were taken to be of international standards and could be utilized in the establishment of ceramics and glazes making industries which are no longer available in Nigeria.
Keywords: production, ceramics, glaze, utilization, locally sourced, Nigerian origin, materials.

1. Introduction

The world of Ceramics cannot be made complete without the introduction of ceramic glaze and its utilization as a ceramic component. Glaze (glass in powder) defines the thin, homogenous, glossy or mathy coat usually applied on ceramic products to enhance quality, strength, attractiveness and beauty [1]. For many centuries, glazes have been used for decorative effects and to render ceramic bodies impermeable to liquids. In recent years, they have also been used to provide large surface compressions and hence to strengthen ceramic bodies. Kingery *et al.* [1] claimed that such strength permits the ceramic wares based on glaze materials to be guaranteed for three years against breakage. Suitable glazes have been developed from feldspar, kaolin, quartz, barium carbonate, dolomite, zircon, ZnO and colour pigments in later years [2]. The advantages conferred by the addition of glaze layer are substantial, and for this reason, glazing has become an integral part of white ware technology. It provides an impermeable layer on porous bodies. It is easy to clean, an important aspect in the case of wall tiles or sanitary wares. It protects under-glaze decoration, either by the use of coloured glazes per se or in terms of the so-called in-glaze decoration. The use of coloured glazes goes back to history, probably to the Egyptians and is responsible for much of the charm of early pottery [3]. It is an extraordinary fact that many wonderful coloured glazes were produced without the benefit of the knowledge of modern theories of glass structure. In addition to aesthetic effects, glaze has important technical characteristics. Thus they can materially increase mechanical strength, provide specific electrical properties. The details of glaze formulation are very complex [4]. For this reason, also most pottery manufacturers do not compound their own glazes, but get them from specialist glaze suppliers. This is part of the limitation of Nigerian ceramic industry.

In the last three decades, advances in ceramic glaze technology and manufacture have brought out beauty, class and variety to the domestic products of ceramics such as dinner wares, table wares, hotel wares, decorative wares, ornament wares, building wares and even electrical wares etc [4, 5, 6].

Consequently, the high taste enjoyed by a sizeable percentage of Nigerians in the use of glazed ceramic wares has led to the huge and foreign exchange cost to the economy. The implication and relevance to the economy is the fact that there is no local production of ceramic glaze in Nigeria and even the tiny percentage of glazed ceramic wares produced in Nigeria, are substandard compared to the imported wares in our markets [5]. It is only the development of good and colourful glazes locally that can raise the competitive level of Nigerian-made ceramic wares, reduce importation costs, expand production capabilities and encourage manufacturing outfits. Recent survey revealed that several ceramic manufacturers have had to close down principally due to lack of glaze supply [5, 6].

The objective of this work is to develop and formulate glazes in order to meet the growing need of the ceramic and allied industries in Nigeria; to develop and produce ceramic glazes from suitable raw materials; to discover

the wide potentialities embedded in our natural endowed non-metallic and metallic raw materials scattered all over the country and to put them into different uses; and identify, select, characterize and utilize of locally available glaze raw materials, thus maintaining quality control and standards for glazes.

2.0 Materials and Methods

2.1 Collection of Raw materials and processing

15 kg each of raw feldspar, quartz and kaolin were collected respectively from Abeokuta and Jos. 5 kg of calcium carbonate ($CaCO_3$) from Abeokuta was also collected. Further raw materials collection includes: 2 kg of zirconium silicate from local agent, 1 kg each of barium carbonate, lead bisilicate (a deflocculant) and zinc oxide from local agents, laboratory and Abeokuta respectively; 10 kg each of ball clay from Nsu (Imo state) and Ijoko (Ogun state). 2kg of borax was collected finally from local agents. These raw materials were characterized as such and labeled. They were thereafter sent for raw material processing for purification. After the processing of the materials, they were separated in the order of the production to be undertaken.

2.2 Composition of the Ceramic Bodies

The ceramic bodies were compounded according to the nature or type required. Here, two bodies were composed: the table wares body composition and the porcelain body composition. Both compositions are as shown in Tables 1 and 2.

2.3 Production Methodology

After weighing on a scale, the weighed samples were compounded or mixed together into an electrical ball mill for proper milling in a wet batch. This was achieved by adding a measurable quantity of water and added to the milling process. The milling was allowed for 30 minutes and checked for homogeneity. The milled, homogeneous, fine powdered slurry was subjected to sieving using a 300-mesh particle size. The sieved slurry was allowed for ageing for a whole day or more. This was to allow for the removal of air bubbles, which may constitute pore spaces, generated as a result of the milling. The aged slurry called slip was ready for slip casting. The slip was caste into different shapes in the cast moulds made of plaster of Paris (POP) – $CaSO_4 .2H_2O$ This was a high absorbent material, which absorbs the water contents of the slip to generate plasticity to the cast slip thereby forming a cast body. The body was thereafter dismembered from the moulds and kept for atmospheric drying. The dried body was then subjected to the kiln firing (bisque firing) to a temperature of 800°C — 1000°C. This was to fully remove the water of plasticity and then kept ready for glazing. The fired body is an irreversible fired mass of body.

2.4 Glaze Formulation

This was quite complex and requires higher level of ingenuity proceeded first by glaze calculation.

Fifteen test trials formulations were made, five were investigated closely and feldspathic glazes were eventually developed, the high temperature glaze, which contained no trace of lead, and low temperature glaze with traces of lead. For the low temperature, the lead contained would not volatilize except at a certain temperature unattained.

After the glaze calculation that gave rise to the compositions in Table 1 and 2 above, the materials were compounded and ball milled. The same process as in the case of ceramic body methodology was followed until the ageing storage. In this case, the ageing was allowed for a longer time up to 3-4 weeks. They were thereafter taken to the furnace for drying at the temperature of between 1 167°C - 1250°C for high temperature glaze and 1080°C - 1120°C for low temperature glaze.

2.5 Glazing

The prepared cast tableware and the porcelain body were subjected to glazing using the produced glaze by immersion. The glaze was made into slurry and the wares were dipped into the slurry, allowed to dry atmospherically before subjecting them to gloss. Adding a calculated amount of water makes the glaze slurry, and if colouring was desired, the colouring matter was added. The gloss firing was attained according to the nature of glaze used.

2.6 Chemical analysis by X-Ray fluorescence X-RF technique theory

X-RF uses the irradiation of x-rays, which raise the orbital electron to higher level, when these excited electrons fall back to have lower energy level, they emit characteristic X-rays which can be used to obtain qualitative and quantitative information about the minerals being irradiated and these forms the basis of the X-RF analytical techniques.

The X-RF consists of a powerful X-ray source, electronic discemator instrument, a detector and a recorder to measure the various intensities. It is a versatile instrument having the capacity to analyse many samples and element simultaneously.

Procedure: 0.5 kg of the sample to be analyzed were ashed by subjecting to a high temperature (above 780°C) and were then placed into the detector of the x ray fluorescence instrument which rotates 100 times on two cycles while the recorder produces the result automatically.

2.7 Test analysis

The following analyses were conducted on the ceramics wears glazed and produced: water of absorption test, apparent porosity, modulus of rupture, compressive strength and acidity test.

3. Results and Discussion

Table 5 is the result of the X-ray fluorescence analysis. Table 6 and 7 are the physical analysis on green wares (unfired) and the ball clay while Table 8 is the same analysis for the glazed wares. Table 9 is the quality control tests on the low and high temperatures glazes that were produced in comparison with the standards. The determination of those elements present in the form of oxide was the basic factor in glaze calculation and formulations. It was on this basis that the scientific incursion unto the theory of glazing makes absolute meaning. The results in Table 3 and 4 confirmed the suitability of the raw materials for glaze formulations and

ceramic wares productions.

The physical and chemical analysis which includes loss on Ignition (LOI) result includes conversion of carbonate to oxides, sulphates to sulphur trioxide, calcium to calcium oxides. These are volatiles (See equation):

$CaCO_3 + Heat \quad CaO + CO_2$

$CaSO_4 + Heat \quad CaO + SO_3$

There were also losses due to combustion of carbon and organic matters.

In Silica determination, fusion of flux mixture, sodium and borax ensured that all silica present was converted to sodium silicate and metallic oxides. Sodium was decomposed with the liberation of silicic acid.

$Na_2SiO_2 + HC1 \quad NaC1 + H_2SiO_3$

Silicic acid was appreciably soluble in dilute mineral acid, so the solution was evaporated to dryness to expel the excess of acid.

The alumina content of the ball clay, were in the range (25.0 - 28.42). These fell within the specification of balls clay suitable for ceramic production. The chemical analysis of the raw materials for glaze formulations showed that they were suitable for glaze, table wares and porcelain formulations and were up to international standard.

The X-RF analysis revealed low Na_2O for Kaolin, quartz and the ball clays. This fell with the specifications of the British Ceramic Association. The kaolin with a low Fe_2O_3 content was most suitable. The quartz was of pure standard having 95.5% of SiO_2 which was the major glass and 0.07% of Fe_2O_3 which made it to fall within the pure grade for glaze productions.

The high SiO_2 content of the quartz (the major source of SiO_2) and virtually for feldspar, kaolin and ball clay that were higher than others, suggested high refractoriness of the ceramic products produced. Refractoriness was the ability to withstand high temperatures without appreciable deformation under service conditions. The apparent porosity and water absorption of the ball clays were consistent with the standard clay of primary geologic origin [8]. The bulk density, volume of shrinkage and refractoriness as deduced from the Tables 3.2 a, b, c were satisfactory in accordance with research specifications. The firing shrinkage of 10.6% was most suitable for the object of this research and reacted in a good binding manner thus presenting increase in compactions.

Ajiwe and Ugochukwu [8] reported that all shrinkage above 100% was considered suitable for tile productions, however, higher shrinkage increased with increase in temperature.

The above empirical deductions coupled with the facts of physical inspections of the products made; the different types of glaze, the electrical porcelain insulators and some table wares which, in the event of productions were limited only to laboratory experiments and few workshop un-automated operations due to inadequate facilities and limited finance confirmed that the wares were comparable to the commercial ones anywhere in the world [8, 9]. This meant that if there were good capital and adequate facilities, the production of these wares would be highly standardized. This work has so far brought to the limelight that good potentials exist for the utilizations of Nigerian non-metallic and metallic raw materials for the development of glazes and ceramics wares and industries.

5. Conclusion

In conclusion, this work has proved that good potentials exist for the use of Nigerian raw materials for glaze formulation, which could be utilized in the making of ceramics. The work particularly highlighted the absolute lack of meaningful research work in this area of glaze manufacture that is so vital to the survival and growth of ceramics industry in Nigeria. The work no doubt brought out the untapped potentials in the use of local materials for glaze development and ceramic productions. The results of chemical analysis of the local feldspar, kaolin, clays and quartz are within limits of standard material properties. With the exception of black clay (Nsu), most raw materials were found suitable for glaze preparation. The trial glaze were tested and found acceptable. This work has succeeded in opening up more research area for meaningful standard glaze development utilizing other raw materials located in Nigeria. It has been recommended that more specific topics of glaze development on low temperature glaze either using Borax or Lead, as the main flux should be conducted. If research in this area was successful, it could lead to the establishment of glaze pilot plant for ceramic and pottery industries.

References

[1] KIngsley, W.D., Bowen, H.K., Uhimann, D.R. (1976). Introduction to Ceramics (2nd Edition). A Woley lnterscience publication, USA. pp. 46, 47.

[2] Men Dinsdale (1985). Potter Science - Materials, processes and products. Ellis Horwood Ltd, Chichester pp 13-33, 69,167-175,191.

[4] Eke, HO. (2001). Chemical analysis and utilization of some clay minerals of south east Nigeria - A masters degree thesis of the Department of Production Technology, Nnamdl Azikiwe University, Awka, pp 1-50

[5] Raw Materials Research and Development Council (RMRDC) (2001). Technical Briefs on Minerals in Nigeria — Limestone/Marble: RMRDC pub., Lagos, Nig. Pp 3-17.

[6] Federal Institute of Industrial Research (FIIRO) (1987). *Scientific Journal on Clay and Glazes* 1 (1), Oshodl, Lagos, pp 6

[7] Raw material Research and development council (2002). Ceramic art ware and toy manufacturing – 6th Technological exposition. pp. 103-104.

[8] Ajiwe, V.l.E. and Ugochukwu C. (1998). Utilization of local clays In emulsion paint manufacture: Research and Development report *Journal of Applied Sciences* 2 (3), 357 — 363

[9] Omowumi, O.J. (2001). Characterization of some Nigerian clay as Refractory Materials for Furnace lining.

Nigerian Journal of Engineering Management 2(3),1-4.

Table 1: Table ware body Composition

Composition	%	Weight (kg)
Ball clay	25%	1.25
Black Imo Clay	15%	0.75
Kaolin	10%	0.5
Quartz (SiO_2)	35%	1.75
Feldspar	155	0.75
Total	**100**	**5kg**

Table 2: Porcelain Body Composition – Total of 5 Kg and 4kg

Composition	%	Weight (kg)
Ball clay (Ijoko)	15%	0.6
Black Imo (Nsu)	40%	1.6
Feldspar	20%	0.8
Quartz	25%	1.0
Total	**100**	**4kg**

Table 3: High Temperature Glaze Formulation (1167°C – 1250°C)

Composition	%	Weight (kg)
Feldspar	27.5	2.75
$CaCO_3$	15.0%	1.5
$BaCO_3$	5.5%	0.55
Clay	6.0%	0.6
Quartz	20%	2
$ZrSiO_2$	16%	1.6
ZnO	5%	0.5
Kaolin	55%	0.5
Total	**100%**	**10kg**

A total of 10kg of high temperature glaze was formulated (HTG)

Table 4: Low Temperature Glaze Formulation (1080^0c-1120^0c)

Composition	%	Weight (kg)
Lead bisilicate	10.0%	1
Borax	12.0%	1.5
$BaCO_3$	3.05%	0.3
Feldspar	25.0%	2.5
Quartz	20.0%	2.0
Marble 14.0	14%	1.4
Clay (Ijoko)	13.0	1.3
	10kg	**1.3**

Table 5: X-Ray Fluorescence Analysis (Raw Material Samples)

Elements present		Kaolin	Feldspar	Quartz	Ball clay (Imo)	Ball clay (Ijoko)
SiO_2		47.40	72.10	95.50	58.63	66.58
$A1_2O$		36.60	15.55	0.60	28.03	25.64
Fe_2O_3		1.61	0.90	0.07	1.41	4.13
TiO_2		0.91	0.35	0.02	1.12	1.08
CaO	Fluxes	0.05	0.32	0.06	0.28	0.30
MgO		0.06	0.04	0.05	0.08	0.68
Na_2O		0.04	2.75	0.08	0.03	0.03
K_2O		0.73	0.25	0.20	0.33	0.17
LOI		12.60	0.44	0.26	9.91	9.33

Table 6: (A) Physical Analysis on Ball Clay (Ijoko)

Parameter	Value	British standard
Apparent porosity (%)	18.60	17.20-20.60
Water of Absorption (%)	7.5	7.0-7.8
Bulk density ($glcm^3$)	1.92	1.0-1.90
Volume of shrinkage (%)	2.8	2.5-3.0
Refractoriness	1680^0	Above 1500^0C

Table 7: (B) Physical Analysis on Green Wares (Unfired)

Parameter	Value measured
Wd (Dried Weight)	12.6250
D (Suspended in water)	20.7599
WS (Weight Soaked in water)	23.8855

Table 8: (C) Physical Analysis on Glazed Wares

Parameter	Valued measured	Standard
Percentage Shrinkage	10.6	STD 9.5-10.5
Modulus of Rapture (MOR)	$7.18kgcm^3$	STD 8.0 Satisfactory
Acidity test	Neutral (Satisfactory)	

Table 9: Quality Control Analysis

Quality control parameter	STD	LTD	HTG
a. Particle Size	200, 300 mesh	300 mesh	300 mesh
b. Melting Temperature	980, 1040^0C	10800^0C - 1120^0C	-
	1080^0C		
c. Hard Glaze Temperature	1200^0C - 1250^0C	-	11670C
d. Thermal Expansion	Glaze	Satisfactory	Satisfactory
e. Thermal Expansion	Body satisfactory	Satisfactory	Satisfactory
f. Autoclave Grazing Test	16/1 hour cycle	-	-

EFFECT OF VOLUME RATIO ON THE TENSILE PROPERTIES OF RICE HUSK FLOUR (RHF) POLYESTER COMPOSITE

Imoisili P. E, Olunlade B. A.,*Tomori W. B.
Engineering Materials Development Institute, P.M.B 611, Km 4 Ondo Road Akure Ondo State
* Department of Chemistry, Federal University Of Technology, Akure. Ondo state
Corresponding author: patrickehis2002@yahoo.com

ABSTRACT
To investigate, the effect of volume ratio of an agricultural waste materials use as reinforcing fillers in thermosetting polymer composite. Polyester was used as the matrix and rice husk flour (RHF) as the reinforcing filler, to prepare a particle-reinforced composite in order to determine the tensile properties of the composite according to the filler loading in respect to thermosetting polymer. In the sample preparation, five levels of filler loading (5, 10, 20, 30 and 40 wt. %) were designed. Test result shows that the Ultimate Tensile Strengths, Modulus, Maximum load and Micro-hardness of the composites did not show any appreciable improvement with increase in filler loading.

Keywords: *polyester composites, rice husk flour (RHF), Ultimate tensile strength, modulus*

INTRODUCTION

Recent investigations of polymer-based composite materials have opened new routes for polymer formulations and have allowed the manufacture of new products with optimal properties for special applications [10, 5]. In most cases, these composites improve the product design and reduce the material and energy consumption. Using natural filler to reinforce the composite materials offers the following benefit in comparison with mineral filler [7, 15], strong and rigid, light weight, environmental friendly, economical, renewable and abundant resource. How ever they have the disadvantage of degradation by moisture, poor surface adhesion to hydrophobic polymers, non-uniform filler sizes, not suitable for high temperature application among others [1]
The improved performance of polymers and their composites in industrial and structural applications by the addition of filler materials has shown great promise and so has lately been a subject of considerable interest. Various kinds of polymers and polymer matrix composites reinforced with metal particles have a wide range of industrial applications such as in heaters, electrodes [19], and composites with thermal durability at high temperature [2]. These engineering composites are desired due to their low density, high corrosion resistance, ease of fabrication, and low cost [1,7,13]. Similarly, ceramic filled polymer composites have been the subject of extensive research in the last two decades. The inclusion of inorganic fillers into polymers for commercial applications is primarily aimed at the cost reduction and stiffness improvement [11, 21]. Along with fiber reinforced composites, the composites made with particulate fillers have been found to perform well in many real-operational conditions.

Studies are ongoing to find ways to use lignocellulosic filler in place of synthetic fillers as reinforcing fillers. These natural fillers are especially being sought since the production of composites using natural substances as reinforcing fillers is not only inexpensive but also able to minimize the environmental pollution caused by the characteristic biodegradability [18], enabling these composites to play an important role in resolving future environmental problems. The need for materials that are non-toxic to the human body and have appropriate characteristics for specific purposes is ever increasing due to the lack of resources and increasing levels of environmental pollution. Thus, research is proceeding to develop composites using various recycled wastes [21], especially in developing composites using most environmentally friendly agro-wastes (lignocellulosic materials) as reinforcing fillers and thermoplastic polymers as matrixes. The convenience of these composites lies in the fact that the ingredients are obtained easily from natural wastes and hence the composites can be made relatively easily. They can be used to resolve environmental problems and to produce products with various physical properties and effective functions. Lignocellulosic materials as reinforcing fillers in plastics, in place of the previously used inorganic substances and synthetic fibers, offer a major benefit in terms of environmental protection.The benefits offered by lignocellulosic materials include making the final product light [10], decreasing the wear of the machinery used, low cost, biodegradability [18], and absence of residues or toxic byproducts.

A number of natural occurring fillers and fiber in composite have been studied in the past. These include wood fillers [4] wheat straw, almond husk, ash rice husk [9,20], pineapple leaf [16], sisal , Coir, and rice husk [6], These fillers introduce some advantages compared to traditional inorganic fillers, including their renewable nature, low density, nonabrasive properties, reasonable strength, and stiffness [17]. Luo and Netravali [13] studies the tensile and flexural properties of pineapple fiber, Belmeres et al [1] studies sisal, henequen, and palm fiber, and found that they have similar physical,

chemical, and tensile properties,. Fuad et al [3] investigated wood base filler derive from oil palm wood flour, khalid et al [12], also studied epoxy composite reinforced with the use of cotton fiber along with glass fiber.

2.0 EXPERIMENTAL

2.1 SAMPLE PREPARATION.

The sample was ground into powder with the use of electric blender. The grounded powder was later sieve with BS/ISO 3310 into particle size of 53 µm. and dried in an oven at 105°c to reduce moisture content. This was used for all the different percentage compositions of Rice Husk filler (RHF) that were used for the Composite preparation.

A commercially available Unsaturated Polyester Resin with Cobalt Octoate as Accelerator and Methyl Ethyl Ketone Peroxide (MEKP) as Catalyst, was used as matrix for the composites. After being thoroughly mixed, the resin was cast onto the cavity of a steel mold, previously coated with a mould releasing agent and allows to cure. Composites with amounts of Rice Husk Flour (RHF), ranging from 5, 10, 20, 30 and 40 wt. % were manufactured

.

The prepared sampled were analyzed using a universal Instron testing machine model 3369, in accordance with ASTM Test Method D638-03, and micro hardness testing was carried out. on the sample using a Leco micro hardness tester, model LM-700AT, in accordance with ASTM E384

3.0 RESULTS AND DISCUSSION.

The tensile strengths of the composites made of lignocellulosic filler (RHF) and polyester
(PE) matrix at different filler loadings are shown in Figure. 4. The tests were conducted at room temperature. Tensile strengths of RHF–PE composites slightly decreased with increasing filler loading

As the filler loading increased, there is increase in the interfacial area, the worsening interfacial bonding between filler (hydrophilic) and matrix polymer (hydrophobic) decreased the tensile strength, which nevertheless remained within acceptable levels [18]

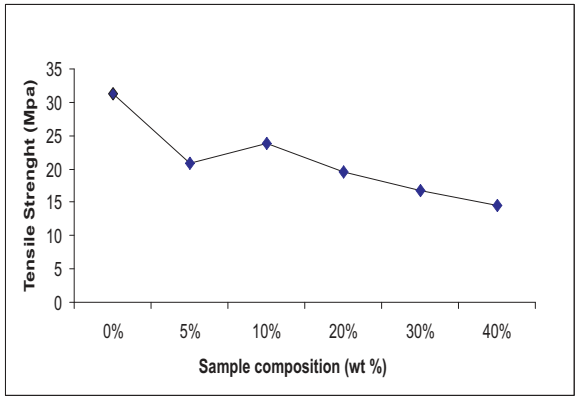


Figure 1 Tensile Test Result for Different Volume Ratio.

Modulus test result are shown in figure 2, for irregularly shape fillers, the strength of the composites decreases due to the inability of the filler to support stresses transferred from the polymer matrix [8].

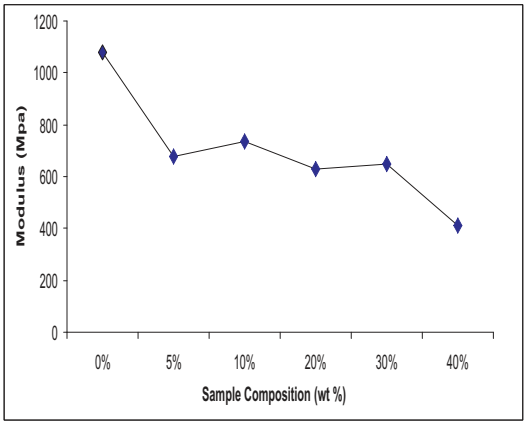


Figure 2: Modulus Test Result for Different Volume Ratio

From figure 3, maximum load at break of the samples show decrease gradually as filler loading increases.

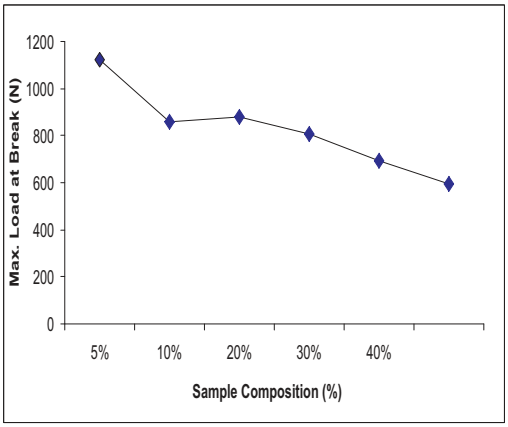


Figure 3: Maximum Load Test Result for Different Volume Ratio.

Micro hardness test result are shown in figure 4,there was gradual increase in hardness as filler level increase from 5% to 10%, after which the value decreases gradually,

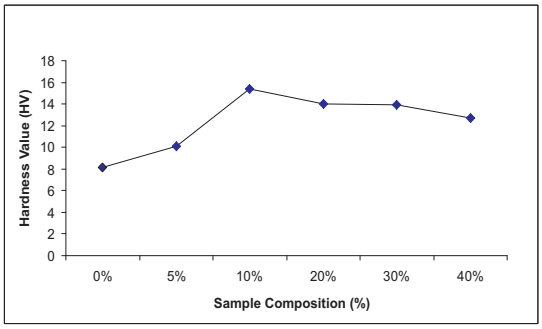


Figure 7: Micro -Hardness Test Result for Different Volume Ratio.

CONCLUSIONS

Tensile strengths of the composites slightly decreased while the tensile modulus improved as the filler loading increased. However the composites had an acceptable strength up to a filler loading of 10-20 wt.%. RHF could be utilized as biodegradable filler at end of- use in polymeric materials to minimize environmental pollution rather than produce strong reinforcing filler
The poor interfacial bonding between filler and matrix polymer caused decreased tensile properties nevertheless, this problem could be reduced by using a compatibilizing or coupling agent, and further extended research is suggested.

REFERENCE

1. Belmares H., Barrera A., and Monjaras M., "New Composite Materials from Natural Hard fibers. Part 2. Fatigue Studies and a Novel Fatigue Degradation Model", *Industrial Engineering Chemical Product Research and Development*, **22** (1983), pp. 643–652.
2. Bucknall, C. B. *Toughened Plastics*, London: Applied Science, 1977.
3. Fuad M.Y.A., Rahmad S. and Azlan M.R.N., "Filler Content Determination of Bio-Based Thermoplastics Composites by Thermogravimetric Analysis" *Proceedings of the Fourth International Conference on Advances in Materials and Processing Technologies, Kuala Lumpur*, 24–28 August, 1998, pp. 268–275.
4. Gattenholm, P.; Berlisson, H.; Mathiasson, A. (1993).The Effect of Chemical Composition of Interphase, On Dispersion of Cellulosic Fiber in Polymer. I.PVC-Coated cellulose in polystyrene. Journal Applied Polymer Science. 49. (2), 197-20
5. George, J., Sreekala, M. S. and Thomas, S. (2001). A review on interface modification and characterization of natural fiber reinforced plastic composites. Polymer Engineering & Science, 41: 1471–1485.
6. Han-Seung Yang , Hyun-Joong Kim ,*, Jungil Son , Hee-Jun Park ,Bum-Jae Lee , Taek-Sung Hwang (2003) Rice-Husk Flour Filled Polypropylene Composites; Mechanical And Morphological Study. Composite Structures 63 (2004) 305–312
7. Herrara-Franco P. A., Valadez-Gonzalez, and M. Cervantes-uc, "Development and Characterization of a HDPE–Sand–Natural Fiber Composite", *Composites Part B: Engineering*, **28B (3)** 1997, pp. 331–343.
8. Ismail H, Edyham MR, Wirjosentono B. (2002) Bamboo fibre filled natural rubber composites: the effects of filler loading and bonding agent. Polym Testing ;21(2):139–144.
9. Ismail, H.; Mega, L.; Abdul-Khalil, H. P. S. (2001). Effect of a silane coupling agent on the properties of white rice husk ash polypropylene/ Natural Rubber Composite. Polymer International.50: (5). 606-611.
10. Jacobson RE, Engineer MS, Caulfield DF, Rowell RM, Sanadi AR. Recent developments in annual growth lignocellulosics as reinforcing fillers in thermoplastics. In: Proceedings of 2nd Biomass Conference of the Americas: Energy, Environment, Agriculture, and Industry, August 21–24, Portland, OR. Golden, CO: National Renewable Energy Laboratory, 1995. p. 1171–1180.
11. Karnani, R., Krishnan, M. and Narayan, R. (1997), Biofiber-reinforced polypropylene composites. Polymer Engineering & Science, 37: 476–483.
12. Khalid A.A., Sahari B., and Khalid Y.A., "Environmental Effects on the Progressive Crushing of Cotton and Glass Fiber/Epoxy Composite Cones", *Proceedings of the Fourth International Conference on Advances in Materials and Processing Technologies, Kuala Lumpur*, 24–28 August, 1998, pp. 680–689.
13. Luo S. and Netravali A.N., "Mechanical and Thermal Properties of Environmentally Friendly "Green" Composites Made from Pineapple Leaf Fibers and Poly (hydroxybutyrate-co-valerate) Resin", *Polymer Composites*, **20 (3)**. (1999), pp. 367–378.
14. Martí-Ferrer, F., Vilaplana, F., Ribes-Greus, A., Benedito-Borrás, A. and Sanz-Box, C. (2006), Flour Rice Husk as Filler in Block Copolymer Polypropylene: Effect of different coupling agents. Journal of Applied Polymer Science, 99: 1823–1831.
15. Maulida A, Nasir M., and Khalil H.P.S.A. "Hybrid Composites Based on Natural Fiber", *Proceedings of Symposium on Polymeric Materials*, *Penang*, 1-2 June 2000, (Published by USM Press, Penang, 2000), pp. 216–219.
16. Mishra S. Hamzah H, Murshidi JA, Deraman M. (2002) Chemical Modification on lignocellulosic Polymeric Oil Palm Empty Fruit Bunch for Advance Material. Advances in Polymer Tech; 20(4):289-295
17. Neus Anglès, M., Salvadó, J. and Dufresne, A. (1999), Steam-Exploded Residual Softwood-Filled Polypropylene Composites. Journal of Applied Polymer Science, 74: 1962–1977
18. Premalal HGB, Ismail H, Baharin A. Comparison of the mechanical properties of rice husk powder filled polypropylene composites with talc filled polypropylene composites. Polym Testing 2002;21(7):833–839.
19. Riffle J. S., I. Yilgor, A. K. Banthia, C. Tran, G. L. Wilkes, and J. E. McGrath in "Epoxy resin chemistry", (ed. R. S. Bauer),*ACS Symposium Series no. 201*. Washington, DC: American Chemical Society, 1983, p. 21.
20. Saroja Devi M., Murugesan V., Rengaraj K, Anand P. (1998). Utilization of flyash as filler for unsaturated polyester resin. Journal of Applied Polymer Science.69: (7)1385-1391.
21. Son JI, Kim HJ, Lee PW. Role of paper sludge particle size and extrusion temperature on performance of paper sludge-thermoplastic polymer composites. J Applied Polymer Science 2001; 82(11):2709–2718.

PRODUCTION OF ALUMINA IN THE ALUMINUM SILICATE AND REFRACTORY SHOP OF THE AJAOKUTA STEEL COMPANY LIMITED

OCHERI C.[1], OYELARAN O.A[2] & BARNABAS A.[3] AGBOOLA, J.B[4] AJI DANIEL [5]
Foundry Shop, Ajaokuta Steel Company Limited, Ajaokuta, Kogi State[1]
Hydraulic Equipment, Development Institute, Kano [2]
Department of Metallurgical & Materials Engineering,Federal University of Technology, Akure[3]
Department of Mechanical Engineering, Federal University of Technology, Minna ,Niger State[4]
Department of Metallurgical Engineering, Federal Polytechnic Idah[5]
E-mail:ocheri4c@yahoo.com

ABSTRACT
The raw material for the production of Alumina in the Aluminum Silicate and Refractory Shop of the Steel plant have aluminum silicate content of high quantity of clay and molasses as blender. The blenders are used in order to increase the plasticity of the clay. The clay composition of aluminum silicate is higher in aluminum content, the better and the more expensive they are .The clay content should not be less than 35% Aluminum. The tonnes of clay needed in the Ajaokuta Steel Company Limited per year is 63,000 tonnes while the molasses is 1, 700 tonnes per year. The clay is collected from a deposit in Abeokuta, while the molasses is being gotten from Basita Sugar Company in Ilorin. This paper further discusses how the materials are handled, processed and making them to meeting the requirement for the production of Alumina.

Keywords: Alumina, Production, Aluminum silicate, Molasses and clay

INTRODUCTION

The Aluminum Silicate Refractory Shop of the Ajaokuta Steel Company Limited, consist of the following units:-
(a) The Raw Material Storage yard
(b) Crushing yard, the types of crushers used are raw crusher for hard materials and roll crusher for raw clay
(c) Clay Drying and Milling Yard
(d) Rotary Kiln / Gas clearing Yard
(e) Mixing and Pressing Yard
(f) Tunnel Kiln
(g) Finish Stock yard.

The raw material for the production of Aluminum silicate consist of high quantity of clay and molasses as blender as by product.

The blenders are used in order to increase the plasticity of the clay. The clay composition of Aluminum silicate, the higher the aluminum content, the better .and the more expensive they are. The clay content should not be less than 35% of aluminium. The tonnes of the clay needed in the Ajaokuta Steel Company Limited per year is 63,000 tonnes, while the tonnes of molasses is 1, 7000 tonnes per year. The clay is being gotten from Abeokuta, while molasses is being gotten from Bastia sugar company, Ilorin.

2.0 The Raw Material Storage yard

The clay are dumped with the aid of the overhead cranes by taking them bit-by –bit to the crushing unit where the jaw crusher is being used for crushing of hard clay and the roll crusher for the raw clay. With the aid of the conveyor belts the crushed materials are taken to the drum drier at a temperature of 1,500^{o}C, After the drying of the clay , the clay are latter taken for grinding either with basket distingrater or the bore milling grinding machine . These are stored as clay powder.

The clay is sent to the rotary kiln where calcinations of the clay take place. There are two rotary kilns in this unit of the same capacity. From the rotary kiln the materials are discharged into the drum cooler where there is water which is used to cool the body of the drum .The temperature of the calcinations is 800°C

3.0 In the Mixing and Pressing Yard

The raw clay is mixed with the calcined clay, water and molasses all in the required ratio, this depend on the type of refractory bricks needed to be produced. The clay are later passed to the pressing machine for pressing, it consists of moulds. The moulded bricks are sent to the tunnel kiln by the kiln car for firing.

3.1 The Tunnel Kiln

This unit consists of four zones:-
(a)The drying chamber zone; - This is the place where the drying of the bricks takes place and hot air is needed for drying.
(b)The Pre-heating zone: - The pre-heating of the bricks are done with the aid of heat gotten from the cooling zone.
(c)Heating Zone: - Heating of the bricks takes place in this zone at a temperature of 1500°C with the aid of natural gas.
(d)The last zone is the cooling zone:- air from outside is being introduced into the zone which is used for the cooling of the bricks.

At the last stage the good bricks are sent to the

At the last stage the good bricks are sent to the storageyard, while the bad ones are sent to the crushing unit for re-crushing.

4.0 Design and Operation data of the major units of Tar- Bonded Refractory Plant

The shop comprises the following major units:
(i)Rotary Kiln and its subsidiaries
(ii)Grinding and milling
(iii)Mixing
(iv) Preheating

(i) **Rotary Kiln and Its Subsidiaries**

The rotary Kiln is a cylindrical shell inclined at an angle of 2° to the horizontal. It has a charging and charging ends. The flow of materials (dolomite) in the kiln is counter current to the flow of the natural gas used to fire the kiln.

The kil n is divided into three temperature zone, with different lining net works, adjoining the charging end is the pre-heating zone with temperature average of 900°C, this zone is lined
with fire clay bricks. The next zone is the heating or calcinations zone lined with chrome –magnestic bricks and the zone temperature ranging between 900°C - 1750°C. The Kiln zone is lined with **periclasepchromite** bricks and the zone temperature is about 1000°C this zone is referred to as the cooling zone. Toward the tail end of the kiln i.e at about 1.7 m to the discharging end there is multite lining.

Directly linked to the rotary kiln are (1) the cooler kiln: - This is also a cylindrical shell like the rotary kiln, it has a uniform lining of clay brick. It is connected to the discharging end of the kiln. The outer shell of the cooler kiln is water cooled with the internal cooling medium is air.

(ii) Gas cleaning plant: At the charging end of the rotary kiln is connected to the gas cleaning plant.

4.0 Design and operating data of the kiln and its subsidiaries are given below:-

(a) Rotary Kiln

(i)Dimension Ø16 x 34 m
(ii) Angle of indentation 2°
(iii) Dolomite mass flow rate 2.5 t /hr
(iv) Dolomite inlet temperature 30°C
(v)Dolomite outlet temperature 1000 °C
(vi) (a) Pre-heating zone lining. Thickness -0.23 m , length 8.67 m
(b) Calculation zone lining. Thickness 0.23 m, length 15.07 m
(c) Cooling zone lining. Thickness 0.30 m, length 8.18 m

(b) The Cooler Kiln

Dimension Ø1.2 x 16 m
(ii) Angle of indentation 2°
(iii) Dolomite mass flow rate 1.05 t /hr
(iv) Dolomite inlet temperature 100°C
(v) Dolomite outlet temperature 1000 °C

(C) **Gas Cleaning Plant**

(i) Temperature of the flue gases -750-850 °C
(ii) Composition of gases (% volume) :
CO – 16.26
H – 13.56
O- 4.86
N_2- 69.32
(iii) Dust content of gases at 0°C ,
CO – 16.26
H – 13.56
O- 4.86
N_2- 69.32
(iii) Dust content of gases at 0°C ,

5.0 Grinding and Milling: Dolomite is first crushed in the roll crushed after when it is screened into sizes; portions of the screened size are sent into the ball mill where it is milled down to a size fraction of between 0-0.1 m. The ball mill is of dimension 1.5 x 5.6 m complete with mill ball.

Milling levels – Dolomite size into the milling yards ± 5. Roll crusher – screened size en-roll crushed (i) 5-3 mm
(ii) 3-1 mm
(iii) 1-0 mm

Ball mill size- into the ball mill (i) + 5 mm (ii) 5-3 mm (iii) 3-1mm (iv) 0.1mm. Milled size ball mill

6.0 Mixing: The mixer is of periodical action model 2000. It is used to pre-heated to a temperature of 80°C before being charged with dolomite that has also charging sequence of dolomite into the mixer is
(i) 5-3mm-15-20% plus tar
(ii) 3-1 mm -2.55% plus more tar
(iii) 1-0 mm -50-55% plus balance of tar up to 6% max. Tar is heated to 1200°C, while the mixing is done at a temperature of 75°C

6.0 Pressing: The press is used in a special hydraulic press of 1600°F. It is boiled to deliver pressure in the range of 1200-1400 kg / cm^2. The press is incorporated with seven different press mould for different product shape.

FLOW CHART THE TAR BONDED DOLOMITE REFRACTORY PLANT

Raw Dolomite
Receiving Yard

REFERENCES

1. Project Report: Ajaokuta steel company limited detailed Project Report (DPR) Vol. IV on Personnel

2 Company Report: Ajaokuta steel company limited detailed Project Report (DPR) Vol. I part II Explanatory Note.

3. Project Report: Ajaokuta steel company limited Detailed Project Report (DPR) Vol. V Repair shop, List of Equipment.

4. Evaluation Report of Ajaokuta steel company limited by Voest-Alhine Industrial Service GmbH Linz / Austria 1997

5. Project Report: Investment Profile of Ajaokuta steel company limited, March 1990

6. Status Report and Business Plan for Ajaokuta steel company limited April 1999.

7. Oisamoje M.D. "The Role of Metallurgy In Diversifying The Nigerian Economy Through The Development Of Viable Upstream And Down Stream Industries", Proceedings Of the NMS, 13, 1995, pp. 1-10.

8. Okonji, P.O: "Steel: Path to Economic Diversification Proceedings", NMS, 13, 1995 PP 11 – 16.

9 Banji Oyeleran Tenuche "The Steel Industry in Nigeria": CAL TOP Publications Nigeria Ltd 1994 pp 52

10. Arc M. Aminu Kani (1999) : Commerical Operation of Ajaokuta Steel Company , Alumino- Silcate Refractory Plant , Held in Kaduna National Steel Raw Materials Exploration Agency 10th March 1999 pg 16

CHARACTERIZATION OF SOLID WASTE IN NIGERIA: AKURE METROPOLIS AS A CASE STUDY

O. P. Fapetu, T. I. Ogedengbe* and O. T. Ajayi
Department of Mechanical Engineering, School of Engineering and Engineering Technology, The Federal University of Technology, Akure.

* Corresponding author: tioged@yahoo.com

Abstract
This study collected and characterized solid wastes in Akure Metropolis using the manual sorting technique. A total of 36323.9 g of solid wastes was collected in the high socioeconomic areas while 32617.3 g was collected in the low socioeconomic areas of Akure. The solid waste collected from the high socioeconomic area was found to have highest percentage of plastic at Ala quarters, glasses at Futa staff quarters, food waste at Ijapo estate and Alagbaka quarters. The high percentage of plastic and glass is due to high consumption of plastic bottled drinks and glass bottled drinks (assorted) in the area while food waste is due to disposal of cooked and uncooked food. Low socioeconomic area has highest percentage of glass (in comparison with other constituents) at three of the studied locations (Rescue area, Solagbade Street and St Leo Street) and food waste at Araromi Street. The high quantity of glass in this area is due to the high consumption of alcoholic and gin bottled drinks while the food waste is as a result of food canteen and disposal of unfinished food or meal. The solid wastes from the high socioeconomic area have 71.39% of it recyclable while 81.71% were found to be recyclable in the low socioeconomic area. The results will assist government and entrepreneurs strategizing for solid waste disposal as well as wealth generation from municipal solid wastes.

Keywords: Solid wastes, characterization, wealth generation.

Introduction

Waste is defined as any substance which constitutes scrap material, effluent waste or other unwanted surplus arising from the application of any process or article which is required to be disposed of or which has been broken, worn-out, contaminated or otherwise spoiled. This is supplemented with anything which is discarded or otherwise dealt with as if it were waste and shall be presumed to be waste unless the contrary is proved. In general, waste is useless, unwanted or discarded material resulting from agricultural, commercial, communal and industrial activities. Waste is also defined as any unwanted material intentionally thrown away for disposal **[1]**.

ste is generated by human activities. Such activities include industrial, communal or agricultural and it can be in form of solid (bottle, glass, tin, etc) or liquid such as industrial waste, sewage etc. Waste products arise from our ways of life and they are generated at every stage of process of production and development. However, certain wastes may eventually become valuable resources to others once they are removed from the waste stream **[2]**.

Waste characterization could be defined as the process of collecting waste at its source and directly sorting it out into its composite materials **[3,4]**. It is the means of finding out how much of paper, glass, food waste, etc, discarded in the waste system or stream. It also involves analysis of the composition of waste streams. Waste characterization is a method used to determine the types of materials being discarded in a waste stream and in what proportion. Solid waste composition varies considerably with community size, socioeconomic status and with the activities which are conducted in any area. Areas which experience population growth will often have increased amounts of construction materials, e.g. wood, insulation, and dirt, in the waste stream **[2].**

Waste composition indicates the components of the waste stream given as a percentage of the mass or volume. The main constituents of solid wastes are similar throughout the world but the proportions vary widely from country to country and even within a city, because the variations are closely related to income level. Waste generated in developing countries contains a large percentage of organic materials, usually three times higher than that of industrialized countries. The waste is also more dense and humid, due to the prevalent consumption of fresh fruits and vegetables, as well as unpackaged food **[5]**. Developed World residents consume more processed food packaged in cans, bottles, jars and plastic containers than those in the developing world. As a result, waste generated in the former contains more packaging materials than in that of the latter.

The volumes of wastes and changing composition have a profound impact on waste management practices **[6]**. Therefore it is important to characterize and identify the major constituents of municipal solid waste

stream in any area. This will help to determine waste generating sources, characterize the waste stream components from each source, and quantify the amount of solid waste generated by each source. It will further facilitate identification of the types and quantities of recyclable materials in the waste streams as well as assessment of the effectiveness of existing recycling programs. The amount of recyclable materials remaining in the waste stream can be determined to evaluate the potential for further reduction of this volume. Hence, in this study, solid wastes were manually collected within Akure metropolis, characterized and analyzed.

2.0 A global overview of issues on solid waste

Solid wastes include wastes from durable goods, nondurable goods, containers and packaging, food scraps, yard trimming, and miscellaneous inorganic materials from residential, commercial, institutional, and industrial sources. It does not include sewage, hazardous wastes, nonhazardous industrial waste, construction and demolition debris, or automobile bodies. Waste comes in many forms but it has three classic general types namely; Solid waste, Liquid waste and Gaseous waste. This classification is based purely on the state of matter of these waste products. Further classifications include Municipal solid waste, commercial waste, industrial waste, medical waste, radioactive waste and hazardous waste. Municipal solid waste, more commonly known as trash or garbage, consists of everyday items that were used and thrown away, such as product packaging, grass clippings, furniture, clothing, bottles, food scraps, newspapers, appliances, paint, and batteries. This comes from our homes, schools, hospitals, and businesses. Commercial waste consists of wastes from premises used mainly for the purpose of trade or business or for the purpose of sport or recreation but not including industrial waste. Industrial waste includes waste produced from industrial activity such as from factories, mills and mines and it has existed since the advent of the industrial revolution. Much industrial waste is neither hazardous nor toxic such as waste fiber produced by agriculture or logging. Medical waste also known as clinical waste and normally refers to waste products that cannot be considered general waste is produced from health care premises such as clinics and hospitals while radioactive waste is usually the product of a nuclear process such as nuclear fission, though industries not directly connected to the nuclear power industry may also produce radioactive waste. Hazardous waste includes waste that is toxic in nature thereby producing substantial or potent threats to public health or the environment.

Waste can also be classified depending on its source. The reason for using a classification by source is that it is the specific composition of each waste category that sometimes recommends a special collection or treatment system for each one. This means that classification of waste will be determined by the socio-economic sector generating the waste. The variety of sources from where waste is usually generated includes households, commercial establishments (e.g. shops, restaurants, etc.), Institutions (e.g. schools, hospitals and government offices) and factories (waste from industrial production).

Waste creation by mankind is inevitable as far as the manipulation of the environment continues. Solid waste composition varies from one area to another according to income level, population, density and predominant activities (residential, commercial, industrial, etc.). Changes in solid waste composition occur seasonally as a result of seasonal changes in food consumption. Changes in lifestyle and increasing dependence on processed food and associated plastic packaging continuously alter the solid waste composition. Solid waste in Nigeria is composed mainly of paper, food scraps, vegetable matter, plastics, metals, textiles, rubber, and glass. All categories of wastes including toxic or non-toxic, biodegradable or non-biodegradable, recyclable or non-recyclable are dumped together making their management very difficult. The reason(s) for this attitudinal occurrence in developing countries may not be farfetched. It could be as a result of lack of awareness, poverty, population growth, and high urbanization rates combine with lack of governments' policies on waste management issues especially on waste management and separation. In places where there are governments' policies, the agencies saddled with the mandate to enforce the policies are either under funded by the governments or are not monitored for efficiency. Therefore the big challenge with solid waste management in major Nigerian cities is not only the volume of the wastes, but also the composition of the wastes.

During typical solid waste collection in Akure, Ondo State, a member of the collection crew walks along the street alerting households by using truck alarms or the truck driver alerts the households using the truck horn, telling people to bring out their waste. Other crew members load waste from bins and containers onto the collection trucks where the waste is later transferred to the landfill site of the Ondo State Integrated Wastes Recycling and Treatment Project (OSIWRTP) at Igbatoro for recycling. Also, due to absence of drainage and seepage control facilities and insufficient gas collection systems at landfill sites, burning of the solid waste is another popular option being used **[7]**.

In most communities solid waste are managed by dumping them in landfills and then through incineration.

Landfills are sites for the disposal of waste materials by burial and are the oldest form of waste treatment. Landfills may include internal waste disposal sites (where a producer carries out their own waste disposal at the place of production) as well as sites used by many producers. Many landfills are also used for other waste management purposes such as the temporary storage, consolidation and transfer, or processing of waste materials. Unless they are stabilized, areas use for landfills could be prone to shaking or liquefaction in a large earthquake **[8]**. The area being filled in developed countries is usually single and a rubberized landfill liner is placed to prevent contamination by leachates migrating downwards through the underlying geographical formation. Land filling as a method of waste disposal in Akure involves obtaining a suitable parcel of land within the confines of the OSIWRTP which is dug to a depth of about 10ft or more. The wall of the hole is then cemented to prevent leachate from leaking into nearby soil formation which if not prevented could lead to contamination of underground water system. A major drawback of landfills is that it is not feasible in congested cities where land space is extremely scarce. In addition, such area which is used for land filling can sparsely be used for another purpose **[8]**.

Incineration otherwise, described as thermal treatment, is a waste treatment technology that involves the combustion of organic materials or substances. Incineration of waste materials converts the waste into incinerator bottom ash, flue gases, particulates and heat which can in turn be used to generate electric power. The flue gases are cleaned of pollutants before they are disposed into the atmosphere. Incineration with energy recovery is one of several waste-to-energy technologies such as gasification, pyrolysis and anaerobic digestion. Incineration may also be implemented without energy and materials recovery.

In Akure, after collection and sorting of waste, giant incinerators (enclosed spaces or incinerators) which causes less pollution due to the closed system it utilizes are used for burning solid waste. The amount of solid waste generated in Akure has increased steadily over time, from an estimated quantity of 60, 000 metric tons per year in 1996 to 75,000 metric tons in 2006 due to the increasing population, industrial and economic development. While the population of Akure was about 283,108 in 1996, it increased to approximately 353, 211 in 2006. In 2004 government conducted a feasibility study of waste management in Ondo State. The study revealed that most of the waste arises from households, abattoirs, poultries, piggeries, markets and small scale industries with a total generation of 280 tons per day. However the total assessment revealed that about 80% of the total waste is organic in nature, followed by plastic/nylon, 15.72% and about 1% metal **[9]**. Recently there has been a considerable increase in plastic and paper in the recycled portion. The reason is due to the high demand for sachet water due to lack of potable water in Akure and the increase in use of packaging materials such as Polyethylene terephthalate (PET) bottles and bags. Therefore, since the types and quantity of materials consume ability by human changes from time to time the constituents of waste will also change from time to time. Hence there is need for periodic characterization of waste constituent which can facilitate periodic review of waste management strategy as well as development of strategies for turning the waste to wealth (e.g. Generation of energy from solid waste).

3.0 Materials and methods

Solid wastes were collected from both dumpsites and dustbins in the high income areas (Ala quarters, Futa staff quarters, Ijapo estate, and Alagbaka quarters) and the low income areas (St Leo Street, Araromi Street, Solagbade Street and Rescue area at futa south gate) of Akure. The collection was done in each of the selected locations for one month. The site-specific approach for estimating waste stream composition which involves sampling, sorting, and weighing the individual components of the waste stream was adopted for the study as it is useful and efficient in defining local waste stream compositions. For each of the locations, the total waste collected was first measured using a digital weighing balance and recorded separately. The waste bag was then emptied onto the sorting table and the waste was sorted one after the other by hand (i.e. using manual separation method) into the appropriate material categories. Sorting of material into various categories was done based on the report of the U.S. Environmental Protection Agency, 2006, so that the waste was sorted into material component categories like plastic, metal, paper, textile, wood, nylon, food waste, glass and rubber. The sorted constituents were then measured using the digital weighing balance. The homogeneity of the component of the waste that fell into the different categories of its constituents was properly monitored during and checked after separation prior to their measurement. The measured weights of the waste in the various categories were recorded appropriately and the percentage composition by weight of each of the constituents was determined.

4.0 Result and discussion

4.1 Analysis of Results for High Socioeconomic Area.

The percentage composition of solid waste in high socioeconomic area of Akure is as presented in Figure 1. The percentage composition ranges from 7.42% nylon to 18.98% food waste. The major components of solid waste from this area were food waste (18.98%), glass (15.32%), papers (14.00%), and plastic (13.99%). Ala quarters produced the highest value of plastics and textile. This was due to high consumption of bottled water and other plastic drinks and plenty of small children clothing's in the area. Futa staff quarters have the highest composition value of glass and wood. This was due to the consumption of wine, soft and alcoholic bottled drinks and nearness of the location to variety of

planted trees. Nylon, food waste and metal are generated in high quantity at Alagbaka. Since this area is government residential area, most of the people living there are senior officers which consumed packaged materials, making them to produce a lot of spoilt cooked and uncooked food. Ijapo generated the highest quantity of paper which is due to usage and consumption of different variety of carton drinks.

4.2 Analysis of Results for Low Socioeconomic Area

The percentage composition of solid waste in Low Socioeconomic Area of Akure is as shown in Figure 1. The percentage composition ranges from 1.86% rubbers to 22.08% glass. The major components of solid waste from this area were glass (22.08%), plastic (14.22%), plastic (13.37), papers (14.00%), nylon (12.46%) and food waste (12.18%).

Solagbade Street has highest composition value of textile, rubber, wood and paper. This location has small commercial activities taking place as the area has people like tailors, vulcanizers and carpenters doing their day to day businesses. The papers generated here are mainly from institutional papers and the carton drinks taken by some of the people. St Leo Street has the highest quantity of plastic and glass. This can be attributed to the hotels and guest house at this particular area. Araromi Street produced the largest composition of metal and food waste. Food waste obtained here is from the unfinished cooked food and spoilt raw food while the metals consist of few canned drinks and food with various spoilt metallic components like stainless plates and cups. Rescue area only produced the largest share of nylon which can be due to the high consumption of sachet water, biscuits and other nylon packaged items. It is an area populated by university students. The low socioeconomic area has three different locations (Rescue area, Solagbade Street and St Leo Street) with the highest quantity of glasses. It can thereby be said that glass is predominant in this socioeconomic area of Akure.

4.3 Comparative Analysis of Solid Waste composition between High and Low Socioeconomic Areas

Figure 1 show that High Socioeconomic Area has the highest value of plastic, textile, and metal compared to the Low Socioeconomic Area which has highest value of glass, paper, nylon and rubber. This is in agreement with pat study **[6]** and it shows that higher income and economic growth have an impact on the composition of wastes. Wealthier individuals consume more packaged products, which result in a higher percentage of organic materials in the waste stream. In this Area (Ala Quarters, Futa staff Quarters, Ijapo Estates and Alagbaka Quarters), most residents depend on processed food with assorted drink while those from Low Socioeconomic Area (Rescue area, Solagbade Street, Araromi and St Leo Street) rely more on unprocessed food cooked at home, thus generating a less amount of inorganic waste due to their economic status.

Though it has been reported that the packaging fractions of solid waste which consists of paper, nylon, plastic, metal and glass have a direct relationship with household income **[10]**, but in this study, High Socioeconomic Area have higher percentage of plastic and metal while Low Socioeconomic Area has the higher percentage of glass, paper, and nylon. The low value of glass, papers and nylon in High Socioeconomic Area, when compared with Low Socioeconomic Area may be due partly to the accessibility of scavengers to waste bins that are usually placed outside the gates of buildings.

The percentage composition of recyclable material is 71.39% in High Income Area and 81.71% in Low Income Area. The high percentage of recyclable materials in Low Income Area was due to high values of glass, paper, nylon and rubber. The percentage of waste that can be used to generate energy varies in both areas. There is 37.82% of energy waste in High Income Area and 26.24% in Low Income Area.

5.0 Conclusion and recommendation

Effective waste management has to do with the proper understanding of the waste components being generated in order to design appropriate collection and disposal techniques. Most of the waste collected and sampled in both high and low socioeconomic area of Akure can be recycled rather being disposed into landfill or incinerator. A heap of papers meant to be incinerated can be processed and recycled into toilet tissues. Also old and broken glasses and bottle can be used in the production of new glassware. Metals too can be processed into scrap metals which could be turned steel after going through metallurgical processes. Likewise nylons can be recycled, so as to prevent indiscriminate disposal of sachet water. With the characterization of solid wastes, waste managers would be able to effectively manage the disposal, collection, treatment and recycling of solid wastes.

References

1. **Oresanya O. (1998).** Waste Control Measures and Responsibility of a Waste Manager within the Framework of Recent Management Methods and Development in Municipal and Industrial Wastes. *Workshop on Effective Waste Management in Nigeria The Nigerian Society of Engineers, Lagos.*
2. **Wei JB, Herbell JD, Zhang S (1997).** Solid Waste Disposal in China –Situation, Problems and Suggestions. *Waste Management & Research, p. 15, pp. 573-583*

1. **Brunner PH, Ernst WR (1986).** Alternative Methods for the Analysis of Municipal Solid Waste. Waste Mana gement and Research 4: 147 160.

Martin J.H., Collins J.H., Diener RGA (1995). Sampling Protocol for Composting, Recycling and Re -use of Municipal Solid Waste. J. Air Waste Manage. Assoc. 45:

1. **United States Environmental Protection Agency, USEPA, (2008).** Municipal Solid Waste in the United States: 2007 Facts and Figures, Office of Solid Waste (5306P) EPA530-R-08-010 *http://www.epa.gov/epaoswer/non-hw/muncpl/pubs/report-00.pdf. pp 4-5, 24-25.*
2. **Cointreau-Levin S (1997).** Occupational and Environmental Health Issues of Solid Waste Management: Special Emphasis on Middle and Lower – Income Countries (Draft). *World Bank Report. Pp. 25.* http://www.ilsr.org/recycling/other/dctransfer/ochealth.pdf.
3. **Olanrewaju O. O. and Ilemobade A. A. *(2009).* Waste to Wealth: A Case Study of the Ondo State Integrated Wastes Recycling and Treatment Project, Nigeria.** *European Journal of Social Sciences, Vol. 8, No. 1. Pp. 7-16.*
4. Eriksen, G., Coale, F., Bollero, G., (1999). *Soil nitrogen dynamics and maize production in municipal solid waste amended soil. Agron. J.* 91, 1009–1016.
5. **Sridhar, M. K. C., Adeoye, G. O., Olaseha, G. O., Tairu, T. T., Tijani, S. P., and Akinyosoye, V.O. (2004):** *An Assessment of Wastes Generated in Akure City, Ondo State*: A rapid appraisal Survey (phase I). *Waste Recycling and Environmental Management Research and Development Group (WREM), University of Ibadan, Ibadan.*
6. **Bolaane B., Ali M. (2004).** Sampling Household Solid waste at Source: Lessons Learnt in Gaborone. *Journal of Waste Management and Research. 22(3): 142-148.*

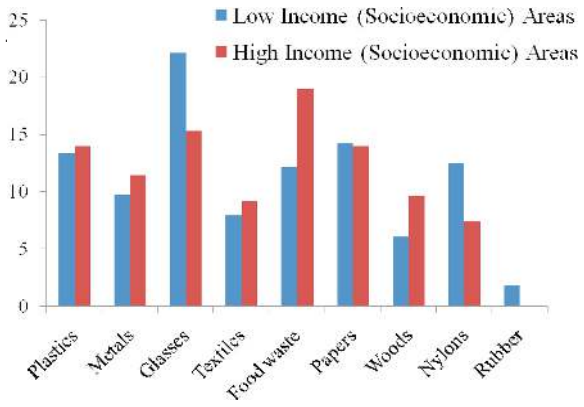


Figure 1: Percentage composition of solid waste in both High and Low Socioeconomic Area of Akure.

FATE OF NANOPARTICLES IN THE ENVIRONMENT

Akpotu, S.O. and Oketola, A.A.
Analytical/Environmental Chemistry Unit, Department of Chemistry, University of Ibadan, Ibadan, Nigeria.
Corresponding author: soulmanlegendry@yahoo.com

ABSTRACT
With increasing technological advancement, the need for more specific products arises, hence the manipulation of materials at the nanoscale level. The benefits of such manipulation are immense. However, at this level (1-100 nm), particles behave differently from the macroscale level. Some materials at macroscale levels are inactive but as they tend towards the nanoscale levels, they become very active e.g., silver, gold etc, as a result of size, form and shape which may present serious environmental and human health concerns. An assessment of the effect on nanoparticles with respect to human health and the environment requires a holistic assessment that takes into consideration the types of nanomaterials, concentrations in the environment, fate and effects. This is of prime importance because there are no known regulatory limits for nanoparticles in the environment. This paper discuss the fate of nanoparticles in the environment such as metals and metal oxides, carbon products (e.g., n-C_{60} fullerenes and carbon nanotubes), quantum dots and semiconductors, nanoclays, dendrimers, and nanoemulsions. Understanding the fate and behaviour of nanoparticles in the environment will assist in policy formulation and assessment of the toxicity of these materials.

1.0 INTRODUCTION

Nanotechnology involves the engineering and manipulation of particles at levels between 1-100 nm, which transform the properties of the materials to be different from the properties at the macroscale levels. This results in marked changes in chemical, physical, magnetic and electrical properties of the particles and has led to large scale manufacturing of these materials worldwide with varied usage. [1] disclosed that titanium dioxide nanoparticles possess photocatalyst activity and are used as antibacterial coatings and in sunscreens. Due to their antibacterial properties, silver nanoparticles are used as medical tools, but they are also of interest in photography, jewelry, electricity and as batteries. The list of actual applications and uses of nanoparticles or nanomaterials are already substantial, and will certainly become exponential in the future. The production, use, and disposal of nanoparticles will inevitably lead to their appearance in air, water, soils and organisms including man [2].

The environmental and health consequences of these materials, their production, and the life-cycle implications of the products merit attention, during the early stages of their development. Recent research has focused largely on the possible toxicity of these materials. Several physico-chemical parameters have been proposed to be critical determinants in nanoparticle toxicity which include size and crystalline structure [3]e.t.c. However, no single parameter has yet been identified as being the one responsible for nanoparticle toxicity. Moreover, another important factor to take into account is the nature of the cell type studied. Indeed, each cell type has its own function and therefore may not respond the same way as another cell type after exposure to one single nanoparticle [3]. The unique physicochemical properties of engineered nanoparticles (NPs) are attributable to their small size, large surface area, chemical composition, surface reactivity, charge, shape, and media interactions ([4]; [5]; [6]; [7]; [8]). Although, impressive from the perspective of material science, the novel properties of NPs could lead to adverse biological effects, with the potential to create toxicity. Indeed, some studies have shown that NPs could exert toxic effects and pose hazards to humans and the environment ([4]; [5]; [6]; [7]; [8]). Nanotoxicology is an emerging science that demands an understanding of the physicochemical properties of nanomaterials that may lead to adverse biological outcomes .Nanoparticles are already present in the environment in large quantities, derived from both natural sources (volcanic dusts or natural bushfire products in air, colloids in aquatic systems and soils), and as a consequence of anthropogenic activities (e.g. smoking, motor vehicle exhausts, industrial stack emissions etc) [9]. Nanoparticles in the size range of 3–7 nm have been shown to account for more than 36–44 % of the total number of particles in some urban air samples with the total size of particles ranging from <10 to 10,000 nm [10].

2.0 ENVIRONMENTAL SOURCES OF NANOPARTICLES

There are various routes by which these NPs enter the environment with atmospheric and aqueous discharge being the most prominent. Releases may come from point sources, such as factories or landfills, and from nonpoint sources, such as wet deposition, storm-water runoff, and attrition from products containing nanomaterials. Long-range atmospheric transport as well as transport in saturated and unsaturated regions in the subsurface is possible. Human exposure is most likely during manufacturing, but inhalation of nanomaterials released to the atmosphere and ingestion in water or food (e.g., fish) that has accumulated nanoparticles may also be possible.

Dermal exposure from sunscreens and cosmetics is also likely [2].

3.0 Classification of nanoparticles or nanomaterials
Naturally occurring nanoparticles can be classified into the following categories, synthetic and manufactured nanoparticles

3.1**. Manufactured or synthetic nanoparticles**
Manufactured nanoparticles can be defined as those that are deliberately produced rather than materials that are by-products of other activities not targeted at its production [9]. The properties of manufactured nanoparticles will vary greatly once released into the environment as interactions occur with other chemicals. Such processes can dramatically affect subsequent biological interactions [9]. Manufactured nanoparticles display physicochemical characteristics that impart upon them unique electrical, thermal, mechanical, and imaging properties that are highly desirable for applications within the commercial, medical and environmental sectors ([11]; [12]; [13]).

3.2 NATURAL NANOPARTICLES
These are nanomaterials that are presently naturally occurring in soil, air and water. These particles have long been documented to cause pollution in the environment. These include natural clay, colloids and macromolecules in natural water which have a size of 1-1000 nm, depending on their degree of aggregation ([14]; [15]).

4.0 TOXICITY OF NANOPARTICLES
In the field of toxicology and/or eco - toxicology research, the effects of particles are deemed correlated to the mass of product to which animals or humans are exposed. The greater the absorbed mass, the greater is the effect ([16]; [9]). In the case of nanoparticles, it has been clearly demonstrated ([17]; [18]; [6]) that the mass of the product is not the most relevant parameter to correlate with measured effects, thus, upsetting the traditional interpretation of the measured toxicity. When dealing with nanoparticles, the concentration or mass metric may not apply, and alternative considerations may involve particle number, surface area (shape), particle composition, or surface reactivity [9].
Studies on toxicity of nanoparticles in humans may be due to several parameters such as specific surface area [24], number of particle size [20], size distribution, concentration, surface state [10], contamination, electric charge, degree of particle agglomeration and site of deposition in the lungs the surface electrical charge, shape, porosity, crystalline structure, the potential of electrostatic attraction, method for particle synthesis, hydrophilic/hydrophobic character and post-synthesis modifications (the surface coating to prevent agglomeration). Particle morphology may also be an important parameter [21].

4.1 **TOXICITY OF NATURAL NANOPARTICLES**
The harmfulness of air pollution was suspected in the reign of Charles II but its real cost in lives lost became clear in the 1930s and 1940s with two episodes, one in the Meuse valley in Belgium and the other in Donora in Pennsylvania. Coal smoke and a winter temperature inversion were a lethal combination [22]. These episodes were followed by the infamous London smog of December 1952 in which some 4000 excess deaths occurred over a week. These deaths mostly appeared to be from lung disease, chronic bronchitis being then a highly prevalent condition in urban Britain, but it was apparent that a proportion was from heart attacks [23].

4.2 TOXICITY OF MANUFACTURED NANOPARTICLES
The ? brogenicity and carcinogenicity of asbestos is now very well known and much research has led to the conclusion that this human toxicity is related primarily to four factors:
(i) A length greater than about 15 mm, below which the ? bre can be removed by lung macrophages;
(ii) A diameter less than about 3 mm, allowing the ? bre to be inhaled to the gas-exchanging part of the lung;
(iii) Insolubility or resistance to dissolution in the lung milieu;
(iv) A sufficient dose to the target organ.
Nanoparticles have a more pronounced effect on in? ammation, cell damage and cell stimulation than an equal mass of particles of the same material of greater size [4]. This appears to hold true for materials as varied as carbon black, titanium dioxide, various metals and polystyrene [24]. Surface area of nanoparticles is the main driving force of the pro-in? ammatory effects and this is evident in both in-vitro) and in-vivo [24] experiments, particles of various sizes producing in? ammatory effects that are directly related to the surface area dose.
Puri? ed SWCNTs containing relatively low amounts of metal were able to induce pulmonary granulomas suggesting that metal contaminants alone were not causal. He concluded that under their test conditions and on an equal-weight basis, SWCNTs can be more toxic than quartz, a particle with recognized occupational health hazards associated with chronic inhalation exposures. [35] performed a more comprehensive comparative toxicity assessment of SWCNTs in rats by examining the ability of these nanoparticles to induce pulmonary in? ammation as well as alter lung cellular proliferation, and pathology following intratracheal instillation of SWCNTs. Pulmonary granuloma formation was also observed following SWCNT exposure.
In contrast to quartz particles, SWCNT-induced multifocal pulmonary granuloma formation occurred without evidence of ongoing pulmonary in? ammation or cellular proliferation. The ability of SWCNTs to induce granulomatus lesions by a unique mechanism within the lung may be consistent with their physicochemical properties which impart to them enhanced structural properties but may also make them more persistent in biological and ecological systems. The bio-persistence of SWCNTs may be a signi? cant occupational safety issue since chronic exposures to low levels of SWCNTs could be associated with adverse health effects [18]. [25] discovered inflammatory and fibrosing pulmonary response in a study conducted in-vivo with multi-walled

carbon nano-tubes (MWCNT) and they compared the effects of nano-tubes with those of asbestos (chrysotile), and hence demonstrated that, at equal doses, asbestos induces a higher respiratory toxicity.

4.3 Mechanisms of toxicity of nanoparticles

There are various routes through which nanoparticles may enter humans, which might result into different degree of toxicity depending on the size, composition, form and shape of these nanoparticles. The routes of entry could be dermal, ingestion, and inhalation. Whether these persisting nanomaterials react with the body, stay inert, or interact with the system will govern their toxic properties and is primarily dependent on their surface properties [27].

The suspension of a particle as an individual particle or as an aggregate depends on surface chemistry. A small aggregate or single particle is presumed to be more toxic than an aggregate of NSPs as the relative surface area could change, determining whether the material has a good wetting characteristic, or has a surface characteristic that catalyzes specific chemical property [27]. The toxicity of NPs increases with particle size albeit concentration. This was shown in a studies on ceria nanoparticles by [28] who found out that particle concentration and particle size have been found to significantly influence the stability ratio and hence the doublet formation time. The doublet formation time of large particles was reported to be a few orders of magnitude higher than the nanoparticles even at a very low concentration. It can be noted that the particle size has an effect on the stability constant and this can be altered by small changes on the particle surface, such as charge distribution. Changes in particle size, such as small changes on the particle surface as regard charge distribution of the particle can have an effect on the stability constant as this is governed by particle size. The surface potential (? V) of a monolayer spread at the air/water interface can be interpreted using the Helmholtz Equation

$$\Delta V = \mu n / \varepsilon_{o} A \quad (1)$$

Where, μn is the effective molecular dipole moment at the interface, ε is the vacuum dielectric permittivity, and A is the surface area per molecule [27].

5. FATE OF NANOMATERIALS IN THE ENVIRONMENT

Though nanomaterials may have key pathways that determine their fate in different environmental media (aquatic systems, terrestrial systems etc), they all have similar pathways that govern their fate in the environment. The higher mobility of nanoparticles in the environment implies a greater potential for exposure as they are dispersed over greater distances and their effective persistence in the environment increases [2]. In environmental media, there are key pathways that govern the fate of nanoparticles these are; aggregation, sedimentation, dissolution, adsorption to particulates and solid surfaces, stabilization via surfactants, biological degradation (aerobic and anaerobic), abiotic degradation (including hydrolysis and pyrolysis) and oxidation and reduction [9].

Table 2 shows the physicochemical characterization and environmental fate of nanoparticles.

Physico–Chemical Properties and Material Characterisation	**Environmental Fate**
•Agglomeration/aggregation • Water solubility • Crystalline phase • Dustiness • Crystallite size •Representative transmission electron microscopy picture(s) • Particle size distribution • Specific surface area • Zeta potential (surface charge) • Surface chemistry (where appropriate) • Photocatalytic activity • Pour density • Porosity • Octanol -water partition coefficient, • Redox potential • Radical formation potential • Other relevant information	•Dispersion stability in water •Biotic degradability •Ready biodegradability • Simulation testing on ultimate degradation in surface water • Soil simulation testing • Sediment simulation testing • Sewage treatment simulation testing • Identification of degradation product(s) • Further testing of degradation product(s) as required • Abiotic degradability and fate • Hydrolysis, for surface modified nanomaterials • Adsorption - desorption • Adsorption to soil or sediment • Bioa ccumulation potential • Other relevant

Exposure Assessment

6.1 What to measure

\The quantification of nanoparticles in the environment is meant to show the level of bioaccumulation, fate and their toxicity as related to living organisms. It will be important therefore to note, that measurements reflect the concentrations and physical and chemical properties of the nanoparticles in the field that are truly representative of exposure. In assessing industrial chemicals, the DEW manual [30] lists fate, partitioning behaviour, and persistence as important parameters. These need to be combined with concentration data in estimating likely exposure. The requirement and the current status of methods for nanoparticle analysis and characterisation have been well summarised in recent reviews by [31] and [32].

6.2 Modelling Exposure

[33] Used a series of simple algorithms to predict the likely concentrations that might be found in soils and waters. For waters, they considered five routes of entry which are the direct entry of manufactured nanoparticles into water bodies from bioremediation, inputs from spray drift following use of agrochemicals, runoff from contaminated soils, aerial deposition and emissions from wastewater treatment plants. For soils, routes comprised: the application of remediation technologies, the application of plant protection products, the excretion of nanomedicines used in veterinary products, aerial deposition and the application of sewage sludge as fertiliser.

7. Developing appropriate guidelines for nanomaterials

The available toxicity data are insufficient to develop reliable guidelines for most nanomaterials in soils. Effects have been inconsistent and studies of high quality grade have not demonstrated an up to date significant adverse effects when soil was the medium used for testing. It is therefore premature to suggest any regulatory limit for any nanomaterial in soils [9].

7.1 Exposure limit values

There are no exposure limit values for the general population, irrespective of the medium considered (air, water, food, etc.).

The guide of good practices of the British Institute of Standardization (BSI) proposes four types of nanoparticles and limit values for exposure, based on the currently established limits for the larger particles.

i) Fibrous materials: The BSI guide suggests as limit value exposure for occupational fibers, the value of 0.01 fibre/ml, counts being carried out in scanning or transmission electron microscopy.

ii) Nanomaterials based on carcinogenic, mutagenic or toxic substances for the reproduction.

iii) **Insoluble nanomaterials:** The BSI guide endorsed the NIOSH work and proposals for mg/m^3 for fine particles but 0.1 mg/m^3 for ultrafine ones.

iv) Soluble nanoparticles: for materials highly soluble regardless of their form, it is unlikely that nanoparticles present a superior bioavailability to those of larger particles.

7.2 International progress on nanoparticle risk assessment

The nanotechnology industry is still in infancy but there is a need for regulation of the nanoproducts on a global scale in a manner that is sustainable. Nations like the USA, UK, Japan are already classifying some nanomaterials as toxic and regulating the use of others. But a conscious effort involving all stakeholders, government agencies, Environmental Protection Agency and countries should ensure a responsible production and use of nanomaterials.

8. Conclusion

Though not so much work has been done on the toxicity of nanoparticles, but the few that has been done is suggestive of an inherent toxicity of nanoparticles at cellular level and for the whole body. Assessing the risk associated with nanoparticles should not be about toxicity in the body alone but their life cycle throughout the environment. Hence, a responsible production and use of these particles is advocated. Necessary guidelines and approvals should be instituted. Toxicity testing method has to be improved, consequently setting threshold levels for all nanoparticles in all environmental media.

REFERENCES

1. Borm, P, Klaessig, F.C, Landry, T.D, Moudgil, B, Pauluhn, J, Thomas, K, Trottier, R, and Wood, S. 2006. Research strategies for safety evaluation of nanomaterials, Part V: role of dissolution in biological fate and effects of nanoscale particles. *Toxicol. Sci.* 90: 23–32.

2 Wiesner R.J, Zsurka, G., Kunz, W.S. 2006. Mitochondrial DNA damage and the aging process: facts and imaginations. *Free Radic Res* 40:1284–1294.

3. Lanone S, Boczkowski, J. 2006. Biomedical applications and potential health risks of nanomaterials: molecular mechanisms. *Curr Mol Med* 6:651-663.

4. Donaldson, K., Stone, V., Gilmour, P. S., Brown, D. M. & MacNee, W. 2000 Ultra?ne particles: mechanisms of lung injury. Phil. Trans. *R. Soc. Lond*. A358: 2741–2749. (doi:10.1098/rsta.2000.0681).

5. The Royal Society and Royal Academy of Engineerings, Nanoscience and nanotechnologies: Opportunities and uncertainties. 2004.

6. Oberdörster, G., Oberdörster, E., Oberdörster, J. 2005. Airborne nanostructured particles and occupational health. *Environ Health Perspect*. 113(7): 823-839.

7. Nel, A., Xia, T., Madler, L., Li, N. 2006. Toxic potential of materials at the nanolevel. *Science* 311: 622-627.

8 Xia, T., Kovochich, M., Brant, J., Hotze, M., Sempf, J., Oberley, T., Sioutas, C., Yeh, J., Wiesner, M. and Nel., A. 2006. Comparison of the Abilities of Ambient and Manufactured Nanoparticles To Induce Cellular Toxicity According to an Oxidative Stress Paradigm *Nano Letters* 6(8): 1794-1807.

9. Batley, G.E. and McLaughlin, M.J. 2010. Fate of Manufactured Nanomaterials in Australian Environment. CSIRO Niche Manufacturing Flagship Report.

10. Shi, J.P., Evans, D.E., Khan, A.A., and Harrison, R.M. (2001). Sources and concentration of nanoparticles (<10 nm diameter) in the urban atmosphere. *Atmos. Environ.* 35: 1193-1202.

11. National Research Council (2002). Small Wonders, Endless Frontiers: A Review of the National Nanotechnology Initiative. pp. 12. Washington, DC, National Academy Press. www.nano.gov.

12. US Environmental Protection Agency. (2003). Proceedings: EPA Nanotechnology and the Environmental: Applications and Implications STAR Progress Review Workshop. EPA Document Number: EPA/600/ 02/080.

13. Masciangioli, T. and Zhang W-X. (2003). Environmental Technologies and the Nanoscale. *American Chemical Society. Envrionmental Science & Technology*. 102A – 108A.

14. Buffle, J., and Leppard, G.G. (1995). Characterisation of aquatic colloids and macromolecules. 1. Structure and behaviour of colloidal material. *Environ. Sci. Technol*., 29: 15. Benoit Hervé – Bazin . 2007. "Les Nanoparticules. Un enjeu majeur pour la santé au travail ?" sous la direction de (INRS), EDP Sciences.

16. Lead, J.R. and Wilkinson, K.J. (2007). Environmental colloids and particles: Current knowledge and future developments. In: *Environmental Colloids and Particles: Behaviour, Separation and Characterisation*, Wilkinson, K.J., and Lead, J.R. (eds), John Wiley and Sons, Chichester, UK., pp 1-16

17. Gaffet, E. 2011. Nanomaterials : a review of the definitions, applications, health effects. How to implement secure development. Nanomaterials Research Group – UMR CNRS 5060.

18. Maynard, D.A, Kuempel , E.D. (2005). Airborne nanostructured particles and occupational health. *Journal of Nanoparticle Research* 7: 587–614.

19. Wittmaack, K. 2007. In search of the most relevant parameter for quantifying lung inflammatory response to nanoparticle exposure: particle number, surface area, or what. *Environ Health Perspect*. 115(2):187-194.

20. Buzea, C., Pacheco, I.I., and Robbie, K. (2007). Nanomaterials and nanoparticles: sources and toxicity. *Biointerphases*, 2, 17-71.

21. McDonald, J. C., Drinker, P. & Gordon, J. E. 1951 The epidemiology and social signi? cance of atmospheric smoke pollution. *Am. J. Med. Sci*.221: 325–342.

22. Seaton, A, Lang Tran, Robert Aitken and Kenneth Donaldson. 2009. Nanoparticles, human health hazard and regulation. *J.R.Soc. Interface* 1-13.

23. Duf? n, R., Tran, C. L., Clouter, A., Brown, D., MacNee, W.,Stone, V.& Donaldson, K. 2002. The importance of surface area and speci? c reactivity in the acute pulmonary in? ammatory response to particles. *Ann. Occup. Hyg*. 46(1): 242–245.

24. Mueller, N.C., and Nowack, B. (2008). Exposure modeling of engineered nanoparticles in the environment. *Environ. Sci. Technol.* 42: 4447-4453.

25. AFSSET – 2006. Nanomaterials: Effects on Human Health and the Environment.

26. Karakoti, A.S, Hench, L.L. and Seal, S. 2006. The Potential Toxicity of Nanomaterials—The Role of Surfaces.

27. Limbach, L.K., **Yuchun, Li., Robert, N., Grass,[†]Tobias J., Brunner, M., Hintermann, M, M., Detlef, G. and Wendelin, J. S.** (2005) "Oxide Nanoparticle Uptake in Human Lung Fibroblasts: Effects of Particle Size, Agglomeration, and Diffusion at Low Concentrations," *Environmental Science & Technology* 39(23): 9370–9376.

28. Brant, J. A.; Lecoanet, H.; Wiesner, M. R. 2005. Aggregation and Deposition Characteristics of Fullerene Nanoparticles in Aqueous Systems. *J. Nanopart. Res*. 7, 545–553.

29. DEW (2007). Environmental risk assessment guidance manual for industrial chemicals. Environment Protection Branch, Department of the Environment and Water Resources Report, Canberra, ACT, Australia.

30. Hassellov, M., Readman, J.W., Ranville, J.F., and Tiede, K. (2008). Nanoparticle analysis and characterisation methodologies in environmental risk assessment of engineered nanoparticles. *Ecotox.*, 17, 344-361.

31. Tiede, K., Boxall, A.B.A, Tear, S.P, Lewis, J, David, H. and Hassellov, M. (2008). Detection and characterization of engineered nanoparticles in food and the environment. *Food Addit. Contam.* **25:** 795-821.

32. http://www.bsi-global.com/upload/Standards%20&%20Publications/Nanotechnologies/PD6699-1.pdf

GOLD NANOPARTICLES: A REVIEW

[1,2]Ogundare, O., [2]Adeoye, M.O., [2, 3]Adetunji, A.R., and *Adewoye, O.O.
[1]Engineering Materials Development Institute, Akure.
[2]Department of Materials Science and Engineering, Obafemi Awolowo University, Ile Ife.
[3]Prototype Engineering Development Institute, Ilesa.
*National Agency for Science and Engineering Infrastructure, Abuja
suppiedee@yahoo.com

Abstract
Gold is found in alluvial placers and primary veins from several parts of supracrustal (schist) belts in the northwest and southwest of Nigeria. Nanotechnology is a multidisciplinary field that covers a vast and diverse array of devices derived from engineering, physics, chemistry, and biology. Gold nanoparticles (AuNPs) have gained increasing interest due to their special features such as unusual optical and electronic properties, high stability and biological compatibility, controllable morphology and size dispersion, and easy surface functionalization. In this review, the preparation, properties and applications of gold nanoparticles are presented. We hope this review will fire-up national interest in gold exploitation for national development.
Keywords: Gold, Nanotechnology, gold nanoparticles, Nigeria

Introduction
Gold is an ancient metal of wealth, commerce and beauty, but it also has a number of unique properties that make it invaluable to industry. These properties include:

Resistance to corrosion
Electrical conductivity
Ductility and malleability
Infrared (heat) reflectivity
Thermal conductivity

Gold's superior electrical conductivity, malleability and resistance to corrosion have made it vital in components used in a wide range of electronic products and equipment, including computers, telephones, cellular phones, and home appliances.
Gold has extraordinarily high reflective powers that are relied upon in the shielding that protects spacecrafts and satellites from solar radiation and in industrial and medical lasers that use gold-coated reflectors to focus light energy. And because gold is biologically inactive, it has become a vital tool for medical research and is even used in the direct treatment of arthritis and other intractable diseases. The demand for gold in industry is steady and growing. [43]

History of Gold Production in Nigeria
Gold in Nigeria is found in alluvial and eluvial placers and primary veins from several parts of supracrustal (schist) belts in the northwest and southwest of Nigeria. The most important occurrences are found in the Maru, Anka, Malele, Tsohon Birnin GwariKwaga, Gurmana, Bin Yauri, Okolom, Dogondaji and Iperindo areas, all associated with the schist belts of northwest and southwest Nigeria.
In the absence of any systematic exploration and development, the Nigerian goldfields have experienced intense artisanal workings which target both the primary gold-quartz reefs and their associated alluvial occurrences.
Officially recorded gold production in Nigeria started by 1913 and peaked in the period 1933-1943 when about 1.4 tonnes of gold were produced. The gold production declined during the Second World War period and never recovered as mines were abandoned by mostly colonial companies.
The Nigerian Mining Corporation started exploration for gold in Nigeria in the early 1980s but failed to be sustained due to lack of funds. The discovery of petroleum and its subsequent domination of the Nigerian economy also contributed to the lack of attention to gold exploration despite the widespread potentials [1]
The Iperindo (Ilesa) primary gold project of the Nigerian Mining Corporation shows the Segilola gold deposit as the most advanced gold exploration project in Nigeria. The deposit potential is estimated at 2 million ounces of gold. Gold occurs as free gold, microscopic inclusions in sulphides as Tellurides. Production at the mine was about 124 grams/ month in 1992, the last known period of production. However, production by artisanal miners, reported by government in 1993, was 1,381 grams from alluvial deposits [2]. Ilesa gold mine has been known to house a large deposit of gold ore. According to [5]**, Ilesa gold mine covered an estimated** 2,276.8 hectares making it the largest deposit in Nigeria.

Extraction Methods
Gold ore extraction may be conducted using either surface or underground techniques. Mining methods are selected based on maximum ore recovery, efficiency, economy, and the character of the ore body (including dip, size, shape, and strength) [3].
Generally, gold mining is conducted using surface mining techniques in open-pit mines. This is primarily because of economic factors related to mining large-volume, low-grade ores and the improvement of

cyanide leaching techniques.
The major categories of commercially viable recovery processes include the following:
1. Gravity separation
2. Flotation
3. Cyanidation
4. Refractory ore processing
5. Alternative lixiviants
6. Amalgamation
Today, cyanide leaching is the method of choice for the recovery of most of the world's gold production. There are however, many other chemical leaching processes that have been sporadically or historically used. In most instances, cyanide leaching will provide a more technologically effective and cost efficient method. Alternative lixiviants include:
1. Bromides (Acid and Alkaline)
2. Chlorides
3. Thiourrea
4. Thiosulfate
Amalgamation is one of the oldest processes available. It relies upon the contact of ore with mercury to form a gold-mercury amalgam. This process is strongly out of favor with the major mining companies, due to the extremely toxic nature of mercury and the processes inferior performance when compared to the available alternatives. The process is still used extensively by artesian mines in third world countries and at small “mom and pop” mines, due to its simplicity [41].

Nanotechnology

There is virtually no area of modern science and technology that has not been touched and revolutionized by nanotechnology [4]. Perceived by many as the next “transformative technology,” like electricity or the Internet, nanotechnology encompasses a broad range of tools, techniques, and applications that manipulate or incorporate materials at the nanoscale (a nanometer is one billionth of a meter) in order to yield novel properties that do not exist at larger scales. These novel properties may enable new or improved solutions to problems that have been challenging to solve with conventional technology. These solutions may include more efficient, effective, and inexpensive water purification devices, energy sources, medical diagnostic tests and drug delivery systems, durable building materials, and other products. Additionally, nanotechnology may significantly increase production capacities by enabling manufacturing processes that create less pollution and have modest capital, land, labor, energy, and material requirements.

Silver, iron, platinum, gold, and copper all form metallic bonds. Unlike covalent bonding, metallic bonding is non-directional. The strong bond consists of positively charged metal atoms in fixed positions, surrounded by delocalized electrons. These delocalized electrons are often referred to as "a sea of electrons," and can help explain why copper and gold are yellow and orange, while most other metals are silver. The color of metals can be explained by band theory, which assumes that overlapping energy levels form bands.

Gold Nanoparticles

What characteristics make gold an ideal material for such wide-ranging applications? The nobility of gold and its resistance to surface oxidation (which would hinder the operation of nano-scale technologies and devices based on other metals) is one important material characteristic. The optical properties of gold at the nanoscale are also exciting, (gold nanoparticles have a colour varying from red to purple depending on particle size, a property that can be successfully exploited in a range of applications) [42].
Gold nanoparticles have unique properties that make them more attractive than other nanoparticles for many therapeutic, imaging, and sensing applications, and particularly in medical applications. Gold nanoparticles are very good at scattering and absorbing light. This unique behaviour makes gold nanoparticles a potent candidate for cancer cell detection and treatment in a simpler, faster and easier approach. Gold nanoparticles have an un-oxidized state, whereas most of the surface of less noble metal gets oxidized to a depth of several nanometers or more, often significantly reducing or obliterating the nanoscale properties of the nanoparticles. Gold nanoparticles are highly reactive. Nanomaterials are of growing importance not only for industrial applications but also in bioscience and medicine.
The choice fell on gold nanoparticles because gold is inert, gold nanoparticles are relatively easy to synthesize, and gold surfaces readily bind a wide range of bio-molecules such as DNA and proteins, a property which is desired for quantitative analyses. Furthermore, gold nanoparticles have photothermal properties that may be of use for localized heating or drug release, increasing their potential for therapeutic applications.
Additionally, gold nanoparticles are now known to be catalytically active for a range of commercially important reactions and they also have a surface chemistry particularly suited to the attachment of sulphur-containing molecules, such as thiols, which permits the 'bottom -up' assembly of interesting and useful structures.
Based on these unique properties, exciting new nanotechnology applications using gold are being developed. These include:

- Low resistance printable gold nanoparticulate inks for flexible electronics
- Gold nanowires for interconnections in future electronic devices
- Nanoparticulate gold colloid for rapid tests and biomedical assays
- Gold nanoparticles used for targeted delivery of anticancer drugs and destruction of cancer cells
- Improved decorative coatings using thiol stabilised gold nanoparticles
- Gold nanoparticle containing paints and textiles exhibiting novel aesthetic effects
- Nano-particulate gold catalysts for pollution

control and chemical synthesis

- Fuel cell electro-catalysts based on carbon supported nano-particulate gold [42]

Nano-gold preparation methods

1. Physical methods

Laser ablation method is used to produce gold nanoparticles by using the pulsed laser irradiation of gold target in water in the absence of any additives, at (532 nm, 10 ns, 10 Hz), or (266 nm) wavelengths [6]. Inert gas condensation can be used for the preparation of gold nanoparticles [7]. In this method, the gold nanoparticles as soon as they are formed rapidly collide with inert gas in a low-pressure environment and thus smaller and controlled nanoparticles are formed. The advantage of these methods is the narrow particle size distribution of the produced gold nanoparticles, while its limitation is the need for expensive equipment.

2. Chemical methods

Emulsification procedure produces gold nanoparticles but with a wide distribution of particle diameters [7]. Nano-gold particles are prepared by reduction of the gold ions in the presence of a dispersant in order to avoid excessive gold agglomeration.[9] and 10 initially introduced a sodium citrate reduction of $HAuCl_4$ for the synthesis of stable gold nanoparticles. In addition there are other reductants such as sodium boro-hydride [11], stannous chloride [12] and ascorbic acid [13]. Amine-containing molecules for example, branched poly (ethyleneimine) (PEI) [14], third-generation poly (propyleneimine) dendrimer (PPI-G3) in the presence of sunlight [15], azacryptand at room temperature [16], amino acid [17], polysaccharide [18], Gallic acid [20], alcohols, chitosan [19] or other organic compounds are also used as a reductant for the synthesis of nano-gold. There are several reported modified chemical methods including seed-mediated growth where small particles produced by other techniques like irradiation were exploited as seeds and fresh Au(III) ions were reduced onto the surface of the seed particles by reducing agents like ascorbic acid [23]; [22], use of reverse micelles which involves reduction of $HAuCl_4$ in sodium bis (2-ethylhexyl) sulfo-succinate/isooctane reverse micelles system using reducing agents like ascorbic acid [24], phase transfer reactions as a representative reaction in a novel water cyclohexane two-phase system, the aqueous formaldehyde is transferred to cyclohexane phase via reaction with dodecylamine to form reductive intermediates in cyclohexane; the intermediates are capable of reducing gold ions in aqueous solution to form gold nanoparticles in cyclohexane solution at room temperature [25]; [26].

3. Biosynthesis methods

Biosynthesis of nanoparticles as an emerging highlight of the intersection of nanotechnology and biotechnology has received considered attention due to a growing need to develop environmentally benign technologies in material syntheses. Nair and Pradeep reported the growth of nanocrystals and nanoalloys using Lactobacillus [27]. Daizy has reported a successful attempt on the extract of Volvariella volvacea, an edible mushroom, as reducing and protecting agent for the synthesis of gold, silver and Au–Ag alloy nanoparticles. Gold nanoparticles of different sizes (20–150 nm) and shapes, from triangular to nearly spherical and hexagonal nanoprisms, are obtained by this novel method. The size and shape of gold nanoparticles are also found to depend on the temperature of the extract [21].

4. Applications of nanogold

4.1. Catalytic properties

Few years ago, nanogold received wide interests due to the availability of small sized nanoparticles which provide large surface-to-volume ratio compared to the bulk materials and thus became active for catalysis. Recent years have witnessed a tremendous growth in the number of gold-catalyzed highly selective chemical transformations [28]. The catalysis of organic reactions by gold compounds has been shown to be a powerful tool in organic synthesis [29].

4.2 Biomedical applications

4.2.1. Biosensing and diagnostic

4.2.1.1. Immunohistochemistry

Gold nanoparticles are useful in the construction of electrochemical immunosensors where it plays a crucial role both in the enhancement of the electrochemical signal transducing the binding reaction of antigens at antibody immobilized surfaces and in the ability of increasing the amount of immobilized immunoreagents in a stable mode. Hepatitis B virus surface antigen was detected using electrochemical impedance spectroscopy (EIS) through immobilization of the antibody onto gold nanoparticles-modified 4-aminothiophenol self-assembled monolayers [30].

4.2.1.2 Detection of disease biomarker.

Gold nanoparticles have been used in the assembly of electrochemical and amperometric biosensors for the diagnosis of patients with germ cell tumors and hepatocellular carcinoma. This is done by the detection of a tumor marker, alpha-fetoprotein (AFP), an oncofetal glycoprotein [33]. Electrochemical detection of these disease markers was accomplished by the amperometric changes occurring before and after the antigen–antibody interaction [34].

4.2.1.3. DNA-modified nanogold electrochemical biosensors.

Gold nanoparticles-modified electrodes are used in the assembly of electrochemical DNA biosensors. They constitute useful analytical tools for sequence-specific DNA diagnosis and detection due to their inherent advantages of low cost, sensitivity and rapidity of response [35].

4.2.2. Therapeutic application of gold nanoparticles

Gold nanoparticles exploit their unique chemical and physical properties for transporting and unloading the

pharmaceuticals. First, the gold core is essentially inert and is their ease of synthesis; monodisperse nanoparticles can be formed with core sizes ranging from 1 to 150 nm [37]. Second advantage is imparted by their ready functionalization, generally through thiol linkages. In addition, their photophysical properties could trigger drug release at remote place [36].

4.2.2.1. Gold nanoparticles in drug delivery.
Drug Delivery Systems (DDSs) provide positive attributes to a 'free' drug by improving solubility, in vivo stability, and biodistribution. They can also alter unfavorable pharmacokinetics of some free' drugs. Moreover, huge loading of pharmaceuticals on DDSs can render 'drug reservoirs' for controlled and sustained release to maintain the drug.

4.2.2.2. Gold nanoparticles in biomolecules delivery.
In addition to the delivery of small molecules, tunable size and functionality of gold nanoparticles make them a useful scaffold for efficient recognition and delivery of biomolecules such as peptides, proteins, or nucleic acids like DNA or RNA. Efficient and safe nonviral gene delivery systems are a prerequisite for the clinical application of therapeutic genes.
[38] have investigated gene delivery in vivo using gold nanoparticles excited with electrical pulses. The result was that gene expression was detected in the major mouse organs. In contrast, the injection of naked DNA resulted in a 10-fold lower level of detection. The degradation of DNA in blood, which occurs in times as short as 5 min, is evidently the reason for the inefficient transfection in the latter case. This study illustrates yet another interesting approach to improve gene delivery using gold nanoparticles.

4.2.2.3. Gold nanoparticles for protein delivery.
Gold nanoparticles can be novel nanocarriers of peptides and proteins of interest. Cationic tetraalkylammonium-functionalized GNPs recognize the surface of an anionic protein through complementary electrostatic interaction and inhibit its activity [31]. The activity was recovered due to the release of free protein by treating the protein–particle complex with glutathione, showing GNPs as potential protein transporters. Pokharkar and coworkers have demonstrated functionalized gold nanoparticles as the carriers of insulin [39]. Chitosan-coated particles strongly adsorb insulin on their surface, and are effective for transmucosal delivery of insulin.

4.2.2.4. Gold nanoparticles for site-directed photothermal applications.
Gold nanoparticles cause local heating when they are irradiated with light (800–1200 nm). El-Sayed et al. have recently reported about the potential use of GNPs in photothermal destruction of tumors (Huang et al., 2007). Citrate-stabilized GNPs (core d= 30 nm) were coated with anti-EGFR (epidermal growth factor receptor) to target HSC_3 cancer cells (Human oral Squamous Cell carcinoma). The use of GNPs enhanced the efficacy of photothermal therapy by 20 times.

4.2.2.5. Gold nanocarriers applied in vivo.
[40] have developed a nanoparticle-based targeted drug delivery system (DDS), which contains cetuximab (C225) anti-epidermal growth factor receptor (EGFR) antibody as the targeting agent, gemcitabine as the anti-cancer drug, and gold nanoparticles as the delivery vehicle. The administration of this targeted delivery system resulted in the significant inhibition of pancreatic tumor cell proliferation in vitro and orthotropic pancreatic tumor growth in vivo. In the near future, this strategy could be used as a generalized approach for the treatment of a variety of cancers including pancreatic cancer.

Conclusion
Gold on the nanoscale is a truly unique material. It is easily synthesized, functionalized and handled; it has opened up a whole new field of research in recent years which has accelerated at a staggering pace. It is already a trusted component of many diagnostic devices; gold nanoparticles are beginning to show their potential across a broad range of fields.

References

1. Ministry of Mines and Steel Development, (2010). Gold Deposit- Exploration opportunities in Nigeria. 1-14.
2. Ekande, S.A. (2004). Unpublished M.Sc Thesis. An Assessment of the Effects of Gold Exploitation on the Environment around Ilesa. Department of Metallurgical and Materials Engineering, Obafemi Awolowo University Ile Ife.
3. Whiteway, P. (1990). Mining Explained: A Guide to Prospecting and Mining. *The Northern Miner.*
4.Babatope, B. (2011) Special College Lecture. The World of Nanotechnology. Osun State University Osogbo Nigeria. p2
5. Nigerian Mining Corporation (2006). Listing of Mining Properties Available For Bidding Section 1: Nigerian Mining Corporation (NMC) Titles 2.
6. Ko, S.H., Choi, Y., Hwang, D.J., Grigoropoulos, C.P., Chung, J., Poulikakos, D., (2006). Nanosecond Laser Ablation of Gold Nanoparticles Films. Applied Physics Letter. **89**, 141126-1–141126-3.
7. Lee, K.M., Park, S.T., Lee, D.J., (2005). Nanogold synthesis by inert gas condensation for immuno-chemistry probes. Journal of Alloys and Compounds. **390**: 297–300.
8. Pal, A., Shah, S., Devi, S., (2007). Preparation of silver, gold and silver– gold bimetallic nanoparticles in w/o microemulsion containing Triton X-100. Colloids Surf. A: Physicochemical Engineering Aspects 302: 483–487.
9. Frens, G., (1973). Controlled nucleation for the regulation of the particle size in monodisperse gold suspensions. Natural Physical Science **241**: 20–22.
10. Turkevitch, J., Stevenson, P.C., Hillier, J., (1951). Nucleation and growth process in the synthesis of colloidal gold. Discuss. Faraday Society. **11**: 55–75.
11. Wagner, J., Tshikhudo, T.R., Ko¨ hler, J.M., (2008). Microfluidic generation of metal nanoparticles by borohydride reduction. Chemical Engineering Journal. **135**: S104–S109.

12. Vaškelis, A., Tarozait_e, R., Jagminien_e, A., Tamasˇi_unait_e, L.T., Jusˇk_enas, R., Kurtinaitien_e, M., (2007). Gold nanoparticles obtained by Au(III) reduction with Sn(II): preparation and electrocatalytic properties in oxidation of reducing agents. Electrochim. Acta **53**: 407–416.
13. Sun, K., Qiu, J., Liu, J., Miao, Y., (2009). Preparation and characterization of gold nanoparticles using ascorbic acid as reducing agent in reverse micelles. Journal of Materials Science. **44**: 754–758.
14. Note, C., Kosmella, S., Koetz, J., (2006). Poly(ethyleneimine) as reducing and stabilizing agent for the formation of gold nanoparticles in w/o microemulsions. Colloids Surface. A **290:** 150–156.
15. Luo, Y., (2008). Size-controlled preparation of dendrimer-protected gold nanoparticles: a sunlight irradiation-based strategy. Material Letter **62**: 3770–3772.
16. Lee, K.Y., Hwang, J., Lee, Y.W., Kim, J., Han, S.W., (2007). One-step synthesis of gold nanoparticles using azacryptand and their applications in SERS and catalysis. Journal of Colloid Interface Science. **316**: 476–481.
17. Selvakannan, P.R., Mandal, S., Phadtare, S., Gole, A., Pasricha, R., Adyanthaya, S.D., Sastry, M., (2004). Water-dispersible tryptophanprotected gold nanoparticles prepared by the spontaneous reduction of aqueous chloroaurate ions by the amino acid. Journal Colloid Interface Science **269**: 97–102.
18. Huang, H., Yang, X., (2004). Synthesis of polysaccharide-stabilized gold and silver nanoparticles: a green method. Carbohydrate Resource **339**: 2627–2631.
19. Shih, C.-M., Shieh, Y.-T., Twu, Y.-K., (2009). Preparation of gold nanopowders and nanoparticles using chitosan suspensions. Carbohydrate Polymer **78**: 309–315
20. Wang, W., Chena, O., Jiang, C., Yang, D., Liu, X., Xua, S., (2007). One-step synthesis of biocompatible gold nanoparticles using gallic acid in the presence of poly-(N-vinyl-2-pyrrolidone). Colloids Surf. A: Physicochemical Engineering Aspects **301**; 73–79.
21. Philip, D., (2009). Biosynthesis of Au, Ag and Au–Ag nanoparticles using edible mushroom extract. Chimica. Acta Part A **73**, 374–381.
22. Jana, N.R., Gearheart, L., Murphy, C.J., (2001). Evidence for seedmediated nucleation in the formation of gold nanoparticles from gold salts. Chemical Materials **13**: 2313–2322.
23. Brown, K.R., Natan, M.J., (1998). Hydroxylamine seeding of colloidal Au nanoparticles in solution and on surfaces. Langmuir **14**: 726– 728.
24. Chiang, C.L., (2000). Controlled growth of gold nanoparticles in aerosol-OT/sorbitan monooleate/isooctane mixed reverse micelles. Colloid Interface Science **230**: 60–66.
25. Esumi, K., Hosoya, T., Suzuki, A. (2000). Preparation of hydrophobically modified poly(amidoamine) dendrimer-encapsulated gold nanoparticles. Journal of Colloid Interface Science **229:** 303–306.
26. Haifeng, Z., Cheng, T., Suping, Z., Junbai, L. (2005). One step synthesis and phase transition of phospholipid-modified Au particles into toluene. Colloids Surf. A: Physicochemical Engineering Aspects **257–258**: 411–414.
27. Nair, B., Pradeep, T., (2002). Coalescence of nanoclusters and formation of submicron crystallites assisted by lactobacillus strains. Crystal Growth Des. **2**: 293–298.
28. Arcadi, A., Di Giuseppe, S., (2004). Recent applications of gold catalysis in organic synthesis. Current Organic Chemistry. **8**: 795–812.
29. Thompson, D., (1999). New advances in gold catalysis part II. Gold Bulletin. **32:** 12–19.
30. Wang, M., Wang, L., Wang, G., Ji, X., Bai, Y., Li, T., Gong, S., Li, J., (2004). Application of impedance spectroscopy for monitoring colloid Au-enhanced antibody immobilization and antibody–antigen reactions. Biosenor Bioelectronics **19**: 575.
31. Verma, A., Simard, J.M., Worrall, J.W.E., Rotello, V.M., (2004). Tunable reactivation of nanoparticle-inhibited beta-galactosidase by glutathione at intracellular concentrations. Journal of American Chemical Society.**126**: 13987–13991.
32. Huang, X., Qian, W., El-Sayed, I.H., El-Sayed, M.A., (2007). The potential use of the enhanced nonlinear properties of gold nanospheres in photothermal cancer therapy. Laser Surgical Medicine. **39**: 747–753.
33. Ying, Z., Ruo, Y., Yaqin, C., Dianping, T., Ying, Z., Na, W., Xuelian, L., Qiang, Z., (2005). A reagentless amperometric immunosensor based on gold nanoparticles/thionine/nafion-membrane-modified gold electrode for determination of a-1-fetoprotein. Electrochemical Communication. **7**: 355–360.
34. Xiao-Hong, F., (2007). Electrochemical immunoassay for carbohydrate antigen-125 based on polythionine and gold hollow microspheres modified glassy carbon electrodes. Electroanalysis, 1831–1839.
35. Odenthal, K.J., Gooding, J.J., (2007). Electrochemical DNA biosensors. Analyst **132**: 603–610.
36. Skirtach, A.G., Javier, A.M., Kreft, O., Kohler, K., Alberola, A.P., Mohwald, H., Parak, W.J., Sukhorukov, G.B., (2006). Laserinduced release of encapsulated materials inside living cells. Angew. Chemistry International edition. **45**: 4612–4617.
37. Connor, E.E., Mwamuka, J., Gole, A., Murphy, C.J., Wyatt, M.D., (2005). Gold nanoparticles are taken up by human cells but do not cause acute cytotoxicity. Small **1:** 325–327.
38. Kawano, T., Yamagata, M., Takahashi, H., Niidome, Y., Yamada, S., Katayama, Y., Niidome, T., (2006). Stabilizing of plasmid DNA in vivo by PEG-modified cationic gold nanoparticles and the gene expression assisted with electrical pulses. Journal of Controlled Release **111**: 382–389.
39. Bhumkar, D.R., Joshi, H.M., Sastry, M., Pokharkar, V.B., (2007). Chitosan reduced gold nanoparticles as novel carriers for transmucosal delivery of insulin. Pharmaceutical Resource. **24**: 1415–1426.
40. Patra, C.R., Bhattacharya, R., Wang, E., Katarya, A., Lau, J.S., Dutta, S., Muders, M., Wang, S., Buhrow, S.A., Safgren, S.L., Yaszemski, M.J., Reid, J.M., Ames, M.M., Mukgerjee, P., Mukhopadhyay, D.,

(2008). Targeted delivery of gemcitabine to pancreatic adenocarcinoma using cetuximab as a targeting agent. Cancer Resource. **68**: 1970–1978.

41.(http://www.nanotechproject.org/44/consumer-nanotechnology)
AZoNano - The A to Z of Nanotechnology

42. (http://www.azonano.com/article.aspx) accessed Sept. 2011

43. Gold Mining Process Development. http://www.denvermineral.com/gold-mining-process-development/ accessed Sept. 2011

43.http://bullion.nwtmint.com/gold_uses.php. Accessed Sept. 2011

Examples of Products that use Nanotechnology and Nanomaterials.

Health and Fitness	Electronics and Computers	Home and Garden	Food and Beverage	Other
Wound dressing Pregnancy test Toothpaste Golf club Tennis Racket Skis Antibacterial socks Waste and stain resistant pants Cosmetics Air filter Sunscreen	Computer displays Games Computer hardware	Paint Antimicrobial pillows Stain resistant cushions	Non-stick coatings for pans Antimicrobial refrigerator Canola oil	Coatings Lubricants

Source: Woodrow Wilson Center Consumer Products Inventory. (http://www.nanotechproject.org/44/consumer-nanotechnology)

Method	Particle size range	Recovery Efficiency
Sluice Boxes	2500 to 100 µm	
Jigs	2500 to 75 µm	As low as 50% for ?100 µm gold to 98% for ? 1000 µm
Shaking Tables	3000 to 15 µm	As low as 20% for 20 - 40µm gold p to 90% for ? 40 µm
Spirals	3000 to 75 µm	65 - 80%
Rotating cones and Bowl concentrators	6000 to 30 µm	up to 99% As low as 65% for ? 75 µm gold
Amalgamation	1500 to 70 µm	up to 98% for ? 500 µm gold
Cyanidation	finer than 200 µm	At least 80% to 99%

Source: British Geological Survey, February 1997

SYNTHESIS AND CHARACTERIZATION OF CHEMICAL BATH DEPOSITED $BaTiO_3$ MIXED OXIDE THIN FILMS ON SEEDED TiO_2

F. I. Ezema1[a], B. A. Ezekoye1, P. O. Ike[1],A. B. C. Ekwealor[1]
[1]Department of Physics and Astronomy, University of Nigeria, Nsukka, Nigeria.
Emails: ikepatrickokezie@gmail.com, fiezema@yahoo.com

ABSTRACT
Barium titanium oxide ($BaTiO_3$) thin films were successfully deposited by chemical bath deposition technique. The optical effects of the various concentration of the deposited thin films such as absorbance and transmittance were determined using spectrophotometer at normal incidence of light in wavelength range of 300-1100nm. The SEM revealed a particle size range of (297.9-116.9) nm. The band gap energy from the direct transition was also found to be at a range of (2.2-2.7) eV. The X-ray diffraction (XRD) results obtained were all amorphous when annealed at 200°C. The result of the $BaTiO_3$ thin film shows that concentration has significant effect on the energy band gap, particle size and the optical properties of the thin film.
Key words: SGD, $BaTiO_3$, Concentration, Band Gap, TiO_2, Epitaxy, Annealing, Particle size.

Introduction.

Ternary compounds thin films of $BaTiO_3$ are known as perovskite materials. These materials have been extensively investigated because of their importance for high temperature oxygen sensors, in photo-catalysis, as substrates for high superconductors and as dielectric materials [1, 2]. Such multinary thin-film materials have also become a field of study that will continue to infatuate and drive material scientists to master both understanding and synthesis of the materials with the goal of exploiting its properties in devices. At present, these materials with its properties are commercialized because they are widely used in anti-corrosion coatings, fuel cells, bio-medical implants and other fields [3].

Based on glass-ceramics, $BaTiO_3$ have shown great potential in certain electronic applications [4]. The advantages of ferroelectric glass–ceramic materials, such as lower sintering temperature and homogeneous mixing of ferroelectric phases with glass, have been utilized in ferroelectric and piezoelectric applications [5,6]. This is due to decreasing crystalline size and novel physical properties in low dimensional structures [7,8]. The crystal size in the glass ceramic structure obtained by regulated crystallization is quite acceptable for ferro electrical properties since it is above the critical level of 20-60nm [4]. And such regulated crystallization time is possible to obtain glass ceramic samples with relatively low dielectric losses and variable permittivity in the range of 30-650nm, which would allow its application as elements regulating the intensity fields in microwave furnaces [9].

The highest dielectric constants of $BaTiO_3$ are observed when the average grain size is ~0.8μm [10]. Reduction of the $BaTiO_3$ layer thickness from 10μm to 3μm with grains sizes of 0.2μm resulted in temperature-stable dielectric properties that met industrial requirements [11]. The sinterability of thin films can be improved significantly if monodisperse $BaTiO_3$ powders with grain sizes below 100nm are employed [12,13]. $BaTiO_3$ nanoparticles with an average size of 100nm can be made by sol–gel technique involving the hydrolysis of titanium tetra-isopropoxide in an alkaline solution of barium acetate [14]. It has been found that stress can significantly change the mechanical, dielectric and optical properties, influence the nature of phase transitions, and enhance the dielectric constant of $BaTiO_3$ greatly [15].

Researchers have investigated on the growth of $BaTiO_3$ under hydrothermal conditions either as powder [16,17] or as thin films [18-22]. Bandale et al[22] proposed a film growth mechanism in which the first step was the formation of a titanium oxide layer. Ishizawa et al [21] reported about a precursor anatase layer between the titanium metal foil and the electrochemically grown $BaTiO_3$ thin film.

Solution growth deposition (SGD) technique was used in this research work.SGD is a low temperature method in which a substrate (glass or quartz) is immersed in a semi-stable precursor solution [23-25]. SGD is the most common solution method used for deposition of wide range of chalcogenide (e.g. CdS, ZnS, PbS, CdSe) and chalcopyrite materials (e.g. $CuInS_2$, and $CuInSe_2$) [26]. The SGD process uses a controlled chemical reaction to achieve thin-film deposition by precipitation which was applied by S. Chopra et al [27-30]. A soluble salt of the required metal is dissolved in an aqueous solution to release cations. The non-metallic element is provided by a suitable source compound that decomposes in the presence of hydroxide ions, releasing the anions. The anions and the cations then react to form the compounds which precipitate onto the exposed substrate. A complexing agent is often used to form metal complexes that limit rates of hydrolysis, imparting some stability to the bath, which would otherwise undergo rapid hydrolysis and precipitation.

2. Experimental details

2.1. Growth procedure

Epitaxial growth of $BaTiO_3$ film on TiO_2 film

was done by SGD technique. The components used comprise of an oven, beakers, glass slides, and the starting reagents are barium acetate, ammonia solution, sodium hydroxide, titanium chloride solution, polyvinyl pyrolidon (PVP) and polyvinyl alcohol (PVA).

Prior to the growth, the glass slides and beakers used were washed with detergents and rinsed sequentially with acetone, deionized water, methanol, and deionized water again. This was done in order to remove stain, dust particles or oily solutions that might have adhered to the surface of the glass slide. And this is to form a thermally stable surface film. The preparation of PVP was done by weighing 4g of its whitish coloured powdered solid in a conical flask. Followed by adding 450ml of distilled water into it and stirred continuously for 30mins with a magnetic stirrer. PVA was also prepared by pouring 400ml of distilled water into a flask of 0.9g of its powder. The solution was heated at a temperature of 90°C for 1hour before it was allowed to edge to room temperature.

2.2. Synthesis of titanium oxide.

The raw materials are titanium chloride solution and sodium hydroxide both analytically pure grade were purchased and used as received. The sodium hydroxide serves as a good complexing agent in the reaction.5ml of titanium chloride was introduced into a beaker followed by 3ml of 1mole sodium hydroxide solution and 35ml of 1mole solution of PVA. The mixtures were stirred properly for 10min before introducing a plain glass substrate into it. The bath was allowed to stand in an oven at a temperature of 75°C for 3hrs. At the end the samples were removed, rinsed so as to remove loosely deposited particles before it was allowed to dry at room temperature. A basic precipitate was left in the bath and titanium oxide film was seen to be formed on the glass slide.
The deposition of TiO_2 has been proposed as

$$TiOH^{3+} + H_2O \leftrightarrow Ti(OH)_2^{2+} + H^+$$
$$Ti(OH)_2^{2+} \rightarrow e^- + Ti(IV)oxy\ Species \rightarrow TiO_2$$

$Ti(OH)_2^{2+}$ will thenbe oxidized to Ti(IV)oxy species. According to Kavan et al [31], the Ti(IV)oxy species is an intermediate between TiO^{2+} and TiO_2, consisting of partly dehydrated polymeric Ti(IV) hydroxide, which will be finally converted into TiO_2 by dehydration during the process of deposition.

2.3 Synthesis of barium titanium oxide.

10ml of 1mole barium acetate solution was introduced into the beaker, followed by 6ml ammonia solution as a complexing agent and 40ml of 1mole solution of PVP. The mixtures were stirred properly for 10mins befo re introducing a titanium oxide substrate into the bath. The bath was left at a temperature of 80 °C in an oven for 9hrs. The samples were removed from the bath, rinsed and kept to dry at room temperature. Deposits of film were formed on the substrate leavi ng a basic precipitate in the beaker. The chemical reaction between the barium and the titanium ions led to the nucleation of $BaTiO_3$ crystals on the substrate.

Similar procedures were also conducted with 0.75mole and 0.5mole concentration of barium acetate.

2.4 Annealing.

All the experimental procedures were carried out in open air. The samples of $BaTiO_3$ thin films at different concentration of barium acetate as reactants were all annealed at a temperature of 200°C for a period of 1hour before the characterisation was carried out.

3. Results and Discussion.

3.1 Composition Study.

The result obtained from Energy Dispersive Spectroscopy (EDS), elements of Ba, Ti and O were found to be present as shown in the Figure 1.At a low concentration of the deposited t hin film, it was observed that the atomic percentage of Ba increased thereby reducing that of the Ti present. This is as a result of the decomposition of the Ti ions so as to form a stable equilibrium state of the compound during the reaction. Ba in both t ables was observed to be the only elements that appeared to be emitting at a higher energy level.The peaks from the results in Figure 1 represent the intensity of the energy observed from the characterization from which Si have the highest followed by O. T i appeared at different energy levels which are at 0.5KeV and 4.5KeV, and of which 0.5KeV has the highest intensity.

3.2 Surface Topography of Thin Films.

3.2.1 SEM Study.

The surface structures of the $BaTiO_3$ thin film shown in fig 2 were taken using a scanning electron microscope at a magnification of 5000X. From the result it was seen that $BaTiO_3$ thin films are irregularly shaped with difference in grain size. The microstructure of the synthesized $BaTiO_3$ thin film as shown gave a grain size range of 133.6nm to 137.5nm for $BaTiO_3$ at 1mole and also a grain size range of 116.9nm to 297.9nm for $BaTiO_3$ at 0.5mole. This suggests the level of deposition that took place during the growth

of the thin films.

3.2.2 X-Ray diffraction Study.

The synthesized films shown in fig 3 were analysed for phase composition using X-ray diffraction (XRD, CuKa, Panalytic, 40kV-40mA) over the 2θ range from 10° to 120° at a scan rate of 20° per min. The XRD pattern of the thin films on glass substrate had no peak corresponding to $BaTiO_3$ crystals annealed at 200°C, indicating that the $BaTiO_3$ thin film is in its amorphous state.

3.3 Optical Studies.

3.3.1 Variation of the absorbance and transmittance of the thin films with respect to wavelength.

The spectral plot of absorbance and transmittancewith respect to wavelength for $BaTiO_3$ thin film prepared was shown in figure 4a and 4b. From the optical studies obtainedfor $BaTiO_3$ thin films,it reveals that the absorption edge shifted toward the shorter wavelength. In fig 4a the films absorbed strongly in the visible region and were highly transmitting in the near infrared region as shown in figure 4b. The effect of increase in concentration of the precursors brought about a decrease in absorbance. The marked difference from the transmittance is that film of 0.75Mole has 70% transmittance while film of 0.5Moles has 40% transmittance.

The transmittance of the films were determined using a ratio of incident flux I_o to reflected flux I given in equation

$$T = \frac{I}{I_0} 1$$

And transmittance was determined by using the thickness of the film and the absorption co - efficient by the use of the equation stated below,

$$T = e^{-\alpha x} \qquad 2$$

were *a* is the absorption co-efficient and x is the thickness of the thin films.

The variation of increased absorbance with wavelength in the visible region can be explained on the basis of concentration and thickness of the deposited films. Incident photons on the surface of the films at greater surface area per unit volume were absorbed more with less transmittance. The property of high transmittance in the infrared region exhibited by the thin films therefore makes them good materials for the construction of poultry roofs [32]. This also suggests that the film could be employed as a host material for optoelectronics application [32,33]. The strong absorbance of thin films in the visible region also suggests that the films could be used for the fabrication of solar cells [34].

3.3.2 Variation of the extinction co-efficient and refractive index of the thin films with respect to wavelength.

From the variation of the extinction co-efficient and refractive index with respect to wavelength for different concentration of the deposition medium are presented in figure 5. The extinction co-efficient for 0.5Mole thin film decreases from k=90 at 350nm to k= 75 at 400nm followed by a gradual increase to k=90 at 1100nm. While its refractive index was just a slight curve which increased from n=0.1 at 350nm to n=2.3 at 1100nm.The extinction co-efficient when at 0.7Mole droppedfrom k=80 at 350nm to k= 75 at 380nm followed by a slight increase and then a gradual decrease to k= 35 at 1100nm. Its refractive index produced a curve that has the highest refractive index which starts at n=0.35 at 350nm to n=2.4 at 800nm.

The extinction co -efficient was obtained using the equation

$$k = \frac{\alpha\lambda}{4\pi}$$

were *a* is the absorption co-efficient and λ is the wavelength.

The refractive index was given by Sellmier dispersion relationwhich explains the variation of refractive index with wavelength in the equation below [35],

$$n^2 - 1 = \frac{So\lambda o^2}{[1-(\frac{\lambda o}{\lambda})^2]} \qquad 4$$

Were λ_o is the average oscillator parameter and s_o is the average oscillator strength.

The performance of the thin film from the results shown, are typically enhanced when it consists of varying thickness obtained from the absorbance and the refractive index.

3.3.3 The study of band gap as a function of photon energy.

The optical band gap energy for $BaTiO_3$ was plotted by considering a direct transition between the valance and conduction bands when the photon energy falls on the materials. This corresponds to transitions between extended states in both valence and conduction bands, where the power law behaviour of Tauc$(\alpha hv)^2 \propto (hv - Eg)$ was given for allowed direct transition[36]. This can also be expressed as shown below in equation 5

From the expression,'α' is the absorption coefficient,'*hv*'photon energy which is related to the direct optical band gap energy'*Eg*'. 'A' is a constant which does not depend on photon energy and 'r' is the characteristic of the type of the optical transition process, which is equal to ½ or 2 for direct and indirect band gap.

$$(\alpha hv) = A(hv - Eg)^r 5$$

From the expression,'α' is the absorption coefficient,'*hv*'photon energy which is related to the direct optical band gap energy'*Eg*'. 'A' is a constant which does not depend on photon energy and 'r' is the characteristic of the type of the optical transition process, which is equal to ½ or 2 for direct and indirect band gap.

The plot between $(\alpha hv)^2$ and hv provides the value for the Eg, which is extrapolated by the linear portion of $(\alpha hv)^2 = 0$, as shown below in fig 6.

The values obtained for the band gap of different concentration of $BaTiO_3$ thin films lies in the range of (2.2-2.7) eV. This was obtained from the linear portion of $(\alpha hv)^2$ versus (hv) plot as shown in fig 5. A close observation of the band gap range shows that a decrease in the concentration of the deposition medium brings about an increase in the band gap. The band gap increase or decrease depends on the concentration of the deposition, film thickness, rate of deposition and annealing temperature [34].

4. Conclusion

Epitaxial deposition of different concentration of $BaTiO_3$ thin film has been successfully deposited onto a TiO_2 film using the method of chemical bath deposition technique. The composition Study of the result EDS reveals the percentage composition of the elements in the thin films and the surface topography reveals the grain size and the amorphous phase of the deposited thin films. And from the optical studies, it showed that the films have high absorbance in the visible region and high transmittance in the infrared region of the solar spectrum. This therefore can be used in the fabrication of solar devices. A close observation from the high transmittance of $BaTiO_3$ thin films can be employed in the construction of solar brooders which reduces the cost of energy and the hazards involved in the use of artificial form of brooders.

.

5. Acknowledgement

The researchers wish to express their gratitude to the management and staff of Sheda Science and Technology Complex, Abuja for carrying out the characterisation (XRD, SEM EDX) and the Engineering Materials Development Institute (EMDI),Akure for carrying out the Photo Spectrometer of the data used for this research work.

References

[1]. M.E. Lines, A.M. Glass, Principles and Applications of Ferroelectrics and Related Materials, Clarendon Press, Oxford, (1977).

[2]. V.E. Henrick, P.A. Cox, The Surface Science of Metal Oxides, Cambridge University Press, New York, (1994).

[3]. S.Y. Lee, M.C.C. Custodio, H.J. Lim, R.S. Feigelson, J.P. Maria, S. Trolier-McKinstry, J. Cryst. Growth **226** (2001) 247.

[4]. Y. Ding, A. Osaka, Y. Miura, J. Non-Cryst. Solids **176** (1994) 200.

[5]. A. Herczog, J. Am. Ceram. Soc. **47** (1964) 107.

[6]. D.R. Ulrich, Solid State Technol. **12** (1969) 30.

[7]. M. Sepliarsky, M.G. Stachiotti, R.L. Migoni, Phys. Rev. Lett. **96** (2006) 137603.

[8]. J.E. Spanier, A.M. Kolpak, J.J. Urban, I. Grinberg, L. Ouyang, W.S. Yun, A.M. Rappe, H. Park, Nano Lett. **6** (2006) 735.

[9]. K. Yao, W. Zhu, J. Mater. Res. **12** (1997) 1131.

[10]. A. Morell, J. C. Niepce, J. Mater. Educ. **13** (1991) 173.

[11]. S. F. Wang, G.O. Dayton, J. Am. Ceram. Soc. **82** (1999) 2677.

[12]. P. Gherardi, E. Matijevic´, Colloids Surf. **32** (1988) 257.

[13]. H. Herrig, R. Hempelmann, Mater. Lett.**27** (1996) 287.

[14]. I. MacLaren, C.B. Ponton, J. Eur. Ceram. Soc. **20** (2000) 1267.

[15]. Y.Yano,K.Iijima, Y. Daitoh, T. Terashima, Y. Bando, Y. Watanabe, J. Appl. Phys**76** (1994) 7833.

[16]. J. O. Eckert Jr, C.C. hung-Houston, B.L. Gersten, M. Lencka, R. Riman, J. Am. Ceram. Soc. **79** (1996) 2929.

[17]. W. Hertl, J. Am. Ceram. Soc,**71** (1988) 879.

[18]. M. Yoshimura, S. Yoo, M. Hayashi, N. Ishizawa,Jpn. J. Appl. Phys. **28** (1989) L 2007.

[19]. S. Venigalla, P. Bendale, J. H. Adair, J. Electrochem. Soc.**142**. (1995) 2101.

[20]. Z. Wu, M. Yoshimura, Solid State Ionics **122** (1999) 161.

[21]. N. Ishizawa, M. Hayashi, H. Banno, S. Mizunuma, H. Yamaguchi, S. E. Yoo,M. Yoshimura. Report of the Reserch Laboratory of Engineering Materials, Tokyo institute of Technology, **16**, (1991)9.

[22]. P. Bendale, S. Venigalla, J. R. Ambrose, E. D.VerinkJr, J. H. Adair, J. Am. Ceram. Soc. **80** (1993) 2619.

[23]. P.O'Brien, T. Saeeda, J. Knowles, J.Mater. Chem. **6** (1996) 1135.

[24]. L.Vayssieres, K.Keis, A.Hagfeldt, S. E. Lindquist, Chem. Matter, **13** (2001) 4395.

[25]. L. Vayssieres, Adv. Mater.**15** (2003) 464.

[26]. C. Levy-Clement, Nanostructured Materials for Solar Energy Conversion (2006) 447.

[27]. S. Chopra, S. Sharma, T.C. Goel,Appl. Surf. Sci. **230** (2004) 207.

[28]. R. Thomas, D.C. Dube, Jpn. J. Appl. Phys. 1 **36** (1997) 7337.

[29]. Y. C. Lai, J. C. Lin, C.P. Lee, Appl. Surf. Sci. **125** (1998) 51.

[30]. D.S. Fu, T. Ogawa, H. Suzuki, Appl. Phys. Lett. **77** (2000) 1532.

[31]. L. Kavan, B.O'regan, A. Kay, M. Gratzel, J. Electroanal. Chem. **346** (1993) 297.

[32]. S. Raghvendra, Y. D. Avinash, C. Pandey, S. S. Sanjay,Chal. Lett.**6**, (2009) 233.

[33]. A. E. Ajuba, S. C. Ezugwu, B. A. Ezekoye, F. I. Ezema, P. U. Asogwa, J. Optoelectronics and Biomedical Mat. **2** (2010) 73.

[34]. R. U. Osuji, S. C. Ezeugwu, F. I. Ezema, P. U. Asogwa, A. B. C. Ekwealor, B. A. Ezekoye, Optoelectronics and Advanced Materials-Rapid Communications. **3**, (2009) 141.

[35]. S. Y. Girgis, A. M. Salem, M. S. Selim,J. Phys.

Condensed. Matter **19** (2006) 116213.
[36]. J.C. Tauc, Amorphous and Liquid Semiconductors, Plenum Press, New York, (1974).

Figure Captions:

Figure 1: EDS peaks of $BaTiO_3$ (a) at 1Mole, (b) at 0.5Mole

Figure 2: SEM of $BaTiO_3$ (a) as 1Mole, (b) at 0.5Mole (c) Cross section.

Figure 3: X-Ray Diffraction of $BaTiO_3$ (a). at 1Mole, (b). at 0.75Mole, (c) at 0.5Mole

Figure 4: (a) Plot of absorbance versus wavelength of $BaTiO_3$, (b) Plot of Transmittance versus wavelength of $BaTiO_3$

Figure 5: (a) Plot of extinction co-efficient versus wavelength of $BaTiO_3$. (b) Plot of Refractive index versus wavelength of $BaTiO_3$.

Figure 6: Plot of $(\alpha hv)^2$ versus hv for $BaTiO_3$ band gap

1) Dr F. I. Ezema
Senior Lecturer
Department of Physics and Astronomy
University of Nigeria, Nsukka
Enugu State, Nigeria.
fiezema@yahoo.com

2) Dr B. A. Ezekoye
Senior Lecturer
Department of Physics and Astronomy
University of Nigeria, Nsukka
Enugu State, Nigeria.
benjaminezekoye@yahoo.com

3) Mr P. O. Ike
M.Sc Student
Department of Physics and Astronomy
University of Nigeria, Nsukka
Enugu State, Nigeria.
ikepatrickokezie@gmail.com

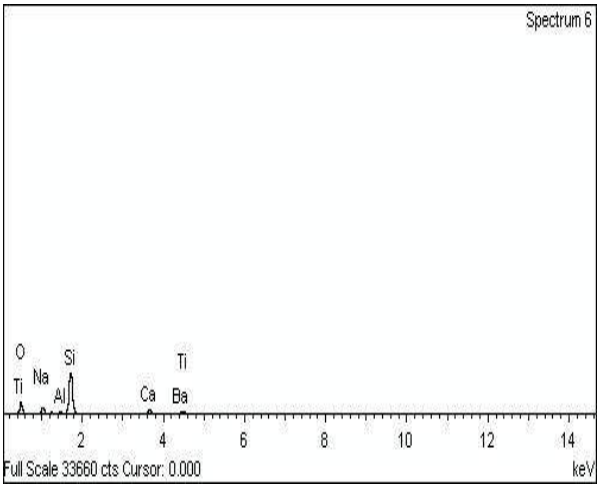


Fig 1a. EDS peaks of $BaTiO_3$ at 1mole

Fig 1a. EDS peaks of $BaTiO_3$ at 1mole

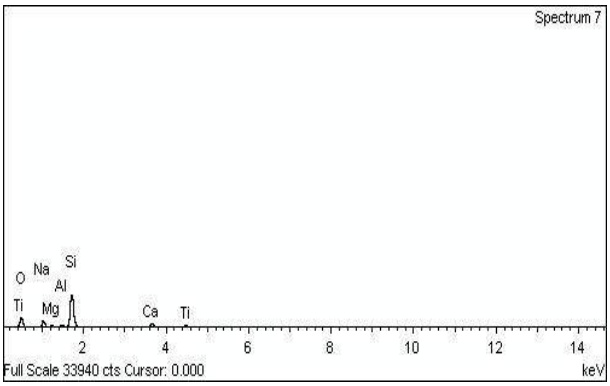


Fig 1b. EDS peaks of $BaTiO_3$ at 0.5mole.

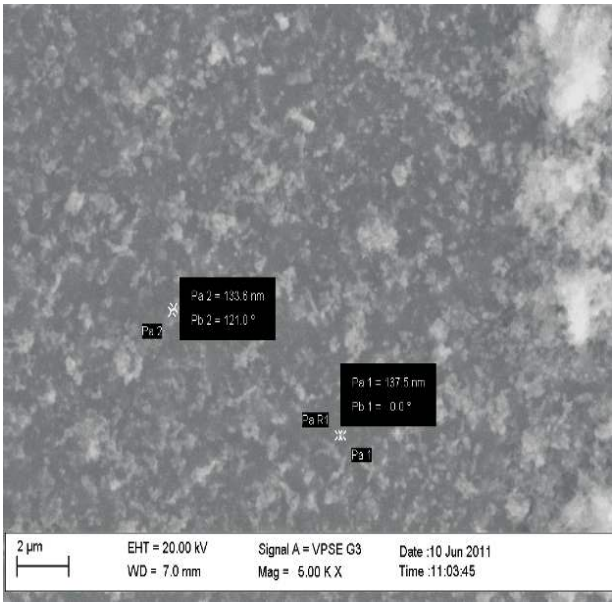


Figure 2a.SEM of $BaTiO_3$ at 1mole.

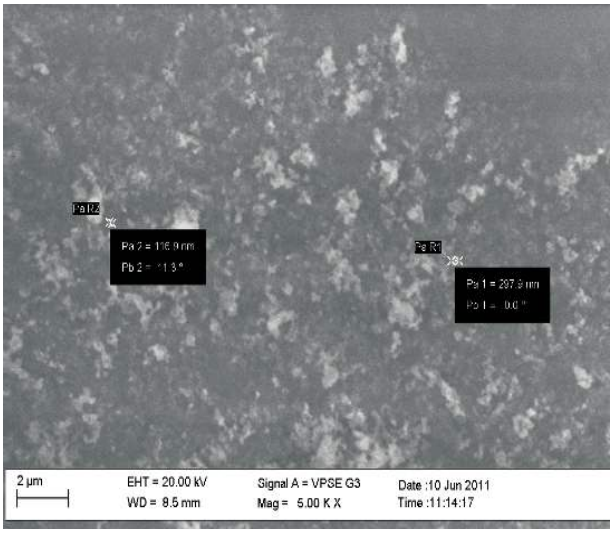


Figure 2b. SEM of $BaTiO_3$ at 0.5mole

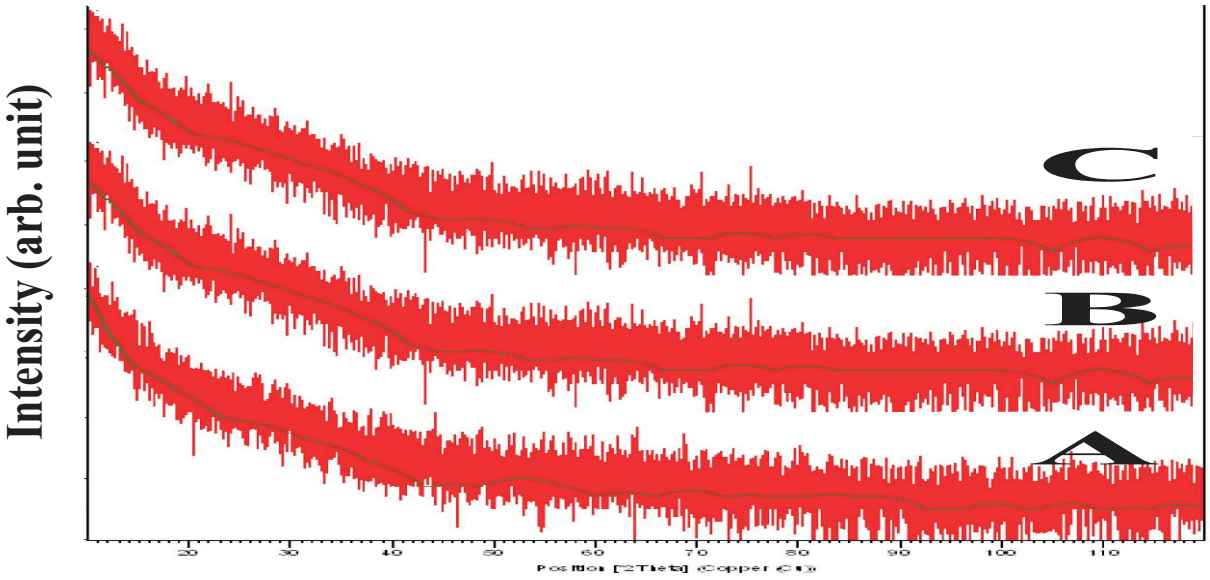


Fig 2c: XRD of $BaTiO_3$ thin films (A) at 1.0M, (B). at 0.75M, (C). at 0.5M all annealed at 200°C.

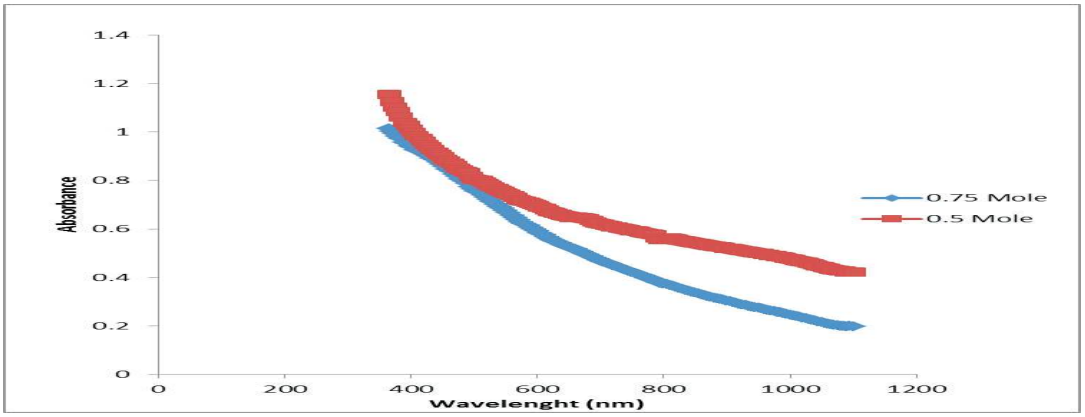


Figure 4a. Plot of absorbance versus wavelength for $BaTiO_3$

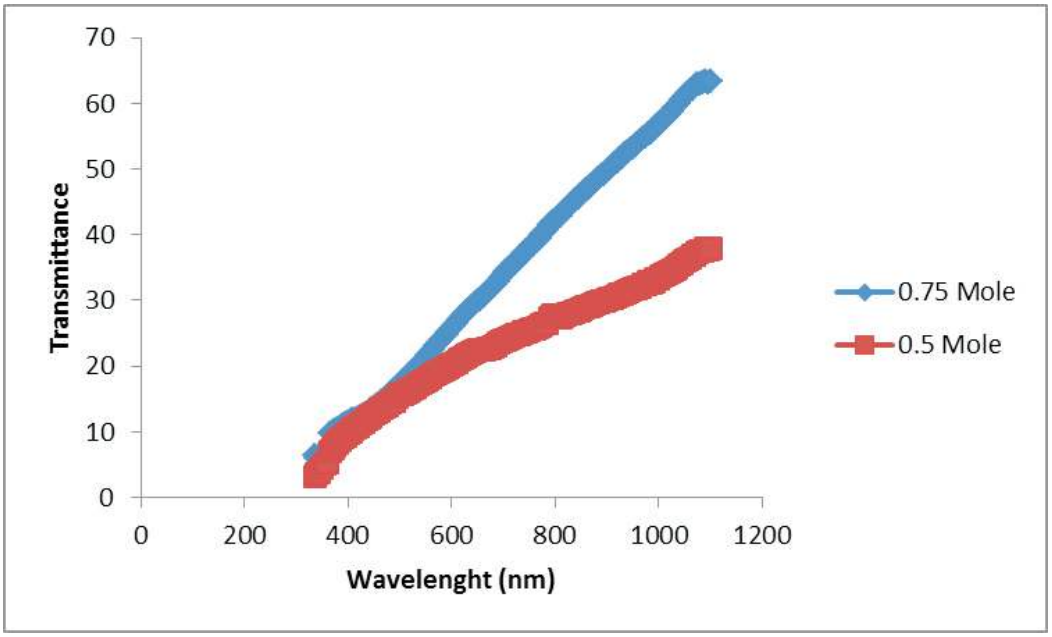


Figure 4b.Plot of transmittance versus wavelength of $BaTiO_3$.

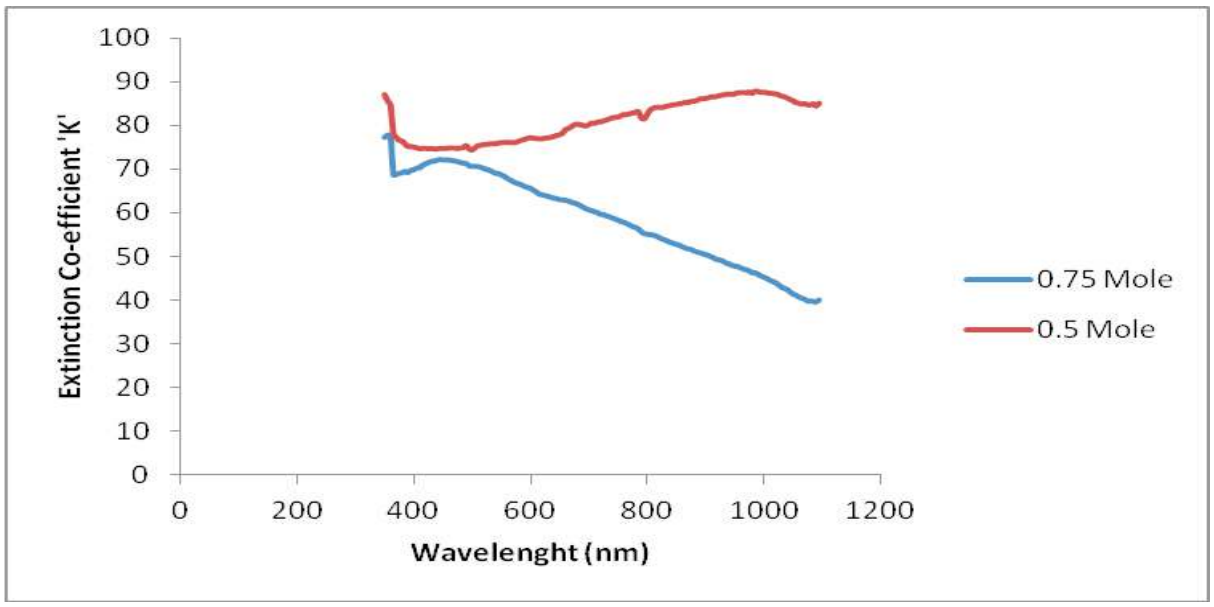


Figure 5a.Plot of extinction co-efficent versus wavelength of $BaTiO_3$.

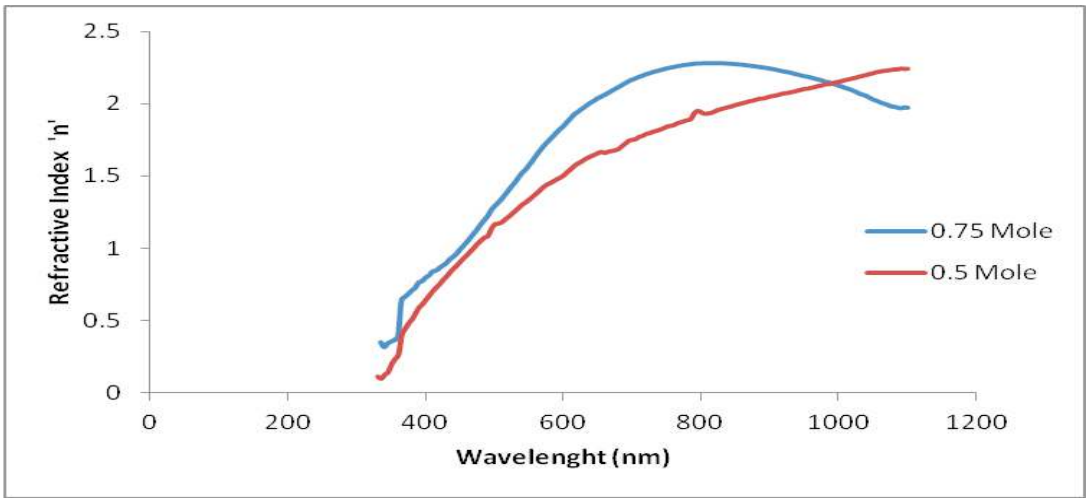


Figure 5b.Plot of Refractive index versus wavelength of $BaTiO_3$.

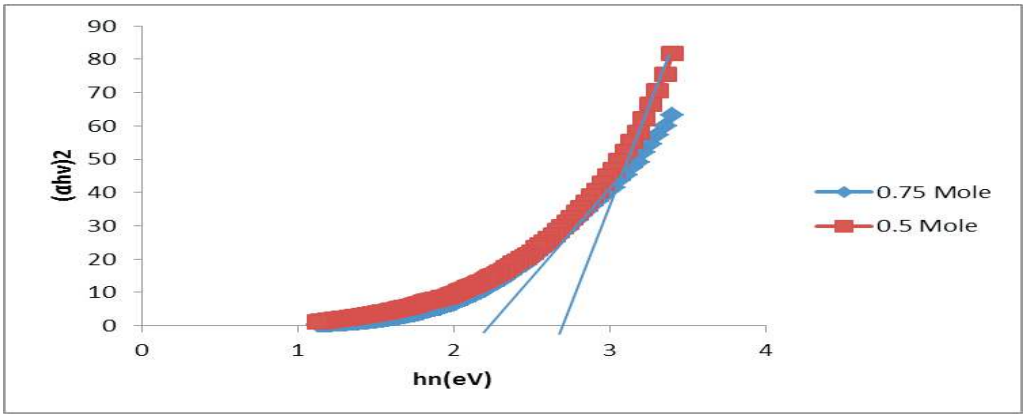


Figure 6. Plot of $(\alpha hv)^2$ versushv for $BaTiO_3$.

CHARACTERIZATION OF SOL-GEL DEPOSITED BARIUM STANNATE FILMS AND POWDER

V. C. ODOH[1], C. I. AMAECHI[1], F. I. EZEMA[1], P. U. ASOGWA[1], and R. U. OSUJI[1,2]
[1]Department of Physics and Astronomy,
[2]Centre for Energy Research and Development,
University of Nigeria, Nsukka, Enugu State, Nigeria

Abstract
Fine layers of barium stannate powder have been synthesized by sol-gel technique from tin chloride pentahydrate ($SnCl_4.5H_2O$) and barium sulphate ($BaSO_4$). Physico-chemical properties of barium stannate, $BaSnO_3$ were characterized by X-ray diffraction (XRD), Fourier transform infrared (FTIR) spectroscopy, scanning electron microscopy (SEM) and UV-Visible spectrophotometry technique. A growth mechanism based on the combination of particle sticking and molecule level heterogeneous growth is proposed. It has been found that the particle size of all the samples was distributed in the range 3.0-6.5? while optical absorption spectrum indicates that $BaSnO_3$ powder have a direct band gap of 3.9eV.

Keywords: Barium stannate, Particle size, Band gap, and Sol-gel.

1.0 Introduction

Tin oxide (SnO_2), with a rutile-type crystalline structure, is an n-type wide band gap (3.6eV) semiconductor that presents a proper combination of chemical, electronic and optical properties that make it advantageous in several applications[1,2]. Following the superfluous electron characterizing this semiconductor, increasing research had been underway in the use of anodes of SnO_2 in lithium batteries [3] and to determine the semiconducting character of material and its potential usefulness as gas sensors for detection of toxic and flammable gases [4].

Stannates with general chemical formula $XSnO_3$, where X are elements of group II (Mg, Ca, Sr & Ba) form a component of dielectric material used in thermally stable capacitors [5]. Supporting the aforementioned usage, it is worth noting that their physical properties such as grain size, morphology semi-conductivity and transparency has guaranteed a wide application as white pigments for conducting coatings, transparent conducting coatings for furnaces and electrodes [6], opto-conducting coatings for solar cells [7], surge arrestors otherwise called varistors [8,9] and catalysts [10,11]. Particulates of SnO_2 have been synthesized by different chemical techniques/routes such as precipitation, hydrothermal, sol-gel, spray pyrolysis and gel-combustion [12-19]. However, the advantages offered by sol-gel method have shown superiority to the convetional solid state reaction because of possibility of mixing starting materials at the molecular level and resulting product expected to be homogenous [20]. This paper describes the synthesis of pure and homogenous powdered $BaSnO_3$ by introduction of various quantities of barium sulphate. The influence of dopant on the crystalline size and optical properties of the synthesized films were studied.

2.0 Experimental procedure

Preparation of thin films and powders

Preparation of transparent $BaSnO_3$ solution was carried out by dissolving a mixture of 3.5g of tin chloride pentahydrate ($SnCl_4.5H_2O$), and ethanol (C_2H_5OH) under vigorous stirring with the magnetic stirrer at ambient temperature ~300K. To the corresponding solution, 7mL of aqueous ammonia solution (27%, ρ =0.88gcm^{-3}) was added drop-wise to obtain a better homogeneity. To investigate optical properties, films for UV-Vis spectrophotometry were produced by dip-coating of degreased quartz substrates in the homogenous gel for 5min. After rinsing in deionized water, they were drip-dried in air. The resulting gel was centrifuged (~1500rpm) for 15min and the sediments collected and dried at 80°C for 5h in order to remove water molecules as shown in the equation [1-2]. Finally, ash coloured barium doped tin oxide powder were calcined at 300°C for 2h.

$$6NH_4^+ + Sn^{2+} \rightarrow [(NH_3)_6Sn]^{2+} \quad [1]$$

$$xBa^{2+} + [(NH_3)_6Sn]^{2+} + yOH^- + 2e^- \rightarrow Ba_xSnO_{2+y} + 6NH_4^+ \quad [2]$$

Characterization of $BaSnO_3$ powder

The X–ray diffractograms of $BaSnO_3$ powder was recorded by using X–ray diffractometer (PANalytical) with CuKα radiation λ = 1.5406Δ in 2theta angle between 20° and 80°. UV-Vis absorption spectra and some other optical parameters for the calcined nanoparticles ~300°C were recorded using UNICO-UV 2102 PC spectrophotometer in the range of 200-1100nm. Fourier Transform Infrared (FTIR) spectra studies were carried out using SHIMADZU – 8400S spectrophometer while Scanning Electron Microscopy (SEM) images were taken with an accelerating voltage of 20kV.

3.0 Results and discussions

3.1 Structural Analysis

The structure of as- synthesized $BaSnO_3$ powder calcined at 300°C for 2h was studied and X–ray diffractograms were recorded in 2theta range, 10 – 80°. Fig.1 shows the XRD patterns of tetragonal rutile crystalline phase of tin oxide resulting from the assignment of diffraction lines (JCPDS # 02-2150). Contributions from characteristic peaks of impurity (BaO) were however not observed. The XRD pattern of the baruim stannate in ethanol shows slight broadening corresponding to the peak 54.87° with preferred orientation of (211). This in agreement with the values and patterns reported by [21]. The average crystallite size of Ba_xSnO_{2+y} nanoparticles was deduced by the inverse proportional relation of full width at half maximum (FWHM), β_2 as predicted by Debye–Scherrer's equation [22]:

$$D = \frac{0.89\lambda}{\beta_{2\Phi}\cos\Phi} \qquad [3]$$

Where D is the crystallite size, λ is the wavelength of CuKα radiation, $\beta_{2\Phi}$ is the full width at half maximum (FWHM) intensity, Φ is the Bragg's angle. The average crystallite size of the barium stannate nanoparticles was found to be distributed in the range 3.0 -6.5? . The result showed a bit ultrafine arrangement o f the particulates dispersed in the ethanol solvent. Inter -planar spacing, d_{hkl} of Ba_xSnO_{2+y} nanoparticles were obtained by the Bragg's law [22] given by the equation

$$d_{hkl} = \frac{n\lambda}{2\sin\Phi} = \frac{a}{\sqrt{h^2+k^2+l^2}} \qquad [4]$$

The microstrain (ε) developed in barium stannate nanoparticles were calculated from the relation [23]:

$$\varepsilon = \frac{\beta_{2\Phi}\cot\Phi}{4} \qquad [5]$$

The dislocation density (ρ) was estimated according to Williamson and Smallnan [24] using the relation

$$\rho = \frac{15\varepsilon}{aD} \qquad [6]$$

Where a is the lattice constant and D is the crystallite size. The average numerical values of the estimated crystalline parameters are summarized in table 1 for calcined (300°C) nanoparticles.

3.2 SEM Characterization

Fig. 2(a-c) shows the SEM of calcined (300°C) barium stannate (Ba_xSnO_{2+y}) nanoparticles with magnification (x500) procured from ethanol. It shows that surface appears rocky-granular having different sizes and shapes of grains without any crack or hole generated on the surface. However, the inhomogeneous distribution of grains suggests a bit ultrafine arrangement. The lower particle size ~ 3.07? reveals the role of the solvent in the control of the nanoparticles nucleation.

3.3 FTIR Characterization

Fig. 3 shows the Fourier transform infrared (FTIR) spectra of the prepared Ba_xSnO_{2+y}, x: y =1:1 nanoparticles dried at 80°C and calcined at 300°C for 2h. The characteristic peaks around ~ 1416.76 and 1627.01 cm^{-1} for sample V_C correspond to the bending vibrations of absorbed water molecules and stretching vibrations of hydroxyl (- OH) group. The weak transmission peaks at 1059.92, and 2860.53cm^{-1} for V_C, 707.90 and 161833 cm^{-1} for V_B, 1166.01, 1459.20, 1615.44 and 2251.60cm^{-1} for V_A belong to the stretching vibrations of aliphatic C-H bonds, and at other points except 543.94 cm^{-1} for V_C, 618.21cm^{-1} for V_B and 751.30cm^{-1} for V_A correspond to the bending vibrations of alkyl group attached to the alcohol solvent which shows that there was permeability of organic groups on the surface of SnO_2 nanoparticles. Gnanam and Rajendran [25] confirmed the assignment of 602cm^{-1} peak to SnO_2 vibration; however the discrepancy in peak for corresponding $BaSnO_3$ nanoparticle samples was obvious that barium ion introduction affected the peak and causing a shift to 751.30cm^{-1}, 618.21cm^{-1} and 543.94 cm^{-1} for V_A, V_B and V_C respectively.

3.4 Optical Absorption Studies

The room temperature UV-Visible spectra in the range of 200-1100nm for as- synthesized Ba_xSnO_{2+y} nanoparticles calcined at 300°C is presented. The optical absorbance of as-synthesized nanoparticles, sample V_A experienced a slight off-shoot within the visible spectrum but decreases near infrared (NIR) region and IR, V_C had almost stable absorbance in both spectra while V_B suffered deviation which is equivalent to a negative gradient straight-line graph along the wavelength axis. At 1100 nm wavelength in the IR, the absorbance measured 0.36, 0.39 and 0.18 revealing a relatively low absorbance for nanoparticle samples (V_A, V_C & V_B).

Fig. 4 shows the transmittance of barium stannate nanoparticles within 200-1100nm wavelength. Sample V_A and V_C possess 40-50% transmittance which assumes a slight increase between the visible and IR, sample V_B has a bit high transmittance of about 66% and this spontaneously becomes proportional to wavelength. The optical band gap energy (E_g) can be determined by the Tauc's relation involving absorption coefficient, α:

$$\alpha = \frac{1}{t}\ln\left(\frac{1}{T}\right) = \theta\left(h\upsilon - Eg\right)^n / h\upsilon \qquad [7]$$

Where θ is a constant, h is planck's constant, Δ is frequency (Hz), T is the transmittance. Fig. 5 depicts the variation of (αhΔ)2 against h? for as- synthesized nanoparticles. For a case of almost linearity in plots, energy band gap, Eg can be deduced by tangent of the intercept on h? axis. This gives a value of ~3.9ev which is in strong agreement with the report of Gnanam and Rajendran [25] on the Cd doped Sno2 Nanoparticles by

Sol-Gel Route. The size of Bohr radius determines the quantum confinement effect of a semiconductor particularly when it is smaller than the Bohr radius. As such, the absorption edge would shift to a higher energy. From the optical absorbance spectrum, absorption edge of the calcined (300°C) barium stannate nanoparticles was estimated to be ~320nm for the samples. However, it was established that a shift in the optical bandgap of polycrystalline thin film semiconductors lowers energy with increase in thickness. This is a prevalent phenomenon in thin film semiconductors obtained by chemical deposition method [26] but no shift was observed in the case of BaxSnO2+y films.

3.0 Conclusion

Barium atoms cross-linking SnO2+y nanoparticles have been synthesized by a chemical sol-gel method at ambient temperature ~300K dissolved in ethanol. The particle size was distributed in the range 3.0? - 6.5? while energy band gap of 3.9eV was confirmed for the nanoparticles by XRD and optical characterization result respectively. Analysis of table 1 also confirmed slight consistency in some crystalline parameters deduced despite the variation of barium sulphate quantities. Optical band gap shift maintained during calcinations irrespective of different quantities of BaSO4 used was in agreement with XRD results where no notable improvement in crystallinity was observed.

References

[1] S. Gnanam, V.Rajendran, J. Sol-Gel Sci.Technol (2010) 53:555-559.

[2] J.M. Jorezebsk, J.P. Marton, J. Electrochem. Soc. (1976) 129:229C.

[3] A.C. Bose, D. Kalpana, P. Thangadurai, S. Ramasamy, j. Power Sources (2002) 107:138.

[4] U. lampe, J, Gerblinger, H. Meixner, Sens. Actuator B Chem. (1995) 24.-25 657.

[5] E.C. Subbarao, Ferroelectrics, (1981) 35 143

[6] Olivi P., Souza Ecp, Longo verela JA, Bulhoes LOS, J. Electrochem Soc. (1993) 140:81

[7] Chopra K.L Major S., Pandya DK Thin solid Films (1983) 102:1

[8] Pianaro S.A, Bueno P.R, Longo E, Verla JA J. Mater. Sci., (1995) 14: 692

[9] Bueno PR, Cassia-Santos M.R. Leite E.R, Longo E.Bisquert J., Garcia-Santiago G., J Appl. Phys(2000) 88: 6545.

[10] Tagawa T, Kataka S, Hattori T, Murakani Y Appl. Catal. (1994) 4:1

[11] Park PW, Kung H.H. Kin DW, Kung MC, J. Catal., (1999) 184:440.

[12] Chen ZW, Lai JKL, SHek CH, Phys. Rev B (2004) 70:165314.

[13] Dieguez A, Rodriguez AR, Vila A, Morante JR, J. Appl. Phys. (2001) 90:1550.

[14] Arai T. j. Phys.Soc. Jpn. (1960) 15:916.

[15] Jeong J. Choi Sp, Chang CI, Shin DC, Park JS, Lee BT, Park YJ, Song HJ, Solid State Commun. (2003) 127:595.

[16] Santos LRB, Chartier T, Pagnoux C, Baumard JF, Santilli CV, Pulcinelli SH, Larbot A, J. Eur. Ceram. Soc. (2004) 24:3713.

[17] Grzeta B, Tkalcec E, Geobbert C, Takeda M, Takahashi M, Nomura K, Jaksic M, J. Phys. Chem. Solids,(2002) 63:765.

[18] Antonio JAT, Baez RG, Sebastian PJ, Vazquez A, J. Solid State Chem. (2003) 174:241.

[19] Zhang J. Gao L, J. Solid State Chem. (2004) 177:1425.

[20] Marina Licheron, G. Jouan and E. Husson; J. of the European Ceram. Soc. (1997) 17:1453-1457.

[21] F. J. Berry, E. Moore, M. Mortimer, X. Ren, R. Heap, P. Slate, M. F. Thomas. J. Solid State Chem., (2008)181:2185-2190.

[22] H. P. Klug, L. E. Alexender, X-ray Diffraction Procedures for Polycrystalline and Amorphous Materials; Woley – New York, 1974.

[23] Poulomi Roy, S. K. Srivastava, Thin Solid Films, (2006) 496, 293-298.

[24] G.B. Willamson, R.C Smallman, Philos. Mag, (1956)1:34.

[25] S.Gnanam.V. Rajendran, J Sol-Gel Sci Technol, DOI 10.1007/s10971-010-2285-7.

[26] M.T.S. Nair, L. Guerrero, O.L. Arenas, P.K.Nair, Applied Surface Science (1999)150:143-151.

List of Figures

Fig.1 - X-ray diffractograms of BaxSnO2+y nanoparticles

Fig. 2 - Scanning electron microscopy (SEM) of barium stannate calcined at 300°C

Fig. 3 – Fourier transform infrared (FTIR) of as-deposited barium stannate nanoparticles

Fig. 4 - Spectral transmittance, T% against wavelength, nm for barium stannate nanoparticles

Fig. 5 - Direct energy bandgap, Eg plot for as-deposited barium stannate nanoparticles.

List of Table

Table 1 - Particle size, dislocation density, microstrain and inter-planar spacing for BaxSnO2+y nanoparticles calcined at 573K.

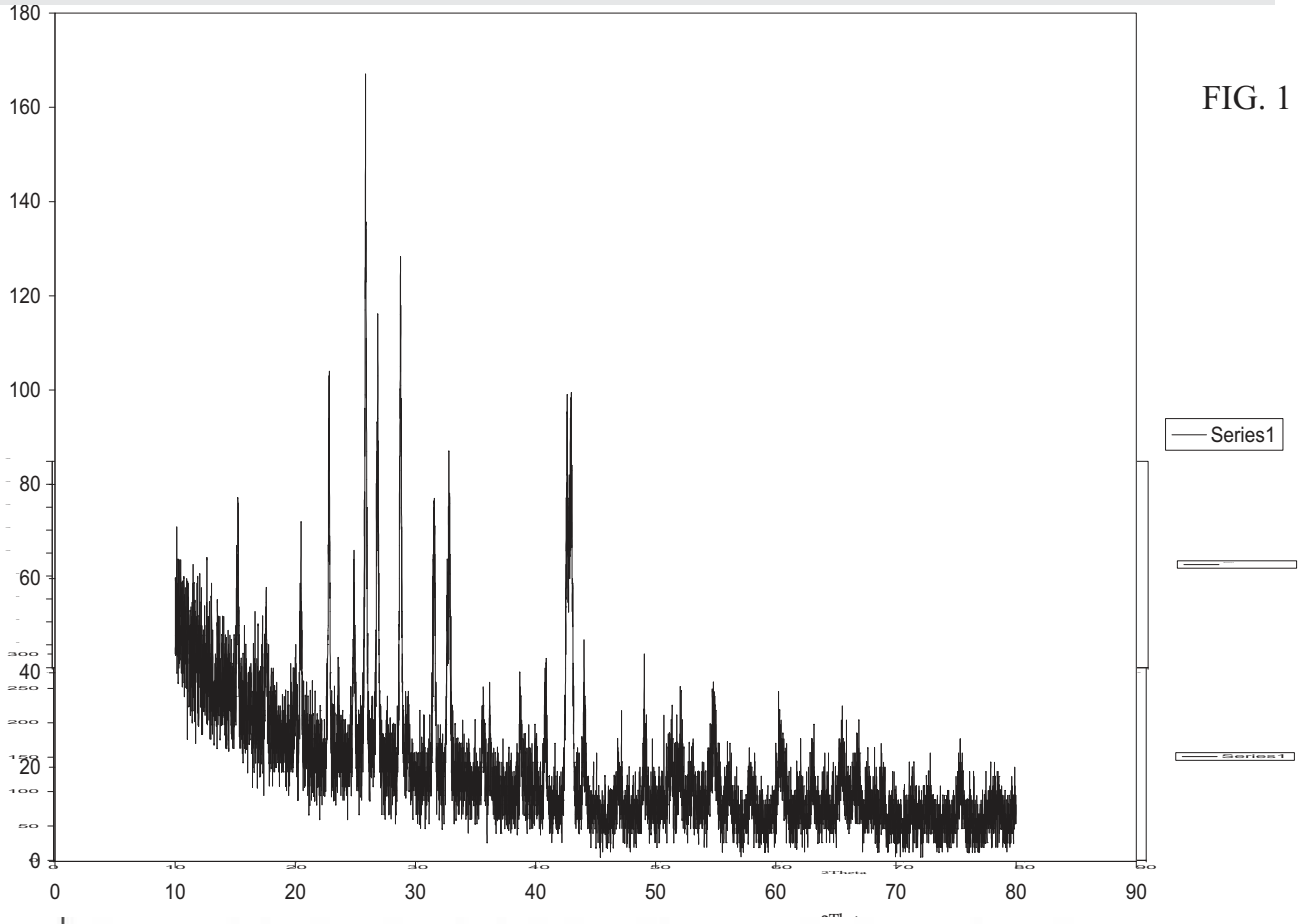

180
160
140
120
100
80
60
40
20
0
0
10
20
30
40
50
60
70
80
90
Series1

FIG. 1

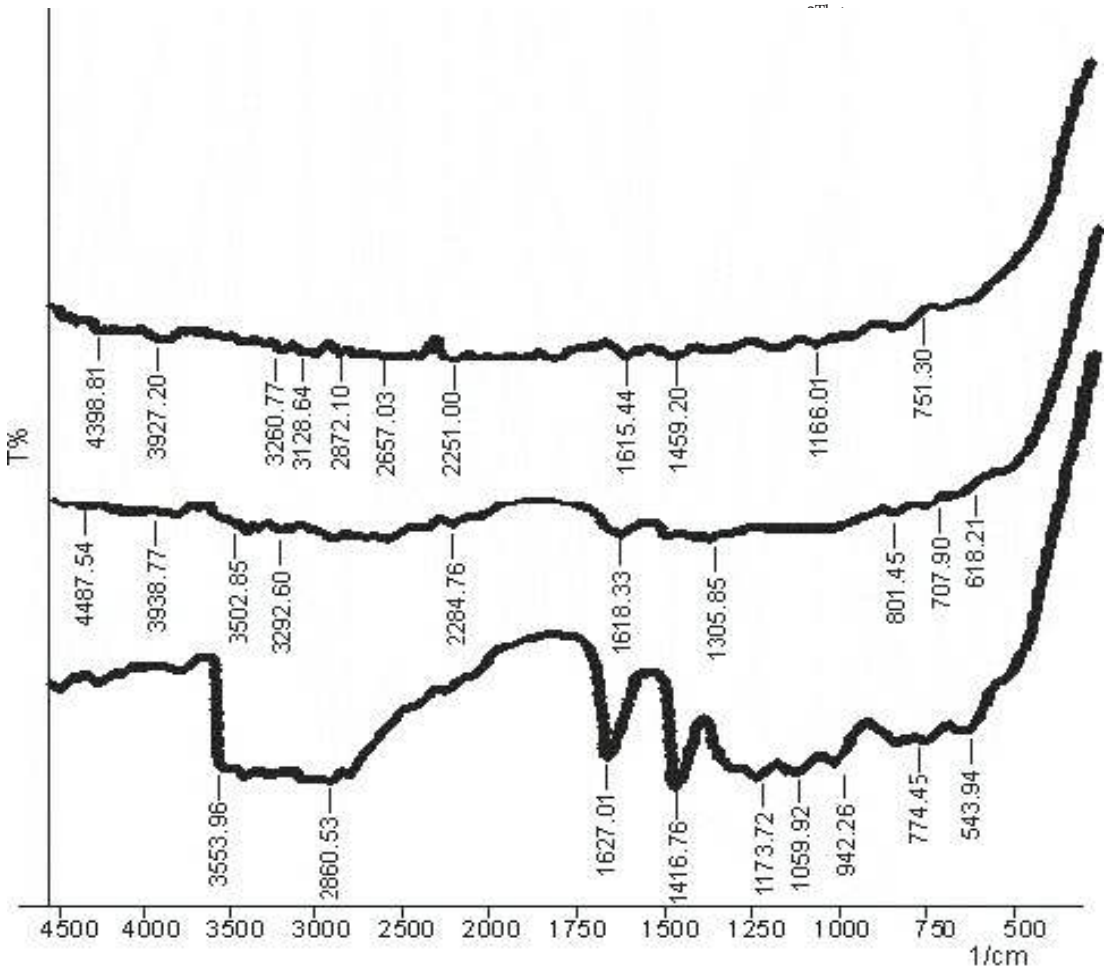
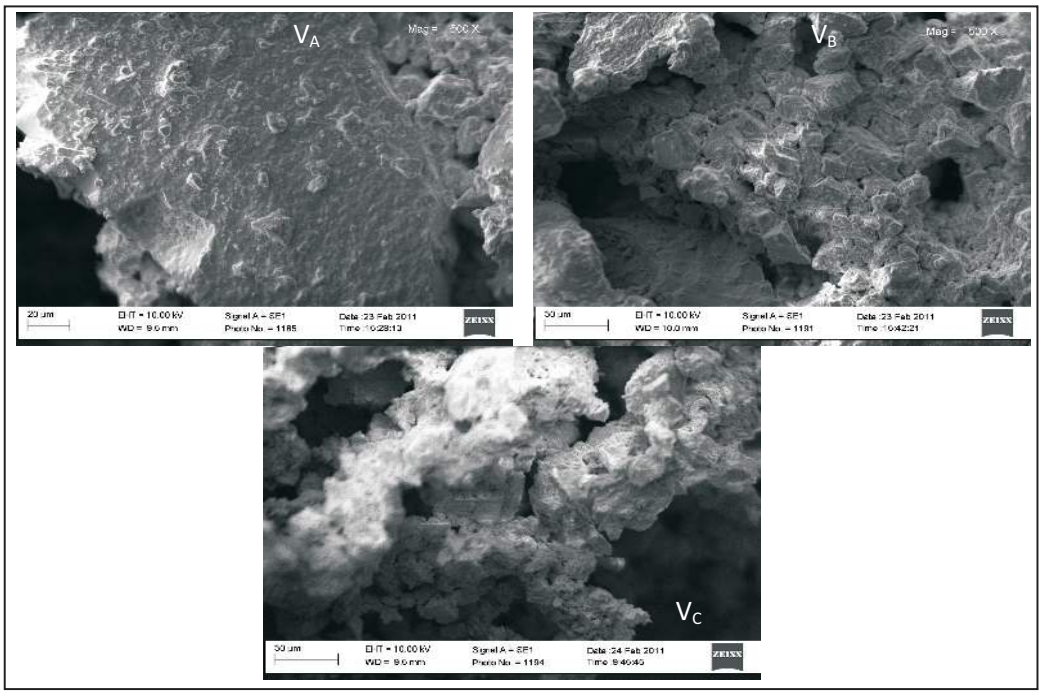

T%
4398.81
3927.20
3260.77
3128.64
2872.10
2657.03
2251.00
1615.44
1459.20
1166.01
751.30
4487.54
3938.77
3502.85
3292.60
2284.76
1618.33
1305.85
801.45
707.90
618.21
3553.96
2860.53
1627.01
1416.76
1173.72
1059.92
942.26
774.45
543.94
4500 4000 3500 3000 2500 2000 1750 1500 1250 1000 750 500
1/cm

FIG. 2



TRANSMITTANCE

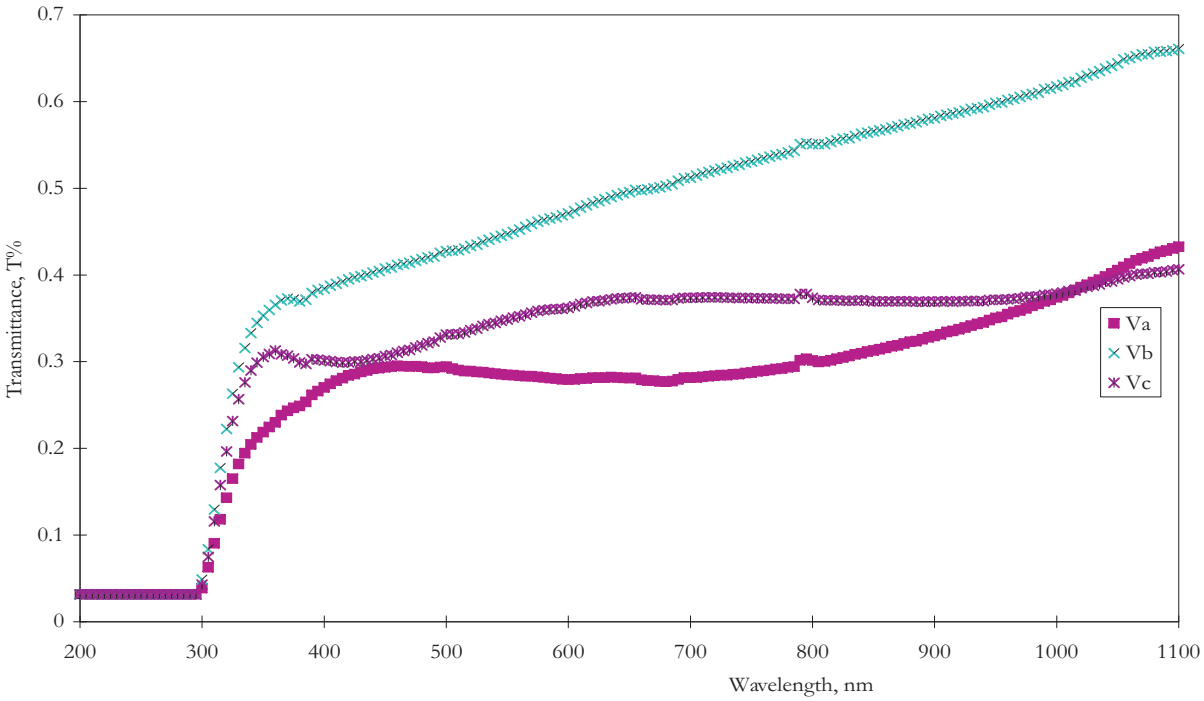


FIG. 3

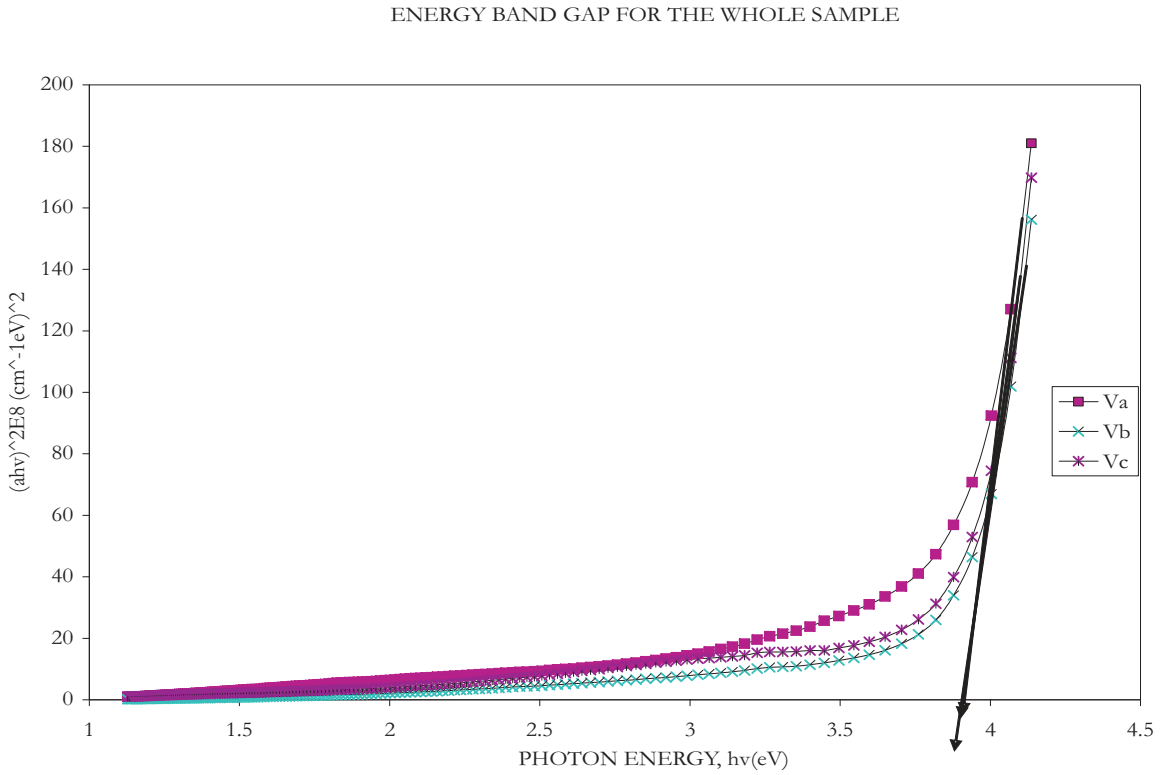


FIG. 4

Sample: Ba_xSnO_{2+y}	Calcination Temperature(°C)	Particle Size(D), <	Dislocation Density (ρ), ? $^{-2}$	Micro-strain (ε)	Inter-planar Spacing (d_{hkl}), ?
V_A	300	3.07	0.29	0.24	1.67
V_B	300	6.13	0.07	0.12	1.67
V_C	300	6.14	0.07	0.12	1.67

TABLE 1.

DECOLOURIZATION AND DEGRADATION OF TEXTILE WASTEWATER USING TiO_2 NANOPARTICLES

A. Giwa*, P.O. Nkeonye, K.A. Bello, E.G. Kolawole
Department of Textile Science and Technology, Ahmadu Bello University, Zaria, Nigeria
**[Email: agiwa@abu.edu.ng; Tel: 08037033052]*

ABSTRACT
The nanophotocatalytic process using semiconducting oxides with a nanostructure is one of the technologies used for the destructive oxidation of organic compounds such as dyes. The photocatalytic oxidation of a textile dye – C. I. Basic Blue 41 (BB41) in aqueous solution was assessed by UV ray irradiation in the presence of TiO_2 nanoparticles. The effect of initial dye concentration, pH and TiO_2 loading were investigated and the optimized conditions for maximum amount of degradation were determined. Analysis of the kinetics showed pseudo-first-order model. The mineralization of the dye was reported by measuring the initial and final chemical oxygen demand of the solution that was irradiated under optimized conditions.

Keywords: Nanophotocatalysis, textile, dye, wastewater, TiO_2, C. I. Basic Blue 41.

INTRODUCTION

Synthetic dyes comprise an important part of industrial water effluents, as they are discharged in abundance by many manufacturing industries. The impact of these dyes on the environment is a major concern because of the potentially carcinogenic properties of these chemicals [1]. Besides this, some dyes can undergo anaerobic decolouration to form potential carcinogens [2]. The wastewater which is coloured in the presence of these dyes can block both sunlight penetration and oxygen dissolution, which are essential for aquatic life. Thus there is a considerable need to treat these coloured effluents before discharging them to various water bodies. Various approaches on handling and decontaminating such effluents have been reported in the literature. Typical techniques include the classical methods such as adsorption [3, 4], coagulation [5,6], ion flotation [7] and sedimentation [8]. All these techniques are versatile and useful, but they all end up in producing a secondary waste product which needs to be processed further. Another set of techniques which are relatively newer, more powerful, and very promising is called Advanced Oxidation Processes (AOPs) which has been developed and employed to treat dye-contaminated wastewater effluents [9]. This methodology would normally utilize a strong oxidizing species such as OH radicals produced in situ, which causes a sequence of reactions thereafter to break down the macromolecules into smaller and less harmful substances as shown in Figure 1.

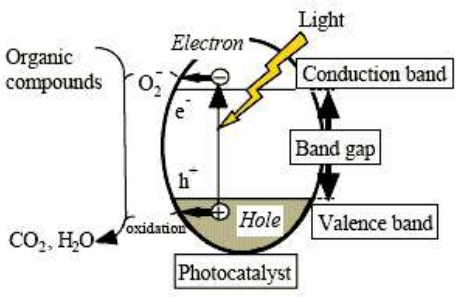


Fig. 1: Mechanism of Photocatalysis

In many cases the macromolecule is completely mineralized into water and carbon dioxide. The AOP technique has drawn considerable attention from various quarters of scientific community as it is easy to handle and produces significantly less residuals as compared to the classical approaches. Amongst the many techniques employed in the AOP approach are the UV photolytic technique [10,11], Fenton process [12,13], photo-Fenton process [14,15], ozonation process [16], sonolysis [17,18], photocatalytic approach [19,20], biodegradation [21,22] and the radiation induced degradation of dyes [23,24].

Various physico-chemical techniques are available for the elimination of dyes from wastewater and in particular photocatalysis is a more promising tool. Moreover, photocatalysis can be used to cause redox transformations and decompose a dye molecule. The use of photosensitive semiconductors such as TiO_2, ZnO, Fe_2O_3, CdS, ZnS and V_2O_5 has been reported in the literature for their use in reducing colour of the dye solutions owing to their environmental-friendly benefits in the saving of resources such as water, energy, chemicals, and other cleaning materials [25,26]. Titanium dioxide (TiO_2) mediated based photodegradation has attracted extensive interest owing to its great advantages in the complete removal of organic pollutants from wastewater [27]. This is mainly because of its various merits, such as optical-electronic properties, low-cost, chemical stability, and non-toxicity [28]. In this research, we have studied the photocatalytic process using TiO_2 in the form of slurry for the decolourization and mineralization of C. I. Basic Blue 41 (BB41).

MATERIALS AND METHODS

BB41, commercially called Cationic Blue GRL (C.I. 11105) is a reactive dye bearing an azo group as chromophore, with a molecular weight of 482.57 and

molecular formula $C_{20}H_{26}N_4O_6S_2$ was provided by Dongwu Dyestuff Co. Ltd. China. Titanium dioxide (Degussa P25) was utilized as a photo-catalyst. Its main physical data are as follow: average primary particle size around 21 nm, purity ~99.5% and BET surface area 50 ± 15 m^2 g/1. A UV–Vis Spectrophotometer, UV–1700 PharmaSpec, Shimadzu was used to determine the decolourization rate.

The photocatalytic activities of the photocatalysts were performed in a 400 ml jacketed glass reactor fitted with a 9W 5" long Philips (PL–S 9W/10/2P Hg) bulb made in Poland.

The slurry composed of dye solution and catalyst placed in the reactor was placed on a magnetic stirrer and stirred magnetically. Samples after photocatalytic treatment were centrifuged (6000 rpm, 10 min) and were filtered through a Millipore filter (0.45 μm) membrane and analyzed for the concentration of the BB41 in the solution using a computer software attached to UV–Vis Spectrophotometer, UV–1700 PharmaSpec, Shimadzu.

Photocatalytic degradation processes were performed using a 200ml solution containing a specified concentration of selected dye. Samples were withdrawn from sample points at certain time intervals and analyzed for decolourization and degradation. Decolourization of dye solutions was checked and controlled by measuring the maximum absorbance of dyes at different time intervals by UV–Vis Spectrophotometer, UV–1700 PharmaSpec, Shimadzu. The maximum absorbance of BB41 in the visible region of UV-Vis spectrum was 608 nm. COD tests were used to assay the mineralization of BB41.

RESULTS AND DISCUSSION

Decolourization kinetics

To estimate the kinetic parameters (k and n), and n^{th}-order rate, an equation of the form

$$-r_{dye} = -\frac{dC}{dt} = k.C^n$$

was used where k is the decolourization rate constant, 1/min). The first-order kinetic model ($n = 1$) was shown as follows:

$$-\ln\frac{C}{C_0} = kt$$

Fig. 1 shows the $-\ln(C/C_0)$ of BB41 versus irradiation time. As it is clear from Fig. 1 that decreasing the dye concentration obeys a linear pattern towards the elapse of irradiation time. This means that the pseudo-first-order kinetics relative to dye is operative.

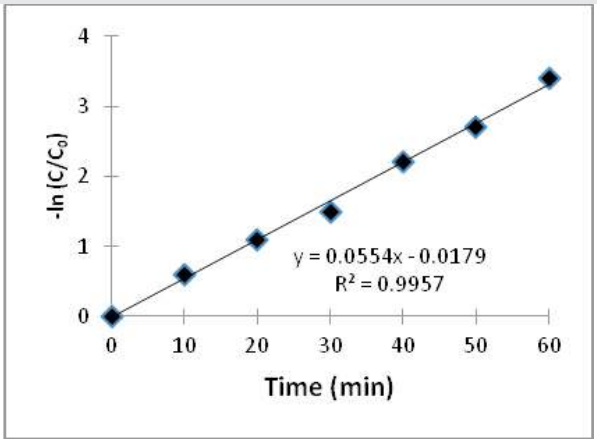


Fig. 2. Pseudo-first-order decolourization rate of BB41.

Effect of TiO_2 loading

The optimum concentration of TiO_2 P-25 required for the decolourization of a 50 mg L^{-1}

BB41 solution was examined with the slurry method by varying the catalyst amount from 0.0 – 1.0 g L^{-1} (Table 1). The results indicate that the required photons, when the concentration of TiO_2 increased to 0.4 g/L, were thoroughly absorbed. This shows that an increase in the amount of catalyst to the level consistent with the optimized level of light absorption increases the amount of decolourization [29-31]. Thus, any further increase of the amount of the catalyst will have no effect on the photodegradation efficiency.

Table : Effect of catalytic loading on photodegradation

S/No.	TiO_2 (gL^{-1})	K ($Lmol^{-1}min^{-1}$)
1	0.0	0.000
2	0.2	0.018
3	0.4	0.023
4	0.6	0.014
5	0.8	0.012
6	1.0	0.011

Effect of initial dye concentration

To study the effect of dye concentration on the rate of decolourization, the BB41 concentrations were varied from 0, 25, 50, 100 & 150 mg L^{-1} while the other variables were kept constant.

Fig. 3 shows the time dependence of unconverted fraction of dye (C/C_0, where C_0 is the initial dye concentration and C is the dye concentration at time t) for the various initial concentrations (0, 25, 50, 100 and 150 mg L^{-1}). Clearly, Table 2 shows that the first-order-kinetic relative to BB41 is operative. However, the apparent decolourization rate constant depends on the initial concentration of dye. As expected by increasing the concentration, the decolourization rate constant (k) is decreased (Table 2).

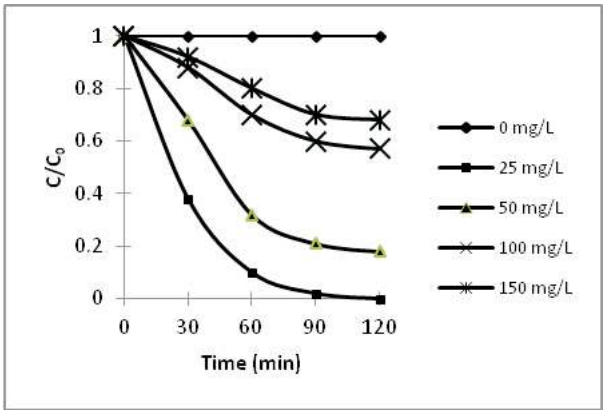


Fig. 3. Photocatalytic decolourization of BB41 with different TiO_2 loadings at different time intervals of irradiation

Table : Effect of dye concentration on photodegradation of Bb41

S/No.	Dye (gL^{-1})	K ($Lmol^{-1}min^{-1}$)
1	0.0	0.000
2	25.0	0.010
3	50.0	0,015
4	100.0	0.005
5	150.0	0.004

The efficiency of dye degradation decreased with an increase in concentration of dye. The reason presumed is that in high dye concentrations, the active sites are covered with dye ions; subsequently, the production of OHC radicals on the surface of catalyst is reduced. Other possible reasons for these results is the effect of UV screening of the own dye. In high dye concentrations a major amount of UV is apt to be absorbed by dye molecules proportional to OH particles and this reduces the efficiency of the catalytic reaction due to the decline in OHC and OH_2C concentrations [32]. Another possible reason is the intervention of the by-products formed during the degradation of mother dye molecules [33].

Effect of pH

Since dyes to degrade can be at different pHs in coloured effluents, comparative experiments were performed at three pH values: one reasonably acidic, one reasonably basic and at the natural pH 5.5 of BB41 (i.e. Natural pH of dye 5.5±2.5). The studies in this report were carried out at pH range 3.0 for the acidic solution and 8.0 for the basic solution.

The pH influences the characteristics of the photocatalyst surface charge, so pH of the solution is a significant parameter in performing the reaction on the surface of semiconductor particles. Point of zero charge (PZC) for TiO_2 particles is pH PZC = 6.8 [34]. The surface of TiO_2 has a positive charge in acidic media (pH <6.8), so there is an electrostatic absorption between positive charge surfaces of TiO_2 and the dye. As the pH of the system increases, the number of surfaces with negative charge increases. Thus, H_2SO_4 and NaOH were used for pH adjustment of dye solutions. The effect of pH on the degradation of dye is shown in Fig. 4.

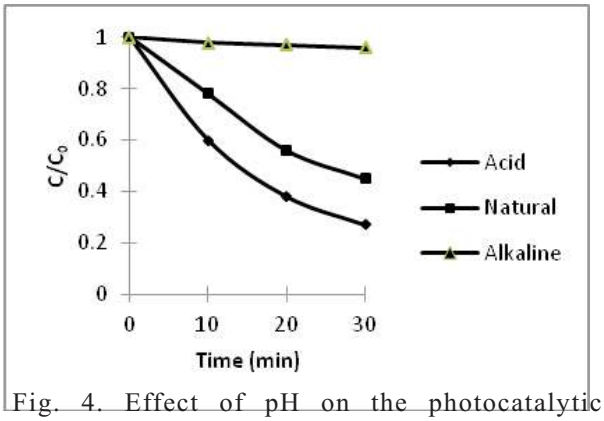


Fig. 4. Effect of pH on the photocatalytic decolourization rate of BB41 (C_0: initial dye concentration, C: dye concentration at time t).

Photocatalytic mineralization of BB41

In order to assess the degree of mineralization reached during the photocatalytic treatment, the COD test was used. Usually, COD decrease with increase in irradiation time whereas the amount of inorganic ions increased with increase in irradiation time. The COD curve has an exponential or sigmoidal shape. The sigma-shaped curves indicate that they are related to the formation of relative tolerant by-products [32]. This pattern means that during the first step of the process where the solution is still coloured there is only a small decrease of the parameter measured (COD) due to the fact that dye molecules are decomposed to lower molecular weight compounds and the resulting intermediates still contribute to the COD of solution. After the decolourization of the solution, the COD decreases sharply, reaching a plateau that corresponds to the oxidation of most stable compounds, indicating that almost complete mineralization of intermediates has occurred. Fig. 5. shows the decrease of COD with irradiation time

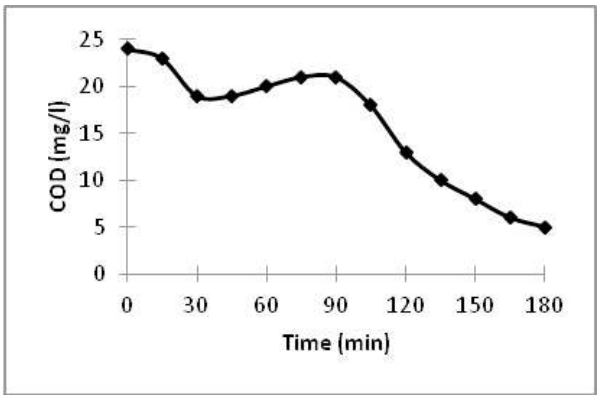


Fig. 5. Decrease of COD with irradiation time.

CONCLUSION

The photocatalytic treatment of a textile dye, C.I. Basic

Blue 41, from aqueous solution in a photocatalytic reactor was studied. The optimum values of the initial dye concentration was 50 g L^{-1} and the operation medium was alkaline. The results of TOC decrease and UV–Vis indicated that photocatalytic process can be used for complete decolorization and mineralization of Bb41.

REFERENCES

[1] S. Parsons, Advanced Oxidation Processes for Water and Wastewater, IWA Publishing, London, UK, 2004.

[2] M. Zubair Alam, S. Ahmad, A. Malik, M. Ahmad, Mutagenicity and genotoxicity of tannery effluents used for irrigation at Kanpur, India, Ecotoxicology and Environmental Safety 73 (2010) 1620–1628.

[3] N. Nasuha, B.H. Hameed, A.T.M. Din, Rejected tea as a potential low-cost adsorbent for the removal of methylene blue, Journal of HazardousMaterials 175 (2010) 126–132.

[4] M.A. Rauf, S.M. Qadri, S. Ashraf, K.M. Al-Mansoori, Adsorption studies of Toluidine Blue from aqueous solutions onto gypsum, Chemical Engineering Journal 150 (2009) 90–95.

[5] A.L. Ahmad, S.W. Puasa, Reactive dyes decolourization from an aqueous solution by combined coagulation/micellar-enhanced ultrafiltration process, Chemical Engineering Journal 132 (2007) 257–265.

[6] M. Riera-Torres, C. Gutiérrez-Bouzán, M. Crespi, Combination of coagulation–flocculation and nanofiltration techniques for dye removal and water reuse in textile effluents, Desalination 252 (2010) 53–59.

[7] K. Shakir, A.F. Elkafrawy, H.F. Ghoneimy, S.G. Elrab Beheir, M. Refaat, Removal of rhodamineB(abasicdye)and thoron(anacidicdye) fromdiluteaqueous solutions and wastewater simulants by ionflotation, Water Research 44 (2010) 1449–1461.

[8] S. Zodi, O. Potier, F. Lapicque, J.-P. Leclerc, Treatment of the industrial wastewaters by electrocoagulation: optimization of coupled electrochemical and sedimentation processes, Desalination 261 (2010) 186–190.

[9] M.A. Rauf, S.S. Ashraf, Application of Advanced Oxidation Processes (AOP) to dye degradation—an overview, in: Arnold R. Lang (Ed.), Dyes and Pigments: New Research, Nova Science Publishers, Inc, 2009.

[10] T.M. Elmorsi, Y.M. Riyad, Z.H. Mohamed, H.M.H. Abd El Bary, Decolourization of Mordant red 73 azo dye in water using H_2O_2/UV and photo-Fenton treatment, Journal of Hazardous Materials 174 (2010) 352–358.

[11] F.H. AlHamedi, M.A. Rauf, S.S. Ashraf, Degradation studies of Rhodamine B in the presence of UV/H_2O_2, Desalination 239 (2009) 159–166.

[12] A. Masarwa, S. Rachmilovich-Calis, N. Meyerstein, D. Meyerstein, Oxidation of organic substrates in aerated aqueous solutions by the Fenton reagent, Coordination Chemistry Reviews 249 (2005) 1937–1943.

[13] C. Bouasla, M.E.-H. Samar, F. Ismail, Degradation of methyl violet 6B dye by the Fenton process, Desalination 254 (2010) 35–41.

[14] J.M. Monteagudo, A. Durán, I.S. Martín, M. Aguirre, Catalytic degradation of Orange II in a ferrioxalate-assisted photo-Fenton process using a combined UV-A/C-solar pilot-plant system, Applied Catalysis B: Environmental 95 (2010) 120–129.

[15] A.K. Abdessalem, N. Bellakhal, N. Oturan, M. Dachraoui, M.A. Oturan, Treatment of a mixture of three pesticides by photo- and electro-Fenton processes, Desalination 250 (2010) 450–455.

[16] A.R. Tehrani-Bagha, N.M. Mahmoodi, F.M. Menger, Degradation of a persistent organic dye from coloured textile wastewater by ozonation, Desalination 260 (2010) 34–38.

[17] S. Merouani, O. Hamdaoui, F. Saoudi, M. Chiha, Sonochemical degradation of Rhodamine B in aqueous phase: effects of additives, Chemical Engineering Journal 158 (2010) 550–557.

[18] X. Wang, Z. Yao, J. Wang, W. Guo, G. Li, Degradation of reactive brilliant red in aqueous solution by ultrasonic cavitation, Ultrasonics Sonochemistry 15 (2008) 43–48.

[19] M.A. Rauf, M.A. Meetani, A. Khaleel, A. Ahmed, Photocatalytic degradation of Methylene Blue using a mixed catalyst and product analysis by LC/MS, Chemical Engineering Journal 157 (2010) 373–378.

[20] R. Xu, J. Li, J. Wang, X. Wang, B. Liu, B. Wang, X. Luan, X. Zhang, Photocatalytic degradation of organic dyes under solar light irradiation combined with Er^{3+}: $YAlO_3$/Fe- and Co-doped TiO_2 coated composites, Solar Energy Materials and Solar Cells 94 (2010) 1157–1165.

[21] L. Ayed, K. Chaieb, A. Cheref, A. Bakhrouf, Biodegradation and decolourization of triphenylmethane dyes by Staphylococcus epidermidis, Desalination 260 (2010) 137–146.

[22] Ö. ÇInar, S. Yasar, M. Kertmen, K. Demiröz, N.Ö. Yigit, M. Kitis, Effect of cycle time on biodegradation of azo dye in sequencing batch reactor, Process Safety and Environmental Protection 86 (2008) 455–460.

[23] A. Vahdat, S.H. Bahrami, M. Arami, A. Motahari, Decomposition and decolouration of a direct dye by electron beam radiation, Radiation Physics and Chemistry 79 (2010) 33–35.

[24] K.A. Mohamed, A.A. Basfar, A.A. Al-Shahrani, Gamma-ray induced degradation of diazinon and atrazine in natural groundwaters, Journal of Hazardous Materials 166 (2009) 810–814.

[25] L. Andronic, A. Enesca, C. Vladuta, A. Duta, Photocatalytic activity of cadmium doped TiO_2 films for photocatalytic degradation of dyes, Chemical Engineering Journal 152 (2009)

64–71.
[26] Z.M. El-Bahy, A.A. Ismail, R.M. Mohamed, Enhancement of titania by doping rare earth for photodegradation of organic dye (Direct Blue), Journal of Hazardous Materials 166 (2009) 138–143.
[27] U. Diebold, The surface science of titanium dioxide, Surface Science Reports 48 (2003) 53–229.
[28] Y.B. Xie, X.Z. Li, Interactive oxidation of photoelectrocatalysis and electro-Fenton for azo dye degradation using TiO_2–Ti mesh and reticulated vitreous carbon electrodes, Materials Chemistry and Physics 95 (2006) 39–50.
[29] A.F. Caliman, C. Cojocarru, A. Antoniadis and L. Poulios, J. Haz. Mat., 144 (2007) 265–273.
[30] A.B. Prevot, M. Vincenti, A. Bianciotto and E. Pramauro, Appl. Catal. B: Environ., 22 (1999) 149.
[31] J.P. Percherancier, R. Chapelon and B. Pouyet, J. Photochem. Photobiol. A: Chem., 87 (1995) 261.
[32] I.K. Konstantinou and T.A. Albanis, Appl. Catal. B,49 (2004) 1.
[33] N.M. Mahmoodi, M. Arami, N.Y. Limaee, K. Gharanjig and F. Doulati Ardejani, Coll. Surf. A: Physicochem. Eng. Aspects, 290 (2006) 125.
[34] F. Zhang, J. Zhaoa, T. Shen, H. Hidaka, E. Pelizzetti and N. Serpone, Appl.Catal. B: Environ., 15 (1998) 147.

EFFECTS OF SOME HEXOSE SUGARS ON THE RETROGRADATION AND STABILITY TO SUNLIGHT OF MAIZE (*Zea mays*) AND WHEAT(*Triticun aestivum*) STARCHES

[1]*Abba, H., [2]Adamu, I. K., [3]Kogo, A.A. and [2]Bello, H.
[1]Department of Chemistry, Ahmadu Bello University, P.M.B. 1045, Zaria, Nigeria.
[2]Nigerian Institute of Leather Science and Technology, P.M.B. 1034, Zaria, Nigeria.
[3]Department of Textile Science and Technology, Ahmadu Bello University, Zaria, Nigeria.
*Author for Correspondence: hamzaabbah@yahoo.com

ABSTRACT
Adhesives were prepared by adding fructose, galactose and glucose to air-dried maize and wheat starch powders in water and exposed to sunlight for four weeks. The extent and rate of retrogradation and stabilization of the prepared and commercial adhesives were comparatively assessed from the changes in their adhesion properties (peel load, relative viscosity and rolling ball distance). From the results, the order: fructose >> glucose > galactose in stabilization of the starches against retrogradation was established. The rate and extent of retrogradation were found to depend on both the botanic source and time of exposure: maize-based adhesives retrograded to higher degree than wheat-based adhesives and all the samples retrograded to greater extent when exposed for longer period. These results are due to maize starch being less dispersed in aqueous solution than the wheat starch and that longer exposure time causes the disordering effect of Brownian motion of the macromolecules to be too intense for association (**retrogradation**) of the samples to take place easily.

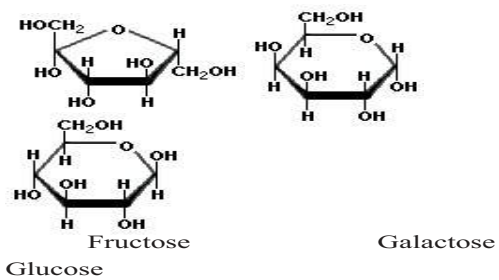
Keywords: adhesion, cere**al,** hexose sugar, retrogradation, starch, viscosity

INTRODUCTION

Interest in both the fundamental and applied sciences of adhesion (molecular attraction exerted between bodies in contact), still grows apace. Adhesive bonding is being increasingly employed in preference to other fastening techniques [8]; [9].

Starch is a highly organized mixture of two carbohydrate polymers, amylose (consisting of linear chains) and amylopectin (composed of branched chains) of glucose units and is used primarily because of its thickening, gelling, adhesive, and film-forming properties [2]. This versatile combination of properties in conjunction with availability, controlled quality, and low cost was reported to be responsible for the widespread domestic and industrial applications of starch [7]; [10]. However, retrogradation (re-association of molecular chains into an ordered structure) limits both the industrial and domestic uses of native starches [5]**;** [6]

Fructose, galactose and glucose are hexose (six-carbon) sugars having $C_6H_{12}O_6$ as their molecular formula and the following molecular structures [3]**;** [4].



Both maize (*Zea mays*) and wheat (*Triticun aestivum*) are annual cereal crops with high (more than 70%) starch content and grown abundantly in northern Nigeria [1].

The aim of this study was to comparatively evaluate the susceptibility and resistance to retrogradation of native maize and wheat starches and in the presence of three hexose sugars in comparison to a commercial adhesive during exposure to sunlight for four weeks.

MATERIALS AND METHODS

Afr**ican millet** grains and potato tubers were purchased at Azare, Bauchi State, Nigeria; f**ructose, galactose and glucose were obtained from Riedel-de Haën Sigma-Aldrich (Seelze, Germany);** commercial adhesive (Araldite AY 1566 GB) was supplied by Ciba-Geigy, Switzerland; Na_2SO_3, NaCl, NaOH and $Mg(OH)_2$ were analytical grade reagents from BDH, Poole, UK and used as-received.

Production of the Native Starches: **1** kg of the African millet grains is thrashed and soaked in 5 litres of 0.2% Na_2SO_3 solution. After soaking for 48 hrs, the resulting native starch is ground and sieved after dewatering in hot air oven at 40 to 50°C to a constant mass. Potato starch is extracted by washing the tubers with water, peeling, slicing, rewashing and grating to obtain the pulp which is then sieved through muslin bag. The filtrate (starch milk) is allowed to stand 24 hrs for the starch to settle before decanting the supernatant to obtain wet starch cake. The cakes are sun dried, ground into fine powder and

packaged into transparent polyethylene bags.

Preparation of the Adhesives: Suspension is prepared by putting 25 g powder of each of the native starches into 100 cm^3 of distilled water in a one-litre beaker containing 10 g of each hexose sugar. The suspension is heated gently with vigorous stirring until gelation occurs. The gel obtained is tackified with 4 cm^3 of 0.1M 1:1 mixture of NaOH and $Mg(OH)_2$. The pure millet and potato starches are used as control for comparison to the sugar-containing formulations.

Measurement of Peel Load: Cardboard laminates measuring 15 cm X 3 cm with bond area of 6 X 3 cm are made by adding 1.5 g of each adhesive formulation. The bonded laminates are exposed rooftop for 4 weeks (average room temperature being 27°C) and the peel strength of the bonds tested each week by clamping one end of the laminate and turning the other end 180° downwards and attaching a load pan to it. Increasing standard weights are added to the pan until the adhesive-laminate bond begins to peel. Three replicate minimum loads needed for the peel to begin are recorded before and after exposure to sunlight and the average value reported for each adhesive formulation as its peel load change.

Measurement of Relative Viscosity: The efflux time (t) it takes 20 cm^3 of each of the adhesive solutions to flow through an Ostwald's viscometer is noted and related to the corresponding efflux time (t_o) for 20 cm^3 of water at room temperature (27°C). The relative viscosity ($\acute{\eta}_{rel}$) of each adhesive solution is then obtained from the expression: $\acute{\eta}_{rel} = \acute{\eta} / \acute{\eta}_o = t / t_o$ where $\acute{\eta}$ is the intrinsic viscosity of the adhesive solution and $\acute{\eta}_o$ is the intrinsic viscosity of water, respectively. 10 minutes were allowed for the viscometer and each of the adhesive solutions to attain thermal equilibrium. Three replicate measurements are taken for each sample before and after exposure to sunlight and the average value reported as its relative viscosity change.

Measurement of Rolling Ball Distance: A flat plane is inclined at 45° to the horizontal and a 120μm-thick adhesive film of each of the adhesive formulations is placed on this surface, the tacky surface uppermost. A small ball or roller is allowed to roll down the plane for 15 cm before rolling on the tacky surface where its movement is arrested. Three replicate distances the ball or roller moves on the tacky surface is recorded before and after exposure to sunlight and the average reported as its change in rolling distance.

RESULTS AND DISCUSSION

Peel load, the amount of weight an adhesive can support before **breaking** off the pure maize and wheat starches in comparison to the hexose sugar-containing and commercial (Araldite) adhesives after being exposed to sunlight for four weeks is shown in Table 1. From the table, it can be observed that the pure (control) maize and wheat starches gave lower values of peel load compared to their hexose sugar-containing counterparts exposed to the same time period. It can also be observed that the peel loads of all the adhesives decrease with increase in period of exposure to sunlight. It can be observed that wheat-based adhesives support about 10 g higher than maize-based adhesives. Further, wheat-based adhesives can be observed to have lost about 3 g weekly in comparison to 5 g lost by maize-based adhesives. This result indicates that maize-based adhesives are inferior to wheat potato-based adhesives in adhesion efficiency. This goes to imply that maize-based adhesives are less stable and retrograded to higher degrees than wheat-based adhesives. A closer look at Table 1 reveals that the efficiency of the three hexose sugars in stabilizing the native starches against retrogradation is in the order: **f**ructose > glucose > galactose. The commercial adhesive is the most stable and decreases by about only 1.1 g per week. It might contain some stabilizers against sunlight

Displayed in Table 2 are the r**elative viscosities** of the pure (control) maize and wheat starches in comparison to the hexose sugar-containing and commercial (Araldite) adhesives exposed to sunlight for four weeks. From the table, it can be observed that the r**elative viscosities** of the sugar-containing adhesives are lower than those of the control starches. It can also be observed that wheat-based adhesives gave about 5.2% higher relative viscosity values than maize-based adhesives. The relative viscosities of maize-based adhesives can be seen to increase by about 4% per week, in contrast to about 2.5% per week for the wheat-based adhesives. These results imply that ma**ize-**based adhesives retrograde (the starch molecules re-associate) at a faster rate than the **wheat-**based adhesives. The commercial adhesive can be observed to be the most stable, as it increases by only about 0.3% on weekly basis. It might contain some visco-static agents that stabilized against the sunlight.

The results of the r**olling ball distances** of both the pure (control) maize and wheat starches, sugar-containing and the commercial (Araldite) adhesives exposed to sunlight for four weeks are shown in Table 3. From the table, it can be observed that the rolling ball d**istances of maize-**based adhesives are about 2.1 **cm longer than wheat-**based adhesives. The rolling ball d**istances of maize** based adhesives can be seen to decrease by about 0.6 cm per week, in contrast to **about** 0.3cm per week for **wheat-**based adhesives. From the inverse relation between viscosity (Table 2) and rolling distance (Table 3), it can seen that the higher the viscosity, the shorter the rolling ball distance, and **the faster the rate of retrogradation. Again, t**he commercial adhesive can be seen to be the most stable, as it increases by only about 0.7 cm every week.

CONCLUSION

On the basis of the results obtained in this study, it can be concluded that, although to varying extents, all the hexose sugars have stabilized the native maize and wheat starches against retrogradation. Maize-based adhesives retr**o**graded more (less stable) than wheat-

based adhesives for the same exposure period. Since the adhesion properties of the prepared adhesives compare favourably to that of the commercial adhesive, the hexose sugars are recommended for use to prolong the shelf life of the two native starches. This is because the single biggest problem facing adhesive chemists and technologists today is that of long term durability of the native adhesive formulations exposed outdoors.

REFERENCES

1. Abdellatif, M., Steven, C. P., Linda, A. G. and Patricia, R-D. (2006). Effect of Jet-Cooked Wheat Gluten/Lecithin Blends on Maize and Rice Starch Retrogradation, *Journal of Cereal Science* 43, 293–300
2. Brown, L. and Holme, T. (2011). Chemistry for Engineering Students, 2nd edn, Brooks/Cole, Centage Learning, Belmont, pp.265-272.
3. Bruice, P.Y. (2011). Organic Chemistry, 6th edn, Pearson Education, Inc., New York, pp.940-975.
4. Carey, F.A. (2008). Organic Chemistry, 7th edn, McGraw-Hill Companies, Inc., New York, pp.1022-1062.
5. Jang, J.K., Lee, S.H., Cho, S.C. and Pyun, Y.R. (2001). Effect of Sucrose on Glass Transition, Gelatinization, and Retrogradation of Wheat Starch, *Cereal Chemistry* 78(2), 186-192.
6. Parker, R. and Ring, S.G. (2001). Some Aspects of the Physical Chemistry of Starch, *Journal of Cereal Science* 34, 1-17.
7. Ratnayake, W. S., Hoover, R. and Warkentin, T. (2002). Pea starch: Composition, Structure and Properties – A Review, *Starch* 54, 217–234.
8. Rubinstein, M. and Colby, R. (2006). *Polymer Physics*, Oxford University Press, Oxford, pp.633-675.
9. Sasaki, T. (2002). Comparison of Physical Properties of Wheat Starch Gels with Different Amylose Content, *Cereal Chemistry* 79, 861–866.
10. Xu, J., Bietz, J.A., Felker, F.C., Carriere, C.J. and Wirtz, D. (2001). Rheological Properties of Vital Wheat Gluten Suspensions, *Cereal Chemistry* 78, 181–185.

Table 1. Peel loads of the pure maize and wheat starches (control) in comparison to the hexose sugar-containing and commercial (Araldite) adhesives exposed to sunlight for four weeks.

Starch	Sugar	Peel load (g)			
		First week	Second week	Third week	Fourth week
Maize	Control	39.3	32.4	25.5	18.3
	Fructose	46.2	41.3	36.1	31.3
	Galactose	41.4	36.3	31.2	26.4
	Glucose	42.1	37.2	32.2	27.3
Wheat	Control	49.5	44.4	39.2	34.1
	Fructose	56.1	53.2	50.3	47.2
	Galactose	50.8	47.7	44.6	41.5
	Glucose	52.3	49.2	46.1	43.2
	Araldite	67.6	65.7	64.5	63.4

Table 2. **Relative viscosities** of the pure maize and wheat starches (control) in comparison to the hexose sugar-containing and commercial (Araldite) adhesives exposed to sunlight for four weeks.

Starch	Sugar	Relative density (%)			
		First week	Second week	Third week	Fourth week
Maize	Control	16.2	19.3	22.2	25.1
	Fructose	10.6	13.5	16.7	19.4
	Galactose	15.1	18.2	21.3	24.1
	Glucose	12.6	15.4	18.5	21.3
Wheat	Control	21.4	23.3	25.2	27.1
	Fructose	15.9	18.8	20.7	22.8
	Galactose	20.2	22.2	24.1	26.2
	Glucose	17.9	15.9	18.1	20.2
	Araldite	12.3	12.7	12.9	13.2

Table 3. Rolling ball distances of the pure maize and wheat starches (control) in comparison to the hexose sugar-containing and commercial (Araldite) adhesives exposed to sunlight for four weeks.

Starch	Sugar	Rolling ball distance (cm)			
		First week	Second week	Third week	Fourth week
Maize	Control	11.9	9.2	8.7	8.2
	Fructose	11.6	6.8	6.3	5.8
	Glactose	11.0	8.7	8.2	7.7
	Glucose	11.1	8.0	7.5	6.9
Wheat	Control	9.8	7.5	6.8	6.0
	Fructose	9.5	5.1	4.5	3.7
	Galactose	9.1	7.1	6.3	5.6
	Glucose	9.2	6.3	5.6	5.1
	Araldite	8.5	8.4	8.3	8.1

MODIFYING MEIONITE SILICATE FOR EFFECTIVE REMOVAL OF ORGANIC CONTAMINANTS FROM SOLUTIONS

Ikhuoria E.U and Enivwenae B.O.
Department of Chemistry University of Benin, Benin City, Nigeria
ikhuoria@uniben.edu.ng

ABSTRACT
Meionite Clay modified with hexadecylpyridinium bromide (HDPB) at 25%, 50%, 75% and 100% of its original C.E.C was used in sorption of phenol and chlorophenol contaminants from solution. Sorption was characterized over a wide range of solute concentrations.
Increase in surfactant loading on the meionite clay up to 100% of its C.E.C, indicated enhanced sorptive property for aromatic organic compounds (phenol and Chlorophenol).
The mechanism supporting the sorption of phenol and chlorophenol onto the meionite inter layers were deduced from the shape of the isotherms. The shapes of the isotherms indicate a double sigmoid isotherm, suggesting multiple mechanisms as responsible for the enhanced sorptive characteristic of the hexadecyl pyridium cation modified meionite. A double sigmoid Isotherm is comprised of a type III isotherm and a sigmoid isotherm. Type III isotherm explains partitioning of organic solutes onto the organoclays while the sigmoid isotherm explains solvation.

Keyword: Organoclay, Meionite, Sorption, hexadecylpyridinium bromide (HDPB)

INTRODUCTION

The environmental impact of organic contaminants is increasingly becoming a major cause of concern. Organic contaminants arising from household chemicals and from the industries do find their way into soil and underground water. The health implications of this have been documented in literature[1].

In Nigeria, the siting of fuel filling stations, the installation of underground oil storage tanks and oil tank farms have also contributed to the contamination of soil and underground water.

Researches had indicated that humic soil to some extent has the ability of removing organic contaminants from water [2]. Further works showed that the ability of soil to remove organic contaminants from solutions was a function of the total organic carbon content of the soil and sediments [3]. These studies indicate that materials with high organic carbon content could be employed in the removal of organic contaminants from solutions.

Minerals are usually low in organic carbon content and are therefore not suitable as sorbents even though they are readily available and relatively inexpensive. However, the clay minerals known to have permanent negative charges on their surfaces can be modified with cationic surfactants of the form $[(CH_3)_3NR]^+$ or $[(CH_3)_2NRR']^+$ in order to raise their organic carbon content and therefore their sorption for organic contaminants. The use of surfactant modified clay (known as organoclay) to remove organic contaminants from water was first introduced by Boyd in1988 [4].

Organoclays are therefore very useful and find applications in the treatment of contaminated waters and as protective barriers in waste disposals and oil reservoirs.

During the modification of the clay, the interlameller spaces of the clay are occupied by the alkyl chains or R groups. The alkyl chains of the surfactants are usually lipophilic. A conglomeration of the alkyl chains on the clay surfaces and interlayer regions result in the formation of an organic phase that controls the sorptive removal of organic contaminants from water [4][5][6][7][8].

In the present study, the effect of surfactant loading on the sorptive properties of organoclay was examined. Clay modified with hexadecylpyridinium bromide (HDPB) at 25%, 50%, 70% and 100% of its original C.E.C was used to sorb organic contaminants from solution. Sorption was characterized over a wide range of solute concentrations. The mechanisms responsible for the sorption property of the organoclay were also deduced

The clay mineral used in this study was meionite. Meionite belongs to the silicate group, tectosilicate, a framework silicate. Like the phyllosilicate clay minerals, meionite has an isomorphous substitution of Aluminium in the silicate structure as shown in the chemical formular, $Ca_4[CO_3][(Al_2Si_2O_8)_3]$.

The quaternary ammonium surfactant used in this study was hexadecyl pyridinium bromide.

EXPERIMENTALS

Clay Extraction:

The clay particles were obtained through wet sedimentation of the ore obtained from Edo north geographical area of Nigeria and subsequent decantation of the <2μm particles through a 2μm mesh filter in accordance with stroke's law. The C.E.C was measured to be 30.10Meq/100g. The major exchangeable cation was Ca^{2+}, with Mg^{+2} and Fe^{+2} in small amounts.

Na-Clay:

Na-Clay was obtained by saturation of the pure clay with sodium chloride and subsequent washing with de-ionized water until pH was 7. Na-Clay obtained was stored in a sealed bottle.

Organoclay:

20g of Na- clay was first dispersed in about 300ml of de – ionized water to which a desired amount of the hexadecyl pyridinium bromide was slowly added. The concentration of the hexadecyl pyridinium cations were 0.25 CEC, 0.50 CEC, 0.75 CEC and 1.00 CEC of the clay respectively.

The reaction mixture was agitated overnight on a magnetic stirrer at room temperature. The organoclays suspensions were then washed with de-ionized water repeatedly until free of bromide ions as indicated by $AgNO_3$ in the classical silver mirror test for bromides. All products were dried at 90^0C in the oven and ground in an agate mortar and than stored in sealed bottles for further use. The organoclays prepared at the concentration of 0.25 CEC, 0.50 CEC, 0.75 CEC and 1.00 CEC were labeled DX, CX BX and AX respectively.

XRD-Characterization

XRD was used to determine the mineralogical composition of the raw material component of the clay. Aqueous suspension of the clay was made by dispersing grains of the clay in few drops of de-ionized water. Drops of the suspension were then placed on the glass slide which was immediately covered with a Teflon tape to prevent vapour loss. X – ray diffraction patterns where recorded using a Philips APD3720 automated X – ray diffractometer.

ADSORPTION OF PHENOL & CHLOROPHENOL USING 25%, 50%, 75% AND 100% HEXADECYL PYRIDINIUM CATION MODIFIED MEIONITE FROM AQUEOUS SOLUTIONS

The batch equilibrium method was implored in obtaining the adsorption isotherms of phenol & chlorophenol on HDPB – modified clay at the various percentages [10].

0.2g of 25%, 50%, 75% and 100% HDPB modified clay were each weighed into corex glass centrifuge tubes. 25ml of phenol or chlorophenol solution at different concentrations were added to the tubes. The tubes were capped with Teflon–backed septa immediately. The tubes were shaken for 24 hours with a mechanical shaker at room temperature. Preliminary experiments showed that sorption reached equilibrium within 18hours. After equilibrium, the tube was centrifuged at 400 rpm for 30 minutes to obtain the supernatant.

Aliquot was taken from the supernatant and its absorbance was measured from the spectrophotometer. From the calibration curve obtained by a set of working standards of phenol or chlorophenol, the concentration of phenol or chlorophenol in the supernatant was determined.

Amounts of phenol or chlorophenol adsorbed were then calculated from the differences between the amount added and that remaining in the final equilibrium solutions.

RESULTS AND DISCUSSIONS.

The C.E.C was determined to know the exchange capacity of cations in the clay as well as that of the modified clay as surfactant loading progresses. The C.E.C values are given in Table 1.

Sorption isotherms of phenol and p-chlorophenol from aqueous solution onto the organoclay at different modifications levels are shown in figures 1 and 2. The distribution and interaction of the surfactant cations in the interlayers of meionite has a pronounced effect on the adsorption of phenol and chlorophenol.

The results indicate that partial replacement of Na^+ (of the Na- clay) with hexadecyl pyridinium cations increases the adsorptive property of meionite to some extent. With increase in surfactant loading, more sodium ions were replaced by the surfactant cations and sorption was further increased. From Table1, it is seen that the C.E.C of the organoclay started diminishing as the percentage of surfactant loading increases. The low values of C.E.C indicate that Na^+ are being exchanged by hexadecyl pyridinium cations that seem to have greater affinity for the inter layers of the meionites. A similar study by Sheng and Boyd, also showed this inverse proportional trend in the adsorption of trimethyl phenyl ammonium (TMPA) cations by a calcium saturated smectite and the subsequent discharge of Ca^{2+} [9].

It is also noticed that subsequent increase in the concentration of both phenol and Chlorophenol had progressive effect on their sorption. This is evidenced in the gradual rise of the curves. This is more pronounced in the adsorption of chlorophenol sorption.

The mechanism supporting the sorption of phenol and chlorophenol onto the meionite inter layers can be deduced from the shape of the isotherms. The shapes of the isotherms indicate a double sigmoid isotherm, suggesting multiple mechanisms as responsible for the solute sorption. A double sigmoid Isotherm comprises of a type III isotherm and a sigmoid isotherm. Type III isotherms explain partitioning of organic solutes onto the organoclays while the sigmoid isotherm explains solvation [11]. From figure 1, the earliest linearity of the isotherms indicate a type III isotherm which indicate partitioning of phenol and chlorophenol onto the modified meionite. With the total organic content increasing, solvation of the ammonium centers by the aromatic compounds occurs, bringing about the wavelike nature of the isotherms pronounced in figure 2.

It has been proposed that multiple mechanism where involved in the sorption of aromatic compounds by hexadecy trimethyl Ammonium clays (HDTMA – Clays) [9]. Aromatic molecules, due to their planar shape and delocalized pi – orbital, interact strongly with HDTMA, causing a re-orientation of the alkyl chains. These solute molecules solvate the cationic ammonium centers and alkyl chains of HDTMA , causing a transition from a parallel to more vertical position relative to the silicate sheets [12]. Solutes molecules are concomitantly adsorbed on the vacated mineral surfaces yielding a sigmoid isotherm. This explains the increase in sorption

with increase in concentration of solutes. It is the combination of the sigmoid isotherm (arising from solvation) and the type III isotherm (arising from solute partitioning) that produces the double sigmoid shaped isotherms which is also observed in this present work.

CONCLUSION

Increase in surfactant loading on meionite clay up to 100% of its C.E.C by hexadecyl pyridinium cations enhances its sorptive property for aromatic compounds (phenol and Chlorophenol).

Multiple mechanisms comprising of partitioning and solvation were also found to be involved in the enhanced sorption characteristic of the hexadecyl pyridium cation modified meionite on aromatic contaminants.

REFERENCES

1. Ademoroti C.M.A (1996) "Environmental Chemistry and Toxicology". Foludex Press Ltd. Ibadan.
2. Chiou C.T, Porter P.E, and Schmedding D.W. (1983) "Partition Equilibria of Nonionic Organic Compounds between Soil Organic matter and Water". Environ Sci Technol 17:22-231
3. Zhaohui L, Daniel A, Lori A. (2002) "Influence of Quaternary Ammonium on Sorption of Selected Metal Cations onto Clinoptilolite Zeolite". Journal of Environmental Quality 31:1106-1114
4. Boyd S.A, Lee J.F, Mortland M.M. (1988) "Attenuating Organic Contaminant Mobility by Soil Modification Nature 333: 345-347.
5. Mortland M.M, Sun S, Boyd S.A. (1986) "Clay-Organic complexes as Adsorbents for Phenol and Chlorophenols". Clay and Clay Miner 34: 581 –585
6. Boyd S.A, Morthland M.M, Chiou Ct. 1988. "Sorption Characteristic of organic compounds on hexadecytrmethlammium-smectite". Soil Sci Am J 52:652-657
7. Boyd S.A, Jaynes W.F, Ross B.S. (1991). "Immobilization of Organic Contaminants by Organo- clays: Organic Substance and sediments in waters". Vol 1. Boca Raton FL. 181- 200.
8. Boyd S.A., Jaynes W.F, Ross B.S. Lee J.F, Mortland M.M. (1988). "Pentachlorophenol Sorption by Organo-clays". Clays Clay miner 36:125-130
9. Sheng G, Xu S, Boyd S.A. (1996). "Mechanisms Controlling Sorption of Neutral Organic Contaminant by Surfactant Derived and Natural Organic Matter". Environ Sci Technol 30: 1553-1557
10. Lee J.F, Mortland M.M, Boyd S.A, Chiou C.T, Kile D.E (1990) "Adsorption of Benzene, Toluene, and Xylene by 2-tetramethylammonium-smectite having Different Charge Densities". Clays and Clay Miners 38:113-120.
11. Gregg S.J, Sing K.S.W (1982) "Adsorption, Surface Area, and Porosity. New York; Academic Pr 303p.
12. Jaynes W.F, Boyd S.A. (1991) "Hydrophobicity of Siloxane Surfaces in Smectites as Revealed by Aromatic Hydrocarbon Adsorption From Water". Clays and Clay Miner 39: 428-436

TABLES AND FIGURES

Table 1: *C.E.C value for Clay/organoclays*

Clay Type	C.E.C (Meq/100g)
Raw Clay	30.10
25% Modification	13.28
50% Modification	9.42
75% Modification	5.30
100% Modification	3.61

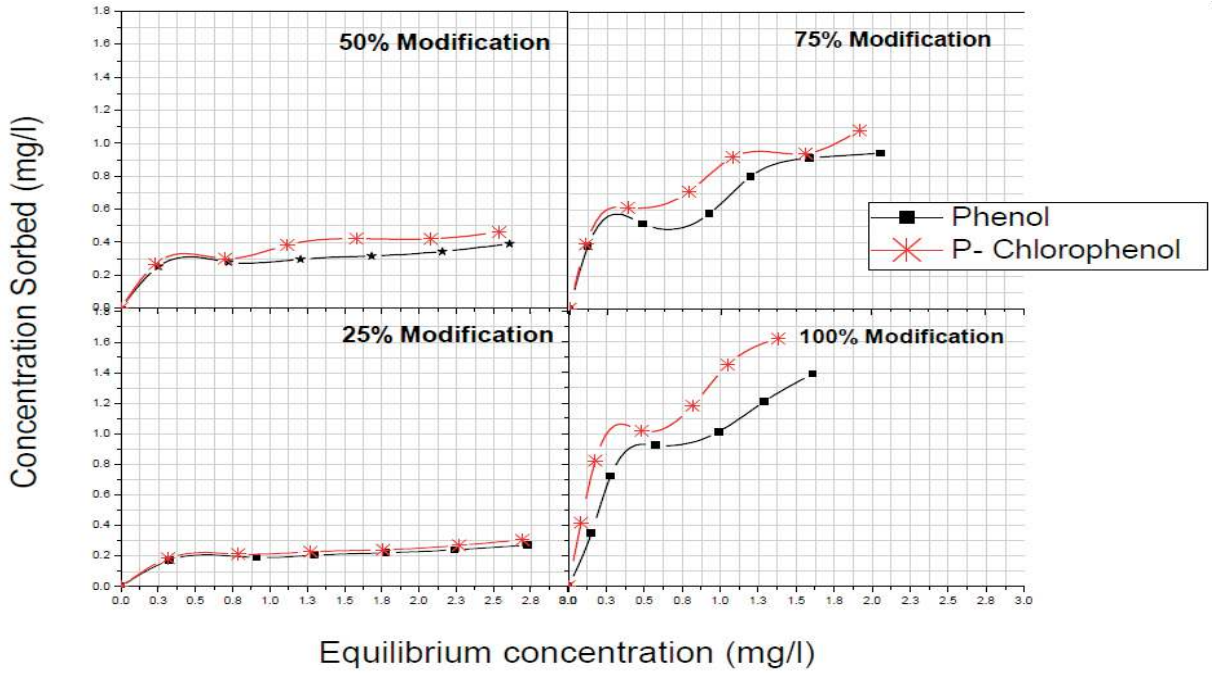


Figure 1: Sorption Isotherm of phenol and p- chlorophenol at 25%, 50%, 75% and 100% modification.

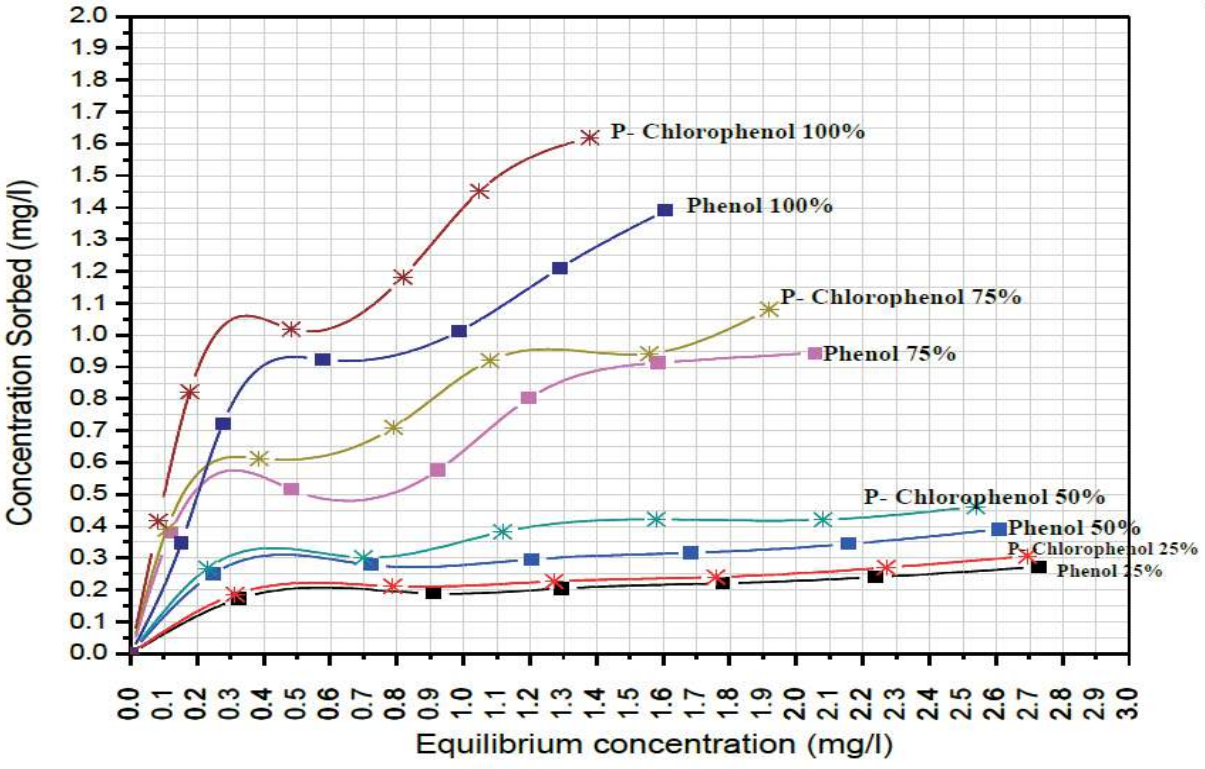


Figure 2: Combined Sorption Isotherms of phenol and p- chlorophenol at 25%, 50%, 75% and 100% modification.

IMPLANTABLE BIOMEMS DEVICES FOR LOCALIZED CANCER DRUG DELIVERY

[1]Danyuo Yiporo, S.O. Dozie-Nwachukwu[2]., G.A. Etuk-Udo[2]., O. Oberiafor[2]., M.C. Ilouno[3]., T.M. Meshack[3]., A. Agwu[4]., O. S. Odusanya[2] and W. O. Soboyejo[1&5]

[1]African University of Science and Technology (AUST), Abuja, [2]Sheda Science and Technology Complex (SHESTCO). [3]University of Jos, [4]Federal University of Technology, Mina. [3]Department of Mechanical and Aerospace Engineering & Princeton Institute of Science and Technology of Materials (PRISM)[5], Princeton University USA.

ABSTRACT

Implantable Bio-Micro-Electro-Mechanical Systems (BioMEMS) represent a new class of devices that can provide localized cancer drug delivery by the combined effect of chemotherapy and hyperthermia which gives it an advantage over prior devices. The current work presents the results of a theoretical and experimental study of a novel implantable drug delivery device. Prototype Poly-di-methyl-siloxane (PDMS) packages with well-controlled micro-channels, and drug storage compartments were fabricated along with a drug storing polymer produced by free radical polymerization of N-isopropylacrylamide and Acrylamide. The swelling due to the uptake of water, bromophenol blue and a bacterial extract - prodigiosin (an apoptotic agent), were studied using weight gain experiments conducted over temperatures within the range in which hyperthermia (28-48°C) could occur during drug delivery. These studies provided understanding of the underlying mechanisms of diffusion and swelling of these PNIPA-based gels. The results show that drug release may be well described by monolithic and membrane diffusion models. The *in-vitro* studies at 43˚C indicate that a lesser amount of drug delivery is achieved when the delivery is accompanied with heat. Morphological studies with an environmental Scanning Electron Microscope (SEM) reveal a polymeric network of the PNIPA-based gels. The diffusion coefficients obtained varied from 2.10 x10^{-12} m^2/s at 28℃ to 4.8162x10^{-6} m^2/s at 48℃. The results obtained from the release exponent as well as the diffusion coefficient from the gels were consistent to prior work. The release exponents were within 0.507- 0.697, indicating a non-Fickian diffusion.

1.0 Introduction

The incidence of cancer in the world today is a public health problem which has fueled philanthropists, the sponsors, researchers, and engineers to actively get involved in finding better strategies for early detection and treatments for cancer. The development of drug delivery devices, a part of which this work addresses, has been the focal point of research in recent years [1, 4].

Cancer is the second leading cause of death in the world [5]. It is second only to cardiovascular diseases [6, 7] and is likely to become the leading cause of death globally by 2030, if the current trends continue [8]. The biggest problem lies on the possibility of early stage detection. Moreover, the existing methods of treatment are based on surgical procedures, radiation therapy, including bulk systemic chemotherapy, which has severe side effects. The current methods of bulk system cancer treatments involve the use of toxic chemical compounds that kill normal /healthy cells as they circulate through the body. There is, therefore, a need for alternative approaches that can reduce the killing of normal /healthy cells during cancer treatments [8].

The field of controlled release has since been born out of this motivation to develop systems that release drugs in a controlled and effective manner.

1.2 Implantable BioMEMS

Implantable Bio-Micro-Electromechanical Systems (BioMEMS) represent new class of devices that can be used to provide localized cancer drug delivery [1]. They can be inserted in regions that surround cancer tissue, and used surgical drugs, in ways that reduces the short and long term effects of bulk chemotherapy.

2. Experimental procedures

2.1 Poly (Di-methyl-Siloxane) (PDMS) Replication

All experiments were carried out at Sheda Science and Technology complex, Abuja where apparatus were available. PDMS packages with different channel lengths and reservoirs were prepared according to the standard sylgard preparation guide[13]. PDMS was prepared by mixing the sylgard184kit to a silicon elastomer curing agent in a 10:1 ratio by volume. The mixture was stirred vigorously, de-gassed with a GALVAC vacuum oven (LTE Scientific LTD., Greenfield, USA) set at -18 in Hg with no heat for 1hour, 15 minutes to remove all bubbles. The de-gassed PDMS was gently poured to flow into Aluminum molds. The rheological nature of PDMS enables it to flow, taken the shape of the molds. The samples were cured at 28 ℃ for 48 hours before being unmolded.

2.2 Preparation of PNIPA-Based Hydrogels

The gels were prepared by free radical polymerization [3, 14]. Co-monomer specie, acrylamide (AM) were co-polymerized with PNIPA, summarized in table 2.1. The ratios of NIPA, methylene-bisacrylamide (MBA) and AM were referenced from prior work [1].

A 100 % PNIPA gel was first prepared by weighing 0.778g of PNIPA, 0.01219g of MBA, and 0.02997g of ammonium persulfate (APS) with an analytical weighing balance. The samples were subsequently topped up with 7ml of distilled water, stirred vigorously until a homogenous mixture was obtained at 24°C. The mixing process was exothermic and energy was released to the environment to ascertain a constant temperature by putting the tubes bearing the solutions on ice and then sonicated, while Nitrogen gas is bubbled through the solution for 20 minutes at 10 bars to remove all dissolved oxygen. 40μl of the initiator, Tetra-methyl-ethylene-diamine (TEMED) was piped into the solution and the mixture was stirred vigorously. The solution was poured into cylindrical molds and opened to terminate the free radical polymerization. The samples were left at 25°C in a water bath to complete the polymerization process for 6 hours. PNIPA gel composites were also prepared by following the same procedure but then acrylamide (AM) was then copolymerized as summarized in table 2.1 above. When the polymerization process was completed, the gels were carefully removed from the cylindrical molds, washed several times with deionized water to remove any chemical residue. They subsequently cut into disc and cylindrical shapes.

2.3 Encapsulating PNIPA into PDMS Package

PNIPA gels were soaked in distilled water, bromophenol blue, and prodigiosin for 5 days before they were inserted into PDMS reservoirs. The reservoir was closed with a PDMS cover by applying a curing agent on both edges (Picture 2.1). The two layers were properly sealed by applying a slight pressure on the axes perpendicular to the edge with a clamping device (picture 2.2), allowed at 28°C for 24 hours to polymerize the two layers.The devices were subjected to resistive heating at (45°C). The time for the fluid to flow across the devices with different channel lengths was taken to ascertain the diffusion coefficient, D:

$$L=\sqrt{Dt} \quad \text{---------- (1)}$$

A plot of L(m) versus $\sqrt{t}$ gives a straight line (figure 2.1) which gives a diffusion coefficient of4.0 x10^{-8} m^2/s.

3. Results and Discussion

3.1 Gel Characterization

The transport characteristics of a conventional PNIPA and PNIPA composite are largely depended on the morphologies of the gel inner matrix. In this present work, EVO^{R} analytical scanning electron microscope (SEM) (Oxford Instrument, MA10., USA) and an LCD Deluxe digital microscope (Celestron, #44345) (Figure 2.3) were used to explore the inner structure of the gels. The SEM analysis revealed an increased in micro-porosity in order of acrylamide copolymers (Fig. 2.2). The optical images of the gels indicated collapsed walls with dangling chain structures. This implies the gels could easily collapse and expand when an external stimulus is applied.

UV-VIS spectrometer (Cecil, 7000 Series) was used to determine the absorbance for bromophenol blue and prodigiosin at 589nm and 538nm, respectively. From Beer-Lambert law, it was possible to determine the molar absorptivity:

$$\varepsilon = \frac{A}{LC} \quad \text{---------- (2)}$$

Where A is the absorbance of the dye(0.911 AU), L is the path length of the quartz cell used (1cm), and C is the concentration of the dye (Fig. 2.4)

3.2 Swelling Ratios and transport measurement

The average swelling ratio (SR_A) was ascertained by soaking the hydrogels in distilled water at different temperatures until equilibrium

(Fig. 2.5):

$$SR_A = \frac{M_t - M_o}{M_o} \quad \text{---------- (3)}$$

The equilibrium swelling ratio $SR_{eq.}$ was obtained from equation[16]

$$SR_{eq.} = \frac{M_{eq} - M_o}{M_o} \quad \text{---------- (4)}$$

Where $M_t$corresponds to the weight of the gel at time t, Mo is the mass of the dried gel at time (t = 0ms), and M_{eq} is the weight of the hydrogel at equilibrium. The water uptake by the gels were obtained with the relative gel mass [17]:

$$M_{rel} = \frac{M_t}{M_s} \quad \text{---------- (5)}$$

Where M_s is the swollen mass at 28°C. The equilibrium volume was achieved via:

$$V_{eq} = \frac{D}{D_o} \quad \text{---------- (6)}$$

Where D_o and D are the diameters of the hydrogels before and after the equilibrium swelling.

3.3 Diffusion and Swelling Mechanisms

The release exponent (n) and the geometric constant via diffusion system (k) were determined [18]:

$$\frac{m_t}{m_\infty} = 4\left(\frac{Dt}{\delta^2}\right)^n = kt^n \quad \text{----(7)}$$

The linear form is expressed by:

A plot of $\ln\left(\frac{m_t}{m_\infty}\right)$ versus ln(t) gives a linear graph where n is the slope (Fig. 2.6).

Where $\frac{m_t}{m_\infty}$ is the drug release fraction at time t, δ is the thickness of the gel, k is the constant relating the structural and geometric characteristics of the controlled release, and n is the release exponent which, indicates the mechanism of drug release. The diffusion coefficient D was obtained by (Table 2.2):

$$D = \frac{k\pi\delta^2}{4} \quad \text{----------(9)}$$

3.2 Modeling of Fluids/ Prodigiosin Release

The loaded gels were released at setting temperatures (28°- 48°C), modeled with the early time approximation:

$$\frac{dM_t}{dt} = 2M_{total}\left(\frac{D}{\pi\delta^2 t}\right)^{1/2} \quad \text{----(10)}$$

Where the coefficient $\frac{2D^{\frac{1}{2}}}{\pi\delta^2}$ relates the gradient from a release rate versus $(t)^{-\frac{1}{2}}$ (Fig. 2.7, fig. 2.8):

Where (dMt)/dt corresponded to the fluid released rate, Mt is the amount of fluid released at time t, Mtotal is the total amount of substance that was dissolved in the PNIPA hydrogels, D is the diffusion coefficient, and δ is the thickness of the dried hydrogel. The diffusion across the micro-channelsis represented by Fick's law:

$$: J = -D\left(\frac{dC_m}{dx}\right) \quad \text{--------(12)}$$

Where J is the flux per unit area (g/cm^2sec), Cm represented the concentration of the drug (mol/cm^3), D is the diffusion coefficient (cm^2/sec) of the drug filled in the PDMS reservoir, and the concentration gradient is represented by $\left(\frac{dC_m}{dx}\right)$ The activation energy for each gel was obtained from a plot of diffusion coefficient as a function of temperature using the Arrhenius equation:

$$D = D_o \exp\left(\frac{-E_a}{RT}\right) \quad \text{------(15)}$$

Where R is the Gas constant, T is temperature; E_a is the activation energy for each gel. The activation energies for the gels is presented in Table 2.3.

4. Conclusion

Diffusion and swelling kinetics of PNIPA gels were presented at temperatures (28˚C - 48˚C). The swelling capacities of the gels were found to decrease with increasing temperature given evidence of the thermo-sensitivity of PNIPA gels (Fig.2.5). The release rates were governed by the earlier time approximation and the diffusion of water molecules were under the influence of temperature. Non-Fickian diffusion dominated in all the results obtained with the power law equation [18].

The biocompatibility of PDMS (Approved by American Food and Drug Association) and the macroporous structure of the PNIPA gel in addition to its sensitivity to an environmental stimuli such as temperature calls for a necessary attention for applications in drug delivery.

Moreover, the synergy of hyperthermia would induce killing of cancer cells surrounded by the device. Since the delivery of the drug is localized, the total quantity of drug needed for a therapeutic effect would be reduced significantly. Hence, the potential side effects associated with localized cancer drug delivery should be much lower than those associated with bulk systemic chemotherapy.

References

[1] Y. Oni, C. Theriault, A. V. Hoek, W. O. Soboyejo, (2011), "Effects of temperature on diffusion from PNIPA-based gels in a BioMEMS device for localized chemotherapy and hyperthermia", Journal of Materials Science and Engineering C

[2] E.S. Matsuo, T. Tanaka, Phase Transitions, 46 (1994) 217.

[3] T. Tanaka (1981) Gels. Sci. Am. 244 124.

[4] Afrassiabi, A.S. Hoffman, L.A. Cadwell (1987), Journal of Membrane Science 33, pg191.

[5] David Cutierrez, (2008), America Cancer Society, "Cancer facts and figures, 2nd edition.

[6] J. Mackay, G.A. Mensah (2004), The Atlas of Disease and Stroke, WHO Non-serial Publication.

[7] Peter Boyle and Bernard Levin (2008), "The World Cancer Report" by World Health Organization

[8] B. Hildebrandt, P. Wust in: W.P. Ceelen (Ed), (2007), Peritoneal Carcinomatosis: A Multidisciplinary Approach, Springer, New York, p. 185.

[9] N.A. Peppas, S.L. Wright, Eur. J. of Pharm. Biopharm. 46 (1998)15.

[10] S.S. Zumdahl, (2005), Chemical Principles, Houghton Mifflin Company, Boston.

[11] D.C. Coughlan, F.P. Quilty, O.I. Corrigan ((2004), Journal of Control Release, 98, p97.

[12] Yucel Dogu, Oguz Okay (2005),"Swelling–Deswelling Kinetics of Poly(N-isopropylacrylamide) Hydrogels Formed in PEG Solutions" Wiley Periodicals.

[13] J. Siepmanna, N.A. Peppas (2000), "Modelling of drug release from delivery systems based on hydroxypropyl methylcellulose (HPMC)", Advanced Drug Delivery Reviews 48 (2001) 139–157

5. Figures and Tables



Picture 2.1 is different sizes of PDMS packages with reservoirs and covers



Picture 2.2 prototype devices

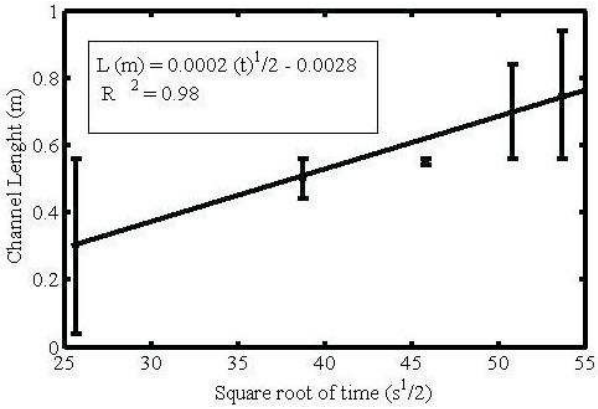


Figure 2.1 Plot of channel length (cm) versus time in seconds.

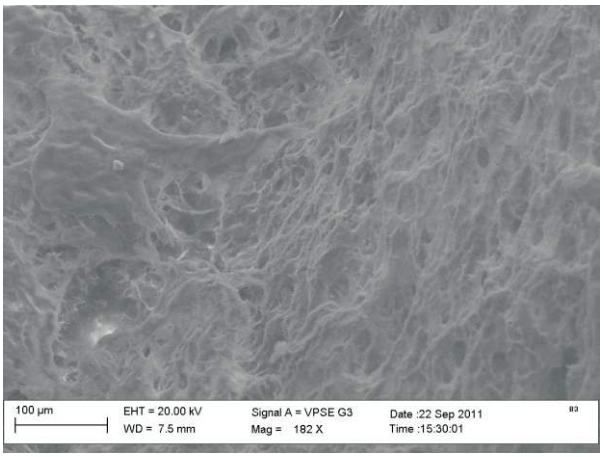


Figure 2.2 SEM image of PNIPA gel composite (15 % acrylamide).

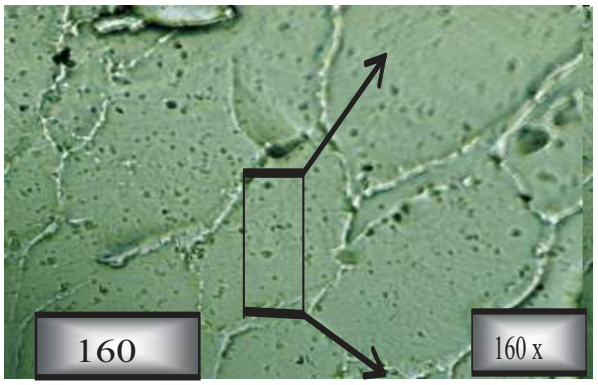


Figure 2.3 LCD microscopy analysis of PNIPA gel

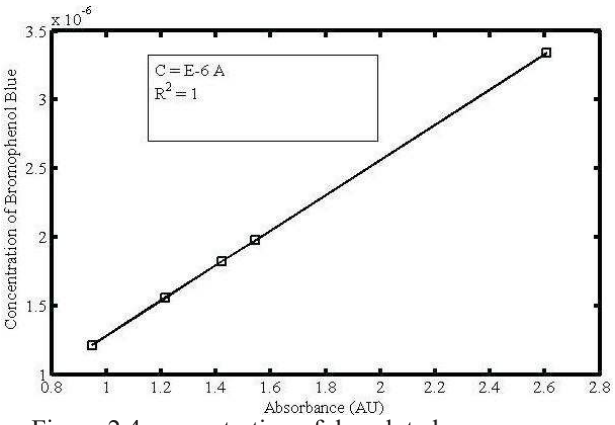


Figure 2.4 concentration of dye eluted versus absorbance at time,

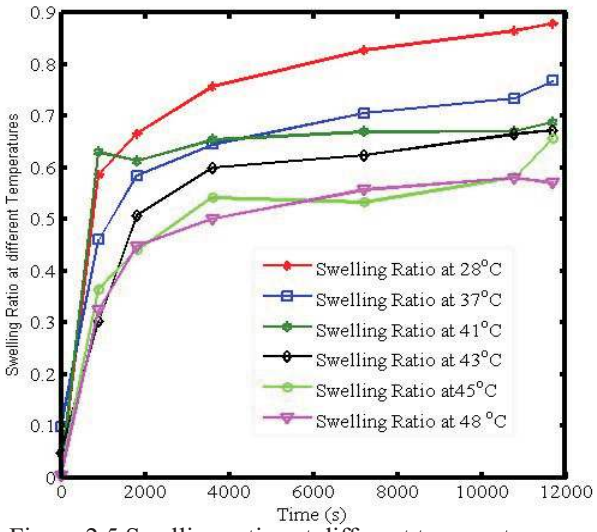
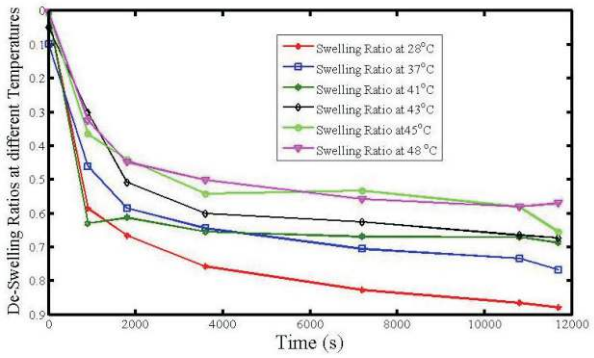


Figure 2.5 Swelling ratios at different temperatures



De-swelling of hydrogels at different temperatures

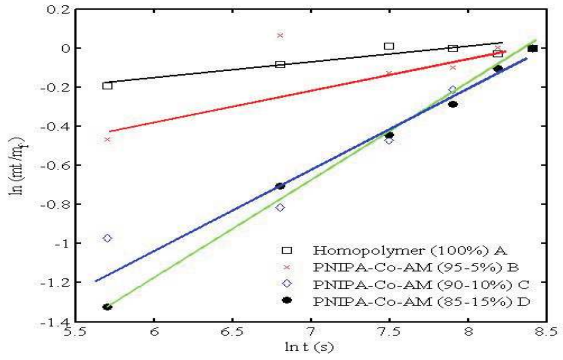


Figure 2.6 Linear plot of the release rate of prodigiosin against time at 37℃ on a log scale

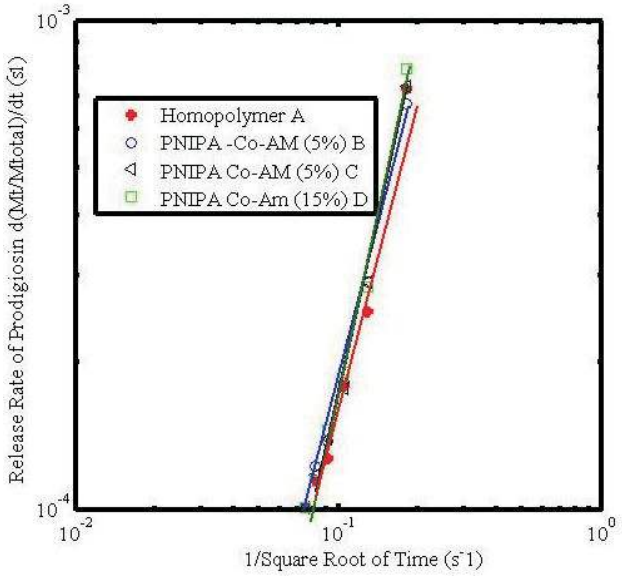


Figure 2.7 Modelled Released Profile versus $t^{-0.5}$,$s^{-0.5}$

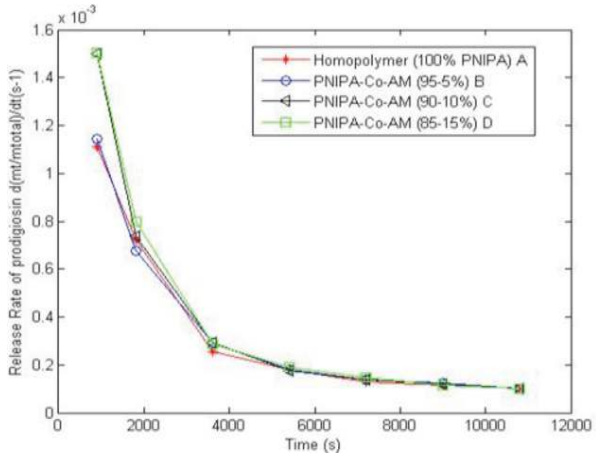


Figure 2.8 Gels release profiles at 43˚C

Table 2.1 PNIPA Gel Configuration and their Compositions

Gel Code	PNIPA (%)	Acrylamide (%)
A	(100%)	-
B	(95%)	(5%)
C	(90%)	(10%)
D	(85%)	(15%)

Table 2.2 D, n, and K at 37℃

Gel	Release expone-nt (n)	Geomet-ric constant (k)	Diffusion Coefficient D (m^2/s)
A	0.507	0.013	3.562E-09
B	0.586	0.007	9.664E-10
C	0.594	0.007	9.650E-10
D	0.697	0.003	1.421E-10

Table 2.3 Activation energy of the gels

Gel Code	Activation Energy (KJ/mole)
A	190.90
B	192.54
C	287.39
D	316.25

BIOSYNTHESIS OF MAGNETIC NANOPARTICLES FOR CANCER DETECTION AND TREATMENT

[1]Obayemi, J. D, E.O. Achi[3], D.O. Olalekan, G.A. Etuk-Udo[2], S.O. Dozie-Nwachukwu[2], E. Paetzell, N. Anuku[5,6], O. S. Odusanya[2], K. Malatesta,[4,6] and W.O. Soboyejo[5,6]

[1]*Department of Materials Science and Engineering, African University of Science and Technology (AUST) Abuja-Nigeria.*
[2]*University of Jos, Plateau State, Nigeria.*
[3]*Sheda Science and Technology Complex (SHESTCO) Abuja, Nigeria,*
[4]*Department of Chemistry, Bronx Community College, New York, NY.*
[5]*Department of Mechanical and Aerospace Engineering, Princeton University, USA,*
[6]*Princeton Institute of Science and Technology of Materials (PRISM), Princeton, USA.*

Abstract
Chemical and physical methods for the synthesis of magnetic nanoparticles for cancer detection and treatment often involve toxic chemicals, high cost and the formation of non-stable nanoparticles. This prompted the development of fundamental understanding of the synthesis of magnetic nanoparticles, which are biocompatible, cost effective, stable, localized and environmentally friendly in the presence of magnetotactic bacteria. In this work, fundamental understanding of the underlying mechanisms involved in the formation of magnetic nanoparticles by magnetotactic bacteria are unraveled. Soil dwelling microbes that respond to magnetic pull were cultured in the presence of ferrous salts. A positive control was designed in which *Magnetospirillum magneticum* was used in the biosynthesis of magnetic nanoparticles. The dependence of particle shape on pH and time, are elucidated using a combination of transmission electron microscopy, UV-visible spectrophotometry and XRD. The implications of the results are discussed for the development of magnetic nanoparticles for the detection and treatment of cancer.

1.0 Introduction and Motivation

Nanotechnology has provides solutions to some critical problem in the areas of energy generation [1, 2], information storage [3], environmental remediation [4, 5] and biological application [6] to mention but a few. In the recent years, there has been increasing interest in the development of nanoparticles for potential and emerging applications in medicine [7]. These include potential emerging application in disease detection and treatment [8, 9], biological labelling [10], biosensors [11], drug delivery [12] etc.

In the case of magnetic nanoparticles (MNPs), there have been significant efforts to develop magnetic nanoparticles for application in cancer detection via magnetic resonance imaging (MRI) [13] and treatment by hyperthermia [14].Their potential has also been explored for use as contrast enhancement agent during MRI of tumour tissue and localized hyperthermia [14] during cancer detection and treatment. Magnetic nanoparticles have been reported to have the ability of binding to drugs, proteins, enzymes, antibodies, or nucleotides and can be directed to an organ, tissue, cells or tumors using an external magnetic field or can be heated in alternating magnetic fields for use in MRI or hyperthermia.

Fe_3O_4 or magnetite nanoparticles are heat-generating nanoparticles which have the ability to convert electromagnetic energy to heat energy. There is several physical and chemical methods use in the synthesis of MNPs. These include: microemulsion, sol-gel synthesis, hydrothermal reactions, flow injection synthesis, thermal decomposition, electrochemical synthesis, pyrolysis, laser pyrolysis, hydrothermal, carbon arc, combustion synthesis, vapour deposition and chemical co-precipitation method etc. However, these synthesis methods often involve the use of toxic chemicals that have harmful effects to the patient and the environment at large. Other set back ranges from the biocompartible, complicacy in the synthesis, localization and cost involve. There is a need for environmentally friendly methods for the synthesis of magnetic nanoparticles which are cost effective and biocompartible; such need has stimulated the recent interest in the biological synthesis of magnetic nanoparticles from magnetotactic bacteria (MTB). There is also a need to understand the underlying mechanisms of magnetic nanoparticle formation in the presence of magnetotactic bacteria.

To this end, most work in this field has been done in improving the biocompatibility of the materials, but no work has been done to unravel the indigenous and different source of MTB. Also, a few scientific investigations and developments have been carried out to develop a fundamental understanding of the synthesis of magnetic nanoparticles, which are biocompatible, cost effective, stable, localized and environmentally friendly in the presence of magnetotactic bacteria. The need to understand the underlying mechanisms involved in the formation of magnetite nanoparticles by these bacteria will contribute positively in improving the quality of magnetic particles, their size distribution, their shape and surface under certain preexisting conditions. This would in turn lead to characterizing them to get a protocol for the quality control and commercialization of these

particles in cancer treatment and detection.It is obvious that biosynthesis of magnetic nanoparticles is not a new thing. Thus, the magnetite synthesis by magnetotactic bacteria occurs in a unique intracellular membrane-like structure called magnetosomes and by metabolic accompanied by some chemical action extracellularly. The magnetosome is a lipid bilayer structure, which houses highly ordered magnetite crystals aligned parallel to the cellular axis. In contrast to physical and chemical synthesis methods, this approach in synthesis of MNPs will be characterized by ambient experimental conditions of pH and time to observe their effect on the morphology of the nanoparticles produce.

The objective of this study is to develop a simple and novel approach how magnetic nanoparticles (magnetite) are formed in the presence of indigenous MTB. The work also develop a fundamental understanding of the mechanism underlying the effects of pH and reaction time on the MNPs produced by well controlled durations of exposure to bacteria. It also shows how the production of the nanoparticles can be optimized in the presence of indigenous MTB under some preexisting condition. This research incorporates theoretical and experimental approach in the biosynthesis of magnetic nanoparticles for cancer detection and treatment.

2.0 MNPs for Cancer Detection and Treatment.

They are several methods apply in the synthesis of magnetic nanoparticles for cancer detection and treatment. It is expected that the synthetic procedure should be relatively simple, inexpensive and reproducible. Magnetic nanoparticles like magnetite depending on their pathway of synthesis were proposed as good contrast agents prior to their use as drug delivery agents for localized therapy. In another sense, it has also been shown to be useful in both targeting and drug delivery in cancer detection and treatment. Essentially, this is explained when anticancer drugs are bound to magnetic compound thereby concentrating them to a target area in the body by means of magnetic effect. However, these concentrated particles tend to allow for magnetic resonance imaging while the particles release the drug or give rise to local heating effect. Recent researches have shown that magnetic and gold nanoparticles can be incorporated together for the detection and treatment of cancer. This idea takes advantage of the magnetic and optical properties

3.0 Experimental Procedure

In this work two samples of MTB as an agent of synthesis were considered for the synthesis. Sample A, a positive control called *Magnetospirillum magneticum* obtained from Princeton in the United States and sample B, an indigenous MTB which we isolated before culturing.

3.1 Isolation of indigenous MTB

Sample B the yet identified indigenous MTB from Sheda environs. The local MTB were obtained from the soil in Sheda located at about 70 from the capital city of Abuja. Precisely, 0.5 kg of the soil sample was collected using a plastic spatula into a new polyethylene container which is closed. These samples were then transferred to the laboratory. The sample was placed in a disinfected bijou bottle which was autoclaved for 20 minutes and distilled water was added to the soil sample so that the solution is about 1 liter. This was then stored under ambient condition of temperature. The magnetotactic bacteria from the sample B were collected using the convectional magnetic collection method [1]. This method deals with magnetic response of magnetotactic bacteria to magnetic field. Here, the sample was subjected to a strong magnetic field by a permanent magnet. After 5 to 6 hours the, 1 ml of the sample near the magnetic axis was collected with a sterile pipette which was then transferred into a sterile test tube for further isolation. Serial dilution was observed to reduce the colonies of bacteria that would appear in each plate for easy quantification. It is expected that the magnetotactic bacteria which are magnetotaxis and motile in nature will move towards the pole of the magnet. Another crucial step was taken to purify and as well produce a single colony of magnetotactic bacteria by a technique called the capillary racetrack method (CRT). In this case, a capillary tube closed at one end with the aid of a gas flame was filled with a chemically defined medium as reported by Flies et al. This was achieved by the use of hypodermic syringe which was fitted the smallest end a Pasteur pipette. Also, at the other large end which acts as a reservoir, wetted cotton was placed. A permanent magnet with high susceptibility was placed at the smallest tip of the arrangement for 3 hours. However, the magnetotactic bacteria which are motile and move under the influence of a magnetic field migrate towards the tip across the cotton plug in the set up. A sterile syringe is use to collect the bacteria at this point for culturing in a *magnetospirillum* growth medium(MSGM) at buffer of PH 4, 6, 6.5, 7, 7.5, 8.5, 9, 9.5 and 12 and an agar-agar MSGM semi solid medium of PH 6.7 distilled water.A similar approach and compositions as in the preparation of the MSGM broth is adopted to prepare the agar-agar semi solid medium. This serves as an alternative secondary method in the purification of the local MTB for inoculation and synthesis in the MSGM medium. Though in this case, an agar-agar constituent was added to the MSGM solution to have a semi-solid MSGM medium. This medium was inoculated andlatter subjected to magnetic field to have a pure MTB.

3.2 Synthesis and quantification of the Magnetite Nanoparticles

Standard magnetic spirillum growth medium (MSGM) was prepare with composition of 0.074 g of succinic acid, 0.068 g of KH_2PO_4, 0.012 g of sodium nitrate, 0.02% of polypeptone, 0.01% of yeast extract, 0.005% of L-cysteine component, 150µg/ml of Chloramphenicol, 1 ml of Wolfe's vitamin, 0.5 ml of Wolfe's mineral and 0.2 ml of ferric quinate. Thereafter, 5 ml of the purified sample A and B was inoculated in the MSGM broth buffer at PH 4, 6, 6.5, 7, 7.5, 8.5, 9, 9.5 and 12 for 24 hours in a shaker incubator (Innova 44 Incubator series). After 24, 48, 72, 96 and 120 hours of inoculation, the samples were obtained for further test.It is expected that as the bacteria grow in the media, the magnetite which grow intracellularly in the magnetosomes of the bacteria and extracellularly by metabolic process evolved as a result of synthesis which is guided by nucleation and growth. 2 ml of the samples each was centrifuge to obtain the pellet and

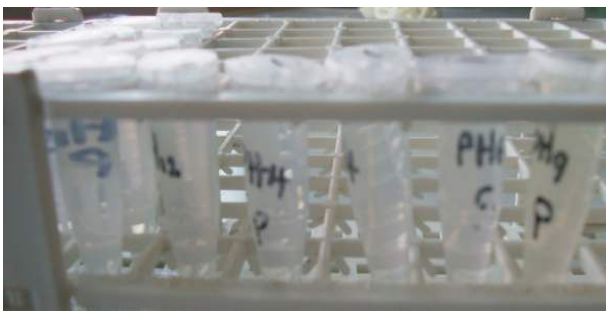
supernatant. The pellets obtained were subjected to 1.0 ml of 12M HCl and 0.5 ml of 1.5M potassium thiocyanate which turns red color. This is to test intracellullarly from the pellet. Extracellular synthesis by the samples was carried out using the supernatant by adding ferric chloride to expose the magnetite contents.A spectrophotometric analysis technique was used afterward to determine the concentrations via absorbance with respect to the magnetite nanoparticles produce by the two samples. This was achieved by taking the absorbance of the samples for the period of five days at different PH. A standard curve as shown in figure 1 of known concentration from chemical synthesis of magnetite was prepared. The known concentration of the chemically synthesized MNPs and that of the samples were taken at an absorbance of wavelength 440 nm.

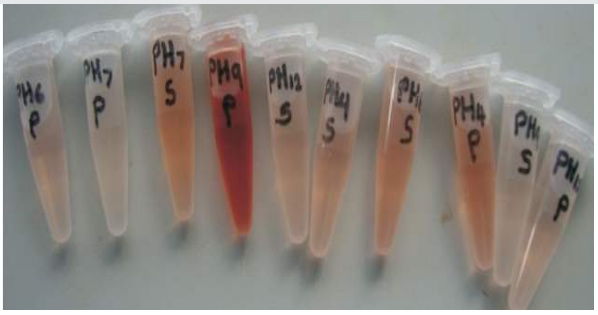
4.0 Result and Discussion

The result obtained for the samples was first based on chemical characterization by the aid of the UV-spectrophotometer. Here, the respective absorbance for the samples was obtained at a wavelength of 440nm. The corresponding concentration of the magnetite formed was quantified with the help of the standard curve for different PH and time as shown in the graph. Optimal production of MNPs which increases with time for the pellet was observed at the PH 7.0 and 9.0 for sample A(*Magnetospirillum Magneticum*) and B respectively as shown in figure 2 and 3.Minimum production of MNPs was obtained at PH 6.5 and 12.0 for sample A and B respectively. This result increases with time for the different PH studied.This overall result increases for the different PH as time increases. Other characterizations done are morphological by the aid of HRTEM and LRTEM

5.0 Conclusion

Despite the increase in the quantity of magnetite with time for different PH.Local bacteria have been able to synthesize MNPs in the form of SPIONs in some cases which can be used in cancer diagnosis and treatment. There is still ongoing work to properly characterize the magnetic nanoparticles produced using VSM, AFM, FITR, MFM, TGA etc. this will detection and treatment. Others areexploring the effectiveness of sizes and shapes morphology in diagnosis and cancer treatment, probing the effect of temperature, and media, probing the thermodynamics and kinetics of the MNPs formed, to model the nucleation and growth of the nanoparticles formation. Future work should probe the growth stage (phase) of microbial cells. Better understanding of the synthesis mechanism on a cellular and molecular level would be necessary.





Picture 2: pellet after complete synthesis

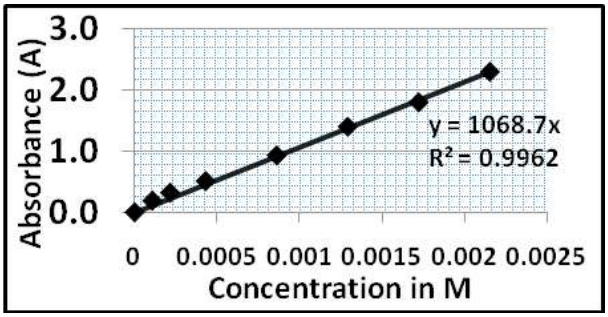


Fig.1: Standard concentration curve

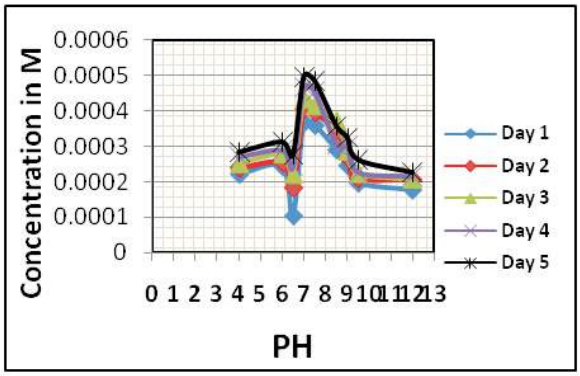


Fig.2: Conc/PH curve for M.magneticum pellet

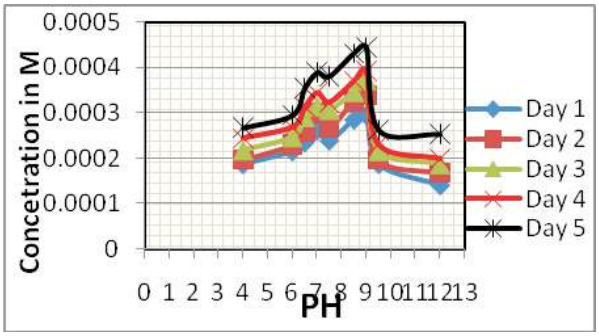
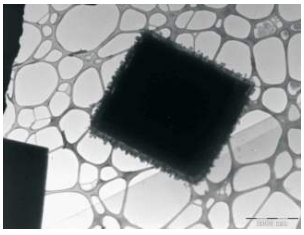
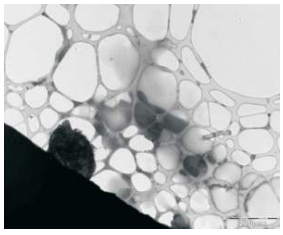


Fig.3: Conc/PH curve for the local strain





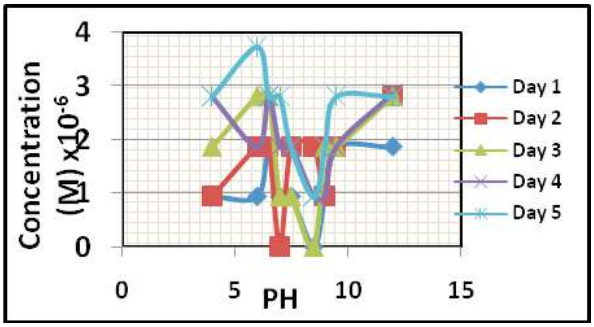


Fig.4: Conc/PH curve for the M.magneticum supernatant

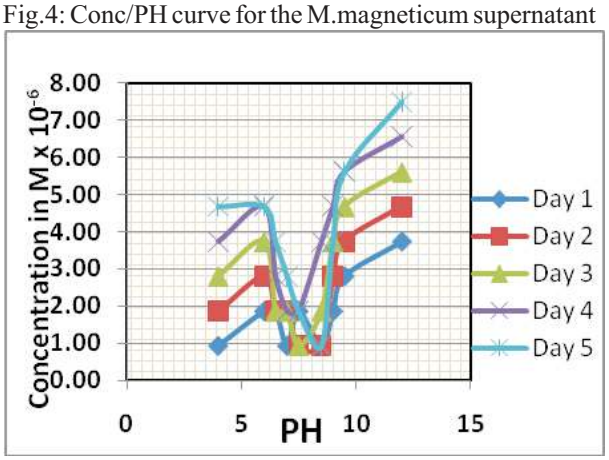
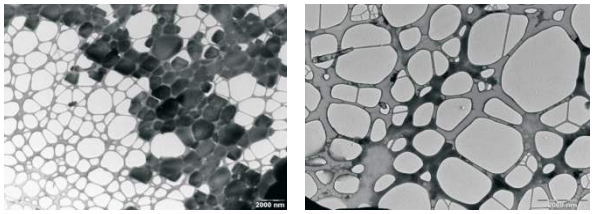
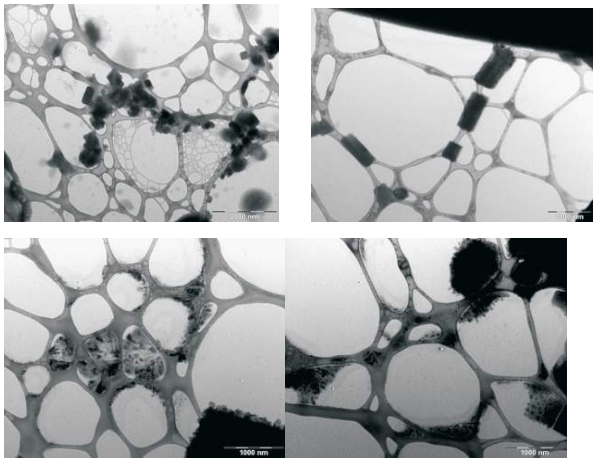
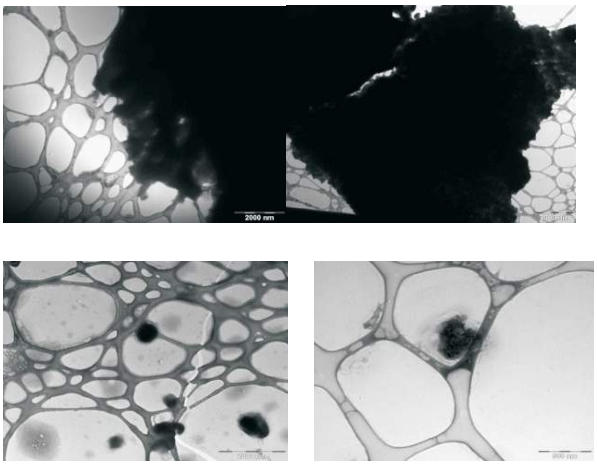


Fig.4: Conc/PH curve for the local strain supernatant



Picture 3: Some TEM images showing of the MNPs formed by the indigenous MTB at different PH and time





Picture 4: Some TEM images showing the MNPs formed by the indigenous MTB and *M.magneticum* at different PH and time

References

[1] Zach,M., Hagglund,C., Chakarov,D. &Kasemo,B. (2006). Nanoscience and nanotechnology for advanced energy systems. Current Opinion in Solid State and Materials Science,10, 132-143.

[2] Serrano,E., Rus,G. & Garcia-Martinez,J. (2009). Nanotechnology for sustainable energy

[3] Sandhu,A. (2008). Data storage: One-track memory. NatureNanotechnology. doi:10.1038/nnano.2008.120.

[4] D. W. Elliott, W.-X. Zhang, Environ. Sci. Technol. 2001, 35, 4922.[5] M. Takafuji, S. Ide, H. Ihara, Z. Xu, Chem. Mater. 2004, 16,1977.

[6] Caruthers,S.D., Wickline,S.A. &Lanza,G.M. (2007). Nanotechnological applications in medicine. Current Opinion in Biotechnology,18, 26-30.

[7] Q A Pankhurst1

PHOTONIC NANOSTRUCTURE FOR THE EFFICIENCY ENHANCEMENT OF CRYSTALLINE SILICON THIN-FILM SOLAR CELLS

A.A. Fashina[1], K.K. Adama[2], ***M.G. Zebaze Kana***[1,2], A.A. Oberafo[2], W.O. Soboyejo[1,3]
[1] Department of Theoretical Physics, African University of Science and Technology, Abuja, Nigeria
[2] Physics Advanced Laboratory, Sheda Science and Technology Complex, Abuja, Nigeria
[3] Department of Mechanical and Aerospace Engineering, Princeton Materials Institute, Princeton University, 1 Olden Street, Princeton, NJ08544, USA

Abstract
In this paper, we have developed a light trapping design **for the efficiency enhancement of** single and multi-junction thin film silicon solar cells. The process involves the reduction of front surface reflection and the increase of the optical path length within the cell. This was achieved by structuring a random pattern on a sub-micron scale realized in the Silicon substrate, on which subsequently a Silicon dioxide layer was thermally grown, before the deposition of the Indium-Tin Oxide (ITO) antireflective coating. Aluminum was used as back contact. The light trapping mechanism was optimized for silicon solar cells by investigating the dependence of the Silicon texturing on the process parameters such as etchant concentration, etching time and temperature. The results obtained from the above optimization were used in the fabrication of Ag/ITO/SiO_2/p-Si/Al solar cell on textured Silicon substrates, which exhibited a significant improvement of **light absorption** over polished Silicon-based cells. **This signifies a potential increase in the efficiency of the device.**

Keywords: Light trapping, texturing, reflectance, c-Si solar cell

1. Introduction

Silicon based photovoltaic cells represent 90% of the photovoltaic panels presently sold in the world [1]. In such cells, more than one third of the cost is due to silicon itself. Indeed, its purification, crystallization and the wafer fabrication have an important energetic and economical cost. This is why the photovoltaic research community is presently looking for ways to have a solar cell structure based on thinner silicon layers. There are nevertheless limitations, already existing for thick cells but becoming crucial for thin cells: the thinner the material, the lower its light absorption, due to the low extinction coefficient of silicon [1,2]. Thus, in order to keep the light absorption high, it is necessary to add light scattering and trapping techniques in the absorbing silicon layer.

Since light absorption is low at long wavelengths for silicon thin film, the cell needs to be assisted by structures that can enhance the absorption probability in this range. These structures need to perform the task usually termed *light trapping*: the photons must easily penetrate into the device, where they will spend a sufficiently long time compared to the absorption time. Light trapping allows cells to absorb sunlight using an active material layer, that is, much thinner than the material's intrinsic absorption length. In addition, light trapping can improve cell efficiency, because thinner cells provide better collection of photo-generated charge carriers, and potentially a higher open-circuit voltage [1].

The theory of light trapping was initially developed for conventional cells where the light-absorbing film is typically thick [1]. From a ray-optics perspective, conventional light trapping exploits the effect of total internal reflection between the semiconductor material (such as silicon, with a refractive index $n \approx 3.5$) and the surrounding medium (usually assumed to be air). However, the light trapping in silicon solar cells mainly falls into two categories; the first is the reduction of front surface reflection and the second involves increasing the optical path length of light within the cell. The concept of reducing the surface reflectivity by introducing intermediate transparent layers has been known since the early 1800's [3].

Combinations of materials, such as silicon dioxide (SiO_2), silicon nitride (Si_3N_4) and some transparent conductive oxides [4,5] are commonly used as intermediate layers. Other methods used to reduce front surface reflection are based on principles of scattering which ranges from random surface texturing [3] to the use of regularly arrayed or inverted pyramidal structures [4-6]. The performance of the front surface texturing can be viewed in reference to the ideal Lambertian scatterer. This is designed to randomly scatter light into a uniform distribution of forward angles, known as a Lambertian distribution. The second category of light trapping in silicon solar cell (i.e., increasing the optical path length of light within the device) involves the modification of both the front and back surfaces of the device. To accomplish this, numerous ideas and designs have emerged ranging from planar reflective surfaces to arrays of ordered nanostructures integrated on the back surface. The main aim behind these designs is to internally reflect incoming light and hence increase the effective thickness towards a maximum factor of $4n^2$ for indirect band gap semiconductors [7] such as crystalline silicon. In our study, an efficient texturing process for solar cell

substrates is reported. The effects of light trapping on the solar cell devices fabricated on the textured substrates are shown.

2. Experimental Procedure

An optimized texturing process for c-Si wafer substrates was achieved using a mixture of potassium hydroxide (KOH) and isopropyl alcohol (IPA) solution. Anisotropic texturing experiments were carried out in GFL-1083 thermo-coupled water bath. The substrates employed in this work for the etching tests were one-side polished (100) c-Si wafer, CZ grown, p-type doped, 1Ωcm in resistivity, and 275μm of thickness. Before the etching process, all samples were dipped in 0.5% HF solution for 100s to remove the native oxide. Various process parameters such as etchant concentration, temperature and etching time were tested. The texturing process was performed at different concentrations and volume ratios of KOH, and IPA respectively as shown in Table 1. Various etching times (30-60min); etchant concentrations and temperatures (60-90^{0}C) were tested using fresh solutions for each sample. At the end of each process, the textured wafers were rinsed thoroughly in deionized water and dried under a stream of high purity nitrogen. The characterization of the un-etched and etched c-Si wafers using a surface profiler (Veeco Dektak 150 Surface Profiler) was initially carried out to determine the roughness of the substrates. Thereafter, the optical reflection measurements were performed with an Avantes Optics UV-VIS-NIR spectrometer, after which a Carl Zeiss EVO MA-10 scanning electron microscope (SEM) was used to image the surface morphology of the textured c-Si wafers.

1 x 1 cm^2 solar cell devices were fabricated using the structure Ag/ITO/SiO_2/p-Si/Al to ascertain the effectiveness of light trapping. In the above device fabrication, the SiO_2 was thermally grown in a furnace at 900^{0}C on the textured Si substrates; the ITO film was deposited by RF magnetron sputtering at an RF power of 50W and subsequently annealed at 250^{0}C for 30mins. To complete the device, the Ag front grid and the Al back contact were both evaporated in an Edwards Auto 306 evaporator, with a vacuum better than 2x10^{-6} Torr.

Table: Volume ratios of etchant concentration

S/N	Volume Ratio (KOH: IPA: DIH_2O)	Composition	Weight (g)	Weight (mL)
1.	1 : 2 : 46	KOH	4.08	----
		IPA	8.16	10.40
		DIH_2O	187.76	187.76
2.	2 : 2 : 46	KOH	8.00	----
		IPA	8.00	10.20
		DIH_2O	184.00	184.00
2.	2 : 4 : 46	KOH	7.69	----
		IPA	15.38	19.61
		DIH_2O	176.92	176.92

3. Results and Discussion

3.1 *Random texturing by KOH solution*

The dependence of the reflectance on the texturing process duration is shown in Fig. 1. This result indicates that increasing the etching time reduces the reflectance.

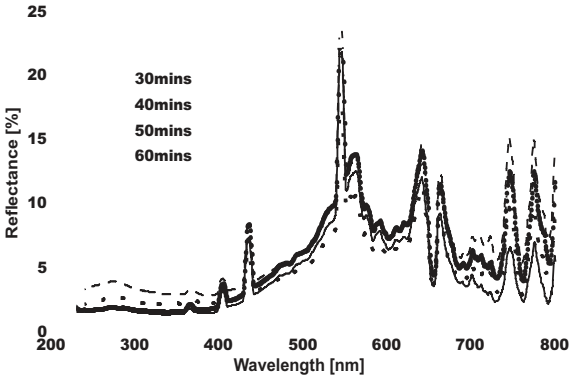


Figure 1: Reflectance spectra of textured wafers for various etching times

Fig. 2 shows the surface reflectance characteristics of different samples processed at various temperatures. It can be seen that the reflectance decreases with an increase in etching temperature. The variation of the reflectance with different etchant concentrations is pictured in Fig. 3. The minimum reflectance is observed for a volume ratio 4:4:46 of **KOH: IPA: DIH_2O**

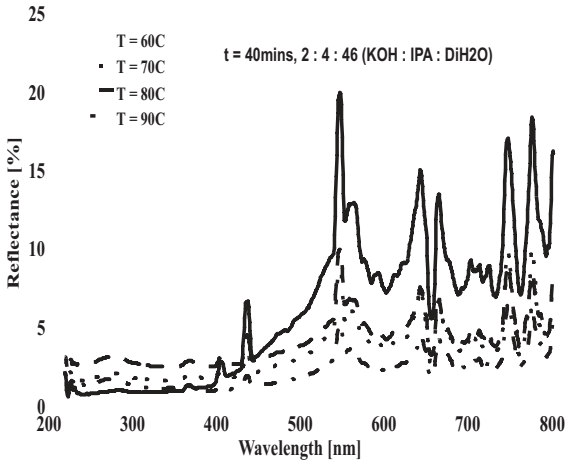


Figure 2: Reflectance spectra of textured wafers at various etching temperatures.

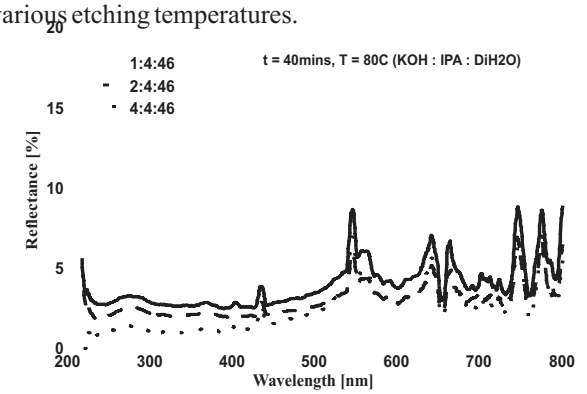


Figure 3: Reflectance spectra of etched wafers at various concentrations.

To investigate the morphological structure of the textured surface, a SEM analysis was carried out on the samples having reflectance characteristics shown in Fig. 2. As it can be seen in Fig. 4 and 5, a complete pyramidal coverage of the wafer is obtained for these samples.

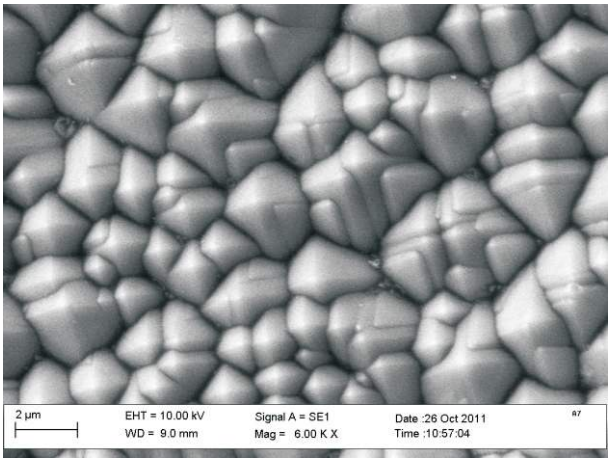
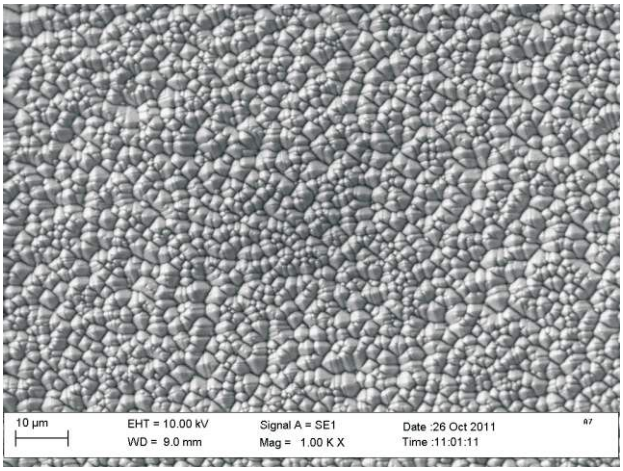


Figure 4: SEM image of a KOH textured wafer sample under the condition: KOH=40%, T=80^{0}C, t=40mins.

The KOH and IPA mixtures reacted with the silicon optimally, thereby forming random pyramids on the surface of the wafer samples and consequently reducing the overall surface reflectance. The pyramids produced are approximately 6 ~10µm in size and the surface roughness of the samples ranges from 679 - 845nm. This random texturing is compatible with device processing (since the pyramid heights are lower than 10µm) and efficient in light trapping enhancement, with the optical reflectivity lower than 15%.



5: SEM image at lower magnification showing a pyramidal coverage obtained on a wafer sample

3.2 *Thermally grown SiO_2 layer*

In the solar cell devices studied in our work, SiO_2 was used as a passivation and an antireflection layer on the front surface. The surface reflections for the thermally grown SiO_2 on both the polished and textured substrates are compared in Fig. 6 which demonstrates a good light trapping effect. The idea of thermally growing SiO2 on the textured substrate has a two-fold reason: from one side, this allows to apply on top of the patterned silicon layer an antireflection coating (ARC), which plays a fundamental role as impedance matching layer; from the other side, the silicon-silica interface can act as a passivating structure preventing a strong electron-hole surface recombination.

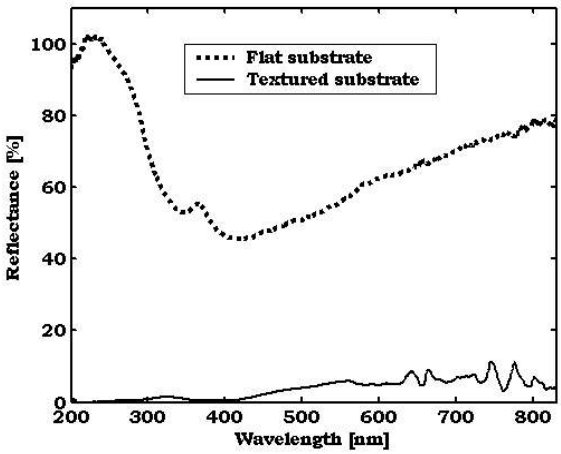


Figure 6: Reflectance spectra of 50nm thermally grown SiO_2 on both flat and textured substrate

3.2.1 ***Optical Simulation of thermally grown SiO_2 layer thickness***

The simulation and optimization of the optical reflectance of the thermally grown SiO_2 has been carried out, using "Optical" software [8] to determine the thickness of the thermally grown SiO_2. Fig. 7 shows the optical simulation of a 50nm thickness of the thermally grown SiO_2. The thickness of the thermally grown SiO_2 has also been confirmed using the standard thermally grown SiO_2 colour chart.

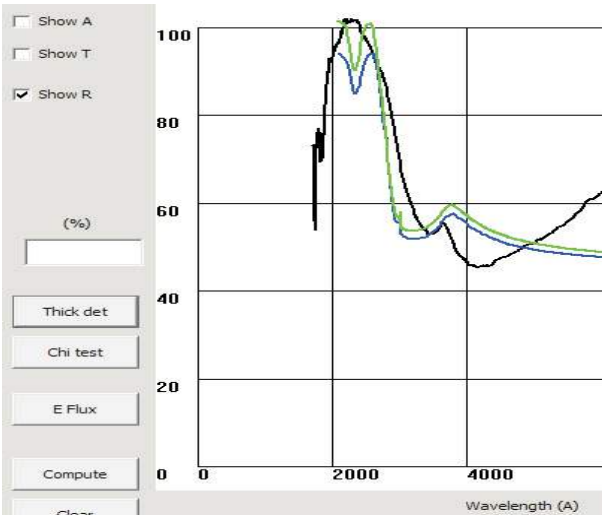


Figure 7: Optical Simulation of the thickness of the 50nm thermally grown SiO_2 on a flat substrate

3.3 *Solar cell device*

In order to investigate the compatibility of the random texturing process with light trapping mechanism, **Ag/ITO/SiO_2/p-Si/Al** solar cell devices were fabricated. The device structure is shown in Fig. 8**.** Since our aim is to study the mechanisms lying behind the light coupling and trapping due to the simultaneous application of a random pattern, SiO_2 passivation layer and an antireflection coating. We verified the total reflection of the complete device after anti-reflection coating deposition, without considering the details of the device efficiency. As can be seen in Fig. 9, the textured front with ARC and SiO_2 passivation layer exhibited good light capture properties that allows light to enter the cell. The texture front structure and small critical angle makes light escape difficult in the front side.

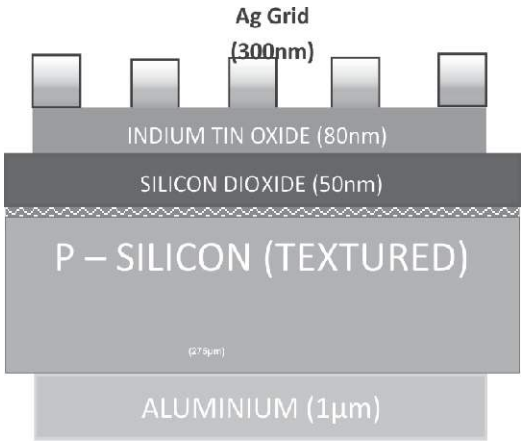


Figure 8: Light trapping structure for c-Si solar cell device.

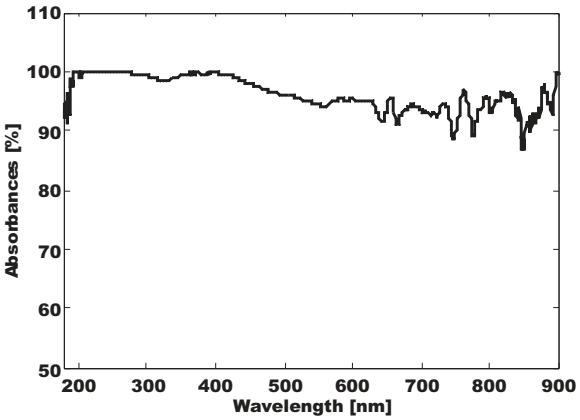


Figure 9: Absorbance spectrum of the solar cell device using flat silicon wafer as reference.

4. Conclusion

A recipe for silicon wafer random pyramidal texturing by KOH anisotropic etching has been developed. A uniform texture on the whole wafer surface with a good light trapping effect (reflectivity lower than 15% in the wavelength region between 400 and 800nm) has been achieved. This surface random texturing has been shown to be compatible with Silicon solar cell device processing and efficient in light trapping enhancement.

Acknowledgements
This research work was carried out at Sheda Science and Technology Complex (SHESTCO), Abuja, under the SHESTCO-AUST-Princeton Programme in Materials Science and funded by the World Bank STEP-B project.

References

[1] Park Y., Drouard E., El Daif O., Letartre X., Viktorovitch P., Fave A., Kaminski A., Lemiti M., Seassal C., "**Absorption enhancement using photonic crystals for silicon thin film solar cells" (2009)**

[2] James G. M., Shouyuan Shi, Caihua Chen, Timothy Creazzo, Allen Barnett, Christiana Honsberg, Dennis W. Prather. **"Thin film silicon solar cell design based on photonic crystal and diffractive grating structures"** Optical Society of America (2008)

[3] J. Muller, B. Rech, J. Springer, and M. Vanecek, "TCO and light trapping in silicon thin film solar cells," Sol. Energy **77,** 917–930 (2004).

[4] D. H. Macdonald, A. Cuevas, M. J. Kerr, C. Samundsett, D. Ruby, S. Winderbaum and A. Leo, "Texturing industrial multi-crystalline silicon solar cells." Sol. Energy 76, 277–283 (2004)

[5] M. A. Green, *Solar Cells: operating principles, technology, and system applications* (Prentice Hall, 1982).

[6] J. Zhao, A. Wang and M. A. Green, "19.8% efficient "honeycomb" textured multicrystalline and 24.4% monocrystalline silicon solar cells." Appl. Phys Letts **73**, 1991 1993 (1998)

[7] A. C. Marsh and J. C Inkson, "Scattering matrix theory of transport in heterostructures," Semiconductor Sci. Technol. **1**, 285 –290, (1986)

[8] E. Centurioni, "*Generalized matrix method for calculation of internal light energy flux in mixed coherent and incoherent multilayers*", Applied Optics, Vol. 44, No. 35 (2005), pp 7532-7539.

ADHESION AND DEGRADATION IN ORGANIC LIGHT EMITTING DEVICES

D.Y. Momodu[1], T. Tong[2,3], M.G. Zebaze Kana[1,4], A.A. Oberafo[4], and W.O. Soboyejo[1,2,5]
[1]*Department of Materials Science and Engineering, African University of Science and Technology, Abuja, Nigeria.*
[2] *Princeton Institute of Science and Technology of Materials (PRISM), Princeton University, Princeton,USA.*
[3] *Department of Electrical and Computer Engineering, Princeton University, Princeton, USA.*
[4] *Physics Advanced Laboratory, Sheda Science and Technology Complex, Abuja,Nigeria.*
[5] *Department of Mechanical &Aerospace Engineering, Princeton University, Princeton, USA.*

ABSTRACT
This paper presents the results of a study of adhesion and surface characteristics between layers that are relevant to organic light emitting devices (OLEDs). Adhesion is studied by atomic force microscopy, which is used to measure the adhesive interactions between bi-material interfaces in model OLED structures. Degradation in these devices is observed over a period of time and microscopic images are reported. The implications of the results are discussed for the improved design of organic light emitting devices.

1. Introduction

Since their original development by Friend et *al* [1] about twenty years ago, organic light emitting devices (OLEDs) have received considerable attention due to their potential for low-cost applications in "soft" lighting and displays [1-6]. Furthermore, the potential to pattern and stamp them into micron- and nano-scale patterns has made them promising candidates to replace liquid crystal displays based on inorganic silicon light emitting devices. However light emitting devices are limited by their relatively low lifetimes, due to the low stability in the presence of oxygen and water vapor [7]. They also have limited quantum efficiencies and undergo a range of degradation mechanisms during exposure to light, water vapor and oxygen in the environment.

The effect of environment has been addressed partly by the development of plastic encapsulation strategies that limit or delay the access of water vapor and oxygen to the devices. There have also been recent efforts to dope the active layers in OLEDs with inorganic materials that can promote improvements in charge and light transport through the resulting hybrid organic/inorganic light emitting devices (HOILEDs). However, there have been no prior studies on the combined effects of adhesion, contact and failure phenomena on the degradation that occur in these organic structures during charge and light transport across the layers. It should be noted that the adhesion energies of these individual layers affect the device lifetime since relatively high current densities in areas of partial contact produce localized heating and oxidation phenomena. As such there is a need to obtain materials with good adhesion energies to aid high surface contact.

This paper presents the results of a combined experimental and analytical study of adhesion, surface contact and failure phenomena in OLED structures. The adhesion of the different layers which constitute a typical OLED is carried out using the Atomic Force Microscopy (AFM) technique. Finally, the current-voltage characteristics of the fabricated OLED and HOILED structures are compared before discussing the failure phenomena that degrade their overall performance.

2. Modeling

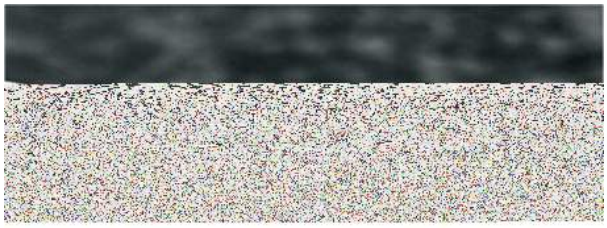
a. AFM Force-Displacement Model

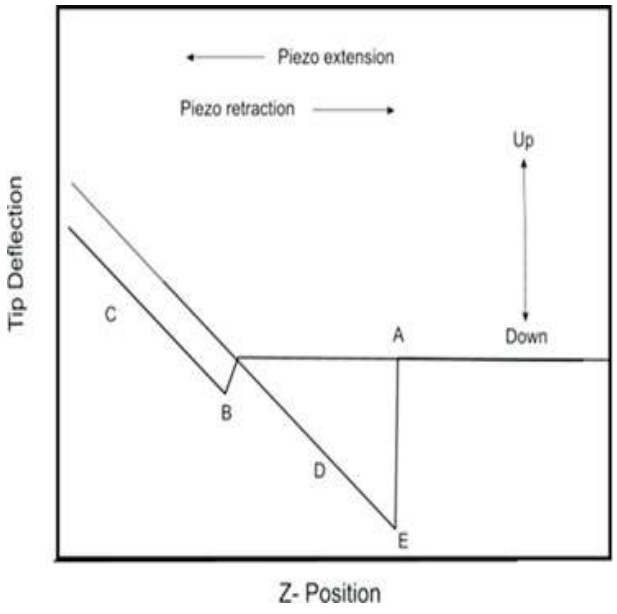
In the contact mode, AFM can be used to measure the pull-off force between two surfaces. The micro-fabricated cantilever probe is attached to a scanner head that is lowered toward the surface at a constant velocity. As the tip (Fig. 1a) is lowered further down, it is eventually pulled into contact with the surface by adhesive force interactions between the tip of the probe and the surface. Hence the reversed loading of the tip must be continued until the adhesive force is eventually overcome at a negative force that corresponds to the pull-off force (Fig. 1b). The measured displacement deflection (Fig. 1c) can then be related to the Hooke's law. This gives:

$$F = -kx \qquad (1)$$

where k is the spring constant, and x is the tip displacement.

However, the accuracy of the AFM measurements of the adhesion force depends significantly on the careful measurement of the spring constant, k, of the AFM cantilever tip. While the values for the spring constant are provided by most tip manufacturers, these are batch estimates, often significantly different from the actual values for each k [9]. The thermal tune method [10] offers a real-time and accurate technique for the measurement of spring constants used in the calculation of pull-off forces. This method involves the measurement of the tip response in the presence of thermal agitations and using a Lorentzian line shape fit to obtain an accurate estimate of the spring constant from the resulting frequency spectrum of harmonic oscillations.





(c)

Figure 1:(a)SEM images of AFM tip,
(b) Contact mode sequence A-E for adhesion measurements on the AFM,
(c) Typical displacement curve.

Note: the deflection of the tip is graphed on the vertical axis while the out of plane displacementof the cantilever tip is along the horizontal axis**.**

b. Surface Roughness and Contact between Layers

Since the surface morphology or roughness of each layer in OLED/HOILED structures can strongly influence the contact and adhesion across each interface [11], there is need to measure the average roughness values and their effects on contacts between the layers.

There is also a need to understand how the adhesion and physical contact, influence electrical contact (between the layers) and the overall device performance. This will be explored in this section using an analytical model of adhesion developed originally by Mastrangelo and Hsu [12,13], and used in a subsequent work by Zong et al [14], and recently by Akande et al [8].

We start by considering the contact of an upper layer around a dust particle on a substrate layer. The upper layer wraps around the dust particle like a cantilever beam until the surfaces come into contact in an s-shaped pattern.

The total energy of the system, UT is now given by:

$$\mathbf{UT = UE + US} \qquad \mathbf{(2)}$$

where UE is the elastic energy stored in the beam (due to bending), US is the adhesion energy for the segment in contact, and Γ is the adhesion [14].

UT can now be written as:

$$U_T = \frac{6EIh^2}{s^3} - \Gamma w(L-s) \qquad \mathbf{(3)}$$

where Γ is the adhesion energy, s is the detached length, I is the 2nd moment of area, h is the final dust particle height, w is the layer width, and E isYoung's Modulus.

De Boer and Michalske [15] further considered this adhesion problem from a fracture mechanics perspective: The detached length s could be thought of as the "crack length". Hence the restoring elastic energy stored in the beam is the "crack driving force", while the adhesion energy is the "crack resistance".

The total energy UT of the system, has a single minimum corresponding to the equilibrium s. This is found by setting

dUT/ds=0 to obtain

$$s = \left(\frac{3Et^3h^2}{2\Gamma}\right)^{\frac{1}{4}} \qquad \mathbf{(4)}$$

where t3= 12 I/w.

From the above equation, it can be seen that as the detach length increases, the adhesion energy decreases which is a good point to note for improved contact and adhesion to improve charge transport. The larger the contact area, the greater the adhesion energy and this increases for materials with lower Young's moduli. As a result, there is a likely improvement in the overall charge transport across such interface.

3 Experimental Methods

3.1 AFM Adhesion Measurements

In the contact mode, Atomic Force Microscopy was used to measure the average pull-off forces (Fpull-off) between thin-film layers. AFM tips (Fig. 1a) were coated with the required complementary material using a dip coating technique, while the other layer was coated on glass slide, depending on the particular adhesion analysis. Since the probe approaches the surface under ambient conditions of temperature (25°C) and humidity (40–50%), the tip experiences negligible interaction with the surrounding medium and its deflection remains close

to zero. This negligible interaction was experienced by the tip with the surrounding medium during the early stages of tip deflection (Fig. 1b(A-E)). After a while, it is eventually pulled into contact by adhesive force interactions with the surface of the substrate layer. There, the tip then bends elastically as it is further displaced in the downwards direction. Upon reversal of the displacement direction, the bending is reversed but the tip does not detach at zero force, due to the adhesive interaction. Hence, a negative force was used to pull-off the tip known as the pull-off force. Using Hooke's law and adhesion models available, force-displacement characteristics and adhesion energies were determined.

3.2 Device Processing and Characterization

All the chemical compounds purchased for preparing the thin-film layer samples and devices were of very high purity (99.99%), with the polymer solutions prepared in the laboratory just before use. In this work, model OLED structures Glass/ITO/PEDOT:PSS/MEH-PPV/Al were fabricated for the surface and optoelectronic characterizations. The device is shown schematically in Fig. 2.

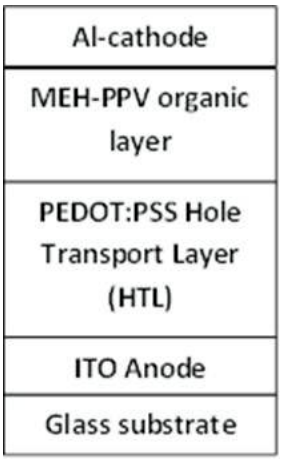


Figure 2:OLED structure showing different layers

The model OLED devices had poly (2-methoxy-5-(2'-ethylhexyloxy)-1,4-phenylenevinylene) (MEH-PPV) as their active layers. The ITO-coated glass structures (~100 nm) were fabricated by rf sputtering from an ITO target, using a magnetron sputtering system (Edwards Auto 306) at the Argon pressure of 3.2 x 10-3 Torr and 50 W rf power. The ITO samples were subsequently annealed at 2500C for 60 min. PEDOT:PSS (Sigma Aldrich, St. Louis, USA) was filtered and spin coated at 1500 rpm for 30 seconds, giving a thickness of 80 nm, as confirmed using a Veeco Dektak 150 surface profiler. MEH-PPV (Sigma Aldrich, St. Louis, USA) was prepared in the laboratory by dissolving 100 mg of MEH-PPV solute in 20 ml of Chloroform (0.5% g/mL). This was stirred at 700 rpm in the dark for 6 hours. It was then filtered using 0.25 µm mesh-sized filter and spin-coated onto the ITO-coated glass at 800 rpm. The above thin film was baked at 110°C for 15 minutes in air before the final aluminium cathode layer was thermally evaporated on the samples at high vacuum to complete the device.

4 Results and Discussions

4.1 Surface Characterization

The results of the surface profilometry measurements of films deposited on glass and ITO-coated glass are presented in Table 1. The lowest average roughness (Ra) recorded for ITO thin film on glass (0.72 ± 0.01 nm) shows a good deposition of anode from the sputtering process. The majority of the layers have roughness average values within reasonable limits, when compared to the actual thickness of the deposited layer.

Table 1: Roughness average, thickness and transmittance (T) for different layered structures

Structure	R_a (nm)	Thickness (nm)	T(%) at 450nm
ITO/Glass	0.70±0.03	100	95
PEDOT:PSS/Glass	3.50±0.30	100	98
PEDOT:PSS/ITO (heated at 100 ^{0}C)	3.90±0.30	100	85
PEDOT:PSS/ITO (heated at 250°C)	3.60±0.2	100	85
MEH-PPV/Glass	11.70±0.80	110	20
Aluminium/Glass	1.70±0.11	200	-

4.2 AFM Adhesion Measurements

The pairwise interactions between the layers are expressed in terms of the average pull-off forces, F_{pull}, and adhesion energies, G. There exists a wide range of adhesive forces exhibited between the surface pair interactions as summarized in Table 2. The highest average pull-off force of 126 N exists between organic-organic PEDOT:PSS/MEH-PPV layers. For the adhesion energy, PEDOT:PSS/MEH-PPV still dominates among the set of layers under analysis and the lowest is organic-inorganic PEDOT:PSS/ITO layers with an average energy of 1.7 J/m^2.This could be explained to be largely due to large covalent bonding between organic/organic layers.

Table 1: Summary of Adhesion results

Tip coat	Substrate coat	Average force (nN)	Adhesion Energy (J/m^2)
ITO	Glass	58.20±4.30	9.30±1.2
ITO	PEDOT:P	30.00±6.70	1.70±0.3
PEDOT:P	MEH-PPV	126.00±28.	32.00±7.

4.3 Current–Voltage Characteristics

The current-voltage curves obtained for the OLED devices fabricated are presented in Figs 3 & 4.

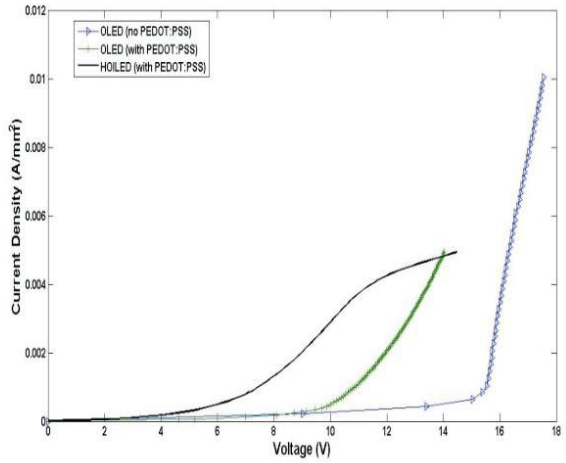


Figure 3 - Current Density – Voltage (J-V) Characteristic curve for OLED with HTL and without HTL

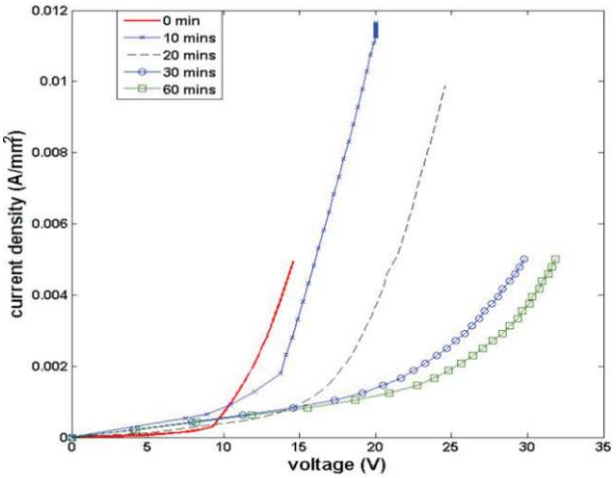


Figure 4 – Current Density –Voltage Characteristic curve showing degradation phenomena

The device fabricated without PEDOT:PSS layer as HTL produced turn-on voltages of 15V at 0 minute. This was repeated for a 6 minute time span and the turn-on voltage increased very little over this period implying that device degradation rather occurrs more significantly over a longer time range. For devices which had the PEDOT:PSS HTL layer, turn-on voltages occurred between 9V – 10V, and with currents of less than 1.0 mA. This shows that the hole transmission layer actually enhances the transport of holes to the active region for recombination of holes with much faster moving electrons from the cathode. The devices were then tested over a longer range period of half an hour to see the degradation trend. It is also observed that as the bias is applied, the surface of the Aluminium cathode undergoes a process that leaves an interesting feature as a result of the hydroscopic nature of the HTL, which dries up the aluminium layer leaving rough-like structures (carbonization) on the cathode surface. Microscopy images (Fig. 5) reveal black spots distributed all over the active region, which increased in size and number with time.

Figure 5:Optical microscope images showing evolution of dark spots and blisters in a degraded OLED

5. Conclusion

We have presented the results of a combined brief analytical and experimental study on the adhesion and degradation phenomena in organic light emitting diode (OLED) / hybrid organic-inorganic light emitting diode (HOILED) devices. It is found that the decrease in the contact lengths of the interfaces within the OLED structures results in increased current densities between the layers; this yields lower turn-on voltages in the OLED devices with PEDOT:PSS hole transport layer (HTL) component compared to those without HTL. Layers with high average pull-off force values exhibit high adhesion energy values, which increase with decreasing void length and as such satisfy the adopted model.

The failure of the OLEDs occur by the initiation and growth of black spots within the OLED structures. These are attributed to a combination of charge- and temperature-induced mass transport (carbonization) and delamination that increases with increased duration of applied bias. A look at the structure of the device under the microscope indicated these blisters with dark spots distributed over the entire active area after a couple of hour.

Acknowledgements

This research work was carried out at Sheda Science and Technology Complex (SHESTCO), Abuja,under the SHESTCO-AUST-Princeton Programme in Materials Science and funded by the World Bank STEP-B project.

REFERENCES

[1]Burroughes, J. H.; Bradley, D. D. C.; Brown, A. R.; Marks, R. N.; MacKay, K.; Friend, R. H.; Burns, P. L.; Holmes, A. B. (1990). Nature 347: 539

[2] C.W. Tang, S.A. Van Slyke, Appl. Phys. Lett. 51 (1987) 913.

[3] M.A. Baldo, D.F. O'Brien, Y. You, A. Shoustikov, S. Sibley, M.E.Thompson, S.R. Forrest,Nature 395 (1998) 151.

[4] Kuo C.H, Peng K.C, Kuo L.C, Yang KH, Lee J.H, Leung M.K, Hsieh K.H.. Chem. Mat. 2006;18:4121-4129.

[5] R.H. Friend, R.W. Gymer, A.B. Holmes, J.H. Burroughes, R.N. Marks, C. Taliani, D.D.C.

Bradley, D.A. Dos Santos, J.L. Bredas, M. Löglund, W.R.Salaneck, Nature 397 (1999) 121.
[6] H. Aziz, Z.D. Popovic, N.-X. Hu, A.-M. Hor, G. Xu, Science 283 (1999).
[7]Saba Zare Zardareh, Farhad Akbari Boroumand, Int. Degradation in Organic Light Emitting Diodes, Journal of Electronics, Circuits and Systems 3:3 (2009)
[8] Wali O. Akande,Yifang Cao,Nan Yao and Wole Soboyejo, J. Appl. Phys. 107, 043519 (2010).
[9] T. Tong, B. Babatope, S. Admassie, J. Meng, O. Akwogu, W. Akande, and W. O. Soboyejo, J. of Appl. Phys 106, 083708 (2009)
[10] Rev. AO, Vol. AN90 (Veeco Instruments Inc., 2005).
[11] Korhan Demirkan, INTERFACES OF ELECTRICAL CONTACTS IN ORGANIC SEMICONDUCTOR DEVICES, PhD Dissertation from the University of Delaware. (2008).
[12] C. H. Mastrangelo and C. H. Hsu, J. Microelectromech. Syst. 2, 33(1993).
[13] C. H. Mastrangelo and C. H. Hsu, J. Microelectromech. Syst. 2, 44(1993).
[14] Z. Zong, Yifang Cao, Nima Rahbar and Wole Soboyejo,J. Appl. Phys, 100,
[15] M. P. de Boer and T. A. Michalske, J. Appl. Phys. 86, 817 (1999).

EFFECTS OF STRETCHING ON FLEXIBLE ORGANIC ELECTRONIC STRUCTURES

O. K. Oyewole[1], J. Asare[1], M.G. Zebaze Kana[1,2], A.A. Oberafo[2], W.O. Soboyejo[1,3]
[1] *Department of Physics, African University of Science and Technology, Abuja, Nigeria*
[2] *Physics Advanced Laboratory, Sheda Science and Technology, Abuja, Nigeria*
[3] *Department of Mechanical and Aerospace Engineering, Princeton University, USA*

ABSTRACT
This work presents the responses of optical properties and microstructures of layers relevant to flexible organic electronics under tension using both analytical modelling and experiments. The optical and surface roughness characterizations of each of the layers of both stretched and as-fabricated structures were carried out to fully understand their dependence on stretching. In order to calculate the interfacial adhesion energies, adhesion forces of interfaces were measured using atomic force microscopy and incorporated into developed models along with material properties of each of the layers. The deformation induced during stretching was also modelled. The finite element was used to simulate stress distributions of the layers and crack driving forces of each of the stretched layers were calculated. The implications of the results obtained are, therefore, summarized for the design of stretchable organic solar cell.

Keywords: stretchable electronic, adhesion, structure, organic solar cell

1 Introduction

In recent years, there has been an increasing interest in the use of solar energy in several applications where stretchability, ductility, weight, cost and durability are priorities [1]. Some of these applications include solar panels which, in many cases, require stretching. There is also a vision of solar cells being integrated into electronic textiles [2] that are stretchable, and energy harvesting devices that are draped over the roof tops of houses [3,4]. Since such solar cells can be subjected to stress, there is a need to develop a basic understanding of the effects of stress on their layers.

In an effort to develop more robust solar cells that can deform by stretching or bending, significant efforts have been made to deposit solar cells on flexible substrates [5-8]. Stephenie *et al* [9] have studied the electrical properties of stretchable gold films and shown that gold films can function as interconnects for power and signal to a fully elastic thin film transistor inverter. The experimental investigations of the elastic-plastic deformation behaviour and cracking of nano/micro thick conducting metal on poly(dimethyl-siloxane) substrates have also been carried out in literature [10,11].

In spite of the tremendous efforts on the study and fabrication of organic electronics, researchers have not yet discussed the effects of stretching on layers of the organic electronic in order to improve charge transport mechanism across the layers during service conditions. In this paper, we study the effects of stretching on the layered structures of stretchable organic solar cells.

2 Modelling

2.1 Mechanical Stress

Since organic electronic structures are being considered for application in stretchable electronic devices, they can deform under service conditions. However, there is an extent to which they can be stretched without significant damage [12]. In this study, a simple composite framework (Fig. 1) is used to model the deformation behaviour of stretchable solar cells.

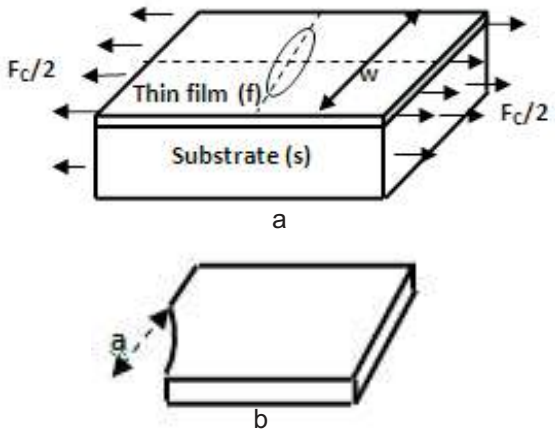


Figure 1*: Composite framework of (a) a stretched thin film on PDMS substrate, (b) a quarter of the thin film*

The stress on the composite is given by [11]:

$$\sigma_c = \frac{1}{t_{total}}\left(E_s\varepsilon_s t_s + E_f\varepsilon_f t_f\right) \qquad (1)$$

where E, ε, and t are Young's modulus, strain, and thickness respectively; t_{total} is the total thickness of the composite, s and f designate substrate and thin film layer, respectively.

Equation (1) is used to estimate the stress-strain behaviour of each of the layers of stretchable organic electronics.

2.2 Adhesion Force Measurement

The contact mode of atomic force microscopy (AFM) is generally used to measure the adhesion force between two surfaces. First, the tip coated with a complementary material, is displaced towards the substrate of the bi-material pair. The tip then jumps to contact with the substrate when adhesive interactions are experienced. The tip is bent under elastic deformation as both surfaces remain in contact. Its displacement is reversed but residual adhesion interactions still keep it in contact with the substrate even at zero loads, until a negative force (pull off force), which eventually overcome the adhesion, is experienced. These various steps have been explained in literature [8,13].

According to Hooke's law, the applied force is directly proportional to the displacement provided that the elastic limit is not exceeded. Hence, the adhesion force is related to the displacement as:

$$F_{adhesion} = -kx \qquad (2)$$

where k is the spring constant and x is the displacement. The negative sign accounts for the negative force experienced.

2.3 Adhesion Energy

Derjaguin-Muller-Toporov (DMT) model is used to describe interactions between stiff materials [13]. Knowing the value of the adhesion force, $F_{adhesion}$, and the effective radius, R, from AFM, we can estimate the adhesion energies of each of the interfaces of the layered organic electronic structures. The adhesion energy is related to adhesion force as [13]:

$$\gamma_{DMT} = \frac{F_{adhesion}}{2\pi R} \qquad (3a)$$

$$\frac{1}{R} = \frac{1}{R_{tip}} + \frac{1}{R_{rms}} \qquad (3b)$$

where R_{tip} and R_{rms} are the radii of the AFM tip and the root mean square roughness of the substrate, respectively.

3 Experimental Procedure

3.1 Fabrication of Layers

First, poly(dimethyl-siloxane) (PDMS) substrate was fabricated by mixing Slygard 184 silicone elastomer base with Slygard 184 silicone elastomer curing agent in 10:1 weight ratio. The mixture was degassed in a vacuum oven of pressure 15inHg for 60min to remove all bubbles. The degassed PDMS was then poured in a glass mold of dimension 25x25x1mm^3. This was cured at different conditions (70°C for 60min, 100° C for 45min, 125°C for 25min, and at room temperature for 3days). The optical transmittance of PDMS substrates was measured using an Avantes UV-VIS Spectrometer while their stress-strain was evaluated using universal tensile machine (TIRA test 2810). A 100nm-thick ITO layer was subsequently sputtered on the PDMS substrates cured at room temperature for 3 days. The sputtering process parameters used were as obtained in our previous work [14], but at room temperature. Furthermore, a 90nm-thick PEDOT:PSS thin film was spin coated on ITO-coated PDMS at 1000 rpm. The spin-coated PEDOT:PSS was baked at 70°C for 5min, after which an 100nm-thick P3HT:PCBM thin film was deposited by spin coating, at a speed of 1500rpm. Finally, a 150nm-thick layer of Al (99.99% pure) was thermally evaporated on the P3HT:PCBM/PEDOT:PSS/ITO-coated PDMS substrates.

3.2 Characterization of the Layers

The optical transmittance of as-deposited and stretched samples (PDMS, ITO/PDMS, PEDOT:PSS/ITO/PDMS, P3HT:PCBM/PEDOT:PSS/ITO/PDMS, and Al/P3HT:PCBM/PEDOT:PSS/ITO/
PDMS) were measured using Avantes UV-VIS-NIR spectrometer. The mechanical tensile test was also carried out on all the layers in order to estimate their stress-strain behaviour. The applied strain was varied from 0-150%. The grain structures of the as-deposited and stretched layers were observed under optical microscope. The scanning electron microscopy (SEM) of the relaxed stretched layers was carried out using a Carl Zeiss EVO MA-10 SEM. The atomic force microscopy technique was used to measure the interfacial adhesion forces of the structures and the root mean square surface roughness of the layers. The thicknesses of the layered structures were measured using Veeco Dektak 150 surface profiler.

4 Results and Discussion

4.1 Finite Element Simulation of Stretching and Crack Driving Forces

In an attempt to further understand the behaviour of layers of organic electronic devices, ABAQUS software package was used to create and implement a 2D model of the system under tensile force. The material properties of the layers used are shown in Table 1.

***Table 1**: Material Properties of the Layers Used for Simulations*

Materials	Young's Mod.(GPa)	Poisson Ratio	Ref.
PDMS	0.003	0.48	[12,13]
Dust	70	0.3	[13]
PEDOT:PSS	1.56	0.3	[13]
P3HT:PCBM	6.02	0.35	[6]
ITO	116	0.35	[11,13]
Al	70	0.3	[6,11]

The results of the simulations are shown in Fig. 2. The results of the stress distribution show that layers with high Young's modulus are liable to fracture first as more stress are being distributed across them. It can be seen that more stress is distributed on ITO layer, followed by Aluminium, while the least stress is on the active layer. Furthermore, the energy release rate was calculated by varying the length of propagated crack across each layer. The results presented in Table 2 show that the energy release rate increases with increase in length of the crack propagated.

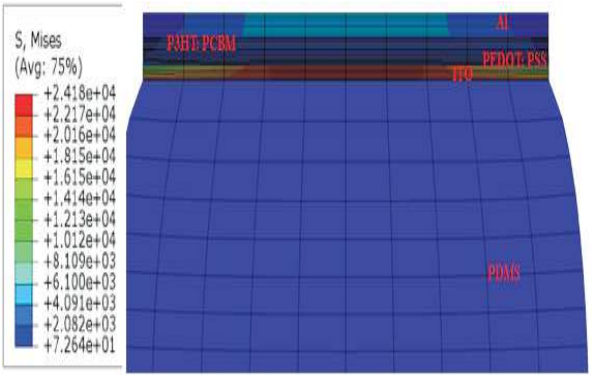


Figure 2: Distribution of Stress across the Layer of a Typical Stretchable Organic Electronics

4.2 Stress-Strain Measurement

The stress-strain curves of various cured PDMS substrates are shown in Fig. 6. The results show that the curing time and temperature, which contribute to the flexibility of PDMS substrates. In other words, the Young's modulus of PDMS decreases with decrease in curing temperature and time. The results obtained from the tensile test of the composites were incorporated into equation (1) for estimation of the stress-strain behaviour of each of the layers.

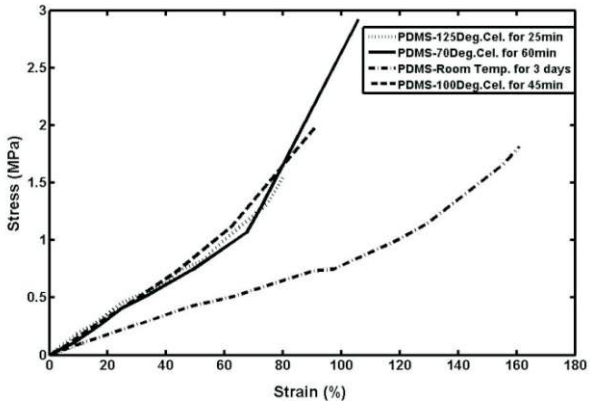


Figure 6: Stress-Strain Curves of PDMS substrates Cured at Different Conditions

The stress-strain curve of ITO layer coated on PDMS substrate is shown in Fig. 4. At points A, B, C, and D, the applied strains are 0, 20, 50, and 70%, respectively.

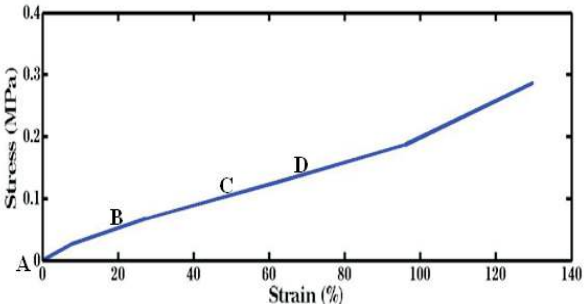


Figure 4: Stress-Strain Curve of ITO Layer on PDMS Substrate

Table 2: Energy Release Rate (G) for Cracks of Different Lengths

Crack Length (mm)	G (Jmm2) for ITO	G (J/mm2) for PEDOT:PSS	G (J/mm2) for P3HT:PCBM	G (J/mm2) for Al
2	0.56	42.72	10.67	0.95
4	1.47	109.33	27.37	2.44
6	3.22	239.22	59.86	5.33
8	7.46	554.78	139.1	12.36

4.3 Optical Transmittance

Fig. 3 shows the changes in the measured optical transmittance of ITO layer due to the applied strain. From the results, increasing applied strain reduces the optical transmittance of the layer. The optical properties of other layers have similar behaviour under monotonic loading.

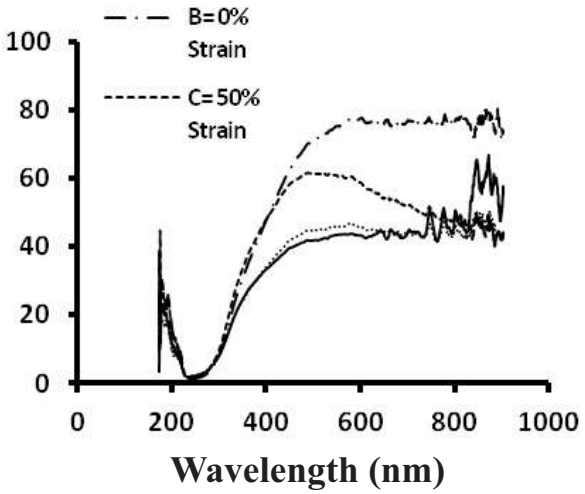


Figure 3: Change in Transmittance of ITO Layer on PDMS Substrate under Stretching

4.4 Changes in Microscopic Structures

The optical microscopy images of microstructures of the ITO layers at different applied strains are shown in Fig. 5. The grain size reduces as the applied strain increases. The same behaviour was observed in other layers of the organic electronic structure. In other words, the grain sizes of the as-fabricated layers of organic electronic structures are larger than the stretched layers. Each of the layers starts to fracture at different applied strains.

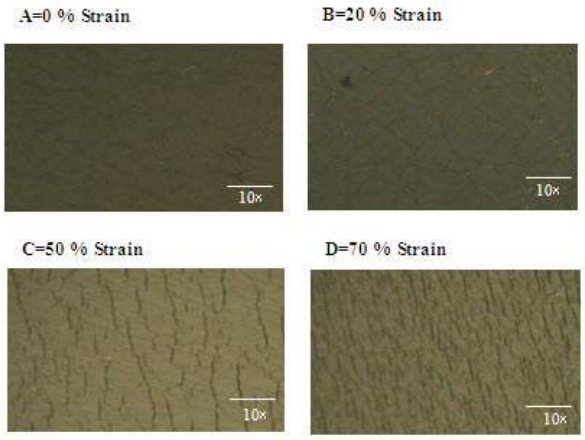


Figure 5: Change in Microscopic Structure of ITO Layer on PDMS Substrate under Stretching

4.5 Surface Roughness and Interfacial Adhesion of the Structure

The values of the measured adhesion forces at the interfaces were used to calculate interfacial adhesion energies of the layered structures. The results show that P3HT:PCBM/PEDOT: PSS interface has the highest adhesion force and energy of 187nm and 40J/m^2 respectively. The root mean square (RMS) roughness values of the layers range from 0.73nm to 9nm.

5 Conclusion

In this work, we have presented the effects of stretching on the optical property and microscopic structure of layers relevant to organic electronics. The optical transmittance of these layers decreases with increase in the applied strain. It has also been found that the energy release rate increases with increase in crack length. The fracture begins to occur in the studied layered structures when strained to about 50%. The interfacial adhesion energy between layers of P3HT:PCBM and PEDOT:PSS is the highest in the investigated layered structures.

Acknowledgements

This research was supported by World Bank Step-B Project. The authors would also like to extend their appreciation to all staff of Physics Advanced Laboratory, Sheda Science and Technology Complex, Abuja and Tifany Tong, Princeton University, USA for their immense contributions to the success of this work.

References

[1] M. Pagliaro, C. Palmisano, and R. Ciriminna, Flexible Solar Cells, (2008), 120

[2] A. Rohatgi, Crystalline Silicon Solar Cells and Modules, NREL 15th Workshop (2005) 11-12

[3] J. Weiss, P. Kukuri, J. Chiguma, J. Gendon, B. Arfaei, P. Borgesen, and W. Jones, Fabrication of low cost flexible solar using solution-based coating techniques, Global Solar Technology (2011) 10-15

[4] G. Dennler, C. Lungenschimied, H. Neugebauer, and N. S. Sariciftci, J. Matter. Res.,Vol. 20, No. 12, (2005)

[5] F. C. Krebs: Sol. Energy Mater – Solar cells 93 (2009) 1968-1977

[6] A.G. Evans and J.W. Hutchinson: The Thermomechanical Integrity of Thin Films and Multilayers, Acta metal. Mater. Vol. 43. No 7, pp. 2507-2530, 1995.

[7] L. Blankenburg, K-Schulthsis, H. Schach, S. Sensfuss, M. Schroder, Sol. Energy Mater. Sol. Cell 93(2009) 476-483

[8] D. R. Hodges, V. Palekis, S.

Bhandaru, K. Singh, D. Morel, E. K. Stefenakos, and C. S. Ferekides: Mater. Res. Soc. Symp. Proc. Vol. 1165 (2009)

[9] Stephanie P. Lacour, Joyelle Jones, Sigurd Wegner: Elastomeric Interconnects, International Journal of High Speed Electronics and System, Vol. 16, No 1 (2006) 397-407

[10] S. Midturi: Stress-Strain Behaviour of Nano/Micro Thin Film Material, ARPN Journal of Engineering and Applied Science, Vol. 5, No. 3, 2010

[11] O. Akogwu, D. Kwabi, S. Midturi, M. Eleruja, B. Babatope, W. O. Soboyejo: Large Strain Deformation and Cracking of Nano-Scale Gold Films on PDMS Substrate, Materials Science and Engineering B 170 (2010) 32-40

[12] Tang, C. W.: Two-layer Organic Photovoltaic Cell. Appl. Phys. Lett. 48,183-185 (1986)

[13] T. Tong, B. Babatope, S. Admassie, J. Meng, O. Akwogu, W. Akande and W. O. Soboyejo: Adhesion in Organic Structures, Journal of Applied Physics 106, 083708 (2009).

[14] M. G. Zebaze Kana, E Centurioni D. Iencinella, C. Summonte, Thin Solid Films 500 (2006) 203 – 208